THE JOURNAL
OF
CHEMICAL PHYSICS

VOLUME 34, NUMBER 6 JUNE, 1961

Effect of Inert-Gas Moderators on the (n, γ) Activated Reaction of I^{128} with CH_4†

EDWARD P. RACK* AND ADON A. GORDUS

Department of Chemistry, The University of Michigan, Ann Arbor, Michigan

(Received November 18, 1960)

In the presence of a large excess of gaseous methane, 54.4±0.5% of I^{128} formed by (n, γ) activation was found to become stabilized in organic combination. The effects of inert-gas additives in moderating the reaction of I^{128} with CH_4 were determined in an effort to ascertain the mechanism. The data, extrapolated to zero mole-fraction methane, indicate that xenon is capable of reducing the organic I^{128} to 11% whereas neon, argon, and krypton each reduce it to only about 36%. These data suggest that of the 54.4% organic I^{128}, about 18.4% forms as a result of hot I^{128} reactions, 11% as a result of excited iodine atoms or I^+ ions in the $^3P_2$, $^3P_1$, and/or $^3P_0$ states, and 25% as a result of reactions of $I^+(^1D_2)$ ions.

INTRODUCTION

HORNIG, Levey, and Willard[1] determined that I^{128} produced by the I^{127} $(n, \gamma)I^{128}$ process is able to react with gaseous methane to form CH_3I^{128}. Further investigations by Levey and Willard[2] indicated that molecules with ionization potentials lower than that of an iodine atom are more effective than inert gases in moderating the $I^{128}+CH_4$ reaction. They interpreted these data as indicating that the positive charge[3] associated with at least 50% of the I^{128} atoms is an important factor in the reaction.

Single displacement and abstraction reactions of thermal iodine atoms or ions with methane are endothermic:

$I+CH_4 \rightarrow CH_3I+H$	1.72 ev
$I^+ + CH_4 \rightarrow CH_3I^+ + H$	0.78
$I^+ + CH_4 \rightarrow CH_3I + H^+$	4.98
$I+CH_4 \rightarrow CH_3+HI$	1.33
$I^+ + CH_4 \rightarrow CH_3^+ + HI$	0.87
$I^+ + CH_4 \rightarrow CH_3 + HI^+$	1.23.

On considering the relative masses of the two colliding bodies, one can argue further that, to have available as internal energy of the activated complex the energies listed above, the iodine atom or ion must possess a minimum kinetic energy that is $(128+16)/16=9$ times as great as the endothermicity of the reaction. This energy for reaction is provided to the I^{128} as a result of the neutron capture-gamma ray recoil. If the neutron binding energy (6.6 Mev)[4] is released as one gamma ray, an I^{128} atom would acquire 182 ev of recoil kinetic energy. There are available, however, data which indicate that the average number of gamma rays emitted as a result of neutron absorption of I^{127} is greater than one. The emission of low-energy gamma rays has been demonstrated.[5] In addition, there is indirect[6] and direct[7] experimental evidence that, following neutron absorption, approximately 1% of the I^{128} fail to dissociate from alkyl iodide molecules. Such failure to bond-rupture could result if there occurs partial cancellation of gamma-ray momenta as a result of multi-gamma emission. Because of the lack of experimental data regarding I^{128} neutron capture-gamma rays, it is impossible to determine precisely the energy spectrum resulting from the gamma recoil. However, if it is assumed that the energy distribution is similar to

† Presented in part at the Symposium on the Chemical Effects of Nuclear Transformations at Prague, October, 1960, sponsored by the International Atomic Energy Agency; supported in part by a grant from the University of Michigan-Memorial Phoenix Project and by the U. S. Atomic Energy Commission, Division of Research.

* Based on work performed in partial fulfillment of the requirements for the Ph.D. degree of E. P. Rack. Receipt of a Proctor and Gamble fellowship is gratefully acknowledged.

[1] J. F. Hornig, G. Levey, and J. E. Willard, J. Chem. Phys. **20**, 1556 (1952).

[2] G. Levey and J. E. Willard, J. Chem. Phys. **25**, 904 (1956).

[3] S. Wexler and H. Davies, J. Chem. Phys. **20**, 1688 (1952).

[4] *American Institute of Physics Handbook* (McGraw-Hill Book Company, Inc., New York, 1957), p. 8–135.

[5] M. Reier and M. H. Shamos, Phys. Rev. **100**, 1302 (1955).

[6] A. A. Gordus and J. E. Willard, J. Am. Chem. Soc. **79**, 4609 (1957).

[7] A. A. Gordus and C. Hsiung, Paper No. 49, IAEA Symposium on the Chemical Effects of Nuclear Transformations, Prague, October, 1960.

Copyright © 1961 by the American Institute of Physics

TABLE I. Percent I^{128} (and I^{131}) stabilized in organic combination in various gaseous mixtures.[a]

Additive	Pressure CH_4-mm	Pressure additive-mm	Mole fraction additive[b]	Percent I^{128} as organic[c]	Percent I^{131} as organic[d]
Neon	594	76	0.113(11)	52.9	
	489	159	0.245(8)	53.1 52.2	
	308	128	0.294(24)	53.3 52.8	2.6 2.2
	362	231	0.390(45)	50.0 54.0	
	205	133	0.394(32)	50.1	
	205	129	0.386(32)	50.1	
Argon	400	189	0.321(27)	54.3 54.5	3.8 3.9
	295	235	0.443(31)	52.2 52.0	3.0 2.0
	109	410	0.765(59)	45.4 47.4	
	50	341	0.872(67)		1.0 1.5
Krypton	595	80	0.119(2)	53.8 53.5	
	483	106	0.180(3)	52.4	5.1
	320	120	0.273(3)	49.5 48.5	
	432	236	0.353(3)	50.5 51.8	6.2 7.3
	194	141	0.421(1)	45.6 45.0	
	143	412	0.742(4)	49.3 49.0	8.8 9.1
	43	456	0.914(3)	48.0	10.8
Xenon	615	40	0.061(2)	50.8 50.5	
	563	61	0.098(4)	48.3 47.3	2.3 3.3
	554	101	0.154(2)	45.2 46.5	
	489	179	0.268(2)	39.6 39.8	
	251	307	0.552(4)	31.6 29.4	7.7 8.0
	179	331	0.649(4)	30.5 29.2	
	72	447	0.865(5)	31.0 30.4	16.0 14.0
	60	454	0.883(5)	29.2 29.3	
	23	515	0.957(5)	24.1 24.5	

[a] All samples contained 0.1±0.02 mm I_2 and 0.5±0.3 mm CH_3I and were irradiated for 7 sec.
[b] Calculated assuming additive pressures. Uncertainty in last figure or figures (given in parenthesis) is based on estimates of determining individual pressures.
[c] An uncertainty of ±0.5 was associated with the positioning of the 25.0 min slope through the decay data.
[d] An uncertainty of ±1.5 was associated with the decay data and possible pre-irradiation I_2—CH_3I exchange.

that resulting in the Cl^{35} (n,γ) Cl^{36} process,[8] then the average recoil energy associated with the I^{128} would be approximately 100 ev; approximately 96% of the I^{128} would acquire more than 45 ev and 99+% more than 7.1 ev. Thus, it would be expected that most of the I^{128} atoms or ions are capable of forming CH_3I or HI via a hot reaction with CH_4.

The formation of CH_3I^{128} need not, however, be limited to the above reactions. It is also possible that a positively charged I^{128} react with CH_4 via an ion-molecule mechanism. For example, the following reactions could occur[9]:

$$I^+ + CH_4 \rightarrow CH_4I^+ \geqq -2.3 \text{ ev},$$

$$CH_4I^+ + e^- \rightarrow CH_3I + H - 6.2 \text{ ev}.$$

The above ion-molecule reaction does not require recoil kinetic energy.

Excited thermal I^+ ions may also react with CH_4. For example, I^+ in the $^1D_2$ state possesses an excitation energy of 1.70 ev.

We have been interested in determining qualitatively the mechanism of the reaction of I^{128} with CH_4. To do this, we have investigated the manner in which the reaction to produce organic I^{128} is inhibited by varying amounts of inert-gas additives.

EXPERIMENTAL

Reaction mixtures. All reaction mixtures were prepared by vacuum-line techniques and sealed in thin quartz bulblets 3–7 ml in size.

Phillips Petroleum Company research-grade CH_4 and Linde Air Products assayed-reagent inert gases were used. I_2 was sublimed from a mixture of Baker reagent I_2 and Merck reagent KI. Eastman Kodak white-label CH_3I was purified by concentrated H_2SO_4 treatment followed by washing and distillation.

Neutron irradiations. The samples were irradiated for 7 sec in a pneumatic tube of the University of Michigan megawatt pool reactor at a thermal neutron flux of about 1.4×10^{12} n/cm²-sec and a background radiation dosage of about 8000 r/min. As discussed below, corrections for radiation-induced reactions were made.

Extraction procedure. In all experiments, the irradiated bulblet was broken in a separatory funnel containing a two-phase mixture of $CHCl_3+I_2$ and approximately 0.5*M* aqueous Na_2SO_3. The organic fraction was separated from the inorganic and each fraction was counted using an Amperex Geiger tube. The data were then corrected for coincidence loss, decay, and relative counting efficiencies.

RESULTS

Summary of data. Summarized in Table I are the observed extents of production of organically bound I^{128} for various methane-inert gas reaction systems. These mixtures contained four substances: methane, inert gas, 0.5 mm CH_3I, and 0.1 mm I_2 scavenger.

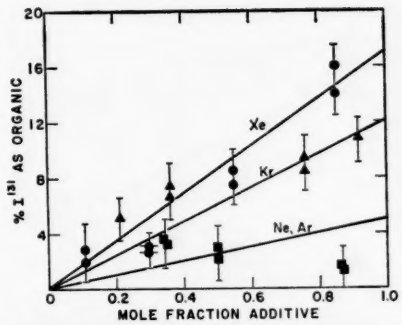

FIG. 1. Reactor-radiation induced pickup of I^{131} in CH_4-inert gas mixtures containing CH_3I and I_2–131. Xenon, ●; krypton, ▲; argon, ■; neon, -●-.

In order to interpret properly the relative effects of the additives, it is necessary to correct these data of Table I for (a) the 1.1% failure to bond-rupture of CH_3I[7] and (b) any radiation-induced reactions.

Radiation induced reactions. Mixtures containing I_2 tagged with I^{131} were also irradiated; the percent I^{131} appearing in organic combination is listed in Table I. These data are also depicted in Fig. 1. Negligible I^{131} pickup was found in I_2–CH_4 systems which did not contain an inert-gas additive.

In order to avoid any possible thermal or photochemical exchange reaction between the I_2–131 and CH_3I, all samples were prepared in a minimum of light and, if neutron irradiation was not immediately feasible, stored at 4°C in the dark. This technique resulted in a pre-irradiation I^{131} organic pickup of only 0–1.5%.

Comparable total pressures (540±60 mm) existed for each sample of Table I. In addition, all samples were (1) irradiated in the same position in the reactor and thus were subjected to the same dose rate; (2) irradiated for the same period of time and thus were subjected to the same total dose; and (3) contained comparable amounts of I_2.

The average energy of the gamma rays in a nuclear reactor is of the order of 2 Mev; therefore, the interaction of such gamma rays with matter proceeds mainly via Compton scattering. To a first approximation the primary interaction probability is related directly to the first power of the atomic number of the material. Levey and Willard[2] found that the amount of organic iodide formed in the I_2–CH_4 system by radiation-induced reactions increased with the pressure of the inert gas and with the number of electrons per atom of inert gas. It would be expected that the data of Fig. 1 should also indicate a similar dependence. The best visual straight lines were drawn through these data and at unit mole-fraction of inert gas (which corresponds to 540±60 mm) extrapolate to about 17%, 12%, and 5%

[8] C. Hsiung, H. Hsiung, and A. A. Gordus, J. Chem. Phys. **34**, 535 (1961).

[9] A. Henglein and G. A. Muccini, Z. Naturforsch. **15a**, 584 (1960).

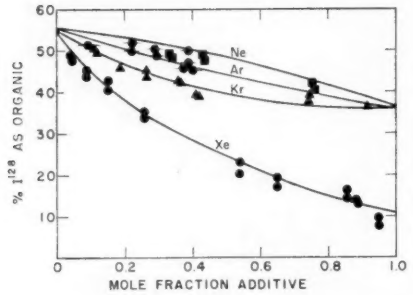

FIG. 2. Percent I^{128} formed as organic activity in CH_4-inert gas mixtures containing CH_3I and I_2. Moderator symbols are listed in caption for Fig. 1. The solid curves are calculated.

for Xe, Kr, and Ar-Ne, respectively. These values are in approximately the same ratio as the number of electrons per atom of inert gas.

If a sample contained I^{131}, the observed percent organic I^{131} was subtracted from the organic I^{128} yield. Since the remaining samples were similar in terms of total pressure and irradiation conditions, we used the data of Fig. 1 to determine the correction for radiation-induced reactions in these systems. To do this, we subtracted a quantity equal to the product of the mole-fraction of the inert gas and the extrapolated maximum extent of I^{131} pickup as determined in Fig. 1.

These I^{128} data of Table I, corrected for failure to bond-rupture and radiation-induced reactions, are depicted in Fig. 2.

Maximum extent of reaction. Extrapolations of the various data[10] to zero mole fraction of additive indicate that $54.4\pm0.5\%$ of the I^{128} reacts with methane to become stabilized in organic combination.

On the basis of previous gas chromatographic analyses,[6] it is known that CH_3I^{128} is the major organic product. The only other observable organic product was CH_2II^{128}, present to the extent of only about 1%.

DISCUSSION

If the CH_3I^{128} is formed only as a result of processes requiring excess kinetic energy, then a large excess of an inert gas should be capable of suppressing completely the formation of CH_3I^{128}. As seen in Fig. 2, the extrapolated data indicate that the inert gases only partially suppress the reaction. Apparently, then, only a fraction of the CH_3I^{128} is formed via hot processes which occur as the result of kinetic energy of the I^{128} atoms or ions. It should be noted that xenon reduces the CH_3I^{128} yield to $11\pm2\%$ whereas the other inert gases reduce this yield to only about $36\pm2\%$. The assumption that the reduction to 36% is a result mainly of excess kinetic-energy reactions is justified by the mathematical analysis given in the next section.

[10] These data include those presented in this paper as well as additional unpublished data concerned with the moderation of the $I^{128}+CH_4$ reaction by molecular additives.

The fact that xenon reduces the extent of formation of CH_3I^{128} by an additional $25\pm3\%$ must be due to a unique ability of xenon to neutralize or quench excited I^{128} ions or atoms. Inert gases, however, are not effective quenching agents.[11] Therefore, this additional inhibition by xenon must be due to a charge-transfer process. For xenon alone to reduce the extent of reaction by charge transfer requires that the energy defect of the reaction approach zero more closely than that for charge transfer with the other inert gases.

The first four excited states of I^+ (ionization potential, 10.454 ev) and their excitation energies are as follows[12]: ($^3P_0$) 0.800, ($^3P_1$) 0.879, ($^1D_2$) 1.702, ($^1S_2$) 4.044 ev. The ionization potential of CH_4 is 12.99 ev.[13] It is unlikely that excited states higher than the $^1D_2$ will exist in the methane environment since charge transfer between CH_4 and I^+ in the $^1S_2$ or higher states is exothermic. Such processes are very probable since the excess energy (energy defect) is assimilated by the various internal degrees of freedom of the methane ion. However, for charge transfer to take place between methane and I^+ ions in ($^1D_2$) or lower energy states requires much greater relative energies of the reacting species than that supplied by the (n,γ) activation.[14]

The ionization potential of xenon is 12.127 ev.[12] Thus, the process $I^+(^1D_2)+Xe\rightarrow I+Xe^+$ is exothermic by 0.029 ev. For this near-resonance charge-transfer process, the cross-section will be maximum for relative energies of about 2 ev and will slowly decrease for energies greater than 2 ev.[14] The smallest energy defect for the possible charge-transfer processes involving the other inert gases is 1.840 ev endothermic for the $I^+(^1D_2)+Kr$ reaction. Hence, these processes involving Kr, Ar, or Ne charge-transfer with I^+ ions in energy states of $^1D_2$ or less have an extremely small probability of occurrence.

It is reasonable to expect the excited iodine ions to react with methane prior to becoming deactivated by fluorescence. The iodine ions would have undergone of the order of 1000 collisions in the 10^{-8}—10^{-7} sec associated with fluorescent deactivation. Only in systems containing a large excess of inert gas would there be a possibility of fluorescent deactivation. This could be the reason that the last xenon data of Fig. 2 are low.

KINETIC-ENERGY MODERATION

Qualitative. If billiard-ball collisions are assumed to occur, then the average kinetic-energy transfer per collision would depend on the atomic weight of the moderator. The most effective inert gas would be xenon and the efficiency would decrease in the order: Kr, Ar, Ne. To interpret Fig. 2, where the data are

[11] K. J. Laidler, *The Chemical Kinetics of Excited States* (Oxford University Press, New York, 1955), p. 103.
[12] C. E. Moore, Natl. Bur. Standards Circ. No. **467**, 108 (1958).
[13] K. Watanabe, J. Chem. Phys. **26**, 542 (1957).
[14] E. F. Gurnee and J. L. Magee, J. Chem. Phys. **26**, 1237 (1957).

presented as a function of the mole fraction of the inert gas, it is also necessary to consider the gas-kinetic cross sections. Again, the order would be as stated above. Thus, qualitatively, the observed inert-gas moderation takes place in a manner characteristic of kinetic-energy removal.

Kinetic theory. Estrup and Wolfgang[15] have developed a kinetic theory of hot-atom reactions and have applied it successfully to the inert-gas moderation of the reaction of gaseous CH_4 with tritium produced by $He^3(n, p)H^3$ activation. Their theory involves three assumptions: (1) the collisions are elastic, (2) the minimum energy required for reaction is large compared with thermal energies; and (3) the energies of the hot atoms form a statistical distribution.

We can assume that the collisions between the inert gases and the I^{128} ions or atoms are elastic. Regarding the second assumption, we have stated earlier that for ground-state I^{128} ions or atoms to react with CH_4 requires that the I^{128} possess at least 7.1 ev of kinetic energy. We must also assume that the I^{128} atoms or ions are formed with energies which are distributed statistically.

Since the neutron capture-gamma ray cascade spectrum for the I^{127} $(n, \gamma)I^{128}$ process is not known, it is not possible to calculate the recoil-energy distribution. However, as discussed above, a distribution of energies does occur. This distribution is probably similar to that resulting in the Br^{79} $(n, \gamma)Br^{80}$ activation.[16] It has been shown[17] that moderation of the reaction of $Br^{80}+CH_4$ can be described in terms of the Estrup-Wolfgang theory. Thus, it may be assumed that there results an approximate statistical distribution of I^{128} energies.

It is important to emphasize that attempts to fit the data of Fig. 2 directly to this kinetic theory were unsuccessful. If, however, we assume that the maximum

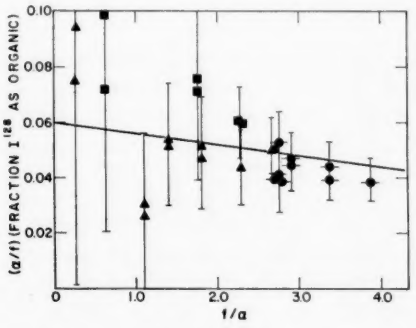

FIG. 3. Plot corresponding to Eq. (15) of reference 15. Moderator symbols are listed in caption for Fig. 1.

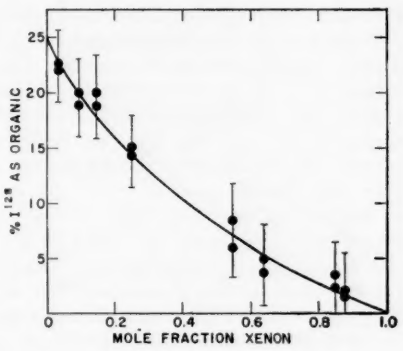

FIG. 4. Effect of xenon in moderating the reaction $I^+(^1D_2)+CH_4 \rightarrow CH_3I^+ + H$. The solid curve is calculated.

inert-gas kinetic-energy moderation is $54.4-36=18.4\%$ we then find that the theory serves to describe the observed effects.

Using the notation of Estrup and Wolfgang, we have calculated α values (which are concerned with the average energy loss per collision) and f values (which are related to the probability of collision between an iodine and an inert gas and thus include the mole-fraction as well as the relative diameters[18] of the colliding species).

Neon, argon, krypton. Thirty-six percent was subtrated from the individual values for the Ne, Ar, and Kr samples. For essentially pure methane, $f/\alpha=4.29$; thus, $(\alpha/f)\cdot$(fraction of I^{128} as organic)$=0.0428$. Figure 3 is a plot of the experimental data corresponding to Eq. 15 of reference 15: $(\alpha/f)\cdot$(fraction of the activity in a given form)$=1-(f/\alpha)K$. A straight line representation indicates agreement with theory. Equally important, all points, regardless of moderator, should fall on the same straight line. The best visual straight line drawn through the data and ending at the point (4.29, 0.0428) has a slope $-K=-0.004\pm0.003$ and an intercept $I=0.06\pm0.01$. It is interesting to note that, within the limits of uncertainty, these values correspond to those found for the $Br^{80}+CH_4$ reaction.[17] The solid curves of Fig. 2 for Ne, Ar, and Kr were calculated using these values of K and I.

Xenon. As stated earlier, the xenon data are not described by the kinetic theory. A lack of agreement still exists even after subtracting 11% from each experimental result. It was suggested in the previous section that xenon could be a more effective moderator since it could easily undergo charge transfer with $I^+(^1D_2)$. To determine the inhibition via the charge-transfer process, we subtracted from the original data: (1) the 1.1% CH_3I failure to bond rupture; (2) the

[15] P. J. Estrup and R. Wolfgang, J. Am. Chem. Soc. **82**, 2665 (1960).

[16] A. A. Gordus (unpublished data).

[17] E. P. Rack and A. A. Gordus, J. Phys. Chem. (to be published).

[18] The diameters used[19] were: I–4.8, Xe–4.9, Kr–4.3, Ar–3.6, Ne–2.6, and CH_4–4.2 A.

[19] S. Chapman and T. J. Cowling, *The Mathematical Theory of Nonuniform Gases* (Cambridge University Press, New York, 1953), p. 229.

radiation-induced production of CH_3I^{128}; (3) the 11% organic I^{128} which is not effected by xenon; and (4) the expected kinetic-energy moderation by xenon. This last factor varied from zero to 18.4% and was calculated in terms of Eq. 15 of reference 15 using the slope and intercept determined from Fig. 3 above. Depicted in Fig. 4 is the percent organic I^{128} remaining after correcting for these four effects.

Let us assume that we may consider the effects separately and that this remaining extent of reaction of I^{128} with methane to produce organically bound I^{128}, R, depends on the probability P that the I^{128} "collides" with CH_4. Thus, $R=25P$. The probability will depend on (1) the mole fraction of methane, $(1-N)$, where N is the mole fraction of additive; and (2) the relative cross sections C for the two types of interactions; $C=\sigma[I^+(^1D_2)+Xe \text{ charge exchange}]/\sigma[I^+(^1D_2)+CH_4$ to yield $CH_3I^{128}]$. Using these definitions, $C=[(25-R)(1-N)]/RN$.

The value of C calculated from the data of Fig. 4 is 2.2 ± 0.6. Considering the various subtractions and uncertainties, it is somewhat fortuitous that the calculated C curves are in reasonable agreement. The solid curve of Fig. 4 was calculated using this value of C.

REACTION PROCESSES

On the basis of the previous discussions, we conclude that of the $54.4\pm0.5\%$ I^{128} found as organic:

$18.4\pm2\%$ is formed via a hot reaction requiring kinetic energy. The experimental evidence, however, is insufficient to conclude whether the hot I^{128} species is an ion or an atom.

$25\pm3\%$ is formed as a result of the $I^+(^1D_2)+CH_4$ reaction. Considering the energy requirements, if the reaction is a simple hydrogen displacement, then the reaction must be $I^+(^1D_2)+CH_4\rightarrow CH_3I^++H$.

$11\pm2\%$ is formed as a result of the reaction of I^{128} ions (or highly excited atoms). Either $^3P_2$, $^3P_1$, or $^3P_0$ I^+ ions are involved since, as stated above, ions in energy states greater than the $^1D_2$ would not exist in the methane environment. If the ionic reaction taking place involves hydrogen displacement, then, considering the energy available, the reaction must also be $I^++CH_4\rightarrow CH_3I^++H$.

The manner in which the CH_3I^+ gains an electron is not known. It is difficult to accept electron capture as the process. The 9.54-ev exothermicity[13] would most probably be dissipated partially in the form of the internal energy of the molecule and thus probably result in C—I bond rupture.[20] If, instead, C—H bond rupture occurred, then, because of the presence of I_2 in the reaction system, CH_2I_2 should be a major product. Gas chromatographic analysis[6] indicated that only a small amount of CH_2I_2 was formed. However, because of the presence of CH_3I and I_2 in the reaction mixture, neutralization of the CH_3I^+ probably takes place via charge transfer.

FURTHER STUDIES

We are also investigating the effects of molecular additives on the moderation of the $I^{128}+CH_4$ reaction. Preliminary evidence indicates that, in addition to kinetic-energy moderation and charge neutralization, the molecular additives may also deactivate the I^{128} via what are probably ion-molecule reactions.

ACKNOWLEDGMENT

The authors appreciate the assistance of the staff of the Michigan Phoenix Reactor and wish to thank Professor Reed A. Howald for helpful discussions.

[20] (a) Reference 11, p. 57; (b) J. L. Magee and M. Burton, J. Am. Chem. Soc. **72**, 1965 (1950).

Quantum Mechanics of Mobile Electrons in Conjugated Bond Systems. I. General Analysis in the Tight-Binding Formulation*

KLAUS RUEDENBERG

Institute for Atomic Research, Department of Chemistry, Department of Physics, Iowa State University, Ames, Iowa

(Received March 16, 1959)

The quantum-mechanical treatment is carried through for a set of electrons in a homonuclear conjugated bond system of arbitrary size, including electronic interaction and including all overlap effects between neighbors. All framework contributions are obtained by explicit integration over the framework Hamiltonian, including the effect of nonconjugated neighbor atoms and differentiating between different types of conjugated atoms (joint, nonjoints, etc.). Expressions are given for the ground-state energy, ionization potential, electron affinity, electronegativity, and for the configuration interaction matrix for the calculation of excited states, assuming singly excited configurations. The results take simple forms permitting instructive interpretations. The partial additivity of one-electron binding-energy contributions, obtained as eigenvalues of topological molecular orbitals, and the approximate validity of the "neglect of differential overlap" is proved.

INTRODUCTION

SINCE its inception, the concept of mobile electrons in conjugated bond systems has provided a remarkably successful model in spite of many limitations, which must largely be attributed to the simplifying assumptions which usually have gone along with it. It is therefore surprising that no rigorous treatment of the quantum-mechanical problem has been carried through. The fruitfulness of the model indicates that it will always remain useful; it lends particular interest to the assumptions and invites a closer scrutiny of their relative significance. But a proper appreciation of the real foundations seems indispensable in order to assess and eliminate the limitations and inconsistencies. Certainly, after so much semi- and sesquiempirical work on the subject, steps towards rigorosity are not out of order.

While the developments given here are essentially written with the pi-electron systems of organic molecules in mind, the essential formulations apply equally to other conjugated bond systems which occur, e.g., in crystals and metals with mobile electrons.

I

The original work of Hückel,[1] which was further developed by Lennard-Jones,[2] Coulson,[3,4] Mulliken and Wheland,[5] Longuet-Higgins,[4,6] and others, is a *one-electron theory* with its shortcomings. The same holds for the free-electron theory, first suggested by Schmidt[7]; in particular the network formulation, developed by Platt,[8] Kuhn,[9] Ruedenberg and Scherr,[10] and others,[11] which was shown to be equivalent to the LCAO formulation,[12] has contributed an illuminating interpretation of the meaning of the model.

The beauty and usefulness of these approaches lies in the elegant simplicity of the mathematical formalism; a simplicity which prevails also when the system becomes arbitrarily large and, as Mulliken and Wheland first showed,[5] when all integrals between neighbor atoms are taken into account and only those involving the overlap between nonneighbors are neglected (*"tight-binding approximation"*). The latter circumstance is extremely gratifying since the quantitative examination of integrals between atomic orbitals shows that the neglect of integrals containing the overlap of nonneighbors can be honestly justified, whereas this is obviously not the case for integrals between neighbors. Thus, the tight-binding approximation is a bona fide first approximation, *whereas the outright neglect of neighbor overlap is not.*

The first step towards a rigorous approach beyond the one-electron model was taken by M. Goeppert-Mayer and A. L. Sklar,[13] who carried through the inclusion of the interaction between electrons in the case of benzene by means of a determinantal wave function. The treatment contained however, a theoretically inconsistent simplifying assumption: use is made, *in integrals between different atomic orbitals*, of

* Contribution No. 665. Work performed in the Ames Laboratory of the U. S. Atomic Energy Commission.

[1] E. Hückel, Z. Physik **70**, 204 (1931); Z. Electrochem. **43**, 752, 827 (1937), review; Z. Physik **72**, 310 (1931); **76**, 628 (1932).

[2] J. E. Lennard-Jones, Proc. Roy. Soc. (London) **A158**, 280 (1937).

[3] C. A. Coulson, Proc. Roy. Soc. (London) **A169**, 413 (1939); C. A. Coulson and G. S. Rushbrooke, Proc. Cambridge Phil. Soc. **36**, 193 (1940); B. H. Chirgwin and C. A. Coulson, Proc. Roy. Soc. (London) **A201**, 196 (1950); C. A. Coulson, R. Daudel, and D. M. Robertson, *ibid.* **A207**, 306 (1951).

[4] C. A. Coulson and H. C. Longuet-Higgins, Proc. Roy. Soc. (London) **A191**, 39 (1947); **A192**, 16 (1947); **A193**, 447, 456 (1948); **A195**, 188 (1948).

[5] R. S. Mulliken, C. Rieke, and S. Brown, J. Am. Chem. Soc. **63**, 41 (1941); see also R. S. Mulliken and C. Rieke, *ibid.* **63**, 1770 (1941); G. W. Wheland, *ibid.* 2025 (1941); P. O. Löwdin, J. Chem. Phys. **18**, 365 (1950).

[6] H. C. Longuet-Higgins, J. Chem. Phys. **18**, 265, 275, 283 (1950).

[7] O. Schmidt, Ber. deut. chem. Ges. **73A**, 97 (1940).

[8] J. R. Platt, J. Chem. Phys. **17**, 484 (1949).

[9] H. Kuhn, J. Chem. Phys. **16**, 840 (1948); **17**, 1198 (1949); Helv. Chim. Acta **31**, 1441 (1948).

[10] K. Ruedenberg and C. W. Scherr, J. Chem. Phys. **21**, 1565 (1953); C. W. Scherr, *ibid.* **21**, 1582 (1953).

[11] N. S. Bayliss, J. Chem. Phys. **16**, 287 (1948); Quart. Revs. **6**, 319 (1952); W. T. Simpson, J. Chem. Phys. **16**, 1124 (1948).

[12] K. Ruedenberg, J. Chem. Phys. **22**, 1878 (1954); N. S. Ham and K. Ruedenberg, *ibid.* **29**, 1199, 1215 (1958).

[13] M. Goeppert-Mayer and A. L. Sklar, J. Chem. Phys. **6**, 645 (1938); C. C. J. Roothaan and R. G. Parr, *ibid.* **17**, 1001 (1949); J. Jacobs, Proc. Phys. Soc. (London) **A62**, 710 (1949); R. G. Parr, D. P. Craig, and I. G. Ross, J. Chem. Phys. **18**, 1561 (1950).

the eigenvalue equation

$$(T+U_P)\chi_P=W_P\chi_P,$$

where T is the kinetic energy, U_P is the part of the framework potential originating from the carbon atom P, χ_P is the AO contributed from the same carbon atom towards the MO's, and W_P is the valence state ionization potential of carbon. Neither is this eigenvalue identity justifiable in principle, nor is it at all close to being satisfied by the particular U_P and χ_P chosen in practice. In spite of this adjustment and in spite of the high symmetry, causing many simplifications, the complexity of this treatment seemed to place it in a class different from the aforementioned models, discouraging its extension to large systems.

The inkling that this apprehension is probably unjustified has been the most important recent advance. It was observed by Parr and Pariser,[14] and also by Pople,[15] that the Goeppert-Mayer-Sklar approach can be cast in a form compatible in mathematical simplicity with the one-electron theories, *if neighbor overlap is neglected and all two-electron integrals, except the two-center Coulomb integrals, are neglected (neglect of differential overlap)*. Moreover Pariser and Parr showed that the results of such a treatment do not essentially deviate from those of the Goeppert-Mayer-Sklar formulation when the same integral values are used, and furthermore that much closer agreement with the experimental spectroscopic data of benzene can be achieved by introducing a semiempirical adjustment of the electron-interaction integrals and of the resonance integral.[14]

In extending the calculations to hydrocarbons larger than benzene, the question arose: how much configuration interaction is appropriate for the satisfactory understanding and prediction of the electronic spectra? Pariser[16] tested a *great* number of interacting one-electron excitations; Pople[17] chose only two such configurations (the "paired excitations," see Sec. 4); Ham and Ruedenberg included those four excited configurations which are analogous to those in benzene.[18] The latter choice, which goes back to J. R. Platt's pioneering interpretation of aromatic spectra,[8] seemed to be the most satisfactory one in comparison with experiment. The last-mentioned calculation was carried out in the free-electron network theory, demonstrating that here too the electronic interaction could be incorporated in a way quite similar to that used in the LCAO theory.

[14] R. G. Parr, J. Chem. Phys. **20**, 1499 (1952); R. Pariser and R. G. Parr, *ibid.* **21**, 466 (1953); **21**, 767 (1953); **23**, 711 (1955); R. Pariser, *ibid.* **21**, 568 (1953).
[15] J. A. Pople, Trans. Faraday Soc. **49**, 1375 (1953).
[16] R. Pariser, J. Chem. Phys. **24**, 250 (1956); **25**, 1112 (1956).
[17] J. A. Pople, Proc. Phys. Soc. (London) **A68**, 81 (1955).
[18] N. S. Ham and K. Ruedenberg, J. Chem. Phys. **25**, 13 (1956).

II

The present investigation would like to contribute some steps towards a more rigorous understanding of the problem. The main objective is to analyze the basic LCAO formulation of the pi-electronic approach with the help of such approximations as are *realistic and bona fide justifiable*, in particular without neglect of nonnegligible overlap terms.

The general formulations are arrived at in the first paper. Formulas are established for the ground-state energy, for ionization potential, electron affinity, electronegativity, and for the calculation of excited states—formulas which permit a simple interpretation and calculation. Concerning the ground state, an old controversy is settled by demonstrating that a major part of the binding energy can be expressed as a sum of the eigenvalues of a one-electron problem; they are of course different from the orbital energies.

These derivations are carried through including electronic interaction and all neighbor overlap effects and with an explicit analysis of the framework contributions. In the second paper the nonneighbor interactions are taken into account, and it is found that they add certain corrections, but will not alter the essential formulations.

For the contraction of the electron-interaction integrals two circumstances prove important. First, the effective Hamiltonian matrix, which determines the basic molecular orbitals, and the overlap matrix are both functions of the topological matrix (or, in the second paper, of a closely related matrix); hence the basic MO's are "topological" MO's and simultaneously eigenvectors of the overlap matrix. Second, the Mulliken approximation for electron interaction integrals is very accurate for $2p\pi$ AO's and therefore adopted. *The conjunction of these facts leads to essential simplifications and also emerges as the real reason for the rather good approximation achieved by the "neglect of differential overlap" under certain conditions.*

The third paper is devoted to a closer examination of the important molecular orbitals of the generalized Hückel type, which are based on the topological matrix. It is found that certain well-known regularities, like the Coulson-Rushbrooke theorem, are only special cases of a more general scheme of interesting cross-relations between bond-order-like quantities.

The last three papers deal with the quantitative aspects. Hitherto underived formulas for framework integrals are established in the fourth paper, and with their help a theoretical calculation of the framework energy contributions is carried out in the sixth paper without introducing unjustified relationships. These theoretical results are compared with the experimental conclusions deduced in the fifth paper. The application of the method to a number of large molecules is under way.

The degree of rigor introduced here shows new

aspects of the pi-electronic approach. A particular instructive part of the formulation is the somewhat intricate cancellation between attractive and repulsive terms, which can be traced in detail. This may lead to a better method for dealing with cases of less complete balancing, e.g., in the presence of hetero-atoms. Furthermore, the quantitative origin of the various energy contributions is established. Finally, certain fundamental quantitative difficulties are isolated, which will require further analysis.

1. HAMILTONIAN AND ATOMIC ORBITALS

General Formulation

The Hamiltonian for N pi electrons is

$$\mathfrak{H}=f(\mathbf{r}_i)+\sum_{i<j}e^2/r_{ij}, \tag{1.1}$$

$$f(\mathbf{r})=(\hbar^2/2m)\Delta+U(\mathbf{r}). \tag{1.1'}$$

The potential energy U can be written as a sum over atomic contributions

$$U(\mathbf{r})=\sum_a V_a(\mathbf{r}), \tag{1.2}$$

where the sum goes over all atoms, carbons and hydrogens. For the hydrogen atoms, $a=h$, let

$$V_h(\mathbf{r})=U_h^{\mathrm{H}}(\mathbf{r})=U^{\mathrm{H}}(\mathbf{r}-\mathbf{r}_h), \tag{1.3}$$

where $\mathbf{r}_h$ is the position vector of the hydrogen nucleus, and the potential energy of an electron in the field of a neutral H atom is given by

$$U^{\mathrm{H}}(\mathbf{r})=-e^2/r+e^2[(1s)^2|, \tag{1.4}$$

where

$$[\Omega| \quad \int dV'\Omega(\mathbf{r}')/|\mathbf{r}-\mathbf{r}'|=f(\mathbf{r}) \tag{1.5}$$

defines the potential of a charge cloud $\Omega(\mathbf{r}')$.

The potential of a carbon atom, $a=P$, is considered as that of the neutral carbon atom minus that of the pi electron which has been contributed to the Schroedinger function of delocalized electrons. The energy of an electron in this potential is therefore

$$V_P=U^{\mathrm{C}}(\mathbf{r}-\mathbf{r}_P)-e^2\int dV'[\chi_P(\mathbf{r}')]^2/|\mathbf{r}-\mathbf{r}'|, \tag{1.6}$$

$$=U_P{}^{\mathrm{C}}-e^2[\chi_P{}^2|, \tag{1.6'}$$

where χ_P is the AO contributed to the pi-electronic wave function. The potential due to the neutral carbon in its valence state, is given by

$$U^{\mathrm{C}}(\mathbf{r})=-e^2(4/r)+e^2[(2s)^2+(2px)^2+(2py)^2+(2pz)^2|, \tag{1.7}$$

i.e., the nucleus $(4e)$ is shielded by the electrons in the four indicated orbitals. The division into short-range and long-range forces, implicit in Eq. (1.6), will be commented upon after Eq. (2.17').

The potential proposed here differs from that introduced by Goeppert-Mayer and Sklar[13] in the following respects:

(1) The hydrogen atoms are taken into account.

(2) The orbital exponent ζ of the atomic orbital χ_P in Eq. (1.6) (AO *orbital exponent*) is not necessarily identical with the orbital exponent ζ_{C} of the four orbitals in Eq. (1.7) (*shielding orbital exponent*).

The following arguments suggest that the two orbital exponents may have to be chosen so that they are different from each other.

The Valence State of Carbon as Gauge

The integral

$$(\chi|(-\hbar^2/2m)\Delta+U^{\mathrm{C}}|\chi) \tag{1.8}$$

is the most sensitive one of the framework integrals, since it is the sum of two large terms (each about 35 ev) of opposite sign which cancel each other almost entirely. Hence a successful computation of framework energy contributions cannot be performed unless the two parts of Eq. (1.8) are properly balanced against each other.

The means for such balancing are the proper choice of the parameters ζ and ζ_{C}.

The criteria for the proper choice should be the known values for the ionization potential and the electron affinity of the valence state of carbon. According to Mulliken, one has[19]

$$\text{electron affinity}=A_{\mathrm{C}}=0.69\text{ ev}, \tag{1.9}$$

$$\text{ionization potential}=I_{\mathrm{C}}=11.22\text{ ev}. \tag{1.10}$$

Since the potential (1.7) corresponds to a neutral carbon, the expression (1.8) represents the energy of an additional electron, and hence it is related to the electron affinity by

$$-A_{\mathrm{C}}=(\chi|(-\hbar^2/2m)\Delta+U^{\mathrm{C}}|\chi). \tag{1.11}$$

Similarly, since Eq. (1.6) is the potential of the C^+ ion in the valence state, the energy of an electron in this potential must be related to the ionization potential; hence[20]

$$-I_{\mathrm{C}}=(\chi|(-\hbar^2/2m)\Delta+V|\chi)$$

$$=-A_{\mathrm{C}}-e^2\int dV_1\int dV_2\chi^2(1)\chi^2(2)/r_{12}. \tag{1.12}$$

That these two equations are consistent with each other can be seen by calculating the energy of *two* electrons,

[19] R. S. Mulliken, J. Chem. Phys. **2**, 782 (1934).

[20] That the one-center Coulomb integrals between the $2p\pi$AO's should equal the difference (I_C-A_C) was first postulated by Pariser. See the second and fourth paper of reference 14. See also W. Moffitt, Proc. Roy. Soc. (London) **A210**, 244 (1951).

occupying the orbital χ with opposing spins, under the influence of the potential (1.6). Their total energy becomes

$$-2I_C+e^2\int dV_1\int dV_2\chi^2(1)\chi^2(2)/r_{12}=-I_C-A_C,$$

i.e., the addition of the second electron lowers in fact the total energy by A_C.

The determination of the framework potential given here is not free of criticism. However, it is consistent and it leads to instructive formulations for the molecular energies. Independent support for this point of view is furnished by an examination of the benzene spectrum [see paper V, after Eq. (2.10)]. We therefore associate with A_C as defined by Eq. (1.11), and with I_C, as defined by Eq. (1.12), the proposed physical meanings, and relegate the analysis of the quantitative aspects to the fifth and sixth paper.

2. MATRIX ELEMENTS IN THE AO BASIS

Overlap Integrals

In the second paper, the error will be analyzed which is incurred when those integrals are neglected which involve the overlap between nonneighbor atomic orbitals. It will be seen that it is a valid approximation to neglect all contributions due to overlap between nonneighbors, but to take into account all contributions due to overlap between neighbors. This "tight-binding approximation" will be adhered to in the present paper.

If all atoms in the conjugated bond system are identical (carbon atoms), then all neighbor overlap integrals are equal, and the overlap matrix is

$$S_{PQ}=\delta_{PQ}+SM_{PQ}, \tag{2.1}$$

where

$$M_{PQ}=\begin{cases}1, & \text{if } P,Q \text{ are neighbors,}\\ 0, & \text{otherwise,}\end{cases} \tag{2.2}$$

is the "topological matrix" of the molecule. Certain properties of this matrix will become important in the subsequent derivations. A discussion of these properties is given in the third paper of this series.[21]

AO Integrals over Neutral Framework and Kinetic Energy

The following integrals have to be considered [see Eqs. (1.2–7)]

$$U_{PQ}=(\chi_P\mid\sum_R U_R{}^C+\sum_h U_h{}^H\mid\chi_Q)$$

$$=\int dV\chi_P\chi_Q\{\sum_R U_R{}^C(\mathbf{r})+\sum_h U_h{}^H(\mathbf{r})\}. \tag{2.3}$$

Since the integral contains the product of two AO's, it has an exponential decrease with distance similar to that of the overlap integral. Consequently only the case of P and Q being neighbors has to be taken into account, i.e.,

$$U_{PQ}=U_{PP}\delta_{PQ}+U_{PQ}M_{PQ}, \tag{2.4}$$

where M_{PQ} is given by Eq. (2.2).

Furthermore the potentials U^C and U^H, coming from neutral spherically symmetric charge distributions, decrease exponentially with distance, and the integral $(\chi_P\mid U_R{}^C\mid\chi_Q)$ decreases in fact more strongly with the distances (RP), (RQ), than do the corresponding overlap integrals. Consequently only those terms in the sum over R have to be kept for which [$R=P$ *or* (R, P) = neighbors] *and simultaneously* [$R=Q$ or (R, Q) = neighbors]. Similarly in the sum over h, only those terms have to be kept for which h is simultaneously a neighbor of P and Q.

Thus one obtains

$$U_{PP}=(\chi_1\mid U_1{}^C\mid\chi_1)+3(\chi_1\mid U_2{}^C\mid\chi_1), \tag{2.5}$$

if P is a joint atom;

$$U_{PP}=(\chi_1\mid U_1{}^C\mid\chi_1)+2(\chi_1\mid U_2{}^C\mid\chi_1)+(\chi_1\mid U_{h1}{}^H\mid\chi_1), \tag{2.5'}$$

if P is a nonjoint atom; and

$$U_{PP}=(\chi_1\mid U_1{}^C\mid\chi_1)+(\chi_1\mid U_2{}^C\mid\chi_1)+2(\chi_1\mid U_{h1}{}^H\mid\chi_1), \tag{2.5''}$$

if P is a free-end atom (end of a conjugated chain). Here the indices (1, 2) denote two neighboring C atoms, and the index $(h1)$ denotes the H atom neighboring to the nonjoint C atom (1). For any pair (PQ) of C atoms one finds

$$U_{PQ}=2(\chi_1\mid U_1{}^C\mid\chi_2). \tag{2.6}$$

The kinetic energy integrals,

$$T_{PQ}=(\chi_P\mid(-\hbar^2/2m)\Delta\mid\chi_Q), \tag{2.7}$$

do *not* contain the *product* $\chi_P\chi_Q$. However, upon closer inspection[22] it is found that T_{PQ} decreases with the distance (PQ) almost exactly as the *square of the overlap integral*. Hence we are again entitled to write

$$T_{PQ}=(\chi_1\mid(-\hbar^2/2m)\Delta\mid\chi_1)\delta_{PQ}+(\chi_1\mid(-\hbar^2/2m)\Delta\mid\chi_2)M_{PQ}, \tag{2.8}$$

where the symbol of Eq. (2.2) is used.

It is expedient to write the matrices U and T together as follows

$$(\chi_P\mid(-\hbar^2/2m)\Delta+\sum_R U_R{}^C+\sum_h U_h{}^H\mid\chi_Q)=(\alpha+\delta\alpha_P)\delta_{PQ}+\beta M_{PQ}, \tag{2.9}$$

where

$$\beta=(\chi_1\mid(-\hbar^2/2m)\Delta\mid\chi_2)+2(\chi_1\mid U_1{}^C\mid\chi_2), \tag{2.10}$$

[21] K. Ruedenberg, J. Chem. Phys. **34**, 1878 (1961).

[22] See Eq. (2.5) of the fourth paper of this series, K. Ruedenberg, J. Chem. Phys. **34**, 1892 (1961).

and α is the mean value of *all* diagonal elements α_P, whereas $\delta\alpha_P$ are the deviations from this mean value for the three types of elements given in Eqs. (2.5, 5′, 5″). One finds for the mean value

$$\alpha=-A_C+(1+\tau)(\chi_1 \mid U_2^C \mid \chi_1) +(2-\tau)(\chi_1 \mid U_{h1}^H \mid \chi_1), \quad (2.11)$$

where

$$-A_C=(\chi_1 \mid (-\hbar^2/2m)\Delta \mid \chi_1)+(\chi_1 \mid U_1^C \mid \chi_1), \quad (2.11')$$

is the negative of the carbon electron affinity given by Eq. (1.11), and τ is defined as follows. Let

$$\left.\begin{aligned} \tau_N &= \text{fraction of nonjoint atoms,} \\ \tau_J &= \text{fraction of joint atoms,} \\ \tau_E &= \text{fraction of free-end atoms,} \end{aligned}\right\} \quad (2.12)$$

so that

$$\tau_N+\tau_J+\tau_E=1,$$

then

$$\tau=\tau_N+2\tau_J. \quad (2.12')$$

The deviations $\delta\alpha_P$ are found to be

$$\left.\begin{aligned} \delta\alpha_E &= -\tau\delta\alpha \\ \delta\alpha_N &= (1-\tau)\delta\alpha \\ \delta\alpha_J &= (2-\tau)\delta\alpha \end{aligned}\right\} \quad (2.13)$$

with

$$\delta\alpha=(\chi_1 \mid U_2^C \mid \chi_1)-(\chi_1 \mid U_{h1}^H \mid \chi_1). \quad (2.13')$$

It is easily verified that indeed

$$\sum_{P=1}^{N}\delta\alpha_P=0.$$

AO Integrals of the Electron Interaction Type

The ionic part of the framework potential as well as electron interaction integrals lead to AO integrals of the form

$$[PQ \mid RS]=[\chi_P\chi_Q \mid \chi_R\chi_S], \quad (2.14)$$

with the definition

$$[\Omega \mid \Omega']=\int dV_1 \int dV_2 \Omega(\mathbf{r}_1)\Omega(\mathbf{r}_2)/r_{12}. \quad (2.14')$$

Our postulate is that the evaluation of these integrals should be carried out to a degree of approximation comparable in quality to the tight-binding approximation. In the light of this criterion, the exact evaluation of the integrals would be too elaborate an approach, whereas the "neglect of differential overlap (between neighbors)," used by Pariser and Parr and by Pople, would be too great a simplification.

An adequate solution seems to be the approximation suggested by R. S. Mulliken.[23] Thereby automatically all those integrals will vanish which are proportional to the overlap of nonneighbors. Thus we put

$$[PQ \mid RS]=S_{PQ}S_{RS}[G(PR)+G(PS)+G(QR) +G(QS)]/4, \quad (2.15)$$

where S_{PQ} is defined by Eq. (2.1), and $G(PQ)$ is the Coulomb integral

$$G(PQ)=G(P,Q)=[PP \mid QQ]=\mathfrak{G}(R_{PQ}). \quad (2.16)$$

Although the Mulliken approximation seems to be the most appropriate one for $2p\pi$ orbitals, it is also possible to use the Sklar-London approximation.[24] It is shown below, that the London approximation can be numerically reproduced[25] if one merely adds to the right-hand side of Eq. (2.15) the "correction term"

$$[PQ \mid RS]'=\tfrac{1}{2}S^2g_2M_{PQ}M_{RS}(\delta_{PR}\delta_{QS}+\delta_{PS}\delta_{QR}), \quad (2.17)$$

where

$$g_2=G(1,1)-G(1,2). \quad (2.17')$$

This term is zero except for the two-center exchange integrals $[12 \mid 12]$. Its effect upon the final results is, however, small.

Short-Range and Long-Range Forces

Two kinds of energy terms can be clearly distinguished. Those due to the short-range forces which result from the neutral parts of the framework potential are given by Eq. (2.9). Those due to the Coulombic long-range forces, *viz.*, ionic attraction by the framework and interelectronic repulsion, are given by Eq. (2.15). It emerges that the short-range terms are essentially determined by the matrix **M** of Eq. (2.2), i.e., by the *topology* of the molecule. The *geometry* of the molecule is only introduced by the long-range terms, *viz.*, via the AO Coulomb integrals $G(PQ)$. It is a conceptual advantage of the tight-binding approximation that it makes the short-range forces strictly topological in character. This is the physical reason for the importance of the properties of the topological matrix **M** discussed in the third paper.[21] In the augmented tight-binding approximation defined in the second paper, the short-range forces are assumed to be determined by the overlap matrix.

AO Integrals for the Transition Moment

In order to calculate spectral intensities and dipole moments, one needs the integrals $(\chi_P \mid \mathbf{r} \mid \chi_Q)$. It is

[23] R. S. Mulliken, J. chim. phys. **46**, 500, 521 (1949); See also K. Ruedenberg, J. Chem. Phys. **19**, 1433 (1951).

[24] A. L. Sklar, J. Chem. Phys. **7**, 990 (1939); A. London, *ibid.* **13**, 417 (1945); See also C. Vroelant, J. chim. phys. **49**, 141 (1952).

[25] See the fifth paper of this series, K. Ruedenberg and E. M. Layton, J. Chem. Phys. **34**, 1897 (1961).

easily seen that

$$\int dV[\chi_P]^2\mathbf{r}=\mathbf{R}_P,$$

$$\int dV\chi_P\chi_Q\mathbf{r}=S\mathbf{R}_m,$$

where m denotes the midpoint between P and Q, and $\mathbf{R}_X$ is the vector from the origin to the point X. Thus the general result is

$$(\chi_P \mid \mathbf{r} \mid \chi_Q)=\tfrac{1}{2}S_{PQ}(\mathbf{R}_P+\mathbf{R}_Q). \qquad (2.18)$$

3. MOLECULAR ORBITALS AND CORRESPONDING MATRIX ELEMENTS

Molecular Orbitals

Since it is our intention to use the molecular orbitals for the ground state as well as for the excited states, the ground-state self-consistent field orbitals are not necessarily the most appropriate ones to use. In fact, the results of the calculations of Pariser[16] and Ham-Ruedenberg[18] with MO's of the type to be discussed below are at least as good as those made with self-consistent field MO's made by Pople.[17]

The point of view taken here is that the MO's should be used as the basis of a configuration interaction type of approach. Hence they should represent good zeroth-order "average" approximations for the several states to be calculated, and secondly they should offer a certain ease of manipulation in view of the configuration interaction calculation. Both requirements are met best by choosing the MO's as the solutions φ_n of a one-electron Schrödinger equation

$$h^{\text{eff}}\varphi_n=\{(-\hbar^2/2m)\Delta+U^{\text{eff}}\}\varphi_n=\epsilon_n{}^{\text{eff}}\varphi_n, \qquad (3.1)$$

with an effective potential U_{eff}. As will now be shown by a careful analysis, the general assumption (3.1) leads in effect to the Hückel orbitals including overlap between neighbors.

The effective potential U_{eff} must represent the average potential felt by any one electron, it must include the shielding of the carbon nuclei by the pi electrons, and thus represents essentially the field exerted by the neutralized atoms. Hence the effective Hamiltonian of Eq. (3.1) must have a form similar to that of the operator whose matrix elements were given in Eq. (2.9) above, i.e.,

$$h_{\text{eff}}=(-\hbar^2/2m)\Delta+\sum_R U_R{}^{\text{C,eff}}+\sum_h U_h{}^{\text{H,eff}}. \qquad (3.2)$$

While the potentials $U^{\text{C,eff}}$, $U^{\text{H,eff}}$ may be different from the neutral-atom potentials, given in Eqs. (1.4) and (1.7) for the many-electron Hamiltonian, they will share with those earlier potentials the property of falling of exponentially, i.e., they will not contain long-range electrostatic forces. The evaluation of AO matrix elements of h_{eff} therefore follows a pattern analogous to that given in Eqs. (2.3)–(2.13), whence

$$(\chi_P \mid h_{\text{eff}} \mid \chi_Q)=(\alpha^{\text{eff}}+\delta\alpha_P{}^{\text{eff}})\delta_{PQ}+\beta^{\text{eff}}M_{PQ}. \qquad (3.3)$$

The molecular orbitals φ_n have to be constructed from the atomic orbitals χ_P discussed in Sec. 1. If there are N carbon atoms, then there will be the ground-state MO's

$$\left.\begin{aligned}&\varphi_n=\sum_{P=1}^{N}c_{Pn}{}'\chi_P, \qquad n=1, 2\cdots(N/2),\\ &\text{and the excited MO's}\\ &\varphi_\nu=\sum_{P=1}^{N}c_{P\nu}{}'\chi_P, \qquad \nu=(N/2)\cdots N.\end{aligned}\right\} \qquad (3.4)$$

According to the variation principle, the coefficients $c_{Pk}{}'$ are determined by the eigenvalue problem characterized by the effective Hamiltonian matrix (3.3) and the overlap matrix (2.1).

In fact, the determination of the MO's (3.4) is the *only* purpose of the matrix (3.3); the matrix itself and the "effective orbital energies" $\epsilon_n{}^{\text{eff}}$ in Eq. (3.1) are not used at all in the further calculations. By virtue of this circumstance, it becomes entirely unnecessary to decide the precise nature of h^{eff} if, for the purpose of determining the MO's, one neglects the small terms $\delta\alpha_P$ in Eq. (3.3). This represents a slight adjustment of the initial molecular orbitals only, and is of little consequence for the further quantitative process. It has, however, the effect of reducing the matrix (3.3) to a function of the topological matrix $\mathbf{M}$ of Eq. (2.2), and therefore the eigenvectors of the effective Hamiltonian matrix (3.3) become those of the topological matrix $\mathbf{M}$.

Let $\{c_{Pn}\}$ be the eigenvectors of $\mathbf{M}$, normalized to unity, i.e.,

$$\left.\begin{aligned}&\sum_Q M_{PQ}c_{Qn}=m_n c_{Pn},\\ &\sum_P c_{Pn}{}^2=1,\end{aligned}\right\}, \qquad (3.5)$$

where the m_n are the eigenvalues of $\mathbf{M}$. For use in the further development we note that the overlap matrix $\mathbf{S}$, defined in Eq. (2.1), is also a function of the topological matrix $\mathbf{M}$ and, therefore, has the same eigenvectors, whence

$$\sum_Q S_{PQ}c_{Qn}=s_n c_{Pn}, \qquad (3.6)$$

where the eigenvalues s_n are given by

$$s_n=1+Sm_n. \qquad (3.7)$$

Under the conditions set forth above, the coefficients for the MO's (3.4) are proportional to the eigenvectors of $\mathbf{M}$. Since, in this case, the *wave functions* φ_n have to

be normalized, one has to put[26]

$$c_{Pn}' = c_{Pn}(s_n)^{-\frac{1}{2}}, \tag{3.8}$$

so that indeed, by virtue of Eq. (3.6),

$$\int dV \varphi_m \varphi_n = \sum_{P,Q} c_{Pm}' S_{PQ} c_{Qn}' = \sum_P c_{Pm}' s_n c_{Qn}' = \delta_{mn}.$$

The MO's defined by Eqs. (3.4) and (3.8) are in fact exactly the Hückel-Wheland MO's. Clearly, the remarkable "power of survival" of these orbitals through all past refinements of the theory (albeit with a reinterpretation of their meaning and their use) is due to the fact that they represent in effect the appropriate "topological molecular orbitals" of the molecule. In view of the remarks made in Sec. 2 [see the section following Eq. (2.17′)] it is understandable that, under the present conditions, the best "compromise MO's" must be topological rather than geometrical in character, since the long-range forces between electrons and nuclei cancel each other out on the average.

Closely connected with this topological character is the fact that different orbitals are primarily distinguished by their different "longitudinal" profiles along the "bond path," while their "transverse" profiles perpendicular to the bond path remain essentially unchanged. Hence the excitations of electrons described by these orbitals are "*bond-path excitations*." [27] It is the merit of J. R. Platt[8] to have first shown that the spectra of aromatic systems can be understood in terms of what has been called the "principle of bond-path excitation,"[27] and that this represents the strongest experimental evidence for the appropriateness of the topological MO's. The topological character and the principle of bond-path excitation represent the common feature shared by the LCAO MO's discussed here and the free electron MO's used by Platt, Ham, and Ruedenberg.[12,27]

MO Integrals over Neutral Framework and Kinetic Energy

The matrix elements between MO's are found by expanding the MO's according to Eqs. (3.4) and (3.8) and then substituting the matrix elements between AO's given by Eq. (2.9). Thus, one finds

$$(\varphi_i \mid (-\hbar^2/2m)\Delta + \sum_R U_R^{\mathrm{C}} + \sum_h U_h^{\mathrm{H}} \mid \varphi_j) = \sum_{P,Q} \sum c_{Pi}' [(\alpha + \delta\alpha_P)\delta_{PQ} + \beta M_{PQ}] c_{Qi}',$$

whence, by virtue of Eqs. (3.5) and (3.8)

$$= (\alpha + \beta m_i)(1 + S m_i)^{-1} \delta_{ij} + \sum_P (c_{Pi}' c_{Pj}') \delta\alpha_P,$$

and, by virtue of Eq. (2.13)

$$= \epsilon_i^{nf} \delta_{ij} + \delta\alpha [J, NJ, E]_{ij}, \tag{3.9}$$

with

$$\epsilon_i^{nf} = \alpha + \gamma m_i/(1 + S m_i),$$

$$\gamma = \beta - \alpha S \tag{3.10}$$

$$[N, NJ, E]_{ij} = (2-\tau) \sum_J c_{Pi}' c_{Pj}' + (1-\tau) \sum_{NJ} c_{Pi}' c_{Pj}' - \tau \sum_E c_{Pi}' c_{Pj}', \tag{3.10′}$$

where α, $\delta\alpha$, β, τ, are defined in Eqs. (2.10)–(2.13′). Furthermore, $\sum_J$, $\sum_{NJ}$, $\sum_E$ indicate summations over all joint atoms, all nonjoint atoms, and all free-end atoms, respectively. Because of the orthonormalization of the c_{Pn}', Eq. (3.10′) can be simplified to

$$[N, NJ, E]_{ij} = (\sum_J c_{Pi}' c_{Pj}' - \sum_E c_{Pi}' c_{Pj}') + (1-\tau)(1 + S m_i)^{-1} \delta_{ij}. \tag{3.10″}$$

In the sequel it will be seen that the quantity γ plays a role which somewhat resembles that attributed to the "empirical resonance integral" in the early semi-empirical approaches. Although the present formulation leads to considerably more complex results, we shall occasionally use the name *resonance integral* to denote γ. (It should be noted that Mulliken[5] uses the nomenclature differently: He calls β what we and most authors call γ; he calls γ what we and most authors call β.)

MO Integrals of the Electron Interaction Type

From Eq. (2.15) for the electron interaction integrals between AO's one finds

$$[\varphi_i \varphi_j \mid \varphi_k \varphi_l] = \tfrac{1}{4} \sum_{P,Q} \sum_{R,S} [G(PR) + G(PS) + G(QR) + G(QS)] \times S_{PQ} c_{Pi}' c_{Qj}' S_{RS} c_{Rk}' c_{Sl}'. \tag{3.11}$$

This equation can be simplified *by taking into account that the c_{Pn}' are also eigenvectors of the overlap matrix*, as given by Eq. (3.6); the result is:

$$[\varphi_i \varphi_j \mid \varphi_k \varphi_l] = \tfrac{1}{4}(s_i + s_j)(s_k + s_l) \sum_{P,Q} G(PQ) \times c_{Pi}' c_{Pj}' c_{Qk}' c_{Ql}', \tag{3.12}$$

where the s_n are the eigenvalues of the orbitals φ_n for the overlap matrix **S**, as given by Eq. (3.7). In this fashion the quadruple sum has been reduced to a double sum. When the coefficients c_{Pn}' are expressed in terms of the coefficients c_{Pn}, according to Eq. (3.8), then Eq. (3.12) takes, also, the form

$$[\varphi_i \varphi_j \mid \varphi_k \varphi_l] = s_{ij} s_{kl} \sum_{P,Q} G(P,Q) c_{Pi} c_{Pj} c_{Qk} c_{Ql}, \tag{3.13}$$

where

$$s_{nm} = \tfrac{1}{2}(s_m + s_n)/(s_n s_m)^{\frac{1}{2}} \tag{3.13′}$$

[26] For a more detailed discussion see K. Ruedenberg, J. Chem. Phys. **22**, 1874 (1954), Sec. 1.

[27] N. S. Ham and K. Ruedenberg, J. Chem. Phys. **25**, 1 (1956), Sec. 2.

is the ratio of the arithmetic and the geometric mean of the respective eigenvalues of the overlap matrix. This ratio becomes unity in the case $m=n$.

The electron interaction integrals between MO's can also be formulated for the case of the Sklar-London approximation. Since in this case the correction term (2.17) has to be added to the AO integrals, one finds for the MO integrals that in addition to the expression (3.12) and (3.13) one has the small correction term

$$[\varphi_i\varphi_j \mid \varphi_k\varphi_l]$$
$$=\tfrac{1}{2}S^2g_2\sum_B(c_{Pi}'c_{Qj}'+c_{Qi}'c_{Pj}')(c_{Pk}'c_{Ql}'+c_{Qk}'c_{Pl}'), \quad (3.14)$$

where $\sum_B$ means the summation over all "bonds," i.e., over all *pairs of neighbor atoms* (each pair taken once), and P, Q denote the two neighbors forming the bond B.

The "Neglect of Differential Overlap"

The formulation (3.13) is convenient to assess the meaning of the assumption of "neglect of differential overlap."[14,15] In the first place it must be noticed that the eigenvalues of $\mathbf{S}$ are positive, in order that the atomic orbitals be linearly independent. Let s_m be the smaller one and s_n be the larger one of the two; then one may write

$$s_{nm}=(1-\tfrac{1}{2}\eta)(1-\eta)^{-\frac{1}{2}}=1+\tfrac{1}{2}\eta^2+\tfrac{3}{2}\eta^3+\cdots$$

with

$$0<\eta=1-(s_m/s_n)<1.$$

Since

$$\eta=S(m_n-m_m)/(1+m_nS),$$

it is seen that the deviation of s_{nm} form unity is quadratic in the overlap integral. Thus, if one wishes to compute the MO integrals *formally* only up to terms linear in S, then one can put $s_{ij}=s_{kl}=1$ in Eq. (3.13). The resulting expression

$$[\varphi_i\varphi_j \mid \varphi_k\varphi_l]=\sum_{P,Q}G(PQ)c_{Pi}c_{Pj}c_{Qk}c_{Ql}$$

is exactly that obtained by the neglect of differential overlap.

Dependence upon the Absolute Magnitude of AO Coulomb Integrals

From Eq. (3.13) follows the interesting identity

$$s_{ij}s_{kl}\sum_{PQ}[G(PQ)+A]c_{Pi}c_{Pj}c_{Qk}c_{Ql}$$
$$=s_{ij}s_{kl}\sum_{PQ}G(PQ)c_{Pi}c_{Pj}c_{Qk}c_{Ql}+A\delta_{ij}\delta_{kl}. \quad (3.15)$$

It shows that the electronic interaction integral (3.13) between molecular orbitals is independent of the absolute value of the Coulomb integrals $G(PQ)$, unless $i=j$ *and* $k=l$. In the latter case, the addition of a constant to all Coulomb integrals changes the MO integrals exactly by the amount of this constant.

By virtue of Eq. (3.15), one obtains

$$s_{ij}s_{kl}\sum_{PQ}G(PQ)c_{Pi}c_{Pj}c_{Qk}c_{Ql}$$
$$=s_{ij}s_{kl}\sum_{PQ}G'(PQ)c_{Pi}c_{Pj}c_{Qk}c_{Ql}+G'\delta_{ij}\delta_{kl}, \quad (3.16)$$

where G' is an arbitrary constant and

$$G'(PQ)=G(PQ)-G'.$$

For G', three particular choices are of interest.

(1) $G'=G(1,1)$. This leads to the elimination of all diagonal elements in the first sum on the right-hand side of Eq. (3.16). Using this device in the calculation of the molecular energy states, it is possible to predict the dependence upon the interaction integral $G(1,1)=[11 \mid 11]$, as will be discussed later.

(2) $G'=G(R_{\max})$, where $R_{\max}$ is the largest internuclear distance in the molecule. This choice quasi-concentrates the effect of the longest range forces in the simple second term on the right-hand side of Eq. (3.16) and minimizes their effect in the complex first term.

(3) $G'=G(R_{mf})$, where R_{mf} is the internuclear distance occurring most frequently in the molecule under investigation. This choice would tend to minimize as much as possible the expected cancellation of Coulomb terms and therefore be computationally advantageous.

Orbital Transition Moments

The orbital transition moment matrix is defined by

$$\mathbf{q}(\varphi_n\varphi_\nu)=(\varphi_n \mid \mathbf{r} \mid \varphi_\nu). \quad (3.17)$$

Substitution of the expansion (3.4) and the AO integrals (2.18) yields

$$\mathbf{q}(\varphi_n\varphi_\nu)=\sum_{P,Q}\tfrac{1}{2}(\mathbf{R}_P+\mathbf{R}_Q)S_{PQ}c_{Pn}'c_{Q\nu}',$$

whence by a transformation similar to that leading to Eq. (3.13)

$$\mathbf{q}(\varphi_n\varphi_\nu)=s_{nm}\sum_P\mathbf{R}_Pc_{Pn}c_{P\nu}, \quad (3.18)$$

where the quantities s_{nm} are defined by Eq. (3.13′).

The off-diagonal elements are required for intensity calculations; the diagonal elements represent the dipole moment of the orbital,

$$\mathbf{q}(\varphi_n\varphi_n)=\sum_P\mathbf{R}_Pc_{Pn}^2.$$

The total dipole moment in the ground state becomes therefore, with $q(P)$ defined by Eq. (4.16′),

$$\mathbf{D}=\sum_P\mathbf{R}_Pq(P)$$

even when neighbor overlap is properly included.

4. ELECTRONIC STATES

Basic Formalism

I

The electronic-state wave functions are constructed as linear combinations of antisymmetrized products (LCAP's) of molecular orbitals. The ground state is given in first approximation by the "closed-shell" determinant containing the N electrons in the $(N/2)=G$ lowest orbitals, $n=1, 2, \cdots G$,

$$\Phi_0=\mathfrak{A}\{(\varphi_1\alpha)^1(\varphi_1\beta)^2\cdots(\varphi_G\alpha)^{N-1}(\varphi_G\beta)^N\}, \quad (4.1)$$

where

$$\mathfrak{A}=(N!)^{-\frac{1}{2}}\sum_P(-1)^P P$$

is the antisymmetrizer. It is assumed that the number of electrons is even and equal to the number of AO's. For each "one-electron orbital excitation" $\varphi_n\rightarrow\varphi_\nu$, there exist four excited wave functions which can be chosen as singlet and triplet states,

$$^{s\sigma}\Phi(\varphi_n,\varphi_\nu)=\mathfrak{A}\{\cdots(\varphi_n\varphi_\nu\eta_{s\sigma})^{2n-1,2n}\cdots\}. \quad (4.2)$$

Here the dotted part is identical with the corresponding part in the ground state (4.1), the Roman suffix indicates a ground-state orbital, the Greek suffix indicates one of the exicted orbitals [see Eq. (3.4)], and $\eta_{s\sigma}$ is one of the four spin eigenfunctions

$$\eta_{10}=(\alpha\beta-\beta\alpha)/\sqrt{2},$$

$$\eta_{31}=\alpha\alpha, \qquad \eta_{30}=(\alpha\beta+\beta\alpha)/\sqrt{2}, \qquad \eta_{3,-1}=\beta\beta. \quad (4.3)$$

In general, the actual excited states of the molecule have to be constructed as superpositions of several one-orbital excitations of the type (4.2), whereas the actual ground state is expected to contain only a small admixture of the LCAP's given by Eq. (4.2). The determination of appropriate superpositions is based on the eigenvalue problems of the respective configuration interaction matrices.

II

The diagonal element of the Hamiltonian with respect to the ground state (4.1), i.e., the ground-state energy, becomes

$$\mathrm{H}_0=(\Phi_0\mid\mathfrak{H}\mid\Phi_0)=\sum_{n=1}^{G}[(\varphi_n\mid f\mid\varphi_n)+\{\varphi_n,\varphi_n\}], \quad (4.4)$$

where f is the *total framework* Hamiltonian defined in Eq. (1.1′) and

$$\{\varphi_i,\varphi_j\}=(\varphi_i\mid f\mid\varphi_j)+\sum_{n=1}^{G}\{2[\varphi_n\varphi_n\mid\varphi_i\varphi_j]-[\varphi_n\varphi_i\mid\varphi_n\varphi_j]\}. \quad (4.5)$$

For $i=j=$a ground-state orbital, this expression represents the energy of one electron in the orbital i due to the framework *and* the field of the $(N-1)$ *other* electrons in the $(N-1)$ other orbital, because of the cancellation occurring in the sum for $n=i$. If one forms the expression (4.5) for $i=j=$an excited orbital, the sum over n still covering the ground-state orbitals, no cancellation occurs. Hence, in this case Eq. (4.5) represents the energy of an electron in orbital i due to the framework and N other electrons occupying all ground-state orbitals.

If one wishes to improve the ground-state wave-function by configuration interaction, one requires the matrix elements for the interaction of the ground state with the excited singlet functions of the type (4.2). They are[28] given by

$$(\Phi_0\mid\mathfrak{H}\mid{}^{10}\Phi(\varphi_n,\varphi_\nu))=\{\varphi_n,\varphi_\nu\}/\sqrt{2} \quad (4.6)$$

and vanish if the φ_n happen to be solutions of the self-consistent field equations. For this reason they are expected to be small for the topological MO's.

The matrix elements describing the interaction between the various one-orbital excitations of the type (4.2) are given by[28]

$$[^{s\sigma}\Phi(\varphi_n,\varphi_\nu)\mid\mathfrak{H}\mid{}^{s'\sigma'}\Phi(\varphi_m,\varphi_\mu)]={}^s\mathrm{H}(\varphi_n\varphi_\nu,\varphi_m\varphi_\mu)\delta_{ss'}\delta_{\sigma\sigma'}, \quad (4.7)$$

As indicated, this matrix is already diagonal with respect to the spin angular momentum. Within one multiplicity the elements are given by

$${}^sH(\varphi_n\varphi_\nu,\varphi_m\varphi_\mu)=H_0\delta_{nm}\delta_{\nu\mu}-\{\varphi_n,\varphi_m\}\delta_{\nu\mu}+\{\varphi_\nu,\varphi_\mu\}\delta_{nm}-{}^s\{\varphi_n\varphi_\nu,\varphi_m\varphi_\mu\}. \quad (4.8)$$

Here H_0 and $\{\varphi_i,\varphi_j\}$ are given by Eqs. (4.4) and (4.5) and

$${}^s\{\varphi_n\varphi_\nu,\varphi_m\varphi_\mu\}=[\varphi_n\varphi_m\mid\varphi_\nu\varphi_\mu]-(1+p_s)[\varphi_n\varphi_\nu\mid\varphi_m\varphi_\mu], \quad (4.9)$$

where p_s is the parity of the space function: $+1$ for singlets and -1 for triplets. Eq. (4.8) can be interpreted as follows: the one-electron excitation $\varphi_n\rightarrow\varphi_\nu$ can be represented as the addition of an electron in orbital φ_ν and a hole in orbital φ_n; then the first term in Eq. (4.8) is the ground-state energy, the second term is the interaction energy of the added hole and the ground state, the third term is the interaction energy of the added electron and the ground state, and the fourth term is the interaction energy of the added electron and the added hole. Another interpretation will be given later.

Only interactions between singly excited antisymmetrized products are taken into account. The inclusion of doubly excited configurations would seem to call for the simultaneous consideration of the sigma electrons.

III

Whereas the *energies* of the excited states are obtained as eigenvalues of the configuration interaction matrix, the *intensity* corresponding to the transition

[28] See reference 27, Sec. 1.

ΔE is characterized by the oscillator strength[29]

$$f=\tfrac{1}{3}\Delta E\mathbf{Q}^2/E_{\mathrm{H}}a^2, \tag{4.10}$$

($a=\hbar^2/e^2m=$ Bohr radius, $E_{\mathrm{H}}=e^2/2a=$ ionization potential of H) where

$$\mathbf{Q}=(\Phi_0 \mid \sum_i \mathbf{R}_i \mid \Phi_{\mathrm{excited}}) \tag{4.11}$$

is the dipole transition moment divided by e, the absolute value of the electronic charge. The latter is a superposition of the transition moments to the one-orbital excitations (4.2) which vanish for the triplets and, for the singlet states, are given by

$$[\Phi_0 \mid \sum_i \mathbf{R}_i \mid {}^{10}\Phi(\varphi_n\varphi_\nu)]=\sqrt{2}\mathbf{q}(\varphi_n\varphi_\nu), \tag{4.12}$$

where the $\mathbf{q}$'s are the orbital transition moments discussed in Eqs. (3.17) and (3.18).

There are also no complications in applying the formulas of Eqs. (3.11), (3.12), and (3.13) to the calculation of the electron-hole interaction (4.9). The insertion of the electron-interaction integrals into the matrix $\{\varphi_i, \varphi_j\}$, as needed for Eq. (4.8), is a little more involved and will be discussed in the following.

Auxiliary Relations Concerning Bond Characteristics

Before carrying on the development it is useful to establish certain properties of quantities of the form

$$f_{PQ}=2\sum_{n=1}^{G} c_{Pn}c_{Qn}f(m_n), \tag{4.13}$$

(bond characteristics) where the m_n are the eigenvalues of $\mathbf{M}$, $\{c_{Pn}\}$ the corresponding eigenvectors [see Eq. (3.5)], and various functions will have to be considered for $f(x)$. The present discussion is based on the analysis given in the third note, to which the reader must be referred for some results.[21]

The following cases will occur in the term $\{\varphi_i, \varphi_j\}$:

$$p(PQ)=2\sum_{n=1}^{G} c_{Pn}c_{Qn}, \tag{4.14}$$

$$p'(PQ)=2\sum_{n=1}^{G} c_{Pn}{}'c_{Qn}{}'=2\sum_{n=1}^{G} c_{Pn}c_{Qn}/(1+Sm_n), \tag{4.15}$$

$$p''(PQ)=2\sum_{n=1}^{G} c_{Pn}{}'c_{Qn}{}'s_n=2\sum_{n=1}^{G} c_{Pn}c_{Qn}(1+Sm_n). \tag{4.16}$$

The quantities $p(PQ)$ form the Coulson bond-order matrix, whose diagonal elements

$$p(PP)=q(P) \tag{4.16'}$$

are Mulliken's "gross atomic populations." The quantities $p'(PQ)$ differ from the Mulliken bond orders merely by the factor $(1+S)$. The quantities $p''(PQ)$ have not been used before, but are also subject to the analysis given in the third paper.[21]

According to Eqs. (2.2), (2.6), and (2.19) of the third paper the following relations are valid,

$$p'(PQ)=\sigma^{-1}\{p(PQ)+\sigma'[\tfrac{3}{2}p(PQ)-(\mathbf{pM})_{PQ}]\}, \tag{4.17}$$

$$p''(PQ)=\sigma\{p(PQ)-\sigma'[\tfrac{3}{2}p(PQ)-(\mathbf{pM})_{PQ}]\}, \tag{4.17'}$$

where

$$\sigma=(1+\tfrac{3}{2}S), \qquad \sigma'=(S/\sigma). \tag{4.17''}$$

The identity (4.17') is exact. The relation (4.17) results from an expansion in term of the small quantity $(\sigma')^2=0.03$, and is a very accurate approximation. The diagonal elements of the matrix $\mathbf{pM}$ are the usual bound valences; in alternant systems

$$(\mathbf{pM})_{PQ}=M_{PQ}, \tag{4.18}$$

if P, Q belong to different classes.

It can be shown that always

$$|\tfrac{3}{2}p(PQ)-(\mathbf{pM})_{PQ}|<1. \tag{4.19}$$

From Eq. (4.17), (4.17') follows

$$p'(PQ)p''(PQ)=[p(PQ)]^2-(\sigma')^2[\tfrac{3}{2}p(PQ)-(\mathbf{pM})_{PQ}]^2.$$

Because of Eq. (4.19), the second term can be neglected to the excellent degree of approximation used in Eq. (4.17), so that

$$p'(PQ)p''(PQ)\cong p(PQ)^2. \tag{4.20}$$

To the same degree of approximation one furthermore finds for a *ground-state orbital* φ_n:

$$s_n p'(PQ)=[1+\sigma'(m_n-\tfrac{3}{2})]\{p(PQ)+\sigma'[\tfrac{3}{2}p(PQ)-(\mathbf{pM})_{PQ}]\},$$

$$s_n^{-1}p''(PQ)=[1-\sigma'(m_n-\tfrac{3}{2})]\{p(PQ)-\sigma'[\tfrac{3}{2}p(PQ)-(\mathbf{pM})_{PQ}]\},$$

and hence, in approximation,

$$\tfrac{1}{2}[s_n p'(PQ)+p''(PQ)/s_n]\cong p(PQ), \tag{4.21}$$

where s_n is the eigenvalue of $\mathbf{S}$ (here, the fact $(m_n-\tfrac{3}{2})<1.5$ has been used).

As an example of the accuracy of the approximations, Table I gives the quantitative results for benzene, with $S=(\tfrac{1}{4})$ substituted in Eq. (4.17''). It is seen that Eq. (4.20), is a nontrivial statement, since p, p', and p'' can be very different from each other. An extensive test of the relation (4.17) was made by Ham and Ruedenberg.[30]

From the definitions (4.14), (4.15), (4.16), and the orthogonality relations for the eigenvectors of $\mathbf{M}$,

[29] See, for example, A. Sommerfeld, "Wave mechanics," *Atomic Structure and Spectral Lines* (Frederick Vieweg, Braunschweig, Germany, 1939), Vol. II, p. 365, Eq. (22). The formulation (4.10) has the advantage of being easily convertible to any units.

[30] N. S. Ham and K. Ruedenberg, J. Chem. Phys. **29**, 1215 (1958).

TABLE I. Numerical values for various bond-order definitions in benzene.

PQ	p	**pM**	p''	p'	$0.9256p$ -0.1322(**pM**)	p^2	$p'p''$
11	1	1.3333	1.3333	0.7579	0.7493	1	1.0105
12	0.6667	1	0.9167	0.4905	0.4848	0.4444	0.4496
13	0	0.3333	0.0833	0.0442	0.0441	0	0.0037
14	−0.3333	0	−0.3333	−0.3115	−0.3085	0.1111	0.1038

there furthermore follows without approximation the matrix relation

$$\sum_R p'(PR)\,p''(RQ)=\sum_R p(PR)\,p(RQ)=2p(PQ),$$

i.e.,

$$\mathbf{p}'\mathbf{p}''=\mathbf{p}^2=2\mathbf{p}. \tag{4.22}$$

Evaluation of the Matrix $\{\varphi_i, \varphi_j\}$

After Eqs. (1.1′), (1.2), (1.3), (1.6) and Eq. (3.12) have been inserted in the definition (4.5), this matrix is conveniently written as follows

$$\{\varphi_i, \varphi_j\}=[\varphi_i, \varphi_j]_1+\{\varphi_i, \varphi_j\}_2+\{\varphi_i, \varphi_j\}_3, \tag{4.23}$$

where

$$\{\varphi_i, \varphi_j\}_1=(\varphi_i\,|\,(-\hbar^2/2m)\Delta+\sum_R U_R{}^{\mathrm{C}}+\sum_h U_h{}^{\mathrm{H}}\,|\,\varphi_j), \tag{4.24}$$

$$\{\varphi_i,\varphi_j\}_2=-e^2\sum_R[\chi_R{}^2|\varphi_i\varphi_j]+e^2\sum_{n=1}^{G}2[\varphi_n\varphi_n|\varphi_i\varphi_j]^0, \tag{4.25}$$

$$\{\varphi_i, \varphi_j\}_3=-e^2\sum_{n=1}^{G}[\varphi_n\varphi_i\,|\,\varphi_n\varphi_j]^0. \tag{4.26}$$

Let us consider these three terms in turn.

The first can be taken over directly from Eq. (3.9),

$$\{\varphi_i, \varphi_j\}_1=\epsilon_i{}^{nf}\delta_{ij}+\delta\alpha[J, NJ, E]_{ij}, \tag{4.27}$$

and originates from the kinetic energy and the neutral part of the framework potential.

An expression for the second is obtained by substituting the Eqs. (2.15) and (3.12) in Eq. (4.25), whence

$$\{\varphi_i, \varphi_j\}_2=-\tfrac{1}{2}(s_i+s_j)\sum_{P,Q}G(PQ)\,c_{Pi}{}'c_{Pj}{}' +\tfrac{1}{2}(s_i+s_j)\sum_{P,Q}G(PQ)\,q(P)\,c_{Pi}{}'c_{Pj}{}',$$

where the $q(P)$ are the gross atomic populations of Eq. (4.16′). Since the terms $G(PQ)$ are symmetric in P and Q, one can write

$$\{\varphi_i, \varphi_j\}_2=\tfrac{1}{4}(s_i+s_j)\sum_{P,Q}G(PQ)\,\{[q(P)-1]c_{Qi}{}'c_{Qj}{}' +[q(Q)-1]c_{Pi}{}'c_{Pj}{}'\}. \tag{4.28}$$

This term contains the "ionic" part of the framework potential and the Coulomb part of the electronic interaction. It is small since the gross atomic populations are in general close to unity, and it vanishes altogether in alternant systems due to the Coulson-Rushbrooke theorem [$q(P)=1$ for all atoms].

The third term of the matrix $\{\varphi_i, \varphi_j\}$ represents the exchange part of the electronic interaction. Substituting Eqs. (3.12) and (3.13) into Eq. (4.26), one obtains

$$\{\varphi_i, \varphi_j\}_3=-\tfrac{1}{16}\sum_{P,Q}G(PQ)[(s_i+s_j)\,p(PQ)+s_is_jp'(PQ) +p''(PQ)](c_{Pi}{}'c_{Qj}{}'+c_{Qi}{}'c_{Pj}{}'), \tag{4.29}$$

where $p(PQ)$, $p'(PQ)$, and $p''(PQ)$ are the matrices defined in Eqs. (4.14), (4.15), and (4.16). While Eq. (4.29) is usable in practice, it can be simplified by virtue of the relations (4.17) and (4.17′), which are good approximations. From the computational point of view it seemed convenient to cast (4.29) in the form

$$\{\varphi_i, \varphi_j\}_3=-\tfrac{1}{16}\sum_{P,Q}G(PQ)[(2\sigma+s_i+s_j)\,p(PQ) +(s_is_j-\sigma^2)\,p'(PQ)](c_{Pi}{}'c_{Qj}{}'+c_{Qi}{}'c_{Pj}{}'), \tag{4.30}$$

$$p'(PQ)=2\sum_{n=1}^{G}c_{Pn}{}'c_{Qn}{}',$$

$$p(PQ)=2\sum_{n=1}^{G}c_{Pn}{}'c_{Qn}{}'s_n. \tag{4.30′}$$

If the Sklar-London approximation is used, the following additional term has to be included in the expression (4.23)

$$\{\varphi_i, \varphi_j\}'=\tfrac{1}{4}S^2g_2\sum_B\{3p'(PQ)[c_{Pi}{}'c_{Qj}{}'+c_{Qi}{}'c_{Pj}{}'] -p'(PP)c_{Qi}{}'c_{Qj}{}'-p'(QQ)c_{Pi}{}'c_{Pj}{}'\}. \tag{4.31}$$

Evaluation of H^0

The term H^0 given in Eq. (4.4) contains the expressions $\{\varphi_n, \varphi_n\}$, for which the result of the preceding subsection can be used. It also contains the terms $\{\varphi_n\,|\,f\,|\,\varphi_n\}$ which are in fact furnished by the expressions (4.24, 4.27) plus the first part of (4.25). When these expressions are inserted in Eq. (4.4), the follow-

ing result is obtained for H^0:

$$H^0+G^0=2\sum_{n=1}^{G}\{\epsilon_n{}^{n\prime}+\delta\alpha[J, NJ, E]_{nn}\}$$
$$+\tfrac{1}{2}\sum_{P,Q}G(PQ)[q(P)-1][q(Q)-1]$$
$$-\tfrac{1}{8}\sum_{P,Q}G(PQ)\{[p(PQ)]^2+p'(PQ)p''(PQ)\}, \quad (4.32)$$

where the constant

$$G^0=\tfrac{1}{2}\sum_{P,Q}G(P,Q) \quad (4.32')$$

is separated out for convenience.[31]

The Sklar-London approximation would add the term

$$-\tfrac{1}{4}S^2g_2\sum_{B}\{3[p'(PQ)]^2-q'(P)q'(Q)\} \quad (4.33)$$

to H^0.

Dependence upon the Absolute Value of the Coulomb Integrals

In Eq. (3.15) it was shown that the MO electron-interaction integrals change in a very simple way if *all* AO Coulomb integrals $G(PQ)$ are increased by a constant amount, A. We shall now discuss the corresponding change of the total matrix elements.

By virtue of Eq. (3.15), the electron-hole interaction (4.9) will change by

$$+A\delta_{\nu\mu}\delta_{nm}. \quad (4.34)$$

By virtue of Eq. (3.15) the exchange term (4.26) will change by

$$-A\delta_{ij}\delta_{i,\text{ground state}}, \quad (4.35)$$

where

$$\delta_{i,\text{ground state}}=\begin{cases}1, & \text{if } i \text{ denotes a ground-state orbital,}\\ 0, & \text{if } i \text{ denotes an excited orbital.}\end{cases}$$

The change of the term $\{\varphi_i, \varphi_j\}_2$ can be inspected by making the substitution $G(PQ)\rightarrow G(PQ)+A$ directly in the expression (4.28). It is found that A is multiplied by the factor

$$\sum_P[q(P)-1]=N-N=0. \quad (4.36)$$

Thus the total configuration interaction matrix (4.8) contains the absolute value of the $G(PQ)$ only in H^0 and in the terms (4.34), (4.35). The latter two are, however, seen to cancel in Eq. (4.8) so that

$${}^nH(\varphi_n\varphi_\nu, \varphi_m\varphi_\mu)-H^0\delta_{nm}\delta_{\nu\mu}=\text{invariant under the substitution } G_{PQ}\rightarrow G_{PQ}+A. \quad (4.37)$$

In order to find the dependence of H^0 upon the absolute value of the $G(PQ)$ we make the substitution $G(PQ)\rightarrow G(PQ)+A$ directly in Eq. (4.32). The Coulomb terms give rise to vanishing terms of the type (4.36) and the exchange terms yield

$$-(A/8)\text{ trace }(\mathbf{p}^2+\mathbf{p}'\mathbf{p}'')=-(A/2)\sum_P q(P)$$
$$=-NA/2,$$

where the identity (4.22) has been used. Hence the substitution changes the expression (H^0+G^0) by the amount

$$-(\tfrac{1}{2})NA. \quad (4.38)$$

The Ground-State Energy

I

The results of the preceding subsection can be used to bring the ground-state energy into an interpretable form.

Let us transform H^0, as given by Eq. (4.32), in the manner illustrated in Eq. (3.16) choosing $G'=G(1,1)$. Furthermore, we express $\epsilon_n{}^{n\prime}$ by means of Eqs. (3.10) ff. and Eqs. (1.12) and (2.11). Thus we obtain

$$H^0=N\alpha'+2\sum_{n=1}^{G}\bar{\epsilon}_n+\bar{G}, \quad (4.39)$$

where

$$\alpha'=\alpha-G(1,1)=-I_C+\bar{\alpha}, \quad (4.40)$$

with

$$-I_C=-A_C-G(1,1), \quad (4.41)$$

$$\bar{\alpha}=(1+\tau)(\chi_1|U_2{}^C|\chi_1)+(2-\tau)(\chi_1|U_{h1}{}^H|\chi_1). \quad (4.42)$$

Furthermore,

$$\bar{\epsilon}_n=\{\gamma m_n+\delta\alpha[(1-\tau)+\sum_J c_{Pn}{}^2-\sum_E c_{Pn}{}^2]\}/(1+Sm_n), \quad (4.43)$$

with

$$\gamma=\beta-\alpha S. \quad (4.43')$$

Finally

$$\bar{G}=\sum_{P<Q}g(PQ)\bar{p}(PQ)-\sum_{P<Q}G(PQ), \quad (4.44)$$

with

$$g(PQ)=[G(1,1)-G(PQ)]>0, \quad (P,Q)\neq(1,1), \quad (4.45)$$

$$\bar{p}(PQ)=\tfrac{1}{4}\{[p(PQ)]^2+p'(PQ)p''(PQ)\}$$
$$-[q(P)-1][q(Q)-1]\}. \quad (4.46)$$

The last equation can be simplified, when the approximation (4.20) is inserted, giving

$$\bar{p}(PQ)=\tfrac{1}{2}[p(PQ)]^2-[q(P)-1][q(Q)-1], \quad (4.46')$$

as a close approximation to (4.46).

The quantities α, β, $\delta\alpha$, τ are defined in Eqs. (2.10)–(2.13'), the quantities I_C, A_C are defined in Eqs. (1.11) and (1.12). In slight deviation from previous usage, we shall call $\bar{\alpha}$, γ, the Coulomb integral and the resonance integral, respectively.

[31] A similar separation was made in the case $S=0$ (neglect of differential overlap) by J. A. Pople, see reference 15.

II

Equation (4.39) has the following interpretation.

All terms involving G's originate from the attraction by the ionic part of the framework potential or from the interelectronic repulsion. It is to be expected that these two effects cancel each other to a large degree. This cancellation is described by the term $[q(Q)-1]\cdot[q(P)-1]$ in Eqs. (4.46) and (4.46′). The effect is largest for alternant systems, since in those one has $q(P)=1$ for all atoms; but also in other systems the term will be small, since it is quadratic in the small quantities $[q(P)-1]$. The cancellation of the two forces cannot be complete however, since, classically speaking, the attraction of N electrons by the N positive ionic charges would be $-\sum_P\sum_Q G(PQ)$, whereas the repulsion between the N electrons is only $+\sum_{P<Q}G(PQ)$. Thus there remains a sizable attraction, and this is described by the term $-G(1,1)$ in Eq. (4.41) and the second sum in Eq. (4.44). There remains a relatively small term in $\bar{G}$, *viz.*, the first term in Eq. (4.46, 46′) which is due to exchange effects and the change in orbital self-energy.[32]

All other terms, containing no G's originate from the attraction of the neutral part of the framework potential and from the kinetic energy.

Another point of view is also instructive and has in fact determined the arrangements of terms in Eq. (4.39). From Eq. (1.12) it is seen that the term I_C of Eq. (4.41) is the ionization potential of C in its valence state, i.e., the energy of *one* electron in the field of *one* C^+ ion in the valence state. Hence $-(NI_C)$ is the bona fide energy of the pi electrons before the formation of the pi bonds so that

$$H^0+NI_C$$

is the energy lowering due to the bond formation. The lowering consists of three parts: $N\bar{\alpha}$=a general effect of the neutral framework on all orbitals, $2\Sigma_n\bar{\epsilon}_n$=an effect of the neutral framework specific for different orbitals, and $\bar{G}$=the effect of the ionic part of the framework minus the electron repulsion.

Thus, one finds again the division into short-range and long-range forces, which was commented upon after Eq. (2.17′). The former described by $\bar{\alpha}$ and $\bar{\epsilon}_n$, arise when atomic orbitals overlap and are responsible for covalent binding. The latter, described by $\bar{G}$, are responsible for ionic effects and electron-penetration effects.[32]

III

In order to assess the bonding power of the pi electrons properly, a further point must be taken into account, however. It must be remembered that the sigma framework contains a certain internal electrostatic-repulsion strain due to the fact that it is considered stripped of the pi electrons and therefore has excess positive charges, giving rise to the framework potential. This positive charge is represented by the last ("ionic") term in Eq. (1.6). The repulsion energy within the sigma framework, due to this ionic part, is therefore

$$E^{f+}=\sum_{P<Q}\{[\chi_P^2\mid\chi_Q^2]-(\chi_P\mid U_Q^C\mid\chi_P)-(\chi_Q\mid U_P^C\mid\chi_Q)\}-\sum_{P,h}\sum(\chi_P\mid U_h^H\mid\chi_P). \quad (4.47)$$

One must separate this energy from the framework and include it instead in the pi-electronic energy, in order to obtain a fair estimate of the strength of the pi-bonding.

By virtue of the arguments following Eq. (2.3), and using the definition (2.16), one finds from Eq. (4.47),

$$E^{f+}=\sum_{P<Q}G(PQ)-2N_B(\chi_1\mid U_2^C\mid\chi_1)-(2N_E+N_N)(\chi_1\mid U_{h1}^C\mid\chi_1),$$

where N_B is the number of bonds, N_N is the number of nonjoint atoms, and N_E is the number of free-end atoms. Now it can be shown that

$$2N_B=N(1+\tau), \qquad (2N_E+N_N)=N(2-\tau),$$

where τ is just the quantity defined in Eq. (2.12′). By virtue of the definition (4.42) of $\bar{\alpha}$, the internal ionic framework repulsion energy can therefore be written

$$E^{f+}=\sum_{P<Q}G(PQ)-N\bar{\alpha}. \quad (4.48)$$

Let us call

$$E^0=H^0+E^{f+}=\textit{effective pi energy of the conjugated system}, \quad (4.49)$$

and, in view of the meaning of (NI_C),

$$E_j=E^0+NI_C=\textit{effective bonding energy of pi electrons with respect to the carbon valence state}. \quad (4.50)$$

Then one obtains for the latter, by combining Eqs. (4.39) and (4.48), finally

$$E_b=2\sum_{n=1}^{G}\bar{\epsilon}_n+\sum_{P<Q}g(PQ)\bar{p}(PQ), \quad (4.51)$$

where all symbols are defined in Eqs. (4.40)–(4.46′). This expression could be used to compute delocalization energies, but this subject is not pursued here because of the well-known uncertainties of interpretation. However, Eq. (4.51) should give an idea of the comparative pi-electron binding in different molecules.

As an example of the energies which are involved and which cancel against each other, we give the quantitative results for benzene.[33]

[32] See K. Ruedenberg (to be published).

[33] The numerical results are taken from the sixth paper in this series, see K. Ruedenberg, J. Chem. Phys. **34**, 1907 (1961).

The binding energy contributions are:

$$2\sum_{n=1}^{G}\tilde{\epsilon}_n = -2.1838\times(88/15) = -12.81 \text{ ev},$$

$$\sum_{P<Q} g(PQ)\bar{p}(PQ) = +6.80 \text{ ev [Eq. (4.46)]},$$

$$\approx +6.77 \text{ ev [Eq. (4.46')]}.$$

Canceled away are the following energy contributions to H^0, in total 260 ev.

One-center attraction (short-range and ionic) contained in the ionization potential of carbon,

$$-NI_C = -6\times(0.69+10.53) = -67.32 \text{ ev}.$$

Many-center attractions canceled by framework repulsion:

short-range:

$$N\bar{\alpha} = -6\times 5.516 = -33.10 \text{ ev}.$$

ionic:

$$-\sum_{P<Q} G(PQ) = -79.70 \text{ ev}.$$

Many-center ionic attraction, canceled by electronic repulsion:

$$-\sum_{P<Q} G(PQ)q(P)q(Q) = -\sum_{P<Q} G(PQ) = -79.70 \text{ ev}.$$

All large energy contributions have canceled out exactly in Eq. (4.51), and it emerges that the term which is finally responsible for the binding, i.e., the first term in Eq. (4.51), is a *sum over the one-electron energies* $\tilde{\epsilon}_n$ *due to the neutral framework potential composed of short-range forces.* Thus $\tilde{\epsilon}_n$ can be called the "*orbital contribution*" to the total energy. This additive orbital contribution must be clearly distinguished from the "*orbital energy*," i.e., the energy of an electron which occupies this orbital. The latter is given by the expression $\{\varphi_n, \varphi_n\}$, as mentioned after Eq. (4.5), and is frequently denoted by ϵ_n, in particular when the ϵ_n's are self-consistent field orbitals.

IV

The original Hückel-Lennard-Jones-Coulson-Wheland theory assumed *ad hoc* and without any analysis the additivity of "one-electron energies," say $\tilde{\epsilon}_n$. At the same time, these $\tilde{\epsilon}_n$ were believed to be "orbital energies," it was in fact hoped that they would be close to the self-consistent field orbital energies. Critics then pointed out the inherent contradiction of these two expectations. The present analysis solves the puzzle by showing that there exist additive orbital energy contributions which are different from the orbital energies and, instead, obtained as eigenvalues of a *topological* one-electron problem. Thus there is an element of truth in the old formula

$$\text{binding energy} \propto 2\sum_{n=1}^{G} m_n/(1+Sm_n);$$

however, Eq. (4.51) provides the additional terms required by the theory.

Thus Eq. (4.51) also furnishes a rigorous justification for the distinction between bonding and antibonding pi orbitals: the orbital is *bonding* (*antibonding*) when the "*orbital energy contribution*" $\tilde{\epsilon}_n$ is negative (positive). In contrast, the orbital is *bound* (*unbound*) if the "*orbital energy*" ϵ_n is negative (positive).

The present derivation furthermore affords understanding of the intricate balancing of energy terms and thereby gives hope for a better treatment of those cases in which the canceling is not complete, e.g., when heteroatoms and substituents enter in. In another investigation this aspect will be pursued further and in fact generalized to arbitrary molecular and crystal systems.[32]

Finally, we wish to comment on the remarkable fact that the electronic interaction terms as given by Eq. (4.46') are *exactly* identical with the ones obtained by Pople[15] under the radical assumption of neglecting *all* overlap integrals from the very beginning. It should be stressed that our Eq. (4.46') is not obtained by a *formal* expansion in S, but from a very accurate approximation, based on a quantitatively checked expansion in terms of the parameter σ' of Eq. (4.17''). As seen above, in benzene use of Eq. (4.46') leads to an error of 0.03 ev in the expression (4.44).

It must be pointed out however that the result (4.46') is *also heavily based on the fact that our MO's are eigenvectors of the topological matrix* **M**, i.e., that they are essentially the Hückel-Wheland orbitals. It may well be that Eq. (4.46') and others are unjustifiable for any other type of molecular orbital. It would seem that the execution of the self-consistent field mechanism, as proposed by Pople, is worth the effort only when it should be possible to establish, under the general assumptions adopted in the present analysis, the validity of Eq. (4.46') and the corresponding simplifications for the self-consistent field operator for the successive iterations in a self-consistent field sequence. Also the difference between joint and nonjoint atoms should be taken into account. The possibility exists that the execution of the self-consistent field formalism, while neglecting differential overlap, leads to results which are less reliable than those derived from Hückel-Wheland orbitals.

Ionization Potential, Electron Affinity, Electronegativity

It can be argued that in a large system the AO's do not change appreciably if only *one* electron out of $N \gg 1$ is removed or added, and for the same reason the topological Hückel-Wheland MO's should not be

appreciably worse approximations than they were in the neutral molecule.

If an electron is removed from the ground-state orbital φ_n, the ground-state energy of the resulting positive ion becomes

$$\mathrm{H}^0-\{\varphi_n,\varphi_n\}.$$

On the other hand, if an additional electron is placed in the excited orbital φ_ν, then the ground-state energy of the resulting negative ion is

$$\mathrm{H}^0+\{\varphi_\nu,\varphi_\nu\}.$$

Hence one has

$$I=-\{\varphi_n,\varphi_n\}=\text{ionization potential of the molecule,} \tag{4.52}$$

$$A=-[\varphi_\nu,\varphi_\nu\}=\text{electron affinity of the molecule,} \tag{4.53}$$

if φ_n is the highest ground-state orbital and φ_ν is the lowest excited orbital. Equation (4.52) is the Hartree-Slater-Koopmans[34] theorem; Mulliken explained its usually good agreement with experiment by a fortunate cancellation of errors. In the case of Eq. (4.53) the errors would tend to add, however.

The ionization potential is obtained from Eq. (4.23) by putting $i=j=n$. Again we make a transformation of the kind which led to Eq. (4.39). Noting Eqs. (4.35) and (4.36), we obtain

$$-I=\{\varphi_n,\varphi_n\}=-I_{\mathrm{C}}+\bar{\alpha}+\bar{\epsilon}_n+\sum_{P<Q}g(PQ)\bar{p}_n(PQ), \tag{4.54}$$

with

$$\bar{p}_n(PQ)=\tfrac{1}{2}\{p(PQ)+\tfrac{1}{2}[s_n p'(PQ)+s_n^{-1}p''(PQ)]\}c_{Pn}c_{Qn} -\{[q(P)-1]c_{Qn}^2+[q(Q)-1]c_{Pn}^2\}, \tag{4.55}$$

where all symbols are defined in Eq. (4.39) ff and Eq. (3.7). Since φ_n is a ground-state orbital, the approximation (4.21) can be used, yielding in close approximation,

$$\bar{p}_n(PQ)=p(PQ)c_{Pn}c_{Qn} -\{[q(P)-1]c_{Pn}^2+[q(P)-1]c_{Qn}^2\}. \tag{4.55'}$$

The electron affinity is obtained in the same way. However, in this case Eq. (4.35) gives the contribution zero, and furthermore approximation (4.21) is not applicable. Hence,

$$-A=\{\varphi_\nu,\varphi_\nu\}=-A_{\mathrm{C}}+\bar{\alpha}+\bar{\epsilon}_\nu+\sum_{P<Q}g(PQ)\bar{p}_\nu(PQ), \tag{4.56}$$

with

$$\bar{p}_\nu(PQ)=\tfrac{1}{2}\{p(PQ)+\tfrac{1}{2}[s_\nu p'(PQ)+s_\nu^{-1}p''(PQ)]\}c_{P\nu}c_{Q\nu} -\{[q(P)-1]c_{Q\nu}^2+[q(Q)-1]c_{P\nu}^2\}. \tag{4.57}$$

[34] T. Koopmans, Physica **1**, 104 (1933). (Strictly Koopmans' theorem applies to SCF orbitals.)

Again the derived equations have a sensible interpretation.

In Eq. (4.57), the electron affinity of the carbon valence state, A_{C}, appears. In Eq. (4.54) the corresponding ionization potential, $I_{\mathrm{C}}=A_{\mathrm{C}}+G(1,1)$, appears. In fact, we expect that the electron in the ground-state orbital φ_n, before its removal, had been subject to a net Coulombic attraction $-G(1,1)$ due to the incomplete shielding of the N nuclei by the $(N-1)$ other electrons, whereas this attraction is absent for the additional electron in the excited orbital φ_ν, which is completely shielded by the N ground-state electrons.

The term $(\bar{\alpha}+\bar{\epsilon}_n)$ in Eq. (4.54) describes the lowering of the orbital energy of the bonding orbital φ_n caused by the short-range, neutral part of the framework potential leading to bond formation. The last term in this equation is the remnant of the long-range Coulombic force, mostly of exchange character, since the appearance of $[q(P)-1]$ indicates that provision has been made for the intrinsic cancellation of ionic framework attraction and electronic repulsion. Again this cancellation is largest for alternants, since here $q(P)=1$.

It is of interest to examine the mean value of the ionization potential and the electron affinity, a quantity which Mulliken has defined as an appropriate measure of the electronegativity of the molecule. From Eqs. (4.54) and (4.56) follows

$$-\tfrac{1}{2}(I+A)=-\tfrac{1}{2}(I_{\mathrm{C}}+A_{\mathrm{C}})+\bar{\alpha}+\tfrac{1}{2}(\bar{\epsilon}_n+\bar{\epsilon}_\nu) +\sum_{P<Q}g(PQ)\tfrac{1}{2}[\bar{p}_n(PQ)+\bar{p}_\nu(PQ)]. \tag{4.58}$$

The quantitative behavior of this expression is best appreciated by considering the case of alternant systems. In this case φ_n and φ_ν are paired orbitals so that

$$m_\nu=-m_n, \qquad c_{P\nu}=J_P c_{Pn},$$

$$J_P=\begin{cases}1, & \text{if } P \text{ is a starred atom,}\\ -1, & \text{if } P \text{ is an unstarred atom,}\end{cases}$$

$$q(P)=1, \tag{4.59}$$

$$\left.\begin{aligned}&p(PQ)=0,\\ &p'(PQ),\ p''(PQ) \text{ are small.}\\ &\text{(see e.g. Table I for benzene)}\end{aligned}\right\} \text{if } P \text{ and } Q \text{ belong to the same class, but } P\neq Q.$$

By virtue of these relations, one obtains

$$\tfrac{1}{2}(\bar{\epsilon}_n+\bar{\epsilon}_\nu)=\{-\gamma S m_n^2+\delta\alpha[(1-\tau) +\sum_J c_{Pn}^2-\sum_E c_{Pn}^2]\}/(1-S^2m_n^2), \tag{4.60}$$

and

$$\tfrac{1}{2}[\bar{p}_n(PQ)+\bar{p}_\nu(PQ)]=\tfrac{1}{4}\begin{Bmatrix}1\\ \\ Sm_n\end{Bmatrix} \times[p'(PQ)+J_Q J_P p''(PQ)(1-S^2m_n^2)^{-1}]c_{Pn}c_{Qn}. \tag{4.61}$$

The expression (4.61) will be small if P and Q belong to the same class, since then p' and p'' are small; if P and Q are of different class, then the minus sign in (4.61) in conjunction with the factor S will make it small. In benzene, e.g., one obtains about -0.15 ev for the total last sum in Eq. (4.58). In contrast the contribution from Eq. (4.60) is about 0.6 ev.

N. S. Hush and J. A. Pople[35] recently suggested that the quantity $(I+A)$ is a constant in alternant systems, basing their conclusions on a treatment neglecting all overlap integrals. However, while the neglect of neighbor overlap introduces only a moderate error in calculating the difference $(\tilde{\epsilon}_n-\tilde{\epsilon}_\nu)$, it introduces a considerable error, e.g., 1.2 ev in benzene, when the sum $(\tilde{\epsilon}_n+\tilde{\epsilon}_\nu)$ is computed. The reason for this is clearly seen from the discussion in the second paper of this series. In fact, the quantity m_n^2 in Eq. (4.60) can vary between 0 and 1 in considering several conjugated systems. As a result, the deviations of the electronegativities (4.58) from a constant value are of the same magnitude as the electronegativity values themselves and as the variations in the ionization potentials. The same is true for the few experimental values quoted by Hush and Pople.

Energies of Excited States

If an electron is promoted from a ground-state orbital φ_n to an excited orbital φ_ν, then the energies of the resulting triplet and singlet states are given by the diagonal element of the matrix (4.8), which we may write

$$^aH(\varphi_n\varphi_\nu, \varphi_n\varphi_\nu)=[H^0-\{\varphi_n, \varphi_n\}] +[\{\varphi_\nu, \varphi_\nu\}-{}^a\{\varphi_n\varphi_\nu, \varphi_n\varphi_\nu\}]. \quad (4.62)$$

In view of the remarks after Eq. (4.5) and of the discussion in the preceding subsection, the first bracket term in (4.62) represents the energy of the system after the electron in φ_n has been removed, and hence the second bracket term must represent the energy addition when the removed electron is now placed in orbital φ_ν, while the orbital φ_n remains empty. Indeed, the remarks after Eq. (4.5) and the discussion in the preceding subsection also show that $\{\varphi_\nu,\varphi_\nu\}$ is the energy of an electron in φ_ν when *all* ground-state orbitals are filled, and that subtracting the term $^a\{\varphi_n\varphi_\nu, \varphi_n\varphi_\nu\}$ amounts to subtracting out the energy of an electron in φ_ν with respect to an electron in φ_n.

This general interpretation is very visibly borne out by our formalism, if we carry out again a transformation of the kind that led to Eq. (4.39). According to Eq. (4.54), this transformation puts in evidence the net Coulomb attraction $-G(1, 1)$ in $\{\varphi_n, \varphi_n\}$, expressing shielding by $(N-1)$ other electrons only. Such a term did not appear in $\{\varphi_\nu, \varphi_\nu\}$, Eq. (4.56), indicating shielding by N other electrons. According to Eq. (4.34) our transformation does however put in evidence such a term in $^a\{\varphi_n\varphi_\nu, \varphi_n\varphi_\nu\}$, indicating that $\{\zeta_\nu, \zeta_\nu\}-{}^a[\varphi_n\varphi_\nu, \varphi_n\varphi_\nu\}$ is the energy of an electron shielded by $(N-1)$ other electrons only.

As a consequence, the integral $G(1, 1)$ cancels out in the excitation energy $^aH(\varphi_n\varphi_\nu,\varphi_n\varphi_\nu)-H^0$, as was already noticed in Eq. (4.37), so that all spectroscopic transitions depend only upon the differences defined in Eq. (4.45). *In view of this circumstance it is rather surprising that the proper adjustment of* $G(1, 1)$ *did play such an important role in the recent advances made in the calculations of spectra.*[20] *In the fourth paper*[25] *we shall in fact see that the primary point of the Pariser-Parr adjustment is the adjustment of the g's of Eq.* (4.45). *This latter adjustment goes considerably beyond changing* $G(1, 1)$ *and requires the adjustment of* $G(1, 1)$ *as a "secondary effect."*

As was discussed after Eq. (4.3), the excited molecular states are in general superpositions of several singly excited states with the configuration interaction matrix (4.8). In alternant systems, it was noted by Moffitt[36] and Pariser[16] that there exists a particularly strong interaction between the "paired one-orbital excitations," *if all overlap integrals are neglected.* Let

φ_ν = the excited orbital *paired* to the ground-state orbital φ_n,

φ_μ = the excited orbital *paired* to the ground-state orbital φ_m,

then the two paired one-orbital excitations are: $\varphi_n\rightarrow\varphi_\mu$ and $\varphi_m\rightarrow\varphi_\nu$, and the strong interaction originated from the fact that the difference of the diagonal elements, *viz.*,

$$\Delta^aH(P)={}^aH(\varphi_n\varphi_\mu, \varphi_n\varphi_\mu)-{}^aH(\varphi_m\varphi_\nu, \varphi_m\varphi_\nu), \quad (4.63)$$

is zero when *all overlap integrals are set equal to zero.* We shall therefore examine this expression under our more rigorous assumptions.

From Eq. (4.62) follows, by changing indices,

$$\Delta^aH(P)=\Delta_1-\Delta_2, \quad (4.64)$$

with

$$\Delta_1=[\{\varphi_m,\varphi_m\}+\{\varphi_\mu,\varphi_\mu\}]-[\{\varphi_n,\varphi_n\}+\{\varphi_\nu,\varphi_\nu\}], \quad (4.65)$$

$$\Delta_2={}^a\{\varphi_n\varphi_\mu, \varphi_n\varphi_\mu\}-{}^a\{\varphi_m\varphi_\nu, \varphi_m\varphi_\nu\}. \quad (4.65')$$

Thus, Δ_1 is composed of the electronegativities which were discussed in Eq. (4.58) ff. Hence the largest contribution to Δ_1 will come from the first term in

[35] N. S. Hush and J. A. Pople, Trans. Faraday Soc. **51**, 600 (1955).

[36] W. Moffitt, J. Chem. Phys. **22**, 1820 (1954). Pariser's independent results,[16] though published later, were communicated in June, 1954, at the Symposium for Molecular Structure and Spectra, Ohio State University, Columbus, Ohio. Subsequent applications were made by M. J. S. Dewar and H. C. Longuet-Higgins, Proc. Phys. Soc. (London) **A67**, 795 (1954), by Pople[17] and by Ham and Ruedenberg.[18]

Eq. (4.60), so that

$$\Delta_1 = -2\gamma S(m_m^2 - m_n^2)/(1 - S^2 m_m^2)(1 - S^2 m_n^2) + \cdots . \quad (4.66)$$

An expression for Δ_2 is obtained by substituting the expressions (4.9) and (3.13) in Eq. (4.65′) and taking into account the properties (4.59) for alternants. Thus results

$$\Delta_2 = -(s_{n\mu}^2 - s_{m\nu}^2)(1 - p_s) \sum_{P<Q} J_P J_Q c_{Pn} c_{Qn} c_{Pm} c_{Qm}, \quad (4.67)$$

where p_s is defined after Eq. (4.9). For the multiplying factor, one finds from the definition (3.13′),

$$(s_{n\mu}^2 - s_{m\nu}^2) = \tfrac{1}{2}[(Sm_m) + (Sm_n)]$$
$$\times [(Sm_m)^2 - (Sm_n)^2]/[(1 - (Sm_m)^2][1 - (Sm_n)^2]. \quad (4.68)$$

In many cases, it seems practical to consider only one-orbital excitations from the 2–3 highest ground-state orbitals to the 2–3 lowest excited orbitals (see footnote 18). In the majority of these cases one has $0 \leq m_n \leq 1$, $0 \leq m_m \leq 1$. With $S = \frac{1}{4}$, it becomes evident that the difference (4.64) is then small in comparison to the diagonal matrix elements themselves.

It is furthermore seen that the two paired one-orbital excitations differ very little in their orbital transition moments. According to Eq. (3.18) and by virtue of Eq. (4.59), one obtains for the difference

$$\mathbf{q}(\varphi_n, \varphi_\nu) - \mathbf{q}(\varphi_m, \varphi_\nu) = (s_{n\mu} - s_{m\nu}) \sum_P J_P \mathbf{R}_P c_{Pn} c_{Pm}, \quad (4.69)$$

and one can again show that the multiplying factor is small in many cases.

Consequently, the present theory including overlap effects appears to substantiate the result that in many cases there is a strong interaction between paired excitation, leading to a strong band and a weak band, in agreement with experiment. However, the interaction does not go quite to a 1:1 mixing, but it is rather of the kind analyzed by Ham and Ruedenberg.[18]

5. VALIDITY OF THE NEGLECT OF DIFFERENTIAL OVERLAP

The foregoing results show that differential overlap cannot be neglected uncritically. The following conclusions seem to be warranted.

Use for Two-Electron Integrals

The neglect of differential overlap represents a valid and effective approximation if the atomic orbitals satisfy Mulliken's approximation *and if* the molecular orbitals are simultaneously eigenvectors of the overlap matrix. Three cases of such orbitals are known so far:

(i) the topological MO's discussed in the present paper;

(ii) the MO's of the augmented tight-binding approximation discussed in the subsequent paper;

(iii) the MO's in cyclic systems, since the effective Hamiltonian and the overlap matrix commute in these systems for symmetry reasons.[37] An example is discussed in the subsequent paper.

To what degree neglect of differential overlap is a bona fide approximation in conjunction with a self-consistent-field procedure, in cases where the SCF MO's are not determined by symmetry, remains questionable. The use of neglect of differential overlap in this situation, and in others, is related to the question, to what degree and under what conditions neglect of differential overlap is a bona fide approximation for Löwdin orbitals.[38] A cogent mathematical analysis of this latter point would be desirable.

Use for One-Electron Integrals

It seems that the neglect of differential overlap introduces little error in the calculation of energy differences, as needed for electronic spectra.

The case of the electronegativities shows however that there are problems where the use of this approximation may have rather little meaning, and a more careful formulation is unavoidable.

[37] P. O. Löwdin, J. Chem. Phys. **18,** 365 (1950).

[38] For further references on this aspect, see R. G. Parr, J. Chem. Phys. **33,** 1184 (1960).

Quantum Mechanics of Mobile Electrons in Conjugated Bond Systems. II. Augmented Tight-Binding Formulation*

KLAUS RUEDENBERG

Institute for Atomic Research, Department of Chemistry, Department of Physics, Iowa State University, Ames, Iowa

(Received March 16, 1959)

The analysis of homonuclear conjugated systems, which has been given within the limits of the tight-binding approximation in the first paper of this series, is extended to include the interactions between nonneighbor atoms and the variation in the interactions between neighbor atoms. Both kinds of interactions are included as perturbation effects on the tight-binding approximation. As a consequence, the formalism developed for the latter is not being complicated and the interpretations remain unchanged. Application to benzene and naphthalene illustrates the approach.

INTRODUCTION

IN the first paper of this series, hereafter referred to as paper I, it has been found possible to formulate the quantum mechanics of conjugated systems in a simple, fairly rigorous manner when the tight-binding approximation is adopted. While it represents progress in that a complete formulation has been achieved with the inclusion of all neighbor overlap effects, the question naturally arises whether the formulation can be extended to include nonneighbor effects.

Clearly, a simple formulation cannot be expected if all nonneighbor interactions are introduced in the most general fashion, nor would this be desirable, as was pointed out in paper I. Since the tight-binding approach is a valid first approximation, it seems, instead, natural to look for a way to include the nonneighbor effects as a correction to the tight-binding approximation. Such a method is here formulated. It is expected to furnish an estimate of the quality of the tight-binding formulas and to yield a meaningful addition. It eliminates, for example, an unpleasant side feature of the tight-binding approximation, viz., the appearance of a spurious linear dependence between atomic orbitals for larger overlap values.

The present formulation also makes provision for taking into account the variations in the neighbor interaction-integrals which are due to the variation in bond distances in homonuclear systems.

The first section discusses the general method; the second section gives, by way of illustration, the application to benzene and naphthalene.

1. MODIFICATION OF THE TIGHT-BINDING FORMULATIONS

The discussion in this section proceeds by examining each step of paper I and introducing the necessary modifications where they are needed.

Matrix Elements in the AO Basis

Overlap Integrals

All overlap integrals are now taken into account, and moreover neighbor atoms can have different overlap integrals. The overlap matrix is therefore no longer a function of the topological matrix, **M**. It is, however, convenient to write **S** again in a form similar to Eq. (2.1) of paper I: Let

$$S_{PQ}=\delta_{PQ}+S\mathfrak{M}_{PQ}, \tag{1.1}$$

where S is the mean value of all *neighbor* overlap integrals, and the matrix $\mathfrak{M}$ is defined by

$$\mathfrak{M}_{PQ}=\begin{cases}0, & \text{if } P=Q\\ (S_{PQ}/S), & \text{if } P\neq Q.\end{cases} \tag{1.2}$$

It differs from the topological matrix M_{PQ} by the small terms (S_{PQ}/S) for nonneighbors, and by the small deviations $[1-(S_{PQ}/S)]$ for neighbors.

AO Integrals of Neutral Framework and Kinetic Energy

The introduction of values for the energy integrals

$$h_{PQ}{}^{nf}=(\chi_P\mid(-\hbar^2/2m)\Delta+\sum_a U_a\mid\chi_Q), \tag{1.3}$$

including the effect of nonneighbors, is the main objective. In Eq. (1.3), the summation means

$$\sum_a U_a=\sum_P U_P{}^C+\sum_h U_h{}^H, \tag{1.4}$$

where $\sum_P$ sums over the C atoms, $\sum_h$ sums over the H atoms, and $\sum_a$ sums over *all* atoms, as defined in Eqs. (1.1)–(1.4) of paper I.

As in Eq. (2.9) of I we write for the diagonal elements

$$h_{PP}{}^{nf}=\alpha_P=\alpha+\delta\alpha_P, \tag{1.5}$$

where α is the mean value of all α_P and $\delta\alpha_P$ the devia-

* Contribution No. 714. Work was performed in the Ames Laboratory of the U. S. Atomic Energy Commission.

TABLE I. Overlap integrals in benzene and naphthalene as function of neighbor overlap integral [for identification, see Eqs. (2.1, 2)].

ρ^a	S_2	S_3	S_4	S_5	S_6	S_7	S_8
1.042	0.90011888	0.74022458	0.67499326	0.52023017	0.44205577	0.35064219	0.32551500
1.540	0.80009691	0.54010059	0.45143178	0.27583702	0.20426654	0.13422361	0.11748042
1.978	0.69987956	0.38375779	0.29366499	0.14270001	0.09254025	0.05083570	0.04209030
2.404	0.60013443	0.26293555	0.18340380	0.07035104	0.03985318	0.01826733	0.01430282
2.850	0.49990653	0.17020241	0.10721210	0.03179981	0.01557253	0.00587897	0.00433630
3.342	0.39956792	0.10143594	0 05686215	0.01260231	0.00523838	0.00159098	0.00109769
3.913	0.30034455	0.05343105	0.02606052	0.00408991	0.00140154	0.00332969	0.00321034
ρ^{*b}	0.24680000	0.03469758	0.01544861	0.00193597	0.00058521	0.00011665	0.00007074
4.657	0.20001350	0.02200372	0.00891440	0.00088562	0.00023527	0.00003955	0.00002276
5.800	0.10070697	0.00516035	0.00156267	0.00007611	0.00001362	0.00000136	0.00000067

[a] $\rho=\zeta(D/a)$, ζ=orbital exponent of $2p\pi$-AO, D=nearest distance, a=Bohr radius, $(D/a)\approx 0.7559$.
[b] $\rho^*=4.2805407$. See Eq. (1.14) of paper VI.

tion from it. One finds

$$\alpha=-A_C+N^{-1}\sum_{Pa}{}'(\chi_P\,|\,U_a\,|\,\chi_P), \tag{1.6}$$

where $-A_C$ is the negative of the electron affinity of carbon as given in Eq. (2.11′) of I, and $\sum'_{Pa}=\sum_P\sum_a$ with omission of the terms $P=a$. Furthermore,

$$\delta a_P=N^{-1}\sum_{Q,a}{}'{}^P[(\chi_P\,|\,U_a\,|\,\chi_P)-(\chi_Q\,|\,U_a\,|\,\chi_Q)], \tag{1.8}$$

with

$$\sum_{Q,a}{}'{}^P=\sum_Q\sum_a$$

with omission of the terms: $a=Q$, $a=P$, $Q=P$.

For the off-diagonal elements

$$h_{PQ}{}^{nf}=\beta_{PQ}=(\chi_P\,|\,(-\hbar^2/2m)\Delta+\sum_a U_a\,|\,\chi_Q),$$

$$P\neq Q, \tag{1.9}$$

it seems reasonable to write

$$\beta_{PQ}=\beta(S_{PQ}/S)+\delta\beta_{PQ}, \tag{1.10}$$

$$=\beta M_{PQ}+\beta[(S_{PQ}-SM_{PQ})/S]+\delta\beta_{PQ}. \tag{1.11}$$

From the formulation (1.11), it is apparent that two corrections to the tight-binding approximation are added. The term involving S_{PQ} provides an estimate for the expected dependence upon the interatomic distance. The correction $\delta\beta_{PQ}$ expresses the fact that β_{PQ} depends still upon the location of the pair (PQ) even when the distance (PQ) is fixed.

To assume the distance dependence of certain integrals proportional to the corresponding overlap integrals is a device which has been used occasionally by other authors. We wish to stress the point, however, that this approximation cannot be invoked without judicious examination of the integrals involved. In the present case the assumption is justifiable because we are dealing with *short-range* forces, as discussed in paper I. Moreover, a quantitative analysis given in the sixth paper of this series[1] supports the approximation. In contrast, the assumption is quite *unjustified* when applied to a Hamiltonian including *long-range* forces.

The constant β can be determined by averaging over all pairs (PQ), i.e., from the equation

$$\sum_{P<Q}\beta_{PQ}=(\beta/S)\sum_{P<Q}S_{PQ}+\sum_{P<Q}\delta\beta_{PQ}, \tag{1.12}$$

but an adequate approximation is the average over neighbor bonds,

$$\beta=N_B{}^{-1}\sum_B\beta_{\langle PQ\rangle}. \tag{1.13}$$

Here $\sum$ indicates summation over all bonds B involving two *neighbor* atoms, and N_B is the number of such bonds. The atoms constituting the bond B are denoted by $\langle P,Q\rangle$.

For nonneighbor atoms the terms $\delta\beta_{PQ}$ represent a second-order effect, hence we put

$$\delta\beta_{PQ}=0, \quad \text{for nonneighbors.} \tag{1.14}$$

Furthermore, the numerical investigation of the naphthalene molecule given below shows that the contributions from nonneighbor atoms with a distance larger than the diameter of benzene are completely negligible, and hence we can put

$$(S_{PQ}/S)=0 \quad \text{for} \quad R(PQ)>2D, \tag{1.15}$$

where D is the average neighbor distance.

With the proposed estimates, the neutral-framework Hamiltonian matrix of Eq. (1.3) can be written

$$h_{PQ}{}^{nf}=(\alpha+\delta\alpha_P)\delta_{PQ}+(\beta+\delta\beta_{PQ})\mathfrak{M}_{PQ}, \tag{1.16}$$

where the symbols have been defined in Eqs. (1.2), (1.6), (1.8), (1.10), (1.13), and (1.14).

[1] K. Ruedenberg, J. Chem. Phys. **34**, 1907 (1961).

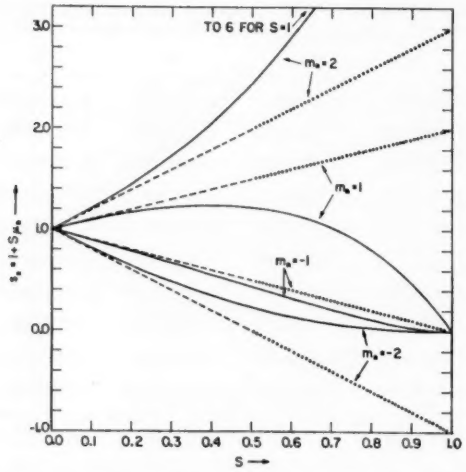

FIG. 1. Eigenvalues of overlap matrix in benzene as functions of neighbor overlap integral. Full lines: exact eigenvalues. Dashed-dotted lines: tight-binding approximation.

In view of the perturbation character of the present approach, it seems practical, furthermore to assume Eq. (1.14) tentatively *also for neighbors* and to admit for the quantity of Eq. (1.8) only three different values, viz., for joints, for nonjoints, and for end atoms. As a compensation the values for β and $\delta\alpha_P$ may be slightly modified. With these simplifications the only differences between the expression (1.16) and the corresponding expression in the tight-binding approximation [Eq. (2.9) of paper I] are merely the numerical change in the values of α, β, $\delta\alpha_P$, and the replacement of the topological matrix $\mathbf{M}$ by the matrix $\mathfrak{M}=(\mathbf{S}-\mathbf{I})/S$ of Eq. (1.2). The subsequent derivations are, however, independent of this simplification.

AO Integrals of the Electron-Interaction Type and of Transition Moments

The derivations of Eqs. (2.14)–(2.18) of paper I can be taken over unchanged, if one merely admits the new values of S_{PQ}.

Molecular Orbitals and Corresponding Matrix Elements

Molecular Orbitals

The arguments in the corresponding section of paper I can be made without change in basic approach. The only difference will be that the place of the matrix $\mathbf{M}$ is now taken by the matrix $\mathfrak{M}$. Hence, let now c_{Pn} be the eigenvector of $\mathfrak{M}$ with the eigenvalue μ_n, i.e.,

$$\sum_Q \mathfrak{M}_{PQ}c_{Qn}=\mu_n c_{Pn},$$

$$\sum_Q c_{Qn}{}^2=1. \tag{1.17}$$

These new eigenvalues and eigenvectors depend, of course, upon the ratios (S_{PQ}/S). Again the overlap matrix has the same eigenvectors, i.e., one has

$$\sum_Q S_{PQ}c_{Qn}=s_n c_{Pn}, \tag{1.18}$$

where now

$$s_n=1+S\mu_n. \tag{1.19}$$

It is easily seen that the molecular orbitals will again be defined by Eqs. (3.4) and (3.8) of paper I, viz.,

$$\varphi_n=\sum_P c_{Pn}{}'\chi_P$$

$$c_{Pn}{}'=c_{Pn}(s_n)^{-\frac{1}{2}}, \tag{1.20}$$

if one now uses for c_{Pn} and s_n the new definitions (1.17) and (1.19).

MO Integrals over Neutral Framework and Kinetic Energy

Instead of Eq. (3.9), of paper I one finds the slightly modified expression

$$(\varphi_i\,|\,(-\hbar^2/2m)\Delta+\sum_a U_a\,|\,\varphi_j)=\epsilon_i{}^{n/}\delta_{ij}+\sum_P c_{Pi}{}'c_{Pj}{}'\delta\alpha_P$$
$$+2\sum_B c_{Pi}{}'c_{Qj}{}'\delta\beta_{PQ}, \tag{1.21}$$

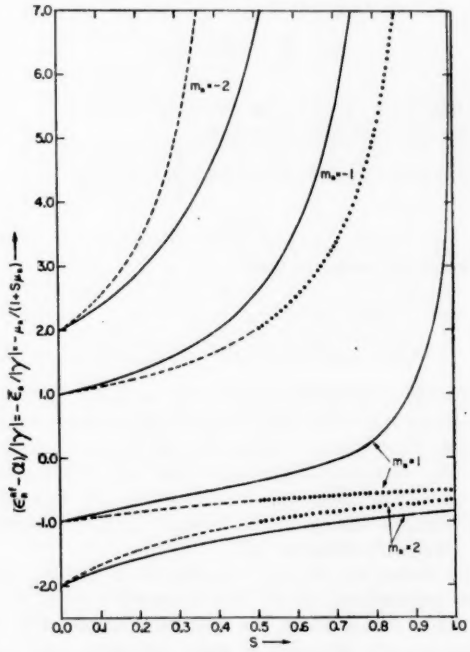

FIG. 2. Eigenvalues of the neutral-framework Hamiltonian matrix in benzene as functions of neighbor-overlap integral. Full-lines: augmented tight-binding approximation. Dashed-dotted lines: tight-binding approximation.

where

$$\epsilon_i^{nf}=\alpha+\gamma\mu_1/(1+S\mu_i) \qquad (1.22)$$

$$\gamma=\beta-\alpha S.$$

MO Integrals of the Electron Interaction Type and of the Orbital Transition Moments

It is noteworthy that the arguments in these two sections remain valid without any change, except that, for the eigenvalues s_n of **S**, one must now substitute the new values of Eq. (1.19). It is seen, in particular, that the discussion of the Parr-Pariser approximation, i.e., the "neglect of differential overlap," is still correct with the present inclusion of many-center interactions.

Electronic States

The derivations and interpretations in this section remain entirely unaltered, and the small changes are self-evident.

In particular, the simplifications based on the Eqs. (4.13)–(4.22) of paper I, which hold for the topological matrix **M** only, must be discarded. This applies, e.g., to Eq. (4.30) of paper I.

For the ground state, Eq. (4.39) of paper I results again, with the following differences. The value of $\bar{\alpha}$ is now

$$\bar{\alpha}=N^{-1}\sum_{Pa}{}'(\chi_P \mid U_a \mid \chi_P), \qquad (1.23)$$

[see Eq. (1.6)]. The value of $\bar{\epsilon}_n$ is now

$$\bar{\epsilon}_n=\{\gamma\mu_n+(\sum_P c_{Pn}{}^2\delta\alpha_P+2\sum_B c_{Pn}c_{Qn}\delta\beta_{PQ})\}/(1+S\mu_n). \qquad (1.24)$$

The approximation (4.46′) of I is not valid.

For the repulsion energy of the sigma framework, one obtains, instead of Eq. (4.47), of I

$$E^{f+}=\sum_{P<Q}[\chi_P{}^2 \mid \chi_Q{}^2]-\sum_{Pa}{}'(\chi_P \mid U_a \mid \chi_Q). \qquad (1.25)$$

The two changes, Eqs. (1.23) and (1.25), have the effect that the Eq. (4.48) of paper I is again valid, leading again to the simple relation (4.51) of paper I for the effective bonding energy of the π electrons.

2. APPLICATION TO BENZENE AND NAPHTHALENE

The two applications given here illustrate the method and, moreover, by way of a numerical comparison with the tight-binding approximation, provide an estimate of the validity of the latter. A result of interest is that, even in larger systems, it entails no loss in accuracy to take into account only the overlap integrals between atoms which lie in the same benzene ring.

We limit ourselves to an analysis of the eigenvalues of the overlap matrix **S** and of the neutral-framework Hamiltonian matrix $\mathbf{h}^{nf}$, since these quantities embody all numerical changes which will occur in introducing the augmented tight-binding approximation.

Overlap Values in Benzene and Naphthalene

In order to exhibit the influence of nonneighbor interactions, the eigenvalues and eigenvectors of **S** and $\mathbf{h}^{nf}$ are calculated as functions of the neighbor-overlap integral S. The latter also determines all nonneighbor overlap integrals. Assuming equidistant neighbors, the corresponding sets of overlap integrals are given in Table I for all internuclear distances occurring in benzene and naphthalene. They are (in terms of the neighbor distance D)

$$R_1=0, \quad R_2=D, \quad R_3=\sqrt{3}D, \quad R_4=2D, \qquad (2.1)$$

in benzene; in naphthalene one has, furthermore,

$$R_5=\sqrt{7}D, \quad R_6=3D, \quad R_7=\sqrt{12}D, \quad R_8=\sqrt{13}D. \qquad (2.2)$$

The effect of variations in neighbor distances will be considered elsewhere.

Rigorous Form of the Matrices S and $\mathbf{h}^{nf}$ in Benzene

Let

$$S_{11}=1, \quad S_{12}=S, \quad S_{13}=S', \quad S_{14}=S'' \qquad (2.3)$$

$$h_{11}{}^{nf}=\alpha, \quad h_{12}{}^{nf}=\beta, \quad h_{13}{}^{nf}=\beta', \quad h_{14}{}^{nf}=\beta''. \qquad (2.4)$$

It is easily seen that the matrices **S** and $\mathbf{h}^{nf}$ can be expressed in terms of the *topological matrix* **M** of Eq. (2.2) of paper I as follows:

$$\mathbf{S}=\mathbf{I}+S\mathbf{M}+S'(\mathbf{M}^2-2\mathbf{I})+S''\mathbf{M}(\mathbf{M}^2-3\mathbf{I})/2, \qquad (2.5)$$

$$\mathbf{h}^{nf}=\mathbf{I}+\beta\mathbf{M}+\beta'(\mathbf{M}^2-2\mathbf{I})+\beta''\mathbf{M}(\mathbf{M}^2-3\mathbf{I})/2, \qquad (2.6)$$

a fact which seems to have remained unnoticed.

Note added in proof. Since termination of this work, Löwdin, Pauncz, and de Heer have shown the generalization of Eq. (2.5) to any cyclic system. It involves Chebyshev polynomials. (Technical Note No. 41 Quantum Chemistry Group, Uppsala, Sweden).

It follows that the matrices **S**, $\mathbf{h}^{nf}$, and **M** still commute, and hence, that the coefficients of the molecular orbitals (1.20) are still given by Eq. (3.8) of paper I, except that s_n now represents the eigenvalues of the matrix (2.5). The invariance of the MO's has therefore been derived without having recourse to group theory.

In addition, Eqs. (2.5) and (2.6) furnish explicit formulas for the eigenvalues s_n of **S** and for the energy eigenvalues $\epsilon_n{}^{nf}$ of the problem

$$(\mathbf{h}^{nf}-\epsilon_n{}^{nf}\mathbf{S})\mathbf{c}_n=0.$$

One obtains

$$s_n=1+Sm_n+S'(m_n{}^2-2)+S''m_n(m_n{}^2-3)/2, \qquad (2.7)$$

$$\epsilon_n{}^{nf}=\alpha+[\gamma m_n+\gamma'(m_n{}^2-2)+\gamma''m_n(m_n{}^2-3)/2]/s_n, \qquad (2.8)$$

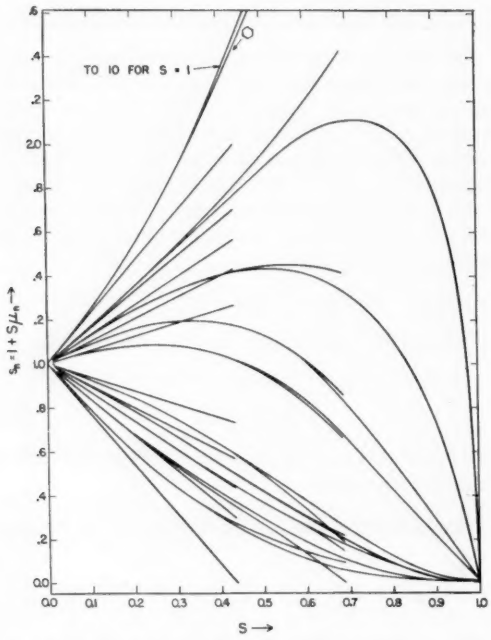

FIG. 3. Eigenvalues of overlap matrix in naphthalene as functions of neighbor-overlap integral. Lines extending to $S=1$: exact eigenvalues. Lines extending to $S=0.69$ and line marked by a hexagon: intra-ring-interaction approximation. Straight lines extending to $S=0.435$; tight-binding approximation.

where

$$\gamma=\beta-\alpha S, \qquad \gamma'=\beta'-\alpha S', \qquad \gamma''=\beta''-\alpha S'', \quad (2.8')$$

and m_n are again the eigenvalues of the topological matrix $\mathbf{M}$.

In view of Eq. (2.5), the simplification of electron-interaction integrals, given in Eqs. (3.11)–(3.18) of paper I, can be carried through with inclusion of *all* overlap integrals. This development was made recently by DeHeer and Pauncz.[2]

Augmented Tight-Binding Approximation for Benzene

When the approximations summarized in Eq. (1.16) are adopted, these Eqs. (2.7) and (2.8) reduce to Eqs. (1.19) and (1.21) given in the foregoing, where now the matrix $\mathfrak{M}$ and its eigenvalues μ_n are given by

$$\mathfrak{M}=\mathbf{M}+(S'/S)(\mathbf{M}^2-2)+(S''/S)(\mathbf{M}^2-3)\mathbf{M}/2, \quad (2.9)$$

$$\mu_n=m_n+(S'/S)(m_n^2-2)+(S''/S)(m_n^2-3)m_n/2. \quad (2.10)$$

In benzene the eigenvalues m_n are -2, -1, 1, 2, the middle two being doubly degenerate. For m_n fixed, μ_n is a function of the neighbor overlap S, which determines also the nonneighbor overlaps S' and S''.

[2] J. de Heer and R. Pauncz, J. Mol. Spectroscopy **5**, 326 (1960).

Figure 1 plots the four eigenvalues s_n, and Fig. 2 plots the four energy values $\bar{\epsilon}_n=\epsilon_n{}^{\pi}/-\alpha$ for the whole range of S. In all cases, the augmented values are given together with the values obtained by the tight-binding approximation.

It is seen that, for $S<0.3$, the deviations are small enough to characterize the tight-binding approach as a valid approximation and a substantial improvement over the neglect of all overlap integrals, which corresponds to the value for $S=0$. Because of the different deviations for the different levels the approximation is particularly good.

(1) For the energy difference between the highest ground-state orbital and the lowest excited orbital; here the error cancels practically completely.

(2) For the total ground-state binding energy $2\sum_n \bar{\epsilon}_n$; here the errors in four of the six levels cancel completely against each other.

The curves corresponding to the tight-binding approximation are only dotted beyond the point $S=0.5$, since the approximation becomes entirely untenable beyond this point, as will be discussed presently.

Linear Dependence and Tight-Binding Approximation

For $S=0.5$, the lowest eigenvalue of $(\mathbf{I}+S\mathbf{M})$ becomes zero, so that the tight-binding approximation

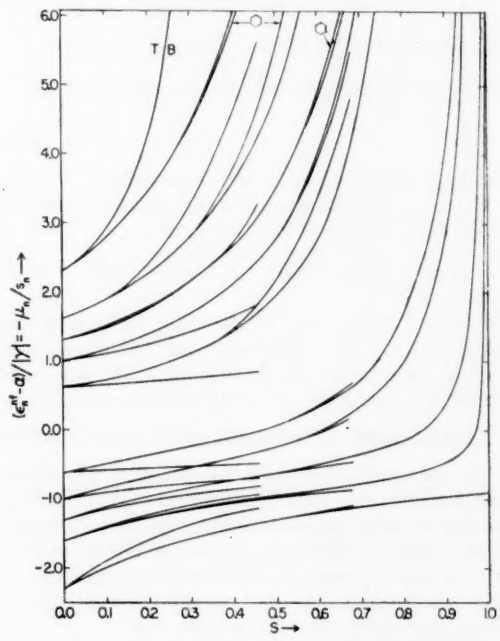

FIG. 4. Eigenvalues of the neutral-framework Hamiltonian matrix in naphthalene as functions of neighbor-overlap integral. Lines extending to $S=0.435$ and line marked TB: tight-binding approximation. Lines extending to $S=0.69$ and lines marked by a hexagon: intra-ring-interaction approximation. Remaining lines: augmented tight-binding approximation with full overlap matrix.

makes the AO's *appear* linearly dependent whereas in reality they are not, since the lowest eigenvalue of **S** reaches zero only for $S=1$.

It is even worse for $S>0.5$. Here the matrix $(\mathbf{I}+S\mathbf{M})$ has a negative eigenvalue, whereas *any* overlap matrix between *any* functions, linearly dependent or independent, always has nonnegative eigenvalues. It must therefore be concluded that this range $(\mathbf{I}+S\mathbf{M})$ can *never* correspond to an overlap matrix between actual orbitals.

The value 0.5 is peculiar to the benzene topology of AO's. In general the corresponding limit is

$$S_{\max}=|\,m_{\min}\,|^{-1},$$

where $m_{\min}$ is the lowest (i.e., most negative) eigenvalue of the topological matrix **M** of the conjugated system in question. It can be shown, however,[3] that always $m_{\min}\geq -3$ and that $m_{\min}$ approaches -3 the larger the system becomes; thus, $S_{\max}$ is never smaller than $\frac{1}{3}$.

Naphthalene

In the case of naphthalene, three degrees of approximation are investigated:

Case 1: tight-binding approximation;

Case 2: "intra-ring interactions only," i.e., neglected are the overlap integrals between all those atoms which are further apart than two neighbor distances;

Case 3: all overlap integrals are taken into account.

The results for the overlap matrix are shown in Fig. 3, the results for the energy matrix are shown in Fig. 4. For the sake of clarity, the curves for Cases 1 and 2 are not drawn beyond the point where they become meaningless due to the fact that the lowest eigenvalue of **S** becomes negative. The over-all behavior is quite similar to that found in benzene.

It emerges, however, that for the overlap values occurring in practice, the results of the "intra-ring approximation" (Case 2) are practically identical with those of the full matrix. This is a practical convenience in that only three overlap values are required for this approach.

[3] K. Ruedenberg, J. Chem. Phys. **22**, 1874 (1954).

Atomic Populations in the Augmented Tight-Binding Approximation

An appropriate measure of the population of an atom in a molecule is Mulliken's "gross atomic population." In the present case it is defined by

$$q(P)=2\sum_n c_{Pn}'\sum_Q c_{Qn}'S_{PQ}, \tag{2.11}$$

which becomes, by virtue of Eqs. (1.18) and (1.20),

$$q(P)=2\sum_n c_{Pn}{}^2. \tag{2.12}$$

In the case of the tight-binding approximation, $\mathfrak{M}=\mathbf{M}$, it can be shown that, for alternant molecules,

$$q(P)=1, \quad \text{at all atoms} \tag{2.13}$$

[see Eq. (3.18) of the subsequent paper]. This "Coulson-Rushbrooke theorem" can no longer be exactly valid in the augmented tight-binding approximation since the matrix is not "class-off diagonal" [see Eq. (3.7) of the subsequent paper]. It is of interest to know how large the deviations are which are introduced by taking into account nonneighbor interactions. For naphthalene one finds

for the joint atom:	$q=0.96235$,
for the nonjoint atom which is neighbor to the joint atom:	$q=1.01117$, (2.14)
for the nonjoint atom which is not neighbor to the joint atom:	$q=1.00766$.

ACKNOWLEDGMENTS

I wish to thank the Midwestern Universities Research Association (Madison, Wisconsin) for solving the naphthalene eigenvalue problems on their IBM 704 computer, and in particular Professor L. J. Laslett of Iowa State University, Department of Physics, for his mediation. Hand computations have been carried out by R. Rue. The work has also profited from a quantitative analysis of some 30 hydrocarbons, according to the present methods, which is carried out presently by R. L. Hummel.

Quantum Mechanics of Mobile Electrons in Conjugated Bond Systems. III. Topological Matrix as Generatrix of Bond Orders*

KLAUS RUEDENBERG

Institute for Atomic Research, Department of Physics, Department of Chemistry, Iowa State College, Ames, Iowa

(Received July 7, 1958)

It is shown that in homonuclear conjugated systems the various bond orders and similar quantities can be written as matrix functions of the topological incidence matrix. This entails the existence of a number of useful general relations between these various quantities. The relations include as special cases: Coulson and Rushbrooke's theorem on charge orders in alternants; G. G. Hall's theorem on bond orders in alternants; McWeeny's theorem on the formal charges; Ham and Ruedenberg's correlation between Coulson and Mulliken bond orders for neighbors in alternants; closely related is Ham-Ruedenberg-Platt's relation between valence-bond bond orders and molecular orbital theory. A number of new relations between bond orders are derived and discussed. The generalization from alternants to nonalternants is given particular attention.

INTRODUCTION

EVER since the definition of molecular orbital bond orders by Coulson,[1] there has been an interest in the properties of these and related quantities which are of characteristic importance in assessing the bond strengths between atoms. This interest has led to the discovery of various useful relationships for these quantities, such as: the theorem of Coulson and Rushbrooke for the charge orders in alternants[2]; R. McWeeny's theorem for the "gross" (or "formal") atomic charges[3]; G. G. Hall's theorem for bond orders in alternants[4]; a similar theorem by the present author[5]; Ham and Rudenberg's relationship[6] between Mulliken and Coulson bond orders for neighbor pairs in alternants; Ham, Ruedenberg, and Platt's relationship between MO theory and VB bond orders.[6,7]

The original bond order definitions just referred to were created with reference to the one-electron molecular orbital approximation. However, the derivations in the first paper of this series show that the same quantities play an important role in the more rigorous formulation of the theory including the many-electron interactions. Thus, the progress from the one-particle model to the N-particle theory increases rather than decreases the interest in bond orders. In fact several types of "bond orderlike quantities" were encountered [see Eqs. (4.14), (4.15), and (4.16) of Paper I]. For all quantities of this type the name "bond characteristics" is suggested.

The present note demonstrates that a quite general account can be given for the basic properties of bond characteristics in conjugated systems when the molecular orbitals are the topological MO's discussed in the beginning of the third section of PapersI.

These MO's are defined as eigenfunction of an effective one-electron Hamiltonian $\mathfrak{H}$ in the tight-binding approximation; they are essentially the Hückel-Wheland MO's. They are important since, in many cases, they do not differ much from the LCAO SCF MO's and, in any case, they provide the best starting MO's for a configuration-interaction treatment. The reason for their usefulness is that they are physically meaningful because, on the average, the *long-range* forces between electrons and nuclei *cancel* those between the electrons so that only the short-range forces are significant for the effective Hamiltonian. It is exactly this *short-range character* which is given expression by the tight-binding approximation.

If the short-range forces are dominant, however, in the effective potential, then it stands to reason that the *topology* of the molecule rather than its *geometry* will shape the form of the molecular orbitals and this, in fact is found to be the case, as was discussedin the preceding paper. As a consequence all mobile bond orders are, in one way or another, an expression of the molecular topology.[8] Therefore the present analysis of bond orders is based on a discussion of certain properties of the topological matrix **M**.

This analysis also leads to an extremely gratifying result concerning the various theorems mentioned in the first paragraph of this introduction. It emerges that all of them are different special cases of one basic relationship of a quite general nature. Further applications beside those already known are immediate, in particular the generalization to nonalternants of certain theorems previously given for alternants.

The present investigation considers conjugated systems consisting of identical atoms, which moreover have the property that analogous integrals between neighbor atom orbitals have the same value for all

* Contribution No. 652. Work was performed in the Ames Laboratory of the U. S. Atomic Energy Commission.

[1] C. A. Coulson, Proc. Roy. Soc. (London) **A169**, 413 (1939).

[2] C. A. Coulson and G. S. Rushbrooke, Proc. Cambridge Phil. Soc. **36**, 193 (1940).

[3] R. McWeeny, J. Chem. Phys. **19**, 1614 (1951); **20**, 920 (1952).

[4] G. G. Hall, Proc. Roy. Soc. (London) **A229**, 254 (1955).

[5] K. Ruedenberg, J. Chem. Phys. **29**, 1232 (1958).

[6] N. S. Ham and K. Ruedenberg, J. Chem. Phys. **29**, 1215 (1958).

[7] N. S. Ham, J. Chem. Phys. **29**, 1229 (1958).

[8] The *geometrical shape of the molecule* is, of course, determined by the hybridization and other energetic effects of the stronger electron-pair bonds.

neighbor pairs. In this case the relation to topology becomes particularly lucid.

Conjugated systems of bonds are found not only in unsaturated organic molecules, but also in crystals and metals. Quite generally such a system is characterized by the fact that the molecule contains more than two atoms, each of which contributes one electron and one AO to the formation of delocalized molecular orbitals associated with the particular bond type. Thus the number of electrons may be well below the number of bonds, in contrast with a systems of electron-pair bonds where the number of electrons is twice the number of bonds.

1. PREMISES

Characterization of the System[9]

If each of the N atoms contributes an AO, $\chi_P (P=1, 2, \cdots N)$, then the molecular orbitals have the form

$$\varphi_n = \sum_{P=1}^{N} c_{Pn}' \chi_P, \qquad (n=1, 2, \cdots N) \qquad (1.1)$$

and, under the conditions set forth in the introduction, the coefficients are determined by the eigenvalue problem characterized by a Hamiltonian matrix

$$\mathbf{H}=\alpha\mathbf{I}+\beta\mathbf{M} \qquad (1.2)$$

and an overlap matrix

$$\mathbf{S}=\mathbf{I}+S\mathbf{M}, \qquad (1.3)$$

where

$$S=(\chi_1 \mid \chi_2), \quad \beta=(\chi_1 \mid \mathbf{H} \mid \chi_2), \quad \alpha=(\chi_1 \mid \mathbf{H} \mid \chi_1). \qquad (1.4)$$

Here χ_1, χ_2 are any two neighbor orbitals; the form of the χ_P's is the same for all atoms. $\mathbf{I}$ is the unit matrix and $\mathbf{M}$ is the topological matrix[10] of the molecule, defined by

$$M_{PQ}=\begin{cases} 1, & \text{if } P \text{ and } Q \text{ are neighbors,} \\ 0, & \text{otherwise.} \end{cases} \qquad (1.5)$$

It is useful to introduce $\mathbf{M}$ as such, since $\mathbf{H}$ and $\mathbf{S}$ can be written as functions of $\mathbf{M}$.[9]

Let $m_n (n=1, 2, \cdots N)$ be the eigenvalues of $\mathbf{M}$, and let

$$\mathbf{c}_n=\begin{pmatrix} c_{1n} \\ c_{2n} \\ \cdot \\ \cdot \\ \cdot \\ c_{Nn} \end{pmatrix} \qquad (1.6)$$

be the corresponding eigenvectors. Then, the molecular orbitals (1.1) are given by

$$c_{Pn}'=(1+Sm_n)^{-\frac{1}{2}} c_{Pn} \qquad (1.7)$$

and the corresponding orbital energies by

$$\epsilon_n=(\alpha+\beta m_n)/(1+Sm_n). \qquad (1.8)$$

Eigenvalue Spectrum of M and Consequences

Since $\mathbf{M}$ has vanishing diagonal elements and the trace is an invariant of the matrix, it follows that

$$\sum_n m_n=0. \qquad (1.9)$$

Positive and negative eigenvalues of $\mathbf{M}$ will therefore occur in such a way as to yield the average zero. It is of importance that they can be shown to be limited by [see Eq. (2.17) of work cited in footnote 9]

$$-3 \leq m_n \leq 3. \qquad (1.10)$$

Since the orbital energies can be written

$$\epsilon_n=\alpha+\gamma m_n/(1+Sm_n), \qquad (1.11)$$

where

$$\gamma=\beta-\alpha S<0, \qquad (1.12)$$

the orbital energies *increase* with *decreasing* m_n values, the lowest orbital being the one with the highest positive m_n value. Hence the indices n are chosen such that m_1 is the largest positive eigenvalue and m_N is the most negative eigenvalue.

In the following we are dealing mainly with the ground state which is characterized by the following orbital occupation numbers g_n:

$$g_n=\begin{cases} 2 & \text{for } 1 \leq n \leq \frac{1}{2}N, \\ 0 & \text{for } (\frac{1}{2}N+1) \leq n \leq N, \end{cases} \qquad \text{if } N \text{ is even,} \qquad (1.13)$$

$$g_n=\begin{cases} 2 & \text{for } 1 \leq n \leq \frac{1}{2}(N-1), \\ 1 & \text{for } n=\frac{1}{2}(N+1), \\ 0 & \text{for } \frac{1}{2}(N+3) \leq n \leq N, \end{cases} \qquad \text{if } N \text{ is odd.} \qquad (1.13')$$

Equations (1.13) and (1.13′) exclude the case of a degeneracy between the highest ground-state orbital and the lowest excited orbital. If such a degeneracy exists, Hund's rule will lead to several singly occupied orbitals. This matter is discussed in some detail in the following in connection with alternant systems [see text following Eq. (3.11)].

For the purpose of the subsequent discussion the following distinctions are convenient:

(1) The number of positive eigenvalues of $\mathbf{M}$ is equal to the number of negative eigenvalues. This is by far the most common situation. In this case, $\det(\mathbf{M}) \geq 0$.

(a) Regular system. All eigenvalues of $\mathbf{M}$ are different from zero. Hence the number N of atoms is

[9] A somewhat more detailed exposition is given in K. Ruedenberg, J. Chem. Phys. **22**, 1878 (1954).

[10] More accurately, $\mathbf{M}$ is the topological incidence matrix corresponding to the valuation 1 of all edges. (In the free electron theory a different valuation is used.) The relation to topology has recently been competently discussed by H. H. Guenthard and H. Primas, Helv. Chim. Acta **39**, 1645 (1956).

even; there are $(\frac{1}{2}N)$ positive and $(\frac{1}{2}N)$ negative m_n's. $\mathbf{M}^{-1}$ exists.

(b) Singular system. There are eigenvalues $m_n=0$. This *must* be the case if N is odd; but occurs also for even N, e.g., in ring systems where the number of atoms is a multiple of 4. In general, the number of vanishing eigenvalues has the same parity as N. Free radicals belong in this class. The inverse of $\mathbf{M}$ does not exist.

(2) The number of positive eigenvalues of $\mathbf{M}$ is *not* equal to the number of negative eigenvalues.

Example for N even: Pentalene ($N=8$). There are four positive and three negative eigenvalues, and one $m_n=0$.

Example for N odd: Ring systems with $(4q-1)$ atoms (q integer). There are $(2q-1)$ positive eigenvalues and $(2q)$ negative ones, counting degeneracies properly.

It is seen that all molecules belonging to class (1) have the following property in their ground state:

$$\begin{aligned} m_n &\geq 0, \quad \text{if} \quad g_n=2, \\ m_n &=0, \quad \text{if} \quad g_n=1, \\ m_n &=0, \quad \text{if} \quad g_n=0. \end{aligned} \tag{1.14}$$

This property is essential for some further conclusions. It will be noticed that this property is also shared by some molecules in class (2), e.g., pentalene. Systems having the property expressed by Eq. (1.14) will be called "normal systems." Some of the relations to be derived hold for all systems, some for normal systems, and some (requiring the existence of $\mathbf{M}^{-1}$) for systems of class (1a).

Equation (1.10) furthermore requires that

$$S<(\tfrac{1}{3}), \tag{1.15}$$

in order that the overlap matrix $\mathbf{S}$ of Eq. (1.3) be always positive definite, i.e., that the atomic orbitals form a linear independent set. The fact that, for $S\geq(\frac{1}{3})$, these functions seem to become linearly dependent indicates that the tight-binding approximation (i.e., neglecting nonneighbor interaction) is inadequate if the overlap between neighbors exceeds 0.333.[11] In the case of unsaturated hydrocarbons, S is generally assumed to be 0.25.

Bond-Orderlike Quantities

Coulson[1] has defined bond orders by the equation

$$p(PQ)=\sum_n g_n c_{Pn} c_{Qn}, \tag{1.16}$$

where the g_n's are given by Eqs. (1.13) and (1.13′). Although the original definition referred to neighbor atoms, it is now generally used for any two atoms, thus generating the Coulson bond-order matrix $\mathbf{p}$.

R. S. Mulliken[12] has defined the bond orders

$$p^m(PQ)=(1+S)\,p'(PQ), \tag{1.17}$$

where [see Eq. (1.7)]

$$p'(PQ)=\sum_n g_n c_{Pn} c_{Qn}'=\sum_n g_n c_{Pn} c_{Qn}/(1+Sm_n), \tag{1.18}$$

giving rise to the bond-order matrix $\mathbf{p}'$. A discussion of the physical meaning has been given elsewhere.[6]

K. Ruedenberg[13] has defined the bond quantities

$$p^{hrp}(PQ)=\sum_n g_n c_{Pn} c_{Qn}/m_n, \tag{1.19}$$

and Ham, Ruedenberg, and Platt discovered[6] that, in the case of neighbors in alternant systems, this definition yielded the valence-bond bond orders $p^v(PQ)$ of L. Pauling. N. S. Ham subsequently explained[7] this agreement by demonstrating the equivalence of the definition (1.19) with the definition of the Pauling bond orders.

The foregoing definitions suggest that one should consider the properties of the general "bond orderlike quantity,"

$$f_{PQ}=\sum_n g_n c_{Pn} c_{Qn} f(m_n), \tag{1.20}$$

where $f(x)$ is an arbitrary function of x. Equation (1.20) defines the matrix $\mathbf{f}$. Quantities of the general form (1.20) will be called "bond characteristics."

Functions of the Topological Matrix

Since $\mathbf{M}$ is a symmetric matrix, any matrix function $f(\mathbf{M})$ satisfies the identity[14]

$$f(\mathbf{M})=\{\sum_{n=1}^{N} c_{Pn} c_{Qn} f(m_n)\}, \tag{1.21}$$

whence in particular also

$$F[f(\mathbf{M}), h(\mathbf{M})]=\{\sum_{n=1}^{N} c_{Pn} c_{Qn} F[f(m_n), h(m_n)]\}. \tag{1.22}$$

The summation on the right-hand side of these two equations differs from the one in Eq. (1.20). The latter goes only over the ground-state orbitals because of the factor g_n, whereas in Eqs. (1.21) and (1.22) we sum over *all* orbitals. The matrices $\mathbf{f}$ and $f(\mathbf{M})$ are therefore different matrices. If $f(x)$ is a polynomial or power series, then $f(\mathbf{M})$ can be computed directly from $\mathbf{M}$ by matrix algebra. Such is not the case for $\mathbf{f}$. *The*

[11] More precisely, the linear independence requires that the smallest eigenvalues of $\mathbf{S}$, i.e. $(1+Sm_{\min})$, is positive. A more explicit discussion of this point was given in Sec. 2 of the preceding paper.

[12] R. S. Mulliken, J. chim. phys. **46**, 675 (1949), Eq. (145b); J. Chem. Phys. **23**, 1833, 1841 (1955).

[13] K. Ruedenberg, J. Chem. Phys. **22**, 1878 (1954), Eq. (4.89).

[14] Equation (1.21) follows from the fact that $f(\mathbf{M})$ has the same eigenvectors as $\mathbf{M}$ and the eigenvalues $f(m_n)$, and that the projection operator in the direction of $\mathbf{C}_n$ is given by $\mathbf{P}_n=\{c_{Pn}c_{Qn}\}$. Eq. (1.21) is the spectral decomposition of $f(\mathbf{M})$. See, e.g., D. C. Murdoch, *Linear Algebra for Undergraduates* (John Wiley and Sons, Inc., New York, 1956), pp. 180–182.

mathematical essence of the following derivations, it may be said, lies in establishing useful relationships between the matrix $\mathbf{f}$ *and the matrix* $f(\mathbf{M})$. We will omit the limits in the summations with the understanding that the sum goes over all orbitals unless the factor g_n is present.

In particular let us consider the matrix $\mathbf{M}_+$ corresponding to the function $f(x)=|x|$, because of its usefulness later on. Apparently

$$\mathbf{M}_+=\{\sum_n c_{Pn}c_{Qn}\,|\,m_n\,|\}=\{\sum_n c_{Pn}c_{Qn}[+(m_n^2)^{\frac{1}{2}}]\}$$
$$=+(\mathbf{M}^2)^{\frac{1}{2}}, \quad (1.23)$$

i.e., $\mathbf{M}_+$ is the positive definite square root of the positive definite matrix $\mathbf{M}^2$ ($\mathbf{M}$ is indefinite). The matrix $\langle\mathbf{M}_+\rangle$ can be obtained directly from $\mathbf{M}$, without recourse to the eigenvectors by a series expansion. In fact, by virtue of Eq. (1.10) one can write

$$+(m_n^2)^{\frac{1}{2}}=(3/\sqrt{2})\,(1-\epsilon)^{\frac{1}{2}}, \qquad \epsilon=1-(m_n^2/4.5).$$

Expanding the square root, one obtains the convergent series

$$\mathbf{M}_+=+(\mathbf{M}^2)^{\frac{1}{2}}=(3/\sqrt{2})\,\{\mathbf{I}-\tfrac{1}{2}\mathbf{A}-\tfrac{1}{8}\mathbf{A}^2-\tfrac{1}{16}\mathbf{A}^3$$
$$-\tfrac{5}{128}\mathbf{A}^4-\cdots\},$$
$$\mathbf{A}=\mathbf{I}-\mathbf{M}^2/4.5. \quad (1.24)$$

A similar series was used, in the case of alternants, for a different but related matrix by G. G. Hall.[4]

2. GENERAL SYSTEMS

First Theorem

It was pointed out after Eq. (1.22) that

$$\mathbf{f}\neq f(\mathbf{M}).$$

One can, however, write

$$\mathbf{f}=F(\mathbf{M}) \quad (2.1)$$

with the definition

$$F(m_n)=g_n f(m_n). \quad (2.1')$$

Applying this device to the definition (1.16) of the Coulson bond order matrix $\mathbf{p}$, one obtains from Eqs. (1.16), (1.21), (1.22), and (1.20)

$$\mathbf{f}=\mathbf{p}f(\mathbf{M})=f(\mathbf{M})\,\mathbf{p}. \quad (2.2)$$

This identity is true without restrictions. It shows that any bond orderlike matrix $\mathbf{f}$ can be computed from $\mathbf{p}$ and $f(\mathbf{M})$ by matrix multiplication without going back to the eigenvalues and eigenvectors.

Second Theorem

For the function $g(x)=[f(x)+f(|x|)]$, Eq. (1.22) yields

$$f(\mathbf{M})+f(\mathbf{M}_+)=\sum_n c_{Pn}c_{Qn}[f(m_n)+f(|m_n|)], \quad (2.3)$$

where the matrix (1.23) has been used.

Now let $f(x)$ be an odd function,

$$f^u(x)=-f^u(-x)$$

and furthermore consider only normal systems in the sense stipulated in connection with Eq. (1.14). It follows immediately that

$$f^u(m_n)+f^u(|m_n|)=g_n f^u(m_n), \quad \text{for all } n,$$

and hence

$$\mathbf{f}^u=f^u(\mathbf{M})+f^u(\mathbf{M}_+). \quad (2.4)$$

Equation (2.4) holds for odd functions in normal conjugated systems. It was mentioned after Eq. (1.23) that $\mathbf{M}_+$ can be computed from $\mathbf{M}$ as a series, without going back to the eigenvectors and eigenvalues.

On the other hand Eq. (2.4) can be combined with Eq. (2.2), whence

$$f^u(\mathbf{M}_+)=(\mathbf{p}-\mathbf{I})f^u(\mathbf{M}), \quad (2.5)$$

for normal systems.

Coulson Bond Orders

Consider now the function $f(x)=x$. Equation (2.4) yields

$$\mathbf{pM}=\mathbf{M}+\mathbf{M}_+ \quad (2.6)$$

for normal systems. And if $\mathbf{M}$ has an inverse, we find

$$\mathbf{p}=\mathbf{I}+\mathbf{M}_+\mathbf{M}^{-1}. \quad (2.7)$$

This equation holds for normal systems with all m_n's different from zero [since $\det(\mathbf{M})$ must be different from zero], Eq. (2.7) is limited to systems belonging to class (1a). Since $\mathbf{M}_+$ can be computed as a series in $\mathbf{M}$ and since, because of the simplicity of $\mathbf{M}$, it is easy to find $\mathbf{M}^{-1}$ by elimination, Eq. (2.7) provides the possibility of computing $\mathbf{p}$ without recourse to eigenvalues and eigenvectors.

In the case of alternant systems, which will be dealt with below, the relation (2.7) can be decomposed into two separate equations. One of them expresses the generalized theorem of Coulson and Rushbrooke,[2] the other is equivalent to the theorem of G. G. Hall.[4] *Thus, Eq. (2.7) has to be considered as the appropriate generalization to nonalternants of these two theorems for alternants.*

From Eq. (2.7) follows

$$(\mathbf{p}-\mathbf{I})^2=\mathbf{M}^{-1}\mathbf{M}_+^2\mathbf{M}^{-1}=\mathbf{M}^{-1}\mathbf{M}^2\mathbf{M}^{-1}=\mathbf{I}, \quad (2.7')$$

i.e., $(\mathbf{p}-\mathbf{I})$ is symmetrical *and* orthogonal. This is equivalent to the identity

$$(\tfrac{1}{2}\mathbf{p})^2=(\tfrac{1}{2}\mathbf{p}),$$

which expresses the fact that $(\frac{1}{2}\mathbf{p})$ is a projection operator in this case.

By virtue of Eq. (2.7) one can now write for the basic relation (2.2),

$$\mathbf{f}=(\mathbf{I}+\mathbf{M}_+\mathbf{M}^{-1})f(\mathbf{M}) \tag{2.8}$$

and for Eq. (2.5),

$$f^u(\mathbf{M}_+)=\mathbf{M}_+\mathbf{M}^{-1}f^u(\mathbf{M}), \tag{2.9}$$

where $f^u(x)$ is an odd function. Eqs. (2.8) and (2.9) are of course limited to systems of class (1a).

Bound Valences

According to Eq. (2.2), the matrix given by Eq. (2.6) is in fact

$$\mathbf{pM}=\{\sum_n g_n c_{Pn} c_{Qn} m_n\}=\mathbf{Mp}; \tag{2.10}$$

we find, therefore,

$$(\mathbf{pM})_{PQ}=\sum_{R(Q)}{}^{NB} p[P, R(Q)]=\sum_{R(P)}{}^{NB} p[Q, R(P)], \tag{2.11}$$

where

$$\sum_{R(X)}{}^{NB}=\text{sum over the neighbors } R \text{ of atom } X.$$

The identity of the second and third member of the equation follows from the symmetry of **pM**, as shown by (2.10).

One recognizes that the diagonal elements of (2.11) are in fact the "bound mobile valences" implied in the definition of free valances by Coulson *et al.*[15] By virtue of Eq. (2.6), the diagonal elements are given by

$$\sum_{R(P)}{}^{NB} p[P, R(P)]=(\mathbf{pM})_{PP}=(\mathbf{M}_+)_{PP}, \tag{2.12}$$

i.e., the bound valences are the diagonal elements of the positive definite square root of $\mathbf{M}^2$. Considering the off-diagonal elements as generalizations, one can call the matrix **pM** the matrix of bound valences.

Mulliken Bond Orders

Consider now the function $f(x)=(1+Sx)^{-1}$. In this case the matrix **f** defined by Eq. (1.20) becomes the matrix $\mathbf{p}'$ of Eq. (1.18), which differs from the Mulliken bond orders (1.17) only by the constant factor $(1+S)$.

Equation (2.2) yields

$$\mathbf{p}'=\mathbf{p}(\mathbf{I}+S\mathbf{M})^{-1}, \tag{2.13}$$

for *any* system, and

$$\mathbf{p}'=(\mathbf{I}+\mathbf{M}_+\mathbf{M}^{-1})(\mathbf{I}+S\mathbf{M})^{-1} \tag{2.14}$$

for molecules of class (1a).

[15] See, e.g., C. A. Coulson and H. C. Longuet-Higgins, Rev. sci. **85**, 929 (1947); also W. Moffitt, Trans. Faraday Soc. **45**, 373 (1949).

Equation (2.13) contains, as a special case, the theorem of R. McWeeny.[3] Indeed, we find from (2.13)

$$\{(\mathbf{I}+S\mathbf{M})\mathbf{p}'\}_{PP}=p(PP).$$

Now the right-hand side of this equation is

$$p(PP)=q(P), \quad \text{the Coulson charge order,}$$

whereas the left-hand side is

$$p'(PP)+S\sum_{R(P)}{}^{NB} p'(PR),$$

i.e., Mulliken's "gross atomic populations." The identity of both quantities is McWeeny's statement.

It is extremely convenient that the right-hand side of Eq. (2.13) can be expanded in a rapidly convergent series. To this end one writes

$$(1+Sm_n)^{-1}=(1+\tfrac{3}{2}S)^{-1}(1-\eta)^{-1}$$

with

$$\eta=(\tfrac{3}{2}-m_n)S/(1+\tfrac{3}{2}S),$$

whence

$$(1+Sm_n)^{-1}=(1+\tfrac{3}{2}S)^{-2}[(1+3S)-Sm_n](1-\eta^2)^{-1}. \tag{2.15}$$

If we now consider normal systems in the sense of Eq. (1.14) ff., then we know that in the definition (1.18) all values m_n are positive or zero; in conjunction with Eq. (1.10) we have, therefore, $0\leq m_n\leq 3$; furthermore, according to Eq. (1.15), we have $S<(\frac{1}{3})$. Thus we find for η^2 the maximum values

$$\eta^2_{\max}=\begin{cases}1/9 \;=0.11, & \text{for } S=\frac{1}{3}\\ 9/121=0.074, & \text{for } S=\frac{1}{4}.\end{cases}$$

The average value with respect to the sum over n is, therefore, 0.03–0.05, so that the expansion of $(1-\eta^2)^{-1}$ should converge very rapidly. Substitution of Eq. (2.15) in Eq. (2.13) and subsequent expansion yields, therefore,

$$\mathbf{p}'=(1+\tfrac{3}{2}S)^{-2}[(1+3S)\mathbf{p}-S\mathbf{pM}][\mathbf{I}-\mathbf{B}]^{-1}, \tag{2.16}$$

$$\mathbf{p}'=(1+\tfrac{3}{2}S)^{-2}[(1+3S)\mathbf{p}-S\mathbf{pM}]\sum_{k=0}^{\infty}\mathbf{B}^k, \tag{2.17}$$

with

$$\mathbf{B}=(\tfrac{3}{2}\mathbf{I}-\mathbf{M})^2[S/(1+\tfrac{3}{2}S)]^2. \tag{2.18}$$

In view of the rapid convergence, the linear approximation should already be very good, i.e.,

$$\mathbf{p}'=(1+\tfrac{3}{2}S)^{-2}[(1+3S)\mathbf{p}-S\mathbf{pM}], \tag{2.19}$$

or by virtue of Eq. (2.6)

$$\mathbf{p}'=(1+\tfrac{3}{2}S)^{-2}[(1+3S)\mathbf{p}-S(\mathbf{M}+\mathbf{M}_+)]. \tag{2.20}$$

These equations make it possible to obtain the Mulliken bond orders from the Coulson bond orders. Since for $S=(1/4)$ one has $(1+3S):S=7:1$, *the Mulliken*

bond orders are essentially a linear function of the Coulson bond orders in the ground state.

The relationship (2.19) includes as a special case the correlation of Ham and Ruedenberg, who found the numerical validity of such a linear relationship in the case of bonds between neighbor atoms and could theoretically justify it approximately for alternant systems. The numerical agreement between their results and Eq. (2.20) is excellent and will be discussed below.[6]

The foregoing results have been derived for normal systems [see after Eq. (2.15)]. However, in the case of other systems we expect, by virtue of Eq. (1.9), only one or at most two ground-state values $m_n<0$, and those will be rather close to zero. Hence the expansion (2.17) should also be fairly good in these cases, so that the approximation (2.19, 2.20) has *general* validity.

3. ALTERNANT SYSTEMS

Characterization

Many molecules of practical interest, e.g., all compositions of six-membered rings, and also many crystals are alternant systems. They are characterized by the fact that the atoms can be divided into two classes, the starred class (*) and the unstarred class (0), in such a fashion that in no case do two neighbor atoms belong to the same class.

Hence the eigenvectors of $\mathbf{M}$ have "starred components" and "unstarred components," i.e., they lie in an algebraic vector space which has a "starred subspace" and an "unstarred subspace." Correspondingly any matrix $\mathbf{A}$ can be decomposed

$$\mathbf{A}=\mathbf{A}^{=}+\mathbf{A}^{\neq}, \tag{3.1}$$

where

$A_{PQ}{}^{=}\neq 0$, *only* if P and Q *do* belong to the same class,

$A_{PQ}{}^{\neq}\neq 0$, *only* if P and Q *do not* belong to the same class. (3.1′)

We call $\mathbf{A}^{=}$ the class-diagonal part of $\mathbf{A}$, and $\mathbf{A}^{\neq}$ the class-off-diagonal part. The class-diagonal part consists of a starred submatrix and and unstarred submatrix,

$$\mathbf{A}^{=}=\mathbf{A}^{=*}+\mathbf{A}^{=0}, \tag{3.2}$$

where

$A_{PQ}{}^{=*}\neq 0$, *only if* P *and* Q are starred atoms,

$A_{PQ}{}^{=0}\neq 0$, *only if* P *and* Q are unstarred atoms.

It is convenient to define the matrix

$$J=\{J_P\delta_{PQ}\}, \tag{3.3}$$

$$J_P=\begin{cases}1, & \text{if } P \text{ is a starred atom,}\\ -1, & \text{if } P \text{ is an unstarred atom,}\end{cases} \tag{3.3′}$$

because then $\mathbf{A}^{=}$ and $\mathbf{A}^{\neq}$ can be characterized by the commutation relations

$$[J, A^{=}]_{-}=\mathbf{J}\mathbf{A}^{=}-\mathbf{A}^{=}\mathbf{J}=0 \tag{3.4}$$

$$[J, A^{\neq}]_{+}=\mathbf{J}\mathbf{A}^{\neq}+\mathbf{A}^{\neq}\mathbf{J}=0. \tag{3.5}$$

Also,

$$\mathbf{J}^2=\mathbf{I}. \tag{3.6}$$

Eigenvalue Spectrum

The interesting properties of alternants are due to the "pairing theorem" concerning their eigenvalue spectrum, which was discovered by Coulson and Rushbrooke.[2]

According to definition (1.5), the topological matrix is class-off-diagonal. Equation (3.5) yields, therefore,

$$\mathbf{J}\mathbf{M}\mathbf{J}=-\mathbf{M}. \tag{3.7}$$

Hence follows the pairing theorem: If $\mathbf{c}_n$ is an eigenvector of $\mathbf{M}$ with eigenvalue m_n, then

$$\mathbf{c}_n{}'=\mathbf{J}\mathbf{c}_n \tag{3.8}$$

is another eigenvector with the eigenvalue

$$\mathbf{m}_n=-m_n. \tag{3.9}$$

On the other hand $\mathbf{M}^2$ is class-diagonal and, by analogy with (3.2), is the sum of its starred submatrix and its unstarred submatrix

$$\mathbf{M}^2=(\mathbf{M}^2)^*+(\mathbf{M}^2)^0. \tag{3.10}$$

According to Eq. (3.4), $\mathbf{M}^2$ commutes with $\mathbf{J}$, and hence $\mathbf{c}_n{}'$ belong to the same, degenerate, eigenvalue of $\mathbf{M}^2$, *viz* $m_n{}^2$. For $\mathbf{M}^2$ one can therefore choose, instead of $\mathbf{c}_n$ and $\mathbf{c}_n{}'$, the orthogonal eigenvectors

$$\mathbf{c}_n{}^*=(\mathbf{c}_n+\mathbf{c}_n{}')/\sqrt{2},$$

$$\mathbf{c}_n{}^0=(\mathbf{c}_n-\mathbf{c}_n{}')/\sqrt{2}, \tag{3.11}$$

(alternant MO's). In $\mathbf{c}_n{}^*$ only the starred elements are $\neq 0$, and hence it is an eigenvector of $(\mathbf{M}^2)^*$; similarly, in $\mathbf{c}_n{}^0$ only the unstarred elements are $\neq 0$, and hence it is an eigenvector of $(\mathbf{M}^2)^0$. Therefore, the eigenvalue problem of $\mathbf{M}$ (of dimension N) can be reduced to the two eigenvalue problems of $(\mathbf{M}^2)^*$ and $(\mathbf{M}^2)^0$, (each *about* of dimension $N/2$).[16] Moreover, these two smaller eigenvalue problems have the same eigenvalues.

The degeneracy between $\mathbf{c}_n{}^*$ and $\mathbf{c}_n{}^0$ is removed, in passing from $\mathbf{M}^2$ to $\mathbf{M}$, if $m_n\neq 0$, but *not* if $m_n=0$. Since the starred and the unstarred submatrix of $\mathbf{M}^2$ have the *same number* of (in fact the same) *nonzero* eigenvalues, the following theorem results for the eigenvalues $m_n=0$:

If the number of starred atoms [and hence the dimension of $(\mathbf{M}^2)^*$] exceeds the number of unstarred atoms [i.e., the dimension of $(\mathbf{M}^2)^0$] by N^*, then the

[16] This was first pointed out by K. Ruedenberg and Ch. W. Scherr, J. Chem. Phys. **21**, 1565 (1953), and later, independently, by W. Moffitt, J. Chem. Phys. **26**, 424 (1957).

eigenvalue $m_n=0$ has $(a+N^*)$ eigenvectors of the form $\mathbf{c}_n{}^*$, when there are a eigenvectors of the form $\mathbf{c}_n{}^0$ (a may be zero or positive). Hence $m_n=0$ is at least N^*-fold degenerate.

The degeneracy of the level corresponding to $m_n=0$ is, therefore, exactly equal to the number of electrons which have to occupy it in the ground state. In accordance with Hund's rule, each of the $(2a+N^*)$ orbitals belonging to $m_n=0$ is assumed to be singly occupied in the ground state.[17]

Functions of M

If $f^g(x)$ is an even function and $f^u(x)$ is an odd function, then the pairing properties (3.8, 3.9) yield

$$c_{Pn}c_{Qn}f^g(m_n)=\pm c_{Pn}{}'c_{Qn}{}'f^g(m_n')$$
$$c_{Pn}c_{Qn}f^u(m_n)=\mp c_{Pn}{}'c_{Qn}{}'f^u(m_n'), \qquad (3.12)$$

where in each case the upper sign holds if P and Q belong to the same class, and the lower sign holds if P and Q do *not* belong to the same class. Under the occupancy assumption adopted in the previous paragraph, these equations hold also for the eigenvalue $m_n=0$.

Substitution of Eq. (3.12) in the definition (1.21) shows immediately that, for alternant systems,

$$f^g(\mathbf{M})=\text{class-diagonal},$$
$$f^u(\mathbf{M})=\text{class-off-diagonal}. \qquad (3.13)$$

Hence an arbitrary function of $\mathbf{M}$ can be decomposed in its class-diagonal part and its class-off-diagonal part as follows:

$$f(\mathbf{M})=f(\mathbf{M})^{=}+f(\mathbf{M})^{\neq},$$
$$f(\mathbf{M})^{=}=f^g(\mathbf{M}),$$
$$f(\mathbf{M})^{\neq}=f^u(\mathbf{M}), \qquad (3.14)$$

where now $f^g(x)$ and $f^u(x)$ are the even and the odd part of the function $f(x)$ defined by

$$f^g(x)=\tfrac{1}{2}[f(x)+f(-x)],$$
$$f^u(x)=\tfrac{1}{2}[f(x)-f(-x)]. \qquad (3.14')$$

Bond Orderlike Quantities

It can roughly be said that, mathematically, the theorems discussed in Sec. 2 served to express bond-orderlike quantities $\mathbf{f}$, defined by Eq. (1.20) in terms of matrix functions $f(\mathbf{M})$ of the topological matrix $\mathbf{M}$.

The new element of interest in the present section is the decomposition of the bond orderlike quantities $\mathbf{f}$ into their class-diagonal and their class-off-diagonal parts, i.e.,

$$\mathbf{f}=\mathbf{f}^{=}+\mathbf{f}^{\neq}. \qquad (3.15)$$

We shall discuss the simplifications which result as a consequence of this decomposition for each of the relations derived in Sec. 2.

Second Theorem

Since alternant systems are normal in the sense of Eq. (1.14) ff., the relation (2.4) is here valid. Now, since $f(|x|)$ is even in x for *any* function, the Eqs. (3.13) show that Eq. (2.4) furnishes, in fact, the decomposition of the bond orderlike quantity $\mathbf{f}^u$, defined by Eq. (1.20) *for an odd function*, into its class-diagonal and its class-off-diagonal part, *viz*,

$$\mathbf{f}^u=(\mathbf{f}^u)^{=}+(\mathbf{f}^u)^{\neq}, \qquad (3.16)$$

where

$$(\mathbf{f}^u)^{=}=f^u(\mathbf{M}_+),$$
$$(\mathbf{f}^u)^{\neq}=f^u(\mathbf{M}). \qquad (3.16')$$

Here $f^u(x)$ is an odd function, and $\mathbf{M}_+$ is the positive definite square root of $\mathbf{M}^2$ [see (1.23) and (2.6)].

Coulson Bond Orders

The identification just discussed, in conjunction with Eq. (2.6) yields immediately that $(\mathbf{p}-\mathbf{I})$ must be class-off-diagonal [see Eq. (3.13)]. It follows, therefore, that the Coulson bond orders can be decomposed.

$$\mathbf{p}=\mathbf{p}^{=}+\mathbf{p}^{\neq}, \qquad (3.17)$$
$$\mathbf{p}^{=}=\mathbf{I}, \qquad (3.18)$$
$$\mathbf{p}^{\neq}=\mathbf{p}-\mathbf{I}, \qquad (3.18')$$

i.e., the class-diagonal part of the Coulson bond-order matrix is the unit matrix. This is the generalized theorem of Coulson and Rushbrooke.[2]

If $\mathbf{M}$ has an inverse (i.e., there are no eigenvalues $m_n=0$), then comparison of Eqs. (2.7) and (3.18') shows that the class-off-diagonal part of $\mathbf{p}$ is also given by

$$\mathbf{p}^{\neq}=\mathbf{M}_+\mathbf{M}^{-1}. \qquad (3.19)$$

This is a simpler and slightly more general statement of the theorem given by G. G. Hall.[4] Since $xf(|x|)$ is an odd function of x, the corresponding matrix function is indeed class-off-diagonal.

First Theorem

Let us now introduce the results (3.17), (3.18), (3.18'), and (3.14) into the first theorem, i.e., Eq. (2.2). Thus is found the decomposition of the bond orderlike quantity obtained for an arbitrary function $f(x)$. The decomposition into the class-diagonal and the class-

[17] For a more detailed investigation of systems with multiple degeneracy for $m_n=0$ ("multiradicals"), from a different viewpoint, see the excellent analysis by H. C. Longuet-Higgins, J. Chem. Phys. **18**, 265 (1950).

off-diagonal part becomes, with the notation of Eq. (3.15),

$$\mathbf{f}^{=}=f^{g}(\mathbf{M})+(\mathbf{p}-\mathbf{I})f^{u}(\mathbf{M}),$$

$$\mathbf{f}^{\neq}=f^{u}(\mathbf{M})+(\mathbf{p}-\mathbf{I})f^{g}(\mathbf{M}), \qquad (3.20)$$

where $f^{g}(x)$ and $f^{u}(x)$ are the even and the odd part of the function $f(x)$, as defined by Eq. (3.14′).

If there are no eigenvalues $m_n=0$, then Eq. (3.19) yields

$$\mathbf{f}^{=}=f^{g}(\mathbf{M})+\mathbf{M}_{+}\mathbf{M}^{-1}f^{u}(\mathbf{M}), \qquad (3.21)$$

$$\mathbf{f}^{\neq}=f^{u}(\mathbf{M})+\mathbf{M}_{+}\mathbf{M}^{-1}f^{g}(\mathbf{M}), \qquad (3.21')$$

and, by virtue of Eq. (2.7′),

$$\mathbf{f}^{\neq}=\mathbf{M}_{+}\mathbf{M}^{-1}\mathbf{f}^{=}. \qquad (3.22)$$

For *even* functions, Eq. (3.21′) represents a simpler statement of the theorem given in footnote 5.

Pauling Bond Orders

For $f(x)=x^{-1}$, the definition (1.20) yields the matrix $\mathbf{p}^{hrp}$ of (1.19) defined by K. Ruedenberg.[13] Eq. (3.20) shows that the class-off-diagonal elements of $\mathbf{p}^{hrp}$ are identical with the elements of $\mathbf{M}^{-1}$. This holds in particular for the elements corresponding to neighbor pairs. The identity of these elements of $\mathbf{M}^{-1}$ with the Pauling bond orders $p^{p}(PQ)$ was shown by N. S. Ham [see text after Eq. (1.19)].[7] Thus of the three matrices $p^{hrp}(PQ)$, $(\mathbf{M}^{-1})_{PQ}$, $p^{p}(PQ)$, the first two agree always when P and Q belong to a different class, and the last two agree when P and Q are neighbors in particular. It is therefore possible, by virtue of Ham's result, to express the Pauling bond orders of valence bond theory in terms of $\mathbf{M}^{-1}$, or alternatively in terms of molecular orbitals.

Mulliken Bond Orders

In order to find the class-diagonal part and the class-off-diagonal part of the Mulliken bond orders, one has to write $(1+Sx)^{-1}$ as the sum of an even and an odd function, *viz*,

$$(1+Sx)^{-1}=1/(1-S^2x^2)+[-Sx/(1-S^2x^2)], \qquad (3.23)$$

and insert the even and the odd function in Eq. (3.20) or (3.21).

We are interested especially, however, in the approximation expressed by Eqs. (2.19) and (2.20). By virtue of the decomposition (3.17) of $\mathbf{p}$, we find immediately

$$\mathbf{p}'=(\mathbf{p}')^{=}+(\mathbf{p}')^{\neq}, \qquad (3.24)$$

with

$$(\mathbf{p}')^{=}=[(1+3S)/(1+\tfrac{3}{2}S)^2]\mathbf{I}-[\mathbf{S}/(1+\tfrac{3}{2}S)^2]\mathbf{M}_{+},$$

$$(\mathbf{p}')^{\neq}=[(1+3S)/(1+\tfrac{3}{2}S)^2](\mathbf{p}-\mathbf{I})-[S/(1+\tfrac{3}{2}S)^2]\mathbf{M}. \qquad (3.24')$$

The excellence of this approximation is seen from an application to neighbor atoms. With $S=1/4$, Eq. (3.24′) yields here

$$p'(PQ)=0.9256p(PQ)-0.1322. \qquad (3.25)$$

As the result of extensive calculations on 17, mostly large, molecules Ham and Ruedenberg have found that the relation

$$p'(PQ)'=0.9388p(PQ)-0.1346 \qquad (3.26)$$

is indeed satisfied within an accuracy of about 0.005 [Eq. (3.26) was the result of a least-squares calculation].[6] The approximation (3.24′) is, therefore, entirely adequate within the framework of this theory.

CONCLUSION

It has been found that all bond characteristics considered here are generated by applying specific operators to the topological matrix. The relations between them are a consequence of this connection with the molecular topology. There may exist still other properties which obtain as functions of the topological matrix.

THE JOURNAL OF CHEMICAL PHYSICS VOLUME 34, NUMBER 6 JUNE, 1961

Quantum Mechanics of Mobile Electrons in Conjugated Bond Systems. IV. Integral Formulas*

KLAUS RUEDENBERG

Institute for Atomic Research, Department of Chemistry, Department of Physics, Iowa State University, Ames, Iowa

(Received March 16, 1959)

Formulas are established for all carbon and hydrogen penetration integrals occurring in the tight-binding approximation of the theory of mobile electrons. The orbital exponents of the penetrated shielding orbitals may differ from the orbital exponent of the penetrating $2p\pi$ electrons. A simple correlation between kinetic energy integral and overlap integral is found.

THE present article furnishes certain new results concerning one-electron integrals in conjugated systems which are needed for a quantitative evaluation of the theory developed in the first paper of this series.[1]

An instructive and useful relationship between the kinetic energy integral and the corresponding overlap integral is reported.

Formulas are derived for all occuring penetration integrals. Up to now, a formula has been given for one case only where, moreover, the orbital exponent of penetrated shielding orbitals and penetrating $2p\pi$ orbital were assumed to be identical.[2] The present investigation covers the various cases generally and also considers the penetration into the hydrogen cores.

1. CONVENTIONS

The atomic orbital on atom P is

$$\chi_P=\chi(\mathbf{r}-\mathbf{r}_P), \tag{1.1}$$

where $\mathbf{r}_P$ is the position vector of nucleus P, and

$$\chi(\mathbf{r})=2p\pi=(\zeta^3/a^3\pi)^{\frac{1}{2}}(\zeta z/a)\exp(-\zeta r/a). \tag{1.2}$$

Here, z is the coordinate perpendicular to the molecular plane, and $\zeta=(\frac{1}{2})Z_{\text{eff}}$. The effective nuclear charge would be about $Z_{\text{eff}}=3.25$ according to Slater's rule; we envisage, however, the possibility of an independent determination of the orbital exponent. Furthermore,

$$a=\hbar^2/me^2=0.529151\text{ A},$$

is the Bohr radius, so that Eq. (1.2) is given in arbitrary units. This is being done to keep a greater flexibility in units. In working with conjugated systems, it is convenient to use as unit of length the mean neighbor distance

$$D=1.40000\text{ A}. \tag{1.3}$$

Two convenient choices exist for the energy unit: either

$$(\hbar^2/2mD^2)=E_{\text{H}}(a/D)^2=1.943\text{ ev}, \tag{1.4}$$

or

$$(e^2/D)=E_{\text{H}}(2a/D)=10.2833\text{ ev}, \tag{1.5}$$

where

$$E_{\text{H}}=e^2/2a=\hbar^2/2ma^2=\text{ionization potential of the hydrogen atom.} \tag{1.6}$$

The expression (1.4) appears as a factor in the kinetic energy terms and is therefore convenient in the FE theory. The expression (1.5) appears as a factor in the potential energy terms and is more convenient in the LCAO theory. The ratio is

$$(e^2/D)/(\hbar^2/2mD^2)=(2D/a)=5.29150 \tag{1.7}$$

(it may be noted that $D=5a^2$ exactly in Angstrom units). From an order-of-magnitude numerical point of view, the unit (1.4) is most convenient.

Besides the neighbor C—C distance D, there appears also the distance D_{H} between a carbon and its neighboring hydrogen atom. One has

$$D_{\text{H}}=1.08\text{ A} \tag{1.8}$$

$$\gamma=(D/D_{\text{H}})=1.2962963. \tag{1.8'}$$

In this context it is also convenient to introduce the quantities

$$\rho=\zeta(D/a) \tag{1.9}$$

and

$$\rho_1=\zeta(D_{\text{H}}/a)=\rho/\gamma, \tag{1.10}$$

which appear in the integrals; ζ is the orbital exponent of the atomic orbital (1.2).

It turns out that the calculation of penetration integrals is greatly facilitated by the results presented in the hybrid-integral paper by Ruedenberg, Roothaan, and Jaunzemis.[3] In particular the formulas for the one-center potentials and the explicit expressions for the C functions given in the "unabridged version",[4] greatly facilitate the present derivations. Frequent references to these papers will therefore be made. For simplicity, footnote 3 will be quoted as "RRJ"

* Contribution No. 701. Work was performed in the Ames Laboratory of the U. S. Atomic Energy Commission.

[1] K. Ruedenberg, J. Chem. Phys. **34**, 1861 (1961).

[2] R. G. Parr and B. L. Crawford, J. Chem. Phys. **16**, 1049 (1948).

[3] K. Ruedenberg, C. C. J. Roothaan, and W. Jaunzemis, J. Chem. Phys. **24**, 201 (1956).

[4] Tech. Rept. 1952–1953, Part Two. Laboratory of Molecular Structure and Spectra, Department of Physics, University of Chicago.

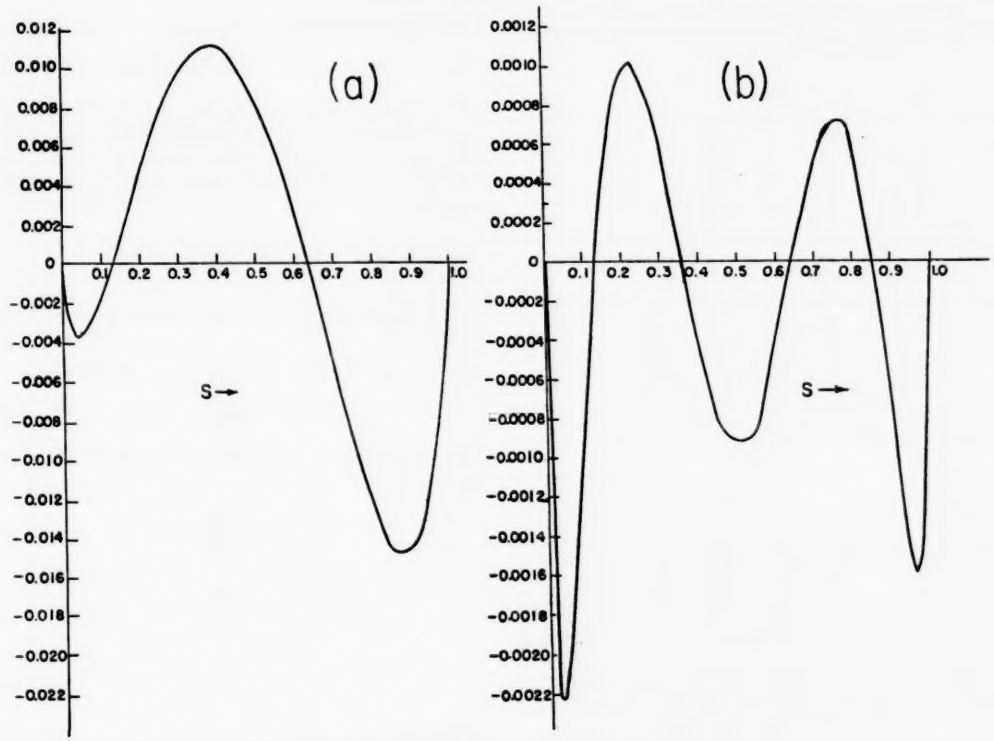

FIG. 1. Kinetic energy integral and overlap integral.
Part (a): $(T_{PQ}/T_{11})-S_{PQ}^2$.
Part (b): $(T_{PQ}/T_{11})-S_{PQ}^3-\frac{3}{4}S_{PQ}(S_{PQ}-1)(S_{PQ}-0.13)(S_{PQ}-0.64)$.

and footnote 4 will be quoted as "RRJu". It may be noted that the results in those papers have to be multiplied by (e^2/a) in order to obtain arbitrary energy units.

2. OVERLAP AND KINETIC ENERGY INTEGRALS

The overlap integral between two AO's is

$$S_{PQ}=(\chi_P \mid \chi_Q)=\exp(-\bar{\rho})[1+\bar{\rho}+(\tfrac{2}{5})\bar{\rho}^2+(\tfrac{1}{15})\bar{\rho}^3], \tag{2.1}$$

where

$$\bar{\rho}=\rho(R_{PQ}/D)=\zeta(R_{PQ}/a), \tag{2.2}$$

with R_{PQ} being the distance between atoms P and Q.

The kinetic energy integral is

$$T_{PQ}=(\chi_P \mid (-\hbar^2/2m)\Delta \mid \chi_Q)$$
$$=T_{11}\exp(-\bar{\rho})[1+\bar{\rho}+(\tfrac{4}{15})\bar{\rho}^2-(\tfrac{1}{15})\bar{\rho}^3], \tag{2.3}$$

where

$$T_{11}=(\chi_P \mid (-\hbar^2/2m)\Delta \mid \chi_P)=E_H\zeta^2=(\hbar^2/2mD^2)\rho^2$$
$$=(e^2/D)\rho^2/5.29150. \tag{2.4}$$

It is of importance that a numerical investigation reveals the relation

$$T_{PQ}/T_{11}=S_{PQ}^2+\tfrac{3}{4}S_{PQ}(S_{PQ}-1)(S_{PQ}-0.13)$$
$$\times(S_{PQ}-0.64), \tag{2.5}$$

to be accurate to one part in one thousand; in fact the first term, viz., S_{PQ}^2, has already an accuracy of 1%. These statements are illustrated by Fig. 1. This result was used in Sec. 2 of paper I, in order to justify the assumptions of the tight-binding approximation for the kinetic-energy integrals.

3. CARBON PENETRATION INTEGRAL $(\chi_1 \mid U_2^C \mid \chi_1)$

The integral to be considered is [See paper I, Eqs. (2.5, 5′, 5″)]

$$(\chi_1 \mid U_2^C \mid \chi_1)=\int dV\chi^2(\mathbf{r}-\mathbf{r}_1)U^C(\mathbf{r}-\mathbf{r}_2), \tag{3.1}$$

where, according to Eq. (1.7) of paper I,

$$U^C(\mathbf{r})=-4e^2/r+e^2[(2s)^2+(2px)^2+(2py)^2+(2pz)^2]. \tag{3.2}$$

TABLE I. Coefficients for the integral $(\chi_1 \mid U_2^C \mid \chi_1)$.

		$k\rightarrow$					
	a_{jk}	0	1	2			
$j\downarrow$	0	330	0	−240			
	1	−126	0	360			
	2	42	0	−168			
	3	−6	0	56			
	4	0	0	−8			

		$k\rightarrow$					
	b_{jk}	0	1	2	3		
$j\downarrow$	0	0	0	0	28		
	1	0	660	0	−76		
	2	0	−252	0	78		
	3	0	84	0	−42		
	4	0	−12	0	14		
	5	0	0	0	−2		

		$k\rightarrow$					
	c_{jk}	0	1	2	3	4	5
$j\downarrow$	0	330	660	420	128	20	4/3
	1	−126	−252	−552	−294	−64	−16/3
	2	42	84	168	210	72	8
	3	−6	−12	−40	−50	−32	−16/3
	4	0	0	4	6	4	4/3

The orbitals in (3.2) have all the same orbital exponent ζ_C (shielding orbital exponent), which may, however, be different from the orbital exponent ζ in the AO (1.2). Upon assuming (2s) to be the nodeless, "Slater type" AO one finds from RRJ, Table I,

$$(2s)^2+(2px)^2+(2py)^2+(2pz)^2=4[3S], \tag{3.3}$$

the symbol on the right-hand side being defined by Eq. (1.3) of RRJ. The orbital exponent of $[3S]$ is again ζ_C. According to Table V and Eqs. (1.5, 18, 19) of RRJ, one finds

$$U^C(\mathbf{r})=-(e^2/a)r^{-1}e^{-s}(4+3s+s^2+\tfrac{1}{6}s^3), \tag{3.4}$$

$$s=2\zeta_C r. \tag{3.4'}$$

Introducing elliptic coordinates according to Eq. (1.5) of RRJ (put atom $1=a$, atom $2=b$), one obtains

$$s=\rho_C(\xi+\eta),$$

where ρ_C is defined by

$$\rho_C=\zeta_C(D/a). \tag{3.5}$$

Furthermore,

$$\chi^2(\mathbf{r}-\mathbf{r}_1)=(\zeta^3/a^3 2\pi)(\rho/2)^2(\xi^2-1)(1-\eta^2)$$
$$\times\exp[-\rho(\xi-\eta)]+\Delta\text{-type distribution.} \tag{3.6}$$

Inserting the expressions (3.4, 6) in the definition (3.1), one obtains the penetration integral in terms of the C functions, defined in Eq. (1.31) of RRJ,

$$(\chi_1 \mid U_2^C \mid \chi_1)=-(e^2/a)(\zeta/16)[4C_{01}^{001}$$
$$+3(\rho_C/\rho)C_{11}^{001}+(\rho_C/\rho)^2C_{21}^{001}+(\tfrac{1}{6})(\rho_C/\rho)^3C_{31}^{001}], \tag{3.7}$$

with the meaning

$$C_{\alpha\beta}^{\gamma\delta\epsilon}=C_{\alpha\beta}^{\gamma\delta\epsilon}(2\rho_C, 2\rho), \tag{3.7'}$$

if $C_{\alpha\beta}^{\gamma\delta\epsilon}(x, y)$ is defined by Eq. (1.31) of RRJ. For the C functions occuring here, explicit expressions are given on page 221 of RRJu. Substitution of those formulas in Eq. (3.7) yields, after some algebraic transformations,

$$(\chi_1 \mid U_2^C \mid \chi_1)=-(e^2/D)[tu^2/(1-u)^7]$$
$$\times\left[(t\sum_{j=0}^{4}a_ju^j+\sum_{j=0}^{5}b_ju^j)\exp(-2\rho_Ct)-t\sum_{j=0}^{4}c_ju^j\right], \tag{3.8}$$

where ρ, ρ_C are defined in Eqs. (1.9), (3.5), and

$$t=\zeta/\zeta_C=\rho/\rho_C, \qquad u=t^2. \tag{3.9}$$

The coefficients in Eq. (3.8) are functions of ρ_C, given by

$$a_j=\rho_C{}^{-2}\sum_{k=0}^{2}a_{jk}\rho_C{}^k,$$

$$b_j=\rho_C{}^{-2}\sum_{k=0}^{3}b_{jk}\rho_C{}^k,$$

$$c_j=\rho_C{}^{-2}\exp(-2\rho_C)\sum_{k=0}^{5}c_{jk}\rho_C{}^k, \tag{3.10}$$

where the constants a_{jk}, b_{jk}, c_{jk}, are given in Table I.

In the case $\zeta=\zeta_C$, i.e., $t=u=1$, one has to use the formulas on p. 246 of RRJu, whence:

$$(\chi_1 \mid U_2^C \mid \chi_1)=-(e^2/D)\exp(-2\rho_C)\rho_C[(35/64)$$
$$+(35/32)\rho_C+(71/80)\rho_C{}^2+(19/60)\rho_C{}^3$$
$$+(9/140)\rho_C{}^4+(2/315)\rho_C{}^5], \tag{3.11}$$

in this case.

TABLE II. Coefficients for the integral $(\chi_1 \mid U_2^C \mid \chi_2)$.

		$k\rightarrow$					
	b_{jk}	0	1	2	3		
$j\downarrow$	0	0	0	0	28		
	1	165	0	−120	112		
	2	297	165	−345	180		
	3	189	297	−375	146		
	4	42	189	−185	60		
	5	0	42	−35	10		

		$k\rightarrow$					
	c_{jk}	0	1	2	3	4	5
$j\downarrow$	0	0	0	0	0	0	0
	1	165	330	210	64	10	2/3
	2	297	759	579	204	36	8/3
	3	189	675	597	240	48	4
	4	42	273	277	124	28	8/3
	5	0	42	49	24	6	2/3

4. CARBON PENETRATION INTEGRAL $(\chi_1 \mid U_2^C \mid \chi_2)$

This integral is defined by

$$(\chi_1 \mid U_2^C \mid \chi_2) = \int dV \chi(\mathbf{r}-\mathbf{r}_1)\chi(\mathbf{r}-\mathbf{r}_2)U^C(\mathbf{r}-\mathbf{r}_1), \tag{4.1}$$

where the potential U_C is again given by Eqs. (3.2, 4). In elliptic coordinates one finds for the orbital product

$$\chi(\mathbf{r}-\mathbf{r}_1)\chi(\mathbf{r}-\mathbf{r}_2) = (\xi^3/a^3 2\pi)(\rho/2)^2(\xi^2-1) \times(1-\eta^2)\exp(-\rho\xi)+\Delta \text{ type distribution.} \tag{4.2}$$

Insertion of Eqs. (3.4) and (4.2) in Eq. (4.1) yields, by methods analogous to those used in the preceding section,

$$(\chi_1 \mid U_2^C \mid \chi_2) = -(e^2/a)\zeta[4C_{01}^{001}+3(2\rho_C/\rho)C_{11}^{001} +(2\rho_C/\rho)^2 C_{21}^{001}+(\tfrac{1}{6})(2\rho_C/\rho)^3 C_{31}^{001}], \tag{4.3}$$

where *now* $C_{\alpha\beta}^{\gamma\delta\epsilon}$ means

$$C_{\alpha\beta}^{\gamma\delta\epsilon} = C_{\alpha\beta}^{\gamma\delta\epsilon}(\rho+2\rho_C, \rho), \tag{4.3'}$$

if $C_{\alpha\beta}^{\gamma\delta\epsilon}(x, y)$ is defined by Eq. (1.31) of RRJ. Substitution of the C functions formulas from p. 221 of RRJu yields, after some transformations,

$$(\chi_1 \mid U_2^C \mid \chi_2) = -(e^2/D)\exp(-\rho_C t)[t^5/(1+t)^7]\sum_{j=0}^{5} a_j t^j, \tag{4.4}$$

where t is again defined by Eq. (3.9). The coefficients are the following functions of ρ_C,

$$a_j = \rho_C^{-2}\left(\sum_{k=0}^{3} b_{jk}\rho_C^k - \exp(-2\rho_C)\sum_{k=0}^{5} c_{jk}\rho_C^k\right), \tag{4.5}$$

where the constants b_{jk} and c_{jk} are given in Table II. The formula applies also in the case $\zeta_C=\zeta$.

5. CARBON PENETRATION INTEGRAL $(\chi_1 \mid U_1^C \mid \chi_1)$

The present integral,

$$(\chi_1 \mid U_1^C \mid \chi_1) = \int dV \chi^2(\mathbf{r}-\mathbf{r}_1)U^C(\mathbf{r}-\mathbf{r}_1), \tag{5.1}$$

is obtained from the two preceding ones by letting atom 2 go into atom 1. This can be done in three different ways.

First, one can start with the expression (3.7) and insert the C functions formulas, given on p. 254 of RRJu for the case $\rho=0$.

Second, one can start with the expression (4.3) and insert the C functions formulas, given on p. 254 of RRJu for the case $\rho=0$.

Third, one can substitute the expressions (3.4) for U^C and (1.2) for $\chi(\mathbf{r})$ directly into Eq. (5.1) and integrate in spherical coordinates.

The result is

$$(\chi_1 \mid U_1^C \mid \chi_1) = -(e^2/D)\rho_C[2t^5/(1+t)^7] \times[14+14t+6t^2+t^3], \tag{5.2}$$

TABLE III. Coefficients for the integral $(\chi_1 \mid U_{1h}^H \mid \chi_1)$.

	$k\rightarrow$				
	a_{jk}	0	1	2	
$j\downarrow$	0	0	0	3/2	
	1	15	0	−7/2	
	2	−3	0	+5/2	
	3	0	0	−1/2	
	$k\rightarrow$				
	b_{jk}	0	1	2	
$j\downarrow$	0	0	0	0	
	1	15/2	0	−8	
	2	−3/2	0	10	
	3	0	0	−2	
	$k\rightarrow$				
	c_{jk}	0	1	2	3
$j\downarrow$	0	0	0	0	0
	1	−15/2	−15	−7	−1
	2	3/2	3	8	2
	3	0	0	−1	−1

where t is again defined by Eq. (3.9). The agreement of the different methods checks Eqs. (3.7) and (4.3).

6. HYDROGEN PENETRATION INTEGRAL $(\chi_1 \mid U_{1h}^H \mid \chi_1)$

In the hydrogen penetration integral,

$$(\chi_1 \mid U_{1h}^H \mid \chi_1) - \int dV \chi^2(\mathbf{r}-\mathbf{r}_1)U^H(\mathbf{r}-\mathbf{r}_{h1}), \tag{6.1}$$

the vector $\mathbf{r}_{h1}$ locates the H nucleus which is neighbor to the carbon nucleus located by $\mathbf{r}_1$. According to Eq. (1.4) of paper I,

$$U^H(\mathbf{r}) = -(e^2/r)+e^2[(1s)^2\,|\,, \tag{6.2}$$

with the shielding orbital exponent $\zeta_H=1$ for the $(1s)$ function. From Table I of RRJ one finds $(1s)^2=[1S]$, and hence, from Table V of RRJ one obtains

$$U^H(\mathbf{r}) = -(e^2/a)r^{-1}e^{-s'}[1+(s'/2)], \qquad s'=2\zeta_H r. \tag{6.3}$$

In elliptic coordinates (put hydrogen$=a$, carbon$=b$ in RRJ), one has

$$s' = \rho_H(\xi+\eta),$$

where now

$$\rho_H = \zeta_H D_H/a, \tag{6.4}$$

with D_H given by Eq. (1.8). For $\chi^2(\mathbf{r}-\mathbf{r}_1)$, one can again use the expression (3.6), if one now only replaces ρ by ρ_1 in that equation [ρ and ρ_1 are defined in Eqs. (1.9, 10)]. Substitution in Eq. (6.1) yields

$$(\chi_1 \mid U_{1h}^H \mid \chi_1) = -(e^2/a)(\zeta/16)[C_{01}^{001} +\tfrac{1}{2}(\rho_H/\rho_1)C_{11}^{001}], \tag{6.5}$$

where $C_{\alpha\beta}{}^{\gamma\delta\epsilon}$ *now* means

$$C_{\alpha\beta}{}^{\gamma\delta\epsilon}=C_{\alpha\beta}{}^{\gamma\delta\epsilon}(2\rho_H, 2\rho_1), \tag{6.6}$$

if $C_{\alpha\beta}{}^{\gamma\delta\epsilon}(x, y)$ is defined by Eq. (1.31) of RRJ. Insertion of the C functions formulas from p. 221 of RRJu and some algebraic transformations and rearrangements yield

$$(\chi_1 \mid U_{1h}{}^H \mid \chi_1) = -(e^2/D)\gamma[u^2/(1-u)^5]$$
$$\times[(t\sum_{j=0}^{3} a_j u^j + \sum_{j=1}^{3} b_j u^j)\exp(-2\rho_H t)$$
$$+\sum_{j=1}^{3} c_j u^j], \tag{6.7}$$

where *now*

$$t=\zeta/\zeta_H=\rho_1/\rho_H=\rho/\gamma\rho_H,$$
$$u=t^2, \tag{6.8}$$

and γ is defined in Eq. (1.8′). The coefficients in Eq. (6.7) are functions of ρ_H and given by

$$a_j=\rho_H{}^{-1}\sum_{k=0}^{2} a_{jk}\rho_H{}^k,$$
$$b_j=\rho_H{}^{-2}\sum_{k=0}^{2} b_{jk}\rho_H{}^k,$$
$$c_j=\rho_H{}^{-2}\exp(-2\rho_H)\sum_{k=0}^{3} c_{jk}\rho_H{}^k. \tag{6.9}$$

The constants a_{jk}, b_{jk}, c_{jk} are listed in Table III.

In the case $\zeta=\zeta_H$, the formulas on p. 246 of RRJu must be used, whence,

$$(\chi_1 \mid U_{1h}{}^H \mid \chi_1) = -(e^2/D)\gamma(\rho_1/16)[1+2\rho_1$$
$$+(22/15)\rho_1{}^2+(4/15)\rho_1{}^3]\exp(-2\rho_1) \tag{6.10}$$

in this case.

7. ELECTRON INTERACTION INTEGRAL

We also include here the formula for the two-center Coulomb integral, defined in Eq. (2.14) of paper I, since it will be used in the subsequent paper. When the atomic orbitals are those of Eq. (1.1), the electron-interaction integral has the formula[5]

$$[PP \mid QQ]=[\chi_P\chi_P \mid \chi_Q\chi_Q]=(e^2/a)\zeta F(\zeta R/a)$$
$$=(e^2/D)\rho F[\rho(R/D)], \tag{7.1}$$

where ρ is the parameter of Eq. (1.9) and the function $F(x)$ is given by

$$F(x)=(x^{-1}-3x^{-3}+20.25x^{-5})-e^{-2x}(20.25x^{-5}+40.5x^{-4}$$
$$+37.5x^{-3}+21x^{-2}+8.5x^{-1}+3.00859375$$
$$+1.0171875x+0.289434523x^2+0.0559523809x^3$$
$$+0.0053571429x^4). \tag{7.2}$$

For $R=0$, i.e., $P=Q$, this expression reduces to

$$[11 \mid 11]=(e^2/D)(501/1280)\rho. \tag{7.3}$$

---

[5] See, e.g., C. C. J. Roothaan, J. Chem. Phys. **19**, 1445 (1951).

Quantum Mechanics of Mobile Electrons in Conjugated Bond Systems. V. Empirical Determination of Integrals between Carbon Atomic Orbitals from Experimental Data on Benzene*

KLAUS RUEDENBERG AND E. MILLER LAYTON, JR.

Institute for Atomic Research, Department of Chemistry, Department of Physics, Iowa State University, Ames, Iowa

(Received March 16, 1959)

It is shown that the experimental information given in the ultraviolet spectrum of benzene uniquely determines the two-center Coulomb integrals between the $2p\pi$ atomic orbitals of carbon as a function of the internuclear distance. The calculations are carried out including all terms involving neighbor overlap. For the many-center electron-interaction integrals, the Mulliken approximation and the London approximation are both considered with little difference in the results. Some peculiar properties of the empirically determined distance dependence are compared with the theoretical behavior of two-center Coulomb integrals. The empirical values for the resonance integral and the Coulomb integral are also found. The investigation differs from similar work of Pariser by the inclusion of overlap effects.

INTRODUCTION

THE preceding papers[1] have developed the general theoretical framework for a fairly rigorous treatment of pi-electron systems in the tight-binding approxiation. In this method, all energy expressions are reduced to a small number of framework integrals and electron-interaction integrals between atomic orbitals.

Furthermore, all integrals of the electron interaction type were reduced to the basic integrals

$$G(PQ)=[PP\mid QQ]=[\chi_P\chi_P\mid\chi_Q\chi_Q]$$
$$=\int dV_1\int dV_2[\chi_P(1)]^2[\chi_Q(2)]^2/r_{12},$$

i.e., two-center Coulomb integrals between $2p\pi$ orbitals at the positions P and Q. Since the two orbitals are of the same kind, the integral is a function of the distance R_{PQ} only,

$$G(PQ)=\mathcal{G}(R_{PQ}).$$

This function will simply be called "the electron-interaction function."

The framework integrals occur only in certain linear combinations, *viz.*, the "Coulomb framework integrals" α, $\delta\alpha$, and the "resonance integral" γ.

Parr and Pariser[2] have proposed for the integrals certain semiempirical values which led to satisfactory results for benzene. These values are then considered as gauged with respect to the aromatic unit and therefore appropriate for use in calculations on other aromatic hydrocarbons.

This procedure raises the question whether or not this set of empirical integral values is unique, i.e., whether it is possible to "go back" from the experimental spectrum to the electron interaction function $\mathcal{G}(R)$. The present note therefore investigates which limitations *must* be imposed upon the energy integrals when the requirement is made, that for benzene, the predicted spectra agrees with the observed one. It is shown that the relevant parameters of $\mathcal{G}(R)$ can be expressed as unique functions of the energy separations observed in the spectrum. The experimental spectrum therefore entirely determines the appropriate interaction function $\mathcal{G}(R)$, and it is therefore possible to inspect whether it possesses the typical characteristics of two-center Coulomb integrals.

The present approach furthermore differs from previous ones in that all neighbor overlaps are carried through all the way, in line with the developments in the preceding papers. This necessitates a decision about the method of approximation for the many-center electron-interaction integrals. Three possibilities are investigated: the Mulliken approximation, the London approximation, and an intermediate formula. It is shown that the resulting electron-interaction functions vary very little, i.e., that the spectrum determines rather uniquely one definite empirical electron-interaction function $\mathcal{G}(R)$. This function represents an improved Pariser-Parr function.

It is shown that this function necessarily has the initial value $\mathcal{G}(0)=10.53$ ev, which was postulated by Pariser[3] on *different* grounds, *viz.*, that $\mathcal{G}(0)$ should be the difference between the ionization potential and the electron affinity of the carbon trigonal valence state. However, it is also shown that the empirical electron interaction function must differ in a rather serious way from the theoretical behavior of two-center Coulomb integrals.

Finally, the gauging by means of the benzene spectrum leads to a definite value of the resonance integral and to a rather peculiar value for the Coulomb integral.

The comparison of the present empirical integral values with theoretically computed ones will be considered in the subsequent note.

* Contribution No. 678. Work was performed in the Ames Laboratory of the U. S. Atomic Energy Commission.

[1] K. Ruedenberg, J. Chem. Phys. **34**, 1861, 1878, 1884, 1892 (1961).

[2] R. Pariser and R. G. Parr, J. Chem. Phys. **21**, 466, 767 (1953), R. G. Parr and R. Pariser, *ibid.* **23**, 711 (1955).

[3] R. Pariser, J. Chem. Phys. **21**, 568 (1953).

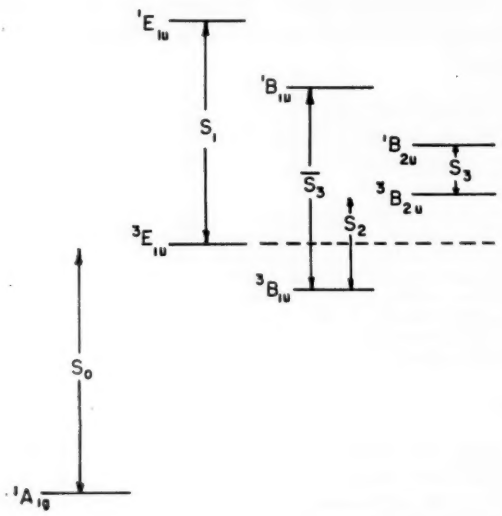

FIG. 1. Schematic diagram of the benzene spectrum. Note: The $^3E_{1u}$ level always lies halfway between the $^3B_{1u}$ and the $^3B_{2u}$ level.

1. THE BENZENE SPECTRUM AS A FUNCTION OF ELECTRON INTERACTION INTEGRALS

Basic Relations

The ground state and lowest excited states of benzene are pictured in Fig. 1.[4] The separations, denoted by s_i, are computed from integrals over molecular orbitals according to the formulas in Table I.[4] Within the tight-binding approximation the molecular orbitals are given as functions of atomic orbitals according to Table II, which also explains our notation.

By virtue of the expansion in Table II the electron-interaction integrals between MO's can be expressed in terms of electron-interaction integrals between AO's. When all integrals involving the overlap of nonneighbors are neglected (tight-binding approximation), the expansions given in Table III result.

TABLE I. Energy separations of the benzene spectrum in terms of MO integrals.

$s_0=\mathcal{E}_c-\mathcal{E}_b+[b_1b_2\,|\,c_1c_2]-[b_1b_1\,|\,c_2c_2]$

$s_1=2[b_1c_1\,|\,b_1c_1]+2[b_1c_1\,|\,b_2c_2]=2[b_1c_2\,|\,b_1c_2]-2[b_1c_2\,|\,b_2c_1]$

$s_2=4[b_1b_2\,|\,c_1c_2]$

$s_3=2[\,[b_1c_1\,|\,b_1c_1]-2[b_1c_1\,|\,b_2c_2]$

$s_3=2[b_1c_2\,|\,b_1c_2]+2[b_1c_2\,|\,b_2c_1]$

$\mathcal{E}_b=\frac{1}{2}\sum_{i=1}^{2}\{(b_i\,|f|\,b_i)+\sum_{n=1}^{3}(2[\phi_n\phi_n\,|\,b_ib_i]-[\phi_nb_i\,|\,\phi_nb_i])\}$

$\mathcal{E}_c=\frac{1}{2}\sum_{i=1}^{2}\{(c_i\,|f|\,c_i)+\sum_{n=1}^{3}(2[\phi_n\phi_n\,|\,c_ic_i]-[\phi_nc_i\,|\,\phi_nc_i])\}$

[4] See N. S. Ham and K. Ruedenberg, J. Chem. Phys. **25**, 13 (1956).

Approximations of AO Electron Interaction Integrals

As discussed in paper I,[1] the approximations given by R. S. Mulliken[5] or A. London[6] shall be used for the evaluation of electron-interaction integrals between AO's which are not of the two-center Coulomb type. It is the purpose of this investigation to find the most suitable approximation of this kind.

Mulliken's approximation is given by

$$[PQ\,|\,RT]^0=S_{PQ}S_{RT}[G(PR)+G(PT)+G(QR)+G(QT)]/4. \quad (1.1)$$

The symbols are explained in paper I, Eqs. (2.1), (2.2), and (2.14)–(2.16).[1]

London's approximation is given by

$$[PQ\,|\,RT]^L=S_{PQ}S_{RT}G(\bar{P}\bar{R}), \quad (1.2)$$

where $\bar{P}$ is the midpoint between P and Q, and $\bar{R}$ is the midpoint between R and T.

TABLE II. Molecular orbitals in the tight-binding approximations.

MO \ AO	χ_1	χ_2	χ_3	χ_4	χ_5	χ_6	Common factor
$a=\phi_1$	1	1	1	1	1	1	$[6(1+2S)]^{-\frac{1}{2}}$
$b_1=\phi_2$	1	0	−1	−1	0	1	$[4(1+S)]^{-\frac{1}{2}}$
$b_2=\phi_3$	1	2	1	−1	−2	−1	$[12(1+S)]^{-\frac{1}{2}}$
$c_1=\phi_4$	1	−2	1	1	−2	1	$[12(1-S)]^{-\frac{1}{2}}$
$c_2=\phi_5$	1	0	−1	1	0	−1	$[4(1-S)]^{-\frac{1}{2}}$
$d=\phi_6$	1	−1	1	−1	1	−1	$[6(1-2S)]^{-\frac{1}{2}}$

In case the points $\bar{P}$ and $\bar{R}$ do not coincide, the Mulliken approximation is obtained from the London approximation by the further "mean-value approximation"

$$G(\bar{P}X)\approx\tfrac{1}{2}[G(PX)+G(QX)], \quad (1.2')$$

which is obviously valid for large distances $\bar{P}X$. We shall find it also perfectly adequate for the short distances, i.e., within a single benzene ring. The only case where the London and Mulliken approximations differ appreciably is that of the two-center exchange integral, where

$$[12\,|\,12]^0=S^2\tfrac{1}{2}[G(1,1)+G(1,2)], \quad (1.3)$$

but

$$[12\,|\,12]^L=S^2G(1,1). \quad (1.3')$$

The Mulliken approximation has the advantage of using only AO's at atomic positions whereas the London approximation introduces AO's at new locations.

[5] R. S. Mulliken, J. Chem. Phys. **46**, 521 (1949).

[6] J. Sklar, J. Chem. Phys. **7**, 990 (1939), A. London, *ibid.* **13**, 417 (1945).

TABLE III. MO electron-interaction integrals in terms of AO electron interaction integrals. Tight-binding approximation.

	[11|11]	[11|22]	[11|33]	[11|44]	[11|12]	[11|23]	[11|34]	[12|12]	[12|23]	[12|34]	[12|45]	C. F.
$[b_1b_2 \mid c_1c_2]$	4	−4	−4	4	0	0	0	−16	16	16	−16	$1/48(1-S^2)$
$[b_1b_1 \mid c_2c_2]$	4	4	4	4	0	0	0	−8	0	0	−8	$1/16(1-S^2)$
$[b_1c_1 \mid b_1c_1]$	4	4	−4	−4	0	0	0	24	−48	48	−24	$1/48(1-S^2)$
$[b_1c_1 \mid b_2c_2]$	4	4	−4	−4	0	0	0	−24	48	−48	24	$1/48(1-S^2)$
$[b_1c_2 \mid b_1c_2]$	4	−4	4	−4	0	0	0	0	0	0	0	$1/16(1-S^2)$
$[b_1c_2 \mid b_2c_1]$	4	−20	20	−4	0	0	0	0	0	0	0	$1/48(1-S^2)$
$[a\,b_1 \mid a\,b_1]$	4	4	−4	−4	24	0	−24	12	12	−12	−12	$1/24(1+2S)(1+S)$
$[a\,c_1 \mid a\,c_1]$	12	−12	−12	12	24	−48	24	12	−12	−12	12	$1/72(1+2S)(1-S)$
$[b_1b_2 \mid b_1b_2]$	4	−4	−4	4	16	−32	16	16	−16	−16	16	$1/48(1+S)^2$
$[b_1b_1 \mid b_1b_1]$	4	4	4	4	16	0	16	8	0	0	8	$1/16(1+S)^2$
$[a\,a \mid b_1b_1]$	4	8	8	4	24	24	24	8	16	16	8	$1/24(1+2S)(1+S)$
$[a\,a \mid c_1c_1]$	12	24	24	12	24	24	24	−24	−48	−48	−24	$1/72(1+2S)(1-S)$
$[b_1b_1 \mid b_2b_2]$	4	20	20	4	16	64	16	−8	32	32	−8	$1/48(1+S)^2$
$[b_1b_1 \mid c_1c_1]$	4	20	20	4	0	0	0	8	−32	−32	8	$1/48(1-S^2)$

In view of the foregoing, we found it practical to define the following "modified London approximation"

$$[PQ \mid RT]^{ML}=[PQ \mid RT]^{0}+[PQ \mid RT]', \quad (1.4)$$

where the first term is identical with the Mulliken approximation (1.1) and the second term is zero except for the two-center exchange integrals where

$$[12 \mid 12]'=\tfrac{1}{2}S^2[G(1,1)-G(1,2)]. \quad (1.5)$$

The approximation (1.4) will turn out to be numerically very close to the London approximation; but it has the advantage of containing only AO's at atomic positions.

TABLE IV. Coefficients for Eq. (1.6).

	a_1	a_2	b_2°	b_2'	a_3	b_3	a_4	b_4	C. F
$[b_1b_2 \mid c_1c_2]$	0	1	0	$-2\sigma_1$	1	0	−1	0	1/12
$[b_1b_1 \mid c_2c_2]$	4	−1	0	$-\sigma_1$	−1	0	−1	0	1/4
$[b_1c_1 \mid b_1c_1]$	0	−1	0	3	1	0	1	0	$\sigma_1/12$
$[b_1c_1 \mid b_2c_2]$	0	−1	0	−3	1	0	1	0	$\sigma_1/12$
$[b_1c_2 \mid b_1c_2]$	0	1	0	0	−1	0	1	0	$\sigma_1/4$
$[b_1c_2 \mid b_2c_1]$	0	5	0	0	−5	0	1	0	$\sigma_1/12$
$[a\,b_1 \mid a\,b_1]$	0	−4	$-\sigma_4$	$6\sigma_4$	4	σ_4	4	σ_4	1/24
$[a\,c_1 \mid a\,c_1]$	0	4	$9\sigma_3$	$2\sigma_3$	4	$9\sigma_3$	−4	$-9\sigma_3$	1/24
$[b_1b_2 \mid b_1b_2]$	0	1	0	$2\sigma_2$	1	0	−1	0	1/12
$[b_1b_1 \mid b_1b_1]$	4	−1	0	σ_2	−1	0	−1	0	1/4
$[a\,a \mid b_1b_1]$	6	−2	0	σ_4	−2	0	−1	0	1/6
$[a\,a \mid c_1c_1]$	6	−2	0	$-\sigma_3$	−2	0	−1	0	1/6
$[b_1b_1 \mid b_2b_2]$	12	−5	0	$-\sigma_2$	−5	0	−1	0	1/12
$[b_1b_1 \mid c_1c_1]$	12	−5	0	σ_1	−5	0	−1	0	1/12

$\sigma_1=1/(1-S^2)$

$\sigma_2=1/(1+S)^2$

$\sigma_3=1/[(1+2S)(1-S)]$

$\sigma_4=1/[(1+2S)(1+S)]$

TABLE V. Energy separations between the excited states in terms of basic integrals.

	M	ML	L
s_1	$(-g_2+g_3+g_4)/3(1-S^2)$	0	0
s_2	$(g_2+g_3-g_4)/3$	$-2g_2S^2/3(1-S^2)$	$(g_2+5g_3-g_4-4g_5-4g_6)S^2/3(1-S^2)$
s_3	0	$g_2S^2/(1-S^2)$	$(g_2-2g_5+2g_6)2S^2/(1-S^2)$
$\bar{s}_3$	$(4g_2-4g_3+2g_4)/3(1-S^2)$	0	0

When Eq. (1.4) is used to simplify the AO integrals, one obtains for the MO integrals expressions of the type

$$a_1G_1+\sum_{i=2}^{4}(a_i+b_iS^2)g_i, \tag{1.6}$$

where

$$G_1=G(1,1), \tag{1.7}$$

$$g_i=G(1,1)-G(1,i). \tag{1.7'}$$

The "correction" (1.5) contributes only to b_2, hence we write

$$b_2=b_2^0+b_2', \tag{1.8}$$

corresponding to the two terms in (1.4). The coefficients a_i, b_i for the various integrals are given in Table IV. It is clear that inclusion of the column b_2' yields the modified London approximation, whereas omission of this column yields the Mulliken approximation.

2. DETERMINATION OF THE ELECTRON INTERACTION FUNCTION FROM THE RELATIVE POSITIONS OF THE EXCITED STATES

Basic Relations

By making the proper substitutions, the separations between the excited states are obtained in terms of the AO Coulomb integrals $G(PQ)$. The expressions resulting from each of the three approximations discussed above are given in Table V. Specifically,

Mulliken approximation = column M;

London approximation = column M + column L;

modified London approximation

$$= \text{column } M + \text{column } ML. \tag{2.1}$$

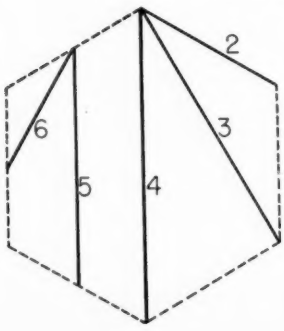

FIG. 2. Labeling of distances in benzene.

The symbols g_i are those of Eq. (1.7'). The London approximation also contains $G(1, 5)$ and $G(1, 6)$; in this case the two AO's are separated by the distances designated correspondingly in Fig. 2.

For $S=0$ the results of Table V reduce to those of Pariser and Parr[2] (neglect of differential overlap). With S different from zero the Mulliken approximation modifies only s_1 and $\bar{s}_3$. The London and modified London approximations contribute additional corrections to s_2 and s_3. All modifications are of the order of S^2.

Table V exhibits the following property: For each approximation the formulas are such that the three separations s_i determine uniquely the distance function $g(R)$ which satisfies

$$g(R_{PQ})=G(1,1)-G(PQ), \tag{2.2}$$

for those distances R_{PQ} occurring in Fig. 2. Thus, from the well-known experimental values[4,7]

$$\begin{aligned} s_1&=1.36000\\ s_2+s_3&=0.57000\\ \bar{s}_3&=1.23000, \end{aligned} \tag{2.3}$$

there is obtained a definite function $g(R)$ for each approximation.

It may be noted that both the London and the modified London approximations predict a small but finite separation s_3 (about 2–3 kK) between the $^1B_{2u}$ and $^3B_{2u}$ levels, the triplet being the lower one.

Approximations with Orbitals at Atomic Positions

Let us consider the approximations PP (Pariser and Parr, $S=0$), M (Mulliken), and ML (modified London). In these cases only three quantities, g_2, g_3, and g_4 occur and one can solve for them if a value for S has been assumed. In a subsequent note we shall justify the value[8]

$$S=0.246800. \tag{2.4}$$

In fact, the calculations are quite insensitive to a variation in S between, say, 0.24 and 0.28. The values of g_2, g_3, g_4 obtained by inverting the equations for s_1, s_2, $\bar{s}_3$, taking into account the figures in Eqs. (2.3) and (2.4),

[7] The unit of length in the present paper is $D=1.4$ A = the average distance of neighbors. The unit of energy is $(\hbar^2/2mD^2)=E_H(a_H/D)^2=1.9432$ ev $=15677$ cm^{-1}. See Eqs. (1.4) to (1.7) of the preceding paper.

[8] K. Ruedenberg, J. Chem. Phys. **34**, 1907 (1961).

are listed in Table VI(b). Furthermore, in Table VI(a) are given the values used by Pariser[9] in his spectral calculations, since they differ from those in the column PP of Table VI(b).

In Figs. 3(a) and (b) are plotted the values $G(1, i)$, obtained from the values g_i of Tables VI(a) and (b) by means of Eq. (1.7′), where for G_1 the value 5.418 is used, which will be justified below. The points $G(1, i)$ must be considered as points on the electron-interaction function

$$\mathcal{G}(R)=G_1-g(R),$$

discussed in the introduction.

The values of $G(1, i)$ follow a pattern of decreasing magnitude as they should. In all cases however, the function $\mathcal{G}(R)$ exhibits an unphysical "buckle" which is alien to the nature of the two-center Coulomb integral. This deficiency is not serious, however, since it can be removed by assuming the value

$$s_2+s_3=0.67, \tag{2.5}$$

instead of the one given in Eq. (2.3). This means that the $^1B_{2u}$ band is placed at 41 kK instead of at 39.5 kK. Actually, the deduction of the exact location of electronic transitions in these systems is usually associated with an uncertainty of 1–2 kK, so that the values in Eq. (2.3) are not absolute, although they were chosen by an unbiased and careful weighing of the various experimental corrections which have to be taken into account.[4] Neither can it be expected that the present theoretical approach yields an over-all agreement with experiment better than 1–2 kK. Therefore, we assume our electron-interaction function to be such that it yields the value 0.67 rather than 0.57 for s_2+s_3 in benzene, without committing ourselves as to the best experimental assignment.

With this assumption the values of the g_i and the $G(1, i)$ become those given in Table VI(c) and plotted in Fig. 3(c). Only the values for the Mulliken approximation are given, those for the PP and the ML approximation being quite similar.

The Value of G_1 in the Mulliken Approximation

From the spectrum, only the *differences* g_i are determined. However, the values of the g_i's are such that, as we shall now see, the absolute value of G_1 is restricted within very narrow limits if the necessary further requirement is taken into account that, at large distances, $\mathcal{G}(R)$ must go into the Coulombic dependence[10]

$$5.29150/R. \tag{2.6}$$

To this end it is convenient to rewrite the results for the Mulliken approximation, given in Table VI(c), in the following form,

$$G_1/5.29150=A+1-0.07902, \tag{2.7}$$

$$G(1, i)/5.29150=A+1/(R_i+1) \quad (i=2, 3, 4), \tag{2.7′}$$

where A is as yet an unknown constant corresponding to the fact that only the differences given by Eq. (1.7′) are known. The fact that the points $G(1, 2)$, $G(1, 3)$, $G(1, 4)$ do fall on the curve (2.7′) seems to be accidental, but it enables us to formulate the condition of transition of $\mathcal{G}(R)$ into (2.6) as follows: It must be possible to form a "splice" function which smoothly joins the curve (2.7′) at the point $R=2$ and joins smoothly with $(1/R)$ at a distance $R\leq 4$. Here, "joining smoothly" signifies a matching of the values of the functions and their derivatives. This process then leads to a value for the constant A and thus for G_1.

Since

$$\left|\frac{d}{dR}\left(A+\frac{1}{R+1}\right)\right|_{R=2}<\left|\frac{d}{dR}\left(\frac{1}{R}\right)\right|_{R<3},$$

the junction with $(1/R)$ cannot be made for R less than 3, since $\mathcal{G}(R)$ may not have a buckle. For the same reason, if it is made at $R=3$, then the splice function must be a straight line and one finds immediately

$$G_1=5.48920. \tag{2.8}$$

This, obviously, is the maximum value possible for G_1. If the junction with $(1/R)$ is made at $R=4$, one can choose a quadratic splice and determine its three constants by matching functions and derivatives at $R=4$ and matching derivatives only at $R=2$. The matching of functions at $R=2$ then yields the constant A, whence

$$G_1=5.37897. \tag{2.9}$$

If a quadratic splice is chosen and determined by also matching second derivatives, the results are hardly different, viz.,

$$G_1=5.38070. \tag{2.10}$$

Equations (2.8)–(2.10) enclose G_1 within 0.2 ev, and it is remarkable that this range includes

5.418 = ionization potential minus electron affinity of carbon in its appropriate valence state.

TABLE VI. Empirical values obtained for the quantities g_i by various approximations.

	(a)	(b)			(c)
	P	PP	M	ML	M
g_2	2.091	2.150	2.071	2.006	2.22112
g_3	2.716	2.895	2.771	2.706	2.92074
g_4	3.078	3.335	3.132	3.132	3.13187

[9] R. Pariser, J. Chem. Phys. **24**, 250 (1956).

[10] In terms of the units defined in footnote 7, one finds

$$e^2/r\rightarrow(2D/a_H)R^{-1}=5.29150/R.$$

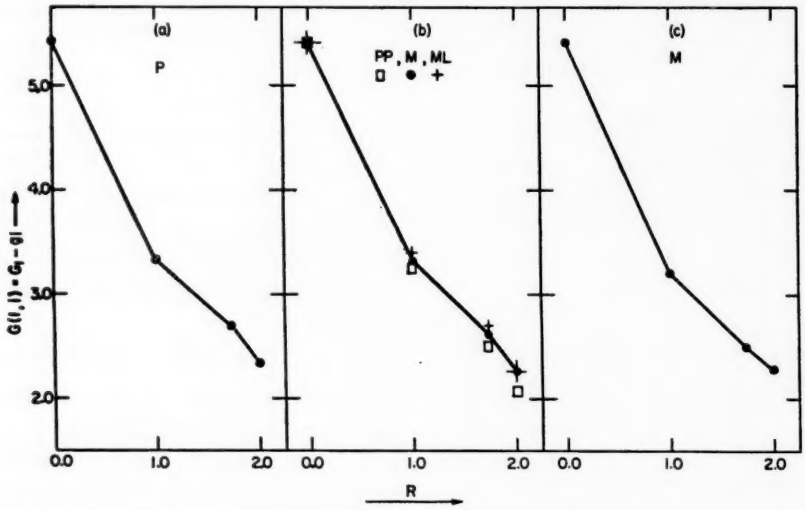

FIG. 3. Values of $G(1, i)$ obtained by various approximations. (a) Values given by Pariser in footnote 9. (b) Values derived from spectral separations of Eq. (2.3): □ Pariser-Parr approximation ($S=0$); ●—Mulliken approximation; + modified London approximation. (c) Values for Mulliken approximation derived assuming the separation (2.5).

That this latter experimental value should agree with G_1 was first postulated by Pariser,[3] and was again discussed in the general theory developed in paper I. *The present derivation, however, does not postulate this agreement but rather demonstrates its existence.* In view of the foregoing results, the choice

$$G_1=5.41800 \tag{2.11}$$

is made.

The Electron-Interaction Function $\mathcal{G}(R)$ for the Mulliken Approximation

It was considered desirable to find, for the electron-interaction function, a form as simple as possible within the general class of appropriate functions. The following form was found practical[10]

$$\mathcal{G}(R)=(5.29150/R)\,(1-e^{-\alpha R}\sum_{k=1}^{5}\gamma_k R^k), \tag{2.12}$$

where $\gamma_0=1$ in order that $\mathcal{G}(0)$ remains finite. The conditions

$$\mathcal{G}(0)=G_1=5.41800, \tag{2.13}$$

$$\mathcal{G}'(0)=0, \tag{2.14}$$

yield

$$\gamma_1=\alpha-G_1=\alpha-5.41800,$$

$$\gamma_2=\tfrac{1}{2}\alpha^2-\alpha G_1=\tfrac{1}{2}\alpha^2-\alpha 5.41800. \tag{2.15}$$

The further requirements

$$\mathcal{G}(1)=G_1-g_2=3.19688,$$

$$\mathcal{G}(\sqrt{3})=G_1-g_3=2.49726,$$

$$\mathcal{G}(2)=G_1-g_4=2.28614, \tag{2.16}$$

provide three linear equations for γ_3, γ_4, γ_5, whose solution yields

$$\gamma_3=1.873161e^{\alpha}-0.358267\exp(\sqrt{3}\alpha)+0.109826e^{2\alpha}$$
$$-0.557940-0.822344\alpha-1.038676\alpha^2,$$

$$\gamma_4=-2.018047e^{\alpha}+0.537400\exp(\sqrt{3}\alpha)-0.173234e^{2\alpha}$$
$$+0.819234+1.150351\alpha+0.683014\alpha^2,$$

$$\gamma_5=0.540733e^{\alpha}-0.179133\exp(\sqrt{3}\alpha)+0.063408e^{2\alpha}$$
$$-0.237388-0.304101\alpha-0.144338\alpha^2. \tag{2.17}$$

The exponent α was then determined by the requirement that $\mathcal{G}(R)$ should go into $5.29150/R$ as fast as possible. Several values of α were chosen and, for each one, $\mathcal{G}(R)$ was calculated and examined in the range $0\leq R\leq 7$. It was found that too high a value of α would generate a buckle whereas, for too low a value, the function $\mathcal{G}(R)$ would approach $5.29150/R$ too slowly. The most satisfactory value was $\alpha=2$. Thus, the parameters in the electron-interaction function (2.12) were found to be

$$\alpha=2,$$
$$\gamma_0=1,$$
$$\gamma_1=0.9760940,$$
$$\gamma_2=-0.0478120,$$
$$\gamma_3=2.0340294,$$
$$\gamma_4=-1.3490009,$$
$$\gamma_5=0.3116263. \tag{2.18}$$

The London Approximation

Since the London approximation contains five g_i's, these cannot be obtained by a direct solution of the three equations expressing s_1, s_2, $\bar{s}_3$. Instead, one must work with a *function* $\mathcal{G}(R)$ (rather than the specific values g_i) from the beginning, and determine its parameters by simultaneously taking into account all required conditions. These are

(1), (2), (3): substitution in the formulas of Table V must give the experimental separations of Eqs. (2.3) and (2.5).

(4) The derivative of $\mathcal{G}(R)$ must vanish at the origin, as for any two-center Coulomb integral.

(5) $\mathcal{G}(R)$ must be buckle-free. In view of (4), this means that $\mathcal{G}(R)$ has only one inflection point, i.e., the equation $d^2\mathcal{G}(R)/dR^2=0$ has only one real root in the R range of interest.

(6) At a reasonable value of R larger than 2, R^* say, the function value $\mathcal{G}(R^*)$ must become equal to $5.29150/R^*$.

(7) For the same value R^*, the derivatives must match, i.e.,

$$d\mathcal{G}(R)/dR=-5.29150/R^2, \qquad \text{for } R=R^*. \quad (2.19)$$

Actually the calculations on the London approximation were carried out with two slight modifications. In the first place, the limiting function

$$(5.29150/R)[1-(3/\rho^2R^2)+(81/4\rho^4R^4)], \quad (2.20)$$

$\rho=\zeta D$, $\zeta=$ orbital exponent of $(2p\pi)$ carbon AO,

$D=$ neighbor distance (1.4 A) in Bohr units, (2.20′)

was used, instead of $(5.29150/R)$. Equation (2.20) represents the long-range part of the exact theoretical expression for the Coulomb integral between $(2p\pi)$ orbitals.[11] The effect of this modification upon the results turns out to be negligible. Second, the value

$$s_2+s_3=0.72 \quad (2.21)$$

was used instead of Eq. (2.5). The effect of this modification is also small.

For the sake of simplicity, we choose $\mathcal{G}(R)$ as a polynomial. However, the following difficulty emerged: Condition (4) requires the absence of the linear term, whereas the other six conditions seem to demand the presence of the linear term, as we shall see. For this reason we consider polynomials of both kinds and later return to a resolution of this difficulty. The following polynomials are considered,

$$\mathcal{G}_c(R)=\sum_{k=0}^{4}c_kR^k \quad (2.22)$$

$$\mathcal{G}_d(R)=d_0+\sum_{k=2}^{5}d_kR^k. \quad (2.23)$$

[11] See Eqs. (7.1), (7.2), and (7.3) of paper IV.

TABLE VII. Coefficients for Eqs. (2.24) and (2.25).

Quartic

c_k \ C_{jk}	C_{1k}	C_{2k}	C_{3k}	C_{4k}
c_1	−3.442823	7.746352	0.732053	−1.647119
c_2	1.427878	−7.817676	−1.520730	3.436811
c_4	−0.135054	1.455109	−0.211324	0.471687

Quintic

d_k \ D_{jk}	D_{1k}	D_{2k}	D_{3k}	D_{4k}
d_2	−5.724066	8.345553	−3.464095	7.879140
d_3	4.702967	−10.581676	7.196133	−16.191299
d_4	−1.128905	3.673434	−4.732043	10.625864

Each contains five coefficients so that, together with R^*, the point of juncture, there are six parameters corresponding to the fact that, besides (4), there are six conditions to be fulfilled.

The process of determination is as follows. From conditions (1), (2), and (3) one finds

$$c_k=(1-2.25S^2)^{-1}[(C_{1k}+C_{2k}S^2)(1-S^2)+(C_{3k}+C_{4k}S^2)c_3] \qquad (k=1,2,4) \quad (2.24)$$

$$d_k=(1-2.25S^2)^{-1}[(D_{1k}+D_{2k}S^2)(1-S^2)+(D_{3k}+D_{4k}S^2)d_5] \qquad (k=2,3,4), \quad (2.25)$$

where C_{jk} and D_{jk} are certain numbers listed in Table VII. That is to say, c_1, c_2, c_4 are expressed as functions of c_3; and d_2, d_3, d_4 as functions of d_5. The conditions (5) and (7) then serve to fix the value of R^* and c_3 or d_5, respectively. The value of c_0 and d_0 is left undetermined by the foregoing procedure and follows then from condition (6).

The only part deserving further comment is the application of conditions (5) and (7). In the case of the quartic, condition (5) signifies that there is no inflection point at all. Since the second derivative is a quadratic, this means that the corresponding discriminant,

$$\Delta_c=3c_3^2-8c_2c_4, \quad (2.26)$$

must be negative. In the case of the quintic the second derivative is a cubic. Since it may have only one real solution, its discriminant,

$$\Delta_d=8d_2d_4^3-3d_3^2d_4^2-30d_2d_3d_4d_5+25d_2^2d_5^2+10d_3^3d_5, \quad (2.27)$$

must be positive. If one inserts the expressions (2.24), (2.25) into (2.26), and (2.27), the discriminants become functions of (S, c_3) or (S, d_5), respectively. Thus the discriminant conditions just mentioned select a

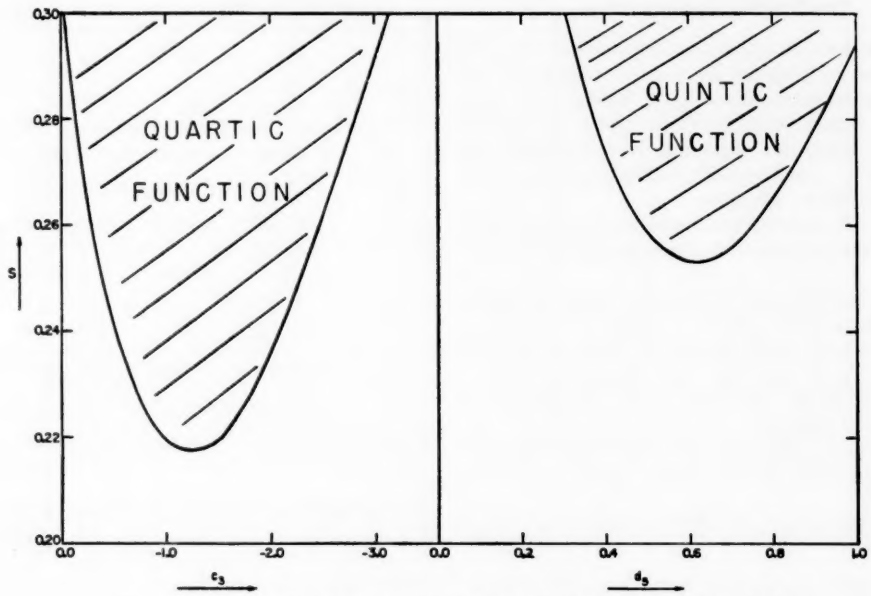

FIG. 4. Admissible regions in the (S, c_3) and in the (S, d_5) plane indicated by shading.

certain admissible region of the (S, c_3) or (S, d_5) plane, respectively. These regions are shown in Fig. 4. It is remarkable that these admissible areas just extend down to where $S=\frac{1}{4}$.

Condition (7), involving derivatives only, does not contain c_0 or d_0 and, in conjunction with Eqs. (2.24) and (2.25), results in an algebraic equation of higher order for the matching point R^*, an equation whose coefficients are functions of (S, c_3) or (S, d_5), respectively. The question arises whether a real solution for R^* exists in the case that the parameters are restricted to the admissible regions of Fig. 4. The answer is positive in the case of the quartic and negative in the case of the quintic. Thus, the quintic cannot fulfill condition (7) whereas the quartic does not fulfill condition (4). Apparently a polynomial is not sufficiently flexible and a function of the kind given in Eq. (2.12) is indispensable to represent $\mathcal{G}(R)$ over the *entire* range.

For the sake of expediency, the difficulty was bypassed by introducing an additional splice function.

TABLE VIII. Comparison between the London approximation and the other approximations.

	PP	M	ML	L_c	L_d
$\bar{g}_2$	2.369	2.290122	2.214774	2.248333	2.254888
$\bar{g}_3$	3.114	2.989744	2.914396	2.947954	2.949540
$\bar{g}_4$	3.335	3.131864	3.131865	3.131866	3.109572
$\bar{g}_5$	...	...	...	2.767332	2.800888
$\bar{g}_6$	...	...	...	2.062820	1.999395

In the case of the quartic, the section between $R=0$ and $R=\frac{1}{2}\sqrt{3}$ was replaced by a cubic, without a linear term, which reproduced the quartic at $R=0$ and at $R=\frac{1}{2}\sqrt{3}$ and the quartic's derivative at the latter point. This splice does not affect the values obtained for the g_i's occurring in Table V since none of them corresponds to a distance less than $R=\frac{1}{2}\sqrt{3}$. The resulting interaction function is as follows:

$$\mathcal{G}_c(R)=\begin{cases}5.470702-6.542174R^2+4.378327R^3, & 0\le R\le\frac{1}{2}\sqrt{3}\\ 5.470702-3.564293R+1.723144R^2 & \\ \quad -0.452386R^3+0.045202R^4, & \frac{1}{2}\sqrt{3}\le R\le 3\\ (5.291500/R)[1-(0.163728/R^2) & \\ \quad +(0.060316/R^4)], & 3\le R.\end{cases}\quad(2.28)$$

This result is based on the use of $S=0.246800$ in Eqs. (2.24, 25) and the corresponding value $\rho=4.280541$ in Eq. (2.20). In the case of the quintic, a quadratic bridge was interposed between the limiting function at $R=3.2$ (match of function values and derivatives) and the quintic itself at $R=2.0$ (match of derivatives). Hence,

$$\mathcal{G}_d(R)=\begin{cases}5.356245-7.402795R^2+7.983113R^3 & \\ \quad -3.335206R^4+0.500000R^5, & 0\le R\le 2.0\\ 3.407436-0.620351R+0.0199863R^2, & \\ \qquad 2.0\le R\le 3.2 & \\ (5.291500/R)[1-(0.171289/R^2) & \\ \quad +(0.066015/R^4)], & 3.2\le R\end{cases}\quad(2.29)$$

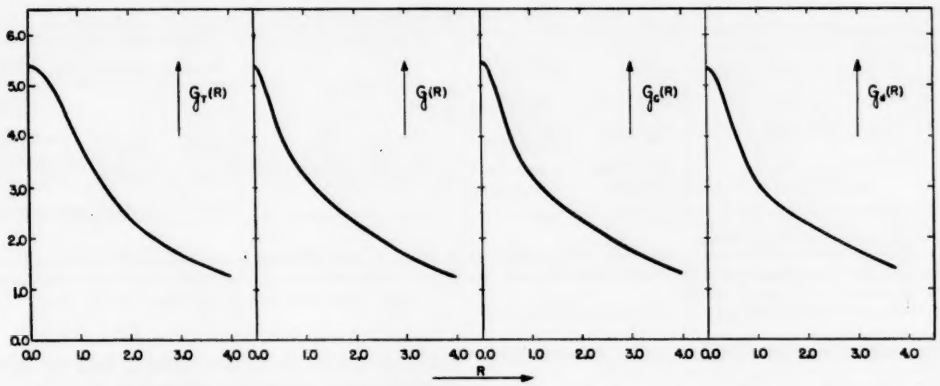

FIG. 5. Electron-interaction functions. $\mathcal{G}_T(R)$: theoretical function of Eq. (7.1) of the preceding paper. $\mathcal{G}(R)$: interaction function in conjunction with Mulliken approximation and neighbor overlap, see Eqs. (2.12) and (2.18). $\mathcal{G}_c(R)$, $\mathcal{G}_d(R)$: interaction functions for London approximation and neighbor overlap, see Eqs. (2.28) and (2.29).

In this case, the values $S=0.260000$ and correspondingly $\rho=4.185000$ were used, since $S=0.246800$ happens to lie just outside the admissible region in Fig. 4. The effect of this change upon the results is, however, very small.

Discussion

The constant terms in the quintic of Eq. (2.29) and the quartic of Eq. (2.28) represent the values of G_1 obtained by carrying through the London approximation in these two ways. Hence,

$$G_{1c}=5.470702 \quad \text{and} \quad G_{1d}=5.356245. \tag{2.30}$$

The agreement of these values with the bracketing values of the Mulliken approximation, discussed in Eqs. (2.8)–(2.10), ff., is perfect.

Furthermore, Table VIII lists the g_i values from the two London approximation functions together with the g_i values which are obtained for the other approximations when the value (2.21) is used instead of the value (2.5). The agreement between the different methods is very close. The similarity is furthermore shown in Fig. 5 which shows the curves for the electron-interaction function obtained in the London approximation as well as the one obtained for the electron-interaction function (2.12) and (2.18) obtained for the Mulliken approximation.

It becomes apparent that the various approximations furnish substantially the same results and that the spectral evidence used quantitatively determines the same form for the interaction function regardless of the analytical approach. It is, however, also seen that a function, such as $\mathcal{G}(R)$, whose derivative vanishes at the origin *and* which has a long nearly linear part, is best represented by a formula of the type of Eq. (2.12). It might be mentioned that the long straight part is the reason that the approximation (1.2′) is quite good, even for the smaller distances.

In conclusion, we infer that the Mulliken approximation with the electron-interaction function (2.12) and (2.18) represents the best way, among those considered, to incorporate the overlap effects. For one thing, it achieves with the simplest means the same semiempirical effect as the other approximations; for another, it is also known to hold more accurately between the theoretical values obtained for the two-center Coulomb integrals and the two-center exchange integrals involving $(2p\pi)$ AO's.

This leads to the final question, viz., whether the electron-interaction function (2.12) and (2.18) which follows so cogently from the spectral identification really bears a close resemblance to the theoretical Coulomb integral G_T between $2p\pi$ orbitals. The formula for the latter is given in Eqs. (7.1), (7.2), and (7.3) of the preceding paper. The most suitable value for the parameter ρ occurring in these formulas is obtained by having the theoretical electron-interaction function $\mathcal{G}_T(R)$ start, for $R=0$, with the initial value of Eq. (2.11), i.e.,

$$\mathcal{G}_T0=G_1=5.418(\hbar^2/2mD^2), \tag{2.31}$$

whence, in the unit (e^2/D),

$$0.391406\rho=1.023906,$$

$$\rho=2.615969. \tag{2.32}$$

This implies a value of ζ which will be discussed in the subsequent paper. For the sake of comparison, the function $\mathcal{G}_T$ corresponding to the ρ value (2.32) is also plotted in Fig. 5. It emerges that there exists a significant difference in the distance dependence of the two curves, amounting to 1.8 ev for the nearest neighbor distance. This discrepancy should be a serious warning against undue optimism.

TABLE IX. Coefficients for Eq. (3.4).[a]

	u_2	v_2	$[v_2']$	$[v_2'']$[b]	u_3	v_3	u_4	v_4	Value[c]
g_b	8	$-\sigma_4$	$[-10\sigma_2-4\sigma_4$	$8(\sigma_2+\sigma_4)]$	0	$-\sigma_4$	4	$-\sigma_4$	1.251076
g_c	$-4\sigma_1-4$	$-9\sigma_3$	$[-6\sigma_1-2\sigma_3$	$-8(\sigma_1+\sigma_3)]$	$4\sigma_1-4$	$-9\sigma_3$	$-8\sigma_1+4$	$9\sigma_3$	-1.363311
g_0	$-4\sigma_1-4$	$-9\sigma_3+\sigma_4$	$\begin{bmatrix}-4\sigma_1+10\sigma_2 \\ -2\sigma_3+4\sigma_4\end{bmatrix}$	$\begin{matrix}-8\sigma_1-8\sigma_2 \\ -8\sigma_3-8\sigma_4\end{matrix}\Big]$	$4\sigma_1+4$	$-9\sigma_3+\sigma_4$	$-8\sigma_1+4$	$9\sigma_3+\sigma_4$	-0.378455

[a] The quantities σ_i are defined in Table IV.

[b] When the Mulliken approximation is used, the bracketed terms are simply ignored. When the modified London approximation is used the bracketed terms must be included, i.e., in Eq. (3.4) one must insert $(v_2+v_2'+v_2'')$ instead of v_2 alone. The additions are due to Eq. (1.5); in particular, v_2' arises from the Coulomb integrals and v_2'' arises from the exchange integrals.

[c] Computed using the Mulliken approximation (see column c of Table VI).

3. DETERMINATION OF FRAMEWORK INTEGRALS

General Formulas

Our attention shifts now to the quantities $\mathcal{E}_b$, $\mathcal{E}_c$, s_0, given in Table I, which involve integrals over the framework potential. According to what has been said in the section starting with Eq. (4.52) in paper I, it is to be expected that $(-\mathcal{E}_b)$ is an approximation to the ionization potential, I, of benzene and $(-\mathcal{E}_c)$ is an approximation to the electron affinity, A, of benzene. According to Fig. 1 of the present paper, s_0 determines the separation between the excited states and the ground state in benzene.

Carrying out the calculations indicated generally in Eqs. (4.54) and (4.56) of paper I, and in Table I of the present paper, one obtains

$$-I=\mathcal{E}_b=-I_C+\bar{\alpha}+\bar{\epsilon}_b+g_b, \tag{3.1}$$

$$-A=\mathcal{E}_c=-A_C+\bar{\alpha}+\bar{\epsilon}_c+g_c, \tag{3.2}$$

$$s_0=\bar{\epsilon}_c-\bar{\epsilon}_b+g_0. \tag{3.3}$$

In these formulas I_C, $\bar{\epsilon}_b$, $\bar{\epsilon}_c$, are defined as

$$I_C=A_C+G_1, \tag{3.4}$$

$$\bar{\epsilon}_b=\gamma/(1+S), \tag{3.5}$$

$$\bar{\epsilon}_c=-\gamma/(1-S), \tag{3.6}$$

and the quantities A_C, $\bar{\alpha}$, γ, are certain linear combinations of one-electron integrals involving the framework potential; γ is called the resonance integral, $\bar{\alpha}$ is called the Coulomb integral. The quantity A_C is the electron affinity of carbon in its valence state.

The quantities g_b, g_c, g_0 depend only upon the g_i defined in Eq. (1.7'), viz.,

$$g_\lambda=\sum_{i=2}^{4} g_i(u_{\lambda i}+v_{\lambda i}S^2)/24, \tag{3.7}$$

where the coefficients $u_{\lambda i}$ and $v_{\lambda i}$ are given in Table IX. Since it was demonstrated in Sec. 2 that the g_i are uniquely determined by the relative positions of the excited states (see Table V), the same holds for the quantities g_b, g_c, g_0. The last column of Table IX contains the numerical values obtained for them when one inserts for the g_i the values resulting from the Mulliken approximation, as given in Table VI(c).

Determination of the Resonance Integral from the Separation between the Ground State and the Excited States

From Eqs. (3.5) and (3.6), it follows that

$$\bar{\epsilon}_c-\bar{\epsilon}_b=-2\gamma/(1-S^2). \tag{3.8}$$

In Eq. (3.3), the quantity g_0 follows from the relative position of the excited states and is given in Table IX. Furthermore, s_0 is spectroscopically found to be[4]

$$s_0=2.24. \tag{3.9}$$

It follows that

$$\bar{\epsilon}_c-\bar{\epsilon}_b=2.618454, \tag{3.10}$$

and

$$\gamma=-1.229482=2.389 \text{ ev}, \tag{3.11}$$

a result obtained uniquely from spectroscopic information.

Determination of the Coulomb Integral from Ionization Potentials and Electron Affinities

When the values of g_b and g_c, given in Table IX, and the value of γ, given in Eq. (3.11), are inserted in Eqs. (3.1) and (3.2), there results

$$\bar{\alpha}=I_C-I-0.264966\equiv I_C-I-0.515 \text{ ev}, \tag{3.12}$$

$$\bar{\alpha}=A_C-A-0.269034\equiv A_C-A-0.523 \text{ ev}. \tag{3.13}$$

According to the interpretation adopted in paper I, A and I should be electron affinity and ionization potential of benzene, whereas A_C and I_C should be electron affinity and ionization potential of the carbon valence state. The experimental values are

$$\begin{aligned} &I_C(\text{ex})=11.22 \text{ ev}, \qquad I(\text{ex})=9.43 \text{ ev}, \\ &I_C(\text{ex})-I(\text{ex})=1.79 \text{ ev}, \\ &A_C(\text{ex})=0.69 \text{ ev}, \qquad A(\text{ex})=0.5 \text{ ev}, \\ &A_C(\text{ex})-A(\text{ex})=0.19 \text{ ev}. \end{aligned} \tag{3.14}$$

Since the Coulomb integral $\bar{\alpha}$ cannot be positive, the best agreement with the experimental values is apparently obtained by letting

$$\bar{\alpha}=0. \tag{3.15}$$

Assuming I_C and A_C to be identical with the experimental values and $\bar{\alpha}$ given by Eq. (3.15), the calculated benzene values become

$$I=10.70 \text{ ev}, \qquad A=0.16 \text{ ev}, \tag{3.16}$$

which would be reasonable Frank-Condon values.

While the empirical value (3.15) might be construed as a sort of support of the free-electron model, it is, however, hardly satisfactory from the point of view of the LCAO theory developed in the first paper, and this matter will have to be examined in the subsequent note.

ACKNOWLEDGMENT

We wish to express our gratitude to A. Wasserman for coding the IBM 650 programs, without which the present investigation could not have been carried through.

THE JOURNAL OF CHEMICAL PHYSICS VOLUME 34, NUMBER 6 JUNE, 1961

Quantum Mechanics of Mobile Electrons in Conjugated Bond Systems. VI. Theoretical Evaluation of Energy Contributions*

KLAUS RUEDENBERG

Institute for Atomic Research, Department of Chemistry, Department of Physics, Iowa State University, Ames, Iowa

(Received March 16, 1959)

The general formulas of the first paper in the series [K. Ruedenberg, J. Chem. Phys. **34**, 1861 (1961)] are used to analyze the energy contributions of the molecular framework for a π-electron system in detail, without use of additional assumptions. The valence-state potential of carbon, used in the framework potential, and the $2p\pi$ atomic orbitals are determined by a minimum principle. The Coulomb integral and resonance integral are evaluated from their constituent integrals in the tight-binding approximation. The agreement with the empirical values [see K. Ruedenberg, J. Chem. Phys. **34**, 1878 (1961)] is unsatisfactory for the Coulomb integral but very good for the resonance integral. The approximate proportionality between energy matrix elements and overlap integrals is proven for a variation of the internuclear distance between 1.26 and 1.54 A.

INTRODUCTION

IN the present note, the energy contributions formulated in the general theory[1] are calculated theoretically from the constituent integrals. In particular, the energy contributions from the framework potential are analyzed in detail, since such an analysis has as yet never been made.

In order to carry out this program, it is necessary to first determine appropriate values for the orbital exponents which appear as parameters in the potential of the neutral-carbon-atom potential and in the $2p\pi$ atomic orbitals. This is done by means of a minimum principle, and it emerges that contrary to previous assumptions, the two orbital exponents cannot be chosen equal to each other.

On this basis, values are calculated for the resonance integral and the Coulomb integral, and these values are then compared with the empirical values deduced in the preceding paper.[2] The agreement found is very good for the resonance integral, but unsatisfactory for the Coulomb integral. Hence, it is possible to predict correctly the framework contributions for the spectral transitions but not for the ionization potentials.

As a side result, it is established that the neighbor elements of the energy matrix are approximately proportional to the overlap integral S when the internuclear distance is varied. This fact formed the basis of the augmented tight-binding approximation in paper II.[3]

In conclusion, it is felt that the analysis of the framework contributions leads to insights as regards the origin of the various energy contributions.

The following units are used, unless otherwise stated:

length: $D=1.4000$ A

energy: $e^2/D=10.2833$ ev.

This energy unit is different from the one used in the preceding paper; see footnote 7 in paper V, and also Eqs. (1.4) to (1.7) of paper IV.

---

* Contribution No. 715. Work was performed in the Ames Laboratory of the U. S. Atomic Energy Commission.

[1] K. Ruedenberg, J. Chem. Phys. **34**, 1861 (1961) hereafter referred to as paper I).

[2] K. Ruedenberg and E. M. Layton, Jr., J. Chem. Phys. **34**, 1897 (1961) (hereafter referred to as paper V).

[3] K. Ruedenberg, J. Chem. Phys. **34**, 1878 (1961) (hereafter referred to as paper II).

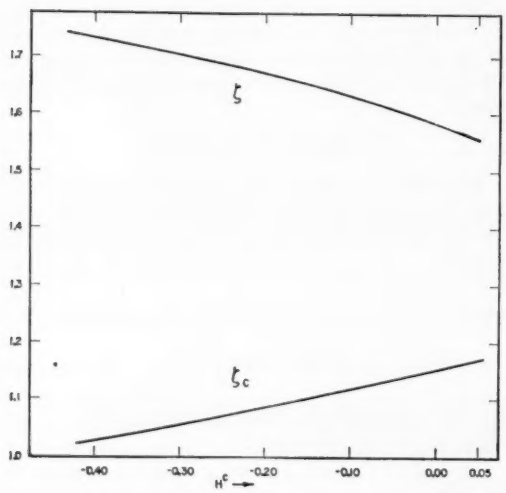

FIG. 1. Orbital exponent of shielding orbitals (ζ_C) and orbital exponent of π-electronic AO's (ζ) as functions of calculated electron affinity of carbon ($A_C=-H_C$).

1. EFFECTIVE VALENCE STATE OF CARBON

Criterion for Choice of Atomic Orbitals

In a large molecule with many π electrons, each of them sees essentially neutral atoms. This surmise is confirmed by the near cancellation of the ionic part of the framework energy against the electron repulsion terms, as shown after Eq. (4.46′) of paper I.[1] For this reason, the most favorable AO's for the construction of MO's would presumably be such $2p\pi$ atomic orbitals which are close to the eigenfunctions of the Hamiltonian

$$\mathfrak{H}^C=(-\hbar^2/2m)\Delta+U^C, \qquad (1.1)$$

where U^C is the neutral carbon potential occurring in the framework potential, i.e., U^C is the potential given in Eq. (1.7) of paper I. Since an ordinary $2p\pi$ AO is not an exact eigenfunction of the Hamiltonian $\mathfrak{H}^C$, the orbital closest to such an eigenfunction will be determined by minimizing the energy integral

$$(\chi\,|\,\mathfrak{H}^C\,|\,\chi)=[\chi\,|\,(-\hbar^2/2m)\Delta\,|\,\chi]+(\chi\,|\,U^C\,|\,\chi), \qquad (1.2)$$

with respect to such parameters as are available in the $2p\pi$ orbital χ. The expression for the orbital was given in Eq. (1.2) of paper IV,[4] the only variation parameter is the orbital exponent ζ of χ. By virtue of Eqs. (2.4), (5.2) of paper IV, one obtains for the energy expression (1.2) the explicit formula

$$(e^2/a)^{-1}(\chi\,|\,\mathfrak{H}^C\,|\,\chi)=(1/2)\zeta_C{}^2t^2 -\zeta_C(14+14t+6t^2+t^3)2t^5/(1+t)^7, \qquad (1.3)$$

with

$$t=\zeta/\zeta_C,$$

where ζ is the orbital exponent of χ, and ζ_C is the orbital exponent of the shielding orbitals occurring in the potential U^C [See Eq. (1.7) of paper I]. Equating the derivative of the expression (1.3) to zero, one obtains the relation

$$\zeta_C=(70+56t+28t^2+8t^3+t^4)2t^3/(1+t)^8, \qquad (1.4)$$

which determines the minimizing value $\zeta=t\zeta_C$ for a given value of ζ_C, i.e., for a given potential U_C.

Criterion for Choice of Neutral Carbon Potential

Equation (1.4) determines the AO exponent as a function of the shielding exponent, viz.,

$$\zeta=\zeta(\zeta_C), \qquad (1.5)$$

and thereby the energy expression (1.3) becomes also a function of ζ_C, i.e.,

$$(\chi(\zeta)\,|\,\mathfrak{H}^C(\zeta_C)\,|\,\chi(\zeta))=H^C(\zeta_C). \qquad (1.6)$$

There remains the question: Which is the appropriate value for the shielding orbital exponent ζ_C? The answer follows from the physical significance of the energy expressions (1.2), (1.3), and (1.6). According to Eq. (1.11) of paper I this energy expression should equal $-A_C$, where A_C is the valence state electron affinity, and hence should be close to the experimentally estimated value of 0.69 ev. We therefore fix ζ_C by equating the function (1.6) to 0.69 ev.

One might have argued that the $2p\pi$ AO's should actually be chosen so as to be close to eigenfunctions of the Hamiltonian $\mathfrak{H}'=(\hbar^2/2m)\Delta+U^C-e^2/rN_a$, $N_a=$ number of atoms, since each electron is only shielded by the *other* electrons. Nevertheless, it would be the quantity of Eqs. (1.2) and (1.3) which would have to have the value -0.69 ev. Therefore, the result for ζ and ζ_C would presumably not change too much, since it is found that the potential U^C contributes about 35 ev, whereas even in benzene, (e^2/rN_a) subtracts only about 3 ev.

Determination of U^C and χ

Since the computations were carried out on an IBM 650 electronic computer, the following procedure was found practical.

First the energy integral (1.3) was computed for fixed ζ_C values as functions of t; specifically for

$$t=0(0.05)2, \quad \rho_C=2.5(0.2)4.5, \quad \text{and} \quad 2.9(0.02)3.1,$$

where

$$\rho_C=2.64575\zeta_C,$$

[4] K. Ruedenberg, J. Chem. Phys. **34**, 1892 (1961) (hereafter referred to as paper IV).

TABLE I. Integrals as functions of the shielding parameter ζ_C.

$\rho_C = (D/a)\zeta_C$ $\quad S = (\chi_1 \mid \chi_2)$

$= 2.64575\zeta_C$ $\quad T_{11} = (\chi_1 \mid (-\hbar^2/2m)\Delta \mid \chi_1)$

$\rho = 2.64575\zeta$ $\quad T_{12} = (\chi_1 \mid (-\hbar^2/2m)\Delta \mid \chi_2)$

$U_{111} = (\chi_1 \mid U_1^C \mid \chi_1)$ $\quad U_{121} = (\chi_1 \mid U_2^C \mid \chi_1)$

$U_{122} = (\chi_1 \mid U_2^C \mid \chi_2)$ $\quad U_{1h1} = (\chi_1 \mid U_h^H \mid \chi_1)$

Energy Unit: $(e^2/D) = 10.2833$ ev

ρ_C	3.0742402	3.0648459	3.0554190	3.0459619	3.0364778
ρ	4.1502243	4.1651256	4.1798132	4.1942895	4.2085582
S	0.26487158	0.26275488	0.26068128	0.25864989	0.25665964
T_{11}	3.2551001	3.2785167	3.3016797	3.3245892	3.3472479
U_{111}	−3.2247735	−3.2582658	−3.2916108	−3.3248065	−3.3578514
T_{12}	0.25537335	0.25322419	0.25110468	0.24901480	0.24695436
U_{122}	−0.29369849	−0.29425592	−0.29481574	−0.29537824	−0.29594340
U_{121}	−0.21592587	−0.21826758	−0.22060139	−0.22297894	−0.22537925
U_{1h1}	−0.058361692	−0.058483732	−0.058602702	−0.058718721	−0.058831833
ρ_C	3.0280269	3.0184985	3.0100121	3.0004485	2.9919347
ρ	4.2210695	4.2349534	4.2471271	4.2606369	4.2724828
S	0.25492430	0.25300926	0.25133936	0.24949621	0.24788879
T_{11}	3.3671791	3.3893660	3.4088801	3.4306013	3.4497041
U_{111}	−3.3870967	−3.4198517	−3.4488365	−3.4812962	−3.5100170
T_{12}	0.24514742	0.24314214	0.24138397	0.23943313	0.23772293
U_{122}	−0.29644814	−0.29701880	−0.29752863	−0.29810519	−0.29862037
U_{121}	−0.22755275	−0.23001822	−0.23223872	−0.23476796	−0.23704030
U_{1h1}	−0.058930105	−0.059038029	−0.059131723	−0.059234719	−0.059324198
ρ_C	2.9834107	2.9545839	2.9481697	2.8085512	
ρ	4.2841778	4.3225562	4.3308613	4.4936819	
S	0.24630979	0.24118351	0.24008530	0.21934442	
T_{11}	3.4686155	3.5310388	3.5446206	3.8161536	
U_{111}	−3.5386119	−3.6341783	−3.6552161	−4.0960820	
T_{12}	0.23603508	0.23050123	0.22930502	0.20601987	
U_{122}	−0.29913810	−0.30090563	−0.30130270	−3.1037706	
U_{121}	−0.23933196	−0.24723201	−0.24902462	−0.29133767	
U_{1h1}	−0.059411748	−0.059693673	−0.059753615	−0.060854818	
ρ_C	2.7041570	2.6030238	2.5058667	2.4130724	
ρ	4.5970669	4.6854428	4.7611467	4.8261448	
S	0.20693949	0.19679362	0.18843076	0.18148719	
T_{11}	3.9937681	4.1487998	4.2839494	4.4017148	
U_{111}	−4.4085408	−4.7004085	−4.9724157	−5.2255651	
T_{12}	0.19148412	0.17927339	0.16900051	0.16033475	
U_{122}	−3.1782044	−3.2566479	−3.3384555	−3.4229199	
U_{121}	−0.32748454	−0.36666003	−0.40855381	−0.45283009	
U_{1h1}	−0.061485077	−0.061984426	−0.062384945	−0.062709785	

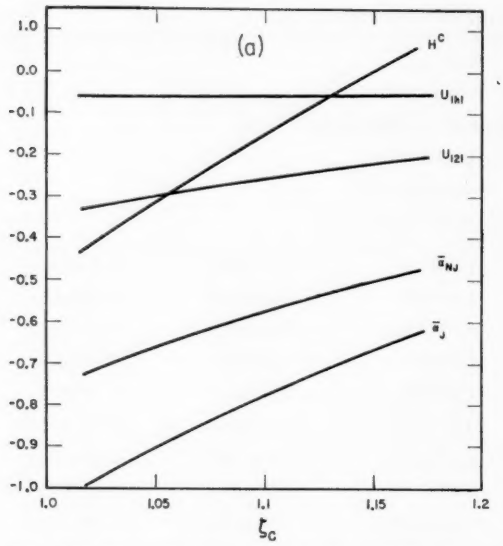

FIG. 2(a). One-center framework energy contributions as functions of shielding orbital exponent. (Definitions of U_{121} and U_{1A1}: see Table I.)

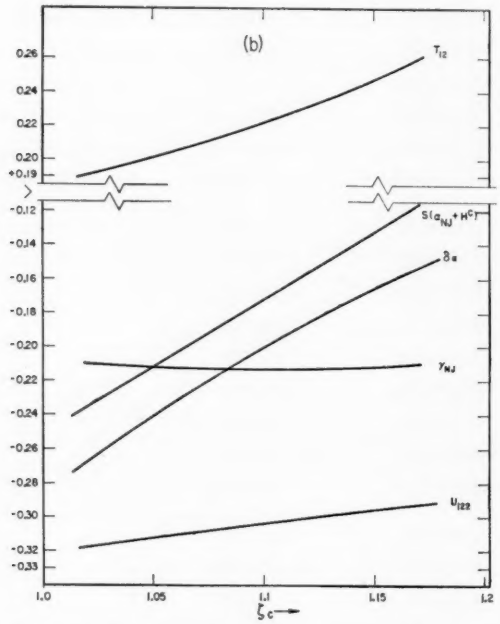

FIG. 2(b). Two-center framework energy contributions as functions of shielding orbital exponent (definitions of T_{12}, U_{122}: see Table I).

is the quantity defined in Eq. (3.5) of paper IV. In the region investigated the energy function was found to have one minimum and one maximum (for fixed value of ζ_C). The minimum value has about the right order of magnitude for values of ρ_C between 2.9 and 3.0, the corresponding t values vary from 1.50 to 1.42.

In the second step, pairs of values (ζ_C, t) satisfying the minimum condition (1.4) in the region of interest were found by computing ζ_C as a function of t for

$$t=1.35(0.001)1.50,$$

and then computing the corresponding energy (1.3).

The simultaneous variation of ζ, ζ_C, H^C is illustrated in Fig. 1 by plotting ζ and ζ_C against H^C. The most notable result is that contrary to previous assumptions, the two orbital exponents must differ from each other. It is very gratifying that, for ζ, one obtains values close to the Slater value

$$\zeta_{S1}=Z_{S1}/2=3.25/2=1.625 \text{ (Z effective charge).} \quad (1.7)$$

It is the shielding orbital exponent ζ_C which turns out to be lower by about 30%. The reason for this result undoubtedly lies in the fact that U^C lumps together several influences; also ζ_C must be a sort of average over four different shielding orbital exponents. Thus the literal interpretation of U^C is somewhat hazardous; the over-all behavior is presumably right, but apparently it needs to be gauged.

It is also seen that H^C is a very sensitive function of ζ_C. This is because H_C is the difference of two large terms, kinetic and potential energy, each about 35 ev, which nearly cancel each other. The delicate balance is shown by the selected values in Table I. The balance is completely upset by the crude assumption $\zeta=\zeta_C=$ Slater value, which leads to a value of about +11 ev for H^C.

In choosing a definite value for ζ_C, it was considered that the semiexperimental value of 0.69 ev=0.067 (e^2/D) has some uncertainty associated with it and that on the other hand, the molecular quantities which are computed in the next section are much less sensitive to ζ_C than H^C. (The latter fact is apparent from Fig. 2.) For these reasons the shielding exponent ζ_C was chosen in such a manner as to give an exact decimal fraction to the overlap integral between two neighbor atoms. Thus the values

$$\zeta_C=1.12863045, \quad (1.8)$$

$$\zeta=1.6178932, \quad (1.9)$$

were adopted.

With these values one finds for one-center kinetic energy, potential energy, and electron affinity,

$$(\chi_1 \mid (-\hbar^2/2m)\Delta \mid \chi_1)=3.4627289, \quad (1.10)$$

$$(\chi_1 \mid U_1{}^C \mid \chi_1)=-3.5296935, \quad (1.11)$$

$$H^C(\zeta_C)=-A_C=-0.066964750. \quad (1.12)$$

The parameters defined in Eqs. (1.9) and (3.5) of paper IV become

$$\rho_C=2.9860740, \quad (1.13)$$

$$\rho=4.2805408, \quad (1.14)$$

TABLE II. Distance dependence of neighbor integrals.[a]

(R/D)	S	T_{12}	U_{122}	U_{121}	β
0.90	0.30993306	0.36740030	−0.42716644	−0.35180098	−0.48693258
0.94	0.28337215	0.30956419	−0.37082935	−0.30169538	−0.43209451
0.98	0.25856031	0.25918611	−0.32136113	−0.25814871	−0.38353615
1.00	0.24680000	0.23655991	−0.29897613	−0.23860942	−0.36139235
1.02	0.23546272	0.21552182	−0.27804245	−0.22042503	−0.34056308
1.06	0.21403064	0.17786365	−0.24020324	−0.18782983	−0.30254283
1.10	0.19420422	0.14554730	−0.20722576	−0.15975252	−0.26890422

[a] R=internuclear distance, D=1.400000 A, for other symbols and energy unit, see Table I.

and substitution of the value for ρ in Eq. (2.1) of paper IV yields the neighbor overlap integral

$$S=0.24680000. \tag{1.15}$$

Ionization Potential and Alternative Choice of the Valence State

According to the arguments given in Eq. (1.12) of paper I, the theoretical expression for the ionization potential of the carbon valence state is

$$I_C=A_C+[11\mid 11], \tag{1.16}$$

where, according to Eq. (7.3) of paper IV,[4] the one-center Coulomb integral is given by

$$[11\mid 11]=G_1=\rho 501/1280. \tag{1.17}$$

The value (1.9) for ζ yields the value (1.14) for ρ' and hence,

$$G_1=1.6754304, \tag{1.18}$$

instead of the experimental value

$$I_C-A_C=10.53 \text{ ev}=1.023906(e^2/D), \tag{1.19}$$

a discrepancy of about 6.5 ev. The suggestion of substituting the empirical value (1.19) for the theoretical one constitutes Pariser's proposal.

In view of this difficulty, it seems natural to ask whether a different choice for the carbon valence state can resolve the discrepancy between Eqs. (1.18) and (1.19). Concretely, this means: Determine ζ and ζ_C such that the expressions (1.2) and (1.3) yields the value −0.067, and that the expression (1.17) yields the value 1.024.

It turns out that these two requirements lead approximately to the result $\zeta\approx\zeta_C\approx 1$. In order to avoid unnecessary complication, and since one has also $\zeta_H=1$ for the hydrogen shielding orbital, let us put exactly

$$\zeta=\zeta_C=\zeta_H=1, \tag{1.20}$$

whence, instead of Eqs. (1.13, 1.14),

$$\rho=\rho_C=2.64575. \tag{1.21}$$

One finds now

$$(\chi_1\mid(-\hbar^2/2m)\Delta\mid\chi_1)=1.3228750, \tag{1.22}$$

$$(\chi_1\mid U_1^C\mid\chi_1)=-1.4468946, \tag{1.23}$$

$$A_C=-H^C=0.1240195, \tag{1.24}$$

$$G_1=[11\mid 11]=1.035563086, \tag{1.25}$$

in satisfactory agreement with the experimental values.

Thus, the AO, orbital exponent ζ would have to be very different from the Slater value in order to yield acceptable values for A_C *and* I_C, and it would lead to the overlap-integral value

$$S=0.54919108. \tag{1.26}$$

It may be that these rather unlikely conclusions must be ascribed to the neglect of explicit interactions with the inner electrons.

2. FRAMEWORK CONTRIBUTIONS TO THE MOLECULAR ENERGIES

Formulas for Framework Contributions

The framework Hamiltonian contributes to the molecular energies the following terms: the resonance integral γ [see Eqs. (4.43′) and (2.10, 2.11, 2.11′) of paper I], the Coulomb integral $\bar{\alpha}$ [see Eq. (4.42) of paper I], the Coulomb integral variation $\delta\alpha$[see Eq. (2.13) of paper I].

The Coulomb integral value depends upon the ratio between the number of joint atoms and the number of nonjoint atoms in a particular molecule. The two extreme cases are

$$\bar{\alpha}_J=3(\chi_1\mid U_2^C\mid\chi_1), \quad \text{if all atoms are joints,} \tag{2.1}$$

$$\bar{\alpha}_{NJ}=2(\chi_1\mid U_2^C\mid\chi_1)+(\chi_1\mid U_{h1}^H\mid\chi_1), \quad \text{if all atoms are nonjoints.} \tag{2.2}$$

The difference between these two extremes is the quantity $\delta\alpha$, viz.,

$$\delta\alpha=\alpha_J-\alpha_{NJ}=(\chi_1\mid U_2^C\mid\chi_1)-(\chi_1\mid U_{h1}^H\mid\chi_1). \tag{2.3}$$

Since the resonance integral depends partly upon the

Coulomb integral, it depends also upon the joint-nonjoint ratio, hence

$$\gamma_J=(\chi_1\mid(-\hbar^2/2m)\Delta\mid\chi_2)+2(\chi_1\mid U_2^C\mid\chi_2)-S(\bar{\alpha}_J+H^C), \quad (2.4)$$

$$\gamma_{NJ}=(\chi_1\mid(-\hbar^2/2m)\Delta\mid\chi_2)+2(\chi_1\mid U_2^C\mid\chi_2)-S(\bar{\alpha}_{NJ}+H^C) \quad (2.5)$$

$$\gamma_{NJ}-\gamma_J=S\delta\alpha. \quad (2.6)$$

Formulas for the calculation of the constituent integrals were given in paper IV.

Theoretical Values

When the atomic orbitals and the neutral carbon potentials are determined by the method outlined in the first section, then the molecular integrals (2.1)–(2.5) also become functions of the shielding orbital exponent ζ_C. For the particular value of ζ_C finally adopted in Eq. (1.8), one obtains the following energy contributions:

$$(\chi_1\mid(-\hbar^2/2m)\Delta\mid\chi_2)=0.23655991, \quad (2.7)$$

$$(\chi_1\mid U_2^C\mid\chi_2)=-0.29897613, \quad (2.8)$$

$$(\chi_1\mid U_2^C\mid\chi_1)=-0.23860942, \quad (2.9)$$

$$(\chi_1\mid U_{h1}^H\mid\chi_1)=-0.059384632, \quad (2.10)$$

$$\bar{\alpha}_J=-0.71582826, \quad (2.11)$$

$$\gamma_J=-0.168199035, \quad (2.12)$$

$$\bar{\alpha}_{NJ}=-0.53660347, \quad (2.13)$$

$$\gamma_{NJ}=-0.21243178, \quad (2.14)$$

$$\delta\alpha=-0.17922479, \quad (2.15)$$

$$S\delta\alpha=-0.044232678. \quad (2.16)$$

Figures 2(a) and 2(b) illustrate the dependence of these energy contributions upon the choice of ζ_C. A listing of the integrals for varying values of ζ_C is given in Table I.

Dependence upon Internuclear Distance

The calculations just quoted were carried out for the neighbor distance $D=1.400000$ A. It is of interest to examine the dependence of the framework contributions upon the neighbor distance, R, since the augmented tight-binding approximation of paper II had introduced certain assumptions concerning this dependence.[3] The energy contributions were calculated for distances between 1.26 and 1.54 A; for ζ_C and ζ the values of Eqs. (1.8) and (1.9) were taken in all cases. The numerical results are given in Table II. Figure 3 gives a graphical representation of the distance dependence for $\delta\alpha$, for β, for γ_{NJ} and for their constituents.

It is now possible to test the assumption expressed in Eq. (1.10) of paper II, viz., that the integral

$$\beta=(\chi_1\mid(\hbar^2/2m)\Delta\mid\chi_2)+2(\chi_1\mid U_1^C\mid\chi_2), \quad (2.17)$$

is approximately proportional to the overlap integral. To this end, Fig. 4 plots some energy contributions, including β, against the corresponding neighbor overlap integral S. It is seen that approximate proportionality exists for α_{NJ}, $\delta\alpha$, and β. A more accurate linear expression is

$$\beta=-1.85352725S+0.09605818, \quad (2.18)$$

$$\beta=-0.36139235\sigma+0.09605818(1-\sigma), \quad (2.18')$$

with

$$\sigma=S/0.24680000.$$

The resonance integral is not a linear function of S. Its dependence upon the internuclear distance is very accurately given by

$$\gamma_{NJ}=-0.21243178[1+1.1850463(1-\tau)-2.9155619(1-\tau)^2], \quad (2.19)$$

with

$$\tau=R/D. \quad (2.19')$$

Comparison with Molecular Experimental Values

The most remarkable fact emerging from Fig. 2 is that the resonance integral γ_{NJ} is extraordinarily

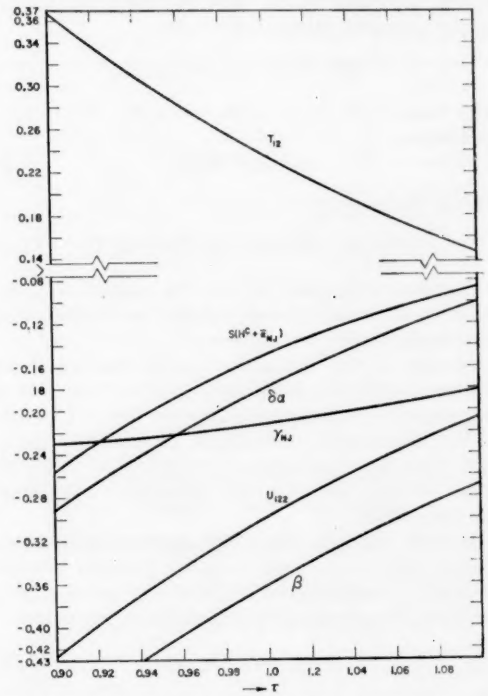

FIG. 3. Framework energies as functions of internuclear distance [definition of τ: see Eq. (2.19′); (definition of T_{12}, U_{122}: see Table I).

constant for a wide range of ζ_C values, as compared to its constituent integrals. This constancy has two consequences. In the first place, it excludes the possibility of a sensitive relationship between the electron affinity $A_C=-H^C$ of the carbon valence state and the resonance integral γ_{NJ}, since the latter is essentially constant when H^C varies from -10 ev to beyond $+3$ ev. By the same token, however, it is impossible to adjust the value of γ_{NJ} by changing the value of ζ_C within limits, which are reasonable for $H^C=-A_C$, so that the present procedure yields essentially *one* value for γ_{NJ}. Thus the comparison with the empirical value becomes the more meaningful. The rather good agreement of Eq. (2.14) with the value deduced from the spectral information of benzene [see Eq. (3.11) of the preceding paper], viz.,

$$\gamma_{NJ}=-0.232350, \tag{2.20}$$

is therefore extremely gratifying.

On the other hand, the theoretical value (2.13) for the Coulomb integral $\bar{\alpha}_{NJ}$ is about -5.473 ev, whereas the semiempirical analysis led to the requirement $\bar{\alpha}_{NJ}=0$ [see Eq. (3.15) of the preceding paper]. It is not surprising that the theoretical value does not keep up with the empirical one on this point; the calculated result is to be expected in principle from the adopted theoretical formalism. It says, entirely reasonably, that the ionization potential of benzene I is larger than that of the carbon valence state I_C. The specific numerical result is

$$I=I_C+4.96=16.18 \text{ ev} \tag{2.21}$$

[see Eqs. (3.12) and (3.14) of paper V]. In the light of the general theoretical framework of the π-electronic approximation [compare the general Eq. (4.54) of paper I], it is in fact very hard to understand why the highest bonding orbital in benzene should in reality be more loosely bound [I(exp)$=9.43$ ev] than the parent valence state of carbon [I_C(exp)$=11.22$ ev]. The origin of this difficulty hardly lies in the tight-binding approximation, as can be seen from the correction which is expected for benzene when nonneighbor effects are included [see Sec. 2 of paper II].[5]

Another unsatisfactory result which seems to point in the same direction is the fact that the molecular ultraviolet spectrum of benzene independently leads to the value (1.19) for G_1 [see Eq. (2.11) of paper V] which is in disagreement with the theoretical value (1.18).

Molecular Energy Contributions Resulting from Alternative Choice of Carbon Valence State

The alternative choice, given in Eq. (1.20) for ζ and ζ_C, which furnishes acceptable values for A_C, I_C, and G_1, leads to the following molecular energy contributions[6]:

$$(\chi_1 \mid -(\hbar^2/2m)\Delta \mid \chi_2)=0.40153626, \tag{2.22}$$

$$(\chi_1 \mid U_2^C \mid \chi_2)=-0.38915505, \tag{2.23}$$

$$(\chi_1 \mid U_2^C \mid \chi_1)=-0.26473775 \tag{2.24}$$

$$(\chi_1 \mid U_{h1}^H \mid \chi_1)=-0.03755303 \tag{2.25}$$

$$\bar{\alpha}_{NJ}=-0.56702853 \tag{2.26}$$

$$\beta=-0.37677359 \tag{2.27}$$

$$\gamma_{NJ}=+0.00274382 \tag{2.28}$$

$$\delta\alpha=-0.22718472. \tag{2.29}$$

While Eq. (2.26) shows no improvement concerning the Coulomb integral, the result (2.28) for the resonance integral has now become extremely unsatisfactory.

It must be considered gratifying that the rather unlikely orbital exponent of Eq. (1.20) does not lead to an improvement but to a worsening of the molecular energy contributions.

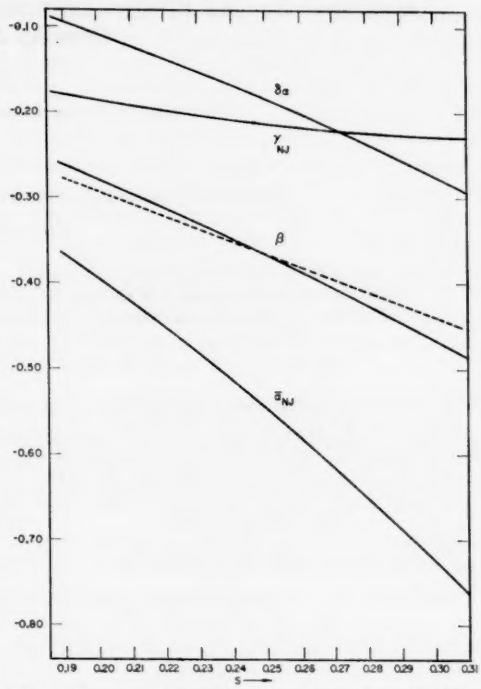

FIG. 4. Framework energies as functions of overlap integral. Dotted line: Corresponds to strict proportionality $\beta=-0.36139\sigma$, obtained by dropping the second term in Eq. (2.18′).

ACKNOWLEDGMENTS

I wish to thank A. Wasserman for preparing most of the IBM 650 codes. I also wish to thank Mr. Hummel for preparing some codes and R. Rue for carrying out the hand computations.

[5] Similar difficulties were noted by R. Pariser and R. G. Parr, J. Chem. Phys. **23**, 711 (1955), in a treatment of ethylene-like molecules. The present results indicate that the neglect of differential overlap, used by Pariser and Parr, is not responsible.

[6] These energy contributions were evaluated for a neighbor distance of 1.39 A.

Energies of Excited Electronic States as Calculated with the Zero Differential Overlap Approximation

J. N. MURRELL

Department of Chemistry, University of Sheffield, Sheffield, England

AND

L. SALEM

Mallinkrodt Chemical Laboratory, Harvard University, Cambridge, Massachusetts

(Received June 22, 1960)

It is shown that electronic excitation energies, calculated using the zero differential overlap approximation, can always be expressed in terms of the difference between two-electron Coulombic integrals. These differences can then be used as empirical parameters for the calculation of excitation energies.

THE matrix elements of the many-electron Hamiltonian $\mathcal{H}=\sum_i H_i+\sum_{ij}G_{ij}$ between the ground state and singly excited states of a closed-shell molecule with $2m$ electrons have the following forms[1,2]:

$$\langle {}^1\chi_{i\to k}|\mathcal{H}|{}^1\chi_0\rangle=\sqrt{2}F_{ki} \tag{1}$$

$$\langle {}^1\chi_{i\to k}|\mathcal{H}|{}^1\chi_{j\to l}\rangle-\delta_{ij}\delta_{kl}E_0=\delta_{ij}F_{kl}-\delta_{kl}F_{ij}+2\langle jk|G|li\rangle-\langle jk|G|il\rangle \tag{2}$$

$$\langle {}^3\chi_{i\to k}|\mathcal{H}|{}^3\chi_{j\to l}\rangle-\delta_{ij}\delta_{kl}E_0=\delta_{ij}F_{kl}-\delta_{kl}F_{ij}-\langle jk|G|il\rangle, \tag{3}$$

where

$$\langle jk|G|il\rangle=\iint\psi_j^*(1)\psi_k^*(2)(e^2/r_{12})\psi_i(1)\psi_l(2)d\tau_1 d\tau_2 \tag{4}$$

$$F_{st}=H_{st}+\sum_{r=1}^{m}\{2\langle rs|G|rt\rangle-\langle rs|G|tr\rangle\}. \tag{5}$$

The ground-state wave function ${}^1\chi_0$, of energy E_0, is a single determinant of the form

$${}^1\chi_0=|\psi_1\bar{\psi}_1\cdots\psi_m\bar{\psi}_m|,$$

in which the lowest m molecular orbitals are doubly occupied. The excited states $\chi_{i\to k}$ are obtained by promoting an electron from an occupied orbital ψ_i to an unoccupied orbital ψ_k, and forming either the singlet or the triplet spin state.

Pariser and Parr[3] and Pople[2] have developed a semiempirical method of calculating the excitation energies of conjugated molecules using the "zero differential overlap approximation." In this approximation, the two-electron integrals between molecular orbitals are evaluated by expanding the molecular orbitals in the LCAO form $\psi_i=\sum_\mu C_{i\mu}\phi_\mu$ and neglecting any integrals which depend on the overlap of two orbitals centered on different atoms. Thus we write, for example,

$$\langle jk|G|il\rangle=\sum_\mu\sum_\nu C_{j\mu}C_{i\mu}C_{k\nu}C_{l\nu}\gamma_{\mu\nu},$$

where

$$\gamma_{\mu\nu}=\langle\phi_\mu\phi_\nu|G|\phi_\mu\phi_\nu\rangle.$$

Empirical values have been assigned to these integrals so as to give the best fit with the experimental energies of certain excited states of benzene.[4] Recently it has been shown[5] that a good fit with the energies of the singlet excited state can be obtained by dropping all γ's except γ_{11} and γ_{12}. It has also been noticed in several specific cases (for example see work cited in footnote 6) that in the expression for the excitation energies the sum of the coefficients of all the two-electron integrals $\gamma_{\mu\nu}$ is zero. This property we will now show to be generally true in the zero differential overlap approximation.

Since the molecular orbitals are orthonormal we have $\sum_\mu C_{s\mu}C_{t\mu}=\delta_{st}$ for all s and t. It follows that the sum of the coefficients of the γ's, Ω, obtained by expanding the expression for F_{st} is

$$\Omega[F_{st}]=\sum_{r=1}^{m}(2\delta_{st}-\delta_{rs}\delta_{rt}).$$

Remembering that r, i, and j refer to occupied orbitals in the ground state, but k and l to unoccupied ones, we have

$$\Omega[F_{ki}]=0,$$

$$\Omega[F_{kl}]=2m\delta_{kl},$$

$$\Omega[F_{ij}]=(2m-1)\delta_{ij}.$$

Likewise

$$\Omega[\langle jk|G|li\rangle]=0,$$

and

$$\Omega[\langle jk|G|il\rangle]=\delta_{ij}\delta_{kl}.$$

From these results it can be seen that the sum of the

[1] C. C. J. Roothaan, Revs. Modern Phys. **23**, 61 (1951).
[2] J. A. Pople, Proc. Phys. Soc. (London) **A68**, 81 (1955).
[3] R. G. Parr, J. Chem. Phys. **20**, 1499 (1952); R. Pariser and R. G. Parr, *ibid.* **21**, 767 (1953).
[4] R. J. Pariser, J. Chem. Phys. **24**, 250 (1956).
[5] H. C. Longuet-Higgins and L. Salem, Proc. Roy. Soc. (London) (to be published).
[6] P. Lykos (private communication to R. G. Parr), 1954.

coefficients of the γ's, obtained by expanding the matrix elements (1), (2), or (3) is zero, and the same result holds for the excitation energies which can all be expressed in terms of these matrix elements.

As a consequence of this important result, the excitation energies can always be written in terms of the set of parameters $(\gamma_{11}-\gamma_{12})$, $(\gamma_{12}-\gamma_{13})$, $(\gamma_{13}-\gamma_{14})$, etc., rather than γ_{11}, γ_{12}, γ_{13}, γ_{14}, etc. Whereas $\gamma_{1\mu}$ is inversely proportional to the interatomic distance $R_{1\mu}$ if 1 and μ are far apart, the new parameter $(\gamma_{1\mu}-\gamma_{1\mu+1})$ falls off more rapidly with distance, being proportional to $R_{1\mu}^{-2}$. There is therefore more reasonable ground for neglecting these differences for remote atoms than there is for neglecting the individual γ's.

With the values $(\gamma_{11}-\gamma_{12})=4.170$ ev, $(\gamma_{12}-\gamma_{13})=1.425$ ev, $(\gamma_{13}-\gamma_{14})=0.810$ ev, and $\beta=H_{12}=-2.371$ ev, the energies of the three singlet excited states of benzene, $^1E_{1u}=6.76$ ev, $^1B_{1u}=5.96$ ev, $^1B_{2u}=4.71$ ev, and the lowest triplet $^3B_{1u}=3.59$ ev, are fitted exactly by the theory. If one equates the parameter $(\gamma_{13}-\gamma_{14})$ to zero, then it is still possible to fit the three singlets by using the values $(\gamma_{11}-\gamma_{12})=6.600$, $(\gamma_{12}-\gamma_{13})=1.425$ ev and $\beta=-2.236$ ev. These parameters are equivalent to the set given by Longuet-Higgins and Salem[5]: $\gamma_{11}=8.025$, $\gamma_{12}=1.425$, $\gamma_{13}=\gamma_{14}=0$, $\beta=-2.236$ ev, and calculations using either of these restricted sets must give the same results. However, the values 6.600 and 1.425 for $(\gamma_{11}-\gamma_{12})$ and $(\gamma_{12}-\gamma_{13})$ are much closer to the values calculated with carbon $2p$ atomic orbitals (8.04 ev and 3.14 ev, respectively),[7] than are Longuet-Higgins and Salem's values of γ_{11} and γ_{12} to the calculated values 16.82 ev and 8.78 ev.[7] It therefore seems more satisfactory to regard the unknown two-electron parameters as differences of γ's rather than as absolute values of these integrals, if only a limited set of parameters is going to be used in the calculations of excitation energies.[8]

ACKNOWLEDGMENT

The authors wish to thank Professor R. G. Parr for stimulating discussions on this topic.

[7] M. Goepert-Mayer, and A. L. Sklar, J. Chem. Phys. **6**, 645 (1938).

[8] Another proof of the theorem contained in this paper is given by K. Ruedenberg, J. Chem. Phys. (to be published).

THE JOURNAL OF CHEMICAL PHYSICS VOLUME 34, NUMBER 6 JUNE, 1961

Vaporization of Iridium and Rhodium

MORTON B. PANISH AND LIANE REIF

Research and Advanced Development Division, Avco Corporation, Wilmington, Massachusetts

(Received October 25, 1960)

The vaporization of iridium and rhodium have been studied by Knudsen effusion and Langmuir evaporation techniques. The vapor pressure of iridium over the temperature range of from 2100° to 2600°K is represented by the equation: $\log p_{mm}=10.46-(33980/T)$, and the vapor pressure of rhodium over the temperature range of from 2050° to 2200°K by the equation: $\log p_{mm}=10.28-(28300/T)$. Third-law analyses of the data yield the following heats of vaporization: iridium, $\Delta H_{298}=158.4\pm0.5$ kcal/mole; rhodium, $\Delta H_{298}=132.8\pm0.3$ kcal/mole. Estimated boiling points for iridium and rhodium are 4800° and 3980°K, respectively.

INTRODUCTION

ALTHOUGH a great deal of information has been obtained on the vaporization of many of the more refractory metals, surprisingly little work has been done on the higher melting platinum metals.

There are only a limited number of vapor-pressure measurement methods which are applicable, with a resonable assurance of success, to materials which do not vaporize appreciably except at very high temperatures. At very low pressures and high temperatures the methods most used and most practical are based upon Langmuir's rate-of-evaporation measurements[1] or Knudsen effusion techniques.[2]

[1] I. Langmuir, Phys. Rev. **2**, 329 (1913).

[2] M. Knudsen, Ann. Physik **29**, 179 (1909).

In Langmuir rate-of-evaporation studies the material to be studied is simply heated in a vacuum in such a manner that virtually all the material which leaves the heated surface condenses elsewhere in the system. The vapor pressure of the material is then obtained by determination of the loss of mass of the heated sample by use of the equation

$$n=paA(2\pi MRT)^{-\frac{1}{2}}, \qquad (1)$$

where n is the number of moles per second which leave the surface of area A (cm^2), M is the molecular weight of the gaseous species, R the gas constant, T the temperature in °K, a the accommodation coefficient, and p the equilibrium vapor pressure.

In this work it is assumed that $a=1$; that is, that the

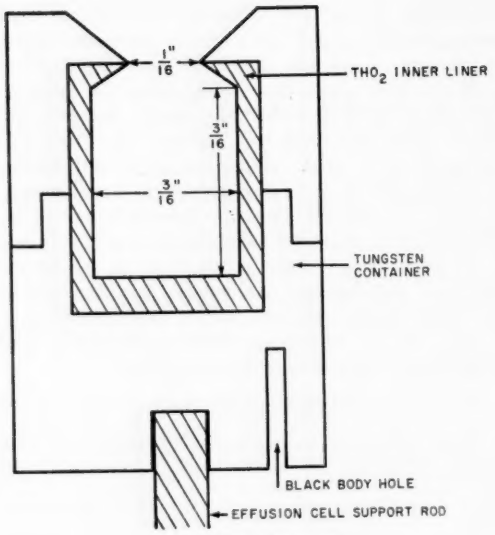

FIG. 1. The effusion cell.

rate at which molecules leave the surface in a vacuum and at equilibrium vapor pressure are the same.

The Knudsen effusion technique requires that the material to be studied be placed in an effusion cell. The effusion cell is, in the ideal case, an inert container with a small orifice. If certain geometrical considerations are met, the number of moles per second of material which effuse from the cell and pass through a collimator whose axis is normal to the center of the orifice is

$$n = paD^2(2\pi MRT)^{-\frac{1}{2}}/(D^2+4L^2), \qquad (2)$$

where p is the pressure (d/cm²), a the orifice area (cm²), D the collimator diameter (cm), L the collimator to orifice distance (cm), M the molecular weight of the effusing species, R the gas constant, and T the temperature (°K).

Detailed descriptions of both methods, discussions of the limiting assumptions, and derivation of the equations from the kinetic theory of gases are available in several standard reference works.[3,4]

EXPERIMENTAL

Knudsen Effusion Studies

In the effusion experiments a thoria-lined tungsten effusion cell was used. The molecular beam effusing from the cell orifice passed through a collimator and struck a cooled target. The rate of effusion of material from the cell was found by determining the amount of material which had condensed upon the target, either by direct weighing of the target or by the use of a radioactive tracer.

[3] S. Dushman, *Scientific Foundations of Vacuum Technique* (John Wiley & Sons, Inc., New York, 1949).
[4] I. E. Campbell, *High Temperature Technology* (John Wiley & Sons, Inc., New York, 1956).

The effusion cell used for the iridium is shown in Fig. 1. It was heated by electron bombardment from two filaments which heated the upper and lower halves independently of each other. Temperature was measured with a "Micro-optical pyrometer" from light collected from the blackbody hole. The optical system and pyrometer were calibrated by measuring the brightness temperature of a tungsten ribbon lamp which had been calibrated by the National Bureau of Standards. The cell halves were held at the same temperature by manual regulation of the power to the two filaments, based upon temperature checks of the cell halves through an observation port in the vacuum system. Temperature in the blackbody hole was thus maintained at $T\pm5$°C, and the cell halves were held within 5° to 10°C of each other during a run.

During a run, the effusion cell orifice was directly below the target magazine which contained a collimator and 12 copper target holders. These were in direct contact with the liquid-nitrogen-cooled copper walls of the magazine. The apparatus was constructed in such a manner that the target holders could be removed from the magazine after the targets had been exposed to the effusion beam without breaking the vacuum. The targets themselves were disks of copper or platinum foil. A magnetically operated shutter could be moved between the effusion cell and the collimator to turn the beam on and off.

TABLE I. Iridium vaporization data.

(T°K)	Experiment type	P_{mm}	Target material	ΔH_{298} (3rd law) (kcal/mole)
2100	Effusion	2.29×10^{-6}	Pt	157.8
2196	Effusion	1.06×10^{-5}	Pt	158.2
2228	Effusion	1.69×10^{-5}	Cu	158.6
2282	Effusion	3.43×10^{-5}	Pt	158.9
2337	Effusion	9.40×10^{-5}	Cu	158.1
2375	Effusion	1.30×10^{-4}	Pt	159.0
2454	Effusion	4.76×10^{-4}	Pt	157.8
2492	Effusion	7.45×10^{-4}	Cu	158.0
2545	Effusion	1.04×10^{-3}	Pt	159.7
2630	Effusion	3.82×10^{-3}	Pt	158.1
		(Effusion) Av $\Delta H_{298}=158.4\pm0.5$ (kcal/mole)		
2123	Langmuir	7.04×10^{-6}	...	155.0
2128	Langmuir	2.77×10^{-6}	...	159.2
2193	Langmuir	6.36×10^{-6}	...	161.3
2293	Langmuir	3.18×10^{-5}	...	160.0
2320	Langmuir	8.45×10^{-5}	...	157.4
2391	Langmuir	3.32×10^{-4}	...	155.6
		(Langmuir) Av $\Delta H_{298}=158.1\pm2$ (kcal/mole)		

The quantity of iridium which had been deposited upon the targets was determined by the use of Ir^{192} as a radioactive tracer. The radioactivity of the target with the condensed sample was compared with that of a previously calibrated sample containing the same ratio of tracer to natural isotopes and a known total weight of the reference material. Counting was done with a standard-well-type crystal counter. For the studies of the vaporization of rhodium no tracer was used. In this case the amount of rhodium deposited upon the target was determined directly by weighing the target before and after exposure to the beam. Weighing was done on a Sartorius microbalance to $\pm 5\mu g$. The targets were far enough away from the effusion cell so that Clausing corrections could be neglected.

The effusion cell used in the studies of the vapor pressure of rhodium was identical to that shown in Fig. 1 except that the thoria liner contained a cylindrical channel of $\frac{1}{8}$-in. diam. The channel in this case was an excellent effusion cell since it was possible to pack the rhodium powder around its walls. The use of such an effusion cell was not possible with iridium powder because it tended to sinter into a small button when heated to very high temperatures in the $\frac{1}{8}$-in. channel. This problem was not encountered when larger quantities of iridium powder were used in the cell shown in Fig. 1.

Langmuir Vaporization Studies

In order to obtain a check upon the data obtained from the effusion studies, several data points were obtained for iridium by a Langmuir technique. An iridium cylinder similar in construction to the lower half of the tungsten container shown in Fig. 1 was used. The cylinder was supported, heated, and its temperature determined in the same manner as for the effusion cells. The total amount of material vaporized was determined by weighing the cylinder and supporting rod before and after each experiment. The vaporizing area was taken as the outside area of the cylinder. If the accomodation coefficient of iridium is unity, the small additional area of the inside walls of the depression in the top of the cylinder will make no contribution to the rate of vaporization. Data from this study are more scattered than that obtained from effusion experiments because the cylinder could not be heated and cooled instantaneously, and because the temperature was determined with a precision of only $\pm 10°K$. Iridium vaporizing from the cylinder condensed upon the cooled walls of the metal vacuum system, and any systematic error due to iridium bouncing back against the cylinder is negligible.

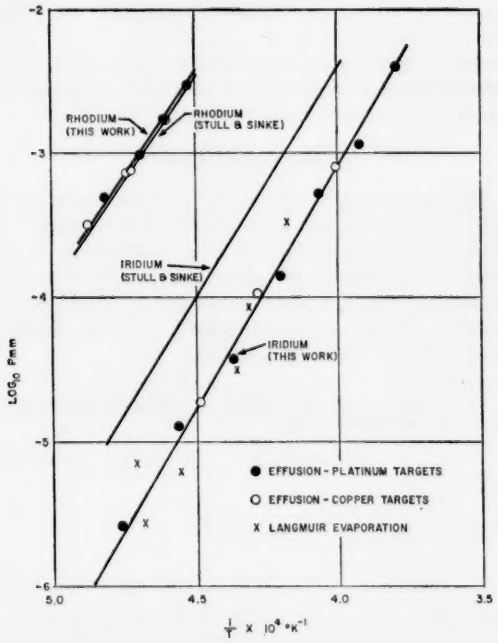

FIG. 2. Log$p$ vs $1/T$ for iridium and rhodium.

TABLE II. Rhodium vaporization data.

T (°K)	P_{mm}	Target material	ΔH_{298} (3rd law) (kcal/mole)
2051	3.20×10^{-4}	Cu	132.4
2077	4.88×10^{-4}	Pt	132.4
2106	7.50×10^{-4}	Cu	132.6
2111	7.66×10^{-4}	Cu	132.8
2130	9.89×10^{-4}	Pt	132.9
2168	1.71×10^{-3}	Cu	133.0
2182	1.70×10^{-3}	Pt	133.8
2205	3.05×10^{-3}	Pt	132.8

Av $\Delta H_{298} = 132.8 \pm 0.3$ kcal/mole

Mass Spectrometric Studies

In order to determine vapor pressure by both the Langmuir and Knudsen techniques it is necessary to know what species are effusing from the cell or vaporizing from the surface. By placing the effusion cell orifice or vaporizing surface close to the entrance slit of a Bendix time-of-flight mass spectrometer, the vaporizing species could be observed. For both iridium and rhodium only monatomic species were observed.

RESULTS

Iridium

The vapor pressures calculated from Eq. (1) and (2) for the vaporization of iridium by Knudsen and Langmuir techniques are given in Table I and are plotted on Fig. 2 along with the estimated data of Stull

and Sinke.[5] The vapor pressures estimated by Stull and Sinke are apparently high because their calculations were based upon a low estimate of the boiling point of iridium. In the effusion studies, the points obtained when copper and platinum targets were used fall upon the same line. If any appreciable fraction of the molecules incident upon the target were reflected, it is probable that this would occur to a different degree for targets of different materials. On this basis it has been assumed here that the amount of reflection was negligible.

The average heat of vaporization of iridium over the temperature range studied was found to be 155±5 kcal/mole from the slope of a line drawn through the effusion data points. Stull and Sinke's $H_T°-H_{298}°$ data[5] were combined with this to yield a ΔH_{298} for sublimation of 158±5 kcal/mole. The error was estimated by picking several possible lines through the points.

A more satisfactory method for checking the results of vapor pressure studies such as that reported here is the so-called third-law calculation utilizing free energy functions.[6]

For any reaction

$$\Delta(F_T-H_{298}/\mathrm{T})_{\text{reaction}}=(F_T-H_{298}/T)_{\text{products}}-(F_T-H_{298}/T)_{\text{reactants}}=(\Delta F/T)-(\Delta H_{298}/T), \quad (3)$$

and

$$\Delta F/T=-R\ln K_{\text{eq}}. \quad (4)$$

In this case $\mathrm{Ir}_{(g)}$ is the product, $\mathrm{Ir}_{(s)}$ is the reactant, and K_{eq} may be taken to be identical with P_{Ir}. The free-energy functions for solid and gaseous iridium have been tabulated from heat capacity and spectroscopic data by Stull and Sinke. The results of third-law calculations in which Stull and Sinke's free-energy function were used are also given in Table I. Although the Langmuir data are quite scattered, they obviously agree quite well with the effusion data. Since this would be expected for a metal, the two methods serve as an excellent check upon each other. A further check is obtained by the excellent agreement between the slope and third law ΔH_{298} values. The measured pressures and calculated heats of vaporization obtained in this work are in essential agreement with those obtained with a Langmuir technique at lower temperatures by Hampson and Walker.[7]

The solid line drawn through the data points for iridium in Fig. 2 was obtained from Eq. (3) using $\Delta H_{298}=158.4$ kcal/mole. This line is represented by

$$\log_{10}P_{mm}=10.46-(33980/T), \quad (5)$$

over the temperature range studied.

The boiling point of iridium was calculated by estimating the average heat of vaporization for liquid iridium from the melting point to 5000°K. This quantity was used with vapor pressure at the melting point and the integrated Clausius-Clapeyron equation to obtain a boiling point of approximately 4800°K.

Rhodium

The data obtained for the vaporization of rhodium by the effusion method are given in Table II and plotted on Fig. 2 along with the estimated vapor-pressure data of Stull and Sinke. There is no appreciable difference between the measured and estimated data. The third-law calculations were done in a manner identical to those described for iridium. The average third-law heat of vaporization of 132.8±0.3 kcal/mole is in excellent agreement with that of 133±2 kcal/mole obtained by the slope method.

The solid line drawn through the data points for rhodium in Fig. 2 was obtained from Eq. (3), using $\Delta H_{298}=132.8$ kcal/mole. This line is represented by

$$\log P_{mm}=10.28-(28300/T), \quad (6)$$

over the temperature range studied. The boiling point of rhodium was estimated to be 3980°K in a manner similar to that described for iridium.

ACKNOWLEDGMENTS

The authors wish to thank Dr. R. J. Barriault for his aid and support, and F. Bourgelas and P. Rosen for their aid in carrying out the experimental part of this work. This research was sponsored by the Advanced Research Projects Agency, monitored by the Materials Central, Wright Air Development Division, Wright-Patterson Air Force Base, Ohio.

[5] D. R. Stull and G. C. Sinke, *Thermodynamic Properties of the Elements* (American Chemical Society, Washington, D. C., 1956).

[6] J. L. Margrave, J. Chem. Educ. **32**, 520 (1955).

[7] R. S. Hampson and R. F. Walker, National Bureau of Standards (private communication).

Potential Curves for Doubly Positive Diatomic Ions

A. C. HURLEY AND V. W. MASLEN

Division of Chemical Physics, C.S.I.R.O. Chemical Research Laboratories, Melbourne, Australia

(Received December 28, 1960)

An integral form of the quantum-mechanical virial theorem, applicable to ionic as well as neutral systems, is established. This theorem is used to derive an approximate expression for the potential curve for a doubly positive diatomic ion in terms of the corresponding curve for a related neutral molecule. The appearance potentials of a number of these ions are calculated and compared with values obtained from electron-impact measurements. Satisfactory agreement is found, but a crucial test of the theory is vitiated by uncertainties in the experimental value of either the appearance potential of the doubly charged ion or the dissociation energy of the corresponding neutral molecule. The accuracy of the approximations underlying the theory is estimated by a series of calculations on two-electron systems.

I. INTRODUCTION

IN recent years a number of appearance potentials of doubly positive diatomic ions has been observed[1,2] and it is therefore of interest to have available theoretical estimates of these quantities. It is to be expected that a calculation of the energies of these systems by conventional quantum-mechanical methods would encounter unusual difficulties. Thus the removal of two electrons from a diatomic molecule cannot be considered as a small perturbation and the use of the same orbitals before and after ionization, as is customary in calculations of ionization potentials, would be very unrealistic. Again, the correlation energy will change markedly in the transition to a system with two fewer electrons.

In this paper an alternative approach is developed. Based on the quantum-mechanical virial theorem, it leads to an approximate relationship between the potential curves of the doubly charged ion and a related neutral molecule and, from this, the relevant appearance potential may be obtained.

II. INTEGRATED VIRIAL THEOREM FOR IONIC MOLECULES

Let $E(s)$, $T(s)$, and $V(s)$ be the total energy, mean kinetic energy, and mean potential energy of a polyatomic molecule $A_1A_2\cdots A_N$ in the electronic state X and with nuclei situated at the points $s\mathbf{R}_1$, $s\mathbf{R}_2\cdots s\mathbf{R}_N$. If, as s tends to infinity with $\mathbf{R}_1$, $\mathbf{R}_2\cdots\mathbf{R}_N$ fixed, the molecule in state X dissociates into atoms and ions $A_1^{Q_1}$, $A_2^{Q_2}$, $\cdots A_N^{Q_N}$, Q_i being the charge on fragment A_i, then the binding energy $B(\mathbf{R}_i)$ for the nuclear configuration $\mathbf{R}_1$, $\mathbf{R}_2$, $\cdots\mathbf{R}_N$ is given by

$$B(\mathbf{R}_i)=E(\infty)-E(1)=-\sum_{i<j}^{N}(Q_iQ_j/R_{ij})+\int_1^\infty\{T(\infty)-T(s)\}ds, \qquad (2.1)$$

where $R_{ij}=|\mathbf{R}_i-\mathbf{R}_j|$.

Proof: The quantum-mechanical virial theorem may be expressed in the form[3,4]

$$2T(s)+V(s)+s[dE(s)/ds]=0. \qquad (2.2)$$

From (2.2) and the relations

$$E(s)=T(s)+V(s) \qquad (2.3)$$

$$T(\infty)=-E(\infty), \qquad (2.4)$$

we obtain

$$(d/ds)\{s[E(s)-E(\infty)]\}=T(\infty)-T(s), \qquad (2.5)$$

which may be integrated over s to yield

$$E(\infty)-E(1)=\int_1^\infty\{T(\infty)-T(s)\}ds-\lim_{s\to\infty}s\{E(s)-E(\infty)\}. \qquad (2.6)$$

Now for large s and the assumed dissociation products

$$E(s)-E(\infty)=\sum_{i<j}^{N}(Q_iQ_j/sR_{ij})+o(1/s),$$

so that

$$\lim_{s\to\infty}s[E(s)-E(\infty)]=\sum_{i<j}^{N}(Q_iQ_j/R_{ij}),$$

and (2.6) is seen to be equivalent to (2.1). The relation (2.1), like the usual differential form of the virial theorem, holds not only for the exact quantities B, T, and E, but also for the same quantities calculated using approximate wave functions of optimum scale.[3,4]

III. APPLICATION TO DOUBLY CHARGED DIATOMIC IONS

For a diatomic system, it is convenient to express T as an explicit function of the distance sR rather than

[1] J. T. Herron and V. H. Dibeler, J. Chem. Phys. **32**, 1884 (1960).

[2] J. D. Morrison (private communication).

[3] C. A. Coulson and R. P. Bell, Trans. Faraday Soc. **41**, 141 (1945).

[4] A. C. Hurley, Proc. Roy. Soc. (London) **A226**, 170 (1954).

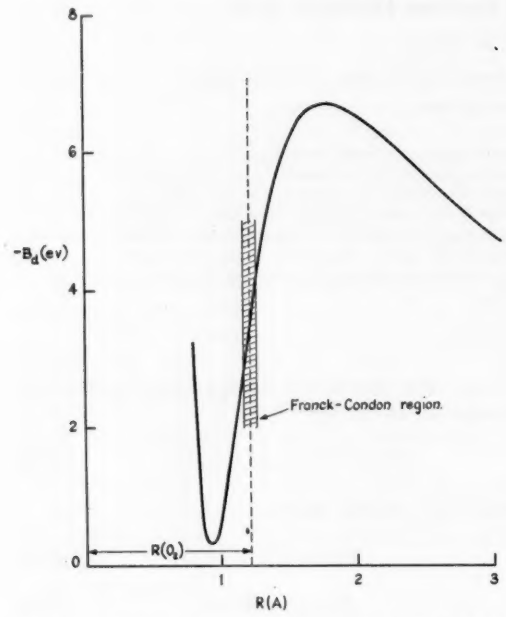

FIG. 1. Calculated potential curve for ground state of O_2^{++}.

the scale factor s. With this modification (2.1) becomes

$$B(R)=-[(Q_1Q_2)/R]+\int_1^\infty\{T(\infty)-T(sR)\}ds$$
$$=-[(Q_1Q_2)/R]$$
$$+(1/R)\int_R^\infty\{T(\infty)-T(R')\}dR', \quad (3.1)$$

where R is the nuclear separation.

Now since the second ionization potential of an atom is always much greater than the first, the ground state and low-lying excited states of a doubly positive diatomic ion (d) will in most cases dissociate adiabatically into two singly positive atomic ions, so that $Q_1=Q_2=1$ and (3.1) becomes

$$B_d(R)=-(1/R)+(1/R)\int_R^\infty\{T_d(\infty)-T_d(R')\}dR'. \quad (3.2)$$

The calculation of $B_d(R)$ is thus reduced to a determination of T_d as a function of nuclear separation. We estimate T_d from the potential curve for the neutral molecule (n) obtained from (d) by reducing both nuclear charges by unity. We expect that as we go from (n) to (d) the most significant change in the wave function will be a more or less uniform contraction caused by the larger nuclear charges of (d). Thus T_d is calculated using the approximate wave function[5];

$$\Psi_d(t, R; x_i)=t^{3m/2}\Psi_n(tR; tx_i), \quad (3.3)$$

[5] This assumption is best suited to homonuclear or almost homonuclear ions. It clearly fails for hydrides.

where $\Psi_n(R; x_i)$ is the exact wave function for (n) and t is a variable scaling factor. The factor $t^{3m/2}$ where m is the number of electrons, ensures that Ψ_d is normalized.

Since for the wave function (3.3)

$$T_d(R)=t^2T_n(tR), \quad (3.4)$$

Eq. (3.2) yields the approximate expression

$$B_d(R)=-(1/R)+(1/R)$$
$$\times\int_R^\infty\{t^2(\infty)T_n(\infty)-t^2(R')T_n(tR')\}dR'. \quad (3.5)$$

So far, we have left t arbitrary. If it were determined as a function of R by minimizing the integral

$$E_d(R)=\int\Psi_d\mathfrak{H}\Psi_d\cdot d\tau,$$

then it follows from the virial theorem for approximate wave functions of optimum scale[3,4] that $B_d(R)$, determined from (3.5), would be identical with

$$B_d(R)=\int\Psi_d(\infty)\mathfrak{H}\Psi_d(\infty)d\tau-\int\Psi_d(R)\mathfrak{H}\Psi_d(R)d\tau. \quad (3.6)$$

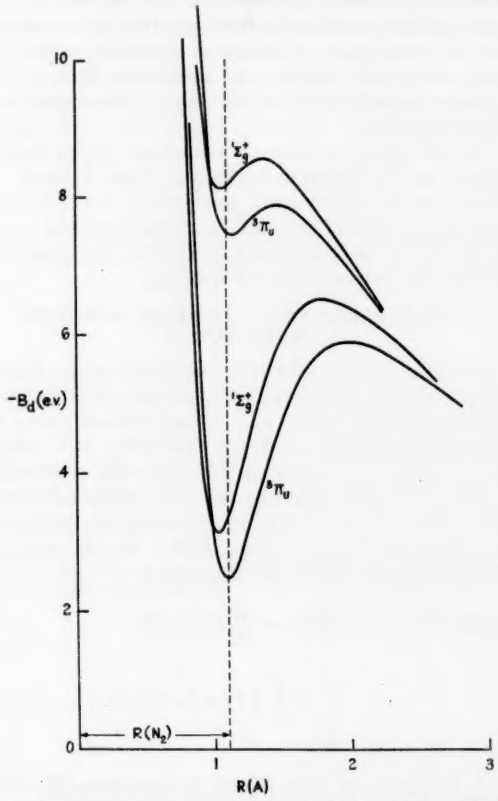

FIG. 2. Calculated potential curves for N_2^{++}. Upper pair assuming $D_0(C_2)=3.6$ ev, lower pair assuming $D_0(C_2)=6.504$ ev.

TABLE I.[a] Predicted appearance potentials (ev).

d	n	$D_0(n)$	$I_p^{++}{}_{calc}$	ΔI_p^{++}	$I_p^{++}{}_{obs}\pm 0.3$ ev	$-[\partial I_p^{++}/\partial D_0(n)]$	$D_0(n)_{est}$
F_2^{++}	O_2	5.114[b]	43.26	0.09	...	1.01	
Cl_2^{++}	S_2	3.6*(3.3, 4.4)[b]	32.57	0.12	32.6[e]	1.19	3.57
Br_2^{++}	Se_2	2.8±.1[b]	29.58	0.06	30.0[e]	1.13	2.43
I_2^{++}	Te_2	2.3±.2[b]	25.74	0.05	...	1.16	
$N_2^{++}(^3\Pi_u)$	C_2	3.6[e] 6.50[b]	46.31 41.32	0.02	42.7[f]	1.71 1.72	5.70
O_2^{++}	N_2	9.756[b]	35.88	0.69	...	1.24	
NO^{++}	CN	7.6*(6.2, 6.9, 8.2)[b]	38.17	0.44	39.8[f]	1.48	6.50
CO^{++}	BN	4[b] 5[e]	42.80 41.17	0 0	41.7[f]	1.63 1.64	4.68
ClF^{++}	SO	5.357[d]	37.20	0.20	...	1.20	
			Excited States				
CO^{++}	BN	4 5	unstable 45.7		45.7[f]		
$N_2^{++}(^1\Sigma_g^+)$	C_2	3.6 6.50	47.0 42.1		43.8[f]		

[a] The parameter $t(\infty)$ employed in these calculations ranges from 1.14 to 1.32. For molecules composed of first row atoms, it was calculated from the tables of Roothaan[7] and in other cases, from Slater functions. An asterisk denotes a favored value.

[b] T. L. Cottrell, *The Strengths of Chemical Bonds* (Butterworths Publications, Ltd., London, 1958), 2nd ed.; A. G. Gaydon, *Dissociation Energies* (Chapman and Hall, Ltd., London, 1953), 2nd ed.

[c] G. Herzberg, work cited in reference 8, p. 513.

[d] L. Brewer, J. Chem. Phys. **31**, 1143 (1959); D. G. H. Marsden, *ibid.* **31**, 1144 (1959).

[e] J. T. Herron and V. H. Dibeler, J. Chem. Phys. **32**, 1884 (1960).

[f] F. H. Dorman and J. D. Morrison J. Chem. Phys. (to be published).

We will usually use the simpler approximation of constant t, determined at infinite nuclear separation. In this case, from (3.4) and (3.5),

$$t(R)=t(\infty)=\{[T_d(\infty)]/[T_n(\infty)]\}^{\frac{1}{2}}, \qquad (3.7)$$

and

$$B_d(R)=-(1/R)+(t^2(\infty)/R)\int_R^\infty\{T_n(\infty)-T_n[t(\infty)R']\}dR'. \qquad (3.8)$$

But from (3.1), assuming that (n) dissociates adiabatically into neutral atoms,

$$B_n\{t(\infty)R\}=(1/t(\infty)R)\int_{t(\infty)R}^\infty\{T_n(\infty)-T_n(R')\}dR'$$
$$=(1/R)\int_R^\infty\{T_n(\infty)-T_n[t(\infty)U]\}dU, \qquad (3.9)$$

so that

$$B_d(R)=-(1/R)+t^2(\infty)B_n\{t(\infty)R\}. \qquad (3.10)$$

Equations (3.7) and (3.10) enable us to calculate $B_d(R)$ very easily from the potential curve for the corresponding state of the isoelectronic neutral molecule and the electronic kinetic energy of the dissociation products.

In deriving Eq. (3.10) two approximations have been made; Eq. (3.3) which assumes that a good wave function for (d) may be obtained simply by rescaling Ψ_n and Eq. (3.7) which assumes further that the optimum scale factor is independent of R. In an appendix to this paper the accuracy of these approximations is investigated for systems isoelectronic with the hydrogen molecule. It appears that (3.7) always provides a good approximation to the optimum $t(R)$ but that the use of the simple scaled function (3.3) will lead to accurate results only when $t(\infty)$ lies in the range $1\leq t(\infty)\leq 1.5$. Fortunately, this range includes most cases of physical interest.

IV. ELIMINATION OF INNER SHELLS

Although Eqs. (3.7) and (3.10) may be used directly to calculate $B_d(R)$, it is probably better to modify these equations by considering electrons in the valence shell apart from those in inner shells. Otherwise the value of the scale factor $t(\infty)$ in (3.7) would be determined primarily by optimizing the wave functions of the most tightly bound inner shells rather than those of the valence shell.

Thus for both (d) and (n) we consider approximate wave functions of the form

$$\Psi=\mathcal{A}\Psi_{k_1}\Psi_{k_2}\Psi_v. \qquad (4.1)$$

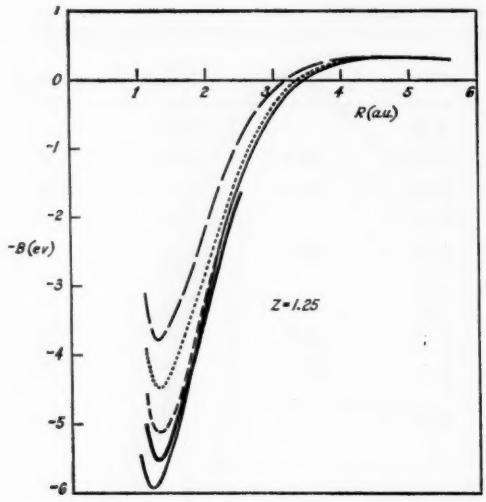

FIG. 3. Potential curves for molecule with $Z=1.25$. Curves A — — — Wang function, B ..... Weinbaum function, C ——— accurate, D ——— virial, constant scale factor [Eqs. (A1)], E ------ virial, variable scale factor [Eqs. (A2), (A3)].

Here $\mathfrak{A}$ is the antisymmetrizing operator and Ψ_{k_1}, Ψ_{k_2}, and Ψ_v are optimum group functions for the inner shell electrons on the nuclei A_1 and A_2 and the valence electrons, respectively. These functions satisfy the generalized orthogonality conditions given by McWeeny.[6] Consequently, the total kinetic energy T is given by

$$T=T_{k_1}+T_{k_2}+T_v. \tag{4.2}$$

Now we expect that the kinetic energies of the inner shell electrons will be almost independent of R, since their wave functions are but little affected by molecular formation. We therefore make the approximations

$$T_{k_1}(R)=T_{k_1}(\infty),$$
$$T_{k_2}(R)=T_{k_2}(\infty) \tag{4.3}$$

and (3.1) reduces to

$$B(R)=-(Q_1Q_2/R)+(1/R)\int_R^\infty\{T_v(\infty)-T_v(R')\}dR'. \tag{4.4}$$

The optimum group function for the valence shell electrons of (d) is now approximated in terms of that for (n)

$$\Psi_{d,v}(t, R; x_i)\approx\beta^{m_v/2}\Psi_{n,v}(tR; tx_i), \tag{4.5}$$

where m_v is the number of electrons in the valence shell. No specific relationship between the inner-shell group functions of (n) and (d) need be assumed, since the kinetic energy of these inner shells has been eliminated by (4.2) and (4.3).

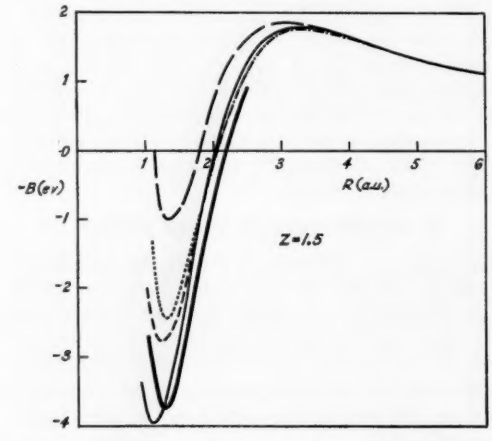

FIG. 4. Potential curves for molecule with $Z=1.5$. Curves as for Fig. 3.

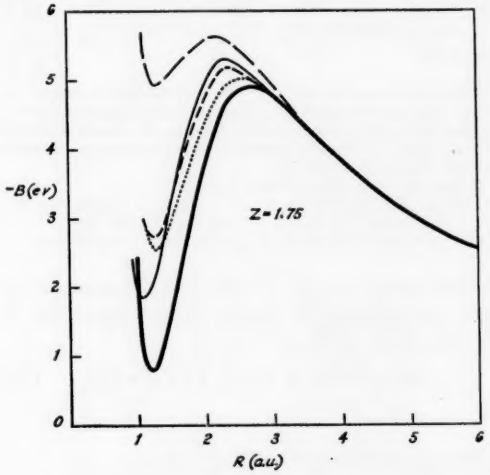

FIG. 5. Potential curves for molecule with $Z=1.75$. Curves as for Fig. 3.

The development of Sec. III may now be repeated, replacing total wave functions and kinetic energies with corresponding quantities for the valence-shell electrons only. We thus obtain, in place of (3.7) and (3.10),

$$t(R)=t(\infty)=\{T_{d,v}(\infty)/T_{n,v}(\infty)\}^{\frac{1}{2}} \tag{4.6}$$

$$B_d(R)=-(1/R)+t^2(\infty)B_n\{t(\infty)R\}. \tag{4.7}$$

V. APPLICATIONS OF (4.7). O_2^{++} AND N_2^{++}

All equations of the preceding sections imply the use of atomic units. When R is expressed in angstroms and

[6] R. McWeeny, Proc. Roy. Soc. (London) **A253**, 242 (1959), Eq. (1.3).

energies in electron volts, Eq. (4.7) must be replaced by

$$B_d(R) = -(14.399/R) + l^2(\infty) B_n\{t(\infty) R\}. \quad (5.1)$$

The modified form (5.1) will be used in the subsequent calculations.

A. O_2^{++}

From Roothaan's computations for first-row atoms,[7] using simple wave functions, we obtain, for O^+

$$T_{O^+,v} = \tfrac{1}{2} T_{d,v}(\infty) = -E_{\text{total}} - T_{\text{inner shell}}$$
$$= 74.2321 - (7.6511)^2 = 15.6928 \text{ a.u.}$$

Likewise, for N,

$$T_{N,v} = \tfrac{1}{2} T_{n,v}(\infty) = 9.8440 \text{ a.u.}$$

Thus, from (4.6) and (5.1)

$$t(\infty) = (15.6928/9.8440)^{\frac{1}{2}} = 1.2626, \quad (5.2)$$

and

$$B_d(R) = -(14.399/R) + 1.5941 B_n(1.2626R). \quad (5.3)$$

Fitting $B_n(r)$ with a Morse curve

$$B_n(r) = D_e\{2\exp[-\beta(r-r_e)] - \exp[-2\beta(r-r_e)]\},$$

where

$$D_e = 9.902 \text{ ev}, \quad \beta = 2.690 \text{ A}^{-1}, \quad r_e = 1.094 \text{ A},^8$$

we obtain, for O_2^{++}, the potential curve

$$B_d(R) = -(14.399/R) + 15.785(2e^{-\alpha} - e^{-2\alpha}), \quad (5.4)$$

where

$$\alpha = 2.943 - 3.397R.$$

This curve is shown in Fig. 1. It may be used to estimate the appearance potential for O_2^{++} in a vertical transition from the ground state of O_2, thus

$$I_p^{++} = D_0(O_2) + 2I(O) - B_d(1.207 \text{ A})$$
$$= 5.082 + 27.228 + 3.567$$
$$= 35.877 \text{ ev}.$$

Because of the width of the ground-state vibrational level of O_2 (Franck-Condon region) O_2^{++} ions may be expected to appear for bombardment energies slightly less than the calculated value.

B. N_2^{++}

For O_2^{++} the value of the dissociation energy of the corresponding neutral molecule is well established. This is not so for N_2^{++} and, in this case, we try two favored values of $D_0(C_2)$, viz., 6.504 ev (150 kcal) and 3.6 ev (83 kcal). A further complication arises here in that C_2 has a low-lying excited state ($^3\Pi_u$) only 610 cm^{-1} above the ground state.[9] Thus, in Fig. 2, we present two pairs of curves for N_2^{++}, using Herzberg's values[8] for β, r_e, etc. and $t = 1.3183$. A point of interest in the figure is that, for N_2^{++}, the state $^3\Pi_u$ is predicted to lie below $^1\Sigma_g^+$, i.e., the situation found in C_2 is reversed in N_2^{++}.

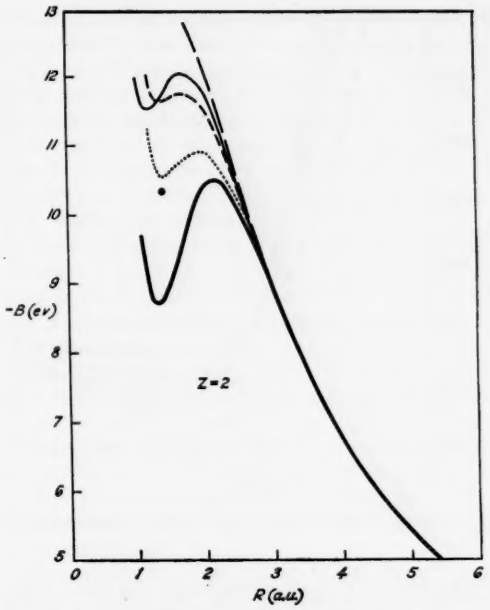

FIG. 6. Potential curves for molecule with $Z=2$ (He_2^{++}) Curves as for Fig. 3, ● local minimum of energy for Weinbaum function.

VI. PREDICTED APPEARANCE POTENTIALS. DISCUSSION

An analysis of the type outlined in Sec. V has been applied to a number of molecular ions, chiefly with component atoms from the first row of the periodic table, but also for several other cases. The results of these calculations are given in Table I. Where doubt exists as to the correct $D_0(n)$, values of $I_p^{++}{}_{\text{calc}}$ have been given either for the favored value or for a number of values of this quantity. For completeness, we have included $-[\partial I_p^{++}/\partial D_0(n)]$ together with an estimate, ΔI_p^{++}, of the possible lowering of I_p^{++} due to the Franck-Condon spread.

The column of Table I labeled $I_p^{++}{}_{\text{obs}}$ has been compiled from electron impact data. Finally, the column on the extreme right of the table gives those $D_0(n)$ which would bring the observed and calculated values of I_p^{++} into agreement. The evidence presented in this column favors the higher of the current values of

[7] C. C. J. Roothaan, Technical Report (1955) of the Laboratory of Molecular Structure and Spectra, Department of Physics, University of Chicago, Chicago, Illinois.

[8] G. Herzberg, *Molecular Spectra and Molecular Structure* I. *Spectra of Diatomic Molecules* (D. Van Nostrand Company, Inc., Princeton, New Jersey, 1950), pp. 551–3.

[9] E. A. Ballik and D. A. Ramsay, J. Chem. Phys. **31**, 1128 (1959).

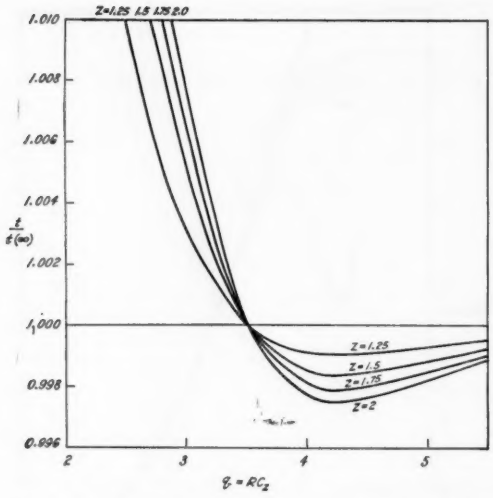

FIG. 7. Variation of scale factor t with scaled nuclear separation $q = RC_z$.

$D_0(BN)$ and $D_0(C_2)$. An extension of the table might profitably be used to clarify other dissociation energy data. Further support for the higher value of $D_0(BN)$ is provided by the observation of a stable excited state of CO^{++}. The calculations predict such a state for $D_0(BN)$ equal to 5 ev, but not for $D_0(BN)$ equal to 4 ev.

It will be noticed in the table that appearance potentials have not been observed for F_2^{++} or O_2^{++}, which are the only cases for which the corresponding $D_0(n)$ is firmly established. Thus, the present method of calculating $B_d(R)$ and I_p^{++} has yet to be subjected to a crucial test and the observation of one or other of these missing entries would seem to provide it.

ACKNOWLEDGMENT

The authors are indebted to Dr. J. D. Morrison for stimulating discussions and permission to quote his experimental results prior to publication.

APPENDIX

We consider the series of hypothetical molecules obtained by varying the charges Z on the nuclei of the hydrogen molecule. Five systems ($Z=1$, 1.25, 1.5, 1.75, 2) are considered. Although only the first and last of these are real molecules (H_2 and He_2^{++}) the results for the other systems enable us to estimate the accuracy of the theory of Sec. III, in particular, Eqs. (3.3) and (3.7).

Figures 3, 4, 5, and 6 show five potential curves for each of the molecules $Z=1.25$, 1.5, 1.75, 2.0.

(1) That calculated from the Hamiltonian integral using a covalent function with optimum orbital exponent c_Z for each value of R (Wang function).

(2) That calculated using covalent and ionic terms, each with the orbital exponent c_Z determined by calculation A (Weinbaum function).[10]

(3) The accurate potential curve. For $Z=1$ and $Z=2$ this curve was obtained from the calculations of Kolos and Roothaan[11] (H_2, He_2^{++}, small R values), Vanderslice *et al.*[12] (H_2, all values of R) and McLean *et al.*[13] (He_2^{++}, large R values). The accurate curves for $Z=1.25$, 1.5, and 1.75 were obtained by interpolation assuming that the logarithm of the error of the Weinbaum calculations B varies linearly with Z for a fixed value of R. This form of interpolation is suggested by the approximately exponential form of the error curves for the Weinbaum calculations on H_2 and He_2^{++}. These accurate curves for $Z=1.25$, 1.5, and 1.75 should be correct to within 0.1 ev and provide a standard for assessing the other potential curves.

(4) The curve obtained from the analogs of Eqs. (3.7) and (3.10). Here the molecule Z replaces (d) and (n) is $H_2(Z=1)$. Since, for molecule Z, $Q_1=Q_2=(Z-1)$ and $T(\infty)=Z^2$, the analogs of (3.7) and (3.10) are

$$B_Z(R) = -[(Z-1)^2/R] + t^2(\infty) B_1\{t(\infty)R\}$$
$$t(\infty) = Z. \qquad \text{(A1)}$$

In this calculation $B_1(R)$ was taken as Vanderslice *et al.*'s[12] "most likely" potential curve for H_2. Since

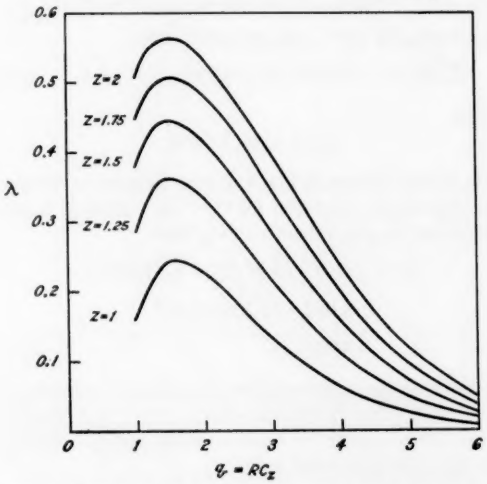

FIG. 8. Variation of λ for the Weinbaum function $\Psi = \Psi_{cov.} + \lambda\Psi_{ionic}$.

[10] For He_2^{++} all parameters were varied independently to obtain the local minimum in the energy for the Weinbaum function (Fig. 6). Since in this extreme case the local minimum lay only 0.2 ev below curve B the orbital exponent was not revaried for the other calculations.

[11] W. Kolos and C. C. J. Roothaan, Revs. Modern Phys. **32**, 219 (1960).

[12] J. T. Vanderslice, E. A. Mason, W. G. Maisch, and E. R. Lippincott J. Mol. Spectroscopy **3**, 17 (1959); **5**, 83 (1960), Errata.

[13] A. D. McLean, A. W. Weiss, and M. Yoshimine (unpublished), referred to by Kolos and Roothaan, see work cited in reference 11.

(3.10) and (3.7), applied to the valence-shell electrons, are the equations used to calculate potential curves for doubly positive diatomic ions (Sec. V) and the appearance potentials of these ions (Sec. VI), the departure of curve D from the accurate curve C enables us to estimate the accuracy of these calculations for a given value of $t(\infty)$.

(5) This calculation dispenses with the assumption that the scaling factor $t(R)$ is independent of R [Eq. (3.7)]. Instead we assume that t varies with R in the same way as for the calculations A. Thus in terms of the variable $q=Rc_Z$ the scaling factor t_Z for the molecule Z is given by

$$t_Z(R)\equiv t_Z(q/c_Z)=[c_Z(q)/c_1(q)]. \qquad \text{(A2)}$$

Having obtained $t_Z(R)$ in this way we obtain $B_Z(R)$ from the analog of Eq. (3.5), i.e.,

$$B_Z(R)=-[(Z-1)^2/R]+(1/R)$$
$$\times\int_R^\infty\{t_Z^2(\infty)T_1(\infty)-t_Z^2(R')T_1(R't_Z)\}dR'. \qquad \text{(A3)}$$

Here $T_1(R)$ is the accurate kinetic energy of the hydrogen molecule derived from Vanderslice *et al.*'s[12] potential curve $E(R)$ and the virial relation

$$T=-E-R(dE/dR).$$

In this calculation we have assumed that the optimum scaling of the exact H_2 wave function for a calculation on the system Z is the same as the optimum scaling of the Wang function. This is clearly a better approximation than the use of the constant scale factor $t(\infty)$. A satisfactory feature of the curves E is that they all lie above the accurate curves for all R values. A curve calculated with a truly optimum t function must have this property, for such a calculation is fully equivalent to one based on the Hamiltonian integral.

The important region of the curves for the calculations of Secs. V and VI is that between the minimum and the maximum. From Figs. 3 and 4 we see that for $Z=t(\infty)\leq 1.5$ the virial curve D differs from the accurate curve by at most 0.5 ev in this region and that for $t(\infty)=1.25$ which approximates most closely to the values used for real molecules (footnote a to Table I) the errors are considerably smaller than this. While it is clearly not possible to set up a unique correspondence between a calculation on a real molecule and on the hypothetical molecule with the same value of $t(\infty)$, these results may indicate the order of magnitude of the errors to be expected in Figs. 1 and 2 and Table I.

Figures 5 and 6 show that for $t(\infty)>1.5$ both the virial curves D and E rapidly become less accurate. The very rapid deterioration of the Wang function for $Z>1.5$ is also apparent; for He_2^{++} $(Z=2)$ it even fails to predict a minimum in the curve. However, even for these large values of $t(\infty)$ there is comparatively little difference between the two virial curves D and E. This indicates that there is little to be gained by replacing the assumption of constant scaling [Eq. (3.7) or (4.6)] by a more refined scaling procedure such as (A2), except that the latter does provide an upper limit to the exact curve.

These points are clearly illustrated in Figs. 7 and 8. Figure 7 shows the ratio $[t/t(\infty)]$ from the Wang calculations A plotted against the scaled nuclear separation $q=Rc_Z$. We see that $[t/t(\infty)]$ is very close to unity except for small values of R where t rises steeply. This region of small R begins to affect the integral (A3) near the minimum of the potential curve. As a result curve D dips sharply below curve E in this region and eventually falls below the accurate curve.

Figure 8 shows the variation with q of the ratio λ between the coefficients of the ionic and covalent terms in the Weinbaum calculation B. If the best wave function for the molecule Z could be obtained simply by rescaling the best wave function for H_2, then any variable parameter in the wave functions, such as λ, would show the same dependence on the scaled nuclear separation q for all values of Z. The progressive departure from this situation as Z increases is evident in Fig. 8.

THE JOURNAL OF CHEMICAL PHYSICS VOLUME 34, NUMBER 6 JUNE, 1961

Effect of Configuration Interactions on the Dissociation Energy and Hyperfine Structure Constants of the NO Molecule*

M. YAMAZAKI,† M. SAKAMOTO, K. HIJIKATA,‡ AND CHUN C. LIN

Department of Physics, University of Oklahoma, Norman, Oklahoma

(Received October 3, 1960)

By means of a 23-dimensional configuration interaction calculation the energy and eigenfunction of the ground $^2\Pi$ state are determined resulting in dissociation energy of 2.2 ev. The magnetic hyperfine and nuclear quadrupole coupling constants are calculated from this molecular function. The contact term $|\Psi(0)|^2$ is obtained as 0.71×10^{-24} cm^{-3} which agrees well with experiment. The values of

$$\langle(3\cos^2\chi-1)\sigma/r^3\rangle_{Av}, \quad \langle\sin^2\chi/r^3\rangle_{Av}, \quad \text{and} \quad \langle r^{-3}\rangle_{Av}$$

are not much affected by the configuration interactions.

I. INTRODUCTION

In a previous paper[1] Lin, Hijikata, and Sakamoto showed the calculations of the hyperfine coupling constants of nitric oxide based on the wave function of Brion, Moser, and Yamazaki.[2] The agreement with experiment was not entirely satisfactory, especially in the case of $|\Psi(0)|^2$. Since the dissociation energy obtained by Brion, Moser, and Yamazaki differs considerably from the experimental value, one might expect some improvement in the results of dissociation energy and the hyperfine coupling constants by means of a thorough configuration interaction calculation. In this article we will describe first how we selected the electronic configurations to obtain the best molecular eigenfunction of the ground state and then give the results of our calculations for the dissociation energy, the magnetic hyperfine and the nuclear quadrupole coupling constants of the ground state.

II. CONFIGURATION INTERACTIONS

Since we are interested only in the ground state of the nitric oxide molecule, we shall first examine the quantity

$$H_{0i}=\int\psi_0^*H\psi_i d\tau \tag{1}$$

for all the 218 states formed by the various ways of assigning the 15 electrons in the eight molecular orbitals[2] (1σ, 2σ, 3σ, 4σ, 5σ, 6σ, 1π, 2π) with 1σ and 2σ always filled. In this paper we shall use ψ for the normalized wave function of a state arising from a particular configuration while Ψ is reserved for the composite wave function obtained by CI calculation, i.e.,

$$\Psi=\sum_i c_i\psi_i. \tag{2}$$

Only 44 states have nonvanishing H_{0i}, which are listed in Table I. The first column of this table defines the electronic configurations, showing the number of electrons in the orbitals. The second column is the labeling of the states, a notation which we will use in the succeeding works. The subscript number refers to the particular spin function to be associated with the configuration. For states with three unpaired electrons, the spin functions are

$$\begin{aligned}\text{Subscript } 1 \quad & (\alpha\alpha\beta-\alpha\beta\alpha)/\sqrt{2},\\ 2 \quad & (2\beta\alpha\alpha-\alpha\alpha\beta-\alpha\beta\alpha)/\sqrt{6}.\end{aligned} \tag{3}$$

When five unpaired electrons are present, the spin functions are taken as[3]

$$\begin{aligned}\text{Subscript } 1 \quad & (\alpha\alpha\beta\alpha\beta-\alpha\alpha\beta\beta\alpha-\alpha\beta\alpha\alpha\beta+\alpha\beta\alpha\beta\alpha)/2,\\ 2 \quad & (-\alpha\alpha\beta\alpha\beta-\alpha\beta\alpha\alpha\beta+\alpha\alpha\beta\beta\alpha+\alpha\beta\alpha\beta\alpha\\ & \quad +2\beta\alpha\alpha\alpha\beta-2\beta\alpha\alpha\beta\alpha)/(12)^{\frac{1}{2}},\\ 3 \quad & (-2\alpha\alpha\alpha\beta\beta+\alpha\alpha\beta\alpha\beta+\alpha\alpha\beta\beta\alpha+\alpha\beta\alpha\alpha\beta\\ & \quad +\alpha\beta\alpha\beta\alpha-2\alpha\beta\beta\alpha\alpha)/(12)^{\frac{1}{2}},\\ 4 \quad & (-2\alpha\alpha\alpha\beta\beta-\alpha\beta\alpha\alpha\beta-\alpha\beta\alpha\beta\alpha+\alpha\alpha\beta\alpha\beta\\ & +\alpha\alpha\beta\beta\alpha+2\alpha\beta\beta\alpha\alpha+2\beta\alpha\alpha\alpha\beta+2\beta\alpha\alpha\beta\alpha-4\beta\alpha\beta\alpha\alpha)/6,\\ 5 \quad & (-\alpha\alpha\alpha\beta\beta-\alpha\alpha\beta\alpha\beta-\alpha\alpha\beta\beta\alpha+\alpha\beta\alpha\alpha\beta\\ & +\alpha\beta\alpha\beta\alpha+\alpha\beta\beta\alpha\alpha+\beta\alpha\alpha\alpha\beta+\beta\alpha\alpha\beta\alpha\\ & \quad +\beta\alpha\beta\alpha\alpha-3\beta\beta\alpha\alpha\alpha)/(18)^{\frac{1}{2}}.\end{aligned} \tag{4}$$

In constructing the wave functions, the unpaired orbitals in the first column of Table I, in the order of right to left, are to be associated, respectively, with each of the α's and β's in the triple or quintuple products of the spin functions in (3) and (4). The matrix elements $H_{ii}-H_{00}$ and H_{0i} are given, respectively, in the

* Supported by the Air Force Cambridge Research Center, Air Research and Development Command, USAF.

† On leave from Kanazawa University, Kanazawa, Japan.

‡ On leave from the University of Electro-Communications, Tokyo, Japan.

[1] C. C. Lin, K. Hijikata, and M. Sakamoto, J. Chem. Phys. **33**, 878 (1960).

[2] H. Brion, C. Moser, and M. Yamazaki, J. Chem. Phys. **30**, 673 (1959).

[3] The matrix element H_{0i} for the states with subscript 5 is always zero. In the work cited in footnote 2 two linear combinations of 8_1, 8_2, 8_3, 8_4, and 8_5 are taken.

TABLE I. $^2\Pi$ states with nonvanishing H_{0i}.

Configurations											Taken by		
3σ	4σ	5σ	6σ	$1\pi^+$	$1\pi^-$	$2\pi^+$	$2\pi^-$	Labeling	$H_{ii}-H_{00}$ (in a.u.)	H_{0i} (in a.u.)	BMY	Ψ	Ψ'
2	2	2	0	2	2	1	0	0	0	...	×	×	×
2	2	2	0	1	2	2	0	1	0.37781	−0.00242			
2	2	2	0	2	1	1	1	2_1	0.33719	0.00767			
2	2	2	0	2	1	1	1	2_2	0.49547	0.00296			
2	2	2	0	2	0	1	2	3	0.81563	0.18126	×	×	×
2	2	2	0	1	1	2	1	4_1	0.79839	0.15540	×	×	×
2	2	2	0	1	1	2	1	4_2	0.90991	0.17483	×	×	×
2	2	1	1	2	2	1	0	6_1	0.90627	0.02535		×	
2	2	1	1	2	2	1	0	6_2	0.71637	0.00596		×	
2	2	1	1	1	2	2	0	7_1	1.24805	0.17193	×	×	×
2	2	1	1	1	2	2	0	7_2	1.03671	−0.00340	×		
2	2	1	1	2	1	1	1	8_1	1.20780	0.12157	(×)	×	×
2	2	1	1	2	1	1	1	8_2	1.36571	0.21057	(×)	×	×
2	2	1	1	2	1	1	1	8_3	1.00017	−0.00241	(×)		
2	2	1	1	2	1	1	1	8_4	0.96528	−0.00417	(×)		
2	2	0	0	2	2	2	1	12	0.58323	−0.04030		×	×
2	2	2	2	2	1	0	0	14	1.20664	−0.00015			
2	2	2	2	2	0	0	1	16_1	1.52263	−0.04520		×	×
2	2	0	2	2	2	1	0	20	1.68099	0.13533	×	×	×
2	2	2	2	2	2	1	0	26_1	1.12235	0.02811		×	
2	1	2	1	2	2	1	0	26_2	1.11091	0.03896		×	×
2	1	2	1	1	2	2	0	27_1	1.50049	−0.04821			×
2	1	2	1	1	2	2	0	27_2	1.45055	0.00908			
2	1	2	1	2	1	1	1	28_1	1.46023	−0.03410			×
2	1	2	1	2	1	1	1	28_2	1.61814	0.05906		×	×
2	1	2	1	2	1	1	1	28_3	1.46353	0.00642			
2	1	2	1	2	1	1	1	28_4	1.39563	0.01112			
2	1	1	2	2	2	1	0	32_1	2.12206	0.02908			
2	1	1	0	2	2	2	1	38_1	1.10035	0.03033			
2	0	2	2	2	2	1	0	42	2.24632	0.07086		×	×
2	0	2	0	2	2	2	1	48	1.30066	−0.08982		×	×
1	2	2	1	2	2	1	0	54_1	1.70302	−0.02144		×	
1	2	2	1	2	2	1	0	54_2	1.58870	0.00288		×	
1	2	2	1	1	2	2	0	55_1	2.03430	−0.10638		×	×
1	2	2	1	1	2	2	0	55_2	1.97726	0.03519			×
1	2	2	1	2	1	1	1	56_1	2.05983	−0.07523		×	×
1	2	2	1	2	1	1	1	56_2	2.21774	0.13029		×	×
1	2	2	1	2	1	1	1	56_3	2.01511	0.02488			
1	2	2	1	2	1	1	1	56_4	1.97448	0.04310			×
1	2	1	2	2	2	1	0	60_1	2.42181	0.08907		×	×
1	2	1	0	2	2	2	1	66_1	1.49960	0.03298			×
1	1	2	2	2	2	1	0	70_1	2.76834	−0.01930			
1	1	2	0	2	2	2	1	76_1	1.92218	0.00276			
0	2	2	2	2	2	1	0	86	3.29518	0.10185			
0	2	2	0	2	2	2	1	92	2.54852	−0.04891			

TABLE II. Ground state wave function 23-dim. Ψ.

ψ_i	Coefficient (c_i)	ψ_i	Coefficient (c_i)
0	0.9669	26_1	0.0015
3	−0.1265	26_2	−0.0315
4_1	−0.1137	28_2	−0.0188
4_2	−0.0861	42	−0.0238
6_1	0.0300	48	0.0488
6_2	−0.0044	54_1	0.0141
7_1	−0.0760	54_2	−0.0018
8_1	−0.0401	55_1	0.0322
8_2	0.0882	56_1	0.0193
12	0.0344	56_2	−0.0387
16_1	0.0249	60_1	−0.0290
20	−0.0516		

third and the fourth column. The molecular orbitals are the LCAO SCF MO's obtained in the "third calculation" of the work cited in footnote 2. Since H_{0i} does not vanish for $i=1$, 2_1 and 2_2, these orbitals are not strictly self-consistent. However, they are orthogonal; this slight self-inconsistency should not appreciably affect the results.

Since the maximum dimension of the secular equation which can be solved by the IBM 650 computer is limited, in the CI calculations we have to choose states which contribute most significantly to the molecular quantities of our interest. Our choice here is partially gauged by energetic considerations and partially by the effects of the states on the hyperfine coupling constants. From the former criterion we discarded the states having no electrons in 3σ. Then we took 15 states for which $|H_{0i}|>0.05$. Of course, states with relatively low value of H_{ii} may also mix appreciably with the ground state unless the corresponding H_{0i} are very small. For this reason we included state 12. The other states are rather immaterial as far as energy is concerned (see next paragraph). However, as indicated in our previous paper,[1] some of the higher states are critical for the value of $|\Psi(0)|^2$. Thus we calculated $\psi_i(0)\psi_j(0)$ and found that 6_1, 6_2, 26_1, 26_2, 54_1, and 54_2 are important (see Sec. III). Finally, state 16_1 is taken as the representative of a particular type of configuration. This totals to 23 states. The 23-term wave function Ψ (normalized) obtained in this way is shown in Table II and this particular function will be referred to as the 23-dim Ψ. The energy of the ground state so calculated is 0.127 a.u. lower than H_{00}, which is 0.050 a.u. higher than the energy of the separated atoms ($^3P+^4S$). The dissociation energy is, therefore, 2.1 ev, which is compared with 1.7 ev calculated by Brion, Moser, and Yamazaki.[2]

In order to examine the effect of the states which were neglected in the 23-dim Ψ, we have calculated the energy by including all the 45 states with nonvanishing H_{0i} (Table I). Since it is difficult to solve a 45×45 secular equation directly by the IBM 650 computer, we have performed a Van Vleck transformation[4] to reduce the 45×45 energy matrix approximately into a 23×23. In this procedure we divide the 45-dimensional energy matrix into a 23×23 (which contains the ground state) and a 22×22 block. A transformation[4] is applied to reduce the matrix elements connecting the two blocks to the second order. In this new form of the energy matrix, the "between-block" elements affect the energy of the ground state only in the fourth order and will be neglected. The energy is then calculated by solving the 23×23 block of the transformed matrix exactly. The dissociation energy obtained in this manner is 2.4 ev which shows little improvement over the result from the 23-dim Ψ.

We have also chosen another set of 23 states by a somewhat different criterion. If we are only concerned with the calculation of energy, the conventional choice is the size of the second-order perturbation term, $|H_{0i}|^2/(H_{00}-H_{ii})$. However, a wave function which gives the "best energy" is not usually the best for the calculations of other molecular quantities. An alternative convenient choice would be the magnitude of $H_{0i}/(H_{00}-H_{ii})$ which is a measure of the first order mixing of the excited states. As we have seen in the preceeding paragraph, inclusion of all the 45 states in the energy matrix changes the dissociation energy by only 0.3 ev. Thus, we shall adopt the second criterion, i.e., choose the 23 states which have the largest values of $H_{0i}/(H_{00}-H_{ii})$. The CI wave function derived from this set of ψ's will be called the 23-dim Ψ'. In this case the ground state becomes 0.130 a.u. lower than H_{00}, which gives a dissociation energy of 2.2 ev. The states which are used in the wave function of Brion, Moser, and Yamazaki (BMY), in 23-dim Ψ, and in 23-dim Ψ' are marked with cross signs in the last column of Table I.

Since the experimental result is 6.6 ev, configuration interactions are not sufficient to account for the discrepancy between the experimental and calculated values. This can be seen in the coefficients in Table II. The states which were not used by the authors of reference 1 do not mix appreciably in the ground state. As a matter of fact, the failure of the CI calculations in NO makes a remarkable contrast to the same kind of treatments in Li_2[5], O_2[6], and F_2[7], where $|D_e(\text{exp})-D_e(\text{calc})|/D_e(\text{exp})$ is less than 30%. From an over-

[4] See, for example, E. C. Kemble, *The Fundamental Principle of Quantum Mechanics* (Dover Publications, New York, 1958), p. 394; E. B. Wilson, Jr., and J. B. Howard, J. Chem. Phys. **4**, 260 (1936).

[5] E. Ishiguro, K. Kayama, M. Kotani, and Y. Mizuno, J. Phys. Soc. Japan **12**, 1355 (1957).

[6] M. Kotani, Y. Mizuno, K. Kayama, and E. Ishiguro, J. Phys. Soc. Japan **12**, 707 (1957).

[7] K. Hijikata, Revs. Modern Phys. **32**, 445 (1960); J. Chem. Phys. **34**, 221, 231 (1961).

TABLE III. Contributions from the various excited configurations to the values of the hyperfine structure constants.

ψ_i	ψ_j	$c_ic_j\psi_i(0)\psi_j(0)$ in a.u.	$c_ic_j(3\cos^2\chi-1/r^3)_{ij}$ in a.u.	$c_ic_j(\sin^2\chi/r^3)_{ij}$ in a.u.	$c_ic_j(1/r^3)_{ij}$ in a.u.	$c_ic_jq_{ij}$ in a.u.
0	0	0	−0.6527	1.2866	1.6035	1.2917
3	3	0	−0.0112	0.0220	0.0018	0.0062
4_1	4_1	0	−0.0090	0.0178	0.0222	0.0051
4_2	4_2	0	−0.0003	0.0033	0.0127	0.0029
7_1	7_1	0	−0.0012	0.0039	0.0145	0.0090
8_1	8_1	0	−0.0011	0.0022	0.0015	0.0025
8_2	8_2	0	−0.0029	0.0071	0.0071	0.0122
12	12	0	−0.0008	0.0016	0.0020	−0.0022
16_1	16_1	0	−0.0004	0.0009	0.0011	0.0031
20	20	0	−0.0019	0.0037	0.0046	0.0073
26_2	26_2	0.0029	0.0013	−0.0005	0.0017	0.0029
6_1	6_1	0	−0.0006	0.0012	0.0015	0.0019
28_2	28_2	0	−0.0001	0.0003	0.0003	0.0009
42	42	0	−0.0004	0.0008	0.0010	0.0026
48	48	0	−0.0017	0.0033	0.0041	−0.0001
55_1	55_1	0	−0.0002	0.0007	0.0026	0.0023
56_1	56_1	0	−0.0003	0.0005	0.0003	0.0008
56_2	56_2	0	−0.0006	0.0014	0.0014	0.0033
54_1	54_1	0	−0.0001	0.0003	0.0003	0.0005
60_1	60_1	0	−0.0002	0.0012	0.0014	0.0028
0	26_2	0.0465	−0.0044	0	0	0
0	6_1	0	0	0	0	−0.0474
0	6_2	0.0031	−0.0040	0	0	0
0	26_1	0	0	0	0	−0.0004
0	54_1	0	0	0	0	0.0047
0	54_2	0.0017	0.0003	0	0	0
7_1	6_1	0	0.0012	−0.0021	0.0026	−0.0012
7_1	55_1	0	0	0	0	0.0009
8_1	8_2	0	0.0010	0.0014	0	0
8_1	6_1	0	−0.0004	0.0008	−0.0010	−0.0004
8_1	56_1	0	0	0	0	0.0003
8_2	8_2	0	−0.0029	0.0071	0.0071	0.0122
8_2	6_1	0	−0.0006	0.0010	−0.0012	−0.0017
8_2	56_2	0	0	0	0	0.0013
20	6_1	0	0	0	0	0.0025
20	6_2	0.0002	−0.0002	0	0	0
20	60_1	0	0	0	0	−0.0008
26_2	6_1	−0.0009	0	0	0	0
26_2	6_2	0.0002	0	0	0	0
26_2	42	0.0012	−0.0001	0	0	0
26_2	26_1	−0.0001	0.0001	0	0	0
26_2	54_1	−0.0006	0	0	0	0
26_2	54_2	0.0001	0	0	0	0
6_1	6_2	0	0.0001	0	0	0
6_1	54_1	0	0	0	0	0.0002
6_2	60_1	0.0001	0	0	0	0
55_1	54_1	0	−0.0002	0.0004	−0.0005	0.0002
56_1	56_2	0	−0.0002	0.0003	0	0
56_1	54_1	0	0.0001	−0.0002	0.0002	0.0001
56_2	54_1	0	−0.0001	0.0002	0.0008	0.0003
54_1	60_1	0	0	0	0	−0.0005

TABLE IV. The hyperfine structure constants and dissociation energy of the ground state of NO.

	$\|\Psi(0)\|^2$ in 10^{24} cm^{-3}	$(3\cos^2\chi-1/r^3)_{Av}$ in 10^{24} cm^{-3}	$(\sin^2\chi/r^3)_{Av}$ in 10^{24} cm^{-3}	$(1/r^3)_{Av}$ in 10^{24} cm^{-3}	eqQ in Mc	D_e in ev
Ground configuration	0	−4.71	9.33	11.6	0.68	−1.4
9-dim. CI	0.0032	...	...	...	0.79	1.6
23-dim. Ψ	0.71	−4.74	9.18	11.38	1.09	2.1
23-dim. Ψ'	0.59	−4.66	9.18	11.36	0.75	2.2
Experimental	0.85	−1.04	13.4	14.9	−2	6.6

simplified picture, NO has one electron outside the closed configuration $(3\sigma)^2(4\sigma)^2(5\sigma)^2(1\pi)^4$. The effective nuclear charge of 2π orbital must be considerably different from that of the lower orbitals. From the other point of view, there is an appreciable amount of mixing of the higher π orbitals. This point must be investigated if a more accurate wave function for the nitric oxide molecule is to be obtained.

III. HYPERFINE STRUCTURE CONSTANTS

The hyperfine structure constants of the NO molecule have been calculated by the 23-term wave function given in Table II. The contributions from the various terms of this wave function to the coupling constants, e.g.,

$$c_ic_j\left(\frac{\sin^2\chi}{r^3}\right)_{ij}=c_ic_j\int\psi_i^*\frac{\sin^2\chi}{r^3}\psi_j d\tau, \text{ etc.,} \qquad (5)$$

are listed in Table III. Of particular interest is the case of $|\Psi(0)|^2$. It may be noticed that the main contributions come from the terms $c_0c_i\psi_0(0)\psi_i(0)$ with $i=6_2, 26_2, 54_2$. These states have unpaired electrons in 5σ, 6σ; in 4σ, 6σ; and in 3σ, 6σ. Especially, the contribution from 26_2 amounts to 90% of $|\Psi(0)|^2$. Thus we know, as in the case of O_2, that the $2s$ electrons play an important role in this quantity. In fact a rough estimation of $|\Psi(0)|^2$ may be made in the following manner. The configurations with unpaired electrons in the σ orbitals are responsible for the contact term. For the states with only one unpaired electron, the contributions to $|\Psi(0)|^2$ arise from terms of the form $c_i^2\psi_i^2(0)$ which are rather small. However, when there are three (or more) unpaired electrons, the cross terms $c_ic_0\psi_i(0)\psi_0(0)$ in the expansion of $|\Psi(0)|^2$ is generally not equal to zero and constitute the major part of the latter quantity. From energetic considerations one might expect that the most relevant states are those having unpaired electrons in

$$(2\pi)(6\sigma)(5\sigma), \qquad (2\pi)(6\sigma)(4\sigma), \qquad (2\pi)(6\sigma)(3\sigma).$$

The coefficient c_i may be taken approximately as $H_{0i}/(E_0-E_i)$ and $c_0\simeq 1$. The value of $|\Psi(0)|^2$ is then simply equal to the sum of $2c_ic_0\psi_i(0)\psi_0(0)$ for these three states which gives 0.804×10^{-24} cm^{-3}.

Unlike the case of $|\Psi(0)|^2$, the mixing of the higher configurations offers practically no improvement in the quantities $\langle(3\cos^2\chi-1)/r^3\rangle_{Av}$, $\langle\sin^2\chi/r^3\rangle_{Av}$ and $\langle r^{-3}\rangle_{Av}$, which was predicted in the previous paper.[1] Also, we may easily see that the greater parts of the values of these quantities are attributed to the ground configuration. The CI has frivolous meaning as far as these quantities are concerned. The discrepancy from the experiment will, therefore, be removed only by improving the atomic orbitals.

Since the atomic orbitals are not suitable for the calculations of the quantities involving r^{-3}, it is difficult to expect significant results on the nuclear quadrupole coupling constant. In the calculation of this quantity we have to sum the contribution of all the electrons. The accumulated error could be so large as to make the usual LCAO MO procedure incredulous. Our result of eQq in the present case is 1.09 Mc.

In Table IV are summarized the hyperfine structure constants and the dissociation energy calculated by several different ways. The first and the second row give the results from the ground-configuration approximation and from the 9-dimensional CI wave function.[1] The molecular quantities calculated by using the 23-term wave function Ψ are shown in the third row. We have also calculated the hyperfine coupling constants by the 23-dim Ψ' and the results may be found in the fourth row of Table IV.

The coupling constants shown in this paper were calculated by using the Slater type wave functions for the atomic orbitals. The values of these constants may be increased by using the Hartree-Fock functions in place of the Slater orbitals. For example, in the case of the ground-configuration approximation, the average values of $(3\cos^2\chi-1)/r^3$, $\sin^2\chi/r^3$, and r^{-3} become -5.7×10^{24}, 10.3×10^{24}, and 12.6×10^{24} cm^{-3}, respectively.[1] Brion and Moser[8] have obtained even higher values of these constants by adopting the semiempirical method of Dousmanis[9] and Mizushima.[10] In their calculations the values of some of the atomic integrals are adjusted by a somewhat *ad hoc* procedure, thus we shall not pursue such approach in this paper.

[8] H. Brion and C. Moser, Phys. Rev. **118**, 675 (1960).
[9] G. C. Dousmanis, Phys. Rev. **97**, 967 (1955).
[10] M. Mizushima, Phys. Rev. **105**, 1262 (1957).

It should be mentioned that the experimental values of $|\Psi(0)|^2$ is derived from the special assumption that the average of $(3\cos^2\chi-1)/r^3$ over the spin distribution is the same as that over the distribution of the orbital angular momentum. This is rigorously correct for the ground configuration but not for most of the excited ones. However, as may be seen from Table IV, $(3\cos^2\chi-1)/r^3$ is rather insensitive to the addition of the excited configurations. Furthermore, if we had used the "exact" molecular orbitals instead of the LCAO MO, the contribution to $(3\cos^2\chi-1)/r^3_{Av}$ from the excited configuration would be less than what we have in this calculation. Hence the value of $|\Psi(0)|^2$ of 0.85×10^{24} cm^{-3} may be expected to be reasonably accurate.

THE JOURNAL OF CHEMICAL PHYSICS VOLUME 34, NUMBER 6 JUNE, 1961

Theory of Vibrational Relaxation in Liquids

ROBERT ZWANZIG

National Bureau of Standards, Washington, D. C.

(Received November 21, 1960)

A new formulation of the theory of vibrational relaxation, based on Zener's semiclassical approximation, is presented here. The relaxation rate is shown to be proportional to the spectral density of the force exerted on the oscillator by its environment. The isolated binary collision theory is derived, but only with the condition that the collision frequency is much smaller than the oscillator frequency. This requirement is not satisfied in a liquid; we conclude that Litovitz's application of the isolated binary collision theory to liquids is not justified. A possible relation between vibrational relaxation and the self-diffusion coefficient in a liquid is discussed.

I

THIS article contains a critique of the application, to the liquid state, of the isolated binary collision (IBC) theory of vibrational relaxation. It also contains some guesses about a more appropriate theory.

In the IBC theory, the rate of vibrational energy transfer is the product of two distinct factors. One of these is the probability of energy transfer as a result of a single collision. The other factor is the average frequency with which collisions occur.

Litovitz[1] (see also Herzfeld and Litovitz[2]) showed that the IBC theory, together with a cell-model estimate of the collision frequency, described experimental data on vibrational relaxation in liquid carbon disulfide. However, the agreement may be fortuitous.

Fixman[3] argued recently that the predictions of the IBC theory are substantially changed when the ordinary intermolecular force between a colliding pair is modified by the addition of a small random force. This extra force, of the sort used in the theory of Brownian motion, is supposed to take account of many body processes in the environment of the colliding pair. Fixman concluded that the IBC theory should not be applied to liquids. Fixman's calculation is in the spirit of the IBC theory, in that the transition rate is still considered to be the product of a collision frequency and a transition probability per collision. He discussed only the second factor.

In this article we present a new form of the transition rate theory, in which the above factorization is not introduced at the beginning. We show (in an approximation due to Zener) that the rate of energy transfer is proportional to the spectral density of the force exerted on the oscillator by its surroundings. We show that the IBC theory is correct only when the collision frequency is much smaller than the oscillator frequency. This condition is met in a dilute gas but not in a liquid.

Finally, we suggest a method of estimating the spectral density in a liquid. This method connects the transition rate to the coefficient of self-diffusion in the liquid. It rests on several plausible conjectures. We do not know of any experimental data with which it can be tested.

There are two reasons why the IBC theory should not be expected to work for liquids. One is that many of the binary collisions overlap in time, and must therefore properly be regarded as parts of triple and higher order collisions. Even if we generalize the IBC theory by including the effects of these multiple collisions, so that the transition rate is now the sum of transition probabilities multiplied by collision frequencies, we still are in trouble. In our derivation of the IBC theory a requirement appears, which has not been stated explicitly in the past: the interval between successive collisions must be much longer than a period of the oscillator. Otherwise the oscillator will "remember" its

[1] T. A. Litovitz, J. Chem. Phys. **26**, 469 (1957). Dr. Litovitz has kindly shown me some recent unpublished work by himself and W. M. Madigorsky, on vibrational relaxation in dense carbon dioxide. They get excellent agreement of experiment with the IBC theory, this time using a cell model with "movable walls."

[2] K. F. Herzfeld and T. A. Litovitz, *Absorption and Dispersion of Ultrasonic Waves* (Academic Press, Inc., New York, 1959).

[3] M. Fixman, J. Chem. Phys. (to be published). (I am indebted to Dr. Fixman for sending me a preprint of his article.)

phase from one collision to the next, and contributions will appear due to interference between different collisions.

The duration of a binary collision is typically about 10^{-13} sec. Even those exceptionally energetic collisions that are supposed to be mainly responsible for energy transfer have roughly the same duration. The period of an oscillator is typically about 10^{-13} sec. In a low-density gas the mean time between collisions is usually about 10^{-10} sec or longer. The conditions for the validity of the IBC theory are met.

In a liquid the duration of a collision, and the period of an oscillator will, of course, remain essentially unchanged. However, the time between collisions is very different. Herzfeld and Litovitz[2] give various estimates, based on several free-volume theories of the liquid state. Their numbers are in the range 10^{-12}–10^{-13} sec. The conditions for the validity of the IBC theory are not met.

II

Our derivation begins with an approximation first used in this context by Zener.[4]

The harmonic oscillator is treated by quantum mechanics. It is described by the Hamiltonian

$$H_0=(1/2\mu)p^2+\tfrac{1}{2}\mu\omega^2q^2, \tag{1}$$

where q is the normal coordinate of the oscillator, p is its conjugate momentum, μ and ω are its reduced mass and frequency.

The environment of the oscillator is treated classically. The dynamical behavior of the environment is assumed to be independent of the state of the oscillator.

The interaction between the oscillator and its environment is specified by the perturbation Hamiltonian,

$$H_1=\lambda qF(t). \tag{2}$$

Here λ is a numerical constant and $F(t)$ is the force[5] exerted on the oscillator by its surroundings at time t; $F(t)$ depends on the state of the environment only; for the present we regard it as a known function of time.

Let us assume that the oscillator is initially in the ground state. The probability $P(t)$ that it will be found in the first excited state at time t, according to first-order time-dependent perturbation theory, is

$$P(t)=(\lambda q_{01}/\hbar)^2\left|\int_0^t ds\,\exp(i\omega s)F(s)\right|^2. \tag{3}$$

In this equation q_{01} is the matrix element of q between the zeroth and first states,

$$q_{01}=(\hbar/2\mu\omega)^{\frac{1}{2}}. \tag{4}$$

If the probability P increases linearly with time, then the limit

$$\lim_{t\to\infty}(1/t)P(t)=R \tag{5}$$

is the *transition rate* R.

The quantity $G(\omega)$, defined by

$$G(\omega)=\lim_{t\to 0}(1/t)\left|\int_0^t dsF(s)\exp(i\omega s)\right|^2, \tag{6}$$

is called the spectral density of F.[6] If this limit exists, then the transition rate is proportional to the spectral density of F at the frequency of the oscillator,

$$R=(\lambda q_{01}/\hbar)^2G(\omega). \tag{7}$$

The rest of this article is concerned with the properties of $G(\omega)$.

The calculation of the spectral density is considerably simplified by use of the Wiener-Khinchin formula of generalized harmonic analysis.[6] This says that $G(\omega)$ is the Fourier transform of an autocorrelation function,

$$G(\omega)=\int_{-\infty}^{+\infty}d\tau\langle F(t)F(t+\tau)\rangle\exp(i\omega t). \tag{8}$$

The average denoted by $\langle\ \rangle$ may be regarded either as a time average,

$$\langle F(t)F(t+\tau)\rangle=\lim_{T\to\infty}(1/T)\int_0^T dtF(t)F(t+\tau); \tag{9}$$

or, if F is ergodic, by an average over a representative statistical ensemble. The latter interpretation is the more useful one.

The result of the preceding derivation can be compared with the IBC theory. There the transition rate depends on the collision frequency ν_c and on the force F_c exerted on the oscillator during a single collision,

$$R(\mathrm{IBC})=\nu_c(\lambda q_{01}/\hbar)^2\,\mathrm{av}\left[\left|\int_{-\infty}^{+\infty}dsF_c(s)\exp(i\omega s)\right|^2\right]. \tag{10}$$

The average av [ ] is taken over all possible kinds of collision.

Now we shall show that the IBC theory is a special case of our general formalism. The purpose of the following discussion is not so much to provide a better theory as to expose clearly the conditions under which the IBC theory may be expected to be valid.

We assume that $F(t)$ can be expressed as a sum of contributions from independent random events.[7] These may be binary, triple, . . . collisions. Each event can be described by a characteristic occurrence time t_k. In the case of binary collisions this may be the time of closest approach during the kth collision; in higher order colli-

[4] C. Zener, Phys. Rev. **38**, 277 (1931); Proc. Cambridge Phil. Soc. **29**, 136 (1933).

[5] $F(t)$ must not be confused with the force exerted on the center of mass of the molecule containing the oscillator.

[6] See, for example, M. C. Wang and G. E. Uhlenbeck, Revs. Modern Phys. **17**, 323 (1945).

[7] The argument is a generalization of that commonly used in the theory of the shot effect.

sions some other time has to be picked, but we do not care what it is. The event can also be described by such parameters as initial relative velocity, angular momentum, etc. We lump all these together and denote them by v_k.

The force during the kth event is $f(v_k; t-t_k)$. Since an event has only a short duration, f differs from zero only when t is in the neighborhood of t_k. The total force is

$$F(t)=\sum_{k=-\infty}^{+\infty} f(v_k; t-t_k). \tag{11}$$

It should be emphasized that the above separation into independent events makes sense only if distinct f's do not overlap in time. If, for example, two binary collisions overlap in time, they should be treated instead as a triple collision. It is hard to imagine an event where two molecules simultaneously exert a force on a third, and yet do not feel each other's presence.

To get the transition rate we need $G(\omega)$. To get the spectral density we calculate first the autocorrelation $\langle F(t)F(t+\tau)\rangle$. Since the force that we have assumed is evidently ergodic, the time average in Eq. (9) may be replaced by an ensemble average. We shall use av[ ] to denote an average over the collision parameters v_k. The average over the arrival times t_k will be done explicitly. It should be remembered that the v_k are independent of the t_k.

Let us break up the autocorrelation into two parts,

$$\langle F(t)F(t+\tau)\rangle=\sum_k \langle f(v_k; t-t_k)f(v_k; t+\tau-t_k)\rangle + \sum_{k\neq j}\sum \langle f(v_k; t-t_k)\times f(v_j; t+\tau-t_j)\rangle. \tag{12}$$

For the moment we shall study the first term only.

Single events occur in a completely random way. Consider a very long time interval T. The probability density that a specific event will occur at a specific time between $t=0$ and $t=T$ is $1/T$. Thus the average $\langle\ \rangle$ may be written as

$$\sum_k \langle f(v_k; t-t_k)f(v_k; t+\tau-t_k)\rangle=\lim_{T\to\infty}\sum_k (1/T) \times\int_0^T dt_k \,\mathrm{av}[f(v_k; t-t_k)f(v_k; t+\tau-t_k)]. \tag{13}$$

Because the duration of any single event is short and remains finite as $T\to\infty$, only a certain number $N(T)$ of terms out of the sum over k will remain: the other terms have arrival times outside the interval (O,T). Having thus restricted the sum over k, we can now extend the time integral over all t from $-\infty$ to $+\infty$. Because of the average over v_k, there is no further basis for distinguishing between terms. (We could be more specific here, and count events according to whether they are binary, triple, etc. collisions. However, in our procedure each event is counted for simplicity just as an event, and the average over v_k includes an average over the various kinds of possible collisions.)

We note also that

$$\lim_{T\to\infty}(1/T)N(T)=\nu_e \tag{14}$$

is the average number of events per unit time.

For the preceding reasons we can rewrite Eq. (13) in the form

$$\sum_k \langle f(v_k; t-t_k)f(v_k; t+\tau-t_k)\rangle =\nu_e\int_{-\infty}^{+\infty} dt_1\,\mathrm{av}[f(v_1; t-t_1)f(v_1; t+\tau-t_1)]. \tag{15}$$

The analysis of the second part of Eq. (12) is much the same, except for the presence of two times. We shall just give the result.

Let $\rho(t_2-t_1)$ be the probability density of any event at t_2, given that any event has occurred at t_1. When t_2-t_1 is large there is no correlation between events and $\rho(t_2-t_1)\simeq\nu_e$. Because different events cannot overlap in time, there is a correlation when t_2-t_1 is small; then ρ must vanish. In terms of the probability $\rho(t_2-t_1)$, the autocorrelation of F is

$$\langle F(t)F(t+\tau)\rangle=\nu_e\int_{-\infty}^{+\infty} dt_1\,\mathrm{av}[f(v_1; t-t_1)f(v_1; t+\tau-t_1)] +\nu_e\int_{-\infty}^{+\infty}\int dt_1 dt_2 \rho(t_2-t_1)\,\mathrm{av}[f(v_1; t-t_1)f(v_2; t+\tau-t_2)]. \tag{16}$$

The next step is to calculate $G(\omega)$. Again we treat the two parts separately. The first part is

$$G_1(\omega)=\int_{-\infty}^{+\infty} d\tau\ (\exp i\omega t)\nu_e\int_{-\infty}^{+\infty} dt_1\,\mathrm{av}[f(v_1; t-t_1) \times f(v_1; t+\tau-t_1)]. \tag{17}$$

We write

$$\exp i\omega t=\exp i\omega(t+\tau-t_1)\times\exp -i\omega(t-t_1) \tag{18}$$

and change variables of integration from t_1 and t_2 to $t+\tau-t_1$ and $t-t_1$. This gives

$$G_1(\omega)=\nu_e\int_{-\infty}^{+\infty}\int dt dt'\,\exp i\omega(t'-t)\,\mathrm{av}[f(v; t)f(v; t')], \tag{19}$$

which is the same as

$$G_1(\omega)=\nu_e\,\mathrm{av}\left[\left|\int_{-\infty}^{+\infty} dt f(v; t)\,\exp i\omega t\right|^2\right]. \tag{20}$$

Here $G_1(\omega)$ has the form that appears in the IBC theory. It is a product of a collision frequency and a quantity characteristic of a single collision. The only difference is that the collisions are not necessarily binary.

The other part of $G(\omega)$ can be handled in the same

way, except that another time integral appears. The result is

$$G_2(\omega)=\nu_c\int_{-\infty}^{+\infty}d\tau\rho(\tau)\exp(i\omega\tau)\times \mathrm{av}\Big[\int_{-\infty}^{+\infty}dt_1 f(v_1;t_1)$$
$$\times\exp(-i\omega t_1)\int_{-\infty}^{+\infty}dt_2 f(v_2;t_2)\exp(+i\omega t_2)\Big]. \quad (21)$$

The factor involving $\rho(\tau)$ is the most interesting part of this equation. Let us write ρ in the form

$$\rho(\tau)=\nu_c+\rho(\tau)-\nu_c. \quad (22)$$

Note that $\rho(\tau)-\nu_c$ is nonvanishing only for small τ. The constant part of ρ gives a delta function,

$$\int_{-\infty}^{+\infty}d\tau\nu_c\exp i\omega t=2\pi\nu_c\delta(\omega). \quad (23)$$

Since we are not interested in the spectral density for zero frequency, this part will be dropped entirely. Therefore the whole Fourier transform, for $\omega\neq 0$, is

$$\int_{-\infty}^{+\infty}d\tau\rho(\tau)\exp(i\omega\tau)=\int_{-\infty}^{+\infty}d\tau(\rho(\tau)-\nu_c)\exp(i\omega\tau). \quad (24)$$

The final result of the derivation is

$$R=(\lambda q_{01}/\hbar)^2[G_1(\omega)+G_2(\omega)]; \quad (25)$$

$G_1(\omega)$ is given by Eq. (20), and $G_2(\omega)$ by Eqs. (21) and (24).

What does this say about the validity of the IBC theory? The contribution $G_1(\omega)$ has the correct form for agreement with the IBC theory, provided that triple collisions can safely be neglected. The contribution $G_2(\omega)$ does not have a counterpart in the IBC theory: it describes the interference between different collisions. If there is no correlation in arrival times, then $G_2(\omega)$ vanishes. But of course there must be a correlation, since events are not allowed to overlap in time. The $G_2(\omega)$ may nevertheless be small.

As a guess, let us call the average duration of an event τ_c, and let us assume that

$$\rho(\tau)=\begin{cases}\nu_c & \text{if} \quad |\tau|>\tau_c;\\ 0 & \text{if} \quad |\tau|<\tau_c.\end{cases} \quad (26)$$

This means that collisions cannot be separated by a time smaller than the duration of a collision, but that they are otherwise uncorrelated. Then

$$\int_{-\infty}^{+\infty}dt\exp(i\omega\tau)(\rho(\tau)-\nu_c)=-\nu_c\int_{-\tau_c}^{+\tau_c}d\tau\exp(i\omega\tau)$$
$$=-(2\nu_c/\omega)\sin\omega\tau_c. \quad (27)$$

In typical cases $\tau_c\sim 10^{-13}$ sec and $\omega\sim 10^{+13}$ sec^{-1}; the factor $\sin\omega\tau_c$ is of order unity, and

$$\int_{-\infty}^{+\infty}d\tau\exp(i\omega\tau)[\rho(\tau)-\nu_c]=O(\nu_c/\omega). \quad (28)$$

The quantity that this multiplies in G_2 is of the same order of magnitude as G_1.

As long as the collision frequency is much smaller than the oscillator frequency, $G_2(\omega)$ can be neglected relative to $G_1(\omega)$. If the collision frequency and the oscillator frequency are comparable in magnitude, $G_2(\omega)$ may not be neglected and the IBC theory no longer holds.

In Litovitz's calculation of the relaxation time in liquid carbon disulfide, the collision frequency is not small compared with the oscillator frequency. The events overlap to such an extent that the separation of $F(t)$ into independent random events does not make sense. The remarkable agreement between his calculation and the experimental data must be regarded as fortuitous.

III

We conclude this article with a few conjectural remarks about the form of the spectral density in liquids.

In many calculations of transition probabilities, the interaction $H'=\lambda qF(t)$ is assumed to be proportional to the force on the center of mass of the molecule containing the oscillator. This is a guess; little is known about the dependence of intermolecular interactions on intramolecular degrees of freedom. We shall assume this proportionality anyhow. We choose the factor λ so that $F(t)$ is the actual force on the center of mass, (or, more correctly, the component of the force along the direction of oscillation). Then $G(\omega)$ is the spectral density of the total force acting on the molecule in the direction of oscillation. Averaging over directions, we write $G(\omega)$ in terms of the total (vector) force $\mathbf{F}(t)$;

$$G(\omega)=\int_{-\infty}^{+\infty}d\tau\exp(i\omega\tau)\times\tfrac{1}{3}\langle\mathbf{F}(t)\cdot\mathbf{F}(t+\tau)\rangle. \quad (29)$$

The force $\mathbf{F}$ is the rate of change of the momentum $\mathbf{P}$ of the center of mass. Then

$$G(\omega)=\int_{-\infty}^{+\infty}d\tau\exp(i\omega\tau)\times\tfrac{1}{3}\langle d\mathbf{P}(t)/d\tau\cdot d\mathbf{P}(t+\tau)/d\tau\rangle. \quad (30)$$

When this is integrated by parts[8] we obtain

$$G(\omega)=\int_{-\infty}^{+\infty}d\tau\exp(i\omega\tau)\times\tfrac{1}{3}\omega^2\langle\mathbf{P}(t)\cdot\mathbf{P}(t+\tau)\rangle. \quad (31)$$

So we have to know the autocorrelation of the total momentum of the molecule.

Now the further conjecture is introduced that the momentum autocorrelation decays exponentially,

$$\langle\mathbf{P}(t)\cdot\mathbf{P}(t+\tau)\rangle=\langle\mathbf{P}(t)\cdot\mathbf{P}(t)\rangle\exp(-\beta|\tau|). \quad (32)$$

[8] Note that $\langle P(t)\cdot P(t+\tau)\rangle=\langle P(0)\cdot P(\tau)\rangle$ is independent of t. This fact is used in the integration by parts.

The coefficient on the right-hand side is

$$\langle \mathbf{P}(t)\cdot\mathbf{P}(t)\rangle = 3MkT, \tag{33}$$

where M is the total mass of the molecule, and T is the temperature. The rate of decay can be found by means of a well-known formula for the coefficient of self-diffusion in the liquid,

$$D_{\text{self}} = \tfrac{1}{3}\int_0^\infty d\tau\,(1/M^2)\,\langle \mathbf{P}(t)\cdot\mathbf{P}(t+\tau)\rangle. \tag{34}$$

Then β is found to be

$$\beta = kT/MD_{\text{self}}. \tag{35}$$

The integration leading to $G(\omega)$ is trivial; one gets

$$G(\omega) = 2\omega^2 MkT[\beta/(\beta^2+\omega^2)]. \tag{36}$$

The corresponding transition rate is

$$R = \lambda^2(kT/\hbar)\,(M/\mu)[\beta\omega/(\beta^2+\omega^2)]. \tag{37}$$

A remarkable feature of this result is that the only way in which collision dynamics enters is through the self-diffusion coefficient. The variation of R with temperature and pressure is determined by the dependence of D_{self} on the same variables. We are not aware of any experimental data with which to check this prediction. Also, the parameter λ can only be guessed at.

Experimental Study of the Shape of the *F* Band Absorption in NaCl

JORDAN J. MARKHAM* AND JOHN D. KONITZER

Zenith Radio Corporation, Chicago, Illinois

(Received August 4, 1960)

The possibility of extending the authors' study of the optical absorption band associated with *F* centers in KCl to KI, KBr, and NaCl is explored. Due to the relative sizes and positions of the *K* and *F* bands in KI and KBr, one cannot resolve the two. The situation in NaCl is unclear; hence, a detailed study has been made. A unique *F* center can be formed in this crystal by various techniques. The optical bleaching properties depend on the means of production. Smakula's equation applies to this center, and it seems to be Pekarian. Our "best equation" for the width at half-height H (in ev), has the form $H^2=0.075 \coth (105.5/\theta) - 0.01$; where θ is the temperature. This study supports the general theory [J. J. Markham, Revs. Modern Phys. **31**, 956 (1959)] although all the experimental problems have not been resolved.

I. INTRODUCTION

IN a recent paper, the optical absorption associated with the *F* center in KCl was studied in detail.[1] Most of the results agreed with the theory,[2] although some unsolved problems remained. One would like to extend these results to other traps in solids. The first step in this direction would be a study of the *F* band in other alkali halides. As stressed previously, we require an isolated band (no overlapping bands) caused by transitions between two bound states. Before a comparison between the data and the theory can be made, a detailed study of the band is required.[3] Here, we report our results on NaCl, KBr, and KI and compare the data of NaCl with the theory.

The absorption in the *F* region for NaCl, KCl, KBr, and KI is shown in Fig. 1. For KCl the *F* and *K* bands are clearly shown. Since the *K* band is small and does not completely overlap the *F*, one may obtain the violet side of the *F* band with a fair amount of accuracy, especially at low temperatures. This is not the case for KBr and KI, where the *K* band or bands overlap the *F* even at 4°K. Many of the features established in KCl hold for KBr and KI; however, a "complete" study seems impossible.

NaCl is an enigma. The long tail to the violet may be due to an unresolved *K* band or bands or to a distortion of the true *F* band, which the present theory cannot explain. We carried through a study, assuming that the *K* band is not important. Later, the authors felt that the violet tail is due to the overlapping of small *K* bands which cannot be resolved. This is our tentative explanation of the lack of correlation with the theory. Since a large fraction of the work on color centers has been done on NaCl, a study of the parameters associated with this band is of general interest.

The equipment and notation has been described previously.[1,2] Some definitions will be given in Table III.

TABLE I. Ranges of half-width values.

Temperature	av H ev	ΔH ev	No. of determinations
5°K	0.254	±0.003	3
78°K	0.278	±0.004	8
300°K	0.46	±0.010	5

II. BAND SHAPE

A. Preparation of Sample

We were able to color NaCl additively by our previous techniques. The crystal temperature was 780°C, while the sodium was held at 570°C. An oil quench[1] does not remove a band at 2.18 ev (room temperature) which we believe is due to colloidal metal. The Göttingen technique[1] was more successful (see Fig. 2). The

TABLE II. Values of H previously reported.

Temperature	H ev	Observer (*s*)
5°K	0.29	Russell and Klick[a]
5°K	0.28	Duerig and Markham[b]
87°K	0.34	Mollwo[c]
81°K	0.31	Russell and Klick[a]
78°K	0.28	Duerig and Markham[b]
300°K	0.47	Mollwo[c]
300°K	0.54	Smakula[d]
300°K	0.50	Russell and Klick[a]
300°K	0.49	Duerig and Markham[b]

* Present address: Physics Division, Armour Research Foundation, Chicago, Illinois.

[1] J. D. Konitzer and J. J. Markham, J. Chem. Phys. **32**, 843 (1960).

[2] J. J. Markham, Revs. Modern Phys. **31**, 956 (1959).

[3] For such a study on KCl, see J. D. Konitzer and J. J. Markham, Phys. Rev. **107**, 685 (1957).

[a] G. A. Russell and C. C. Klick, Phys. Rev. **101**, 1473 (1956).

[b] W. H. Duerig and J. J. Markham, Phys. Rev. **88**, 1043 (1952).

[c] E. Mollwo, Z. Physik **85**, 56 (1933).

[d] A. Smakula, Z. Physik **59**, 603 (1930).

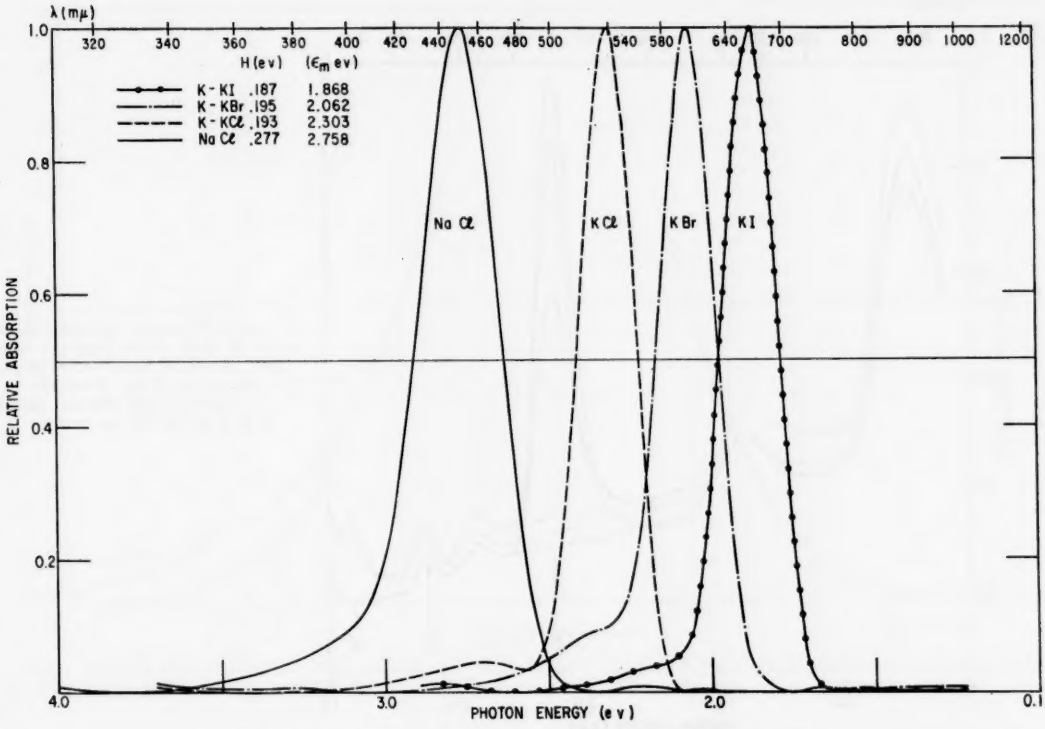

FIG. 1. Optical absorption of KI, KBr, KCl, and NaCl measured at 78°K.

bands to the violet of the *F* seem to be those discussed by Etzel and Patterson.[4] To the red, an *M* and *N* are indicated. We believe that the 2.2 ev structure is due to a combination of *R*'s and colloidal centers. The width at half-height *H* of the *F* band, is small (0.279 ev the same as that for x-ray samples). Bleaching with *F* light causes *H* to increase from 0.279 to 0.328 ev. Light in the Etzel-Patterson bands (3.1 to 5.2 ev) cause the *F* band to rise and *H* decreases to 0.297 ev.

Coloration produced by soft x rays is primarily limited to the surface next to the x-ray equipment. Bleaching produces the *R*, *M*, and *N* bands and broadens the *F* as in KCl[3] (0.474 to 0.510 ev at room temperature). An overnight bleach with a tungsten lamp blackens the crystal. Shielded 140-kvp and 50-kvp x rays produce coloration which is nearly uniform with depth into the crystal. The *F* band also bleaches upon exposure to light; however, only an extremely small structure is formed to the red; prolonged bleaching makes the crystal transparent. Depending on the sample *H* can be changed from 0.275 to 0.290 or 0.333 ev.

From these studies, we conclude that bleaching properties of the *F* band in NaCl depend on the way the centers are formed. Limited observation indicates that the *F* band does not widen in the dark at room temperature.

B. Values of *H* at Fixed Temperatures

Is the *F* band independent of the way it is formed? This is the case in KCl. Samples of very high absorption gave a larger *H*, while those of very low absorption gave a lower value. On the samples with low absorption, the base line cannot be determined accurately. We do not believe that one can make sufficiently accurate measurements on the Beckman DU, when the maximum density is above 1.5, to determine the *F* shape accurately. We have, therefore, been forced to do some "selection" of the data. Eight measurements of *H* at 78°K indicate that it is independent of the way it was formed. In Table I, the average values of the "selected" data are reported. The variation in NaCl is much larger than that for KCl. There are three reasons for this: the uncertainty in the base line; the nonresolvable character of the band or bands to the violet; and further *H* has a larger value, hence the sides are less steep. In Table II, some values of *H* previously reported are given.

[4] H. W. Etzel and D. A. Patterson, Phys. Rev. **112**, 1112 (1958).

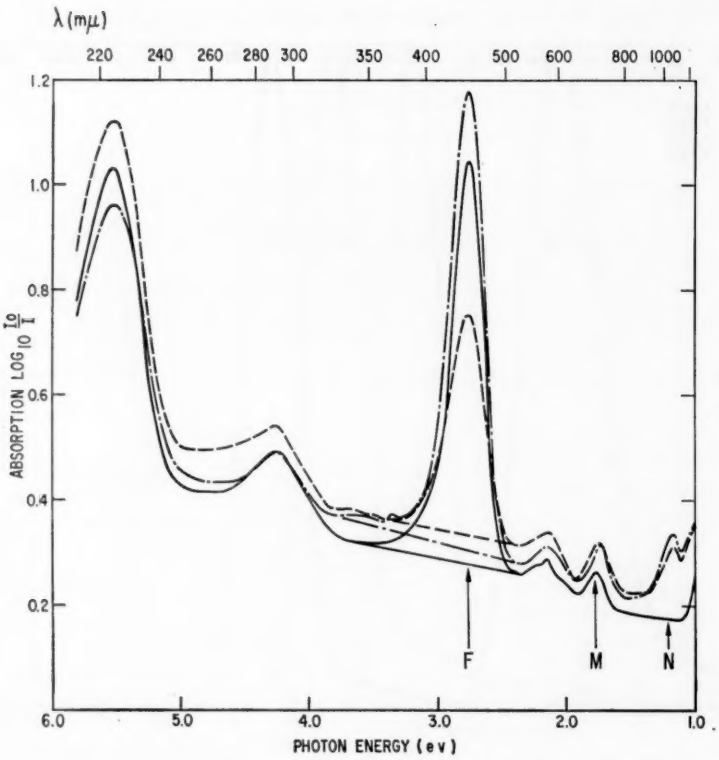

FIG. 2. Bleach of Na-NaCl measured at 78°K. ——: quenched from 790°C, $H=0.279$ ev; — — —: 10-min F bleach at R.T., $H=0.328$ ev; —·—: 2-hr uv (240–400 mμ) bleach at R.T., $H=0.297$ ev.

The conclusion from Tables I and II is that the data presented here is on a narrower band and applies to the pure center. While this center can be made by all three methods described above, the data is limited to those produced by hard x rays, since in this case, the best base line is obtained.

C. H and ϵ_m versus Temperature

Figure 3 shows plots of H and ϵ_m against temperature θ. The theoretical value of $dH/d\theta$ is zero at $\theta=0$°K; hence, the curve was made to have zero slope at 0°K. The spread of points is larger than in the case of KCl. The scatter of ϵ_m did not allow a detailed analysis.

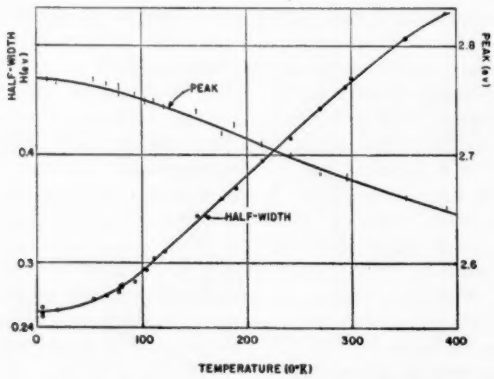

FIG. 3. F center in NaCl (ϵ_m and H vs θ°K).

D. Shape of F Band

The F band in KCl can be represented by two Gaussians or by a Pekarian curve. This fact permitted us to write down a reliable equation for the shape. In Fig. 4, we have again eliminated the thermal broadening (by dividing the photon energy by H and shifting the origin of the x axis). No significance can be attached to the small differences between the two experimental curves. A Pekarian curve[2] (with $S=30$) has been added to the figure. While the red side and the central portion of the band do resemble this curve, the violet side shows a deviation. The shape is not Gaussian, nor can it be represented by two such curves (see work cited in footnote 1, Fig. 6).

E. The Moments

The theory is in terms of the moments defined in Table III (also work cited in footnote 1). In KCl, it was possible to relate them to H and ϵ_m in a manner predicted by the theory. Table III summarizes our calculations on NaCl. The data does not justify elaborate calculations. To a fair approximation, M_0 is tem-

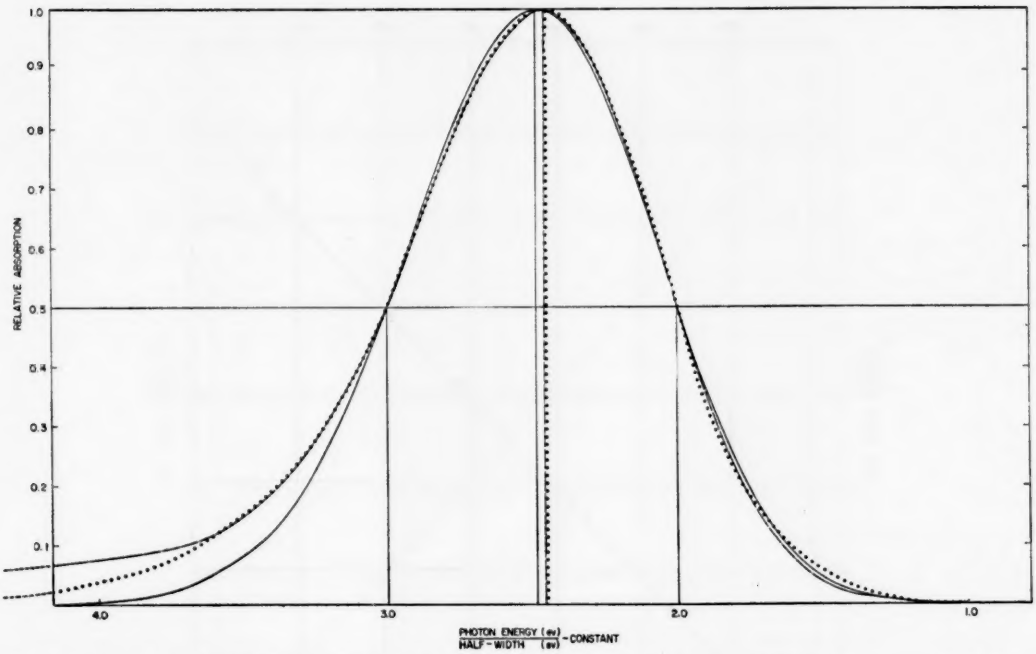

FIG. 4. Shape of *F* band in NaCl.—: Pekarian ($30^n/n!$); — — —: NaCl *F* band at 4.5°K (Constant = 8.4301); . . . : NaCl *F* band at 300°K (constant = 3.373).

perature independent and the ratio of $\alpha_m H$ to M_0 (Smakula's constant) is almost constant. The average value 1.17 is large compared to 1.04 for KCl, 1.06 for a Gaussian, and 1.07 for a Pekarian curve. Doyle[5] has previously obtained this ratio at room temperature. His value is 1.19±0.05, in agreement with our result. These facts establish Smakula's equation for NaCl, if we ignore the thermal variations of M_0.

Of special interest is the ratio of H to m. For a Gaussian curve, this ratio is 2.35, while for a Pekarian,

TABLE III. Properties of *F* center in NaCl x-irradiated at room temperature.

Temperature °K	Concentration[e] $Nf\times10^{-16}$ cm^{-3}	Half-width ev	Absorption coefficient α_m cm^{-1}[d]	ϵ_m[a] ev	ϵ_v[b] ev	ϵ_r[c] ev	$\frac{\epsilon_m-\epsilon_r}{\epsilon_v-\epsilon_m}$	m ev	H/m	M_0 ev cm^{-1}	$\frac{M_0}{\alpha_m H}$
5	5.3	0.255	19.01	2.768	2.904	2.649	0.88	0.198	1.29	5.76	1.19
5	5.8	0.254	20.77	2.772	2.903	2.649	0.94	0.198	1.28	6.26	1.19
Average		0.255		2.770	2.904	2.649	0.91		1.28		1.19
78		0.275	18.84	2.760	2.909	2.634	0.85	0.232	1.18	6.22	1.20
78		0.275	20.61	2.757	2.905	2.630	0.86	0.182	1.51	6.61	1.17
Average		0.275		2.758	2.907	2.632	0.86		1.34		1.18
176	2.6	0.358	6.77	2.725	2.918	2.560	0.86			2.74	1.13
300		0.468	11.33	2.676	2.930	2.462	0.84	0.275	1.70	6.04	1.14
300		0.470	12.37	2.677	2.935	2.465	0.82	0.264	1.78	6.73	1.16
Average		0.469		2.676	2.932	2.463	0.83		1.74		1.15
Over-all average							0.86				1.17

[a] ϵ_m-point of maximum absorption.
[b] ϵ_v-point on the violet which has half the maximum absorption.
[c] ϵ_r-point on the red which has half the maximum absorption.
[d] α-absorption coefficient; α_m-maximum value of α; $M_n=\int\alpha\epsilon^n d\epsilon$; $m^2=M_1/M_2-(\bar{\epsilon})^2$; f=oscillator strength.
[e] The concentration in column 2 is the rounded-off average value taken at the various temperatures. This is also the case for column 3 of Table II in the work cited in footnote 1. The column heading there should read $Nf\times10^{-18}$ cm^{-3}. The value of Nf varies slightly, depending on the value of n (index of refraction) employed.

[5] W. T. Doyle, Phys. Rev. **111**, 1072 (1958).

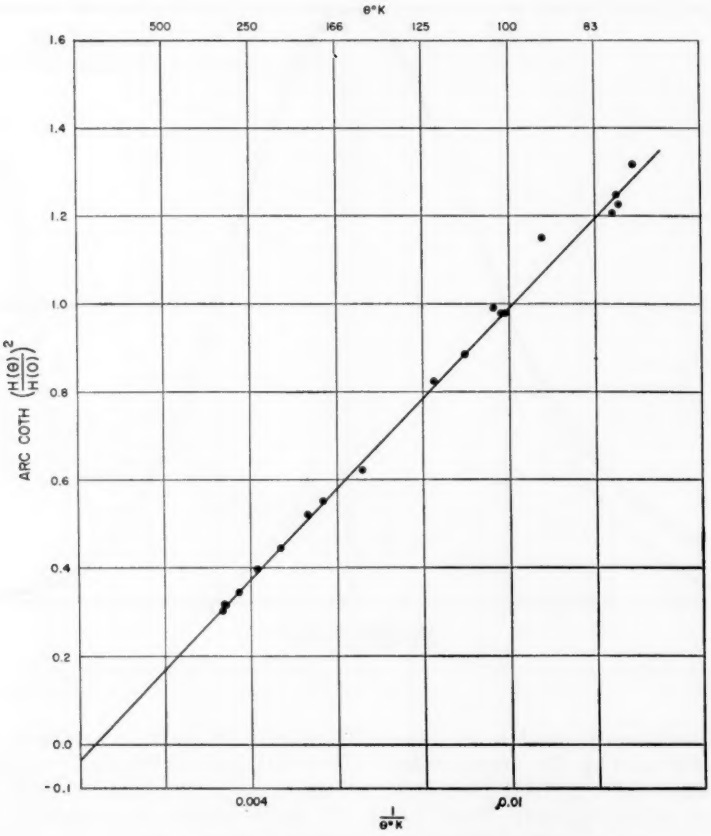

FIG. 5. F center in NaCl. $\omega=2\pi\times4.31\times10^{12}$ sec$^{-1}\approx0.0178$ ev.

it is 2.36. For a pure F band in KCl, it is 2.5; while for a composite F band, the ratio varied from 1.4 (at 5°K) to 2.2 (at 300°K). Table III indicates that in NaCl, the ratio varies from 1.3 to 1.8. By subtracting some of the violet tail of the band in a completely arbitrary manner, one may make the ratio vary from 2.2 to 2.4. This ratio suggests that there may be another band to the violet.

III. ANALYSIS

Again the temperature dependence of H has to be established. We assume that H is a better measure of m for the pure band than the calculated one. Hence, we wish to test the validity of the equation:

$$H^2(\theta)=D\coth(\hbar\omega/2k\theta)+C,$$

where ω is the effective angular frequency of the modes which interact with the trapped electron, and $\hbar$ and k have their usual meaning. Note that the constant C (see work cited in footnote 2; Sec. II) has been added. It may arise from additional terms in the derivation of the equation relating m to θ. In Fig. 5, arc coth$[H^2(\theta)/H^2(0)]$ is plotted against $1/\theta$. A straight line is obtained, but it does not go through the origin; this may indicate that $C\neq0$. In Fig. 6, arc coth$\{[H^2(\theta)-C]/[H^2(0)-C]\}$ is plotted against $1/\theta$ for $C=-0.01$ ev^2. Figure 6 gives a straight line which passes through the origin. The line in Fig. 6 is partly subjective. It seems to us that the method of least squares is of little assistance, since the spread in the points has to be weighted carefully to take account of the nature of the arc coth function. The lines drawn in Figs. 5 and 6 are the "best lines in the authors' opinion." The slope of the curve determines the effective angular frequencies of the modes associated with the center. It is $2\pi\times4.4\times10^{12}$ sec^{-1} or 0.0182 ev. This value is near the gap between the optical and acoustical branches according to calculations on NaCl.[6]

One is tempted to conclude from Fig. 6 that $C\neq0$ for NaCl. In view of the inconsistencies of the data, and exceptionally large value of C, the authors hesitate to make this conclusion. They believe that the techniques

[6] E. W. Kellermann, Phil. Trans. Roy. Soc. London **A238**, 513 (1940); J. J. Markham, J. Chem. Phys. **16**, 580 (1948).

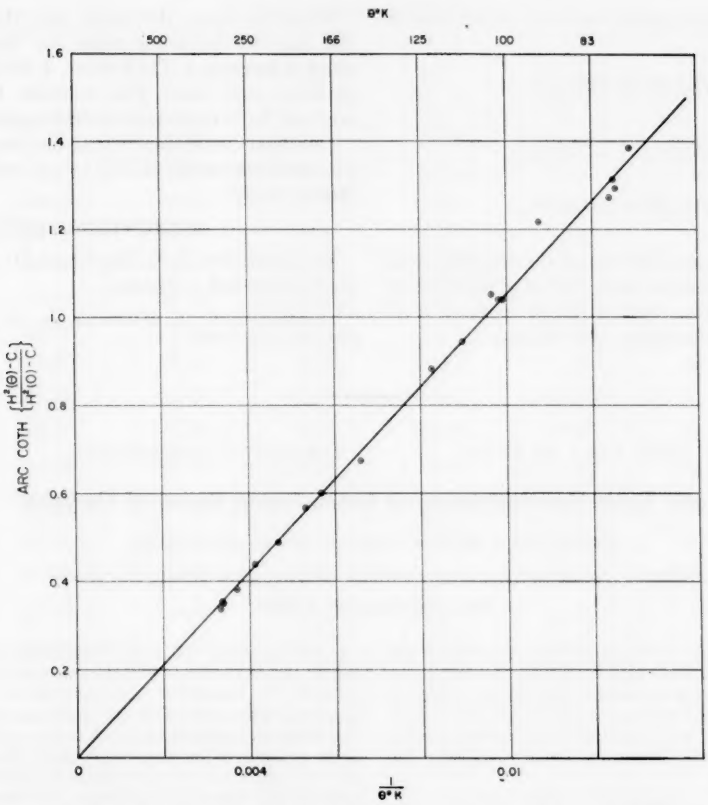

FIG. 6. F center in NaCl, $C=-0.01$ ev^2. $\omega=2\pi\times4.40\times10^{12}$ sec$^{-1}\approx0.0182$ ev.

developed in the work cited in footnote 2 should first be applied to more absorption and emission centers.

To obtain a value of the Huang-Rhys S factor,[2] a relation between m and H must be found. Further, we must consider the effect of C. The theory suggests that one can use the equation

$$S=m^2(0)/\hbar^2\omega^2=(D/\hbar^2\omega^2)(m^2/H^2).$$

Four possible values of S are shown in Table IV; 2.13 is the square of the average value of the ratio of H/m obtained from Table III. Since this value cannot be trusted, we also use the square of the ratio obtained for a Pekarian curve, i.e., 5.56 which results in $S=40$. This is in line with the value obtained for KCl.

TABLE IV.

	2.13	2.13	5.56	5.56
H^2/m^2	$C=0$	$C=-0.01$	$C=0$	$C=-0.01$
D	0.0650	0.0750	0.0650	0.0750
$\hbar\omega$(ev)	0.0172	0.0182	0.0172	0.0182
S	104	106	39.6	40.8

IV. CONCLUSIONS

Our conclusions for NaCl are not as definite as those for KCl. They will be limited to items firmly established.

(1) A unique F center can be produced by various coloring processes. Additive coloration does not produce one main band and the percentage of "secondary" centers is large. The shape of the F band is not affected, however.

(2) The bleaching property of the F center depends on the way it is produced, and the shape does not change in the dark at room temperature.

(3) The area under the absorption curve, i.e., M_0 is almost temperature independent.

(4) M_0 is proportional to $\alpha_m H$ the constant of proportionality; Smakula's constant is 1.17. This does not completely establish Smakula's equation because of item (3).

(5) Figure 4 indicates that the shape of the absorption band, in proper units, is temperature independent; hence, Eq. (9) of the work cited in footnote 1 holds approximately. The approximation occurs because the behavior of H is more complex here.

(6) The following equation holds for the half-width, i.e.,

$$H^2 = D \coth(\hbar\omega/2k\theta) + C,$$

with

$$D = 0.075; \qquad C = -0.01;$$

$$\omega = 2\pi(4.40) \times 10^{12} \text{ sec}^{-1}.$$

The value of ω suggests that we are dealing with local modes. It happens to agree with the value reported by Russell and Klick (see work cited in footnote a to Table II) although the values of H do not.

Recently, Karo, McCombie, and Murray,[7] calculated the effective frequency using the theory of the work cited in footnote 2. Their value, 4.40×10^{12} sec^{-1}, agrees perfectly with ours. This indicates that local modes may not be as important as first suggested.[1]

Our final conclusion is that one may not generalize the consistent result of KCl to any other band without further study.

ACKNOWLEDGMENTS

We thank Dr. H. N. Hersh and Dr. G. A. Noble for their advice and assistance.

[7] A. M. Karo, C. W. McCombie, and A. M. Murray, Phys. Rev. **119**, 504 (1960).

THE JOURNAL OF CHEMICAL PHYSICS VOLUME 34, NUMBER 6 JUNE, 1961

Shock Tube Determination of Dissociation Rates of Oxygen*

JOHN P. RINK,† HERBERT T. KNIGHT, AND RUSSELL E. DUFF

University of California, Los Alamos Scientific Laboratory, Los Alamos, New Mexico

(Received November 2, 1960)

The rate of dissociation of oxygen in Xe-O_2 mixtures was measured over a temperature range of 3000°K to 6000°K. An x-ray densitometer was used to measure the density during the dissociation process behind a shock wave. It was possible to match the experimental data with theoretical density profiles over a wide range of compositions and initial conditions. The reactions considered were

$$O_2 + M \underset{k_r}{\overset{k_d}{\rightleftarrows}} 2\,O + M,$$

where M can be Xe, O_2, or O. Considering these species as third bodies, the deduced recombination rates in cc^2 mole^{-2} sec^{-1} were $4.7 \times 10^{17}\ T^{-1}$, $1.6 \times 10^{18}\ T^{-1}$, and $4.8 \times 10^{18}\ T^{-1}$, respectively. The third-body efficiencies of O_2 and O relative to Xe are 3 and 10. Experimental conditions were such that an accurate measurement of the exponent of the temperature could not be made. However, since the data showed it to be within the limits of $-\frac{1}{2}$ and -2, a value of -1.0 was arbitrarily chosen. The agreement between results reported here and previous work demonstrates the potential utility of this method for kinetic studies of other reactions.

INTRODUCTION

THIS study has a twofold purpose, i.e., to demonstrate the feasibility of using x-ray densitometry of shock waves to determine chemical reaction rates and to obtain an accurate, independent measurement of the dissociation rate of oxygen. Previous measurements of the dissociation rate of oxygen in shock tubes have employed techniques based on interferometric measurements of density[1,2] and on ultraviolet light absorption to determine oxygen concentration.[3,4] An independent method of determining reaction rates is presented here. Density as a function of time behind a shock wave in Xe-O_2 mixtures was measured by x-ray absorption. Then an IBM 704 computer was utilized to calculate a density profile by integrating the simultaneous chemical kinetic equations which describe the system, subject to the appropriate hydrodynamic constraints. The reaction-rate coefficients were deduced from the experimental data by obtaining agreement between the measured and calculated density profiles.

Rates have been determined in mixtures of 95% Xe-5% O_2, 85% Xe-15% O_2, 50% Xe-50% O_2, and 30% Xe-70% O_2 at pre-shock pressures from 9 mm Hg to 30 mm Hg. The temperature range for these experiments was 3000°K to 6000°K.

THEORETICAL CONSIDERATIONS

The equation for the over-all rate of change of oxygen concentration at a given condition behind a shock wave in a mixture of Xe and O_2 is

$$(\partial[O_2]/\partial t)_v = -k_{d1}[O_2][Xe] - k_{d2}[O_2]^2 - k_{d3}[O_2][O] + k_{r1}[O]^2[Xe] + k_{r2}[O]^2[O_2] + k_{r3}[O]^3. \quad (1)$$

* Work done under the auspices of the U. S. Atomic Energy Commission.

† Material taken from thesis submitted in partial fulfillment of requirements for master of science degree in physics at the University of New Mexico, 1961.

[1] S. R. Byron, J. Chem. Phys. **30**, 1380 (1959).

[2] D. L. Matthews, Phys. Fluids **2**, 170 (1959).

[3] M. Camac and A. Vaughan, Avco Everett Research Laboratory, Research Report 84, AFBMD-TR-60-22.

[4] S. A. Losev, Doklady Akad. Nauk S.S.S.R. **120**, 1291 (1958); Soviet Phys.-Doklady **120** (467).

TABLE I. Resume of experiments.

No.	Composition % Xe	Composition % O_2	T_0 °C	P_0 mm Hg	Shock velocity mm/μsec	% Dis. of O_2	No-Reaction temperature °K
1	30.11	69.89	25.6	20.0	1.576	0.9	2710
2	30.11	69.89	27.3	10.0	1.814	8.9	3436
3	30.11	69.89	26.8	10.3	1.858	11.0	3580
4	30.11	69.89	25.8	9.9	2.001	17.1	4062
5	50.02	49.98	28.0	20.2	1.757	14.7	4520
6	50.02	49.98	26.0	20.1	1.548	7.0	3621
7	50.02	49.98	27.6	20.2	1.498	5.6	3422
8	85.00	15.00	26.1	20.1	1.315	34.2	4459
9	85.00	15.00	25.8	19.9	1.339	37.6	4609
10	85.00	15.00	26.0	20.1	1.318	34.6	4478
11	85.00	15.00	25.3	30.4	1.239	22.8	3998
12	95.01	4.99	24.4	20.0	1.432	99.5	6014
13	95.01	4.99	23.5	20.1	1.340	97.3	5300
14	95.01	4.99	26.0	19.9	1.229	81.9	4510
15	95.01	4.99	24.3	29.9	1.179	70.7	4173
16	95.01	4.99	25.2	18.9	1.267	90.1	4774

Ozone was not considered as an intermediate in the dissociation process since it has been shown to be unimportant under the conditions of this experiment.[4,5] If rotational and vibrational equilibrium is assumed, one can say that the rate coefficients in Eq. (1) are related to K, the equilibrium constant, by

$$K = k_{d1}/k_{r1} = k_{d2}/k_{r2} = k_{d3}/k_{r3}. \quad (2)$$

Glick and Wurster[6] and Losev[4] have observed a separation between vibrational relaxation and the O_2 dissociation process in a shock tube. Camac and Vaughan[3] have made a similar observation at temperatures below 8000°K. Above this temperature they found that the two rates become comparable. Thus the assumption that rotational and vibrational equilibrium is established before appreciable dissociation occurs appears to be valid, and Eq. (2) should hold for the shock conditions used in this work.

Since the rate coefficients are related by Eq. (2), and the entire course of dissociation from the very early stages to equilibrium is considered in the data analysis, logically either the dissociation or the recombination rate coefficient may be used to define the reaction rate for a given third body. In this paper the rate coefficients are expressed in terms of the recombination rate k_r in the form

$$k_{ri} = A_i T^{mi}. \quad (3)$$

The index differentiates between the three possible third bodies as indicated in Eq. (1). The activation energy for the recombination process is assumed to be zero which implies that the activation energy for dissociation is the dissociation energy.

Rate determinations were made by comparing calculated density-distance profiles behind shock waves with those obtained experimentally. The computation of a density vs distance profile was made with an IBM 704 code by Duff.[7] Briefly, the code calculates density as a function of time or distance behind the shock as the kinetic processes proceed subject to the appropriate hydrodynamic constraints. For these calculations the following data must be supplied: either a dissociation or recombination rate coefficient for each reaction pair considered; the shock velocity; and parameters specifying the state of the gas assuming vibrational and rotational equilibrium but no chemical reaction. These no-reaction parameters of pressure, density, temperature, and particle velocity behind the shock front for a given shock velocity were calculated in the usual way from the conservation laws for mass, momentum, and energy and the perfect gas law. Values of enthalpy and free energy as function of temperature needed in these calculations were obtained from quartic polynomial fits of the O_2 data of Johnston *et al.*[8] and the NBS tabula-

[5] R. E. Duff, Phys. Fluids **1**, 242 (1958).
[6] H. S. Glick and W. H. Wurster, J. Chem. Phys. **27**, 1224 (1957).
[7] R. E. Duff, J. Chem. Phys. **28**, 1193 (1958).
[8] H. Johnston, L. Savedoff, and J. Belyer, Ohio State Project RF-316, TR-316-4.

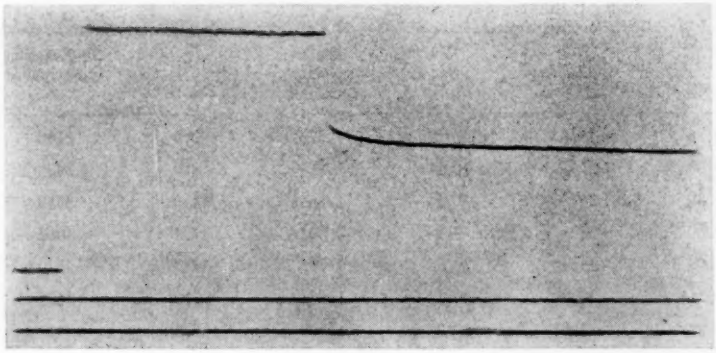

FIG. 1. A typical oscilloscope record of the change in x-ray transmission across a shock in a 95% Xe–5% O_2 mixture at an initial pressure of 19.9 mm Hg. This record corresponds to experiment No. 14 in Table I. The three sweep traces from top to bottom are the x-ray signal, a displaced base line, and 100-μsec timing marks. Shock velocity was 1.229 mm/μsec.

tions for O atom.[9] The heat of formation of O was assumed to be 58.98 kcal/mole.[10]

An iterative procedure was used to deduce the k_{ri} from the experimental density-time profiles. The first step was to derive an approximate Xe rate by fitting the 95% Xe-5% O_2 data. In this fitting the rates for O_2 and O as third bodies given by Camac and Vaughan[3] were used, and the Xe rate was varied until agreement was obtained. Using this value for the Xe rate and the 30% Xe-7% O_2 data, new values for the O_2 and O rates were obtained. This cycle was repeated until a consistent set of k_{ri} was obtained which fit the experimental profiles equally well over the entire experimental range of composition and temperature. The profiles calculated for intermediate compositions lacked sensitivity to variations of a single rate coefficient. However, they were useful as an over-all check of the final set of rates.

EXPERIMENTAL PROCEDURE

The shock tube and x-ray densitometer as described by Knight and Venable[11] were used in the experiment. However, several modifications to improve the accuracy and reliability of the apparatus and experimental techniques were made.

The driver section was a brass tube, 4 ft long and 4 in. i.d., wrapped with heating tapes so that it could be heated to 100°C. The expansion chamber was a circular cross-section brass tube, 3 in. i.d. and 15 ft in length. The x-ray slits, located 14 ft from the diaphragm, were $\frac{3}{4}$ mm wide. A pure tungsten emitter consisting of 20 turns of 0.020-in. wire was used as the cathode in the demountable x-ray tube. A modified RCA 2020 photomultiplier tube having only 7 amplification stages was used in conjunction with a terphenyl-in-polystyrene scintillator to detect the x-rays. The entire x-ray detection circuitry had a time constant of less than 0.4 μsec. The ionization probes[12] used to detect the arrival of the shock wave at various points along the shock tube were equipped with a 0.5-mm step which projected into the flow immediately downstream of the electrodes. This design markedly improved the performance of the ionization probes in the lower part of the velocity range studied.

In order to determine the magnitude of the shock front curvature and/or tilt, an endplate of $\frac{3}{4}$ in. thick steel was fitted with 6 ionization probes ground flush with the endplate. Of the 6 probes, 4 were arranged on one diameter and 3 on a diameter normal to the first—a probe in the center was common to both diameters. Four of these probes were located on a circle with a radius of 1.44 in., and one probe was located 1.13 in. from the center. Signals from these probes were delayed from 1 to 6 μsec at 1-μsec intervals and displayed on an oscilloscope.

The diaphragm material used in these experiments usually consisted of one to four sheets of 0.005-in. Mylar. For the strongest shocks, 0.032-in. copper plates variously scribed 0.010 in. to 0.015 in. deep were used. In all experiments helium driver-gas pressure was raised until the diaphragm ruptured spontaneously. Bursting pressures varied from 80–600 psig. Helium was used instead of hydrogen to eliminate shock perturbations due to burning at the contact surface. In experiments where a strong shock was desired, the driver section was heated to a temperature of 100°C.

The expansion chamber could be evacuated to a pressure of 0.4μ of Hg. The leak rate, measured prior to every experiment, was usually less than 1 μ in 5 min, and was never more than 1 μ in 3 min. Since 10 min was the normal time from the start to completion of an experiment, the impurity level was negligible.

During an experiment two oscilloscope traces of the x-ray signal were obtained simultaneously. One showed the full x-ray signal, including the zero transmission level. The other, at a five times faster sweep speed, showed only the shock front and dissociation region. Records of the anode voltage of the x-ray tube and shock velocity signals were also obtained for every experiment. Endplate probe signals were recorded when desired. The wave form of the x-ray pulse was very reproducible. Monitor traces were obtained after

[9] *Selected Values of Chemical Thermodynamic Properties* (National Bureau of Standards, Washington, D. C., 1947), Ser. III, Table 7.
[10] P. Brix and G. Herzberg, Can. J. Phys. **32**, 110 (1954).
[11] H. T. Knight and D. Venable, Rev. Sci. Instr. **29**, 92 (1958).
[12] H. T. Knight and R. E. Duff, Rev. Sci. Instr. **26**, 257 (1955).

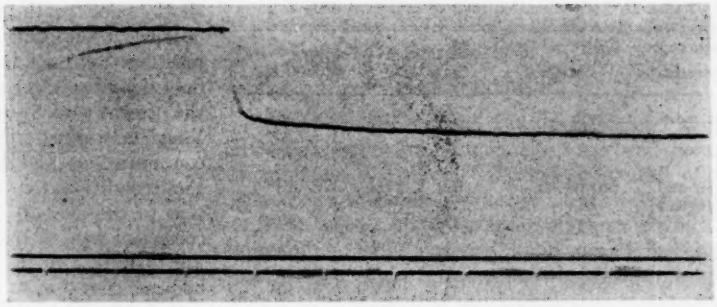

FIG. 2. Same signal as Fig. 1, except that a faster sweep speed was used, 10-μsec timing marks. The base line is not displaced in this record.

each experiment by again pulsing the x-ray tube. These monitor traces were used in the data reduction procedure to establish what the x-ray output would have been in the absence of the shock.

The signals from four ionization probes were displayed on a rasterscope and used for velocity measurement. The distance between the first and last probe was 1.114 m; the x-ray station was located midway between the last two probes. Shock wave attenuation, measured for each experiment, amounted to approximately 1%/m. The shock velocity at the x-ray station was inferred with an accuracy of 0.2% from a curve of average velocity between successive pairs of probes vs position in the tube. This measurement was quite important since the no-reaction temperature depends strongly upon it. A 1% error in the shock velocity would result in a 1.5% to 1.9% error in the no-reaction temperature, depending upon the shock strength and initial composition.

The xenon used in the experiment was obtained from the Mansanto Chemical Company, Mound Laboratory, Miamisburg, Ohio, and was 99.8% pure. It had an unnatural isotopic composition as follows: xenon 131—10.7%; xenon 132—16.9%; xenon 134—28.9%; and xenon 136—43.5%. The oxygen used was ordinary Linde tank grade, 99.8% pure. None of its impurities could have resulted in an observable change in the final rate values, since the impurities have been found to be less efficient than O_2 or O in producing dissociation.[1]

Calibration and data reduction procedures have been described in detail elsewhere.[11] Calibration runs were made at an x-ray anode voltage of 25 kv and the results reproduced within 0.6% in transmission. The calibration curve for a given mixture was calculated from density-transmission data for individual components. The x-ray anode voltage during shock experiments was held at 25±0.1 kv. Separate calibration experiments and calculations were made which showed that in the worst possible case a 0.1-kv variation in the x-ray anode voltage would have produced only a 0.2% change in the final density, an uncertainty small compared to other errors.

Profiles representing the change in density as a function of distance behind the shock front were derived from photographs of oscilloscope traces of the amplitude of the detected x-ray signal as a function of time. Pulse height as a function of distance from a reference point on the trace and a distance-time relationship for the film were read from the records using an optical comparator. This information was combined, by means of a simple IBM 704 code, with calibration, pertinent shock-wave parameters and monitor trace data to yield the experimental density profiles.

The error in measured densities was usually less than 1%. However, in the oxygen-rich mixtures it became necessary to go to lower initial pressures to obtain shocks strong enough to produce measurable dissociation. The lower initial density and smaller changes in transmission across the shock led to a larger but still less than 2% error in measured density as determined by a comparison of the observed and calculated equilibrium densities.

RESULTS

A total of 16 experiments were performed with varying composition, initial temperature and pressure, and degree of dissociation. Details of the compositions, shock velocities, shock temperatures, and degrees of dissociation attained are reported in Table I. Typical x-ray records from experiment No. 14 in Table I are shown in Figs. 1 and 2. Figure 1 shows the entire x-ray signal, and Fig. 2 is a delayed, expanded signal showing in more detail the region in the vicinity of the front of the same shock. The mixture was 95% Xe-5% O_2 at an initial pressure of 19.9 mm Hg. The shock velocity was 1.229 mm/μsec. Figure 3 is a plot of the density profile calculated from these two records. The circles represent densities derived from the record in Fig. 1, and the X's are points from the record in Fig. 2. The solid line is the profile calculated using the rates determined by this work. The dotted lines represent a ±15% change in the Xe rate. The no-reaction density is observable in Figs. 1 and 2 as the start of the trace immediately following the abrupt change in x-ray signal due to the shock. As can be seen from Fig. 3, this no-reaction point is 3.8 mm behind the shock front. This delay varied from 2 mm to 8 mm and was produced mainly by vibrational relaxation, but included transit time across the beam and response time of the electronic circuitry. Endplate measurements have eliminated the possibility of devia-

TABLE II. Recombination rates of oxygen at 3500°K.

Investigator	Method	Type third body	k_r, cc² mole⁻² sec⁻¹ at 3500°K
This paper	x ray	O_2	4.6×10^{14}
		Xe	1.3×10^{14}
		O	1.4×10^{15}
Camac and Vaughan	ultraviolet	O_2	1.6×10^{14}
		Ar	5.2×10^{13}
		O	1.3×10^{15}
Byron	light-interferometer	O_2	4.8×10^{14}
		Ar	4.5×10^{13}
		O	9.9×10^{14}
Matthews	light-interferometer	O_2	8×10^{14}
Losev	ultraviolet	O_2	2×10^{14}
Chesick & Kistiakowsky	x ray	O_2-Xe	2×10^{14}

tions from a planar shock contributing to this delay. At no time did wave curvature and/or tilt cause the wave front to deviate from a diametral plane by as much as the x-ray slit width, i.e., $\frac{3}{4}$ mm. Normally these effects were less than half the slit width.

A set of rate coeficients k_{ri} was found with which it was possible to fit all 16 experiments. The recombination rates for each of the third bodies, Xe, O_2, O, as determined in this experiment are listed below,

$$k_{r\mathrm{Xe}}=4.7\times10^{17}T^{-1}\pm15\%$$

$$k_{rO_2}=1.6\times10^{18}T^{-1}\pm20\%$$

$$k_{r\mathrm{O}}=4.8\times10^{18}T^{-1}\pm20\% \quad \mathrm{cc}^2 \quad \mathrm{mole}^{-2} \quad \mathrm{sec}^{-1}.$$

Analysis of the data obtained in this work revealed that the 3000°K to 6000°K temperature range covered was insufficient to do more than establish the limits of $-\frac{1}{2}$ to -2 for the temperature exponents m_i. Therefore they were arbitrarily set equal to -1.0. The error limits were obtained by varying successively the recombination rates until the calculated density profiles deviated significantly from the experimental density profiles as shown in Fig. 3 for $k_{r\mathrm{Xe}}$. This procedure is legitimate because each of the three dissociation reactions predominates over the other two for some range of composition and extent of reaction.

COMPARISON WITH OTHER RESULTS

The recombination rate coefficients reported by different investigators for various third bodies evaluated at 3500°K are presented in Table II. A value of 8.36×10^{-7} moles/cc for the equilibrium constant at 3500°K was used in converting the dissociation rates to recombination rates.

Camac and Vaughan[3] utilized an ultraviolet light absorption technique to observe the rate of disappearance of O_2 behind shock waves in Ar-O_2 mixtures. From this information and knowledge of initial conditions and shock velocity, the published rate coefficients were obtained. According to their report recombination reactions were not included in their calculations. The only significant disagreement between their results and the present work is over the value of k_{rO_2}. Camac and Vaughan worked with relatively small initial oxygen concentrations and high shock temperatures. Under these conditions the O_2 reaction made a small contribution to the over-all dissociation process, and its rate coefficient was, therefore, difficult for them to measure. For these reasons the value of 8 reported for the third-body efficiency of O relative to O_2 disagrees with the value of 3 which we obtained. Since our value of k_{rO_2} was obtained by a detailed analysis of the entire dissociation process from the onset of reaction to equilibrium including the effects of recombination in gas mixtures at higher initial pressures and higher oxygen concentrations, we suggest that it is probably the more reliable result. In this paper the relative efficiency of one third body to another will be defined as the ratio of their respective rate coefficients at 3500°K.

Byron,[1] using an optical interferometer and drum camera, measured the time required for half the density change due to dissociation to occur. From this he deduced rates of dissociation. He worked with both pure oxygen and oxygen diluted with argon. Recombination effects were not included in his calculations. Therefore, his results also are probably somewhat low. However the third-body efficiency of O relative to O_2 reported by Byron is not in serious disagreement with our value.

Matthews[2] obtained Mach-Zehnder interferograms of shocks in pure oxygen. From these he derived a density vs distance profile behind the shock. He then compared the experimental profiles with profiles calculated using a collision theory rate equation. He was the first to consider both dissociation and recombination in the analysis of his data. Matthews was unable to measure the rate of dissociation caused by the O_2–O collisions, so for his calculation he used Byron's work

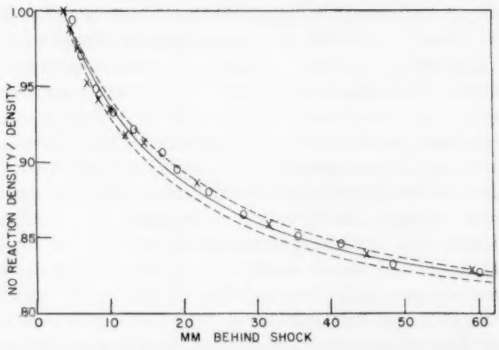

FIG. 3. Plot of density profile. Circles represent density points from record in Fig. 1, and X's are points from record in Fig. 2. Solid line is profile using rates which fit all the experimental density profiles. The dotted lines represent a ±15% change in the Xe rate.

to obtain information concerning O to O_2 third-body efficiency ratio. If the O to O_2 efficiency ratio were larger than that given by Byron, as reported by both Camac and Vaughan and this work, the rate quoted by Matthews would tend to be too high.

Losev[4] employed ultraviolet absorption to measure the temperature distribution behind shocks in pure oxygen. He worked with strong shocks, 2.7-3 mm/μsec, and a low initial pressure of 7.6 mm of Hg. Under these conditions the results of Camac and Vaughan suggest that he was probably observing vibrational relaxation and dissociation simultaneously. The rate quoted in Table II was taken from a graph and is probably only accurate to 50%.

The rate reported by Chesick and Kistiakowsky[13] is the average of only two experiments. There was no mention of any attempts to separate the rates of the different third bodies; so this rate is probably an average of effects of all third bodies present. A mixture of 25.1% Xe-74.9% O_2 was used in their experiment.

[13] J. P. Chesick and G. B. Kistiakowsky, J. Chem. Phys. **28**, 956 (1958).

CONCLUSIONS

The combination of the x-ray densitometer and an IBM 704 computer for data analysis has been shown to be adaptable to a study of the dissociation rate of oxygen. With a single set of rate coefficients it was possible to fit the density profiles of 16 experiments in which the composition, initial pressure, and degree of dissociation were varied. Fair agreement with previous work is obtained. It is felt that this investigation demonstrates the feasibility of using this method in kinetic studies of other gases.

ACKNOWLEDGMENTS

The authors take pleasure in acknowledging many fruitful discussions with Dr. Garry L. Schott and are indebted to Richard E. Johnston for his help in performing the experiments.

Effect of Pressure on the Resistance of Iodine and Selenium*

A. S. Balchan and H. G. Drickamer

Department of Chemistry and Chemical Engineering, University of Illinois, Urbana, Illinois

(Received December 15, 1960)

The effect of pressure from 60 to over 400 kbar has been measured on the resistance of selenium and iodine. Selenium exhibits a very rapid drop in resistance between 60 and 128 kbar; at 128 kbar it shows a discontinuous drop. At higher pressures its behavior is apparently metallic. Iodine shows a rapid drop in resistance from 60 kbar to the region of 225–255 kbar where there is relatively abrupt change of slope. At higher pressures the change in resistance with pressure is much smaller. It is interesting to note that the optical energy gap of selenium extrapolates to zero at about 130 kbar, while the optical gap for iodine extrapolates to zero at 240 kbar.

WITH the use of apparatus previously described,[1] the resistance of selenium and iodine has been measured from 60 to over 400 kbars pressure. The selenium used was from the same stock as that used for previous high-pressure optical studies.[2] The iodine was resublimed single-crystal material.

The relative resistance of selenium as a function of pressure is shown in Fig. 1. The first reliable resistances could be obtained at about 60 kbar. It drops by about five orders of magnitude to 128 kbar where there is a transition involving a further decrease of about three orders of magnitude. The behavior near the transition was erratic and sluggish. On six runs it apparently occurred at low as 115 kbar and as high as 140 kbar. Above the transition the resistance drops slowly and the selenium is almost certainly metallic. The relative resistance of the metallic phase is shown in Fig. 2 on an expanded resistance scale. It is difficult to estimate absolute resistances; however, two different methods (a) comparison with previous measurements for metals, e.g., barium in the same apparatus; (b) estimation of sample dimensions) give values of $50–100\times10^{-6}$ ohm cm at 140 kbar. The dotted curve in Fig. 1 shows Bridgman's[3] results with his pressures corrected to the present

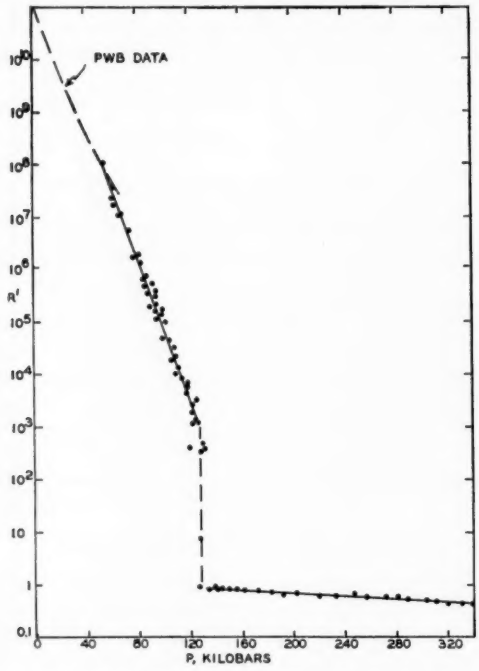

FIG. 1. Selenium, relative resistance vs pressure.

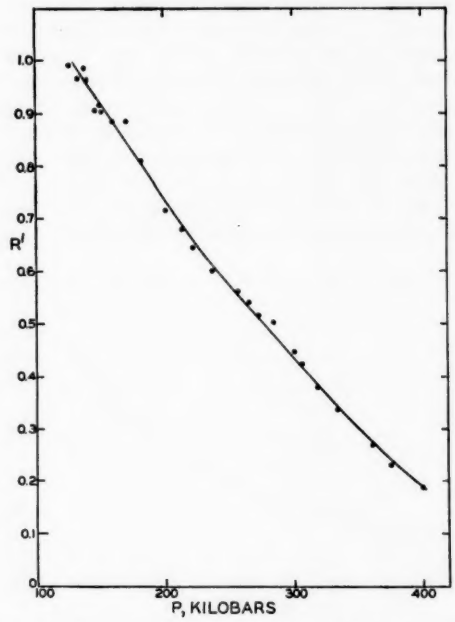

FIG. 2. Selenium (metallic phase), relative resistance vs pressure.

* This work was supported in part by the U. S. Atomic Energy Commission.

[1] A. S. Balchan and H. G. Drickamer, Rev. Sci. Instr. **32**, 308 (1961).

[2] H. L. Suchan and H. G. Drickamer, J. Chem. Phys. **31**, 355 (1957).

[3] P. W. Bridgman, Proc. Am. Acad. Arts and Sci. **81**, 165 (1952).

scale.[1] There is reasonable agreement on the slope. It is interesting to note that pressure measurements on the optical absorption edge[2] indicate that it extrapolates to zero at about 130 kbar. There are a number of reasons why one would not expect this close a comparison, but the agreement cannot be entirely fortuitous.

The effect of pressure on the relative resistance of iodine is shown in Fig. 3. It was not possible to obtain resistances below about 80 kbar. There is a rapid drop in resistance in the low-pressure region. No discontinuity in the resistance occurs, but in the region from 225 to 255 kbar there is a rather abrupt change of slope, and above this pressure the resistance drops relatively slowly. This is illustrated more clearly on the enlarged scale of Fig. 4. By extrapolation of the resistances of both sections of the curve a pressure of about 235 kbar is estimated for the "transition to the metallic phase," although one cannot really state that a transition occurs. Again, it is interesting to note that

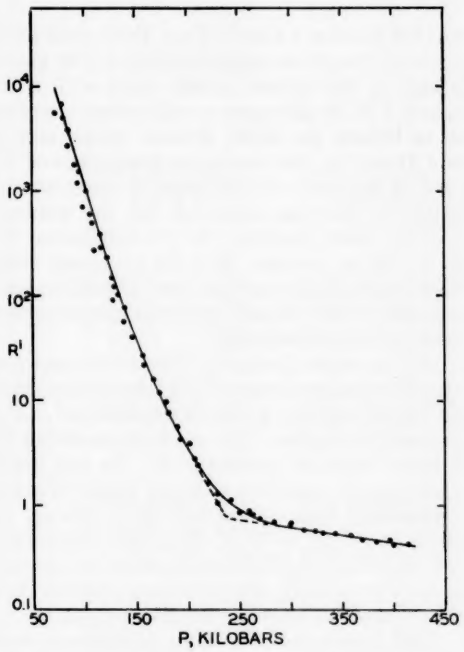

FIG. 3. Iodine, relative resistance vs pressure.

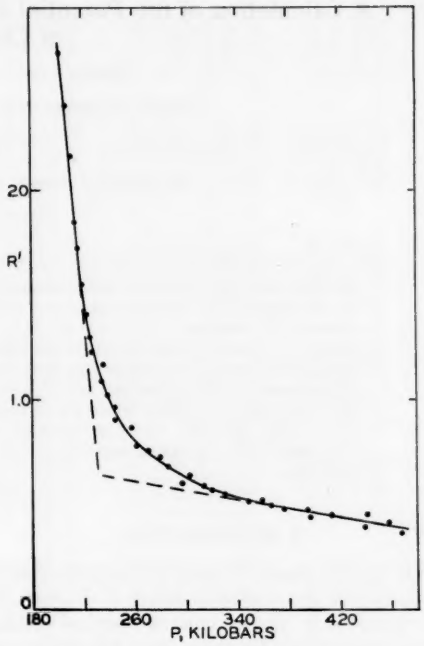

FIG. 4. Iodine (high pressure region), relative resistance vs pressure.

the optical energy gap extrapolates to zero at about 240 kbar.[2] Estimates by various methods (see above) give a resistivity of $60\text{–}120\times10^{-6}$ ohm cm at 350 kbar.

It seems clear that an insulator could become a metal by the continuous approach and eventual overlap of the valence and conduction bands with no first-order phase transition. This seems to be the case with iodine. Alternatively, the attainment of the metallic state could be accompanied by a rearrangement of the atoms involving a discontinuous volume change and generally a discontinuous resistance change (first-order phase transition). Selenium would appear to illustrate this latter behavior. Most good metals have a relatively simple, compact crystal structure, so that one would expect that iodine would ultimately undergo a first-order transition, although it might be too sluggish to run at any measurable rate at room temperature and any attainable pressure.

A Calculation of the Potential Energy Curves for Some Electronic States of Carbon Monoxide

HÉLÈNE LEFEBVRE-BRION AND C. M. MOSER

Centre de Mécanique Ondulatoire Appliquée, 155 rue de Sèvres, Paris

AND

R. K. NESBET

Department of Physics, Boston University, Boston, Massachusetts

(Received November 8, 1960)

The LCAO-MO SCF orbitals for the $^1\Sigma^+$ ground state of carbon monoxide, constructed from 1*s*, 2*s*, and 2*p* atomic functions, have been calculated for 11 internuclear distances between 1.5 and 4.0 a.u. Using the unoccupied SCF orbitals a number of lower excited states have been calculated. The equilibrium distances, force constants, and ν_{00} energies have been calculated from the curves of E vs R for these various states. As these calculated curves do not separate at infinity into the atoms in their proper spectroscopic states, configuration interaction has been carried out with functions which cross the computed curves and separate into the atoms in their ^3P states. The lower states of carbon monoxide seem to be divided into three classes: (a) those which are reasonably well represented by our functions, namely, $X\,^1\Sigma^+$, $e\,^3\Sigma^-$, $a'\,^3\Sigma^+$, $A\,^1\Pi$, and $a\,^3\Pi$; (b) those which are not at all well represented by our functions, namely, $b\,^3\Sigma^+$, $B\,^1\Sigma^+$, and $C\,^1\Sigma^+$; (c) those states for which the experimental assignment may be in error, namely, $d\,^3\Pi$ and $F\,^1\Pi$.

I. INTRODUCTION

ONE cannot expect a very satisfactory characterization of the electronic states of diatomic molecules using only the calculated vertical excitation energies particularly for those cases where the experimental data is subject to more than one assignment. It is evidently desirable to obtain potential curves to describe the electronic states, but this has only recently become a feasible project with the completion of digital computer programs capable of doing these tedious calculations rapidly and accurately.

Recently we have discussed some of the lower electronic states of carbon monoxide from the vertical excitation energies calculated from the LCAO-MO SCF orbitals for the ground state, these orbitals being linear combinations of 1*s*, 2*s*, and 2*p* atomic functions on each center.[1] From this calculation it would seem that this simple method is rather satisfactory for some of the lower states, but the states which lie near the ionization potential appear to require functions built on a larger basis set.

While the computer programs used in the present work make it possible to carry out calculations using any desired basis set, our knowledge of the applicability of simple wave functions to a study of excited states is so meager that it seems worthwhile to construct potential curves based on only 1*s*, 2*s*, and 2*p* functions, before considering more complicated functions.

We have recently pointed out that programs written by one of us (R.K.N.) for the IBM 704 computer make it possible to calculate the LCAO-MO SCF orbitals for carbon monoxide with the basis set 1*s*, 2*s*, and 2*p* atomic functions in less than 10 min (for a given set of parameters).[2] The calculation was repeated for 12 different values of R between 1.5 and 4.0 a.u. From these point, the curves of E vs R were constructed for the $^1\Sigma^+$ ground state and for four lowest excited states $a\,^3\Pi$, $a'\,^3\Sigma^+$, $e\,^3\Sigma^-$, and $A\,^1\Pi$. In this paper we will extend our calculation to include the triplet d state (which may be either $d\,^3\Pi$ or $d\,^3\Delta$) and four higher-lying states of $^1\Sigma^+$s $^3\Sigma^+$, and $^1\Pi$ symmetry. For all these 10 states we shall calculate the following quantities: (a) the quadratic term of the force constant; (b) the equilibrium distance; (c) the ν_{00} energies. With the previously calculated vertical excitation energies these properties should make possible a fairly detailed understanding of some of the states of carbon monoxide.

We wish to emphasize the fact that in this paper we will use the usual spectroscopic notation for the lowest excited states only as a guide for discussion of the results of our calculations. Thus we have calculated the three lowest states of symmetry $^1\Sigma^+$, the two lowest $^3\Sigma^+$, the lowest $^3\Sigma^-$, and the two lowest $^1\Pi$ and $^3\Pi$ states. For *convenience* these states have been labeled, respectively, as $X\,^1\Sigma^+$, $B\,^1\Sigma^+$, $C\,^1\Sigma^+$, $a'\,^3\Sigma^+$, $b\,^3\Sigma^+$, $e\,^3\Sigma^-$, $A\,^1\Pi$, $F\,^1\Pi$, $a\,^3\Pi$, and $d\,^3\Pi$. In doing so we do not wish to imply any necessary correspondence between these calculated wave functions and the observed spectra.

It is well known that the single determinant wave function which is at least qualitatively suitable to describe a molecule near the equilibrium distance is quite unsuitable when the internuclear distance becomes large. We have thus recalculated the molecular properties (a)–(c) from curves which at least have proper behavior at infinity. Finally, we have compared these curves with the best available experimental results.

II. CALCULATIONS

The LCAO-MO SCF method is by now so well known that only a very brief description of the calculations need be given here.

[1] H. Brion and C. Moser, J. Chem. Phys. **32**, 1194 (1960).

[2] P. Merryman, C. Moser, and R. K. Nesbet, J. Chem. Phys. **32**, 631 (1960).

TABLE I. LCAO coefficients and orbital energies of SCF orbitals for carbon monoxide (atomic units).

$R=$		1.5	1.75	2.0	2.1319	2.25	2.5	2.75	3.0	3.25	3.5	3.75	4.0
$\mathcal{E}^c1\sigma$		−35.92682	−35.35657	−34.92907	−34.74392	−34.59654	−34.33043	−34.11262	−33.93104	−33.77732	−33.64550	−33.53124	−33.43129
$\mathcal{E}^c2\sigma$		−23.27080	−22.50967	−21.93834	−21.69088	−21.49395	−21.13848	−20.84768	−20.60535	−20.40026	−20.22443	−20.07203	−19.93868
$\mathcal{E}^c3\sigma$		−11.57495	−10.85850	−10.23198	−9.95175	−9.72980	−9.34282	−9.05260	−8.83715	−8.67686	−8.56585	−8.48830	−8.42330
$\mathcal{E}^c4\sigma$		−9.59538	−9.20368	−8.78362	−8.54236	−8.31357	−7.80310	−7.30503	−6.87144	−6.52101	−6.25686	−6.05494	−5.88969
$\mathcal{E}^c5\sigma$		−6.94596	−6.82433	−6.78662	−6.80123	−6.83223	−6.92890	−7.00094	−6.96078	−6.71749	−6.33427	−6.01741	−5.77655
$\mathcal{E}^c6\sigma$		−7.06120	−7.54481	−7.79249	−7.83712	−7.84031	−7.77450	−7.67096	−7.60378	−7.67206	−7.81379	−7.85908	−7.83919
$\mathcal{E}^c1\pi$		−9.31377	−8.90320	−8.57390	−8.42650	−8.30815	−8.09691	−7.93809	−7.84348	−7.85031	−7.90887	−7.90939	−7.86629
$\mathcal{E}^c2\pi$		−7.90158	−7.68509	−7.44715	−7.32001	−7.20682	−6.97055	−6.73561	−6.48431	−6.17333	−5.84663	−5.60875	−5.44079
$\mathcal{E}1\sigma$		−20.99977	−20.89971	−20.83434	−20.80409	−20.77812	−20.72565	−20.67611	−20.62797	−20.57634	−20.52896	−20.50588	−20.50518
$\mathcal{E}2\sigma$		−11.61067	−11.50518	−11.45397	−11.43946	−11.43123	−11.42353	−11.42322	−11.42551	−11.42398	−11.41222	−11.39781	−11.38260
$\mathcal{E}3\sigma$		−1.84073	−1.72265	−1.59493	−1.53153	−1.47860	−1.38000	−1.29937	−1.23345	−1.17608	−1.12896	−1.10215	−1.09303
$\mathcal{E}4\sigma$		−0.79981	−0.78496	−0.76749	−0.75830	−0.75063	−0.73767	−0.73036	−0.72792	−0.72751	−0.72665	−0.72509	−0.72128
$\mathcal{E}5\sigma$		−0.53929	−0.52363	−0.51133	−0.50517	−0.49911	−0.48243	−0.45846	−0.42695	−0.39158	−0.36834	−0.35814	−0.35077
$\mathcal{E}6\sigma$		1.20706	1.14040	0.96530	0.86408	0.77745	0.61718	0.49178	0.39957	0.34553	0.32962	0.31998	0.30539
$\mathcal{E}1\pi$		−0.86759	−0.75243	−0.65571	−0.61054	−0.57327	−0.50379	−0.44657	−0.40144	−0.37040	−0.35512	−0.35142	−0.35627
$\mathcal{E}2\pi$		0.39693	0.31723	0.25245	0.22383	0.20101	0.16012	0.12763	0.10275	0.08824	0.08726	0.09191	0.09871
1σ	$1s_C$	−0.00121	−0.00045	0.00002	0.00015	0.00022	0.00029	0.00028	0.00026	0.00022	0.00018	0.00015	0.00012
	$1s_O$	0.99621	0.99643	0.99667	0.99679	0.99687	0.99702	0.99713	0.99720	0.99724	0.99726	0.99727	0.99729
	$2s_C$	−0.01709	−0.01119	−0.00731	−0.00591	−0.00493	−0.00346	−0.00250	−0.00186	−0.00141	−0.00108	−0.00084	−0.00065
	$2s_O$	0.03022	0.02319	0.01848	0.01680	0.01564	0.01394	0.01291	0.01229	0.01193	0.01174	0.01161	0.01151
	$2p_{\sigma C}$	−0.01094	−0.00842	−0.00620	−0.00530	−0.00462	−0.00352	−0.00274	−0.00216	−0.00173	−0.00139	−0.00112	−0.00089
	$2p_{\sigma O}$	0.01116	0.00833	0.00603	0.00509	0.00438	0.00320	0.00237	0.00176	0.00131	0.00090	0.00059	0.00038
2σ	$1s_C$	0.99491	0.99661	0.99702	0.99711	0.99717	0.99727	0.99735	0.99742	0.99746	0.99748	0.99749	0.99750
	$1s_O$	−0.00660	−0.00230	−0.00069	−0.00030	−0.00009	−0.00013	0.00020	0.00021	0.00019	0.00017	0.00015	0.00012
	$2s_C$	0.00544	0.01273	0.01410	0.01394	0.01363	0.01285	0.01218	0.01171	0.01142	0.01128	0.01121	0.01118
	$2s_O$	0.00727	−0.00218	−0.00441	−0.00444	−0.00420	−0.00344	−0.00270	−0.00208	−0.00160	−0.00124	−0.00097	−0.00076
	$2p_{\sigma C}$	0.00253	0.00549	0.00560	0.00517	0.00468	0.00365	0.00276	0.00205	0.00145	0.00094	0.00060	0.00040
	$2p_{\sigma O}$	0.01307	0.00461	0.00071	−0.00028	−0.00082	−0.00130	−0.00135	−0.00122	−0.00103	−0.00086	−0.00072	−0.00060
3σ	$1s_C$	−0.22786	−0.16529	−0.12785	−0.11413	−0.10409	−0.08748	−0.07479	−0.06449	−0.05546	−0.04578	−0.03564	−0.02632
	$1s_O$	−0.22878	−0.21777	−0.21264	−0.21213	−0.21269	−0.21612	−0.22114	−0.22644	−0.23142	−0.23637	−0.24075	−0.24398
	$2s_C$	0.00462	0.13261	0.20477	0.22596	0.23791	0.24747	0.24260	0.22914	0.20952	0.17957	0.14287	0.10695
	$2s_O$	0.87218	0.77873	0.75918	0.76758	0.78143	0.82070	0.86296	0.90109	0.93320	0.96213	0.98622	1.00339

TABLE I.—Continued.

	$R=$	1.5	1.75	2.0	2.1319	2.25	2.5	2.75	3.0	3.25	3.5	3.75	4.0
	$2p_{\sigma C}$	0.09516	0.13546	0.15435	0.15660	0.15550	0.14711	0.13482	0.12233	0.11121	0.09699	0.07924	0.06186
	$2p_{\sigma O}$	0.45471	0.36226	0.27645	0.23761	0.20640	0.15007	0.10495	0.06872	0.03853	0.01640	0.00446	−0.00159
	$1s_C$	−0.14561	−0.12997	−0.13720	−0.14580	−0.15505	−0.17626	−0.19543	−0.21012	−0.22055	−0.22708	−0.23071	−0.23278
	$1s_O$	0.10939	0.12001	0.12387	0.12355	0.12196	0.11497	0.10434	0.09211	0.07958	0.06654	0.05332	0.04100
4σ	$2s_C$	0.06825	0.27843	0.45357	0.53634	0.60603	0.73757	0.84067	0.91352	0.96238	0.99113	1.00613	1.01439
	$2s_O$	−0.50358	−0.61750	−0.65490	−0.65235	−0.64022	−0.59161	−0.52424	−0.45182	−0.38216	−0.31452	−0.24952	−0.19073
	$2p_{\sigma C}$	0.02293	0.04793	0.06036	0.05984	0.05562	0.03803	0.01576	−0.00357	−0.01510	−0.01441	−0.00736	−0.00013
	$2p_{\sigma O}$	0.88307	0.78332	0.68761	0.63641	0.58980	0.48425	0.37900	0.28130	0.19343	0.12791	0.08961	0.06654
	$1s_C$	0.12461	−0.13709	0.13898	0.13607	0.13124	0.11478	0.09251	0.06767	0.04155	0.02174	0.01246	0.00844
	$1s_O$	−0.04397	0.02639	−0.01008	−0.00181	0.00539	0.01943	0.03061	0.03872	0.04519	0.04658	0.01465	0.03459
5σ	$2s_C$	−0.94253	0.88022	−0.80709	−0.76156	−0.71531	−0.60025	−0.47035	−0.33713	−0.20384	−0.10496	−0.05914	−0.03937
	$2s_O$	0.19635	−0.09156	0.00178	−0.04097	−0.07706	−0.14469	−0.19520	−0.22932	−0.25541	−0.25432	−0.22134	−0.18005
	$2p_{\sigma C}$	0.53751	−0.54548	0.55582	0.56201	0.56852	0.58723	0.61672	0.66856	0.76488	0.86822	0.92483	0.95335
	$2p_{\sigma O}$	0.27712	−0.34359	0.41265	0.44995	0.48277	0.54378	0.58071	0.57721	0.50227	0.37448	0.27893	0.21818
	$1s_C$	−0.08251	0.02632	0.07757	0.08939	0.09431	0.09387	0.08604	0.07586	0.06503	0.05289	0.04178	0.03294
	$1s_O$	−0.09942	−0.12142	−0.12184	−0.11738	−0.11189	−0.09793	−0.08295	−0.06785	−0.05159	−0.03514	−0.02325	−0.01559
6σ	$2s_C$	−2.13342	−1.58385	−1.17186	−1.00628	−0.88223	−0.67771	−0.53046	−0.42294	−0.34077	−0.26686	−0.20478	−0.15763
	$2s_O$	2.55884	1.88868	1.37993	1.17440	1.02002	0.76418	0.57653	0.43137	0.30563	0.19714	0.12492	0.08072
	$2p_{\sigma C}$	−1.92395	−1.63587	−1.38771	−1.28314	−1.20357	−1.06952	−0.96539	−0.86742	−0.73546	−0.57045	−0.44120	−0.35001
	$2p_{\sigma O}$	1.02244	1.02538	0.97519	0.94541	0.92053	0.87799	0.85350	0.85525	0.89869	0.95286	0.97774	0.98717
1π	$2p_{\pi C}$	0.42445	0.44714	0.45830	0.46151	0.46311	0.46233	0.45359	0.42817	0.36110	0.25597	0.16875	0.10813
	$2p_{\pi O}$	0.72644	0.73884	0.75925	0.77103	0.78175	0.80466	0.82882	0.85861	0.90372	0.95137	0.97817	0.99061
2π	$2p_{\pi C}$	−1.05317	−0.98679	0.94544	0.93057	0.92038	0.90680	0.90280	0.91021	0.93607	0.96857	0.98667	0.99467
	$2p_{\pi O}$	0.87270	0.79234	−0.72625	−0.69603	−0.67115	−0.62335	−0.57780	−0.52402	−0.43579	−0.31390	−0.21252	−0.14056

TABLE II. Molecular constants for some electronic states of carbon monoxide.

Electronic states	Assumed single excitation	Schematic representation of second function used in CI	Vertical excitation energy obs. (ev)[e]	Vertical excitation energy calc. (ev)[d]	r_e (obs) A[e]	r_e (calc. before CI) A	r_e (calc. after CI) A	k (obs)[e]	10^5 dyne cm^{-1} k (calc. before CI)	k (calc. after CI)	ν_{00}[e] (obs) including zero-point energy ev	ν_{00} (calc. before CI) ev	ν_{00} (calc. after CI) ev
$X\,^1\Sigma^+$		a	0	0	1.128	1.176	1.200	19.02	21.06	16.55	0	0	0
$a\,^3\Pi$	$5\sigma\rightarrow 2\pi$	b	6.22	6.17	1.209	1.270	1.283	12.22	13.98	11.58	6.04	5.13	5.57
$a'\,^3\Sigma^+$	$1\pi\rightarrow 2\pi$	a	8.25	7.41	1.359	1.360	1.392	6.12	11.63	8.50	6.92	4.70	4.92
$e\,^3\Sigma^-$	$1\pi\rightarrow 2\pi$	a	8.68–8.91	9.56	1.393	1.374	1.419	4.83	10.79	6.85	8.10	6.62	6.75
$A\,^1\Pi$	$5\sigma\rightarrow 2\pi$	b	8.74	9.23	1.235	1.325	1.357	9.28	9.43	6.75	8.07	7.59	7.84
$d\,^3\Pi$	$1\pi\rightarrow 6\sigma$	a	8.96	24.2	1.396	unstable		5.23			7.73		
$d\,^3\Delta$	$1\pi\rightarrow 2\pi$			8.48		1.367	1.418		11.22	6.60		5.66	5.74
$b\,^3\Sigma^+$	$5\sigma\rightarrow 6\sigma$		10.39	23.05	1.088	(1.63)							
$B\,^1\Sigma^+$	$1\pi\rightarrow 2\pi$		10.8	23.14	1.12	(1.33)							
$C\,^1\Sigma^+$	$5\sigma\rightarrow 6\sigma$		11.4	27.37	1.125	(1.48)							
$F\,^1\Pi$	$1\pi\rightarrow 6\sigma$		12.37	25.97		unstable							

[a] $5\sigma\rightarrow 6\sigma$, $1\pi\rightarrow 2\pi$ from ground-state configuration.
[b] $5\sigma\rightarrow 6\sigma$, $5\sigma\rightarrow 2\pi$, $1\pi\rightarrow 2\pi$ from ground-state configuration.
[c] Data taken from Y. Tanaka, A. S. Jursa, and F. Le Blanc, J. Chem. Phys. **26**, 862 (1957) and H. Herzberg, *Molecular Spectra and Molecular Structure, Spectra of Diatomic Molecules* (D. Van Nostrand Company, Inc., Princeton, N. J., 1950), 2nd ed.
[d] See work cited in footnote 1.

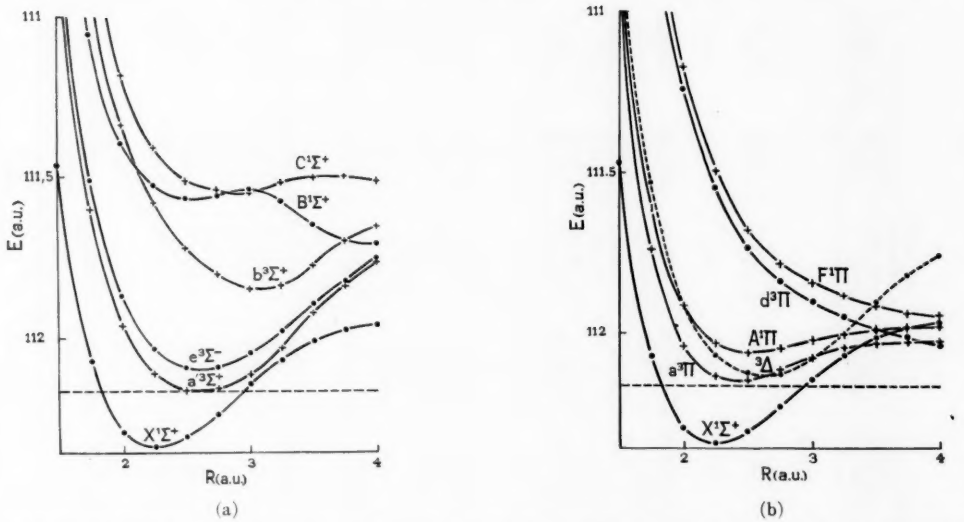

FIG. 1. (a)–(b). Calculated potential energy curves for some electronic states of carbon monoxide (SCF calculation). The dotted line is the calculated sum of atomic energies.

The SCF orbitals have been calculated[3] for the $^1\Sigma^+$ ground state of CO using the 704 program mentioned above. These orbitals minimize the energy of the Slater determinant,

$$\psi_0 = \det|(1\sigma)^2(2\sigma)^2(3\sigma)^2(4\sigma)^2(1\pi)^4(5\sigma)^2|.$$

These orbitals are linear combinations of $1s$, $2s$, and $2p$ atomic functions on each center. The exponents have been chosen to be those (slightly rounded off) which minimize the energy of the atoms,[4] viz.,

	Carbon	Oxygen
Z_{1s}	5.67	7.66
Z_{2s}	1.61	2.25
Z_{2p}	1.57	2.23.

The SCF calculation was carried out at the following 12 internuclear distances (in a.u.): 1.5, 1.75, 2.0, 2.1319, 2.25, 2.5, 2.75, 3.0, 3.25, 3.5, 3.75, and 4.0. The coefficients of the orbitals are given in Table I along with the orbital energies.

In the simplest possible approximation the excited states will be represented by single electron excitations from the ground state to one of the unoccupied virtual orbitals (1 of σ symmetry and 1 of π symmetry). The particular single excitation which has been used to describe each excited state is given in Table II. The excitation energies which have been calculated are matrix elements of the true Hamiltonian for properly symmetrized linear combinations of Slater determinants. In this way we have calculated the energies of the states $X\ ^1\Sigma^+$, $b\ ^3\Sigma^+$, $C\ ^1\Sigma^+$, $B\ ^1\Sigma^+$, $e\ ^3\Sigma^-$, $a'\ ^3\Sigma^+$, $A\ ^1\Pi$, $a\ ^3\Pi$, $F\ ^1\Pi$, $d\ ^3\Pi$, and $d\ ^3\Delta$ at the 12 distances given above and the results are shown in Figs. 1 and 2.

In order to obtain the molecular properties which we are interested in, polynomials were fitted to the points representing only the electronic part of the total energies. This curve fitting was carried out on the IBM 650 machine. Nuclear repulsion was added analytically. The value of R for which $dE/dR=0$ is, of course, r_e and $(d^2E/dR^2)R=r_e$ is the force constant. The energy of the ν_{00} transition is the difference in energy of two states taken at their respective calculated r_e values. The results are collected in Table II in the columns headed "before CI."

The single determinantal wave function which best represents the ground state of a molecule near the equilibrium position, no longer is satisfactory at larger internuclear distances, for this function will separate into atoms which are not in their lowest spectroscopic states. For example, it can be readily shown that the function ψ_0 separates at infinity to carbon and oxygen atoms both in a mixture of ^1D and ^1S states rather than to the atoms in their ^3P ground states. Thus the curves given in Figs. 1(a) and 1(b) are not a very satisfactory approximation to the physical problem we are attempting to study.

If we accept the D_e value for the ground state of carbon monoxide to be 11.11 ev, then there is no difficulty in saying that the states $X\ ^1\Sigma^+$, $a\ ^3\Pi$, $a'\ ^3\Sigma^+$, $d\ ^3\Delta$, $e\ ^3\Sigma^-$, and $A\ ^1\Pi$ should all dissociate into atoms in their

[3] We have examined in detail the accuracy of the program used for the present calculation by comparing the integrals produced by the program for CO at the equilibrium distance and those obtained earlier[1] either by hand or from other machine programs. The agreement was always at least six significant figures.

[4] C. C. J. Roothaan, *Technical Report, Laboratory of Molecular Structure and Spectra* (University of Chicago, Chicago, Illinois, 1955), p. 24.

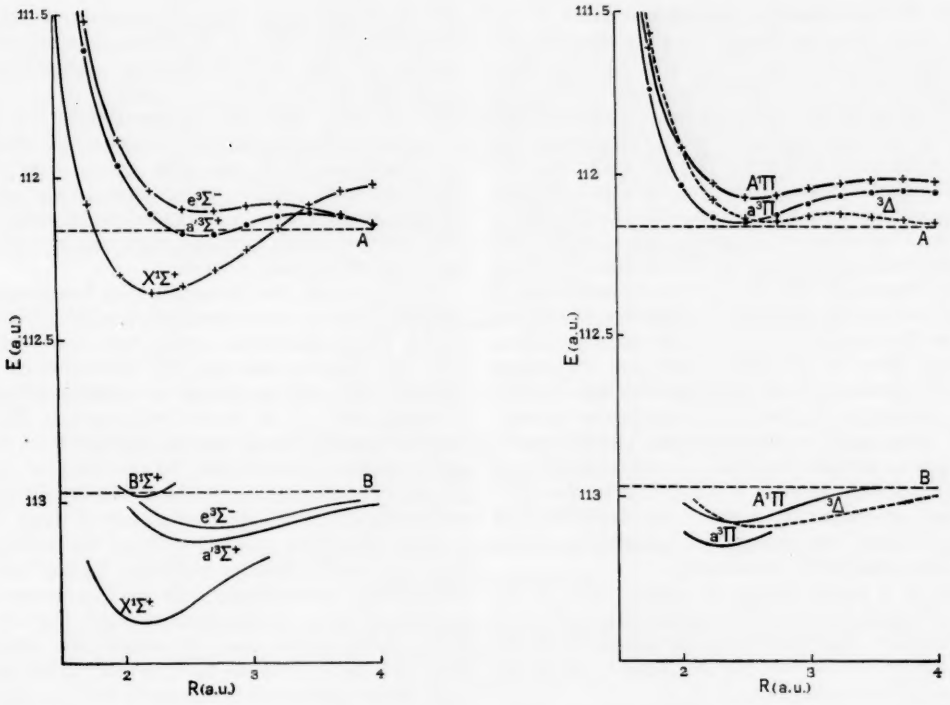

FIG. 2(a)–(b). Calculated and observed potential energy curves for some electronic states of carbon monoxide. The calculated curves at the top of the graph are after configuration interaction. The dashed line A is the calculated sum of atomic energies. The observed curves are at the bottom and are taken from the work cited in footnote 6. Dashed line B is the observed sum of atomic energies.

^3P states.[5] We have thus been led to modify the results given in Figs. 1(a) and 1(b) by including configuration interaction which is limited to the excited configurations which cross the previously calculated curves beyond the r_e distances and go to the atoms in their ^3P states.

From Table I it is easy to ascertain the asymptotic behavior of the orbitals. In particular it will be seen that when $R\rightarrow\leq$, 5σ will be entirely $2p\sigma_c$, $6\sigma\rightarrow 2p\sigma_0$, $1\pi\rightarrow 2p\pi_0$, $2\pi\rightarrow 2p\pi_c$. It is straightforward to construct a determinant of proper Λ and multiplicity which will give at infinity the atoms in their ^3P states. One can then use the projection operator technique to find the eigenfunctions of S^2.

The interacting functions are indicated schematically in Table II. For each state the configuration interaction matrix was of second order. In some symmetries it would have been possible to construct a third function which would eventually cross the curves given in Figs. 1(a) and 1(b), but in each case this additional function has zero interaction with the function originally used and crosses the curves at $R>4.0$ a.u. The curves obtained after configuration interaction are given in Figs. 2(a) and 2(b) along with the experimental curves given by Tobias, Fallon, and Vanderslice.[6]

III. DISCUSSION

In our previous work studying the spectra of carbon monoxide from the computed vertical excitation energies, it seemed that the lower excited states could be divided into two groups: (a) those that seemed to be reasonably well represented by our simple approximation of obtaining excited-state energies from the SCF orbitals for the ground state. These states included $a\,^3\Pi$, $a'\,^3\Sigma^+$, $e\,^3\Sigma^-$ and $A\,^1\Pi$; (b) those which did not appear to be at all satisfactorily represented in our approximation. These states included $b\,^3\Sigma^+$, $B\,^1\Sigma^+$, $C\,^1\Sigma^+$, $F\,^1\Pi$ and $d\,^3\Pi$. However, if we followed Mulliken[7] and assumed the d state was not $^3\Pi$ but was rather $^3\Delta$, then the d state could be included in group (a).

A study of the potential curves given in Figs. 1(a)–(b) and 2(a)–(b) seems to bear out this division. The curves for the states $a\,^3\Pi$, $a'\,^3\Sigma^+$, $e\,^3\Sigma^-$, and $A\,^1\Pi$ all have well-defined minima at a slightly larger inter-

[5] A. G. Gaydon, *Dissociation Energies and Spectra of Diatomic Molecules* (Chapman and Hall, Ltd., London, 1953) 2nd ed. revised.

[6] I. Tobias, R. J. Fallon, and J. T. Vanderslice, J. Chem. Phys. **33,** 1638 (1960).

[7] R. S. Mulliken, Can. J. Chem. **36,** 11 (1958).

nuclear distance than the r_e value calculated for the $X\ ^1\Sigma^+$ state. The discrepancy between observed and calculated force constants is no more than one might reasonably expect from such simple calculations. The error in the ν_{00} values is perhaps larger than one might wish but this is less important than the inversion in the order of the states $a\ ^3\Pi$ and $a'\ ^3\Sigma^+$ and $e\ ^3\Sigma^-$ and $A\ ^1\Pi$.

The changes brought about by our limited configuration interaction of these states are all in the same direction for all the states in this group. The r_e values[8] and ν_{00} energies all become larger and the k values all become smaller. Bratoz and Bessis[9] have already noted that in H_2 and LiH a more complete configuration interaction than we have carried out lowers the calculated force constant. Since for the ground state and the excited states the predicted value of k was too high (except $A\ ^1\Pi$), accounting for the proper asymptotic behavior of the curves seems to be important. The changes in computed ν_{00} energies were all in the right direction.

The conclusion seems to be clear. Our simple wave functions are apparently adequate for describing this group of states even though the quantitative agreement is not always very satisfactory.

There is a second group of states: $b\ ^3\Sigma^+$, $B\ ^1\Sigma^+$, $C\ ^1\Sigma^+$, $d\ ^3\Pi$, and $F\ ^1\Pi$ for which our functions are not at all satisfactory. But it will make our discussion of this group clearer if we include the first three in one group and the last two in another.

The Σ^+ states all appear to be bound, but the curves have a peculiar shape and the minima are observed to be at r_e values which are larger than that observed for the $X\ ^1\Sigma^+$ ground state when in fact they should be smaller. It seems evident we will need functions with larger basis sets to describe these states and we are now actively investigating this problem.[10] The states $d\ ^3\Pi$ and $F\ ^1\Pi$ appear to fall into a different category of problem. These states are not found to have any minima at all. Configuration interaction between our states $A\ ^1\Pi$ and $F\ ^1\Pi$ and between $a\ ^3\Pi$ and $d\ ^3\Pi$ is nearly negligible and would have no important effect on the curves given in Fig. 2(a). As we have already mentioned Mulliken[7] has suggested that the d state is not $^3\Pi$ but $^3\Delta$ and our calculation of vertical excitation energy supported this suggestion. But the calculation reported here is far more substantial evidence in support of Mulliken's hypothesis. If we assume the state has $^3\Delta$ symmetry, it has a well-defined minima and the agreement with experiment for r_e, k, and ν_{00} is no worse than with the group of states we feel are definitely well represented by our functions. Available experimental data on $F\ ^1\Pi$ are very limited, but it may be significant that Gaydon[5] suggests that the symmetry assignment is in doubt. It may be, of course, that calculations carried out with functions built on a larger basis set would indicate that there is another low-lying bound Π state. We are in the process of investigating this point.

On the results of a single calculation on one molecule one should not draw too many general conclusions. But if, as seems possible, even simple calculations can indicate where errors in the experimental assignment may have occurred, then the usefulness of these calculations will be quite evident.

Finally, we will wish to inquire as to how our curves compare with the experimental curves [Figs. 2(a) and 2(b)]. The experimental curves have been deduced from experimental data using the Rydberg-Klein-Rees method.[6] Not only are our curves considerably higher in energy, but they are by no means parallel. The two most striking differences are: (a) the calculated curves are much more shallow than the experimental curves; (b) all the calculated curves have pronounced humps while only the $A\ ^1\Pi$ experimental curves seems likely to have one. Point (a) follows from the well-known fact than an SCF function built on a limited basis set considerably underestimates the binding energy. Expanding the basis set should considerably improve the shape of our curves near the equilibrium distance. Point (b) results from the fact that our curves are the result of the interaction of one curve which is approximately a parabola with another curve which is approximately a hyperbola. The resulting lower curve is the energy mean value of a wave function that up to a certain point is nearly completely represented by one configuration and after that nearly completely represented by another configuration. If more functions had been used the hump would be considerably flattened out. But one might expect that even in the infinite matrix some such turnover might occur. That is, up to a certain point the exact solution of the Schrödinger equation could be represented by an expansion where the configuration suitable for the equilibrium distance would have the largest coefficient and where toward larger internuclear distances the dominant term would be another configuration.

IV. CONCLUSION

One important conclusion to our work is that the SCF orbitals for the ground state are reasonably satisfactory for simple descriptions of excited states. Some work in progress (see e.g. the work cited in footnote 10) clearly indicates that at least some of the difficulties described here can be solved by moderately increasing the basis set. Coulson[11] has recently stated that "it hardly seems worthwhile to find the best Roothaan-like orbitals . . . if we are to include 10 or 20 more con-

[8] See, e.g., H. A. Aghajanian, Quarterly Progress Report, Solid State and Molecular Theory Group, M.I.T. July 15, 1957, p. 29.
[9] S. Bratoz and G. Bessis, J. chim. phys. **56**, 1042 (1959).
[10] H. Brion-Lefebvre, C. M. Moser, and R. K. Nesbet, J. Chem. Phys. **33**, 931 (1960).
[11] C. A. Coulson, Revs. Modern Phys. **32**, 170 (1960).

figurations, this simplification is hardly worth the additional labor of first determining SCF coefficients." This surely is a question of relative labor, for in the present state of affairs there is no additional *human* labor involved in determining SCF coefficients but there would be an enormous amount in finding the matrix elements of a 20th-order matrix. Far more important, the concept of single excitations, which has been the basis of so much experimental interpretation would be lost in a 20th-term function.

ACKNOWLEDGMENTS

This work has been supported in part by a grant from the Ordnance Corps, U. S. Department of the Army, the National Science Foundation, and the Martin Aircraft Company. In particular, we should like to express our deep appreciation to the RIAS division of the Martin Company for hospitality accorded to two of us (C.M. and R.K.N.) and to the Baltimore division of the Martin Company for the use of their IBM 704 computer.

THE JOURNAL OF CHEMICAL PHYSICS VOLUME 34, NUMBER 6 JUNE, 1961

Isotopic Separation Factor for the System Potassium Amalgam-Aqueous Potassium Hydroxide*

H. H. GARRETSON* † AND J. S. DRURY

Chemistry Division, Oak Ridge National Laboratory, Oak Ridge, Tennessee

(Received August 31, 1960)

The isotopic fractionation of potassium between potassium amalgam and aqueous potassium hydroxide was measured at room temperature. The single-stage separation factor was 1.006±0.002 (95% C. I.).

INTRODUCTION

LEWIS and McDonald,[1] and Perret *et al.*[2] studied the fractionation of lithium isotopes between lithium amalgam and solutions of lithium salts. They observed a concentration of the light isotope in the amalgam phase, and estimated the isotopic equilibrium constant at room temperature to be >1.025 and ~1.05, respectively. It was of interest to us to measure the isotopic equilibrium constant for the corresponding potassium system. Since potassium amalgam is more stable than lithium amalgam, it was feasible for us to employ an aqueous solution in our system; the previously mentioned workers used systems in which the alkali metal salt was dissolved in various organic solvents.

EXPERIMENTAL

Materials and Methods

Triple-distilled Hg was further purified by bubbling air through it in the presence of dilute HNO_3. Reagent grade KOH was obtained from J. T. Baker Company.

At the beginning of a run, 200 ml of 9.644*M* KOH solution and 500 ml of Hg were placed in a 1-liter cylindrical electrolysis vessel fitted with Pt electrodes and a glass stopcock drain. Amalgam was formed by electrolysis until the concentration of the KOH was reduced one-half. The amalgam and KOH phases were then stirred for 5 hr to ensure isotopic equilibrium. The aqueous phase was removed from the reaction flask and stored for subsequent use. Both phases were

TABLE I. Conditions for the multistage batch run [K(Hg)−KOH system].

Pass no.	KOH(aq.) (*M*)	K(Hg)$_x$ (*M*)	K in aq. phase (%)	Equil. time (min)	Temp. (°C)
	Amalgam phase equilibration				
0	9.644				
1	4.468	1.723	48	300	31
2	2.016	0.881	45	370	33
3	1.147	0.409	50	270	35
4	0.470	0.206	47	240	34
5	0.247	0.0956	50	270	35
	Aqueous phase equilibration				
1	4.468	1.723	48	300	31
2	1.886	0.732	52	130	34
3	0.992	0.338	53	240	
4	0.534	0.140	60	300	29
5	0.256	0.0832	56	210	

* This paper is based on work performed for the U. S. Atomic Energy Commission by Union Carbide Corporation.

† Present address: Lynchburg College, Lynchburg, Virginia.

[1] G. N. Lewis and R. T. McDonald, J. Am. Chem. Soc. **58**, 2519–24 (1936).

[2] L. Perret, L. Rozand, and E. Säito, *Proceedings of the Second United Nations International Conference on the Peaceful Uses of Atomic Energy, Geneva* (United Nations, New York, 1958), Vol. 4, p. 595.

TABLE II. Isotopic analyses of fifth-pass samples from a multistage batch run K(Hg)−KOH system.

	Atom ratio K^{39}/K^{41} for amalgam phase	
	Amalgam leg	Aqueous leg
	13.65	13.92
	13.33	13.74
	13.95	14.19
	13.65	14.01
Mean	13.65	13.97

Total separation, $\frac{(K^{39}/K^{41})\text{aq.}}{(K^{39}/K^{41})\text{amal.}}=1.023$

sampled. Water was then added to the amalgam phase in the reaction vessel and half the potassium in the amalgam phase was electrolyzed into the water. These phases were equilibrated, separated, and sampled as before. Fresh water was added, and the cycle was repeated until five successive equilibrations were made, following the amalgam phase. The reaction vessel was then emptied, and the aqueous phase from the first pass, together with 500 ml of mercury, was placed in the reaction vessel. Half the potassium of the aqueous phase was then electrolyzed into the mercury to form amalgam. These phases were equilibrated as before, and the process was continued until five passes were made on the aqueous phase. The conditions for each pass are shown in Table I. The concentration of potassium in each phase was determined by taking weighed samples and titrating them with standard hydrochloric-acid solution. In order to compute the percentage of potassium in each phase, it was necessary to calculate the weight of water produced during the formation of the amalgam and the amount of water decomposed when the amalgam was leached. Samples from each phase were obtained from the fifth pass when the aqueous phase was followed, and from the fifth pass when the amalgam phase was followed. These samples were analyzed by the thermal emission method on a 6-in. radius, 60°-sector mass spectrometer. The results are shown in Table II.

RESULTS AND DISCUSSION

From Table II it may be seen that a total separation of 1.023 was observed in the ratio of K^{39}/K^{41} ratios of amalgam samples taken from the fifth passes of the aqueous and amalgam legs, respectively. This total separation corresponds to that for four theoretical plates. The observed single-stage fractionation factor is thus equal to 1.006 ± 0.002 (95% C.I.), with the heavy isotope concentrating in the amalgam phase.

The enrichment of the heavy isotope in the amalgam phase is opposite to that found in the lithium amalgam systems. This effect is probably due to differences in the solvation energies of the two alkali metal ions.

Paramagnetic Susceptibility of Polycrystalline Praseodymium Metal

SIGURDS ARAJS, R. V. COLVIN, AND J. M. PECK

Edgar C. Bain Laboratory for Fundamental Research, U. S. Steel Corporation Research Center, Monroeville, Pennsylvania

(Received November 14, 1960)

The paramagnetic susceptibility of polycrystalline praseodymium metal has been measured between 300 and 1500°K. The measurements are in good agreement with the predictions of the Van Vleck theory of paramagnetism based on a localized f-electron model of noninteracting Pr^{3+} ions. By making a reasonable correction for the contribution of conduction electrons to the paramagnetism, a best fit to the experimental results is obtained by using a screening constant $\sigma=34$.

INTRODUCTION

THE purpose of this report is to present further results on the paramagnetic behavior of the polycrystalline rare earth metals. Up to the present time we have studied neodymium, samarium, gadolinium, terbium, dysprosium, holmium, erbium, and thulium. The results on these metals have already been reported and described from the viewpoint of the localized f-electron model.[1-4] In this paper we discuss our measurements on polycrystalline praseodymium from 300 to 1500°K.

THEORETICAL CONSIDERATIONS

We may look at the metallic praseodymium as a collection of weakly interacting Pr^{3+} ions imbedded in a sea of electrons. This electron sea is by no means a simple free electron gas. Fortunately, for understanding the paramagnetic behavior of praseodymium metal, these electrons are of secondary importance only because the localized f electrons of Pr^{3+} ions are the main source for the paramagnetic behavior. This has been quite successfully demonstrated for other rare earth metals in earlier papers.[1-4] The theoretical method which we shall apply for explaining the paramagnetic properties of praseodymium has been given in detail in two of these.[3,4] However, a short description of this approach, specific to the praseodymium problem, will be presented here.

The electronic configuration of a Pr^{3+} ion is $1s^2$, $2s^2\ 2p^6$, $3s^2\ 3p^6\ 3d^{10}$, $4s^2\ 4p^6\ 4d^{10}\ 4f^2$, $5s^2\ 5p^6$. The lowest energy level multiplet consists of three energy levels $^3H_4$, $^3H_5$, and $^3H_6$ (Fig. 1). The ground state is $^3H_4$. The width of the multiplet ΔE can be calculated from the modified Goudsmit formula[3,5]

$$\Delta E=(8\pi^4me^2/c^3h^5)\frac{2L+1}{n^3l(l+1)(2l+1)}(Z-\sigma)^4, \quad (1)$$

where m is the mass of an electron, c the velocity of light, h the Planck constant, n the principal quantum number, l the orbital quantum number of an electron, L the total orbital quantum number of the incomplete $4f$ shell, Z the atomic number, and σ the nuclear screening constant. If the width of the multiplet, is known its detailed structure can be found by applying the Lande interval rule[6]

$$E_{J-1}-E_J=AJ, \quad (2)$$

where E's represent the energy levels, J is the quantum number associated with the total angular momentum $\mathbf{J}$ of the incomplete $4f$ shell. The results of such calculations for a Pr^{3+} ion are summarized in Table I. This table also shows more refined energy level calculations made by Elliott and Stevens,[7] and Runciman and Wybourne,[8] and some of the experimental values of the energy levels.

The paramagnetic susceptibility of the noninteracting Pr^{3+} system can be determined from the calculated energy levels E_J by means of the Van Vleck theory.[9] When the thermal energy kT is comparable with the energy intervals of the lowest multiplet, the paramagnetic susceptibility per gram can be written as

$$\chi=\frac{(N/M)\sum_J[\{g_J^2\beta^2J(J+1)/3kT\}+\alpha](2J+1)\exp(-E_J/kT)}{\sum_J(2J+1)\exp(-E_J/kT)}, \quad (3)$$

where N is the Avogadro number, M the atomic weight of praseodymium metal, k the Boltzmann constant, T the absolute temperature, β the Bohr magneton, and

$$\alpha=[\beta^2/6(2J+1)][F_{J+1}/(E_{J+1}-E_J)-F_J/(E_J-E_{J-1})] \quad (4)$$

with

$$F_J=(1/J)[(S+L+1)^2-J^2][J^2-(S-L)]^2. \quad (5)$$

[1] S. Arajs, J. Chem. Phys. **32**, 951 (1960).
[2] S. Arajs and D. S. Miller, J. Appl. Phys. **31**, 325S (1960).
[3] S. Arajs, Phys. Rev. **120**, 756 (1960).
[4] S. Arajs and R. V. Colvin, J. Appl. Phys. **32**, 336S (1961).
[5] S. Goudsmit, Phys. Rev. **31**, 946 (1928).
[6] E. V. Condon and G. H. Shortley, *The Theory of Atomic Spectra* (The Macmillan Company, New York, 1935), p. 193.
[7] R. J. Elliott and K. W. H. Stevens, Proc. Roy. Soc. (London) **A218**, 553 (1953).
[8] W. A. Runciman and B. G. Wybourne, J. Chem. Phys. **29**, 1149 (1959).
[9] J. H. Van Vleck, *The Theory of Electric and Magnetic Susceptibilities* (Oxford University Press, New York, 1932), p. 226.

TABLE I. Energy levels of the lowest multiplet of Pr^{3+}.

	$\dot{E}_J$[cm^{-1}]									
Term	$\sigma=32$	$\sigma=33$	$\sigma=34$	$\sigma=35$	$\sigma=36$	Elliott and Stevens	Runciman and Wybourne		Experimental	
$^3H_6$	6353	5463	4670	3966	3345	4400	4212	4477	4274[a]	~5200[b]
$^3H_5$	2888	2483	2123	1803	1521	2000	2050	2190	2171[a]	
$^3H_4$			0			0	0			0

[a] From W. A. Runciman and B. G. Wybourne (the work cited in reference 8).
[b] F. H. Spedding, Phys. Rev. **58**, 255 (1940).

The quantity g_J is the Lande splitting factor

$$g_J=1+\frac{S(S+1)+J(J+1)-L(L+1)}{2J(J+1)}. \quad (6)$$

The paramagnetic susceptibility given by Eq. (3) can be expressed in Bohr magnetons μ_{eff} according to the equation

$$\mu_{\text{eff}}=[(3kM/N\beta^2)\chi T]^{\frac{1}{2}}. \quad (7)$$

It should be emphasized that due to the fact that the separations between the energy levels of the Pr^{3+} multiplet are comparable with kT, the paramagnetic behavior of the noninteracting Pr^{3+} ions does not follow the Curie law. Hence, also, the effective Bohr magneton number is a function of temperature.

EXPERIMENTAL PROCEDURE

The magnetic susceptibilities of praseodymium metal were measured using the Faraday method. The apparatus and the experimental techniques have been described before.[10]

Two samples of praseodymium (designated by 1 and 2) have been used in this investigation. Sample 1 was obtained from the Research Chemical Division of the Nuclear Corporation of America. It was in a cast form, and its chemical analysis is given in Table II. Sample 2, also in a cast form, was purchased from the St. Eloi Corporation. No detailed analysis for this material is available but the manufacturer claims that the purity is at least 99.5%.

Each sample, having a mass of about 5 g, was wrapped in a tantalum foil and enclosed in a silica capsule filled with gaseous argon at 20 cm Hg pressure at room temperature.

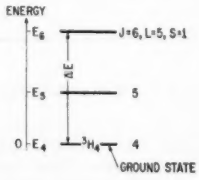

FIG. 1. Schematic representation of the lowest energy multiplet of Pr^{3+}.

[10] S. Arajs and D. S. Miller, J. Appl. Phys. **31**, 986 (1960).

RESULTS AND DISCUSSION

Values of the paramagnetic susceptibility of praseodymium metal were obtained from the experimental magnetic susceptibility data by correcting for the diamagnetic contribution which was taken to be -0.14×10^{-6} g^{-1} cm^3.[11] The inverse susceptibility vs temperature behavior of praseodymium metal is shown in Fig. 2 together with all the known previous investigations.[12–17] It should be noted that our room-temperature measurements are in satisfactory agreement with those of Spedding *et al.*,[15] Lock,[16] and Leipfinger.[17] The only known previous work on the paramagnetic behavior of praseodymium at high temperatures is that due to Henry la Blanchetais.[14] However, her data does not agree with our measurements as can be seen in Fig. 2. It is suspected that the differences are due to impurities in the sample used by Henry la Blanchetais.

TABLE II. Analysis of praseodymium metal (sample 1).

Impurity	Amount [wt.%]
Lanthanum	0.1
Oxygen	0.06
Magnesium	0.05
Iron	0.01
Tantalum	Not detected

[11] H. H. Landolt and R. Börnstein, *Zahlenwerte and Funktionen aus Physik, Chemie, Astronomie, Geophysik, Technik* (Springer Verlag, Berlin, 1950), Vol. I, Part I, p. 398.
[12] M. Owen, Ann. Physik **37**, 657 (1912).
[13] W. Klemm and H. Bommer, Z. anorg. u. allgem. Chem. **241**, 264 (1939).
[14] Ch. Henry la Blanchetais, Compt. rend. **234**, 1353 (1952); J. recherches centre nat. recherche sci. Lab. Bellevue (Paris) **28**, 32 (1954); **29**, 103 (1954).
[15] F. H. Spedding, S. Legvold, A. H. Daane, and L. D. Jennings, *Progress in Low Temperature Physics*, edited by C. J. Gorter (North-Holland Publishing Company, 1957), Vol. II, p. 368.
[16] J. M. Lock, Proc. Phys. Soc. (London) **B70**, 566 (1957).
[17] H. Leipfinger, "Magnetic properties of rare earth metals at very low temperatures," Physikalisches Institut der Technischen Hochschuhle München, 1957, Tech. Rept., under contract; Z. Physik **150**, 415 (1958).

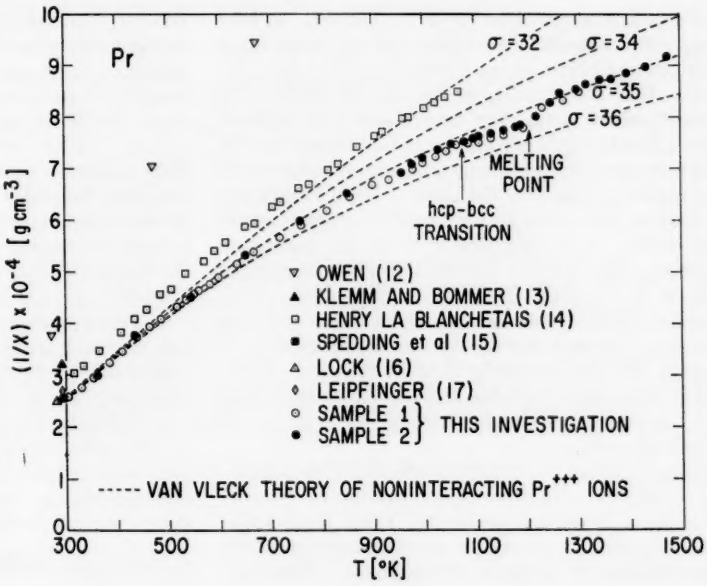

FIG. 2. Inverse paramagnetic susceptibility of Pr as a function of temperature.

It is known that praseodymium metal, which has a hexagonal crystal structure at room temperatures, changes to a body-centered cubic structure at 1071°K.[18] The melting point of praseodymium is at 1208°K.[15] Our magnetic studies show a very slight anomaly in the plot of the inverse paramagnetic susceptibility vs temperature at the hexagonal-bcc transition and a considerably larger anomaly at the melting point. It is significant that there are no finite discontinuities in susceptibility at these phase transformations indicating that the interactions between Pr^{3+} ions are indeed small. The idea of weak interactions is also supported by the quite satisfactory agreement between the theoretical calculations and the experimental observations on the magnetic behavior of praseodymium as shown in Fig. 2. The theoretical curves for various σ values have been calculated from Eq. (3). It appears from Fig. 2 that the energy level structure associated with $\sigma=35$ approximately explains the temperature dependence of the paramagnetism in praseodymium metal. This is in agreement with our findings on metallic neodymium.[2]

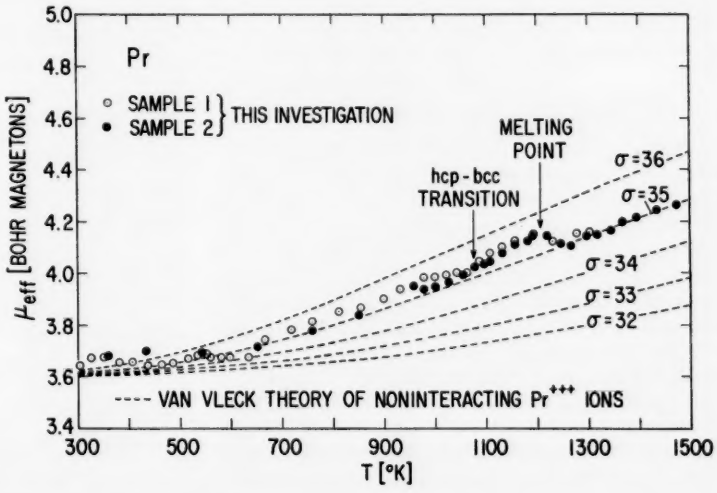

FIG. 3. Bohr magneton number of Pr as a function of temperature.

[18] J. J. Hanak, Ph.D. thesis, Iowa State University of Science and Technology, Ames, Iowa, 1959.

It should be emphasized, however, that so far we have completely neglected the contribution to the paramagnetic susceptibility arising from the conduction electrons. This contribution is not exactly known for praseodymium metal. For dysprosium it is believed to be 1.15×10^{-6} g^{-1} cm^3 [4] and it can be assumed that for praseodymium this additional temperature independent susceptibility term is of the same order of magnitude. By making this correction for a number of points on the plot in Fig. 2, an approximate fit to the theoretical curve associated with $\sigma=34$ is obtained. The same is also true of the magnetic behavior of neodymium metal described before.[2] This correction provides even better agreement between the theory and the measurements because the experimentally determined energy levels of Pr^{3+} ions given in Table I are in closer agreement with the calculated levels obtained by using $\sigma=34$ instead of $\sigma=35$.

Figure 3 shows the measured effective Bohr magneton numbers as a function of temperature in comparison with the theoretical predictions. This is just another way of looking at the temperature dependence of the magnetization of metallic praseodymium. These experimental results indicate that the tripositive ion approximation and the Van Vleck theory of paramagnetism satisfactorily account for the major features of the observed paramagnetic behavior of polycrystalline praseodymium metal.

Finally, it should be mentioned that the magnetic status of praseodymium at low temperatures is still relatively unexplored. The only work of significance in this temperature region is that due to Lock.[16] He has measured the magnetic susceptibility of praseodymium metal from room temperatures down to 1.3°K. Above about 100°K the susceptibility obeys a Curie law $\chi=(11.25/T)\times10^{-3}$ g^{-1} cm^3, from which the effective Bohr magneton number is calculated to be 3.56 which compares favorably with the theoretical value 3.58 in this temperature region. Below 100°K, according to Lock, the magnetic susceptibility first increases above the Curie-law value and then flattens out at a value of 1.55×10^{-3} g^{-1} cm^3 below 4°K.

The heat capacity of praseodymium at low temperatures has been studied by Parkinson *et al.*[19] They report a minimum in the specific heat curve at about 100°K whose origin is not understood.

It definitely appears that the magnetic behavior of metallic praseodymium should be reinvestigated at low temperatures. One should especially look for possible evidence for an antiferromagnetic ordering. Work along these lines is being considered in this Laboratory.

ACKNOWLEDGMENTS

The authors are indebted to R. C. Peak for technical assistance and R. W. Whitmore for numerical calculations with Burroughs Datatron 205. Stimulating discussions with D. S. Miller have been greatly appreciated.

[19] D. H. Parkinson, F. E. Simon, and F. H. Spedding, Proc. Roy. Soc. (London) **A207**, 137 (1951).

On the Theory of Helix-Coil Transition in Polypeptides*

SHNEIOR LIFSON†

Departments of Chemistry, Harvard University, Cambridge, Massachusetts, and University of Oregon, Eugene, Oregon,‡ and Physics Section, Convair, Division of General Dynamics Corporation, San Diego, California

AND

A. ROIG§

Department of Chemistry, Massachusetts Institute of Technology, Cambridge, Massachusetts

(Received November 7, 1960)

The evaluation of the configurational partition function of a polypeptide molecule, with the internal rotation angles as variables, leads to an improved treatment of the phenomenon of helix-coil transition in polypeptide molecules. The conditional probabilities of occurrence of helical and coiled states of the peptide units are obtained in the form of a 3×3 matrix. The order of this matrix is the lowest possible for the model employed, and is derived by a logical procedure which serves to eliminate redundancies in the enumeration of states. The eigenvalues of this matrix yield the various molecular averages as functions of the degree of polymerization, temperature, and molecular constants. Explicit formulas are given for the degree of intramolecular hydrogen bonding, average number of helical sequences, and the distribution of their lengths, as well as the number average and the weight average of these lengths.

INTRODUCTION

THE statistical thermodynamics of the helix-coil transition in polypeptide chains has been studied extensively in recent years by a number of authors.[1–8] In the present paper we propose a solution of the same problem from a different point of view, by applying the internal rotation angles of the polypeptide chain molecule as the variables which determine the microscopic configurations of the molecule. A comparison of the other theories with the present treatment will show that the latter, being more rigorous, improves upon the former, and yet, in a sense, it is simpler. Like Zimm and Bragg,[4] we apply a matrix representation of the partition function, from which the degree of helicity and other related quantities are calculated. Our choice of the matrix elements is, however, different. Zimm and Bragg,[4] as well as Gibbs and DiMarzio[5] and Nagai,[8] consider the probability that a chain element is hydrogen bonded as being dependent on the state of the neighboring chain elements, but assume that the probability of a chain element being nonbonded is independent of the state of its neighbors. However, the probability of a chain element being nonbonded is actually smaller if its two neighbors are bonded than if they are not. Although the effect of that assumption on the final results might be small in many cases, it is not always negligible. Moreover, it appears that while eliminating this assumption, the order of the matrix of conditional probabilities can be reduced from eight in the theory of Zimm and Bragg, to three in our present treatment. This simplification makes it possible to calculate the various molecular averages of interest in terms of all three eigenvalues of the probability matrix and their corresponding eigenvectors. Thus, one obtains a solution to the polypeptide helix-coil transition problem for low as well as intermediate molecular weights, and a clearer insight into the effect of the various eigenvalues on the quasi-phase-transition in finite, one-dimensional systems.

CONFIGURATIONAL PARTITION FUNCTION

We consider a chain molecule of $n+2$ peptide units (amino acid residues), embedded in a solvent. The units are numbered, 0, 1, $\cdots$, i, $\cdots$, n, $n+1$, with the zeroth and the $(n+1)$ units carrying the free carboxyl and the free amine, respectively. The peptide bonds connecting the adjacent peptide units are known to have a partial double-bond character, and are assumed to be fixed. The two other bonds of each peptide have a partial freedom of rotation, and the instantaneous values of the respective internal rotation angles (ϕ_i, ψ_i) determine the microscopic configuration of the chain (see Fig. 1). The nitrogen of the zeroth unit is assumed to form an intramolecular hydrogen bond with the oxygen of the fourth unit if, and only if, the units 1, 2, and 3

* Partly presented at the Fourth Annual Meeting of the Biophysical Society, Philadelphia, Pennsylvania, February, 1960.

† On leave from the Weizmann Institute of Science, Rehovot, Israel.

‡ Supported in part by a research grant from the Heart Institute, U. S. Public Health Service.

§ On leave from the Institute of Physical Chemistry, C.S.I.C., Madrid, Spain.

[1] J. A. Schellman, Compt. rend. trav. lab. Carsberg, Ser. chim. **29**, No. 15 (1955); J. Phys. Chem. **62**, 1485 (1958).

[2] L. Peller, thesis, Princeton University, 1951; J. Phys. Chem. **63**, 1194 (1959).

[3] S. A. Rice, A. Wada, and E. P. Geiduschek, Discussions Faraday Soc. **25**, 130 (1958).

[4] (a) B. H. Zimm and J. K. Bragg, J. Chem. Phys. **28**, 1246 (1958); (b) **31**, 526 (1959).

[5] (a) J. H. Gibbs and E. A. DiMarzio, J. Chem. Phys. **28**, 1247 (1958); (b) **30**, 271 (1959).

[6] S. A. Rice and A. Wada, J. Chem. Phys. **29**, 233 (1958).

[7] T. L. Hill, J. Chem. Phys. **30**, 383 (1959).

[8] K. Nagai, J. Phys. Soc. Japan **15**, 407 (1960).

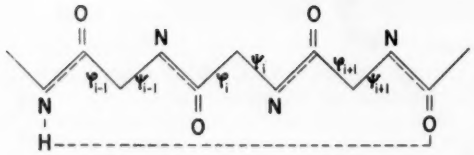

FIG. 1. Polypeptide chain, a schematic representation in the extended zigzag configuration.

are in the α-helix conformation.[9] Similarly, any pair of units $(i-2,\ 1+2)$ is bonded by a hydrogen bond provided the three peptide units $i-1$, i, $i+1$, are in the α-helix conformation. The energy of the intramolecular hydrogen bonds together with the interaction between the R groups of the amino acid residues, tend to stabilize the α-helix structure, while the free energy of the partial freedom of internal rotation and the solvent-polymer interactions tends in general to favor the random, i.e., coiled, conformation. By calculating the configurational partition function of the system, one obtains a quantitative measure of the interplay between these two tendencies.

The solvent polypeptide interactions may be of various kinds, including solvent peptide hydrogen-bonding. We shall not discuss them here in detail. For our purpose it is sufficient to consider the total configurational energy $V^{(n)}(\phi_1, \psi_1, \cdots, \phi_n, \psi_n)$ as a function of the $2n$ internal rotation angles, obtained after properly averaging[10] over all possible configurations of the solvent molecules, as well as over the internal rotation angles of the peptide units 0 and $(n+1)$ which do not participate directly in stabilizing the helical structure.

We shall assume that the configurational energy $V^{(n)}$ is given by

$$V^{(n)}=\sum_{i=1}^{n} V_i^{(1)}(\phi_i,\psi_i) + \sum_{i=2}^{n-1} V_i^{(3)}(\phi_{i-1},\psi_{i-1},\phi_i,\psi_i,\phi_{i+1},\psi_{i+1}). \quad (1)$$

The terms $V_i^{(1)}(\phi_i, \psi_i)$ represent the potential of hindered rotation, namely, the part of the energy of each peptide unit which is independent of other units. They also include the energy of solvent-peptide hydrogen bonds or other particular interactions whenever such interactions are present. The terms $V_i^{(3)}(\phi_{i-1}, \cdots, \psi_{i+1})$ represent the energy of formation of the helix.[11] They include the energy change accompanying the formation of a hydrogen bond between the NH group of the $(i-2)$ peptide unit and the oxygen of the $(i+2)$ unit, and also other interactions such as interactions between side chains which help to stabilize the α helix and are presumably essential in determining the right- or left-handedness of the helix.[12] The term $V_i^{(3)}$ is assumed to be different from zero if, and only if, all three pairs of internal rotation angles have the values $\phi_{i-1}^{(h)}\cdots\psi_{i+1}^{(h)}$ assigned to them in the α-helix conformation, within a narrow range of variation

$$\Delta\phi_{i-1}^{(h)}, \quad \Delta\psi_{i-1}^{(h)}, \cdots, \Delta\phi_{i+1}^{(h)}, \quad \Delta\psi_{i+1}^{(h)}.$$

The configurational partition function of the system is given by

$$Z=\int_{\phi_1=0}^{2\pi}\cdots\int_{\psi_n=0}^{2\pi}\exp[-\beta V^{(n)}]d\phi_1\cdots,d\psi_n, \quad (2)$$

where $\beta=1/kT$.

Evidently, the multiple integral of Eq. (2) cannot be factorized; however, it can be reduced to a sum of products and the summation performed with the help of matrix methods. For this purpose we divide the integration region of each pair of internal rotation angles (ϕ_i, ψ_i) into two parts: the coil region c_i and the helix region h_i. These regions are shown schematically in Fig. 2.

The integration over the coil region c_i can be performed over each pair of angles independent of the state of the adjacent peptide units, since $V_i^{(3)}=0$ holds over the entire region c_i, and we may write

$$\int_{c_i}\exp(-\beta V_i^{(1)})d\theta_i d\psi_i=u, \qquad i=1 \text{ or } n \quad (3)$$

$$\int_{c_i}\exp(-\beta V_i^{(1)}-\beta V_i^{(3)})d\phi_i d\psi_i=u, \qquad i=2,\ \cdots,\ n-1. \quad (4)$$

The integration over the helical region h_i does depend on the state of the adjacent peptide units. When both the $i-1$ and $i+1$ peptide units are in the helix region,

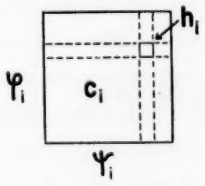

FIG. 2. Range of integration of a pair of internal rotation angles (ϕ_i, ψ_i).

[9] L. Pauling, R. B. Corey, and H. R. Branson, Proc. Natl. Acad. Sci. U. S. **37**, 205, 241 (1951).

[10] A detailed discussion of the nature of $V^{(n)}$ for polymer molecules in general is given in a recent paper by S. Lifson and I. Oppenheim, J. Chem. Phys. **33**, 109 (1960), where $V^{(n)}$ is shown to be the potential of the average torque acting on the internal rotation angles. It has, roughly speaking, the nature of a free energy with respect to the solvent molecules and of an internal energy with respect to the intra-polypeptide interactions.

[11] The attributions of $V_i^{(3)}$ $(\phi_{i-1}\cdots\psi_{i-1})$ to the ith unit is arbitrary. We could just as well attribute it to any of the units between $i-2$ and $i+2$. It has, however, the advantage of symmetry. We shall sometimes say that the ith unit is hydrogen bonded meaning merely that $v_i^{(3)}\neq 0$.

[12] E. R. Blout, C. de Lozé, S. M. Bloom, and G. D. Fasman, J. Am. Chem. Soc. **82**, 3787 (1960).

the energy $V_i^{(3)}$ is different from zero, and we have

$$\int_{h_i} \exp(-\beta V_i^{(1)} - \beta V_i^{(3)}) d\phi_i d\psi_i = w, \qquad i=2, \cdots, n-1; \text{ both } i-1 \text{ and } i+1 \text{ in the helix region.} \tag{5}$$

Otherwise the energy $V_i^{(3)}$ vanishes, and we have

$$\int_{h_i} \exp(-\beta V_i^{(1)} - \beta V_i^{(3)}) d\phi_i d\psi_i = v, \qquad i=2, \cdots, n-1; \text{ either } i-1 \text{ or } i+1 \text{ or both are in the coil region.} \tag{6}$$

Similarly, integration over the helical regions of the peptide units at both ends gives always

$$\int_{hi} \exp(-\beta V_i^{(1)}) d\phi_i d\psi_i = v, \qquad i=1 \text{ or } n, \tag{7}$$

irrespective of the state of the adjacent unit.

Consider now a compound state of the polypeptide chain defined by specifying the state of each peptide unit as being either in the helix region or in the coil region. The contribution of such a state to the partition function can be expressed as a product of n factors, each of which is either u, v, or w. As an example, let us examine a sequence with $n=15$ in the state described by

$$hhhhhccchhchccc, \tag{8}$$

[the units 0 and 16 were omitted; see the discussion preceding Eq. (1)], in which the first five peptide units are in the helix region, the three succeeding units are in the coil region, etc. The contribution of this state to the partition function is seen to be

$$vwwvuuuvvuvuuu. \tag{9}$$

The rules in constructing such terms follow directly from Eqs. (3)–(7):

(1) A peptide unit in the coil state always contributes a factor u.

(2) A peptide unit at the beginning or at the end of an uninterrupted sequence of helical states contributes a factor v.

(3) A peptide unit at the interior of an uninterrupted sequence of (more than two) helical states contributes a factor w.

The product given in (9) is proportional to the probability of occurrence of the sequence (8), the the proportionality factor being Z^{-1}. The factors u, v, and w represent *conditional* probabilities of occurrence of their corresponding events, the conditions being given by the above three rules. Since the terms u, v, and w are not normalized, only ratios between them are significant. If one of these factors is arbitrarily set equal to unity, this is equivalent to fixing arbitrarily the zero point of the energy in Eq. (1), and does by no means limit the generality of the discussion. *We shall later make use of this freedom, by setting $u=1$, and shall consider the different quantities of interest as functions of v and w only.*

Note also that, in general,

$$v \ll u \tag{10}$$

because the region h is much smaller than the region c. Also

$$v \ll w \tag{11}$$

because $V^{(3)}$ must be negative if a helix-coil transition is to be expected.

At this point it seems instructive to compare the set of statistical weights, or conditional probabilities, introduced by Zimm and Bragg with those employed here. Our w corresponds to their s. Also our v corresponds to their $\sigma^{\frac{1}{2}}$. This last correspondence is somewhat disguised by the fact that they attribute the factor σ to the *beginning* of a helical sequence, while we attribute a factor v, namely, $\sigma^{\frac{1}{2}}$, to both the beginning and the end of a helical sequence which, nevertheless, amounts to the same final effect. Our statistical weight of the coil region, u, however, does not correspond exactly to their statistical weight of the unbonded segment. It follows from our definitions of u, v, and w that the (unnormalized) probability of a segment to be unbonded[11] is $u+v$ if either of its neighbors is in the coil region, but it reduces to u if its two neighbors are both in the helical region. Zimm and Bragg did not distinguish between these two possibilities and attributed the same statistical weight (unity) to the unbonded segment, irrespective of the state of its neighbors. The effect of this approximation is small as long as $v \ll u$. The approximation, however, is unnecessary since the more rigorous treatment is also simpler. It should be noted that the above remarks hold, with minor differences, with respect to Gibbs and DiMarzio,[5] and Nagai.[8]

To obtain the partition function we sum over all possible terms which can be constructed following the rules 1 through 3. To do this we define a variable index ρ which stands for either h or c, and introduce the following notation

$$\int_{\phi_i=0}^{2\pi} \int_{\psi_i=0}^{2\pi} d\phi_i d\psi_i = \sum_{\rho_i=h,c} \int_{\rho_i} d\phi_i d\psi_i. \tag{12}$$

The partition function can be written now as

$$Z = \sum_{\rho_1=h,c} \cdots \sum_{\rho_n=h,c} \int_{\rho_1} \cdots \int_{\rho_n} \exp(-\beta V_1^{(1)}) \prod_{i=2}^{n-1} \times \exp(-\beta V_i^{(1)} - \beta V_i^{(3)}) \exp(-\beta V_n^{(1)}) d\phi_1 d\psi_1 \cdots d\phi_n d\psi_n \tag{13}$$

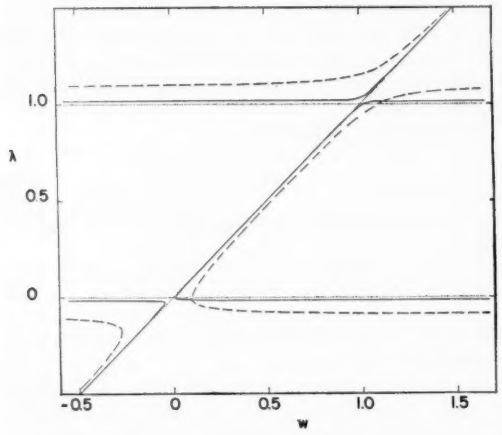

FIG. 3. Secular equation for $v=0.1$ (dashed lines) and (see footnote 15 in text) $v=0.0141$ (solid lines). The dotted lines represent the asymptotic behavior in the limit $v\to 0$.

or

$$Z=\sum_{\rho_1=h,c}\cdots\sum_{\rho_n=h,c}u_{\rho_1}w_{\rho_1\rho_2\rho_3}\cdots w_{\rho_{n-2}\rho_{n-1}\rho_n}u_{\rho_n}, \tag{14}$$

where $u_{\rho_i}(i=1 \text{ or } n)$ is either u or v according to whether ρ_i is c_i [Eq. (3)] or h_i [Eq. (7)]. Similarly $w_{\rho_{i-1}\rho_i\rho_{i-1}}$ is either u or v or w according to whether the sequence $\rho_{i-1}\rho_i\rho_{i+1}$ corresponds to the conditions of Eqs. (4), (6), or (5), respectively.

The values of $w_{\rho_{i-1}\rho_i\rho_{i+1}}$ may be represented by a 3×3 matrix $\mathbf{W}_i=\{W_{rs}\}$ in which the rows correspond to the value of $\rho_{i-1}\rho_i$ and the columns to those of $\rho_i\rho_{i+1}$:

$$\mathbf{W}_i=\{W_{rs}\}=\begin{array}{cc|ccc} & \rho_{i+1} & h & c & h\cup c \\ \rho_{i-1} & \rho_i & h & h & c \\ \hline h & h & w & v & 0 \\ h & c & 0 & 0 & u \\ c & h\cup c & v & v & u \end{array}. \tag{15}$$

The notation $h\cup c$ means "h or c." The third row is denoted by $(c, h\cup c)$ which means that ρ_{i-1} is determined, $\rho_{i-1}=c$, while ρ_i can be either h or c and is determined for each element in the row by the column to which it belongs. Similarly, the third column has $\rho_i=c$, while ρ_{i+1} is either h or c. As long as $\mathbf{W}_i$ is considered alone, the value of ρ_{i+1} in the third column is not determined and is also irrelevant. However, when we form, for example, the matrix product $\mathbf{W}_i\mathbf{W}_{i+1}$, elements of the third row of $\mathbf{W}_{i+1}$ always multiply elements of the third column of $\mathbf{W}_i$ and thereby the value of ρ_{i+1} becomes determined for each element of the product.

By the rules of matrix multiplication the sum in Eq. (14) is represented exactly by the product

$$Z=\mathbf{u}\mathbf{W}^{n-2}\mathbf{u}^{+}, \tag{16}$$

where $\mathbf{u}$ and $\mathbf{u}^{+}$ are, respectively, the row and column vectors

$$\mathbf{u}=(v, v, u), \qquad \mathbf{u}^{+}=(v, u, v+u)^{*}, \tag{17}$$

and represent the peptide units at the two ends of the chain. We use the asterisk to denote a transpose of a vector or matrix, but note that $\mathbf{u}^{+}$ is not the transpose of $\mathbf{u}$. The elements of the vector $\mathbf{u}$ correspond to the states h, h, c which are the values of the variable index ρ_{i-1} in $\mathbf{W}_i$. Similarly, the elements of the vector $\mathbf{u}^{+}$ correspond to the states h, c, $h\cup c$ of ρ_{i+1} in $\mathbf{W}_i$.

The introduction of the logical symbol $\cup$, as in the third row and column, serves to reduce the four possible values of $\rho_{i-1}\rho_i$ (as well as of $\rho_i\rho_{i+1}$) to three.[13] Its applicability is quite general; it helps to reduce considerably the high orders of matrices which represent the partition function of more complicated problems, such as the detailed balance between intra- and intermolecular hydrogen bonding, or between right-handed and left-handed helices when both are feasible. A detailed discussion of such systems will be published separately.

In very small chains, where the end effects are of major importance, the terms v and u in $\mathbf{u}$ and $\mathbf{u}^{+}$ might be considered as different from those in the interior of the chain, mainly due to the particular structure of the end groups. If, however, we do not wish to make this distinction, it appears preferable for later applications to define the row and column vectors

$$\mathbf{e}=(0, 0, 1), \qquad \mathbf{e}^{+}=(0, 1, 1)^{*} \tag{18}$$

so that

$$\mathbf{u}=\mathbf{e}\mathbf{W}, \qquad \mathbf{u}^{+}=\mathbf{W}\mathbf{e}^{+}, \tag{19}$$

[13] Instead, we might represent $w_{\rho_{i-1}\rho_i\rho_{i+1}}$ by a 4×4 matrix. Let the rows and columns correspond to the 4 pairs hh, ch, hc, cc. The partition function is then given by

$$Z=\mathbf{u}'\mathbf{W}'^{n-2}\mathbf{u}'^{+}=(vuvu)\begin{pmatrix} w & o & v & o \\ v & o & v & o \\ o & u & o & u \\ o & u & o & u \end{pmatrix}^{n-2}\begin{pmatrix} v \\ v \\ u \\ u \end{pmatrix}.$$

To show that this expression is equivalent to Eq. (16) we introduce a similarity transformation

$$\mathbf{X}=\begin{pmatrix} 1 & 0 & 0 & 0 \\ 0 & -1 & 1 & -1 \\ 0 & 1 & 0 & 0 \\ 0 & 1 & 0 & 1 \end{pmatrix}, \qquad \mathbf{X}^{-1}=\begin{pmatrix} 1 & 0 & 0 & 0 \\ 0 & 0 & 1 & 0 \\ 0 & 1 & 0 & 1 \\ 0 & 0 & -1 & 1 \end{pmatrix},$$

and obtain $Z=(\mathbf{u}'\mathbf{X})(\mathbf{X}^{-1}\mathbf{W}'\mathbf{X})^{n-2}(\mathbf{X}^{-1}\mathbf{u}'^{+})$ which is equal to $\mathbf{u}\mathbf{W}^{n-2}\mathbf{u}^{+}$ of Eq. (16), except that it has all 4th rows and columns zero. Since the matrix $\mathbf{W}$ is regular, there can be no further reduction of order.

and the partition function may be written as

$$Z=\mathbf{e}\mathbf{W}^n\mathbf{e}^+, \tag{20}$$

where each peptide unit is represented by a matrix $\mathbf{W}$.

An evaluation of Z is effected by transforming $\mathbf{W}$ into a diagonal matrix $\mathbf{\Lambda}$ according to the transformation

$$\mathbf{T}^{-1}\mathbf{W}\mathbf{T}=\mathbf{\Lambda}. \tag{21}$$

The diagonal elements λ_1, λ_2, λ_3, of the diagonal matrix $\mathbf{\Lambda}$ are the eigenvalues of the matrix $\mathbf{W}$, namely, solutions of the secular equation

$$f(\lambda; w, v, u)=(\lambda-w)(\lambda^2-u\lambda-uv)-uv^2=0. \tag{22}$$

After introducing $\mathbf{W}=\mathbf{T}\mathbf{\Lambda}\mathbf{T}^{-1}$ into Eq. (20), the partition function Z can be written as

$$Z=\mathbf{e}\mathbf{T}\mathbf{\Lambda}^n\mathbf{T}^{-1}\mathbf{e}^+. \tag{23}$$

The columns of $\mathbf{T}$ are right-hand eigenvectors of $\mathbf{W}$ which satisfy the equations $\mathbf{W}\mathbf{x}_r^*=\lambda_r\mathbf{x}_r^*(r=1, 2, 3)$, and are seen to be proportional to $[uv/(\lambda_r-w), u, \lambda_r]^*$; the proportionality factor will be set here as λ_r^{-1},

$$\mathbf{x}_r^*=[uv/\lambda_r(\lambda_r-w), u/\lambda_r, 1]^*, \qquad r=1, 2, 3. \tag{24}$$

Similarly the rows of $\mathbf{T}^{-1}$ are left-hand eigenvectors of $\mathbf{W}$ which satisfy the equations $\mathbf{y}_r\mathbf{W}=\lambda_r\mathbf{y}_r$ and are given by

$$\mathbf{y}_r=[uv/\lambda_r(\lambda_r-w), (1-u/\lambda_r), u/\lambda_r]C_r. \tag{25}$$

The normalizing factor $C_r=C_r(\lambda_r)$ is determined by $\mathbf{T}^{-1}\mathbf{T}=1$ which requires $\mathbf{y}_r\mathbf{x}_r^*=1$, and is given by

$$C_r^{-1}=u^2v^2/\lambda_r^2(\lambda_r-w)^2+u(2\lambda_r-u)/\lambda_r^2, \tag{26}$$

or

$$C_r=\lambda_r^2(\lambda_r-w)/u(\lambda_r-\lambda_s)(\lambda_r-\lambda_t); \qquad r\neq s\neq t=1, 2, 3, \tag{26'}$$

or

$$C_r=\lambda_r^2v^2/[\mu_r^2+(2\lambda_r-u)uv^2], \tag{26''}$$

where

$$\mu_r=\lambda_r^2-u\lambda_r-uv. \tag{27}$$

The various forms of C_r are introduced for later application and are obtained by using the secular equation (22) and the symmetric functions of its coefficients

$$\sum_{r=1}^{3}\lambda_r=w+u, \qquad \sum_{r<s}^{3}\lambda_r\lambda_s=u(w-v),$$

$$\lambda_1\lambda_2\lambda_3=-uv(w-v). \tag{28}$$

By using Eqs. (24)–(26) to obtain $\mathbf{e}\mathbf{T}$ and $\mathbf{T}^{-1}\mathbf{e}^+$,

$$\mathbf{e}\mathbf{T}=(1, 1, 1), \qquad \mathbf{T}^{-1}\mathbf{e}^+=(C_1, C_2, C_3)^*, \tag{29}$$

the partition function Z is finally derived, after introducing Eq. (29) into Eq. (23):

$$Z=\sum_{r=1}^{3}Z_r \tag{30}$$

with

$$Z_r=\lambda_r^nC_r. \tag{31}$$

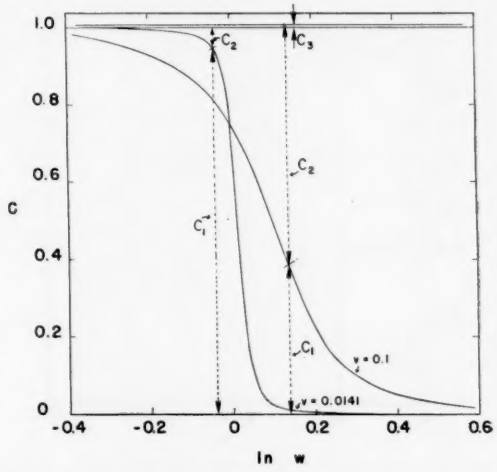

FIG. 4. Dependence of C_r on $\ln w$ for $v=0.1$ and $v=0.0141$.

A fair insight into the problem of the helix-coil transition and its relation to the eigenvalues of the probability matrix $\mathbf{W}$ can be obtained by analyzing the dependence of the three eigenvalues λ_1, λ_2, and λ_3 on the parameters w and v. We shall put $u=1$ since, as indicated before, only ratios between the parameters w, v, and u have physical significance.[14] The secular equation may be rearranged for that purpose in the form

$$w=\lambda-[v^2/(\lambda^2-\lambda-v)], \qquad (u=1). \tag{32}$$

In Fig. 3, $\lambda(w)$ is plotted from this equation, for two values of v, $v=0.1$ and $v=0.0141$.[15] The dotted lines indicate the asymptotic behavior of $\lambda(w)$ in the limit $v\to 0$. The point of intersection of the dotted lines is the point of a true sharp phase transition which may occur only in the limit $v\to 0$, as was pointed out by Zimm and Bragg.[4] The region of the actual diffuse transition is in the vicinity of that point,[16] where the values of the eigenvalues λ_1 and λ_2 deviate from their asymptotic values to an extent dependent on the value of v. In this region the difference between λ_1 and λ_2 is

[14] The relationship between these parameters and observable quantities such as temperature or chemical potential has been discussed by other authors and will not concern us here; the significance of $\ln w$ is briefly mentioned in Eq. (33).

[15] This value was chosen for comparison with Zimm and Bragg's results (see footnote 4).

[16] The midpoint of the transition for large n is approximately $w=1+v$, $\lambda_1=1+2v$, $\lambda_2=1$. We shall refer sometimes to this point as the transition point or simply the transition.

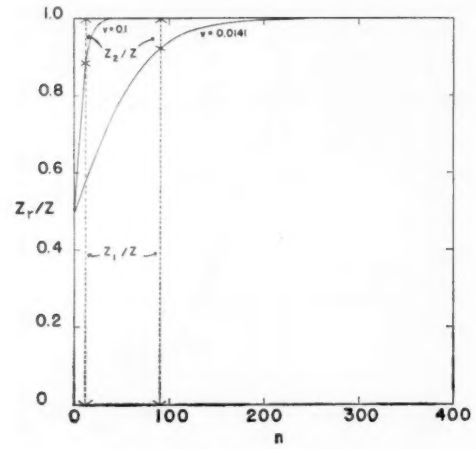

FIG. 5. Dependence of Z_1/Z and Z_2/Z on n for $v=0.1$ and $v=0.0141$ at $w=1+v$.

small, of the order of v, and the contribution of λ_2 to the partition function, the degree of helicity etc., may not be neglected unless n is very large. On the other hand, λ_3 is seen to be always small and essentially independent of w. Its contribution to the transition, therefore, is negligible except at extreme conditions of very small n and relatively large v. Since λ_3 is always negative, its main contribution to the partition function changes sign according to whether n is odd or even. A corresponding significant difference between the properties of polypeptides with odd and even numbers of peptide units evidently may occur only when n is small.

The mathematical procedure leading from the formulation of the configurational partition function, Eq. (2), to its final evaluation, Eq. (30), may be viewed as a series of transformations of the state variables which determine the state of the peptide units of the polypeptide chain. The first transformation replaced the $2n$ continuous variables ϕ_i and ψ_i by n discrete state variables, one for each unit, each with two values c and h. Represented by these variables, the partition function, Eq. (14), was given as a sum over the corresponding 2^n configurations of the whole system. When we next applied the matrix representation of the partition function, Eq. (20), we introduced in fact as our new state variables the states of the $n-1$ pairs of adjacent units, each with three values, (h, h), (h, c), and $(c, h \cup c)$. The representation of the 2^n configurations of the whole system was unaltered by this transformation. Finally, the similarity transformation $\mathbf{T}$, which diagonalized the matrix of conditional probabilities $\mathbf{W}$, may also be considered as a transformation to new $n-1$ state variables whose values determine the state of the n units of the system. Since the matrix of conditional probabilities is diagonal in these variables, it follows that the whole system can be found, in this representation, in one of the three states $r=1, 2, 3$ with a probability Z_r/Z for each. We shall consider Z_r as the partition function for the rth state. It is to be expected, therefore, that any average molecular property should be calculated by averaging its values over these three states, with Z_r/Z as the corresponding statistical weights. In the next section we shall derive explicitly such formulas for various average molecular properties.

The expression $Z_r=\lambda_r{}^n C_r$ suggests that λ_r is the contribution of each unit to Z_r while C_r is a factor which represents the contribution of end effects to the partition function Z_r. In Fig. 4 we see the dependence of these end effects on $\ln w$; this variable was chosen because of its correlation with the temperature, which we assume to be

$$\ln w = -\Delta H/kT + \Delta S/k. \tag{33}$$

Here ΔH is the energy change accompanying the formation of an intramolecular hydrogen bond, and ΔS is the corresponding charge of entropy. Both ΔH and ΔS include, in general, contributions from solvent interactions. It is easy to show that $C_1+C_2+C_3=1$ and that $C_3<0$. The latter is essentially independent of w and is very small; for $v=0.1$, C_3 is less than 1% of the largest of C_1 or C_2 and for smaller values of v, such as $v=0.0141$, it is completely negligible. On the other hand, the relative importance of C_1 and C_2 depends strongly on $\ln w$; at low values of w (coil region) C_1 is near unity, whereas C_2 is small, the end effect thus being appreciable only in Z_2. On the other hand, at large values of $\ln w$ (helical region) only Z_1 is appreciably reduced by the end effect while C_2 is near unity; at the transition point, $C_1 \simeq C_2$.

The three partition functions Z_r are strongly dependent on n through the factor $\lambda_r{}^n$. Even for very low values of n, the value of $\lambda_3{}^n$ is small; this together with the behavior of C_3 makes Z_3 completely negligible. The relative magnitude of Z_1 and Z_2 is determined essentially by $(\lambda_2/\lambda_1)^n$; as seen from the secular equation (22) and Fig. 3, this factor has a maximum at the transition point. The sharpness of this maximum increases and its value decreases when n and/or v increases and makes Z_2 important only in the transition region, i.e., around $w=1+v$, and even then only if n and/or v are not too large. In Fig. 5 the values of Z_1/Z and Z_2/Z at $w \cong 1+v$ (where $C_1=C_2$) are plotted vs n, which show the change of their relative magnitude with increasing n for $v=0.1$ and for $v=0.0141$. The value of n at which Z_2 is negligible within a specified degree of approximation can be calculated as follows, according to Eqs. (30), (31), and (26′):

$$Z \cong Z_1[1+(\lambda_2/\lambda_1)^n(C_2/C_1)]$$

$$\cong Z_1[1+(\lambda_2/\lambda_1)^{n+1}(w-\lambda_2)/(\lambda_1-w)], \tag{34}$$

if we assume that $Z_3 \cong 0$ and that $(\lambda_1-\lambda_3)/(\lambda_2-\lambda_3) \cong \lambda_1/\lambda_2$. The maximum of $(\lambda_2/\lambda_1)^{n+1}$ occurs at the transition point but that of the bracket is shifted slightly toward larger w since C_2/C_1 is an increasing function of w as can be seen from Fig. 4. This shift is very small, though; at a point such as $\lambda_1 \cong 1+3v$, $(w \cong 1+\frac{5}{2}v$, $\lambda_2 \cong 1+\frac{1}{2}v)$, at which $(w-\lambda_2)/(\lambda_1-w) \cong \frac{4}{5} \cong 1$ the derivative $\partial(Z_2/Z_1)/\partial w$ is already negative for any value of v and n. Then,

$$(Z_2/Z_1)_{\max} \cong (\lambda_2/\lambda_1)_{\max}{}^{n+1} \cong (1+2v)^{-n}$$
$$= \exp[-n \ln(1+2v)] \cong e^{-2nv}. \quad (35)$$

Therefore, to have $(Z_2/Z_1)_{\max} < 0.01$, n has to be such that $nv > 2.3$. For $nv \geq 3$, the term Z_2/Z_1 is negligible within an error of less than 1/300, and one might adopt this as a criterion for the negligibility of Z_2, i.e.,

$$Z_2 \cong 0, \qquad Z_1 \cong Z, \qquad \text{if } nv \geq 3. \quad (36)$$

To sum up the above discussion, we observe that among the three terms which comprise Z, one, Z_3, is practically always negligible. Among the others, Z_2 contributes to the partition function only in the transition region, i.e., in the vicinity of $w=1+v$, and provided $nv<3$; the effect of the ends of the chain, through C_2/C_1, is negligible at the coil region, but tends to increase slightly the relative weight of Z_2 at the helix side of the transition, within the narrow range $1+v \leq w \leq 1+2.5v$. Beyond this range Z_2 is negligible, unless nv is significantly smaller than 3.

MOLECULAR AVERAGES

Degree of Intramolecular Hydrogen Bonding

The average number of intramolecular hydrogen bonds, $\bar{n}_{\text{bond}}$, and the relative number or degree of hydrogen bondings, $\theta = \bar{n}_{\text{bond}}/n$, are both functions of n, w, and v (we set $u=1$ without loss of generality). By standard methods of statistical mechanics we have

$$\theta = n^{-1} \partial \ln Z / \partial \ln w. \quad (37)$$

On using Eq. (30) we may write

$$\theta = \sum_{r=1}^{3} \theta_r Z_r / Z, \quad (38)$$

where θ_r is given by

$$\theta_r = n^{-1} \partial \ln Z_r / \partial \ln w. \quad (39)$$

Thus, it appears that θ_r is the same function of Z_r as θ is of Z and may, therefore, be considered as the degree of intramolecular hydrogen bonding for the rth state. Equation (38) then gives θ as the average value of θ_r with statistical weights Z_r/Z, as pointed out in the preceding section. After introducing Eq. (31) into Eq. (39) we obtain

$$\theta_r = \partial \ln \lambda_r / \partial \ln w + n^{-1} \partial \ln C_r / \partial \ln w \equiv \theta_r{}^0 [1 + n^{-1} \theta_r{}'], \quad (40)$$

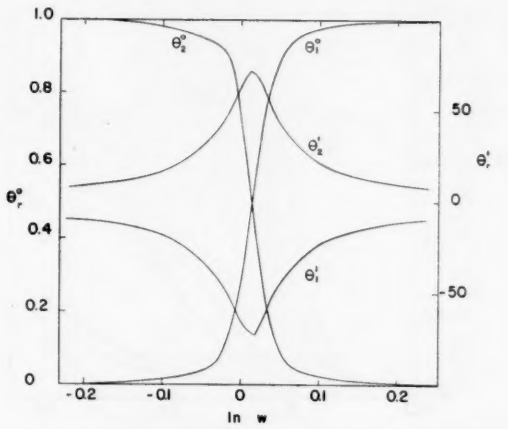

FIG. 6. Dependence of $\theta_1{}^0$, $\theta_2{}^0$, $\theta_1{}'$, and $\theta_2{}'$ on $\ln w$ for $v=0.0141$.

where the last term, $n^{-1}\theta_r{}'$, is a correction due to end effects, linear in n^{-1}, whereas $\theta_r{}^0$ represents the limiting value of θ_r for large n. The explicit expressions for $\theta_r{}^0$ and $\theta_r{}'$ are easily found from Eqs. (40), (26″), (27), and (22):

$$\theta_r{}^0 = \frac{\mu_r}{\lambda_r} \frac{\lambda_r \mu_r - v^2}{v^2(2\lambda_r - 1) + \mu_r{}^2}$$
$$\theta_r{}' = 2\left[1 - \lambda_r \frac{\mu_r(2\lambda_r - 1) + v^2}{v^2(2\lambda_r - 1) + \mu_r{}^2}\right]. \quad (41)$$

Thus, we have $\theta_r{}^0$ and $\theta_r{}'$ in terms of v and $\lambda_r(w, v)$, i.e., as functions of the variables of physical interest, v and w. The molecular weight dependence of θ is represented explicitly by the factors Z_r/Z in Eq. (38) and the factor n^{-1} in Eq. (40), while $\theta_r{}'$ are independent of n. As Z_3 is usually negligibly small, only $\theta_0{}^0$, $\theta_1{}'$, $\theta_2{}^0$, and $\theta_2{}'$ will be considered. In Fig. 6 these functions are plotted vs $\ln w$, with $v=0.0141$. It is seen that the contributions of $\theta_2{}^0$ and $\theta_2{}'$ to θ counteract those of $\theta_1{}^0$ and $\theta_1{}'$, respectively, $\theta_2{}^0$ tends to zero when $\theta_1{}^0$ tends to one, and vice versa, while $\theta_2{}'$ and $\theta_1{}'$ have opposite signs.[17] It should be noted also that $\theta_2{}'$ and $\theta_1{}'$ are rather large in absolute value in the transition region, and increase with decreasing v.

We can now see in a more quantitative fashion at which value of n and v can $\theta_2{}^0$ and the end effects be considered negligible within a certain error. Equation (38) can be rewritten as

$$\theta = \theta_1 \frac{1 + \theta_2 Z_2/\theta_1 Z_1}{1 + Z_2/Z_1}. \quad (42)$$

By using Eqs. (40), (41), (31), (26″), (22), and (28) and by approximating again $(\lambda_1-\lambda_3)/(\lambda_2-\lambda_3)$ by

[17] In fact, it can be shown rigorously that $\Sigma_r \theta_r{}^0 = 1$, and that $\theta_3{}^0$ and $\theta_3{}'$ are relatively negligible, thus $\theta_2{}^0 \cong 1 - \theta_1{}^0$, $\theta_2{}' \sim -\theta_1{}'$.

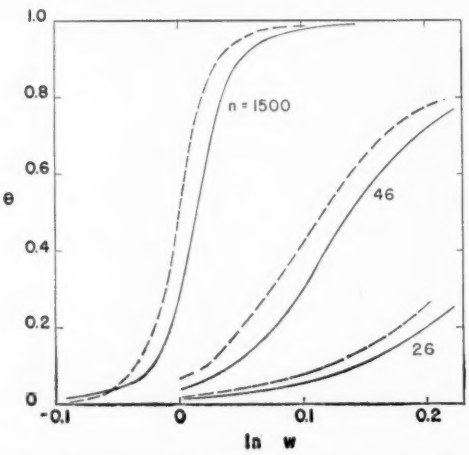

FIG. 7. Dependence of the degree of intramolecular hydrogen bonding, θ, on $\ln w$ for $v=0.0141$ and $n=26$, 46, and 1500. Comparison of the present theory (solid lines) with that (see footnote 4 in text) of Zimm and Bragg (dashed lines).

λ_1/λ_2 we have

$$\frac{\theta_2 Z_2}{\theta_1 Z_1} \cong (\lambda_2/\lambda_1)^n \frac{n(\lambda_1-\lambda_2)+2\lambda_2}{n(\lambda_1-\lambda_2)-2\lambda_1}. \qquad (43)$$

The last fraction shows a maximum near the midpoint of the transition $w \cong 1+v$ and tends to unity with increasing values of n and/or v since then $n(\lambda_1-\lambda_2)$ becomes larger. The maximum value of the whole expression, $\theta_2 Z_2/\theta_1 Z_1$, then lies quite near the point $w \cong 1+v$, as can be shown by making $\partial(\theta_2 Z_2/\theta_1 Z_1)/\partial w = 0$. The condition for maximum is, after minor simplifications,

$$\lambda_1 = (\lambda_1+\lambda_2)(\partial\lambda_1/\partial w).$$

This equation cannot be solved analytically for w but it can be shown that the solution lies in the narrow range: $(1-\frac{1}{2}v) < w < 1+v$ in which the last fraction in Eq. (43) is very close to 2, if $nv=3$. Then, according to Eq. (35) and its discussion,

$$(\theta_2 Z_2/\theta_1 Z_1)_{\max} \cong 2e^{-2nv}$$

and

$$\theta = \theta_1 = \theta_1^0(1+n^{-1}\theta_1') \quad \text{if } nv \geq 3, \qquad (44)$$

within an error of less than 1%.

The influence of the end effects, included in θ_1', however, is still important and vanishes only at relatively large values of n, at which $n^{-1}\theta_1' \cong 0$. The actual value of n at which that happens is easily found from Eqs. (40), (41), and the secular equation; according to them,

$$\theta_1 = \theta_1^0\left(1-\frac{2\lambda_1^2}{\lambda_1-\lambda_3}\frac{1}{n(\lambda_1-\lambda_2)}\right).$$

Obviously the maximum value of the fraction will occur at the transition, where $\lambda_1-\lambda_2 \cong 2v$, as seen in Fig. 6. Then, when $1/nv$ is negligible compared with 1, Eq. (38) becomes

$$\theta = \theta_1^0 \quad \text{if } nv \gg 1, \qquad (45)$$

that is, θ reaches its limiting value. This result could be obtained directly from Eq. (37) if we assume that, at high values of n, $\ln Z \cong n \ln\lambda_1$.

As a summary of the results, θ has been plotted vs $\ln w$ in Fig. 7 for $v=0.0141$ and several values of n together with the results of Zimm and Bragg,[4] (for $\sigma = 2\times10^{-4}$ in their notation). Except for a shift in the scale of $\ln w$, the agreement between the two theories is fairly good. While in our theory the transition point is at $w=1+v$, in the theory of Zimm and Bragg it occurs at $w=1$. The difference can be traced to the different ways of assigning conditional probabilities, which has been discussed in the preceding section.

The experimental data of Doty and Young,[18] and Zimm, Doty and Iso,[19] on the optical rotation of poly-γ-benzyl-L-glutamate were analyzed according to our theory, by using Eq. (33) to determine the relation of $\ln w$ to T. We obtain $\Delta H = 950$ cal/mol, which is comparable to $\Delta H = 850$ cal/mol obtained by Zimm, Doty, and Iso.

Average Number of Helical Sequences and Number-Average Length of a Sequence

When the degree of hydrogen bonding θ is different from its extreme values 0 and 1, the question arises how strong is the tendency of helical states to group into long sequences. The smaller the average number of sequences for a given θ, the longer is the average length of a sequence. Let $\bar{n}_{seq}$ denote the average number of helical sequences having at least 2 helical states in a sequence, then the number-average length $\bar{l}_n$ of a helical sequence is given by

$$\bar{l}_n = (\bar{n}_{bond}+2\bar{n}_{seq})/(n)_{seq} = \theta/\eta+2, \qquad (46)$$

where $\eta = \bar{n}_{seq}/n$. The term $2\bar{n}_{seq}$ represents the two nonbonded units in the helical state which start and end each sequence.

To obtain η (or $\bar{n}_{seq}$), we make the following observation. In the matrix **W**, Eq. (15), the three elements (31), (12), and (32), though having the same value v, represent three distinguishable states of nonbonded helical units. Let us denote them, respectively, by v_{31}, and v_{12}, and v_{32}. Then v_{31} belongs to a peptide unit which starts a helical sequence. This is evident from the values of $\rho_{i-1}\rho_i\rho_{i+1}$ for this element, namely *chh*. Similarly v_{12} belongs to a peptide unit at the end of a helical sequence because it is determined by $\rho_{i-1}\rho_i\rho_{i+1} = hhc$, while v_{32} corresponds to $\rho_{i-1}\rho_i\rho_{i+1} = chc$ and, there-

[18] P. Doty and J. T. Yang, J. Am. Chem. Soc. **78**, 498 (1956).
[19] B. H. Zimm, P. Doty, and K. Iso, Proc. Natl. Acad. Sci. U. S. **45**, 1601 (1959).

fore, belongs to a lonely helical state. Since each helical sequence of two or more units has one beginning and one end, the average number of v_{31}, denoted by $\bar{n}_{31}$, equals the average number $\bar{n}_{12}$ of v_{12} and the average number of sequences, $\bar{n}_{seq}$,

$$\bar{n}_{12}=\bar{n}_{31}=\bar{n}_{seq}. \tag{47}$$

To obtain these averages we distinguish between the three v's in the secular equation (22), and thus have

$$f(\lambda; w, v_{12}, v_{31}, v_{32})=(\lambda-w)(\lambda^2-\lambda-v_{32})-v_{12}v_{31}=0. \tag{48}$$

Now λ_r and Z are functions of the different v's and we have

$$\eta=\bar{n}_{12}/n=n^{-1}\partial \ln Z/\partial \ln v_{12}. \tag{49}$$

By following the same reasoning which led from Eqs. (37) to (40), we have

$$\eta=\sum_{r=1}^{3}\eta_r Z_r/Z, \tag{50}$$

where

$$\eta_r=\eta_r^0(1+n^{-1}\eta_r'). \tag{51}$$

Again η_r represents the relative number of helical sequences for the rth state. Explicit expressions can be obtained by using Eqs. (51), (26″), (27), (22), and (41):

$$\eta_r^0=\frac{v^2\mu_r}{\lambda_r[v^2(2\lambda_r-1)+\mu_r^2]}=\theta_r^0[(\lambda_r-w)/w]$$
$$\eta_r'=\theta_r'+(\lambda_r\mu_r/v^2). \tag{52}$$

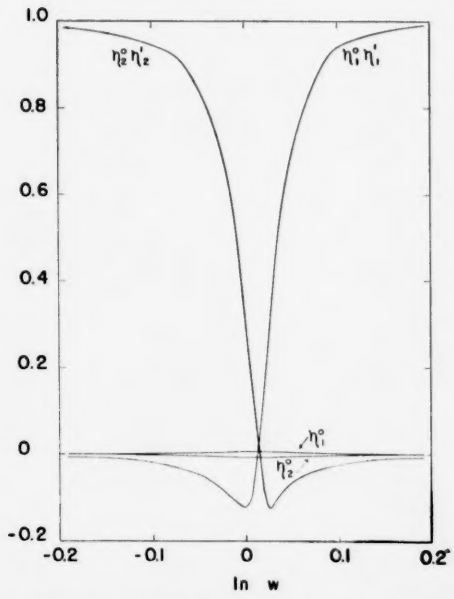

FIG. 8. Dependence of η_1^0, η_2^0, $\eta_1^0\eta_1'$, and $\eta_2^0\eta_2'$ on ln$w$ for $v=0.0141$.

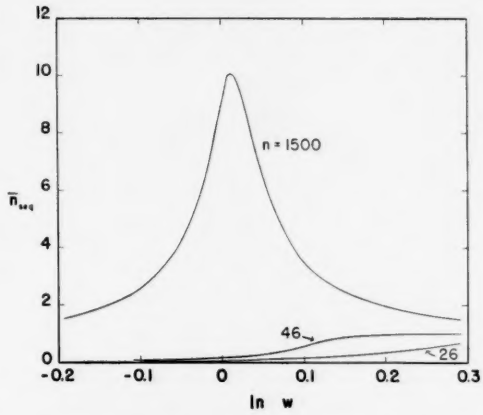

FIG. 9. Dependence of the average number of helical sequences, $\bar{n}_{seq}$, on ln$w$ for $v=0.0141$ and $n=26$, 46, and 1500.

We neglect η_3 since its statistical weight Z_3/Z is very small; therefore, only η_1 and η_2 have to be considered. According to Eq. (52) η_r^0 is always small, because when θ_r^0 tends to unity, $(\lambda_r-w)/w$ tends to zero. Both η_1^0 and $-\eta_2^0$ have a shallow maximum in the transition region, as seen in Fig. 8. On the other hand η_r' undergoes very large changes. For example, η_1' increases indefinitely with increasing w, because of the term $\lambda_1\mu_1/v^2$, while η_1^0 tends at the same time to zero. It appears more instructive, therefore, to consider the molecular weight dependence of η_r through the product $\eta_r^0\eta_r'$ which is plotted vs ln$w$ in Fig. 8. We see that $\eta_1^0\eta_1'$ and $\eta_2^0\eta_2'$ are approximately symmetric with respect to a line through the transition point. At the extreme helical region, when θ tends to unity, $\eta_1^0\eta_1'$ tends also to unity and η tends to $1/n$; namely, the molecule consists of a single helical sequence. In following arguments similar to those used in the discussion of θ, we find that η is given to a good approximation by η_1 provided nv is of the order of three or larger,

$$\eta=\eta_1=\eta_1^0(1+n^{-1}\eta_1') \quad \text{for } nv\geq 3. \tag{53}$$

As a summary of these results, the average number of helical sequences, $\bar{n}_{seq}$, is plotted in Fig. 9 vs ln$w$ for $v=0.0141$ and $n=26$, 46, and 1500. All three curves tend to zero in the coil region, and to unity (single, unbroken helix) in the helical region, but only when the molecular weight is high is the average number of helical sequences significantly larger than one, and its maximum value occurs in the transition region. The number average length of a helical sequence [Eq. (46)] increases with increasing helicity monotonously and smoothly irrespective of whether η has a maximum in the transition region or not. This is seen in Fig. (10), where $\bar{l}_n/n$ is plotted vs ln$w$ with the values of n and v the same as in Fig. 9.

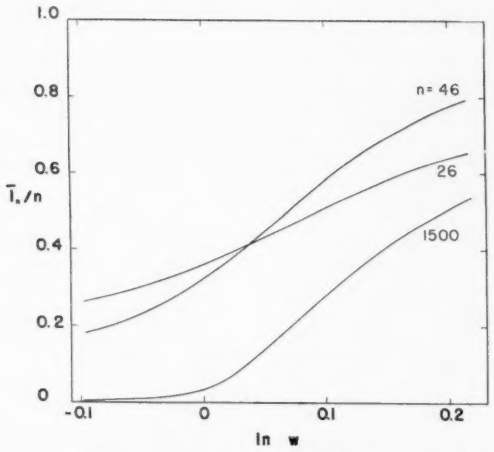

FIG. 10. Dependence of the relative number average length of a helical sequence, $\bar{l}_n/n$ on $\ln w$ for $v=0.0141$ and $n=26$, 46, and 1500.

Distribution of Lengths of Helical Sequence

We now ask what is the average number $\bar{n}_x$ of helical sequences of length x (i.e., sequences of x peptide units) for a molecular chain of n units, and given values w and v. To answer this and other similar questions we need a more general method of averaging over molecular properties than that used in the preceding examples. We shall now derive such a method, which is a modification of a method used by one of us[20] in calculating average dimensions of polymers, and which takes advantages of the simplicity of the matrix representation of the partition function.

It was observed before, that the three v's in the matrix $\mathbf{W}$ represent three distinguishable states of nonbonded helical units. The same is true for each element of the matrix, i.e., the corresponding state is determined by the sequence $\rho_{i-1}\rho_i\rho_{i+1}$ to which it belongs. For example, the element u_{23} [in position (23)] starts a random sequence, the element u_{33} continues such a sequence while w evidently belongs to a bonded unit in the interior of a helical sequence. (A better distinction between different u's is obtained when the 4×4 matrix representation[13] is followed.)

We ask now, what is the probability $p_{rs}(i)$ that a particular peptide unit, the ith, will be found in one of the above-mentioned positions. It should be clear that the answer cannot be u, v, or w since these are conditional probabilities determined by the unit under consideration *and* its neighbors, while we are interested in the probability of finding the ith element in a given state (rs) irrespective of, and therefore averaged over, all the admissible positions of all other peptide units.

The probability of finding the whole chain in a specified state, $\rho_1\cdots\rho_n$, is given by the summand in Eq. (14). To obtain $p_{rs}(i)$ we fix the ith unit in the state (rs) and sum over all the states of the $i-1$ units on the left and the $n-i$ units on the right, which are consistent with the state (rs) of the ith unit. In matrix notation,

$$p_{rs}(i)=\mathbf{e}\mathbf{W}^{i-1}(W_{rs}\mathbf{E}_{rs})\mathbf{W}^{n-i}\mathbf{e}^{+}/Z, \qquad (54)$$

where W_{rs} is the element (rs) of $\mathbf{W}$, and $\mathbf{E}_{rs}$ is a 3×3 matrix with the digit one in position (rs) and zero elsewhere. Note that $\mathbf{E}_{rs}$ does not commute with $\mathbf{W}$. The factor $W_{rs}\mathbf{E}_{rs}$ represents our requirement that the ith elements be in the (rs) position, while $\mathbf{e}\mathbf{W}^{i-1}$ and $\mathbf{W}^{n-i}\mathbf{e}^{+}$ represent the summation, or averaging, over all possible states of the other peptide units, consistent with the ith unit in (rs); $1/Z$ is the normalization factor. That these probabilities are normalized, i.e.,

$$\sum_{r,s}p_{rs}(i)=1; \qquad i=1,\cdots,n \qquad (55)$$

follows directly from the identity

$$\mathbf{W}=\sum_{r,s}W_{rs}\mathbf{E}_{rs}. \qquad (56)$$

Equation (54) can be transformed to enable direct summation over i. We first diagonalize $\mathbf{W}$ by Eq. (21), and obtain

$$p_{rs}(i)=W_{rs}\mathbf{e}\mathbf{T}\mathbf{\Lambda}^{i-1}\mathbf{T}^{-1}\mathbf{E}_{rs}\mathbf{T}\mathbf{\Lambda}^{n-1}\mathbf{T}^{-1}\mathbf{e}^{+}/Z. \qquad (57)$$

Now let $\mathbf{l}_\alpha$ and $\mathbf{l}_\alpha{}^*$ be a row and a column vector, respectively, whose components are the diagonal elements of Λ^α, where α is any integer; and let $\mathbf{T}_r{}^+$ and $\mathbf{T}_s$ be diagonal matrices whose diagonal elements are, respectively, the rth column of $\mathbf{T}^{-1}$ and the sth row of $\mathbf{T}$. Let us further denote

$$\mathbf{a}_r=\mathbf{e}\mathbf{T}\mathbf{T}_r{}^+ \qquad \mathbf{a}_s{}^+=\mathbf{T}_s\mathbf{T}^{-1}\mathbf{e}^+. \qquad (58)$$

Equation (56) can then be written as

$$p_{rs}(i)=W_{rs}\mathbf{a}_r\mathbf{l}_{i-1}{}^*\cdot\mathbf{l}_{n-i}\mathbf{a}_s{}^+/Z, \qquad (59)$$

where $\mathbf{l}_{i-1}{}^*\cdot\mathbf{l}_{n-1}$ is the diadic product of the two vectors.

As examples of the use of the probabilities p_{rs} we shall first obtain the functions θ and η derived already above, Eqs. (38) and (50). Thus, the degree of hydrogen bonding θ is given by

$$\theta=n_{\text{bond}}/n=\sum_{i=1}^{n}p_{11}(i)/n=\mathbf{a}_1\mathbf{L}_{n-1}\mathbf{a}_1{}^*/Zn, \qquad (60)$$

where $\mathbf{a}_1$ and $\mathbf{a}_1{}^*$ are obtained from Eq. (58) with the help of Eqs. (24), (25), and (29), setting $u=1$,

$$(\mathbf{a}_1)_r=vC_r/\lambda_r(\lambda_r-w); \qquad (61)$$

$\mathbf{a}_1{}^*=\mathbf{a}_1{}^+$ is the transpose of $\mathbf{a}_1$; and $\mathbf{L}_{n-1}$ is the symmetric matrix

$$\mathbf{L}_{n-1}=\sum_{i=1}^{n}\mathbf{l}_{i-1}{}^*\cdot\mathbf{l}_{n-i}; \qquad (\mathbf{L}_{n-1})_{rr}=n\lambda_r{}^{n-1};$$

$$(\mathbf{L}_{n-1})_{rs}=(\lambda_r{}^n-\lambda_s{}^n)/(\lambda_r-\lambda_s). \qquad (62)$$

[20] S. Lifson, J. Chem. Phys. **30**, 964 (1959).

The equivalence of Eqs. (60) and (38) can be easily shown, and will not be given here.

Similarly η can be obtained by

$$\eta=\bar{n}_{12}/n=\sum_{i=1}^{n}p_{12}(i)/n=\mathbf{a}_1L_{n-1}\mathbf{a}_2^{+}/nZ, \quad (63)$$

where a_2^{+} is obtained like a_1^{+} above, and is given by

$$(\mathbf{a}_2^{+})_r=C_r/\lambda_r, \quad (64)$$

and again Eqs. (63) and (50) can be shown to be equivalent.

This formulation of probabilities can be applied to states involving more than one peptide unit. For example, we may ask what is, in terms of the matrices $\mathbf{W}$ and $\mathbf{E}_{rs}$, the probability $p(x, i)$ that a helical sequence of length x (i.e., having x peptide units) starts at the unit $i-x+1$ and ends at i, $(x\leq i)$. The above considerations lead directly to the answer

$$p(x, i)=\mathbf{e}\mathbf{W}^{i-x}(v\mathbf{E}_{21})(w\mathbf{E}_{11})^{x-2}(v\mathbf{E}_{12})\mathbf{W}^{n-i}\mathbf{e}^{+}/Z, \quad 2\leq x\leq i, \quad (65)$$

which is reduced to

$$p(x, i)=(v^2w^{x-2})\mathbf{e}\mathbf{W}^{i-x}\mathbf{E}_{22}\mathbf{W}^{n-i}\mathbf{e}^{+}/Z, \qquad 2\leq x\leq i \quad (66)$$

by using the identities

$$\mathbf{E}_{ri}\mathbf{E}_{is}=\mathbf{E}_{rs}. \quad (67)$$

We are now in a position to answer the question stated at the beginning of this section: The average number $\bar{n}_x$ of helices of length x is given by

$$\bar{n}_x=\sum_{i=x}^{n}p(x, i)=(v^2w^{x-2})\,\mathbf{a}_3\mathbf{L}_{n-x}\mathbf{a}_2^{+}/Z \qquad 2\leq x\leq n, \quad (68)$$

where $\mathbf{L}_{n-x}$ is obtained from Eq. (62) by replacing n by $n-x+1$; $\mathbf{a}_3$ is obtained from Eq. (58) with the help of Eqs. (25) and (29), and the result is the same as Eq. (64), i.e., $\mathbf{a}_3=(\mathbf{a}_2^{+})^{*}$. Thus,

$$\bar{n}_x=(v^2w^{x-2}/Z)\,\mathbf{a}_3\mathbf{L}_{n-x}\mathbf{a}_3^{*}. \quad (69)$$

For the special case $x=1$, when $\bar{n}_1$ is the average number of lonely helical states, Eq. (66) has to be slightly modified: The factor v replaces (v^2w^{x-2}), so that

$$\bar{n}_1=(v/Z)\,\mathbf{a}_3L_{n-1}\mathbf{a}_3^{*}. \quad (70)$$

It is seen that $\bar{n}_x$ of a chain of n units is related to $\bar{n}_1$ of a chain of $n-x+1$ units by

$$\bar{n}_x^{(n)}=(vw^{x-2}Z^{(n-x+1)}/Z^{(n)})\,\bar{n}_1^{(n-x+1)}, \quad (71)$$

where superscripts such as (n) and $(n-x+1)$ will denote henceforth, when necessary, the respective numbers of peptide units in the whole chain. An expression for $\bar{n}_1$ may be obtained also by using the common method of calculating molecular averages

$$\bar{n}_1=(v_{32}/Z)\partial Z/\partial v_{22}, \quad (72)$$

where Z is a function of v_{32} through the eigenvalues of the secular equation given in Eq. (48). By following again the same path which led to Eq. (38) for θ, we obtain for any x

$$\bar{n}_1^{(x)}/x=\sum_{r=1}^{3}\xi_rZ_r^{(x)}/Z^{(x)}, \quad (73)$$

where

$$\xi_r=\xi_r^{0}(1+x^{-1}\xi_r'), \quad (74)$$

$$\xi_r^{0}=\partial\ln\lambda_r/\partial\ln v_{32}, \quad (75)$$

$$\xi_r'=(\partial\ln C_r/\partial\ln v_{32})/(\partial\ln\lambda_r/\partial\ln v_{32}). \quad (76)$$

By introducing Eq. (73) into Eq. (71) we have after replacing x by $n-x+1$ in Eq. (71),

$$\bar{n}_{n-x+1}^{(n)}=(vw^{n-1}/Z^{(n)})\sum_{r=1}^{3}C_r\xi_r^{0}(x+\xi_r')(\lambda_r/w)^{x}. \quad (77)$$

If $n\geq 3$ we may write, according to Eq. (36), $Z^{(n)}=Z_1^{(n)}$, and

$$\bar{n}_{n-x+1}^{(n)}=(v/\lambda_1)(w/\lambda_1)^{n-1}\sum_{r=1}^{3}(C_r/C_1)\xi_r^{0}(x+\xi_r')(\lambda_r/w)^{x}. \quad (78)$$

For a large part of the range of variation of x we may also reduce the sum in Eq. (78) to only its first term, and we obtain then for most of the distribution

$$\bar{n}_x^{(n)}=(v/\lambda_1)\xi_1^{0}(n+1-x+\xi_1')(w/\lambda_1)^{x-2}. \quad (79)$$

Equations (77)–(79) indicate that the distribution of lengths of helical sequences is rather broad on both sides of the transition region, although the actual value of all $\bar{n}_x$ increases steeply with the transition from the coil to the helix region.

After having derived $\bar{n}_x$ we obtain directly the distribution of peptide units among the various helical sequences

$$\bar{m}_x=x\bar{n}_x \quad (80)$$

and the "weight-average" length $\bar{l}_A$ of a helical segment, where the statistical weight of each sequence is proportional to the number of peptide units comprising the sequence. Since the distribution $\bar{n}_x$ is rather broad, $\bar{l}_A$ is, in general, much larger than $\bar{l}_n$. It is given by

$$l_w=\sum_{x=2}^{n}x\bar{m}_x/\sum_{x=2}^{n}\bar{m}_x=\sum_{x=2}^{n}x^2\bar{n}_x/\sum_{x=2}^{n}x\bar{n}_x$$

$$=\sum_{x=2}^{n}x^2\bar{n}_x/n(\theta+2\eta). \quad (81)$$

The distribution of helical sequences or the weight-average length of such sequences may be helpful in the study of the hydrodynamic behavior of polypeptides at and above the transition region. According to Eq. (79) $\bar{n}_x$ tends to zero when x is large enough for any fixed value $w/\lambda_1<1$. Therefore, when n is large enough the

polypeptide molecule must exhibit a hydrodynamic behavior of a kinked chain of rigid rods, whereas a short or medium length molecule might behave as a rigid helix under the same conditions of temperature and solvent. It is appropriate to note in this connection that Nagai,[8] has discussed the hydrodynamic behavior of polypeptide chains in the transition region by calculating the mean-square end-to-end distance of a partially helical chain. His results may be simplified considerably by replacing his 7×7 matrices by our 3×3 ones.

ACKNOWLEDGMENTS

The authors are grateful to W. H. Stockmayer and P. Doty for interesting discussions related to the subject of this paper. One of us (A. R.) gratefully acknowledges an appointment supported by the International Cooperation Administration under the Visiting Research Scientists Program administered by the National Academy of Sciences, U.S.A. One of us (S.L.) gratefully acknowledges the financial support given by National Science Foundation Grant NSF G-7487 during his stay at Harvard.

THE JOURNAL OF CHEMICAL PHYSICS VOLUME 34, NUMBER 6 JUNE, 1961

Theory of Solutions. III. Thermodynamics of Aggregation or Polymerization*

TERRELL L. HILL†

Department of Theoretical Chemistry, Cambridge University, Cambridge, England

(Received November 21, 1960)

Polymeric and colloidal systems are usually polydisperse, containing possibly hundreds or thousands or more, of subspecies differing only in degree of polymerization n. The required thermodynamic approach is that appropriate to a highly multicomponent system. Let $P(n)$ be the fraction of polymer molecules of size n. The distribution function $P(n)$ will depend on one or more parameters, for example, the mean $\bar{n}$ and standard deviation σ in the case of a Gaussian distribution. The thermodynamic problem becomes tractable if we replace, as composition variables, the numbers of molecules of all the polymer subspecies by the total number of polymer molecules N and the parameters of $P(n)$. The new set of variables may be only two, three, etc., in number. Our main interest in this paper is to investigate how the thermodynamic functions of the system change when the distribution function $P(n)$ changes, as, for example, in a kinetic study in which $P(n)$ evolves sufficiently slowly with time or in thermodynamic studies on different samples of the same polymer.

I. INTRODUCTION

IN systems such as a solution of a natural or synthetic polymer, a gas of liquid droplets or nuclei, inorganic colloidal particles or nuclei suspended in a liquid, etc., the "polymer," which is the general term we shall use for brevity in all these cases, does not exist, in general, as a single component but rather as a whole series of components differing in the degree of polymerization or aggregation, i.e., in molecular weight. In other words, the polymer is usually polydisperse (heterogeneous). The required thermodynamic approach here is that appropriate to a highly multicomponent system: the number of polymer subspecies may range, say, from ten to thousands or more.

Let n be the number of monomers (repeat units) or molecular units (e.g., water molecules in a water droplet) in a given polymer subspecies, and let $P(n)$ be the fraction of all polymer molecules containing n monomers. In this paper we shall be concerned primarily with the question of how the thermodynamic functions of the system change when the distribution function $P(n)$ changes. Such a discussion should be of use in equilibrium studies comparing different samples [with differing distributions $P(n)$] of the same polymer or in kinetic studies on a polymeric system in which the distribution evolves with time (e.g., polymerization of a polymer, aggregation of a colloidal suspension, or formation of condensation nuclei in a gas). In the kinetic case the rate must be sufficiently slow so that quasi-equilibrium is attained at each stage of evolution.

In any given application the mathematical form of $P(n)$ must be sufficiently general to encompass the complete range of alterations in $P(n)$ to be encountered. Thus P will be a function not only of n but also of a sufficient number of parameters $\alpha_1, \alpha_2, \cdots$. The number of parameters in practical cases would usually be in the range one to four. Ordinarily the degree of polymerization will be sufficiently large so that a continuous distribution $P(n)$[normalized by $\int P(n)dn=1$] can

* Supported in part by a research grant from the Heart Institute, Public Health Service. The first two papers of the series are T. L. Hill, J. Am. Chem. Soc. **79**, 4885 (1957); J. Chem. Phys. **30**, 93 (1959).

† Public Health Service Special Research Fellow, 1960–61, and Alfred P. Sloan Foundation Fellow. Permanent address: Department of Chemistry, University of Oregon, Eugene, Oregon.

be used. Two important examples are

$$P(n, \bar{n}, \sigma) = \frac{\exp[-(n-\bar{n})^2/2\sigma^2]}{(2\pi)^{\frac{1}{2}}\sigma}, \quad (1)$$

$$P(n, \bar{n}) = (1/\bar{n}) \exp(-n/\bar{n}). \quad (2)$$

In the Gaussian distribution (1) the parameters are the mean $\alpha_1=\bar{n}$ and standard deviation $\alpha_2=\sigma$, while in the exponential distribution (2) the only parameter is the mean $\alpha_1=\bar{n}$. As we shall see in Sec. II, there is considerable advantage in any case to choosing $\alpha_1=\bar{n}$.

We now come to the essential point: although a polydisperse polymeric system ordinarily has a hopelessly large number of components to take into account thermodynamically, the problem becomes tractable if we introduce as thermodynamic composition variables for the polymer $\alpha_1, \alpha_2, \cdots$ and N, the total number of polymer molecules of all subspecies.

Although it is desirable to apply the equations we derive to statistical mechanical models of linear polymer coils, helical rods, liquid droplets, colloidal particles, etc., we shall not attempt this here (see, however, Appendix II) but rather confine ourselves to a purely thermodynamic discussion. Even with this restriction we shall not give an exhaustive catalog of all the possible thermodynamic relations. In particular, we shall work primarily with the Gibbs free energy F.

II. PRESSURE AS INDEPENDENT VARIABLE

Consider a solution at pressure p and temperature T containing solvent (component 1) and a large number (perhaps thousands or more) of polymer subspecies (components 2, 3, $\cdots$). Then

$$dF = -SdT + Vdp + \mu_1 dN_1 + \sum_{i\geq 2} \mu_i dN_i, \quad (3)$$

where F = Gibbs free energy. If the solvent is in fact a mixed solvent of *fixed* composition with a total number of molecules N_1 and numbers of molecules of the different solvent components $N'=x'N_1$, $N''=x''N_1$, etc., where x', x'', etc., are constants, then we can define μ_1 by the relation

$$\mu_1 N_1 = \mu' N' + \mu'' N'' + \cdots = (\mu' x' + \mu'' x'' + \cdots) N_1.$$

Thus Eq. (3) also applies to a mixed solvent of *constant* composition.

The large number of independent variables N_2, N_3, $\cdots$, in Eq. (3) can be replaced by a relatively small number of variables if we now make use of the distribution $P(n)$. Each of the numbers $N_2, N_3, \cdots$, is determined by the total number of polymer molecules $N(=N_2+N_3+\cdots)$ and $P(n)$, that is, by N, $\alpha_1, \alpha_2, \cdots$. Hence we can use $N, \alpha_1, \alpha_2, \cdots$, as thermodynamic variables instead of $N_2, N_3, \cdots$; N is an extensive property while $\alpha_1, \alpha_2, \cdots$, are intensive.

We therefore rewrite Eq. (3) in the alternative form

$$dF = -SdT + Vdp + \Gamma_1 d\alpha_1 + \Gamma_2 d\alpha_2 + \cdots + \mu_1 dN_1 + \mu dN. \quad (4)$$

The important quantities $\Gamma_1, \Gamma_2, \cdots$ (extensive) and μ (intensive) are defined, by this equation, as differential coefficients;

$$\Gamma_i = (\partial F/\partial \alpha_i)_{T,p,N_1,N,\alpha_j}, \qquad \mu = (\partial F/\partial N)_{T,p,N_1,\alpha} \quad (5)$$

(α means all of the α's and α_j means all but the one involved in the derivative). Integration of Eq. (4), holding intensive properties constant, yields

$$F = \mu_1 N_1 + \mu N. \quad (6)$$

From Eq. (3),

$$F = \mu_1 N_1 + \sum_{i\geq 2} \mu_i N_i$$

so that

$$\mu = N^{-1} \sum_{i\geq 2} \mu_i N_i = \sum_n \mu(n) P(n) = \int \mu(n) P(n) dn, \quad (7)$$

where $\mu(n)$ is the chemical potential of $n$mers in the solution. We shall use the integral notation below for the summation over n. It will be understood that summation is to be substituted where necessary (e.g., small n or a small number of polymer subspecies). The quantities μ and $\mu(n)$ (and all other intensive properties of the system) are functions of p, T, and the composition, which is determined by $m=N/N_1$ (essentially the total molality of polymer) and all the α's. It is clear from Eq. (7) that μ is the mean value of $\mu(n)$ with respect to the distribution $P(n)$. Equations such as (7) and (12), below, in which one needs to know a partial molal quantity as a function of n are more likely to be useful in theoretical work (statistical mechanics) than in experimental work, though there is no obstacle in principle to making the necessary measurements.

If $P(n)$ is held constant (i.e., if the α's are constant), we see from Eqs. (4) and (6) that we have, in effect, an ordinary two-component solution. This point will be emphasized below in Eqs. (41) and (42).

Let G be any extensive property of the system. Then

$$dG = (\partial G/\partial T)dT + (\partial G/\partial p)dp + \sum_{k\geq 1} G_k^* d\alpha_k + \bar{G}_1 dN_1 + \bar{G} dN, \quad (8)$$

where $\bar{G}_1$ is an ordinary partial molal quantity and

$$G_k^* = (\partial G/\partial \alpha_k)_{T,p,N_1,N,\alpha_j}, \qquad \bar{G} = (\partial G/\partial N)_{T,p,N_1,\alpha}.$$

The G_k^* are extensive quantities (like $\partial G/\partial T$ and $\partial G/\partial p$) while $\bar{G}$ is intensive. Integration of Eq. (8) gives

$$G = \bar{G}_1 N_1 + \bar{G} N, \quad (9)$$

and hence

$$N_1 d\bar{G}_1 + N d\bar{G} = (\partial G/\partial T)dT + (\partial G/\partial p)dp + \sum_k G_k^* d\alpha_k \tag{10}$$

$$= \sum_k G_k^* d\alpha_k \qquad (p,\ T \text{ constant}) \tag{11}$$

$$= 0 \qquad (p,\ T,\ \alpha \text{ constant}). \tag{12}$$

These are Gibbs-Duhem equations. Special cases of Eqs. (10) and (11) are ($G = F$, $\bar{F}_1 = \mu_1$, $\bar{F} = \mu$),

$$N_1 d\mu_1 + N d\mu = -SdT + Vdp + \sum_k \Gamma_k d\alpha_k \tag{13}$$

and

$$G_i^* = N_1(\partial \bar{G}_1/\partial \alpha_i)_{T,p,m,\alpha_j} + N(\partial \bar{G}/\partial \alpha_i)_{T,p,m,\alpha_j}. \tag{14}$$

For a given distribution (α's constant) $\bar{G}(T,\ p,\ m)$ may be found experimentally by use of the standard methods of binary solution thermodynamics since in this case $\bar{G}$ behaves just like a partial molal property of a single solute. To find the dependence of $\bar{G}$ on the α's, different distributions must be used.

Just as in Eqs. (6) and (7) we have

$$\bar{G} = N^{-1} \sum_{i \geq 2} \bar{G}_i N_i = \int \bar{G}(n) P(n) dn, \tag{15}$$

where $\bar{G}(n)$ is the ordinary partial molal quantity for $n$mers. Thus $\bar{G}$ is the mean of $\bar{G}(n)$ with respect to $P(n)$. Equation (7) is a particular case ($G = F$) of Eq. (15). If we put Eq. (15) in Eq. (14) and use the ordinary Gibbs-Duhem equation

$$0 = N_1 d\bar{G}_1 + \sum_{i \geq 2} N_i d\bar{G}_i = N_1 d\bar{G}_1 + N \int P(n) d\bar{G}(n) dn \quad (p,\ T \text{ constant}),$$

we find

$$G_i^* = N \int \bar{G}(n)(\partial P/\partial \alpha_i)_{n,\alpha_j} dn. \tag{16}$$

Special cases of Eqs. (14) and (16) are ($G = F$)

$$\Gamma_i = F_i^* = N_1(\partial \mu_1/\partial \alpha_i)_{T,p,m,\alpha_j} + N(\partial \mu/\partial \alpha_i)_{T,p,m,\alpha_j} \tag{17}$$

$$= N \int \mu(n)(\partial P/\partial \alpha_i)_{n,\alpha_j} dn. \tag{18}$$

Other but less practical expressions for Γ_i follow from

$$d(F - \mu_1 N_1) = d(\mu N) = -SdT + Vdp + \Gamma_1 d\alpha_1 + \cdots - N_1 d\mu_1 + \mu dN$$

$$d(F - \mu N) = d(\mu_1 N_1) = -SdT + Vdp + \Gamma_1 d\alpha_1 + \cdots + \mu_1 dN_1 - Nd\mu.$$

Then

$$\Gamma_i = (\partial \mu N/\partial \alpha_i)_{T,p,\mu_1,N,\alpha_j} = N(\partial \mu/\partial \alpha_i)_{T,p,\mu_1,\alpha_j}$$

$$= (\partial \mu_1 N_1/\partial \alpha_i)_{T,p,N_1,\mu,\alpha_j} = N_1(\partial \mu_1/\partial \alpha_i)_{T,p,\mu,\alpha_j}. \tag{19}$$

There are of course many cross-derivative relations. For example, from Eq. (4),

$$-\partial S/\partial \alpha_i = -S_i^* = \partial \Gamma_i/\partial T, \qquad \partial V/\partial \alpha_i = V_i^* = \partial \Gamma_i/\partial p \tag{20}$$

$$\partial \Gamma_j/\partial \alpha_i = \Gamma_{ji}^* = \partial \Gamma_i/\partial \alpha_j = \Gamma_{ij}^* \tag{21}$$

$$-\partial S/\partial N = -\bar{s} = \partial \mu/\partial T, \qquad \bar{v} = \partial \mu/\partial p, \qquad \partial \Gamma_i/\partial N = \bar{\Gamma}_i = \partial \mu/\partial \alpha_i \tag{22}$$

$$-\bar{s}_1 = \partial \mu_1/\partial T, \qquad \bar{v}_1 = \partial \mu_1/\partial p, \qquad \partial \Gamma_i/\partial N_1 = \bar{\Gamma}_{i1} = \partial \mu_1/\partial \alpha_i. \tag{23}$$

Using these, we have

$$d\mu = -\bar{s}dT + \bar{v}dp + \sum_k \bar{\Gamma}_k d\alpha_k + (\partial \mu/\partial m)dm \tag{24}$$

$$d\mu_1 = -\bar{s}_1 dT + \bar{v}_1 dp + \sum_k \bar{\Gamma}_{k1} d\alpha_k + (\partial \mu_1/\partial m)dm \tag{25}$$

$$d\Gamma_i = -S_i^* dT + V_i^* dp + \sum_k \Gamma_{ik}^* d\alpha_k + \bar{\Gamma}_{i1} dN_1 + \bar{\Gamma}_i dN. \tag{26}$$

Integration of Eq. (26) gives

$$\Gamma_i = \bar{\Gamma}_{i1} N_1 + \bar{\Gamma}_i N,$$

as expected [see Eq. (9)].

Closed System

As implied in Sec. I, an important application arises when the colloidal or polymeric system is closed and the distribution function $P(n)$ changes. In this case, the total number of monomers in the system $\bar{n}N$ is a constant, as is also[1] N_1. It is convenient, then, to select $\alpha_1=\bar{n}$ and to change independent variables from $\bar{n}$, α_2, α_3, $\cdots$, N to $\bar{n}$, α_2, α_3, $\cdots$, $\bar{n}N$. Thus Eq. (4) becomes

$$dF=-SdT+Vdp+[\Lambda-(\mu N/\bar{n})]d\bar{n}+\Gamma_2 d\alpha_2 +\Gamma_3 d\alpha_3+\cdots+\mu_1 dN_1+(\mu/\bar{n})d(\bar{n}N), \quad (27)$$

where we use the special symbol Λ for Γ_1 when $\bar{n}$ is chosen as α_1. Consequently, when the distribution $P(n)$ is varied in a closed system at constant T and p,

$$dF=[\Lambda-(\mu N/\bar{n})]d\bar{n}+\Gamma_2 d\alpha_2+\Gamma_3 d\alpha_3+\cdots. \quad (28)$$

Since $dF=DW_{\text{non}-pV}$[on] (the non-pV reversible work done on a closed system at constant T and p), the terms on the right of Eq. (28) specify the non-pV reversible work required (positive or negative) to alter the distribution $P(n)$ in an arbitrary way. If no non-pV work is done on or by the system $dF\leq 0$ where the inequality holds for a spontaneous change in $P(n)$, as in a closed kinetic experiment at constant T and p, and the equality holds when a final equilibrium $P(n)$ is reached,

$$0\geq[\Lambda-(\mu N/\bar{n})]d\bar{n}+\Gamma_2 d\alpha_2+\Gamma_3 d\alpha_3+\cdots. \quad (29)$$

If $P(n)$ changes spontaneously in such a way that α_2, α_3, $\cdots$, are constant and only the mean $\bar{n}$ shifts, then the sign of $d\bar{n}$ must satisfy $[\Lambda-(\mu N/\bar{n})]d\bar{n}<0$. Similarly, if $\bar{n}$, α_3, $\cdots$, are constant, $\Gamma_2 d\alpha_2<0$; etc. At equilibrium

$$\Lambda/N=\mu/\bar{n}, \qquad \Gamma_2=0, \qquad \Gamma_3=0, \qquad \cdots. \quad (30)$$

These relations are equal in number to the number of parameters in $P(n)$ and are therefore just sufficient to determine the equilibrium values of $\bar{n}$, α_2, α_3, $\cdots$, since T, p, N_1, and $\bar{n}N$ are all preassigned and constant.

The quantity Λ/N is essentially a chemical potential per monomer associated with the process of adding monomers to a fixed number of polymer molecules (N constant), since $\Lambda=(\partial F/\partial\bar{n})_N$. On the other hand, $\mu/\bar{n}$ is a chemical potential per monomer associated with the process of adding monomers in the form of additional polymer molecules ($\bar{n}$ constant), since $\mu=(\partial F/\partial N)_{\bar{n}}$. At equilibrium, these two chemical potentials are equal, according to Eq. (30) (see Appendix II for an example).

It is helpful to keep in mind that the type of process we are considering in this subsection, a change in the distribution $P(n)$ in a closed system, is a very special case of a "chemical reaction" (i.e., a rearrangement of units into different aggregates of units) occurring in a closed system (see Appendix I). The thermodynamic treatment is basically that appropriate to a chemical reaction.

The change in any extensive property (e.g., H, S, V, etc.) attending an arbitrary change in $P(n)$ in a closed system at constant p and T follows from Eq. (8),

$$dG=[G_{\bar{n}}^*-(\bar{G}N/\bar{n}]d\bar{n}+\sum_{k\geq 2}G_k^* d\alpha_k. \quad (31)$$

Equation (28) is a special case ($G=F$). The quantity

$$(\partial G/\partial\bar{n})_{nN}=G_{\bar{n}}^*-(\bar{G}N/\bar{n})=(\partial G/\partial\bar{n})_N -(N/\bar{n})(\partial G/\partial N)_{\bar{n}} \quad (32)$$

$$=N\int\bar{G}(n)[(\partial P/\partial\bar{n})-(P/\bar{n})]dn, \quad (33)$$

might be termed the differential heat ($G=H$, $dH=$ heat absorbed since $p=$constant), entropy ($G=S$), etc., of *aggregation* or *polymerization*. The differential Gibbs free energy of polymerization is $\Lambda-(\mu N/\bar{n})$. If $\sigma=(\overline{n^2}-\bar{n}^2)^{\frac{1}{2}}$, the standard deviation of $P(n)$, is chosen as α_2 and we use the special symbol Δ for Γ_2, then

$$(\partial G/\partial\sigma)_{\bar{n},\bar{n}N}=G_\sigma^*=(\partial G/\partial\sigma)_{N,\bar{n}}=N\int\bar{G}(n)(\partial P/\partial\sigma)dn, \quad (34)$$

may be referred to as the differential heat ($G=H$), entropy ($G=S$), etc., of *dispersion*; the differential Gibbs free energy of dispersion is Δ.

Expansions in Powers of Molality

Consider a solution with a multicomponent solute, as in Eq. (3). The chemical potential of solute component i expressed as a series in powers of all the $m_k=N_k/N_1$, can be written[2]

$$\mu_i/kT=[\mu_i^0(T)/kT]+\ln\kappa_i(p,T)+\ln m_i+\sum_{j\geq 2}C_{ij}^{(2)}(p,T)m_j+\sum_{j,k\geq 2}C_{ijk}^{(3)}(p,T)m_j m_k+\cdots, \quad (35)$$

where the C's are analogous to virial coefficients [see Eq. (36) and Sec. III], the order of subscripts on the C's is immaterial (e.g., $C_{233}^{(3)}=C_{323}^{(3)}$), μ_i^0 is the chemical potential of gaseous component i at unit fugacity, and κ_i is

[1] This is true for aggregation and addition polymerization but not for condensation polymerization. In the latter case a solvent species is usually produced during the process. This complication, which proves to be minor, is ignored in the text but is illustrated in Appendix I.

[2] See paper I of this series, for example.

the Henry's law constant for component i. The corresponding (i.e., self-consistent) series for μ_1 is[2]

$$-\mu_1'/kT=\sum_{i\geq 2}m_i+\sum_{i,j\geq 2}C_{ij}^{(2)}(p,T)m_im_j+\sum_{i,j,k\geq 2}C_{ijk}^{(3)}m_im_jm_k+\cdots, \tag{36}$$

where

$$\mu_1'=\mu_1(p,T,m_2,m_3,\cdots)-\mu_1(p,T,0,0,\cdots).$$

In the special case of interest to us, we have

$$\mu(n)/kT=[\mu^\dagger(n,p,T)/kT]+\ln m+\ln P(n,\alpha)+2m\int C^{(2)}(n,n',p,T)P(n')dn'$$

$$+\tfrac{3}{2}m^2\int C^{(3)}(n,n',n'',p,T)P(n')P(n'')dn'dn''+\cdots \tag{37}$$

$$-\mu_1'/kT=m+m^2\int C^{(2)}(n,n')P(n)P(n')dndn'+m^3\int C^{(3)}(n,n',n'')P(n)P(n')P(n'')dndn'dn''+\cdots, \tag{38}$$

where

$$\mu_1'=\mu_1(p,T,m,\alpha)-\mu_1(p,T,0)$$

$$\mu^\dagger=\mu^0(n,T)+kT\ln\kappa(n,p,T).$$

Then, from Eq. (7),

$$\mu/kT=(1/kT)\int\mu^\dagger(n)P(n)dn+\ln m+\int P(n)\ln P(n)dn+2m\int C^{(2)}(n,n')PP'dndn'$$

$$+\tfrac{3}{2}m^2\int C^{(3)}(n,n',n'')PP'P''dndn'dn''+\cdots \tag{39}$$

$$F/N_1kT=[\mu_1(0)/kT]+(\mu_1'/kT)+(m\mu/kT)$$

$$=[\mu_1(0)/kT]+(m/kT)\int\mu^\dagger Pdn+m\ln m+m\int P\ln Pdn-m+m^2\int C^{(2)}PP'dndn'$$

$$+(m^3/2)\int C^{(3)}PP'P''dndn'dn''+\cdots, \tag{40}$$

where $P'=P(n')$, etc. The integral of $P\ln P$ in these equations is an "entropy of mixing" term.

It is easy[2] to write down similar formal expansions for $\bar{v}_1$, $\bar{v}$, V, $\bar{H}_1$, $\bar{H}$, H, $\bar{s}_1$, $\bar{s}$, S, etc., by introducing pressure and temperature derivatives of $\mu^\dagger$, $C^{(2)}$, $C^{(3)}$, etc., but we omit these.

If, in Eqs. (38), (39), and (40), we introduce "effective" quantities

$$C_{\rm eff}^{(2)}=\int C^{(2)}PP'dndn', \qquad C_{\rm eff}^{(3)}$$

$$=\int C^{(3)}PP'P''dndn'dn'' \tag{41}$$

$$\mu_{\rm eff}^\dagger=\mu_{\rm eff}^0+kT\ln\kappa_{\rm eff}$$

$$\mu_{\rm eff}^0=\int P(\mu^0+kT\ln P)dn, \qquad \ln\kappa_{\rm eff}=\int P\ln\kappa dn, \tag{42}$$

we obtain equations appropriate to a two-component solution.[2] However, this "effective" or "pseudo" two-component-solution point of view will be useful only in experiments in which $P(n)$ is held constant.

From either Eqs. (5) and (40) or (18) and (37) we find for Γ_i

$$\Gamma_i/NkT=(kT)^{-1}\int\mu^\dagger(\partial P/\partial\alpha_i)dn+(\partial/\partial\alpha_i)\int P\ln Pdn$$

$$+2m\int C^{(2)}P'(\partial P/\partial\alpha_i)dndn'$$

$$+\tfrac{3}{2}m^2\int C^{(3)}P'P''(\partial P/\partial\alpha_i)dndn'dn''+\cdots. \tag{43}$$

The second term on the right can also be written as

$$\int(\partial P/\partial\alpha_i)\ln Pdn.$$

An Example. Gaussian Distribution

In order to put a few of the above equations into more explicit form (but still within the framework of thermodynamics), we consider here a particular distribution, namely, the Gaussian distribution of Eq. (1). The two parameters on which $P(n)$ depends in this case are $\alpha_1=\bar{n}$ and $\alpha_2=\sigma$; also, $\Gamma_1=\Lambda$ and $\Gamma_2=\Delta$. The degree of polymerization is assumed large enough so that $P(n)$ may be considered a continuous function of n.

Because the Gaussian $P(n)$ is concentrated about $n=\bar{n}$, it is necessary to have information about thermodynamic functions such as $\mu^\dagger(n)$, $C^{(2)}(n, n')$, etc., only in the neighborhood of $n=\bar{n}$. Hence we employ Taylor expansions of these thermodynamic functions about $n=\bar{n}$. Thus we make use of the following:

$$\partial P/\partial\bar{n}=(n-\bar{n})P/\sigma^2,$$

$$\partial P/\partial\sigma=\{[(n-\bar{n})^2/\sigma^3]-(1/\sigma)\}P$$

$$\int P\ln P dn=-\tfrac{1}{2}(1+\ln 2\pi\sigma^2) \tag{44}$$

$$\mu^\dagger(n)=\mu^\dagger(\bar{n})+(\partial\mu^\dagger/\partial n)_{n=\bar{n}}(n-\bar{n})+\cdots$$

$$C^{(2)}(n, n')=C^{(2)}(\bar{n}, \bar{n})+(\partial C^{(2)}/\partial n)_{n=n'=\bar{n}}(n-\bar{n})+(\partial C^{(2)}/\partial n')_{n=n'=\bar{n}}(n'-\bar{n})+\cdots,$$

etc. It should be noted that Eq. (44) is not valid when σ is too small, for in this case we have to use $\Sigma_n P\ln P$ which goes to zero when $\sigma\to 0$ (a single polymer species). We now substitute the above relations in Eqs. (38), (39), and (43), carry out the integrations over n, and find

$$-\mu_1'/kT=m+m^2[C^{(2)}(\bar{n}, \bar{n})+C_{n^2}{}^{(2)}\sigma^2+\tfrac{1}{4}(C_{n^4}{}^{(2)}+C_{n^2n'^2}{}^{(2)})\sigma^4+\cdots]+\cdots \tag{45}$$

$$\mu/kT=(1/kT[\mu^\dagger(\bar{n})+\tfrac{1}{2}\mu_{n^2}{}^\dagger\sigma^2+\tfrac{1}{8}\mu_{n^4}{}^\dagger\sigma^4+\cdots]+\ln m-\tfrac{1}{2}(1+\ln 2\pi\sigma^2)+2m[\text{ as in (45)}]+\cdots \tag{46}$$

$$\Lambda/NkT=(1/kT)(\mu_n{}^\dagger+\tfrac{1}{2}\mu_{n^3}{}^\dagger\sigma^2+\tfrac{1}{8}\mu_{n^5}{}^\dagger\sigma^4+\cdots)+2m[C_n{}^{(2)}+\tfrac{1}{2}(C_{n^3}{}^{(2)}+C_{nn'^2}{}^{(2)})\sigma^2+\tfrac{1}{8}(C_{n^5}{}^{(2)}+2C_{n^3n'^2}{}^{(2)}+C_{nn'^4}{}^{(2)})\sigma^4+\cdots]+\cdots \tag{47}$$

$$\Delta/NkT=(1/kT)(\mu_{n^2}{}^\dagger\sigma+\tfrac{1}{2}\mu_{n^4}{}^\dagger\sigma^3+\cdots)-(1/\sigma)+2m[C_{n^2}{}^{(2)}\sigma+\tfrac{1}{2}(C_{n^4}{}^{(2)}+C_{n^2n'^2}{}^{(2)})\sigma^3+\cdots]+\cdots, \tag{48}$$

where

$$\mu_{n^a}{}^\dagger=(\partial^a\mu^\dagger/\partial n^a)_{n=\bar{n}}, \qquad C_{n^an'^b}{}^{(2)}=(\partial^{a+b}C^{(2)}/\partial n^a\partial n'^b)_{n=n'=\bar{n}}.$$

In using these series, the following properties of the derivatives are helpful

$$(\partial/\partial\bar{n})\mu_{n^a}{}^\dagger=\mu_{n^{a+1}}{}^\dagger, \quad C_{n^an'^b}{}^{(2)}=C_{n^bn'^a}{}^{(2)}$$

$$(\partial/\partial\bar{n})C_{n^an'^b}{}^{(2)}=C_{n^{a+1}n'^b}{}^{(2)}+C_{n^an'^{b+1}}{}^{(2)}.$$

In the limit $\sigma\to 0$ (a single polymer species with $n=\bar{n}$—but $\bar{n}$, the degree of polymerization, is variable), we have

$$-(\mu_1'/kT)=m+m^2C^{(2)}(\bar{n}, \bar{n})+m^3C^{(3)}(\bar{n}, \bar{n}, \bar{n})+\cdots \tag{49}$$

$$\mu/kT=(1/kT)\mu^\dagger(\bar{n})+\ln m+2mC^{(2)}(\bar{n}, \bar{n})+\tfrac{3}{2}m^2C^{(3)}(\bar{n}, \bar{n}, \bar{n})+\cdots \tag{50}$$

$$\frac{\Lambda}{NkT}=(kT)^{-1}\frac{\partial\mu^\dagger(\bar{n})}{\partial\bar{n}}+m\frac{\partial C^{(2)}(\bar{n}, \bar{n})}{\partial\bar{n}}+\tfrac{1}{2}m^2\frac{\partial C^{(3)}(\bar{n}, \bar{n}, \bar{n})}{\partial\bar{n}}+\cdots; \tag{51}$$

Δ is of course not defined in this case. Incidentally, the term $-\sigma^{-1}$ in Eq. (48) [which arises from $-\ln\sigma$ in Eq. (46)] becomes inadequate for very small σ, as we should expect. The first correction term can be shown to be of order σ^{-3}.

Also, for a Gaussian distribution, if we expand $\bar{G}(n)$ in Eq. (33) about $n=\bar{n}$ and integrate, we find

$$(1/N)(\partial G/\partial\bar{n})_{nN}=\left[\left(\frac{\partial\bar{G}(n)}{\partial n}\right)_{n=\bar{n}}-\frac{\bar{G}(\bar{n})}{\bar{n}}\right]+\tfrac{1}{2}\left[\left(\frac{\partial^3\bar{G}(n)}{\partial n^3}\right)_{n=\bar{n}}-(1/\bar{n})\left(\frac{\partial^2\bar{G}(n)}{\partial n^2}\right)_{n=\bar{n}}\right]\sigma^2+\cdots. \tag{52}$$

Only the leading term on the right remains when $\sigma\to 0$. An equivalent but alternative expression, when $\sigma=0$, follows from Eq. (32)

$$N^{-1}(\partial G/\partial\bar{n})_{\bar{n}N}=m^{-1}(\partial\bar{G}_1/\partial\bar{n})_{m,p,T}+(\partial\bar{G}/\partial\bar{n})_{m,p,T}-(\bar{G}/\bar{n}). \tag{53}$$

Actually, Eq. (53) is valid for any $P(n)$ which depends only on the parameter $\alpha_1=\bar{n}$.

III. OSMOTIC PRESSURE

Osmotic pressure (and light scattering) measurements are common with colloidal or polymeric solutions. In an osmotic system the solvent (component 1), which may be multicomponent without complication, can pass through a semipermeable membrane and hence is present in both "inside" and "outside" systems. The solute species cannot pass through the membrane and are present only in the "inside" system. The outside system is characterized by p, μ_1, T and the inside by $p+\Pi$, μ_1, T, μ_2, μ_3, $\cdots$, where Π = osmotic pressure.

An exact thermodynamic analogy can be drawn between the present system and that of Sec. II. Once we establish the analogy, the equations of Sec. II can be translated immediately into the required osmotic form. Hence we shall write down here only a few of the more fundamental equations, especially those setting up the notation; the reader can fill in the omitted equations as desired.

We start with Eq. (3) for the inside system, but replace p by $p+\Pi$. We define the function

$$\mathfrak{F}=F-\mu_1N_1-(p+\Pi)V=\sum_{i\geq 2}\mu_iN_i-(p+\Pi)V. \tag{54}$$

Then

$$d\mathfrak{F}=-SdT-N_1d\mu_1-(p+\Pi)dV+\sum_{i\geq 2}\mu_idN_i. \tag{55}$$

This equation is analogous, term by term, to Eq. (3). Thus $F\leftrightarrow\mathfrak{F}$, $V\leftrightarrow N_1$, $p\leftrightarrow-\mu_1$, $\mu_1\leftrightarrow-(p+\Pi)$, $\mu_1(0)\leftrightarrow-p$, $\mu_1'\leftrightarrow-\Pi$, $N_1\leftrightarrow V$. Corresponding to Eq. (4), we have

$$d\mathfrak{F}=-SdT-N_1d\mu_1+\Gamma_1d\alpha_1+\Gamma_2d\alpha_2+\cdots-(p+\Pi)dV+\mu dN \tag{56}$$

$$\mathfrak{F}=-(p+\Pi)V+\mu N. \tag{57}$$

Intensive properties of the system are functions of μ_1, T, $\rho=N/V$, and the α's. Instead of Eq. (8), we have

$$dG=(\partial G/\partial T)dT+(\partial G/\partial\mu_1)d\mu_1+\sum_{k\geq 1}G_k^{\ddagger}d\alpha_k+\bar{G}_vdV+\bar{G}'dN, \tag{58}$$

with

$$G=\bar{G}_vV+\bar{G}'N, \tag{59}$$

where

$$G_k^{\ddagger}=(\partial G/\partial\alpha_k)_{T,\mu_1,V,N,\alpha_j},\qquad \bar{G}_v=(\partial G/\partial V)_{T,\mu_1,N,\alpha},\qquad \bar{G}'=(\partial G/\partial N)_{T,\mu_1,V,\alpha}. \tag{60}$$

Equation (15) is replaced by

$$\bar{G}'=N^{-1}\sum_{i\geq 2}\bar{G}_i'N_i=\int\bar{G}'(n)P(n)dn, \tag{61}$$

where

$$\bar{G}_i'=(\partial G/\partial N_i)_{T,\mu_1,V,N_j}. \tag{62}$$

The Gibbs-Duhem relation following Eq. (15) becomes

$$0=Vd\bar{G}_v+\sum_{i\geq 2}N_id\bar{G}_i'\qquad(\mu_1,\ T\ \text{constant}). \tag{63}$$

In the special case $G=\mathfrak{F}$,

$$\mathfrak{F}_v=-(p+\Pi),\ \bar{\mathfrak{F}}'=\mu=\bar{F},\ \mathfrak{F}_k^{\ddagger}=\Gamma_k=F_k^{*},\ \bar{\mathfrak{F}}_i'=\mu_i=\bar{F}_i. \tag{64}$$

The first of these relations is the analog of $\bar{F}_1=\mu_1$. Equation (63) can be written as

$$d\Pi=\sum_{i\geq 2}(N_i/V)d\mu_i\qquad(\mu_1,\ T\ \text{constant}), \tag{65}$$

since p is constant when μ_1 and T are constant. This is a well-known relation in solution thermodynamics.

The analog of Eq. (28) is

$$d\mathfrak{F}=[\Lambda-(\mu N/\bar{n})]d\bar{n}+\Gamma_2d\alpha_2+\Gamma_3d\alpha_3+\cdots\qquad(T,\ \mu_1,\ V,\ \bar{n}N\ \text{constant}). \tag{66}$$

In place of Eqs. (35) and (36) we use[3]

$$\mu_i/kT=[\mu_i^{0}(T)/kT]+\ln\kappa_i(\mu_1,T)v_1(\mu_1,T)+\ln\rho_i+\tfrac{2}{1}\sum_{j\geq 2}B_{ij}^{(2)}(\mu_1,T)\rho_j+\tfrac{3}{2}\sum_{j,k\geq 2}B_{ijk}^{(3)}(\mu_1,T)\rho_j\rho_k+\cdots \tag{67}$$

$$\Pi/kT=\sum_{i\geq 2}\rho_i+\sum_{i,j\geq 2}B_{ij}^{(2)}(\mu_1,T)\rho_i\rho_j+\sum_{i,j,k\geq 2}B_{ijk}^{(3)}(\mu_1,T)\rho_i\rho_j\rho_k+\cdots, \tag{68}$$

[3] See paper II of this series, for example.

where $\rho_i = N_i/V$, v_1 is the volume per molecule of the pure solvent, and the B's are osmotic pressure virial coefficients. The Henry's law constant κ_i is the same as in Eq. (35), only the independent variables are different. The transcription of the remaining equations of Sec. II to the osmotic case is then obvious. A few examples are,

Eq. (38):

$$\Pi/kT = \rho + \rho^2 \int B^{(2)}(n, n') P(n) P(n') dn dn' + \cdots.$$

Eq. (40):

$$\mathfrak{F}/VkT = -(p/kT) + (\rho/kT)\int \mu^{\square} P dn + \rho \ln\rho + \rho \int P \ln P dn - \rho + \rho^2 \int B^{(2)} P P' dn dn' + \cdots \tag{69}$$

$$\mu^{\square} = \mu^{\dagger} + kT \ln v_1 = \mu^0(n, T) + kT \ln \kappa(n, \mu_1, T) v_1(\mu_1, T)$$

Eq. (48):

$$\Delta/NkT = (kT)^{-1}(\mu_n{}^{2\square}\sigma + \cdots) - \sigma^{-1} + 2\rho(B_n{}^{(2)}\sigma + \cdots) + \cdots. \tag{70}$$

An important special case of an osmotic system is a gas of colloidal particles with no solvent (e.g., liquid droplets or nuclei). Then the "outside" system is missing, $p=0$ and Π is the total pressure of the gas. Equation (67) becomes

$$\mu_i/kT = [\mu_i{}^0(T)/kT] + \ln\rho_i + \sum_{j\geq 2}^{s} B_{ij}{}^{(2)}(T)\rho_j + \cdots, \tag{71}$$

etc. If the gas is very dilute so that all virial coefficients can be dropped, we have, in the Gaussian distribution case [see Eqs. (45)–(48)],

$$\Pi = \rho kT \tag{72}$$

$$\mu/kT = (1/kT)[\mu^0(\bar{n}) + \tfrac{1}{2}\mu_n{}^{2\,0}\sigma^2 + \cdots] + \ln\rho - \tfrac{1}{2}(1 + \ln 2\pi\sigma^2) \tag{73}$$

$$\Lambda/NkT = (1/kT)(\mu_n{}^0 + \tfrac{1}{2}\mu_n{}^{2\,0}\sigma^2 + \cdots) \tag{74}$$

$$\Delta/NkT = (1/kT)(\mu_n{}^{2\,0}\sigma + \tfrac{1}{2}\mu_n{}^{4\,0}\sigma^3 + \cdots) - (1/\sigma). \tag{75}$$

APPENDIX I

The object of this Appendix is to introduce the "chemical reaction" point of view in the present problem. Let X_n be the chemical symbol for an $n$mer. Equation (37) can be written

$$\mu(n)/kT = [\mu^{\dagger}(n)/kT] + \ln a(n),$$

$$a(n) \to mP(n) \quad \text{as} \quad m \to 0,$$

where $a(n)$ is the activity of $n$mers. Thus $\mu^{\dagger}(n)$ is the "standard" [i.e., $a(n)=1$] chemical potential or free energy of $n$mers.

Consider the reaction

$$X_1 + X_n \to X_{n+1}; \qquad \Delta F_1{}^{\dagger} = \mu^{\dagger}(n+1) - \mu^{\dagger}(n) - \mu^{\dagger}(1). \tag{I}$$

If n is large,

$$\Delta F_1{}^{\dagger} = [\partial\mu^{\dagger}(n)/\partial n] - \mu^{\dagger}(1).$$

There is, of course, an arbitrary zero of free energy in $\mu^{\dagger}(1)$. On the other hand, $\Delta F_1{}^{\dagger}$ is a quantity with operational (i.e., experimental) significance which does not contain an arbitrary zero. Hence $\partial\mu^{\dagger}(n)/\partial n$ has the same arbitrary zero as $\mu^{\dagger}(1)$.

The above is a "differential" reaction. The corresponding "integral reaction" is

$$nX_1 \to X_n; \qquad \Delta F_2{}^{\dagger} = \mu^{\dagger}(n) - n\mu^{\dagger}(1). \tag{II}$$

Clearly

$$\Delta F_2{}^{\dagger}(n) = \sum_{n'=1}^{n} \Delta F_1{}^{\dagger}(n') \cong \int_1^n \Delta F_1{}^{\dagger}(n') dn'.$$

A third reaction of interest is

$$(n+1)X_n \to nX_{n+1};$$

$$\Delta F_3{}^{\dagger} = n\mu^{\dagger}(n+1) - (n+1)\mu^{\dagger}(n). \tag{III}$$

For large n,

$$\Delta F_3{}^{\dagger} = n\frac{\partial\mu^{\dagger}(n)}{\partial n} - \mu^{\dagger}(n) = n^2\frac{\partial\mu^{\dagger}/n}{\partial n}.$$

There is no arbitrary zero of free energy in $\partial(\mu^{\dagger}/n)/\partial n$. The three ΔF's are interrelated by

$$\Delta F_3{}^{\dagger} = n\Delta F_1{}^{\dagger} - \Delta F_2{}^{\dagger}.$$

We might note from Eqs. (46)–(48) and (52) that μ and $\Lambda = (\partial F/\partial\bar{n})_N$ contain an arbitrary zero of free energy but that Δ and $(\partial F/\partial\bar{n})_{\bar{n}N}$ do not. A change in $\bar{n}$ with $\bar{n}N$ constant, as in Eq. (28), is closely related to reaction (III) above.

Solvent in Reaction

As an example of the solvent being involved in the polymerization reaction, suppose that

$$X_1+X_n\rightarrow X_{n+1}+S,$$

where S=solvent (component 1). Thus, X_n is built up by forming $n-1$ bonds with the evolution of one molecule of S per bond formed. Let B be the total number of these bonds in the system,

$$B=N\int(n-1)P(n)dn=\bar{n}N-N.$$

In a closed system, $\bar{n}N$ is constant and $dN_1=dB=-dN=(N/\bar{n})d\bar{n}$. Hence, instead of passing from Eq. (27) to Eq. (28), we find

$$dF=[\Lambda-(\mu N/\bar{n})+(\mu_1 N/\bar{n})]d\bar{n}+\Gamma_2 d\alpha_2+\Gamma_3 d\alpha_3+\cdots.$$

The quantity in parentheses is of order $F/\bar{n}$ or $\mu N/\bar{n}$ or $\mu_1 N_1/\bar{n}$. Ordinarily the concentration of monomers is less than the concentration of solvent, though possibly of the same order of magnitude: $\bar{n}N=O(N_1)$ and $N=O(N_1/\bar{n})$. Thus, when $\bar{n}\gg 1$, as is usually the case, the last term in parentheses in the above equation is unimportant.

In a similar way, Eq. (32) is modified to read

$$(\partial G/\partial\bar{n})_{\bar{n}N}=G_{\bar{n}}{}^*-(\bar{G}N/\bar{n})+(\bar{G}_1 N/\bar{n}).$$

APPENDIX II

As an example, consider a gas of spherical liquid droplets with a Gaussian distribution in n. Equations (72)–(75) are then applicable. We assume that $\mu^0(n, T)$ has the form

$$\mu^0(n, T)/kT=a_1(T)n+a_2(T)n^{\frac{2}{3}},$$

where $a_2>0$. Thus, a_1 is the free energy per molecule (chemical potential) of bulk liquid and the other term is a surface tension term. We have omitted terms, varying slowly with n and negligible for large n, associated with the moment of inertia (rotation) and mass (translation). Then we find

$$\Lambda/NkT=a_1+\tfrac{2}{3}a_2\bar{n}^{-\frac{1}{3}}[1+\tfrac{2}{9}(\sigma^2/\bar{n}^2)+\cdots]$$

$$\Delta/NkT=-\tfrac{2}{9}a_2\bar{n}^{-\frac{1}{3}}[(\sigma/\bar{n})+\tfrac{1.4}{9}(\sigma^3/\bar{n}^3)+\cdots]-\sigma^{-1}$$

$$(\Lambda/NkT)-(\mu/\bar{n}kT)=-\tfrac{1}{3}a_2\bar{n}^{-\frac{1}{3}}[1-\tfrac{7}{9}(\sigma^2/\bar{n}^2)+\cdots]+\bar{n}^{-1}[\ln\bar{n}+\ln(V/\bar{n}N)]+(2\bar{n})^{-1}(1+\ln 2\pi\sigma^2);$$

Δ/NkT is always negative (all terms in the series are positive) so σ increases as equilibrium is approached spontaneously [see Eq. (29)]. Here $(\Lambda/N)-(\mu/\bar{n})$ is also negative for large $\bar{n}$ (only the first term remains); hence $\bar{n}$ increases spontaneously in a closed system. The conditions for equilibrium are found by setting the last two expressions, above, equal to zero and solving for $\bar{n}$ and σ with V, T, and $\bar{n}N$ preassigned and constant. The solution is $\sigma\rightarrow\infty$, $\bar{n}\rightarrow\infty$, in such a way that $\sigma/\bar{n}\rightarrow 0$.

THE JOURNAL OF CHEMICAL PHYSICS VOLUME 34, NUMBER 6 JUNE, 1961

Entropy of Mixing of Interconvertible Species. Some Reflections on the Gibbs Paradox

RICHARD M. NOYES

Department of Chemistry, University of Oregon, Eugene, Oregon

(Received November 21, 1960)

Expressions are derived for the change of state when two separated but interconvertible species are allowed to mix and come to chemical equilibrium. These expressions are unaffected by the possible existence of an exchange process involving simultaneous interconversion of two molecules. The results emphasize that entropy concepts are intimately connected with the distinguishability of chemical species and that the original concern of Gibbs arose because distinguishability is usually employed as a discontinuous concept. The discontinuity could be removed in specific cases by recognizing the finite limits to distinguishability imposed by existing analytical procedures.

INTRODUCTION

THE so-called "Gibbs Paradox"[1] is associated with the entropy of mixing of gases. Let two samples of ideal gas at the same temperature and pressure consist of n_1 moles of A_1 and of n_2 moles of A_2, respectively. If the gases are allowed to mix without change in temperature or total volume available to them, there are two possible values for the entropy change. Thus,

$$\Delta S = R[(n_1+n_2)\ln(n_1+n_2) - n_1\ln n_1 - n_2\ln n_2] \quad (1)$$

if the chemical species A_1 and A_2 are distinguishable in any way, but

$$\Delta S = 0 \quad (2)$$

if A_1 and A_2 are indistinguishable.

Gibbs was obviously concerned that Eq. (1) retained its full value during successive examples in which A_1 and A_2 became more and more similar, but that the entropy of mixing vanished apparently discontinuously when A_1 and A_2 became identical. Of course no real paradox exists, and these consequences follow automatically in a quantum statistics that recognizes the existence of indistinguishable particles as Schrödinger[2] has pointed out.

Klein[3] has recently considered the situation where A_1 and A_2 are nuclear isomers of monatomic species and where these isomers interconvert in a time long compared to the time of mixing. This example is a special case of the general situation in which A_1 and A_2 are interconvertible. Consideration of this general case provides some insight into the problems associated with the definition of entropy.

FORMULATION OF PROBLEM

Let A_1 and A_2 be distinguishable but interconvertible by the process

$$A_1 \rightarrow A_2. \quad (3)$$

Furthermore, let X be the mole fraction of A_1 in an equilibrium mixture at temperature T, and let ΔH° be the standard enthalpy change at this temperature. Examples can be quite general. Thus, A_1 and A_2 may be identical in energy and in statistical weights if they are optical isomers; they may differ in statistical weights but not significantly in energy if they are ortho and para hydrogen at moderate temperatures; or they may differ in both energy and entropy if they are chemical or nuclear isomers. The standard entropy change associated with process (3) is

$$\Delta S^\circ = \Delta H^\circ/T - R\ln[(X/(1-X)]. \quad (4)$$

Let the initial state of a hypothetical system consist of n_1 moles of A_1 and n_2 moles of A_2 in separate flasks each at 1 atm and at temperature T, and let the final state consist of an equilibrium mixture containing a total of n_1+n_2 moles at 1 atm and the same temperature. This change of state can be accomplished by two obvious paths, and the entropy changes calculated for each must, of course, be identical.

Let path I be to mix the two gases and then let them come to equilibrium. For the initial mixing process, $\Delta S(\text{mix})$ is given by Eq. (1). The subsequent equilibration process can be written

$$n_1A_1\left(P=\frac{n_1}{n_1+n_2}\right)+n_2A_2\left(P=\frac{n_2}{n_1+n_2}\right) \rightarrow (n_1+n_2)XA_1(P=X) + (n_1+n_2)(1-X)A_2(P=1-X), \quad (5)$$

where the parentheses indicate pressures in atmospheres. The entropy change can be calculated for the hypothetical path of converting both species to their standard states, causing $[n_1-(n_1+n_2)X]$ moles to react by process (3), and converting the products from their standard states to the final pressures. The entropy

[1] J. Willard Gibbs, *Collected Works* (Yale University Press, New Haven, Connecticut, 1948), Vol. I, p. 167.
[2] E. Schrödinger, *Statistical Thermodynamics* (Cambridge University Press, New York, 1952), pp. 58–62.
[3] M. J. Klein, Am. J. Phys. **26**, 80 (1958).

change for process (5) is then

$$\Delta S(\text{reaction}) = n_1 R \ln\frac{n_1}{n_1+n_2} + n_2 R \ln\frac{n_2}{n_1+n_2} + [n_1-(n_1+n_2)X]\Delta H^\circ/T - [n_1-(n_1+n_2)X]R \times \ln[X/1-X)](n_1+n_2)XR\ln X - (n_1+n_2)(1-X)R\ln(1-X). \quad (6)$$

Finally, the maintenance of constant temperature may require exchange of thermal energy with the surrounding thermostat. Then

$$\Delta S(\text{thermostat}) = [(n_1+n_2)X-n_1]\Delta H^\circ/T. \quad (7)$$

The total entropy change for path I is the sum of $\Delta S(\text{mix})+\Delta S(\text{reaction})+\Delta S(\text{thermostat})$. We obtain

$$\Delta S(\text{total}) = -n_1 R\ln X - n_2 R\ln(1-X). \quad (8)$$

In contrast, let path II be for both gas samples to react isothermally to form equilibrium mixtures which are then mixed. For the sample that is initially A_1, the reaction process is

$$n_1 A_1(P=1) \rightarrow n_1 X A_1(P=X) + n_1(1-X)A_2(P=1-X). \quad (9)$$

The entropy change of the gas during this process is

$$\Delta S(1) = n_1(1-X)\Delta H^\circ/T - n_1(1-X)R\ln[X/(1-X)] - n_1 XR\ln X - n_1(1-X)R\ln(1-X). \quad (10)$$

By similar reasoning, the entropy change for reaction of the gas that is initially A_2 is given by

$$\Delta S(2) = -n_2 X\Delta H^\circ/T + n_2 XR\ln[X/(1-X)] - n_2 XR\ln X - n_2(1-X)R\ln(1-X). \quad (11)$$

The thermal effects accompanying these reactions cause a total entropy change in the thermostat identically equal to the value in Eq. (7). Finally, when the two reacted gases are mixed, we obtain $\Delta S(\text{mix}')=0$. The total entropy change for path II is the sum of $\Delta S(1)+\Delta S(2)+\Delta S(\text{thermostat})+\Delta S(\text{mix}')$ and gives

$$\Delta S(\text{total}) = -n_1 R\ln X - n_2 R\ln(1-X) \quad (12)$$

identical with Eq. (8). The identical final results are obtained even though one path used Eq. (1) for the entropy of mixing and the other path used Eq. (2).

DISCUSSION

The above treatment neglects the conceivable process

$$A_1{}^* + A_2 \rightarrow A_2{}^* + A_1, \quad (13)$$

where the asterisks serve to designate the individual molecules. If the molecules initially present in the A_1 and A_2 flasks can be distinguished by some technique such as isotopic labeling, it is possible to follow the rate of process (13). This rate is apt to be very fast if A_1 and A_2 are different electronic states of the same atom or molecule; it is probably very slow if they are *cis* and *trans* isomers of an olefinic compound.

If it were indeed possible to distinguish in some way which container or molecular state a particular molecule had been in at the start of an experiment, additional terms would be needed to calculate ΔS for the change of state considered above. If the molecules are only distinguishable by whether their state is A_1 or A_2 at the time of the observation, it is meaningless to attempt to describe process (13) in terms of quantum mechanics. We may have a personal prejudice that this process is still taking place at very nearly the same rate as it did when the species were isotopically distinguishable, but we cannot devise any experiment to confirm or deny this prejudice. The equations of the previous section are valid independent of any philosophical questions about the existence of process (13).

The absence of any effect due to the occurrence or nonoccurrence of process (13) serves to emphasize that entropy changes are affected not by processes we can imagine to occur but by processes we can imagine ourselves being able to detect. Problems in entropy of mixing are intimately tied up with the distinguishability of molecular species. Gibbs was unaware of the existence of isotopes. After they had been discovered but before they could be separated, their existence did not affect the entropy change computed for any process that seemed possible of attainment. Once they could be separated, they needed very much to be considered.

Entropy resembles potential energy and other thermodynamic properties in that the absolute scale must be arbitrarily defined. The zero adopted is by convention a perfect crystal of indistinguishable species at 0°K. If any supposedly pure chemical is found to contain distinguishable subspecies, its entropy will *ipso facto* be increased by this discovery.

Gibbs was disturbed by the apparent discontinuity in the entropy of mixing as the gases that were mixed became more and more similar. However, distinguishability as used here is a discontinuous concept that does or does not apply to two molecules, and the discontinuity in mathematical equations is entirely to be expected. The discontinuity disappears when real analytical procedures are considered. If it were postulated that the mole fraction of A_1 in a mixture could be measured with an uncertainty of $\pm\varepsilon$, it should be possible to develop a thermodynamics such that the calculated entropy of mixing would vary continuously from Eq. (1) for $\varepsilon=0$ to Eq. (2) for $\varepsilon=1$. This argument to eliminate the discontinuity in the concept of distinguishability was conceived before it was realized that Landé[4] had developed many of the concepts of quantum mechanics from a similar consideration of the lack of a discontinuity in the separability of species. Shannon[5] has associated entropy with communication theory by somewhat similar concepts.

[4] A. Landé, Am. Scientist **41**, 439 (1953).
[5] C. E. Shannon, Bell System Tech. J. **27**, 379, 623 (1948).

Gibbs developed his ideas in the nineteenth century when properties of systems were regarded as independent of the methods used to study them. During the twentieth century, the development of special relativity involved recognition of a finite maximum available signal velocity, the development of quantum mechanics involved recognition of a finite minimum time needed for an interaction leading to transfer of a significant amount of energy, and the development of Fermi-Dirac statistics involved recognition of the existence of indistinguishable elementary particles. It has become apparent that even a completely hypothetical system cannot be discussed clearly and unambiguously unless care is taken to define the properties of the observer as well as those of the system.

ACKNOWLEDGMENT

The development of these ideas was supported in part by the U.S. Atomic Energy Commission under contract. Professor J. A. Schellman and Professor D. F. Swinehart suggested helpful references and made useful comments during discussions of this manuscript.

Crystal Field Parameters for Erbium in Er $(C_2H_5SO_4)_3 \cdot 9H_2O$

EDWARD H. ERATH*

Physics Department, University of California, Los Angeles, California

(Received September 26, 1960)

Intermediate coupling wave functions and eigenvalues for f^{11} were used to compute the effective operator equivalent factors for the free-ion levels of erbium. The Stark splitting of the ground level $^4I_{15/2}$ was used in a first-order perturbation calculation on the ground state to determine the crystal field parameters. The parameters that fit the experimental data best are; $\langle r^2\rangle A_2 = 125.80$, $\langle r^4\rangle A_4 = -31.06$, $\langle r^6\rangle A_6 = -81.19$, $\langle r^6\rangle A_6^6 = 387.19$. The parameters were used to calculate the Stark splitting of the free-ion levels and the results compared with experimentally observed values for ten levels. For the 46 Stark levels involved the calculation predicts the splitting with an average deviation of 3.4 cm^{-1}.

INTRODUCTION

WYBOURNE[1] has diagonalized the complete intermediate coupling approximation matrices for the f^3 and f^{11} configurations. Wong[2] completed this calculation separately and obtained the following electrostatic and spin-orbit interaction parameters for erbium; $F_2 = 433.64$ cm^{-1}, $F_4 = 67.522$ cm^{-1}, $F_6 = 7.0900$ cm^{-1}, $\zeta_{4f} = 2471.0$ cm^{-1}, and term energies in good agreement with Wybourne. Both calculations predict that the term $^4I_{13/2}$, which is the first excited state of erbium, is approximately 6800 cm^{-1} above the ground term $^4I_{15/2}$. Since these terms are separated by such a large energy it is reasonable to assume that the influence of the crystal field on the ground term could be determined to within a few percent by a first-order perturbation calculation, and that the calculation would yield a good set of crystal field parameters.

In this work intermediate coupling wave functions were used to determine the effective operator equivalent factors for the free-ion terms of erbium. These factors were used, along with experimentally determined crystal field parameters for Er^{+3} in a field of D_{3h} symmetry, to compute by a first-order perturbation calculation the Stark splitting of the free-ion terms. The crystal field parameters were determined using the experimentally observed splitting of the ground term in the matrices of the perturbation calculation on this term. Because the excited states of erbium are in most cases separated by fairly large energy intervals, a first-order perturbation calculation should yield splittings that agree fairly well with experimentally observed values, provided one has at his disposal a good set of parameters.

Here the splittings of ten free-ion levels determined by a first-order perturbation calculation are compared with experimental values. The average deviation for the 46 Stark levels involved is 3.4 cm^{-1}.

EXPERIMENTAL DETAILS

Rare-earth ethylsulphate salt solutions were prepared by reacting the rare-earth sulphate with barium ethylsulphate. The necessity of using large quantities of water to dissolve the fairly insoluble rare-earth sulphate was avoided by first mixing the two salts dry and then adding to the mixture only that amount of water necessary to completely dissolve the product of the reaction. The barium ethylsulphate dissolves readily and reacts with whatever rare-earth sulphate has gone into solution. Highly insoluble barium sulphate precipitates and allows the dissolution of more rare-earth sulphate. In this manner the reaction goes to completion and very little water is required. Agitation of the solution speeds the reaction and an almost

* Hughes Staff Doctoral Fellow.

[1] B. G. Wybourne, J. Chem. Phys. **32**, 639 (1960).

[2] Eugene Y. Wong, J. Chem. Phys. (to be published).

TABLE I. Operator equivalent factors for Er^{+3}.

Term	Energy cm^{-1} Calc	Operator equivalent factors α	β	γ
$^4I_{15/2}$	0	$+2.6947\times10^{-3}$	$+4.5187\times10^{-5}$	$+1.9993\times10^{-6}$
$^4I_{13/2}$	6776	$+3.1414\times10^{-3}$	$+5.6546\times10^{-5}$	$+1.7793\times10^{-6}$
$^4I_{11/2}$	10 415	$+3.0065\times10^{-3}$	$+4.7676\times10^{-5}$	$+1.7388\times10^{-6}$
$^4F_{9/2}$	12 497	-0.0335×10^{-3}	$+1.7901\times10^{-4}$	$+3.7779\times10^{-5}$
$^4I_{9/2}$	15 447	-5.5440×10^{-3}	$+1.9305\times10^{-4}$	-8.8316×10^{-6}
$^4S_{3/2}$	18 522	-4.1486×10^{-2}		
$^2H_{11/2}$	19 406	$+6.6214\times10^{-3}$	-7.1658×10^{-5}	$+3.7354\times10^{-6}$
$^4F_{7/2}$	20 717	-1.2232×10^{-2}	-1.9906×10^{-4}	$+8.6970\times10^{-5}$
$^4F_{5/2}$	22 320	-7.1188×10^{-3}	-5.5951×10^{-4}	
$^4F_{3/2}$	22 701	-5.2393×10^{-2}		
$^2G_{9/2}$	24 892	-2.0067×10^{-3}	$+1.6796\times10^{-4}$	$+3.1415\times10^{-5}$
$^4G_{11/2}$	26 889	-7.7444×10^{-4}	-1.3714×10^{-4}	$+2.8561\times10^{-6}$
$^2K_{15/2}$	27 406	$+7.3342\times10^{-3}$	$+7.4081\times10^{-5}$	-4.0018×10^{-7}
$^4G_{9/2}$	27 938	$+5.1951\times10^{-4}$	-8.2378×10^{-5}	-2.8031×10^{-6}
$^4G_{7/2}$	28 354	-1.8842×10^{-3}	$+1.5604\times10^{-4}$	$+2.3716\times10^{-5}$
$^2D_{3/2}$	32 057	-6.4868×10^{-2}		
$^2K_{13/2}$	32 854	$+8.7419\times10^{-3}$	$+1.1104\times10^{-4}$	$+6.7514\times10^{-7}$
$^2P_{1/2}$	33 623	0		
$^4G_{5/2}$	33 969	-3.5547×10^{-3}	-3.9926×10^{-3}	
$^2G_{7/2}$	34 650	-1.1080×10^{-2}	-3.8057×10^{-4}	-5.8047×10^{-6}

saturated solution of rare-earth ethylsulphate can be obtained in several hours. Solutions were saturated by evaporation in a vacuum.

Crystals were grown by slow evaporation at constant temperature and by slow temperature decline from about 40°C. Both techniques produced good clear crystals up to 2 cm thick suitable for spectroscopic work.

The spectrum was recorded from 2 μ to 2200 A at both liquid-nitrogen and liquid-helium temperatures in both polarizations. The visible and photographic infrared regions were photographed using a 21-ft radius grating spectrograph and the remainder of the spectrum recorded on a Cary ultraviolet spectrophotometer, for which a liquid-helium Dewar[3] was designed and constructed.

CRYSTAL FIELD INTERACTION

The reduced matrix elements calculated by Judd[4] and Racah coefficients[5] were used to compute the operator equivalent factors between states within a manifold of constant J according to the method described by Elliott, Judd, and Runciman.[6] These factors and the intermediate coupling wave functions were used to compute the effective operator equivalent factors for the terms of erbium. The effective operator equivalent factors are listed in Table I.

A first-order perturbation calculation was carried out on the ground multiplet $^4I_{15/2}$ of erbium using the crystal field parameters for Tm^{+3} in $Tm(C_2H_5SO_4)_3\cdot 9H_2O$ as determined by Wong and Richman,[7] and the reduced matrix elements of the crystal field potential as calculated by Stevens,[8] and Elliott and Stevens.[9] The Stark splitting of the ground term calculated in this manner agreed well with experimental measurements. In fact three of the experimental energy values agreed to within three percent of the calculated values. Crystal quantum numbers were assigned to the Stark levels of the ground term on the basis of this calculation and the polarization selection rules used to verify the assignment by study of the transitions to the states $^4S_{3/2}$, $^4F_{5/2}$, and $^4I_{9/2}$. In each case the rules were strictly obeyed. Finally the observed splittings were used to calculate the crystal field parameters from the matrices of the crystal field perturbation on the term $^4I_{15/2}$. Because the uppermost Stark level of the ground term had not been observed

[3] Description to be published.
[4] B. R. Judd, Proc. Roy. Soc. (London) **A227,** 552 (1955).
[5] A. Simon, J. H. Vander Sluis, and L. C. Biedenharn, Oak Ridge National Lab. Rept. No. 1679 (1954).
[6] J. P. Elliot, B. R. Judd, and W. A. Runciman, Proc. Roy. Soc. (London) **A240,** 509 (1959).
[7] E. Y. Wong and I. Richman, J. Chem. Phys. **34,** 1182 (1961).
[8] K. W. H. Stevens, Proc. Phys. Soc. (London) **A65,** 209 (1952).
[9] R. J. Elliot and K. W. Stevens, Proc. Roy. Soc. (London) **A219,** 387 (1953).

TABLE II. Calculated and observed Stark levels for the states of erbium.

Term	Term energy cm^{-1} Calc	Term energy cm^{-1} Exptl	μ	Stark energy cm^{-1} Calc	Stark energy cm^{-1} Exptl	ΔE	ν^a	ν^b
$^4I_{15/2}$	0	0	±5/2′	−147.3	−147.3	0.0	0.0	0.0
			±3/2″	−104.5	−103.3	−1.2	44.0	43.8
			±3/2′	−72.2	−72.6	0.4	74.7	74.6
			±1/2″	−36.7	−37.1	−0.4	110.2	110.7
			±5/2	26.4	25.2	1.1	172.6	173.0
			±3/2	62.5	68.5	−6.0	215.8	
			±1/2′	113.5	107.9	5.5	255.2	
			±1/2	158.3	156.7	1.6	304.0	
$^4I_{13/2}$	6775.6		±5/2′	−51.3				
			±3/2′	−40.6				
			±1/2″	−37.4				
			±1/2′	−17.0				
			±5/2	17.7				
			±3/2	52.0				
			±1/2	79.7				
$^4I_{11/2}$	10 414.8		±3/2′	−19.8				
			±1/2′	−19.4				
			±5/2′	−15.7				
			±1/2	2.3				
			±5/2	16.3				
			±3/2	36.2				
$^4F_{9/2}$	12 496.6	12 366.5	±3/2′	−87.7	−87.6	−0.1	12 426.2	
			±5/2′	−71.6	−73.9	2.3	12 439.9	
			±3/2	8.8	11.2	−2.4	12 525.0	
			±1/2	25.5	26.4	−0.9	12 540.2	
			±5/2	125.1	123.9	1.2	12 637.7	
$^4I_{9/2}$	15 447.4	15 207.2	±3/2′	−46.7	−48.5	1.8	15 306.0	15 307.24
			±1/2	−18.0	−15.1	−2.9	15 339.4	15 339.83
			±5/2′	−1.7	−6.0	4.3	15 348.5	15 346.91
			±3/2	18.9	22.7	−3.8	15 377.2	15 377.70
			±5/2	47.5	47.1	0.4	15 401.6	15 402.11
$^4S_{3/2}$	18 522.0	18 326.8	±3/2	−15.7	−13.0	−2.7	18 461.1	18 460.72
			±1/2	15.7	13.0	2.7	18 487.1	18 488.34
$^2H_{11/2}$	19 406.5	19 087.1	±5/2′	−64.6	−65.1	0.5	19 169.3	19 169.01
			±3/2′	−26.4	−17.3	−9.1	19 217.1	19 218.56
			±5/2	−12.4	−7.7	−4.7	19 226.7	19 199.41
			±1/2′	5.6	11.3	−5.7	19 245.7	19 245.75
			±3/2	36.3	24.0	12.3	19 258.4	19 258.23
			±1/2	61.5	54.9	6.6	19 289.3	19 288.90
$^4F_{7/2}$	20 716.6	20 457.3	±5/2′	−49.7	−48.2	−1.5	20 556.4	20 555.61
			±3/2	−19.7	−16.5	−3.2	20 588.1	20 586.91
			±5/2	20.6	18.4	2.2	20 623.0	20 596.41
			±1/2	48.8	46.5	2.3	20 651.1	20 650.32
$^4F_{5/2}$	22 319.6	22 121.6	±3/2	−6.4	−13.1	6.7	22 255.8	22 256.04
			±5/2	−6.2	1.8	−8.0	22 270.7	22 268.71
			±1/2	12.6	11.2	1.4	22 280.1	22 280.35
$^4F_{3/2}$	22 701.3	22 460.9	±3/2	−19.8	−23.4	3.4	22 584.8	22 586.06
			±1/2	19.8	23.4	−3.4	22 631.6	22 635.77

TABLE II.—*Continued.*

Term	Term energy cm^{-1} Calc	Exptl	μ	Stark energy cm^{-1} Calc	Exptl	ΔE	ν^a	ν^b
$^2G_{9/2}$	24 891.7	24 515.4	±3/2′	−77.4	−80.8	3.4	24 581.9	24 581.82
			±5/2′	−56.5	−58.6	2.1	24 604.1	24 573.05
			±3/2	4.5	1.6	2.9	24 661.1	24 658.51
			±1/2	24.8	24.4	0.4	24 687.1	24 688.93
			±5/2	104.6	116.6	−12.0	24 779.3	
$^4G_{11/2}$	26 888.7	26 348.1	±5/2′	−63.6	−59.1	−4.5	26 436.5	
			±3/2′	−23.6	−23.2	−0.4	26 472.4	
			±5/2	−20.5	−13.9	−6.6	26 481.7	
			±3/2	22.0	16.5	5.5	26 512.1	
			±1/2′	28.5	22.3	6.2	26 517.9	
			±1/2	57.1	57.5	−0.4	26 553.1	
$^2K_{15/2}$	27 406.0		±1/2″	−140.2				
			±3/2″	−104.9				
			±5/2′	−46.2				
			±3/2′	9.7				
			±5/2	30.7				
			±1/2′	71.1				
			±3/2	81.2				
			±1/2	98.6				
$^4G_{9/2}$	27 937.8		±5/2′	−18.7				
			±5/2	−3.3				
			±3/2′	2.1				
			±1/2	5.0				
			±3/2	14.9				
$^4G_{7/2}$	28 354.2		±5/2′	−14.0				
			±3/2	−3.9				
			±1/2	1.4				
			±5/2	16.6				
$^2D_{3/2}$	32 057.4		±3/2	−24.5				
			±1/2	24.5				
$^2K_{13/2}$	32 853.8		±1/2″	−102.6				
			±3/2′	−79.8				
			±5/2′	−35.6				
			±1/2′	2.1				
			±5/2	28.8				
			±3/2	85.8				
			±1/2	102.6				
$^2P_{1/2}$	33 623.0		±1/2	0				
$^4G_{5/2}$	33 969.5		±3/2	−57.5				
			±5/2	15.0				
			±1/2	42.5				
$^2G_{7/2}$	34 650.4		±5/2′	−29.8				
			±5/2	−15.7				
			±3/2	9.0				
			±1/2	36.5				

[a] Observed energy of Stark levels above the lowest Stark level of the ground state. Values are averages obtained using all of the transitions observed terminating on a given level at 77°K.

[b] Values reported by Hellwege, Hüfner, and Kahle.

only five cubic and two quadratic equations were solved simultaneously to determine the parameters with the following results:

$$\langle r^2\rangle A_2 = 125.80 \qquad \langle r^4\rangle A_4 = -31.06$$

$$\langle r^6\rangle A_6 = -81.19 \qquad \langle r^6\rangle A_6^6 = 387.19.$$

These parameters were then used to compute the splitting of excited states by the crystal field. Table II shows the results of this calculation compared with the experimental results and those of Hellwege, Hüfner, and Kahle.[10]

DISCUSSION

Generally the experimental results agree with those of Hellwege *et al.* There is excellent agreement for lines that remain at liquid helium temperature. Since some levels cannot be observed at 4.2°K we chose to determine the energy level diagram primarily from data recorded at 77°K for the sake of consistence. The position of each level reported in Table II is an average obtained using data from all of the transitions observed terminating on the level at 77°K. Helium temperature data were used only to verify quantum number assignments.

Hellwege has reported crystal quantum number assignments for 31 Stark levels. Our quantum number assignments agree for all of these and we have observed fifteen others. All of the data reported are compared with the calculated Stark splittings in Table II. We differ with Hellwege's experimental energy values for three levels; $\mu=\pm\frac{5}{2}$, $\mu=\pm\frac{5}{2}$, and $\mu=\pm\frac{5}{2}'$ in the groups $^2H_{11/2}$, $^4F_{7/2}$, and $^2G_{9/2}$, respectively. Our energy value for each deviates from the calculated value by a small amount when our experimental data are used to determine the centers of gravity of the groups, while Hellwege's values have large deviations (+22.6, +28.8, and +31.1 cm^{-1}, respectively). If his data are used to compute the centers of gravity the deviation for his energy values for the levels in question improve slightly, but the average deviation degenerates for each group. In the group $^2H_{11/2}$ for example, the deviation for $\mu=\pm\frac{5}{2}$ changes to +18.1 cm^{-1}, but the average deviation for the group increases to 11.7 cm^{-1}. Deviations of 20 or 30 wave numbers seem uncommonly large compared with the excellent agreement obtained between observed and calculated splittings for the other 43 Stark levels. Our energy values for the three levels appear to be more likely, but it should be reported that the levels could not be located without the aid of the calculated splittings. In all three cases only weak transitions were observed to the levels.

ACKNOWLEDGMENTS

The author wishes to express his gratitude to Dr. Eugene Wong who diagonalized the intermediate coupling matrices using the IBM 709 computer and to Dr. Paul Fletcher of the Hughes Research Laboratories for helpful discussion.

[10] K. H. Hellwege, S. Hüfner, and H. G. Kahle, Z. Physik **160**, 149 (1960).

THE JOURNAL OF CHEMICAL PHYSICS VOLUME 34, NUMBER 6 JUNE, 1961

Analysis of the Absorption and Fluorescence Spectrum of $NdCl_3$ Diluted with $LaCl_3$ †

EUGENE Y. WONG

Department of Physics, University of California, Los Angeles, California

(Received October 3, 1960)

The Stark splitting of the identified levels of Nd^{+3} in $LaCl_3$ were calculated by first-order perturbation. Intermediate coupling wave functions and crystal-field interaction parameters reported by Judd were used. The calculated spectrum agrees with the spectrum observed by Carlson to 5 cm^{-1}.

INTRODUCTION

A RATHER complete work on the absorption and fluorescence spectrum of $NdCl_3$ diluted with $LaCl_3$ was reported by Carlson.[1] In that report Russell-Saunders wave functions were used to calculate the Stark splitting. This is adequate for the ground ^4I term because it is separated quite far from the other terms. However, for the excited levels, the Russell-Saunders approximation is not adequate because the different levels are much closer to each other. Wybourne[2] reported a rather successful intermediate coupling calculation for the Nd^{+3} ion. It seems that this wave function whould be used in order to get a better result.

Judd[3] has reported a very successful analysis of the Stark splitting of the fluorescence spectrum of $NdCl_3$ diluted with $LaCl_3$. In this paper his work is extended to the excited levels by using first-order perturbation and intermediate coupling wave functions.

† This work is supported by the Office of Ordnance Research, U. S. Army.

[1] E. H. Carlson, "Absorption and fluorescence spectra of $NdCl_3$ and states of the neodymium ion" (Johns Hopkins Spectroscopic Report No. 18, March, 1960).

[2] B. G. Wybourne, J. Chem. Phys. **32**, 639 (1960).

[3] B. R. Judd, Proc. Roy. Soc. (London) **A251**, 134 (1959).

TABLE I. Effective operator equivalent factors and effective g for Nd^{+3}. (Energy in cm^{-1}).

Level	E_{cal}	E_{exp}	α	β	γ	g
$^4I_{9/2}$	0.00	0.00	-6.127×10^{-3}	-2.710×10^{-4}	-3.630×10^{-5}	0.733
$^4I_{11/2}$	1928.28	1881.53	-4.052×10^{-3}	-9.536×10^{-5}	-2.904×10^{-6}	0.966
$^4I_{13/2}$	3974.75	3864.31	-3.109×10^{-3}	-5.652×10^{-5}	-1.796×10^{-6}	1.107
$^4I_{15/2}$	6099.07		-2.610×10^{-3}	-4.459×10^{-5}	-2.039×10^{-6}	1.198
$^4F_{3/2}$	11 523.34	11 292.44	5.054×10^{-2}			0.431
$^4F_{5/2}$	12 606.77	12 329.03	1.413×10^{-2}	1.376×10^{-3}		1.031
$^2H_{9/2}$	12 612.05	12 459.15	5.775×10^{-3}	2.650×10^{-5}	2.288×10^{-5}	0.999
$^4S_{3/2}$	13 453.73	13 382.81	5.074×10^{-3}			1.953
$^4F_{7/2}$	13 611.08	13 293.20	1.217×10^{-2}	1.800×10^{-4}	-8.839×10^{-5}	1.213
$^4F_{9/2}$	14 902.45	14 576.10	6.810×10^{-3}	-2.109×10^{-4}	-1.140×10^{-6}	1.238
$^2H_{11/2}$	15 986.02	15 286.74	1.172×10^{-3}	-1.304×10^{-5}	-1.894×10^{-6}	1.099
$^2G_{7/2}$	17 353.65	17 000.56[a]	3.670×10^{-3}	-2.477×10^{-5}	-3.471×10^{-5}	0.942
$^4G_{5/2}$	17 357.56	17 000.56[a]	3.588×10^{-3}	4.142×10^{-3}		0.576
$^2K_{13/2}$	18 977.79	18 614.97	-9.617×10^{-3}	-9.812×10^{-5}	5.681×10^{-7}	0.937
$^4G_{7/2}$	19 228.93	18 885.24	9.382×10^{-3}	4.318×10^{-4}	8.029×10^{-5}	0.960
$^4G_{9/2}$	19 718.72	19 293.88	-1.116×10^{-3}	4.427×10^{-5}	-5.863×10^{-6}	1.146
$^2K_{15/2}$	21 027.21		-7.606×10^{-3}	-4.692×10^{-5}	-1.879×10^{-6}	1.063
$^2D_{3/2}$	21 248.27	21 028.25	2.441×10^{-2}			1.072
$^2G_{9/2}$	21 254.58	20 889.24[a]	7.826×10^{-3}	1.746×10^{-4}	2.653×10^{-7}	1.134
$^4G_{11/2}$	21 825.83	21 289.36	4.169×10^{-4}	2.234×10^{-4}	-4.815×10^{-6}	1.259
$^2P_{1/2}$	23 147.36	23 068.46				0.621
$^2D_{5/2}$	23 878.23	23 640.97	3.706×10^{-2}	7.93×10^{-4}		1.196
$^2P_{3/2}$	26 349.94	25 972.22	6.963×10^{-2}			1.074
$^4D_{3/2}$	28 640.13	27 827.81	-1.823×10^{-2}			1.132

[a] Calculated from the average of the observed lines.

METHOD OF CALCULATION

An intermediate coupling calculation for Nd^{+3} was carried out by using the spin-orbit interaction matrix elements reported by Judd and Loudon[4] and the parameters reported by Wybourne.[2] The matrix elements of the electrostatic interaction were calculated according to the method outlined by Elliott, Judd, and Runciman.[5] The results agree with those reported by Wybourne to within a few wave numbers which is within the accuracy of the parameters used. The calculated eigenvalues do not fit the observed spectrum of $NdCl_3$ diluted with $LaCl_3$ very well as indicated in Table I. The calculated values are almost always about 150 cm^{-1} higher than the observed results, suggesting that the ground state of $^4I_{9/2}$ was used as the zero-energy point instead of the center of the $^4I_{9/2}$ level. These intermediate coupling wave functions were still used because the errors they produced were expected to be less than those introduced by other means such as the first-order perturbation approximation and mixing of other configurations. These so-called errors introduced by other means are expected to amount to about 5 cm^{-1} which is the average deviation obtained by Judd[6] in an analysis of $PrCl_3$ spectrum.

The crystal field acting on the f electrons is written as follows,

$$V=A_2^0(3z^2-r^2)+A_4^0(35z^4-30r^2z^2+3r^4)+A_6^0(231z^6-315r^4z^2+105r^2z^4-5r^6)+A_6^6(x^6-15x^4y^2+15x^2y^4-y^6).$$

All the other terms that will give zero matrix elements are neglected. The parameters used here are those reported by Judd.[3] They are as follows,

$$A_2^0\langle r^2\rangle=103.7\ cm^{-1},\quad A_4^0\langle r^4\rangle=-36.0\ cm^{-1},$$
$$A_6^0\langle r^6\rangle=-44.5\ cm^{-1},\quad A_6^6\langle r^6\rangle=426.2\ cm^{-1}.$$

[4] B. R. Judd and R. Loudon, Proc. Roy. Soc. (London) **A251,** 127 (1959).

[5] J. P. Elliott, B. R. Judd, and W. A. Runciman, Proc. Roy. Soc. (London) **A240,** 509 (1957).

[6] B. R. Judd, Proc. Roy. Soc. (London) **A241,** 414 (1957).

TABLE II. Calculated Stark splitting, $g_\parallel$ and $g_\perp$ vs experimental results. (Energy in cm^{-1}, within a level a constant energy is subtracted from E to give E'.)

		Experimental values				Calculated values			
Level	$\lvert\mu\rvert$	E	E'	$g_\parallel$	$g_\perp$	E	$g_\parallel$	$g_\perp$	E
	5/2	0.00	−148.79	4.01	1.76	−143.52	4.11	1.88	−5.27
	1/2	115.39	−33.40			−35.14	0.73	3.67	1.74
$^4I_{9/2}$	3/2	123.21	−25.58			−16.56	4.24	0.00	−9.02
	3/2	244.40	95.61			95.61	0.38	0.00	0.00
	5/2	249.35	100.56			99.61	2.64	1.88	0.95
	3/2	1973.85	−55.72			−55.72	8.14	0.00	0.00
	1/2	2012.58	−16.99			−14.69	4.23	4.14	2.30
	5/2	2026.90	−2.67			−5.99	6.42	2.10	3.32
$^4I_{11/2}$	1/2	2044.19	14.62			13.93	3.24	3.69	0.69
	3/2	2051.60	22.03			24.84	2.35	0.00	−2.81
	5/2	2058.90	29.33			37.63	2.30	4.14	−8.30
	1/2	3931.84	−78.43			−84.35	11.14	0.83	5.92
	3/2	3974.88	−35.39			−39.34	6.82	0.00	3.95
	1/2	3998.89	−11.38			−5.04	2.83	4.77	−6.34
$^4I_{13/2}$	5/2	4012.92	2.65			−0.91	1.85	4.92	3.56
	1/2	4031.86	21.59			22.53	11.63	2.15	−0.91
	3/2	4042.08	31.81			34.37	0.18	0.00	−2.56
	5/2	4083.00	72.73			72.73	0.37	4.92	0.00
$^4F_{3/2}$	1/2	11 423.90	−15.05	0.93	0.80	−15.70	0.43	0.86	0.65
	3/2	11 453.91	15.05	1.25	0	15.70	1.29	0.00	−0.65
	1/2	12 458.37	−17.42	1.22	2.89	−17.66	1.03	3.09	0.24
$^4F_{5/2}$	3/2	12 480.65	4.86	2.80	0.00	5.99	3.09	0.00	−1.13
	5/2	12 487.47	11.68			11.68	5.16	0.00	0.00
	5/2	12 536.14	−77.85			−71.24	3.62	2.54	−6.61
	3/2	12 555.37	−58.26	0.4		−58.26	0.52	0.00	0.00
$^2H_{9/2}$	3/2					21.16	6.51	0.00	
	1/2	12 643.52	29.53			25.24	1.00	5.00	4.29
	5/2	12 662.91	48.92			83.09	5.62	2.55	33.17
$^4S_{3/2}$	1/2	13 527.22	−2.01	2.10	2.96	−1.58	1.95	3.90	−0.43
	3/2	13 531.23	2.01	5.96	0.91	1.58	5.85	0.00	0.43
	1/2	13 396.05	−44.97	1.05	4.64	−47.21	1.21	4.85	3.14
$^4F_{7/2}$	5/2	13 400.02	−40.10			−35.87	2.63	2.73	−4.23
	3/2	13 474.53	34.41			34.41	3.64	0.00	0.00
	5/2	13 488.08	47.96			48.66	5.35	2.73	−0.70
	5/2	14 705.73	−15.79	7.63	0.15	−13.66	3.57	3.78	−2.13
	5/2	14 710.20	−10.82	8.46	0.22	−7.23	6.04	3.78	−3.59
$^4F_{9/2}$	3/2	14 715.30	−6.22	3.99	0.35	−9.32	3.71	0.00	3.10
	1/2	14 721.87	0.35	1.33	5.76	−7.55	1.24	6.19	7.90
	3/2	14 759.24	37.72	10.90	0.00	37.72	11.14	0.00	0.00
	3/2	15 907.08	−36.82	9.10	0	−23.56	7.64	0.00	−13.26
	5/2	15 923.91	−19.99		2.59	−5.43	3.27	4.68	−14.56
$^2H_{11/2}$	1/2	15 948.12	4.22	0.65	3.86	−16.63	0.62	6.35	20.85
	3/2	15 953	9.10		3.74	5.03	1.04	0.00	4.07
	1/2	15 960.77	16.87	11.35	0.17	16.87	11.61	0.24	0.00
	5/2					23.83	0.67	4.68	
	1/2	18 554.39	−60.52			−55.39	12.16	0.00	−5.14
	1/2					−40.78	10.29	0.00	
	3/2	18 579.68	−35.22			−40.36	8.30	0.00	5.14
$^2K_{13/2}$	5/2					−23.25	5.69	2.22	
	5/2					20.39	3.82	2.22	
	3/2					57.62	2.69	0.00	
	3/2	18 993.59	−35.96	2.94	0	−46.48	2.88	0.00	10.52
$^4G_{7/2}$	5/2	19 012.88	−16.67		2.47	−12.03	3.53	1.62	−4.64
	1/2	19 042.34	12.79	0.91	3.46	−0.48	0.96	3.84	12.27
	5/2	19 078.02	48.47			58.98	1.32	1.62	−10.41
	5/2					−17.61	6.34	0.98	
	1/2	19 430.93	−10.15	0.60	5.01	−10.15	1.15	5.73	0.00
$^4G_{9/2}$	3/2	19 434.75	−6.33	9.95	0	−6.79	0.65	0.00	0.45
	3/2	19 454.60	13.52	2.19	0.83	13.73	7.53	0.00	−0.21
	5/2	19 458.72	17.64			20.82	4.05	0.98	−3.18

TABLE II.—*Continued.*

		Experimental values				Calculated values			
Level	$1\mu1$	E	E'	$g_\parallel$	$g_\perp$	E	$g_\parallel$	$g_\perp$	ΔE
$^2D_{3/2}$	1/2	21 161.71	−13.01	1.13	1.53	−7.59	1.07	2.14	−5.42
	3/2	21 187.72	13.00			7.59	3.21	0.00	5.42
	1/2	21 369.56	−68.04	1.40	5.81	−65.61	0.15	6.95	−2.43
	3/2	21 393.35	−44.25	5.75	0.29	−44.25	5.92	0.00	0.00
$^4G_{11/2}$	1/2	21 407.90	−29.70	11.24	1.02	−6.98	12.64	0.60	−22.72
	3/2	21 465.95	28.35			14.82	1.64	0.00	13.53
	5/2					15.16	1.53	3.27	
	5/2	21 527.55	89.95	5.18	1.22	86.86	0.99	3.27	3.09
$^2P_{1/2}$	1/2	23 214.93	0.00	0.59	0.60	0.00	0.62	0.62	
	1/2	23 759.73	−27.70	1.16	3.41	−34.18	1.20	3.59	6.48
$^2D_{5/2}$	3/2	23 778.42	−9.01	3.42	0	−2.55	3.59	0.00	−6.64
	5/2					36.72	5.98	0.00	
$^2P_{3/2}$	1/2	26 134.85	−16	1.06	2.14	−21.65	1.07	2.14	5.65
	3/2	26 167	16			21.65	3.21	0.00	−5.65
$^4D_{3/2}$	3/2	27 972.88	−0.90			−5.67	3.39	0.00	4.77
	1/2	27 975.68	0.90			5.67	1.13	2.26	−4.77

The matrix elements of the crystal-field interaction were calculated by the method outlined by Stevens.[7] The effective operator equivalent factors were calculated from the intermediate coupling wave functions and the reduced matrix elements reported by Judd.[8] The calculated effective operator equivalent factors and the effective g are listed in Table I. Both the calculated and observed energy levels are also listed in the same table for purposes of identification. The observed values of the center of the levels were calculated by averaging all of the Stark states of the same level whenever all the Stark states were reported. Where only some of the Stark states were reported, the center is then calculated by assuming that the theoretical Stark splitting is correct.

The Stark splitting was calculated by first-order perturbation. These results together with the spectrum reported by Carlson[1] are listed in Table II. A constant energy was subtracted from each level in order to give the best fit to the calculated Stark splitting. These values are listed as E' in Table II.

Here $g_\parallel$ and $g_\perp$ were calculated by assuming no mixing of different nondegenerate states by the magnetic field, that is, by a first-order perturbation approximation. The formulas for $g_\parallel$ and $g_\perp$ used here are the same as those reported by Carlson[1] except for $g_\perp$ of the $\mu=\pm\frac{5}{2}$ state where his expression is incorrect by a factor of two. Carlson's experimental values for $g_\parallel$ and $g_\perp$ are listed in Table II as the experimental results. In the case of $^4F_{9/2}$ the low-field values are listed for the reason discussed in the following section.

[7] K. W. H. Stevens, Proc. Phys. Soc. (London) **A65,** 209 (1952).
[8] B. R. Judd, Proc. Roy. Soc. (London) **A250,** 562 (1959).

DISCUSSION

$^4I_{9/2}$

The theoretical calculation indicates that the highest energy state is a $\mu=\pm\frac{5}{2}$ state and the next one is a $\mu=\pm\frac{3}{2}$ state. This disagrees with Carlson's experimental result. However, looking more closely at Table 14 of Carlson's report one finds only two lines that give polarization information on these two states. They are as follows,

Table 14-A	13 284.85 cm^{-1}	π	$A_6 \leftrightarrow Z_5$
Table 14-F	19 302.30 cm^{-1}	σ	$F_5 \leftrightarrow Z_4$;

A_6 was identified in Table 7 as a $\mu=\pm\frac{3}{2}$ state, since the only transition that gives π polarization is from $\mu=\pm\frac{3}{2}$ to $\mu=\pm\frac{3}{2}$. This identified Z_5 as a $\mu=\pm\frac{3}{2}$ state as claimed by Carlson. However, F_5 was identified as a $\mu=\pm\frac{1}{2}$ state in Table 7. A σ-polarized transition to Z_4 identified Z_4 as a $\mu=\pm\frac{3}{2}$ state. Since one has to be a $\mu=\pm\frac{5}{2}$ state (because there cannot be more than two $\mu=\pm\frac{3}{2}$ states, and one of them is already identified) the two identifications are in conflict with one another. Actually Carson did not identify these two states experimentally but did identify it according to Judd's calculation. Since Judd's included second-order crystal-field interaction, his calculation must be better than the present one. Most likely, Carson's identification is correct.

$^4F_{9/2}$

The separation between different states in this level is about 5 cm^{-1} except for the upper $\mu=\pm\frac{3}{2}$ state. This is a very poor case for first-order perturbation because a 35-kgauss magnetic field will give a 5 cm^{-1} splitting

for $g \simeq 3$. This is the reason that $g_\perp$ does not at all fit the observed values. When H is parallel to the c axis of the crystal, only the two $\mu = \pm\frac{5}{2}$ states will be seriously mixed with each other. This is why the three remaining states have a good fit for $g_{||}$. Assuming that the two $\mu = \pm\frac{5}{2}$ states are separated by 5 cm^{-1} and allowing mixing of the two states, $g_\perp$ is as follows,

$H = 12\,060$ gauss $\quad g_\perp = 2.68 \quad g_\perp' = 5.16,$

$H = 35\,100$ gauss $\quad g_\perp = 2.01 \quad g_\perp' = 4.56.$

These values somehow deviate more than those obtained from the first-order perturbation calculation.

Since a lower field gives better agreement with the first-order perturbation calculation, the low-field values are listed in Table II as experimental values.

$^4F_{5/2}$ and $^2H_{9/2}$

The energy separation between these two levels is very small. However, there is very little mixing due to the crystal-field interaction between them, because one of them is a quartet level and the other is mainly a doublet level.

$^2G_{7/2}$ and $^4G_{5/2}$

Wybourne identified these two levels as group D. These two levels are close enough to each other to be both in group D, and there will be quite serious mixing between them due to the crystal-field interaction. Since the first-order perturbation is not adequate and the crystal field quantum number for the Stark states are not identified experimentally, no calculation is done for these two levels.

$^2K_{13/2}$

This level was not identified by Wybourne. However, in Carlson's report there are two lines E_1 and E_2 which fit in this level quite nicely as shown in Table I. However, Carlson listed these two lines as due to the impurity of U. The author grew these crystals and it is difficult to see how there can be any U in it. Some crystals from the same batch were used in a magnetic resonance experiment and no resonance of U^{+3} was detected[9]; U^{+3} gives a very strong magnetic resonance signal, if no resonance signal was detected, the possibility that some U^{+3} exists is very small. For these reasons these two lines are identified here as the $^2K_{13/2}$ level.

From the polarization of these two lines one can identify the upper energy state as a $\mu = \pm\frac{3}{2}$ state and the other as a $\mu = \pm\frac{1}{2}$ state. The theoretical calculation gives a fair fit for these two states as shown in Table II.

$^2K_{15/2}$ and $^2G_{9/2}$

Wybourne identified these two levels as group G and H. These two levels are very close to each other. For the same reason mentioned before, no calculation was carried out for these two levels.

CONCLUSIONS

The average deviation for this calculation is about 4.9 cm^{-1}, which is the same as that obtained by Judd in the analysis of the spectrum of $PrCl_3$. This is a fair agreement because in most of the levels the states appear as expected. If one assumes that there is no crystal field interaction and considers all the Stark splitting as deviations, then the average deviation is about 31 cm^{-1}.

The g values are also in fair agreement because the magnetic-field splitting is rather large for a first-order perturbation approximation.

ACKNOWLEDGMENT

The author wishes to acknowledge the aid offered by Edward Erath in checking the calculation of the effective operator equivalent factors.

[9] Using some crystal from the same batch Don Halford found many weak lines about 1/10 of the intensity of the hyperfine lines of Nd^{+3}. One of these lines has a $g_\perp = 1.552$ which is very close to $g_\perp$ of U^{+3}.

Crystallography of the Ru-B and Os-B Systems

C. P. KEMPTER AND R. J. FRIES

Los Alamos Scientific Laboratory, University of California, Los Alamos, New Mexico

(Received November 3, 1960)

The Ru-B and Os-B systems were investigated by x-ray powder diffraction. In addition to Aronsson's hexagonal Ru_7B_3 phase, two new hexagonal Ru-B phases were found: RuB_2 (D_{6h}^1-P6/mmm, $a_0=2.852$ A, $c_0=2.855$ A) and Ru_2B_5 (D_{6h}^4-P6/mmc, $a_0=2.89$ A, $c_0=12.81$ A. In the Os-B system, two new hexagonal phases, isomorphous with the latter Ru-B phases, were found: OsB_2 ($a_0=2.876$ A, $c_0=2.871$ A) and Os_2B_5 ($a_0=2.91$ A, $c_0=12.91$ A). RuB_2 and OsB_2 are isomorphous with MoB_2; Ru_2B_5 and Os_2B_5 are isomorphous with W_2B_5.

THE Ru–B and Os–B systems were first investigated by Buddery and Welch[1] who claimed to have prepared the phases Ru_2B, RuB, Ru_2B_3, RuB_2, OsB, and OsB_2 by heating the components in stoichiometric proportions in evacuated silica capillaries at 1000–1200°C. They stated further that RuB and OsB were cubic with $a=6.97$ A and $a=7.03$ A, respectively. No x-ray data and no further structural information were presented.

Recently, Aronsson[2] reported on the crystal structure of Ru_7B_3, which he found to be hexagonal (space group $C_{6v}^4-P6_3mc$; structurally similar to Cr_7C_3) with $a=7.467$ A, $c=4.713$ A, $c/a=0.631$, and $Z=2$.

In the present investigation, all preparations were made by mixing weighed quantities of the finely divided elements, pressuring into ½-in. diam briquettes at 20 000 psi, and firing in vacuo on boron nitride disks in a globar furnace at temperatures ranging from 1200 to 1735°C and times from 5 min to 20 hr. The Shield-Alloy Corporation "min 99% purity"—325 mesh boron contained 0.01–0.1% Mg, Si, Ca, Mn, and Fe as the main spectral impurities. Two sources of Ru were used, Varlacoid Chemical Company Ru, which contained 0.001–0.01% Na, K, Pd, and Os as main impurities,

TABLE I. X-ray powder data for RuB_2 and OsB_2.

RuB_2			OsB_2		
hk.l	*d*, A	$I_{rel.}$	*hk.l*	*d*, A	$I_{rel.}$
00.1	2.832	40	00.1	2.847	30
10.0	2.454	80	10.0	2.470	50
10.1	1.859	90	10.1	1.871	70
00.2, 11.0	1.422	50	11.0, 00.2	1.434	40
11.1	1.273	50	11.1	1.283	60
10.2, 20.0	1.233	60	20.0, 10.2	1.241	70
20.1	1.132	50	20.1	1.140	60
11.2	1.008	40	11.2	1.015	40
00.3	0.9510	10	00.3	0.9566	10
20.2, 12.0	0.9333	50	12.0, 20.2	0.9405	50
10.3	0.8876	80	12.1	0.8942	90
12.1	0.8867	80	10.3	0.8923	70
30.0	0.8230	30	30.0	0.8301	30
11.3	0.7913	70	30.1	0.7976	80
30.1	0.7909	70	11.3	0.7962	50
12.2	0.7812	100	12.2	0.7871	100

TABLE II. X-ray powder data for Ru_2B_5 and Os_2B_5.

Ru_2B_5			Os_2B_5	
hk.l	*d*, A	$I_{rel.}$	*d*, A	$I_{rel.}$
00.2	6.38	5	6.38	5
00.4	3.18	30	3.20	10
10.0	2.50	10	2.51	40
10.1	2.46	20	2.46	30
10.2	2.315	50	2.334	50
10.3	2.161	20	2.167	60
00.6	...	...	2.146	30
10.4	1.973	10	1.982	20
10.5	1.792	50	1.800	90
10.6	1.627	10	1.634	30
00.8	1.599	10	1.611	30
10.7	1.453	20	1.487	10
11.0	1.445	40	1.454	80
11.2	...	...	1.420	5
10.8	1.345	20	1.359	40
11.4	1.323	50	1.327	100
00.10	1.281	20	1.291	40
20.0	...	...	1.261	30
20.1	1.251	5	1.254	60
10.9	1.239	40	1.247	100
20.2	1.229	60	1.238	10
20.3, 11.6	1.201	10	1.206	70
20.4	1.161	40	1.172	60
10.10			1.150	60

[1] J. H. Buddery and A. J. E. Welch, Nature **167**, 362 (1951).
[2] B. Aronsson, Acta Chem. Scand. **13**, 109 (1959).

and Baker and Company Ru, which had 0.01–0.1% Pt and 0.001–0.01% Rh, Pd, and Au. The J.A. Samuel Company Os contained 0.001–0.01% Al, Si, K, Fe, Pd, Ir, Pt, and Au as main spectral impurities.

The Ru_7B_3 phase reported by Aronsson was verified on examination of a 2 Rus:1B mixture heated at 1300°C for 20 hours. An isomorphous Os_7B_3 phase was not observed on examination of 4 Os:1B and 2 Os:1B mixtures heated under the same conditions. On heating 1 Ru:1B mixtures at 1300°C and 1320°C for 18 hr, the "cubic" RuB phase was not observed; however, a new hexagonal phase isomorphous with MoB_2 (D_{6h}^1—$P6/mmm$) was found, with a secondary phase of Ru metal. Therefore, 1 Ru:2B mixtures were heated at 1200°C and 1300°C and the same hexagonal RuB_2 phase was found with no Ru metal detectable. The hexagonal lattice parameters (symmetrical back reflection focusing camera, Cu radiation, Ni filtered) and their standard deviations were determined by the method of Vogel and Kempter[3], assuming systematic errors in $\Delta a_0/a_0$ and $\Delta c_0/c_0$ directly proportional to $\phi \tan\phi$, where ϕ is the complement of the Bragg angle. The values obtained were $a_0=2.8517\pm0.0001$ A $c_0=2.8548\pm0.0001$ A, and $c_0/a_0=1.001$, uncorrected for refraction. For 1 (RuB_2) per unit cell, the calculated density is 10.136 g/cc. On heating 1 Os:1B mixtures at 1300°C and 1685°C, the "cubic" OsB phase was not observed; however, a new hexagonal phase isomorphous with MoB_2 and RuB_2 was found, with a secondary phase of Os metal. The lattice parameters were determined using the above methods and it was found for hexagonal OsB_2 that $a_0=2.8761\pm0.0001$ A, $c_0=2.8709\pm0.0001$ A, and $c_0/a_0=0.998$, uncorrected for refraction. For 1(OsB_2) per unit cell, the calculated density is 14.809 g/cc. In the above mentioned attempts to prepare Os_7B_3, this same OsB_2 phase and Os metal were found. Debye-Scherrer data (Cu target, Ni filter) for the RuB_2 and OsB_2 are shown in Table I.

Mixtures of 1 Os:2B were then heated at 1300°–1400°C, but it was found that OsB_2 was produced as a minor phase, with a new hexagonal phase isomorphous with W_2B_5(D_{6h}^4—$P6/mmc$) as the major phase, and an unknown phase as the secondary phase. The Os_2B_5 approximate lattice parameters are $a_0=2.91$ A, $c_0=12.91$ A, and $c_0/a_0=4.44$. For 2 (Os_2B_5) per unit cell, the calculated density is 15.2 g/cc. Mixtures of 2 Os:5B heated at 1300°C and 1735°C produced a secondary phase of Os_2B_5 and a major phase of the same unknown phase. Mixtures of 2 Ru:5B heated at 1300°C and 1540°C produced a new hexagonal phase, isomorphous with W_2B_5 and Os_2B_5, as a secondary phase, and an unknown phase isomorphous with the one observed in the Os–B system as the major phase. The Ru_2B_5 approximate lattice parameters are $a_0=2.89$ A, $c_0=12.81$ A, and $c_0/a_0=4.43$. For 2(Ru_2B_5) per unit cell the calculated density is 9.19 g/cc. Ru_2B_5 is not isomorphous with Mo_2B_5. Debye-Scherrer data (Cr target, V filter) for Ru_2B_5 and Os_2B_5 are shown in Table II. The intensities are only approximate because of possible line overlap with the unknown phases.

Mixtures of 1 Ru:3B and 1 Os:3B heated at 1300°C for 18 hr produced only the above mentioned unknown isomorphous phases. The phases are not isomorphous with ReB_3.

ACKNOWLEDGMENTS

The authors thank J. A. Mariner for the spectrographic analyses, L. A. Wahman for the x-ray film reading, and D. L. Cooper for the IBM 704 lattice parameter fits.

[3] R. E. Vogel and C. P. Kempter, Los Alamos Scientific Laboratory Rept. LA-2317 (April, 1959); Acta Cryst. (to be published).

Theory of the Diamagnetic Susceptibilities of the Alkanes

H. F. HAMEKA

The Johns Hopkins University, Department of Chemistry, Baltimore 18, Maryland

(Received November 21, 1960)

A general theory of the diamagnetic susceptibilities of the alkanes is developed. It is found that the molecular susceptibilities are obtained as sums of contributions from the 1*s* electrons of the carbon atoms, from the various C—C and C—H bonds, and from interactions between various pairs of adjacent C—C and C—H bonds. It is possible to express the theory in a semi-empirical form so that all susceptibilities of the alkane molecules are expressed in terms of three parameters. For the most reliable series of experimental data, the susceptibilities of 24 different hydrocarbons may be described by these parameters within an accuracy of 0.5%. Theoretical values of diamagnetic susceptibilities are given for 54 alkane molecules, namely for all isotopes up to and including octane, for the normal alkanes from nonane to hexadecane and for a few other molecules for which experimental data have been reported. The accuracy of the theoretical values is compatible with the accuracy of the measurements.

I. INTRODUCTION

IT has recently been shown[1-3] that a satisfactory theory of molecular diamagnetic susceptibilities may be developed by employing gauge invariant atomic orbitals. The necessary conditions for the validity of this theory are: (1) that the wave functions of the ground state and of the lower excited states of the molecule may be written as functions of atomic orbitals and (2) that these molecular wave functions are a subgroup of a complete set of ortho-normal functions. In particular, if the molecular wave functions may be approximated by products of molecular orbitals, each of which may be written as a linear combination of atomic orbitals,[4] the calculation of the diamagnetic susceptibility can be performed in a straightforward fashion. In this special case the diamagnetic susceptibility may be expressed in terms of various monoelectronic one- or two-center atomic integrals and of certain molecular excitation energies. The integrals will depend on the functional form of the atomic orbitals involved and, in the case of two-center integrals, on the internuclear distance.

In this paper it will be assumed that the molecular wave functions have the form mentioned above. Although it may appear that this assumption imposes rather stringent restrictions on the molecular wave functions that may be employed for susceptibility calculations, at the present stage of quantum chemistry, these conditions are fulfilled by practically all calculated wave functions for molecules other than H_2. It may be mentioned in this connection that gratifyingly accurate wave functions of this type for various diatomic and triatomic molecules were obtained by Roothaan's self consistent field method.[5]

For the N_2 molecule the diamagnetic susceptibility was calculated from SCF LCAO MO functions[3] obtained by Scherr[6]; for the H_2 and CH_4 molecules,[1,2] the diamagnetic susceptibilities were computed from LCAO MO wave functions that are equally and slightly less accurate, respectively. The results of these calculations show that diamagnetic susceptibilities may be calculated from LCAO MO functions with accuracies between 1 and 10%. This seems to indicate that calculations of diamagnetic susceptibilities from LCAO MO functions will yield very accurate results if the LCAO MO functions are chosen as accurately as possible. This has encouraged us to propose a general theory of the diamagnetic susceptibilities of the alkanes.

This theory will be based on the following assumptions: (1) that each C—C and C—H bond in an alkane molecule may be represented by a localized LCAO orbital, (2) that these localized orbitals for either C—C or C—H bonds are identical for all C—C or C—H bonds in all alkane molecules, and (3) that all C—C and C—H bondlengths have the same values in all alkanes. In the theory we will also consider the excitation energies that are required to transfer an electron from a bonding C—C or C—H orbital to an antibonding C—C or C—H orbital belonging to an adjacent bond; apparently there are then four different sets of excitation energies. We will assume that, within each set, the excitation energies will be the same for each corresponding pair of bonds in all alkane molecules.

In the next section we will develop a general theory of the magnetic susceptibilities of the alkanes on the basis of the above assumptions.

II. CALCULATIONS

Let us consider an alkane molecule C_NH_{2N+2} and let us set out to construct the ground-state wave function of this molecule according to the assumptions made in Sec. I. We will denote the nuclei by an index i, so that $i=1, 2, 3, \cdots, N$ denotes carbon nuclei, and $i=N+1, N+2, N+3, \cdots, 3N+2$ denote hydrogen nuclei. The bonds may either be denoted by indexes m or by sets of indexes (i_m, j_m), so that i_m and j_m refer to

[1] H. F. Hameka, Z. Naturforsch. **14a**, 599 (1959).
[2] H. F. Hameka, Physica **25**, 626 (1959).
[3] H. F. Hameka, J. Chem. Phys. **34**, 366 (1961).
[4] These functions will be referred to as LCAO MO functions.
[5] C. C. J. Roothaan, Revs. Modern Phys. **23**, 69 (1951).
[6] C. W. Scherr, J. Chem. Phys. **23**, 569 (1955).

the nuclei that are connected by bond m. Since there are $N-1$ C—C bonds and $2N+2$ C—H bonds, the C—C bonds will be denoted by $m=1, 2, 3, \cdots, N-1$ and the C—H bonds by $m=N, N+1, N+2, \cdots, 3N+1$. If we now impose the condition that $j>i$ we have

$$\begin{aligned} &1\leq i_m\leq N \quad i_m<j_m\leq N \qquad \text{for} \quad 1\leq m\leq N-1,\\ &1\leq i_m\leq N \quad N+1\leq j_m\leq 3N+2 \quad \text{for} \quad N\leq m\leq 3N+1. \end{aligned} \tag{1}$$

All bonds may now be represented by molecular orbitals

$$\begin{aligned} \phi_m(k)&=A[u(i_m;k)+u(j_m;k)] \qquad 1\leq m\leq N-1,\\ \phi_m(k)&=B[v(i_m;k)+\lambda h(j_m;k)] \qquad N\leq m\leq 3N+1, \end{aligned} \tag{2}$$

where u, v, and h are appropriate atomic orbitals, presumably hybridized, i and j denote the corresponding nuclei, m the directions into which the orbitals should point, and k refers to the coordinates of electron k. The quantities A and B are normalization constants and λ is an electronegativity constant. If the inner electrons of the carbon atoms are described by atomic orbitals $s_i(k)$, the ground-state molecular wave function may be written as

$$\begin{aligned} \Psi_0=[(8N+2)!]^{-\frac{1}{2}}\sum_P P\delta_P\{\prod_{i=1}^{N}[s_i(2i-1)s_i(2i)\\ \times\alpha(2i-1)\beta(2i)]\prod_{m=1}^{3N+1}[\phi_m(2N+2m-1)\\ \times\phi_m(2N+2m)\alpha(2N+2m-1)\beta(2N+2m)]\}. \end{aligned} \tag{3}$$

In some excited states the electrons may also occupy antibonding orbitals:

$$\begin{aligned} \phi_m'(k)&=A'[u'(i_m;k)-u'(j_m;k)] \qquad 1\leq m\leq N-1,\\ \phi_m'(k)&=B'[v'(i_m;k)-\lambda' h'(j_m;k)] \qquad N\leq m\leq 3N+1. \end{aligned} \tag{4}$$

The singlet wave functions of the states where an electron has been transferred from a bonding orbital belonging to one bond to an antibonding orbital belonging to another bond are then

$$\begin{aligned} \Psi_{n,l}=[2(8N+2)!]^{-\frac{1}{2}}\sum_P P\delta_P\{\prod_{i=1}^{N}[s_i(2i-1)s_i(2i)\\ \times\alpha(2i-1)\beta(2i)]\prod_{m\neq n}[\phi_m(2N+2m-1)\phi_m(2N+2m)\\ \times\alpha(2N+2m-1)\beta(2N+2m)][\phi_n(2N+2n-1)\\ \phi_l'(2N+2n)+\phi_n(2N+2n)\phi_l'(2N+2n-1)]\\ \times\alpha(2N+2n-1)\beta(2N+2n)\}. \end{aligned} \tag{5}$$

It is now possible to calculate the diamagnetic susceptibility of the C_NH_{2N+2} molecule according to the method developed in a previous paper.[3] If we follow the notation of this paper, we have

$$\begin{aligned} \chi&=-\chi_1-\chi_2+\chi_3,\\ \chi_1&=2LE_{00}^{(2)}/S_{00},\\ \chi_2&=2L\{\partial^2/\partial H^2[HE_{00}^{(1)}/S_{00}]\}_{H=0},\\ \chi_3&=2L\sum_{j=0}^{\infty}E_{0j}^{(1)}E_{j0}^{(1)}/(S_{00}E_j-S_{jj}E_0), \end{aligned} \tag{6}$$

where the summation over j implies a summation over all excited states and where the quantities $E_{kl}^{(i)}$, E_k, and S_{kl} have been defined in the work cited in reference 3. L is avogadro's number.

Let us first focus our attention on χ_1. According to Eqs. (13) and (16) of the work cited in reference 3,

$$\chi_1=(e^2L/6mc^2)\langle\Psi_0|\sum_j(\mathbf{r}_j-\mathbf{q}_j)^2|\Psi_0\rangle, \tag{7}$$

where the summation extends over all electrons and the vectors $\mathbf{q}_j$ are determined by the condition that, after breaking up the expression into one- and two-center one-electron integrals, $\mathbf{q}_j$ has to be taken as the position of the nucleus corresponding to the atomic orbital following the operator. Bearing this condition in mind, substitution of Eq. (2) into Eq. (7) yields

$$\begin{aligned} \chi_1=(e^2L/3mc^2)[\sum_{i=1}^{N}\langle s_i(k)|(\mathbf{r}_k-\mathbf{q}_k)^2|s_i(k)\rangle\\ +\sum_{n=1}^{3N+1}\langle\phi_n(k)|(\mathbf{r}_k-\mathbf{q}_k)^2|\phi_n(k)\rangle] \end{aligned} \tag{8}$$

or, if we define

$$\begin{aligned} J_C&=(e^2L/3mc^2)\langle s_i(k)|(\mathbf{r}_k-\mathbf{q}_k)^2|s_i(k)\rangle,\\ J_{CC}&=(e^2L/3mc^2)\langle\phi_n(k)|(\mathbf{r}_k-\mathbf{q}_k)^2|\phi_n(k)\rangle\\ &\qquad 1\leq n\leq N-1,\\ J_{CH}&=(e^2L/3mc^2)\langle\phi_n(k)|(\mathbf{r}_k-\mathbf{q}_k)^2|\phi_n(k)\rangle\\ &\qquad N\leq n\leq 3N+1, \end{aligned} \tag{9}$$

we can also write

$$\chi_1=NJ_C+(N-1)J_{CC}+(2N+2)J_{CH}, \tag{10}$$

since for all C—C and C—H bonds J_{CC} and J_{CH} are supposed to be equal according to our assumptions.

According to Eqs. (8) and (13) of footnote 3, the contribution χ_2 to the magnetic susceptibility is obtained by computing the matrix elements of the operators

$$\Lambda_i^{(v)}(j)=(e\hbar i/2mc)[\mathbf{H}(\mathbf{r}_{jv}\nabla_j)], \tag{11}$$

where $\mathbf{r}_{ji}$ denotes the position of electron j with respect to nucleus v. After expressing the matrix elements in terms of one- and two-center atomic integrals, v is to be taken as the nucleus belonging to the atomic orbital

following the operator, whereas the atomic orbitals preceding the operators have to be multiplied by an appropriate phase factor representing a gauge transformation from the position of their corresponding nuclei to the position of the nucleus v. The molecular orbitals containing these transformed atomic orbitals will be denoted by $\tilde{\phi}_m(k)$ and $\tilde{\phi}_m'(k)$.

In order to calculate χ_2 it is helpful to observe that

$$\langle\tilde{\phi}_m(k)\,|\,\Lambda_1^{(v)}(k)\,|\,\phi_m(k)\rangle=0(H^2),$$
$$\langle\tilde{\phi}_m(k)\,|\,1\,|\,\phi_m(k)\rangle=1+0(H^2),$$
$$\langle\tilde{\phi}_m(k)\,|\,1\,|\,\phi_n(k)\rangle+\langle\tilde{\phi}_n(k)\,|\,1\,|\,\phi_m(k)\rangle=0(H^2)\,n\neq m,$$
$$\langle\tilde{\phi}_m(k)\,|\,\Lambda_1^{(v)}(k)\,|\,s_i(k)\rangle=0. \tag{12}$$

It then follows from Eq. (6) that

$$\chi_2=2L\{\partial^2/\partial H^2[2\sum_{m=1}^{3N+1}\langle\tilde{\phi}_m(k)\,|\,\Lambda_1^{(v)}(k)\,|\,\phi_m(k)\rangle]\}_{H=0}. \tag{13}$$

After averaging over all different orientations of the molecule with respect to the magnetic field, this may be written as

$$\chi_2=(N-1)K_{CC}+(2N+2)K_{CH}, \tag{14}$$

where

$$K_{CC}=4L[\partial^2/\partial H^2\langle\tilde{\phi}_m(k)\,|\,\Lambda_1^{(v)}(k)\,|\,\phi_m(k)\rangle_{Nv}]_{H=0} \qquad 1\leq m\leq N-1,$$
$$K_{CH}=4L[\partial^2/\partial H^2\langle\phi_m(k)\,|\,\Lambda_1^{(v)}\,|\,\phi_m(k)\rangle_{Nv}]_{H=0} \qquad N\leq m\leq 3N+1. \tag{15}$$

In calculating χ_3 only terms linear in H of E_{0j} and E_{j0} need to be considered, so that, taking into account Eq. (12),

$$\chi_3=(4L/H^2)\sum_m\sum_j\langle\tilde{\phi}_m\,|\,\Lambda_1^{(v)}\,|\,\phi_m{}^{(j)}\rangle \times\langle\tilde{\phi}_m{}^{(j)}\,|\,\Lambda_1^{(v)}\,|\,\phi_m\rangle/(\epsilon_{m,j}-\epsilon_{m,0}), \tag{16}$$

where the summation over j should be extended over all excited molecular orbitals $\phi_m{}^{(j)}$ with energies $\epsilon_{m,j}$. In order to evaluate this expression it is useful to consider $\Lambda_1^{(v)}|\phi_m\rangle$. Let us consider bond m between nuclei i and j and let us take the positive z axis as pointing from i to j. Let us then assume that the functions $\phi_m(k)$ may be written as

$$\phi_m(k)=A[\alpha_1 s(r_{ki})+\alpha_2 z_{ki}p(r_{ki})+\alpha_1 s(r_{kj})-\alpha_2 z_{kj}p(r_{kj})] \qquad 1\leq m\leq N-1,$$
$$\phi_m(k)=B[\beta_1 s(r_{ki})+\beta_2 z_{ki}p(r_{ki})+\lambda\gamma_1 h_s(r_{kj}) -\lambda\gamma_2 z_{kj}h_p(r_{kj})] \qquad N\leq m\leq 3N+1. \tag{17}$$

Actually, Eq. (17) goes further than the assumptions expressed in Sec. I, but since χ_1 is the main contribution to the susceptibility and χ_3 is only a correction, we may calculate χ_3 less accurately than χ_1 without affecting the over-all accuracy of χ. It follows from Eqs. (11) and (17) that

$$\Lambda_1^{(v)}(k)\,|\,\phi_m(k)\rangle=(e\hbar i/2mc)\,A\alpha_2\{H_x[y_{ki}p(r_{ki}) -y_{kj}p(r_{kj})]-H_y[x_{ki}p(r_{ki})-x_{kj}p(r_{kj})]\} \qquad 1\leq m\leq N-1,$$
$$\Lambda_1^{(v)}(k)\,|\,\phi_m(k)\rangle=(e\hbar i/2mc)\,B\{H_x[\beta_2 y_{ki}p(r_{ki}) -\lambda\gamma_2 y_{kj}h_p(r_{kj})]-H_y[\beta_2 x_{ki}p(r_{ki})-\lambda\gamma_2 x_{kj}h_p(r_{kj})]\} \qquad N\leq m\leq 3N+1. \tag{18}$$

To a fairly good approximation these functions may now be expressed as linear combinations of the functions $\phi_{m(i)}$, $\phi_{m(j)}$, $\phi_{m(i)}'$ and $\phi_{m(j)}'$ if we denote by $m(i)$ and $m(j)$ the bonds starting from nuclei i and j:

$$\Lambda_1^{(v)}(k)\,|\,\phi_m(k)\rangle=\sum_{m(i)}\{H_x[a_{m(i)}\phi_{m(i)}+a_{m(i)}'\phi_{m(i)}'] +H_y[b_{m(i)}\phi_{m(i)}+b_{m(i)}'\phi_{m(i)}']\} +\sum_{m(j)}\{H_x[a_{m(j)}\phi_{m(j)}+a_{m(j)}'\phi_{m(j)}']+H_y[b_{m(j)}\phi_{m(j)} +b_{m(j)}'\phi_{m(j)}']\} \qquad m(i),\ m(j)\neq m. \tag{19}$$

It then follows from Eq. (6) that

$$\chi_3=(4L/3)\sum_m\{\sum_{m(i)}[|a_{m(i)}'|^2+|b_{m(i)}'|^2]/(\epsilon_{m(i)}'-\epsilon_m) +\sum_{m(j)}[|a_{m(j)}'|^2+|b_{m(j)}'|^2]/(\epsilon_{m(j)}'-\epsilon_m)\} \qquad m(i),\ m(j)\neq m. \tag{20}$$

The reader will easily verify that the expressions

$$g[m;m(i)]=[|a_{m(i)}'|^2+|b_{m(i)}'|^2]/[\epsilon_{m(i)}-\epsilon_m] \tag{21}$$

depend only on m and $m(i)$. More specifically

$$g[m;m(i)]=u(\mathrm{CC};\mathrm{CC}) \qquad 1\leq m\leq N-1 \qquad 1\leq m(i)\leq N-1,$$
$$g[m;m(i)]=u(\mathrm{CH};\mathrm{CC}) \qquad 1\leq m\leq N-1 \qquad N\leq m(i)\leq 3N+1$$
$$N\leq m\leq 3N+1 \qquad 1\leq m(i)\leq N-1,$$
$$g[m;m(i)]=u(\mathrm{CH};\mathrm{CH}) \qquad N\leq m\leq 3N+1 \qquad N\leq m(i)\leq 3N+1. \tag{22}$$

If one now compares Eqs. (6), (10), (14), (20), and (22), it will appear that χ may be written as

$$\chi=N_C\chi_C+N_{CC}\chi_{CC}+N_{CH}\chi_{CH}-N_{CC;CC}\chi_{CC;CC} -N_{CC;CH}\chi_{CC;CH}-N_{CH;CH}\chi_{CH;CH}, \tag{23}$$

where N_C is the number of C atoms, N_{CC} the number of C—C bonds, N_{CH} the number of C—H bonds, $N_{CC;CC}$ the number of pairs of adjacent C—C bonds, $N_{CC;CH}$ the number of pairs of adjacent C—H bonds. The other quantities on the right-hand side of Eq. (23) may then be taken as adjustable parameters.

TABLE I. The molar diamagnetic susceptibilities of 54 alkane molecules expressed in terms of A, B, and C.[a]

Compound		χ_t	χ_e	References
methane	$A+C$	18.89	12.4	9
			17.4	b
ethane	$A+B$	29.58	27	9
			26.8	b
propane	$A+2B$	40.84	39.6	10
			40.5	9
			38.6	b
butane	$A+3B$	52.10	57.4	9
			50.3	b
2-methyl-propane	$A+3B+C$	52.67	56.3	9
			51.7	10
			50.5	b
pentane	$A+4B$	63.36	63.05	8
			63.3	b
			61.5	b
2-methyl-butane	$A+4B+C$	63.93	64.40	8
			63.0	b
2,2-dimethyl-propane	$A+4B+3C$	65.07	63.1	10
			63.0	b
hexane	$A+5B$	74.62	74.3	8,11,12
			73.63	c
2-methyl-pentane	$A+5B+C$	75.19	75.26	8
3-methyl-pentane	$A+5B+C$	75.19	75.52	8
2,2-dimethyl butane	$A+5B+3C$	76.33	76.24	8
2,3-dimethyl-butane	$A+5B+2C$	75.76	76.22	8
heptane	$A+6B$	85.88	85.24	8,13
			85.83	c
2-methyl-hexane	$A+6B+C$	86.45	86.24	8,13
3-methyl-hexane	$A+6B+C$	86.45		
3-ethyl-pentane	$A+6B+C$	86.45		
2,2-dimethyl-pentane	$A+6B+3C$	87.59	86.97	8,13
2,3-dimethyl-pentane	$A+6B+2C$	87.02	87.51	8,13
2,4-dimethyl-pentane	$A+6B+2C$	87.02	87.48	8,13
3,3-dimethyl-pentane	$A+6B+3C$	87.59		
2,2,3-trimethyl-butane	$A+6B+4C$	88.16	88.36	8,13
octane	$A+7B$	97.14	96.63	8,11, 13,14
			96.93	c
2-methyl-heptane	$A+7B+C$	97.71		
3-methyl-heptane	$A+7B+C$	97.71	97.99	8,13
4-methyl-heptane	$A+7B+C$	97.71		
3-ethyl-hexane	$A+7B+C$	97.71		
2,2-dimethyl-hexane	$A+7B+3C$	98.85		
2,3-dimethyl-hexane	$A+7B+2C$	98.28	98.77	8,13
2,4-dimethyl-hexane	$A+7B+2C$	98.28		
2,5-dimethyl-hexane	$A+7B+2C$	98.28	98.15	8,13
3,3-dimethyl-hexane	$A+7B+3C$	98.85		
3,4-dimethyl-hexane	$A+7B+2C$	98.28	99.06	8
2,2,3-trimethyl-pentane	$A+7B+4C$	99.42	99.86	8,13
2,2,4-trimethyl-pentane	$A+7B+4C$	99.42	98.34	8,13
2,3,3-trimethyl-pentane	$A+7B+4C$	99.42		
2-methyl-3-ethyl-pentane	$A+7B+2C$	98.28		
3-methyl-3-ethyl-pentane	$A+7B+3C$	98.85	99.9	13
2,2,3,3-tetramethyl-butane	$A+7B+6C$	100.56		
nonane	$A+8B$	108.40	108.13	8,13,14
4-methyl-octane	$A+8B+C$	108.97	109.6	14
decane	$A+9B$	119.66	119.51	8,14
4-methyl-nonane	$A+9B+C$	120.23	121.4	14
2,6-dimethyl-octane	$A+9B+2C$	120.80	122.5	14
undecane	$A+10B$	130.92	131.8	14
2,4-dimethyl-nonane	$A+10B+2C$	132.06	134.7	14
3,4-dimethyl-nonane	$A+10B+2C$	132.06	134.7	14
4,5-dimethyl-nonane	$A+10B+2C$	132.06	134.5	14
dodecane	$A+11B$	142.18		
tridecane	$A+12B$	153.44		
tetradecane	$A+13B$	164.71		
pentadecane	$A+14B$	175.97		
hexadecane	$A+15B$	187.23	187.63	8
2,2,4,7,9,9-hexa-methyl-decane	$A+15B+8C$	191.78	191.52	8

[a] The resulting theoretical values χ_t and experimental values χ_e are expressed in terms of 10^{-6} cgs units. In the last columns the references from which the experimental values are derived are listed.

[b] C. Barter, R. G. Meisenheimer, and D. P. Stevenson, J. Phys. Chem. **64**, 1312 (1960).

[c] W. R. Angus, G. I. W. Llewelyn, and G. Scott, Trans. Faraday Soc. **55**, 887 (1959).

III. APPLICATIONS

In order to apply Eq. (23) we wish to find a class of hydrocarbons that fulfill the conditions laid down in Sec. I. According to the current ideas of quantum chemistry the alkanes satisfy these conditions within a very good approximation. The cyclic compounds show various features, such as bent bonds, different bond energies, etc., that have induced us not to include them in this discussion. Equation (23) shows χ expressed in terms of six adjustable parameters, but we have found

that for the alkanes χ may even be expressed in terms of the following three parameters:

$$A=\chi_C+4\chi_{CH}+\chi_{CC;CC}-2\chi_{CC;CH}-5\chi_{CH;CH},$$
$$B=\chi_C+\chi_{CC}+2\chi_{CH}-\chi_{CC;CC}-4\chi_{CC;CH}-\chi_{CH;CH},$$
$$C=-\chi_{CC;CC}+2\chi_{CC;CH}-\chi_{CH;CH}. \quad (24)$$

The diagmagnetic susceptibilities of 38 alkane molecules have been reported,[7] but we share the opinion of the author of the work cited in reference 7 that the most accurately known values are those measured by Broersma[8] for 24 alkane molecules.

In Table I we have listed the magnetic susceptibilities of 54 alkane molecules as functions of A, B, and C. If we determine A, B, and C in such a way as to give the best possible agreement with the experimental data of Broersma[8] by means of the method of least-square deviations, we find that $A=18.318\times10^{-6}$, $B=11.260\times10^{-6}$ and $C=0.570\times10^{-6}$. By employing these values we obtain the theoretical molar diamagnetic susceptibilities of Table I, which should be compared with the experimental values obtained by various authors[8–14] as far as they are known.

IV. DISCUSSION

It will be noticed that there is a very close similarity between our theory and the semiempirical determination of susceptibilities by means of Pascal's constants.[15] According to Pascal, magnetic susceptibilities may be determined from

$$\chi_M=\sum(n_A\chi_A)+\lambda, \quad (25)$$

where n_A is the number of atoms of susceptibility χ_A in the molecule and λ is a correction depending on the nature of the bonds between the atoms. The main difference between Pascal's description and ours is that Pascal assigns susceptibilities to the various atoms in the molecule whereas in our theory the susceptibilities of the various bonds are considered. However, if we allow for the assumption that the various atomic orbitals of one particular kind of atom in different bonds are basically the same and, in particular, if these differences and the effects of the interactions between adjacent bonds are accounted for by the choice of λ, Pascal's approach to the theory of diamagnetic susceptibilities becomes identical with ours. There is one essential difference between the two methods: our description has a sound theoretical basis whereas Pascal's method is not more than a clever guess, justified by the success with which the method has been applied.

The agreement between theoretical and experimental susceptibility values, as shown in Table I, is satisfactory: for Broersma's data, which are the most reliable, the deviations between theoretical and experimental values vary between 0.9 and 8.2 per mil and the square root of the mean-square deviation is 4.5 per mil. It may be added that Broersma claims an accuracy of 1.5 per mil, but we believe that it is probably closer to 5 per mil. For the other experimental data the deviations are slightly larger for the higher hydrocarbons (between 0.5% and 1.5%) and they become much larger for the gaseous compounds (8% for the best fitting experimental values). These deviations are very close to the possible errors in the experimental values: an inspection of Table I will show that the discrepancies between experimental and theoretical values are not greater than the discrepancies between various experimental values reported by different authors.

We believe that this theory enables us to predict the diamagnetic susceptibilities of the alkanes with an accuracy of about 1%, especially for the higher alkanes this assertion seems to be supported by the values of Table I.

[7] G. Foëx, *Tables de Constantes et Données Numériques*, 7, *Constantes Sélectionnées, Diamagnétisme et Paramagnétisme*, (Masson et Cie, Editeurs, Paris, France, 1957).
[8] S. Broersma, J. Chem. Phys. **17**, 873 (1949).
[9] F. Bitter, Phys. Rev. **33**, 389 (1929).
[10] J. R. Lacher, J. W. Pollock, W. E. Johnson, and J. D. Park, J. Am. Chem. Soc. **73**, 2838 (1951).
[11] A. Fava and A. Iliceto, Ricerca sci. **24**, 1652 (1954).
[12] B. Cabrera, J. chim. phys. **38**, 1 (1941).
[13] R. Manzoni-Ansidei, Boll. sci. fac. chim. ind. univ. Bologna **5**, 5 (1944).
[14] V. C. G. Trew, Trans. Faraday Soc. **49**, 604 (1953).
[15] P. W. Selwood, *Magnetochemistry* (Interscience Publishers, Inc., New York, 1956), p. 91.

THE JOURNAL OF CHEMICAL PHYSICS VOLUME 34, NUMBER 6 JUNE, 1961

Theory of the Surface Tension of Molten Salts*

H. REISS AND S. W. MAYER

Atomics International,† Research Department, Canoga Park, California

(Received November 22, 1960)

A theory of the surface tension of molten salts is presented, based on a result obtained by Reiss, Frisch, Helfand, and Lebowitz and a theory of corresponding states. This theory allows one to compute the surface tension of a salt if the diameters of the ionic hard cores are known along with the densities of the salts at a given temperature. Agreement with experiment is very good.

I. INTRODUCTION

THE literature contains a wealth of experimental information concerning the surface tension of molten salts, but to date there has been no satisfactory molecular theory for this parameter. The principal objective of the present paper is to supply an improved theory.

The starting point is a relation furnished by Reiss, Frisch, Helfand, and Lebowitz[1] in a recent treatment of the molecular theory of fluids. This relation will be modified with the aid of a theory of corresponding states for molten salts.[2] The relation we have in mind is Eq. (1.2) of Reiss *et al.* It specifies the surface tension σ of a one-component liquid of spherical molecules possessing hard cores of diameter a. The equation follows

$$\sigma=(kT/4\pi a^2)\{[12y/(1-y)]+[18y^2/(1-y)^2]\}-(pa/2). \quad (1.1)$$

Here k is the Boltzmann constant, T the absolute temperature, p the pressure, and

$$y=\pi a^3\rho/6, \quad (1.2)$$

where ρ is the concentration of molecules in the liquid. Usually the term $pa/2$ is of negligible magnitude and can be ignored. Thus, given the temperature, the concentration (density), and the hard-core diameter, one can compute the surface tension.

Strictly speaking, Eq. (1.1) does not specify the surface tension of a liquid against its own vapor, but rather that of a liquid in contact with a perfectly rigid wall which has no attraction for the molecules of the liquid. Nevertheless, the original authors[1] thought that the two tensions ought to have been very similar so that Eq. (1.1) could be used as a good approximation to the real surface tension. The rationale for this was the idea that because a real interface existed between vapor and liquid, a set of boundary forces equivalent to an external wall was actually present in the real case. Excellent agreement with experiment was indeed achieved[1] for the liquids neon, argon, helium, hydrogen, nitrogen, oxygen, and benzene.

Before developing this theory to suit our present needs, it is probably worthwhile to consider, at least briefly, the foundations upon which it rests. For the rigorous justification of such ideas the reader must refer to the original papers,[1,3] but still some sense of the central theme can be given in a few paragraphs.

Everything rests on the fact that it is possible to express $W(r)$, the reversible work which must be expended in the production of a spherical cavity of radius r in the fluid, in the following form,

$$W(r)=(\tfrac{4}{3}\pi r^3)p+4\pi r^2\sigma[1-(4\delta/r)]+\epsilon. \quad (1.3)$$

The only parameters in Eq. (1.3) which have not been defined previously are δ and ϵ. The quantity δ has the dimension of length and may depend upon ρ and T, while ϵ is another quantity (very small) which may depend upon ρ and T and has the dimensions of energy. Actually, the validity of Eq. (1.3) is limited to the range $r>a/2$.

Although Eq. (1.3) can be derived from strictly molecular considerations,[3] it is both instructive and satisfying to find it consistent with the macroscopic requirements of thermodynamics. For example, consider Eq. (1.3) when r/a is very large compared to unity. Since δ is of the order of a and ϵ is very small, the asymptotic form of $W(r)$ is

$$W(r)=(\tfrac{4}{3}\pi r^3)p+4\pi r^2\sigma. \quad (1.4)$$

The first term on the right is just pv, where v is the volume of the cavity, and represents simply the volume work performed in pushing back the liquid to form the cavity. The second term is σA, where A is the interfacial area between the cavity and the liquid. Thus, the second term is the surface work associated with the production of the cavity. Since $r/a\gg1$, we are dealing with a macroscopic cavity to which thermodynamic reasoning should apply. In fact, Eq. (1.4) has exactly the form required by thermodynamics.

* Work performed under contract to the U. S. Atomic Energy Commission.

† A division of North American Aviation.

[1] H. Reiss, H. L. Frisch, E. Helfand, and J. L. Lebowitz, J. Chem. Phys. **32**, 119 (1960).

[2] H. Reiss, S. W. Mayer, and J. Katz, J. Chem. Phys. (to be published).

[3] H. Reiss, H. L. Frisch, and J. L. Lebowitz, J. Chem. Phys. **31**, 369 (1959).

TABLE I. Calculated and observed surface tensions of molten salts.

Molten salt	Temp. (°C)	Density (g/cm³)	Gas equilibrium distance (A)	σ obs (d/cm)	σ calc (d/cm)
			Uni-univalent		
NaCl	1000	1.448[a]	2.361[e]	98[d]	111
NaBr	900	2.217[a]	2.502[e]	91[d]	95
NaI	700	2.704[a]	2.712[e]	84[d]	75
KCl	900	1.452[a]	2.667[e]	90[d]	96
KBr	800	2.073[a]	2.821[e]	85[d]	87
KI	800	2.334[a]	3.048[e]	69[d]	76
RbCl	828	2.024[b]	2.787[e]	89[b]	81
RbBr	831	2.542[b]	2.945[e]	81[b]	83
RbI	772	2.719[b]	3.177[e]	72[b]	72
CsF	826	3.456[b]	2.345[e]	96[b]	85
CsCl	830	2.592[b]	2.906[e]	78[b]	79
CsBr	808	2.915[b]	3.072[e]	72[b]	76
CsI	821	2.953[b]	3.315[e]	63[b]	70
			Uni-divalent		
$BaCl_2$	1000	2.982[e]	2.82[i]	157[j]	152
$CdCl_2$	600	3.366[f]	2.21[i]	83[k]	79
$HgCl_2$	293	4.670[g]	2.29[i]	56[l]	36
$HgBr_2$	241	5.113[b]	2.41[i]	65[l]	37
			Uni-trivalent		
$BiCl_3$	271	3.554[b]	2.48[m]	66[b]	52
$BiBr_3$	281	4.099[b]	2.63[m]	64[b]	47

[a] L. Yaffe and E. R. Van Artsdalen, J. Phys. Chem. **60**, 1125 (1956).
[b] F. M. Jaeger, Z. anorg. Chem. **101**, 1 (1917).
[c] A. Honig, M. Mandel, M. L. Stitch, and C. H. Townes, Phys. Rev. **96**, 629 (1954).
[d] H. Bloom and J. O'M. Bockris, *Modern Aspects of Electrochemistry* (Academic Press, Inc., New York, 1959), Vol. 2, p. 198.
[e] P. W. Huber, E. V. Potter and H. W. St. Clair. U. S. Bureau of Mines, Report of Investigations, No. 4858 (1952).
[f] N. K. Boardman, A. Dorman and E. Heymann, J. Phys. Chem. **53**, 375 (1949).
[g] G. J. Janz, C. Solomons, and H. J. Gardner, Chem. Revs. **58**, 481 (1958).
[h] G. J. Janz and J. D. McIntyre, Ann. N. Y. Acad. Sci. **79**, 790 (1960).
[i] P. A. Akishin and V. P. Spiridonov, Kristallografiya **2**, 475 (1957).
[j] J. S. Peake and M. R. Bothwell, J. Am. Chem. Soc. **76**, 2656 (1954).
[k] N. K. Boardman, A. Palmer, and E. Heymann, Trans. Faraday Soc. **51**, 277 (1955).
[l] E. B. R. Prideaux and J. R. Jaratt, J. Chem. Soc. **1938**, 1203.
[m] H. A. Skinner and L. E. Sutton, Trans. Faraday Soc. **36**, 681 (1940).

A little thought should be given to the nature of σ. The cavity envisioned here is one from which the *centers* of all molecules are excluded. Thus, there can be no vapor in the cavity; it is not a bubble. As a result, the interface is not the usual one separating a liquid from its vapor; and the surface tension is not the usual interfacial tension. Instead, the cavity may be regarded as having been produced by the insertion of a rigid sphere of diameter b into the fluid, such that

$$r=(a+b)/2. \tag{1.5}$$

In Eq. (1.5), $a/2$ has been added to $b/2$ because when the boundary of the hard core of a molecule is in contact with the sphere of radius $b/2$, its *center* is still removed from the center of the hard sphere by an additional distance $a/2$ equal to its own radius. Since the cavity is defined in terms of the exclusion of the *centers* of molecules, its radius is given by Eq. (1.5). It is assumed by Reiss *et al.* that σ furnishes a good approximation to the usual liquid-vapor interfacial tension.

It is implicit in what has been said that the theory applies to spherical molecules strictly, and to those spherical molecules which possess cores that are reasonably rigid with well defined diameters a. Most spherical molecules meet this requirement; and we shall have more to say about it later.

Thermodynamic arguments[4] have been given to show that surface tension should depend upon curvature when the latter becomes very high (when r/a becomes small). In fact, the asymptotic dependence (for r small but not too small) can be accounted for by multiplying σ by a factor

$$1-(2\delta/r). \tag{1.6}$$

This is just the factor which appears in Eq. (1.3), except that 4 occurs where 2 should. This is because surface tension is usually defined as the coefficient of dA in the differential expression dW. Integration to obtain Eq. (1.3) introduces another factor of 2. Thus $W(r)$ continues to agree with thermodynamic requirements as r/a becomes smaller. The important point, however, is that molecular considerations[1,3] suggest that it is valid until $r/a=\frac{1}{2}$.

When $r/a=\frac{1}{2}$ or $r=a/2$, b in Eq. (1.5) is zero. This means that the hard sphere we have added to produce the cavity has shrunk to a point. Still, it produces a cavity of radius $a/2$ in the fluid. However, for $r\leqslant a/2$ the cavity is of such dimension that the center of only one molecule at a time could occupy the region occupied by the cavity if the latter were not present. This fact makes it possible co compute $W(r)$ *exactly* for $r\leqslant a/2$. The uniqueness of the point $r=a/2$ is such that Eq. (1.3) does not apply for values of r less than this.

The calculation of $W(r)$ for $r\leqslant a/2$ depends upon a general theorem[5] of statistical mechanics which says that if P is the probability of a molecular event (or series of coordinated events) and W is the reversible work required to produce the event through the application of constraints, then

$$P=\exp(-W/kT). \tag{1.7}$$

[4] R. C. Tolman, J. Chem. Phys. **16**, 758 (1948); **17**, 118, 333 (1949); J. G. Kirkwood and F. P. Buff, *ibid.* **17**, 338 (1949); F. P. Buff, *ibid.* **23**, 419 (1955).
[5] L. D. Landau and E. M. Lifshitz, *Statistical Physics* (Pergamon Press, New York, 1958), p. 351.

Thus, if we can calculate the probability of the random occurrence (by fluctuation) of a cavity of size r, we can use Eq. (1.7) to calculate W.

Now, the chance that a molecule is present in the region which would otherwise constitute the cavity is the sum of the chances that either one molecule, or two, or three, etc., are present. In this case only *one* molecule can be present, so it is the chance that one molecule is present. But this is simply

$$\tfrac{4}{3}\pi r^3\rho, \tag{1.8}$$

that is, the volume of the region times the bulk average concentration. The chance that the molecule is absent (the chance that the cavity exists) is just one minus this value, or

$$P=1-\tfrac{4}{3}\pi r^3\rho=\exp(-W/kT). \tag{1.9}$$

On taking logarithms,

$$W(r)=-kT\ln(1-\tfrac{4}{3}\pi r^3\rho). \tag{1.10}$$

Now, Reiss, Frisch, and Lebowitz[3] have shown that although the function $W(r)$ changes at $r=a/2$, still W, dW/dr, and d^2W/dr^2 are continuous at $r=a/2$. This means that W, dW/dr, and d^2W/dr^2 must be equal at $r=a/2$, whether computed from Eqs. (1.3) or (1.10). Thus we have three relations, which are sufficient to determine the functional forms of σ, δ, and ϵ in Eq. (1.3). This is precisely how σ of Eq. (1.1) is computed.

Equation (1.1) applies to a one-component system. The continuity conditions applied at $r=a/2$ have been derived only for a one-component system. However, they should apply also to a multicomponent solution, provided that the individual molecular species, though different, all have the same hard-core diameter a. A real molten salt is a multicomponent fluid, which seldom satisfies the latter requirement. Thus it will be necessary to modify the theory to account for this difference in core diameters.

In a paper to be published shortly the authors demonstrate that it is possible to develop a theory of corresponding states for molten salts. The result from this theory which is pertinent to our present development is that the equation of state for a purely ionic salt depends (aside from valence) only on the distance of closest approach between ions of opposite sign. Therefore, if the hard-core diameter of the cation is d_c and that of the anion d_a the properties of the salt do not depend upon d_c and d_a individually, but only on

$$a=\tfrac{1}{2}(d_c+d_a). \tag{1.11}$$

As a result we can employ Eq. (1.1) to compute σ for a hypothetical salt in which

$$d_c=d_a=a/2, \tag{1.12}$$

and in which, therefore, all distances of closest approach (cation-cation, anion-anion, anion-cation) are the same and equal to a. The result will be applicable to the surface tension for the real salt in which $d_c\neq d_a$ as long as Eq. (1.11) applies. This principle has been used in connection with Eq. (1.1) to compute the results which appear in the next section.

II. COMPARISON WITH EXPERIMENT

In order to compare Eq. (1.1) with experiment, it is necessary to have values for a. Since these represent distances of closest approach and not bond distances, reliable data are hard to acquire. However, a ought not to be much smaller than the corresponding bond distance. As an approximation, therefore, in view of the absence of the required data, we have used the equilibrium bond distances. The details of this choice are as follows.

The bond distance in the molecular salt (measured in the gas by electron diffraction or microwave techniques) was chosen for a.

The surface tensions computed with this choice should be slightly larger than the observed, since these values of radius are larger than the distance of closest approach.

In Table I we have collected the results of these calculations and compared them with experiment. Uni-univalent, uni-divalent, and uni-trivalent salts have been included. Column 5 lists the observed surface tension, while column 6 shows the result calcaulted, using Eq. (1.1) and employing the data on the corresponding line in columns 2–4. We observe that the agreement is good in all cases, except in the case of the salts of mercury.

Both $HgBr_2$ and $HgCl_2$ are known to have anomalously low conductivities in the molten state, and are thought to be un-ionized. This means that the radius of the separate particle is that of the molecule rather than the ion; that is, it is larger than would be expected for an ion. Thus the actual surface tension is larger; and the value computed with Eq. (1.1), assuming ionic radii, is relatively too small. It appears as though the anomalous state of ionization of the mercuric salts is reflected in the present data.

Madelung Constants for Several Structures*

QUINTIN C. JOHNSON† AND DAVID H. TEMPLETON

Lawrence Radiation Laboratory and Department of Chemistry, University of California, Berkeley, California

(Received December 12, 1960)

Madelung constants are given for 38 structures, some of which are relatively complex. The Madelung constants for binary compounds are compared with an empirical rule previously formulated.

DURING a series of calculations of the variation of lattice energy with respect to atomic parameters,[1] we have incidentally calculated many Madelung constants of known structures. These constants are reported here in the hope that other workers will find them useful.

The calculations were made with the IBM 704 computer according to Bertaut's method[2] with correction for series termination.[3] Some details of the computer program are described elsewhere.[4]

The structures, together with the values of the parameters that were used, are given in Table I. (The obvious cubic structures without parameters are not listed.) Table I gives the chemical formula of the compound, the space group, the cell constants (a, b, c, β), the symbol for the first element followed by its Wyckoff symmetry as described in the International Tables,[5] the x, y, and z parameters, the symbol of the second element, etc. If any cell constant or parameter is not necessary, no entry is made, and the next piece of information is listed. For example, consider β LaOF. The space group is $R\bar{3}m$, $a=4.0507$ A, $c=20.213$ A; lanthanum is in Wyckoff symmetry c, with $x=0.242$; oxygen is in Wyckoff symmetry c with $x=0.122$; and fluorine is also in Wyckoff symmetry c with $x=0.370$. No exhaustive survey of the literature was made in order to ascertain the latest values of the parameters.

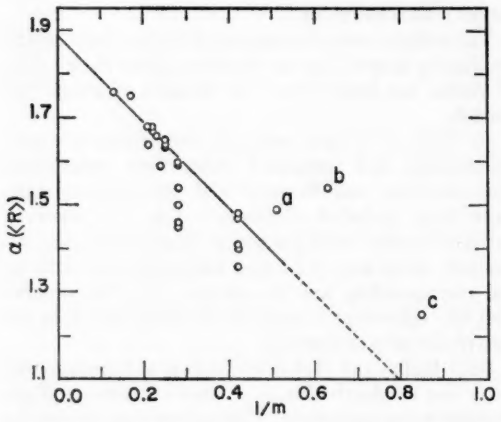

FIG. 1. Plot of the reduced Madelung constant, $\alpha(\langle R\rangle)$ vs the reciprocal of the weighted-harmonic-mean coordination number m. The lettered points are (a) V_2O_5, (b) LaF_3 considering only five nearest neighbors in the calculation of $\langle R\rangle$, and (c) SiF_4. The straight line is given by $\alpha=1.89-1/m$.

The results of the calculations are given in Table II. The shortest interatomic distance is denoted by R_0. In many cases more digits are listed than have chemical significance in order to ensure that (except in cubic cases) the mathematics is not the determining factor in the accuracy with which the Madelung constant is known. The second entry in Table II is the series termination correction for the Madelung constant. The Madelung constant based on R_0 as unit distance is denoted $A(R_0)$. Care should be exercised so that this is not mistaken for the Madelung constant based on the average shortest distance. For certain applications, this latter has more significance; it may readily be computed by multiplying the sixth entry in Table II $\langle R\rangle$ by $A(R_0)$ and dividing by R_0. The sixth entry in this table $\langle R\rangle$ was determined by taking the average distance of the p_c nearest neighbors of the cation.

The fourth entry β/π is a measure of where the series was terminated.[3] Because of the sensitivity of the Madelung constant to changes in the values of the structural parameters, no conscious effort was made to carry most of the calculations past a meaningful number of digits. Experience has shown that the last digit of $A(R_0)$ as listed here must be considered to be known with the accuracy of ± 1. This can be verified by comparison of the results for CaF_2, CsCl, Cu_2O, NaCl, and ZnS with more accurate values already published.[6] The values for the two CdI_2 structures confirm the results of Hartman[7] rather than the earlier values quoted by Sherman.[8]

* This work was performed under the auspices of the U. S. Atomic Energy Commission.

† Present address: Department of Chemistry, Lawrence Radiation Laboratory, University of California, Livermore, California.

[1] Q. C. Johnson, Lawrence Radiation Laboratory Report UCRL-9350 (August, 1960).

[2] E. F. Bertaut, J. phys. radium **13**, 499 (1952).

[3] D. H. Templeton, J. Chem. Phys. **23**, 1629 (1955); R. E. Jones and D. H. Templeton, *ibid.* **25**, 1062 (1956).

[4] D. H. Templeton and Q. C. Johnson, Proceedings of the Conference on Computing Methods and the Phase Problem in X-Ray Crystal Analysis, Glasgow, Scotland, August, 1960 (to be published).

[5] *International Tables for X-Ray Crystallography*, edited by N. F. M. Henry and K. Lonsdale (The Kynoch Press, Birmingham, England, 1952), Vol. 1.

[6] Y. Sakamota, J. Chem. Phys. **28**, 164 (1958).

[7] P. Hartman, Acta Cryst. **11**, 365 (1958).

[8] J. Sherman, Chem. Revs. **11**, 93 (1932).

TABLE I. Description of structures for which Madelung constants were calculated.

Compound	Structure
$AlCl_3$	*C2/m*; 5.93, 10.24, 6.17, 108°; Al-*g*, 0.167; Cl-*i*, 0.226, 0.219; Cl-*j*, 0.250, 0.175, 0.781
αAl_2O_3	*R*$\bar{3}$*c*; 4.7628, 13.0082; Al-*c*, 0.355; O-*e*, 0.303
$BeCl_2$	*Ibam*; 9.86, 5.36, 5.26; Be-*a*; Cl-*j*, 0.109, 0.203
BeO	$P6_3mc$; 2.698, 4.380; Be-*b*, (0.0); O-*b*, 0.365
BiSCl	*Pnma*; 7.70, 4.00, 9.87; Bi-*c*, 0.140, 0.138; S-*c*, 0.77, 0.04; Cl-*c*, 0.50, 0.79
$CaCl_2$	*Pnnm*; 6.25, 6.44, 4.21; Ca-*a*; Cl-*g*, 0.275, 0.325
$CaTiO_3$[a]	*Pm3m*; 3.84; Ca-*a*; Ti-*b*; O-*c*
$CdCl_2$	*R*$\bar{3}$*m*; 3.86, 17.50; Cd-*a*; Cl-*c*, 0.25
CdI_2 (Bozorth)	*P*$\bar{3}$*m*1; 4.240, 6.855; Cd-*a*; I-*d*, 0.25
CdI_2 (Hassel)	$P6_3mc$; 4.240, 13.710; Cd-*b*, 0.00; I-*b*, 0.625; I-*a*, 0.375
$LaCl_3$	$P6_3/m$; 7.483, 4.375; La-*d*; Cl-*h*, 0.287, 0.382
LaF_3	$P6_3/mmc$; 4.148, 7.354; La-*c*; F-*b*; F-*f*, 0.57
La_2O_3	*P*$\bar{3}$*m*1; 3.9373, 6.1299; La-*d*, 0.245; O-*a*; O-*d*, 0.645
LaOCl	*P4/nmm*; 4.119, 6.883; La-*c*, 0.178; O-*a*; Cl-*c*, 0.635
βLaOF	*R*$\bar{3}$*m*; 4.0507, 20.213; La-*c*, 0.242; O-*c*, 0.122; F-*c*, 0.370
γLaOF	*P4/nmm*; 4.091, 5.837; La-*c*, 0.778; O-*a*; F-*b*
$MgAl_2O_4$	*Fd3m*; 8.0800; Mg-*a*; Al-*d*; O-*e*, 0.387
MgF_2	$P4_2/mnm$; 4.623, 3.052; Mg-*a*; F-*f*, 0.31
SiF_4	*I*$\bar{4}$*3m*; 5.41; Si-*a*; F-*c*, 0.165
βSiO_2[b]	$P6_222$; 5.02, 5.48; Si-*c*; O-*j*, 0.197
$SrBr_2$	*Pnma*; 11.44, 4.31, 9.22; Sr-*c*, 0.811, 0.108; Br-*c*, 0.103, 0.119; Br-*c*, 0.614, 0.842
$TiCl_2$	*P*$\bar{3}$*m*1; 3.561; 5.875; Ti-*a*, Cl-*d*, 0.25
TiO_2 (rutile)	$P4_2/mnm$; 4.5929, 2.9591; Ti-*a*; O-*f*, 0.3056
TiO_2 (anatase)	$I4_1/amd$; 3.785, 9.514; Ti-*a*; O-*e*, 0.2064
TiO_2 (brookite)	*Pbca*; 9.184, 5.447, 5.145; Ti-*c*, 0.128, 0.098, 0.863; O-*c*, 0.008, 0.147, 0.182; O-*c*, 0.229, 0.110, 0.530
UD_3	*Pm3n*; 6.64; U-*a*; U-*c*; D-*k*, 0.155, 0.31
V_2O_5	*Pmmn*; 11.519, 3.564, 4.373; V-*f*, 0.1486, 0.105; O-*f*, 0.149, 0.458; O-*f*, 0.320, 0.000; O-*a*, 0.000
YCl_3	*C2/m*; 6.92, 11.94, 6.44, 111.0°; Y-*g*, 0.166; Cl-*i*, 0.211, 0.247; Cl-*j*, 0.229, 0.179, 0.760
YF_3	*Pnma*; 6.353, 6.850, 4.393; Y-*c*, 0.3686, 0.0595; F-*c*, 0.527, 0.577; F-*d*, 0.180, 0.074, 0.364
Y_2O_3	*Ia*3; 10.604; Y-*b*; Y-*d*, 0.970; O-*e*, 0.385, 0.145, 0.380
YOCl	*P4/nmm*; 3.903, 6.597; Y-*c*, 0.18; O-*a*; Cl-*c*, 0.64
ZnO	$P6_3mc$; 3.2495, 5.2069; Zn-*b*, (0.0); O-*b*, 0.345
ZnS	$P6_3mc$; 3.819, 6.246; Zn-*b*, (0.0); S-*b*, 0.375

[a] Ideal perovskite.
[b] High-temperature quartz.

The last two columns in Table II prove useful in checking against blunders in computation. Templeton has observed that the reduced Madelung constant,

$$\alpha(R_0)=2A(R_0)/z_a z_c n,$$

for several binary salt structures is approximately

$$\alpha=1.89-1/m,$$

where m, the weighted-harmonic-mean coordination number, is defined as[9]

$$1/m=(\sum n_i/p_i)/(\sum n_i).$$

In these relations, R_0 is the nearest-neighbor distance, z_a and z_c are the charge numbers of the anion and cation, respectively, n is the number of atoms per formula unit, and n_i is the number of atoms of one kind with coordi-

[9] D. H. Templeton, J. Chem. Phys. **21**, 2097 (1953).

TABLE II. Results of Madelung-constant calculations.

Compound	R_0	Correction	$A(R_0)$	β/π	p_c	$\langle R\rangle$	$1/m$	$\alpha(\langle R\rangle)$
$AlCl_3$	2.2953	0.002	8.303	3	6	2.3165	0.42	1.40
αAl_2O_3	1.8478	0.006	24.242	3	6	1.9174	0.22	1.68
$BeCl_2$	2.0170	0.0011	4.086	3	4	2.0170	0.42	1.36
BeO	1.5987	0.002	6.368	3	4	1.6493	0.25	1.64
BiSCl	2.7226	0.003	10.388	3	4	2.7367	...	...
$CaCl_2$	2.7083	0.0011	4.730	3	6	2.7501	0.28	1.601
CaF_2	2.360352	0.00007	5.03879	5	8	2.360352	0.21	1.68
$CaTiO_3$	1.92000	0.0004	24.7550	5	6	1.92000	...	...
$CdCl_2$	2.6633	0.0011	4.489	3	6	2.6633	0.28	1.50
CdI_2 (Bozorth)	2.988222	0.00007	4.38190	5	6	2.988222	0.28	1.46
CdI_2 (Hassel)	2.988222	0.00007	4.38409	5	6	2.988222	0.28	1.46
CsCl	3.570623	0.00002	1.76268	5	8	3.570623	0.13	1.76
Cu_2O	1.841170	0.00007	4.44249	5	2	1.841170	0.42	1.48
$LaCl_3$	2.9503	0.002	9.129	3	9	2.9801	0.28	1.54
LaF_3	2.3533	0.002	9.119	3	5 11	2.3782 2.5735	0.63 0.23	1.54 1.66
La_2O_3	2.3711	0.006	24.179	3	4	2.3913	0.25	1.63
LaOCl	2.3964	0.003	10.923	3	4	2.3964	...	...
βLaOF	2.4194	0.003	11.471	3	8	2.5038	...	...
γLaOF	2.42141	0.0002	11.3914	5	8	2.51619	...	...
$MgAl_2O_4$	1.9173	0.007	31.475	3	4	1.9173	...	...
MgF_2	1.9677	0.0011	4.762	3	6	1.9874	0.28	1.60
NaCl	2.813840	0.00002	1.74756	5	6	2.813840	0.17	1.75
βSiO_2	1.6191	0.004	17.609	3	4	1.6191	0.42	1.47
SiF_4	1.5461	0.004	12.489	3	4	1.5461	0.85	1.25
$SrBr_2$	3.1605	0.0011	4.624	3	7	3.2544	0.24	1.59
$TiCl_2$	2.5267	0.0011	4.347	3	6	2.5267	0.28	1.45
TiO_2 (anatase)	1.93743	0.0003	19.0691	5	6	1.94618	0.28	1.60
TiO_2 (brookite)	1.8424	0.004	18.066	3	6	1.9595	0.28	1.60
TiO_2 (rutile)	1.94511	0.0003	19.0803	5	6	1.95840	0.28	1.60
UD_3	2.0584	0.002	8.728	3	12	2.3252	0.21	1.64
V_2O_5	1.5437	0.01	44.32	3	5	1.8188	0.51	1.49
YCl_3	2.5845	0.002	8.313	3	6	2.6365	0.42	1.41
YF_3	2.1630	0.002	8.899	3	9	2.3213	0.28	1.59
Y_2O_4	2.2532	0.006	24.844	3	6	2.2741	0.22	1.67
YOCl	2.2844	0.003	10.916	3	4	2.2844	...	...
ZnO	1.796380	0.00009	5.99413	5	4	1.980843	0.25	1.65
ZnS (cubic)	2.340867	0.00009	6.55222	5	4	2.340867	0.25	1.64
ZnS (hexagonal)	2.339051	0.00009	6.56292	5	4	2.339850	0.25	1.64

nation number p_i. For structures with several nearest neighbors at slightly different distances, it is perhaps more useful to consider a reduced Madelung constant derived from $A(\langle R\rangle)$ rather than from $A(R_0)$. In Fig. 1 points are plotted corresponding to the $\alpha(\langle R\rangle)$ and $1/m$ values listed in Table II. The new values fall on or below the previously derived empirical line except for SiF_4, V_2O_5, and LaF_3—three structures which involve some of the atoms in onefold coordination. This coordination number was not encountered in the previous study, and the correlation is not accurate in such cases. The LaF_3 case is ambiguous in that La has one neighbor at 2.35 A, four at 2.39 A, and six others at 2.74 A. The correlation fails if only the five shortest distances are considered but agrees well if all 11 are included. Only the former case corresponds to onefold coordination for some of the fluorine atoms.

It is interesting that the reduced Madelung constant for an isolated tetrahedral SiF_4 molecule is 1.23, compared with 1.25 for the crystal; the crystal, therefore, has hardly any Coulomb contribution to its molecular cohesion.

THE JOURNAL OF CHEMICAL PHYSICS VOLUME 34, NUMBER 6 JUNE, 1961

Positive and Negative Ion Formation in CCl_3F

R. K. CURRAN

Westinghouse Research Laboratories, Pittsburgh 35, Pennsylvania

(Received November 23, 1960)

A mass spectrometer with an ion source utilizing nearly monoenergetic electrons was used to measure appearance potentials of positive and negative ions in CCl_3F. Kinetic energy measurements were made on the negative ions. The results have lead to values for the ionization potentials of CCl_3, CCl_2F, and $CClF$. The C—F and C—Cl bond energies have been determined from measurements on the negative fluorine and chlorine ions. A value is given for the electron affinity of the CCl_3 radical.

I. INTRODUCTION

THE CCl_3F molecule has been studied by Warren and Craggs[1] who measured appearance potentials for positive ion formation. Negative ion formation by electron impact has not been reported. It is the purpose of this paper to report the results of a recent study of positive and negative ion formation in CCl_3F.

II. APPARATUS

The mass spectrometer used has been described previously.[2] Ion detection for the present work was accomplished with a Faraday cage and a vibrating-reed electrometer. Sinde the analyzer was operated at high voltage and the collector at ground potential, the retarding curve for ion kinetic energy could be traced out by varying the potential of the ion source with respect to ground.

The ion source was equipped for the RPD method.[3] The maximum half-width of the electron distributions used was about 0.3 ev. The energy scale for positive ions was calibrated with Xe^+ from Xe and CO^+ from CO. The energy scale for negative ions was calibrated from the electron retarding curve. The onset for the fastest electrons in the distribution was taken as zero energy.

Linear extrapolation or vanishing current were used to determine potentials for positive ions depending on the shape of the ionization efficiency curve. Vanishing current was used whenever the ionization efficiency exhibited tailing which could not be attributed to the finite width of the electron distribution. Linear extrapolation is the preferred method, since once a linear region is established, the position of the extrapolated intercept with the electron-energy scale is independent of ion detection sensitivity.

Negative ion appearance potentials were determined as the electron energy at vanishing ion current. All data shown are representative data with corrected electron energy scales.

III. RESULTS

The results for positive ions are shown in Table I along with the results of Warren and Craggs.[1] The large discrepancy between the present value of 12.77 ± 0.15 ev for the appearance potential of CCl_3^+ and that obtained by Warren and Craggs is undoubtedly due to the difficulty they encountered with appearance potential measurements for low abundance ions or ions with unusual ionization efficiency curves. The CCl_3^+ has a low abundance and furthermore has breaks in its ionization efficiency. A linear extrapolation, such as

[1] J. W. Warren and J. D. Craggs, *Mass Spectrometry* (Institute of Petroleum, London, 1952), p. 36.
[2] R. E. Fox, *Advances in Mass Spectrometry* (Pergamon Press, New York, 1959), p. 397.
[3] R. E. Fox, W. M. Hickam, D. J. Grove, and T. Kjeldaas, Jr., Rev. Sci. Instr. **26**, 1101 (1955).

TABLE I. Positive ion appearance potentials and breaks in the ionization efficiency curves.

	Appearance potential	Breaks	Footnote 1 appearance potentials
CCl_3^+	12.77±0.15	14.3±0.2, 15.5±0.2	13.8±0.2
CCl_2F^+	11.97±0.07	...	12.27±0.05
$CClF^+$	17.41±0.15	18.8±0.2	17.0±0.1

Warren and Craggs suggest, from above the break at 14.3±0.2 ev would give a value near 14 ev for the appearance potential. The CCl_3^+ ion current versus electron energy is shown in Fig. 1.

No structure was observed in the ionization efficiency of CCl_2F^+. The ionization efficiency has, however, a region of curvature for about 1.5 v above threshold.

Three low-energy processes were observed leading to negative ion formation. Figure 2 shows the F^- current versus electron energy. The appearance potential of this ion is 1.80±0.10 ev. Figure 3 is a plot of F^- kinetic energy versus electron energy. It clearly shows the onset of a new process at 2.60±0.05 ev. It therefore seems reasonable that the structure in Fig. 2 between threshold and 2.7 ev represents processes leading to F^- formation with zero kinetic energy.

Figure 4 shows the Cl^- current versus electron energy. It appears in the range 0–0.05 ev. The shape of the Cl^-/CCl_3F current curve is very similar to the shape of the Cl^-/CCl_4 current curve.[4] The true cross section apparently rises very sharply at zero electron energy and then tapers slightly toward high energies, thus having the over-all "triangular" shape mentioned in footnote 4 for Cl^- from CCl_4. The Cl^-/CCl_3F process does not exhibit a second peak at low energy as does[4] Cl^-/CCl_4. This is presumably because of the loss of some symmetry in the molecule as a result of replacing a Cl atom by an F atom. The kinetic energy of Cl^-/CCl_3F was measured as 0.40±0.05 ev. This is the same value[4] obtained for Cl^-/CCl_4.

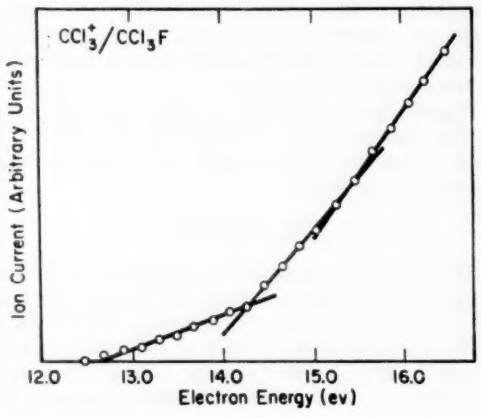

FIG. 1. CCl_3^+ current vs electron energy. The electron energy scale has been corrected with the Xe^+ ion.

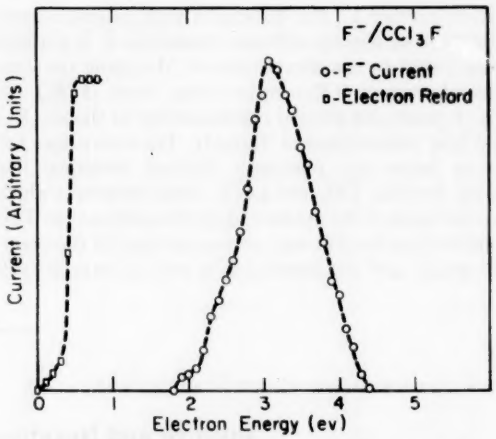

FIG. 2. F^- current vs electron energy. The structure above onset presumably represents processes with zero kinetic energy as verified in Fig. 3. The electron retarding curve determines the zero of the energy scale.

Figure 5 is the CCl_3^- current versus electron energy. The onset for this process is 2.75±0.10 ev. No kinetic energy was observed for this ion.

IV. DISCUSSION

1. $D(CCl_3—F)$

A measure of the dissociation energy of the C—F bond $D(CCl_3-F)$ is obtained by noting that

$$D(CCl_3-F)+KE_{total}\leq AP(F^-)+EA(F).$$

The measured kinetic energy of the F^- ion was zero thus, $KE_{total}=0$. The appearance potential of F^- is $AP(F^-)=1.80\pm0.10$ ev; and the electron affinity[5] of F

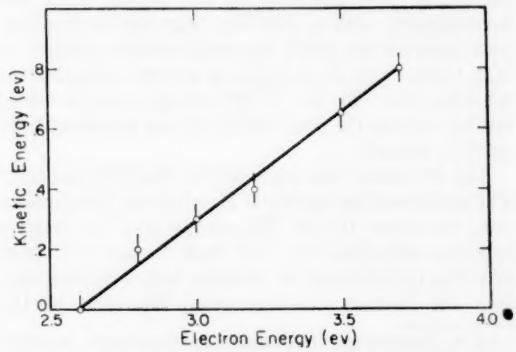

FIG. 3. Kinetic energy of F^- ion vs electron energy. The intercept at 2.60 ev shows that F^- current in Fig. 1 below 2.6 ev must arise from processes yielding F^- ions with zero kinetic energy.

[4] R. E. Fox and R. K. Curran (to be published).

[5] H. O. Pritchard, Chem. Revs. **52**, 529 (1953).

is $EA(F)=3.62\pm0.09$ ev. Substitution of these values in the above equation yields $D(CCl_3-F)\leq5.42\pm0.15$ ev. This is to be compared with $D(CCl_3-F)$ derived from the dissociation energy[6] $D(CCl_3-Cl)=78.2$ kcal/mole or 3.39 ev obtained thermochemically. Using this value of $D(CCl_3-Cl)$ with [6,7]$\Delta H_f(CCl_4)=-25.5$ kcal/mole and $\Delta H_f(Cl)=28.5$ kcal/mole, one has $\Delta H_f(CCl_3)=24.2\pm4$ kcal/mole. Then from[8] $\Delta H_f(CCl_3F)=-70\pm4$ kcal/mole, and $\Delta H_f(F)=18.5\pm4$ kcal/mole, one obtains $D(CCl_3-F)=112.7\pm7$ kcal/mole or 4.85 ± 0.30 ev, in agreement with the results obtained above.

2. $I(CCl_3)$

Recalling that the appearance potential of CCl_3^+ was $AP(CCl_3^+)=12.77\pm0.15$ ev and since

$$D(CCl_3-F)+I(CCl_3)+KE_{total}\leq AP(CCl_3^+),$$

one may calculate $I(CCl_3)$ using the value $D(CCl_3-F)\leq5.42\pm0.15$ ev obtained above. It will be assumed that $KE_{total}=0$. Although the kinetic energy of the CCl_4 was observed as being less than 0.05 ev, the fluorine atom fragment could have been carrying as much as 0.3 ev kinetic energy. The assumption of $KE_{total}=0$ will thus result in any estimate of $I(CCl_3)$ being too high by at most about 0.3 ev in the event that the CCl_3^+ ion carries some kinetic energy in the range of zero to 0.05 ev.

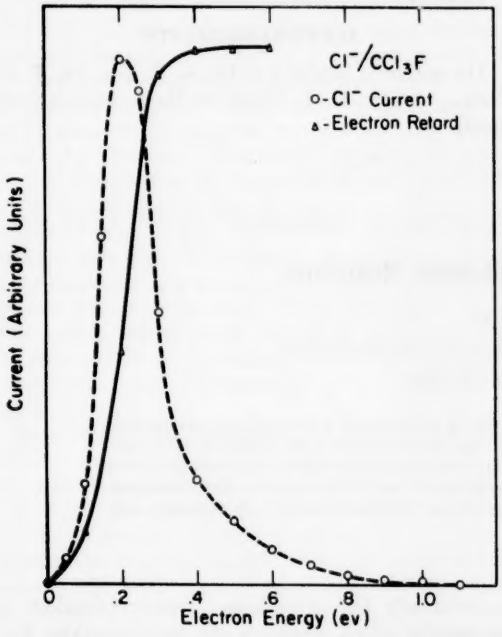

FIG. 4. Cl^- current vs electron energy. This closely resembles the Cl^-/CCl_4 of footnote 4. The electron retarding curve determines the zero of the energy scale.

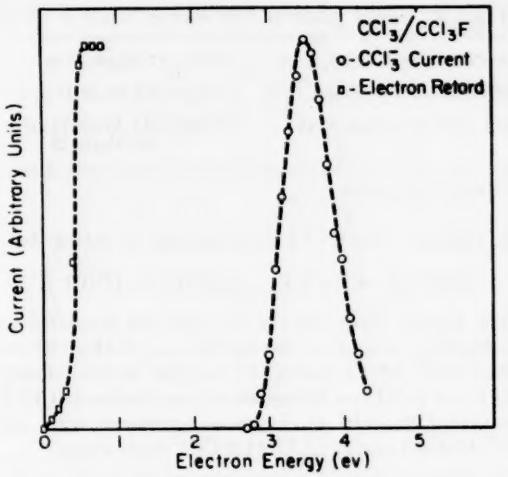

FIG. 5. CCl_3^- current vs electron energy. The electron retarding curve determines the zero of the energy scale.

On substitution for $AP(CCl_3^+)$ and $D(CCl_3-F)$ in the above equation it should be noted that $AP(CCl_3^+)-D(CCl_3-F)\geq7.35\pm0.25$ ev. Thus one obtains $I(CCl_3^+)\geq7.35\pm0.25$ ev.

This value for $I(CCl_3^+)$ is to be compared with that obtained using the thermochemical value[6,7] of $D(CCl_3-Cl)=3.39$ ev, which has been verified by electron impact[4] in CCl_4. From electron impact experiments[4,9] the appearance potential of CCl_3^+ from CCl_4 is 11.67 ± 0.10 ev, which then requires that $I(CCl_3)\leq8.28\pm0.15$ ev. The results of Farmer *et al.*[9] give $I(CCl_3)=8.78\pm0.05$ ev which requires $D(CCl_3-Cl)=2.89$ ev in disagreement with thermochemical[6,7] and other electron impact[4] data.

It should be pointed out that if one assumes the thermochemical value of $D(CCl_3-F)=4.85\pm0.30$ ev is more nearly correct than the electron impact value of $D(CCl_3-F)\leq5.42\pm0.15$ ev, by allowing for some internal energy to be carried off by the CCl_3 fragment in the F^- formation from CCl_3F, the present value of $I(CCl_3)$ would become 7.92 ± 0.35 ev in agreement with the value $I(CCl_3)\leq8.28\pm0.15$ ev. Thus, it seems reasonable to conclude that the value $I(CCl_3)\leq8.28\pm0.15$ obtained by electron impact in CCl_4 is the more accurate value for the ionization potential of the CCl_3 radical.

3. $D(CCl_2F—Cl)$

The measurement of the appearance potential and the kinetic energy of the Cl^- ion in CCl_2F allows one

[6] T. L. Cottrell, *The Strengths of Chemical Bonds* (Butterworths Scientific Publications, Ltd., London, 1958).
[7] A. G. Gaydon, *Dissociation Energies* (Chapman and Hall, Ltd., London, 1953).
[8] F. W. Kirkbride and F. G. Davidson, Nature **174**, 79 (1954).
[9] J. B. Farmer, I. H. S. Henderson, F. P. Lossing, and D. G. H. Marsden, J. Chem. Phys. **24**, 348 (1956).

TABLE II. Derived quantities from electron impact in CCl_3F.

$D(CCl_3-F) \leq 5.42 \pm 0.15$ ev	$I(CCl_3) \geq 7.92 \pm 0.35$ ev
$D(CCl_2F-Cl) \leq 3.28 \pm 0.10$ ev	$I(CCl_2F) \leq 8.69 \pm 0.15$ ev
$EA(CCl_3) \geq 2.10 \pm 0.35$ ev	$I(CClF) \leq 13.33 \pm 0.25$ or[a] 10.85 ± 0.25

[a] Cf. discussion in text.

to determine the C—Cl bond strength by noting that

$$D(CCl_2F-Cl)+KE_{total} \leq EA(Cl)+AP(Cl^-).$$

The kinetic energy of the Cl^- ion was measured as 0.40 ± 0.05 ev and so one has $KE_{total}=0.54 \pm 0.05$ ev. Now with $AP(Cl^-)=0 \pm 0.05$ and the electron affinity of Cl as[5] $EA(Cl)=3.82 \pm 0.06$ ev one obtains $D(CCl_2F-Cl) \leq 3.28 \pm 0.10$ ev in good agreement with the C—Cl bond energy of 3.39 for CCl_4 given above.

4. $EA(CCl_3)$

For the process leading to CCl_3^- formation in CCl_3F one may write

$$D(CCl_3-F)+KE_{total} \leq AP(CCl_3^-)+EA(CCl_3).$$

As in the case of CCl_3^+ the kinetic energy of CCl_3^- was measured as less than 0.05 ev. The assumption made here that the $KE_{total}=0$ may result in about a 0.3 ev error at maximum in the derived $EA(CCl_3)$. In the discussion of $I(CCl_3)$ it was pointed out that the thermochemical value of $D(CCl_3-F)=4.85 \pm 0.30$ ev is probably more reliable than that obtained by electron impact formation of F^- since the CCl_3 fragment can carry off internal energy and for this reason the thermochemical value is used here. With $AP(CCl_3^-)=2.75 \pm 0.10$ ev the resultant value for the electron affinity of CCl_3 is $EA(CCl_3) \geq 2.10 \pm 0.35$ ev.

5. $I(CCl_2F)$

Since $AP(CCl_2F^+)=11.97 \pm 0.07$ ev and $I(CCl_2F)+D(CCl_2F-Cl) \leq AP(CCl_2F^+)$, one has $I(CCl_2F) \leq 8.69 \pm 0.15$ ev using the value $D(CCl_2F-Cl) \leq 3.28 \pm 0.10$ ev obtained above.

6. $I(CClF)$

Taking $AP(CClF^+)=17.41 \pm 0.15$ ev as measured and assuming neutral Cl atom fragments with zero kinetic energy one obtains from

$$I(CClF^+)+2D(CCl_2F-Cl) \leq AP(CClF^+)$$

that $I(CClF^+) \leq 10.85 \pm 0.25$ ev. If the neutral fragment is a Cl_2 molecule then $I(CClF^+) \leq 13.33 \pm 0.25$ ev, using[7] $D(Cl_2)=2.48$ ev. There is no *a priori* reason for preference of either one of these values for the ionization potential.

Table II summarizes the above results.

ACKNOWLEDGMENTS

The author is indebted to Dr. R. E. Fox, Dr. A. V. Phelps, and Dr. G. J. Schulz for their valuable comments.

THE JOURNAL OF CHEMICAL PHYSICS VOLUME 34, NUMBER 6 JUNE, 1961

Kinetic Model for Solid-State Reactions

R. E. CARTER

General Electric Research Laboratory, Schenectady, New York

(Received November 25, 1960)

A model for solid-solid or solid-gas reactions between spherical particles and a fine powder or gas has been developed. The oxidation of uniformly sized nickel spheres has been shown to fit this model to 100% reaction. Previously reported models are inadequate because they do not meet the boundary conditions set down and because the volume of the product was assumed to equal that of one of the reactants. The inadequacy of earlier experimental results has been explained by the failure to experimentally meet the boundary conditions imposed.

INTRODUCTION

IN 1927, Jander published a model of the kinetics of solid-state reactions.[1] Since then a number of workers have analyzed their data in terms of this model.[2-4] Unfortunately Jander made two oversimplifications in his analysis which invalidate the final equation. The purpose of this study was to develop an equation for the rate of reaction of spherically shaped particles with either another solid or a gas.

THEORY

Jander considered a sphere of radius r of component A, the complete surface of which was reacting with

[1] W. Jander, Z. anorg. u. allgem. Chem. **163**, 1 (1927).
[2] G. Economos and T. R. Clevenger, Jr., J. Am. Ceram. Soc. **403**, 48 (1960).
[3] Y. Iida, J. Japan Soc. Powder Met. **6**, 11 (1959).
[4] P. J. Jorgensen, M. E. Wadsworth, and I. B. Cutler, J. Am. Ceram. Soc. **42**, 613 (1959).

component B and developing a reaction product of thickness y. Furthermore he assumed that the reaction was diffusion limited. The rate of thickening of the reaction product was assumed inversely proportional to its thickness

$$dy/dt = k/y. \tag{1}$$

Integration of (1) gave

$$y^2 = 2kt. \tag{2}$$

The volume of unreacted material at time t was given as

$$V = (4/3)\pi(r-y)^3 \tag{3}$$

$$V = (4/3)\pi r^3(1-x), \tag{4}$$

where x is the fraction of the original sphere which has reacted. Equating the right-hand sides of Eqs. (3) and (4) yields

$$y = r[1-(1-x)^{\frac{1}{3}}], \tag{5}$$

and on substituting y into (2) the well-known Jander relationship is obtained

$$[1-(1-x)^{\frac{1}{3}}]^2 = 2kt/r^2 = Kt. \tag{6}$$

A plot of $[1-(1-x)^{\frac{1}{3}}]^2$ versus t should therefore be a straight line.

There are two weaknesses in the above analysis. First, Eq. (1) is for the reaction of a plane surface. Obviously the rate of thickening of a spherical shell of the reaction product must depend upon the ratio of the areas of the outer to inner surfaces. This analysis would therefore be expected to hold for only small values of x where the ratio of these two surfaces is near unity and the surface can be considered to be plane.

The second simplification was made in equating the right-hand sides of Eqs. (3) and (4). These volumes are equal *only* when the volume of the sphere consisting of the unreacted part of component A and the reaction product is equal to the initial volume of component A. This equality will hold only if $x=0$, i.e., at the start of the reaction, or if the volumes of an equivalent of component A and an equivalent of the product are equal.

Since both of these criticisms become of greater importance as x increases, it is not surprising that all of the reported data examined[1-3] deviate from Eq. (6) at large values of x. Jander's own data fit the best of any, apparently because of greater care in experimentally meeting the boundary conditions of the model. Even here the experimental points depart from a straight line for values of x greater than 0.75. In addition these data depart from Eq. (6) for small values of x. The straight line drawn through the experimental points does not pass through the zero reaction point at zero time but cuts the time axis at about 4% of the time required to reach $x=0.75$.

In the analysis developed here, a sphere of component A of radius r_0 (Fig. 1) is considered to react over all of its surface with either a finely divided powder or a gas.

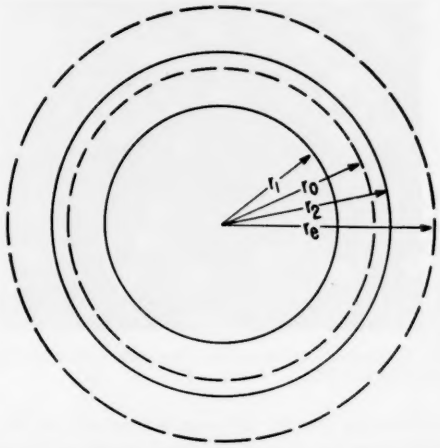

FIG. 1. Model for the reaction of a sphere of component A with component B. r_0=initial radius of A; r_1=instantaneous radius of A; r_e=radius of product at $x=1.0$; and r_2=instantaneous radius of unreacted A plus product.

Again the reaction is considered to be diffusion controlled. Let r_1 be the instantaneous value of the radius of component A, which must decrease from r_0 to zero as x goes from zero to one, r_e be the radius of the sphere of reaction product at $x=$one, and r_2 be the instantaneous radius of the sphere of unreacted component A plus the reaction product which must vary from r_0 to r_e. Finally allow z to represent the volume of product formed per unit volume of component A consumed, i.e., the ratio of the equivalent volumes.

The quantity Q_A of A present at any time t is

$$Q_A = (4/3)\pi r_1^3. \tag{7}$$

The rate of change of Q_A, equal to the flux of material diffusing through the spherical shell of thickness r_2-r_1, is given by[5]

$$dQ_A/dt = -4\pi k r_1 r_2/(r_2-r_1), \tag{8}$$

where k is the reaction rate constant.

Equation (8) is for a steady-state condition, one in which the gradient is fixed by the activity of the diffusing species at each interface and the thickness of the diffusion layer. The area for diffusion through a spherical shell increases as the square of the radius. The flux across each incremental thickness of the shell must be equal at all times, except for the small variation allowed by changes in the stoichiometry giving the gradient dc/dy. The product of the diffusion coefficient and the concentration gradient, Ddc/dy, at any time t must therefore vary across the diffusion layer as $1/r^2$.

A related assumption is made in deriving the parabolic law for the reacting of plane surfaces;

$$dy/dt = k/y. \tag{9}$$

[5] R. M. Barrer, Phil. Mag. **35**, 802 (1944).

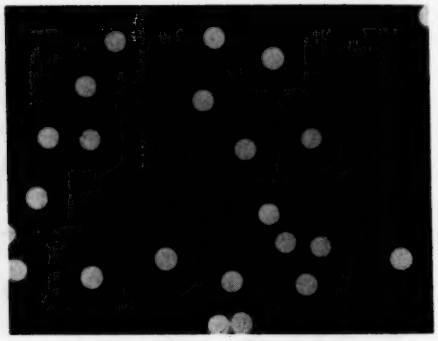

FIG. 2. Shadow photograph of 74-μ nickel spheres sized by double screening 48X.

Here since the area for diffusion is constant the product Ddc/dy must be a constant across the film. The parabolic law has been repeatedly shown to be valid for plane films and is so well accepted that experimental agreement with Eq. (9) has become the criterion for determining if an oxidation reaction is diffusion controlled.

The total volume of the sphere is made up of unreacted A plus the product layer, hence,

$$r_2^3 = zr_0^3 + r_1^3(1-z). \tag{10}$$

Allowing x to equal the fraction of A that has reacted, the radius of the reacted core may be written as

$$r_1 = (1-x)^{\frac{1}{3}} r_0. \tag{11}$$

Differentiating Eq. (7) with respect to time and equating to the right-hand side of Eq. (8), gives

$$r_1 dr_1/dt = -kr_2/(r_2 - r_1). \tag{12}$$

Substituting for r_2 from Eq. (10) yields

$$\left\{ r_1 - \frac{r_1^2}{[zr_0^3 + r_1^3(1-z)]^{\frac{1}{3}}} \right\} dr_1 = -kdt. \tag{13}$$

Integrating Eq. (13) from r_0 to r_1 with the substitution of $y^3 = (1-z)r_1^3 + zr_0^3$ one obtains

$$[(1-z)r_1^3 + zr_0^3]^{2/3} - (1-z)r_1^2 = zr_0^2 + 2(1-z)kt. \tag{14}$$

Substituting for r_1 from Eq. (11) gives

$$[1+(z-1)x]^{2/3} + (z-1)(1-x)^{2/3} = z + 2(1-z)kt/r_0^2. \tag{15}$$

A plot of the left-hand side of Eq. (15) against time should therefore give a straight line.

EXPERIMENTAL

None of the data in the literature are suitable for a critical examination of Eq. (15). First, most studies have not been carried out to sufficiently large values of x, and second, none of the data have been gathered from experiments which closely approach the boundary conditions of uniformly sized spheres with reaction occurring over all of the surface. Many investigators have made no effort to size their samples while the most careful workers have only screened out a so-called uniform size fraction. The openings of adjacent screens in even the close Tyler series, however, differ by a factor of 1.19. The ratio of the volumes of spheres whose diameter differ by this factor is 1.68. The small spheres will be completely reacted while an appreciable fraction of the largest spheres remain unreacted. A sample having this range of sizes will therefore have a reaction rate much faster during the early part of the reaction than during the later stages of the reaction. In addition no effort has been made to prepare spherical particles. Instead the poor assumption has been made that ground brittle materials consist of spheres. The initial surface area of a sample of such irregularly shaped particles will therefore be much larger than if the sample were made up of spheres. After the reaction has partially consumed the sample, however, the unreacted core of the particles will approach a spherical shape. The reacting surface area of such a powder will therefore decrease faster than allowed for in the above analysis and so the reaction rate will again be too low to fit Eq. (15) for large values of x.

Equation (15) was tested by measuring the oxidation rate of sized nickel spheres. Nickel was chosen because it forms only one oxide at normal oxidizing temperatures in one atmosphere of oxygen and because it is known to oxidize by the parabolic law.[6]

Spheres were made by dropping a +250 mesh carbonyl nickel powder through a shot tower held near 1600°C and filled with approximately half an at-

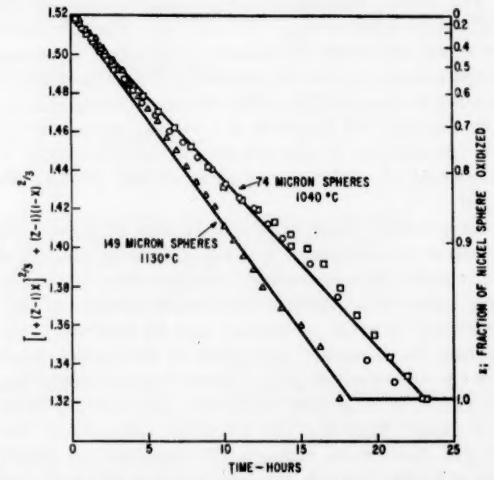

FIG. 3. Plots of $(1+(z-1)x)^{2/3} + (z-1)(1-x)^{2/3}$ vs time for the oxidation of nickel spheres in oxygen. □, ○, 74-μ spheres, 1040°C; △, 149-μ spheres, 1130°C.

[6] O. Kubaschewski and B. E. Hopkins, *Oxidation of Metals and Alloys* (Academic Press, Inc., New York, 1953).

mosphere of hydrogen. The spheres were then sized on almost new screens of the $2^{\frac{1}{4}}$ Tyler series. A $-80, +100$ and $a\ -170, +200$ mesh fraction were selected for the oxidation study. Because of the wide size variation in these fractions, the spheres were sized further as follows: Both fractions were screened again on 100 and 200 mesh screens, respectively, and the small amount of material which passed the screens was taken for the oxidation study. This sizing method although extremely wasteful of material gave very uniformly sized spheres.

The size and size distribution of the spheres so selected was measured microscopically. Because of their curvature and the shallow depth of field of the microscope at the 400 magnification used here, direct measurement of the spheres was impossible. Shadows cast by the spheres on the other hand could be accurately measured. A few spheres were spread on a microscope slide and shadowed with gold from a point source held ten inches away. This distance, which was at least 3400 times as great as the distance from the slide to the parallel great circle of the largest sphere, insured within the accuracy of these measurements that the shadow had a diameter identical to that of the sphere. After knocking the spheres from the slide, the shadows were measured at 400 magnification by means of a filar-eyepiece. A typical shadow pattern is shown in Fig. 2.

The measurement of one sphere ten times gave the standard deviation of the measurement to be 0.56% of the mean. The measurement of 20 spheres, after subtracting the variance in the measurement from the variance in the batch, gave a standard deviation of the sample of 1.65%. Assuming a Gaussian distribution, the diameters of essentially all of the spheres fall within $\pm 5\%$ of the mean (99.7% fall within ± 3 standard deviations of the mean). Although the size distribution of a sample falling between adjacent screens of the $2^{\frac{1}{4}}$ series is only twice the above limits, the distribution of such a sample is probably more than twice the distribution found for the double screened spheres. There are two reasons for this. A fraction cut by adjacent screens from a sample having a wide size distribution, such as the spheres from the shotting operation, can be expected to have a near rectangular size distribution. Second, because the screens and screening are never perfect, a wider distribution than the $2^{\frac{1}{4}}$ screen opening ratio is expected. To illustrate this point, a $-170, +200$ mesh fraction was measured as above, and again assuming a Gaussian distribution the standard deviation was 4.0% of the mean. Thus, 99.7% of the spheres fall within $\pm 12\%$ of the mean, exceeding the $\pm 9.5\%$ spread expected from the listed screen sizes. It must be admitted, however, that the specifications allow the maximum opening to exceed the design opening by up to 60%.

The nickel spheres were oxidized in $\frac{1}{4}$-in. diam platinum buckets, the bottoms of which were covered

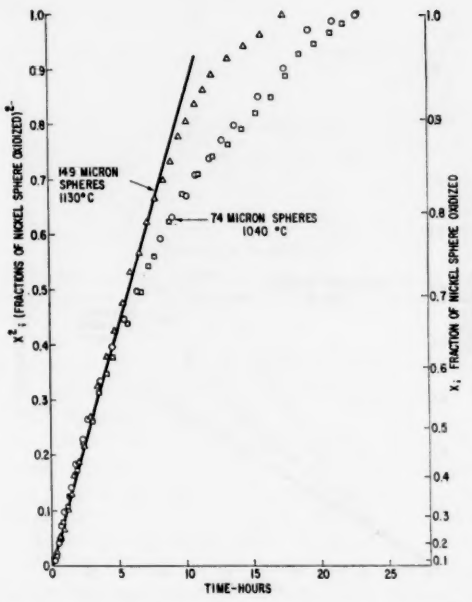

FIG. 4. Plots of x^2 vs time for the oxidation of nickel spheres in oxygen. □, ○, 74-μ spheres, 1040°C; △, 149-μ spheres, 1130° C.

with 80 mesh platinum screening. This screening prevented the spheres from piling up and so held them to approximately a single layer across the bottom of the bucket. All of the surfaces of the spheres were therefore free to oxidize. About 5 mg of spheres were placed in weighed buckets and reweighed, all weighings having an uncertainty of ± 10 μg. The buckets were suspended in cold furnaces from a continuously recording quartz torsion thermomicrobalance (Sartorius Electrona Micro-Balance, Model II). The sample and counterweight were then brought at the same rate to the oxidation temperature with a linear nitrogen flow of 165 cm/min over both assemblies. After about two hours at temperature, by which time the balance had become steady, ± 10 μg, the atmosphere was changed to oxygen at the same flow rate. Since it was impossible to calculate exactly when the oxygen replaced the nitrogen in contact with the sample, zero time was taken when the balance first recorded a weight gain, about two minutes after the gas change. Oxidation then proceeded isothermally until no further weight gain. Because the weight-time curve asymptotically approached a constant weight-time line, the time when gain in weight or oxidation ceased was difficult to determine. The run was therefore continued for several hours after the oxidation was thought to be complete. The last part of the weight-time curve was then extrapolated backwards as a constant weight line, and where it departed from the observed curve was taken as the time when oxidation was complete.

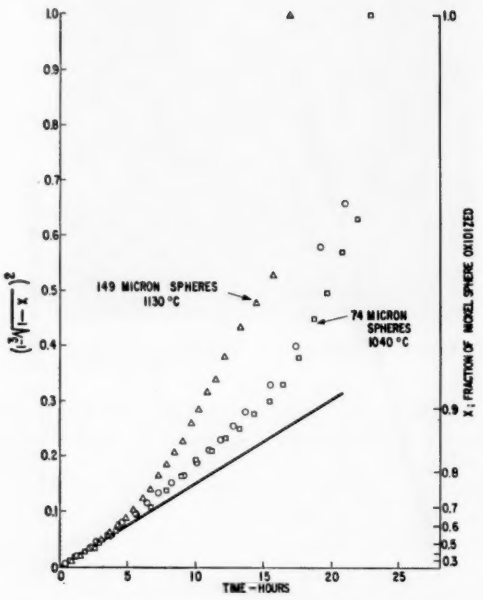

FIG. 5. Plots of $[1-(1-x)^{1/3}]^2$ vs time for the oxidation of nickel spheres in oxygen. □, ○, 74-μ spheres, 1040°C; △, 149-μ spheres, 1130°C.

RESULTS

The results for both sizes of spheres are plotted according to Eq. (15) in Fig. 3. For the oxidation of nickel to NiO, z equals 1.52. As shown both sizes of spheres gave good straight lines from $x=0$ to 1.0. Because of the difficulty of determining exactly when oxidation was complete and because the left side of Eq. (15) expands faster than x as x approaches one, the points at long oxidation times show increased scatter. Nevertheless, there is no systematic deviation from a straight line.

The "S" shaped deviation of the experimental points about the straight line may be real. If so, its cause is unknown. The departure from a straight line for the small spheres is the mirror image of the departure for the large spheres which would suggest that the "S" shape is an artifact.

Platinum is known to lose weight in oxygen at 1200°C.[7,8] During this study a surprisingly large loss was found at 1040°C. In 24 hr, the 0.4-g buckets lost about 90 μg which was an appreciable fraction of the 1350-μg weight gain of the oxidation. Fortunately the difference in weight loss between the sample and counterweight buckets was only about 15 μg, which could be ignored.

[7] R. E. Carter and F. D. Richardson, Research, Correspondence, **VII,** S3 (1954).
[8] A. Schneider and U. Esch, Z. Elektrochem. **49,** 55 (1943).

DISCUSSION

The good agreement between model and experiment shown in Fig. 3 demonstrates that experimentally the boundary conditions of the model can be successfully met. By such experiments most solid-solid or solid-gas reactions may be studied.

The slopes of the curves of Fig. 3 are proportional to (the reaction rate constant)/r_0^2. A plot of the reaction rate constant vs $1/T$ gave an energy of 67.3 kcal/mole. Considering that this energy was obtained from measurements at only two temperatures and that no effort was made to ensure the accuracy of the temperature or to ensure the purity of the nickel spheres, this energy is in reasonable agreement with reported energies for the migration of nickel ions in NiO.

Gulbransen and Andrew[9,10] report an energy of 41.2 kcal from an oxidation study, in good agreement with the 45 kcal given in the compendium of Kubaschewski and Hopkins.[6] Gulbransen and Andrew also report an energy of 68.3 kcal for oxidation above 900°C but believe that this value is without significance since the oxide layer cracked repeatedly during formation.[10] Shim and Moore[11] give 44.2 kcal, for the self-diffusion of nickel in NiO. From a slightly earlier study Lindner and Akerström[12] report 56 kcal for self-diffusion in NiO. J. Moore believes that there is probably a range of experimental values owing to differences in sample preparation.[13] He has recently found energies for diffusion of nickel in NiO ranging from 42–60 kcal, depending upon the experimental method used.

The inadequacy of the assumptions of earlier workers that the particle shape of ground brittle materials is spherical and the inadequacy of their sizing causes all of their data, when plotted according to Eq. (15), to curve below a straight line for values of x greater than approximately 0.5. These reactions appear to be too rapid during the early stages, due to the large surface area of the irregularly shaped particles. During the last stages of the reaction the rate is too slow, firstly because only a few larger particles are left to react, and secondly because of sintering of the particles together.

To plot the square of the amount of oxidation against time, Eq. (2), is to assume that the nickel spheres are planes of infinite extent. Such a plot, however, does not deviate from a straight line until values of x are between 0.6 and 0.8, Fig. 4. This is a slightly larger value of x than is reached on a Jander plot, Eq. (6), where departure is found at x between 0.5 and 0.6,

[9] E. A. Gulbransen and K. F. Andrew, J. Electrochem. Soc. **101,** 128 (1954).
[10] E. A. Gulbransen and K. F. Andrew, J. Electrochem. Soc. **104,** 451 (1957).
[11] Moon Taik Shim and W. J. Moore, J. Chem. Phys. **26,** 802 (1957).
[12] R. Linder and A. Akerstrom, Discussions Faraday Soc. No. **23,** 133 (1957).
[13] W. J. Moore, University of Indiana, Bloomington, Indiana (private communication).

Fig. 5. The straight-line portion of Fig. 4 is of course without significance except to illustrate that the mass of a sphere is proportional to r^3 while the area is proportional to r^2, so that for small amounts of reaction a sphere can be considered to be a plane. The earlier departure of the Jander plot from a straight line is probably due to equating the right-hand sides of Eqs. (3) and (4), as has been discussed.

Serin and Ellikson[14] have applied to solid-state reactions the well-known equation[15]

$$(1-x)=\frac{6}{\pi^2}\sum_{n=1}^{\infty}\frac{1}{n^2}\exp\left(-\frac{n^2\pi^2Dt}{r_0^2}\right)=\frac{6}{\pi^2}\sum_{n=1}^{\infty}\frac{1}{n^2}\exp(-n^2kt) \tag{16}$$

governing the flow of heat into a sphere having a zero initial temperature and a constant surface temperature. They have shown that Jander's[1] data on the reaction of $CaCO_3$ with SiO_2 and with MoO_3 follow Eq. (16) to a little less than 25% completion, where the data terminated.

Unfortunately experimental data cannot be easily plotted according to Eq. (16). A master plot of x vs kt, however, will give the value of kt for each experimental value of x. Knowing the experimental t for each experimental x, then allows the calculation of a k for each x. A plot of k vs x is shown in Fig. 6 for the oxidation of the nickel spheres. As shown, k is approximately constant to $x=0.9$ for 1040°C oxidations. The 1130°C data, however, depart at $x=0.7$. In all cases k increases sharply for x greater than 0.9 where the unreacted spheres have been reduced to approximately half their initial diameters. This increase may result because no volume change was allowed for in the development of Eq. (16).

The fit of the experimental data to oversimplified models up to 80% reaction illustrates the danger of drawing conclusions from data which extend even this far. To warrant any conclusions as to the validity of a model the data must fit the model to 100% reactions.

To determine if a solid state reaction is diffusion controlled, to determine the energy of activation, or to determine the relative reactivities of powders is relatively easy. The reacting particles need not be spherical nor of uniform size. It is only necessary that the sample be identical in all experiments, i.e., the particle shape and size distribution and the reacting areas be constant. The thickness of the reaction product is then proportional to the amount reacted for small amounts of reaction and the x^2 vs time plot will give all of the information required. If, however, the entropy is desired or the final stages of the reaction are to be studied,

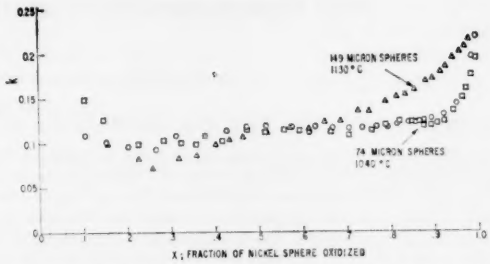

FIG. 6. Plot of k vs x [Eq. (16)] for the oxidation of nickel spheres in oxygen. □, ○, 74-μ spheres, 1040°C; △, 149-μ spheres, 1130°C.

the experimental conditions must meet the conditions of the model very closely, and the reaction must be followed to 100% completion.

The slope of the x^2 vs time plot is a function of both the particle size and shape as well as the temperature. If the particle size distribution and particle shape are constant between experiments, the slope of the straight line plot of the log of the slope of the x^2 vs time line against $1/T$ is proportional to the activation energy. The absolute slope of the x^2 vs time line is without significance so that the intercept of the log slope vs $1/T$ plot is not the entropy. The entropy can only be obtained by plotting the data to 100% reaction according to Eq. (15). The intercept of the plot of the log k vs $1/T$ is then proportional to the entropy.

CONCLUSIONS

A mathematical model of the kinetics of solid-state reactions has been developed and shown to be obeyed by the oxidation of nickel spheres to 100% reaction. The need to experimentally meet the boundary conditions of the model has been stressed and shown to be attainable. The lack of fit between the model and earlier experimental data is due to failure of earlier investigators to meet the boundary conditions of the model.

The fit between earlier, but simplified models and published rates, for small amounts of reaction, results because any shape of particle approximates a plane if only a thin layer of the particle is reacted. Inevitably, however, the observed rates depart from the models because of inadequacies in the models and because of insufficient experimental control over the size and shape of the reacting particles.

ACKNOWLEDGMENTS

The author wishes to thank R. L. Cormia for assistance in making the nickel spheres, P. D. S. St. Pierre for measuring the oxidation rate of the spheres, J. G. Leschen for the solution of Eq. (13), and W. J. Moore for permission to quote unpublished data.

[14] B. Serin and R. T. Ellickson, J. Chem. Phys. **9**, 742 (1941).
[15] H. S. Carslaw and J. C. Jaeger, *Conduction of Heat in Solids* (Clarendon Press, Oxford, England, 1959), 2nd ed.

Fluid Superposition Approximation and the Fourth Virial Coefficient

G. H. A. COLE

Physics Division, Clarke, Chapman & Co. Ltd., Gateshead, England

(Received November 14, 1960)

A new superposition approximation is given for relating the triplet distribution for a classical system of identical particles in interaction (fluid) to the pair distribution. The new approximation is based upon the well-known expression due to Kirkwood, but explicitly accounts for the particle density through a power series expansion. It is proposed that the coefficients of this expansion should be chosen in order to ensure internal consistency in the calculation of the virial coefficients of the pressure (when expressed in powers of the density) from either the pressure equation or the relative compressibility equation, and the necessary formulas are given. The equations are checked numerically for the ideal case of a gas of rigid spheres, as far as the fourth virial coefficient. The modified form of the original Kirkwood superposition approximation, which is the new approximation, is found for this case to be $g^{(3)}(r, s, t)=g^{(2)}(r)g^{(2)}(s)g^{(2)}(t)[1+0.1014bn]$ where $g^{(3)}$ is the triplet distribution, $g^{(2)}$ the pair distribution, n the particle number density, and b is equal to four times the volume of each particle. The theory then leads to a fourth virial coefficient of value $0.2885b^3$ which is to be compared with the exact value $0.2869b^3$. This value is found to be a marked improvement on the values calculated by previous authors. The higher powers of n in the new superposition approximation necessary for the correct calculation of higher virial coefficients than the fourth are not considered in this paper.

I. INTRODUCTION

ACCORDING to the modern kinetic theory of classical simple fluids, developed by Kirkwood,[1] Born and Green,[2] Yvon,[3] and others,[4] the thermodynamic properties can be related explicitly to the normalized dimensionless pair distribution function, written $g^{(2)}(\mathbf{r}_1, \mathbf{r}_2)$, where $\mathbf{r}_1$ and $\mathbf{r}_2$ are the simultaneous position vectors for the two particles. The pair distribution can be calculated by solving a first-order nonlinear integro-differential equation such as that given by Born and Green[2] [see Eq. (3) below], or the equivalent equation of Kirkwood and Boggs[5]; alternatively a second-order equation[6] can be used.

By invoking the virial theorem[2,4] the fluid pressure has been related to $g^{(2)}$, and for a monatomic fluid

$$p=nkT-(n^2/6)\int_0^\infty g^{(2)}(r)[\partial\psi(r)/\partial r]4\pi r^3 dr, \quad (1)$$

where $\psi(r)$ is the potential of the interparticle force, $n=N/V$ is the particle number density for the fluid composed of N identical particles contained in a volume V, and the remaining symbols have their usual significance. On the other hand, Ornstein and Zernike[7] have shown from the theory of fluctuations that the relative compressibility is related to $g^{(2)}$ by

$$kT(\partial n/\partial p)=1+4\pi n\int_0^\infty [g^{(2)}(r)-1]r^2 dr. \quad (2)$$

To obtain the knowledge of $g^{(2)}$ necessary for the evaluation of the integrals in these two expressions we shall, in what follows, appeal to the Born-Green-Yvon equation[2]

$$[\partial g^{(2)}(\mathbf{r}_{12})/\partial \mathbf{r}_{12}]+(1/kT)[\partial\psi(\mathbf{r}_{12})/\partial \mathbf{r}_{12}]g^{(2)}(\mathbf{r}_{12})$$
$$=-(n/kT)\int_0^\infty [\partial\psi(\mathbf{r}_{13})/\partial \mathbf{r}_{13}]g^{(3)}(\mathbf{r}_{12}, \mathbf{r}_{13}, \mathbf{r}_{23})d\boldsymbol{\tau}_{13}. \quad (3)$$

Other equations could be used for this purpose but we choose this one for convenience. In Eq. (3) $g^{(3)}(\mathbf{r}_{12}, \mathbf{r}_{13}, \mathbf{r}_{23})$ is the triplet-distribution function giving the probability that the particles 1, 2, and 3 are simultaneously at the locations $(\mathbf{r}_1, \mathbf{r}_2, \mathbf{r}_3)$ and $|\mathbf{r}_i-\mathbf{r}_j|=r_{ij}$ for spherical particles.

Equation (3) is conventionally arranged to involve $g^{(2)}$ alone by introducing a superposition approximation due originally to Kirkwood[1] and which may be written

$$g^{(3)}(\mathbf{r}_{12}, \mathbf{r}_{13}, \mathbf{r}_{23})=g^{(2)}(\mathbf{r}_{12})g^{(2)}(\mathbf{r}_{13})g^{(2)}(\mathbf{r}_{23}). \quad (4)$$

In the arguments to follow we shall consider the possibility of modifying this approximation, which it is convenient to denote by $g_k^{(3)}$, by adding terms involving powers of the density [see Eq. (12)].

For the case of a fluid at not too high density (compressed gas) it is known[4] that $g^{(2)}(\mathbf{r})$ can be expanded in the form

$$g^{(2)}(\mathbf{r})=\exp\{-\psi(\mathbf{r})/kT\}$$
$$\times[1+a_1(\mathbf{r})n+a_2(\mathbf{r})n^2+a_3(\mathbf{r})n^3+\cdots]. \quad (5)$$

The insertion of Eq. (5) into Eq. (3) allows the coefficients of the expansion $a_1, a_2, a_3, \cdots$ to be determined within the Born-Green-Yvon theory and under a superposition approximation, by considering the coefficients of successive powers of n. Equation (5) can then be used in combination with either Eq. (1) or (2) to yield the well-known virial expansion of the pressure,

$$p=nkT[1+Bn+Cn^2+Dn^3+En^4+\cdots], \quad (6)$$

with the virial coefficients $B, C, D, E, \cdots$ defined as

[1] J. G. Kirkwood, J. Chem. Phys. **3**, 300 (1935).
[2] M. Born and H. S. Green, *A General Kinetic Theory of Liquids* (Cambridge University Press, New York, 1949).
[3] J. Yvon, Actualités sci. et ind. **1937**, 542.
[4] For a review see, e.g., J. de Boer, Repts. Progr. in Phys. **12**, 305 (Phys. Soc., London, 1949).
[5] J. G. Kirkwood and E. M. Boggs, J. Chem. Phys. **10**, 394 (1942).
[6] G. H. A. Cole, J. Chem. Phys. **28**, 912 (1958).
[7] L. S. Ornstein, and F. Zernike, Proc. Acad. Sci. Amsterdam **17**, 795 (1914).

integrals which involve the interparticle force potential $\psi(r)$ (see Sec. II).

Equations (1), (2), and (3) are exact; approximation is introduced into the theory by the independent assumption of superposition such as (4). Rushbrooke and Scoins[8] have shown that the set of equations (1), (3), (4), and (5) provide correct values for the second and third virial coefficients B and C, but that the fourth coefficient D is not given correctly. In addition, these authors show that the set of equations (2), (3), (4), and (5) also provide correct values for B and C and that D is again wrong, but that the value of D calculated from these two sets of equations is different. Thus the superposition approximation (4) introduces an inconsistency into the theory which appears explicitly in connection with D. For the case of rigid spheres (where the various formulas may be treated explicitly) if a subscript p refers to the pressure equation (1) while a subscript c refers to the compressibility equation (2), with the absence of any subscript denoting an exact value, then Rushbrooke and Scoins find that using (4), $D_c > D > D_p$. The same results were derived independently by Nijboer and van Hove.[9] These authors in addition consider the possibility of altering the Kirkwood superposition approximation with the aim of improving the calculated value of D for a gas of hard spheres. The inconsistency within the theory between the pressure equation (1) and the compressibility equation (2), however, remains. Internal consistency was later achieved by Rodriguez[10] while using a superposition approximation, but at the expense of replacing the Kirkwood form of the approximation (4) by an asymmetric modified expression with no apparent theoretical backing. While providing correct values for the second and third virial coefficients, the theory still gives an incorrect value for the fourth coefficient although the value is an improvement over the values of Rushbrooke and Scoins, and of Nijboer and van Hove (see Sec. V). Perhaps the strongest objection to the Rodriguez form of the superposition approximation is that although it provides a value of D which is consistent with both Eqs. (1) and (2), it is not of sufficient generality to ensure that consistency is simultaneously maintained for the higher virial coefficients such as the fifth and sixth.

In the present paper we are concerned with modifying the original Kirkwood form of the superposition approximation (4) in a natural way which maintains its symmetry of form, and further which is able also to ensure complete internal consistency for all the virial coefficients simultaneously. The value of the fourth virial coefficient for a gas of hard spheres calculated using this approximation will be found (Sec. V) to be in excellent agreement with the known exact value. This gives some confidence in the use of this modified superposition approximation for the determination of the structure of real fluids at not too high densities.

II. EXPRESSIONS FOR THE VIRIAL COEFFICIENTS

It is well known that the insertion of the expansion (5) into Eq. (1) or (2) leads at once to expressions for the virial coefficients B, C, D, E, $\cdots$. We write them down now for completeness, since it will be necessary to refer to them later.

As usual write

$$\exp[-\psi(r)/kT]-1\equiv\alpha(r):$$

$$-(1/kT)[\partial\psi(r)/\partial r]\exp[-\psi(r)/kT]$$

$$=[\partial\alpha(r)/\partial r]\equiv\alpha'(r). \quad (7)$$

Then the virial coefficients derived from the pressure equation (1) are

$$B_p=\tfrac{1}{6}\int_0^\infty 4\pi r^3\alpha'(r)\,dr, \quad (8a)$$

$$C_p=\tfrac{1}{6}\int_0^\infty 4\pi r^3\alpha'(r)a_1(r)\,dr, \quad (8b)$$

$$D_p=\tfrac{1}{6}\int_0^\infty 4\pi r^3\alpha'(r)a_2(r)\,dr, \quad (8c)$$

$$E_p=\tfrac{1}{6}\int_0^\infty 4\pi r^3\alpha'(r)a_3(r)\,dr, \quad (8d)$$

and so on. Alternatively, from the compressibility equation (2) it follows that

$$B_c=-2\pi\int_0^\infty \alpha(r)r^2dr, \quad (9a)$$

$$C_c=\tfrac{4}{3}B_c^2-(4\pi/3)\int_0^\infty a_1(r)[\alpha(r)+1]r^2dr, \quad (9b)$$

$$D_c=3B_cC_c-2B_c^3-\pi\int_0^\infty[\alpha(r)+1]a_2(r)r^2dr, \quad (9c)$$

$$E_c=(16/5)B_c[D_c+B_c^3-(9/4)B_cC_c]+(9/5)C_c^2$$

$$-(4\pi/5)\int_0^\infty[\alpha(r)+1]a_3(r)r^2dr, \quad (9d)$$

and so on. Clearly, in a theory possessing the proper internal consistency subscripts would be superfluous.

The expressions (8) and (9) must ultimately be reconciled with the alternative exact expressions which

[8] G. S. Rushbrooke, and H. I. Scoins, Phil. Mag. **42**, 582 (1951) and Proc. Roy. Soc. (London) **A216**, 203 (1953).
[9] B. R. A. Nijboer, and L. van Hove, Phys. Rev. **85**, 777 (1952).
[10] A. E. Rodriguez, Proc. Roy. Soc. (London) **A239**, 373 (1957).

are as follows[11]:

$$B=-2\pi\int_0^\infty \alpha(r)r^2dr, \tag{10a}$$

$$C=-\tfrac{1}{3}\iint \alpha_{12}\alpha_{13}\alpha_{23}d\tau_3, \tag{10b}$$

$$D=-\tfrac{1}{8}\iiint[\alpha_{12}\alpha_{13}\alpha_{23}\alpha_{24}\alpha_{34}+6\alpha_{12}\alpha_{23}\alpha_{13}\alpha_{14}\alpha_{24} +3\alpha_{12}\alpha_{23}\alpha_{34}\alpha_{14}]d\tau_2d\tau_3d\tau_4, \tag{10c}$$

and so on. Here $\alpha_{ij}=\alpha(r_{ij})$ and $d\tau_i$ denotes a volume element about the point r_i.

The evaluation of the integrals in Eqs. (8) and (9) involves a knowledge of the coefficients of the expansion (5), and it is in this way that the superposition approximation controls the values of the virial coefficients.

III. MODIFIED SUPERPOSITION APPROXIMATION

The Kirkwood superposition approximation $g_K^{(3)}$, given by Eq. (4), is exactly only in the limit of infinite dilution and also for infinite particle separation. It does not, as it stands, include the fluid density explicitly although this does implicitly appear through its effect upon the pair distribution.[12] Nevertheless it yields the correct value for $a_1(r)$, i.e., the first density term appearing in the expansion (5) for the radial distribution function.

A natural way of including the density explicitly into the argument is to express $g^{(3)}$ as a power series in n [analogous to (5)], and so to write

$$g^{(3)}(r_{12}, r_{13}, r_{23})=g_K^{(3)}(r_{12}, r_{13}, r_{23})[1+X_1n+X_2n^2+\cdots]. \tag{11}$$

The coefficients in this expansion are to be expected in the general case to be each a function of the three separation distances (r_{12}, r_{13}, r_{23}) as well as of both ψ and T.

In our present arguments the expression (11) will be accepted as the superposition approximation to be introduced into the theory in place of the original form (4), and functions $X_1, X_2, X_3, \cdots$ determined in such a way that internal consistency is assured for the theory with respect to Eqs. (1) and (2). It is a straightforward matter to confirm that when the expression (11) is inserted into Eq. (3), together with the expansion (5), then the coefficient $a_1(r)$ is unaffected by any of the functions X_i; that the coefficient $a_2(r)$ is affected by the function X_1 but not by any higher functions such as X_2 or X_3; that the coefficient $a_3(r)$ is affected by both the functions X_1 and X_2 but not by higher functions such as X_3 or X_4, and so on. Equations (8) and (9) then show that X_1 affects the fourth virial coefficient, and that the subsequent functions X_i affect the higher virial coefficients. The functions X_i can therefore be successively selected to provide the required consistency between the corresponding members of the two schemes of Eqs. (8) and (9).

We proceed now to use the expression (11) as a means of closing the equations of the theory in such a manner as to retain internal consistency in the arguments. Only the fourth virial coefficient will be calculated so that the expansion (11) need be taken only as far as the linear term in the density, i.e., assume

$$g^{(3)}(r_{12}, r_{13}, r_{23})=g_K^{(3)}(r_{12}, r_{13}, r_{23})[1+X_1n]. \tag{12}$$

IV. CONDITION FOR CONSISTENCY

By inserting the expressions (12) and (5) into the Born-Green-Yvon equation (3) and equating the coefficients of corresponding powers of n in the resulting expansion it follows that

$$a_1(r)=-\pi\int_0^\infty\int_{-s}^{s}[(t+r)/r](s^2-t^2) \times\alpha(t+r)dt\alpha'(s)ds, \tag{13a}$$

$$a_2(r)=\tfrac{1}{2}a_1^2(r)-\pi\int_0^\infty\int_{-s}^{s}[(t+r)/r](s^2-t^2)a_1(t+r) \times[\alpha(r+t)+1]dt\alpha'(s)ds -\pi\int_0^\infty\int_{-s}^{s}[(t+r)/r](s^2-t^2)\alpha(t+r)dta_1(s)\alpha'(s)ds -\pi\int_0^\infty\int_{-s}^{s}X_1(r, s, t)[(t+r)/r](s^2-t^2)\alpha(t+r)dt\alpha'(s)ds, \tag{13b}$$

where to conform with previous authors we have made the substitution $r\equiv r_{12}$; $s\equiv r_{13}$; $t\equiv r_{23}$. The original Kirkwood assumption (4) is retrieved from (12) if we set $X_1=0$: in this case the expressions (13) become identical with those previously given by Rushbrooke and Scoins.[8] In an obvious notation, (13b) can be written more simply as

$$a_2(r)=a_2^K(r)-\pi\int_0^\infty\int_{-s}^{s}X_1(r, s, t)[(t+r)/r] \times(s^2-t^2)\alpha(r+t)dt\alpha'(s)ds, \tag{13c}$$

where $a_2^K(r)$ stands for the first two terms on the right-hand side of (13b). It will be convenient later to introduce the function $\Xi(r)$ according to

$$\Xi(r)=-\pi\int_0^\infty\int_{-s}^{s}X_1(r, s, t)[(t+r)/r](s^2-t^2) \times\alpha(r+t)dt\alpha'(s)ds, \tag{13d}$$

so that

$$a_2(r)=a_2^K(r)+\Xi(r). \tag{13e}$$

The insertion of (13e) into the expressions (8) and (9) gives each of the coefficients D_p and D_c appropriate to

[11] See e.g., R. H. Fowler and E. A. Guggenheim, *Statistical Thermodynamics* (Cambridge University Press, New York, 1939).
[12] G. H. A. Cole, Advances in Phys. **8**, 225 (1960).

the superposition approximation (12) as the sum of the corresponding coefficient derived on the basis of the Kirkwood approximation (4), and written, respectively, D_p^K and D_c^K, and an additional term involving X_1 through Ξ.

The theory will have internal consistency as far as the fourth virial term if $D_c=D_p$. Using (13e), (8c), and (9c), the condition for consistency is that

$$4\pi/6\int_0^\infty \alpha'(r)\Xi(r)r^3dr+D_p^K$$

$$=-\pi\int_0^\infty[\alpha(r)+1]\Xi(r)r^2dr+D_c^K,$$

which can be rearranged to become

$$4\pi/6\int_0^\infty\{r\alpha'(r)+\tfrac{3}{2}[\alpha(r)+1]\}\Xi(r)r^2dr=D_c^K-D_p^K. \quad (14)$$

This is the condition which the function X_1 is required to satisfy.

The procedure is immediately applicable to further coefficients in the expansion (11), e.g., to X_2. By using the expansion (5) as far as the term $a_3(r)n^3$. Eq. (3) then provides an expression for $a_3(r)$ in terms of $a_2(r)$ and $a_1(r)$ which is to be added to the right hand side of (13b). The requirement of internal consistency is met for the fifth virial coefficient E by choosing X_2 such that E_p given by (8d) is equal to E_c given by (9d). The expressions which can be derived for X_2, X_3, $\cdots$ will not be written down here since they will not be used in what follows.

To proceed further we will make an assumption, the utility of which will be shown numerically in Sec. V for the case of a fluid of rigid spheres. Let us assume that X_1 varies sufficiently slightly with changing particle separation that it may adequately be treated as a constant. Expressed alternatively, the constant value selected for X_1 is to be regarded in some sense as an average of the correct function X_1. Such a procedure can be expected to lead to reasonable numerical results for rigid spheres at least, since it will be found later (Sec. V) that the value of the fourth virial coefficient for this case is dictated very largely by the behaviour of $a_2(r)$ in the region $r<2\sigma$ (where σ is the particle diameter); it is required of X_1 that it should be reasonably constant only in this region. If this is admitted, then from (13d) and (13b) it follows that

$$\Xi(r)=X_1a_1(r), \quad (15a)$$

so that (13e) becomes now

$$a_2(r)=a_2^K(r)+X_1a_1(r). \quad (15b)$$

The left-hand side of the condition (14) becomes

$$(C_p-\tfrac{3}{4}C_c+B_c^2)X_1.$$

Since there is no need to distinguish the source of the second and third virial coefficients,[8] the condition (14)

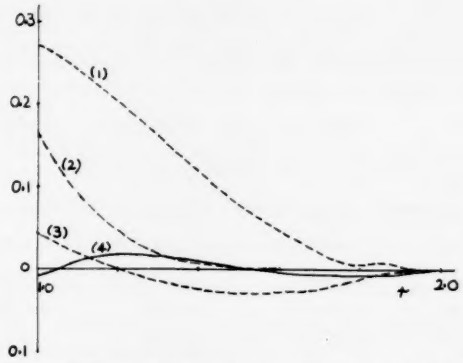

FIG. 1. Difference between the exact function $a_2(r)$ for hard spheres and the approximate functions: (1) Kirkwood approximation $(a_2-a_2^K)$; (2) Nijboer and van Hove $(a_2-a_2^N)$; (3) Rodriguez $(a_2-a_2^R)$; (4) present calculations involving the new modified Kirkwood approximation $(a_2-a_2^M)$. (Particle diameter taken as unit of length.)

becomes, when (15a) is valid,

$$X_1=\frac{D_c^K-D_p^K}{C/4+B^2}. \quad (16)$$

This is the final expression for X_1 in terms of various virial coefficients. It should be remembered that X_1 will be a function of (ψ/T). It is proposed that the superposition approximation resulting when (16) is inserted into (12) is superior to the original Kirkwood assumption (4) for the calculation of classical fluid properties. Further improvement can be expected to result from the inclusion of further terms of the general expression (11).

V. TEST FOR HARD SPHERES

Some indication of the general usefulness of the arguments set down so far, together with the utility of the assumption (15a), is obtained by using the formulas for the calculation of D for a fluid composed of rigid spheres. The exact values of B, C, and D are known for this case[13] so that a direct test of the theory is possible (see also work cited in reference 11, Sec. 707).

The interparticle potential for hard spheres can be written

$$\psi(r)=\infty \quad \text{for} \quad 0\leq r\leq 1$$
$$=0 \quad \text{for} \quad r>1, \quad (17)$$

where the molecular diameter 2σ is taken as the unit of length. It follows from the definition (7) for α that now

$$\alpha(r)=-1 \quad \text{for} \quad 0\leq r\leq 1$$
$$=0 \quad \text{for} \quad r>1, \quad (18a)$$

and that

$$\alpha'(r)=\delta(r-1), \quad (18b)$$

where δ is the Dirac delta function.

[13] L. Boltzmann, Verslag Gewone Vergader Afdeel. Natuurk., Ned. Akad. Wetenschap. **7**, 484 (1899); H. Happel, Ann. Physik **21**, 342 (1906); R. Majumdar, Bull. Calcutta Math. Soc. **21**, 10 (1929).

TABLE I. Numerical values of the coefficient of the term proportional to n^2 in the expansion (5) of the pair distribution for a gas of hard spheres derived from several arguments: $a_2(r)$ is the exact function; $a_2^M(r)$ is derived from the present paper using (12); $a_2^K(r)$ is derived from the Kirkwood theory using (4); $a_2^N(r)$ is due to Nijboer and von Hove, and Rushbrooke and Scoins; and $a_2^R(r)$ has been given by Rodriguez. The function $a_1(r)$ is due to Kirkwood [Eq. (19a)]. (Particle diameter taken as unit of length.)

r	$a_2(r)$	$a_2^M(r)$	$a_2^K(r)$	$a_2^R(r)$	$a_2^N(r)$	$a_1(r)$
1.00	1.2587	1.2659	0.9879	1.2163	1.0966	1.3090
1.08	0.8237	0.8145	0.5755	0.7994	0.7234	1.1256
1.16	0.4531	0.4366	0.2342	0.4456	0.3948	0.9530
1.24	0.1434	0.1258	−0.0425	0.1502	0.1123	0.7923
1.32	−0.1087	−0.1237	−0.2605	−0.0912	−0.1235	0.6439
1.40	−0.3071	−0.3173	−0.4253	−0.2823	−0.3131	0.5088
1.48	−0.4551	−0.4598	−0.5422	−0.4265	−0.4570	0.3878
1.56	−0.5564	−0.5561	−0.6159	−0.5282	−0.5567	0.2816
1.64	−0.6139	−0.6099	−0.6506	−0.5889	−0.6140	0.1914
1.72	−0.6308	−0.6251	−0.6501	−0.6111	−0.6308	0.1175
1.80	−0.6087	−0.6066	−0.6174	−0.5968	−0.6087	0.0507
1.88	−0.5528	−0.5500	−0.5547	−0.5472	−0.5528	0.0222
1.96	−0.4634	−0.4630	−0.4635	−0.4628	−0.4634	0.0025
2.04	−0.3506	−0.3506	−0.3506	−0.3506	−0.3506	...
2.12	−0.2542	−0.2542	−0.2542	−0.2542	−0.2542	...
2.20	−0.1781	−0.1781	−0.1781	−0.1781	−0.1781	...
2.28	−0.1198	−0.1198	−0.1198	−0.1198	−0.1198	...
2.36	−0.0767	−0.0767	−0.0767	−0.0767	−0.0767	...
2.44	−0.0460	−0.0460	−0.0460	−0.0460	−0.0460	...
2.52	−0.0254	−0.0254	−0.0254	−0.0254	−0.0254	...
2.60	−0.0126	−0.0126	−0.0126	−0.0126	−0.0126	...
2.68	−0.0053	−0.0053	−0.0053	−0.0053	−0.0053	...
2.76	−0.0017	−0.0017	−0.0017	−0.0017	−0.0017	...
2.84	−0.0003	−0.0003	−0.0003	−0.0003	−0.0003	...
2.92	−0.0000	...	...	...	...	...
3.00	...	...	...	...	...	...

Kirkwood[1] showed long ago that now

$$a_1(r)=\tfrac{2}{3}\pi(2-\tfrac{3}{2}r+\tfrac{1}{8}r^3) \quad \text{for} \quad r\leq 2$$
$$=0 \quad \text{for} \quad r>2, \qquad (19a)$$

a result which also follows directly from (13a). Further, Nijboer and van Hove[9] and also Rodriguez[10] have shown that for the original Kirkwood assumption (4)

$$a_2^K(r)=\omega_2(r)+\chi_2(r), \qquad (19b)$$

where

$$\omega_2=\pi^c\left[\tfrac{27}{70}\cdot(1/r)-\tfrac{9}{4}+\tfrac{9}{5}r-\tfrac{1}{4}r^2-\tfrac{1}{6}r^3+\tfrac{1}{20}r^4-\tfrac{1}{1260}r^6\right]$$
$$\text{for} \quad 1\leq r\leq 3$$
$$=0 \quad \text{for} \quad r>3, \qquad (19c)$$

and

$$\chi_2=\pi^2\left[-\tfrac{9}{35}\cdot(1/r)+\tfrac{29}{9}-\tfrac{101}{80}r+\tfrac{3}{4}r^2+\tfrac{5}{16}r^3-\tfrac{2}{15}r^4+\tfrac{43}{10080}r^6\right] \quad \text{for} \quad 1\leq r\leq 2$$
$$=0 \quad \text{for} \quad r>2. \qquad (19d)$$

This also follows directly from (13b). Appropriate values of the virial coefficients are also available in the literature. Thus it is known[8,11] that

$$B=b; \qquad C=0.6250b^2, \qquad (20)$$

where $b/4=\frac{4}{3}\pi\sigma^3$, which is the molecular volume. Further, Rushbrooke and Scoins[8] and Nijboer and van Hove[9] give

$$D_p^K=0.2252b^3; \qquad D_c^K=0.3424b^3. \qquad (21)$$

These several values allow X_1 to be deduced from (16):

$$X_1=0.1013_6 b, \tag{22}$$

which is independent of the temperature for hard spheres. The superposition approximation in the modified form (12) is, consequently,

$$g^{(3)}(\mathbf{r}_{12},\mathbf{r}_{13},\mathbf{r}_{23}) = g^{(2)}(\mathbf{r}_{12})g^{(2)}(\mathbf{r}_{13})g^{(2)}(\mathbf{r}_{23})[1+0.1014bn]. \tag{23}$$

By multiplying the function $a_1(\mathbf{r})$ by the value (22) to form Ξ according to (15a), the function $a_2(\mathbf{r})$ appropriate to the superposition approximation (23) follows from Eqs. (19) and (13e); the fourth virial coefficients which then result from (8c) and (9c) will be denoted, respectively, by $D_p{}^M$ and $D_c{}^M$. It follows easily from Eq. (8c) that $D_p{}^M=D_p{}^K+X_1C=D_p{}^K+0.06337b^3$ using (20), so that with the value (21) for $D_p{}^K$

$$D_p{}^M=0.2885_7 b^3. \tag{24a}$$

Also from Eq. (9c), $D_c{}^M=D_c{}^K+X_1(\frac{3}{4}C-B^2)$ so that from (20), (21), and (22), $D_c{}^M=D_c{}^K-0.05387b^3$. So that

$$D_c{}^M=0.2885_3 b^3. \tag{24b}$$

A comparison between the values (24a) and (24b) shows that internal consistency is fully maintained in the calculations. We may take as the mean value

$$D^M=0.2885b^3. \tag{25}$$

The exact value for D for rigid spheres is known[11,13] to be

$$D=0.2869b^3.$$

It is seen, therefore, that the value of D calculated according to the arguments of the present paper and using the modified superposition approximation is in excellent agreement with the exact value, differing from it (being larger) by little more than $\frac{1}{2}\%$. Further, the theory is internally consistent.

The value of D^M derived above and based on the modified superposition approximation (12) should be compared with the values of D previously derived by other authors. Thus, Rushbrooke and Scoins[8] and Nijboer and van Hove[9] in their papers obtain the two values, denoted by $D_p{}^N$ and $D_c{}^N$:

$$D_p{}^N=0.2500b^3; \qquad D_c{}^N=0.2969b^3,$$

while Rodriguez finds for his form of superposition for D^R

$$D^R=D_p{}^R=D_c{}^R=0.2773b^3.$$

The complete set of values can be conveniently compared by forming the difference between each calculated value for D and the known exact value: let this difference be denoted by ΔD. Then

$$\Delta D_p{}^K=-0.0617b^3; \qquad \Delta D_c{}^K=0.0555b^3$$

[Kirkwood approx. (4)],

$$\Delta D_p{}^N=-0.0369b^3; \qquad \Delta D_c{}^N=0.0100b^3$$

(Rushbrooke-Scoins; Nijboer and Van Hove),

$$\Delta D^R=\Delta D_p{}^R=\Delta D_c{}^R=-0.0096b^3 \quad \text{(Rodriguez)},$$

$$\Delta D^M=\Delta D_p{}^M=\Delta D_c{}^M=+0.0016b^3$$

[present calculations using new approximation (12)].

The numerical superiority of the present approach over the previous work is clear.

It is of interest to compare the values of $a_2(\mathbf{r})$ over a range of the separation distance $\mathbf{r}$ with the corresponding values given by the previous authors. Reference to the expression (5) shows that this is essentially a comparison between the pair distribution functions predicted by the various theories. This data is collected in the table where the columns have the following sources: $a_2(\mathbf{r})$ is the exact function as given by Nijboer and van Hove[9]; $a_2{}^M(\mathbf{r})$ is the function derived from the present theory using Eq. (15b) and the superposition approximation (12); $a_2{}^K(\mathbf{r})$ is derived from the Kirkwood approximation (4) and the expansions (19); $a_2{}^R(\mathbf{r})$ is the function given by Rodriguez[10]; while $a_2{}^N(\mathbf{r})$ is the best function given by Nijboer and van Hove and also by Rushbrooke and Scoins. In the final column of the table is contained for completeness the function $a_1(\mathbf{r})$ derived from the Kirkwood formulas (19a). The table shows that the function $a_2{}^M(\mathbf{r})$ compares quite well with $a_2(\mathbf{r})$, and especially that it is a marked improvement over the previous functions for the smaller values of $\mathbf{r}$. The assumption (15a), *viz.*, that X_1 is constant, affects each value of $a_2{}^M(\mathbf{r})$ and causes deviations from the correct function in addition to those introduced by the superposition approximation (12). Such deviations have less effect on the calculated values of D since the formulas (8) and (9) show that $a_2(\mathbf{r})$ is to be integrated over the whole range for D_p, or alternatively, for hard spheres, evaluated only at the point $\mathbf{r}=1$ for D_c. It is tempting to hope that the numerical agreement between the present formulas and the exact expressions would be still closer if the condition (X_1 = constant) could be relaxed and Eq. (14) itself properly satisfied by X_1 without approximation.

It is intended to use the arguments of the present paper for the calculation of the fifth virial coefficient for a fluid of hard spheres, to be considered in a later paper.

ACKNOWLEDGMENT

My best thanks are due to Dr. A. E. Rodriquez for helpful discussion.

Electrical Properties of Organic Solids. IV. Charge Carrier Diffusivity in Metal-Free Phthalocyanine

DAVID R. KEARNS* AND MELVIN CALVIN

Department of Chemistry and Lawrence Radiation Laboratory,† University of California, Berkeley, California

(Received October 31, 1960)

The pulsed light technique has been applied to determine the charge carrier mobility in microcrystalline or amorphous, metal-free phthalocyanine layers. This appears to be of the order of 10^{-3} to 10^{-2} cm^2 sec^{-1} v^{-1}, and the positive holes are the majority carriers. The low values are attributed to the physical state of the layer.

INTRODUCTION

IN a previous paper[1] we presented the results of an investigation of the kinetic and steady-state behavior of metal-free phthalocyanine photoconductivity. The steady-state conductivity measurements have now been extended, and from the information obtained from these measurements it has been possible to apply pulse light techniques to the measurements of charge carrier mobilities in phthalocyanine. Experimental apparatus and sample preparation were as described earlier.[1]

RESULTS AND DISCUSSION

Some interesting conclusions can be drawn from a consideration of the intensity dependence of the photoconductivity of phthalocyanine surface cells of varying thicknesses (see Fig. 1). In these experiments, either the front (surface with electrodes) or back (surface away from the one with electrodes) face of a sample was illuminated with strongly absorbed 6000–7000 A light (Fig. 1). The results are given in Fig. 2 where log photocurrent is plotted as a function of log relative light intensity.

In order to determine film thickness, the phthalocyanine film of each surface cell was completely dissolved in a known volume of concentrated sulfuric acid. Absorption spectra were then measured and the phthalocyanine content was determined by comparison with the spectrum of a concentrated sulfuric solution of known phthalocyanine concentration. These measurements allowed us to calculate the amount of phthalocyanine present in each film and from this, an average film thickness would be estimated.

In order to account for these data, it is necessary to assume that phthalocyanine does possess bulk conductivity, but charge carriers in the region near the phthalocyanine-glass interface make a greater contribution to the cell conductivity than do carriers some distance from this interface. The observed photoconductivity thus is primarily due to charge carriers in this region of higher conductivity. According to this assumption, it is possible to have contribution to the photocurrent from carriers generated in two different regions of the sample: (1) current i_a from carriers generated in the highly conducting region near the phthalocyanine-glass interface, and (2) current i_b from carriers generated some distance from the highly conducting region, but which diffuse into the conducting region.

Lyons[2] has formulated a theory of photoconductivity based upon the assumption that excitons migrate to the surface of the solid before they can generate carriers. This process will be governed by the diffusion of the excitons and Lyons derives the result that the photocurrent will vary linearly with light intensity. This theory has been modified by Compton[3] to include the case where carriers may be formed in the bulk of the solid, but must diffuse to the electrode surface of the solid before they can conduct. Again, a linear relationship between photocurrent and light intensity is predicted.

Therefore, the contribution i_b to the photoconductivity due to diffusion of charge carriers into the region of higher conductivity will vary linearly with the light intensity. As indicated elsewhere,[1] at high light intensities the photocurrent i_a due to carriers generated near the surface will vary as the fourth root of the light intensity L. The relative contribution of i_a and i_b to the photoconductivity will then determine the over-all observed steady-state intensity dependence. For front face illumination, the photoconductivity varies with L^Z where Z goes from $\frac{1}{3}$ to a maximum value of $\frac{1}{2}$ as sample thickness is increased (see Fig. 2, curves $1F$, $2F$, and $3F$). Thus, even for front-face illumination, there appears to be a significant contribution of i_b to the photocurrent. Over the same range of light intensities, the photoconductivity produced by back-face illumination varies as L^Z where Z goes from $\frac{1}{2}$ to 1 as sample thickness is increased (see Fig. 2, curves $1B$, $2B$, and $3B$). When the back face of the thick sample is illuminated almost all of the photocurrent is due to diffusion of carriers produced at the back

* Present address: Department of Physics, University of Chicago, Chicago, Illinois.

† The work described in this paper was sponsored by the U. S. Atomic Energy Commission.

[1] G. Tollin, D. R. Kearns, and M. Calvin, J. Chem. Phys. **32**, 1013 (1960).

[2] L. E. Lyons, J. Chem. Phys. **23**, 220 (1955).

[3] D. M. J. Compton, W. G. Schneider, and T. C. Waddington, J. Chem. Phys. **27**, 160 (1957).

surface into the conducting region near the front surface.

Obviously, as the sample thickness is increased, the i_a contribution to the photoconductivity becomes insignificant for back-face illumination. For front-face illumination both types contribute even in the thickest samples measured.

Measurement of the Carrier-Diffusivity and Mobility

The conclusions reached with regard to the discussion of intensity dependence of the steady-state photoconductivity suggest a method by which the diffusivity of charge carriers and hence their mobility in phthalocyanine can be measured. Consider the following experiment: If a thick sample (thick with respect to the region of high conductivity) receives a short pulse of strongly absorbed light on the back surface, there should be a time lapse between the light pulse and the arrival of carriers in the region of high conductivity. Although the concentration of excited phthalocyanine molecules may be initially well localized near the back surface, exciton migration would extend the region of excitation to greater than 10^{-5} cm from the surface[4] and so, in practice, a few carriers are produced almost immediately in the conducting region. The arrival peak of the photocurrent, however, should have a rather large time lag between it and the peak of the flash, provided a thick enough sample is used. As will be shown later, this time delay can be related to the diffusivity of the charge carriers and the distance between their site of production and the region of "high conductivity."

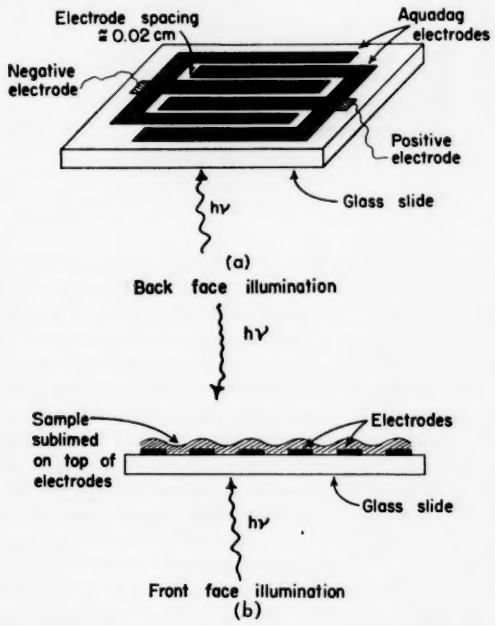

FIG. 1. (a) Schematic diagram of a phthalocyanine surface cell, showing arrangement of electrodes. (b) Cross-sectional view of (a).

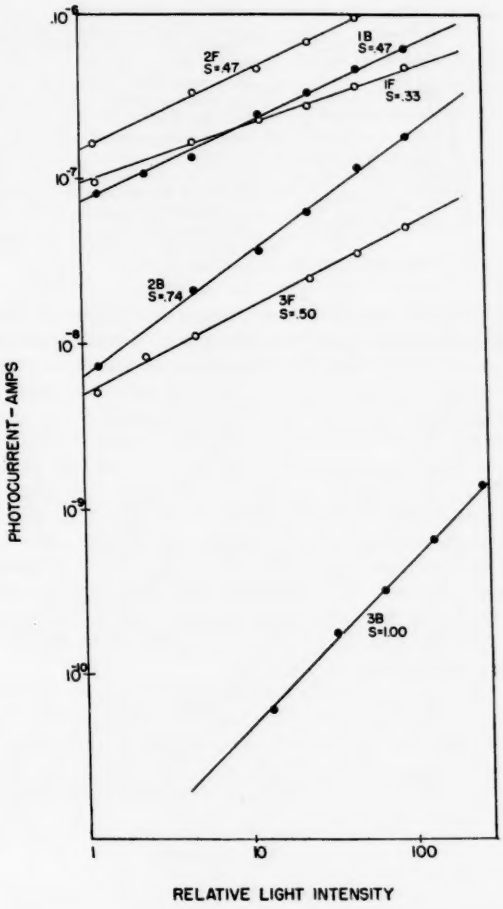

FIG. 2. Intensity dependence of steady-state photoconductivity for front- or back-face illumination of phthalocyanine surface cells of varying thickness. 6000- to 7000-A light was used. $1F$ = front-face illumination of $\sim 10^{-5}$ cm thick cell, $1B$ = back-face illumination of $\sim 10^{-5}$ cm thick cell, $2F$ = front-face illumination of 10^{-4} cm thick cell, $2B$ = back-face illumination of 10^{-4} cm thick cell, $3F$ = front-face illumination of 8×10^{-4} cm thick cell, and $3B$ = back-face illumination of 8×10^{-4} cm thick cell.

In the following experiments, phthalocyanine surface cells of different thicknesses were illuminated by the light pulse from the FT503 flash tube operated at 2200 v with a load capacitance of 256 μf (see reference 1). In each case, either the back or front face of a sample was illuminated, and a 6000- to 7000-A band-pass filter was interposed between the flash tube and the sample.

[4] D. S. McClure, *Solid State Physics* (Academic Press, Inc., New York, 1959), Vol. 8, p. 1.

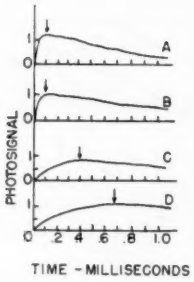

FIG. 3. Carrier diffusion experiment. Curve A: Rise and decay characteristics of FT503 light pulse with a 6000- to 7000-A band-pass filter. This light pulse was used to obtain curves B, C, and D. Curve B: Photocurrent pulse for front-face illumination of 4×10^{-4} cm thick surface cell. Curve C: Photocurrent pulse for back-face illumination of 4×10^{-4} cm thick surface cell. Curve D: Photocurrent pulse for back-face illumination of 8×10^{-4} cm thick surface cell.

Illumination of a semitransparent sample in this manner produced a photocurrent pulse whose maximum corresponded with the maximum of the light pulse regardless of whether the front or back face was illuminated. In Fig. 3(b), the flash photocurrent produced by front-face illumination of a sample 4×10^{-4} cm thick is compared with the shape of the light pulse [Fig. 3(a)]. Again, as expected, the peak of the photocurrent coincides with the peak of the light pulse. When the back surface of this sample was flashed with the 6000- to 7000-A light [Fig. 3(c)], there was a 300-μsec delay between the peak of the light pulse and the current pulse, and this delay increases to over 500 μsec when the sample thickness is increased to 8×10^{-4} cm as shown in Fig. 3(d).

In order to calculate the diffusivity we use the following model. Consider a semi-infinite solid bounded by the planes $x=0$ and $x=l$. Assume that we now introduce at time $t=0$ a quantity of charge carriers into the region $0<x<h$ such that the concentration of charge carriers C is, at $t=0$,

$$C=C_0 \quad \text{for} \quad 0<x<h$$

$$C=0 \quad \text{for} \quad x>h.$$

Due to the concentration gradient, carriers will diffuse out of the region $0<x<h$ toward the region of high conductivity δx located at $x=l$. The time dependence of the carrier concentration C at $x=l$ for such a system can be expressed, as shown by Barrer,[5] by the following equation,

$$C=C_0\{(h/l)+(2/\pi)\sum_{n=1}^{n=\infty}[(1/n)\exp-(n\pi/l)^2Dt \cdot \cos(n\pi x/l)\cdot\sin(n\pi h/l)]\}, \quad (1)$$

where D is the diffusivity of the charge carriers. Since strongly absorbed light was used in these experiments, the charge carriers will be initially 90% contained in the region within 10^{-5} cm of the illuminated surface. Therefore, $h\cong10^{-5}$ cm should be used in Eq. (1), and assuming various values for l and D, the curves shown in Fig. 4 can be obtained. Because charge carrier recombination has been neglected so far, these theoretical curves approach a limiting value of $C_0(h/l)$ rather than going through a maximum. Reference to Fig. 3 demonstrates that the rise of the flash photocurrent is quite a bit more rapid than the decay. It is, therefore, reasonable to assume that the peak of the photocurrent pulse will occur at the time when the rate of diffusion of carriers into the region of high conductivity is beginning to decrease. From the theoretical curves of Fig. 4 we might expect this to occur at approximately 0.8 $[C_0(h/l)]$. For the 4×10^{-5} cm thick sample, one would estimate a diffusivity of $\sim10^{-4}$ cm^2/sec from the data given in Fig. 3(c) and the theoretical curves of Fig. 4. For the 8×10^{-4} cm thick sample, the data again yield a diffusivity of $\sim10^{-4}$ cm^2/sec. This is probably an upper limit on the diffusivity for the following reasons:

(a) The effect of recombination may have been

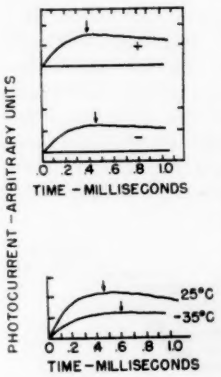

FIG. 5. (a) Field effect on the photocurrent pulse. The $\pm$ signs indicate the polarity of back face with respect to the front face. These results were obtained with back-face illumination of the 4×10^{-4} cm thick surface cell. (b) Temperature effect on the photocurrent pulse of the 4×10^{-4} cm thick surface cell.

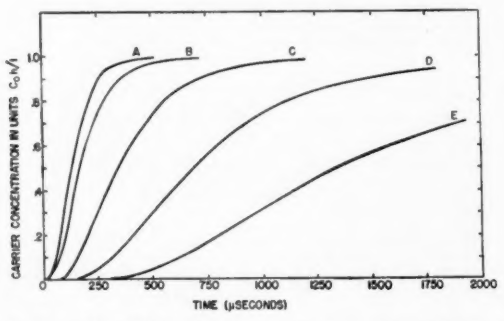

FIG. 4. Theoretical photocurrent rise curves: $h=10^{-5}$ for all curves, A: $D=10^{-5}$ cm^2/sec, $l=10^{-4}$ cm, B: $D=10^{-4}$ cm^2/sec, $l=3.5\times10^{-4}$ cm, C: $D=4\times10^{-4}$ cm^2/sec, $l=10^{-3}$ cm, or: $D=5\times10^{-5}$ cm^2/sec, $l=3.5\times10^{-4}$ cm, D: $D=5\times10^{-5}$ cm^2/sec, $l=5\times10^{-4}$ cm, or: $D=10^{-4}$ cm^2/sec, $l=7\times10^{-4}$ cm, or: $D=2\times10^{-4}$ cm^2/sec, $l=10^{-3}$ cm, E: $D=10^{-4}$ cm^2/sec, $l=10^{-3}$ cm.

[5] R. M. Barrer, *Diffusion In and Through Solids* (Cambridge University Press, New York, 1941), p. 14.

underestimated and consequently the peak photocurrents may be occurring at less than 80% theoretical maximum.

(b) The region of high conductivity (δx) may not be completely negligible and this would result in a smaller value for l than that used in the calculations. Again, this would lead to a high value for the diffusivity.

Since the mobility $\mu=(e/kT)D$ a value of $\mu=4\times10^{-3}$ $cm^2/secv$ may be calculated from the room-temperature value of the diffusivity.

The effect on the current pulse, of the application of an electric field perpendicular to the plane of the sample, was investigated. Two plates of conducting glass were positioned on opposite faces of a surface cell, but insulated from the cell. When the back-surface plate was maintained at +1200 v with respect to the front plate the conductivity pulse arrived 70 μsec earlier than when 1200 v were applied to the back plate. This is shown in Fig. 5(a). These results indicate that positive holes are the majority carriers.

When the temperature of a sample is lowered from 25° to −35°, the delay between the flash and the photocurrent maxima increased from 470 μsec to 600 μsec. This is shown in Fig. 5(b). Due to the broadness of the conductivity pulse, it was difficult to accurately locate the peak of the photocurrent. However, it is clear that the diffusivity of the carriers decreases slightly with a decrease in temperature.

Kepler[6] and LeBlanc[7] have measured charge carrier mobilities in anthracene crystals and found $\mu\simeq1$. Our measurements were carried out on sublimed films which were essentially amorphous and this is probably the reason why our mobilities are so much lower.

[6] R. G. Kepler in Proceedings of Conference on "Electronic Conductivity in Organic Solids," Duke University, April 1960.
[7] O. H. LeBlanc, Jr., J. Chem. Phys. **33**, 626 (1960).

Solid State Ionization Potentials of Some Aromatic Organic Compounds

DAVID R. KEARNS* AND MELVIN CALVIN

Department of Chemistry and Lawrence Radiation Laboratory,† University of California, Berkeley, California

(Received October 31, 1960)

The ionization potentials of a number of solid aromatic organic compounds have been determined by photoelectric threshold measurements. These are compared with literature values of the gaseous ionization potentials and the solid-state surface values seem to be approximately $1\frac{1}{4}$ v smaller. The relation between the ionization potential of a molecule within a crystalline lattice and that in the surface of the lattice is described, and the significance of the bulk ionization for conductivity of organic molecular lattices is discussed.

THEORIES of the electrical properties of organic molecular crystals have often involved solid-state ionization potentials.[1,2] The gaseous ionization potential is an important property governing molecular behavior and, correspondingly, the solid-state ionization potential is an important parameter governing the behavior of molecules in the solid state. Because of our general interest in the electronic and electrical behavior of organic solids,[3–5] the solid-state ionization potential is a parameter of great interest to us.

In 1957 Lyons[1] calculated the energy required to ionize a molecule in the ground state in a molecular crystal and compared this value with the energy required to ionize the molecule in the gaseous state. Since there is polarization energy arising from the presence of a charged ion in a polarizable molecular crystal, less energy is required to ionize a molecule in a crystal than in the gaseous state. Using classical equations, Lyons estimated the polarization energy contribution to the lowering of the ionization potential to be 0.8 ± 0.3 ev for naphthalene and 1.0 ± 0.3 ev for anthracene.

The gaseous ionization potential of anthracene has been estimated from uv absorption to be 7.2 ev[6] and, consequently, a crystal ionization potential as low as 5.9 ev might be expected. This is barely within the quartz ultraviolet spectral region. Tetracene, on the other hand, has a gaseous ionization potential of 6.6 ev[6,7] and, therefore, should have a crystal ionization potential easily within the quartz uv energy region if Lyons' calculations are valid. Measurements involving photoionization of organic solids were actually carried out as early as 1913 by Pauli,[8] who studied the photoionization of anthracene, β-naphthylamine, and eosin. Subsequent workers have studied the ionization of other compounds (rosaniline[9] and cyanine dyes[10]). However, Lyons appears to be the only one who has attempted to determine the threshold of photoionization. He reported a value of 5.6 ev for the threshold of photoionization in anthracene, but gave no information as to how the threshold was determined. It therefore seemed useful to examine the materials with which we have been concerned[3–5] to determine the energy required to produce ions in the solid state.

EXPERIMENTAL PROCEDURE

In the following experiments the light from a Bausch and Lomb hydrogen arc illuminator was passed through a Bausch and Lomb 500-mm grating monochromator and then focused onto the sample in a vacuum chamber. A diagram of the experimental apparatus is shown in Fig. 1. Electrons ejected from the organic sample are collected by a platinum gauze which was held at +90 v with respect to the sample. A vibrating reed electrometer was used to measure the current flowing through a 5×10^{11}-ohm resistor R which was placed in series with the sample and battery.

The following organic compounds were chosen for these initial experiments: metal-free phthalocyanine, nickel phthalocyanine, ferric phthalocyanine, violanthrene, decacyclene, tetracene, pentacene, perylene, etioporphyrin, and phenothiazine.

The phthalocyanine and the hydrocarbons were of particular interest to us because a number of other solid-state measurements (electrical and magnetic) had been performed on these compounds which suggested that they had a relatively low ionization potential.[5] Phenothiazine was expected, on the basis of its chemical behavior, as well as calculation,[11] to have a very low ionization potential and was included in order to check this supposition.

* Present address: Department of Physics, University of Chicago, Chicago, Illinois.

† The work described in this paper was sponsored by the U. S. Atomic Energy Commission.

[1] L. E. Lyons, J. Chem. Soc. **1957**, 5001.

[2] C. G. B. Garrett, in *Semiconductors*, edited by N. B. Hannay, (Reinhold Publishing Corporation, New York, 1959), p. 634.

[3] G. Tollin, D. R. Kearns, and M. Calvin, J. Chem. Phys. **32**, 1013 (1960).

[4] D. R. Kearns, G. Tollin, and M. Calvin, J. Chem. Phys. **32**, 1020 (1960).

[5] D. R. Kearns and M. Calvin, J. Am. Chem. Soc. (to be published).

[6] R. M. Hedges and F. A. Matsen, J. Chem. Phys. **28**, 950 (1958); K. Watanabe, *ibid.* **26**, 542 (1957).

[7] I. Bergman, Trans. Faraday Soc. **50**, 829 (1954).

[8] W. Pauli, Ann. Phys. **40**, 677 (1913).

[9] A. Predwoditelew and N. Netchaewa, Z. Physik **29**, 332 (1924).

[10] R. Fleischmann, Ann. phys. **5**, 73 (1930).

[11] Calculations by A. Pullman and B. Pullman referred to by A. Szent-Gyorgyi, I. Isenberg, and G. Karreman, Science **130**, 1191 (1959).

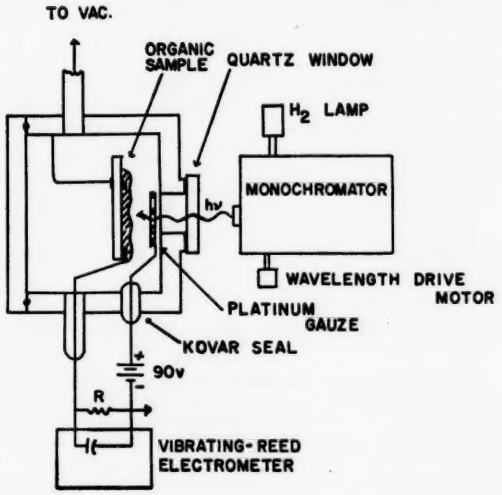

FIG. 1. Diagram of experimental apparatus for measurement of solid-state ionization potentials of aromatic organic compounds.

These compounds were first purified by vacuum sublimation in a muffle furnace. The purified material was then sublimed onto a glass slide to which an annular ring of graphite had been applied. A diagram of a sample cell prepared in this manner is shown in Fig. 2. The sample was then mounted in the vacuum chamber (Fig. 1) and light from the monochromator was focused at the center of the circle formed by the graphite electrode. In this manner, no light was allowed to reach the graphite and a photoelectric effect from graphite was eliminated. Uv light which was not absorbed by the organic sample was absorbed by the supporting glass slide. Photoemission of electrons from the glass was measured and found to be two orders of magnitude smaller than that from the organic solids; the threshold was at 2300 A.

During the measurements the monochromator wavelength drive was turned at a rate of 11 A/min and slit

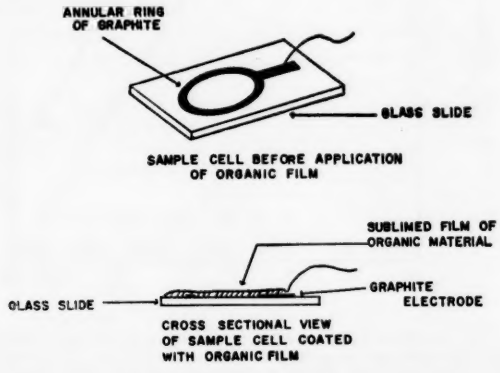
ANNULAR RING OF GRAPHITE
GLASS SLIDE
SAMPLE CELL BEFORE APPLICATION OF ORGANIC FILM
SUBLIMED FILM OF ORGANIC MATERIAL
GRAPHITE ELECTRODE
GLASS SLIDE
CROSS SECTIONAL VIEW OF SAMPLE CELL COATED WITH ORGANIC FILM

FIG. 2. Diagram of sample cell.

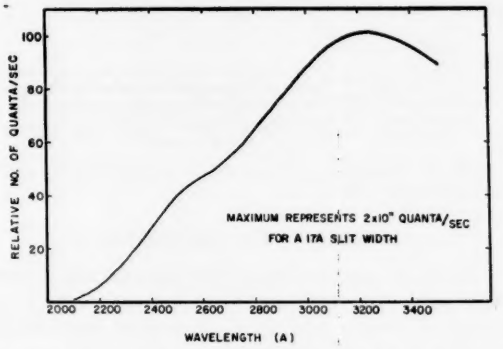

FIG. 3. Spectral distribution of relative number of quanta from the monochromator.

widths of 0.25 or 0.5 mm, corresponding to approximately 9 A and 17.5 A, respectively, were used. The spectral distribution through the monochromator in number of quanta/sec relative to 100 at 3200 A is given in Fig. 3. These data were used to convert the measured photoelectric currents to currents that would be observed for equal rate of input of quanta at all wavelengths. In Fig. 4 the measured photoelectric current as a function of wavelength is given for a tetracene sample. Qualitatively the same curves were obtained for the other compounds studied. It is difficult from this type of plot to determine the threshold wavelength for photoionization because of the "tail".

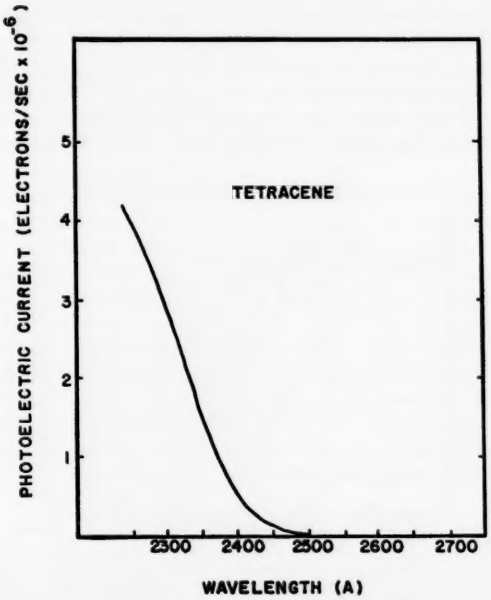

FIG. 4. Plot of photoelectric current as a function of wavelength for tetracene.

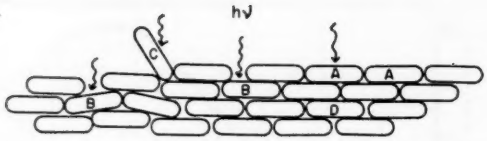

FIG. 5. Schematic representation of cross-sectional view of sublimed organic film.

RESULTS AND DISCUSSION

As can be seen in Fig. 4, the photoelectric current approaches the wavelength scale asymptotically instead of linearly and there are several possible explanations for this behavior.

(a) The sample contains impurities which have ionization potentials lower than the host material. Unfortunately, we have no accurate way of estimating how important a role impurities played in our measurements.

(b) The molecules at the surface will have a variety of dielectric environments and this correspondingly will give rise to a distribution of ionization potentials.

Figure 5 is a schematic representation of a cross-sectional view of a sublimed organic film. Type *A* molecules are surrounded on three sides by other polarizable molecules and, as indicated in the diagram, we expect this to be the most probable environment. Type *B* molecules are almost completely surrounded by other molecules and hence have an ionization potential very nearly that of molecules located in the bulk of the layer (type *D* molecules) Type *C* molecules will have an ionization potential very nearly equal to that of a molecule in the gas phase. According to this discussion, we should expect to find a distribution of ionization potentials determined by the distribution of molecules in various types of surface sites.

If we assume that the number of molecules $N(I)$ which have ionization potentials I which differ from

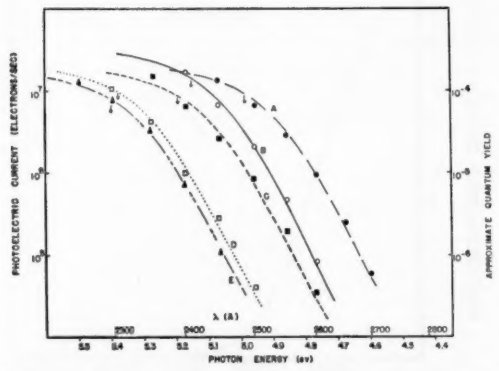

FIG. 6. Plot of log photoelectric current as a function of the energy of the incident photons for: *A*—Phenothiazine, *B*—Metal-free Phthalocyanine, *C*—Violanthrene, *D*—Tetracene, and *E*—Decacyclene. Arrows under the curves indicate the most probable surface ionization potentials.

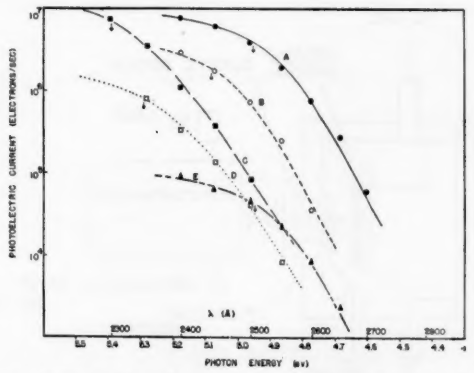

FIG. 7. Plot of log photoelectric current as a function of the energy of the incident photons for: *A*—Ferric Phthalocyanine, *B*—Pentacene, *C*—Perylene, *D*—Etioporphyrin, and *E*—Nickel Phthalocyanine. Arrows under the curves indicate the most probable surface ionization potentials.

the most probable surface value I_{surface} by an amount $\Delta I=(I_{\text{surface}}-I)$ is given by

$$N(I)\alpha \exp -h(\Delta I)^2, \tag{1}$$

where h is a constant which determines the "spread" in ionization potentials (the higher the value of h, the more uniform is the surface), then it is possible to calculate the shape of the photoelectric current $i(E)$

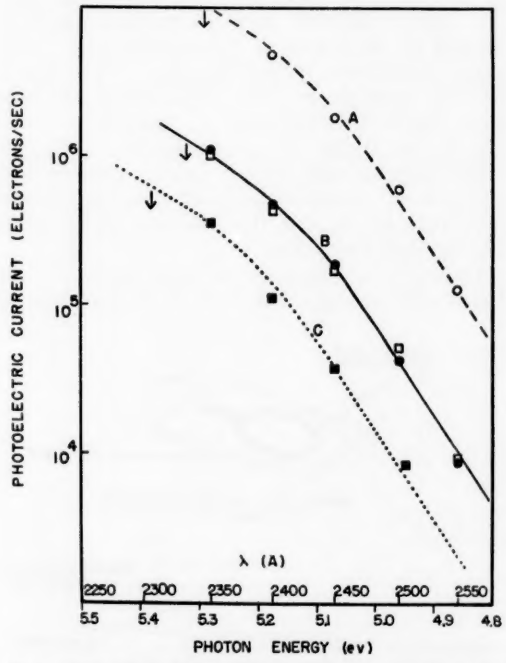

FIG. 8. Plot of log photoelectric current as a function of incident photo energy for ortho-chloranil layer backed by: *A*—Metal-free Phthalocyanine, *B*—Ferric Phthalocyanine or Violanthrene, and *C*—Phenothiazine.

TABLE I. Gaseous and solid-state ionization potentials of some aromatic organic compounds.

Compound	Gaseous ionization potential, (ev)[a] (Ig)	$I_{surface}$ (ev)	$I_g - I_{surface}$ (ev)[b]	Estimated solid-state ionization potential (ev)
Phenothiazine	...	4.99±0.05	...	4.36
Nickel phthalocyanine	...	4.95	...	4.32
Metal-free phthalocyanine	...	5.15	...	4.52
Ferric phthalocyanine	...	4.95	...	4.32
Violanthrene	6.40	5.20	1.20	4.57
Perylene	6.82	5.39	1.43	4.76
Tetracene	6.63	5.38	1.26	4.75
Pentacene	6.23	5.08	1.15	4.45
Decacyclene	6.76	5.40	1.36	4.77
Etioporphyrin	...	5.29	...	4.66

[a] See reference 6.
[b] Average value of $(I_g - I_{surface}) \simeq 1.28$ ev. Estimated average polarization energy associated with an ion in a solid = 1.91 ev.

vs excitation energy E curves for various values of h. This can be done by integrating

$$i(E) \alpha \int_{\Delta I=(I_{surface}-0)}^{\Delta I=(I_{surface}-E)} \exp -h(\Delta I)^2 d(\Delta I). \qquad (2)$$

Curves of this type were constructed for various h values and then compared with the experimentally determined data. This comparison is most easily carried out if log (photoelectric current) is plotted against excitation energy and this has been done in Figs. 6 and 7 for the various compounds studied. The points are experimental, however, the curve drawn through the points in every case is the integral of a Gaussian curve $[i(E)$ with $h=30$ (except perylene and etioporphyrin)$]$. For etioporphyrin and perylene, $h=20$ gave the best fit. Arrows under each curve indicate the most probable ionization potential $I_{surface}$. There is gratifyingly close agreement between the experimental points and the theoretical curves.

In Table I we have presented the most probable surface ionization potential $I_{surface}$ determined in the manner described above.

While surface ionization potentials are interesting, it would be more useful to be able to determine the energy required to ionize a molecule located inside such a solid. It is clear from Fig. 5 that the average surface molecule will not have as many polarizable molecules around it as will a bulk molecule and hence will have a higher ionization potential than bulk molecules. The average difference between the gaseous ionization potential and the most probable surface ionization potential is 1.28 ev and this represents some fraction (between one-half and one) of the polarization energy which would be obtained if the ionized molecule were completely surrounded by polarizable molecules.

If we assume this fraction to be two-thirds, then it is possible to estimate the ionization potential of a molecule completely surrounded by other molecules. Since 1.28 represents two-thirds of the total possible polarization energy, 0.63 ev must be subtracted from the most probable surface ionization potential to give the bulk ionization potential. These values are tabulated in the last column of Table I.

In a preliminary series of experiments ortho-chloranil was applied by sublimation or spraying to the exposed surface of a photoelectric cell of either phthalocyanine, ferric phthalocyanine, phenothiazine, or violanthrene. The photoemission of electrons from the exposed layer of ortho-chloranil molecules thus supported was then studied. (No photoelectric current was observed from pure ortho-chloranil sample cells with exciting light down to 2200 A.) In Fig. 8 results of the above experiments are presented. The points are experimental. However, again, the curve drawn through the points in every case is the integral of a Gaussian curve $[i(E)$ of Eq. (2)$]$ with $h=20$.

Again, as with the data obtained with the one-component systems, arrows under each curve indicate the most probable ionization potentials ($I_{surface}$) which are tabulated in Table II. To a high degree of approximation, in all four of the two component sys-

TABLE II. $I_{surface}$, the most probable surface ionization potential of ortho-chloranil supported on a layer of donor molecules.

Donor layer	$I_{surface}$
Ferric phthalocyanine	5.32±0.05
Metal-free phthalocyanine	5.29
Phenothiazine	5.38
Violanthrene	5.32
	Average 5.33

tems, $I_{surface}$ is about the same in every case, 5.35 ev, and this value is always higher than the measured $I_{surface}$ of the molecules supporting the ortho-chloranil layer.

We propose the following explanation for these observations. As can be seen from Table I, the four compounds (donor molecules) used as the supporting layer for the ortho-chloranil layer all have rather low ionization potentials. Ortho-chloranil, on the other hand, in solution has a very high electron affinity and correspondingly, in the more polarizable solid state, will have an even higher electron affinity due to polarization energy. Other experiments[5] have already indicated that when layers of ortho-chloranil and violanthrene are placed in contact with each other, electrons are transferred from the violanthrene layer to the ortho-chloranil layer. The other three donor molecules used as bases for the ortho-chloranil layer all have smaller solid-state ionization potentials than violanthrene, so again, we should expect electron transfer to the ortho-chloranil layer. Photoionization of pure ortho-chloranil requires photon energies greater than 5.6 ev and we propose that in the ortho-chloranil lamellar systems the photoemission of electrons is a result of photoionization of ortho-chloranil negative ions.

The fact that the ortho-chloranil negative ions will be located in such close proximity to a positively charged donor layer will make removal of electrons from the ortho-chloranil layer more difficult than if no field effects were present. This we believe is the reason why the ionization energy is so high. In view of the fact that electron transfer from violanthrene to ortho-chloranil does take place, the bulk solid electron affinity should be at least 4.6 ev.

Color Centers in ZnS Single Crystals

A. HALPERIN AND R. PINKER

Department of Physics, The Hebrew University of Jerusalem, Jerusalem, Israel

(Received November 25, 1960)

Absorption bands induced in ZnS crystals by uv (0.366 μ) are described. The two main absorption bands peaked at or below 0.6 μ and at 1.2 μ. Two weaker bands at 0.8 and 1.35 appear as shoulders of the main bands. Thermal and optical bleaching properties are also described, and the results are shortly discussed in light of a formerly proposed model.

INTRODUCTION

SUITABLE excitation, e.g., by x rays or uv light, induces in many crystals additional absorption bands not present in the unexcited crystals. The defects responsible for such additional absorption are usually named *color centers*.

Color-center research is very common in alkali-halide crystals, and it has provided much valuable information on the nature of the defects in these crystals. Very little is, however, known about color centers in the sulfide phosphors. Much effort has been devoted to the investigation of the luminescence and the associated *luminescence centers* in the sulfide crystals, but only a few investigators have reported on color-center absorption in these crystals.

It appears that Lenard[1] was the first to report on excited absorption in ZnS. Upon irradiation of ZnS:Cu with uv light Lenard observed absorption bands at 0.43 and 0.56 μ. Hoch[2] extended the measurements to 1 μ, and found a broad absorption band over the whole range for excited ZnS:Cu phosphors. More recently, Antonov-Romanovski and Shchukin[3] found, for uv-excited ZnS:Cu:Co phosphors, absorption bands at 0.45, 0.8, and 1.3 μ.

All the mentioned investigations were carried out on powders. Color centers in single crystals of CdS were described by Halperin and Garlick.[4] The aim of the present work is to report the observation of color centers in single crystals of ZnS, and to describe some of their properties.

The same crystals were also subjected to a more thorough investigation in which their luminescence, thermoluminescence, photoconductivity, effects of infrared radiation, and some other properties were examined. Some of the results were reported in previous communications.[5,6] The additional information obtained in the present work might help toward a better understanding of the defect energy levels in the sulfide phosphors.

EXPERIMENTAL

The crystals used were grown by Hamilton who used the Reynolds-Czyzak method with some modifications.[7] They were found in this laboratory to show only green luminescence at room temperature with a blue component appearing at lower temperatures. Out of a few batches examined by us, only crystals of one batch exhibited the color-center absorption. Small crystals were picked out from each of the batches and were used for qualitative spectrographic examination. The batch exhibiting the color centers was found to be richer in copper content (about 10^{-4} in weight) compared to others whose copper content was found to be near 10^{-5}.

The dimensions of the crystals used were about $1\times1\times3$ mm. They were mounted in a vacuum cryostat, the construction of which was essentially the same as that described previously.[8]

The crystal was fitted into the sample compartment of a Beckman DK spectrophotometer. Minor modifications in the sample compartment of the DK (Fig. 1) made possible exposure of the crystal to uv-exciting light (0.366 μ) while measuring its absorption. The light beam from the DK monochromator is shown in Fig. 1 to enter the sample compartment, where it is split up into the reference beam (B_1) and the sample beam (B_2) by alternative switching between the two paths with aid of the rotating mirrors R_1 and R_2 and the stationary ones M_1 and M_2. The crystal (C) is mounted in the cryostat, which is provided with two pairs of fused silica windows to let the reference and sample beams through. Exciting light from the mercury compact arc L (Mazda MD/E, 250w) was filtered by a uv-transmitting filter F_1 (Corning 5860), condensed by a quartz lens Q, and then reached the crystal by reflection from the semitransparent adjustable mirror M_4. The filter F_2 (Wratten 16) blocked the exciting light and the luminescence from the detector.

[1] P. Lenard, Handbuch Exptl. Phys. **23,** 690 (1928).
[2] A. Hoch, Ann. Physik **38,** 485 (1940).
[3] V. V. Antonov-Romanovski and I. P. Shchukin, Doklady Akad. Nauk. S.S.S.R. **71,** 445 (1950).
[4] A. Halperin and G. F. J. Garlick, Proc. Phys. Soc. (London) **B68,** 758 (1955).
[5] A. Halperin and H. Arbell, Phys. Rev. **113,** 1216 (1959).
[6] H. Arbell and A. Halperin, Phys. Rev. **117,** 45 (1960).
[7] D. R. Hamilton, J. phys. radium **17,** 797 (1956); Brit. J. Appl. Phys. **9,** 103 (1958). We are indebted to Dr. Hamilton for providing the crystals, and for valuable information regarding their preparation.
[8] A. A. Braner and A. Halperin, Phys. Rev. **108,** 932 (1957).

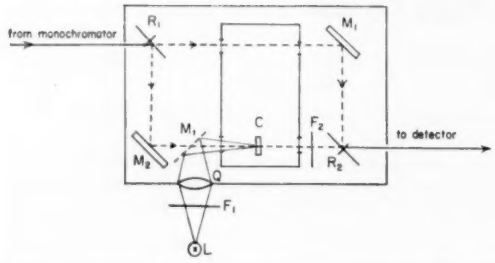

FIG. 1. Diagram of the sample compartment of the Beckman DK spectrophotometer adopted for color-center measurements. R_1 and R_2 are rotating mirrors; M_1 and M_2 are stationary ones; C is the crystal in the cryostat, L is a mercury lamp, F_1 and F_2 are filters, M_1' is a semitransparent mirror, and Q is a quartz lens.

This arrangement enabled *continuous* recording of absorption spectra of the crystals *before* and *after* uv excitation from which the additional absorption could be obtained by subtraction. However, measurements carried out separately for each point out of a series of chosen wavelengths proved, more accurate. The unexcited crystal was bleached thermally in each of the latter measurements by being warmed up to 500°K which removed any absorption due to previous excitations. It was then cooled down in the dark to the measurement temperature, and its absorption at the chosen wavelength was recorded *before* and *during* uv excitation up to saturation. The additional absorption at a given wavelength could thus be determined accurately from the curve. The same procedure was repeated for many points in the spectral range under investigation, from which the spectrum of the additional absorption was plotted. Care was taken to keep the measuring beam as weak as possible in order to minimize optical bleaching of the induced absorption. Nearly the same intensity of the measuring beam was kept throughout the whole spectral range. This was secured by the slit servo-mechanism of the DK spectrophotometer. Some of the records were continued after stopping the excitation when the measuring beam, at a suitably chosen intensity, served for optical bleaching experiments.

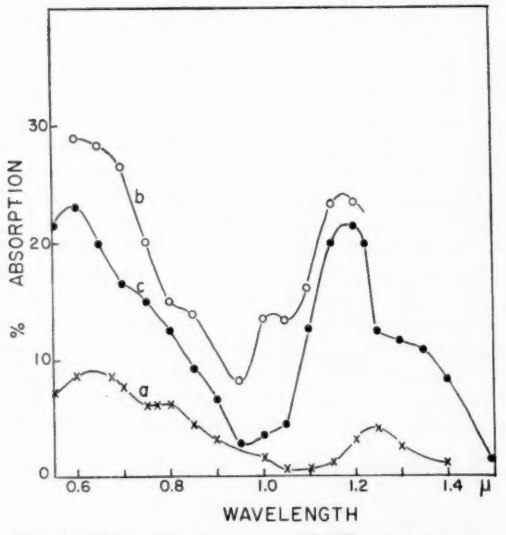

FIG. 2. Color-center absorption of ZnS crystals. Curves a: at room temperature; b: at 80°K after cooling down the crystal from 500°K; c: as b but after cooling from 325°K.

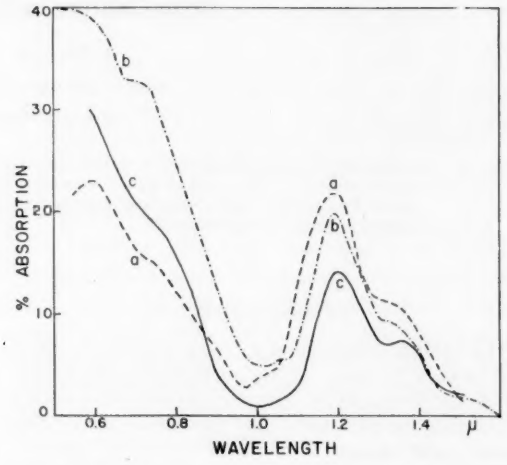

FIG. 3. Curves a and b: color-center absorption of two specimens of ZnS. Curve c: as b but recorded continuously (see text).

RESULTS

A. Spectrum of Color Center Absorption

Absorption measurements at 80°K and at room temperature with the unexcited crystals did not show any noticeable band structure. Previous to these

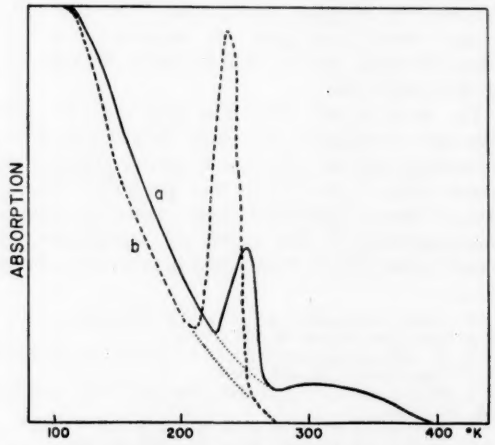

FIG. 4. Thermal bleaching of color centers in ZnS. Rate of warmup is about 20°/min. Curve a: at 0.6 μ; b: at 1.1 μ.

measurements the crystals were warmed up to 500°K which removed any formerly induced absorption, and then cooled down in the dark to the measurement temperature. Subsequent irradiation with uv (0.366 μ) induced absorption bands in the crystal. This is shown in Fig. 2. Curve a shows the induced absorption excited and measured at room temperature. In Fig. 2, curve b shows the same results but with the crystal excited at 80°K and the induced absorption measured at this temperature. In c the crystal was again excited and measured at 80°K. This time, however, it had been warmed up to 325°K between successive points, which only partially bleached the formerly induced absorption. The induced absorption as measured in curve c indicates, therefore, the additional absorption which can be induced at 80° compared to 325°K. In fact, curves a and c add to give approximately curve b except at about 1 μ where a pronounced maximum appears in curve b. This maximum might be related with defects produced by rapid cooling of the crystal from 500° to liquid-air temperature.[9]

The absorption spectra in Fig. 2 show two main bands. One lies at about 0.6 μ[10] with a shoulder at 0.8 μ, and another at 1.2 μ with a shoulder at 1.35 μ. Different crystals showed the same bands but with different relative densities. Curves a and b (Fig. 3) show the absorption spectra for two samples. The curves were obtained point by point at 80°K and with thermal bleaching nearly at room temperature between successive points. In Fig. 3, curve c belongs to the same crystal as does curve b, but was obtained from a continuous record (see Experimental section above). The curves look very similar, but the absorption obtained by the continuous record (curve c) is generally lower by about 25% when compared to that obtained point by point. The difference might be attributed to better saturation at each wavelength in the point-by-point method.

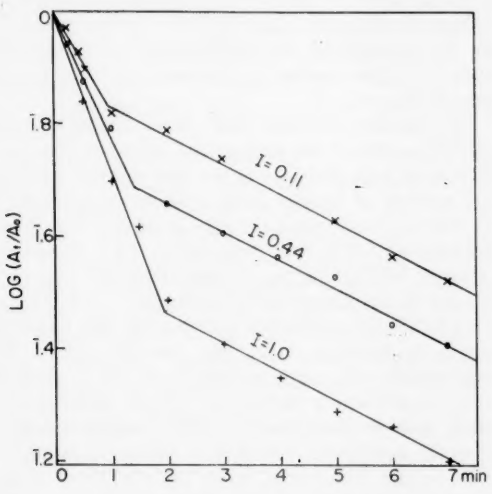

FIG. 5. Optical bleaching decay curves for absorption of ZnS at 0.6 μ and 80°K for different intensities I of the bleaching beam (0.6 μ). A_0 is absorption at $t=0$, and A_t—at time t.

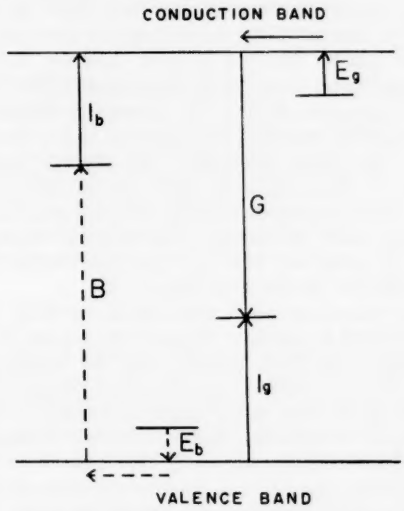

FIG. 6. An energy band model for ZnS:Cu:Cl crystals. Solid lines indicate electron transitions, and dashed lines indicate hole transitions. Transition E_b releases holes which give the blue glow peak at 120°K, and E_g releases electrons to give the green peak at 160°K. For the meaning of the other transitions see text.

B. Bleaching of Color Centers

The small dimensions of the used crystals, their rough diffusing faces, and the long optical path from the crystal to the detector in the Beckman DK spectrophotometer made the absorption measurements very sensitive to small changes in the position of the crystal in the optical path. Such changes occurred upon switching on the heating coil in the cryostat which introduced tensions in its metal Dewar. To enable continuous records of thermal bleaching curves, the measuring system was replaced by another in which a photomultiplier just near the window of the cryostat served as detector. An E.M.I. 6256B photomultiplier was used up to 0.6 μ, and a Dumont 1430K for longer wavelengths. Thermal bleaching curves were then taken at 0.6, 0.8, and 1.1 μ.[11] Figures 4(a) and (b) show the bleaching curves at 0.6 and 1.1 μ, respectively. The curves were normalized at 80°K to enable compari-

[9] Similar quenching effects were observed in CdS; see reference 4.

[10] It should be noted that the peak wavelength of the 0.6 μ band might have been affected by some transmission of the green luminescence through the Wratten 16 filter. The real peak seems to be at shorter wavelengths.

[11] This wavelength is on the short wavelength side of the 1.2-μ band. The sensitivity of the 1430 K photomultiplier was too low at the peak itself.

son of their bleaching temperatures. Both the curves start to drop at 115°K and undergo the main bleaching below 200°K. The 1.2 μ band, however, seems to decrease faster in the lower temperature region than in the 0.6 μ region. In both the curves a peak appears at about 250°K, and the curves seem to be just continued when this peak disappears. The thermal bleaching curve at 0.8 μ was very similar to the one at 0.6 μ [Fig. 4(a)] except that in this case the peak at 250°K was still more pronounced. The origin of these peaks is as yet unknown, and it is not clear whether it is a real effect or just an interference.

The measuring beam was used to optically bleach the induced absorption. Results were similar to those obtained with CdS crystals[4] and the decay curves could be analyzed into components of constant slopes. Initial slopes were again found to depend on the intensity of the bleaching beam, while later components were almost independent of it. This is shown in Fig. 5, where a few decay curves, obtained at 0.6 μ with different intensities of the bleaching beam, are given.

DISCUSSION

The peak wavelengths of the color-center absorption observed in the present work appear also in connection with other phenomena in ZnS crystals. Peaks at 0.8, 1.2, and 1.35 μ were observed[12–14] in the stimulation of the visible luminescence of ZnS. At certain conditions wavelengths of 0.7–0.8 and 1.3 μ were found[14,15] to quench the visible luminescence. Broser and Broser-Warminsky[16] found stimulation at temperatures up to 120°K by 1.2 μ, while above 170°K there was a quenching effect by 1.3 μ.

The same wavelengths also appear in excitation spectra for the infrared emission of ZnS.[14,17,18] Meijer[18] stresses the remarkable similiarity between the green stimulation spectrum, the quenching spectrum, and the infrared excitation spectrum of ZnS:Cu phosphors. He concluded that the three processes were governed by the same transitions.

As the same wavelengths appear in the absorption induced in ZnS upon excitation with uv, it seems that this absorption is also related to the mentioned group of phenomena and it involves the same transitions.

The experimental difficulties with the small needle-type crystals used in the present work did not enable more accurate and more detailed measurements. These crystals were also used with their rough faces which caused high scattering of the measuring beam. Grinding and polishing did not help as it reduced the thickness of the crystal; with it the whole effect was reduced. Unfortunately all the attempts to detect induced absorption in batches which contained larger crystals were unsuccessful. These difficulties did not enable us to clarify the nature of the peak at 250°K in the thermal bleaching curve (Fig. 4), or to obtain higher accuracy in the spectra of the induced absorption. The present discussion will therefore be given in short with the hope that it will be more helpful once larger crystals exhibiting color-center absorption become available.

Previous work in this laboratory[6] has shown the thermoluminescence of our ZnS crystals to be composed of a blue glow peak at 120°K, a green one at 160 and another weak green peak at about 360°K. Infrared of 1–1.4 μ was found to enhance the green glow peak at 160°K and to quench the blue one, while shorter wavelengths (0.6–0.8 μ) quenched generally both the peaks.

Two models have been proposed (reference 6, Fig. 8) to account for the experimental results. One of these models is given again in Fig. 6. Taking 3.8 ev as the forbidden gap of ZnS, and taking the green center to be at about 2.3 ev below the conduction band, there remain 1.5 ev (about 0.8 μ, transition I_g) between the green center and the valence band. Once the green centers are excited by uv light, (transition G) infrared of 0.8 μ might be absorbed, raising electrons from the valence band to the empty centers. Similarly about 1 ev (1.2 μ) might be absorbed on raising electrons from the excited blue centers to the conduction band (transition I_b, Fig. 6).

The number of excited blue centers should decrease at 120°K when holes at the blue traps are freed and recombine with electrons in the blue centers. Similarly the number of excited green centers should decrease at 160°K. As a result, the 1.2-μ absorption should decrease at 120°K, and that of 0.6–0.8 μ should decrease at 160°K. This really seems to be the case (Fig. 4), and the 1.2-μ band seems to decrease faster than the 0.6-μ band. The separation between the two bleaching curves is, however, not clear enough, and further experiments with larger crystals is needed to establish it. It is worth noting that curve a (Fig. 4) shows another small drop in absorption at 360°K, which is a good fit to the weak green glow peak at this temperature.

In reality there seem to be discrete levels in the forbidden gap in addition to those given in our simplified model. Hence the structure (see Fig. 2) in the color-center absorption of the crystals. The various slopes in the decay curves (Fig. 5) also indicate that more energy levels contribute to the color-center absorption.

[12] G. R. Fonda, J. Opt. Soc. Am. **36**, 382 (1946).
[13] G. F. J. Garlick and D. E. Mason, J. Electrochem. Soc. **96**, 90 (1949).
[14] P. F. Browne, J. Electronics **2**, 1 (1956).
[15] N. T. Melamed, J. Electrochem. Soc. **97**, 33 (1950).
[16] I. Broser and R. Broser-Warminsky, J. phys. radium **17**, 791 (1956).
[17] R. E. Halsted, E. F. Apple, and J. S. Prener, Phys. Rev. Letters **1**, 134 (1958).
[18] G. Meijer, J. Phys. Chem. Solids **7**, 153 (1958).

Proton Resonance Line Shape for a Polycrystalline Aromatic Radical

ROLAND LEFEBVRE

Centre de Mécanique Ondulatoire Appliquée, 155 Rue de Sèvres, Paris XV°, France

(Received November 28, 1960)

A calculation is made of the resonance line shape for an in-plane proton of a polycrystalline aromatic radical in the case where the electron-proton hyperfine interaction is the only factor responsible for the resonance shift. Even with the inclusion of the anisotropic part of the electron-proton hyperfine interaction the position of the peak is linearly related to the unpaired π-electron density on the neighboring carbon atom, ρ_c. The relation is very close to the one found for the solution. The line shape is very symmetrical, with a width which increases for an increasing ρ_c. This behavior is in good agreement with the recent results of Gutowsky and collaborators.

INTRODUCTION

In nuclear magnetic resonance experiments performed on paramagnetic molecules, the nuclei are under the influence of a magnetic field which is the resultant of the external field and a strong internal field. The latter field is essentially that due to the unpaired electron distribution. This should produce very large electron hyperfine splittings in the nuclear magnetic resonance spectrum.

With very strong electron exchange interactions or a very short electron relaxation time, the internal field has to be averaged over the various electron spin states.[1] This has the effect of reducing the nuclear resonance shifts to a few gauss. McConnell and Chesnut[1] have shown how in these circumstances the proton shifts for a radical in solution depend on the isotropic coupling constants, which can be related in turn, for an aromatic radical, to the unpaired π-electron densities on the neighboring carbon atoms. Such shifts have been observed and discussed for a number of paramagnetic molecules.[2–4]

Observations have also been made on polycrystalline substances[2,5,6] and the shifts have again been related to the isotropic coupling constants. A more correct procedure is to take into account both the isotropic and anisotropic parts of the hyperfine interaction. Averaged nuclear resonance shifts in both the solution and the solid state have been derived by McConnell and Robertson[7] from the spin Hamiltonian. Rather than determining an averaged nuclear resonance shift in this paper the proton resonance line shape itself for a polycrystalline radical will be calculated by procedures similar to those which have been recently developed[8,9] for obtaining the electron spin resonance line shape of a polycrystalline radical. An application is made to the case of a proton belonging to a CH bond of an aromatic radical.

LINE SHAPE FORMULA

The proton shift for a given orientation of a radical trapped in a solid can be obtained by an obvious extension of the formula valid for the solution.[1] For each proton the total spin Hamiltonian for the radical contains a term of the form[10]

$$\mathfrak{A}\mathbf{S}_x\mathbf{I}_x+\mathfrak{B}\mathbf{S}_z\mathbf{I}_z+\mathfrak{C}\mathbf{S}_y\mathbf{I}_y, \qquad (1)$$

which expresses the interaction between the unpaired electron distribution and this proton. x, y, and z are the axes which diagonalize this interaction. $\mathfrak{A}$, $\mathfrak{B}$, and $\mathfrak{C}$ are its principal values, which we assume to be expressed in gauss. $\mathbf{S}_x$, $\mathbf{S}_y$, $\mathbf{S}_z$ and $\mathbf{I}_x$, $\mathbf{I}_y$, $\mathbf{I}_z$ are the components of the electron and proton spin operators.

In current magnetic resonance experiments the electron spin is quantized along the direction of the external magnetic field, and the term (1) can be interpreted[10,11] as a coupling between the proton spin and an internal magnetic field, the components of which are

$$-\mathfrak{A}(g\beta/g_p\beta_p)M_s\cos\theta, \qquad -\mathfrak{B}(g\beta/g_p\beta_p)M_s\sin\theta\cos\phi,$$
$$-\mathfrak{C}(g\beta/g_p\beta_p)M_s\sin\theta\sin\phi$$

along the axes z, x, and y. The $g\beta$ and $g_p\beta_p$ are the electron and proton gyromagnetic ratios, M_s the electron spin quantum number of values $\pm\frac{1}{2}$, θ and ϕ the polar angles giving the direction of the external magnetic field in the xyz axes. If the proton sees only a field averaged over the two electron spin states, on account of the difference in Boltzmann factors the components are transformed into [see (1) or (6) for a similar

[1] H. M. McConnell and D. B. Chesnut, J. Chem. Phys. **28**, 107 (1958).
[2] H. M. McConnell and C. H. Holm, J. Chem. Phys. **27**, 314 (1957).
[3] A. Forman, J. N. Murrell, and L. E. Orgel, J. Chem. Phys. **31**, 1129 (1959).
[4] W. D. Phillips and R. E. Benson, J. Chem. Phys. **33**, 607 (1960).
[5] H. S. Gutowsky, H. Kusumoto, T. H. Brown, and D. H. Anderson, J. Chem. Phys. **30**, 860 (1959).
[6] T. H. Brown, D. H. Anderson, and H. S. Gutowsky, J. Chem. Phys. **33**, 720 (1960).
[7] H. M. McConnell and R. E. Robertson, J. Chem. Phys. **29**, 1361 (1958).
[8] H. Sternlicht, J. Chem. Phys. **33**, 1128 (1960); S. M. Blinder, *ibid.* **33**, 748 (1960).
[9] R. Lefebvre, J. Chem. Phys. **33**, 1826 (1960).
[10] H. M. McConnell, C. Heller, T. Cole, and R. W. Fessenden, J. Am. Chem. Soc. **82**, 706 (1960).
[11] N. M. Atherton and D. H. Whiffen, Mol. Phys. **3**, 1 (1960).

derivation]:

$$\mathfrak{A}(g\beta/g_p\beta_p)(g\beta H/4kT)\cos\theta,$$

$$\mathfrak{B}(g\beta/g_p\beta_p)(g\beta H/4kT)\sin\theta\cos\phi,$$

$$\mathfrak{C}(g\beta/g_p\beta_p)(g\beta H/4kT)\sin\theta\sin\phi,$$

where H is the external magnetic field intensity. As these components are proportional to those of the external field we can write the spin Hamiltonian for the proton in the form

$$\mathcal{H}_p=\beta_p\mathbf{I}\cdot\mathbf{G}\cdot\mathbf{H}. \tag{2}$$

$\mathbf{G}$ is a coupling tensor given by the relation

$$\mathbf{G}=g_p[\mathcal{E}+(g\beta/g_p\beta_p)(g\beta/4kT)\mathfrak{I}]. \tag{3}$$

In (3) $\mathcal{E}$ is the unit tensor, and $\mathfrak{I}$ the electron-proton coupling tensor, of principal values $\mathfrak{A}$, $\mathfrak{B}$, $\mathfrak{C}$.

The levels associated with (2) are given by[12]

$$E(M_I)=\beta_p M_I G H; \tag{4}$$

M_I is the proton spin quantum number for a projection $\pm\frac{1}{2}$ along the direction of an effective magnetic field, and G the quantity

$$G=\{G_x^2\sin^2\theta\cos^2\phi+G_y^2\sin^2\theta\sin^2\phi+G_z^2\cos^2\theta\}^{\frac{1}{2}}, \tag{5}$$

where G_x, G_y, and G_z are the three principal values of $\mathbf{G}$ In an experiment at fixed frequency ν, there is absorption for the field

$$H=h\beta^{-1}G^{-1}\nu. \tag{6}$$

Numerical calculations show the internal field to be ordinarily of the order of a few gauss. From this the following observations can be made: (a) the spin of the proton is always very nearly quantized along the direction of the external magnetic field. This circumstance will help in discussing the qualitative features of the proton resonance line shapes. (b) Each proton can be treated independently so far as there is no nearby proton producing a static dipolar interaction of comparable magnitude. This will not be always so. In that circumstance two or more protons should be treated together each in its own effective field and taking into account the direct spin-spin interactions.

We now assume that for a given orientation the line shape is a normalized Gaussian centered at H of formula (6), of width λ between points of maximum and minimum slope,

$$F(H')=\lambda^{-1}(2/\pi)^{\frac{1}{2}}\exp-[2(H'-H)^2/\lambda^2]. \tag{7}$$

The line shape for the polycrystalline substance is obtained by multiplying (7) by the probability density for a given orientation of the radical and integrating over all possible orientations, thus giving

$$g(H')=(4\pi\lambda)^{-1}(2/\pi)^{\frac{1}{2}}\int_0^{\pi}d\theta\int_0^{2\pi}d\phi\{\sin\theta \times\exp-[2(H'-H)^2/\lambda^2]\}. \tag{8}$$

Integrals similar to (8) have been calculated[9] by numerical integration on the IBM 704 to obtain the electron spin resonance line shape of a polycrystalline CH π-electron radical. A similar program has been written for the calculation of (8). The component linewidth λ has been assumed to be orientation independent.

APPLICATION TO A POLYCRYSTALLINE AROMATIC RADICAL

McConnell and Strathdee[13] have developed the theory of hyperfine interactions for an aromatic radical in the solid state. The following somewhat simplified version of their treatment is probably sufficient for our purpose.

The electron-proton hyperfine interaction given as (1) combines the contact and dipolar electron-proton interactions and can be also written as

$$ha_H\mathbf{S}\cdot\mathbf{I}-g\beta g_p\beta_p\int\rho(r)\left[\frac{\mathbf{S}\cdot\mathbf{I}}{r^3}-3\frac{(\mathbf{S}\cdot\mathbf{r})(\mathbf{I}\cdot\mathbf{r})}{r^5}\right]dv, \tag{9}$$

where a_H is the isotropic coupling constant for the proton under consideration, and $\rho(r)$ the unpaired electron density function. It is now well established both experimentally and theoretically[1,14,15] that the isotropic coupling constant for a given in-plane proton in an aromatic radical is proportional to the π-electron spin density at the neighboring carbon atom. In the simplest approximation this means that if the unpaired electron density function contains the term

$$\rho(r)=\rho_c\pi^2(r)+\cdots, \tag{10}$$

where π is the $2p\pi$ atomic orbital centered at a carbon atom, then the isotropic coupling constant for the neighboring proton is given by

$$a_H=Q\rho_c, \tag{11}$$

where Q is a negative constant of the order 22–25 gauss.

Turning now to the dipolar part of the hyperfine interaction, it is reasonable to expect that it will be determined essentially by the term shown in (10). Therefore, except for a change of $\pi^2(r)$ into $\rho_c\pi^2(r)$, we have the same coupling tensor as that for a CH fragment. This means that the interaction is diagonal in a local system of axes, with z along the CH bond and x along the $2p\pi$ orbital axis. The principal values of the

[12] E.g., B. Bleaney, Phil. Mag. **42**, 441 (1951).

[13] H. M. McConnell and J. Strathdee, Mol. Phys. **2**, 129 (1959).

[14] H. M. McConnell, Ann. Rev. Phys. Chem. **8**, 105 (1957).

[15] A. D. McLachlan, H. H. Dearman, and R. Lefebvre, J. Chem. Phys. **33**, 65 (1960).

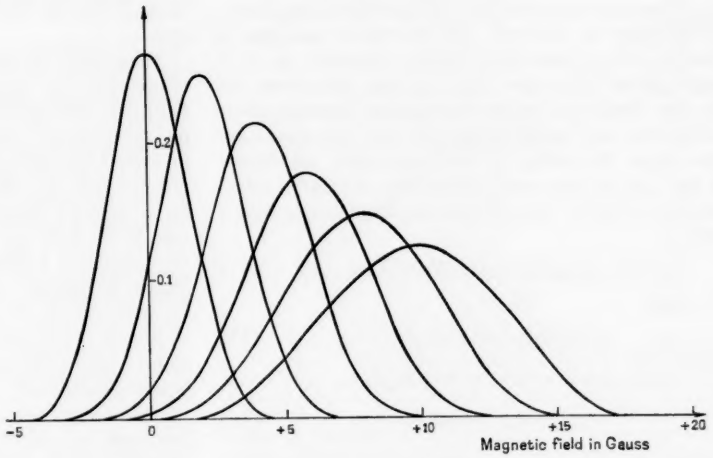

FIG. 1. Proton resonance line shapes for a component linewidth of 3 gauss, and π-electron spin densities ranging from 0.00 (first curve on the left) to 0.25 (last curve on the right) with an interval of 0.05.

coupling tensor are simply proportional to the principal values in the case where the density function is just $\pi^2(r)$. Combining the two parts of the hyperfine interaction we write

$$\mathfrak{Z}=\rho_c\mathbf{T}, \tag{12}$$

where $\mathbf{T}$ is the coupling tensor of principal values, A, B, and C for a standard CH bond, with a π-electron spin density on the carbon integrating to one, and $\mathfrak{Z}$ the coupling tensor of principal values $\mathfrak{A}$, $\mathfrak{B}$, and $\mathfrak{C}$ for the CH bond at which there is found a π-electron spin density integrating to ρ_c. Therefore there is for each in-plane proton in an aromatic radical a tensor coupling its spin to the external field and given by

$$\mathbf{G}=g_p[\mathcal{E}+\rho_c(g\beta/g_p\beta_p)(g\beta/4kT)\mathbf{T}]. \tag{13}$$

We note that (12) is only an approximate relation, because in a more elaborate treatment a_H is only related to the π-electron spin density, while the dipolar interaction depends also on the σ-electron spin density.

In an experiment carried out at a given absolute temperature and for a given external magnetic field intensity, the line shape for a particular proton depends in the present approximation only on ρ_c, the π-electron spin density on the neighboring carbon, which can be positive or negative. Because A, B, and C for the reference CH bond are all of the same sign and negative,[10] it follows from (13) and (6) that the proton resonance occurs for all orientations at a higher field if ρ_c is positive and at a lower field if ρ_c is negative. For an infinitely narrow component line, the line shape would extend only toward either higher fields or lower fields. This is not necessarily so with a finite component linewidth.

Figure 1 gives the line shapes which have been obtained for a component linewidth independent of ρ_c and equal to 3 gauss; ρ_c has been taken positive, with values ranging from 0.00 to 0.25, with an interval of 0.05. We take T and H to be the same as in the experiments of Brown, Anderson, and Gutowsky,[6] namely, 77°K and 6300 gauss. For A, B, and C the values derived by McConnell, Heller, Cole, and Fessenden[10] from a study of the electron spin resonance spectrum of the $(COOH)_2CH$ radical were used (that is $A\sim-10.4$ gauss, $B\sim-21.8$ gauss, $C\sim-32.5$ gauss).

There are three properties of these line shapes which follow from an inspection of Fig. 1: (a) the line shapes are all very symmetrical and approximately Gaussian, (b) the peak is displaced to higher fields as ρ_c is increased. This displacement is linearly related to ρ_c, (c) the width increases progressively.

It is difficult to make more precise statements concerning the dependence on ρ_c of the line shape given in (8) because of the complicated form of this integral. However, as we shall see below, the line shape referring to an infinitely narrow component linewidth can be discussed in the same way as Sternlicht[8] has discussed the electron spin resonance line shape of the CH π-electron radical, in the case where the proton spin is quantized along the direction of the external magnetic field. Formula (6) can be rewritten

$$H=h\beta_p^{-1}g_p^{-1}\nu(G/g_p)^{-1}=H_0(G/g_p)^{-1}, \tag{14}$$

and because of the small anisotropy in the tensor $\mathbf{G}$, we have

$$(G|g_p)^{-1}\simeq 1-\rho_c(g\beta/g_p\beta_p)(g\beta/4kT)[A\cos^2\theta + B\sin^2\theta\cos^2\phi+C\sin^2\theta\sin^2\phi]. \tag{15}$$

Therefore absorption occurs at a field differing from the normal resonance field H_0 by (Note that A, B, and C are negative),

$$-\rho_c(g\beta/g_p\beta_p)(g\beta H_0/4kT)[A\cos^2\theta+B\sin^2\theta\cos^2\phi + C\sin^2\theta\sin^2\phi]. \tag{16}$$

A similar expression is found in Sternlicht's treatment, except that the electron spin resonance spectrum is made up of a symmetrical doublet. However, as A, B, and C are all of the same sign, the lines never cross and the line shape for the present problem corresponds to one of the two halves of the electron spin resonance line shape. According to this treatment transposed to the case of (16) and taking into account the fact that $|A|<|B|<|C|$, the line shape will extend from a field,

$$-\rho_c(g\beta/g_\mu\beta_\mu)(g\beta H_0/4kT)A, \tag{17}$$

to a field,

$$-\rho_c(g\beta/g_\mu\beta_\mu)(g\beta H_0/4kT)C, \tag{18}$$

with a peak going to infinity at a field,

$$-\rho_c(g\beta/g_\mu\beta_\mu)(g\beta H_0/4kT)B. \tag{19}$$

This suffices to explain completely the behavior of the line shape in the case of a finite component linewidth. (a) the line is very nearly symmetrical because $(A-B)\sim(B-C)$. (b) the peak displacement is linearly related to ρ_c [cf. (19)]. In addition as $|B-a_H|$ is a rather small quantity both on experimental[10] and theoretical[13] grounds, the relation is nearly that valid for the solution (in that case $A=B=C=a_H$). (c) the width increases with ρ_c as this is $[\rho_c(g\beta)^2H_0(A-C)]/4kTg_\mu\beta_\mu$ for the line shape with zero component linewidth.

These three properties of the proton resonance line shapes are just those which have been observed by Gutowsky and collaborators[5,6] in experiments performed on polycrystals containing diphenyl-picryl hydrazyl and *tris-p* chlorophenylaminium perchlorate. In particular the fact that the peak displacement is nearly that for a solution enabled them to make a reasonable correlation between the observed displacements and the calculated π-electron spin densities on the carbon atoms. It appears from the present calculations that the hyperfine interaction alone produces a distribution of proton resonances that can explain the increase in width without any appreciable contribution from static dipolar interactions.

Although in this paper only the proton resonance line shape in aromatic radicals was treated the method could be readily extended to the magnetic resonance of other nuclei of nonzero spin in polycrystalline radicals.

ACKNOWLEDGMENTS

Thanks are due to Mr. Bessis for writing the program for the calculation of expression (8) and to the Institut Européen de Calcul Scientifique for grant of 704 machine time.

THE JOURNAL OF CHEMICAL PHYSICS VOLUME 34, NUMBER 6 JUNE, 1961

Gaseous Detonations. XV. Expansion Waves in Gaseous Detonations

HAJIME MIYAMA* AND PAUL KYDD†

Gibbs Chemical Laboratory, Harvard University, Cambridge, Massachusetts

(Received November 23, 1960)

The ultraviolet absorption spectrum of OH and the visible light emission profile in the rarefaction wave following a detonation in $C_2H_2+H_2+2O_2$ have been measured. Analysis of the absorption spectrum at an initial pressure of 60 mm Hg gives an average rotational temperature of 3164°K during the first 310 μsec. after the detonation wave front. The gas temperature calculated by using detonation theory and necessary thermodynamic data is 392°K higher than the experimental rotational temperature. The difference is very close to the difference of 350°K which has been predicted by T. C. James theoretically.

The emission profiles demonstrated the presence of double waves at initial pressures higher than 90 mm and the appearance of these waves coincides with an increase in detonation velocity to that calculated using a "frozen" sound velocity.

In expansion waves produced by bursting a thin diaphragm with the detonation wave, the emission intensity was found to be far higher than predicted and the velocity of the expanding gas and the shock wave ahead of it to be somewhat lower than expected.

AS is well known, a detonation wave consists of the reaction zone between the wave front and the C–J plane and the rarefaction zone which follows the C–J plane. Measurements of OH radical concentration,[1] light emission,[2] and rotational[3] or vibrational[4] temperature of OH radicals in the reaction zone have already been published by several researchers; however, meas-

* Present address: Department of Chemistry, Defense Academy, Yokosuka, Japan.

† Present address: General Electric Research Laboratory, Schenectady, New York.

[1] T. Just and H. G. Wagner, Z. Elektrochem. **61**, 678 (1957).

[2] A. L. Bennett and H. W. Wedaa, J. Chem. Phys. **23**, 1359 (1955).

[3] G. B. Kistiakowsky and F. D. Tabbutt, J. Chem. Phys. **30**, 577 (1959).

[4] G. B. Kistiakowsky and R. K. Lyon, J. Chem. Phys. (to be published).

urements of these quantities in the rarefaction zone have not been reported.

Measurements of the absolute intensity of OH absorption are especially interesting to determine the correct values of a (the ratio of collision broadening to Doppler broadening) and f (the f value of dispersion theory) for the OH absorption spectrum in a detonation. This can be done by comparing the spectroscopic results with the calculated results of detonation theory. These quantities can then be used to obtain the concentration of OH in the rarefaction wave.

For this purpose, we measured the velocity of the detonation wave, the ultraviolet absorption spectrum of OH, and the light emission in the rarefaction wave of the detonation of $C_2H_2+H_2+2O_2$ mixture.

The light emission has also been measured in the expansion wave produced in vacuum by rupturing a diaphragm with a detonation wave in the above mentioned mixture, and strong shock waves have been qroduced in argon by the same method. The shock velocity and the emission profile behind them have been obtained. Very little data on this subject is available.[5,6]

EXPERIMENTAL DETAILS

The procedure used to obtain the OH absorption spectrum was almost the same as that described in the previous papers[3,4] except for the dimensions of the detonation tube and the structure of the flash lamp.

The new detonation tube has an internal diameter of 10 cm and a total length of 472 cm with a spark plug

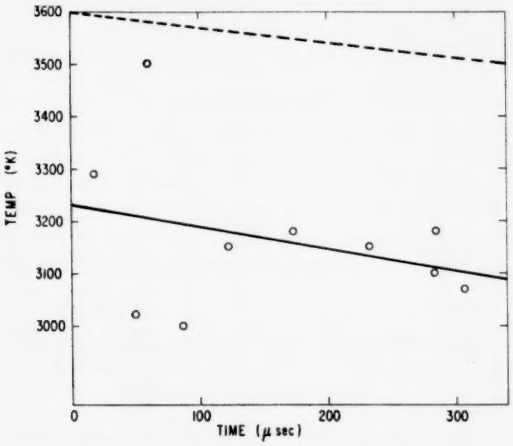

FIG. 1. Variation of rotational temperature and calculated gas temperature with time after detonation front. Open circles, experimental rotational temperature; solid line, the least square line for experimental values; dotted line, the calculated gas temperature.

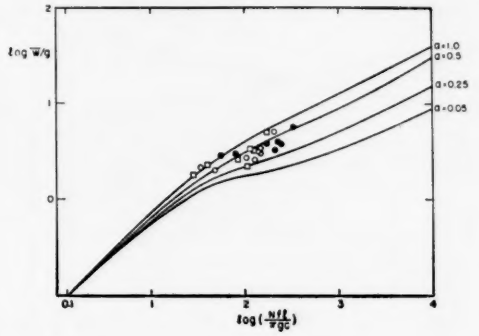

FIG. 2. Curve of growth with experimental values. Open circles, a run at 306.7 μsec after detonation front; closed circles, a run at 128.5 μsec; open squares, a run at 284.2 μsec. $\bar{W}$ is the equivalent linewidth calculated from the observed absorption line dividing its area by the incident intensity; N is the concentration of absorbing OH radicals; l, the effective path length; f, the f value of dispersion theory; c, the velocity of light; g, the total width of a Doppler broadened line; and a, the ratio of collision broadening to Doppler broadening.

at one end for igniting the mixture. At a distance of 411 cm from this end of the tube, there were placed two quartz windows which had a width of 0.55 cm in the direction of propagation of the wave and a height of 2.5 cm. The inside surface of the windows was almost perfectly flush with the walls of the tube. A photomultiplier gauge used for triggering a raster sweep oscilloscope, four ionization gauges for velocity measurement, and another photomultiplier gauge for triggering the flash lamp were placed in line for 100 cm upstream of the windows and one more velocity gauge was placed on the downstream end plate (61 cm from the window section).

The light source for absorption measurements was the short flash of strong continuous radiation from a condensed spark discharge between two tungsten electrodes. These were enclosed in a quartz capillary of 2 mm i.d. and 3 mm wall thickness, and were mounted in a housing filled with 65 mm Hg of oxygen. A 3μf condenser at 4.3 kv was discharged through them by a trigger electrode. This was actuated, through a delay circuit and an amplifier, by the photomultiplier gauge 17.8 cm ahead of the quartz windows. The duration of the flash was less than 2 μsec at the wavelengths around 3000 A. Compared with the flash lamp described in the previous papers,[3,4] this one had much higher intensity and this made possible more precise measurements of rotational temperature and concentration of OH. The rotational temperature and OH concentration were obtained by analyzing the R_2 branch of the O–O transition of the $^2\Sigma^+ \rightarrow {}^2\pi$ band system.

Emission measurements were made with a photomultiplier and a cathode follower, the rise times of which were less than 3 μsec. This emission intensity was adjusted with sheets of Lektromesh filter of known transparency, and two 1 mm slits were placed between

[5] G. A. Bird, "A note on combustion driven shock tube," RAE Tech. Note Aero., 2511 (May, 1957).

[6] H. F. Waldron, "An Experimental investigation of the flow properties behind strong shock waves in nitrogen," UTIA Rept. No. 50 (March, 1958).

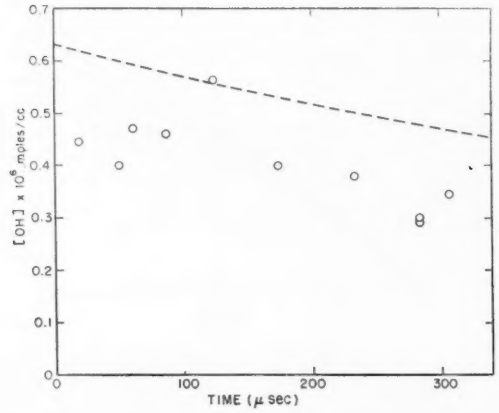

FIG. 3. Variation of measured and calculated OH concentration with time after the detonation front. Open circles are experimental OH concentrations obtained by assuming $F=1.45\times10^{-4}$ and $a=0.5$. The dotted line is the calculated OH concentration.

the tube and the phtomultiplier to obtain an optical time resolution of less than 5 μsec. Most of the measurements were made with a Baird atomic interference filter with a transmission peak at 4163 A, but a 4362-A filter was sometimes used.

For measurements in the expansion wave, produced by breaking a diaphragm with a detonation wave, the diaphragm (usually 0.0005-in. thick Mylar sheet) was placed 2, 4.2, 6.2, 9.7, or 52.7 cm ahead of the window section. Five more velocity gauges were placed between the window section and the downstream end plate. Shock waves in argon were produced in the same way.

EXPERIMENTAL RESULTS

Measurements of Rotational Temperature, Concentration of OH, and Light Emission in the Rarefaction Wave

OH rotational temperatures were obtained[7] by plotting the logarithms of the intensity of lines in the R_2 branch vs their energy. The temperature was calculated by using only lines $R_2$3, $R_2$4, $R_2$7, $R_2$8, $R_2$14, and $R_2$15. This was done because these lines are strong and easily measured, and the results agreed with the values obtained by using the iso-intensity method.[3,7] Rotational temperatures obtained in this way for detonations in 60 mm Hg of the mixture $C_2H_2+H_2+2O_2$ are shown in Fig. 1 as a function of the time behind the wave front. In these measurements the detonation wave was very stable and had a mean velocity of 2561±0.9 m/sec.

The OH concentration is calculated by using the method of the curve of growth,[8,9] an example of which is shown in Fig. 2. Since g, l, and c are known or can be calculated, by choosing suitable values of a and f, N can be obtained from the measured values of $\bar{W}$ and the curve. By using the rotational and vibrational partition functions, the total concentration of OH in the ground state (N_0) can be obtained. The numerical values of these quantities which have been used are as follows: $T=3555.5°K$, $a=0.5$, $l=10$ cm, $F=1.45\times10^{-4}$ and $N/N_0=0.001422(2J''+1)\exp(-E_k/kT)$; F is related to the f value by the following expression:

$$f=FS_{J'J''}/(2J''+1), \qquad (1)$$

where $S_{J'J''}$ is the rotational transition probability. Justication for using the above values of temperature, a and f, will be given later. The measured values of the OH concentration are plotted in Fig. 3 for detonation at an initial pressure of 60 mm.

The detonation velocity and light emission profiles were measured at various initial pressures as shown in Figs. 4 and 5. Emission measurements with both 4326-A filter and 4163-A filter gave the same result, and therefore all of the later measurements were done with 4163-A filter. The shape of the emission profile changes strikingly as the initial pressure is changed. Almost the same behavior was observed in the mixture $C_2H_2+H_2+3O_2$ but was not observed in the mixture $C_2H_2+H_2+O_2$ which gave unstable waves.

Measurements of Light Emission in the Expansion Waves Produced by Detonation Waves

Emission profiles were measured at distances of 2, 6.2, 9.7, and 52.7 cm from the diaphragm and with initial pressures of 60, 120, and 150 mm Hg of detonable

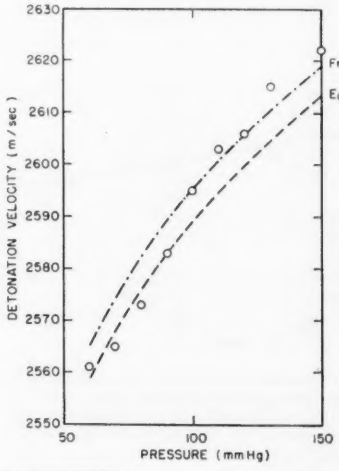

FIG. 4. Variation of detonation velocity with initial pressure. Open circles, experimental values; dashed line, calculated frozen value; dotted line, calculated equilibrium value.

[7] G. H. Dieke and H. M. Crosswhite, Bumble Bee Series Rept. 87, The Johns Hopkins University (1948).

[8] A. C. G. Mitchell and M. W. Zemansky, *Resonance Radiation and Excited Atoms* (Cambridge University Press, New York, 1934).

[9] T. Carrington, J. Chem. Phys. **31**, 1243 (1959).

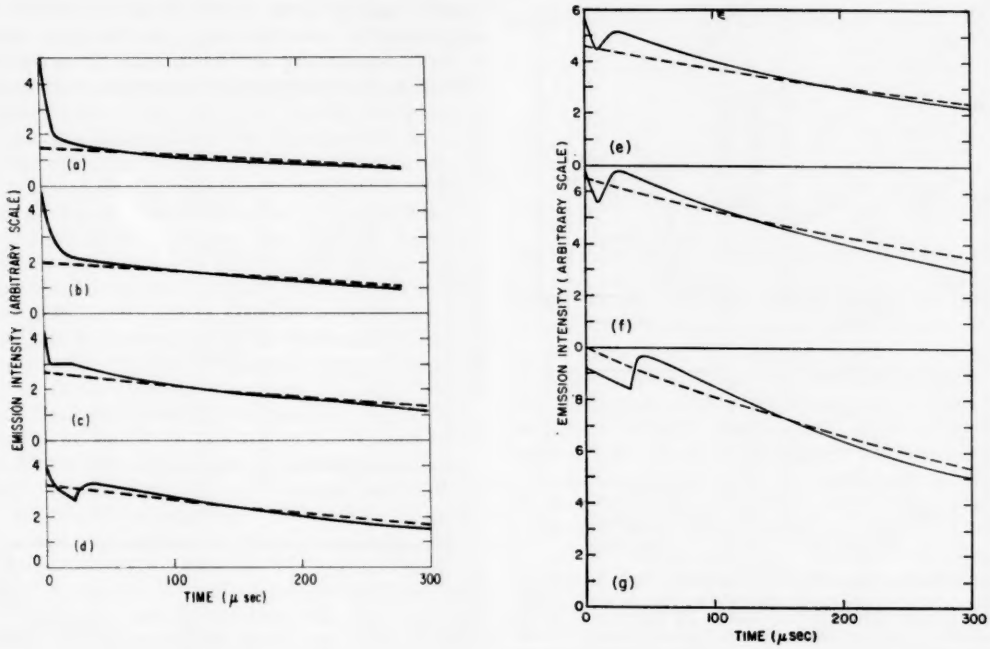

FIG. 5. Variation of the emission intensity and the calculated value of the quantity [CO][O] with time after the detonation front. The ordinate scale is in arbitrary units chosen to agree with the calculated curve at 150 μsec; a: at 60 mm Hg; b: at 70 mm; c: at 80 mm; d: at 90 mm; e: at 100 mm; f: at 120 mm; g: at 150 mm. Solid lines, experimental curves; dotted line, calculated curves.

mixture. Results with 0.001 in. thick cellophane diaphragms were almost the same as those with 0.0005-in. Mylar, but measurements with 0.001-in. Mylar gave somewhat higher emission intensity that started about 20 μsec later. The emission measured at 2 cm was very irreproducible, and therefore this measurement is omitted in Fig. 6. The intensity was calibrated by using the emission from a detonation which was produced under the same conditions but without the diaphragm, after each expansion experiment. The ordinate 1.0 corresponds to the emission intensity at the $C-J$ plane.

Measurements of the Shock Velocity and Light Emission behind Shock Waves in Argon Produced by Detonation

Measurements of shock wave velocity are shown in Fig. 7 where 120 mm of detonable mixture in the driver section and 10, 60, or 120 mm of argon in the expansion section was used. In the case of 120 mm of argon, emission was measured at 6.2-, 9.7-, and 52.7-cm distances from the diaphragm as shown in Figs. 8(a)–(c). For 60 mm and 10 mm of argon, this was measured only at 52.7 cm as shown in Figs. 8(d) and (e).

DISCUSSION

Measurements of Rotational Temperature

By using the detonation theory[10] and necessary thermodynamic data,[11] various quantities at the $C-J$ plane and in the rarefaction wave can be calculated. The $C-J$ conditions for denonation in the mixture used in this research were calculated using the IBM 704 program made available to us by J. A. Fay of M.I.T. Conditions in the isentropic rarefaction wave were calculated using tables computed by W. G. Browne of the General Electric Company.

In Fig 1, the calculated translational temperature is compared with the experimental rotational temperature. The average value of the rotational temperature for 310 μsec after the arrival of the detonation wave is 392°K lower than the corresponding calculated value. In a previous paper,[3] a difference of 400°K in the same direction was found for a $2H_2+O_2$ detonation. It was suggested that this could be due to instrumental error, but according to the recent paper of James,[12] the observed rotational temperature for the 0—0 transition

[10] B. Lewis and G. Von Elbe, *Combustion, Flames, and Explosions of Gases* (Academic Press, Inc., New York, 1951).
[11] Selected Values of Thermodynamic Properties (National Bureau of Standards, Washington, D. C.), Ser. III, Vol. 1.
[12] T. C. James, J. Chem. Phys. **32**, 1770 (1960).

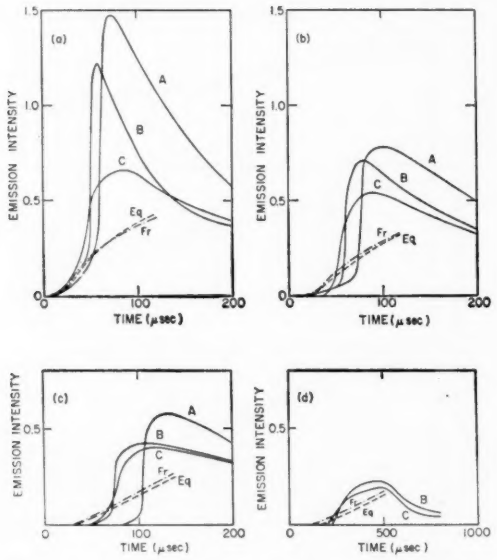

FIG. 6. Emission intensity as a function of time in the free expansion of the products of detonation into vacuum. Initial pressure of detonable mixture: curve A, 60 mm; curve B, 120 mm; curve C, 150 mm. Distance from the diaphragm: 6(a), 4.2 cm; 6(b), 6.2 cm; 6(c), 9.7 cm; 6(d), 52.7 cm. Calculated frozen —·— and equilibrium — — — curves shown for comparison.

of the $^2\Sigma^+ \rightarrow {}^2\pi$ band system must be lower than the true temperature as a result of theoretical consideration of rotation-vibration interaction in electronic transitions. He predicts that for the R_2 branch used in the present research, if the true temperature were 3000°K the measured temperature would be 2650°K, a difference of 350°K. Since the calculated temperature in the present case is in the neighborhood of 3500°K, the effect should be somewhat bigger, and the results appear to be in satisfactory agreement with the prediction. Therefore, it seems reasonable to use the calculated gas temperature in further discussion instead of the experimental rotational temperature.

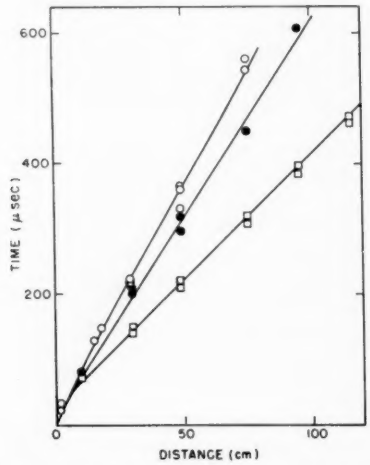

FIG. 7. Velocity plots of argon shock waves driven by a detonation at 120 mm initial pressure. Argon pressure, 10 mm □, 60 mm ●; 120 mm ○.

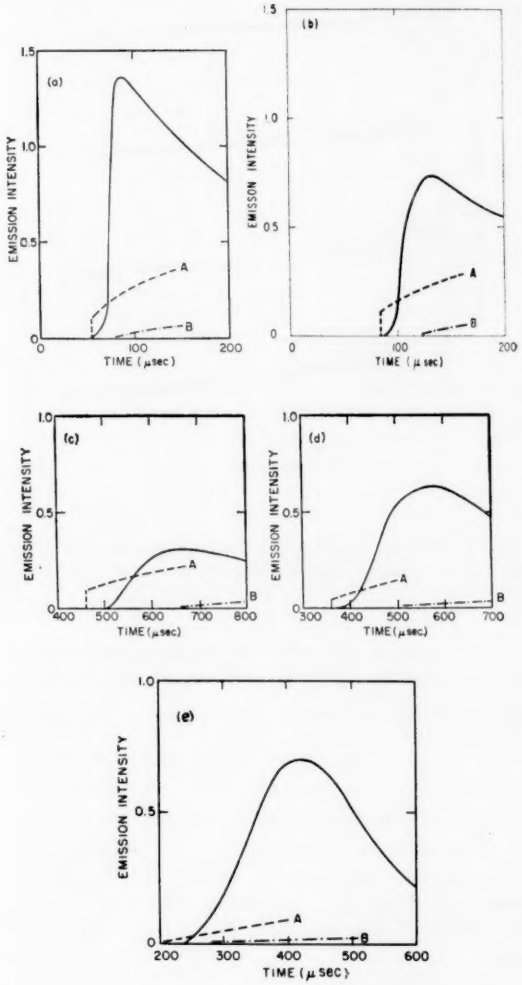

FIG. 8. Emission intensity as a function of time behind shock waves driven into argon by a detonation at 120 mm initial pressure. Argon pressure Figs. 8(a)–(c), 120 mm; 8(d), 60 mm; 8(e), 10 mm. Distance from the diaphragm: 8(a), 6.2 cm; 8(b), 9.7 cm; 8(c)–(e), 52.7 cm. Calculated curves for cases A and B shown for comparison.

Measurements of OH Concentration

To obtain experimental values of OH concentration, it is necessary, as mentioned previously, to choose suitable values of a and f (or F). For OH in flames,

Kaskan[13] obtained the following empirical formula for a:

$$a=450\ \mathrm{P/T}, \qquad (2)$$

where P is the pressure in atmospheres and T is the absolute temperature. In the present experiment, pressure and temperature were averaged for the first 310 μsec after the detonation front to obtain values of 1.99 atm and 3555°K, respectively, which gives $a=0.25$. There are two groups of values for F, i.e., Carrington's value[9] 3.24×10^{-4} which agrees very well with the value of Oldenberg[14] and also is supported by Kaskan,[15] and on the other hand Dyne's value[16] 1.45×10^{-4}. If Dyne's value is applied to our results with $a=0.25$, the OH concentration becomes twice the theoretical value. In order to decrease this difference, a bigger value of a must be used. To obtain the values of a and F which agree best with our results, the intensities of seven lines measured in each of ten experiments have been used to determine values of the product FN_0 using the curves of growth corresponding to values of a equal to 0.05, 0.25, 0.5, and 1.0. When the product is divided by N_0 calculated from the detonation theory, the values of F shown in Table I were obtained. The standard deviation of the F values was taken as an indication of the accuracy of the fit between the data and the curves of growth. This indicates that $a=0.5$ and $F=1.13\times10^{-4}$ give the best agreement. Therefore, experimental values of OH concentration calculated with the combination of Dyne's value for F and $a=0.5$ are shown in Fig. 3 for the comparison with the theory.

TABLE I.

a	F	Standard deviation
1.0	6.53×10^{-5}	65.5%
0.5	1.13×10^{-4}	53.5%
0.25	3.33×10^{-4}	59.7%
0.05	1.13×10^{-3}	64.3%

Measurements of Emission Intensity

As shown in Fig. 5 the change of the emission intensity agrees fairly well with the change of the calculated value of the product [CO][O] except at the wave front. It is well known that the flame of carbon monoxide burning with oxygen shows strong emission in the blue to near ultraviolet region (4500–3500 A). According to Gaydon[17] and Kaskan,[18] this continuous emission is due to the reaction $CO+O=CO_2+h\nu$. The use of an interference filter at 4163 A removes the light emitted by other species such as OH, CH, C_2, and HCO, therefore it seems reasonable that the measured emission is due to the CO+O reaction.

Concerning the shape of the emission profile at the wave front in Fig. 5, the first peak seems due to chemiluminescence during the reaction zone which has been observed in acetylene and oxygen detonation by Bennett.[2] Above 90 mm Hg a second peak appears and the separation between the two peaks increases at higher pressure. The same phenomenon has been observed previously[19] in several hydrocarbon-oxygen mixtures and explained as being due to an entropy increase in the rarefaction wave caused by further reaction. This explanation appears to be confirmed by the present results. The sudden transition to a lower detonation velocity below 100 mm pressure shown in Fig. 4 correlates with abrupt reduction in intensity of the second emission peak relative to the first. This indicates that the second wave seen in the light emission plot supplies energy to the first wave front as long as the secondary reactions are proceeding rapidly enough to maintain it. When the pressure is reduced so that the second wave is not maintained, the detonation velocity and temperature decrease. This effect may be related to the abnormally large diameter effect and low pressures observed behind detonation waves in low pressure gases.[20]

Measurements of Light Emission in the Expansion Waves Produced by Detonation Waves

As described above, there was good agreement between the light emission profile in the normal rarefaction wave and the calculated change of the quantity [CO][O]. In an attempt to measure the chemical reaction rates for the recombination of radicals in an expansion wave, emission measurements, in the very rapid expansion wave produced by rupturing a diaphragm with a detonation, were conducted. In Fig. 6 the intensity scale was calibrated by using the emission from a detonation wave, produced under the same conditions but without the diaphragm, after each expansion experiment. The difference between the calculated profiles for expansion with chemical equilibrium and for frozen expansion is not very great. Equilibrium profiles were obtained by assuming that all chemical species in the expansion wave are equilibrated at all times and that equilibrium values of γ and the sound velocity may be used. The others were obtained by assuming that chemical composition in the expansion wave is frozen and that frozen values of γ and sound velocity must also be used. In the former case, the $x-t$ diagram[21] which is necessary to obtain the change of [CO][O] with time during the expansion was

[13] W. E. Kaskan, J. Chem. Phys. **31**, 944 (1959).
[14] O. Oldenberg and F. F. Rieke, J. Chem. Phys. **6**, 349 (1938).
[15] W. E. Kaskan, J. Chem. Phys. **29**, 1420 (1958).
[16] P. J. Dyne, J. Chem. Phys. **28**, 999 (1958).
[17] A. G. Gaydon, *The Spectroscopy of Flames* (Chapman and Hall, Ltd., London, 1957), p. 91.
[18] W. E. Kaskan, Combustion and Flame **3**, 39 (1959).
[19] M. Cher and G. B. Kistiakowsky, J. Chem. Phys. **29**, 506 (1958).
[20] D. H. Edwards, G. T. Williams, and J. C. Breeze, J. Fluid Mech. **6**, 497 (1959).
[21] G. Rudinger, *Wave Diagram for Nonsteady Flow in Ducts* (D. Van Nostrand Co., Princeton, New Jersey, 1951).

TABLE II.

Pressure of argon	Experimental shock velocity (m/sec)	Calculated shock velocity (m/sec) Case A Fr.	Case A Eq.	Case B Fr.	Case B Eq.
10 mm Hg	2600	3216	3284	2396	2540
60	1650	1947	2000	1415	1450
120	1450	1563	1595	1118	1139

constructed by following an isentropic change from the $C-J$ condition in a table obtained from the General Electric Company. In the latter case, it was constructed by using the condition that the Riemann variable P must be constant [21] during expansion,

$$P=2a/(\gamma+1)+u, \tag{3}$$

where u is flow velocity and a the sound velocity. Strictly speaking, the effect of the rarefaction wave which follows the detonation front must also be taken into account. This wave interacts with the expansion wave produced by rupturing the diaphragm, but for the initial part of expansion profile, this effect can be neglected and the above described methods can be used as the first approximation.

As shown in Fig. 6, the difference between the experimental results and the calculated values is very large, particularly with regard to the peak intensity, though the emission appears at the time which is predicted by the theory. Two possible reasons for this difference may be considered. One is that the diaphragm does not break properly and another is the effect of emission from some impurities. As described in the experimental section, measurements with different diaphragms show that the diaphragm does not rupture immediately. therefore, the flow is complicated by a reflected wave and the gas in the expansion wave may be much hotter than calculated at short distances from the diaphragm. This effect is expected to become smaller at longer distance from the diaphragm and at higher pressure. Actually, measurements at the distance of 52.7 cm from the diaphragm show that this is the case, and flow approaches the equilibrium condition. The effect of the emission from impurities cannot be important because several emission measurements without any filter gave almost the same profiles, both in shape and in peak intensity relative to the detonation wave, as those with a filter. This suggests that the light being observed is concentrated in the blue continuum from the reaction under study.

Measurements of the Shock Velocity and Light Emission behind Shock Waves in Argon Produced by Detonation

To investigate further the rupturing of the diaphragm and the behavior of the expanding gas from the detonation wave, experiments on driving shock waves in argon were conducted.

As explained by Bird,[5] when a detonation takes place in the high pressure end of a shock tube, a diaphragm which is just able to withstand the pressure of the unburnt gas will be instantly ruptured by the detonation wave (case A). The subsequent flow will then be determined by the condition at the $C-J$ plane of the detonation. If the diaphragm is sufficiently strong to withstand the pressure and temperature behind the detonation wave, the burnt gas will come to rest before the diaphragm is broken and the flow will be in accordance with the classical shock tube theory (case B). If the diaphragm is intermediate in strength between these two extreme cases, the flow will be more complex than in either.

In order to compare the experimental results with the theoretical values, calculations were conducted for these two extreme cases. For case A, the effect of the rarefaction wave after the detonation front was neglected for the same reason as in the expansion experiment. By using the same methods as were used in the calculation of detonation-driven expansion waves into vacuum, the relation between pressure and flow velocity in the expansion wave can be calculated from the condition of the burnt gas in the driver section. In case A, this gas is moving forward and in case B it is at rest. For the relation of flow velocity and pressure in the region between the shock wave and contact surface to those in the unshocked argon, there is the following Hugoniot equation[22]:

$$u_2=u_1+(p_2-p_1)\{2/\rho_1[(\gamma_1-1)p_1+(\gamma_1+1)p_2]\}^{\frac{1}{2}},$$

where u, p, and ρ are flow velocity, pressure, and density, respectively. At the contact surface, p and u of the shocked gas must be equal to the corresponding quantities of the expanding gas. Therefore, by plotting these two relationships between u and p in the $u-p$ plane and finding the intersection point of these two curves, the pressure and flow velocity can be calculated. The velocity of shock wave is given by the following relationship[22].

$$w_1=a_1[\beta_1(1+\alpha_1 p_2/p_1)]^{\frac{1}{2}}, \tag{4}$$

where $\alpha_1=(\gamma_1+1)/(\gamma_1-1)=4.00$, $\beta_1=(\gamma_1-1)/2\gamma_1=0.200$ and $a_1=321.5$ m/sec for argon at 300°K. Calculated values of the shock velocity are shown in Table II. There is not much difference between values using the frozen assumption and those using the equilibrium assumption. However, there is a big difference between values for cases A and B. By using the results of these calculations, theoretical profiles of [CO][O] for the equilibrium case are also calculated as shown in Fig. 8 for comparison with the experimental data.

According to the results of Fig. 8 the light emission appears almost at the time which is predicted by the

[22] I. I. Glass and G. N. Patterson, J. Aeronaut. Sci. **22**, 73 (1955).

calculation for the case A. However the contact surface between argon and luminous gas appears to be rather broad, especially at 52.7 cm from the diaphragm. By comparing the midpoint of the rise in luminosity with the predicted time of arrival of the contact surface, the actual situation appears to lie between cases A and B. The most ideal case occurs with the highest pressure of argon used. Measurements at 120 mm Hg of argon show that the emission peak height becomes lower at longer distances from the diaphragm as was described in the free expansion experiments. The measured shock velocity is also intermediate between cases A and B as shown in Table II. Again the best agreement with the ideal situation (case A) is obtained at the highest pressure of argon. The observed shock velocity record shows an acceleration of the shock wave to a distance of about 9 cm from the diaphragm at all argon pressures, but after that the velocity becomes constant within experimental error. Waldron[6] observed a strong attenuation of the velocity of detonation-driven shock waves in nitrogen, but this was observed at a distance of more than five feet from the diaphragm in a 2×2-in. shock tube. Up to this distance, the velocity was almost constant. In his report, there was no comparison between the measured shock velocity and the calculated value. The deviation of the measured shock velocity from the calculated values for the case A is probably due to losses in the expansion process, since the discrepancy is worst at the lowest argon pressure. If the discrepancy were mostly due to nonideal diaphragm rupture, the pressure dependence should be in the other direction, since the force on the diaphragm is greatest with the lowest argon pressure.

Results at lower pressures of argon show that the intensity of emission is unusually strong compared with the calculated value of [CO][O]. A compression wave will be formed by the interaction of the expansion waves with the contact surface, but this is too weak[5] to explain this strong emission. As a result of the calculation of shock temperature by using the experimental shock velocity, the temperature behind shock waves at 10 mm, 60 mm, and 120 mm Hg of argon are 6360°K, 2720°K, and 2150°K respectively. Only the temperature with 10 mm of argon can ionize argon to give strong emission[23], but the emission with 60 mm of argon cannot be explained by this effect. At present, our data are not sufficient to explain this strong emission. It is interesting to note that quite high shock strengths can be produced in light tubes by this method because of the very high temperature and forward mass velocity of the gas behind the detonation wave. The Mach number of the shock wave produced in 10 mm argon by 120 mm of detonable mixture was 8.1.

ACKNOWLEDGMENTS

We wish to express our thanks to Professor G. B. Kistiakowsky for his helpful advice. Also, we are grateful to Professor D. H. Menzel for allowing us to use a microdensitometer; to Professor H. W. Emmons, Professor A. E. Bryson, and Dr. W. E. Kaskan for their helpful advice; to Dr. W. G. Browne for allowing us to use the General Electric Tables; to Professor J. A. Fay for allowing us to use the IBM 704 Code; and to Dr. W. Gardiner for help in our calculations. One of us (H. M.) wishes to thank the National Science Foundation and the Milton Fund for post doctoral fellowships. This work was supported by the funds of the Office of Naval Research to which we express our thanks.

[23] H. E. Petschek, P. H. Rose, H. S. Glick, A. Kane, and A. Kantrowitz, J. Appl. Phys. **26**, 83 (1955).

Effect of Electron Energy on Some Electron-Impact Processes

SEYMOUR MEYERSON

Research and Development Department, American Oil Company, Whiting, Indiana

(Received December 27, 1960)

Decomposition processes induced by electron impact have been inferred from appearance potentials and from isotopic distributions of fragment ions in mass spectra of labeled compounds. Implicit in such inferences is an assumption that the paths by which the fragment ions are formed are the same near the appropriate appearance potentials as at the higher electron energies usually employed. For five ions that were the subjects of earlier studies—$C_7H_7^+$ from two deuterated *p*-xylenes and $C_5H_5^+$ from two deuterated toluenes and a deuterated benzyl chloride—isotopic distribution has been found to be essentially independent of electron energy. These results support the assumption made in earlier studies.

MASS spectra are obtained conventionally by bombardment with electrons accelerated to 50 to 75 v. In attempts to clarify the reactions underlying the spectra, data obtained at such electron energies are often correlated with appearance potentials—the minimum energies at which ions of particular masses are formed. Such correlations assume that the ions, and the paths by which they are formed, are unchanged by lowering the electron energy to a value close to the appearance potential. At such a low energy, one can reasonably hope that all ions observed stem from a single process. But, at higher energies, additional processes are likely to set in; processes with different energy requirements have been shown to give rise to ions of the same mass.[1]

TABLE I. Low-voltage spectra of xylenes.

	α-d			*x-d*	
	Peak height at mass:			Peak height at mass:	
Ionizing voltage	91	92	Ionizing voltage	91	92
		Repeller voltage=1.5			
9.5	3.3	4.4	10.0	11.4	24.0
10.0	14.7	18.6	10.5	33.6	72.9
10.5	42.6	57.6	11.0	60.0	127.5
11.0	78.6	108.6	11.5	99	212
11.5	131.7	178	12.0	147	321
12.0	201	272	12.5	201	447
12.5	285	378	13.0	257	569
13.0	359	478	13.5	321	720
13.5	459	602	14.0	393	889
14.0	565	739			
		Repeller voltage=10.0			
4.3	1.1	1.5	a		
4.8	6.0	8.0			
5.3	27.5	33.3			
5.8	75.9	96.0			
6.3	148	186			
6.8	257	329			
7.4	391	495			
7.8	540	670			
8.4	720	903			
8.9	906	1143			

[a] Not measured.

In electron-impact studies in this laboratory, labeling evidence obtained with 70-v electrons, taken together with appearance potentials and other data, has provided a basis for inferring processes by which ions are formed. Such interpretation requires that the isotopic distributions obtained at electron energies close to the appearance potentials be the same as those at 70 ev. Accordingly, the isotopic distributions of $C_3H_3^+$ ions from propyne-3-d_3[2] and of $C_6H_5^+$ and CH_3^+ ions from deuterated toluenes[3] at electron energies near the appearance potentials have been found essentially the same as at higher energies. Data on $C_3H_5^+$ ions from 1-butene-4-d_3 have been interpreted as showing that the deuterium content of these ions increases markedly as the electron energy approaches the appearance potential.[4] However, this interpretation rests on the assumption that the intensities of variously deuterated $C_3H_4^+$ and $C_3H_3^+$ ions are negligible throughout the range of ionizing voltages studied. This assumption is open to serious question; consequently, no effect of ionizing voltage in this system has been clearly established.

The possible dependence of isotopic distribution upon electron energy has now been investigated for five additional ions that were the subjects of earlier studies: $C_7H_7^+$ from two deuterated *p*-xylenes[5] and $C_5H_5^+$ from two deuterated toluenes[6] and a deuterated benzyl chloride.[7] We have also included a second variable, ion-repeller voltage. As repeller voltage is increased, residence time of the ions in the chamber is decreased;

[1] J. D. Morrison, J. Chem. Phys. **22,** 1219 (1954); Rev. Pure Appl. Chem. (Australia) **5,** 22 (1955); J. Appl. Phys. **28,** 1409 (1957).
[2] J. Collin and F. P. Lossing, J. Am. Chem. Soc. **80,** 1568 (1958).
[3] P. N. Rylander and S. Meyerson, J. Chem. Phys. **27,** 1116 (1957).
[4] W. A. Bryce and P. Kebarle, Can. J. Chem. **34,** 1249 (1956); W. A. Bryce, in *Advances in Mass Spectrometry*, edited by J. D. Waldron (Pergamon Press, New York, 1959), p. 392.
[5] S. Meyerson and P. N. Rylander, J. Phys. Chem. **62,** 2 (1958).
[6] P. N. Rylander, S. Meyerson, and H. M. Grubb, J. Am. Chem. Soc. **79,** 842 (1957).
[7] S. Meyerson, P. N. Rylander, J. D. Eliel, and E. L. McCollum, J. Am. Chem. Soc. **81,** 2606 (1959).

TABLE II. Low-voltage spectra of toluenes.

Ionizing voltage	α-d Peak height at mass: 64	65	66	67	Ionizing voltage	x-d Peak height at mass: 64	65	66	67
				Repeller voltage = 1.5					
13.5	0	0	0.8	1.3	13.5	0	0	0.5	1.0
14.0	0	0	0.9	2.0	14.0	0	0	0.8	1.7
14.5	0	0	1.6	2.8	14.5	0	0	1.5	3.0
15.0	0	1.0	3.6	3.6	15.0	0	1.6	4.0	4.0
15.5	0	4.0	8.0	5.2	15.5	0	4.7	8.5	4.9
16.0	0.3	8.8	15.0	7.0	16.0	0.7	7.7	15.0	6.0
16.5	0.7	15.1	26.9	8.9	16.5	1.2	15.2	26.2	8.1
17.0	1.5	24.1	40.3	10.9	17.0	1.8	25.0	40.8	10.1
17.5	2.3	35.3	57.8	13.5	17.5	2.4	35.0	58.6	13.3
18.0	3.6	48.2	76.8	16.0	18.0	3.6	47.5	77.4	15.2
18.5	4.5	60.2	96.6	18.7	18.5	4.7	60.0	97	17.3
19.0	6.2	72.2	115.5	21.8	19.0	6.0	72.5	117	20.0
				Repeller voltage = 10.0					
10.5	0	0	2.7	5.4	10.5	0	0	2.7	5.4
11.0	0	1.0	5.0	8.5	11.0	0	0.9	4.9	7.8
11.5	0.6	3.4	8.2	11.0	11.5	0.4	3.2	8.8	10.0
12.0	1.3	9.6	17.7	16.6	12.0	1.1	9.2	19.0	14.6
12.5	1.9	19.8	34.8	21.5	12.5	1.8	19.1	34.7	19.0
13.0	3.2	37.0	61.5	28.7	13.0	3.2	36.5	61.7	25.2
13.5	5.0	60.5	99.0	34.3	13.5	5.0	60.3	99.0	31.3
14.0	7.0	87.5	145	41.4	14.0	7.2	88.0	145	38.7
14.5	9.8	114.3	185	48.3	14.5	10.2	118.5	194	43.3
15.0	14.6	151	229	55.0	15.0	13.6	149	244	51.6
15.5	18.0	187	289	63.6	15.5	17.3	178	295	58.0
16.0	22.8	221	338	69.2	16.0	21.3	216	352	64.4

conceivably, the extent of hydrogen "scrambling" in the dissociation processes might be affected.

EXPERIMENTAL

Labeled compounds were selected from those used in earlier work.[5–7] The materials and their isotopic purities are: *p*-xylene-α-*d*, 95.2%; *p*-xylene-*x*-*d*, 79.2%; toluene-α-*d*, 98.7%; toluene-*x*-*d*, 88.2%; and benzyl chloride-*x*-*d*, 80.5%. Spectra were recorded on a Consolidated model 21–103c mass spectrometer.

The spectra of the xylenes were measured from mass 90 to 92; those of the toluenes and the benzyl chloride, from 64 to 67. These regions were scanned repeatedly at electron energies from a value near the appearance potential to 4 or 5 ev above the appearance potential at intervals of about 0.5 ev. Nominal values of electron energies were deemed adequate; no attempt was made to correct them for contact potentials, thermal energy spread, etc. Measurements were made at two different repeller voltages, 1.5 and 10.0 v, except that *p*-xylene-*x*-*d* was studied only at 1.5 v. Residence time is inversely proportional to the square root of repeller voltage; hence, the two sets of data correspond to residence times differing by a factor of about 2.5. The experimental data for the xylenes, toluenes, and benzyl chloride are presented in Tables I, II, and III, respectively. Peak heights are expressed in arbitrary units.

DISCUSSION

At electron energies near the appearance potentials of the ions, both total ion yield and the distribution of ionic products are steeply varying functions of electron

TABLE III. Low-voltage spectra of benzyl chloride-*x*-*d*.

Ionizing voltage	Peak height at mass: 64	65	66
	Repeller voltage = 1.5		
13.5	0	1.2	1.6
14.0	0	2.9	3.9
14.5	0	6.0	9.0
15.0	0	9.9	15.4
15.5	0	15.8	24.2
16.0	0	22.4	34.5
16.5	0.5	30.3	47.3
17.0	1.5	37.8	59.0
17.5	1.9	46.1	72.0
18.0	3.1	54.9	84.8
18.5	3.7	63.9	96.9
	Repeller voltage = 10.0		
9.4	a	1.2	1.2
9.9		4.2	4.7
10.3		9.4	13.0
10.9		21.0	27.5
11.4		35.6	48.0
11.8		55.6	77.1
12.2		81.0	110.4
12.9		105	146
13.4		123	177
13.8		152	217
14.3		176	246
14.8		202	285

[a] Not measured.

TABLE IV. Labeling of $C_7H_7^+$ from *p*-xylenes.

α-d Ionizing voltage 70	*α-d* Percent labeling 56[a]	*x-d* Ionizing voltage 70	*x-d* Percent labeling 89[a]
	Repeller voltage = 1.5		
9.5	59	10.0	85
10.0	57	10.5	85
10.5	59	11.0	85
11.0	60	11.5	85
11.5	59	12.0	86
12.0	59	12.5	86
12.5	58	13.0	86
13.0	59	13.5	87
13.5	58	14.0	87
14.0	58		
	Repeller voltage = 10.0		
4.3	58		
4.8	58		
5.3	56		
5.8	57		
6.3	57		
6.8	57		
7.4	57		
7.8	57		
8.4	57		
8.9	57		

[a] See the work cited in footnote 5.

energy. The difficulty of precisely reproducing conditions in the ionizing chamber in two separate runs argues against any treatment of the data requiring that ion yields and distributions from a labeled compound be equal to those from its unlabeled counterpart. Therefore, the general procedure[5] used to compute isotopic distributions of fragment ions in 70-ev spectra is not suitable at low electron energies. Each such distribution must be computed from data derived from a single spectrum.

In the xylene-*d* spectra, peak height at mass 90 was zero in all the low-voltage measurements. This finding, in agreement with the similar observation made on the

TABLE V. Labeling of $C_6H_6^+$ from toluenes.

α-d Ionizing voltage 70	*α-d* Percent labeling 59[a]	*x-d* Ionizing voltage 70	*x-d* Percent labeling 68[a]
	Repeller voltage = 1.5		
15.0	69	15.0	59
15.5	60	15.5	63
16.0	59	16.0	69
16.5	61	16.5	67
17.0	60	17.0	66
17.5	60	17.5	68
18.0	60	18.0	67
18.5	60	18.5	67
19.0	60	19.0	67
	Repeller voltage = 10.0		
11.0	63	11.0	61
11.5	54	11.5	61
12.0	55	12.0	63
12.5	58	12.5	64
13.0	58	13.0	65
13.5	59	13.5	66
14.0	60	14.0	67
14.5	60	14.5	67
15.0	58	15.0	67
15.5	59	15.5	68
16.0	59	16.0	68

[a] See the work cited in footnote 6.

70-ev spectrum of unlabeled *p*-xylene,[5] establishes the absence of $C_7H_6^+$ and consequently of $C_7H_5D^+$. Thus, the peak at 91 can be attributed solely to $C_7H_7^+$, and the distribution of labeled and unlabeled ions of this species can be obtained readily from the peak heights at 92 and 91. The observed peak height at 92 was corrected for $C_7H_7^+$ containing C^{13} in natural abundance;[8] that at 91, for the contribution of unlabeled xylene. The values thus found for the isotopic distribution of the $C_7H_7^+$ ions from xylenes are shown in Table IV.

In the toluene spectra, the $C_5H_4^+$ intensity at 64 was negligible in all the low-voltage measurements; the contributions of $C_6H_3D^+$ at 65 are therefore also pre-

[8] D. R. McAdams, *Isotope Correction Factors for Mass Spectra of Petroleum Fractions* (Esso Standard Oil Company, Baton Rouge, Louisiana, 1957).

sumed negligible. However, a peak at 67 shows the presence of $C_5H_5D^+$ and, by inference, of $C_5H_6^+$ of mass 66. Intensity of the $C_5H_6^+$ ion is far lower than that of $C_5H_5^+$ at 70 ev; but, because $C_5H_6^+$ has a lower appearance potential, its intensity is much closer to or even greater than that of $C_5H_5^+$ at sufficiently low energies. In order to make the necessary correction at 66, $C_5H_6^+$ was assumed to be formed with the same isotopic distribution at low voltages as at 70 ev[9]: 72.5% labeled from toluene-*α-d* and 75.2% labeled from toluene-*x-d*.[10] The observed peak height at 66 was corrected for this interference and for $C_5H_5^+$ containing naturally occurring C^{13}; that at 65, for the contribution of unlabeled toluene. The corrected peak heights are attributed to $C_5H_4D^+$ and $C_5H_5^+$. The values found for the isotopic distribution of the $C_5H_5^+$ ions from toluenes are shown in Table V.

Benzyl chloride gives rise to no $C_5H_6^+$ ions and, in the low-voltage range studied, to a negligible yield of $C_5H_4^+$ ions. Therefore, the benzyl chloride data needed to be corrected only at 66 for $C_5H_5^+$ containing naturally occurring C^{13}, and at 65 for the contribution of unlabeled benzyl chloride. The isotopic distribution of the $C_5H_5^+$ ions from benzyl chloride is shown in Table VI.

In Tables IV, V, and VI, the isotopic distributions shown vary but little throughout the low-voltage ranges studied and, within narrow limits, agree with the distributions obtained with 70-v electrons. Largest variations, appearing at the lowest voltages, may reflect little more than the decrease of signal-to-noise ratio as the electron energy approaches the appearance potential. The toluene experiments with 10 v on the repellers show small but possibly real drifts in isotopic distribution.

To a good approximation, the data support the assumption that most of the ions in each instance are formed by the same path when the electron energy is 70 ev as when it is close to the appearance potential. Ionizing voltage has almost no effect on isotopic distributions of fragment ions. If the ion yield at 70 ev includes contributions from two or more processes with differing energy requirements, such processes would appear to involve states of the parent ion that dissociate by a common path. A similar conclusion was indicated by evidence[7] that the $C_7H_7^+$ ions formed from benzyl chloride near the appearance potential and those formed at electron energies high enough to cause them to dissociate further to $C_5H_5^+$ and C_2H_2 both have the tropylium structure and presumably result from a common reaction path.

TABLE VI. Labeling of $C_5H_5^+$ from benzyl chloride-*x-d*.

Ionizing voltage 70	Percent labeling 74[a]
Repeller voltage = 1.5	
13.5	68
14.0	70
14.5	74
15.0	75
15.5	74
16.0	75
16.5	75
17.0	75
17.5	75
18.0	75
18.5	74
Repeller voltage = 10.0	
9.4	58
9.9	64
10.3	71
10.9	69
11.4	70
11.8	71
12.2	71
12.9	71
13.4	72
13.8	72
14.3	71
14.8	72

[a] See the work cited in footnote 7.

[9] This assumption seems justified because it leads to self-consistent results despite variation of the 67/66 peak-height ratio from 0.61 to 0.14 in the toluene-*α-d* spectrum and from 0.55 to 0.12 in the toluene-*x-d* spectrum as electron energy is increased from 15.5 to 19 ev. Moreover, within experimental error, the assumption is consistent with the 67/66 peak-height ratio at ionizing voltages below the appearance potential of the $C_5H_5^+$ ion and, presumably, of the $C_5H_4D^+$ ion.

[10] The spectra of the deuterated toluenes are reported in the work cited in footnote 6 and the computing procedure is described in the work cited in footnote 5.

THE JOURNAL OF CHEMICAL PHYSICS VOLUME 34, NUMBER 6 JUNE, 1961

Deviations from Thermal Equilibrium among Reactant Molecules*

B. WIDOM

Department of Chemistry, Cornell University, Ithaca, New York

(Received December 27, 1960)

A model of a chemically reacting system is considered in which the reactant molecules are dilutely dispersed in an inert gas and reaction is the result of binary collisions between inert and reactant species. It is noted that during reaction the distribution of reactants over their internal states is not that characteristic of equilibrium. It is shown that if κ is the rate constant of the reaction and κ_{eq} the rate constant that would have characterized the reaction had the reactants been in equilibrium, then $\kappa = \kappa_{eq} - \bar{\tau}(\langle q^2\rangle - \langle q\rangle^2)$, where $\bar{\tau}$ is a mean relaxation time, q is the reaction probability per unit time from a particular reactant state, and $\langle\ \rangle$ is an average over reactant states with an equilibrium distribution. The rate constant κ_{eq} is itself $\langle q\rangle$. A number of illustrations are given, and it is concluded that in real chemical systems $\langle q^2\rangle$ is probably of the order of magnitude of $\langle q\rangle^{1+\gamma}$ with $0<\gamma<1$. This has as a consequence that κ is of the form $(1-B\kappa_{eq}{}^{\gamma})\kappa_{eq}$. The quantity in parentheses describes the effect on κ of deviations from equilibrium, and it is a decreasing function of temperature. It is suggested that this might possibly be the explanation of the observed temperature-decreasing pre-exponential factor in the rate constant for dissociation of diatomic molecules.

1. INTRODUCTION

IT is a well-established result of kinetic theory that during the course of a chemical reaction the reactant molecules are not distributed over their internal states in the same way that they would be if the system were in equilibrium. This perturbation of the Boltzmann distribution by the reaction may be extensive if the reaction is very rapid or negligible if the reaction is slow. The purpose of this paper is to derive and discuss an explicit formula for the relation of the true rate constant κ to the value κ_{eq} that it would have if the reactant molecules were in thermal equilibrium;

$$\kappa = \kappa_{eq} - \bar{\tau}(\langle q^2\rangle - \langle q\rangle^2), \tag{1.1}$$

where $\bar{\tau}$ is a certain mean relaxation time, q is the reaction probability per unit time from a given reactant state, and $\langle\ \rangle$ represents an average over reactant states with the Boltzmann distribution as weighting factor. The rate constant κ_{eq} is itself $\langle q\rangle$. The theory applies to the model described in the following paragraph.

The system is taken to be one in which the reactant molecules are dilutely dispersed in a constant-temperature inert gas, the molecules of which do not have variable internal states, and which is itself so dilute that reaction is the result entirely of binary collisions between the inert and reactant molecules. Then if X is an inert gas molecule and A is a reactant, the reaction being considered is

$$X + A \rightarrow X + \text{products}$$

and specifically excluded from consideration are those cases in which reaction proceeds by the initial formation of a long-lived complex between X and A (or between X and a fragment of A) which itself undergoes collisions with X. It is assumed that the relative translational motion of the particles is at all times the same as though the system were in equilibrium at the fixed temperature of the diluent gas, that is, that translational relaxation is instantaneous. It is to be imagined, further, that the reaction is truly bimolecular, so that reactant and product molecules are distinguished by their internal states,[1] which are defined by the specification of the values of independent action variables equal in number to the number of internal degrees of freedom of the reactant molecule.[2]

Two further assumptions are made, neither of which is essential to the model, and which do not appear explicitly in the general formula of Eq. (1.1), but which lead to great simplification of notation and description. The first is that classical mechanics may be used instead of quantum mechanics, this assumption being already inherent in the definition of state given above. The second is that there is an upper limit to the range of interaction between the inert and reactant molecules, so that there exists a finite, constant collision number Z, and every reactant molecule, whatever its state, suffers Z collisions per unit time with inert gas molecules.[1] This does *not* mean that the effective size of a reactant molecule is independent of its state, but merely that there is a *largest* effective size, and that molecules in states associated with a smaller spatial extension undergo a larger number of ineffective collisions, i.e., more zero-angle scattering, than do the largest molecules. This is automatically taken account of by the transition probability.

In Sec. 2 the rate constant of the reaction is expressed in terms of an eigenvalue of a symmetrized transition kernel, following a well-known procedure. In Sec. 3 a relation is derived connecting κ and κ_{eq} and containing the reaction probability per unit time, q; terms are

* This research was supported by the U. S. Air Force through the Air Force Office of Scientific Research of the Air Research and Development Command. Presented at the Symposium on Experimental and Theoretical Advances in Elementary Gas Reactions, American Chemical Society meeting, St. Louis, Missouri, March 27–30, 1961.

[1] B. Widom, J. Chem. Phys. **31**, 1387 (1959).
[2] B. Widom, J. Chem. Phys. **32**, 913 (1960).

classified according to order of magnitude in q and Eq. (1.1) results from the approximation of neglecting terms of high order. Several illustrative cases are discussed in Sec. 4, and it is suggested that the deviations from thermal equilibrium caused by reaction may perhaps be responsible for the observed negative temperature coefficient of the pre-exponential factor in the rate constant for dissociation of diatomic molecules.

2. RATE EQUATION AND RATE CONSTANT

Let x (or y) symbolize the internal state of a reactant molecule; it is a point in the internal action space of a molecule and is therefore really a set of several variables. Let dx (or dy) be an element of volume in this space of states, and symbolize by $\mathfrak{R}$ the region of the space identified as *reactant*, the remainder of the space corresponding to *product* states. Suppose $k(x, y)dy$ is the probability per unit time that a reactant molecule in state x will make a transition (due to collisions with inert gas molecules) to some state in the region dy in the neighborhood of y, and suppose further that $c(x, t)dx$ is the number of reactant molecules which, at time t, are in states in the region dx in the neighborhood of x. Then for all reactant states x the rate equation is[1]

$$\partial c(x, t)/\partial t = \int_{\mathfrak{R}} k(y, x)c(y, t)dy - Zc(x, t). \qquad (2.1)$$

Here, Z is the number of collisions per unit time suffered by each reactant molecule, and, according to the assumed model, it is finite and constant. Equation (2.1) assumes that product molecules are removed from the system as soon as they are formed, and it correctly describes those reactions in which either (*i*) the products really are removed as soon as formed, or (*ii*) the reaction is followed only for a time sufficiently short so that the reverse reaction of products to form reactants may be neglected. An alternative problem which often arises is that of determining the rate at which reactants form products (and the equal rate of the reverse reaction) when the reactants and products are in equilibrium; but then the rate constant for the reaction *reactants→products* is exactly κ_{eq}, by definition. The point of the present analysis is to determine the deviation from κ_{eq} of the rate constant κ that characterizes Eq. (2.1), and it is this equation which is appropriate for most of the experimental situations of interest.

A significant feature of Eq. (2.1) is that it does not require the transition probability $k(x, y)$ to be defined when either x or y is outside the range of reactant states. This is of little interest when the reaction is an isomerization, but when it is a dissociation, had the product states been relevant they would have needed to be treated differently from reactant states because some internal degrees of freedom become translations. As long as the rate equation contains no explicit reference to the product states, however, the nature of the products is irrelevant, and that this is the case here is due to the assumption that products are instantaneously removed from the system. If the reaction is indeed a dissociation then the inverse reaction is a recombination, which cannot be treated directly by the present theory. On the other hand, if the reaction is an isomerization then so is its inverse, which can then be treated by the same theory.

Suppose $f(x)dx$ is proportional to the fraction of all reactant molecules that would be found with states in the region dx in the neighborhood of x if these molecules were in thermal equilibrium at the temperature of the diluent gas. Then as a consequence of detailed balance the kernel

$$S(x, y) = S(y, x) = [f(x)/f(y)]^{\frac{1}{2}}k(x, y) \qquad (2.2)$$

is symmetric.[2] Let μ_i and $\phi_i(x)$ $(i=0, 1, 2, \cdots)$ be its eigenvalues and its mutually orthogonal eigenfunctions in the region $\mathfrak{R}$, so that

$$\int_{\mathfrak{R}} S(x, y)\phi_i(y)dy = \mu_i\phi_i(x). \qquad (2.3)$$

Then the solution of Eq. (2.1) with an arbitrarily prescribed $c(x, 0)$ is[2]

$$c(x, t) = f(x)^{\frac{1}{2}}\sum_{i=0}^{\infty} h_i\phi_i(x)\ \exp[-(Z-\mu_i)t], \qquad (2.4)$$

where

$$h_i = \int_{\mathfrak{R}} f(x)^{-\frac{1}{2}}c(x, 0)\phi_i(x)dx \Big/ \int_{\mathfrak{R}} \phi_i^2(x)dx.$$

The eigenvalues μ_i may be numbered in such a way that

$$Z > \mu_0 > \mu_1 > \mu_2 > \cdots. \qquad (2.5)$$

That the largest eigenvalue is less than Z corresponds to the fact that reactants are continually disappearing, so $c(x, t)$, for any reactant state x, must approach 0 as $t\to\infty$. Equation (2.4) may now be interpreted in a way which, from recent discussions,[3–11] has become very familiar:

Only in the case that

$$Z-\mu_0 \ll Z-\mu_1 \qquad (2.6)$$

will the reaction have a clearly defined rate constant

[3] E. E. Nikitin, Doklady Akad. Nauk S.S.S.R. **116,** 584 (1957).
[4] E. E. Nikitin and N. D. Sokolov, J. Chem. Phys. **31,** 1371 (1959).
[5] E. E. Nikitin, Zhurn. Fiz. Khim. **33,** 572 (1959).
[6] E. W. Montroll and K. E. Shuler, Advances in Chem. Phys. **1,** 361 (1958).
[7] K. E. Shuler, *Seventh Symposium (International) on Combustion* (Butterworths Scientific Publications, Ltd., London, 1958), p. 87.
[8] S. K. Kim, J. Chem. Phys. **28,** 1057 (1958).
[9] I. Prigogine and T. A. Bak, J. Chem. Phys. **31,** 1368 (1959).
[10] T. A. Bak and I. W. Plesner, Technical Note No. 1 prepared under contract with the Aeronautical Research Laboratory, Wright Air Development Center (1959).
[11] F. P. Buff and D. J. Wilson, J. Chem. Phys. **32,** 677 (1960).

κ, that is, only in such a case will the total number of reactant molecules

$$C(t)=\int_{\mathfrak{R}} c(x,t)\,dx$$

satisfy

$$-dC(t)/dt=\kappa C(t)$$

for all time after a (relatively) very short induction period $(Z-\mu_1)^{-1}$. Thus, when the condition of Eq. (2.6) is satisfied there exists a single effective rate constant κ given by

$$\kappa=Z-\mu_0. \tag{2.7}$$

The quantities

$$\tau_i=(Z-\mu_i)^{-1}\ (i=1,2,3,\cdots) \tag{2.8}$$

are the relaxation times, the longest of which, τ_1, is identified as *the* relaxation time. Then after the time τ_1, which is much smaller than the characteristic reaction time κ^{-1}, the reactants reach a condition in which the further evolution of the system is characterized by the single rate constant κ. This condition reached by the reactants after time τ_1 is called a steady state, because for all $t\gg\tau_1$, and all reactant states x and y, it follows from Eq. (2.4) that

$$c(x,t)/c(y,t)=f(x)^{\frac{1}{2}}\phi_0(x)/f(y)^{\frac{1}{2}}\phi_0(y) \tag{2.9}$$

independently of t. On the other hand, $\phi_0(x)$ may deviate considerably from $f(x)^{\frac{1}{2}}$, so the ratio $c(x,t)/c(y,t)$ in the steady state may be significantly different from its equilibrium value $f(x)/f(y)$. The reaction is then said to have perturbed the equilibrium distribution. When the reaction is sufficiently slow, however, the steady-state distribution is only a slightly perturbed Boltzmann distribution, so $\phi_0(x)\approx f(x)^{\frac{1}{2}}$.

If *the reaction probability per unit time from reactant state* x is symbolized by $q(x)$, then by the hypotheses that define the present model

$$q(x)=Z-\int_{\mathfrak{R}} k(x,y)\,dy \tag{2.10}$$

and in terms of this quantity,[1]

$$\kappa_{\rm eq}=\langle q\rangle, \tag{2.11}$$

where $\langle\ \rangle$ symbolizes an average over reactant states with the Boltzmann distribution as weighting factor. Analogously, it follows from Eqs. (2.2), (2.3), (2.7), and (2.10) that the true rate constant κ is itself the average of $q(x)$ over all reactant states x, with the steady-state distribution $f(x)^{\frac{1}{2}}\phi_0(x)$, rather than the Boltzmann distribution $f(x)$, as weighting factor. Necessarily, $q(x)\leqslant Z$ for every x. The reaction is slow, and the deviation of the steady-state distribution from the equilibrium distribution is slight, when in some sense $q(x)$, and therefore also $\langle q\rangle$ and $\langle q^2\rangle$, are small. This is the point of view from which Eq. (1.1) is derived in Sec. 3.

That $\phi_0(x)$ may in some sense be approximated by $f(x)^{\frac{1}{2}}$, as suggested above, leads to an important conclusion about the relation of κ to $\kappa_{\rm eq}$. From Eqs. (2.3) and (2.7) it follows that

$$\kappa=Z-\int_{\mathfrak{R}}\int_{\mathfrak{R}} S(x,y)\phi_0(x)\phi_0(y)\,dx\,dy\Big/\int_{\mathfrak{R}}\phi_0^2(x)\,dx. \tag{2.12}$$

The approximate κ that then follows from the approximation $\phi_0(x)\approx f(x)^{\frac{1}{2}}$ is, according to Eqs. (2.2), (2.10), and (2.11), precisely $\kappa_{\rm eq}$. It is a well-known consequence of variational principles, however, that the value of a ratio of integrals such as that in Eq. (2.12) is relatively insensitive to changes in the function $\phi_0(x)$, so even if the approximation $\phi_0(x)\approx f(x)^{\frac{1}{2}}$ for the eigenfunction is very crude, the approximation $\kappa\approx\kappa_{\rm eq}$ might nevertheless be close. Therefore, merely demonstrating for a model system that the steady-state distribution differs substantially from the Boltzmann distribution does not in itself invalidate the approximation $\kappa\approx\kappa_{\rm eq}$. This point has been largely overlooked in the past.

3. RELATION OF κ TO $\kappa_{\rm eq}$

Normalize $f(x)^{\frac{1}{2}}$ and each $\phi_i(x)$ in such a way that the integral of its square over $\mathfrak{R}$ is unity,

$$\int_{\mathfrak{R}} f(x)\,dx=\int_{\mathfrak{R}}\phi_i^2(x)\,dx=1\ (i=0,1,2\cdots). \tag{3.1}$$

Then

$$f(x)^{\frac{1}{2}}=\sum_{i=0}^{\infty} a_i\phi_i(x) \tag{3.2}$$

and

$$a_0^2+\epsilon=1, \tag{3.3}$$

where

$$a_i=\int_{\mathfrak{R}} f(x)^{\frac{1}{2}}\phi_i(x)\,dx \tag{3.4}$$

and

$$\epsilon=\sum_{i=1}^{\infty} a_i^2. \tag{3.5}$$

Let $\{\ \}$ symbolize an average over $i=1,2,3,\cdots$ in which the weighting factor is a_i^2, so that in particular, because of Eqs. (2.8) and (3.5),

$$\epsilon\{\tau^{-1}\}=\sum_{i=1}^{\infty} a_i^2(Z-\mu_i)$$

$$\epsilon\{\tau^{-2}\}=\sum_{i=1}^{\infty} a_i^2(Z-\mu_i)^2. \tag{3.6}$$

From Eqs. (2.2), (2.3), (2.10), and (3.2), the reaction probability per unit time from reactant state x is

$$q(x)=Z-f(x)^{-\frac{1}{2}}\sum_{i=0}^{\infty} a_i\mu_i\phi_i(x). \tag{3.7}$$

The symbol $\langle\ \rangle$ was defined in Sec. 2 to represent an average over reactant states with $f(x)$ as weighting factor, so from Eqs. (2.7), (2.8), (3.1), and (3.3)–(3.7),

$$\langle q\rangle=(1-\epsilon)\kappa+\epsilon\{\tau^{-1}\} \tag{3.8}$$

$$\langle q^2\rangle=(1-\epsilon)\kappa^2+\epsilon\{\tau^{-2}\}. \tag{3.9}$$

Eliminating ϵ between Eqs. (3.8) and (3.9) leads to a quadratic equation for κ, the appropriate root being the one which goes to zero when $\langle q\rangle$ and $\langle q^2\rangle$ go to zero. The result is an exact expression for κ in terms of $\langle q\rangle=\kappa_{eq}$, $\langle q^2\rangle$, $\{\tau^{-1}\}$ and $\{\tau^{-2}\}$.

Since κ is expected to be close to κ_{eq} when the reaction is slow, the initial deviation of κ from κ_{eq} is obtained by expanding the exact expression obtained above in increasing powers of $\langle q\rangle$ and $\langle q^2\rangle$ and discarding all but the first few terms. The terms to be retained are those in $\langle q\rangle$, $\langle q\rangle^2$, and $\langle q^2\rangle$. All other terms, if both $\langle q\rangle$ and $\langle q^2\rangle$ can be looked upon as small, are negligible compared to one or another of the terms which are retained. Furthermore, when the reaction rate vanishes the relaxation times approach finite, positive limits, so both $\{\tau^{-1}\}$ and $\{\tau^{-2}\}$ are, as far as $\langle q\rangle$ and $\langle q^2\rangle$ are concerned, of the order of magnitude of unity. The formula for κ which then results is

$$\kappa=\kappa_{eq}-(\langle q^2\rangle-\langle q\rangle^2)\{\tau^{-1}\}/\{\tau^{-2}\}, \tag{3.10}$$

where it is to be recalled that κ_{eq} and $\langle q\rangle$ are interchangeable.

Defining $\bar{\tau}=\{\tau^{-1}\}/\{\tau^{-2}\}$, it is seen from Eqs. (2.8) and (3.6) that

$$\bar{\tau}=\sum_{i=1}^{\infty}a_i^2\tau_i^{-1}/\sum_{i=1}^{\infty}a_i^2\tau_i^{-2},$$

that is, $\bar{\tau}$ is an average of τ_i over $i=1, 2, 3, \cdots$ with the weighting factor $a_i^2\tau_i^{-2}$. From Eqs. (2.5) and (2.8), each τ_i is necessarily positive, and from the definition of *the* relaxation time τ_1, each τ_i with $i>1$ is less than τ_1. Therefore,

$$\bar{\tau}\doteq\alpha\tau_1, \qquad 0<\alpha<1. \tag{3.11}$$

For most practical purposes it would be quite sufficient to identify $\bar{\tau}$ with the relaxation time τ_1 itself, though it should be recognized that τ_1 is actually an upper limit to $\bar{\tau}$. In terms of this mean relaxation time, Eq. (3.10) becomes

$$\kappa=\kappa_{eq}-\bar{\tau}(\langle q^2\rangle-\langle q\rangle^2), \tag{3.12}$$

which is the result anticipated in Eq. (1.1). The neglected terms are of higher order in $\langle q\rangle$ or in $\langle q^2\rangle$ than the terms retained.

It follows from Eq. (3.12) that $\kappa_{eq}>\kappa$, as it must be.[8] The reason for this is that it is the most reactive states, i.e., those with the largest $q(x)$, which are most depleted by the reaction, so that in the steady state the fraction of reactant molecules in the most reactive states is less, and in the least reactive states greater, than at equilibrium.

According to Eq. (3.12) there is no difference between κ and κ_{eq} in either of two quite distinct cases: (*i*) $\bar{\tau}=0$, (*ii*) $\langle q^2\rangle=\langle q\rangle^2$. Both these extreme cases are easily interpreted physically. (*i*) In the absence of reaction, the relaxation time τ_1 is a measure of the time required for the system to come to equilibrium starting from an arbitrary initial distribution. If $\bar{\tau}=0$ then each τ_i, including τ_1, is zero, so during reaction the equilibrium distribution is being continually re-established in a time infinitesimal compared to that during which significant reaction can occur. Then the hypothesis that the reactants are always at equilibrium among themselves is correct, and $\kappa=\kappa_{eq}$. (*ii*) If $\langle q^2\rangle=\langle q\rangle^2$ then $q(x)$ is independent of x, that is, reaction occurs equally effectively from any reactant state. But in such a case the actual distribution of reactants among states is irrelevant to the reaction rate, so *any* assumption about the distribution, including the equilibrium hypothesis, necessarily leads to the correct rate constant. Therefore, again, $\kappa=\kappa_{eq}$. It should be noted that in this case, even though the assumption of an equilibrium distribution is irrelevant, it is nevertheless correct, just as it was correct in case (*i*); for if $q(x)$ is independent of x then, according to Eqs. (2.2) and (2.10), the quantity $f(x)^{\frac{1}{2}}$ is an eigenfunction of $S(x, y)$ with eigenvalue $Z-q$; but now this eigenvalue is $Z-q=Z-\kappa_{eq}=Z-\kappa=\mu_0$, that is, it is the largest eigenvalue; therefore $\phi_0(x)=f(x)^{\frac{1}{2}}$, so the steady-state and equilibrium distributions are indeed identical.

In Eq. (3.12) no assumptions have been made about the magnitudes of $\langle q^2\rangle$ and $\langle q\rangle$ relative to each other. It will be seen in Sec. 4 that if $\langle q^2\rangle\sim\langle q\rangle^n$ with $1\leq n\leq 2$, then the extremes $n=1$ or 2 can arise in simplified models but probably not in real physical situations, while the intermediate condition $1<n<2$, which probably always holds, may have important implications for the temperature dependence of the pre-exponential factor in the rate constant.

The quantity $\bar{\tau}(\langle q^2\rangle-\langle q\rangle^2)$ for a reaction is not related in any simple way to the corresponding quantity for the inverse reaction. If the superscripts f and b refer to reaction in the forward and backward directions, then $\kappa_{eq}{}^f/\kappa_{eq}{}^b$ is equal to the equilibrium constant K for the reaction, but if κ differs significantly from κ_{eq} then, as was pointed out by Nikitin and Sokolov,[4] and as is here verified, $\kappa^f/\kappa^b\neq K$. It is suggested in Sec. 4 that deviations from the equilibrium distribution among dissociating diatomic molecules may perhaps be responsible for the observed negative temperature coefficient of the pre-exponential factor in the rate constant. If this is really the case then the common practice of assuming $\kappa^f/\kappa^b=K$ in order to relate the dissociation and recombination processes is quite fallacious. The error becomes more serious the higher the temperature, because the higher the temperature the greater the rate and hence the greater the dis-

crepancy between κ and κ_{eq}. The earlier assertion[1] that the equilibrium hypothesis makes the same percentage error in estimating both κ^f and κ^b, so that $\kappa^f/\kappa^b = \kappa_{eq}{}^f/\kappa_{eq}{}^b = K$, is incorrect.

As a final remark in the interpretation of Eq. (3.12), it may be noted that if $f(x)$ is normalized as in Eq. (3.1), then it follows from Eq. (2.10), and from the condition of detailed balance, $f(x)k(x,y) = f(y)k(y,x)$, which led to the symmetry of $S(x,y)$ in Eq. (2.2), that

$$\langle q^2\rangle - \langle q\rangle^2 = \int_{\mathfrak{R}}\int_{\mathfrak{R}} f(x)k_2(x,y)\,dxdy - \left[\int_{\mathfrak{R}}\int_{\mathfrak{R}} f(x)k_1(x,y)\,dxdy\right]^2,$$

where $k_1(x,y)$ is the first iterate of $k(x,y)$, that is, $k(x,y)$ itself, while $k_2(x,y)$ is the second iterate of $k(x,y)$, that is,

$$k_2(x,y) = \int_{\mathfrak{R}} k(x,w)k(w,y)\,dw.$$

But if $k_n(x,y)$ is the nth iterate of $k(x,y)$, then

$$Z^{-n}\int_{\mathfrak{R}} k_n(x,y)\,dy$$

is a measure of the probability that a molecule initially in reactant state x will survive n consecutive collisions without reacting.[1] Thus, $\langle q^2\rangle - \langle q\rangle^2$ is, for an equilibrium distribution of reactants, a measure of the difference between the average probability of a reactant molecule surviving two consecutive collisions and the square of the average probability of its surviving one. It is, therefore, a measure of the effect on the reaction probability of the correlation of the state of a molecule after a second collision with its state after a first collision. From this point of view, the fact that necessarily $\langle q^2\rangle \geqslant \langle q\rangle^2$ means that, on the average, if a molecule suffers a collision without reacting it then finds itself in a state of less than average reactivity. Only when $q(x)$ is independent of x could the correlation between consecutive reactant states fail to influence the reaction probability; but in such a case $\langle q^2\rangle = \langle q\rangle^2$, which is clearly consistent with the present interpretation.

4. ILLUSTRATIONS AND APPLICATIONS

Of the two factors, $\bar{\tau}$ and $\langle q^2\rangle - \langle q\rangle^2$, which determine the deviation of κ from κ_{eq}, the second is by far the more significant. As already noted, $\bar{\tau}$ can for practical purposes be identified with the relaxation time τ_1, which for any reactant species is likely to lie between a few Z^{-1} and a few thousand Z^{-1}. On the other hand, $\langle q^2\rangle - \langle q\rangle^2$, as is already obvious from its second term, which is $\kappa_{eq}{}^2$, is subject to a very much wider range of variation in its order of magnitude. Furthermore, it is very sensitive to temperature, just as a rate constant is, while by comparison the mean relaxation time changes very slowly with temperature.

If $\langle q^2\rangle$ is of the order of magnitude of $\langle q\rangle^2 = \kappa_{eq}{}^2$, then the deviation of κ from κ_{eq} is indeed small and probably negligible. On the other hand, if $\langle q^2\rangle$ is of the order of magnitude of $\langle q\rangle = \kappa_{eq}$, then the deviation of κ from κ_{eq} is so large that not only is the approximation $\kappa \approx \kappa_{eq}$ unacceptable, but a formal application of Eq. (3.12) might even lead to $\kappa < 0$, showing that even the higher powers of $\langle q\rangle$ and $\langle q^2\rangle$ which were discarded in obtaining the equation are not negligible. In the intermediate case in which $\langle q^2\rangle \sim \langle q\rangle^n$, with $1 < n < 2$, the deviation of κ from κ_{eq} would be easily noticeable but not extreme. Each of these three possibilities can be illustrated by a specific model.

(a) $n = 1$

In a recent discussion of the kinetics of dissociation of diatomic molecules[12] it was assumed, as is commonly done, that the reaction probability per unit time $q(x)$ is zero unless the energy of state x is within about kT of the dissociation limit, and is then equal to βZ, where β is an unspecified constant of the order of magnitude of, though necessarily less than, unity, and k and T are Boltzmann's constant and the absolute temperature, respectively. For such a $q(x)$,

$$\langle q^2\rangle = \beta Z\langle q\rangle \gg \langle q\rangle^2,$$

with $\langle q^2\rangle$ and $\langle q\rangle$ both proportional to $\exp(-\epsilon^*/kT)$, and the very much smaller $\langle q\rangle^2$ proportional to $\exp(-2\epsilon^*/kT)$. Here, ϵ^* is the activation energy, which for dissociating diatomic molecules may be identified with the dissociation energy. Since $\langle q\rangle^2$ is now negligible compared to $\langle q^2\rangle$, the rate constant κ as given by Eq. (3.12) becomes

$$\kappa = (1 - \beta Z\bar{\tau})\kappa_{eq}.$$

But typically $Z\bar{\tau}$ is between a few and a few thousand, so with β about unity, the formally calculated rate constant κ is negative. The general conclusion to be drawn from this is that if the entirety of a reaction occurs from reactant states of energy within a few kT of the minimum energy required for reaction, then deviations from the equilibrium distribution during reaction are so extensive that in no sense can κ_{eq} be considered an adequate approximation to κ. Though κ_{eq} remains an upper bound to κ, the lowest order correction to κ_{eq}, as given by Eq. (3.12), is not sufficient to provide an estimate of κ itself.

(b) $n = 2$

Behavior at the opposite extreme is found in the model of the string oscillator suffering impulsive collisions with particles of mass identical to its own,

[12] B. Widom, J. Chem. Phys. **31**, 1027 (1959).

incident along its line of oscillation.[13] If the string breaks, i.e., if the molecule dissociates, when the magnitude of the momentum of the oscillating particle exceeds the value x^*, then the dissociation rate from a state in which the magnitude of the oscillator's momentum is x is[1]

$$q(x)=\int_{x^*}^{\infty} z(y)\,dy$$

independently of x; here, $z(y)dy$ is the number of collisions per unit time suffered by the oscillator in which the magnitude of the momentum of the incident particle lies in the range y to $y+dy$. Since $q(x)$ is now constant, $\langle q^2\rangle=\langle q\rangle^2$ and $\kappa=\kappa_{eq}$ exactly; there is no significant deviation from equilibrium during the course of the reaction. If the string does not break but the oscillator is just formally counted as dissociated when, at the end of any collision, the magnitude of its momentum is found to exceed x^*, then the result is slightly different,[1]

$$q(x)=h'(x^*)x,$$

where $h(x)$ is a certain auxiliary function which is defined in connection with the analysis of the model,[13] though $h'(x^*)$, being just a constant, is of no interest here. This $q(x)$ is not constant so $\langle q^2\rangle\neq\langle q\rangle^2$, but it is a slowly varying function of x so $\langle q^2\rangle$ and $\langle q\rangle^2$ may be expected to be of the same order of magnitude and both proportional to $\exp(-2\epsilon^*/kT)$, where $\epsilon^*=x^{*2}/2m$, with m the mass common to the oscillator and the incident particles. Calculation shows that this is indeed the case, and when $\epsilon^*\gg kT$,

$$\langle q^2\rangle-\langle q\rangle^2=(\tfrac{1}{2}-1/\pi)Z^2(kT/\epsilon^*)\exp(-2\epsilon^*/kT).$$

There is again no significant deviation from equilibrium provided kT is small compared to ϵ^*.

(c) $1<n<2$

An intermediate case, in which $\langle q^2\rangle$ is neither as large as $\langle q\rangle$, as in the first illustration, nor as small as $\langle q\rangle^2$, as in the second, is provided by the two-dimensional model of rough-sphere collisions between molecules and inert gas atoms,[2] if it is assumed that a molecule dissociates centrifugally as soon as the magnitude of its angular momentum exceeds x^*. Let I be the molecular moment of inertia, m the reduced mass of the atom-molecule system, a the sum of the atomic and molecular radii, $b=I/ma^2$, and $\epsilon^*=x^{*2}/2I$. Then by calculation from the known properties[2] of the system, $q(x)$ is found to be a rapidly decreasing function of the difference between x^* and the angular momentum x. When $\epsilon^*\gg kT$,

$$\langle q\rangle=\kappa_{eq}=(kT/\pi\epsilon^*)^{\frac{1}{2}}Z\exp(-\epsilon^*/kT)$$

whatever the value of the parameter b, this result being identical to that for the second string oscillator model described above; and, in addition, still assuming $\epsilon^*\gg kT$,

$$\langle q^2\rangle=(n-1)^{-\frac{1}{2}}(kT/n\pi\epsilon^*)Z^2\exp(-n\epsilon^*/kT),$$

where

$$n=1+2/(b+b^{-1}).$$

Thus, $\langle q^2\rangle\sim\langle q\rangle^n$, with $1<n\leqslant 2$. The case $n=2$, which would result in this illustration being classed with the string oscillator models discussed above, arises *only* when $b=1$, that is, when $I=ma^2$; but it is already known that when this holds then the present two-dimensional rotor model is in many ways dynamically equivalent to the string-oscillator model. When, however, the parameter b has any value other than unity, then this system does indeed provide an example of a case intermediate between the two extremes already illustrated.

The first example, illustrating the extreme in which $\langle q^2\rangle\sim\langle q\rangle$, arose from an assumption which is sometimes made for calculational convenience, but which otherwise has no experimental or theoretical justification, *viz.*, that $q(x)$ is *identically zero* for all states x which have energies differing by more than a few kT from the minimum energy required for reaction. The string oscillator model, which is known to be highly artificial in a number of ways, led to the extreme in which $\langle q^2\rangle\sim\langle q\rangle^2$, and was seen to be associated with a reaction probability per unit time $q(x)$ which is independent, or nearly independent, of the reactant state x. Finally, the intermediate case of $\langle q^2\rangle\sim\langle q\rangle^n$ with $1<n<2$ was illustrated by a model which is certainly the most realistic of those discussed, and is, furthermore, characterized by a $q(x)$ which is a rapidly decreasing function of the difference between the energy of state x and the minimum energy required for reaction, but is nevertheless not identically zero when this difference exceeds a few kT. Even though there is as yet no real experimental or theoretical basis for deciding which of these three kinds of $q(x)$ characterizes real chemical systems, it is surely the last which seems most probably correct at the present time. It may therefore be conjectured with reasonable assurance that in chemical reactions

$$\langle q^2\rangle\sim\langle q\rangle^n=\kappa_{eq}{}^n,\qquad 1<n<2.$$

Then $\langle q\rangle^2$ may be neglected in comparison with $\langle q^2\rangle$, and Eq. (3.12) becomes

$$\kappa=(1-B\kappa_{eq}{}^{\gamma})\kappa_{eq},\qquad 0<\gamma<1,\qquad (4.1)$$

where B contains $\bar{\tau}$ and the factor of proportionality that relates $\langle q^2\rangle$ to $\langle q\rangle^n$. It is extremely likely that the temperature dependence of B is trivial compared to that of $\kappa_{eq}{}^{\gamma}$ in all cases, just as it is known to be in the two-dimensional rough-sphere model. Therefore the quantity in parentheses acts as a pre-exponential factor

[13] B. Widom, J. Chem. Phys. **28**, 918 (1958).

multiplying that which is already present in κ_{eq}, this additional factor being a decreasing function of temperature. That the deviations from thermal equilibrium in a chemical reaction manifest themselves in a temperature-decreasing pre-exponential factor has been noted previously by Stupochenko and Osipov.[14] The important point in Eq. (4.1) is that deviations from equilibrium become noticeable as soon as kT becomes comparable to a *fraction* of ϵ^*, though just how small this fraction is seems to depend significantly on the details of the system.

It should be noted that Eq. (4.1) can only be used to estimate accurately the *initial* effects of deviations from equilibrium, but that as soon as these are so large that $B\kappa_{eq}^{\gamma}$ is comparable to unity, then the terms which have been neglected become important. The κ calculated formally from the uncorrected Eq. (4.1) may be negative, just as it was with $\gamma=0$ in the first illustration.

It seems entirely possible that the observed temperature-decreasing pre-exponential factor in the rate of dissociation of diatomic molecules[15] is due to deviations from thermal equilibrium among the reactants, these deviations necessarily causing a lowering of the rate constant below κ_{eq} and necessarily becoming more extreme with increasing temperature. Two of the alternative explanations which have been considered in the past are (i) that the reaction does not proceed by the binary collision mechanism $X+A\rightarrow X+$ products, but rather by the initial formation of a long-lived complex between X and A, the equilibrium concentration of which decreases with temperature; or (ii) that the binary collision mechanism is correct, and that deviations from equilibrium are of no significance, but that due to a peculiarity of the transition probability a temperature-decreasing pre-exponential factor is already contained in κ_{eq}. However, an explanation in terms of deviations from equilibrium which increase with temperature seems to be at least as straightforward as either of these two alternatives, and at the present time there are no experimental or theoretical grounds on which this possibility could be excluded.

[14] E. V. Stupochenko and A. I. Osipov, Zhurn. Fiz. Khim. **33**, 1526 (1959).

[15] H. B. Palmer and D. F. Hornig, J. Chem. Phys. **26**, 98 (1957)

Effects of Diffusion in Nuclear Magnetic Resonance Spin-Echo Experiments

D. E. WOESSNER

Field Research Laboratory, Socony Mobil Oil Company, Inc., Dallas, Texas

(Received December 27, 1960)

The spin-echo attenuation by molecular self-diffusion in an inhomogeneous magnetic field has been calculated for three- and four-pulse sequences. The method employed avoids the question of an averaging procedure as discussed by Das and Saha. Experimental measurements yield confirmation of the three-pulse results.

I. INTRODUCTION

SINCE Hahn's discovery of nuclear magnetic resonance spin-echoes[1] in liquids, much theoretical and experimental work elucidating spin-echo phenomena has been performed.[2–17] Physical models explaining spin-echo formation in an inhomogeneous magnetic field have been presented for a variety of rf pulse sequences. The dependences of the spin-echo amplitudes on longitudinal (T_1) and transverse (T_2) relaxation have been investigated thoroughly.

The role of molecular self-diffusion in liquids in attenuating the spin-echo amplitudes for an inhomogeneous magnetic field has been less thoroughly studied for general multi-pulse sequences. Diffusion causes the precessional frequency ω_0 of a given nucleus to be time dependent. Hence, because of the random nature of thermal diffusion, a group of nuclei which possess a given frequency at the time of the first pulse will, at a later time, be distributed over a range of frequency values. A distribution of precessional phase angles $\int\omega_0(t)dt$ for nuclei of this group exists at this later time. A second rf pulse reverses the algebraic signs of the phase angles of all, or part, of the nuclei. As time passes, the nuclei which are thus affected tend towards their initial phase angles and yield a spin-echo. However, the ever-present random diffusion produces a dispersion of phase angles even at the maximum in-phase condition, the peak of the spin-echo, and thus reduces the spin-echo amplitude. Different approaches to the calculation of this attenuation for two-pulse and more complicated pulse sequences have yielded several different results.

The purpose of this paper is to calculate the diffusion attenuation terms for all the spin-echoes in three- and four-pulse sequences.

II. MATHEMATICAL METHODS

The mathematical analysis is performed by applying the basic Bloch equations[18] and their solutions successively in the presence and absence of the applied intense rectangular rf pulses. The general equations describing U, V, and M_z, the in-phase, out-of-phase, and longitudinal components, respectively, with respect to the conventional rotating coordinate system are:

$$U=-(\omega_0-\omega)V-U/T_2 \tag{1}$$

$$V=(\omega_0-\omega)U-V/T_2-\omega_1M_z \tag{2}$$

$$M_z=(M_0-M_z)/T_1+\omega_1V, \tag{3}$$

in which ω_0 is the nuclear precessional frequency, and ω is the frequency of the rotating coordinate system. T_2 is the transverse (spin-spin) relaxation time; T_1 is the longitudinal (spin-lattice) relaxation time; M_0 is the equilibrium magnetization in the absence of a rf field; and $\omega_1=\gamma H_1$, γ being the nuclear gyromagnetic ratio and H_1 being the magnitude of the effective rotating component of the rf field.

In the absence of a pulse, $\omega_1=0$; and the solutions to the Bloch equations may be written as

$$M_z(t'')=M_0\{1-[1-M_z(t')/M_0]\times\exp[-(t''-t')/T_1]\} \tag{4}$$

$$F(t'')=F(t')\exp[-(t''-t')/T_2+i\int_{t'}^{t''}(\omega_0-\omega)dt], \tag{5}$$

where $F=U+iV$ is the rotating component of the nuclear magnetization.

If the rf field is applied at time t for a duration t_w which is small compared to T_1, T_2, and $1/|\omega_0-\omega|$, and if H_1 is large so that $\omega_1\gg|\omega_0-\omega|$, $1/T_1$, $1/T_2$,

[1] E. L. Hahn, Phys. Rev. **80**, 580 (1950).
[2] T. P. Das and A. K. Saha, Phys. Rev. **93**, 749 (1954).
[3] H. Y. Carr and E. M. Purcell, Phys. Rev. **94**, 630 (1954).
[4] T. P. Das and D. K. Roy, Phys. Rev. **98**, 525 (1955).
[5] E. T. Jaynes, Phys. Rev. **98**, 1099 (1955).
[6] A. L. Bloom, Phys. Rev. **98**, 1105 (1955).
[7] G. J. B. Crawford, Phys. Rev. **99**, 600 (1955).
[8] T. P. Das, A. K. Saha, and D. K. Roy, Proc. Roy. Soc. (London) **A227**, 407 (1955).
[9] S. Fernbach and W. G. Proctor, J. Appl. Phys. **26**, 170 (1955).
[10] A. G. Anderson, R. L. Garwin, E. L. Hahn, J. W. Horton, G. L. Tucker, and R. M. Walker, J. Appl. Phys. **26**, 1324 (1955).
[11] B. Herzog and E. L. Hahn, Phys. Rev. **103**, 148 (1956).
[12] H. C. Torrey, Phys. Rev. **104**, 563 (1956).
[13] J. W. Horton, IBM J. Research Develop. **1**, 93 (1957).
[14] T. Ghose, S. K. Ghosh, and D. K. Roy, Indian J. Phys. **31**, 265 (1957).
[15] T. Ghose, S. K. Ghosh, and D. K. Roy, Nuovo cimento **5**, 751 (1957).
[16] B. M. Banerjee, S. K. Ghosh, and A. K. Saha, Indian J. Phys. **31**, 211 (1957).
[17] D. C. Douglass and D. W. McCall, J. Phys. Chem. **62**, 1102 (1958).
[18] F. Bloch, Phys. Rev. **70**, 460 (1946).

TABLE I. Echo terms for three pulses.

Position of maximum	Trigonometric part	Relaxation damping	Diffusion phase term	Diffusion damping of echo
$2\tau_2$	$M_0 \sin\theta_1 \cos^2\frac{1}{2}\theta_2 \sin^2\frac{1}{2}\theta_3$	$\exp[-2\tau_2/T_2]$	$\exp[i(-\phi_{10}-\phi_{21}+\phi_{t2})]$	$\exp\{-\frac{2}{3}k\tau_2^3\}$
$2\tau_2-\tau_1$	$M_z(\tau_1) \sin\theta_2 \sin^2\frac{1}{2}\theta_3$	$\exp[-(2\tau_2-2\tau_1)/T_2]$	$\exp[i(-\phi_{21}+\phi_{t2})]$	$\exp\{-\frac{2}{3}k(\tau_2-\tau_1)^3\}$
$2\tau_2-2\tau_1$	$-M_0 \sin\theta_1 \sin^2\frac{1}{2}\theta_2 \sin^2\frac{1}{2}\theta_3$	$\exp[-(2\tau_2-2\tau_1)/T_2]$	$\exp[i(\phi_{10}-\phi_{21}+\phi_{t2})]$	$\exp\{-\frac{2}{3}k[\tau_1^3+(\tau_2-2\tau_1)^3]\}$
$\tau_2+\tau_1$	$\frac{1}{2}M_0 \sin\theta_1 \sin\theta_2 \sin\theta_3$	$\exp[-2\tau_1/T_2-(\tau_2-\tau_1)/T_1]$	$\exp[i(-\phi_{10}+\phi_{t2})]$	$\exp\{-\frac{1}{3}k[2\tau_1^3+3\tau_1^2(\tau_2-\tau_1)]\}$

then the solutions of Eqs. (1)–(3) at the end of the pulses are

$$U(t+t_w)=U(t) \tag{6}$$

$$V(t+t_w)=V(t)\cos\theta-M_z(t)\sin\theta \tag{7}$$

$$M_z(t+t_w)=V(t)\sin\theta+M_z(t)\cos\theta, \tag{8}$$

where $\theta=\omega_1 t_w$. The value of F immediately following the pulse is given by the following equation obtained from (6) and (7):

$$F(t+t_w)=F(t)\cos^2\tfrac{1}{2}\theta+F^*(t)\sin^2\tfrac{1}{2}\theta-iM_z(t)\sin\theta. \tag{9}$$

The value of M_z may be written as

$$M_z(t+t_w)=M_z(t)\cos\theta-\tfrac{1}{2}i[F(t)-F^*(t)]\sin\theta. \tag{10}$$

Equation (9) shows that a pulse separates the rotating magnetization into two parts: one part which is proportional to the initial value and the other part which is proportional to the complex conjugate of the initial value. A solution of the time-dependent Schrödinger equation leads to the result[19] that the fraction of nuclei which undergo the quantum transition $(\pm\frac{1}{2}\rightarrow\mp\frac{1}{2})$ due to the pulse is $\sin^2\frac{1}{2}\theta$, and the fraction remaining unchanged in orientation $(\pm\frac{1}{2}\rightarrow\pm\frac{1}{2})$ is $\cos^2\frac{1}{2}\theta$. Hence, the first part is due to those nuclei remaining unchanged, and the second part, whose phase angle is reversed because it involves the complex conjugate, is due to those nuclei which have undergone the quantum transition. The phase reversal allows these nuclei to approach a pre-pulse in-phase condition and form a spin-echo. This is the so-called primary-echo mechanism.

Another spin-echo mechanism, the stimulated mechanism, occurs through the action of the pulse on M_z. The M_z after a pulse includes a term proportional to the initial F value and a term proportional to the initial F^*, as in Eq. (10). The longitudinal magnetization from these terms is transformed to rotating magnetization by a subsequent pulse so that the F^* term can approach later the in-phase condition and form an echo called the stimulated echo. The F term behaves after this subsequent pulse as if its previous in-phase condition were moved forward in time by a time interval equal to the pulse interval, insofar as echo formation by still another pulse is concerned. Hence, it forms a "virtual" stimulated echo.

[19] I. I. Rabi, Phys. Rev. **51**, 652 (1937).

III. EFFECTS OF MOLECULAR DIFFUSION

The diffusion effects under consideration are those observable only when a magnetic field gradient exists.[20] The gradient causes a spread of $(\omega_0-\omega)=\Delta\omega$ values over the volume containing the sample. Diffusion of molecules into regions of different magnetic field values causes $\Delta\omega$ for any given nucleus to be time dependent. The phase integral in Eq. (5) for a nucleus then becomes

$$\int_{t'}^{t''}(\omega_0-\omega)dt=\Delta\omega(t''-t')+\phi_{t''t'}, \tag{11}$$

where $\phi_{t''t'}$ is the phase shift due to diffusion. The random character of diffusion produces a distribution of $\phi_{t''t'}$ values for a group of nuclei which initially had a particular $\Delta\omega$ value. The net rotating magnetization for these nuclei is found by substituting Eq. (11) in (5),

$$F(t'')=F(t')\exp[-(t''-t')/T_2+i\Delta\omega(t''-t')+i\phi_{t''t'}], \tag{12}$$

and then integrating (12) over the distribution of $\phi_{t''t'}$ values. The result is an attenuation of $F(t'')$. The total rotating magnetization is then found by integrating the resultant over the distribution of $\Delta\omega$ values. This procedure is applicable as long as $\phi_{t''t'}$ is independent of $\Delta\omega$ and position in the sample; these conditions hold when the field gradient is constant over the sample volume.

The diffusion effects on M_z are entirely negligible even though M_0 is proportional to H_0. No phase is associated with the time dependence of M_z. In practice, the fractional variation of H_0 which the nuclei experience during the pulse sequence because of diffusion is very small. Hence, the effect of molecular diffusion on the time dependence of M_z, which would be cal-

[20] Nuclear spin relaxation effects are negligible because the variation of magnetic field over the molecular volume due to the gradient of H_0 is extremely small compared to the instantaneous local magnetic fields.

culated by making M_0 in Eq. (4) time dependent, is insignificant.

IV. CALCULATION OF SPIN-ECHO TERMS FOR THREE AND FOUR PULSES

The various spin-echo terms are easily calculated by starting with the initial conditions $U=V=0$ and $M_z=M_0$ and applying Eqs. (9) and (10) to find the effects of the pulses and using Eqs. (4) and (12) to evaluate the time dependences of the nuclear magnetizations following the pulses. The peaks of the spin-echoes occur when the $\Delta\omega$ terms in Eq. (12) are zero, that is, when nuclei of different $\Delta\omega$ values have the same precessional phase angles except for the random distributions of diffusion phase shifts ϕ.

The $F(t)$ terms which yield spin-echoes in the free precession following the last pulse in three- and four-pulse sequences are tabulated in Tables I and II, respectively. The first three pulses are applied at $t=0$, τ_1, and τ_2; the fourth pulse is at τ_3. These times are chosen so that $\tau_2>2\tau_1$ and $\tau_3>2\tau_2$. The pulse durations are neglected. The symbol θ_i represents the $\gamma H_1 t_w$ product for the ith pulse.

V. CALCULATION OF THE PHASE SHIFT DISPERSION

The problem is to calculate the distributions of ϕ_t values for the free precession interval in which the echoes occur. Two effects must be considered. One is a difference of algebraic signs for the ϕ's in two successive free precession intervals; this indicates a phase reversal at the intervening pulse. The occurrence of the same sign for the two ϕ's indicates no phase reversal, and, hence, the phase dispersion proceeds as if the intervening pulse had not occurred. The other effect is the absence of a ϕ for a free precession interval. The ϕ preceding this interval is reversed by the pulse at the end of the interval in the stimulated echo mechanism; its sign is unchanged in the virtual stimulated echo mechanism.

The calculation follows a procedure similar to those of Das and Saha[2] and Carr and Purcell[3] for the phase dispersion following a single pulse and that of Carr and Purcell[3] for their special multi-pulse sequence. The basic idea of the method is to follow the phase shift accumulated as the molecule moves into spatial regions of different precessional frequencies. The method will be illustrated by two examples. The first is the phase reversal by a pulse at τ_j. The phase angle of a nucleus at time t following the initial pulse may be written as follows by dividing the entire time interval into a large number n of small increments Δt,

$$\phi_t=\gamma G\{d_1\Delta t+d_2\Delta t+\cdots+d_j\Delta t+d_{j+1}\Delta t+d_{j+2}\Delta t+\cdots+d_n\Delta t\}, \quad (13)$$

in which G is the constant uniform magnetic field gradient existing over the sample, and d_i is the displacement in the direction of the magnetic field gradient

TABLE II. Echo terms for four pulses.

Position of maximum	Trigonometric part	Relaxation damping	Diffusion phase term	Diffusion damping of echo
$2\tau_3$	$M_0\sin\theta_1\cos^2\frac{1}{2}\theta_2\cos^2\frac{1}{2}\theta_3\sin^2\frac{1}{2}\theta_4$	$\exp[-2\tau_3/T_2]$	$\exp[i(-\phi_{10}-\phi_{21}-\phi_{32}+\phi_{43})]$	$\exp\{-\frac{2}{3}k\tau_3^3\}$
$2\tau_3-\tau_1$	$M_z(\tau_1)\sin\theta_2\cos^2\frac{1}{2}\theta_3\sin^2\frac{1}{2}\theta_4$	$\exp[-(2\tau_3-2\tau_1)/T_2]$	$\exp[i(-\phi_{21}-\phi_{32}+\phi_{43})]$	$\exp\{-\frac{2}{3}k(\tau_3-\tau_1)^3\}$
$2\tau_3-2\tau_1$	$-M_0\sin\theta_1\sin^2\frac{1}{2}\theta_2\cos^2\frac{1}{2}\theta_3\sin^2\frac{1}{2}\theta_4$	$\exp[-(2\tau_3-2\tau_1)/T_2]$	$\exp[i(\phi_{10}-\phi_{21}-\phi_{32}+\phi_{43})]$	$\exp\{-\frac{2}{3}k[\tau_1^3+(\tau_3-2\tau_1)^3]\}$
$2\tau_3-\tau_2+\tau_1$	$-\frac{1}{2}M_0\sin\theta_1\sin\theta_2\sin^2\frac{1}{2}\theta_3\sin^2\frac{1}{2}\theta_4$	$\exp[-(2\tau_3-2\tau_2+2\tau_1)/T_2-(\tau_3-\tau_1)/T_1]$	$\exp[i(-\phi_{10}-\phi_{32}+\phi_{43})]$	$\exp\{-\frac{1}{3}k[3\tau_1^2(\tau_3-\tau_1)+2(\tau_3-\tau_2+\tau_1)^3]\}$
$2\tau_3-\tau_2$	$M_z'(\tau_2)\sin\theta_3\sin^2\frac{1}{2}\theta_4$	$\exp[-(2\tau_3-2\tau_2)/T_2]$	$\exp[i(-\phi_{32}+\phi_{43})]$	$\exp\{-\frac{2}{3}k(\tau_3-\tau_2)^3\}$
$2\tau_3-\tau_2-\tau_1$	$-\frac{1}{2}M_0\sin\theta_1\sin\theta_2\sin^2\frac{1}{2}\theta_3\sin^2\frac{1}{2}\theta_4$	$\exp[-(2\tau_3-2\tau_2)/T_2-(\tau_3-\tau_1)/T_1]$	$\exp[i(\phi_{10}-\phi_{32}+\phi_{43})]$	$\exp\{-\frac{1}{3}k[2\tau_1^3+3\tau_1^2(\tau_3-\tau_1)+2(\tau_3-\tau_2-\tau_1)^3]\}$
$2\tau_3-2\tau_2+2\tau_1$	$M_0\sin\theta_1\sin^2\frac{1}{2}\theta_2\sin^2\frac{1}{2}\theta_3\sin^2\frac{1}{2}\theta_4$	$\exp[-(2\tau_3-2\tau_2+2\tau_1)/T_2]$	$\exp[i(-\phi_{10}+\phi_{21}-\phi_{32}+\phi_{43})]$	$\exp\{-\frac{2}{3}k[\tau_1^3+(\tau_3-2\tau_1)^3+(\tau_3-2\tau_2+2\tau_1)^3]\}$
$2\tau_3-2\tau_2+\tau_1$	$-M_z(\tau_1)\sin\theta_2\sin^2\frac{1}{2}\theta_3\sin^2\frac{1}{2}\theta_4$	$\exp[-(2\tau_3-2\tau_2)/T_2]$	$\exp[i(\phi_{21}-\phi_{32}+\phi_{43})]$	$\exp\{-\frac{2}{3}k[(\tau_2-\tau_1)^3+(\tau_3-2\tau_2+\tau_1)^3]\}$
$2\tau_3-2\tau_2$	$-M_0\sin\theta_1\cos^2\frac{1}{2}\theta_2\sin^2\frac{1}{2}\theta_3\sin^2\frac{1}{2}\theta_4$	$\exp[-(2\tau_3-2\tau_2)/T_2]$	$\exp[i(\phi_{10}+\phi_{21}-\phi_{32}+\phi_{43})]$	$\exp\{-\frac{2}{3}k[\tau_2^3+(\tau_3-2\tau_2)^3]\}$
$\tau_3+\tau_2$	$\frac{1}{2}M_0\sin\theta_1\cos^2\frac{1}{2}\theta_2\sin\theta_3\sin\theta_4$	$\exp[-2\tau_3/T_2-(\tau_3-\tau_2)/T_1]$	$\exp[i(-\phi_{10}-\phi_{21}+\phi_{43})]$	$\exp\{-\frac{1}{3}k[2\tau_2^3+3\tau_2^2(\tau_3-\tau_2)]\}$
$\tau_3+\tau_2-\tau_1$	$\frac{1}{2}M_z(\tau_1)\sin\theta_2\sin\theta_3\sin\theta_4$	$\exp[-(2\tau_3-2\tau_1)/T_2-(\tau_3-\tau_2)/T_1]$	$\exp[i(-\phi_{21}+\phi_{43})]$	$\exp\{-\frac{1}{3}k[2(\tau_2-\tau_1)^3+3(\tau_3-\tau_1)^2(\tau_3-\tau_2)]\}$
$\tau_3+\tau_2-2\tau_1$	$-\frac{1}{2}M_0\sin\theta_1\sin^2\frac{1}{2}\theta_2\sin\theta_3\sin\theta_4$	$\exp[-(2\tau_3-2\tau_1)/T_2-(\tau_3-\tau_2)/T_1]$	$\exp[i(\phi_{10}-\phi_{21}+\phi_{43})]$	$\exp\{-\frac{1}{3}k[2\tau_1^3+3(\tau_3-2\tau_1)^2(\tau_3-\tau_2)+2(\tau_3-2\tau_1)^3]\}$
$\tau_3+\tau_1$	$\frac{1}{2}M_0\sin\theta_1\sin\theta_2\cos\theta_3\sin\theta_4$	$\exp[-2\tau_1/T_2-(\tau_3-\tau_1)/T_1]$	$\exp[i(-\phi_{10}+\phi_{43})]$	$\exp\{-\frac{1}{3}k[2\tau_1^3+3\tau_1^2(\tau_3-\tau_1)]\}$

[a] $M_z'(\tau_2)$ is the initial M_z value for the third pulse with omission of the phase-containing terms.

of the nucleus from the initial position at the ith time increment. Let a pulse at the jth increment reverse the phase angle accumulated up to time $j\Delta t=\tau_j$. Then, for $t>\tau_j$,

$$\phi_t=\gamma G\{-[d_1\Delta t+d_2\Delta t+\cdots+d_j\Delta t]+[d_{j+1}\Delta t+d_{j+2}\Delta t+\cdots+d_n\Delta t]\}. \quad (14)$$

By substituting the relations

$$\begin{aligned} d_2&=d_1+(d_2-d_1)\\ d_3&=d_1+(d_2-d_1)+(d_3-d_2)\\ &\cdots\\ d_n&=d_1+(d_2-d_1)+(d_3-d_2)+\cdots+(d_n-d_{n-1}) \end{aligned} \quad (15)$$

in Eq. (14) and collecting the coefficients of the (d_i-d_{i-1}), we obtain the relation

$$\begin{aligned}\phi_t=\gamma G\Delta t\{&(n-2j)d_1+(n-2j+1)(d_2-d_1)\\ &+\cdots+(n-j-1)(d_j-d_{j-1})+(n-j)(d_{j+1}-d_j)\\ &+(n-j-1)(d_{j+2}-d_{j+1})+\cdots+(d_n-d_{n-1})\}. \end{aligned} \quad (16)$$

A result from diffusion theory is that each (d_i-d_{i-1}) is a normally distributed (Gaussian) independent variable. Hence, ϕ_t is a linear function of independent normally distributed stochastic variables and its dispersion is[21]

$$\begin{aligned}\langle\phi_t^2\rangle_{Av}=\gamma^2G^2(\Delta t)^2\{&[(n-2j)^2\langle d_1^2\rangle_{Av}\\ &+(n-2j+1)^2\langle(d_2-d_1)^2\rangle_{Av}+\cdots+(n-j-1)^2\\ &\times\langle(d_j-d_{j-1})^2\rangle_{Av}]+[(n-j)^2\langle(d_{j+1}-d_j)^2\rangle_{Av}\\ &+(n-j-1)^2\langle(d_{j+2}-d_{j+1})^2\rangle_{Av}\\ &+\cdots+\langle(d_n-d_{n-1})^2\rangle_{Av}]\}, \end{aligned} \quad (17)$$

and it is normally distributed. Another result from diffusion theory is

$$\langle d_1^2\rangle_{Av}=\langle(d_2-d_1)^2\rangle_{Av}=\cdots=\langle(d_n-d_{n-1})^2\rangle_{Av}=2D\Delta t, \quad (18)$$

where D is the molecular self-diffusion coefficient. After applying the series

$$\sum_{r=1}^{N}r^2=N(N+1)(2N+1)/6\approx N^3/3 \quad (19)$$

for large N, Eq. (17) becomes

$$\langle\phi_t^2\rangle_{Av}=\tfrac{2}{3}\gamma^2G^2D(\Delta t)^3[2(n-j)^3-(n-2j)^3]. \quad (20)$$

After making the further substitutions $n\Delta t=t$, $j\Delta t=\tau_j$, and $\gamma^2G^2D=k$, the dispersion becomes

$$\langle\phi_t^2\rangle_{Av}=\tfrac{2}{3}k[2(t-\tau_j)^3-(t-2\tau_j)^3]. \quad (21)$$

This result is the same as that derived by Douglass and McCall[17] by a different method, and it is in agreement with the results of Herzog and Hahn[11] and of Carr and Purcell.[3] It gives the diffusion attenuation for the two-pulse echo.

The second example is the stimulated-echo mechanism in which the phase shift for a free precession interval is absent. The phase shift accumulated preceding this interval is reversed by the pulse at the end of the interval. Let pulses occur at the jth and kth time increments with $k>j$. No phase shift is accumulated during the interval between $\tau_j=j\Delta t$ and $\tau_k=k\Delta t$. Then, for $t>\tau_k$,

$$\phi_t=\gamma G\{-[d_1\Delta t+d_2\Delta t+\cdots+d_j\Delta t]+[d_{k+1}\Delta t+d_{k+2}\Delta t+\cdots+d_n\Delta t]\}. \quad (22)$$

Apply Eq. (15), collect the coefficients of the (d_i-d_{i-1}), and write the dispersion:

$$\begin{aligned}\langle\phi_t^2\rangle_{Av}=\gamma^2G^2(\Delta t)^2\{&(n-k-j)^2\langle d_1^2\rangle_{Av}\\ &+(n-k-j+1)^2\langle(d_2-d_1)^2\rangle_{Av}+\cdots+(n-k-1)^2\\ &\times\langle(d_j-d_{j-1})^2\rangle_{Av}+(n-k)^2[\langle(d_{j+1}-d_j)^2\rangle_{Av}+\cdots\\ &+\langle(d_k-d_{k-1})^2\rangle_{Av}]+(n-k)^2\langle(d_{k+1}-d_k)^2\rangle_{Av}\\ &+(n-k-1)^2\langle(d_{k+2}-d_{k+1})^2\rangle_{Av}+\cdots+\langle(d_n-d_{n-1})^2\rangle_{Av}\}. \end{aligned} \quad (23)$$

Then use of (18) and (19) yields the result

$$\langle\phi_t^2\rangle_{Av}=\tfrac{2}{3}k[2(t-\tau_k)^3+3(t-\tau_k)^2(\tau_k-\tau_j)-(t-\tau_k-\tau_j)^3]. \quad (24)$$

which produces the same diffusion attenuation for a three-pulse sequence as that derived by Hahn[1] and Herzog and Hahn.[11]

The above examples illustrate a method which can be applied to any sequence of phase-shift reversals and phase-shift omissions. The other phase terms needed for a four-pulse sequence are the following:

(a) For two-phase reversals, one at τ_j and the other at τ_k,

$$\langle\phi_t^2\rangle_{Av}=\tfrac{2}{3}k[2(t-\tau_k)^3-2(t-2\tau_k+\tau_j)^3+(t-2\tau_k+2\tau_j)^3]. \quad (25)$$

(b) For three-phase reversals, at τ_j, τ_k, and τ_m,

$$\langle\phi_t^2\rangle_{Av}=\tfrac{2}{3}k[2(t-\tau_m)^3+2(t-2\tau_m+2\tau_k-\tau_j)^3-2(t-2\tau_m+\tau_k)^3-(t-2\tau_m+2\tau_k-2\tau_j)^3]. \quad (26)$$

(c) For a stimulated echo due to pulses at τ_j and τ_k followed by a phase reversal at τ_m,

$$\langle\phi_t^2\rangle_{Av}=\tfrac{2}{3}k[2(t-\tau_m)^3+3(t-2\tau_m+\tau_k)^2(\tau_k-\tau_j)-2(t-2\tau_m+\tau_k)^3+(t-2\tau_m+\tau_k+\tau_j)^3]. \quad (27)$$

(d) For a virtual stimulated echo due to pulses at τ_j and τ_k followed by a reversal at τ_m,

$$\langle\phi_t^2\rangle_{Av}=\tfrac{2}{3}k[2(t-\tau_m)^3+3(t-2\tau_m+\tau_k)^2(\tau_k-\tau_j)-(t-2\tau_m+\tau_k-\tau_j)^3]. \quad (28)$$

[21] M. E. Munroe, *Theory of Probability* (McGraw-Hill Book Company, Inc., New York, 1951), p. 92.

(e) For a phase reversal at τ_j followed by a stimulated echo mechanism by pulses at τ_k and τ_m,

$$\langle\phi_t^2\rangle_{Av}=\tfrac{2}{3}k[2(t-\tau_m)^3+3(t-\tau_m)^2(\tau_m-\tau_k) -2(t-\tau_m-\tau_k+\tau_j)^3+(t-\tau_m-\tau_k+2\tau_j)^3]. \quad (29)$$

The initial pulse occurs at $t=0$. These results are for $\tau_m>\tau_k>\tau_j$, and are not subject to the limitations used in Sec. IV.

The diffusion damping at the echo maxima tabulated in Tables I and II are obtained from the diffusion phase terms by using the above relations and letting t be the time of the echo maxima. In doing this, the role of a nonreversing pulse for a given echo must be recognized as resulting in relations as, for example,

$$\phi_{10}+\phi_{21}-\phi_{12}=\phi_{20}-\phi_{t2}. \quad (30)$$

VI. EXPERIMENTAL RESULTS AND DISCUSSION

Values of the diffusion damping terms for three-pulse spin-echoes were measured by use of three-pulse spin-echo apparatus in which each pulse is adjusted independently. Apparatus and procedures previously described[22] were used to establish and measure the various field gradients used in these measurements. The results are in agreement with the attenuation terms in Table I.

Several useful generalizations may be made by inspection of the calculations. Consider the echo produced by the primary echo mechanism acting on an in-phase condition, either a free decay immediately following a pulse or an echo. The diffusion damping of the resultant echo with respect to the pre-pulse in-phase amplitude is

$$E(t+\tau)/E(t)=\exp(-k\tau^3/12), \quad (31)$$

where τ is the time between the maximum of the in-phase condition and the maximum of the subsequent echo. This result has been used to measure self-diffusion coefficients[23] by use of 90°–180°–180° pulse sequences and measuring the ratio of the two spin-echo amplitudes as a function of τ. This generalization also predicts the counteraction of diffusion damping in the special Carr and Purcell technique.[3]

A second generalization is that the diffusion damping of the echo produced by action of a two-pulse stimulated-echo mechanism on an in-phase condition is

$$E(t+\tau_1+\tau_2)/E(t)=\exp\{-\tfrac{1}{3}k[2\tau_1^3+3\tau_1^2(\tau_2-\tau_1)]\}, \quad (32)$$

where τ_1 and τ_2 are the times of application of the pulses with respect to the time t of the maximum of the in-phase condition.

Equation (28), of course, leads to an expression for the echo observable from the virtual stimulated-echo mechanism.

The method used here for calculating the phase shift dispersions avoids the necessity for deciding upon averaging procedures as has been discussed by Das and Saha.[2] In addition, it shows that the diffusion attenuation of an echo is independent of the rf pulse angles θ, as is observed experimentally.[22]

[22] D. E. Woessner, Rev. Sci. Instr. **31**, 1146 (1960).

[23] R. L. Garwin and H. A. Reich, Phys. Rev. **115**, 1478 (1959).

Interaction of Hydrogen and of Nitrogen with a Molybdenum Ribbon*‡

R. A. PASTERNAK AND HANS U. D. WIESENDANGER

Stanford Research Institute, Menlo Park, California

(Received August 15, 1960)

Adsorption and desorption studies—by flash-filament and ion gauge techniques—gave information on surface coverages, sticking probabilities, atom formation, and surface mobilities for the interaction of gases with a molybdenum ribbon. For hydrogen, saturation surface coverages were independent of pressure (10^{-6}–10^{-3} mm Hg), within experimental errors, but depended strongly on temperature (225°–500°K). Adsorption below 320°K proceeded in two steps. Two layers were successively adsorbed and completed at 320° and 225°K, respectively; each contained close to two hydrogen atoms per surface molybdenum atom. The sticking probability was 0.35; it remained constant during the formation of the first layer. At about 700°K, no measurable amounts of hydrogen were retained on the ribbon surface, but the kinetics of atom formation above 1200°K suggested that traces of hydrogen might be adsorbed at much higher temperatures. Finally, adsorbed hydrogen was readily replaced by other gases, such as nitrogen, even at room temperature. For the adsorption of nitrogen, the saturation surface coverage decreased only about 30% from 225°–710°K; its value at room temperature was about one nitrogen atom per surface molybdenum atom. The initial sticking probability, in the same temperature range, decreased from 0.7 to 0.2.

INTRODUCTION

INVESTIGATIONS of interactions of gases with solid surfaces are of great importance for the understanding of solid state in general, and of catalysis in particular. Research on gas-metal interactions has been going on for many years, but the significance of a number of the earlier studies is open to question because of the limitations in techniques: often the surfaces were ill-defined; contaminants were present; and pressures were so high that the initial rates of adsorption were immeasurably fast.

The recent developments in ultra-high vacuum techniques, the invention of the field emission microscope, and the flash-filament technique have provided powerful tools for the detailed study of adsorption and desorption processes. This paper describes a flash-filament study of the hydrogen-molybdenum and nitrogen-molybdenum systems and some experiments illuminating the effects of contamination.

EXPERIMENTAL

Apparatus

The apparatus employs the flash-filament principle described by others,[1–3] but with important modifications designed to reduce the problem of contamination, to improve the resolution of desorption steps, and to drop the temperature of the filament rapidly from desorption to adsorption conditions.

One of the main features of the apparatus (Fig. 1) is a high steady-state flow rate. High pumping speeds of about 15–25 liter/sec for H_2 were obtained with an oil-diffusion pump and a nonrefrigerated molecular sieve trap[4] described previously,[5] and high conductances were maintained between the ribbon and the variable leak. The leak hole normally used had a conductance of 12 liter/sec for H_2, and the volume of the apparatus between the leak and the Alpert valve was 2.3 liters. Base pressures of below 3×10^{-10} mm Hg were easily maintained after bakeout.

The principal pressure gauge was a stripped Westinghouse gauge mounted in a half-liter bulb, not in direct view of either the sample filament or the exit hole. This arrangement assured immediate response to fast pressure changes and considerably reduced heating and degassing of the glass walls. The gauges were left on continuously throughout the study to minimize transitory effects. The gauges were used in conjunction with modified Veeco RG21A ion gauge controls and a two-channel Brush recorder (0.01 sec rise time, 12.5 cm/sec chart speed). The gauge sensitivity found by calibration with a McLeod gauge was 0.4 for H_2 relative to air, in fair agreement with previous data.[6]

By cooling the leads and passing a low heating current through the ribbon at an appropriate time after flashing to 2000°K, the time required for the filament temperature to decay to about ambient was reduced by a factor of 2 to about 1 min. The temperature of the ribbon was determined from its resistance using literature data,[7] cross checked experimentally.

Of the two approaches for determining the sticking probabilities and the total number of adsorbed gas

* This work was done in part for the Lawrence Radiation Laboratory at Livermore, California, under the auspices of the Atomic Energy Commission.

‡ Presented in part at the symposium "The Chemistry of Solid State Phenomena," 137th National Meeting of the American Chemical Society, Cleveland, Ohio, April 1960.

[1] J. A. Becker and C. D. Hartman, J. Phys. Chem. **57**, 157 (1953).

[2] J. A. Becker, *Advances in Catalysis* VII (Academic Press, Inc., New York, 1955), p. 135.

[3] T. W. Hickmott and G. Ehrlich, J. Phys. Chem. Solids **5**, 47 (1958).

[4] M. A. Biondi, Rev. Sci. Instr. **39**, 831 (1959).

[5] H. U. D. Wiesendanger and R. A. Pasternak, Experientia **16**, 467 (1960).

[6] D. Alpert, J. Appl. Phys. **24**, 860 (1953).

[7] Goldsmith, A. and T. E. Waterman, WADC Technical Rept. 58–476 (1959). See also A. G. Worthing in *Molybdenum* edited by L. Northcott (Academic Press, Inc., New York, 1956).

atoms, the method involving measurement of the pressure increase on flash-heating the filament after different adsorption times was used by preference. Correction factors for gas losses by pump-out through the large exit hole were derived from a comparison with equivalent data obtained with a smaller exit hole for which pump-out was found to be negligible. For our standard heating rate of 10 000°K/sec these factors were 1.5 for H_2, and 1.2 for N_2, independent of the height of the pressure peak within the accuracy of our measurements. The rapid pumping rate reduced the relative importance of contaminants and improved the resolution of consecutive desorption steps. However, the desorption curves became distorted, thus precluding the evaluation of the kinetics of desorption.

Materials

The gases used in this study—Air Reduction Company reagent-grade H_2 (0.15 mole % maximum impurities), and 99.996% purity N_2 from Matheson—were dried over liquid nitrogen and stored in a baked reservoir (Fig. 1).

The molybdenum ribbon (15.0×0.065×0.0005 cm) was rolled from 99.9% purity stock (Fansteel, <0.03% C) without lubricants, and cut along the rolling direction. X-ray photographs showed that the [110] crystal direction coincided approximately with the ribbon axis, and that the (311) and (411) faces were preferentially exposed, as also reported for tungsten ribbons.[8] Grain growth occurred in the course of the experiments, and a surface roughness factor of 1.2 was estimated from electron micrographs. The ribbon was conditioned by heating it to 2000°K in H_2 for 5 hr, for several minutes every day, and intermittently for seconds before each experiment. In the course of the experiments, a thin molybdenum film gradually deposited on the walls of the cell; it did not affect the measurements. Only in the very last few experiments a reversible adsorption of hydrogen by the film could be detected. Robinson reported that such films seal the pores of the glass walls and reduce the release of contaminants.[9]

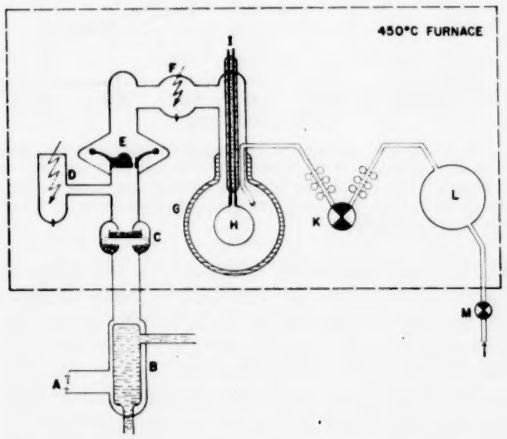

FIG. 1. Ultra-high vacuum unit. (A) Oil diffusion pump and backing pump; (B) water baffle; (C) high-conductance isolation trap charged with activated alumina; (D) ionization gauge (Veeco); (E) variable mechanical leak; (F) ionization gauge (Westinghouse, modified); (G) flash filament cell; (H) Molybdenum ribbon; (I) tungsten leads; (K) Granville-Phillips valve; (L) gas reservoir; (M) Hoke valve.

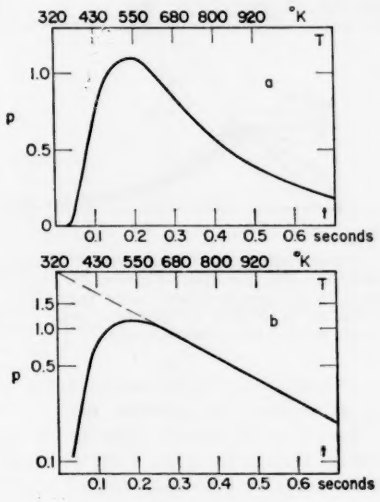

FIG. 2. Desorption curve at intermediate heating rate. Steady state pressure $p_0 \simeq 3.9 \times 10^{-7}$ mm Hg; flash-heating rate 1300°/sec; adsorption temperature 330°K. p in arbitrary units. (a) pressure vs time plot; (b) log pressure vs time plot.

INTERACTION OF HYDROGEN WITH MOLYBDENUM

Characteristics of the Desorption Curves

When the molybdenum ribbon was flash-heated after adsorption of hydrogen above 320°K, single desorption pressure peaks were obtained. Figure 2 shows a typical desorption curve for an adsorption temperature of 330°K and a maximum flash temperature of 1500°K. The log p vs time plot for this desorption curve (Fig. 2b) approached a straight line soon after the pressure maximum was reached; this is characteristic for simple pump-out through a hole. The conductance of the exit hole was calculated from the slope and agreed within 15% with that calculated from the geometric dimensions; this indicates that hydrogen pumping by the gauge and by the walls was not severe. Similar desorption curves were obtained at maximum flash temperatures of 2000°K. (see also Fig. 7.) These curves discount the existence of another distinct desorp-

[8] J. A. Becker, *Solid State Physics* edited by F. Seitz (Academic Press, Inc., New York, 1958), Vol. VII, p. 379.

[9] N. W. Robinson, Brit. J. Appl. Phys. **10**, 383 (1959).

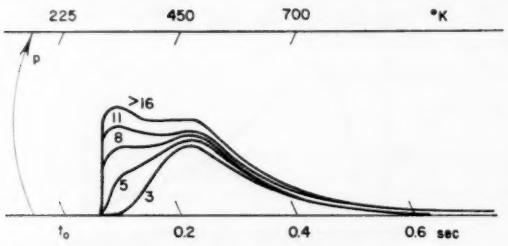

FIG. 3. Desorption curves as function of adsorption time. $p_0 \cong 7.2\times10^{-9}$ mm Hg; flash-heating rate = 1300°/sec; adsorption temperature 225°K; curves labeled with adsorption times in minutes. Peak at ~340°K is forming after peak at 550°K has approximately reached its maximum height.

tion step of hydrogen at higher temperatures. The temperatures at which these pressure maxima occurred did not depend on adsorption temperature (if above 320°K) or on surface coverage. They depended, however, on the rates of pump-out and of heating, and ranged from about 450°–700°K for heating rates from 250°–10 000°K/sec.

The different desorption pattern for hydrogen adsorbed below 320°K is illustrated in Fig. 3. These curves, for adsorption at 225°K were obtained by slowly heating the ribbon. For short adsorption times, only one desorption peak was observed at about 550°K. For longer times of adsorption, a second step appeared at about 350°K; its height increased with time, whereas the height of the first peak remained approximately constant. Thus, the first stage of adsorption was practically completed before the second became noticeable. The amounts of hydrogen released in the two desorption steps could not be evaluated from these overlapping curves, but flash experiments carried out at high heating rates showed that on saturation at 225°K approximately twice the amount of hydrogen was adsorbed as at 320°K. The desorption proceeded in two steps for adsorption temperatures up to 320°K, but with increasing adsorption temperature, the low temperature desorption peak decreased in height and shifted to higher temperatures. (See Fig. 4.)

Surface Coverage as a Function of Pressure and Temperature

Saturation surface coverages were determined over a pressure range of 6.5×10^{-9} to 4.2×10^{-6} mm Hg, and at adsorption temperatures between 225° and 470°K. At the lower temperatures, precision of the measurements was better than 5% on immediate repetition, and better than 10% throughout the investigation. In Fig. 5 the observed surface coverages in atoms/cm² are plotted against the ribbon temperatures for the two steady-state pressures of 7.8×10^{-7} and 2.3×10^{-8} mm Hg. The numerous data for pressures of 7.8×10^{-8}, 1.6×10^{-7}, 3.9×10^{-7}, and 4.2×10^{-6} mm Hg lie within the range defined by the reproduced curves, but a few data obtained at 6.5×10^{-9} mm Hg are about 20% lower.

The saturation surface coverage depended little on pressure within the accuracy of the measurements; the observed variance might arise in part from wall effects.

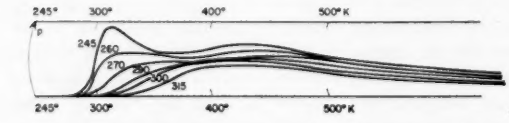

FIG. 4. Desorption curves as function of adsorption temperature. $p_0 \cong 1.6\times10^{-7}$ mm Hg; flash-heating rate = 210°/sec. Curves labeled with adsorption temperatures in °K.

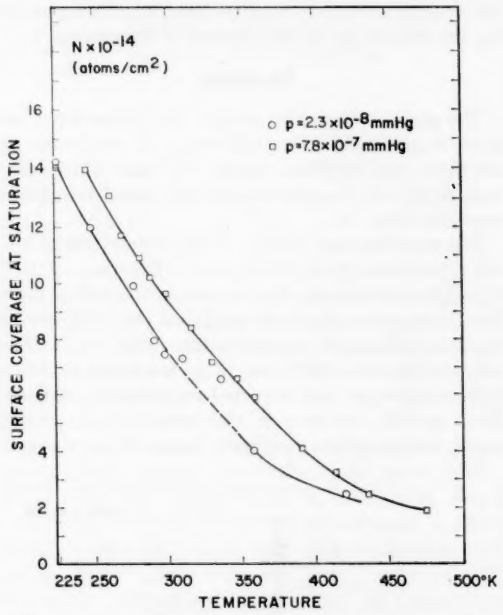

FIG. 5. Surface coverages at saturation vs adsorption temperatures at two pressures. All experimental values obtained at pressures of 2×10^{-8} to 4.2×10^{-6} mm Hg fall into the range between the given curves. The apparent pressure dependence is within experimental errors.

The two-step adsorption mechanism at low temperatures was not significantly affected by pressure changes; the limiting temperature of 320°K for the appearance of the second step remained unchanged over the whole range of pressures studied. The measured experimental surface coverage at high temperatures is undoubtedly high and the effects of pressure on coverage might be masked, because the amount of gas adsorbed on the cold ends of the filament must be substantial.[10,10a]

The points given in Fig. 5 may indicate a plateau at about 320°K at a coverage of about 7×10^{14} atoms/cm², and a second plateau at 225°K at a coverage of

[10] I. Langmuir, S. MacLane, and K. B. Blodgett, Phys. Rev. **35**, 479 (1930).

[10a] However, at room temperature, the total amount of gas adsorbed was increased by less than 10% on cooling of the leads.

about 14×10^{14} atoms/cm^2. The existence of such plateaus would agree with the two-step adsorption mechanism indicated by the desorption curves.

Sticking Probabilities

The sticking probabilities as functions of surface coverage and temperature obtained by the flash-desorption technique are shown in Fig. 6. (Maximum sticking probabilities calculated from the pressure-time curves during adsorption were lower by about 30%.) Measurements made several months later gave sticking probability curves of the same character, but the absolute values were about one third lower. This decrease might have been caused by increased wall pumping, or by changes in the surface properties of the ribbon.[2,3,11] The former explanation is more likely, because an equivalent decrease in apparent surface saturation coverages was also observed in these latest experiments.

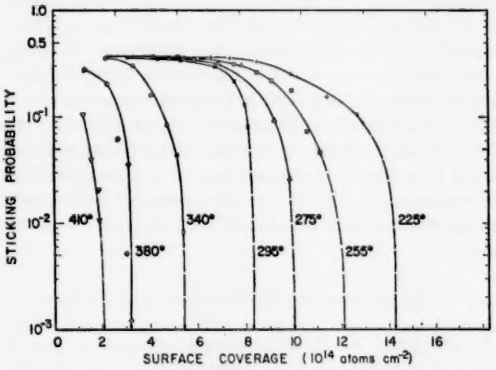

FIG. 6. Sticking probabilities vs surface coverages. $p_0\cong1.6\times10^{-8}$ mm Hg. Curves labeled with adsorption temperatures in °K.

Figure 6 shows that for lower surface coverages the sticking probability is virtually independent of coverage, and of temperature. The curves appear to extrapolate to about 0.35 even for the highest adsorption temperatures. At temperatures below about 320°K, the sticking probability remains constant until approximately the amount of hydrogen characteristic for this limiting temperature has been adsorbed; it then drops off—the more gradually the lower the adsorption temperature. It is reasonable to assign the range of constant sticking probability to the adsorption of the first stage, and the range of decreasing sticking probability to the adsorption of the second stage.

Hydrogen Atom Formation

Since Langmuir,[12] many effects observed in studies involving hot tungsten filaments have been ascribed to

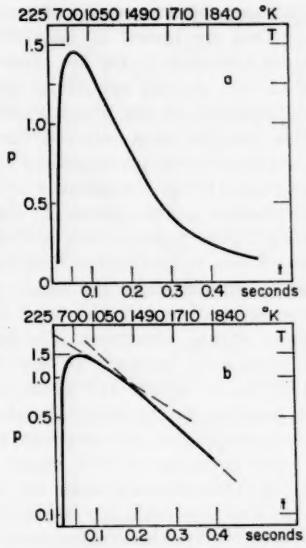

FIG. 7. Desorption curve at maximum heating rate. $p_0\cong3.9\times10^{-7}$ mm Hg; flash-heating rate approximately 10 000°/sec; adsorption temperature 330°K. p in arbitrary units. (a) Pressure vs time plot; (b) log pressure vs time plot.

atomic hydrogen.[13–15] Evidence for the formation of atomic hydrogen and its adsorption by the glass walls of the unit was also found in the present investigation.

The desorption curves obtained at high heating rates showed accelerated pump-out when the ribbon reached a temperature of about 1400°K. The declining branch of the log$p$ vs time plot of such a desorption curve (Fig. 7b) was composed of two straight lines intersecting at about 1450°K. The slope of the first line corresponded to that found for simple pump-out through the exit hole. The increase in slope shows that a second removal mechanism became effective at this temperature, probably the production of hydrogen atoms on the hot filament and their subsequent adsorption by the glass walls. The linearity of this second part of the curve indicates that the formation of hydrogen atoms is first order with respect to pressure, and independent of ribbon temperature above 1450°K. The difference in slope of the two straight lines is a measure of the rate

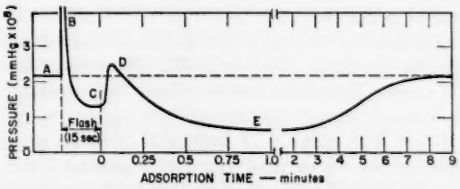

FIG. 8. Pressure-time relationship during adsorption experiment. (A) Steady-state pressure $p_0\cong2.15\times10^{-8}$ mm Hg; (B) flash peak; (C) pressure when ribbon at 2000°K; (D) pressure surge when heating discontinued; (E) normal decrease of pressure due to pumping by the ribbon.

[11] J. Eisinger, J. Chem. Phys. **29,** 1154 (1958).
[12] I. Langmuir, J. Am. Chem. Soc. **34,** 1310 (1912).
[13] T. W. Hickmott, J. Appl. Phys. **31,** 128 (1960).
[14] J. C. P. Mignolet, Rec. trav. chim. **74,** 685, 701 (1955).
[15] D. Brennan and P. C. Fletcher, Proc. Roy. Soc. (London) **A250,** 389 (1959).

of hydrogen atom formation. Assuming that all hydrogen atoms are buried in the wall, the efficiency of H-atom formation on the hot ribbon was calculated to be 0.12; i.e., at least one out of eight hydrogen molecules impinging on the ribbon dissociated.

This interpretation received further support from the analysis of the pressure-time curves for hydrogen adsorption. In Fig. 8 segment A represents the steady-state pressure in the system; B, the pressure peak on flashing; C, the approach to a new equilibrium pressure as the ribbon is kept at the flash temperature; D, the pressure increase above the steady state when heating is discontinued; and E, the usual range of decreasing pressure during adsorption. The pressure decrease C was found to be constant for any ribbon temperature of 1200°K, or higher, and again suggested hydrogen atom pumping by the walls. The observed pressure decrease corresponded to a minimum efficiency of hydrogen atom formation of 0.15, closely agreeing with the value of 0.12 obtained from the slope of the flash curves. The true efficiency is even higher, because at room temperature the sticking probability of hydrogen atoms on the walls is probably less than unity, and the rate of recombination of atoms on the walls is significant. Recombination is indicated by the pressure surge D corresponding to the release of hydrogen molecules formed by such a mechanism.

DISCUSSION

For chemisorption on metal surfaces one generally accepts the model of a monolayer containing a small number of adsorbate atoms per surface metal atom. In the case of hydrogen on molybdenum, a monolayer cannot be defined by simple adsorption measurements, because the saturation coverage shows a strong continuous dependence on temperature. This was found to arise from two consecutive adsorption stages, both temperature dependent, and not differing greatly in stability. The hydrogen in both layers is undoubtedly bound to the surface by chemical forces and is probably dissociated, since the temperatures are too high for physisorption. The maximum amount of hydrogen adsorbed in each of these steps can be assumed to represent a monolayer.

To derive the ratio of gas to surface metal atoms, let us assume that only (311) and (411) planes are present, both occupying equal areas; then, the number of molybdenum atoms per cm^2 of the surface is about 4×10^{14}.[15a] The number of hydrogen adatoms per cm^2 of the surface in each of the two observed layers is about 7×10^{14}. Thus, it appears that each chemisorbed layer contains close to two hydrogen atoms per surface molybdenum atom. Since the average distance between the Mo atoms for the assumed surface density is about 5 A, whereas the diameter of Mo is only 2.7 A, the H atoms of the first layer can easily be accommodated in the wells between them and form bonds with Mo atoms located below the surface. The H atoms in the second layer would, then, form bonds with the surface metal atoms.

The virtually complete desorption at 600°K and the large temperature dependence of coverage down to 225°K suggest that the H atoms have a high surface mobility and can readily interchange with molecules in the gas phase. This is further supported by the easy replacement of adsorbed hydrogen by nitrogen and oxygen which shall be discussed in a later section. The constancy of the observed sticking probability over a wide range of coverages also suggests a very high mobility of hydrogen on the surface; the mobile hydrogen might be present in a transitory state between physisorbed molecules and chemisorbed atoms. The constancy of sticking probability with respect to temperature shows that the activation energy for the adsorption is negligibly small from 225°–400°K. Sticking probabilities may remain constant to much higher temperatures, even though only a very small amount of hydrogen is adsorbed in the steady state. This is indicated by the observation that the rate of hydrogen atom formation on the hot filament is independent of temperature, although the activation energy of this reaction must equal, at least, the heat of dissociation of 104 kcal/mole. Thus, the dissociation reaction is preceded by a rate-determining step of very small activation energy, very likely the adsorption of hydrogen; it is followed by fast evaporation of H atoms from the surface

$$H_2(\text{gas}) \xrightarrow{\text{slow}} 2H(\text{ads}) \xrightarrow{\text{fast}} 2H(\text{gas}).$$

The efficiency of H atom formation would then be identical with the sticking probability of the hydrogen molecules on the surface at the particular temperature. The observed efficiency of 0.15, a minimum value, is close to the sticking probability of 0.35 observed at lower temperatures and, thus, appears to confirm this mechanism of atom formation on a hot filament, and the constancy of sticking probability.[15,16]

No data on hydrogen adsorption under ultra-high vacuum conditions on molybdenum filaments have been published, but data on the hydrogen-tungsten system obtained by field emission and flash-filament techniques are available for comparison.

Müller[17] and Gomer[18,19] observed virtually complete desorption of hydrogen at about 600° and 700°K, respectively; Müller also reported two-step adsorption at temperatures below 300°K. According to Becker,[20] most hydrogen is released below 575°K, but tempera-

[15a] This estimate is in good agreement with the data on nitrogen adsorption reported below.

[16] G. Ehrlich, J. Chem. Phys. **31**, 1111 (1959).

[17] E. W. Müller, Ergeb. exakt. Naturwiss. **27**, 290 (1953).

[18] R. Gomer and E. R. Wortman, J. Chem. Phys. **23**, 1741 (1955).

[19] R. Gomer, *Advances in Catalysis* VII (Academic Press, Inc., New York, 1955), p. 93.

[20] J. A. Becker (private communication). (Paper read at International Congress on Catalysis, Paris, 1960.)

tures as high as 1100°K are needed for its complete removal. Redhead[21] found a main hydrogen desorption peak at 550°K; a much smaller peak at 1050°K was composed of hydrogen and carbon monoxide.

These desorption temperatures are very close to those obtained for the hydrogen-molybdenum system. Eisinger,[22] however, found two desorption peaks at 1100° and 1800°K; their relative heights changed with adsorption time. Moreover, at 610°K the total equilibrium coverage was only about 30% lower than at 310°K. Two stages of adsorbed hydrogen were postulated, although the possibility of contamination effects was recognized. However, inspection of his curves shows that the rate of pump-out for the 1800°K peak is much lower than that for the 1100°K peak. Thus, desorption of a heavier molecular species at 1800°K is indicated. The apparently high desorption temperature of hydrogen, 1100°K, may reflect large end effects due to the short filament used.

Recently, Becker[20] has found a maximum sticking probability of 0.2 for hydrogen on loosely packed tungsten crystal planes, such as (411). He also found two hydrogen atoms adsorbed per tungsten atom at room temperature.

After the present experiments were completed, Hickmott[23] reported that the equilibrium amount of hydrogen chemisorbed on tungsten increased continuously with decreasing temperature from 373°K (the higher limit of his measurements) to a temperature somewhere between 194°K and 77°K where a temperature-insensitive coverage was attained. At 77°K a second layer of low coverage was formed and ascribed to molecular adsorption of hydrogen. Closer inspection of the published desorption curves reveals an additional discontinuity in their slopes, indicating the possibility of two-step atomic adsorption. Finally, Hickmott found a small increase of coverage with pressure of a magnitude which would fall within our limits of precision. For the observed high coverages, Langmuir's isotherm cannot be applied and the effect of pressure on coverage cannot be predicted. However, for constant coverage, temperatures may be thermodynamically related to pressure. If one assumes a molal heat of adsorption of 20 kcal for hydrogen, the effect of a hundred-fold pressure increase at 300°K would be canceled by a temperature increase of only about 40°.

INTERACTION OF NITROGEN WITH MOLYBDENUM

A limited flash-filament study of the nitrogen-molybdenum system was carried out, mainly for internal calibration. Adsorption and desorption of nitrogen were studied at the steady-state pressure of 2.5×10^{-8} mm Hg as functions of adsorption time and temperature. Only one desorption peak between 1300° and 1700°K was found. The initial pressure surge was followed by an exponential decrease from which the effective area of the exit hole was calculated; it agreed within 10% with the value calculated from its geometry.

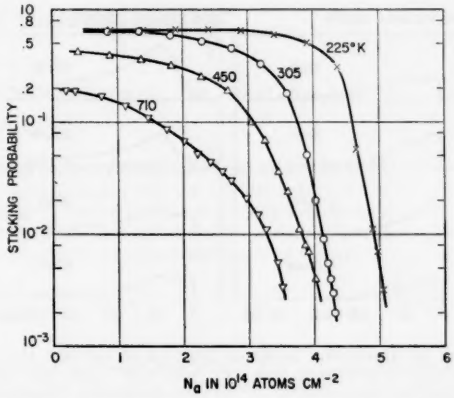

FIG. 9. Sticking probabilities of nitrogen vs surface coverages $p_0\simeq2.5\times10^{-8}$ mm Hg.

Sticking probabilities and surface coverages were determined both from flash-desorption curves, and from pressure-time curves during adsorption; the results agreed within 5%. In Fig. 9 the dependence of the sticking probability on the surface coverage and the adsorption temperature is shown. At 225°K, the sticking probability remained constant at 0.7 until about three-fourths of the maximum coverage. At higher adsorption temperatures, the sticking probability declined more rapidly with increasing coverage. The amount of nitrogen adsorbed at saturation decreased from 5.5×10^{14} atoms/cm² at 225°K to 4×10^{14} atoms/cm² at 710°K; this trend is less marked than with hydrogen. These numbers indicate that the ratio of nitrogen adatoms to surface Mo atoms is unity.

We find no indication for a low-temperature desorption peak equivalent to the α peak described by Ehrlich for the nitrogen-tungsten system.[3,24] Our sticking probabilities agree fairly well with those reported by Becker.[2,8] Finally, our ratio of nitrogen adatoms to surface molybdenum atoms agrees with Kisliuk's most recent data[25] which supercede Eisinger's higher value.[26]

PROBLEM OF CONTAMINATION

In previous flash-filament studies, contaminant gases have often introduced artifacts. Possible contaminants in such systems are carbon monoxide, hydrocarbons, nitrogen, oxygen, and water vapor. Interactions of these gases with tungsten surfaces have been studied,

[21] P. A. Redhead, paper read at 6th National Symposium on Vacuum Technology, Philadelphia (1959).
[22] J. Eisinger, J. Chem. Phys. **29**, 1154 (1958).
[23] T. W. Hickmott, J. Chem. Phys. **32**, 810 (1960).
[24] G. Ehrlich, J. Phys. Chem. **60**, 1388 (1956).
[25] P. Kisliuk (private communication).
[26] J. Eisinger, J. Chem. Phys. **28**, 165 (1958).

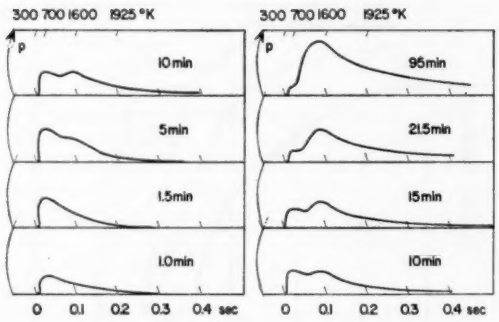

FIG. 10. Desorption curves as functions of exposure time to hydrogen contaminated with air. $p_0 \simeq 3 \times 10^{-8}$ mm Hg; flash-heating rate approximately 10 000°/sec; adsorption temperature 300°K. Hydrogen (peak at 500°K) is gradually replaced by contaminants (nitrogen peak at 1600°K; no oxygen peak).

and approximate desorption temperatures have been reported.[8,13,21] The similarity of tungsten and molybdenum with respect to hydrogen and nitrogen suggests that these data hold for the gas-molybdenum systems, too. Some experiments were carried out in the present study using hydrogen contaminated with air, and moist air, for obtaining information about the mechanism of simultaneous adsorption of two or more gases.

During our study of hydrogen, a small amount of air was admitted to the system. Even after pumping down the unit and passing pure hydrogen through it for many hours, complex desorption curves were still obtained. A series of desorption curves as a function of adsorption time is shown in Fig. 10. Two peaks were found: The first at about 500°K is attributed to hydrogen, the second at 1600°K to nitrogen. The height of the nitrogen peak increased continuously, whereas the hydrogen peak increased at first, but decreased again on longer adsorption times. However, the hydrogen peak did not completely disappear even after adsorption overnight. The following mechanism is indicated: Both gases are adsorbed competitively as long as the surface of the metal is only partly covered. When all sites are occupied, displacement of adsorbed hydrogen by nitrogen occurs. The final equilibrium might depend on the partial pressures of the gases, or on the existence of some sites which will hold hydrogen but not nitrogen atoms. The replacement of hydrogen by nitrogen is expected, because the heat of adsorption of nitrogen is much higher. The results suggest that hydrogen adsorbed on a molybdenum surface must have appreciable mobility even at room temperature.[27] A thorough flash-filament study of nitrogen-hydrogen-metal systems would be of considerable interest.

Double-peak desorption patterns showing a similar dependence on adsorption time as in the nitrogen-hydrogen-molybdenum system have also been reported for the nitrogen-tungsten,[3,24] and for the hydrogen-tungsten system.[22] However, they have been ascribed to different states of binding of the pure gases.

In the interaction of the molybdenum ribbon with moist air at a pressure of about 2.5×10^{-7} mm Hg, desorption curves consisting of two peaks at 500° and 1600°K again indicated the desorption of hydrogen and nitrogen. The height of the nitrogen peaks declined on each repetition of the experiment. Apparently, water decomposed, and oxygen was incompletely removed, even at the maximum flash temperature of 2000°K. Thus, on repetition, less free surface was available for the adsorption of water and nitrogen. Strong bonding of oxygen is also found for tungsten surfaces.[21]

In the present study of hydrogen and nitrogen sorption, no spurious peaks attributable to impurities appeared in any of the desorption experiments. A low level of contamination was also indicated by the good reproducibility of the hydrogen desorption curves; for fixed experimental conditions the height and shape of the desorption peak remained constant for two hours after saturation. However, on longer exposures the height gradually decreased—in two days by about 50%. No second pressure desorption peak appeared, but slow desorption of a contaminant was indicated by slow apparent pump-out of the unit on high-temperature flashing. Furthermore, the ribbon had to be heated to at least 1500°K in hydrogen for about 10 sec before the amount of hydrogen adsorbed at saturation approached the well-reproducible maximum value characteristic for a clean surface. The contaminants were very likely traces of oxygen or water from the walls rather than from the hydrogen gas, for the rate of contamination was not dependent on pressure.

ACKNOWLEDGMENTS

We are indebted to Norman Milleron of the Lawrence Radiation Laboratory, Livermore, for his valuable advice, and to E. M. Carr of our laboratory for his assistance in the earlier stages of the investigation. This research was greatly aided by discussions with Dr. A. P. Brady and Dr. A. G. Brown.

[27] R. Gomer, R. Wortman, and R. Lundy, J. Chem. Phys. **26**, 1147 (1957).

Binding Energies of Alkali Halide Molecules*

G. M. ROTHBERG†

Columbia Radiation Laboratory, Department of Physics, Columbia University, New York 27, New York

(Received July 28, 1959)

The repulsive part of the energy of interaction of an alkali ion and a halogen ion may be written $fe^{-z/r}$, where f and r are constants appropriate to the ions and z is the internuclear distance. In alkali halide crystals and monomers, f and r may be determined empirically, but in the case of the dimers the necessary data are lacking. In this paper the repulsive energy is examined qualitatively with use of the Thomas-Fermi model, and an approximation is found for the dimer constants that enables accurate calculations to be made of the binding energies of the dimers.

I. INTRODUCTION

THE cohesive energies of alkali halide crystals and the binding energies of the diatomic molecules can be accurately calculated with the use of a relatively simple model of the molecules which treats the binding as being completely ionic.[1–4] Calculations of the dissociation energies of the alkali halide dimers,[5,6] however, have been considerably less accurate, and it is the purpose of this paper to present a method for improving these calculations. A model that correctly predicts the energies may, of course, have considerable value in the calculation of other molecular properties.

The energies to be discussed are associated with the following reactions:

$$MX = M^+ + X^-; \tag{1}$$

$$M_2X_2 = 2M^+ + 2X^-; \tag{2}$$

$$M_2X_2 = 2MX. \tag{3}$$

M represents an alkali atom and X a halogen atom. The binding energies of the reactants relative to the products are, respectively, W_1, W_2 and $\Delta E = W_2 - 2W_1$. These energies are negative. The ΔE is the dissociation energy of the dimer. In the ionic model the binding energies are the sums of three parts, electrostatic, van der Waals, and repulsive. In this paper the electrostatic energy will include the dipolar polarization of the ions. The repulsive energy of all the ions in the dimer will be included, not only that of the unlike ions. It turns out that the van der Waals energy of a dimer and the repulsive energy due to the like ions are small and approximately cancel each other.

With the temperature set equal to 0°K and with the zero-point energy neglected, the binding energy W_1 is given by[4]

$$W_1 = -e^2/z - (\alpha_1+\alpha_2)e^2/2z^4 - l/z^6 - 2\alpha_1\alpha_2 e^2/z^7 + f\exp(-z/r), \tag{4}$$

where z is the internuclear distance, e is the electronic charge, α_1 and α_2 are the polarizabilities of the alkali and halogen ions, l is the van der Waals constant, and f and r are the repulsion constants.

The first result of the ionic model with respect to a dimer is that it is planar and has the general configuration shown in Fig. 1. If the ions were hard charged spheres, the most stable configuration would be the one shown. Making the ions soft and polarizable does not destroy the stability of the planar configuration. The binding energy W_2 is given by[5]

$$W_2 = -(4e^2/z) + (e^2/x) + (e^2/y) - \alpha_1[(x/z^3) - (1/x^2)]eF_1 - \alpha_2[(y/z^3) - (1/y^2)]eF_2 - (4l/z^6) - (m/x^6) - (n/y^6) + 4f\exp(-z/r) + g\exp(-x/q) + h\exp(-y/t). \tag{5}$$

The quantities x and y are the interalkali and interhalogen distances. The quantities m and n are the van der Waals constants for the plus-plus and minus-minus ion attractions, and the constants g and q and h and t characterize the plus-plus and minus-minus ion repulsions. F_1 and F_2 are the electric fields at the alkali ion and at the halogen ion. The electric field at an ion is the field that would exist at the position of the nucleus if the ion were removed from the molecule, all other charges being held fixed. From reference 5,

$$F_2 = B_2/C, \tag{6}$$

where

$$B_2 = [(y^3+2\alpha_2)(x^3-z^3)z^5 + \tfrac{3}{2}\alpha_2 x^3 y^2 (y^3-z^3)](x^5y^3z^8)^{-1}e, \tag{7}$$

and

$$C = [(x^3+2\alpha_1)(y^3+2\alpha_2)z^{10} - (\tfrac{9}{4})\alpha_1\alpha_2 x^5 y^5](x^3y^3z^{10})^{-1}. \tag{8}$$

The field F_1 is obtained from the same equations when x and y and α_1 and α_2 are interchanged.

* This research was supported in part by the United States Air Force, monitored by the AF Office of Scientific Research of the Air Research and Development Command.

† Present address: Department of Physics, Rutgers University, New Brunswick, New Jersey.

[1] M. Born and J. E. Mayer, Z. Physik **75**, 1 (1932).

[2] F. Seitz, *The Modern Theory of Solids* (McGraw-Hill Book Company, Inc., New York, 1940), Chap. II.

[3] M. Born and K. Huang, *Dynamical Theory of Crystal Lattices* (Oxford University Press, New York, 1954), Chap. I.

[4] E. S. Rittner, J. Chem. Phys. **19**, 1030 (1951).

[5] C. T. O'Konski and W. I. Higuchi, J. Chem. Phys. **23**, 1175 (1955).

[6] J. Berkowitz, J. Chem. Phys. **29**, 1386 (1958).

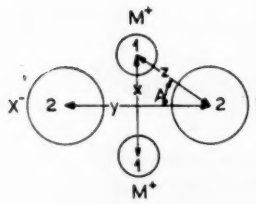

FIG. 1. Typical shape of a dimer. M^+ is an alkali ion and X^- is a halogen ion.

The electrostatic and van der Waals terms in Eqs. (4) and (5) are derived on the assumption of nonoverlapping of the electron clouds of the ions, and the polarizabilities and van der Waals constants are assumed to be those of the free ions. On the other hand, the source of the repulsive energy is precisely the overlapping of the electron clouds, and the repulsion constants are dependent upon the relative configuration of the ions in the molecule and are determined empirically from properties of the configuration of interest, as for example, internuclear distances and vibrational frequencies. In the cases of the alkali halide crystals and monomers, enough experimental data are available for all the repulsion constants to be determined. In the case of the dimers data are lacking, and one must, in effect, guess the constants in some systematic way. If the calculations turn out well, one may then hope that the procedure has some intrinsic merit. Previous investigators have guessed that the dimer and monomer constants were equal and have ignored the like-ion repulsions. In this paper the nature of the repulsive energy is considered and a better guess is made for the repulsion constants.

Pauling[7] and Milne and Cubicciotti[8] have a very different approach to the ionic model. They completely ignore the van der Waals energy and the polarization of the ions, and instead of an exponential form for the repulsion between two ions they use a term of the form K/z^n, where K and n are constants characteristic of the two ions and are the same for monomers and dimers. The calculations are immensely simplified in this way, and the resulting values for ΔE agree with the experimental values as closely as the ones obtained in this paper. The energies W_1 and W_2, however, are less accurate than the ones in this paper, and thus the good agreement for ΔE results from a cancellation of errors. Nevertheless, the simplicity of this method makes it useful.

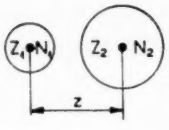

FIG. 2. Two interacting ions with rigid electron clouds. The atomic number is Z_i and the number of electrons is N_i.

[7] L. Pauling, Proc. Nat. Acad. Sci. (India) **25**, Sec. A, Part I (1956). Quoted in reference 8.
[8] T. A. Milne and D. Cubicciotti, J. Chem. Phys. **29**, 846 (1958).

II. INTERACTION OF M^+ AND X^-

In this section only the constants f and r for the unlike-ion repulsions will be discussed, since the like-ion repulsions are relatively unimportant. A particularly suitable description of the interaction energy is afforded by the Thomas-Fermi statistical model, since in this model the concept of electron clouds plays a direct role.[3,9] The statistical model will be used to obtain two results, namely (1) that when the equilibrium separation between the ions is reduced from its value in the crystal to its value in the monomer the constant f must assume a much larger value than in the crystal, but the constant r is approximately unchanged, and (2) that the polarization of the ions increases f by a factor roughly linear in the fields as shown by Eq. (12). These two results suggest a means for interpolating the dimer constants between those of the crystal and monomer, and this is pursued in the succeeding sections. It should be emphasized at the outset that the statistical model is used only to indicate the qualitative behavior of the repulsion constants and not to yield quantitative results.

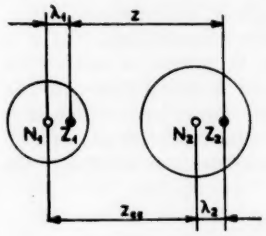

FIG. 3. Two interacting ions with deformable electron clouds. The nuclei are at ●, and the centers of the electron clouds are at ○. Ion 1 is the alkali and ion 2 is the halogen.

1. Rigid Ions

For the time being, ions with rigid charge distributions will be considered. In such ions the polarization and van der Waals energies vanish. Two interacting ions are shown schematically in Fig. 2. To a first approximation the electron density ρ of the system is just the sum of the densities of the free ions: $\rho=\rho_1+\rho_2$. The ions have been drawn with finite radii for clarity, but the Lenz-Jensen[9,10] density functions will be used for convenience in calculations, and these decrease exponentially at large distances. The interaction energy u relative to the free ions can be written $u=u_c+u_s$, where u_c is the electrostatic energy of the ions treated as point charges and u_s is the energy arising from the overlap. The overlap energy can in turn be written $u_s=u_e+u_n+u_k$. Small exchange and correlation effects have been neglected. Because of the overlap the electrons of each ion are less shielded from the nucleus of the other ion, and the electrostatic energy is reduced; this effect gives rise to u_e, which is therefore

[9] P. Gombás, *Die Statistische Theorie des Atoms und Ihre Anwendungen* (Springer-Verlag, Berlin, Germany, 1949).
[10] H. Jensen, Z. Physik **77**, 722 (1932).

negative. When the electron clouds overlap the nuclei, the shielding between the nuclei is reduced, and the electrostatic energy is increased; the energy u_n is therefore positive. It was a quantum-mechanical discussion of this effect that led Born and Mayer[1,11] to first propose the exponential form for the repulsive energy. The energy u_k is completely quantum mechanical in origin. In accordance with the Pauli principle no more than two electrons can occupy each h^3 of volume in electron phase space. When electron clouds overlap, the volume density is increased in the region of overlapping and there must be a compensating decrease in the momentum density. In other words the kinetic energy of the electrons must increase. Thus the term u_k is positive.

The separation of the interaction energy into u_c and u_s corresponds to the separation made in the ionic model, so u_s must correspond to the repulsive energy $f\exp(-z/r)$,

$$f=u_s(z)\,\exp(+z/r). \tag{9}$$

When the internuclear distance of the two ions is varied by a large amount, say from the equilibrium separation in the crystal to the equilibrium separation in the monomer, the variation of the repulsive energy cannot be described by a simple exponential. Hence f and r are not strictly independent of z as is assumed in the ionic model. For small variations in z about some value such as the equilibrium distance z_0, f and r may be considered constant but must then be evaluated at $z=z_0$. Thus,

$$f=u_s(z_0)\,\exp(+z_0/r). \tag{10}$$

For small variations in z if f is to be constant near z_0, $(df/dz)_{z_0}=0$. One can use Eq. (9) to find the value of r, assumed constant, that makes $(df/dz)_{z_0}=0$, and then f may be determined from Eq. (10).

This calculation was carried out for the typical case of K^+ and Cl^- with use of an approximation for u_s given by Gombás[9] that is good for internuclear distances greater than about four Bohr radii. For the KCl crystal $z_0=5.94$ Bohr radii and for the KCl monomer $z_0=5.05$ Bohr radii. In addition certain terms were dropped that contribute only about 5% to u_s. In view of the qualitative nature of the calculations it would be inappropriate to go into further details here; the results are in the case of the crystal

$$f=845\text{ ev}\quad\text{and}\quad r=0.468\text{ A},$$

and in the case of the monomer

$$f=1585\text{ ev}\quad\text{and}\quad r=0.427\text{ A}.$$

These results are, of course, quantitatively inaccurate, but the qualitative variation of f and r from crystal to monomer should be correct. The value of r decreases only by 10% from crystal to monomer, but f increases by almost 100%. The f and r for an internuclear distance appropriate to the dimer would be intermediate between the crystal and monomer values. It is clear from the strong dependence of f upon z_0 that a calculation of the binding energy W_2 with use of the monomer values for f and r cannot yield an accurate result.

These qualitative results are completely verified by the empirical values of the constants. The determination of the constants is described in Section IV. In all cases the monomer f is more than twice as large as the crystal f, while the average value of r for all the species differs only slightly from monomer to crystal.

2. Deformable Ions

The distortion of the electron clouds that gives rise to the polarization and van der Waals energies also affects the repulsive energy. The relatively small effect of the van der Waals energy will be ignored, and it will be assumed that the distortion of the charge distribution of each ion is merely a displacement of the center of the electron cloud so that it no longer coincides with the nucleus, the electron cloud retaining its spherical symmetry. Two interacting ions are shown schematically in Fig. 3, where ion 1 is the alkali and ion 2 is the halogen. The displacement of each electron cloud is λ_i, and the distance between the centers of the clouds is z_{ee}. A single ion placed in a uniform electric field and distorted as above has a change in energy relative to the field-free undistorted ion equal to the increase in Coulomb energy between the nucleus and the electron cloud plus the energy of interaction of the electron cloud and the nucleus with the external field. To second order in the field the change in energy is equal by definition to $-\frac{1}{2}\alpha F^2$, where α is the polarizability of the ion and F is the field. This relation defines the polarizability.

In the case of two interacting ions and no external field the interaction energy may be expanded to second order in F_i, the field at ion i in the sense used in Sec. I. In the limit of small displacements λ_i and large charge densities the interaction energy can again be written $u=u_c+u_s$, where now u_c is the electrostatic energy of a system of point charges and dipoles exactly as in the ionic model. The repulsive energy u_s is now approximately a function of z_{ee} instead of z and with the same functional form as for rigid ions. The analog of Eq. (9) becomes

$$f_e=u_s(z_{ee})\,\exp(+z_{ee}/r_e), \tag{11}$$

where f_e and r_e are the repulsions constants. The values of f_e and r_e are the same as the values of f and r determined at $z_0=z_{ee}$. Since r changes very little from the crystal z_0 to the monomer z_0, and since $z_{ee}=z+\lambda_1-\lambda_2\approx z$, then r_e may be set equal to r. Hence, in the form

[11] A. Unsöld, Z. Physik **43**, 563 (1927).

used in the ionic model,

$$u_s = f\exp(-z/r) = \{f_e \exp[+(\lambda_2-\lambda_1)/r]\}_{z_0} \times \exp(-z/r),$$

where the subscript z_0 indicates that f is to be considered a constant and evaluated at $z=z_0$. For sufficiently small λ_i

$$f \approx (f)_{z_0}(1+\lambda_2/r-\lambda_1/r)_{z_0},$$

where f_e has been replaced by $(f)_{z_0}$ given by Eq. (10). Since $\lambda_i=\alpha_i F_i/N_i e$,

$$f \approx (f)_{z_0}[1+(\alpha_2/N_2 e r)F_2-(\alpha_1/N_1 e r)F_1]. \quad (12)$$

When more than a single pair of ions are present, as in the dimer, the electric fields F_1 and F_2 acting on the ions of a particular pair are no longer parallel to the internuclear axis and neither are the displacements λ_1 and λ_2. For the repulsive energy only the components of the λ_i along the internuclear axis are important, and hence the fields in Eq. (12) should be replaced by their components along this axis.

This treatment of the effect of polarization is analogous to one given by Dick and Overhauser.[12] These authors calculated the interaction energy of two helium atoms by means of the Heitler-London method and showed that when the electron clouds were displaced as above the repulsive energy was of the form implied by Eq. (11). Because they used wave functions appropriate to the free atoms all kinetic energy terms disappeared from the interaction energy, and they attributed the entire repulsive energy to electrostatic interactions. However, when free atom wave functions are used the quantum-mechanical virial theorem is not satisfied and neither the potential energy nor the kinetic energy are individually correctly represented. In the case of undistorted ions they obtain an expression like $f\exp(-z/r)$, but the variation of f and r with internuclear separation is opposite to the one found here. If wave functions are used that satisfy the virial theorem, the increase of the effective nuclear charges of the atoms as the internuclear distance is decreased might result in the proper variation of f and r.

III. APPROXIMATIONS FOR f AND r IN THE DIMER

Three approximations for the dimer repulsion constants f and r will be examined in the rest of this paper. The first is simply the assumption that the dimer constants have the same value as in the monomer, and it will be shown that the energies ΔE calculated with use of this approximation are in poor agreement with experiment. The second approximation follows in a plausible way from the preceding discussion, and the third approximation is a simplification of this one; both will be shown to result in good agreement with experiment. The particular form of the second approximation was partially motivated by a desire to preserve the simplicity of the ionic model. Since the constant r does not depend strongly upon the internuclear distance of the ions, one value may be used in all calculations, for crystals and monomers as well as for dimers. In the next section it will be found convenient to use the average value $\bar{r}$ rather than the value r assumes in each molecule. The $\bar{r}$ to be used in all calculations is chosen to be the crystal one[1]

$$\bar{r}=0.345 \text{ A}. \quad (13)$$

The second approximation for f is based upon Eq. (12). The factor $(f)_{z_0}$ is a function of the internuclear distance and depends upon F_1 and F_2 through the effect of the fields in determining this distance; the larger the attractive fields the smaller the internuclear distance. It will be assumed that the large but unknown variation of $(f)_{z_0}$ with z_0 can be adequately described by taking $(f)_{z_0}$ to be linear in the fields. The terms in Eq. (12) within the square brackets, representing the effect of polarization, are also linear in the fields but tend to give more importance to F_2, for the factor α_2/N_2 is more than twice as large as α_1/N_1 when the Pauling[13] values for α_1 and α_2 are used; that is, the distortion of the halogen is larger than the distortion of the alkali. Therefore, only terms linear in F_2 will be retained, and since F_2 in the dimer makes an angle A with the internuclear axis as in Fig. 1, it is the component $F_2\cos A$ along the axis that is important. The resulting approximation for f is then

$$f=(f_0+ef'F_2\cos A)_{z_0}, \quad (14)$$

where f_0 is the empirical crystal value for f and f' is a constant to be determined from some property of the monomer; the subscript z_0 means f is to be evaluated for the ions at their equilibrium separation. This equation enables one to interpolate the dimer f between the crystal and monomer values. In the crystal $F_2=0$ and f equals the usual crystal constant f_0. In the monomer F_2 is just the field produced by a point charge and dipole located at the nucleus of the alkali ion. When the monomer f and z_0 are known, the constant f' may easily be calculated. In the dimer the equilibrium internuclear distances x_0 and y_0 are unknown, but f and the binding energy W_2 may be found by an iteration procedure discussed in the following section.

The third approximation for f is a simplification of Eq. (14), namely,

$$f=f_0+ef'F_2(x,y)\cos A(x,y). \quad (15)$$

This f is a function of the variables x and y instead of the constant equilibrium distances x_0 and y_0 and consequently no iterations need be made, which represents a considerable computational improvement over Eq. (14). Because of this the third approximation was

[12] B. G. Dick, Jr., and A. W. Overhauser, Phys. Rev. **112**, 90 (1958).

[13] L. Pauling, Proc. Roy. Soc. (London) **A114**, 191 (1927).

TABLE I. Primary constants.

	Substance	z_0[a] (A)	ω_e[a] (cm^{-1})	α_1[b] (A^3)	α_2[b] (A^3)	μ_A[c] (at. wt. units)	D_0[d] (ev)	I_1[e] (ev)	I_2[e] (ev)	E[f] (ev)	T[g] (°K)
Li	F	1.39[h]		0.029	1.05		5.95	5.40	75.7	3.62	1127
	Cl	1.96[h]			3.69		5.00			3.83	870
	Br	2.1704	480		4.81	6.3872	4.35			3.54	803
	I	2.3919	450		7.16	6.582	3.50			3.24	720
Na	F	1.98[h]		0.181			4.65	5.14	47.3		1170
	Cl	2.3606	380			13.9508	4.24				920
	Br	2.5020	315			17.8588	3.80				
	I	2.7115	286			19.4692	3.07				817
K	F	2.21[h]	405	0.84			5.00	4.34	31.7		1009
	Cl	2.6666	305			18.599	4.40				897
	Br	2.8207	230			26.260	3.94				
	I	3.0478	200			29.896	3.32				823
Rb	F	2.15[h,i]	390	1.42			5.35	4.17	27.3		951
	Cl	2.7868	270			25.068	4.50				866
	Br	2.9448	181			41.313	4.00				
	I	3.1769	147			51.089	3.35				
Cs	F	2.3453	385	2.44		16.6277	5.50	3.89	23.4		863
	Cl	2.9062	240			27.998	4.60				
	Br	3.0720	171			49.921	4.10				
	I	3.3150	120			64.935	3.40				

[a] See reference 15.
[b] See reference 13.
[c] G. H. Herzberg, *Molecular Spectra and Molecular Structure. I. Spectra of Diatomic Molecules* (D. van Nostrand Company, Inc., Princeton, New Jersey, 1950) 2nd ed.
[d] A. G. Gaydon, *Dissociation Energies and Spectra of Diatomic Molecules* (Chapman and Hall, Ltd., London England, 1953), 2nd ed.
[e] *Landolt-Bornstein Zahlenwerte und Funktionen*, edited by A. Euchen (Springer-Verlag, Berlin, Germany, 1950), Vol I, part 1, p. 211.
[f] H. O. Pritchard, Chem. Revs. **52**, 529 (1953).
[g] For sources see ΔE in Table III.
[h] Calculated in Sec. IV.
[i] Experimentally z_0=2.26554 A. See reference 17.

TABLE II. Secondary constants; van der Waals and repulsion constants.

							First approximation		Second and Third approximations Monomer		
	Substance	l (ev)	m (ev)	n (ev)	g (ev)	h (ev)	r (A)	f (ev)	f (ev)	f_0[a] (ev)	f'[b] (A)
Li	F	0.158	0.048	2.99	19.6	292				62	27
	Cl	0.585		39.1		2420				178	155
	Br	0.708		61.4		5000	0.397	1210	1120	255	280
	I	0.968		125		14600	0.410	2020	1840	437	553
Na	F	0.958	1.16		125					197	88
	Cl	3.55					0.320	1510	1390	567	305
	Br	4.30					0.333	2100	1910	814	459
	I	5.89					0.342	3500	3150	1390	872
K	F	4.30	16.8		751					483	124
	Cl	16.1					0.312	2880	2620	1390	541
	Br	19.3					0.342	4110	3690	2000	844
	I	26.5					0.357	7030	6280	3420	1690
Rb	F	7.15	41.3		1640				1120	715	61(357) Δ
	Cl	26.4					0.292	3890	3490	2060	656
	Br	32.1					0.336	5520	4940	2960	1030
	I	44.2					0.361	9560	8500	5060	2140
Cs	F	12.0	104		3590		0.285	1610	1480	1060	111
	Cl	44.4					0.309	5380	4820	3040	830
	Br	54.1					0.313	7780	6890	4380	1340
	I	74.6					0.386	13700	12000	7480	2910
					$q=l=0.345$ A		$\bar{r}=0.340\pm0.03$ A			$\bar{r}=0.345$ A	

[a] See reference 14
[b] The force eF_2 is in units of ev/A. Δ calculated with use of experimental value of z_0.

used to calculate the energies W_2 for all the species, whereas the second approximation was used only in three representative cases. It will be seen in Sec. IV that the W_2 values determined with the two approximations should agree within a few percent in all cases and both sets of values agree well with experiment. It should be pointed out that although Eq. (14) is based upon the original assumption of the ionic model that f is a constant and Eq. (15) is inconsistent with this assumption, until more is known about the dimers there is no physical reason for choosing one approximation over the other. In the calculation of the binding energies W_1, however, the use of approximation 3 would result in poor agreement with experiment.

IV. CALCULATION OF W_1, W_2, AND ΔE

The binding energies are given by Eqs. (4) and (5) and $\Delta E = W_2 - 2W_1$. Most of the calculations were performed in 1957 on the IBM 650 of the Watson Scientific Computing Laboratory at Columbia University. All primary and secondary constants needed for the calculations are given in Tables I and II, and the symbols will be explained in the course of the discussion.

1. Evaluation of Constants

The van der Waals constants are[2]

$$l = \tfrac{3}{2}\alpha_1\alpha_2 I_2 E/(I_2+E), \tag{16}$$

$$m = \tfrac{3}{4} I_2 \alpha_1^2, \tag{17}$$

and

$$n = \tfrac{3}{4} E \alpha_2^2, \tag{18}$$

where I_2 is the second ionization potential of the alkali atom and E is the electron affinity of the halogen atom. The dimer constants for the like-ion repulsions were taken to be the same as in the crystals.[14] Since the repulsive energy arising from the like ions is small, the variation in the constants from crystal to dimer may be neglected.

With use of approximation 1, two molecular properties of the monomers are required to determine f and r. For each of the 15 monomers whose equilibrium separations z_0 and vibrational frequencies ω_e were known[15] when these calculations were made, the repulsion constants were at first determined by requiring that

$$(dW_1/dz)_{z_0} = 0, \tag{19}$$

and

$$(d^2W_1/dz^2)_{z_0} = p. \tag{20}$$

The force constant p is related to the frequency by

$$p = 5.89\times 10^{-2}\mu_A\omega_e^2 \text{ d/cm}, \tag{21}$$

where ω_e is in cm^{-1} and μ_A is the reduced mass of the monomer in atomic weight units. The resulting values of r, shown in Table II under the heading First Approximation, are nearly constant, the mean value being $\bar{r} = 0.340 \pm 0.03$ A, where the plus-minus indicates the average deviation from the mean. With use of $\bar{r}$ and Eq. 19 the values of f were redetermined; it is these values which are given in Table II under First Approximation.

The use of a mean value of r to determine f does not lead to a significant departure of W_1 from the value that would be obtained if both f and r were found for each molecule. On the other hand, the averaging process allows calculations to be made of the energies W_1 for the five monomers with unknown separations, as is done later. Because the internuclear distances used in the present calculations are smaller than those used by Rittner,[4] the present values of f are considerably smaller than his and $\bar{r}$ is larger. More recent values for the vibrational frequencies[16] have been shown to yield an average r for only six monomers of 0.346 ± 0.01 A, in agreement with the value used here. The crystal $\bar{r}$ is 0.345 ± 0.02 A, which is essentially the same as the monomer value.

With use of approximations 2 and 3 only f' must be determined, and only one molecular property of the monomers is required. For the 15 monomers with known equilibrium separations the f were obtained as above and the f' were calculated from Eq. (14). The results are given in Table II under the heading Second and Third Approximations; the f do not differ much from the first approximation because the $\bar{r}$ are practically the same. The constant f' is in units of angstroms, since f is in ev and eF_2 is in ev/A. Also shown are the crystal values f_0. The monomer f is always considerably larger than f_0.

The five monomers whose internuclear distances were not known at the time these calculations were made are LiF, LiCl, NaF, KF, and RbF. The distance in RbF has since been measured,[17] and the calculation of f' has been repeated on a desk calculator with use of this measurement. For these five monomers, z_0 and f' were found by using Eqs. (4) and (19) and requiring that the calculated energy W_1 equal the experimental one; the results are in Tables I and II. It can be seen that RbF has a calculated internuclear distance smaller than that of KF, which is certainly incorrect and must result from poor experimental values for W_1. This will be discussed further in Sec. IV–3.

The determination of the dimer f from Eq. (14) is complicated by the fact that the equilibrium separations x_0 and y_0 are experimentally unknown. The W_2 must satisfy the relations

$$(\partial W_2/\partial x)_{x_0,y_0} = 0,$$

and

$$(\partial W_2/\partial y)_{x_0,y_0} = 0, \tag{22}$$

[14] M. L. Huggins and J. E. Mayer, J. Chem. Phys. **1**, 643 (1933).
[15] A. Honig, M. Mandel, M. L. Stitch, and C. H. Townes, Phys. Rev. **96**, 629 (1954).
[16] S. A. Rice and W. Klemperer, J. Chem. Phys. **27**, 573 (1957).
[17] H. Lew, F. E. Geiger, Jr., and J. T. Eisinger, Can. J. Phys. **36**, 171 (1958).

TABLE III. Binding energies W_1 and W_2 and dissociation energies ΔE.

	Substance	First approximation $-W_1$ (ev)	First approximation $-W_2$ (ev)	First approximation $-\Delta E$ (ev)	Third approximation $-W_1$ (ev)	Third approximation $-W_2$ (ev)	Third approximation $-\Delta E$ (ev)	Experimental $-W_1$(exp) (ev)	Experimental $-\Delta E$(exp)[a] (ev)	Experimental $-\Delta E(0)$[b] (ev)
Li	F					19.04	3.58	7.73	2.56	2.76
	Cl					15.65	2.51	6.57	2.21	2.36
	Br	6.18	14.00	1.62	6.15	14.66	2.36	6.21	2.00	2.14
	I	5.84	13.40	1.72	5.83	13.86	2.20	5.66	1.81	1.94
Na	F					15.17	2.83	6.17	2.36	2.57
	Cl	5.61	12.86	1.64	5.58	13.33	2.17	5.55	2.08	2.24
	Br	5.39	12.44	1.66	5.38	12.82	2.06	5.40		
	I	5.13	11.94	1.68	5.11	12.20	1.98	4.97	1.73	1.87
K	F					13.75	2.31	5.72	2.07	2.14
	Cl	5.05	11.66	1.56	5.03	12.01	1.95	4.91	1.81	1.97
	Br	4.84	11.25	1.56	4.83	11.53	1.87	4.74		
	I	4.60	10.75	1.56	4.58	10.95	1.79	4.42	1.59	1.73
Rb	F				5.65 Δ	13.60	1.79	5.91	1.82	1.98
	Cl	4.88	11.26	1.51	4.86	11.58	1.86	4.85	1.73	1.88
	Br	4.68	10.87	1.51	4.67	11.12	1.78	4.64		
	I	4.44	10.37	1.50	4.42	10.55	1.71	4.29		
Cs	F	5.60	12.61	1.40	5.59	13.02	1.84	5.77	1.64	1.79
	Cl	4.75	10.94	1.44	4.74	11.23	1.75	4.66		
	Br	4.54	10.83	1.44	4.53	10.77	1.71	4.45		
	I	4.29	(no calculation)		4.28	10.20	1.64	4.05		

[a] The sources for ΔE are: (1) all fluorides: M. Eisenstadt, G. M. Rothberg, and P. Kusch, J. Chem. Phys. **29,** 797 (1958); (2) NaCl: M. Eisenstadt, V. S. Rao, and G. M. Rothberg, *ibid.* **30,** 605 (1959); (3) LiI: L. Friedman, *ibid.* **23,** 477 (1955); (4) all others: S. H. Bauer, R. M. Diner, and R. F. Porter, *ibid.* **29,** 991 (1958). A re-analysis of data of R. C. Miller and P. Kusch, J. Chem. Phys. **25,** 860 (1956) and **27,** 981 (1957).

[b] Obtained by subtraction of $2kT$ from ΔE (exp.) Δ calculated with use of experimental value of z_0.

and one method of determining x_0, y_0, and f is to (1) guess at x_0 and y_0, (2) calculate f, (3) determine if this f allows Eqs. (22) to be satisfied, and (4) continue until Eqs. (22) are satisfied. This procedure constitutes approximation 2 and was applied only to LiF, NaCl, and CsF. Their results are representative of what may be expected in all cases, for the energies and internuclear distances are determined by the primary and secondary constants of Tables I and II, and in these three species the constants assume a wide range of

TABLE IV. Interalkali and interhalogen distances x_0 and y_0 in the dimers and apex angle $2A$ at the halogens.

	Substance	First approximation x_0 (A)	First approximation y_0 (A)	First approximation $2A$ (deg)	Third approximation x_0 (A)	Third approximation y_0 (A)	Third approximation $2A$ (deg)
Li	F				2.38	2.34	91.0
	Cl				2.75	3.51	76.2
	Br	2.53	4.20	62.2	2.95	3.85	75.0
	I	2.63	4.59	59.6	3.05	4.33	70.4
Na	F				3.23	2.77	98.8
	Cl	3.09	4.27	71.8	3.39	3.91	81.8
	Br	3.15	4.55	69.4	3.46	4.24	78.4
	I	3.23	4.95	66.2	3.54	4.71	73.8
K	F				3.65	3.13	98.8
	Cl	3.72	4.55	78.6	3.97	4.19	87.0
	Br	3.84	4.83	77.0	4.07	4.53	83.8
	I	3.93	5.29	73.2	4.17	5.03	79.4
Rb	F				3.67	3.23	97.2
	Cl	4.03	4.63	82.0	4.21	4.31	88.6
	Br	4.13	4.93	80.0	4.31	4.64	85.8
	I	4.23	5.39	76.2	4.45	5.15	81.6
Cs	F	4.03	3.53	97.6	4.06	3.25	102.6
	Cl	4.37	4.65	86.4	4.49	4.36	91.6
	Br	4.47	4.97	84.0	4.61	4.71	88.8
	I	(no calculation)			4.77	5.21	85.0

TABLE V. Results of second approximation for f. W_1 is the same as with the third approximation.

Substance	x_0 (A)	y_0 (A)	$2A$ (deg)	$-W_2$ (ev)	$-\Delta E$ (ev)
LiF	1.83	2.74	67	17.93	2.47
NaCl	2.99	4.21	71	13.19	2.03
CsF	3.96	3.35	100	13.01	1.83

values. When Eq. (15) is used to determine the dimer f no preliminary guess need be made for x_0 and y_0.

Although the second and third approximations have been discussed as if the dimer f were actually calculated, as a matter of fact, this was not done, since for the calculation of W_2 the f need not be determined explicitly. Only in the case of NaCl have the dimer values of f been explicitly calculated in all approximations, and these are, in order of approximation, (1) 1510 ev, (2) 1200 ev, and (3) 1060 ev.

2. Evaluation of Energies

The method of calculating W_1 is straightforward and requires no further comment. The calculation of W_2, x_0 and y_0 with use of the *first* and *third* approximations for f and r was accomplished by selecting the minimum value of W_2 for each dimer from a group of energies calculated by varying x and y in Eq. 5 in steps of 0.02 A over appropriate intervals. The energies are shown in Table III; x_0, y_0, and the angle $2A$ subtended at a halogen ion by the alkali ions are shown in Table IV. As far as only the mathematical procedure is concerned x_0 and y_0 are accurate to 0.01 A, the apex angle $2A$ is accurate to 0.5 deg, and the energies are accurate to 0.005 ev. The dissociation energies ΔE are also in Table III.

When the *second* approximation was used, W_2, x_0, and y_0 were calculated by means of the iteration procedure outlined above. This calculation was done on a desk calculator, and x_0 and y_0 are accurate to about 0.05 A, the angle $2A$ is accurate to about 2 deg, and W_2 is accurate to several hundredths of an ev. The results are given in Table V. The results for LiF, NaCl, and CsF may be generalized by comparison with the results of the *third* approximation. The larger the ions the closer are the results of the two approximations, because W_2 and f, given as a function of x and y by Eq. (15), become increasingly insensitive to variations in x and y. Hence, the values of x_0 and y_0 that satisfy Eqs. (22) with f a function of x_0 and y_0, as in approximation 2, become closer to the values of x_0 and y_0 that satisfy Eqs. (22) with f a function of x and y, as in approximation 3. In LiF the two approximations yield energies W_2 that differ by 6% of the value for approximation 3, and in NaCl and CsF the energies differ by less than 1%. The internuclear distances in LiF differ by about 20% of the values for approximation 3, and in NaCl and CsF the differences are about 10 and 2%, respectively. In all cases, then, the two approximations should yield values of W_2 within a few percent of each other, and the internuclear distances should differ by less than about 20%. The W_2 resulting from use of approximation 2 must always be more positive than the W_2 from approximation 3, for the former must be contained in the group of energies from which the latter was selected as minimum.

As an illustration of the magnitudes of the various energy terms which contribute to W_2, results of approximations 1 and 2 for the case of NaCl are given in Table VI. It can be seen that the repulsive energy of the like ions and the van der Waals energy are small and tend to cancel each other. The second approximation for f has resulted in $f=1200$ ev, to be compared with $f=1510$ ev for the first approximation. The reduction in f permits an increase in the electrostatic energy, although the repulsive energies in the two approximations are about the same. From Table III it can be seen that for a given alkali ion the binding energies W_1 and W_2 decrease in magnitude with increasing size of the halogen ion, and for a given halogen ion the binding energies decrease in magnitude with increasing size of the alkali. This variation results from the fact that the electrostatic attractions are principally responsible for the binding, and these attractions are smaller the further apart the ions are.

3. Comparison with Experiment

The experimental values of W_1 are given by

$$-W_1\,(\text{exp}) = D_0 + I_1 - E, \tag{23}$$

where D_0 is the energy of dissociation of the monomer into atoms at $T=0°$K, and I_1 is the first ionization potential of the alkali atom. The zero-point energy is included in W_1(exp) but not in the calculated energies; this extra energy is completely negligible for the present purposes. The experimental values are given in Table III, and the differences between the calculated and

TABLE VI. Energy terms contributing to the binding energy W_2 of the NaCl dimer. Calculated with the first and second approximations for f and r.

	First approximation (ev)	Second approximation (ev)
Electrostatic energy of point charges	−13.82	−14.07
Polarization energy	− 1.61	− 1.79
Van der Waals energy	− 0.05	− 0.06
Repulsive energy of like ions	+ 0.03	+ 0.03
Repulsive energy of unlike ions	+ 2.59	+ 2.70
Total binding energy W_2	−12.86	−13.19

TABLE VII. Differences between calculated and experimental energies. These differences are (calculated energy) − (experimental energy) in percent of calculated energy. For W_1 and δW_1 the second and third approximations are identical.

Substance	First approximation			Second approximation			Third approximation	
	$-\delta W_1$ (%)	$-\delta W_2$ (%)	$-\delta\Delta E$ (%)	$-\delta W_1$ (%)	$-\delta W_2$ (%)	$-\delta\Delta E$ (%)	$-\delta W_2$ (%)	$-\delta\Delta E$ (%)
Li F					−2	−12	4	23
Cl							1	6
Br	−1	−4	−32	−1			1	9
I	3	1	−13	3			4	12
Na F							2	9
Cl	1	−4	−37	1	−1	−10	0	−3
Br	0			0				
I	3	1	−11	3			3	6
K F							1	7
Cl	3	−1	−26	2			2	−1
Br	2			2				
I	4	2	−11	4			3	3
Rb F				−6			−1	−11
Cl	1	−3	−24	0			0	−1
Br	1			1				
I	3			3				
Cs F	−3	−6	−28	−3	−2	0	−2	0
Cl	2			2				
Br	2			2				
I	6			5				
Average	2	3	23	2			2	7

experimental values are given in Table VII in percent of the calculated value. Both the first and the second (or third) approximations give energies in good agreement with experiment, the worst cases being, respectively, CsI and RbF, where the differences are 6%. On the average the difference is only 2%.

The experimental W_1 for KF and RbF do not have the proper relative sizes, since the binding energy of KF should be the more negative. The experimental z_0 for RbF is given in Table I; it is larger than the calculated distance, which indicates that the present experimental W_1 for RbF is more negative than the true value. The f' calculated with use of the experimental z_0 is shown in Table II, and when this is used in the calculation of W_1, the calculated W_1 is more positive than the experimental one by about 6% of the calculated value.

Before comparing calculated and experimental values of W_2 and ΔE it is of interest to ask what kind of agreement may be expected between them. Calculated values of the cohesive energy of alkali halide crystals differ from the experimental values by less than about 1%,[2,3] and the calculated and experimental values of W_1 have an average difference of about 2% of the calculated value. The small difference in both crystals and monomers, despite their greatly different molecular structures, leads one to expect that the average difference between calculated and experimental values of W_2 might also be 2% if suitable constants are used in the interactions. Since the energies ΔE are given by $\Delta E = W_2 - 2W_1$, one should, in comparing the calculated and experimental values of ΔE, consider a difference of about 10% to be good agreement.

The experimental ΔE are in Table III. A correction must be made for the fact that zero-point energies were neglected in the calculations and the temperature was set equal to 0°K, whereas the experimental ΔE were obtained at the temperatures shown in Table I. The average thermal energy of a vibration through terms of first order in the frequency is just kT, and this *includes* the zero-point energy. The total thermal energy of a dimer is thus $9kT$, and the thermal energy of two monomers is $7kT$. One need only subtract $2kT$ from the experimental ΔE to reduce them to 0°K and no zero-point energy. These energies, $\Delta E(0)$, are given in Table III. The inaccuracy of this correction is much less than the experimental inaccuracy of ΔE. The experimental values listed in this table for W_2 are derived from $\Delta E(0)$ and $W_1(\text{exp})$ and include a negligible contribution from the zero-point energy of the monomer.

The differences between the calculated and experimental energies are given in Table VII in percent of the calculated value. With use of the *first* approximation the calculated ΔE are in poor agreement with experiment except in the cases of LiI, NaI, and RbI; the average difference is 23%. The *second* and *third* approximations produce a striking improvement in the dissociation energies. In the third approximation all the energies except LiF are in good agreement with experiment, the average difference being only 7%. In

the case of LiF the difference is 23%, and this is reduced to only 12% when the second approximation is used. The calculated and experimental values of W_2 agree on the average to 3% in the first approximation and 2% in the second and third approximations.

The relatively simple calculations of Milne and Cubicciotti discussed in Sec. I yield values of W_1, W_2, and ΔE with an average difference from experiment of 6, 4, and 6%, respectively.

In conclusion, the experimental evidence supports the present derivation of the repulsion constants for the dimers. The eventual experimental determination of the dimeric internuclear distances and vibrational frequencies will not only yield the correct repulsion constants, but also information about the dependence of the repulsive energy on the overlapping of the electron clouds.

ACKNOWLEDGMENTS

I wish to thank Professor P. Kusch for his encouragement and helpful suggestions and J. P. Auffray for programming the calculations for the IBM 650.

THE JOURNAL OF CHEMICAL PHYSICS VOLUME 34, NUMBER 6 JUNE, 1961

Line Shape of Ultraviolet Absorption in Solid Noble Gases

PAUL H. E. MEIJER

Catholic University of America and National Bureau of Standards, Washington, D. C.

(Received April 7, 1960)

The absorption of ultraviolet radiation in solid noble gases shows lines that are a few hundred inverse centimeters broad. An attempt is made to explain and calculate the width and shape of these lines on the basis of a tentative curve of energy versus configuration. It is shown that the width has the proper order of magnitude. The line shape can be easily calculated at the short wave length end. It should show an exponential tail. If we inspect the expression for small values of the energy, we find a rapidly rising exponential, which will give rise to a smeared-out edge appearance. The line will have a nonsymmetrical shape.

1. INTRODUCTION

OBSERVATIONS of vacuum ultraviolet absorption in solid xenon by Schnepp and Dressler[1] show strong and broad "lines" at 1405 A (67 340 cm^{-1}) and 1305 A (76 630 cm^{-1}). The widths are 500 cm^{-1} and 300 cm^{-1}, respectively. There are in addition two weaker absorption bands 1508 A (66 310 cm^{-1}, 200 cm^{-1} wide) and 1360 A (73 530, 500 cm^{-1} wide).

Similar absorptions were found by the same authors in krypton. They consisted of one strong band and one weak band. Nelson and Hartman[2] found two absorption peaks in argon with their far ultraviolet detection technique; part of their spectrum was, however, not confirmed by the first two authors.

The general conclusion is that we find in the neighborhood of the atomic resonance wavelength, a line which is broadened to a few hundred inverse centimeters. The displacement with respect to the atomic line has been calculated with the tight-binding approximation.[3] There is, however, an uncomfortable disagreement between experiments and calculations. Our main consideration is with respect to the linewidth or line shape instead of with this displacement of these lines.

Mulliken[4] has constructed a set of tentative potential curves of the xenon molecule. The main features of these curves are the following: The ground state is a practically flat curve, except for distances shorter than about 1 A, where repulsion becomes important. The excited states show pronounced minima at a similar distance. We assume an energy configuration diagram to hold for the solid, that is of similar shape, with the difference, of course, that it is symmetrical with respect to a point midway between two lattice sites. (See Fig. 1). The exact shape will of course depend on the direction. We assume (in our estimates below) the center at 3.3 A nuclear separation,[5] which corresponds to the average distance in these facecentered cubic lattices. (All noble gases condense in this system with the exception of helium which we do not consider.)

In order to have an idea about the amplitude of the zero-point vibrations we estimate the force constant. Both from the shape of the argon potential curves as well as from the constants in the Lennard-Jones potential we find that $K=2V/x^2$ is between 10^3 and 10^4 d/cm. The half-width of the Gaussian wave function, using the mass of a xenon atom is 0.08 A. Although

[1] O. Schnepp and K. Dressler, J. Chem. Phys. **33**, 49 (1960).
[2] J. R. Nelson and P. L. Hartman, Bull. Am. Phys. Soc. **4**, 371 (1959).
[3] R. S. Knox, J. Phys. Chem. Solids **9**, 238, 265 (1959).
[4] Mullikin (unpublished data).
[5] E. R. Dobbs and G. O. Jones. Repts. Progr. in Phys. **19**, 516 (1956). (This is the $T=0$ value extrapolated from higher temperatures.)

the well is very shallow, the large mass causes the amplitude of the zero-point vibrations to be very small. Higher states are not excited since the distance between the vibration energy levels is about 4.10^{-3} ev or 40°K. The experiment of Schnepp and Dressler was conducted at much lower temperatures (4.2°K).

What will take place in a localized excitation is easy to see. The potential curve for the excited atom is unstable, and lattide vibrations will be "emitted" to the surrounding atoms. The excited atom may go off center and sink gradually into one of the surrounding potential wells. This would lead to a local distortion. We do not think, however, that this picture is correct and will discuss this point in a separate paper.

Before we consider the alternative nonlocalized description, we will consider the dipole transition matrix element of the configuration coordinate. From its energy dependence we can obtain an expression for the line shape.

2. MATRIX ELEMENTS DUE TO NUCLEAR MOTION

In order to calculate the part of the transition matrix element which is due to the motion of the nuclei, one has to make assumptions about the potential curve in a certain direction. After the calculation, an averaging over all directions has to be performed. Since the potential curves are poorly known, and actually apply to a diatomic molecule instead of a lattice, we will refrain from doing such an averaging and restrict ourselves to a given direction.

The characteristic feature of the lower potential curve is a very shallow parabola which is due to the van der Waals binding. This would suggest that the nuclear wave function is spread out, but due to the large atomic mass this is not the case. As a matter of fact, it is well known that only in helium do the zero-point vibrations have detectable effects.

The upper potential curves all have the same feature. They have a slightly convex plateau in the middle and two valleys at each side. Compare Fig. 7 in Schnepp and Dressler.[1] There is no convenient way of indicating the energy levels in closed form and hence we will make some crude approximations. The main point of interest is to explain the width of the observed "line." Since transitions can take place in principle to any "vibrational" level in the upper potential curve, the question arises, which matrix element gives the largest contribution. Or, to formulate it differently; if we consider increasing values of energy from what value on do the matrix elements become negligibly small? The wave functions of the energy levels within the potential curves are of oscillatory character in the middle. If this wavelength becomes smaller than the width of the zero-point wave function of the lower state, the integral will approximately average out. (The wave functions of odd parity will always give a zero result.)

If we assume that for energy levels far enough above the potential energy maximum the wave function

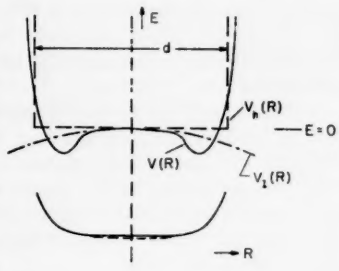

FIG. 1. $V(R)$ indicates the potential curve of the upper or excited state as a function of the configuration coordinate R. V_l is the approximation used for the low-energy side of the line, V_h the approximation for the high side. The dotted line in the lower curve is from the dipole-dipole effect and is strongly exaggerated.

behaves like a "box" wave function, which has the energy eigenvalues

$$E=(\pi\hbar n)^2/2md^2,$$

the condition mentioned above becomes

$$2d/n_1=\delta,$$

where δ is the width of the wave function in the lower electronic level

$$\delta=(2/\pi)^{\frac{1}{2}}\alpha^{-1}=(2/\pi)^{\frac{1}{2}}(\hbar^2/mK)^{\frac{1}{4}},$$

and K the force constant of that level. The corresponding energy E_1 for which the wavelength becomes comparable with the width δ is

$$E_1=(\pi^3\hbar/m)(mK)^{\frac{1}{2}}. \quad (1)$$

If we take $K=0.16$ ev/A^2 by using the data of Mulliken[4] for xenon and $m=2.2\ 10^{-22}$ g (the mass of krypton) we find that the order of magnitude for E is 100 cm^{-1}. Since this proves only that the above explanation for the linewidth is at least not excluded, we need a more accurate expression for the line shape in order to confirm this picture.

3. LINE SHAPE

The value of the matrix element as a function of E depends mainly on the wave function in the very small region of length δ around the center. The only way to determine the wave function in this region for the actual potential is to solve the Schrödinger equation.

For the high-energy side of the line, one can use the box potential V_h as a reasonable approximation. The two normalized wave functions are

$$\phi=[\alpha/(\pi)^{\frac{1}{4}}]^{\frac{1}{2}}\exp(-\tfrac{1}{2}\alpha^2x^2) \quad (2)$$

for the lower state, and

$$\psi=(2/d)^{\frac{1}{2}}\cos(n\pi/d)x=(2/d)^{\frac{1}{2}}\cos(2mE/\hbar^2)^{\frac{1}{2}}x \quad (3)$$

for the upper state; hence the transition matrix element is

$$m=\int\phi\psi d\tau=[2\alpha/d(\pi)^{\frac{1}{2}}]^{\frac{1}{2}}\int_{-\infty}^{\infty}\cos[\hbar^{-1}(2mE)^{\frac{1}{2}}x]$$

$$\times\exp(-\tfrac{1}{2}\alpha^2x^2)dx=[(\pi)^{\frac{1}{2}}/\alpha d]^{\frac{1}{2}}\exp(-mE/\alpha^2\hbar^2), \quad (4)$$

which gives a transition probability which goes to zero as an exponential function of E. The limits of the integral have been taken from $-\infty$ to $+\infty$, since the exponential wave function (2) becomes very small outside the box.

For low-energy values we will approximate the potential by an inverted parabola and calculate the wave function with the W.K.B. method. Ordinary perturbation theory, starting with a square well potential, and perturbing it with the two valleys, it excluded since the depth of the valley is considerably larger than the separation of the levels.

The wave number as a function of the distance is, according to the W.K.B. method

$$k=\hbar^{-1}\{2m(E+\tfrac{1}{2}K'x^2)\}^{\frac{1}{2}}, \tag{5}$$

where K' is the proportionality constant in $V_l=-\frac{1}{2}K'x^2$. For low-energy values this is, approximately,

$$k=\hbar^{-1}(mK')^{\frac{1}{2}}|x|(1+E/K'x^2). \tag{6}$$

The wave function is proportional to

$$\chi=N\exp[i\hbar^{-1}(mK')^{\frac{1}{2}}\{\tfrac{1}{2}\epsilon x^2+(E/K')\ln|x|\}], \tag{7}$$

where $\epsilon=|x|/x$.

The resulting integral is of the type[6] (γ, α, and β are constants),

$$\int_0^\infty \exp(-\gamma x^2)\exp[i(\kappa x^2+\beta\lg x)]dx$$
$$=\tfrac{1}{2}(\gamma-i\kappa)^{-\frac{1}{2}(1+i\beta)}\Gamma[(i\beta/2)+\tfrac{1}{2}]. \tag{8}$$

The imaginary part is of no interest since this part of the integrand is of odd parity and will cancel on the total domain ($-\infty$ to ∞) of the integration. In order to determine the line shape for small E, we study this expression for small β. The Γ function has no poles or other irregularities around the value $\frac{1}{2}$. Hence, for small β it can be replaced by a Taylor series around this point.[7] The β dependence of this integral will be dominated by the factor in front of the gamma function. By evaluating the real part, we find the behavior proportional to $\exp[\frac{1}{2}\beta\tan^{-1}(\alpha/\gamma)]$. From our estimates $\alpha\approx\gamma$; hence the order of magnitude of the constant in front of the energy is: $\hbar^{-1}(m/K')^{\frac{1}{2}}$ since by comparing (7) with (8) $\beta=\hbar^{-1}(mK')^{\frac{1}{2}}E/K'$. This implies a very steep behavior since K' is very small. We want to mention again that this is only an estimate. Since it is impossible to normalize the W.K.B. wave function, the energy dependence of the normalization constant cannot be determined, unless one takes the complete contour of the potential into account. The normalization constant is a function of E, hence our result holds only if the normalization factor is more or less constant in the neighborhood of $E=0$ and in particular it should not undergo a sharp decline. It can be shown from the square well model that, if the wells are sufficiently deep the normalization factor is nearly constant in the neighborhood of $E=0$ (see Appendix). This result becomes independent of the depth and also of the over-all width of the potential contour for sufficiently large depth. Hence we can conclude that if we modify the potential into a more realistic curve, the above statement will remain valid. It turns out that the function $N=N(E)$ for $E\gg0$ is increasing for the square well potential model.

The general conclusion of this section is that for a potential of the type sketched by Schnepp and Dressler the line shape will be such that the low-energy side is a smoothed-out edge, while the high-energy side has an exponential decay with a factor indicated in Eq. (4).

4. EXCITON THEORY

So far the picture we considered was essentially three atoms on a line in which the middle one was excited. We want to incorporate this in an infinite crystal. The general theory has been given by Davydov[9] and goes back to theories by Frenkel and Peierls. We will refer to the paper of the first author and describe what changes have to be made to include the nuclear motion. We will refer to the corresponding coordinate as the configuration coordinate.

In the adiabatic approximation, the total wave function is assumed to be a product of nuclear and electronic coordinates. There is little doubt that this approximation holds in this case. To illustrate this point we use a criterion formulated by Herring[10]

$$(\hbar\omega/\Delta E)(\Delta X/\Delta X')\ll1,$$

where $\hbar\omega$ refers to the lattice vibrations, ΔE to the electron transition, ΔX to the amplitude of the lattice vibrations and $\Delta X'$ to the configuration displacement required to give a large change in the electronic wave function. Not only is the first factor small, of the order of magnitude of 10^{-3}, as estimated before, but the second factor makes it probably still smaller, since the relatively flat potential curves would seem to indicate that the wave functions do not overlap substantially even when brought a few angstroms closer together.

The electronic transition probability still depends

[6] The argument of the logarithm is not dimensionless; this is usually taken care of by the limits of the integral. Since we want to study the behavior of the wave function in the neighborhood of $E=0$, we assume the additional term to be incorporated in the normalization factor.

[7] A better approximation is given in the tables by Jahnke and Emde.[8] The formula shows that, inside a convergence circle of radius one around the origin, the function is roughly proportional to $\exp(i\beta)$.

[8] E. Jahnke and F. Emde, *Tables of Functions* (Dover Publications, New York, 1945).

[9] A. S. Davydov, J. Exptl. Theoret. Phys. (U.S.S.R.) **18**, 210 1958. Translation by M. Kasha, Dept. of Chemistry, University of California, Berkeley, February, 1949, distributed under contract N6-ori-211, T.O. 3, by the Office of Naval Research.

[10] C. Herring, *Photo Conductivity Conference* (John Wiley & Sons, Inc., New York, 1956), p. 81.

[11] D. L. Dexter, Solid State **6**, 353 (1958).

parametrically on the position of the nuclei, a fact which we will also neglect (Condon approximation).[11] The considerations are restricted to absorption only, i.e., we take the value of the configuration coordinate that corresponds to the equilibrium situation of the *lower* potential curve.

Since the nuclear wave functions of the excited states belong to a different set of functions, the calculation of the matrix element M_{nm} of the secular equation (reference 7, Eq. 8) will now contain an integral over the volume element of configuration volume element $d\tau_c$ as well as over the electron coordinates $d\tau_e$:

$$M_{nm}=\int[\eta_m^*(E)\xi_n^*(0)\varphi_m'(\mathrm{I})\varphi_n(\mathrm{II})V_{nm}\xi_m(0)\eta_n(E)\varphi_m(\mathrm{I})\varphi_n'(\mathrm{II})$$
$$-\eta_m^*(E)\xi_n^*(0)\varphi_m'(\mathrm{I})\varphi_n(\mathrm{II})V_{nm}\xi_m(0)\eta_n(E)\varphi_m(\mathrm{II})\varphi_n'(\mathrm{I})]d\tau_e d\tau_e, \quad (9)$$

where φ_n represents the electronic wave function around the nth site in the ground state, φ' the same but for the excited level. The nuclear wave function ξ is an eigenfunction of the potential curve of the bottom level. The quantum number is zero, the argument (not shown) is the configuration coordinate and n refers again to the lattice site. A similar but different set of wave functions for the excited state is indicated by η. The almost continuous quantum number is E, the energy measured from the value of the excited state at the (metastable) equilibrium distance.

Since the overlap of the nuclear wave functions is negligible compared to the electron overlap which is already neglected, the only contribution of the configuration space integral is due to the nuclear wave functions at the same site. This integral can be factored out, and we have

$$M_{nm}=|m|^2M'_{nm}; \qquad m(E)=\int\eta^*(E)\xi(0)d\tau_e, \quad (10)$$

where M'_{nm} represents the integral over the electronic coordinates. The integral for the diagonal element in the secular equation can be evaluated in the same way. Since this integrand contains factors like

$$\eta_m^*(E)\eta_m(E)\xi_n^*(0)\xi_n(0),$$

the net result is a factor 1 in front of the electronic integral.

The complete secular equation is now

$$\sum_n a_n m^2(E)M_{mn}-(E+\epsilon)a_m=0, \quad (11)$$

where a_n is the amplitude of the state in which the excitation is at site n and M_{nm} the electronic (exchange) matrix element. $E+\epsilon$ is the total energy, and E the energy above the plateau of the upper configuration state. Since $E\ll\epsilon$, we can disregard E in the second term and the equation can be solved in the normal way, taking E as a parameter. The difference is that instead of a band made up of levels we will now have a band made up of bands. The latter are much narrower than the exciton bandwidth, hence the picture is basically the same. The transition takes place mainly to the $k=0$ state of the exciton band, but the transition probability is weighed by the factor m, which gives rise to the line shape as described in the previous section.

ACKNOWLEDGMENTS

The author wishes to acknowledge many very stimulating discussions with Dr. O. Schnepp who also read the manuscript and offered valuable suggestions. I wish to thank Dr. R. S. Mulliken for permission to use his unpublished results on the potential curves of diatomic xenon.

APPENDIX. SQUARE WELL MODEL

In order to investigate the behavior of the matrix element m as a function of E around $E=0$ we calculate this function for a square well potential

$$V=0 \quad \text{if} \quad -a<x<a; \qquad V=-V_0 \quad \text{if} \quad -b<x<-a$$

and

$$a<x<b; \qquad V=\infty \quad \text{if} \quad x<-b \quad \text{and} \quad x>b.$$

The general form of a wave function of even parity is

$$\psi_1=A[\exp(-\beta x)+\exp(\beta x)] \quad \text{if} \quad -a<x<a. \quad (\mathrm{A1a})$$

$$\psi_2=B\exp(i\gamma x)+C\exp(-i\gamma x) \quad \text{if} \quad |a|<|x|<|b|. \quad (\mathrm{A1b})$$

The coefficient $\beta=(-2mE/\hbar^2)^{\frac{1}{2}}$ is either positive real ($E>0$) or pure imaginary ($E<0$). The coefficient $\gamma=[2m(V_0+E)/\hbar^2]^{\frac{1}{2}}$ is always positive real in the region in which we are interested.

The boundary conditions at $\pm b$ and the matching conditions at $\pm a$ lead to the equation

$$\beta^{-1}(\cosh\beta a/\sinh\beta a)$$
$$=-\gamma^{-1}\{[\sin\gamma(b-a)]/[\cos\gamma(b-a)]\}, \quad (\mathrm{A2})$$

which determines the eigenvalues. Due to the relatively heavy mass of the atoms the eigenvalues lie rather dense and in order to obtain the E dependence of the total expression we have first of all to know the density function.

The condition that $E\gg -Vo$ is certainly fulfilled near $E\sim 0$ as long as the two wells are sufficiently deep. Hence γ is large and the right-hand side of (A2)

is practically zero for

$$[(h-\tfrac{1}{2})\pi]/(b-a)<\gamma<[(h+\tfrac{1}{2})\pi]/(b-a)$$

$$h=0, 1, 2\cdots.$$

If, however, $\gamma\approx(h+\frac{1}{2})\pi(b-a)^{-1}$ the right-hand side has a sharp peak and behaves like the derivative of a delta function. The roots in the neighborhood of $E=0$ are approximately given by

$$\gamma=(h+\tfrac{1}{2})\pi/(b-a) \qquad \text{(A3)}$$

and hence the density of states is constant.

The normalization constant can be expressed in terms of A, B, and C

$$1=2\left[\int_0^a \psi_1^2(x)dx+\int_a^b \psi_2^2(x)dx\right].$$

Two constants can be eliminated using the boundary and matching conditions and after some manipulation we find

$$(2A^2)^{-1}=(\sinh 2\beta a/\beta)[1-(\beta^2/\gamma^2)]$$

$$\times-2(\beta/\gamma)\{\sinh 2\beta a/[\sin 2\gamma(b-a)]\}(b-a)+2a. \qquad \text{(A4)}$$

If β is large positive the positive exponential in the sinh will dominate everything and hence A will tend to zero. If β is pure imaginary the expression is, neglecting terms that contain γ in the denominator,

$$(2A^2)^{-1}\approx 2a([\sin(2\beta a)/2\beta a]+1), \qquad \text{(A4a)}$$

which means a sharp rise in A as a function of E.

The behavior of $A=A(E)$ is sufficient for our purpose since the integral is

$$(\psi\phi)\propto\int\exp(-\alpha^2x^2)2A\cos\beta x dx\approx A\alpha^{-1}.$$

The first conclusion from (A4) is that in both cases $(E>0)$ and $(E<0)$ the function ϕ considered as a function of β is even, hence has a slope which is practically zero in the origin. The other conclusion from the example is that already for a flat potential curve the transition matrix element is "in the large" an increasing function of E. In this case the matrix element is proportional to the normalization constant. Hence if we introduce a convex potential the result obtained by the W.K.B. method will be enhanced by the previously established behavior of the normalization constant.

THE JOURNAL OF CHEMICAL PHYSICS VOLUME 34, NUMBER 6 JUNE, 1961

Heat Capacity of Thulium from 15° to 360°K*

L. D. JENNINGS,† EMMA HILL, AND F. H. SPEDDING

Institute for Atomic Research and Department of Chemistry, Iowa State University, Ames, Iowa

(Received September 12, 1960)

Thulium shows a lambda anomaly in its heat capacity near 55°K which is associated with magnetic ordering and which shows thermal hysteresis. In addition, there are anomalous changes in the slope of the heat capacity curve near 88°, 162°, and 180°K. These changes and the unexpectedly low value of the slope near room temperature complicate the analysis of the data, but there is evidence that the effective exchange integral in thulium is appreciably larger than that for neighboring rare earths. The results in the temperature range from 14° to 21°K support a T^3 dependence of the magnetic specific heat as predicted by spin wave theory for an antiferromagnet. The thermodynamic functions are tabulated for the temperature range studied.

INTRODUCTION

THE group of rare-earth metals with 7 to 14 4*f* electrons (except Yb which is divalent) form a particularly interesting series for they are all hexagonal close packed with approximately the same axial ratio. They thus do not present the problem of a variety of crystal structures which is typical of the light rare earths. This report, in addition to one on lutetium,[1] concludes the initial investigation of the heat capacity, from 15°K to room temperature, of the trivalent rare-earth metals.

Thulium, in addition to having unusual thermal properties which are discussed below, has electrical[2] and magnetic[3–5] properties which are out of the ordinary. Unfortunately, the results are not yet complete, but the magnetic moment vs temperature curves show a maximum near 12°K as well as one near 55°K. It appears that with moderate applied fields the metal is

* Contribution No. 931. Work was performed in the Ames Laboratory of the U. S. Atomic Energy Commission.

† Present address: Ordnance Materials Research Office, Watertown, Massachusetts.

[1] L. D. Jennings, R. E. Miller, and F. H. Spedding, J. Chem. Phys. **33**, 1849 (1960).

[2] R. V. Colvin, S. Legvold, and F. H. Spedding, Phys. Rev. **120**, 741 (1960).

[3] B. L. Rhodes, S. Legvold, and F. H. Spedding, Phys. Rev. **109**, 1547 (1958).

[4] D. D. Davis and R. M. Bozorth, Phys. Rev. **118**, 1543 (1960).

[5] W. E. Henry, J. Appl. Phys. Suppl. **31**, 3235 (1960).

TABLE I. The thermodynamic functions of thulium, joule/g atom-deg. Atomic weight of thulium=168.94; 273.15°K=0°C.

T, °K	C_p	$S°$	$(H°-H_0°)/T$	$-(F°-H_0°)/T$	T, °K	C_p	$S°$	$(H°-H_0°)/T$	$-(F°-H_0°)/T$
2[a]	0.02	0.010	0.007	0.003	95	25.18	42.794	21.443	21.351
4[a]	0.08	0.041	0.028	0.013	100	25.25	44.087	21.631	22.456
6[a]	0.22	0.097	0.066	0.031	110	25.40	46.501	21.967	24.534
8[a]	0.57	0.201	0.142	0.059	120	25.55	48.718	22.260	26.458
10[a]	1.09	0.362	0.260	0.102	130	25.69	50.768	22.518	28.250
12[a]	2.04	0.640	0.474	0.166	140	25.80	52.674	22.748	29.926
14	3.47	1.055	0.792	0.263	150	25.91	54.456	22.956	31.500
16	5.37	1.638	1.242	0.396	155	25.96	55.307	23.052	32.255
18	7.56	2.395	1.819	0.576	160	26.02	56.131	23.143	32.988
20	9.97	3.317	2.514	0.803	165	26.10	56.933	23.231	33.702
25	16.25	6.213	4.629	1.584	170	26.21	57.714	23.317	34.397
30	22.06	9.705	7.061	2.644	175	26.31	58.475	23.402	35.073
35	27.12	13.498	9.573	3.925	180	26.39	59.217	23.483	35.734
40	31.56	17.419	12.051	5.368	185	26.44	59.942	23.563	36.379
45	35.14	21.351	14.424	6.927	190	26.47	60.647	23.639	37.008
50	38.16	25.213	16.651	8.562	195	26.49	61.335	23.712	37.623
51	38.73	25.974	17.078	8.896	200	26.52	62.006	23.782	38.224
52	39.29	26.732	17.499	9.233	210	26.56	63.300	23.913	39.387
53	39.83	27.486	17.916	9.570	220	26.61	64.536	24.034	40.502
54	40.35	28.235	18.327	9.908	230	26.65	65.720	24.147	41.573
54.5	40.58	28.608	18.530	10.078	240	26.70	66.855	24.253	42.602
55	40.60	28.979	18.730	10.249	250	26.75	67.947	24.352	43.595
55.5	39.91	29.333	18.924	10.409	260	26.81	68.997	24.445	44.552
56	35.51	29.689	19.099	10.590	270	26.86	70.010	24.534	45.476
56.5	27.93	29.971	19.211	10.760	273.15	26.88	70.321	24.561	45.760
57	24.91	30.196	19.266	10.930	280	26.92	70.988	24.618	46.370
58	24.30	30.622	19.357	11.265	290	26.97	71.933	24.698	47.235
59	24.23	31.037	19.440	11.597	298.15	27.02	72.682	24.761	47.921
60	24.22	31.444	19.520	11.924	300	27.03	72.849	24.775	48.074
65	24.35	33.387	19.885	13.502	310	27.08	73.737	24.849	48.888
70	24.51	35.196	20.209	14.987	320	27.13	74.598	24.919	49.679
75	24.67	36.892	20.501	16.391	330	27.19	75.434	24.987	50.447
80	24.83	38.490	20.767	17.723	340	27.24	76.247	25.053	51.194
85	25.02	40.001	21.011	18.990	350	27.31	77.037	25.116	51.921
90	25.12	41.434	21.237	20.197	360	27.37	77.806	25.178	52.628

[a] Extrapolated value.

antiferromagnetic between these temperatures and ferromagnetic at lower temperatures. Davis and Bozorth[4] extrapolate their magnetization curves to zero applied field and estimate that the ferromagnetic Curie temperature is 22°K. This anomaly does not show, however, in the resistivity results.

The heat capacity results are sufficiently anomalous that we are not able to separate the magnetic contribution in a clear-cut way. The results are not, however, inconsistent with the point of view that the entropy of ordering is $R\ln(2J+1)$, where J is the angular momentum quantum number given by Hund's rule for the tripositive ion. The estimated energy of ordering, on the other hand, is unexpectedly high.

EXPERIMENTAL

The adiabatic calorimeter used was the same as that previously used for other rare earths.[6] The sample container has also been described in detail.[6] Thulium was prepared by reducing the oxide of the metal with lanthanum under vacuum and collecting it in a tantalum crucible. The procedure is identical to that used to prepare samarium.[7] The metal was then cast in two parts and machined to fit into the sample container. The sample contained 439.92 g, and the atomic weight of thulium was taken as 168.94. Spectrographic analysis showed all the rare earths other than thulium to be present to less than 0.02%. This value was the upper limit of detection by the spectrographic method used to analyze the block. Magnesium was less than 0.01% and iron varied from 0.02% to 0.005%, depending on the position of the block analyzed. Since the distilled thulium was remelted in tantalum, it picked up an appreciable amount of tantalum from the crucible. This amount was determined to be 0.4% by weight. This amount of impurity is barely sufficient to give rise to

[6] L. D. Jennings, R. M. Stanton, and F. H. Spedding, J. Chem. Phys. **27**, 909 (1957).

[7] L. D. Jennings, E. D. Hill, and F. H. Spedding, J. Chem. Phys. **31**, 1240 (1959).

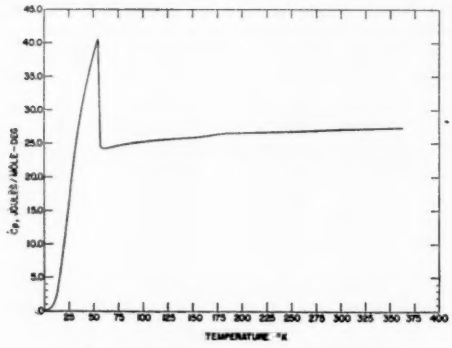

FIG. 1. The heat capacity of thulium.

the anomalies at 88°K and 180°K if the impurity gave Schottky-type anomalies at these temperatures. It seems unlikely, however, that such anomalies would be at so high a temperature in a thulium compound.

The joule is used as the unit of energy. The temperature scale is that of the National Bureau of Standards, using 273.16°K as the temperature of the triple point of water.

RESULTS

The results of the measurements, $\Delta H/\Delta T$ as a function of the average temperature of the point are tabulated in the Appendix. A smooth curve was fitted to the points and extrapolated to absolute zero in the way described below. The thermodynamic functions were then calculated and values which have been corrected for the tantalum impurity[1] are given in Table I. The heat capacity is plotted in Fig. 1.

The precision, as judged from the scatter of points about a smooth curve, was better than 0.1% above 30° except for the region just above the anomaly at 55°, where the slope of the heat capacity curve is very large, and for the anomalous regions near 85° and 170° where the scatter increased to 0.2%. Because of increased difficulty in maintaining adiabatic conditions, the precision decreased below 30° to about 1.5% at 15°.

The heat capacity showed a lambda-type anomaly peaked near 55°K. This temperature is near that at which the magnetic moment shows a maximum. The anomaly was not so sharp as for, say, terbium, having a maximum second derivative of about 3 joule/mole-deg.[3] It is not known whether this lack of sharpness is a property of the pure metal or of our particular sample. As shown by the data of series 3, 5, and 6, the sample showed thermal hysteresis under this peak; if the sample was cooled to a temperature just below the peak, the first few heat capacity points were up to 0.4% low. As this amount was barely greater than our precision, it was not feasible to study this behavior in detail. The actual value of the heat capacity through this region was taken as that which was obtained when the sample had been cooled to a temperature well below the anomaly.

There were anomalous changes in slope near 88°, 162°, and 180°K. The origin of these changes is not known, but the curve was studied in some detail near these temperatures. Although the points scattered somewhat more than at other parts of the curve, we could find no systematic dependence of the heat capacity on the thermal history of the sample. Fig. 2 shows the heat capacity in these regions.

We examined the temperature dependence of the heat capacity in the range of temperature from 13° to 21°K in order to extrapolate our data to absolute zero. As a convenient method of displaying the data, we subtracted the expected electronic contribution, $10^{-2}T$ joule/mole-deg, from each point and then calculated the Debye temperature which would yield the remaining heat capacity at each point. The amount subtracted was only about 7% near 13°K and 2% near 21°K so that a change in the coefficient of the electronic term would not alter the results significantly. The resulting Debye temperatures vs temperature are plotted in Fig. 3. One observes that although there is not a marked temperature dependence, the values of the Debye temperature are much less than would be expected from an extrapolation of the values for neighboring rare earths. Such an extrapolation would suggest a value of about 185° at absolute zero. It is thus clear that there is a considerable magnetic contribution to the heat capacity at 13°K. In order to extrapolate our results to absolute zero, we have assumed the electronic contribution mentioned above and have assumed that the lattice and magnetic contributions together are given by the extrapolation shown in Fig. 3. This assumption ignores the possibility of a specific heat anomaly below 13°K as suggested by the magnetic data. However, in view of the fact that we find no anomaly near 22°K, the apparent ferromagnetic Curie temperature, it appears possible that thulium either does not become ferromagnetic in zero applied field or else the entropy difference between the antiferromagnetic and ferromagnetic states is too small to be detectable. Recent measurements in this laboratory of the small field susceptibility using the inductance technique show the anomaly near 22° and thus support the latter point of view. This result

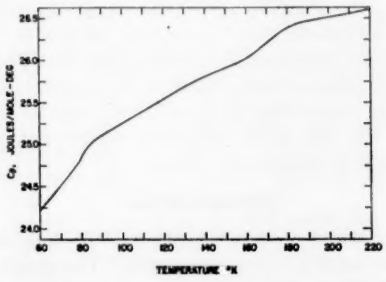

FIG. 2. The heat capacity of thulium in the region of two anomalies in the slope.

is not necessarily in conflict with the lack of an anomaly in the resistivity, for if the entropy change is small, one would not expect the electron mean free path to change greatly. In either event, our extrapolation procedure would be approximately correct.

DISCUSSION

Magnetic Contribution to Thermodynamic Functions

In order to examine the effects of magnetic coupling, one would like to separate the magnetic part of the heat capacity from the lattice and conduction electron part. In the case of the rare-earth metals which have been studied previously,[6] it has been possible to make this separation in a reasonably satisfying way by assuming that the conduction electron contribution did not differ greatly from the conduction electron contribution in lanthanum,[8] that the lattice contribution had the same form as does that of the nonmagnetic rare earths,[1] and that the total entropy of the magnetic contribution was $R\ln(2J+1)$. The lattice contribution is given as a function of a parameter Θ/T. This function does not differ greatly from a Debye function and Θ is chosen so that the entropy near room temperature is the same as for a Debye function with the Debye temperature $\Theta_D=\Theta$. As shown in the work cited in reference 1, Θ differs but little from a Debye temperature. The value of the Θ parameter and the slope and value of the heat capacity near room temperature then served as checks. In the case of thulium, the room-temperature entropy is in fair agreement with the value calculated using these assumptions and a Θ value of 167°, the value which one might anticipate from the work on other rare earths. The room-temperature slope of the heat capacity curve, on the other hand, is much less than would be calculated on the basis of a conduction electron term of $1\times10^{-2}T$, the value for lanthanum. Thus it is possible to make an estimate of the energy of magnetic ordering, but not with good confidence.

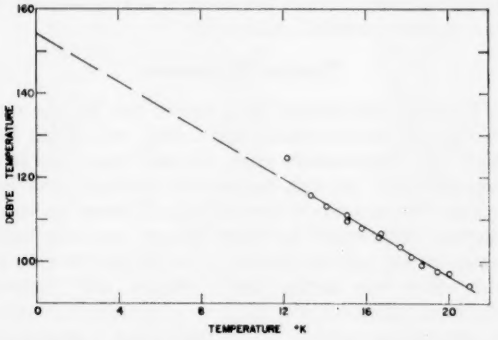

FIG. 3. The effective Debye temperature vs temperature for the lowest experimental points. The straight-line continuation was used to extrapolate our data to absolute zero. This continuation should come into temperature zero with zero slope, but the difference in the thermodynamic functions thus calculated would be negligible.

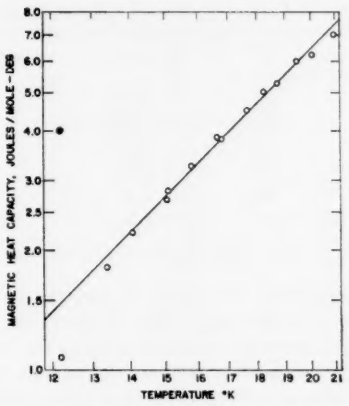

FIG. 4. A logarithmic plot of the magnetic contribution to the lowest temperature heat capacity points. The lowest points do not lie off the line by more than the amount of error possible in the first point of an experimental run. The straight line has slope three.

In this connection, it should be observed that it is currently believed that the mechanism for the magnetic ordering of the rare earths is a coupling of the magnetic moments of the rare-earth ions through the conduction electrons.[9,10] If this is indeed the case, it would not be possible to rigorously separate the heat capacity of the magnetic moments from that of the conduction electrons. It may be, then, that this effect shows up more strongly in thulium and is somehow responsible for the changes in slope near 88°, 162°, and 180°.

In an attempt to understand the magnetic part of the heat capacity at low temperatures, we have assumed that the lattice contribution is given by a Θ value of 167°. Using the heat capacity of the nonmagnetic rare earths[1] as a guide, this value corresponds to a Debye temperature of 168 at 13°K and 161 at 21°K. The magnetic contribution was then calculated for each of the low-temperature points and the results are shown on a logarithmic plot in Fig. 4. Within the experimental accuracy, these points fall on the straight line whose slope is three, yielding a magnetic heat capacity $C=8.0\times10^{-4}T^3$ joule/mole-deg. This result is in agreement with the previous statement that the lattice and magnetic contributions have approximately the same temperature dependence. This temperature dependence is in accord with that predicted for an antiferromagnet on the basis of spin wave

[8] A. Berman, M. W. Zemansky, and H. A. Boorse, Phys. Rev. **109,** 70 (1958).

[9] P. G. deGennes, Compt. rend. **247,** 1836 (1958).
[10] K. Yosida, Phys. Rev. **106,** 893 (1957).

TABLE II. Calculated values of exchange integrals.

	T_c	$\mathcal{J}/k$(from T_c)	$\mathcal{J}/k$(from W)
Gd	292	2.95	2.7
Tb	228	3.56	3.4
Dy	174	3.95	3.9
Ho	132	4.7	4.3
Er	84	5.3	4.7
Tm	55	7.6	10.7

theory,[11] and would be consistent with the supposition that there is no ferromagnetism at low fields.

In connection with the question as to the reason for there being no anomaly in the heat capacity near 22°, it is clear that any hypothesis must yield a very small difference both in energy and in entropy between the ferromagnetic and the antiferromagnetic states in thulium. That this is the case is borne out by the magnetization vs temperature curves[4] which show that at 12 koe the maximum magnetization is as great in the antiferromagnetic region of temperature as in the ferromagnetic region. The same type of effect is manifested in the behavior of terbium, where a small effect is noted in the heat capacity at the antiferro- to ferromagnetic transition, no detectable effect in the magnetization at moderate applied field, and a tremendous effect in the magnetization with applied fields of about 1 oe.

Value of Exchange Integral

From our data and with the assumption that the ordering arises from isotropic nearest-neighbor exchange, it is in principle possible to compute the effective exchange integral $|\mathcal{J}|$ in three ways. The internal consistency of these results is then a measure of the applicability of the assumptions.

If one can separate the magnetic heat capacity from the total, the area under the resulting curve yields the total magnetic energy which is given by $NzS^2|\mathcal{J}|$.[12] Here, N is the number of magnetic sites, z the number of nearest neighbors, and S the spin. It is not necessary to make any assumptions or calculations about the details of the ordering mechanism for this relation to hold. Values of $|\mathcal{J}|$ calculated from this relation for the heavy trivalent rare earths are given in Table II. The value for thulium itself is most in doubt as shown by the above discussion.

The ordering temperature depends on the value of $|\mathcal{J}|$. We have taken for the relationship between them values obtained by extrapolating the work of Brown and Luttinger[13] and of Brown[14] using the more exact results of Wood and Rushbrooke[15] for low spin values as a guide. Their results, which were calculated for magnetism arising from spin only, may be adapted to the rare-earth case by replacing $\mathcal{J}$ by $\mathcal{J}(S^2/J^2)$ and S by J in their expressions.[9] We find for values of momentum greater than 1 and within the precision of the extrapolation that $kT_c=6.28\ S(S+1)|\mathcal{J}|$. We thus note that the momentum dependence is the same as that given by a molecular field calculation which yields $kT_c=8S(S+1)|\mathcal{J}|$.[16] Values of $|\mathcal{J}|$ obtained with the help of the quantum expression are given in Table II.

Finally, the spin-wave heat capacity is determined by the form of the ordering and by the value of the exchange integral.[11] Unfortunately, the form of the ordering is not known for thulium and it is not therefore possible to make an exact calculation of the exchange integral with this method. If, however, one uses as an approximation the result derived on a two sublattice model, we calculate from our experimental result that $|\mathcal{J}|/k=11.6$, in fair agreement with the results given in Table II.

Examination of Table II shows that there is better agreement of the values of $|\mathcal{J}|$ for each rare earth obtained from different methods than there is from one rare earth to another. There is in fact a clear trend for the effective exchange integral to increase with atomic number. This result indicates that $|\mathcal{J}|$ is not roughly constant as is often assumed in connection with magnetic data.

Recent treatments of the ordering energy in the rare earths show that the coupling is more complicated than nearest-neighbor exchange, but the expression for the energy of coupling has essentially the same form as does that used here.[9,10] The interaction does, however, extend over a longer range than simply nearest neighbors and so it will be necessary to modify the detailed results. We may thus take the values of $|\mathcal{J}|$ obtained here as an indication of the strength of the interaction, but reserve a detailed explanation.

Thermal Hysteresis

Previous experiments have shown that for the rare earths, all lambda peaks below that one which lies highest in temperature show thermal hysteresis. It is supposed that the high-temperature magnetic ordering is such that it tends to maintain itself below the equilibrium temperature for phase change in a way analogous to the supercooling of a liquid. In the case of the other rare earths which display this thermal hysteresis phenomenon, there is a significant fraction of the ordering entropy under the highest temperature anomaly, and there is a correspondingly significant reduction of the heat capacity in the regions showing thermal hysteresis. Thulium presents a particularly

[11] J. van Kranendonk and J. H. van Vleck, Revs. Modern Phys. **30**, 1 (1958).
[12] J. A. Hofmann, A. Paskin, K. J. Tauer, and R. J. Weiss, J. Phys. Chem. Solids **1**, 45 (1956).
[13] H. A. Brown and J. M. Luttinger, Phys. Rev. **100**, 685 (1955).
[14] H. A. Brown, Phys. Rev. **104**, 624 (1956).
[15] P. J. Wood and G. S. Rushbrooke, Proc. Phys. Soc. (London) **A70**, 765 (1957).
[16] L. Neel, Compt. rend. **206**, 49 (1938).

TABLE III. Heat capacity determinations for thulium. For necessary corrections, see text.

T_{Av}	ΔT	$\Delta H/\Delta T$
	Series 1	
12.20	0.19	1.909
13.36	1.86	2.935
15.04	1.52	4.341
16.74	1.85	6.050
18.71	2.08	8.297
20.99	2.42	11.045
23.19	1.93	13.889
25.66	2.97	16.925
29.18	4.02	21.059
33.42	4.41	25.462
37.82	4.35	29.561
42.18	4.35	33.002
46.35	3.98	35.853
50.21	3.72	38.150
53.85	3.54	39.935
58.32	5.27	25.706
63.76	5.48	24.266
69.20	5.38	24.450
74.54	5.28	24.612
82.50	10.62	24.911
92.98	10.34	25.148
103.23	10.14	25.280
113.28	9.96	25.431
123.17	9.81	25.580
132.92	9.68	25.709
141.74	9.57	25.800
151.26	9.47	25.912
161.08	10.16	26.022
171.19	10.03	26.214
182.05	11.78	26.421
193.33	10.80	26.476
204.08	10.73	26.522
214.76	10.67	26.569
224.34	10.61	26.618
234.89	10.55	26.668
245.38	10.50	26.716
255.81	10.44	26.757
266.16	10.36	26.902
276.43	10.34	26.887
286.66	10.28	26.958
296.84	10.24	27.008
306.95	10.19	27.074
317.01	10.15	27.112
327.03	10.11	27.174
336.99	10.07	27.226
346.89	10.03	27.281
	Series 2	
14.08	2.03	3.544
15.80	1.40	5.179
17.66	2.28	7.120
20.04	2.44	9.967
22.23	1.91	12.736
24.93	3.45	16.094
28.49	3.62	20.376
32.94	5.21	25.038
38.69	2.12	30.397
41.74	3.92	32.790
45.54	3.62	35.384
50.09	5.47	38.078
53.08	0.50	39.749
53.58	0.49	40.008
54.08	0.49	40.261
54.57	0.49	40.447
55.12	0.59	40.274
55.66	0.49	38.711
56.20	0.58	32.298
56.96	0.93	24.736
57.81	0.75	24.292
58.67	0.95	24.188
59.62	0.94	24.167
61.54	2.88	24.181
66.60	4.75	24.361
71.65	5.33	24.510
78.77	8.90	24.763
87.89	9.33	25.064
98.23	11.33	25.210
109.44	11.10	25.374
120.45	10.90	25.531
131.27	10.74	25.675
139.30	5.31	25.766
147.23	10.54	25.859
157.71	10.43	25.978
167.47	10.31	26.151
177.67	10.17	26.391
188.18	10.90	26.447
199.18	10.84	26.483
209.97	10.78	26.534
220.16	9.65	26.589
230.29	10.66	26.641
240.89	10.61	26.684
251.43	10.54	26.807
261.91	10.50	26.794
272.32	10.45	26.853
282.69	10.40	26.916
291.21	10.36	26.948
301.47	10.32	27.008
311.66	10.27	27.067
321.80	10.23	27.127
331.87	10.18	27.185
341.91	10.14	27.237
351.88	10.10	27.304
	Series 3	
51.95	0.95	38.951
52.79	0.71	39.491
53.60	0.88	39.984
54.26	0.44	40.301
54.68	0.39	40.441
54.97	0.19	40.484

TABLE III.—*Continued.*

T_{Av}	ΔT	$\Delta H/\Delta T$
	Series 3—*Continued*	
55.31	0.47	40.007
55.82	0.53	37.328
56.51	0.85	28.041
	Series 4	
15.09	1.15	4.485
16.62	1.72	6.049
18.21	1.33	7.846
19.46	1.12	9.360
21.46	2.86	11.774
24.03	2.24	14.983
27.12	3.91	18.670
32.06	5.91	23.998
36.94	3.82	28.828
40.64	3.43	31.971
43.96	3.17	34.411
48.25	5.39	37.069
51.47	0.64	38.905
52.54	1.49	39.461
53.44	0.29	39.931
53.81	0.43	40.130
54.25	0.45	40.326
54.72	0.46	40.525
55.19	0.47	40.340
55.50	0.15	29.766
55.73	0.30	38.519
56.04	0.30	34.883
56.36	0.32	30.130
56.72	0.38	25.013
	Series 5	
49.40	0.48	37.537
49.88	0.47	37.820
	Series 6	
53.05	0.48	39.573
53.54	0.48	39.841
54.03	0.48	40.082
	Series 7	
79.46	0.40	24.731
80.43	1.54	24.777
81.97	1.53	24.887
83.52	1.52	24.946
85.04	1.51	24.980
86.56	1.51	25.037
88.07	1.50	25.079
89.58	1.50	25.097
91.08	1.49	25.107
92.58	1.49	25.137
	Series 8	
166.50	0.71	26.027
167.91	2.08	26.069
169.99	2.07	26.140
172.06	2.07	26.180
174.12	2.06	26.230
176.18	2.06	26.273
178.23	2.05	26.310
180.28	2.05	26.378
182.32	2.04	26.401
184.36	2.04	26.418
	Series 9	
83.41	3.91	24.931
86.61	2.47	25.063
89.76	3.81	25.104
93.57	3.79	25.135
97.50	4.06	25.190
101.56	4.04	25.239
	Series 10	
159.15	1.67	25.959
162.03	4.05	26.014
166.09	4.03	26.073
170.12	4.01	26.185
174.12	3.99	26.308
178.10	3.97	26.355
182.07	3.96	26.398
186.02	3.95	26.436
190.11	4.21	26.452
194.31	4.20	26.461
	Series 11	
73.61	5.36	24.534
78.49	4.36	24.718
83.01	4.67	24.917
87.66	4.61	25.047
92.38	4.81	25.113
99.49	9.39	25.209
109.23	10.08	25.362
119.42	10.28	25.515
129.63	10.13	25.651
	Series 12	
140.51	5.27	25.724
146.65	6.98	25.797
152.75	5.20	25.866
157.95	5.17	25.922
163.13	5.15	25.971
168.29	5.12	26.042
173.40	5.08	26.211
178.47	5.05	26.318
183.51	5.03	26.385

TABLE III.—*Continued.*

T_{Av}	ΔT	$\Delta H/\Delta T$
	Series 12—*Continued*	
188.54	5.01	26.407
196.15	10.21	26.426
206.34	10.15	26.477
216.46	10.10	26.530
226.52	10.04	26.583
	Series 13	
65.14	2.20	24.333
76.92	6.12	24.652
82.99	5.99	24.874
87.81	5.91	25.005
93.69	5.83	25.096
99.50	5.77	25.156
105.24	5.71	25.242
111.02	5.65	25.347
116.68	5.59	25.497
	Series 14	
148.01	5.36	25.856
153.37	5.33	25.877
158.71	5.31	25.942
164.06	5.29	25.981
169.32	5.23	26.171
174.60	5.33	26.301
179.87	5.18	26.335
185.05	5.17	26.359
190.21	5.15	26.385
195.89	5.12	26.468
201.01	5.10	26.474
206.11	5.09	26.475
211.21	5.08	26.485
216.29	5.07	26.500
	Series 15	
73.40	6.46	24.466
79.80	6.33	24.692
86.06	6.20	24.939
92.23	6.12	25.049
98.32	6.05	25.121
104.34	5.99	25.222
110.30	5.93	25.310
116.21	5.87	25.412

interesting case, for here there is only a very small reduction in the heat capacity in the region showing thermal hysteresis and correspondingly only a small amount of entropy under the anomalies at temperatures above 55°. This observation, however, increases our confidence that the anomalies in slope at the higher temperatures are a fundamental property of the metal and not an impurity effect, but we offer no mechanism to explain the form of these anomalies.

These considerations suggest that it would be of interest to examine the region near 20° for thermal hysteresis. Unfortunately, the existence of the magnetic transition near this temperature came to our attention only after the sample had been dissolved to make the tantalum analysis and it was not possible to make such an investigation at this time.

ACKNOWLEDGMENTS

We should like to thank Dr. J. Powell and his group for preparing the thulium salts and Gene Wakefield for preparing the metal. We have benefitted from discussions with the personnel of the Ordnance Materials Research Office at Watertown, Massachusetts, especially with Dr. A. Paskin and Dr. R. J. Weiss. Roger Miller, Bernard Gerstein, and Robert Stanton helped in the taking of data.

APPENDIX

Table III gives the results of the individual measurements of $\Delta H/\Delta T$. They have not been corrected for curvature or for the presence of the tantalum or other impurity.

Magnetic Properties of Uranium Tetrafluoride*

M. J. M. Leask,† Darrell W. Osborne,‡ and W. P. Wolf§

Clarendon Laboratory, Oxford University, England

(Received August 23, 1960)

The magnetic susceptibility of a number of UF_4 samples has been measured in the temperature range 1.3°–20.4°K, using the mutual inductance method of McKim and Wolf. Although some of the samples were highly purified, initial measurements indicated appreciable differences between their susceptibilities below 4.2°K. These differences were eventually overcome by subjecting the specimens to the same heat treatment just before susceptibility measurement. The effect of the heat treatment is not entirely understood, but a number of possibilities have been investigated. Theoretically, the main features of the susceptibility variation have been explained on a simple crystal field model of noninteracting ions, and this also accounts for the recent specific heat measurements of Burns, Osborne, and Westrum. An even better theoretical fit has been obtained by introducing a small, adjustable interaction between neighboring uranium ions. Below 2°K the measured susceptibility was anomalous: Samples which at higher temperatures were very similar (±1%), showed considerable differences (~25%), the susceptibility in some cases increasing rapidly with decreasing temperature, and becoming dependent on measuring field. This behavior is unexplained but it is probably not a property of "pure" UF_4.

INTRODUCTION

GENERAL interest in the magnetic and thermodynamic properties of U^{4+} compounds has been in evidence for some years.[1–5] One of the earliest experiments on these compounds was the measurement of the specific heat of uranium tetrafluoride between 20° and 350°K by Brickwedde, Hoge, and Scott[6] (BHS). In this temperature range they observed no anomalous behavior, but no detailed interpretation of the results could be made because the magnetic contribution to the entropy could not be separated from the lattice contribution. Interest in this particular compound was revived when Jones, Gordon, and Long[7] showed that the specific heat of uranium dioxide exhibits a λ-type anomaly at 28.7°K. This suggested that even though no anomalous behavior had been observed in the tetrafluoride down to 20°K, its properties below 20°K might well be very interesting. The original BHS results on the uranium tetrafluoride specific heat were then reexamined by Lohr, Osborne, and Westrum,[8] who measured the specific heat of thorium tetrafluoride—taken to represent the lattice contribution to the UF_4 specific heat—and hence obtained the magnetic entropy of uranium tetrafluoride. This entropy was some 30% lower at room temperature than that obtained for uranium dioxide, and therefore indicated that an anomaly might occur in the specific heat of uranium tetrafluoride below 20°K. The extrapolation of the original BHS results below 20°K had given no hint of this, so Lohr, Osborne, and Westrum made further heat capacity measurements on purified samples of uranium tetrafluoride down to 5°K[9] (1954), and later Burns, Osborne, and Westrum made measurements down to 1.3°K.[10] Their results showed that the magnetic contribution to the specific heat indeed exhibits an anomaly but of the Schottky type, and not the λ form as in the dioxide. The peak occurs at about 6°K where the magnetic C_p has a maximum value of 0.26 cal deg^{-1} mole^{-1}. This confirmed earlier heat capacity measurements carried out on uranium tetrafluoride by C. A. Bailey,[11] which had indicated an anomaly of this type with the maximum at about the same temperature. The magnetic susceptibility measurements which form the subject of this paper were carried out in order to complement the heat capacity measurements and to find an explanation consistent with both sets of results.

Previous measurements of the magnetic susceptibility have all been carried out at higher temperatures, *viz.*, in the range 77°–500°K. Elliott[2] and Dawson[3] both found that the high temperature susceptibility followed a Curie-Weiss law $[\chi=C/(T+\theta)]$ with large values of θ(~100°K) which they ascribed to a combination of large crystalline electric field and exchange effects. The observed value of C was compared with that expected for various theoretical models. Thus, if the

* This research was supported in part by the United Kingdom Atomic Energy Authority, and in part by the United States Atomic Energy Commission.

† Shell Commonwealth Research Scholar.

‡ John Simon Guggenheim Memorial Fellow, on leave from Argonne National Laboratory, Argonne, Illinois.

§ Imperial Chemical Industries Research Fellow.

[1] C. A. Hutchison, Jr., and N. Elliott, J. Chem. Phys. **16**, 920 (1948).

[2] N. Elliott, Phys. Rev. **76**, 431 (1949).

[3] J. K. Dawson, J. Chem. Soc. (London) **1951**, 429.

[4] J. K. Dawson, J. Chem. Soc. (London) **1952**, 1185.

[5] C. A. Hutchison, Jr., and G. A. Candela, J. Chem. Phys. **27**, 707 (1957).

[6] F. G. Brickwedde, H. J. Hoge, and R. B. Scott, J. Chem. Phys. **16**, 429 (1948).

[7] W. M. Jones, J. Gordon, and E. A. Long, J. Chem. Phys. **20**, 695 (1952).

[8] H. R. Lohr, D. W. Osborne, and E. F. Westrum, Jr., J. Am. Chem. Soc. **76**, 3837 (1954).

[9] D. W. Osborne, E. F. Westrum, Jr., and H. R. Lohr, J. Am. Chem. Soc. **77**, 2737 (1955).

[10] J. H. Burns, D. W. Osborne, and E. F. Westrum, Jr., J. Chem. Phys. **33**, 387 (1960).

[11] C. A. Bailey, D. Phil. thesis, Oxford, 1959.

orbital contribution to the magnetic moment were completely quenched, the two unpaired electrons on the U^{4+} ion would exhibit "spin-only" paramagnetism, with $C=1.00$. This behavior might be expected if the electron configuration were $6d^2$, since these electrons are relatively unshielded from electric crystal fields. On the other hand, the configuration $5f^2$ would, in general, lead to a value of C different from 1.00, depending on the crystal field. Both Elliott[2] and Dawson[3] observed appreciable departures from the spin-only value ($C=1.36$ and 1.18, respectively) and explained this in terms of a $5f^2$ configuration. This confirmed the earlier predictions of Wu and Goudsmit[12] and Mayer,[13] who showed theoretically that for elements with $Z>90$, $5f$ electrons may occur in ground-state structures.

However, Dawson[4] also performed a later series of susceptibility measurements on solid solutions of UF_4 in ThF_4 with the object of distinguishing by progressive dilution of the U^{4+} ion in diamagnetic ThF_4. He found that the Curie constant extrapolated to exactly 1.0 at infinite dilution—i.e., that expected for "spin-only" behavior—and hence considered this as evidence for a $6d^2$ ground state. This apparent contradiction has since been resolved by Hutchison and Candela,[5] who show that under certain conditions the energy level system of a $5f^2$ U^{4+} ion in a cubic crystalline electric field is such that the Curie constant is just the same as would be expected at infinite dilution and high temperatures for a quenched $6d^2$ ground state. The present susceptibility results confirm the work of Hutchison and Candela, in that the main features of the low temperature susceptibility of UF_4 are explained satisfactorily in terms of a $5f^2$ ground state.

EXPERIMENTAL METHOD

The apparatus used for the measurement of magnetic susceptibility was similar to an earlier design by McKim and Wolf,[14] so that only the basic principles will be described here.

In this method, one uses an ac Hartshorn bridge to measure the mutual inductance of a specially wound coil, before and after moving a paramagnetic specimen through a fixed, predetermined distance along the coil axis. The change in mutual inductance is then directly proportional to the susceptibility χ of the specimen. The mutual inductance coil is immersed in liquid helium or hydrogen, and the vapor pressure of the liquid is used to measure the temperature. Susceptibility measurements were thus carried out in the oscillatory (175 cps) magnetic field produced by the primary winding of the coil (1 gauss/ma). From considerations of sensitivity and power dissipation it was found convenient to operate at a field of approximately 40 gauss. This relatively small value of measuring field made the method very sensitive to small amounts of ferromagnetic impurities present in specimens. By the same token, however, these were very easy to detect, particularly since the out-of-phase component of susceptibility at 175 cps in ferromagnetic substances is usually several orders of magnitude larger than that in paramagnetic substances, and this was measurable directly on the Hartshorn bridge. The detailed procedure for the detection of ferromagnetic impurities is described in detail in another paper,[15] since all the UF_4 specimens used in this research were found to be completely free of such impurity when tested at 4.2°K, the starting point of each experiment.

Specimen containers were made from Teflon, which was chosen for ease of machining and subsequent cleaning. Their susceptibility, which was measured beforehand, was applied as a correction to the total magnetic susceptibility, and this never amounted to more than 0.3% at any temperature. Calibration of the apparatus was carried out by making susceptibility measurements on a known weight of manganous ammonium sulphate hexahydrate. The calibration constant was usually checked before each experiment, and was found to exhibit a long-term variation not greater than 0.7%. The sensitivity of the apparatus was such that the susceptibility of a typical UF_4 specimen (approx 1g) could be measured to one part in 5000 at 4.2°K. Measurements made at other temperatures during any particular experiment were always self-consistent to one part in 1000. However, since repeated experiments on other substances have shown systematic differences of a few tenths of a percent, it is believed that the absolute accuracy of the method is probably about $\pm\frac{1}{2}$%.

The magnetic susceptibilities of all the UF_4 specimens were measured as a function of temperature from 4.2°K down to 1.3°K (liquid helium) and from 20.4°K down to 13.94°K (liquid hydrogen) at one value only of measuring field, usually 40 gauss. Cooperative effects, such as those observed below 2°K, were detected and investigated by making additional susceptibility measurements at a number of different primary fields between 1 and 40 gauss.

SPECIMENS

Preliminary experiments on relatively impure UF_4 specimens showed appreciable differences between their magnetic susceptibilities. Great care was taken, therefore, to ensure that the materials used in this investigation were of the highest purity obtainable. The specimens fall into three classes: (1) Specimens H1 and H2, obtained from AERE Harwell, on which the preliminary measurements were made. These compounds were of relatively ill-defined purity, and susceptibility measurements on these indicated the necessity of obtaining much purer specimens.

[12] T. Y. Wu and S. Goudsmit, Phys. Rev. **43**, 496 (1933).
[13] M. G. Mayer, Phys. Rev. **60**, 184 (1941).
[14] F. R. McKim and W. P. Wolf, J. Sci. Instr. **34**, 64 (1957).
[15] M. J. M. Leask, L. E. J. Roberts, and W. P. Wolf (to be published).

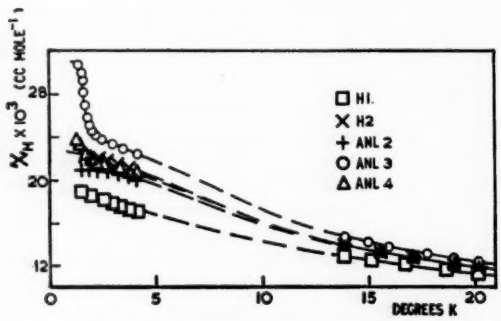

FIG. 1. Molar susceptibilities of the five starting materials, all nominally pure UF_4.

(2) Specimens ANL2, ANL3, and ANL4, obtained from the Argonne National Laboratory, Argonne, Illinois. These were very much purer than the Harwell specimens, and had been extensively analyzed, both spectrographically for trace impurities and chemically for correct stoichiometry. Susceptibility measurements on these specimens were more precise than those on the Harwell specimens, and were carried out to lower temperatures. Analytical data on these materials may be found in Appendix 1.

(3) Specimens ANL2FG and ANL4FG. These were prepared from the specimens ANL2 and ANL4 by fusion at the melting point, (as described in Appendix 2), followed by coarse grinding of the product in a porcelain mortar. Reasons for doing this will be discussed in the next section.

RESULTS

The magnetic susceptibilities of each of the five starting materials—H1, H2, ANL2, ANL3, ANL4—are shown in Fig. 1, in which χ is plotted as a function of temperature for the range 1.3°–20.4°K. All values of χ above 1.6°K were found to be independent of measuring field, indicating purely paramagnetic behavior and the absence of any ferromagnetic or cooperative effects. Leaving aside for a moment the results below 2°K, Fig. 1 shows that although the general behavior of all the specimens is qualitatively the same between 2° and 20.4°K, the systematic differences between the various specimens are much too large to be accounted for by experimental error in the susceptibility measurements. The most obvious explanation for these differences would appear to lie in the presence of impurities in the specimens, but closer examination shows that this cannot be the only reason. When considering the possible effect that impurities might have on the susceptibility, it is convenient to consider each of the possible types of impurities in turn.

Diamagnetic impurities can be dismissed as a possibility since the large susceptibility differences observed experimentally would require such large amounts (15%) that these would have been detected by chemical analysis. The small amounts of UO_2F_2 could account for only a fraction of the observed susceptibility differences.

Ferromagnetic impurities are unlikely, since in the first place routine tests for ferromagnetism in each specimen proved negative, and second, the contribution to the susceptibility from such an impurity would almost certainly be independent of temperature, whereas none of the curves in Fig. 1 differ from each other by a constant amount.

Paramagnetic impurities were certainly present in all the specimens, but again, in the case of ANL2, ANL3, and ANL4, the spectrographically determined concentrations were much too low to account for the susceptibility differences. In the case of the less pure specimens H1 and H2, one might have expected the paramagnetic impurities to *raise* the susceptibility above that expected for pure UF_4. It is surprising, therefore, that instead of having a greater susceptibility than any of the other specimens, H1 in fact has a lower susceptibility at all temperatures, and H2 was comparable with ANL4. However, in view of the uncertainty in the purity of these two specimens, it was decided to concentrate only on the results from the highly purified specimens ANL2, ANL3, and ANL4 in an attempt to reconcile these with each other and a theoretically predicted susceptibility. It will be seen that the reconciliation of these results does in fact lead to a possible explanation for the anomalous behavior of H1 and H2.

Visual examination of the ANL specimens showed clearly that they were powders of widely differing particle size. This was certainly a consequence of the different heat treatments which the specimens had undergone in the course of preparation. ANL3, for instance, had been melted, whereas ANL2 had been purified by sublimation in vacuum. In view of the possibility that this might be the reason for the differing

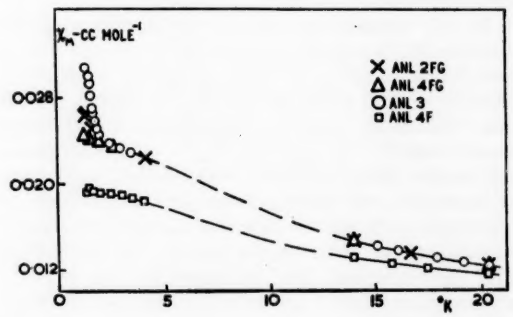

FIG. 2. Susceptibilities of three different samples (ANL2FG, ANL4FG and ANL3) after melting and grinding to a powder. Note the close similarity down to 2°K and the relatively large differences below 2°K. The fourth set of results (□=ANL4F) refer to one of the samples fused but not ground. The difference is due to partial crystallization during the fusion, and indicates a large magnetic anisotropy for the individual ions.

susceptibilities, it was decided to subject ANL2 and ANL4 to the same heat treatment as ANL3, and see what effect this had on the susceptibility. The melting process is described in Appendix 2. In both cases the product (labeled ANL2F, ANL4F) showed signs of crystal growth in a preferred direction, and this was confirmed by checking the ANL4F lump for anisotropy at 4.2°K by an oscillation method. A large anisotropy was observed for this specimen and correspondingly the total susceptibility measured in one direction was much lower than that of the starting material at all temperatures (see Fig. 2). In order to avoid anisotropy effects, therefore, both ANL2F and ANL4F were roughly ground to a powder (and labeled ANL2FG and ANL4FG, respectively,) just before being inserted into the apparatus. Figure 2 shows results on these two specimens compared with the results of ANL3. The three sets of results are seen to agree to within ±1% at all temperatures above 2°K, reasonable agreement in view of the extensive treatment of the specimens. This may be taken to be strong evidence that these three results approximate closely to the true behavior of pure UF_4. The precise effect of melting is not yet fully understood, but three obvious possibilities may be considered.

TABLE I. Molar susceptibility of UF_4.

T(°K)	χ_M (cm³ mole⁻¹)
20	0.0124
18	0.0131
16	0.0138
14	0.0146
Interpolated values	
12	0.0159
10	0.0172
8	0.0189
6	0.0209
4	0.0224
3.5	0.0230_5
3	0.0233_5
2.5	0.0237
2	0.0238_5
Extrapolated value	
0	0.0240

Related Compounds

U_2F_9 and U_4F_{17} are two compounds closely related to UF_4 in that they have similar crystal structures[16,17] and a stoichiometric U/F ratio which is very close to that of UF_4. One cannot therefore overlook the possibility that even supposedly pure UF_4 might contain small amounts of either or both of these compounds. However, the stoichiometric analysis on ANL3 (which had been melted prior to analysis) was so near the theoretical U/F ratio that the possibility of even small percentages of these compounds being present is rather remote. Again this is good evidence that the susceptibility of ANL3 really does represent that of UF_4.

Particle Size Effect

Because the U^{4+} ion has an even number of unpaired electrons it may be expected on theoretical grounds (see below) that increasing the distortion of the immediate surroundings of the individual ions would reduce the low temperature susceptibility below that of similar ions within a uniform UF_4 crystal. Such a distorted condition could arise at or near the surface of a crystal, and if each crystal were extremely small (i.e., if the substance were very finely powdered) an appreciable percentage of the U^{4+} ions would find themselves in surface layers, and therefore in distorted surroundings. Such an aggregate of microcrystals would then exhibit a smaller bulk susceptibility at low temperatures than a powder containing much larger microcrystals, and simple calculation shows that the particle size necessary to account for the observed effect on the susceptibility would be $\sim 10^{-6}$ cm. Since the most obvious effect of melting would be to increase the particle size by several orders of magnitude, it was decided to seek information on the particle sizes of some of the original specimens. ANL4 and H2 were chosen for this purpose, the latter because it was obviously a much finer powder than any of the ANL specimens. We are greatly indebted to the following people for the determinations which were carried out:

(1) Doctor R. W. D'Eye, of Atomic Energy Research Establishment (AERE), Harwell, England made estimates of the particle sizes from the broadening of lines in an x-ray diffraction photograph. His estimates were:

$$\text{ANL4} \sim 10^{-4} \text{ cm}$$

$$\text{H2} \sim 10^{-5} - 10^{-6} \text{ cm}.$$

(2) Doctor J. V. Shennan, United Kingdom Atomic Energy Authority (U.K.A.E.A.), Capenhurst, England, determined the total surface areas of the powders by the nitrogen adsorption method, and Doctor L. Tomlinson, U.K.A.E.A. Springfield, England repeated these determinations by the more accurate krypton adsorption method. Both these methods agreed well with each other but indicated particle sizes of the order of ten times larger than those given by the x-ray

[16] W. H. Zachariasen, Acta Cryst. **2**, 390 (1949).
[17] P. Agron, A. Grenall, R. Kurrin, and S. Weller, U.S.A.E.C. Report, MDDC1588 (1948).

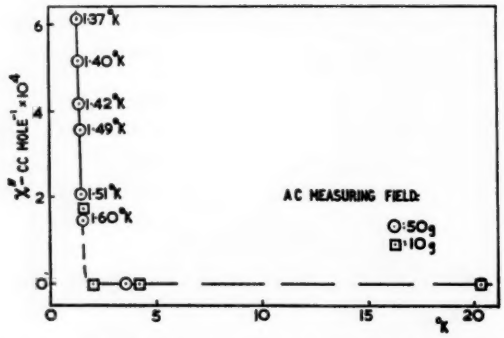

FIG. 3. Variation of the out-of-phase susceptibility χ'' with temperature, for one of the samples (ANL3) which was anomalous below 2°K. Note that the largest value is only 3% of the corresponding χ', suggesting that possibly only a small part of the sample is giving rise to the cooperative effects which may also be responsible for the anomalous variation of χ'.

method. This is probably not too surprising since the x-ray method would presumably see dislocations within the microcrystals, whereas the gas adsorption methods would not. Since dislocations also produce distortions of local surroundings, they would affect the susceptibility in the same way as surface layers, and so the x-ray determination is probably a better estimate of the effective microcrystallite size. Thus, although on theoretical grounds there is good reason to expect the susceptibility to depend on particle size, it is difficult so see how ANL4, for instance, could have been subject to this effect since the microcrystallite size is two orders of magnitude too large.

Hydrates

A third possibility is that hydrates may have formed on the surface of the finely powdered UF_4 specimens. Such compounds would tend to reduce the bulk susceptibility and would certainly be decomposed during the fusion process. To test this possibility, a portion of ANL4 was heated to 450°C for 1 hr in vacuum, which should have been[18] more than sufficient to decompose any hydrates. The susceptibility of this "dehydrated" sample was approximately 1% lower than that of ANL4, a difference which was not regarded as significant.

The general conclusion to be drawn is that none of the mechanisms appears to explain the observed increases in susceptibility, and the effect of melting the specimens is therefore not understood. Nevertheless the very close agreement between the three different fused samples over the range 2°–20°K is strong evidence that these results represent the true behavior of UF_4 in this temperature range. Table I gives smoothed values of the mean susceptibility between 2° and 20.4°K and the extrapolated value for $T=0$. In making the extrapolation the anomalous behavior of the susceptibility below 2°K is neglected.

RESULTS BELOW 2°K

The behavior of the susceptibility below 2°K is anomalous both from an experimental and theoretical point of view, and all the specimens appear to behave quite differently from one another in this temperature region. Nevertheless it is possible to describe the behavior of all the specimens in terms of varying amounts of two distinct effects superimposed on the smooth variation predicted by the results above 2°K. Effect A begins at about 2°K as the temperature is lowered. The susceptibility is still paramagnetic, but rises very steeply to a peak at about 1.5°K. Effect B begins at 1.6°K as the temperature is lowered, and is cooperative, in that the suceptibility becomes dependent on measuring field. This effect is much smaller than the first and is superimposed upon it. The cooperative nature is demonstrated clearly by the variation of the loss component of susceptibility with temperature, as shown for ANL3 in Fig. 3. The sudden increase below 1.6°K accompanies the dependence of the in-phase susceptibility on the magnitude of the measuring field. It may be noted that the relatively impure specimen H1 showed no sign of either of these effects down to 1.5°K. This was also the case with ANL2, the only purified sample to show no anomalous effects. It is interesting to note that the amount of effect A was *reduced* by the melting process in the case of ANL4 but *increased* in the case of ANL2. Effect B seemed to be unaffected by the melting process, being much larger in ANL3 than in any of the other specimens.

DISCUSSION

Hutchison and Candela[5] have recently explained the magnetic behavior of $[(CH_3)_4N]_2UCl_6$, another U^{4+} compound, in terms of a very simple model. They assumed that the unpaired electrons on the U^{4+} ions belong to the $5f^2$ configuration and that Russell-Saunders coupling is large compared with crystal field effects, and they calculated the splitting of the $^3H_4$ free ion ground multiplet produced by the crystal field, estimated from a point charge model. In the particular substance which they considered the field has octahedral symmetry, which splits the $J=4$ multiplet into states Γ_1, Γ_3, Γ_4, and Γ_5 (Bethe's notation),[19] and they were able to show that for all values of the relative magnitude of fourth- and sixth-order crystal field terms, the Γ_1 (singlet) state was lowest. This result was borne out by the experimentally determined magnetic susceptibility, which was found to be independent of temperature. The magnitude of this susceptibility allowed the calculation of the energy separation to the next higher levels, which was then compared with the spectroscopic evidence on the overall splitting between

[18] J. K. Dawson, R. W. M. D'Eye, and A. E. Truswell, J. Chem. Soc. (London) **1954**, 3922.

[19] H. A. Bethe, Ann. Phys. **3**, 133 (1929).

the $^3H_4$ and $^3H_5$ multiplets, to check the assumption on the relative magnitudes of the Russell-Saunders coupling and crystal field effects. This showed that the spin-orbit coupling is indeed larger than the crystal field effects, but only by a factor of about three, so that in some cases admixtures of higher multiplets into the ground state may not be entirely negligible. This has been confirmed by Conway,[20] whose spectroscopic work on U^{4+} ions in CaF_2 indicates that the ground state of the U^{4+} ion is 87.7% $^3H_4$ plus 11.3% $^1G_4$. In addition, further work by Candela and co-workers[21] on the magnetic susceptibilities of other U^{4+} and Pu^{4+} compounds having cubic symmetry has indicated for some of these compounds the possibility of a reduction in L due to partial breakdown in Russell-Saunders coupling. In general, however, we may conclude that it is still a reasonable approximation to specify the ground multiplet by pure Russell-Saunders coupling of the $5f^2$ configuration, with crystal field effects larger than for similar rare-earth compounds but still relatively small.

In applying these conclusions to UF_4 we are faced with the difficulty that the symmetry of the crystal field at the U^{4+} ions is not known precisely, so that we must make some further assumptions regarding the splitting of the $^3H_4$ multiplet. Zachariasen[22] has determined the unit cell dimensions and space group for UF_4 and its isomorphs, so the positions of the U^{4+} ions in unit cell are well established, but the exact positions of the fluorine atoms surrounding each U^{4+} ion are not known. However, these have been estimated from theoretical F–F and U–F spacings[23] and it appears that each U^{4+} ion is surrounded by a somewhat distorted cube of eight fluorine atoms. The distortions are of prime importance in determining the final removal of degeneracy from the ground multiplet, but it is not possible to discuss their effect in quantitative detail when the experimental datum is an averaged quantity like powder susceptibility or specific heat.

From the estimated structure it seems reasonable to regard the crystal fields acting on each U^{4+} ion as being made up of two parts: (a) a dominant term of cubic symmetry due to a regular cube of negative charges to which the fluorine atoms approximate, and (b) terms of lower symmetry and smaller magnitude to account for the displacement of the fluorine atoms from the regular cube positions surrounding each uranium ion. For this type of cubic field, i.e., that due to a cube of negative charges, Hutchison and Candela have shown in detail that for some values of the ratio between fourth- and sixth-order crystal field parameters[24] the Γ_5 (triplet) state is lowest, while for the remaining values of the crystal field parameter ratio, the Γ_1 (singlet) state may be lowest. They also show that the Γ_5 triplet may be described in terms of a fictitious spin $S'=1$ with an effective $g=2$. For temperatures at which the three Γ_5 states but none of the others are populated, this predicts a behavior indistinguishable from that of "spin only" paramagnetism, as observed in diluted UO_2.[25] In deciding whether Γ_1 or Γ_5 is lowest in the particular case of UF_4, we note the following facts:

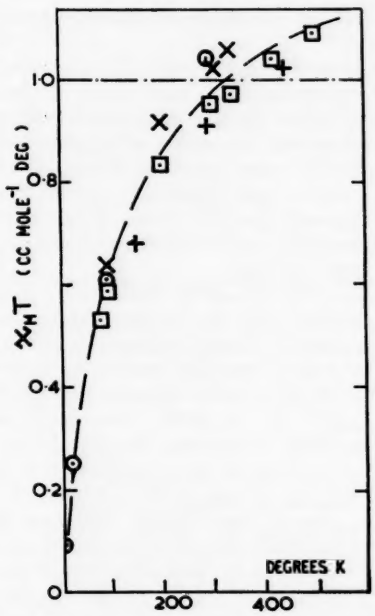

FIG. 4. High temperature susceptibility of UF_4: ⊡, × Dawson[3,4]; + Elliott,[2] ⊙ this work (sample ANL4). The points at 77° and 300°K were kindly obtained for us by Dr. R. Lazenby o this Laboratory.

(i) The low-temperature magnetic susceptibility is quite large and strongly temperature dependent in the region 2°–20°K (see Fig. 2).

(ii) Disregarding the anomalous susceptibility observed below 2°K in some of the samples, the results above 2°K indicate that the susceptibility flattens off as T tends to zero.

(iii) Specific heat results[10] on UF_4 indicate the splitting between the lowest energy levels to be 15.4°K.

(iv) In the energy matrix of the Zeeman Hamiltonian there are no off-diagonal terms coupling Γ_1 with any of the Γ_5 states.

(v) By 300°K, $\chi_M T$ for UF_4 is very nearly 1.0 (see Fig. 4, giving the high temperature results of different

[20] J. G. Conway, J. Chem. Phys. **31**, 1002 (1959).
[21] G. A. Candela, C. A. Hutchison, Jr., and W. B. Lewis, J. Chem. Phys. **30**, 246 (1959).
[22] W. H. Zachariasen, Acta Cryst. **2**, 388 (1949), Wyckoff Vol. II.
[23] R. D. Burbank, U.S.A.E.C.D. Report, 3216 (1951).
[24] The estimate of the crystal field parameters depends not only on the position of the negative ions but also on the estimate of $\langle r^4 \rangle_{Av}$ and $\langle r^6 \rangle_{Av}$ for the $5f$ electrons, which is rather uncertain.
[25] W. Trzebiatowski and P. W. Selwood, J. Am. Chem. Soc. **72**, 4504 (1950).

workers) and the total magnetic entropy is just greater than $R\ln 3$.[9]

This evidence strongly favors a Γ_5 triplet lowest, for the following reasons. If Γ_1 were lowest, the susceptibility would indeed become temperature independent as T tended to zero, but with a value much less than the experimental value since, by virtue of (iv), a nearby Γ_5 triplet state would not contribute to the susceptibility, and Γ_3 and Γ_4 states, which could, are on Hutchison and Candela's evidence almost certainly at much higher energies.

If, on the other hand, Γ_5 were lowest, the 15.4° splitting obtained from the specific heat results (iii) could be regarded as being between two of the three levels of the triplet, the third level being sufficiently high so that all three levels appeared degenerate (by exhibiting $\chi_M T=1.0$) at 300°K. This would explain not only the 300°K susceptibility but also the fact that the magnetic entropy at this temperature is of the order of $R\ln 3$. The splitting of the Γ_5 triplet into three singlet levels spread over roughly 300° may be explained in terms of the distortions of the crystal structure from cubic symmetry, since even without knowing anything explicit about the distortions one may be fairly certain from the estimated fluorine positions that the symmetry is as low as rhombic, which is all that is needed to remove the Γ_5 degeneracy in the manner suggested. The fact that the entropy at 300°K is just greater than $R\ln 3$, and that $(\chi_M T)_{300°K}$ is just greater than 1.0, could possibly mean that the singlet is beginning to be populated at this temperature, and is therefore relatively close to Γ_5.

DETAILED THEORY

In order to compare the experimentally observed susceptibility with theory in more detail, it is necessary to write down an expression for the susceptibility of an individual U^{4+} ion in terms of the three nondegenerate states arising from the splitting of the Γ_5 ground multiplet described by $S'=1$, $g=2$. If we require to calculate the powder susceptibility this may be done in a very general way. Within a manifold spanned by Γ_5, the effect of any small noncubic crystal field potential can be described as giving rise to three nondegenerate states $|A\rangle$, $|B\rangle$, and $|C\rangle$, each of which can be written in terms of a general linear combination of the states $S_z'=|0\rangle$, $|\pm 1\rangle$, of the fictitious spin $\mathbf{S}'=1$. The effect of a magnetic field is calculated from the first- and second-order perturbations of

$$\mathcal{H}_M=g_J\beta\mathbf{H}\cdot\mathbf{J},$$

which within the Γ_5 triplet is identical with

$$\mathcal{H}_M=2\beta\mathbf{H}\cdot\mathbf{S}'. \tag{1}$$

The powder susceptibility is found by averaging the effect of applying $\mathbf{H}$ in turn along each of the principal axes x, y, and z of each ion. Substituting into the general formula for susceptibilities in small fields[26] we find

$$\chi_{\text{powder}}=\frac{(4N\beta^2/3)\sum_{\nu=x,y,z}\sum_{i=A,B,C}\sum_{\substack{j=A,B,C\\ j\neq i}}\{(|\langle i|S_\nu|i\rangle|^2/kT)-[2|\langle i|S_\nu|j\rangle|^2/(E_i-E_j)]\}\exp(-E_i/kT)}{\sum_{i=A,B,C}\exp(-E_i/kT)}. \tag{2}$$

This may be simplified considerably. From the fact that any static electric field is invariant to time reversal, while $\mathbf{S}'$ is not, we note that all diagonal matrix elements $\langle i|S_\nu|i\rangle$ must vanish. Further, using the identities

$$\begin{aligned}\langle i|\mathbf{S}'^2|i\rangle&=S'(S'+1)=2\\&=\sum_j\sum_{\nu=x,y,z}|\langle i|S_\nu|j\rangle|^2 \qquad i,j=A,B \text{ or } C\end{aligned} \tag{3}$$

and the fact that

$$\langle i|S_\nu|i\rangle=0, \tag{4}$$

we find that $\sum_\nu|\langle i|S_\nu|j\rangle|^2\equiv 1$ for any pair of states

$$|i\rangle\neq|j\rangle=|A\rangle, \qquad |B\rangle \text{ or } |C\rangle.$$

Thus we may write an expression for the powder susceptibility as

$$\chi_p=(8N\beta^2/3)\sum_i[\exp(-E_i/kT)/(E_i-E_j)]/\sum_i\exp(-E_i/kT). \tag{5}$$

If we express the energies relative to the ground state, $E_B-E_A=\Delta_1 k$, $E_C-E_A=\Delta_2 k$, where Δ_1 and Δ_2 are in °K, this becomes

$$\chi_{\text{powder}}=\frac{(8N\beta^2/3k)\{(1/\Delta_1+1/\Delta_2)+[1/(\Delta_2-\Delta_1)-1/\Delta_1]\exp(-\Delta_1/T)+[-1/\Delta_2-1/(\Delta_2-\Delta_1)]\exp(-\Delta_2/T)\}}{1+\exp(-\Delta_1/T)+\exp(-\Delta_2/T)}\cdots. \tag{6}$$

[26] J. H. Van Vleck, *Theory of Electric and Magnetic Susceptibilities* (Oxford University Press, New York, 1932), p. 182.

Other than the general assumptions outlined above, the only approximations which have been made in deriving this formula have been to neglect matrix elements of both the crystal field and the magnetic moment to states outside the Γ_5 manifold, which seems well justified if the cubic crystal field splittings are large and the deviations from cubic symmetry are reasonably small. The off-diagonal matrix elements of the magnetic moment contribute a term to the susceptibility which is independent of temperature (until the Γ_3 and Γ_4 states are populated) and which may be appreciable near room temperature ($\sim$10–20%), but which is quite negligible at low temperatures.

ENTROPY UNDER THE SCHOTTKY ANOMALY AND χ_M AT ABSOLUTE ZERO

The specific heat results indicate the splitting between the two lowest lying levels to be 15.4°K, whence it follows from the expression for the magnetic susceptibility that $(\chi_M)_{T=0}$ should be approximately equal to (1/15.4) or 0.065 cgs units per mole, since $\Delta_2 \gg 15.4$°K ($\Delta_2 \sim 300$°K, from the high temperature susceptibility). However, the experimental results above 2°K (Fig. 5) indicate that χ_M tends to 0.024 cgs units per mole at absolute zero, approximately one-third of the predicted 0.065. Furthermore, the magnetic entropy associated with the Schottky specific heat anomaly was found to be $0.228R$, (i.e., $0.203R$ found experimentally up to 20°K,[10] and $0.025R$ calculated on the assumption of a $1/T^2$ magnetic specific heat above 20°K), again approximately one-third of the $R \ln 2 = 0.693R$ expected for a two-level system. Since the 12 U^{4+} ions in unit cell fall into two classes, eight of one and four of the other (hereafter referred to as U_2 and U_1 type ions, respectively, in conformity with previous notation[22]), the factor of one-third in both these results can be explained very simply by assuming that only the U_1 type ions contribute to the magnetic susceptibility and specific heat at low temperatures. This would be the case if the axial and rhombic distortions of the local crystal field at each of the other eight ions in unit cell were of such a magnitude and sign as to leave a singlet level very much below the other two levels of the triplet.

Thus the general features of both the magnetic susceptibility and the specific heat results are explained adequately on the assumption that two-thirds of the ions in unit cell contribute to neither of these quantities at low temperatures. This assumption is not strictly correct, however, since high temperature susceptibility and specific heat measurements indicate that all the ions in unit cell are equivalent by 300°K. This means that the two-thirds ions having a singlet level lowest (U_2) must in addition have another two levels within about 300°K of the ground state; these two levels will contribute to the susceptibility (but not the specific heat) even at very low temperatures with terms proportional to $1/\Delta_1'$ and $1/\Delta_2'$, where for the U_2-type ions $E_B - E_A = \Delta_1' k$ and $E_C - E_A = \Delta_2' k$. Moreover, there are twice as many ions of this type as of the other. We have also neglected up to now the effect, proportional to $1/\Delta_2$, of the second excited state Δ_2 of the U_1 ions. If we assume that Δ_1', Δ_2', and Δ_2 are all of the order of 300°K, as indicated qualitatively by the high temperature susceptibility, these terms increase the total susceptibility to $(\chi_M)_{T=0} = 0.027$ cgs units, 15% greater than the experimental value, and well outside the limits of experimental error. We shall now discuss several refinements of the simple theory which could remove this discrepancy, and in particular we shall consider mechanisms which are likely to reduce the magnetic moment of the ground state.

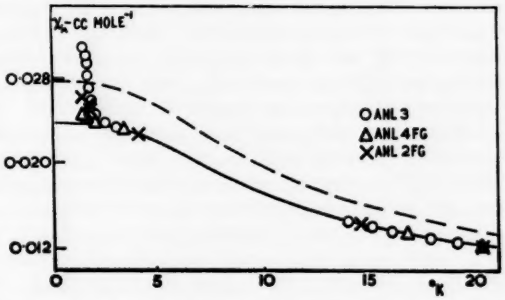

FIG. 5. Theoretical variation of susceptibility. Broken line represents Eq. (6), assuming that $\Delta_1 = 15.4$°K, for one-third of the U^4 ions, and that Δ_2, Δ_1' and Δ_2' are all about 300°K. Solid line represents Eq. (7), fitted with the factor $p = 0.844$, and the Δ's as before.

A typical effect of this nature is the breakdown of Russell-Saunders coupling, and there is, in fact, good evidence as mentioned previously, that the U^{4+} ground state in UF_4 contains small admixtures of terms other than $^3H_4$. The effect of these is very small, however, and Conway's results[20] show that the resultant reduction in moment is less than 2%. Another mechanism leading to a reduction in the moment is that of orbital overlap, or partial covalent bonding of the magnetic electrons with the surrounding fluorines, of the type discussed by Stevens.[27] One effect of such an orbital overlap would be a large shift in the nuclear magnetic resonance frequency of the fluorines, but this has not been found experimentally.[28] On the other hand, Bleaney, Llewellyn, and Jones[29] did find evidence for overlap from electron spin resonance experiments in the rather similar case of U^{3+} in CaF_2, so that while at present there is no evidence in the case of UF_4, the possibility cannot be ruled out entirely.

Another rather unlikely possibility is that the noncubic crystal field potential is not negligible compared

[27] K. W. H. Stevens, Proc. Roy. Soc. (London) **A219,** 542 (1953).

[28] R. G. Shulman and V. Jaccarino, Phys. Rev. **108,** 1219 (1957).

[29] B. Bleaney, P. M. Llewellyn, and D. A. Jones, Proc. Phys. Soc. (London) **B69,** 858 (1956).

with the effect of the cubic field, so that the states from higher Γ's are admixed into the lowest triplet. From existing data it is impossible to estimate this effect quantitatively, but it does seem that 15% is a rather large discrepancy to account for in this way.

A fourth and much more likely possibility is that of interactions between adjacent U^{4+} ions. In fact, it might be asked why this effect does not dominate the low temperature susceptibility, as it does in UO_2, which undergoes an antiferromagnetic transition at 28°K.[7] One reason for this may be the fact, suggested by a comparison of the transition temperatures of various known antiferromagnetic compounds, that fluorine ions do not provide such a strong path for superexchange mechanisms as oxygen ions. A second and more important reason is peculiar to the type of crystal structure of UF_4. As we have shown, the low symmetry crystal field completely removes the ground state degeneracy of all the ions, thereby "quenching" their effective angular momentum [Eq. (4)]. Under these conditions there can be no first-order interaction between the ions, and any coupling must arise from the off-diagonal matrix elements of the interaction potential V_{int}. The effect of these on the susceptibility will depend inversely on the unperturbed crystal field splittings of each one of any pair of the interacting ions, and if these are large for one of the ions, the total effect will be small. If we assume that any interaction is between nearest neighbors only, this is precisely the situation which applies in UF_4. As we have shown, two thirds of the ions are virtually nonmagnetic at low-temperatures, with a large energy separation between the ground state and other crystal field states, and an examination of the structure shows that the eight nearest neighbors to the U_1 magnetic ions with the 15.4°K splitting are all of the U_2 (nonmagnetic) type.

Even so, the interaction effect is not zero and we may estimate its order of magnitude in terms of a specific form for V_{int}. The simplest form of coupling is that of isotropic exchange

$$\mathcal{H}_{\text{ex}}=\sum_{j>i}\tau_{ij}\mathbf{S}_i\cdot\mathbf{S}_j,$$

between the real spins $\mathbf{S}_i$ and $\mathbf{S}_j$. Within the manifold spanned by $|{}^3H_4, \Gamma_5\rangle$ this may be expressed in terms of a coupling between fictitious spins $\mathbf{S}'=1$

$$\mathcal{H}_{\text{ex}}=\sum_{j>i}[2(g_J-1)/g_J]^2\tau_{ij}\mathbf{S}_i'\cdot\mathbf{S}_j'=\sum_{j>i}K_{ij}\mathbf{S}_i'\cdot\mathbf{S}_j',$$

where g_J is the Landé factor, which equals 5/4. By analogy with UO_2 the value of K_{ij} may be of the order of 1° to 10°K. To estimate the effect of this interaction on any one U_1-type ion i we use the molecular field approximation, which consists in replacing $\sum_j K_{ij}\mathbf{S}_j'$ by $\sum_j K_{ij}(1/2N\beta)\mathbf{M}_j$, where the summation is taken over the eight nearest neighbors of type U_2 and $\mathbf{M}_j$ is their average magnetic moment. In an applied field $\mathbf{H}_0$, $\mathbf{M}_j$ is given to a first approximation by $\mathbf{M}_j=\chi_j\cdot\mathbf{H}_0$, where χ_j is the unperturbed susceptibility. Strictly speaking, the susceptibility of any one U_2 ion χ_j is anisotropic with principal axes which are different for each of the eight ions in unit cell, but to derive an order of magnitude estimate for the exchange effect we can replace χ_j by its average powder value. If we consider only temperatures low compared with Δ_1' and Δ_2', i.e., $kT\ll 250$°K, χ_j is constant and given by

$$\chi_j=8N\beta^2/3k[1/\Delta_1'+1/\Delta_2']\sim 16N\beta^2/750k.$$

The Hamiltonian for the susceptibility of any one U_1-type ion is then

$$\mathcal{H}=-2\beta\mathbf{H}_0\cdot\mathbf{S}_i'[1-(1/2\beta)zK_{ij}/2N\beta(16N\beta^2/750k)],$$

where $z=8$=the number of nearest U_2-type ions. If K_{ij} is positive, corresponding to antiferromagnetic coupling, the effect of the term in the square bracket is to reduce the susceptibility by a factor $[1-(32/750K_{ij}]^2$. This would account for the discrepancy at $T=0$ if $K_{ij}\sim 1.8k$, a reasonable order of magnitude. Interactions of this kind are also not in disagreement with the low temperature magnetic specific heat results,[10] which show a variation close to that of an ideal Schottky anomaly, but with small systematic discrepancies. At temperatures above the peak the experimental values lie above the ideal Schottky curve, while at low temperatures the difference is in the opposite sense, and this is consistent with the general effect of interactions.[30]

In the above discussion we have neglected altogether the exchange effect on the U_2-type ions, but although this may be relatively quite large, its effect on the total susceptibility and specific heat will be unimportant since the contribution from these ions is small.

LOW TEMPERATURE VARIATION OF SUSCEPTIBILITY

We are now in a position to compare in more detail the experimentally observed variation of χ_M between 2° and 20°K with the theoretical model. When $kT\ll\Delta_2$, Δ_1' and Δ_2' Eq. (6) may be written as

$$\chi_M=\tfrac{1}{3}p\cdot 8N\beta^2/3k\cdot(1/\Delta_1)\{[1-\exp(-\Delta_1/T)]/[1+\exp(-\Delta_1/T)]\}+\alpha, \quad (7)$$

where the factor $p=0.844$ has been included to allow for the reduction in moment as discussed above. The estimated value of α, based on $\Delta_2=\Delta_1'=\Delta_2'\sim 300$°K is 0.0057 cgs units per mole. The factor $\frac{1}{3}$ allows for the abundance of the U_1 type ions, for which $\Delta_1=15.4$°K. With these assumptions, Eq. (7) is completely determined and may be compared with experimental values (see Fig. 5). It can be seen that the agreement is excellent, although it must be emphasized that the power susceptibility is not very sensitive to some specific details of the calculation. If the strength and

[30] J. H. Van Vleck, J. Chem. Phys. **5**, 320 (1937).

symmetry of the local crystalline field and its directions relative to the unit cell axes could be estimated more precisely from a determination of the fluorine positions, single crystal measurements could be compared with the calculated susceptibilities. Comparison of the principal values would then constitute a much more sensitive check on the theory. Of course, direct spectroscopic evidence for the crystal field splittings would also help to confirm the various assumptions. As it is, the main features of the magnetic and thermal properties can be accounted for by making a few simple assumptions, and a detailed fit can be obtained by including a few reasonable refinements.

ACKNOWLEDGMENT

We wish to thank Professor B. Bleaney for some stimulating discussions regarding the crystal field theory of the U^{4+} ion.

APPENDIX 1

Uranium Tetrafluoride Samples

H1.—No analyses are available for this sample, which was obtained from the Atomic Energy Research Establishment, Harwell, England. It was a very fine powder.

H2.—This sample also was a very fine powder and was obtained from Harwell. Chemical analyses showed about 2% UO_2F_2 and 0.35% carbon, and spectroscopic analyses showed the presence of the following elements, in parts per million: Al, 5; Ca, <2; Cr, 15; Cu, <5; Fe, 135; Mg, 2; Mn, 4; N, 25; Ni, 15; Si, 15; V, 5.

ANL2.—This was a portion of the purified sample used by Osborne, Westrum, and Lohr[9] for measurements of the heat capacity from 5° to 300°K. It had been prepared by two vacuum sublimations of uranium tetrafluoride manufactured by the Mallinckrodt Chemical Works and had been ground in a mortar to a fine powder. Chemical analyses showed 75.83±0.07% uranium (theoretical, 75.80%), 24.18±0.06% fluorine (theoretical, 24.20%) and 0.006±0.003% oxygen (corresponding to 0.05% UO_2F_2). It was handled and stored in an inert atmosphere until the time it was loaded into a container for the magnetic susceptibility measurements. Spectroscopic analyses, after removal from the specimen container, showed the presence of the following elements in parts per million: Al, 75; Ba, 0.5; Ca, 20; Cr, 3; Cu, 10; Fe, 10; Li, 0.4; Mg, 10; Mn, 1.5; Na, 10; Ni, 3; Pb, 2; Si, 20; Th, 40; Ti, 0.7; Zr, 15. The following elements, for which the limits of sensitivity in parts per million were as indicated by the numbers, were not detected: Ag, 1; As, 10; B, 0.1; Be, 0.01; Bi, 1; Ce, 2; Co, 5; Dy, 1; Er, 0.4; Eu, 0.1; Gd, 1; Ho, 1; K, 20; La, 0.4; Lu, 0.1; Mo, 20; Nd, 2; P, 50; Pr, 2; Pt, 100; Sb, 1; Sc, 0.1; Sn, 5; Sr, 1; Ta, 30; Tb, 2; Tm, 2; Y, 0.05; Zn, 50; Yb, 0.05.

ANL3.—This was part of the "granular" sample used by Burns, Osborne, and Westrum[10] for heat capacity measurements from 1.3° to 20°K. It had been prepared in the same way as ANL2, had been melted at about 1000°C in a platinum crucible in a helium atmosphere, and then had been gently broken into pieces larger than 1 mm in diameter. Chemical analyses showed 75.81% uranium (theoretical 75.80%), 24.18% fluorine (theoretical 24.20%) and 0.009% oxygen (corresponding to 0.09% UO_2F_2). The sample was handled and stored in an inert atmosphere. For the susceptibility measurements it was ground briefly in a mortar in an argon atmosphere and was then quickly loaded into a container. Spectroscopic analyses after removal from the specimen container indicated the following elements in parts per million: Al, 10; Ba, 0.2; Cr, 0.8; Cu, 6; Li, 0.1; Mg, 5; Mn, 0.1; Mo, 40; Ni, 1; Si, 30; Zr, 2. The following elements, for which the limits of detection were as indicated (in parts per million) were not detected: Ag, 1; As, 10; B, 0.1; Be, 0.01; Bi, 1; Ca, 20; Ce, 2; Co, 5; Dy, 1; Er, 0.4; Eu, 0.1; Fe, 2; Gd, 1; Ho, 1; K, 20; La, 0.4; Lu, 0.1; Na, 10; Nd, 2; P, 50; Pb, 1; Pr, 2; Pt, 1000; Sb, 1; Sc, 0.1; Sn, 5; Sr, 1; Ta, 2000; Tb, 2; Th, 2; Ti, 0.5; Tm, 2; Y, 0.05; Yb, 0.05; Zn, 50.

ANL4.—This was a fine powder from the same stock used for the preparation of ANL3. No analyses are available, but presumably it contained about 2% UO_2F_2 and was otherwise very pure.

APPENDIX 2

Melting Process

UF_4 reacts very readily at elevated temperatures with water vapor and oxygen, and great care was therefore taken to devise a process of melting the specimens which would avoid the possibility of contamination by the atmosphere.

The specimen was placed in a platinum tube 5 mm i.d., 0.5 mm wall, 20 cm long, crimped and fused shut at one end and connected through a soft-glass seal at the other end to a vacuum system. The specimen was pumped to a high vacuum for 24–28 hr at room temperature before slowly raising the temperature by slipping a tube furnace over the platinum tube. Pumping on the specimen was maintained to a temperature of 850°C to ensure the removal of any volatile compounds, and pure helium gas was then admitted to 1 atm pressure to prevent sublimation near the melting point. The temperature was held at 1030°C (mp 960°C) for one hour and then lowered quite rapidly (4 hr to room temperature). The final product was found to be a hard, dark green polycrystalline glassy mass, very similar in appearance to ANL3.

Role of Exchange Energy in Intermediate-Range Interactions*

FRANK O. ELLISON

Department of Chemistry, Carnegie Institute of Technology, Pittsburgh 13, Pennsylvania

(Received August 26, 1960)

Computations have been made of the Coulomb and exchange parts of the interaction energies of a proton with a hydrogen atom and of two hydrogen atoms. It is found that the exchange energy becomes a *more* important and Coulomb energy becomes a *less* important fraction of the first-order interactions (i.e., interaction of ground-state atoms with no configuration interaction) as the internuclear distance is increased. It is also shown that the first-order contribution is necessary to bring the perturbation calculations of Coulson on H_2^+ and of Löwdin and Hirschfelder on H_2 into good agreement with experiment for intermediate separations.

INTRODUCTION

DETERMINATIONS and discussions of forces between chemical species can often be placed in one of three categories depending upon the separations considered: short range, intermediate range, or long range. Long-range force studies are nearly always characterized by the assumption that exchange forces are negligible. Justification of this supposition customarily rests upon the statement that Coulomb interactions depend upon inverse powers of the separation, while exchange forces diminish in an exponential manner with increasing distance. The dividing line between intermediate and long ranges can be defined as the minimum separation at which this assumption allows results that are correct to some prescribed accuracy. It is the purpose of this paper to bring together in one place results of some theoretical calculations on the two simplest examples of interaction, with explicit attention being devoted to the role of exchange energy at intermediate up to the lower limit of long-range separations.

The importance of exchange energy in this context was suggested long ago by Pauling[1]; more recent studies of the proton-hydrogen atom interaction[2] has led Roe[3] to the same conclusions.

INTERACTION OF A PROTON WITH A HYDROGEN ATOM

Let us consider a most general wave function for the hydrogen molecule-ion, namely,

$$\psi_N=\alpha_N+\beta_N, \tag{1}$$

where

$$\alpha_N=\sum_{n=1}^{N}c_n a_n, \qquad \beta_N=\sum_{n=1}^{N}c_n b_n, \tag{2}$$

in which the c_n are linear variational coefficients, a_n and b_n denote Slater-type atomic orbitals[4] centered on nuclei a and b, respectively, having principal quantum number n, azimuthal quantum number $n-1$, magnetic quantum number zero, and each having a common orbital exponent ζ (e.g., $a_1=1s_a$, $b_3=3dz^2{}_b$, etc.).[5] The number N of such basis functions could be extended to yield a potential energy curve having any desired accuracy for a given range of internuclear distance.

The expectation value of the total molecular energy for nuclei fixed at distance R is given by

$$E_N=(H_{\alpha\alpha}+H_{\beta\alpha})/(S_{\alpha\alpha}+S_{\beta\alpha}), \tag{3}$$

where

$$H_{fg}=\int f_N H g_N d\tau \quad \text{and} \quad S_{fg}=\int f_N g_N d\tau.$$

If one were to neglect exchange and overlap effects in calculating the energy, this would simplify to $E_C=H_{aa}/S_{aa}$. Equation (3) can be rewritten

$$E_N-E_H=(E_C-E_H)+X=C+X, \tag{4}$$

where E_H is the ground-state energy of a hydrogen atom, $X=(H_{\beta\alpha}-E_C S_{\beta\alpha})/(S_{\alpha\alpha}+S_{\beta\alpha})$ is the exchange contribution and C is the Coulomb contribution to the interaction energy E_N-E_H.

In order to assess the relative importance of C and X in the interaction energy, calculations have been carried out for $N=1$ and $N=2$, each with $\zeta=1$ and with variable ζ.[6] These interaction energies are listed in Table I, together with the best possible theoretical results of Bates, *et al.*[7] Eq. (1) can be written

$$\psi_N=\sum_{n=1}^{N}c_n(a_n+b_n) \tag{5}$$

$$=\sum_{n=1}^{N}h_n N_n(a_n+b_n), \tag{6}$$

* Supported in part by a research grant from the National Science Foundation.

[1] L. Pauling, Chem. Revs. **5**, 173 (1928).

[2] See, for example, F. C. Brooks, Phys. Rev. **86**, 92 (1952).

[3] G. M. Roe, Phys. Rev. **88**, 659 (1952).

[4] R. S. Mulliken, Revs. Modern Phys. **32**, 232 (1960).

[5] Such a set of orbitals on one center form a complete set for this problem, and are identical with those used by J. O. Hirschfelder and P. O. Löwdin, Mol. Phys. **2**, 229 (1959) and by P. O. Löwdin and H. Shull, Phys. Rev. **101**, 1730 (1956).

[6] These calculations will be recognized as those originally done by B. Finkelstein and G. Horowitz, Z. Physik **48**, 118 (1928) and by B. Dickenson, J. Chem. Phys. **1**, 317 (1933).

[7] D. R. Bates, K. Ledsham, and A. L. Stewart, Phil. Trans. Roy. Soc. (London) **246**, 215 (1953).

TABLE I. Interaction energies for the hydrogen molecule-ion.[a]

R	E_1-E_H $\zeta=1$	E_1-E_H ζ variable	E_2-E_H $\zeta=1$	E_2-E_H ζ variable	$E-E_H$ Expt[b]
0.5	1.07865	0.76824	1.04014	0.76618	
1.0	0.21164	0.05900	0.18824	0.05081	0.04822
1.5	0.00499	−0.06712	−0.01069	−0.07931	
1.9		−0.08596		−0.09921	
2.0	−0.05377	−0.08651	−0.06591	−0.09980	−0.10263
2.1		−0.08610		−0.09938	
2.4	−0.06454		−0.07523		−0.09654
2.5	−0.06483	−0.07876	−0.07525	−0.09142	
2.6	−0.06450		−0.07468		−0.09083
3.0	−0.05908	−0.06445	−0.06841	−0.07563	−0.07756
3.5	−0.04817	−0.04996	−0.05644	−0.05936	
4.0	−0.03687	−0.03733	−0.04393	−0.04494	−0.04608
5.0	−0.01920	−0.01921	−0.02368	−0.02372	−0.02442
6.0	−0.00907	−0.00908	−0.01151	−0.01152	−0.01196
7.0	−0.00404	−0.00405	−0.00529	−0.00531	−0.00559
8.0	−0.00173	−0.00173	−0.00239	−0.00240	−0.00257
9.0	−0.00072	−0.00072	−0.00110	−0.00110	−0.00120
10.0	−0.00030	−0.00030	−0.00052	−0.00052	−[0.00059]

[a] Distances R expressed in atomic units, 1 a.u. = 0.5292 A; energies in Hartree units, 1 h.u. = 27.210 ev.
[b] From reference 7; value in brackets is extrapolated.

where N_n is a factor that normalizes the function a_n+b_n. The variational coefficients h_n, as well as the best values of the orbital exponents ζ are displayed in Table II.

Inspection of Table I shows that the interaction energies for $R\geq 5$ a.u. are not improved significantly by variation of the oribital exponent ζ. For these separations, E_2-E_H differs from experiment by less than 0.02 ev or $\frac{1}{2}$ kcal.

Table III lists the Coulomb energy C and exchange energy X calculated using $\zeta=1$ in the functions ψ_1 and ψ_2. It is noted that the exchange energy is greater than the Coulomb energy for all internuclear distances less than at least 10 a.u. In fact, when considering the simplest function ψ_1, which yields the *first-order* contribution, it is perfectly valid to assume that only exchange forces significantly contribute to the interaction for $R>4$ a.u.

A better understanding of the relative importance of exchange and Coulomb energy at large separations is possible by expressing the interaction energy in a form somewhat different from that done in Eqs. (3) and (4), namely,

$$E-E_H=\sum_{n=1}^{N}\sum_{m=1}^{N}c_m c_n(J_{mn}+K_{mn}), \qquad (7)$$

where

$$J_{mn}=\int a_m H_n' a_n dv, \quad K_{mn}=\int b_m H_n' a_n dv,$$

and

$$H_n'=(n-1)/r_a-1/r_b+1/R.$$

The derivation of Eq. (7) is given in the Appendix. The J_{mn} and K_{mn} are Coulomb and exchange integrals, respectively. Calculations show that the coefficient c_1 increases and the coefficients c_n, $n>1$, decrease monotonically with increasing R. Furthermore, the products c_n^2 and c_1c_n, $n>1$, both decrease with increasing R (Plotting their natural logarithms against R yields nearly straight lines for $N=2$, indicating that they are falling off exponentially with R).

The very first term in Eq. (7), $c_1^2(J_{11}+K_{11})$, can be called the first-order interaction energy; in conventional perturbation analyses of long-range interaction this part is often neglected. Here it is seen from Table I that $J_{11}+K_{11}$ constitutes roughly 75 and 50% of the experimental interaction energy at R equal 3 and 10, respectively. As pointed out above, a very good approximation of this first-order part for $R>4$ is secured by neglecting the Coulomb part J_{11} and retaining only the exchange term K_{11}. It is easy to show by referring to

TABLE II. Best variational parameters for H_2^+ wave functions.

	Orbital exponents[a]		Linear variational coefficients[b]			
R	I	II	I	II	III	IV
0.5	1.7781	1.7620	0.8519	0.2216	0.9785	0.0342
1.0	1.5391	1.5283	0.8859	0.1712	0538	0.0771
1.5	1.3625	1.3682	0.9088	0.1460	0.9400	0.1067
1.9	1.2598	1.2746			0.9354	0.1216
2.0	1.2385	1.2543	0.9226	0.1340	0.9350	0.1242
2.1	1.2193	1.2359			0.9348	0.1266
2.5	1.1547	1.1738	0.9319	0.1295	0.9350	0.1243
3.0	1.0953	1.1141	0.9400	0.1275	0.9360	0.1328
3.5	1.0555	1.0725	0.9484	0.1246	0.9416	0.1314
4.0	1.0286	1.0422	0.9576	0.1190	0.9538	0.1223
5.0	1.0031	1.0090	0.9754	0.0990	0.9757	0.0994
6.0	0.9961	0.9971	0.9881	0.0741	0.9880	0.0742
7.0	0.9961	0.9954	0.9949	0.0529	0.9948	0.0530
8.0	0.9977	0.9961	0.9978	0.0379	0.9978	0.0380
9.0	0.9992	0.9974	0.9991	0.0280	0.9990	0.0281
10.0	1.0000	0.9990	0.9996	0.0216	0.9996	0.0216

[a] Column I lists best ζ in ψ_1; column II lists best ζ in ψ_2.
[b] Columns I and II list best h_1 and h_2, respectively, in ψ_2 using $\zeta=1$; columns III and IV list best h_1 and h_2, respectively, in ψ_2 using best possible values of ζ.

formulas for the basic integrals[8] that make up J_{11} and K_{11} that the former varies like $\exp(-2R)$ while the latter decreases more slowly like $\exp(-R)$.

For $n>1$, it can be shown that the terms J_{1n} and K_{1n} are both negative (and hence contribute to binding), that $|J_{1n}|$ varies like R^{-n} and $|K_{1n}|$ like $\exp(-R)$. For large R, K_{1n} could probably be neglected. In Eq. (7), these are both multiplied by $c\,c_n$, which in turn decrease in approximately exponential ways with increasing R. This second-order part becomes a more significant fraction of the experimental interaction energy as R increases.

Integrals of the type $J_{nn}+K_{nn}$, $n>1$, appearing in Eq. (7) are always positive, and hence tend to lessen the interaction energy. Finally, terms of the type $c_nc_m(J_{mn}+K_{mn})$, $m>n>1$, are probably of little chemical significance since the coefficient products c_nc_m are very small.

INTERACTION OF TWO HYDROGEN ATOMS

In this study the Heitler-London and Wang calculations were repeated and analyzed for a large range of internuclear distances. The wave functions are, of course,

$$\psi=a_1(1)b_1(2)+a_1(2)b_1(1), \tag{8}$$

in which for the Heitler-London treatment the orbital exponents ζ are unity, while for the Wang treatment ζ is a variational parameter. The resulting interaction energies and best values of ζ are given in Table IV. Also listed are the "experimental" values found by interpolating Rydberg's and Beutler's analysis of the first ten vibrational levels of molecular hydrogen.[9]

In the same general way that Eq. (4) was derived for H_2^+, the interaction energy of two hydrogen atoms can be expressed as the sum of Coulomb and exchange energies[10]

$$E-2E_H=C+X, \tag{9}$$

where

$$C=H_{11}-2E_H$$
$$X=(H_{12}-S^2H_{11})/(1+S^2), \tag{10}$$

in which

$$H_{11}=\int a_1(1)b_1(2)Ha_1(1)b_1(2)dv_1dv_2$$
$$H_{12}=\int a_1(1)b_1(2)Ha_1(2)b_1(1)dv_1dv_2. \tag{11}$$

The values of C and X calculated for the Heitler-London function are given in Table IV. The exchange contribution exceeds the Coulomb contribution for all values of the internuclear distance considered.

DISCUSSION

In considering the hydrogen molecule-ion, it was shown that the *first-order* interaction of the proton with H constitutes a significant part of the energy at all distances less than 10 a.u. Furthermore, since the Coulombic part of the *first-order* term decays like $\exp(-2R)$ while the exchange part varies like $\exp(-R)$, the former can be neglected for $R>4$ a.u.

TABLE III. Coulomb and exchange energies for H_2^+.[a]

	Using w.f. ψ_1		Using w.f. ψ_2	
R	$-C$	$-X$	$-C$	$-X$
3	0.00331	0.06239	0.01496	0.05345
4	0.00042	0.03729	0.00724	0.03669
5	0.00005	0.01925	0.00317	0.02051
6	0.00001	0.00908	0.00150	0.01001
7	0.00000	0.00404	0.00081	0.00448
8	0.00000	0.00173	0.00048	0.00191
9	0.00000	0.00072	0.00030	0.00080
10	0.00000	0.00030	0.00020	0.00032

[a] See reference a, Table I.

[8] C. C. J. Roothaan, J. Chem. Phys. **19**, 1445 (1951).

[9] See J. O. Hirschfelder, C. F. Curtiss and R. B. Bird, *Molecular Theory of Gases and Liquids* (John Wiley & Sons, Inc., New York, 1954), p. 1060.

[10] See S. Fraga and R. S. Mulliken, Revs. Modern Phys. **32**, 254 (1960).

TABLE IV. Results of calculations on the hydrogen molecule.[a]

R	$E-E_H$ H.L.	$E-E_H$ Wang	ζ Wang	$-(E-E_H)$ Expt[b]	C H.L.	X H.L.
0.5	0.76841	0.51120	1.4937			
1.0	0.00358	−0.08895	1.2859	0.121		
1.3	−0.09254	−0.13656	1.1944	0.170		
1.35		−0.13834	1.1816	0.173		
1.4	−0.10547	−0.13905	1.1699	0.1742	−0.00227	−0.10320
1.45		−0.13887	1.1579			
1.5	−0.11272	−0.13796	1.1467	0.173		
1.65	−0.11596					
2.0	−0.10355	−0.10804	1.0620	0.140		
3.0	−0.04167	−0.04170	0.9951	0.056	−0.00692	−0.03475
4.0	−0.01129	−0.01136	0.9914	0.016[c]	−0.00161	−0.00968
5.0	−0.00252	−0.00253	0.9966		−0.00032	−0.00220
6.0	−0.00051	−0.00051	0.9994		−0.00006	−0.00045
7.0	−0.00010	−0.00010	0.9995		−0.00001	−0.00009
8.0	−0.00002	−0.00002	0.9998		−0.00000	−0.00002
9.0	−0.00000	−0.00000	0.9999		−0.00000	−0.00000

[a] See reference a, Table I.
[b] From reference 9.
[c] Extrapolated.

Coulson[11] applied perturbation theory to the H_2^+ problem, deriving a formula for the interaction which he contended to be exact for $R \geq 6$ only, since exchange was neglected. Values calculated from his formula are displayed in Table V. In order to partially account for the neglected exchange, we have added to Coulson's results the exact first-order contribution (from column 2 of Table I)[12]; it is noteworthy that the values thus corrected compare quite well with experiment.

In the Heitler-London treatment of H_2, it can be shown, by referring to the basic integrals[13] that make up C and X, that C behaves asymptotically like $R^2 \exp(-2R)$ while X varies like $R^3 \exp(-2R)$. Thus X gains in relative importance over C as R increases.

Löwdin and Hirschfelder[5] have recently published calculations on the long-range H—H interaction, in which exchange was entirely neglected. In Table VI, we have listed their values, together with the results of adding to them the full amount[12] of first-order interaction. These sums are seen to compare relatively well with the Hirschfelder-Linnett and Pauling-Beach calculations.[14]

Fraga and Mulliken[10] have recently shown how Coulomb energy might well play a much more important role in the valence-bond theory of chemical binding than heretofore recognized; applications of this method have often neglected the Coulomb contribution completely. Conversely, in long-range studies, the practice has often been to ignore the first-order exchange energy, which has been shown here to be of significance for separations less than $10a_0$ for H_2^+ and less than $8a_0$ for H_2.

APPENDIX

Using the wave function as expressed by Eq. (5), the total molecular energy for fixed nuclei takes the following form,

$$E=\sum_n\sum_m c_n c_m\left[\int a_m H a_n d\tau+\int b_m H a_n d\tau\right]/(\Delta_1+\Delta_2), \quad \text{(A1)}$$

where

$$\Delta_1=\sum_n\sum_m c_n c_m \delta_{nm} \quad \text{and} \quad \Delta_2=\sum_n\sum_m c_n c_m S_{nm'},$$

[11] C. A. Coulson, Proc. Roy. Soc. Edinburgh **A61**, 2D (1941); See also reference 9, p. 1009.
[12] The first-order contribution would actually be reduced, probably by about 10 to 15%, because of the coefficient C_1^2 present in a complete treatment.
[13] K. S. Pitzer, *Quantum Chemistry* (Prentice-Hall, Inc., Englewood Cliffs, New Jersey, 1953), p. 420.
[14] J. O. Hirschfelder and J. W. Linnett, J. Chem. Phys. **18**, 130 (1950); L. Pauling and J. Y. Beach, Phys. Rev. **47**, 686 (1935). (In reference 5 it is noted that the Pauling-Beach results, especially the R^{-8} term, are probably in error.)

TABLE V. Interaction energies for H_2^+ from amended perturbation theory.[a]

R	Perturbation theory[b]	First-order interaction	Sum	Exptl[c]
5	−0.01040	−0.01920	−0.02960	−0.02442
6	−0.00234	−0.00907	−0.01141	−0.01196
8	−0.00062	−0.00173	−0.00235	−0.00257
10	−0.00024	−0.00030	−0.00054	−0.00059

[a] See reference a, Table I.
[b] Calculated from Eq. (13) in reference 11.
[c] From Table I.

in which $S_{nm}'=\int b_m a_n dv$. The Hamiltonian operator H can be split into two parts, $H=H_n^0+H_n'$, in which

$$H_n^0=-\tfrac{1}{2}\nabla^2-n/r_a \tag{A2}$$

$$H_n'=(n-1)/r_a-1/r_b+1/R, \tag{A3}$$

where $H_n^0 a_n=E_H a_n$, E_H being the ground-state energy of the hydrogen atom. The interaction energy can then be written

$$E-E_H=\sum_n\sum_m c_n c_m(J_{mn}+K_{mn})/(\Delta_1+\Delta_2), \tag{A4}$$

in which the J_{mn} and K_{mn} are defined just following Eq. (7) above. Eq. (A4) would become

$$E-E_H=\sum_n\sum_m c_n c_m J_{mn}/\Delta_1=C \tag{A5}$$

if one were to neglect all overlap and exchange effects.

TABLE VI. Interaction energies for H_2 from amended perturbation theory.[a]

R	Perturbation theory[b]	First-order interaction[c]	Sum	H.L. and P.B.[d]
5	0.000787	0.00252	0.00331	0.00296
6	0.000236	0.00051	0.00075	0.00064
7	0.000080	0.00010	0.00018	0.00015
8	0.000033	0.00002	0.00005	0.00004
9	0.000016	0.00000	0.00002	0.00002
10	0.000008	0.00000	0.00001	0.00001

[a] See reference a, Table I.
[b] Calculated from equation in abstract of reference 5.
[c] From column 2 of Table IV.
[d] From reference 9.

Suppose that for each internuclear distance, the coefficients c_n are chosen so that $\Delta_1+\Delta_2=1$. Then Eq. (A4) can be written

$$E-E_H=\sum_n\sum_m c_n c_m(J_{mn}+K_{mn}). \tag{A6}$$

Equation (7) is thus proved. Furthermore, the Coulomb energy C [Eq. (A5)] becomes

$$C=\sum_n\sum_m c_n c_m J_{mn}/(1-\Delta_2)\simeq\sum_n\sum_m c_n c_m J_{nm}, \tag{A7}$$

since, for large distances $\Delta_2<1$ (inasmuch as all S_{mn}' are small compared with 1, and hence $(1-\Delta_2)^{-1}\simeq 1+\Delta_2\simeq 1$. Subtracting C from Eq. (A6) gives the exchange contribution $X\simeq\sum_n\sum_m c_n c_m K_{mn}$.

"Floating" Hydrogen Densities in Some Molecules of the Type XH_n

K. E. BANYARD

Department of Physics, The University of Leicester, Leicester, England

(Received October 13, 1960)

The model of "floating" hydrogen densities was suggested initially by McDonald in an analysis of the electron density for NH_4^+. The model, as used here, is an attempt to represent the molecular radial distribution as a superposition of the radial densities obtained from the "best" electronic wave functions (in the sense of the variation method) for the constituent atoms, the centers of the unperturbed hydrogen distributions being allowed to "float" inward along the bonds. The model was applied to H_2O and CH_4 and the molecular and bond dipole moments were calculated. Thus for H_2O, which alone possesses a resultant moment, some insight could be obtained into the accuracy of the angular dependence of the density pref dicted by such a model. Comments were also made on NH_4^+ and NH_3. Further, the application of an approximate formula of Carter enabled a determination to be made of the paramagnetic contribution to the molar diamagnetic susceptibility.

INTRODUCTION

RECENT experimental work of McDonald[1] has suggested a model for the electron distribution in the ammonium ion in which a spherical, but electron deficient, central atom is surrounded by four unperturbed hydrogen electron clouds, centered, however, inside the protons. Banyard and March[2] have shown that the above model is in keeping with a self-consistent radial electron distribution obtained earlier by Bernal and Massey.[3] As was pointed out in the work cited in reference 2, however, a more stringent test of McDonald's model should reside in the angularity it predicts for the electron distribution.

Although no suitable theoretical distribution, with angular terms included, is available at present for NH_4^+, it seemed that further insight into the model of "floating" hydrogen densities might be obtained by a study of H_2O. This seemed a particularly appropriate choice since evidence from the x-ray scattering factor[4] and the diamagnetic susceptibility[5] indicates that the radial density distribution is now known to some accuracy. A comparison of the dipole moment, found from the model of "floating" hydrogen densities, with experiment should then help to throw light on the validity of the angular dependence of the density given by such a scheme.

In view of the results obtained for H_2O, together with those deduced for NH_4^+, it seemed of interest to apply a similar procedure to CH_4, for which a fairly suitable radial density also exists.

ANALYSIS OF THE RADIAL DENSITY DISTRIBUTION

The radial density resulting from the ten-electron Roothaan treatment of H_2O by Ellison and Shull[6] was obtained by Banyard and March[4] and is shown in curve (a) of Fig. 1. The radial density distribution is such that when integrated with respect to the radial distance r it will yield the total number of electrons within the system, namely, ten for the case of H_2O. In accordance with the general model of "floating" densities, an attempt will be made to express this radial distribution as a superposition of the "best" unperturbed radially symmetric oxygen density, centered on its nucleus, along with the density of two unperturbed hydrogen atoms, the distance of their centers of distribution from the oxygen nucleus being regarded as a variable parameter yet to be determined.

At present the "best" atomic oxygen density, in the sense of the variation method, is provided by the Hartree-Fock treatment,[7] see curve (b) of Fig. 1. Subtraction of this radial density from curve (a) leads to the distribution shown by curve (c) of Fig. 1, this will now be compared with the spherical density given by two "floating" unperturbed hydrogen atoms after averaging over angles about the oxygen nucleus as the new origin.

However, owing to the Hartree-Fock oxygen density being somewhat more concentrated in the region of the origin than the molecular density, it is seen that curve (c) becomes negative. Such a result may arise, in part, from the fact that the Slater atomic orbitals used for oxygen in the Roothaan treatment of H_2O do not possess (as is well known) the flexibility of Hartree-Fock functions. Hence, in this case, it was thought to be physically more reasonable to attempt a fit to curve (c) in the outer regions of the molecule, say $r > 1.81$ a.u. (i.e., the O—H bond length expressed in atomic units), where it might be expected that the "hydrogen densities" will be predominant.

The radial electron density distribution $D_{nH}(r) = 4\pi r^2 \rho(r)$ obtained by averaging n normalized hydrogen

[1] T. R. R. McDonald, Acta Cryst. **13**, 113 (1960).
[2] K. E. Banyard and N. H. March, Acta Cryst. **14**, 357 (1961).
[3] M. J. M. Bernal and H. S. W. Massey. Monthly Notices Roy. Astron. Soc. **114**, 172 (1954).
[4] K. E. Banyard and N. H. March, J. Chem. Phys. **26**, 1416 (1957).
[5] K. E. Banyard, J. Chem. Phys. **33**, 832 (1960).
[6] F. O. Ellison and H. Shull, J. Chem. Phys. **23**, 2348 (1955); **21**, 1420 (1953).
[7] D. R. Hartree, W. Hartree, and B. Swirles, Phil. Trans. Roy. Soc. **238A**, 240 (1940).

atom densities, each of the form[8]

$$P(r_h)=\pi^{-1}Z^3\exp(-2Zr_h),$$

about a new origin, located at a distance r_0 from each of the original centers of distribution, may be derived in closed form by using

$$\rho(r)=(n/2rr_0)\int_{|r-r_0|}^{(r_0+r)}P(r_h)\cdot r_h\cdot dr_h.$$

In the above, r_h is the radial distance from a hydrogen nucleus and for the case of unperturbed hydrogen densities then $Z=1$. Thus, it can be readily shown that

$$D_{nH}(r)=Z(nr/2r_0)[\exp(-2Z|r-r_0|)\cdot\{1+2Z|r-r_0|\}$$
$$-\exp[-2Z(r+r_0)]\cdot\{1+2Z(r+r_0)\}], \qquad (1)$$

where

$$\int_0^\infty D_{nH}(r)dr=n.$$

Use of Eq. (1) for unperturbed hydrogens reveals that for $n=2$ and $r_0=1.0$ (see the broken curve of Fig. 1) an almost perfect fit is obtained, to within graphical accuracy, with the extracted curve (c) over the region $r>1.8$. A better fit with the peak of curve (c) may be obtained at the expense of the agreement in the outer region by relaxing the condition that $Z=1$ for the hydrogens and choosing for $n=2$, values of $r_0=0.9$ and $Z=1.1$, see the ringed dots of Fig. 1.[9]

For CH_4 we used the Hartree-Fock radial electron density of Mills[10] which, to within a first approximation, allows for the influence on the radial density of the first few angular components with the symmetry of the molecule; see curve (a) of Fig. 2. Subtracting from this curve the "best" radial density for atomic carbon,[11] see curve (b) of Fig. 2, leads to the extracted density distribution for the four "hydrogen electrons" shown in curve (c), a small region of negative density occuring once again near the origin. For the region $r>2$ a.u. (i.e., the C—H bond length), the best fit to curve (c) obtained by using Eq. (1), with $n=4$ and $Z=1$, is given by choosing an r_0 of between 1.6 and 1.7; see, respectively, the broken line curve and that indicated by crosses in Fig. 2. Allowing for the relaxation of $Z=1$ a slightly better fit in the outer region may be obtained, to within graphical accuracy, by choosing $r_0=1.7$ and $Z=1.1$, see the ringed dot curve of Fig. 2.

DISCUSSION OF RESULTS

The excellent agreement for H_2O between curve (c) of Fig. 1 and the $r_0=1.0$ unperturbed hydrogen curve, in the region $r>1.8$, indicates that only a fairly small error may exist in the present choice of r_0, say ± 0.03. Thus, the centers of the unperturbed "floating" hydrogen distributions are located along the bonds at a distance of 0.55 ± 0.02 of the O—H separation.

For CH_4, with r_0 ranging from 1.6 to 1.7, the centers of distribution of the unperturbed hydrogen densities are located tetrahedrally at a distance of 0.83 ± 0.03 of the bond length from the carbon nucleus. This result is in good agreement with the theoretical value of Tomiie[12] (i.e., 0.86 of the experimental bond length) obtained by an alternative analysis for the C—H bond within crystals. Our result also compares quite favorably with the measured values which are quoted in Table I of Tomiie.

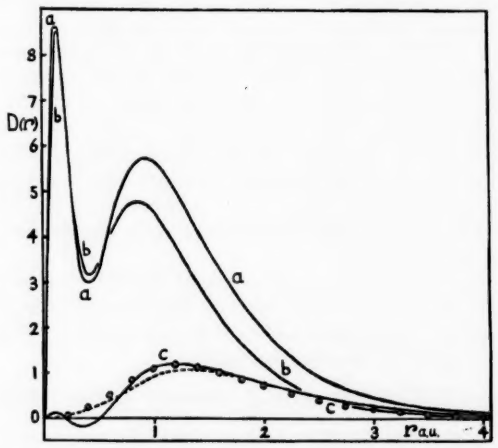

FIG. 1. Analysis for H_2O. Curve (a): Radial density for H_2O from Ellison and Shull. Curve (b): Hartree-Fock density for O atom. Curve (c): Density obtained by subtracting curve (b) from curve (a). Hydrogen distributions for $n=2$ are shown by: – – – for $r_0=1.0$ and $Z=1.0$ and ⊙⊙⊙ for $r_0=0.9$ and $Z=1.1$.

[8] All equations are expressed in atomic units which were used throughout this work.

[9] A possible alternative analysis for H_2O is as follows: The oxygen density given by the Slater orbitals used in the work cited in reference 6 was subtracted from the corresponding molecular radial electron density. The resulting extracted hydrogen distribution was now found to possess no regions of negative density. This curve was best fitted in the outer region, using the unperturbed form of Eq. (1) with $n=2$, by choosing a value of $r_0=1.5$. However, the best fit over the region of the maximum was given by $r_0=1.6$ and $Z=1.1$. In each case the discrepancy between the extracted and the theoretical curves was quite small.

However, owing to the superiority of the Hartree-Fock functions over those of Slater, it is felt that, on the whole, the representation of the molecular radial density shown in Fig. 1, when expressed as a superposition of the "best" constituent atomic densities, will be more satisfactory than that indicated in the preceding paragraph.

[10] The results of I. M. Mills, Mol. Phys. **1**, 99 (1958), although now considered to be somewhat approximate [see A. F. Saturno and R. G. Parr, J. Chem. Phys. **33**, 22 (1960)], are still thought to provide, in a very convenient form, a fairly reasonable first-order representation of the radial electron density distribution within CH_4. Other wave functions for CH_4, which for our purposes are presented in a less convenient form, have been given recently by S. Koide, H. Sekiyama, and T. Nagashima, J. Phys. Soc. Japan **12**, 1016 (1957); R. K. Nesbet, J. Chem. Phys. **32**, 1114 (1960) and A. F. Saturno and R. G. Parr, *ibid.* **33**, 22 (1960).

[11] See the Hartree-Fock treatment of A. Jucys, Proc. Roy. Soc. (London) **A173**, 64 (1939).

[12] Y. Tomiie, J. Phys. Soc. Japan **13**, 1030 (1958).

The dipole moment resulting from this density representation may be calculated in a straightforward manner. For H_2O, we obtain a result of $2.5\pm0.1D$[13] compared with the experimental value of $1.84D$;[14] the dipole moment arising from the Roothaan treatment of Ellison and Shull was $1.51D$, all values being in the sense $H_2^+O^-$. Our result, although not good, is by no means displeasing when one considers the approximate nature of our model and the sensitivity of the quantity in question with respect to the electron distribution.

For the C—H bond in CH_4, a dipole moment of $0.9\pm0.1D$ in the C^-—H^+ sense is obtained. From such a model, it is therefore not surprising that, for this rather difficult C—H example, the result is unsatisfactory when compared with the usually accepted bond moment within methane of $0.3\sim0.4D$,[15] the sense being in the reverse direction, i.e., C^+—H^-. It is seen from the table that for NH_4^+ the analysis of Banyard and March[2] provides a bond dipole moment which agrees quite well with the generally accepted value.[15]

An interesting feature of this atomic superposition representation of the molecular radial density is that it now enables us to use the approximate formula of Carter[16] for the evaluation of χ[17] the molar diamagnetic susceptibility. He showed that, for a similar model, it was possible to express χ for CH_4, for example, as

$$\chi=-0.7923\{\sum_{\text{all electrons}}\langle r_i^2\rangle_{\text{At}}-4R^2\}, \qquad (2)$$

where the first term is the well-known purely diamagnetic contribution, χ_r[18] to the total susceptibility. The second term corresponds to a paramagnetic contribution to χ and may be expressed as

$$\chi_p=+0.7923nR^2, \qquad (3)$$

where R is the distance from the origin (i.e., the "central" atom of the molecule which in this case is the carbon atom) to the centers of the n unperturbed hydrogen distributions.

Use of Eq. (3) together with the present results for $R=r_0$ for CH_4, H_2O, and NH_4^+[19] enabled χ_p to be compared with the "experimental" paramagnetic contribution $\chi_{h.f.}$ quoted in the work cited in reference 5 and based on values given by Weltner[20] derived from

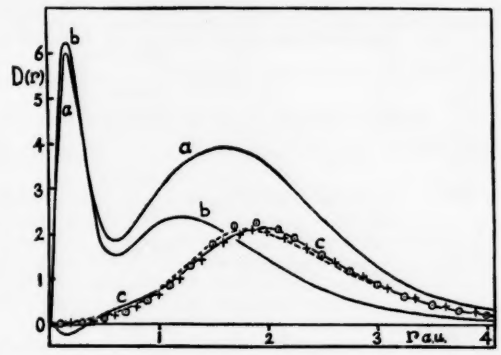

FIG. 2. Analysis for CH_4. Curve (a): Radial density with angular term allowance for CH_4 from Mills. Curve (b): Hartree-Fock density for C atom. Curve (c): Density obtained by subtracting curve (b) from curve (a). Hydrogen distributions for $n=4$ are shown by: − − − for $r_0=1.6$ and $Z=1.0$, +++ for $r_0=1.7$ and $Z=1.0$, and ⊙⊙⊙ for $r_0=1.7$ and $Z=1.1$.

observations of the molecular rotational magnetic moment. The results for χ_p and $\chi_{h.f.}$ are recorded in Table I; also tabulated are the "experimental" values of r_0 required in Eq. (3) to reproduce $\chi_{h.f.}$. It is to be noted that all contributions to the molar diamagnetic susceptibility quoted here are expressed with respect to the center of mass of the molecule as the origin, while for convenience all values of r_0, both theoretical and "experimental," are referred to the "central" atomic nucleus as origin.

From the table it is seen that the agreement between the "experimental" and theoretical values for r_0 is quite pleasing. Thus, it would seem not unreasonable to suggest that for some molecules of the type XH_n a useful first approximation might be obtained for the radial electron density from a knowledge of the experimental molecular rotational magnetic moment. Such an observation would enable $\chi_{h.f.}$ to be determined[21] and a corresponding value of r_0 could then be found by using Eq. (3). The superposition of the radial distribution of the n unperturbed hydrogen densities, centered along the bonds at a distance of r_0 from the X-atomic nucleus, along with the "best" radial density for the X atom would then yield the molecular radial distribution. It is felt that such a density might well provide a reasonable starting point for a subsequent Hartree-Fock treatment.

Contained in the table are the "experimental" values of $\chi_{h.f.}$ and the equivalent r_0 for NH_3. The dipole moment obtained by using, in this case only, the "experimental" r_0 gives $1.54D$ which is somewhat in excess of the observed value of $1.48D$,[14] both results are in the sense $N^-H_3^+$. A theoretical r_0 is obtainable by applying the present analysis to the radial electron density distribution arising from the Roothaan treat-

[13] Dipole moments are expressed in Debye units (D). The physical dimensions for H_2O and NH_3 are taken from K. E. Banyard and N. H. March, Acta Cryst. **9**, 385 (1956).

[14] G. W. C. Kaye and T. H. Laby, *Tables of Physical and Chemical Constants* (Longman's Green and Company, Inc., New York, 1958).

[15] J. W. Smith, *Electric Dipole Moments* (Butterworths Scientific Publications, London, 1955), pp. 120–125.

[16] C. Carter, Proc. Roy. Soc. (London) **A235**, 321 (1956).

[17] All values of χ, χ_r, χ_p, and $\chi_{h.f.}$ are expressed in terms of 10^{-6} emu/mole.

[18] The evaluation of χ_r for these molecules is discussed in the work cited in reference 5.

[19] The results for NH_4^+ obtained in the work cited in reference 2 are quoted here in terms of the experimental bond length of 1.937 a.u.

[20] W. Weltner, J. Chem. Phys. **28**, 477 (1958).

[21] See work cited in reference 20, also N. F. Ramsey, *Molecular Beams* (Oxford University Press, New York, 1956), Chap. 6.

TABLE I. Comparison of the paramagnetic contributions to the molar diamagnetic susceptibility.

	Theoretical			"Experimental"		
	r_0	Dipole moment (D)	χ_P[a]	r_0	Dipole moment (D)	$\chi_{h.f.}$[a]
H_2O	1.00±0.03	2.5±0.1 ($H_2^+O^-$)	+1.47±0.09	1.00	1.84[d] ($H_2^+O^-$)	+1.46
CH_4[c]	1.65±0.05	0.9±0.1 (C^--H^+)	+8.7±0.6	1.71	0.3~0.4[e] (C^+-H^-)	+9.3
NH_4^+[c]	1.47±0.10[b]	1.2±0.2 (N^--H^+)	+6.8±0.9	1.39	1.31[e] (N^--H^+)	+6.1
NH_3	...	1.54 ($N^-H_3^+$)	...	1.37	1.48[d] ($N^-H_3^+$)	+4.3

[a] See reference 17.
[b] See reference 19.
[c] See reference 23.
[d] See work cited in reference 14.
[e] See work cited in reference 15.

ments of NH_3.[22] However, such a calculation was not performed owing to the labor involved in extracting the radial density from the appropriate molecular orbitals.

CONCLUSION

The model of "floating" hydrogen densities, although somewhat crude, does provide a dipole moment for H_2O and NH_4^+ [23] which is of the correct order of magnibond dipole moment appears to be unsatisfactory.[24] Nevertheless, it is felt that for H_2O (which alone has a resultant dipole moment) the outer region of the first angular term arising from such a model, although perhaps not too unreasonable, will not possess any detailed accuracy.

For H_2O, a possible "experimental" value for r_0 might be provided by performing a three-dimensional x-ray analysis of ice after the manner of McDonald for ammonium bifluoride.

An interesting feature arising from this work is that the results for H_2O, CH_4, NH_4^+ and, to some extent, NH_3 indicate the possibility that for some molecules of the type XH_n a knowledge of the molecular rotational magnetic moment might well provide a means of obtaining, in a rather simple manner, a fairly reasonable first approximation to the molecular radial electron density.

Note added in proof. The suggestion contained in the conclusion, concerning a possible application of the "floating" hydrogen density model, has been carried out in detail for NH_3 and H_2S. The results are very pleasing and will be reported in the near future.

Also, the "approximate" Hartree-Fock density with angular allowance for CH_4 obtained by Mills[10] has now been recalculated and corrected [see I. M. Mills, Mol. Phys. **4**, 57 (1961)]. The results for CH_4 presented here may therefore suffer corresponding changes, these are, however, thought to be fairly small. This is now under investigation.

ACKNOWLEDGMENT

It is a pleasure to thank Dr. N. H. March for a critical and helpful reading of this paper.

[22] See H. Kaplan, J. Chem. Phys. **26**, 1704 (1957); also A. B. F. Duncan, *ibid.* **27**, 423 (1957).
[23] These molecules possess bond dipole moments only.
[24] It is not surprising, however, to observe that the results of calculations for the quadrupole and octopole moments, based on this model, are somewhat less satisfactory than those for the dipole moments.

Studies in Molecular Structure. IV. Potential Curve for the Interaction of Two Helium Atoms in Single-Configuration LCAO MO SCF Approximation*

BERNARD J. RANSIL

Laboratory of Molecular Structure and Spectra, Department of Physics, The University of Chicago, Chicago 37, Illinois

(Received October 17, 1960)

Single-configuration LCAO MO SCF wave functions and corresponding total energies were calculated for two ground-state He atoms interacting over an extensive range (0.4 to 12.0 A). Comparison with available experimental data is made; remarkably good agreement is obtained for distances greater than 1.5 A. For the first time, it is believed, an *a priori* account is given of both the van der Waals minimum and the repulsion region with a wave function of sufficient flexibility to deal with both. The details of repulsion and of bonding in the van der Waals region are analyzed in terms of atomic and overlap populations.

THE APPROXIMATION

SINGLE-configuration wave functions were computed as a function of internuclear distance (R) for two ground-state He atoms in LCAO MO SCF approximation using $1s$, $2s$, and $2p\sigma$ STO's (Slater-type orbitals). The orbital exponents were set equal and varied for each value of R until the total energy was minimized. The function so obtained is hereafter designated as the best limited MO(BLMO) function. The results of these calculations, which include MO (molecular orbital) coefficients, molecular orbital energies (ϵ), the optimum ζ (orbital exponent) values and total molcular energy (E_M), are given in the Appendix. Table I summarizes the energy data and Table II compares the energy data of this calculation with the available experimental data, and with other theoretical curves. Curves for the repulsion and van der Waals region are given in Figs. 1 and 2.

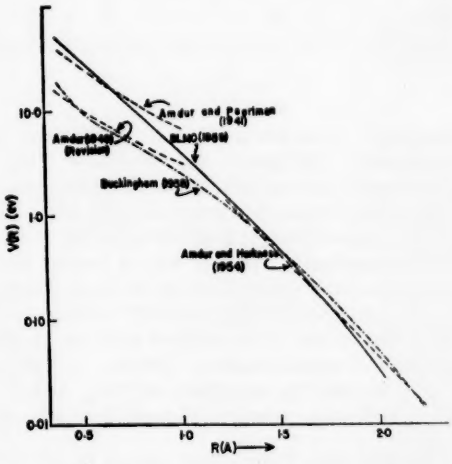

FIG. 1. Repulsive region for interaction for two He atoms. See Table II for references.

* This work was assisted by the National Science Foundation and by the Office of Ordnance Research.

CALCULATION OF THE POTENTIAL FUNCTION

The interaction potential of two He atoms at any given value of the internuclear distance is computed as the difference between the total molecular energy at the given value of $R[E_M(R)]$ and the computed energy of two He atoms in their ground-state: $V(R)=E_M(R)-2E(\mathrm{He})$. At large values of the internuclear distance, the molecular energy E_M rapidly approaches the asymptotic energy of two He atoms in their ground state approximated with $1s$ STO's having $\zeta=1.6875$; and the single-configuration ground-state wave function goes over smoothly and unambiguously to $1s$ atomic functions.

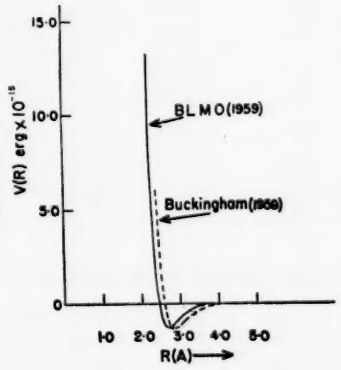

FIG. 2. Van der Waals region for interaction of two He atoms. BLMO, this calculation. Buckingham: Table II, reference g.

It is because of the smooth, asymptotic behavior of both E_M and the single configuration ground state wave function (which is a result of the interaction of completely filled orbitals) that the potential function has been defined and calculated in the above manner. Potential functions (and dissociation energies) for all first-row diatomic molecules with the exceptions of He_2, Be_2, and Ne_2 cannot be so conveniently defined if the SCF approximation is employed because (1) the SCF total energy fails to approach the energy of the ground-state dissociation products and (2) the ground-state molecular SCF function fails to go over smoothly to the appropriate atomic ground-state configuration.

TABLE I. Potential curve for He_2 single determinant LCAO MO SCF approximation

A	R a.u.	$\zeta_{1s}=\zeta_{2s}=\zeta_{2p\sigma}$	E_M (a.u.)	[a] $V(R)$ a.u.	ev
0.4	0.7559	1.6618	−3.9506 8029 5	1.7446 3220 5	47.47
0.5	0.944875	1.6409	−4.5619 9249 2	1.1333 2000 8	30.84
0.6	1.13385	1.6356	−4.9387 1440 7	0.7565 9809 3	20.59
0.75	1.4173125	1.6465	−5.2787 3492 8	0.4165 7757 2	11.34
0.8	1.5118	1.6530	−5.3543 2090 4	0.3409 9160 4	9.278
1.0	1.88975	1.6774	−5.5444 9624 5	0.1508 1625 5	4.104
1.25	2.362188	1.6898	−5.6432 8135 8	0.0520 3114 2	1.416
1.5	2.834625	1.6902	−5.6785 6432 4	0.0167 4817 6	0.4557
1.75	3.307063	1.6881	−5.6904 5713 9	0.0048 5536 1	0.1321
2.0	3.7995	1.6868	−5.6941 2778 4	0.0011 8471 6	0.03324
2.2	4.15745	1.6865	−5.6950 1290 3	0.0002 9959 7	0.0081 52
2.4	4.5354	1.6866	−5.6952 7887 1	0.0000 3362 9	0.0009 150
2.5	4.724375	1.6867	−5.6953 2117 1	−0.0000 0867 1	−0.0002 359
2.6	4.91335	1.6868	−5.6953 3755 8	−0.0000 2505 8	−0.0006 818
2.7	5.102325	1.6870	−5.6953 4090 0	−0.0000 2840 0	−0.0007 728
2.8	5.2913	1.6871	−5.6953 3837 0	−0.0000 2587 0	−0.0007 039
3.0	5.66925	1.6873	−5.6953 2892 8	−0.0000 1642 8	−0.0004 470
3.4	6.42515	1.6875	−5.6953 1669 8	−0.0000 0419 8	−0.0001 142
3.8	7.18105	1.6875	−5.6953 1332 9	−0.0000 0082 9	−0.0000 225
4.0	7.5590	1.6875	−5.6953 1284 7	−0.0000 0034 7	−0.0000 0944
4.5	8.503875	1.6875	−5.6953 1249 6	0	0
5.0	9.44875	1.6875	−5.6953 1250 0	0	0
6.0	11.3385	1.6875	−5.6953 1250 0	0	0
12.0	22.677	1.6875	−5.6953 1250 0	0	0

[a] Calculated using asymptotic value $E(2He) = -5.6953125$ a.u.

COMPARISON WITH PREVIOUS CALCULATIONS

He_2, like H_2, has been given a great deal of attention by theoretical physicists and chemists; most of the early work has been summarized by Hirschfelder, Curtiss, and Bird.[1] Of particular interest here will be a few of the most recent calculations done on the He_2 system. Selection of these calculations was made for any or all of the following reasons: (1) the functional forms adopted have begun to achieve the degree of complexity and flexibility required for a reasonably accurate representation; (2) the calculations were done, in whole or in part, with the aid of high-speed digital equipment, considerably decreasing the human source of error; (3) historical importance having direct bearing on this calculation.

Huzinaga[2] (completely manual calculation) and independently, Phillipson and Mulliken[3] (manual and mechanical calculation), employ the MO ζ method[4] of varying the orbital exponent: the $\sigma_g 1s$ MO is permitted a ζ value different from the $\sigma_u 1s$ MO. Both are varied independently. Another way of looking at this is to assume that a double basis set has been chosen for each atom, $1s(\zeta_g)$ and $1s(\zeta_u)$, and MO's constructed as defined. This is *not* to be confused with the so-called "open-shell" approximation [where $1s \sim 1s(\zeta) + \lambda 1s'(\zeta')$] because the assignment of the ζ and ζ' are made according to *symmetry*, whereas the "open-shell"

[1] J. O. Hirschfelder, C. F. Curtiss, and R. B. Bird, *Molecular Theory of Gases and Liquids* (John Wiley & Sons, Inc., New York, 1954).

[2] S. Huzinaga, Prog. Theoret. Phys. (Kyoto) **18**, 139 (1957); T. Hasino and S. Huzinaga, *ibid.* **20**, 631 (1958).

[3] P. Phillipson and R. S. Mulliken (to be published).

[4] MO-ξ method: Each MO is characterized by a distinct, variationally chosen set of ξ's. STO-ξ method: The ξ's of each STO are independently optimized, but remain the same for every MO. See R. S. Mulliken, Revs. Modern Phys. **32**, 232 (1960).

TABLE II. Summary of experimental and theoretical data on interaction of two He Atoms. (Potential energy in units of erg$\times 10^{-11}$)

		Experimental							Theoretical			
R(A)	This Calculation (BLMO)	Amdur 1949[a]	Amdur and Jordan[b] 1958, 1959	Amdur and Colgate[c] 1959	Amdur and Harkness[d] 1954	From 2nd virial coefficient data at high temperature[e]	From compressibility and viscosity data for helium[f]	Buckingham composite[g]	Phillipson and Mulliken;[h] Huzinaga[i]	Griffing and Wehner[j]	Rosen, Page Margenau[k]	Moore and Margenau[l]
0.4	7.605							2.851		11.99		
0.5	4.940	1.705						1.683	4.585	7.15		
0.6	3.298	1.291						1.185				4.04
0.75	1.816	0.886						0.807	1.804	2.27		2.28
0.8	1.486	0.788				1.157		0.715				1.84
1.0	0.657	0.510	0.520	0.580		0.760		0.421	0.678	0.772	0.425	0.729
1.25	0.227		0.168	0.191		0.266		0.190	0.244	0.257	0.220	0.244
1.5	0.0730		0.0663	0.0771	0.0671	0.0832		0.0748	0.0831	0.0846	0.0830	0.0798
1.75	0.0212				0.0215	0.0247		0.0259	0.0266	0.0258	0.0287	
2.0	0.00516				0.0069	0.00692	0.0068	0.00773	0.00785	0.00785	0.00928	
2.2	0.00131				0.00278	0.00230	0.0027	0.00251		0.00305	0.00355	
2.4	0.000147					0.000634	0.00093	0.000601		0.00113	0.00124	
2.5	−0.0000378					0.000276		0.000207	0.000487	0.000680	0.000688	0.000286
2.6	−0.000109					0.0000742		0.00000074	0.000254		0.000349	
2.7	−0.000124					−0.0000338		−0.0000952	0.000128			
2.744												−0.0000207
2.8	−0.000113					−0.0000870		−0.000130	0.0000588		0.0000262	
3.0	−0.000072					−0.000113		−0.000118	0.00000607		−0.0000714	
3.11										−0.000093[m]		−0.0000733
3.4	−0.000018					−0.0000778		−0.0000479	−0.00000402		−0.0000777	
3.606												−0.0000397
3.8	−0.000004					−0.0000436		−0.0000140			−0.0000481	
4.0	−0.000001					−0.0000255		−0.0000072	−0.00000057		−0.0000367	
5.0	0					−0.0000084		−0.0000002			−0.0000096	

[a] I. Amdur, J. Chem. Phys. **17,** 844 (1949).
[b] I. Amdur and J. E. Jordan (private communication from Professor Amdur, 1960).
[c] I. Amdur and S. O. Colgate (private communication from Professor Amdur, 1960).
[d] I. Amdur and A. L. Harkness, J. Chem. Phys. **22,** 664 (1954).
[e] From data by Schneider and Intema as quoted by P. Rosen, J. Chem. Phys. **18,** 1182 (1950).
[f] R. A. Mason and W. E. Rice, J. Chem. Phys. **22,** 522, 843 (1954).
[g] R. A. Buckingham, Trans. Faraday Soc. **54,** 453 (1958).
[h] P. Phillipson and R. S. Mulliken (private communication).
[i] S. Huzinaga, Progr. Theoret. Phys. (Kyoto) **18,** 139 (1957); **20,** 631 (1958).
[j] V. Griffing and F. Wehner, J. Chem. Phys. **23,** 1024 (1955).
[k] P. Rosen, C. H. Page, and H. Margenau as given by J. O. Hirschfelder, C. F. Curtiss, and R. Bird, *Molecular Theory of Gases and Liquids* (John Wiley & Sons, Inc., New York, 1954).
[l] N. Moore and H. Margenau, Ph.D. thesis, Yale University, 1959.
[m] This value was obtained using MO's constructed from 1s and 2$p\sigma$ STO's on both centers; the other values quoted in this column were obtained using functions constructed from 1s STO's only.

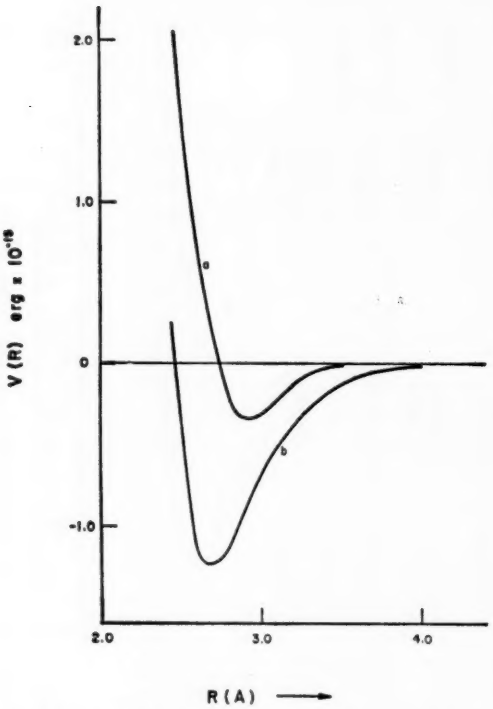

FIG. 3. Effect of basis set choice on the He_2 potential curve; J. S. Dooling and P. Piper, reference 6. Curve (a) $1s$, $2p\sigma$, STO's only, curve (b): $1s$, $2s$, $2p\sigma$, STO's.

method employes ζ and ζ' for both symmetries and hence is classificable under the STO-ζ procedure.[4] Griffing and Wehner[5] (completely manual calculation) performed the prototype of the calculation reported here. They employed only $1s$ STO's and retained $\zeta = 1.6875$ throughout. $2p\sigma$ character ($\zeta = 1.6875$) was introduced for one calculation at the expected distance for the van der Waals minimum ($R = 3.11$ A) and binding obtained.

Recently Dooling and Piper[6] (integrals computed mechanically, SCF performed manually) computed an interaction curve by the same methods as Griffing, Wehner, and the present paper, for the range 2.51 A to 3.76 A, keeping $\zeta = 1.6875$. In one case, $1s$ and $2p\sigma$ STO's were used; and in a second $1s$, $2s$, and $2p\sigma$. Both curves showed a minimum as would be expected. Inclusion of the $2s$ STO lowered the minimum and shifted it toward smaller internuclear distance, an effect which is predicted by the superposition of the results of the present calculation with the Griffing and Wehner spot calculation at 3.11 A. See Fig. 3.

The calculation reported here (completely mechanical) utilizes $1s$, $2s$, $2p\sigma$ STO's, giving all a common variable ζ which was optimized at each R value over an extensive range.

Although the coefficients for $2s$ and $2p\sigma$ are themselves rather small (of the order of 0.001, cf. Appendix), enough $2p\sigma$ character is introduced to produce sufficient polarization to give an energy minimum in the proper region.

Moore[7] (completely manual) recently used a trial state function analogous to Hirschfelder and Linnett for H_2 in an attempt to introduce the necessary polarization. Because the single configuration (VB) function constructed from $1s$ STO's only "can offer only repulsion," the terms of the determinant were modified in a complex manner to achieve a degree of polarization. The disadvantages of this technique as a general method from the standpoint of (1) calculational difficulties and (2) extensibility are obvious upon comparison. The results are in general agreement with those produced by more straightforward, extensible techniques.

AGREEMENT WITH EXPERIMENTAL DATA

In general, the agreement among the methods which account for polarization in some fashion is good considering the uncertainty of the data derived from experiment. The MO-ζ technique (Huzinaga, Phillipson-Mulliken) although primarily intended to describe short range interaction, nevertheless gives some binding in the van der Waals region. The simple LCAO MO SCF function (Griffing-Wehner) gives good account of the region roughly between 1 and 2 A; the extended LCAO MO SCF function (this calculation, Dooling-Piper, and the single Griffing-Wehner point) gives reasonably good account of the region from 1.0 A on, and closely parallels the MO-ζ calculation from 1.0 to 0.4 A.

The discrepancy of roughly 20 ev between the best calculated energy and Amdur's experimentally derived value at $R = 0.5$ A however requires explanation: Can it be attributed to Amdur's data (or its interpretation), to the inadequacy of the LCAO approximation, or both?

Theoretical considerations support a larger value of the interaction potential at 0.5 A than the 1.70 erg$\times 10^{-11}$ obtained from Amdur's potential function for that region.

One line of argument begins with the fact that for the hydrogen molecule the single configuration function utilizing $1s$, $2s$, and $2p\sigma$ STO's has been shown to be energetically comparable to the molecular Hartree-Fock function, *especially if the ζ's are independently varied*[8] (i.e., the STO-ζ calculation[4]). One can assume that the same approximation should give a close-to-Hartree-Fock energy for He_2, which, together with the correlation correction, should give agreement with the

[5] V. Griffing and F. Wehner, J. Chem. Phys. **23**, 1024 (1955).
[6] J. S. Dooling and P. Piper, Bull. Am. Phys. Soc. **5**, 339 (1960).
[7] N. Moore, "Energy of interaction of two He atoms," (preprint, Yale University, 1960).
[8] B. J. Ransil, J. Chem. Phys. (to be published).

TABLE III. He_2: Overlap populations as function of internuclear distance.

R(A)		$n(1s_A, 1s_B)$	$n(1s_A+2s_B)$ + $n(2s_A+1s_B)$	$n(1s_A, 2p\sigma_B)$ + $n(2p\sigma_A, 1s_B)$	$n(2s_A, 2s_B)$	$n(2s_A, 2p\sigma_B)$ + $n(2p\sigma_A, 2s_B)$	$n(2p\sigma_A, 2p\sigma_B)$	$n(i)$
0.5	$1\sigma_g$	0.807786	−0.149186	0.077368	0.041508	0.006002	−0.001976	0.781502
	$1\sigma_u$	−3.978162	−0.482682	0.715314	−0.088229	−0.036455	+0.034306	−3.835908
	Total	−3.170376	−0.631868	0.792682	−0.046721	−0.030453	0.032330	−3.054406
1.00	$1\sigma_g$	0.483983	−0.058886	0.035854	0.001488	−0.000570	0.000169	0.462038
	$1\sigma_u$	−0.856657	−0.031520	0.166658	−0.000241	0.000820	−0.002059	−0.723017
	Total	−0.372674	−0.090406	0.202512	0.001247	0.000232	−0.001890	−0.260979
1.50	$1\sigma_g$	0.200105	−0.004840	0.011628	0.000018	−0.000070	0.000086	0.206927
	$1\sigma_u$	−0.246769	−0.002258	0.032347	−0.000004	−0.000084	−0.000542	−0.212470
	Total	−0.046664	−0.002258	0.043975	0.000014	−0.000154	−0.000456	−0.005543
2.0	$1\sigma_g$	0.068680	0.000552	0.003364	0.000000	0.000008	0.000025	0.072629
	$1\sigma_u$	−0.073618	0.002115	0.005437	−0.000010	−0.000046	−0.000061	−0.066183
	Total	−0.004938	0.002667	0.008801	−0.000010	−0.000038	−0.000036	0.006446
2.5	$1\sigma_g$	0.020639	0.000260	0.000640	0.000000	0.000002	0.000003	0.021544
	$1\sigma_u$	−0.021070	0.000464	0.000763	−0.000002	−0.000005	−0.000004	−0.019854
	Total	−0.000431	0.000724	0.001403	−0.000002	−0.000003	−0.000001	0.001690
2.6	$1\sigma_g$	0.016057	0.000192	0.000439	0.000000	0.000002	0.000002	0.016692
	$1\sigma_u$	−0.016317	0.000323	0.000505	−0.000001	−0.000003	−0.000003	−0.015496
	Total	−0.000260	0.000515	0.000944	−0.000001	−0.000001	−0.000001	0.001196
2.7	$1\sigma_g$	0.012455	0.000144	0.000298	0.000000	0.000001	0.000001	−0.012899
	$1\sigma_u$	−0.012611	0.000218	0.000332	−0.000001	−0.000002	−0.000001	−0.012065
	Total	−0.000156	0.000362	0.000630	−0.000001	−0.000001	0.000000	0.000834
2.8	$1\sigma_g$	0.009640	0.000102	0.000199	0.000000	0.000001	0.000001	0.009943
	$1\sigma_u$	−0.009733	0.000147	0.000218	0.000000	−0.000001	−0.000001	−0.009370
	Total	−0.000093	0.000249	0.000417	0.000000	0.000000	0.000000	0.000573
3.0	$1\sigma_g$	0.005739	0.000050	0.000087	0.000000	0.000000	0.000000	0.005876
	$1\sigma_u$	−0.005772	0.000064	0.000092	0.000000	0.000000	0.000000	−0.005616
	Total	−0.000033	0.000114	0.000179	0.000000	0.000000	0.000000	0.000260
3.4	$1\sigma_g$	0.001994	0.000010	0.000015	0.000000	0.000000	0.000000	0.002019
	$1\sigma_u$	−0.001998	0.000011	0.000015	0.000000	0.000000	0.000000	−0.001972
	Total	−0.000004	0.000021	0.000030	0.000000	0.000000	0.000000	0.000047
4.0	$1\sigma_g$	0.000392	0.000001	0.000001	0.000000	0.000000	0.000000	0.000394
	$1\sigma_u$	−0.000392	0.000001	0.000001	0.000000	0.000000	0.000000	−0.000390
	Total	0.000000	0.000002	0.000002	0.000000	0.000000	0.000000	0.000004

experimental value to at least the first significant figure.

Checking on this, it is found that the STO-ζ calculation for He_2 at 0.5 A improves the total electron energy by 2.68 ev over the equal-ζ calculation. (The improvement in the H_2 case was only 0.037 ev, which gives an indication of how much poorer this approximation is for He_2). The best theoretical energy so far for the He_2 interaction at 0.5 A is 28.618[9] ev. The correlation correction should be close to that for the united atom Be (2.6 ev), which reduces the best calculated energy to 26.0 ev, a factor of 2.4 greater than the "experimental." If our assumptions about the correlation correction are valid, the difference of roughly 15 ev must then be ascribed to the difference between the calculated energy and the true Hartree-Fock energy for He_2; but a difference of 15 ev is rather difficult to believe. However, this should be further tested by calculations with larger basis sets.

Another argument makes use of the known united atom energy and the behavior of the calculated electronic energies as the internuclear distance decreases. This argument is best illustrated using the MO-ζ function and consequently is discussed by Phillipson and Mulliken.[3] Their conclusions are that the true value at R=0.5 A should be about 18 ev, which splits the

[9] P. Phillipson, R. S. Mulliken (private communication).

TABLE IV. He_2: Atomic populations as function of internuclear distance.

R(Å)	$n(1\sigma_g;1s)$	$n(1\sigma_g;2s)$	$n(1\sigma_g;2p\sigma)$	$n(1\sigma_g)$	$n(1\sigma_u;1s)$	$n(1\sigma_u;2s)$	$n(1\sigma_u;2p\sigma)$	$n(1\sigma_u)$	Totals $n(i;1s)$	Totals $n(i;2s)$	Totals $n(i;2p\sigma)$
0.5	1.907872	0.048083	0.044045	2	1.732665	−0.181645	0.448980	2	3.640537	−0.133562	0.493025
1.0	2.004661	−0.023309	0.018648	2	1.922915	−0.014801	0.091886	2	3.927576	−0.038110	0.110534
1.5	1.996233	−0.002363	0.006130	2	1.981491	0.001263	0.017246	2	3.977724	−0.001100	0.023376
2.0	1.997891	0.000284	0.001825	2	1.996007	0.001081	0.002912	2	3.993898	0.001365	0.004737
2.5	1.999507	0.000138	0.000335	2	1.999336	0.000247	0.000417	2	3.998873	0.000385	0.000772
2.6	1.999653	0.000103	0.000244	2	1.999550	0.000172	0.000278	2	3.999203	0.000275	0.000522
2.7	1.999756	0.000078	0.000166	2	1.999699	0.000117	0.000184	2	3.999455	0.000195	0.000350
2.8	1.999833	0.000055	0.000122	2	1.999801	0.000079	0.000120	2	3.999634	0.000134	0.000232
3.0	1.999924	0.000027	0.000049	2	1.999916	0.000034	0.000050	2	3.999840	0.000061	0.000099
3.4	1.999988	0.000006	0.000006	2	1.999986	0.000006	0.000008	2	3.999974	0.000012	0.000014
4.0	1.999999	0.000000	0.000001	2	2.000000	0.000000	0.000000	2	3.999999	0.000000	0.000001

discrepancy in a fairly proportionate manner: the theoretical calculations so far are too high by 5–8 ev; the experimentally derived data are too low by 5–8 ev, i.e., by close to a factor of two.

The "experimental" values[10] are not obtained directly but are inferred from atomic beam collision data using both wide and narrow aperture apparatus. The data are quoted for limited ranges of R. The most reliable points fall at the midsection of each range. The fact that data from both apparatus give fairly consistent agreement at $r=1.0$ A indicates that the data at $R=1.0$ A is reliable. The average of the three measurements 0.54 ± 0.4 erg$\times10^{-11}$ differs from the theoretical average (Ransil and Phillipson-Mulliken: 0.668 erg$\times10^{-11}$) by 0.8 ev. The experimental data exhibit a wide spread (where duplication exists) and not too much confidence can be put in the slopes. On the other hand, until investigated thoroughly, one cannot be sure how close our approximation is, energetically, to an accurate Hartree-Fock molecular function. And once assured of that point, the validity of the correlation correction argument, except at very small and very large nuclear separations, would have to be looked into. The functional dependence of the correlation correction on the internuclear distance is not known; it is believed to obey a simple exponential law, assuming the united atomic correlation correction at $R=0$ and the dissociated atom correction at large R. But the actual behavior would depend on electron coupling details as the internuclear distance changes, and they need not be simple.

DETAILS OF BONDING AND REPULSION IN TERMS OF POPULATION ANALYSES

Overlap and atomic populations were computed as a function of internuclear distance and are given in Tables III and IV. Although population analyses must be used with caution as an interpretive tool, they do provide an interesting picture of the He_2 interaction. It is seen that the total overlap oppulation is strongly negative (i.e., antibonding) in the region 0.5 A$\leq R\leq$1.0 A, an effect arising from the exceptionally strong antibonding character of the $2\sigma_u$ MO. Somewhere between 1.5 and 2.0 A, the bonding character of $2\sigma_g$ begins to predominate and the total overlap population exhibits slight bonding character, going through a maximum around $R=2.0$ A and continuing bonding, going to nonbonding as the internuclear separation increases. This behavior correlates well in a qualitative fashion with the repulsive potential and van der Waals minimum. More accurate functions might perhaps produce quantitative agreement, i.e., coincidence of the crossover point in the potential curve with the change of sign of overlap population, and coincidence of the point of maximum overlap with the van der Waals minimum.

The atomic populations display strong promotion to

[10] Table II, references a, b, c, and d.

at $2p\sigma$ at small internuclear distances. At all times the $2s$ interaction is present, but enters in less significantly than $2p\sigma$; at the same time its contribution is not negligible because it lowers the energy and displaces the minimum toward small R values. (See Fig. 3.) As the internuclear separation becomes larger, the population becomes entirely $1s$ which correlates with the dissociation into two He atoms of configuration $1s^2$.

REPULSION REGION AND THE VAN DER WAALS MINIMUM

The magnitude of the interaction energies involved in the repulsion and van der Waals regions (1–20 ev for the powerful exchange repulsion; 10^{-3} ev for the van der Waals region) has always provided a strong reason for treating them as two different problems. However it should be possible, given a function of sufficient flexibility, to consider them together as one problem, characterized by competitive binding and repulsion phenomena which diminish or increase in importance as the internuclear distance varies. It is therefore of considerable interest that the approximation used in this work displays sufficient flexibility to deal with both regions with (for the most part) acceptable accuracy. Interesting also is the fact that this is achieved without π functions because from VB theory we would expect equally important contributions from configurations involving $(1s\ 2p\sigma)$, $(1s\ 2p\pi^+)$ and $(1s\ 2p\pi^-)$. Inclusion of π functions in the context of LCAO MO SCF theory necessarily implies configuration interaction (CI). CI should achieve its greatest effect in the repulsion region and should have a slight lowering and displacing effect in the van der Waals region. The fact that the van der Waals minimum is dealt with as successfully as it is with only $1s$, $2s$, and $2p\sigma$ STO's argues against weighting the π-function contributions *equally* throughout the entire interaction range. Undoubtedly radial correlation effects introduced by π-type configurations are extremely important in the exchange repulsion region; however their importance would be expected to dwindle considerably (relative to the σ contributions) as the internuclear disance increases.

ACKNOWLEDGMENTS

The author is indebted to the staff of the Computation Section, Wright Air Development Center, Wright Patterson Air Force Base, Ohio for their courteous cooperation. He also acknowledges the invaluable assistance of Tracy Kinyon in the hand computational work.

He is especially grateful to Professor R. S. Mulliken for a critical reading of the manuscript and suggestions for its improvement, and to Professor I. Amdur for preprints on his He_2 work, and for a most informative and enjoyable discussion of the interpretation of both experimental and theoretical results.

APPENDIX. BLMO WAVE FUNCTIONS AND ENERGIES FOR THE INTERACTION OF TWO HE ATOMS

	R(au)	0.7559		0.944875		1.13385		1.417313	
	ζ_{1s}	1.6618		1.6409		1.6356		1.6465	
	ζ_{2s}	1.6618		1.6409		1.6356		1.6465	
	$\zeta_{2p\sigma}$	1.6618		1.6409		1.6356		1.6465	
		c_{ip}	ϵ_i (au)	c_{ip}	ϵ_i (au)	c_{ip}	ϵ_i (au)	c_{ip}	ϵ_i (au)
$1\sigma_g$	$c_{11}=c_{14}$	0.51086		0.53292		0.55369		0.58136	
	$c_{12}=c_{15}$	-0.16528	-2.07752	-0.13979	-1.77831	-0.11395	-1.55326	-0.07833	-1.32552
	$c_{13}=c_{16}$	0.03538		0.03292		0.02890		0.02253	
$1\sigma_u$	$c_{21}=-c_{24}$	1.39952		1.18264		1.04744		0.92804	
	$c_{22}=-c_{25}$	0.34446	-0.09372	0.20381	-0.21882	0.11698	-0.33486	0.05008	-0.48415
	$c_{23}=-c_{26}$	-0.15661		-0.13715		-0.11450		-0.08426	
$2\sigma_g$	$c_{31}=c_{34}$	0.18133		0.16196		0.14447		0.12782	
	$c_{32}=c_{35}$	0.48264	0.68441	0.49134	0.75522	0.49495	0.83317	0.48550	0.94693
	$c_{33}=c_{36}$	-0.26136		-0.30708		-0.35289		-0.42434	
$2\sigma_u$	$c_{41}=-c_{44}$	1.54203		-3.10140		0.56634		0.33861	
	$c_{42}=-c_{45}$	-0.57434	2.69154	-0.63952	2.16528	-0.63439	1.87215	-0.59280	1.64810
	$c_{43}=-c_{46}$	0.64036		-0.57066		0.54352		0.53454	
$3\sigma_g$	$c_{51}=c_{54}$	-0.43556		-0.41515		-0.39233		-0.35381	
	$c_{52}=c_{55}$	0.32206	2.37384	0.33810	2.20374	0.35738	2.06333	0.39597	1.88052
	$c_{53}=c_{56}$	1.50108		1.19794		0.98114		0.74261	
$3\sigma_u$	$c_{61}=-c_{64}$	37.27691		19.72472		11.34494		5.55179	
	$c_{62}=-c_{65}$	14.69674	6.94769	8.32845	6.10703	5.19840	5.47855	2.97967	4.75696
	$c_{63}=-c_{66}$	9.81077		6.53826		4.65307		3.03555	
	E_M(au)	-3.9506 80295		-4.5619 92492		-4.9387 14407		-5.2787 34922	

	R(au)	1.5118		1.88975		2.362188		2.834625	
	ζ_{1s}	1.6530		1.6774		1.6898		1.6902	
	ζ_{2s}	1.6530		1.6774		1.6898		1.6902	
	$\zeta_{2p\sigma}$	1.6530		1.6774		1.6898		1.6902	
		c_{ip}	ϵ_i (au)	c_{ip}	ϵ_i (au)	c_{ip}	ϵ_i (au)	c_{ip}	ϵ_i (au)
$1\sigma_g$	$c_{11}=c_{14}$	0.58867		0.61891		0.64789		0.66946	
	$c_{12}=c_{15}$	-0.06780	-1.27094	-0.03511	-1.11950	-0.01357	-1.01785	-0.00426	-0.96391
	$c_{13}=c_{16}$	0.02060		0.01446		0.01021		0.00812	
$1\sigma_u$	$c_{21}=-c_{24}$	0.90012		0.82341		0.77149		0.74344	
	$c_{22}=-c_{25}$	0.03823	-0.52636	0.01413	-0.65945	0.00284	-0.76291	-0.00204	-0.82225
	$c_{23}=-c_{26}$	-0.07587		-0.05054		-0.03169		-0.02034	
$2\sigma_g$	$c_{31}=c_{34}$	0.12571		0.13559		0.16426		1.20504	
	$c_{32}=c_{35}$	0.47696	0.98125	0.40480	1.07575	0.21466	1.07583	0.02268	1.00147
	$c_{33}=c_{36}$	-0.44917		-0.54912		-0.63495		-0.63241	
$2\sigma_u$	$c_{41}=-c_{44}$	-2.29621		0.18855		0.12033		0.08158	
	$c_{42}=-c_{45}$	-0.57767	1.60469	-0.52618	1.49289	-0.48126	1.39955	-0.44459	1.33063
	$c_{43}=-c_{46}$	-0.03546		0.54539		0.56131		0.58013	
$3\sigma_g$	$c_{51}=c_{54}$	-0.33980		-0.27657		-0.18029		-0.10041	
	$c_{52}=c_{55}$	0.41233	1.82486	0.49661	1.62426	0.60956	1.45238	0.64986	1.37845
	$c_{53}=c_{56}$	0.67649		0.43913		0.14256		-0.08175	
$3\sigma_u$	$c_{61}=-c_{64}$	4.47246		2.07350		0.94403		0.48212	
	$c_{62}=-c_{65}$	2.55352	4.55406	1.57424	3.84645	1.08185	3.13548	0.86908	2.60194
	$c_{63}=-c_{66}$	2.67936		1.75592		1.18804		0.88295	
	E_M(au)	-5.3543 20904		-5.5444 96245		-5.6432 81358		-5.6785 64324	

	R(au)	3.307063		3.7795		4.15745		4.5354	
	ζ_{1s}	1.6881		1.6868		1.6865		1.6866	
	ζ_{2s}	1.6881		1.6868		1.6865		1.6866	
	$\zeta_{2p\sigma}$	1.6881		1.6868		1.6865		1.6866	
		c_{ip}	ϵ_i (au)	c_{ip}	ϵ_i (au)	c_{ip}	ϵ_i (au)	c_{ip}	ϵ_i (au)
$1\sigma_g$	$c_{11}=c_{14}$	0.68445		0.69413		0.69903		0.70218	
	$c_{12}=c_{15}$	-0.00042	-0.93412	0.00101	-0.91734	0.00133	-0.90935	0.00130	-0.90432
	$c_{13}=c_{16}$	0.00671		0.00533		0.00423		0.00320	
$1\sigma_u$	$c_{21}=-c_{24}$	0.72766		0.71865		0.71432		0.71156	
	$c_{22}=-c_{25}$	-0.00375	-0.85586	-0.00374	-0.87461	-0.00319	-0.88329	-0.00248	-0.88858
	$c_{23}=-c_{26}$	-0.01308		-0.00832		-0.00574		-0.00392	
$2\sigma_g$	$c_{31}=c_{34}$	0.12133		0.08559		0.06161		0.04271	
	$c_{32}=c_{35}$	-0.08215	0.93872	-0.13169	0.91597	-0.14782	0.92309	-0.14882	0.94456
	$c_{33}=c_{36}$	-0.61335		-0.61163		-0.62099		-0.63582	
$2\sigma_u$	$c_{41}=-c_{44}$	0.05773		0.04198		0.03261		0.02495	
	$c_{42}=-c_{45}$	-0.40619	1.28173	-0.36001	1.24621	-0.31549	1.22273	-0.26512	1.20108
	$c_{43}=-c_{46}$	0.60325		0.63052		0.65354		0.67485	
$3\sigma_g$	$c_{51}=c_{54}$	-0.05850		-0.03720		-0.02707		-0.02008	
	$c_{52}=c_{55}$	0.65045	1.35124	0.64969	1.34259	0.65316	1.34290	0.66012	1.34757
	$c_{53}=c_{56}$	-0.18503		-0.22156		-0.22424		-0.21118	
$3\sigma_u$	$c_{61}=-c_{64}$	0.26046		0.14377		0.08947		0.05530	
	$c_{62}=-c_{65}$	0.76792	2.21644	0.72249	1.94445	0.70901	1.78909	0.70658	1.67634
	$c_{63}=-c_{66}$	0.68880		0.54537		0.44811		0.35954	
	E_M(au)	-5.6904 57139		-5.6941 27784		-5.6950 12903		-5.6952 78871	

	R(au)	4.724375		4.91335		5.102325		5.2913	
	ζ_{1s}	1.6867		1.6868		1.6870		1.6871	
	ζ_{2s}	1.6867		1.6868		1.6870		1.6871	
	$\zeta_{2p\sigma}$	1.6867		1.6868		1.6870		1.6871	
		c_{ip}	ϵ_i (au)	c_{ip}	ϵ_i (au)	c_{ip}	ϵ_i (au)	c_{ip}	ϵ_i (au)
$1\sigma_g$	$c_{11}=c_{14}$	0.70328		0.70414		0.70482		0.70[illegible]	
	$c_{12}=c_{15}$	0.00122	-0.90258	0.00111	-0.90121	0.00102	-0.90014	0.00090	-0.89931
	$c_{13}=c_{16}$	0.00274		0.00232		0.00196		0.00163	
$1\sigma_u$	$c_{21}=-c_{24}$	0.71060		0.70983		0.70923		0.70876	
	$c_{22}=-c_{25}$	-0.00215	-0.89038	-0.00184	-0.89178	-0.00153	-0.89286	-0.00128	-0.89370
	$c_{23}=-c_{26}$	-0.00323		-0.00265		-0.00217		-0.00178	
$2\sigma_g$	$c_{31}=c_{34}$	0.03511		0.02863		0.02318		0.01865	
	$c_{32}=c_{35}$	-0.14470	0.95812	-0.13803	0.97235	-0.12939	0.98672	-0.11926	1.00039
	$c_{33}=c_{36}$	-0.64415		-0.65254		-0.66067		-0.66824	
$2\sigma_u$	$c_{41}=-c_{44}$	0.02160		0.01854		0.01577		0.01328	
	$c_{42}=-c_{45}$	-0.23882	1.19060	-0.21259	1.18035	-0.18700	1.17056	-0.16280	1.16108
	$c_{43}=-c_{46}$	0.68395		0.69167		0.69792		0.70268	
$3\sigma_g$	$c_{51}=c_{54}$	-0.01731		-0.01489		-0.01278		-0.01090	
	$c_{52}=c_{55}$	0.66451	1.35111	0.66922	1.35526	0.67406	1.36018	0.67877	1.36526
	$c_{53}=c_{56}$	-0.20023		-0.18706		-0.17220		-0.15635	
$3\sigma_u$	$c_{61}=-c_{64}$	0.04333		0.03388		0.02640		0.02057	
	$c_{62}=-c_{65}$	0.70740	1.63281	0.70870	1.59624	0.71008	1.56620	0.71121	1.54103
	$c_{63}=-c_{66}$	0.31880		0.27911		0.24254		0.20902	
	E_M(au)	-5.6953 21171		-5.6953 37558		-5.6953 40900		-5.6953 38370	

	R(au)	5.66925		6.42515		7.18105		7.5590	
	ζ_{1s}	1.6873		1.6875		1.6875		1.6875	
	ζ_{2s}	1.6873		1.6875		1.6875		1.6875	
	$\zeta_{2p\sigma}$	1.6873		1.6875		1.6875		1.6875	
		c_{ip}	ϵ_i (au)	c_{ip}	ϵ_i (au)	c_{ip}	ϵ_i (au)	c_{ip}	ϵ_i (au)
$1\sigma_g$	$c_{11}=c_{14}$	0.70607		0.70675		0.70699		0.70704	
	$c_{12}=c_{15}$	0.00068	-0.89815	0.00035	-0.89705	0.00015	-0.89668	0.00010	-0.89659
	$c_{13}=c_{16}$	0.00112		0.00048		0.00020		0.00013	
$1\sigma_u$	$c_{21}=-c_{24}$	0.70810		0.70746		0.70723		0.70718	
	$c_{22}=-c_{25}$	-0.00087	-0.89484	-0.00036	-0.089592	-0.00016	-0.89629	-0.00010	-0.89637
	$c_{23}=-c_{26}$	-0.00117		-0.00049		-0.00020		-0.00013	
$2\sigma_g$	$c_{31}=c_{34}$	0.01186		0.00457		0.09448		0.00103	
	$c_{32}=c_{35}$	-0.09668	1.02475	-0.05457	1.05841	-0.02678	1.07572	-0.01812	1.08055
	$c_{33}=c_{36}$	-0.68107		-0.69676		-0.70324		-0.70475	
$2\sigma_u$	$c_{41}=-c_{44}$	0.00917		0.00398		0.00159		0.00099	
	$c_{42}=-c_{45}$	-0.11996	1.14392	-0.05992	1.11817	-0.02780	1.10323	-0.01854	1.09879
	$c_{43}=-c_{46}$	0.70841		0.71081		0.70949		0.70880	
$3\sigma_g$	$c_{51}=c_{54}$	-0.00776		-0.00361		-0.00150		-0.00094	
	$c_{52}=c_{55}$	0.68723	1.37604	0.69850	1.39593	0.70365	1.40956	0.70493	1.41403
	$c_{53}=c_{56}$	-0.12383		-0.06790		-0.03279		-0.02206	
$3\sigma_u$	$c_{61}=-c_{64}$	0.01243		0.00453		0.00167		0.00101	
	$c_{62}=-c_{65}$	0.71242	1.50315	0.71154	1.45991	0.70960	1.43986	0.70885	1.43441
	$c_{63}=-c_{66}$	0.15161		0.07422		0.03398		0.02255	
	E_M(au)	-5.6953 28928		-5.6953 16698		-5.6953 13329		-5.6953 12847	

	R(au)	8.503875		9.44875		11.3385		15.1180	
	ζ_{1s}	1.6875		1.6875		1.6875		1.6875	
	ζ_{2s}	1.6875		1.6875		1.6875		1.6875	
	$\zeta_{2p\sigma}$	1.6875		1.6875		1.6875		1.6875	
		c_{1p}	ϵ_1 (au)	c_{1p}	ϵ_1 (au)	c_{1p}	ϵ_1 (au)	c_{1p}	ϵ_1 (au)
$1\sigma_g$	$c_{11}=c_{14}$	0.70709		0.70711		0.70705		0.70711	
	$c_{12}=c_{15}$	0.00003	-0.89651	0.00001	-0.89649	0.00000	-0.89648	0.00000	-0.89648
	$c_{13}=c_{16}$	0.00004		0.00001		0.00000		0.00000	
$1\sigma_u$	$c_{21}=-c_{24}$	0.70713		0.70711		0.70716		0.70711	
	$c_{22}=-c_{25}$	-0.00003	-0.89646	-0.00001	-0.89648	0.00000	-0.89648	0.00000	-0.89648
	$c_{23}=-c_{26}$	-0.00004		-0.00001		0.00000		0.00000	
$2\sigma_g$	$c_{31}=c_{34}$	0.00029		0.00008		0.00001		0.00000	
	$c_{32}=c_{35}$	-0.00636	1.08673	-0.00208	1.08885	-0.00019	1.08975	0.00000	1.08984
	$c_{33}=c_{36}$	-0.70641		-0.70690		-0.70709		-0.70711	
$2\sigma_u$	$c_{41}=-c_{44}$	0.00028		0.00008		0.00001		0.00000	
	$c_{42}=-c_{45}$	-0.00641	1.09292	-0.00208	1.09083	-0.00019	1.08993	0.00000	1.08984
	$c_{43}=-c_{46}$	0.70772		0.70730		0.70712		0.70711	
$3\sigma_g$	$c_{51}=c_{54}$	-0.00028		-0.00008		-0.00001		0.00000	
	$c_{52}=c_{55}$	0.70643	1.42029	0.70690	1.42266	0.70709	1.42372	0.70711	1.42383
	$c_{53}=c_{56}$	-0.00766		-0.00249		-0.00023		0.00000	
$3\sigma_u$	$c_{61}=-c_{64}$	0.00028		0.00008		0.00001		0.00000	
	$c_{62}=-c_{65}$	0.70773	1.42745	0.70731	1.42501	0.70712	1.42394	0.70711	1.42383
	$c_{63}=-c_{66}$	0.00771		0.00249		0.00023		0.00000	
	E_M(au)	-5.6953 12496		-5.6953 12500		-5.6953 12500		-5.6953 12500	

Electrostatic Binding Energy in a Body-Centered Structure of Parallel Charge Doublet Chains

P. J. JACKSON

Department of Physics, University of the Witwatersrand, Johannesburg, South Africa

(Received November 2, 1960)

The binding energy between chains in a body-centered tetragonal structure, consisting of infinite charge doublet chains parallel to the c axis, is considered as a function of two lattice parameters. Graphs are plotted of the variation of the binding energy with these parameters. The results are applied to the particular case of metaldehyde.

INTRODUCTION

CONSIDER a body-centered tetragonal structure, consisting of charge doublets parallel to the c axis at each lattice point. Let the sides of the unit cell be a, a, and c. The structure is then made up of parallel charge doublet chains as in Fig. 1. Each charge doublet is rigidly bound to those above and below in the same chain. The electrostatic binding between the chains will be considered below. It will be shown that there is an equilibrium separation of the chains in such a structure.

Let the chains in the body-centered positions be called class E chains, as shown in Fig. 1. Let the identical chains at the corners of the unit cell, which are displaced by $c/2$ parallel to the c axis relative to the class E chains, be called class F chains. Consider the electrostatic potential at P, the positive end of a doublet (Fig. 1), which is due to all the chains except that containing P; let this potential be Φ. Then that part of the energy required to dissociate unit volume of an infinite crystal into separate chains, which is due to electrostatic interaction between the charge doublets, is

$$W=\tfrac{1}{2}(2e\Phi N)=e\Phi N,$$

where e is the charge on the end of a doublet and N is the number of doublets per unit volume. The potential

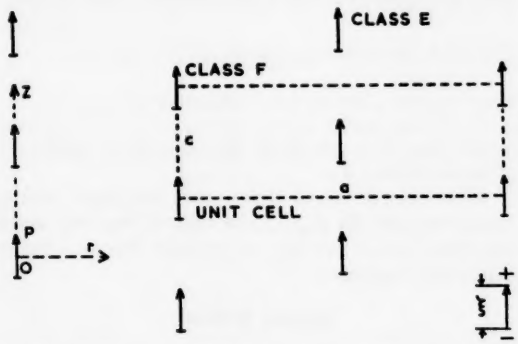

FIG. 1. Projection of lattice consisting of parallel charge doublet chains onto ac plane, showing coordinate system used in the evaluation of the potential of a single chain.

Φ has to be evaluated at both ends of the same doublet, at which points, however, it is equal and opposite. The product $e\Phi$ is thus of the same sign at both these points and leads to the factor 2 in the above expression. The factor $\frac{1}{2}$ is inserted to avoid double counting of the contribution from each doublet. The problem is thus to evaluate Φ.

POTENTIAL OF A SINGLE CHAIN

Consider the potential ϕ due to a single doublet chain at any point (r, θ, z) in cylindrical polar coordinates referred to the center of a doublet as origin (Fig. 1). Let the dipole moment of a single doublet be $e\xi$, where ξ is the length of a doublet. Introduce the parameters $\alpha=\xi/c$, $\beta=r/c$, $\gamma=z/c$. Then ϕ can be written

$$\phi(\alpha,\beta,\gamma)=e/c\{[\beta^2+(\gamma-\tfrac{1}{2}\alpha)^2]^{-\frac{1}{2}}-[\beta^2+(\gamma+\tfrac{1}{2}\alpha)^2]^{-\frac{1}{2}}$$

$$+\sum_{n=1}^{\infty}\langle[\beta^2+(n+\gamma-\tfrac{1}{2}\alpha)^2]^{-\frac{1}{2}}-[\beta^2+(n+\gamma+\tfrac{1}{2}\alpha)^2]^{-\frac{1}{2}}$$

$$+[\beta^2+(n-\gamma+\tfrac{1}{2}\alpha)^2]^{-\frac{1}{2}}-[\beta^2+(n-\gamma-\tfrac{1}{2}\alpha)^2]^{-\frac{1}{2}}\rangle\}. \quad (1)$$

This series converges as

$$e/c\sum_{n=1}^{\infty}2\alpha\gamma n^{-3}$$

for sufficiently large n, the value of n beyond which the convergence is rapid depending on β. (When β is less than about 0.8 it was found that a sum to 15 terms is adequate.)

Two methods of evaluating Φ will now be described, the first using Eq. (1) to compute Φ directly, the second making use of an expression due to Madelung.[1] The first method is convenient for small β, the second for large β.

EVALUATION OF Φ IN TERMS OF ϕ

First Method

The potential at P due to a chain of class E (Fig. 1) is $\phi(\alpha, \beta, \frac{1}{2}\xi)$ and that due to a chain of class F is

[1] E. Madelung, Physik Z. **19**, 524 (1918).

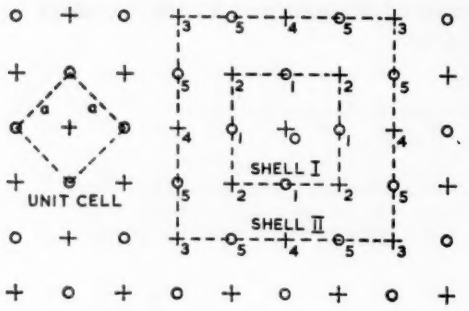

FIG. 2. Projection of lattice on to aa plane, showing the grouping of chains into shells. Here 0=chain of class F, +=chain of class E.

$\phi(\alpha, \beta, \frac{1}{2}+\frac{1}{2}\xi)$. Also,

$$\phi(0, \beta, \tfrac{1}{2}\xi)=0=\phi(0, \beta, \tfrac{1}{2}+\tfrac{1}{2}\xi)$$

and

$$\phi(1, \beta, \tfrac{1}{2}\xi)=0=\phi(1, \beta, \tfrac{1}{2}+\tfrac{1}{2}\xi),$$

since the dipoles vanish at $\alpha=0$ or 1.

In general,

$$\phi(1-\alpha, \beta, \tfrac{1}{2}\xi)=\phi(\alpha, \beta, \tfrac{1}{2}\xi)$$

and

$$\phi(1-\alpha, \beta, \tfrac{1}{2}+\tfrac{1}{2}\xi)=\phi(\alpha, \beta, \tfrac{1}{2}+\tfrac{1}{2}\xi),$$

so that any function of $\phi(\alpha, \beta, \frac{1}{2}\xi)$ and $\phi(\alpha, \beta, \frac{1}{2}+\frac{1}{2}\xi)$ need only be evaluated in the range $0<\alpha\leq 0.5$.

Consider the projection of the lattice on to the aa plane (Fig. 2). Let P lie on the chain 0. Consider the potential Φ_I due to the group of chains marked 1 and 2, which we shall call shell I. Let $a/c=\beta_0$.

For the class F chains marked 1; $r=2^{-\frac{1}{2}}a$; $\beta=2^{-\frac{1}{2}}\beta_0$. For the class E chains marked 2; $r=a$; $\beta=\beta_0$ and Φ_I is thus given by

$$\Phi_I(\alpha, \beta_0)=4\phi(\alpha, 2^{-\frac{1}{2}}\beta_0, \tfrac{1}{2}+\tfrac{1}{2}\xi)+4\phi(\alpha, \beta_0, \tfrac{1}{2}\xi).$$

Consider shell II, which consists of chains marked 3, 4, 5. For the class E chains marked 3; $r=2a$; $\beta=2\beta_0$. For the class E chains marked 4; $r=2^{\frac{1}{2}}a$; $\beta=2^{\frac{1}{2}}\beta_0$. For the class F chains marked 5; $r=(\frac{5}{2})^{\frac{1}{2}}a$; $\beta=(\frac{5}{2})^{\frac{1}{2}}\beta_0$. Thus the potential Φ_{II} at P, due to shell II, is

$$\Phi_{II}(\alpha, \beta_0)=4\phi(\alpha, 2\beta_0, \tfrac{1}{2}\xi)+4\phi(\alpha, 2^{\frac{1}{2}}\beta_0, \tfrac{1}{2}\xi)$$
$$+8\phi(\alpha, (\tfrac{5}{2})^{\frac{1}{2}}\beta_0, \tfrac{1}{2}+\tfrac{1}{2}\xi).$$

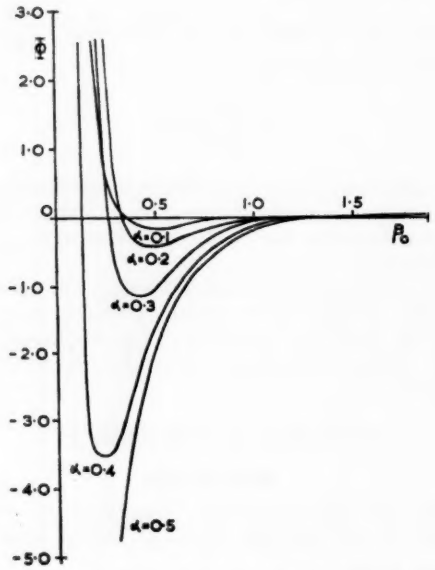

FIG. 3. Showing the variation of binding energy between chains (W) with α and β_0($W=e\Phi N$).

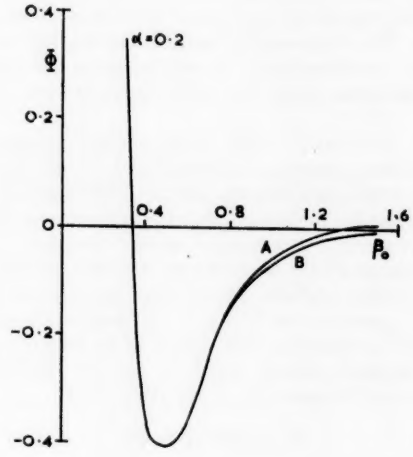

FIG. 4. Comparison of the two methods used in the evaluation of the binding energy between chains. Curve A: Φ calculated using first method. Curve B: Φ calculated using second method.

Finally Φ the required potential at P, is given by

$$\Phi=\Phi_I+\Phi_{II}+\Phi_{III}+\cdots,$$

where Φ_{III} etc., are given by expressions similar to those for Φ_I and Φ_{II}.

A few sample values of Φ_{III} were calculated, and it was found that for $\beta_0\geq 0.1$ the value of Φ_{III} was much less than that of $\Phi_I+\Phi_{II}$. Accordingly Φ_{III} and higher terms were neglected.

Second Method

Madelung[1] showed that the potential, $\phi(r, z)$, due to an infinite line of equidistant like point charges of magnitude e, separated by distances c, could be written

as

$$\phi(r, z) = 4e/c \sum_{m=1}^{\infty} K_0(2\pi mr/c) \cos(2\pi mz/c) + 2e/c \ln(2c/r) + \text{constant}, \quad (2)$$

where K_0 is a Bessel function of the second kind. When the potential of a chain consisting of equal numbers of opposite charges is considered, as is the case with the present problem, the last two terms on the right-hand side cancel. It can easily be seen that, using Eq. (2) with the appropriate values of $\beta = r/c$,

$$\Phi_{\mathrm{I}} = 16e/c \sum_{m=1}^{\infty} [1 - \cos(2\pi m\alpha)][K_0(2\pi m\beta_0) + (-1)^m K_0(2^{\frac{1}{2}}\pi m\beta_0)]$$

and

$$\Phi_{\mathrm{II}} = 16e/c \sum_{m=1}^{\infty} [1 - \cos(2\pi m\alpha)][2K_0(10^{\frac{1}{2}}\pi m\beta_0) + (-1)^m\{K_0(4\pi m\beta_0) + K_0(2^{\frac{1}{2}}\pi m\beta_0)\}].$$

Similar expressions for Φ_{III} and Φ_{IV} can be obtained. Again shells higher than the second may be neglected. These expressions are convenient for the evaluation of Φ for $\beta_0 > 0.5$.

RESULTS

The first method was used to evaluate Φ for values of α in the range $0 < \alpha \leq 0.5$ and β_0 in the range $0.1 \leq \beta_0 \leq 1.5$. The results are shown graphically in Fig. 3. A Burroughs E 101 computer was used to evaluate the sums in each case to 15 terms.

The first method gave values of Φ which were slightly positive in the range $0.8 \leq \beta_0 \leq 1.5$, although for large values of β_0 the attraction between nearest neighbors must predominate. This is due to the sum being taken to only 15 terms.

The second method was used to evaluate Φ in the range $0.1 \leq \beta_0 \leq 1.5$ for $\alpha = 0.2$. A graph is plotted (Fig. 4.) of β_0 against Φ as computed by the two methods for $\alpha = 0.2$.

DISCUSSION

It will be seen from Fig. 3 that Φ has a minimum for values of $\beta_0 \approx 0.5$ and $0 < \alpha < 0.5$. When $\alpha = 0.5$ there is no short-range repulsion. This is to be expected since the nearest-neighbor chains are of class F and must, for $\alpha = 0.5$, give rise to an infinite attraction when $\beta_0 = 0$.

The short-range repulsion increases less rapidly as β_0 tends to zero for $\alpha = 0.1$ than for larger values of α. The reason for this is as follows. The repulsion between chains for small β_0 is independent of α provided $\beta_0 \ll \alpha$. The stage at which this occurs depends on the value of α. Thus when $\alpha = 0.1$, the value of β_0 at which the repulsion becomes independent of α is smaller than is the case for larger α, and the repulsion for $\alpha = 0.1$, $0 < \beta_0 < 0.4$ is less marked than for larger α.

Consider a polar crystal in which the permanent charge doublets are arranged as described above. If the size of the molecules is such as to allow them to adopt a value of $\beta_0 \approx 0.5$, then the binding between chains could be largely due to the electrostatic interaction of the permanent doublets. The van der Waals interaction is between instantaneous dipoles and should be smaller than the permanent doublet interaction when $\beta_0 \approx 0.5$.

An example of such a polar crystal is metaldehyde, in connection with which this work arose. Metaldehyde is tetragonal and the structure has been shown by Pauling and Carpenter[2] to consist essentially of dipole chains parallel to the c axis. The values of α and β_0 for metaldehyde are approximately 0.2 and 2.6, respectively. Since $\beta_0 \gg 0.5$, the binding between chains cannot be attributed to the permanent dipole interaction. The value of this contribution, as calculated by the above methods, is only 0.9 cal/mole. Sasada and Atoji[3] calculated that the binding energy due to the permanent dipoles in orthorhombic hexachloroethane was only 0.4% of the total binding energy. In the case of metaldehyde, although the electrostatic binding between chains contributes only a small amount to the total binding energy, the electrostatic binding in the chains is strong and may contribute substantially to the total binding energy.

ACKNOWLEDGMENTS

Thanks are due to Burroughs (S.A.) Ltd., for making their E 101 computer in Paris available for the evaluation of the sums, and to Professor F.R.N. Nabarro for valuable discussions.

[2] L. Pauling and D. C. Carpenter, J. Am. Chem. Soc. **58**, 1274 (1936).

[3] Y. Sasada and M. Atoji, J. Chem. Phys. **21**, 145 (1953).

NMR Spectra of Some Halogenated Propenes

J. D. SWALEN AND C. A. REILLY

Shell Development Company, Emeryville, California

(Received November 21, 1960)

The 40-Mc/sec nuclear magnetic resonance (NMR) spectra of $CF_3CF{=}CF_2$, *cis* and *trans* isomers of $CF_3CCl{=}CFCl$, and $CF_3CCl{=}CF_2$ have been analyzed in terms of the NMR parameters of the molecules; i.e., the magnetic shielding constants of the various fluorine nuclei and the spin-spin coupling constants between them.

The spectrum of perfluoropropylene, $CF_3CF{=}CF_2$, has been analyzed adequately by a first-order perturbation treatment. The spectrum of each of the isomers of $CF_3CCl{=}CFCl$ has been analyzed exactly as an AB_3 system of spins by the use of the trace relations only. In a previous analysis of the *cis*-isomer, a small signal from the *trans*-isomer was not identified. This small signal has now been proved to arise from the *trans*-isomer. The spectrum of $CF_3CCl{=}CF_2$ has been analyzed by an iterative scheme on an electronic computer. Here the nuclei were treated as an ABC_3 system of spins.

The various magnetic parameters determined by these analyses have been compared with the molecular structures and have been briefly discussed in terms of the theories of the magnetic properties of molecules.

INTRODUCTION

THE nuclear magnetic resonance (NMR) spectra of a number of halogenated olefins have been reported by McConnell, McLean, and Reilly.[1–3] Each of these spectra was analyzed in terms of the various magnetic shielding constants and spin-spin coupling constants by perturbation theory. In all cases except two, the calculated spectra agreed satisfactorily with those observed and only minor refinements could be accomplished by more complete analyses. The two exceptions, which we have now analyzed successfully by the techniques described in this paper, were spectra of the compounds

$$CF_3CCl{=}CFCl \qquad (I)$$

and

$$CF_3CCl{=}CF_2. \qquad (II)$$

The spectra of both compounds possess several lines between the main CF_3 "doublets." McConnell and Reilly[3] called these lines in the spectrum of compound I, "signal X," and were unable to account for their presence. Recently, Fessenden and Waugh[4] suggested that "signal X" must be due to some impurity, probably an isomer of the main component. The analysis given below proves that such is the case and that the impurity is the *trans* isomer of the main component, which is the *cis* isomer. The central lines in the spectrum of compound II are in agreement with theory and are in general to be expected in an ABC_3 system of spins.[4]

In addition to these results on the NMR spectra of compounds I and II, we have analyzed the spectrum of perfluoropropylene, $CF_3CF{=}CF_2$. In this case, first-order perturbation theory gave sufficiently accurate results.

Finally, the various magnetic parameters derived from all the spectra are discussed in terms of the molecular structures and the current theories of magnetic interactions in molecules.

ANALYSIS OF THE $CF_3CF{=}CF_2$ NMR SPECTRUM

The 40-Mc/sec NMR spectrum of perfluoropropylene is shown in Fig. 1. Since the multiplets are so well separated from one another, this spectrum was analyzed quite well by first-order perturbation theory. In Table VII the NMR parameters as determined from the spec-

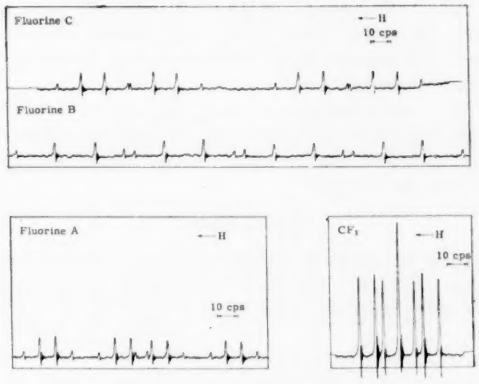

FIG. 1. NMR spectrum of

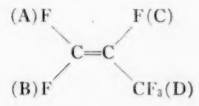

at 40 Mc/sec.

[1] H. M. McConnell, A. D. McLean, and C. A. Reilly, J. Chem. Phys. **23**, 1152 (1955).
[2] H. M. McConnell, C. A. Reilly, and A. D. McLean, J. Chem. Phys. **24**, 479 (1956).
[3] H. M. McConnell and C. A. Reilly, J. Chem. Phys. **25**, 184 (1956).
[4] R. W. Fessenden and J. S. Waugh, J. Chem. Phys. **30**, 944 (1959).

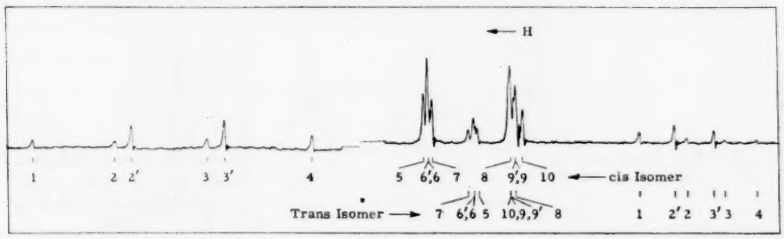

FIG. 2. NMR spectrum of $CF_3CCl{=}CFCl$ at 40 Mc/sec.

trum are listed. The chemical shift values (δ) are given in ppm from the CF_3 group in CF_3CF_2COOH used as an external reference. The absolute values of the coupling constants are in cycles per second. The spectra were not, however, sufficiently perturbed to allow the signs of these constants to be determined. The coupling constants given in Table VII are believed to have been determined somewhat more accurately than those previously published.[2]

ANALYSIS OF $CF_3CCl{=}CFCl$ SPECTRA

The NMR spectrum of a mixture of the two isomers of $CF_3CCl{=}CFCl$,

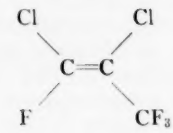

(*cis* isomer)

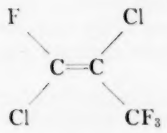

(*trans* isomer),

recorded at 40 Mc/sec is shown in Fig. 2. The assignment of the lines to the two isomers assumes $J_{AB}>0$ in each case, and is as shown in Figs. 2 and 3.

Lines labeled 5, 6, 6′, and 7 in the spectrum of the *trans* isomer were previously called "signal X" and lines labeled 1, 2, 2′, 3, 3′, and 4 in this spectrum were previously assigned to an impurity.[3] The high-energy members (8, 9, 9′, 10) of the CF_3 "doublet" in the spectrum of the *cis* compound exhibit an unsymmetrical pattern because of the presence of the corresponding members of the *trans* "doublet" superimposed on them. The resonances from the single fluorine atom in both compounds are split into six lines. On the basis of first-order perturbation theory the pattern would be a 1:3:3:1 quartet. Here the higher perturbation splits each of the middle lines into two lines. The stronger lines (2′ and 3′) arise from transitions between those energy levels with the symmetry of the E species of the C_3 symmetry group (see Fig. 3). The weaker lines (2 and 3) arise from the corresponding A levels. The intensity ratio follows from the twofold degeneracy of the E levels so that $E{:}A=2{:}1$.

In Fig. 4 the 56.4-Mc/sec NMR spectrum of this mixture of isomers is shown. The lines labeled 5, 6, 6′, and 7 in the spectrum of the *trans* isomer are clearly shifted from the center of the CF_3 doublet in the spectrum of the *cis* isomer proving that the lines 5, 6, 6′, and 7 did not arise from the same nuclei as the stronger CF_3 multiplets.

Each of the spectra was analyzed from its derived energy levels according to the method of Reilly and Swalen[5] using the results of Pople, Schneider, and Bernstein.[6] The appropriate NMR energy level diagram is shown in Fig. 3. An interesting and useful short cut in the analyses was pointed out by L. L. van Reijen[7] and is based on the invariance of the traces, i.e., the sum of the energy levels of each F_z submatrix is equal to the sum of the diagonal elements of this submatrix. Since in the present case there are only

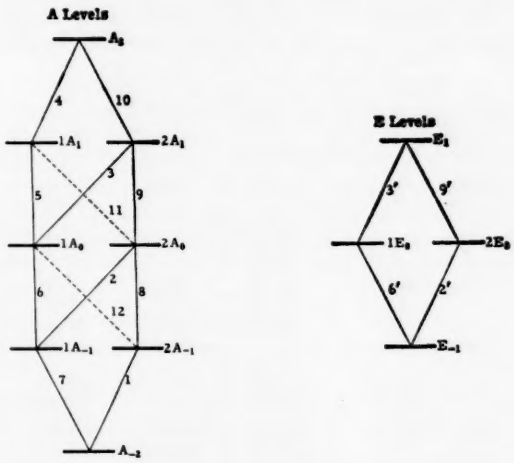

FIG. 3. NMR energy level diagram for an AB_3 system of spins.

[5] C. A. Reilly and J. D. Swalen, J. Chem. Phys. **32**, 1378 (1960).
[6] J. A. Pople, W. G. Schneider, and H. J. Bernstein, *High-Resolution Nuclear Magnetic Resonance* (McGraw-Hill Book Company, Inc., New York, 1959).
[7] L. L. van Reijen, (private communication).

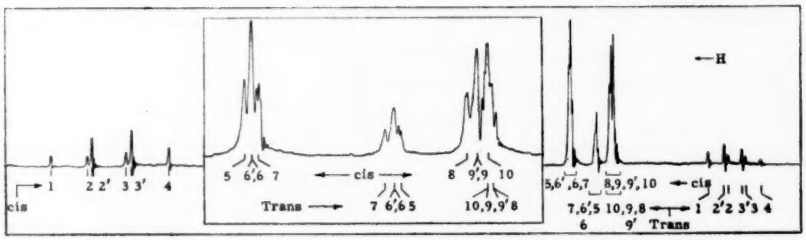

FIG. 4. NMR spectrum of $CF_3CCl{=}CFCl$ at 56.4 Mc/sec.

three parameters,

$$h_A=\tfrac{1}{2}\eta_A H_0(1-\sigma_A),$$

$$h_B=\tfrac{1}{2}\eta_B H_0(1-\sigma_B),$$

$$J=J_{AB},$$

to be determined, a sufficient number of relations can be obtained from the energy levels A_2, A_{-2}, E_1, and E_{-1}, and the traces of the matrices for $F_z=1, 0$, and -1:

$$1A_1+2A_1=4h_B-2J,$$

$$1A_0+2A_0=-2J,$$

$$1A_{-1}+2A_{-1}=4h_B-2J,$$

$$1E_0+2E_0=-2J.$$

The use of this method eliminated any necessity for diagonalization of the matrices.

The labeling scheme we have adopted for the transitions of an AB_3 system of spins is such that the lines increase in energy in both alphabetical and numerical order when $\sigma_A \gg \sigma_B$ and $J_{AB}>0$. Note that our labeling differs from that of reference 6, but is consistent with that of reference 5.

For the assignments of Figs. 2 and 4 the observed and calculated transition energies (relative to line No. 1 of the *cis* isomer) are given in Tables I and II. The energy levels obtained from the observed transitions are given in Tables III and IV and a summary of the NMR parameters determined from these levels by the method outlined above is given in Table VII. The identification of which isomer was *cis* and which one was *trans* was determined from the magnitudes of the coupling constants to the CF_3 group. In $CF_3CF{=}CF_2$ these coupling constants are 22.0 cps and 8.7 cps for the F nuclei *cis* and *trans* to the CF_3 group, respectively (see Table VII). These compare well with the values 24.3 cps and 10.4 cps for the isomer assignment we have made. The intensities in the spectra indicate that the *cis* to *trans* ratio in this mixture is about 3:1.

It is noted that, in this particular case, the spectra at 40 Mc/sec could have been analyzed equally well

TABLE I. NMR transitions in *cis* $CF_3CCl{=}CFCl$ (positions relative to transition No. 1).

Transition No.	Energy at 39.996 Mc/sec Obs	Calc	Energy at 56.4 Mc/sec Obs	Calc
1	0 cps	−0.04 cps	0 cps	−0.21 cps
2	21.3	21.40	22.2	22.26
2′	25.3	25.35	25.1	25.08
3	45.1	45.24	46.3	46.40
3′	49.7	49.61	49.5	49.44
4	72.6	72.32	72.7	72.65
5	231.2	231.04	313.7	313.80
6′	232.5	232.31	314.6	314.54
6	232.5	232.54	314.6	314.66
7	233.4	233.44	315.5	315.47
8	254.9	254.88	338.0	337.94
9	256.4	256.38	338.9	338.80
9′	256.4	256.57	338.9	338.90
10	258.2	258.12	340.2	340.05
11	...	442.18	...	606.20
12	...	466.02	...	630.34

TABLE II. NMR transitions in *trans* $CF_3CCl{=}CFCl$ (positions relative to transition No. 1 of the *cis* isomer).

Transition No.	Energy at 39.996 Mc/sec Obs	Calc	Energy at 56.4 Mc/sec Obs	Calc
11	...	188.29 cps	...	251.23 cps
12	...	198.48	...	260.91
7	243.2 cps	243.33	329.2 cps	329.09
6′	244.7	244.47	330.2	330.06
6	244.7	244.76	330.2	330.39
5	245.7	246.03	331.0	331.23
10	254.9	254.32	340.2	339.85
9	254.9	254.95	340.2	340.07
9′	254.9	255.05	340.2	340.28
8	256.4	256.22	340.8	340.91
1	289.8	289.61	398.8	398.57
2′	299.1	299.07	407.9	407.82
2	302.4	302.50	410.1	410.39
3′	309.7	309.65	418.0	418.04
3	312.5	312.69	420.0	420.07
4	321.0	320.98	428.6	428.69

TABLE III. NMR energy levels (experimental) in *cis* $CF_3CCl{=}CFCl$.

39.996 Mc/sec				56.4 Mc/sec			
A_2	402.97 cps	...	...	A_2	526.70 cps	...	...
$1A_1$	330.49	...	...	$1A_1$	453.85	...	...
$2A_1$	144.69	E_1	147.00 cps	$2A_1$	186.45	E_1	188.10 cps
$1A_0$	99.47	$1E_0$	97.45	$1A_0$	140.13	$1E_0$	138.65
$2A_0$	−111.66	$2E_0$	−109.50	$2A_0$	−152.30	$2E_0$	−150.80
$1A_{-1}$	−133.03	E_{-1}	−134.95	$1A_{-1}$	−174.53	E_{-1}	−175.95
$2A_{-1}$	−366.51	...	...	$2A_{-1}$	−490.20	...	...
A_{-2}	−366.46	...	...	A_{-2}	−490.10	...	...

from the transitions themselves instead of from the derived energy levels because the unresolved multiplets of lines in the CF_3 resonances made an accurate measurement of some of the line positions impossible. Several of the energy levels were consequently located by only one measurement so no improvement in accuracy was to be expected by using the derived energy levels. The agreement between the observed and calculated spectra is about as good as can be expected in view of the large number of overlapping lines.

ANALYSIS OF $CF_3CCl{=}CF_2$ SPECTRUM

The 40-Mc/sec NMR spectrum of

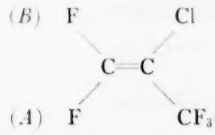

is shown in Fig. 5. The line positions relative to transition No. 5 as zero are given in Table V. The 56.4-Mc/sec NMR spectrum was also obtained, but it was not sufficiently simpler than the one shown in Fig. 5 to be of any assistance in the analysis. Indeed some information was lost since fewer lines were resolved and no combination lines appeared.

The CF_3 resonance consists of a number of weaker lines between two main multiplets, which are separated by approximately $J_{AX}+J_{BX}$. These central lines are to be expected from an ABC_3 system of spins and are not analogous to "signal X" in the $CF_3CCl{=}CFCl$ spectra as previously thought.[3] The AB pattern is seen to be well mixed and consequently caused considerable difficulty in the analysis. One would expect, from a first-order perturbation by the AC and BC coupling on an AB pattern, to obtain a pattern similar to that shown in Fig. 6 in which the AB pattern consists of four lines each split into quartets. However, the observed spectrum shows only a vague resemblance to this pattern.

The ABX_3 approximation (see references 4 and 6) was applied next. The results of this approximate calculation are given below and were used to start the ABC_3 analysis.

ABX_3 APPROXIMATE ANALYSIS

From the CF_3 pattern the separation of the strongest transitions (18, 18′ and 27, 27′) gave the sum $4j=J_{AX}+J_{BX}$ (approx). The measured value of 32.8 cps was compared with the results on *cis* and *trans* $CF_3CCl{=}CFCl$ (see Table VII) where a value of 34.7 cps was obtained for this sum. Hence, J_{AX} and J_{BX} were assumed to be of equal sign. Also, from the

TABLE IV. NMR energy levels (experimental) in *trans* $CF_3CCl{=}CFCl$.

39.996 Mc/sec				56.4 Mc/sec			
A_2	535.74 cps	...	...	A_2	717.51 cps	...	...
$1A_1$	214.36	...	...	$1A_1$	288.63	...	...
$2A_1$	281.01	E_1	279.70 cps	$2A_1$	377.46	E_1	376.57 cps
$1A_0$	−31.49	$1E_0$	−29.90	$1A_0$	−42.67	$1E_0$	−41.38
$2A_0$	26.24	$2E_0$	24.70	$2A_0$	37.33	$2E_0$	36.37
$1A_{-1}$	−276.26	E_{-1}	−274.50	$1A_{-1}$	−372.84	E_{-1}	−371.58
$2A_{-1}$	−229.99	...	...	$2A_{-1}$	−303.37	...	...
A_{-2}	−519.59	...	...	A_{-2}	−702.07	...	...

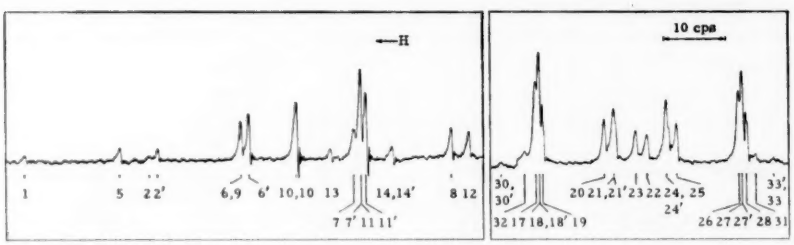

FIG. 5. NMR spectrum of $CF_3CCl{=}CF_2$ at 40 Mc/sec.

analysis of $CF_3CF{=}CF_2$ it was evident that $|J_{AX}|>|J_{BX}|$. We further assumed for convenience that both J_{AX} and J_{BX} are positive in $CF_3CCl{=}CF_2$. Therefore, $j'{=}1/4\ (J_{AX}-J_{BX})$ was also positive. From a comparison of the observed spectrum with that given in Fig. 6, it was probable that $h_A<h_B$. Since

$$D_{\pm\frac{1}{2}}{}^2=[(h_B-h_A)\mp 3j']^2+4j^2,$$

and

$$D_{\pm\frac{1}{2}}{}^2=[(h_B-h_A)\mp j']^2+4J^2,$$

both $D_{-\frac{1}{2}}$ and $D_{-\frac{1}{2}}$ would then be positive and either or both $D_{+\frac{1}{2}}$ or $D_{+\frac{1}{2}}$ might be negative.

There were two cases which we considered: (1) If $3j'<(h_B-h_A)$ then

$$D_{-\frac{1}{2}}>D_{-\frac{1}{2}}>|D_{+\frac{1}{2}}|>|D_{+\frac{1}{2}}|.$$

(2) If $(h_B-h_A)<3j'$ then

$$D_{-\frac{1}{2}}>D_{-\frac{1}{2}}>|D_{+\frac{1}{2}}| \quad \text{and} \quad |D_{+\frac{1}{2}}|<D_{-\frac{1}{2}}.$$

Up to this point, it had not been established which case applied to the spectrum of Fig. 5. However, it was possible to determine various sums and differences between the D's from the group of lines in the central portion of the CF_3 pattern (20 through 25) together with the combination lines observed as satellites to this pattern. The results were found to be

$$D_{-\frac{1}{2}}=18.75 \text{ cps}, \qquad (h_B-h_A)=6.1 \text{ cps},$$
$$D_{-\frac{1}{2}}=12.95 \text{ cps}, \qquad j'=3.5 \text{ cps},$$
$$D_{+\frac{1}{2}}=8.85 \text{ cps}, \qquad |J_{AB}|=4|J|=17.2 \text{ cps},$$
$$D_{+\frac{1}{2}}=-9.75 \text{ cps}.$$

The J_{AX} and J_{BX} were now determined from the value of $j(=8.2 \text{ cps})=1/4(J_{AX}+J_{BX})$ found earlier and the value of $j'(=3.5 \text{ cps})$ given above,

$$J_{AX}=23.4 \text{ cps}$$
$$J_{BX}=9.4 \text{ cps}.$$

An approximate value of 35.1 cps for (h_A+h_B) was found from the estimated weighted mean position in the AB pattern (cf. Fig. 6).

Since (h_B-h_A) was 6.1 cps then

$$\begin{cases} h_A=14.5 \text{ cps} \\ h_B=20.6 \text{ cps}. \end{cases}$$

The remaining parameter h_X needed for calculating line positions and intensities was found from the center of the CF_3 pattern to be 268.7 cps.

ABC_3 SOLUTION

All line positions and intensities could now be calculated as an ABX_3 and at least a partial assignment

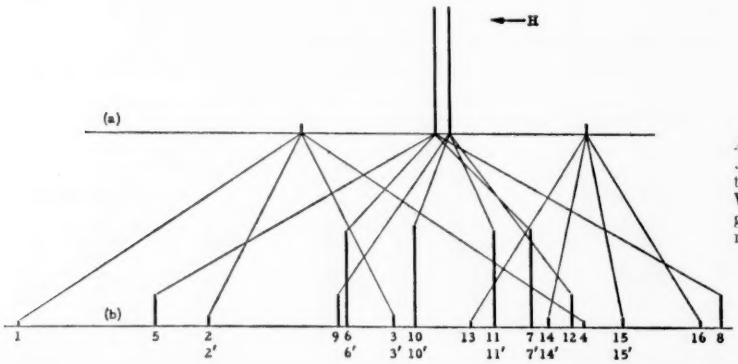

FIG. 6. Calculated AB pattern for an ABX_3 system of spins, assuming $J_{BX}<J_{AB}<J_{AX}$, $h_A<h_B$. (a) Without perturbation by the group of 3 spins, (b) With first-order perturbation by the group of 3 spins. Lines 1–8 from A nucleus, 9–16 from B nucleus.

TABLE V. Observed and calculated 40 Mc/sec NMR spectrum of $CF_3CCl{=}CF_2$.

Transition No.	Obs ν	Calc ν	Relative intensity calc	Transition No.	Obs ν	Calc ν	Relative intensity calc
1	−16.7	−16.56	0.49	29	...	504.91	0.04
5	0	0.10	1.25	30	515.6	515.08	0.31
2	5.2	5.09	0.36	30′	515.6	515.82	0.18
2′	6.6	6.57	0.68	32	518.9	518.74	0.55
6	21.7	21.77	1.54	17	520.6	520.35	3.21
9	21.7	21.75	1.32	18	521.1	521.00	4.27
6′	23.1	23.23	3.15	18′	521.1	520.96	2.13
3	...	25.91	0.07	19	521.6	521.57	3.19
3′	...	27.12	0.10	20	531.5	531.64	3.02
10	32.1	31.83	1.56	21	533.1	533.13	3.77
10′	32.1	32.26	3.19	21′	533.1	533.44	1.86
13	38.5	38.41	0.57	23	536.5	536.79	2.49
4	...	42.35	0.10	22	538.2	538.25	2.47
7	42.8	42.59	1.99	24′	541.5	541.50	1.80
7′	43.9	43.78	4.05	24	541.5	541.81	3.65
11	43.9	43.96	1.98	25	543.1	543.22	2.89
11′	44.8	44.75	4.04	26	553.2	553.31	2.82
14	49.0	48.51	0.39	27	553.9	553.95	3.74
14′	49.0	48.92	0.72	27′	553.9	553.99	1.79
8	59.1	59.02	2.06	28	554.6	554.58	2.80
15	...	60.64	0.07	31	556.2	556.30	0.47
15′	...	61.41	0.08	33′	559.0	559.13	0.15
12	62.3	61.86	2.11	33	559.0	559.86	0.26
16	...	78.52	0.15	34	...	569.95	0.03

should be possible. Instead, two spectra and their associated matrices were calculated on a Bendix G-15 computer with the ABX_3 parameters, one with J_{AB} positive and one with J_{AB} negative. At this stage the spectra were equally well fitted with either assumption.

On the basis of these calculations, an assignment, shown in Fig. 5, was made assuming J_{AB} to be positive. The NMR energy level diagram for this ABC_3 system of spins is shown in Fig. 7. Note here also that our labeling differs from that of references 4 and 6. The labeling of the transitions is appropriate for a spectrum that approaches an ABX_3 type and the lines increase in energy in numerical order if $h_A < h_B \ll h_X$ and also if both $3j'$ and $2J$ are less than $(h_B - h_A)$. If the latter conditions were not satisfied, then it could be expected that the numbers of some of the transitions as labeled would not fall in the order of their energy. For example, in $CF_3CCl{=}CF_2$ the orders of transitions 31 and 32 as well as 22 and 23 were found to be inverted for this reason. If the spectrum should approximate an XBC_3 type,

$$h_X \ll h_B < h_C,$$

then the more appropriate labeling would be different from that shown in Fig. 7. Furthermore, instead of the combination lines shown in this figure, a different group of 12 such lines might be expected to appear. In a true ABC_3 spectrum any of the 46 possible transitions may occur with nonzero intensity.

The experimental energy level matrix Λ_{exp} was next determined in the usual way[5] from these line positions and are given to the nearest hundredth of a cps in Table VI. This energy level matrix together with the eigenvectors S_{ij} obtained during the diagonalization of the approximate Hamiltonian matrix calculated earlier, were then fed into another Bendix G-15 program which calculated the products

$$(H_{exp})_{nn} = \sum_i S_{ni}^2 (\lambda_{exp})_i.$$

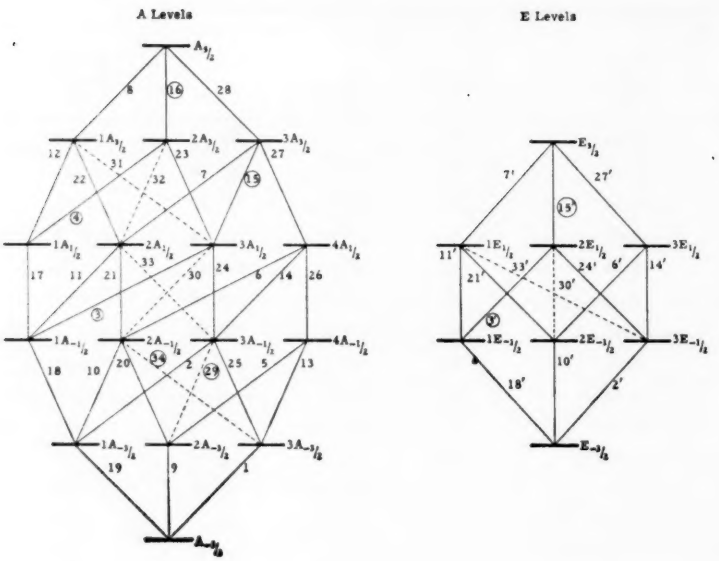

FIG. 7. NMR energy level diagram for ABC_3 system of spins. Circled transitions are missing in $CF_3CCl{=}CF_2$. Combination lines are shown dashed.

These 24 linear equations were solved by least squares to give new values for the 6 NMR parameters: h_A, h_B, h_C, J_{AB}, J_{AC}, and J_{BC}. The whole process was iterated until a consistent solution was obtained. The J_{AC} and J_{BC} were found to converge rather slowly to their final values. In order to speed up the convergence, next approximations were estimated by extrapolation after each step or so and these values were fed into the computer. The convergent parameters for this molecule at $\nu_0=39.996$ Mc/sec were found to be

$$h_A=15.03 \text{ cps}, \qquad J_{AB}=+16.65 \text{ cps},$$
$$h_B=21.12 \text{ cps}, \qquad J_{AC}=+23.83 \text{ cps},$$
$$h_C=268.58 \text{ cps}, \qquad J_{BC}=+9.20 \text{ cps},$$
$$\frac{(2h_C-2h_A)\times 10^6}{\nu_0}=\delta_{AC}=12.68 \text{ ppm},$$
$$\frac{(2h_C-2h_B)\times 10^6}{\nu_0}=\delta_{BC}=12.37 \text{ ppm}.$$

TABLE VI. NMR energy levels at 40 Mc/sec for $CF_3CCl{=}CF_2$ (transition No. 5 as reference point).

A Symmetry		E Symmetry	
$A_{3/2}$	870.78	...	...
$1A_{1/2}$	811.87	...	...
$2A_{1/2}$	792.53	$E_{3/2}$	317.15
$3A_{1/2}$	316.22		
$1A_{1/2}$	749.93	$1E_{1/2}$	273.30
$2A_{1/2}$	273.34	$2E_{1/2}$	255.65
$3A_{1/2}$	255.68	$3E_{1/2}$	−236.82
$4A_{1/2}$	−237.73	...	...
$1A_{-1/2}$	229.50	$1E_{-1/2}$	228.70
$2A_{-1/2}$	−259.63	$2E_{-1/2}$	−259.95
$3A_{-1/2}$	−286.19	$3E_{-1/2}$	−285.75
$4A_{-1/2}$	−791.14	...	...
$1A_{-3/2}$	−291.47	$E_{-3/2}$	−292.25
$2A_{-3/2}$	−791.20	...	...
$3A_{-3/2}$	−829.54	...	...
$A_{-3/2}$	−812.97	...	...

The parameters were fed into another program which calculated the line positions and intensities shown in Table V. The agreement with the observed spectrum is believed to be within experimental error. The square root of the sum of the squares of all the deviations

$$(\sum_i d_i^2/24)$$

of the observed from the calculated positions was calculated to be 1.5 cps.

Similar calculations to the above were then made assuming J_{AB} to be negative. The value of

$$(\sum_i d_i^2/24)$$

was found to be 1.9 cps. Hence, it was concluded that J_{AB}, J_{AC}, and J_{BC} are most likely all of the same sign in this molecule. It is not possible, however, to state whether they are all positive or all negative. For convenience it will be assumed that they are all positive.

The 56.4-Mc/sec spectrum was also calculated with appropriate values of the parameters derived from

TABLE VII. Summary of NMR parameters for some halogenated propenes

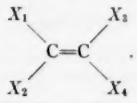

				ppm from external reference: CF_3 group in CF_3CF_2COOH				Cycles per second					
X_1	X_2	X_3	X_4	δ_1	δ_2	δ_3	δ_4	J_{12}	J_{13}	J_{14}	J_{23}	J_{24}	J_{34}
F	F	F	CF_2	11.6	25.1	110.6	−13.0	60.0	40.3	8.7	120.2	22.0	13.2
F	Cl	Cl	CF_2	−25.0	...	...	−23.7	...	...	10.4	...	...	...
Cl	F	Cl	CF_3	...	−18.4	...	−23.5	...	...	...	...	24.3	...
F	F	Cl	CF_3	−6.2	−5.9	...	−18.6	16.65	...	9.20	...	23.83	...

those given above. Agreement within the rather large estimated experimental uncertainties of up to 0.5 cps was obtained.

DISCUSSION AND CONCLUSIONS

A summary of the NMR parameters obtained for the halogenated propenes discussed in this paper is presented in Table VII. As indicated, the chemical shifts have all been referred to the CF_3 group of CF_3CF_2COOH used as an external reference. Rather large differences in these shifts are noted. However, in all four compounds the resonance of the fluorine *trans* to the CF_3 group occurs at lower applied field than the one *cis* to this group. In $CF_3CF{=}CF_2$, the resonance of the fluorine α to the CF_3 group occurs at a remarkably large applied field.

It is seen that $|J_{14}|$ and $|J_{24}|$ are each about the same in those molecules in which they were observable. Furthermore, $|J_{24}| > |J_{34}|$, i.e., the magnitude of the *cis* coupling to the CF_3 group is greater than that of the *trans* coupling to this group. This is opposite to what is usually found for the coupling between two fluorine or hydrogen nuclei bonded directly to C atoms connected by a double bond. It is not at present known if a similar inversion occurs for the analogous coupling of an H nucleus to a CH_3 group across a double bond, although there is some evidence that such may be the case.[8,9]

It will also be noted that $|J_{12}|$ is quite different in the two molecules in which it was observable. It has been shown[10] that the spin-spin coupling constant between the H nuclei in a CH_2 group is a sensitive function of the HCH angle, decreasing with increasing angle. If the theoretical treatment is also applicable to the CF_2 coupling (which is questionable), then the difference in J_{12} would reflect a difference in the FCF bond angle.

Ramsey[11] has developed a general theory of nuclear spin-spin coupling. Three terms contribute to this coupling. They are an orbital term, a dipole-dipole term, and a Fermi term. With protons the Fermi term is dominant. With fluorine nuclei, McConnell[12] has shown that the dipole-dipole term can give a sizeable contribution and that the orbital term gives only a small one. If such is the situation in these compounds, then comparisons between analogous H—H and F—F spin-spin couplings will be difficult.

If the Fermi term is very much larger than the other terms, or if the other terms contribute equally in both $CF_3CCl{=}CF_2$ and $CF_3CF{=}CF_2$, and if $J_{12}>0$ in $CF_3CF{=}CF_2$, then the larger coupling constant in $CF_3CF{=}CF_2$ would reflect a smaller angle. This seems, however, somewhat unlikely on steric grounds. Possibly all the coupling constants are negative or else the dipolar terms are masking any change in the J_{12} coupling constant due to an FCF angular change from $CF_3CF{=}CF_2$ to $CF_3CCl{=}CF_2$.

ACKNOWLEDGMENTS

We wish to thank Roy Johnson and J. Shoolery, Varian Associates, for obtaining the 56.4-Mc/sec spectra. We are also greatly indebted to R. U. Bonnar of these laboratories for programming the Bendix G-15 computer for this type of NMR spectral analysis.

[8] S. Alexander, J. Chem. Phys. **28,** 358 (1958).
[9] E. B. Whipple, J. H. Goldstein, and L. Mandell, J. Am. Chem. Soc. **82,** 3010 (1960).
[10] H. S. Gutowsky, M. Karplus, and D. M. Grant, J. Chem. Phys. **31,** 1278 (1959).
[11] N. F. Ramsey, Phys. Rev. **91,** 303 (1953).
[12] H. M. McConnell, J. Chem. Phys. **24,** 460 (1956).

Phosphorescence Spectra of Acenaphthene at Low Temperatures*

ADNAN ZMERLI†

Department of Physics, Duke University, Durham, North Carolina Laboratoire des Recherches Physiques de la Sorbonne—Paris Laboratoire Aime Cotton—Bellevue (S. et. O.)—France

(Received September 26, 1960)

The phosphorescence spectra of acenaphthene, both of single crystals and of solutions in different solvents (polystyrolene, benzene, or E.P.A.), were photographed at low temperatures. At 4° and 77°K unpolarized spectra of the crystal were obtained using a phosphoroscope, and at 20°K the polarized spectra along the three crystallographic axes had been photographed without the phosphoroscope. Some peculiarities linked to the existence of two different sets of molecules in the unit cell have been observed. Two progressions, here called "normal," connected to each set of molecules have been distinguished in the 4° and 77°K spectra but not in the 20°K spectrum. The interval between the corresponding bands of the two progressions is 28 cm^{-1}. In the 20°K spectrum two new series, here called "nonnormal," and which appear also in the 77°K spectrum have been observed. An attempt of interpretation of these "nonnormal" series has been advanced.

I. INTRODUCTION

THIS study is a continuation of research done on the polarized singlet-singlet absorption spectra of acenaphthene.[1,2]

The elementary cell of acenaphthene belongs to the orthorhombic group C_{2v}^2 and has two distinct sets of two molecules each.[3,4] This indicates that there are in the crystal two exciton bands containing both the two exciton levels for one excited level of the free molecule.

It has been verified that acenaphthene, molten between two fused quartz disks, crystallizes parallel to its cleavage plane σ_{ac}.

The spectra of many flakes of different thickness have been photographed and analyzed.[1,2] The polarized bands located at 30 547 cm^{-1} (medium strong) and at 30 836 cm^{-1} (very weak) in the c spectrum, and at 30 608 cm^{-1} (weak) and at 30 680 cm^{-1} (strong) in the a spectrum have been ascribed to the exciton transitions. The calculations using first-order perturbation theory (dipole-dipole approximation for the intermolecular potential)[5] with adjustable parameters agreed with the experimental results fairly well. It was concluded that the first singlet-singlet electronic transition of acenaphthene molecules is polarized along the short axis of the naphthalene ring. It is noteworthy that the relative intensities of the exciton bands observed agreed very well with those predicted by the molecules' orientation in the elementary cell as far as the last conclusion is concerned. Furthermore the $\Delta W+D_s$ (ΔW represents the energy of the free molecule transition and D_s, the Coulomb energy of exciton) terms in Davydov's formula,[6]

$$\Delta E=\Delta W+D_s+\epsilon_i \tag{1}$$

(ΔE stands for the energy of crystal transitions and ϵ_i for the resonance energy term of exciton), were located at 30 750 cm^{-1} for the first set and at 30 609 cm^{-1} for the second set.

In the case of the $T-S$ transition in crystals, it has been predicted[7] that the resonance energy term is so weak that the exciton splitting would not appear in the spectra. Hence, in this case Davydov's formula should be reduced to

$$\Delta E_T=\Delta W+D_T. \tag{2}$$

(The subscript T stands for the triplet state as S did for the singlet state.)

The Coulomb energy represents, as is known, the variation of the interaction energy between the molecules and its neighbors in a transition from the ground state to the excited state. Evans[8] showed that the $T-S$ spectra of many aromatic substances as solutes in different solvents are only slightly shifted from each other, contrary to the $S-S$ spectra for which, in some cases, the shift could reach several hundred wave numbers. Recently it has been seen that the $0'\rightarrow 0''$ transitions of the $T-S$ spectra of aromatic molecules in crystalline state and in rigid solution are located almost at the same energy; see, for instance, toluene[9] and naphthalene[10–13]—this means, in other words, that the Coulomb energy term D_T is not as strongly affected, in general, by changing the neighborhood of the excited molecule as is the D_S term.

* This work was supported at Duke University by the Office of Ordnance Research, U. S. Army.

† Present address: Faculté des Sciences de Tunis, 8 Rue de Rome, Tunis, Tunisia, North Africa.

[1] H. Poulet and A. Zmerli, Compt. rend. **248,** 3148 (1959).

[2] H. Poulet and A. Zmerli, talk given at the Spectroscopy International Congress at Bologna (Italy) September, 1959 (to be published in Mol. Spectroscopy).

[3] A. I. Kitajgordskii, Zhur. Fiz. Khim. **23,** 1036 (1949).

[4] J. P. Mathieu, M. Ecollan, and J. F. Ecollan, J. chim. phys. **51,** 250 (1954).

[5] D. P. Craig and P. C. Hobbins, J. Chem. Soc. **1955,** 539.

[6] A. S. Davydov, Zhur. Eksp. i Teort. Fiz. **18,** 210 (1948).

[7] R. E. Merrifield, J. Chem. Phys. **23,** 402 (1955).

[8] D. F. Evans, Nature **178,** 534 (1956).

[9] Y. Kanda and H. Sponer, J. Chem. Phys. **28,** 798 (1958).

[10] M. Kasha and R. V. Nauman, J. Chem. Phys. **17,** 516 (1949).

[11] J. Ferguson, T. Iredale, and J. A. Taylor, J. Chem. Soc. **1954,** 516.

[12] A. Terenin and Ermolaev, Trans. Faraday Soc. **52,** 1042 (1956).

[13] A. Zmerli, J. chim. phys. **56,** 405 (1959).

Nevertheless, in the case of $S-S$ transitions in crystalline solutions (guest molecule in a host crystal) in which the guest and host molecules have almost the same size and the crystals of the guest and host molecule are also much alike the shift is very small; the spectrum of crystalline solution starts almost from the middle of the exciton band of the pure crystal of the guest molecule. Two outstanding examples deserve to be recalled: light and heavy naphthalene in durene[14,15] and benzene in hexadeuterobenzene.[16,17]

In some $T-S$ spectra, a shift of one or two hundred wave numbers to the shorter wavelength has been observed when going from the crystal to the solution in E. P. A., see for instance the xylenes.[18] The case of benzene is even more striking.[19,20]

The $T-S$ spectra of acenaphthene at 4° and 77°K were studied with a phosphoroscope in an attempt (1) to discover some peculiarities linked to the existence of two different sets of molecules in the elementary cell and (2) to get more information concerning the interpretation of the polarized spectra obtained at 20°K under a steady illumination, some years ago (1956). At that time the author was working under the guidance of Dr. P. Pesteil in Paris.

TABLE I. Phosphorescence spectrum of acenaphthene in solution in polystyrolene at 20°K, obtained without phosphoroscope.

Wave numbers	Intensity	$\nu_0-\nu$	Assignment
20 650±10	s	0	$0'\rightarrow 0''$
20 150±20	w	500	20 650–500
20 080±20	w	570	20 650–229–343
19 500±15	m	1150	20 650–500–634
19 380±10	vs	1270	20 650–229–1051 or 20 650–2×634
19 100±10	s	1550	20 650–500–1051 or 20 650–1570
18 680±15	m	1970	20 650–544–1409 or 20 650–500–1476
18 000±15	s	2650	20 650–1217–1409
17 890±10	s	2760	20 650–1358–1409 or 20 650–500–1051–1217
17 720±10	s	2930	20 650–1358–1570 or 20 650–2×1476

[14] D. S. McClure and O. Schnepp, J. Chem. Phys. **23,** 1575 (1955).
[15] D. S. McClure, J. Chem. Phys. **24,** 1 (1956).
[16] A. Zmerli, H. Poulet, and P. Pesteil, talk given at "Colloque du C. N. R. S." at Bellevue (France) in July, 1957; Compt. rend. **245,** 517 (1957).
[17] A. Zmerli, J. chim. phys. **56,** 387 (1959).
[18] L. A. Blackwell, Y. Kanda, and H. Sponer, J. Chem. Phys. **32,** 1463 (1960).
[19] H. Shull, J. Chem. Phys. **17,** 296 (1949).
[20] P. Pesteil and A. Zmerli, Ann. phys. **10,** 1077 (1955).

TABLE II. Phosphorescence spectrum of acenaphthene in benzene solution at 20°K, obtained without phosphoroscope.

Wave numbers	Intensity	$\nu_0-\nu$	Assignment
20 650±10	s	0	$0'\rightarrow 0''$
20 575±10	w	75	?
20 150±20	w	500	20 650–500
19 440±10	w	1210	20 650–1217
19 260±10	m	1390	20 650–229–343–804
19 050±10	m–w	1600	20 650–1599
19 000±10	vs	1650	20 650–229–1409
18 805±10	vw	1845	20 650–804–1051
18 440±10	vs	2210	20 650–985–1217 or 20 650–804–1409

II. EXPERIMENTAL RESULTS

A. Apparatus

All results at 20°K have been achieved in Paris using a Huet visible spectrograph and a Cotton mercury arc coupled with a Wood filter as phosphorescence excitation source. The crystal samples employed in this work were the same as those used by Mathieu[4] in his Raman study and Pesteil[21] in his fluorescence work. The way of obtaining such crystals has already been published.[2,4,21] The work on the spectra at 77° and 4°K has been carried out at Duke University. Here a General Electric AH-6 high-pressure mercury arc served as the excitation source and the spectra were obtained with a Bausch & Lomb spectrograph. Dewars used in both laboratories are described elsewhere.[9,20]

B. Phosphorescence Spectra of Solutions of Acenaphthene

Two phosphorescence spectra of acenaphthene in solutions have been photographed at 20°K under a steady illumination: solution of acenaphthene in polystyrolene and solution of acenaphthene in benzene. The solution spectrum of acenaphthene in E. P. A. was obtained at 77°K using a phosphoroscope. The author will limit himself to the description and analysis of the two former spectra.

1. Spectrum of Acenaphthene in Solution in Polystyrolene at 20°K.

This spectrum, which consists of bands of medium width, starts with a band located at 20 650±10 cm^{-1}. All the other bands could be interpreted by starting from the 20 650±10 cm^{-1} band and subtracting from it the Raman vibrations of liquid acenaphthene, published by Luther and Reichel,[22] or their combinations (see Table I). Only the vibrations 500 and 1570

[21] P. Pesteil, Ann. phys. **10,** 128 (1955).
[22] H. Luther and C. Reichel, Z. physik. Chem. (Leipzig) **195,** 103 (1950).

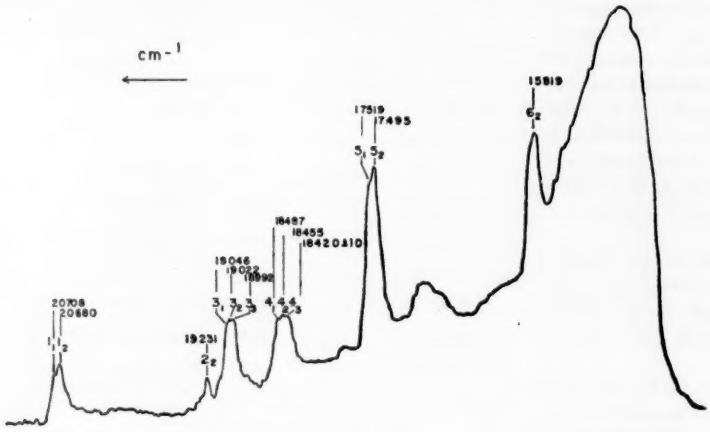

FIG. 1. Microphotometer tracing of a representative plate of the phosphorescence spectrum of acenaphthene crystal at 4°K.

cm^{-1} appear alone in the combinations. The vibrations 228, 343, 544, 634, 1051, 1217, 1358, 1409, and 1476 cm^{-1} are only involved in the combinations.

2. Spectrum of Acenaphthene in Benzene Solution at 20°K

This spectrum, the bands of which are narrower than those of the last spectrum, starts also at 20 650±10 cm^{-1} but does not look at all like the spectrum under 1, above. If one excepts the two bands located at 20 650± 10 cm^{-1} and 20 150±20 cm^{-1} all the other bands are not common. Nevertheless the spectrum could be interpreted also by starting from the 20 650±10 cm^{-1} and subtracting from it the wave numbers of the Raman vibrations of liquid acenaphthene or their combinations (see Table II). The vibration 1217 cm^{-1} which was involved in two combinations in the interpretation of the last spectrum and 1599 cm^{-1} appear here alone. The vibrations 804 and 985 cm^{-1}, which are missing in the last interpretation, appear here in the combinations. It is worth noting that the bands involving 500, 1217, and 1599 cm^{-1} alone are weak ones.

TABLE III. Phosphorescence spectrum of acenaphthene crystal at 4°K, taken with phosphoroscope.

Bands	Peaks	Wave numbers	Intensity	Assignment
1	1_1	20 708	w	$0' \rightarrow 0''$
	1_2	20 680	m	$0' \rightarrow 0''$
2	2_2	19 231	w	20 680–1449 (α_1)
3	3_1	19 046	w	20 708–227 (α_1)–1427 (α_1)
	3_2	19 022	m	20 680–227 (α_1)–1427 (α_1) or 20 708–227 (α_1)–1449 (α_1)
	3_3	18 992	m	20 680–227 (α_1)–1449 (α_1)
	3_4	18 962?	vw?	20 680–543 (α_1)–1173 (α_1)
4	4_1	18 487	w	20 708–638 (α_1)–1591 (α_1)
	4_2	18 455	m	20 680–638 (α_1)–1591 (α_1) or 20 708–2×543 (α_1)–1173 (α_1)
	4_3	18 420±10	m	20 680–2×543 (α_1)–1173 (α_1)
5	5_1	17 519	m	20 708–2×1591 (α_1)
	5_2	17 495	s	20 680–2×1591 (α_1)
6	6_1	15 845?	?	20 708–227 (α_1)–1449 (α_1)–1591 (α_1)
	6_2	15 819	s	20 680–227 (α_1)–1449 (α_1)–1591 (α_1)

C. Description and Analysis of Phosphorescence of Acenaphthene Crystal

1. Unpolarized Spectrum at 4°K Taken with a Phosphoroscope

This spectrum consists essentially of narrow bands numbered from 1 to 6. All exhibit a resolution which is clearly demonstrated on the microphotometer tracing (see Fig. 1). The first band shows two peaks located at 20 708 and 20 680 cm^{-1}. The second of them is much stronger than the first, which appears almost like a shoulder. The second band, the weakest of this spectrum, exhibits only one peak which would correspond to the strong peak 1_2 in the first band. The peak corresponding to the weak one at 20 708 cm^{-1} does not appear because of the weakness of the band. The bands 5 and 6 present the same shape as the first one. On the other hand, in the bands 3 and 4 it is possible to distinguish three peaks instead of two as in the bands 1, 5, and 6. Let us consider the third band and let us denote its peaks 3_1, 3_2, and 3_3. The peak 3_1 is the weakest one, much weaker than the two others. The peak 3_2 is the strongest one but not much stronger than the third one 3_3. The intervals between peaks 3_1 and 3_2 (19 046−19 022=24 cm^{-1}) and peaks 3_2 and 3_3 (19 022−18 992=30 cm^{-1}) are almost equal to the interval of the doublet of the first band (20 708−20 680=28 cm^{-1}). This observation leads to the possibility that bands 3 and 4 might result from a superposition of two doublets—the second and strong component of the first one coinciding with the first and weak component of the second doublet (see Table III).

This spectrum consists of two progressions. The weaker one contains all the weak components of the doublets and starts with the peak 1_1 at 20 708 cm^{-1}. The second progression, containing the strong component of the doublets begins with the peak 1_2 at 20 680 cm^{-1}. It is worth noting that this spectrum does not look like any spectrum of acenaphthene in solution (benzene, polystyrolene, or E. P. A.); nevertheless this spectrum and the spectrum of acenaphthene in solution in benzene seem to have some common bands: The peaks 1_2 (20 680 cm^{-1}), 3_2 (19 022 cm^{-1}), and 4_2 (18 455 cm^{-1}) would correspond to the bands at 20 650 cm^{-1} ($0' \rightarrow 0''$), 19 000 cm^{-1}, and 18 440 cm^{-1} of the solution spectrum.

The vibrational structure may be explained also by involving the vibrations α_1 (227, 543, 648, 1173, 1427, 1449, and 1591 cm^{-1}) observed in the Raman spectrum of acenaphthene crystal.[4] If one excepts the vibration 1449 cm^{-1} which appears alone, all the vibrations (1449 cm^{-1} included) appear in combinations with each other. The case of 1591 cm^{-1} is the most striking example. It is very hard to explain why 1591 cm^{-1} occurs in many combinations and in its second harmonic form (2×1591 cm^{-1}) and not alone.

TABLE IV. Phosphorescence spectrum of acenaphthene crystal at 20°K, obtained without phosphoroscope in the three *a*, *b*, and *c* polarizations.

Wave numbers	Intensity *a*	*b*	*c*	Assignments
19 070	...	m	vs	Head of the first progression
19 015	vvs	m	vs	Head of the second progression
18 992	m	...	vw	?
18 972	w	...	...	?
18 600	vvw?	...	...	19 015–418(α_1)
18 574	m	vw	w	19 015–447(α_2)
18 528	...	vw	w	19 070–543(α_1)
18 518	m	...	m	19 015–503(α_2)
18 483	...	...	w	19 070–582(α_1)
18 470	m	...	w	19 015–543(α_1)
18 436	m	m	w	19 015–582(α_1)?
18 411	m	...	...	19 070–237(β_1)–418(α_1)
18 403	...	...	w	19 070–668(?)
18 286	?	m	...	19 070–237(β_1)–543(α_1)?
18 239	?	m	vw	19 015–237(β_1)–543(α_1)?
18 175	w	...	vw	19 015–2×418(α_1)
18 121	...	...	vw	19 070–447(α_2)–503(α_2)
18 066	vw	...	vw	19 015–447(α_2)–503(α_2)
17 892	...	vw	m	19 070–1173(α_1)
17 842	m	vw	w	19 015–1173(α_1)
17 728	...	...	m	19 070–543(α_1)–804(α_1)
17 684	m	vw	w	19 015–543(α_1)–804(α_1)
17 637	...	m	s	19 070–1427(α_1)
17 588	s	m	m	19 015–1427(α_1)
17 462	...	m	s	19 070–1602(α_1)
17 411	s	m	m	19 015–1602(α_1)
17 233	?	m	w	19 015–237(β_1)–543(α_1)–999(α_1)
17 024	?	...	w	19 070–447(α_2)–1602(α_1)
16 969	?	...	w	19 015–447(α_2)–1602(α_1)

TABLE V. Phosphorescence spectrum of acenaphthene crystal at 77°K, taken with phosphoroscope.

Wave numbers	Intensity	Assignment
19 354	vw	20 725–1368
19 046	m	20 708–227(α_1)–1427(α_1)
19 023	m	20 680–227(α_1)–1427(α_1)
18 573	w	19 015–447(α_2)
18 522	w	19 070–582(α_1)
18 492	m	20 708–638(α_1)–1591(α_1)
18 461	m	20 680–638(α_1)–1591(α_1)
17 624	s	19 070–1427(α_1)
17 572	s	19 015–1427(α_1)
17 456	s	19 070–1602(α_1)
17 414	s	19 015–1602(α_1)
16 924	s	19 070–543(α_1)–1602(α_1)
16 008	s	19 070–3059(α_1)
14 833	s	19 070–1173(α_1)–3059(α_1)

2. *Polarized Spectra at 20°K, Obtained without a Phosphoroscope*

The polarized spectra of the sample have been photographed along the direction of the three crystallographic axes. The reader will find in Table IV the wave numbers of the bands forming these spectra, their intensity along the axes *a*, *b*, and *c*, and their vibrational analysis.

These spectra start at 19 070 cm^{-1}, a band which does not exist in the 4°K spectrum, and they obviously contain two progressions of different polarization. The bands located, for instance, at 19 070, 17 637, and 17 462 cm^{-1}, the strongest of the first progression, appear only along the *b* and *c* axes. They are missing in the *a* spectrum, even when the plate has been overexposed. On the other hand, their corresponding bands in the second progression located, respectively, at 19 015, 17 588, and 17 411 cm^{-1}, which are visible in the three directions, are stronger along the *a* axis than the *b* and *c* axes. The interval between the corresponding

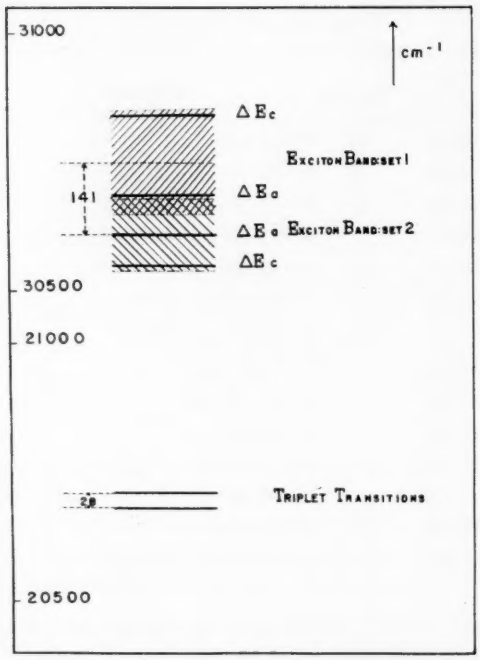

FIG. 2. Levels scheme for the lowest transitions of acenaphthene. The region between 21 000 and 30 500 cm^{-1} is not scaled for reasons of proportion.

bands of these two progressions is on the average equal to 52 cm^{-1}. One finds for the strongest doublet 19 070/015 cm^{-1} $\Delta\nu=55$ cm^{-1}, for the doublet of medium intensity 17 728/684 cm^{-1} $\Delta\nu=44$ cm^{-1}, and for the very weak doublet 18 121/18 066 cm^{-1} $\Delta\nu=55$ cm^{-1}, for instance.

Bands in each progression can be linked to the bands at 19 070 and 19 015 cm^{-1} by subtracting from them the wave number of one vibration α_1 for most of them, or a combination of α_1 vibrations for the rest of them. Only the doublet 18 121/066 cm^{-1} involves two vibrations α_2, in which case the symmetry of the combinations is α_1.

It is obvious that the two progressions found here do not correspond at all to the series under 1 above.

Many bands show up between 18 700 and 18 300 cm^{-1}. By comparing their relative intensities along the three directions, with those of the bands at 19 070 and 19 015 cm^{-1}, it has been possible to link the bands at 18 528, 18 483, 18 411, and 18 403 cm^{-1} to 19 070 cm^{-1} and the bands at 18 574, 18 518, and 18 470 cm^{-1} to 19 015 cm^{-1}. The α_2 vibrations 447 and 503 cm^{-1} have been used for interpreting the 18 574 and 18 518 cm^{-1} bands. The combinations 447 and 503 have been used for the doublet 18 121/066 cm^{-1} cited above. One combination of symmetry $\beta_1[237(\beta_1)+418(\alpha_1)]$ has been employed for the interpretation of the 18 411 cm^{-1} band which appears only along the a axis, in contrast to the 19 070 cm^{-1} band which is visible only in the b and c spectra. The vibration 668 cm^{-1} which appears in the liquid[22] and not in the crystal Raman spectrum[4] might fit fairly well for the interpretation of the 18 403 cm^{-1}. Because of its relatively strong intensity along the b axis, it is very hard to give a satisfactory explanation of the band at 18 436 cm^{-1} although the interval 19 015–18 436 = 579 cm^{-1} fits very well with the α_1 vibration 582 cm^{-1}.

The very weak bands appearing at 18 992 and 18 972 cm^{-1} seem to correspond to the peaks 3_2 and 3_3 of the 4°K spectrum, but this coincidence is perhaps fortuitous.

3. *Phosphorescence Spectrum at 77°K, Taken with a Phosphoroscope*

This spectrum starts with a very weak band located at 19 354 cm^{-1}, which does not appear at 4° or at 20°K. The origin of this band will be discussed later. Some doublets like the ones observed at 4°K appear at 19 046/023 and 18 492/61 cm^{-1} in this spectrum which contains also the following doublets pointed out at 20°K: 17 624/572 and 17 460/414 cm^{-1}. The bands found at 18 573 and 15 522 cm^{-1} have already been observed at 20°K. Hence, with the exception of a few bands including the first and very weak one at 19 354 cm^{-1} cited above, the spectrum is a mixture of bands already noticed at 20° and at 4°K (see Table V).

III. INTERPRETATION AND DISCUSSION

The 4°K spectrum is not difficult to interpret. By analyzing the $T-S$ spectra of acenaphthene in solution in benzene and polystyrolene at 20°K, which start with the same zero transition at 20 650 cm^{-1} (see Tables I and II), and comparing them with the 4°K spectrum, one can assign the bands at 20 708 and at 20 680 cm^{-1} as zero transitions of two sets of molecules in the unit cell. As expected the interval between the two $T-S$ zero transitions (20 708 − 20 680 = 28 cm^{-1}) is small compared to the corresponding interval between the centers of gravity of the exciton S_1 bands. (30 750 − 30 609 = 141 cm^{-1}); S_1 stands for the first excited state. From these results and those formerly obtained from the $S-S$ absorption spectra,[1,2] it is possible now to draw a level scheme for the lowest transitions of acenaphthene. It is represented in Fig. 2.

The most serious and difficult problem which remains to be solved concerns the explanations of the existence of the two series which appear at 20°K alone and at 77°K together with the series mentioned above, observed at 4°K. By comparing the 77°K spectrum with the 20° and 4°K spectra, one can see that the first bands of the 4°K crystal spectrum 20 708–20 680 cm^{-1}, called here the "normal" series, and the first bands of the 20°K crystal spectrum, 19 070–19 015 cm^{-1}, called here the "nonnormal" series, are missing at 77°K. The "normal" series start with the bands at 19 046–19 023 cm^{-1} at 77°K instead of the bands at 20 708 and 20 680

cm^{-1} at 4°K (compare Tables III and V). The "nonnormal" series begin with the bands 17 624 and 17 572 cm^{-1} at 77°K instead of the bands at 19 070 and 19 015 cm^{-1} at 20°K, as far as the strong bands are concerned (compare Tables IV and V). Hence, it seems that the effect of raising the temperature is to suppress some first bands of the series appearing at lower temperature.

The last remark should also be valid for the "nonnormal" series observed at 20°K. Hence we should look for their zero transitions on the shorter wavelength's side. As the doublet 19 070–19 015 cm^{-1} of the "nonnormal" series appearing at 20°K seems to correspond to the doublet 19 046–19 023 cm^{-1} of the "normal" series appearing at 4° and 77°K, it appears reasonable to locate their zero transitions at 20 725 and 20 670 cm^{-1}, which would be very close to the 20 708 and 20 680 cm^{-1} zero transitions of the normal series. These two "nonnormal" series may be attributed to molecules located in some lattice defect sites. In these lattice defects the molecules have obviously a neighborhood different from the one they would have in their normal sites. Consequently their correspondent term D_T of Eq. (2) written above would be different. The interval of 55 cm^{-1} is still much smaller than the corresponding interval between the centers of gravity of the exciton S_1 bands (141 cm^{-1}).

This last assumption could help to explain the polarization of the bands of the nonnormal series, which the author has been unable to elucidate, in spite of many attempts, from the normal positions of molecules in unit cells. A similar assumption could also help in understanding the different phosphorescence spectra of naphthalene obtained under a steady illumination at 20°K, with different samples (monocrystal, powder, flakes from alcoholic solution, sublimed naphthalene, etc.[23]). The few common bands of these different spectra may be attributed to a transition linked to molecules located in their normal sites; the other bands may be attributed to a molecule trapped in lattice defects which differ with the sample preparation.

This assumption leads also to an interpretation of the very weak band at 19 354 cm^{-1} observed in the 77°K spectrum. The difference $20\,725-19\,354=1371$ cm^{-1} almost coincides with the wave number of the vibration α_1 1368 cm^{-1} of an acenaphthene crystal.

It is worth noting that a similar assumption had been used in order to explain the weak series of bands appearing in the polarized absorption spectra of 2,6-dimethylnaphthalene beside the strong exciton series.[24]

IV. CONCLUSION

This study of phosphorescence spectra of acenaphthene crystal shows, as expected, some peculiarities which are attributed to the existence of two different sets of molecules in the unit cell. Two series have been observed. A tentative explanation of the "nonnormal" progressions appearing at 20° and 77°K has been advanced. Nevertheless, many questions remain unanswered. Full understanding of the mechanism involving the $T-S$ spectra of aromatic crystals still remains an open question.

ACKNOWLEDGMENTS

The author wishes to thank Professor H. Sponer for many discussions in connection with this work, for reading the manuscript and offering many helpful suggestions for its improvement. He acknowledges several stimulating and interesting discussions with Professor J. P. Mathieu, Dr. P. Pesteil, and Dr. H. Poulet at the Sorbonne, Paris.

[23] A. Zmerli, L. Pesteil, and P. Pesteil, Compt. rend. **242,** 2822 (1956).

[24] Talk given at the 26th annual meeting of the Southeastern Section of American Physical Society, in Gatlinburg, Tennessee, April 1960; A. Zmerli and H. Poulet, J. Chem. Phys. **33,** 1177 (1960).

NMR Spectra of Vinyl Chloride and the Chloroethylenes

E. B. WHIPPLE,* W. E. STEWART, G. S. REDDY, AND J. H. GOLDSTEIN

Department of Chemistry, Emory University, Atlanta 22, Georgia

(Received November 29, 1960)

The NMR spectra of vinyl chloride, the three dichloroethylenes, and trichloroethylene have been obtained and analyzed. Three deuterated species of vinyl chloride were used to facilitate the analysis and to obtain all the C^{13}—H couplings in this molecule. The C^{13}—H couplings were also obtained for the other chloroethylenes. The NMR parameters are compared for the entire series of compounds, and it is shown that a definite parallelism exists between the chemical shifts and the C^{13}—H couplings. The results are discussed in terms of the inductive and mesomeric properties of the chlorine substituent.

INTRODUCTION

THE application of the methods of microwave spectroscopy, in particular the analysis of hyperfine structure produced by quadrupolar nuclei, has permitted a reappraisal of the bonding situation in the vinyl halides, leading to a more modest estimate of the importance of lone-pair conjugation.[1,2] This approach has been employed in a recent study of vinyl chloride by Kivelson, Wilson, and Lide[3] who were able to obtain improved structural parameters and quadrupole coupling constants with the aid of isotopically substituted species.

Nuclear magnetic resonance spectroscopy is also capable, in principle, of providing new insights into the structure and electron distribution of the vinyl halides. For example, interest has been expressed in the values of the spin coupling constant in the CH_2 group, since this has been shown by Gutowsky *et al.*[4] to depend on the value of the HCH bond angle. Thus the value $J=-1.6$ cps obtained for vinyl bromide[5] is particularly interesting since it implies an HCH bond angle greater than 125°.[4]

This communication reports the results of a detailed study of vinyl chloride by NMR methods. The analysis was simplified considerably by the use of deuterated species of very high purity, which also permitted us to obtain all the C^{13}—H coupling constants in the molecule. In addition, NMR parameters have been obtained for all the dichloroethylenes and for trichloroethylene, and these have been compared with the results of the vinyl chloride analysis.

These studies were carried out with a Varian Associates model 4300-B high-resolution NMR spectrometer, equipped with flux stabilizer, and operating at 40 Mc. The calibrations were performed by the side-band modulation procedure, using a Krohn-Hite Model 440-B push-button audio oscillator.

Vinyl Chloride and Deuterated Vinyl Chlorides

The sample of normal vinyl chloride, $H_2C{=}CHCl$ (I), was the commercially available material, used without further purification. Three deuterated species were employed,

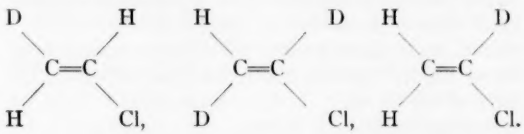

(II) (III) (IV)

The isotopic purity of these species was judged to be in excess of 95%, as indicated by their NMR spectra.

The analysis was originally carried out using the normal material I and species II and III. The α-substituted form (IV) was later analyzed separately as a check. For species I–III cyclohexane served as solvent and internal reference. The final values of the chemical shifts were converted to an internal TMS reference in cyclohexane, based on our measured value of the TMS peak relative to cyclohexane, 57.7 cps.

A typical spectrum of the mixed deuterated species, II and III, in cyclohexane is shown in Fig. 1. The three lines designated *C* correspond to the spectrum of III, while the lines designated *A* and *B* constitute the spectrum of II, as was verified by observations on the individual species. The six *A* lines are assigned to the proton adjacent to the halogen atom.

The chemical shifts for this deuterated mixture were measured at 4.56% and 11% total concentration, by weight, in cyclohexane, and no appreciable concentration shifts were observed in this range. The spectrum of C_2H_3Cl (I) was then calibrated at an intermediate concentration 8.67% giving the observed spectrum shown in Table I. The normal species (I) is an *ABC* system,[6] requiring for its analysis a rather laborious process of matching experimental and numerically computed results, but a considerable simplification is achieved by using initial values taken directly from the calibrated spectrum of the deuterated mixture

* Present address: Union Carbide Research Institute, Box 324, Tuxedo, New York.

[1] J. H. Goldstein, J. Chem. Phys. **24**, 507 (1956).

[2] J. H. Goldstein, J. Chem. Phys. **24**, 106 (1956).

[3] D. Kivelson, E. B. Wilson, and D. R. Lide, J. Chem. Phys. **32**, 205 (1960).

[4] H. S. Gutowsky, M. Karplus, and D. M. Grant, J. Chem. Phys. **31**, 1278 (1959).

[5] G. S. Reddy and J. H. Goldstein (to be published).

[6] R. W. Fessenden and J. S. Waugh, J. Chem. Phys. **31**, 996 (1959).

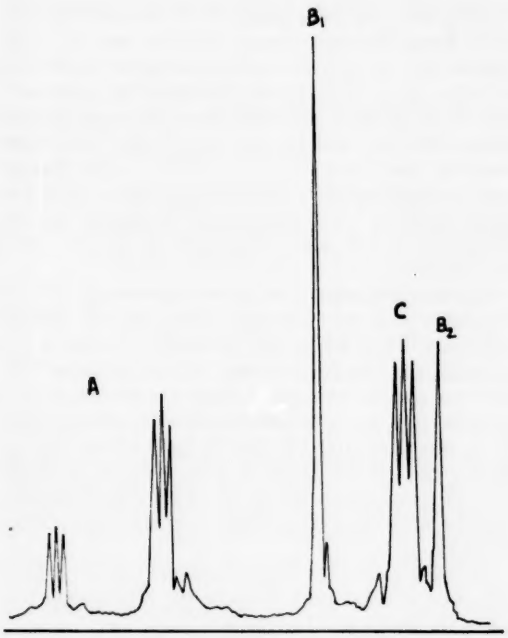

FIG. 1. NMR spectrum of mixture of CHD=CHCl and CHD=CDCl in cyclohexane solution.

(Fig. 1). These were adjusted, admitting both positive and negative values for the J's, until all lines in the spectrum of C_2H_3Cl agreed within the indicated experimental error. The ranges of adjustment were: $\omega_A = -189.5$ to -190.0 cps; $\omega_B = -157.3$ to -158.6 cps; $\omega_C = -152.5$ to -153.5 cps; $J_{AB} = 14.7 \pm 0.1$ cps; $J_{AC} = 6.5 \pm 1.1$ cps; and $J_{BC} = -2.0$ to $+2.0$ cps. The factor $\gamma_H/\gamma_D = 6.45$ was used to convert J_{HD} to the corresponding J_{HH}. The failure to observe splitting in the B lines (Fig. 1) fixes the limits of J_{BC} at ± 2.0 cps. The final adjusted values of the six parameters for C_2H_3Cl are shown in Table I; the agreement obtained for both the frequencies and intensities is seen to be quite satisfactory.

The analyses for the three deuterated species are quite straightforward. Table II gives the values of the parameters obtained for all the species studied, with the chemical shifts based on an internal TMS reference.

The C^{13}—H couplings were measured on pure liquid samples of the deuterated species. Because of the simplicity of the spectra this presented no difficulty, and the variety of species available made it possible to obtain this coupling for every position in the vinyl chloride molecule. The results are given in Table III.

Spectra of Dichloroethylenes and Trichloroethyenes

For purposes of comparison with vinyl chloride the chemical shifts were measured for *cis*- and *trans*-dichloroethylene, 1,1-dichloroethylene, and trichloroethylene in TMS solution. These values are given in Table III for a concentration of 5%. Dilution to 3% changes these values by no more than about 0.5 cps. Values of all the C^{13}—H couplings, as well as of the H—H couplings in the 1,2-dichloroethylenes, were obtained from the spectra of the pure liquids. Table III

TABLE I. Proton magnetic resonance shifts[a] and couplings for vinyl chloride in dilute[b] cyclohexane solutions.

I. Assignments

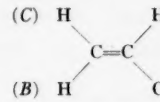

$\omega_A = -189.8$ $J_{AB} = 14.7$
$\omega_B = -158.5$ $J_{AC} = 7.5$
$\omega_C = -153.4$ $J_{BC} = -1.3$

II. Spectrum

Line	Calc freq.	Obs freq.	Dev.	Calc int.	Obs int.
1	−202.67	−202.7	0.03	0.498	0.46
2	−197.14	−197.2	0.06	0.277	0.30
3	−194.05	−194.1	0.05	0.378	0.34
4	−189.59	−189.5	−0.09	0.504	0.34
5	−186.49	−186.5	0.01	0.617	0.58
6	−180.97	−181.0	0.03	1.74	1.44
7	−164.54	−164.50	−0.04	1.501	1.501
8	−163.75	−163.7	−0.05	1.355	1.42
9	−156.98	−156.95	−0.03	1.234	1.12
10	−156.19	−156.20	0.01	1.156	1.14
11	−150.67	−150.70	0.03	1.484	1.34
12	−148.37	−148.5	0.13	1.257	1.20

[a] Expressed in cps at 40 Mc, from cyclohexane internal reference.
[b] 8.67% by weight.

TABLE II. NMR parameters for the isotopic vinyl chlorides.[a]

Parameter	H_2C=CHCl (I)	HDC=CHCl (II)	HD=CDCl (III)	H_2C=CDCl (IV)
ω_A	−247.6	−247.3	...	...
ω_B	−216.3	−215.2	...	−217.6
ω_C	−211.2	...	−210.4	−212.5
J_{AB}[b]	14.7	14.7	...	14.9±0.7
J_{AC}[b]	7.5	6.5±0.7	6.5±0.7	7.8±0.7
J_{BC}	−1.3	...	...	−1.3

[a] All values in cps at 40 Mc. The shifts are referred to TMS (internal). An uncertainty of ±0.5 cps is to be allowed in the chemical shifts of I–III since they were not extrapolated to infinite dilution. The shifts of IV refer to a concentrated solution (~30%) and will probably increase about 1.0–1.5 cps on extrapolation. Unless otherwise indicated the estimated uncertainty for the coupling constants is ±0.1 cps.
[b] J_{AB} is the *trans* H—H coupling constant, or the *trans* H—D coupling constant converted to the H—H value. J_{AC} is the *cis* H—H coupling, or the converted H—D value.

TABLE III. Summary of NMR results for the chloroethylenes.[a]

Compound			J(HH)		J(C^{13}H)
cis-$C_2H_2Cl_2$		−251.1	5.3		198.5
trans-$C_2H_2Cl_2$		−249.6	12.1		199.1
1,1-$C_2H_2Cl_2$		−215.3	...		166
C_2HCl_3		−252.9	...		201.2
C_2H_3Cl	α	−247.6	gem −1.3	α	195
	β-*cis*	−216.2	*cis* 7.5	β-*cis*	160
	β-*trans*	−211.1	*trans* 14.7	β-*trans*	161

[a] All values in cps at 40 Mc; shifts are referred to TMS (internal).

summarizes the results obtained for all the undeuterated chloroethylenes.

DISCUSSION

The values of J_{BC} for vinyl chloride (−1.3 cps) would imply, on the basis of Karplus' theory,[4] an HCH angle of 126.7°, intermediate between the vinyl fluoride and vinyl bromide values. It is worth noting that the corresponding coupling in 2-chloropropene is 1.38 cps[7] and that for 2-bromopropene is 1.9±0.2 cps. This suggests that the methyl group does not greatly affect this coupling and that, by inference, the $=CH_2$ couplings in the 2-halopropenes are also negative.

It should be noted that the apparent effect of D substitution on the chemical shifts (Table II) is outside the estimated experimental error. The effect of D substitution on J_{HC} is less certain due to the larger experimental error here, but is nevertheless believed to be real.

Several interesting observations emerge from the summary in Table III. It is quite striking that for all the compounds listed the value of ω falls between −247 and −252 cps whenever the proton is adjacent (α) to chlorine, and between −211 and −216 for protons β to chlorine. Comparing vinyl chloride with ethylene (−211.5 cps) under similar conditions we have ascertained that the effects of a single chlorine substitution on the three proton shifts are: −36, −5, and 0 cps at the α, β(*cis*) and β(*trans*) positions. This reflects the larger inductive withdrawal by chlorine at the nearest position, and possibly some cancellation of the inductive effect at the β positions by lone-pair conjugation. From the shift values obtained here, it is apparent that the α effect is rather insensitive to multiple chlorine substitution. In vinyl bromide the α, β(*trans*), and β(*cis*) protons are lower than the vinyl chloride values by 7, 22, and 14 cps, respectively.[5] This might result in part from a correspondingly larger diamagnetic deshielding effect. However, the *trans* value is so much lower in vinyl bromide as to suggest that the difference in lone-pair conjugation of Cl and Br is involved.

There is a marked parallelism between the C^{13}—H couplings and the chemical shifts for the chloroethylenes. Thus, for all cases in which a proton is α to chlorine, the coupling constant falls in the range 195–201 cps and for the cases where the proton is β to chlorine (but not α to another chlorine) the couplings lie in the range 160–166 cps. In light of the work of Muller and Pritchard,[8] this is to be expected, since the C^{13}—H couplings are shown by these workers to vary linearly with the charge density on the carbon atom involved.

We have attempted also to compute the C—H bond distances in vinyl chloride using the relationship proposed by Muller and Pritchard,

$$R(\text{C—H}) = 1.1597 - 4.17\times10^{-4}J_{\text{CH}} \text{ (in angstroms)}, \quad (1)$$

and have obtained the following results: 1.093 A for the β C—H distances and 1.078 A for the α C—H distance. The recent microwave investigation of Kivelson, Wilson, and Lide, on the other hand, gave 1.090 A (β-*cis*), 1.078 A (β-*trans*) and 1.079 A (α), so that our calculations are in good agreement with two of the microwave values.

ACKNOWLEDGMENTS

The authors wish to express their gratitude to the Public Health Service for a grant in partial support of this investigation. They are indebted to Dr. Frank Regenass of the B. F. Goodrich Company Research Center for supplying pure samples of the deuterated compounds, and to Anthony A. Lea of the International Business Machines Company, Educational Center, Atlanta, for assistance with the calculations.

[7] E. B. Whipple, J. H. Goldstein, and L. Mandell, J. Am. Chem. Soc. **82**, 3010 (1960).

[8] N. Muller and D. E. Pritchard, J. Chem. Phys. **31**, 768, 1471 (1959).

Diffusional Transport of Atomic Hydrogen through Molecular Hydrogen at Elevated Temperatures*

HENRY WISE

Chemical Physics Department, Stanford Research Institute, Menlo Park, California

(Received December 5, 1960)

Changes in the transport properties of a gas mixture of atomic and molecular hydrogen were measured in a temperature range from 300° to 700°K. The steady-state distribution of atoms diffusing from a source towards a catalytically active surface was determined in a cylinder of finite length. The experimental parameter of interest is the diffusion Reynolds number which contains the ratio of interdiffusion coefficient to recombination coefficient. If the catalytic activity of the surface is known, one may relate the atom-concentration gradient to the diffusion coefficient. In the temperature region studied the change in the binary diffusion coefficient for the system H, H_2 was evaluated. Based on the results obtained, the intermolecular force fields applicable to the atom-molecule encounters were examined.

INTRODUCTION

MEASUREMENTS of the transport properties of pure gases and gas mixtures have led to a detailed analysis of the dynamics of molecular encounters and of the intermolecular force fields. In particular, experimental data on the coefficient of diffusion as a function of temperature yields information on the force law governing the interaction of different gaseous species, as contrasted to measurements of viscosity where interaction between like molecules makes some contribution to the bulk properties of the mixture. Theoretical formulas relating the intermolecular forces with transport parameters have been derived[1,2] and the accuracy of the various approximations and mixing rules examined.[3] Recent measurements of the variation of diffusion coefficients of molecular gases with temperature have been interpreted in terms of an intermolecular force field represented by a purely repulsive potential.[4]

The determination of the diffusion coefficient of labile species, such as atoms, in a gas mixture is of special interest since the first theoretical approximation to the transport properties is characterized by spherically symmetrical interaction potentials corresponding to elastic collisions. Such a requirement is approximated satisfactorily by monoatomic gases without any internal degrees of freedom. At the same time the chemical reactivity of labile species, such as for example, the homogeneous and heterogeneous recombination of atoms, makes the experimental determinations more difficult. As a result, special experimental techniques have to be designed to carry out these measurements. The viscosities of gas mixtures containing atomic and molecular hydrogen have been determined by Harteck.[5] Based on a van der Waals-Sutherland model, according to which the attractive forces between hard elastic spheres vary as an inverse power of the distance, the collision diameters[6] were computed from the measured viscosity data. In addition, experimental values of elastic collision cross sections for scattering of hydrogen atoms in molecular hydrogen at room temperature have led to the computation of the average repulsive potential function between a hydrogen atom and molecule.[7] However, the energy range of the atoms involved (200 to 800 ev) makes the data less applicable at separation distances encountered in collisions of such particles whose average thermal energy is less than 0.1 ev.

The experimental arrangement employed for the study of the catalytic activity of solid surfaces for the recombination of atoms[8] is well suited for an investigation of the relative change in transport parameters resulting from variations in physical properties, such as composition[9] or temperature, of the gas-containing atoms. In such a system atoms diffuse into a cylinder of finite length and catalytic activity. The atom concentration profile in the cylinder is established as a balance between diffusion and atom removal by surface reaction. The experimental parameter of interest is δ, the diffusion Reynolds number,[10] which contains a ratio of interdiffusion coefficient D_{ij} and recombination coefficient γ. Consequently, if the catalytic activity of the surfaces is known, one may relate the atom-concentration gradient to the interdiffusion coefficient.[9] At the same time, changes in the transport properties of the gas may be measured quantitatively

* This work was sponsored by Project Squid, which is supported by the Office of Naval Research, Department of the Navy.

[1] S. Chapman and T. G. Cowling, *The Mathematical Theory of Nonuniform Gases* (Cambridge University Press, New York, 1953).

[2] J. O. Hirschfelder, C. F. Curtiss, and R. B. Bird, *Molecular Theory of Gases and Liquids* (John Wiley & Sons, Inc., New York, 1954).

[3] E. A. Mason, J. Chem. Phys. **27**, 75, 782 (1957).

[4] R. E. Walker and A. A. Westenberg, J. Chem. Phys. **29**, 1147 (1958).

[5] P. Harteck, Z. physik. Chemie **139**, 98 (1928).

[6] I. Amdur, J. Chem. Phys. **4**, 339 (1936).

[7] I. Amdur, J. Chem. Phys. **11**, 157 (1943).

[8] H. Wise and C. M. Ablow, J. Chem. Phys. **29**, 634 (1958).

[9] H. Wise, J. Chem. Phys. **31**, 1414 (1959).

[10] H. Motz and H. Wise, J. Chem. Phys. **32**, 1893 (1960).

TABLE I. Variation of binary diffusion coefficient D_{H,H_2} with temperature at 1 atm.

T °K	$(D_{ij})_2/(D_{ij})_1$	D_{ij} cm²/sec	D_{ij}(theoret)[b] cm²/sec A	B
293	1.00	1.76[a]	1.87	1.74
349	1.29	2.26	2.44	2.26
372	1.67	2.92	2.72	2.52
375	1.42	2.48	2.76	2.55
422	1.76	3.08	3.37	3.14
450	2.25	3.94	3.70	3.46
498	2.14	3.75	4.37	4.13
518	2.60	4.56	4.66	4.40
666	3.10	5.42	7.11	6.67
719	4.10	7.19	8.14	7.58

[a] Reference 6.
[b] Calculation based on interaction potential[13]; Model A: atom approaching along bisector of molecular axis; Model B: atom approaching along molecular axis.

from the relative variation in the parameter δ if the recombination coefficient remains constant or varies in a known and predictable manner.[11] As a result, the effect of temperature on the binary diffusion coefficient of atomic hydrogen in molecular hydrogen may be evaluated by such an experimental arrangement.

APPARATUS

The apparatus[11] consists of a vertical tube (2.5 cm in radius) made of Pyrex glass through which the hydrogen gas is pumped at a suitable rate by means of a mechanical pump and mercury diffusion pump. In this cylinder the atoms are produced with an electrodeless rf discharge (17 to 18 Mc/sec). A fraction of the atoms produced is allowed to diffuse into a horizontal side arm (1.25 cm in radius) attached to the vertical tube at one side and closed off at the other. The temperature of the side arm can be adjusted and maintained with the aid of a multiple resistance-wound furnace with a relatively flat temperature profile. The total gas pressure is kept constant during the course of an experiment. In general, the pressure is maintained at less than 100 μ Hg to reduce the contribution of the homogeneous, three-body, atom-recombination reaction. The atomic hydrogen-atom concentration along the side arm is measured with a microcalorimeter composed of a tungsten filament of known catalytic activity whose temperature can be adjusted and maintained with an external dc circuit. The filament forms part of a Wheatstone bridge. The energy contributed to the filament as a result of heterogeneous atom recombination can be measured directly. From such measurements of the relative atom concentration at the probe as a function of distance from the atom source, the diffusion Reynolds number δ can be evaluated at various gas temperatures. Since the tungsten-filament activity does not vary with temperature[11] ($\gamma'=0.07$), the variations in the concentration profiles observed in a series of experiments are a direct measure of the change in binary diffusion coefficient with gas temperature. It can be shown readily that the ratio of the interdiffusion coefficients at the two gas temperatures T_1 and T_2 is given by

$$[(D_{12})_{T_2}/(D_{12})_{T_1}]=(\delta'_2/\delta'_1)(T_2/T_1)^{\frac{1}{2}}, \qquad (1)$$

where $\delta'=4\ D_{12}[1-(\gamma'/2)]/\gamma' cR$, and γ', the recombination coefficient of the filament probe; c the mean atomic velocity, and R the radius of the side arm.[10]

The evaluation of the atom concentration profile is complicated by the contribution of radial diffusion due to the finite catalytic activity of the Pyrex walls of the side arm. The theoretical analysis presented[4] considers this effect in some detail. Such effects of the catalytic wall on the diffusion gradients were taken into account. As a matter of fact, the experimental data demonstrated the variation in surface activity of Pyrex glass for hydrogen-atom recombination with changes in surface temperature.[12]

RESULTS

Over the range of temperatures studied the relative increase in the binary diffusion coefficient has been computed from the observed change in the diffusion Reynolds number δ_T' [cf. Eq. (1)]. These results are summarized in Table I. Since the experimental technique described does not permit an absolute measurement of the diffusion coefficient the values of D_{ij} shown in column 3 (Table I) are based on the value of D_{ij} computed at 293°K from the data given by Amdur.[6]

DISCUSSION

For an encounter between a hydrogen atom and a hydrogen molecule the energy of interaction has been examined theoretically by the semiempirical method of Eyring[13,14] and the calculations of Margenau[15] in-

TABLE II. Calculated binary diffusion coefficients D_{H,H_2} at 1 atm.

Temperature °K	D_{H,H_2} Model: A	Model: B	Model: hard sphere
300	1.9	1.8	1.9[a]
500	4.4	4.1	4.1
1000	13.3	13.1	11.6
1500	27.1	25.3	21.0
2000	44.1	41.3	32.7
2500	63.9	60.1	45.7

[a] Reference value.

[11] B. J. Wood and H. Wise (to be published).
[12] B. J. Wood and H. Wise (to be published).
[13] H. Eyring and M. Polanyi, Z. physik Chem. **B12**, 279 (1931).
[14] J. O. Hirschfelder, J. Chem. Phys. **9**, 645 (1941).
[15] H. Margenau, Phys. Rev. **66**, 303 (1944).

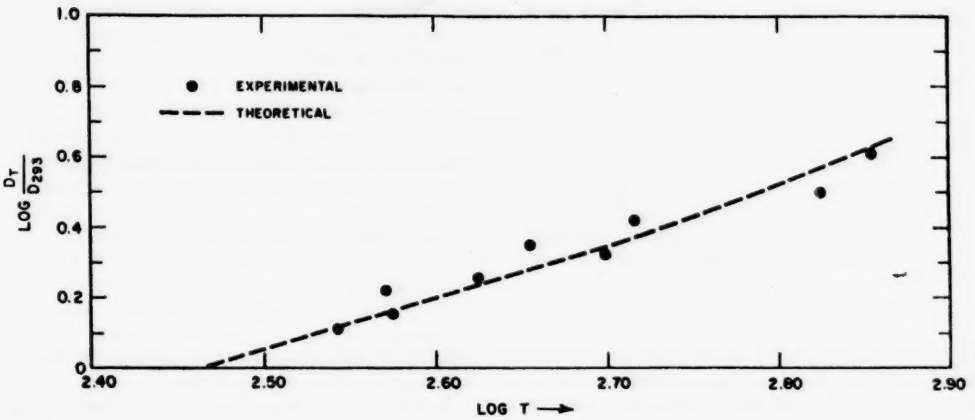

FIG. 1. Comparison of experimental results with theoretical analysis. (Lennard Jones 6-12 potential $\sigma_{12}=2.85$ A, $\epsilon_{12}=5\times10^{-15}$ erg.)

volving an approximation of the three-center exchange integrals. In the latter analysis two configurations were taken into consideration: (a) an approach of the atom perpendicular to the line of the nuclei of the molecule (Model *A*), and (b) an approach of the atom along the line of the nuclei of the molecule (Model *B*). By combining the repulsive part of the potential energy and the dispersion energy, a theoretical potential of interaction was obtained which yielded for Model *A* a collision diameter of $\sigma_{12}{}^{A}=2.85$ A and a potential depth of $\epsilon_{12}{}^{A}=5\times10^{-15}$ erg, while for Model *B*, $\sigma_{12}{}^{B}=3.03$ A and $\epsilon_{12}{}^{B}=3.5\times10^{-15}$ erg.

For the coefficient of binary diffusion both the Chapman-Cowling[1] and the Kihara[16] procedures yield to a first approximation

$$[D_{12}]_1=(3/8n\sigma_{12}{}^{2})(RT/2\pi)^{\frac{1}{2}}\times[(M_1+M_2)/M_1M_2]^{\frac{1}{2}}(1/\Omega_{12}{}^{(1,1)*}), \quad (2)$$

where $\Omega_{12}{}^{(1,1)*}$ is a dimensionless collision integral,[2] which is a function of the temperature and the interaction potential, n the total gas density, and M_1 and M_2 the molecular weight of the two components. Higher approximations to the diffusion coefficient have been presented.[16] The integrals $\Omega_{12}{}^{(1,1)*}$ for the Lennard-Jones (6–12) potential have been tabulated in reference 2. For these two configurations in the atom-molecule collision[17] the interdiffusion coefficients were calculated from Eq. (2).

The results are shown in columns 4 and 5 of Table I. The change in the diffusion coefficient with temperature as predicted from the theoretical analysis for low-energy collisions is in good agreement with the experimental results (Fig. 1). The configuration involving an atom situated along the line connecting the two nuclei (Model *B*) appears to offer a more suitable representation of the collision process. However, the temperature range over which the data were obtained is insufficient for such a distinction.

It is of interest to consider the magnitude of the deviation of the transport properties of a gas mixture containing atomic and molecular hydrogen from those computed on the basis of simple kinetic theory. For the interaction of rigid, elastic spheres of diameter σ the collision integral $\Omega_{1,2}{}^{*}$ reduces to unity in Eq. (2). The diffusion coefficients computed from such an expression based on simple kinetic theory are compared with those derived on the basis of an intermolecular force field.[15] It is apparent from the data shown in Table II that, with increasing temperature, marked deviations occur from the values computed for a hard-sphere model. The magnitude of this divergence can be further demonstrated by consideration of the effect of chemically reactive species on the thermal conductivity of a gas mixture. With the assumption of chemical equilibrium, a relatively simple expression may be derived for the thermal conductivity of a chemically reactive gas in which the energy conducted by molecular collisions is augmented by the transport of chemical enthalpy as a result of the existing concentration gradients.[2,19,20] For hydrogen in chemical and thermal equilibrium at 2500°K and a pressure of 1 atm, the ratio of the thermal conductivity of the gas (λ_R), due to energy transport by diffusion of atoms, to the thermal conductivity of molecular hydrogen, λ, is calculated to be 1.3. On the other hand, a similar computation yields $(\lambda_R/\lambda)=1.0$ at 2500°K when collisions between rigid elastic spheres are considered.

[16] E. A. Mason, J. Chem. Phys. **27**, 175 (1957).
[17] Quantum deviations have been shown to be small[18] at temperature greater than 250°K.
[18] E. A. Mason and W. E. Rice, J. Chem. Phys. **22**, 522 (1956).
[19] J. O. Hirschfelder, J. Chem. Phys. **26**, 274 (1957).
[20] J. N. Butler and R. S. Brokaw, J. Chem. Phys. **26**, 1636 (1957).

Twist in Alumina Whiskers

G. W. SEARS, R. C. DEVRIES, AND C. HUFFINE

General Electric Research Laboratory, Schenectady, New York

(Received April 8, 1960)

Eshelby twists have been microscopically observed at the tapered tips of alumina whiskers grown by the reaction

$$Al_2O_{(g)}+2H_2O_{(g)}\rightleftharpoons 2H_{2(g)}+Al_2O_{3(s)}.$$

It has been found that the twist and associated screw dislocation can be removed by nonuniform bending occurring during breakage of the whisker from its base.

STUDIES of the growth of near-perfect crystalline whiskers[1–3] have led to the conclusion that each whisker contains an axial screw dislocation while it is growing. The possibility of preferential poisoning leading to this unusual morphology has been virtually eliminated by a recent study of mercury crystals.[4]

It has been shown[5,6] that a circular cylinder containing an axial screw dislocation must be uniformly twisted along its axis by an amount equal to the Burger's vector of the dislocation divided by the cross-sectional area of the cylinder. Recently Eshelby[7] has treated the twist in a whisker of noncircular cross section and has found that $\alpha=(b/A)K$, where α is the twist in rad/cm, b is the Burgers vector, A is the cross-sectional area, and K is a constant ($\sim$1) characteristic of the cross-section shape. It was assumed that the dislocation was coaxial to the center of the polygonal cylinder.

Webb and Forgeng[8,9] have measured axial twists in aluminum oxide whiskers by x-ray diffraction. Their whiskers were grown by passing wet hydrogen over an aluminum-titanium alloy at 1400°C for several hours. The twists corresponded to multiple Burgers vectors, respectively, five and 12 times the unit Burgers vector in the [0001] direction. Webb[10] summarized the evidence for twisted whiskers in 1958.

Gomer[11] has indirectly demonstrated the presence of axial screw dislocations in growing mercury whiskers.[1,2] At electric fields sufficient to give appreciable electron-field emission, the whiskers were under an axial tension of about 100 000 psi. By changing the field and associated tensile stress, reversible rotation of the whisker tip was observed. The Eshelby twist should be a function of the tensile stress.

Recently it has been shown that the twist in lithium fluoride whiskers[12] grown from aqueous solution can be directly observed microscopically at 500×. The whiskers grew as ribbons so that the twist morphology was quite readily visible. Frequently a twisted whisker would grow onto the substrate at two points. The thickening would proceed from the points of attachment and would drive almost all of the original twist into the thinnest section between the pins.

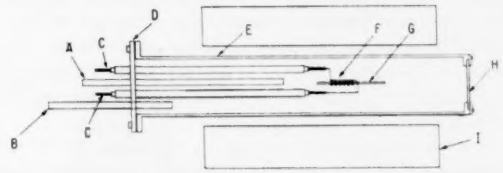

FIG. 1. Growth apparatus: A, hydrogen inlet; B, hydrogen outlet; C, molybdenum lead-in; D, asbestos gasket; E, inconel tube; F, tungsten coil; G, alumina rod; H, quartz sight-glass; I, external furnace.

Detailed studies[13–15] have been made on the growth of alumina whiskers by the reaction

$$Al_2O_3+2H_{2(g)}\rightleftharpoons Al_2O_{(g)}+2H_2O_{(g)}.$$

The role of screw dislocations in the whisker growth process was convincingly demonstrated.

The original growth apparatus was modified on the basis of the previous results so as to grow larger whiskers. The present apparatus is shown in Fig. 1. The growth was carried out in a 36-in. length of 1.62-in. o.d. inconel tubing. One end of the tube was provided with a flange which served as a support for a circular plate bearing four 0.25-in. diam steel tubes. Two tubes served as hydrogen inlet and outlet, respectively. The other two served as conduit for two 0.06-in. diam

[1] G. W. Sears, Acta Met. **1**, 457 (1953).
[2] G. W. Sears, Acta Met. **3**, 361 (1955).
[3] G. W. Sears, Acta Met. **3**, 367 (1955).
[4] G. W. Sears (to be published).
[5] E. H. Mann, Proc. Roy. Soc. (London) **A199**, 376 (1949).
[6] J. D. Eshelby, J. Appl. Phys. **24**, 176 (1953).
[7] J. D. Eshelby, Phil. Mag. **3**, 440 (1958).
[8] W. W. Webb and W. D. Forgeng, J. Appl. Phys. **28**, 1449 (1958).
[9] W. W. Webb, R. D. Dragsdorf, and W. D. Forgeng, Phys. Rev. **108**, 498 (1957); J. Appl. Phys. **29**, 817 (1958).
[10] W. W. Webb, *Growth and Perfection of Crystals*, edited by R. H. Doremus, B. W. Roberts, and D. Turnbull (John Wiley & Sons, Inc., New York, 1958), p. 230.
[11] R. Gomer, J. Chem. Phys. **28**, 458 (1958).
[12] G. W. Sears, J. Chem. Phys. **31**, 53 (1959).
[13] R. C. DeVries and G. W. Sears, J. Chem. Phys. **31**, 1256 (1959).
[14] G. W. Sears and R. C. DeVries, J. Chem. Phys. **32**, 93 (1960).
[15] G. W. Sears and R. C. DeVries (to be published).

molybdenum electrical leads. A tungsten heating coil was mounted from the leads. It had a helical diameter of 0.25-in. and a length of 0.75-in. It was wound with 15 turns of 0.020-in. tungsten wire. The other end of the inconel tube was provided with an internal flange against which a quartz observation port was mounted. Asbestos gaskets were used at both ends. An alumina rod was mounted on a bracket so that it passed through the tungsten coil.

Line hydrogen was passed through the vessel until it was purged of air. The output hydrogen was ignited and the tube was inserted into a 24-in. long kanthal wound furnace so that the tungsten coil was at the hottest zone. After the inconel tube had come to temperature, the tungsten coil was heated above the furnace temperature by passage of an electric current. Typical operating parameters are: wall temperature, 1150°C; coil temperature, 1730°C; and hydrogen flow rate, 1 liter/sec. After about 90 min the growth tube was removed from the furnace. When cool, the hydrogen was turned off, and the tungsten coil assembly was removed for microscopic observation.

As expected, the maximum whisker length was about 20 mm as compared to 1.5 mm in earlier experiments.[14] Much more important to the mechanism of whisker growth, was the observation that whiskers of alumina having a $[11\bar{2}0]$ axial direction, were in some cases helically twisted at their free end. This type of whisker has been previously[15] called A_2 whiskers. They grow as very thin ribbons and have a tapered growing end. The twist was observed at 40× with a binocular microscope and is sketched in Fig. 2. The tip had a definite helical morphology. As expected, the amount of twist was greatest near the tip and diminished to an amount unobservable with the binocular microscope. When such a whisker was snapped off at its base, the helical twist disappeared at the free end of the whisker and it became flat.

Eshelby[5] has shown that a whisker containing an axial screw dislocation must be twisted along its axis. Although he did not consider the configuration of a tapered whisker, it seems fair to assume that the twist would become smaller (rad/cm) as the whisker cross section became larger, as was observed. The twisted end is taken as evidence for a screw dislocation parallel to the whisker axis. Eshelby[5] also pointed out that a screw dislocation could be forced out of a whisker by nonuniform bending. The local bending at the base of the whisker corresponds to a stress of 2–3 000 000 psi at fracture and to nothing a short distance away. This nonuniform bending removed the helical tip morphology and the associated axial screw dislocation.

FIG. 2. Twisted alumina whiskers.

In any attempt to study whisker growth mechanisms by examination of the state of twist of the product whiskers, it must be demonstrated that the dislocation has not been removed in handling. In addition, the calculations of Hirth and Frank[16] indicate that in some cases the active dislocations can be removed by thermal fluctuation from the growing whisker, either during the growth process to cause its abrupt cessation, or after the whisker growth has ceased by removal of the driving energy.

[16] J. P. Hirth and F. C. Frank, Phil. Mag. **3**, 1110 (1958).

On the Kinetic Theory of Dense Fluids. VI. Singlet Distribution Function for Rigid Spheres with an Attractive Potential

STUART A. RICE* AND ALAN R. ALLNATT†

Department of Chemistry and Institute for the Study of Metals, University of Chicago, Chicago, Illinois

(Received August 18, 1960)

A new integro-differential equation for the singlet distribution function in a model dense fluid is derived and solved. In the model considered, the pair interaction potential is represented as a rigid core plus a soft attraction. Interactions between two rigid cores are handled as in the theory of the dense rigid-sphere fluid, while interactions between the soft attractions are handled, following Kirkwood, in the Fokker-Planck approximation. The use of coarse graining in time to provide a time scale permitting the above separation, the relaxation in momentum space, the kinetic flux vectors, and the physical basis of the analysis are all discussed.

I. INTRODUCTION

IN the Gibbsian formulation of classical equilibrium statistical mechanics, the state of the system is completely specified once the distribution function in the N-body Γ space is specified. Similarly, the goal of the Kirkwood formulation of transport theory[1] is the calculation of the distribution function descriptive of the stationary nonequilibrium state. Although the relationship which any n-body distribution function ($n<N$) must satisfy is easily derivable from the Liouville theorem, the resultant equation is not closed in the sense that a solution requires knowledge of the $(n+1)$st distribution function. In the Kirkwood approach, the solution to this dilemma is sought by approximating the mean force acting on a selected set of molecules in a manner similar to that employed in the theory of Brownian motion. This procedure leads to a set of generalized Fokker-Planck equations for the lower-order distribution functions. It is well known that the Brownian motion approximation is valid only in the limit of small momentum transfer. For this reason the Kirkwood formulation has been criticized on the grounds that in a one component system in which all molecules are of equal mass, the presence of a steep repulsive core in the intermolecular pair potential, ensures that there will be a significant number of large momentum transfers.

A model fluid ideally suited to the examination of large momentum transfer is the dense rigid-sphere liquid. The kinetic theory of the dense rigid-sphere fluid was first studied by Enskog,[2a] who derived a modified Boltzmann equation for the rate of change of the distribution function in singlet space. The theory has since been reanalyzed by several workers[2b] from various points of view, since, once this system is well understood, one may hope to use it as a model relative to which other more approximate theories can be tested and evaluated. Recently, Rice, Kirkwood, Ross, and Zwanzig[3,4] have established sufficient conditions for the derivation of a modified Boltzmann equation for a dense rigid-sphere fluid starting from the Liouville equation. The first of these conditions is that the interval of time τ during which the basic dynamical event occurs, be allowed to tend to $+0$, an arbitrarily small, positive quantity. The dynamics of the system is thus determined by binary collisions only. The second condition is that the pair correlation function be taken independent of momentum. The hypothesis that correlated successive binary, triple, etc., collisions can be neglected, may be expected to hold at finite densities for the rigid-sphere model in the limit as τ approaches $+0$, but clearly it does not hold for any molecular model at a finite density and finite τ, where the dynamics will be influenced by the higher-order collisions.

However, Harris and Rice[5] have shown that for the case of equilibrium in configuration space with a perturbation in momentum space, the longest relaxation time for return to equilibrium of the rigid-sphere fluid is one collision at liquid densities. This result supports the conjecture that the truncated collision series is a useful approximation. It is evident that further modification of the theory to include finite densities and molecules with an attractive potential along the lines so far discussed, is not easy, involving, among other difficulties, multiple collisions for which analytical solutions for the trajectories are not known.

In the present paper we consider a dense fluid from a point of view which is related to both the methods cited above. Clearly, whereas in the rigid-sphere model a molecule will, during the interval between collisions, travel on a trajectory uninfluenced by any of the other molecules, yet, in a real fluid, the molecule will in the time between strongly repulsive interactions, be continuously undergoing small momentum changes as

* Alfred P. Sloan Fellow.
† NATO Fellow.
[1] J. G. Kirkwood, J. Chem. Phys. **14**, 180 (1946).
[2] (a) D. Enskog, Kgl. Svenska Vetenskapsakad. Handl. **63**, N4 (1922); (b) F. C. Collins and H. Raffel, J. Chem. Phys. **22**, 1728 (1954); H. C. Longuet-Higgins and J. Pople, *ibid.* **25**, 884 (1956); J. T. O'Toole and J. S. Dahler, *ibid.* **32**, 1097 (1960).
[3] S. A. Rice, J. G. Kirkwood, J. Ross, and R. W. Zwanzig, J. Chem. Phys. **31**, 575 (1959).
[4] S. A. Rice, J. Chem. Phys. **31**, 584 (1959).
[5] R. A. Harris and S. A. Rice, J. Chem. Phys. (to be published).

the result of the attractive interaction of neighboring molecules. If the repulsive potential is of the hard-core type, then the molecule in the period between hard-core collisions, undergoes a form of Brownian motion.[6] This may be characterized by a friction constant, the expression for which is similar to that appearing in the Kirkwood theory except that it involves only the nonrigid-core part of the intermolecular potential. The reader may object that in a fluid such as argon, at the boiling temperature the attractive interactions are very weak relative to the repulsive interactions, and therefore that the trajectory between repulsive interactions is almost rectilinear. We do not believe this to be an accurate description of the motion of a molecule. Rather we assert that deviations from free particle flow are nonnegligible and frequent. This must, of course, be viewed as a basic assumption in the theory which is developed in this paper.

In this paper equations for the singlet distribution function are derived and solved by the Chapman-Enskog[7] procedure, and hence expressions for the kinetic contribution to the coefficients of thermal conductivity and viscosity obtained. The longest relaxation time for return to equilibrium, for a distribution function perturbed in momentum space but always at equilibrium in configuration space, is calculated. The result is compared with the corresponding result for the right-sphere model and the significance of the calculations is discussed.

In succeeding papers we shall deal with the calculation of the pair distribution function, of the frictional coefficient, and of the fluxes of matter, momentum, and energy.

II. DERIVATION OF THE TRANSPORT EQUATION

We consider a system of N structureless particles of equal mass m, with positions and momenta specified by $2N$ vectors $\mathbf{R}_1\cdots\mathbf{R}_N$, $\mathbf{p}_1\cdots\mathbf{p}_N$. The dynamical state of the system is specified by the normalized specific distribution function, which satisfies the Liouville equation

$$\frac{\partial f^{(N)}}{\partial t}+\sum_{j=1}^{N}\{(\mathbf{p}_j/m)\cdot\nabla_{R_j}f^{(N)}+\mathbf{F}_j\cdot\nabla_{p_j}f^{(N)}\}=0, \quad (1)$$

where $\mathbf{F}_j$ is the intermolecular force extended on molecule j due to all the other molecules in the system. It will be assumed that $\mathbf{F}_j$ can be expressed as the sum of pair forces,

$$\mathbf{F}_j=\sum_{i\neq j}\mathbf{F}_{ij}(|\mathbf{R}_j-\mathbf{R}_i|). \quad (2)$$

The reduced distribution function $f^{(n)}$ is defined by the relation

$$f^{(n)}(\mathbf{rp};t)=\frac{1}{(N-n)!}\iint f^{(N)}(\mathbf{rpQP};t)d\mathbf{P}d\mathbf{Q}, \quad (3)$$

where $\mathbf{r}$ and $\mathbf{p}$ are the coordinates of the subset of n particles and $\mathbf{Q}$ and $\mathbf{P}$ are the coordinates of the remaining set of $(N-n)$ particles. We shall be concerned in the following with distribution functions, coarse grained in time, defined by the relation

$$\bar{f}^{(n)}(\mathbf{rp};t)=\tau^{-1}\int_0^\tau f^{(n)}(\mathbf{rp};t+s)ds, \quad (4)$$

where τ is the interval of coarse graining.

We consider first the equation for the singlet distribution function obtained from the Liouville equation by a $(2N-2)$-fold integration, the use of Green's theorem, and coarse graining in time. The equation is

$$(\partial\bar{f}^{(1)}/\partial t)+(\mathbf{p}_1/m)\cdot\nabla_{R_1}\bar{f}^{(1)}=\Omega_R+\Omega_S, \quad (5)$$

where

$$\Omega_S=-\tau^{-1}\int_0^\tau\int\cdots\int\mathbf{F}_{12}^{(S)}\cdot\nabla_{p_1}f^{(2)}(\mathbf{R}_1\mathbf{R}_2\mathbf{p}_1\mathbf{p}_2;t+s)d\mathbf{R}_2d\mathbf{p}_2ds$$

$$\Omega_R=-\tau^{-1}\int_0^\tau\int\cdots\int\mathbf{F}_{12}^{(R)}\cdot\nabla_{p_1}f^{(2)}(\mathbf{R}_1\mathbf{R}_2\mathbf{p}_1\mathbf{p}_2;t+s)d\mathbf{R}_2d\mathbf{p}_2ds. \quad (6)$$

The force on molecule 1 due to molecule 2, $\mathbf{F}_{12}$, has been separated into two components, $\mathbf{F}_{12}^{(R)}$ the repulsive force between the molecules, and $\mathbf{F}_{12}^{(S)}$ the attractive force between the molecules.

It is convenient to introduce at this point the transformation function $K^{(N)}$, the conditional probability of finding the system at $\{\mathbf{RP}\}$ in phase space at time $(t+s)$ if it was at $\{\mathbf{R'P'}\}$ at time t, defined by the equation

$$f^{(N)}(\mathbf{RP};t+s)=\int\cdots\int K^{(N)}(\mathbf{RP}/\mathbf{R'P'};s)f^{(N)}(\mathbf{R'P'};t)d\mathbf{R'}d\mathbf{P'}. \quad (7)$$

[6] The separation into hard and soft parts of a potential energy has been used in plasma theory. For general comments see J. G. Linhart, *Plasma Physics* (North-Holland Publishing Company, Amsterdam, 1960). We wish to thank the referee for calling this to our attention.

[7] See for example, S. Chapman and T. G. Cowling, *The Mathematical Theory of Nonuniform Gases* (Cambridge University Press, New York, 1953).

Substitution of Eq. (7) in Eq. (1) shows that $K^{(N)}$ satisfies the Liouville equation

$$\frac{\partial K^{(N)}}{\partial s}+\sum_{j=1}^{N}\{(\mathbf{p}_j/m)\cdot\nabla_{R_j}K^{(N)}+\mathbf{F}_j\cdot\nabla_{p_j}K^{(N)}\}=0. \tag{8}$$

The general solution of Eq. (8) can be written as

$$K^{(N)}(\mathbf{RP}/\mathbf{R'P'};\tau)=\prod_{j=1}^{N}\delta[\mathbf{R}_j-\mathbf{R}_j'-\Delta\mathbf{R}_j(\tau)]\delta[\mathbf{p}_j-\mathbf{p}_j'-\Delta\mathbf{p}_j(\tau)], \tag{9}$$

where $\Delta\mathbf{R}_j(\tau)$ and $\Delta\mathbf{p}_j(\tau)$ are the increments in $\mathbf{R}_j$ and $\mathbf{p}_j$ in the time τ as determined from the equations of motion of the N-body system.

The definition of the relative probability density $f^{(n/N-n)}$ by the equation

$$f^{(N)}(\mathbf{rpQP};t)=f^{(n)}(\mathbf{rp};t)f^{(n/N-n)}(\mathbf{rp/QP};t), \tag{10}$$

allows us to write, using Eqs. (7) and (2),

$$f^{(n)}(\mathbf{rp};t+s)=\int\cdots\int K^{(n)}(\mathbf{rp/r'p'};s)f^{(n)}(\mathbf{r'p'};t)d\mathbf{r'}d\mathbf{p'}, \tag{11}$$

where

$$K^{(n)}(\mathbf{rp/r'p'};s)=\int\cdots\int K^{(N)}(\mathbf{rpQP/r'p'Q'P'};s)f^{(n/N-n)}(\mathbf{r'p'/Q'P'};t)d\mathbf{P}d\mathbf{Q}d\mathbf{P'}d\mathbf{Q'} \tag{12}$$

is the conditional probability density that the subset of n molecules will have coordinates and momenta $\mathbf{rp}$ at time $(t+s)$ if their coordinates and momenta were $\mathbf{r'p'}$ at time t. From Eqs. (12) and (8) it is found that

$$(\partial K^{(2)}/\partial s)+(\mathbf{p}_1/m)\cdot\nabla_{R_1}K^{(2)}+(\mathbf{p}_2/m)\cdot\nabla_{R_2}K^{(2)}+\mathbf{F}_{12}\cdot\nabla_{p_1}K^{(2)}+\mathbf{F}_{21}\cdot\nabla_{p_2}K^{(2)}$$

$$=-\sum_{j=3}^{N}\int\cdots\int\{\mathbf{F}_{1j}\cdot\nabla_{p_1}+\mathbf{F}_{2j}\cdot\nabla_{p_2}\}K^{(N)}(s)f^{(2/N-2)}(\mathbf{R}_1'\mathbf{R}_2'\mathbf{p}_1'\mathbf{p}_2'/\mathbf{Q'P'};t)d\mathbf{P}d\mathbf{Q}d\mathbf{P'}d\mathbf{Q'}, \tag{13}$$

and from Eqs. (6) and (11)

$$\Omega_R=-\tau^{-1}\int_0^{\tau}\int\cdots\int\mathbf{F}_{12}^{(R)}\cdot\nabla_{p_1}K^{(2)}(s)f^{(2)}(\mathbf{R}_1'\mathbf{R}_2'\mathbf{p}_1'\mathbf{p}_2';t)d\mathbf{R}_2d\mathbf{p}_2dsd\mathbf{R}_1'd\mathbf{R}_2'd\mathbf{p}_1'd\mathbf{p}_2'. \tag{14}$$

Until now, we have made no commitment as to the nature of the interatomic potential. We have, however, in the integration resulting in Eq. (5), implicitly assumed that the potential is continuous. We now consider as a model liquid the special case when the repulsive potential is representable as a rigid core. We make no assumption about the attractive part of the potential. Mathematically this means that $V^{(R)}$ may be represented as, say, $(\sigma/R)^n$ and for our model we take the limit as $n\to\infty$. Since the resultant equations are identical in form with Eqs. (13) and (14) there is no need to display them here. It is important to note, however, that we have taken the limit leading to the infinitely repulsive hard-core potential only at this juncture, and not at the outset of the calculation.

We are now in a position to consider the evaluation of Ω_R and Ω_S. We suppose that at the start of the time interval 0 to τ the molecule undergoes a collision, which occupies the time 0 to $+0$, and that in the remainder of the period it undergoes a kind of Brownian motion due to the attractive forces with the other molecules. It will be assumed that a time τ can be chosen long enough to allow a friction constant, whose value is given explicitly below, to achieve a plateau value, but short enough so that no further hard-core collisions occur, other than that in the time 0 to $+0$.

The quantity $\mathbf{F}_{12}^{(R)}\nabla_{p_1}K^{(2)}$ can be eliminated between Eqs. (13) and (14). The force $\mathbf{F}_{12}^{(R)}$, and hence also the integral Ω_R, will be zero except in the time 0 to $+0$. It will be assumed that to evaluate Ω_R in this time interval, it will be an adequate approximation to take $V^{(S)}\approx$ constant, and $\mathbf{F}_{1j}=0\,(j\geq 3)$. Note that $\mathbf{F}_{1j}^{(R)}=0\,(j\geq 3)$ by

definition in the time interval specified and $\mathbf{F}_{1j}^{(S)} \approx 0$ by the assumed constancy of $V^{(S)}$. The expression for Ω_R is therefore

$$\Omega_R = \tau^{-1} \int_0^\tau \int \cdots \int \{ (\partial K_0^{(2)}/\partial s) + (\mathbf{p}_1/m) \cdot \nabla_{R_1} K_0^{(2)} + (\mathbf{p}_2/m) \cdot \nabla_{R_2} K_0^{(2)} \}$$
$$\times f^{(2)}(\mathbf{R}_1' \mathbf{R}_2' \mathbf{p}_1' \mathbf{p}_2'; t) d\mathbf{R}_2 d\mathbf{p}_2 ds d\mathbf{R}_1' d\mathbf{R}_2' d\mathbf{p}_1' d\mathbf{p}_2'. \quad (15)$$

With the assumptions so far made it is now easy to see that Ω_R is identical with the collision term of the modified Boltzmann equation of RKRZ, and fuller details of this derivation will be found in their paper.[3] Briefly, we use the fact that $K_0^{(2)}$ satisfies the Liouville equation in pair space, the formal solution of which is

$$K_0^{(2)}(\mathbf{R}_1 \mathbf{R}_2 \mathbf{p}_1 \mathbf{p}_2 / \mathbf{R}_1' \mathbf{R}_2' \mathbf{p}_1' \mathbf{p}_2'; s) = \prod_{i=1}^{2} \delta[\mathbf{R}_i - \mathbf{R}_i' - \Delta\mathbf{R}_i(s)] \delta[\mathbf{p}_i - \mathbf{p}_i' - \Delta\mathbf{p}_i(s)]. \quad (16)$$

It is consistent with the rigid-sphere analysis of RKRZ, and also with the treatment of Ω_S below, to approximate the pair correlation function by the local equilibrium pair correlation function, $g_0^{(2)}$. With this assumption substitution of (16) into Eq. (15) and integration over $\mathbf{p}_1'$, $\mathbf{p}_2'$, $\mathbf{R}_1'$, $\mathbf{R}_2'$, and s leads to

$$\Omega_R = \tau^{-1} \iint [g_0^{(2)}(\mathbf{R}_1 - \Delta\mathbf{R}_1, \mathbf{R}_2 - \Delta\mathbf{R}_2) f^{(1)}(\mathbf{R}_1 - \Delta\mathbf{R}_1, \mathbf{p}_1 - \Delta\mathbf{p}_1; t) f^{(1)}(\mathbf{R}_2 - \Delta\mathbf{R}_2, \mathbf{p}_2 - \Delta\mathbf{p}_2; t)$$
$$- g_0^{(2)}(\mathbf{R}_1 \mathbf{R}_2) f^{(1)}(\mathbf{R}_1 \mathbf{p}_1; t) f^{(1)}(\mathbf{R}_2 \mathbf{p}_2; t)] d\mathbf{R}_2 d\mathbf{p}_2$$
$$+ \tau^{-1} \int_0^\tau \iint [(\mathbf{p}_1/m) \cdot \nabla_{R_1} + (\mathbf{p}_2/m) \cdot \nabla_{R_2}] f^{(2)}(\mathbf{R}_1 \mathbf{R}_2 \mathbf{p}_1 \mathbf{p}_2; t+s) d\mathbf{R}_2 d\mathbf{p}_2 ds. \quad (17)$$

The second integral of Eq. (17) was omitted by RKRZ. The first integral may be evaluated in the following manner. The function is zero except in the time 0 to $+0$. As $+0$ approaches an infinitesimally small interval, $\Delta\mathbf{R}_1$ and $\Delta\mathbf{R}_2$ approach zero. Further, the positions of 1 and 2 differ by just one hard-sphere diameter σ in this limit. We erect a cylindrical coordinate system (z, b, ϵ) with origin on molecule 1 and z axis antiparallel to the initial relative momentum vector. Complete collisions in an interval τ' occur a filamentary volume in relative configuration space

$$(p_{12}/\mu) \tau' b db d\epsilon,$$

and in the usual case we should take $\tau' = +0$. However, since in the time 0 to τ the molecule undergoes only one rigid-core collision (in the time 0 to $+0$), and since Ω_R is zero except in the range 0 to $+0$ we can extend the length of the cylinder within which completed collision occurs to

$$(p_{12}/\mu) \tau b db d\epsilon,$$

without altering the result. The final value for the first integral of Eq. (17) is now seen to be

$$g_0^{(2)}(\mathbf{R}_1, \mathbf{R}_2) \int (p_{12}/\mu) [f^{(1)}(\mathbf{R}_1, \mathbf{p}_1 - \Delta\mathbf{p}_1; t) f^{(1)}(\mathbf{R}_2, \mathbf{p}_2 - \Delta\mathbf{p}_2; t) - f^{(1)}(\mathbf{R}_1, \mathbf{p}_1; t) f^{(1)}(\mathbf{R}_2, \mathbf{p}_2; t)] d\mathbf{p}_2 b db d\epsilon. \quad (17')$$

To evaluate the second integral of Eq. (17) we first expand $f^{(2)}$ in a Taylor series about time t and neglect all terms but the first, since these involve double or higher gradients of $f^{(2)}$. After transformation of coordinates and integration over all space with the constraint that $|\mathbf{R}_{21}| \geq \sigma$ this term is

$$\sigma^2 \iint \mathbf{k} \cdot (\mathbf{p}_{12}/\mu) f^{(2)}(\mathbf{R}_1, \mathbf{R}_1 + \sigma\mathbf{k}; t) d\mathbf{k} d\mathbf{p}_2.$$

We now separate the integration in this term into integrals over two hemispheres $\mathbf{k} \cdot \mathbf{p}_{12} > 0$ and $\mathbf{k} \cdot \mathbf{p}_{12} < 0$. After transforming the volume element of integration in the expression and adding the contribution from the first

integral of Eq. (17) the expression for Ω_R is found to be

$$\Omega_R=\int(p_{12}/\mu)[g_0^{(2)}(\mathbf{R}_1,\mathbf{R}_1+\sigma\mathbf{k})\bar{f}^{(1)}(\mathbf{R}_1,\mathbf{p}_1-\Delta\mathbf{p}_1;t)\bar{f}^{(1)}(\mathbf{R}_1+\sigma\mathbf{k},\mathbf{p}_2;t)$$
$$-g_0^{(2)}(\mathbf{R}_1,\mathbf{R}_1-\sigma\mathbf{k})\bar{f}^{(1)}(\mathbf{R}_1,\mathbf{p}_1;t)\bar{f}^{(1)}(\mathbf{R}_1-\sigma\mathbf{k};\mathbf{p}_2;t)]d\mathbf{p}_2bdbd\epsilon.$$

(The further time smoothing performed will not affect the value of Ω_s which is already time smoothed in the same interval.) Thus Ω_R is identical with the collision term of the Enskog equation for hard spheres. It is convenient to expand the distribution functions centered on $\mathbf{R}_1+\sigma\mathbf{k}$, and $\mathbf{R}_1-\sigma\mathbf{k}$ retaining only first-order terms. Equation (17) becomes

$$\Omega_R=J_1+J_2$$

$$J_1=g_0^{(2)}(\mathbf{R}_1,\sigma)\iint[\bar{f}^{(1)}(\mathbf{R}_1,\mathbf{p}_1-\Delta\mathbf{p}_1;t)\bar{f}^{(1)}(\mathbf{R}_1,\mathbf{p}_2-\Delta\mathbf{p}_2;t)-\bar{f}^{(1)}(\mathbf{R}_1,\mathbf{p}_1;t)\bar{f}^{(1)}(\mathbf{R}_1,\mathbf{p}_2;t)](p_{12}/\mu)bdbd\epsilon d\mathbf{p}_2$$

$$J_2=g_0^{(2)}(\mathbf{R}_1,\sigma)\iint[\bar{f}^{(1)}(\mathbf{R}_1,\mathbf{p}_1-\Delta\mathbf{p}_1;t)\sigma\mathbf{k}\cdot\nabla_{R_1}\bar{f}^{(1)}(\mathbf{R}_1,\mathbf{p}_2-\Delta\mathbf{p}_2;t)$$
$$+\bar{f}^{(1)}(\mathbf{R}_1,\mathbf{p}_1;t)\sigma\mathbf{k}\cdot\nabla_{R_1}\bar{f}^{(1)}(\mathbf{R}_1,\mathbf{p}_2;t)](p_{12}/\mu)bdbd\epsilon d\mathbf{p}_2, \quad (17'')$$

where $\mathbf{k}$ is a unit vector in the direction of the line of centers of colliding spheres at contact.

We consider now the evaluation of Ω_S. We have previously assumed that $\mathbf{F}_{12}^{(S)}$ is zero in the time 0 to $+0$. Equation (6) therefore becomes

$$\Omega_s=-\tau^{-1}\int_{+0}^{\tau}\int\cdots\int\mathbf{F}_{12}^{(S)}\cdot\nabla_{r1}f^{(N)}(\mathbf{R}_1\mathbf{R}_2\mathbf{p}_1\mathbf{p}_2\mathbf{Q}\mathbf{P};t+s)d\mathbf{Q}d\mathbf{P}d\mathbf{R}_2d\mathbf{p}_2ds. \quad (18)$$

In the interval $+0$ to τ, molecule 1 undergoes a Brownian motion under the influence of the attractive forces. This can be treated in a manner similar to that described by Ross,[8] and earlier by Kirkwood.[1] We refer the reader to these papers for a fuller description of the details of the procedure. Denoting the values of coordinates and momenta at time $+0$ by the subscript zero we again introduce the phase-space transformation function defined by Eq. (7).

Following the perturbation procedure of Ross we replace $\mathbf{F}_j$ in the Liouville equation for $K^{(N)}$ by $\lambda\mathbf{F}_j$, giving

$$\frac{\partial K^{(N)}}{\partial s}+\sum_{j=1}^{N}\{(\mathbf{p}_j/m)\cdot\nabla_{R_j}K^{(N)}+\lambda\mathbf{F}_j\cdot\nabla_{p_j}K^{(N)}\}=0, \quad (19)$$

and expand $K^{(N)}$ in powers of the perturbation parameter,

$$K^{(N)}=\sum_{n=0}^{\infty}\lambda^nK_n^{(N)}. \quad (20)$$

Substituting (19) into (7) and equating powers of λ gives an infinite set of differential equations for the $K_n^{(N)}$. To terms of order λ^2 the expression for $K^{(N)}$ is found to be

$$K^{(N)}(\mathbf{RP}/\mathbf{R}_0\mathbf{P}_0;s)=[1-\lambda\sum_{j=1}^{N}\Delta p_j(s)\cdot\nabla_{p_j}]\prod_{k=1}^{N}\delta(\mathbf{R}_k-\mathbf{R}_{k0}-\Delta\mathbf{R}_k^0)\,\delta(\mathbf{p}_k-\mathbf{p}_{k0}). \quad (21)$$

The increment $\Delta\mathbf{R}_k^{(0)}(s)$ is the distance traveled by a free particle k in time s, and $\Delta\mathbf{p}_k^{(1)}(s)$ is the change in momentum of the particle in the same time due to the force $\mathbf{F}_k$ acting on the particle moving on a linear trajectory. The analysis of Ross[8] is valid for the case when the momentum changes in time s are small. Since in the present case the only momentum changes are due to attractive potentials, this might be expected to be a better approximation than in the case when $\mathbf{F}_{12}$ includes the repulsive part of the interaction, which gives the hard-core collisions.

[8] J. Ross, J. Chem. Phys. **24**, 375 (1956).

From Eqs. (7), (18), and (21) the expression for Ω_s is

$$\Omega_s=\tau^{-1}\int_{+0}^{\tau}\int\cdots\int \mathbf{F}_{12}^{(S)}(R_{12})\{1-\sum_{j=1}^{N}\Delta\mathbf{p}_j^{(1)}(s)\cdot\nabla_{p_j}\}\prod_{k=1}^{N}\delta(\mathbf{R}_k-\mathbf{R}_{k0})\,\delta(\mathbf{p}_k-\mathbf{p}_{k0})f^{(N)}$$

$$\times(\mathbf{R}_{10}\mathbf{R}_{20}\mathbf{p}_{10}\mathbf{p}_{20}\mathbf{P}_0\mathbf{Q}_0;\,t)\,d\mathbf{P}d\mathbf{Q}d\mathbf{R}_2d\mathbf{P}_2dsd\mathbf{R}_{10}d\mathbf{R}_{20}d\mathbf{p}_{10}d\mathbf{p}_{20}d\mathbf{P}_0d\mathbf{Q}_0, \quad (22)$$

where $\delta(\mathbf{R}_k-\mathbf{R}_{k0}-\Delta\mathbf{R}_k^0)$ has been replaced by $\delta(\mathbf{R}_k-\mathbf{R}_{k0})$ on the assumption that the distribution functions have only macroscopic dependence on configuration space coordinates. The remainder of the development for Ω_s follows identically the development given by Ross. It is necessary to assume that $g^{(2)}$ can be approximated by its local equilibrium value; and that in performing differentiations with respect to $\mathbf{p}_{10}$, $\mathbf{p}_{20}$ the dependence of $f_0^{(2/N-2)}$, the local equilibrium relative probability density, can be neglected and deviations of the singlet distribution functions from equilibrium values disregarded. The expression fo Ω_s is found to be

$$\Omega_s=\nabla_{p_1}\cdot\zeta\{[(\mathbf{p}_1/m)-\mathbf{u}]\bar{f}^{(1)}(\mathbf{R}_1\mathbf{p}_1;\,t)+kT\nabla_{p_1}\bar{f}^{(1)}(\mathbf{R}_1\mathbf{p}_1;\,t)\}-\nabla_{p_1}\cdot\mathbf{F}_1^{*}\bar{f}^{(1)}(\mathbf{R}_1\mathbf{p}_1;\,t), \quad (23)$$

where

$$\zeta=(3kT\tau)^{-1}\int_{+0}^{\tau}\int_{-S}^{+0}\iint \mathbf{F}_{12}^{(S)}(\mathbf{R}_{12})\,\mathbf{F}_1^{(S)}[\mathbf{R}_1+(s+s')(\mathbf{p}/m)]\,f_0^{(1/N-1)}(\mathbf{R}_1\mathbf{p}_1/\mathbf{PQ})\,d\mathbf{P}d\mathbf{Q}dsds' \quad (24)$$

and

$$\mathbf{F}_1^{*}={}^{(1)}\langle\mathbf{F}_1^{(S)}\rangle^0+{}^{(1)}\mathbf{F}_1^{+}, \quad (25)$$

where ${}^{(1)}\langle\mathbf{F}_1^{(S)}\rangle^0$ is the average total intermolecular attractive force on a molecule at $\mathbf{R}_1$ when the average is performed in a canonical ensemble over all other molecules, and ${}^{(1)}\mathbf{F}_1^{+}$ is a perturbation arising from the departure of $f^{(2/N-2)}$ from its equilibrium value.

The final equation for the singlet distribution function can therefore be written in the form

$$D\bar{f}^{(1)}=J_1+J_2+\zeta\mathfrak{A}\bar{f}^{(1)}, \quad (26)$$

where

$$D\bar{f}^{(1)}=(\partial\bar{f}^{(1)}/\partial t)+(\mathbf{p}_1/m)\cdot\nabla_{R_1}\bar{f}^{(1)}+\nabla_{p_1}\cdot\mathbf{F}_1^{*}\bar{f}^{(1)}, \quad (27)$$

$$\mathfrak{A}\bar{f}^{(1)}=\nabla_{p_1}\cdot\{[\mathbf{p}_1/m-\mathbf{u}]\bar{f}^{(1)}+kT\nabla_{p_1}\bar{f}^{(1)}\}. \quad (28)$$

III. PERTURBATION SOLUTION

Equation (26) is readily solved by the Chapman-Enskog procedure. The distribution function is expanded as a series in a perturbation parameter ϵ,

$$\bar{f}^{(1)}=\sum_{l=0}^{\infty}\epsilon^l\bar{f}_l^{(1)}, \quad (29)$$

and the transport equation written in the form

$$D\bar{f}^{(1)}=(1/\epsilon)[J_1+\zeta\mathfrak{A}\bar{f}^{(1)}]+J_2. \quad (30)$$

Substituting the series (29) into the terms in the right-hand side of (30), and equating the coefficients of equal powers of ϵ we obtain the following equations:

$$0=J_1[\bar{f}_0^{(1)}(1),\,\bar{f}_0^{(1)}(2)]+\zeta\mathfrak{A}[\bar{f}_0^{(1)}(1)], \quad (31)$$

$$D\bar{f}_0^{(1)}=J_1[\bar{f}_0^{(1)}(1),\,\bar{f}_1^{(1)}(2)]+J_1[\bar{f}_1^{(1)}(1),\,\bar{f}_0^{(1)}(2)]+J_2[\bar{f}_0^{(1)}(1),\,\bar{f}_0^{(1)}(2)]+\zeta\mathfrak{A}[\bar{f}_1^{(1)}(1),\,\bar{f}_0^{(1)}(1)], \quad (32)$$

where

$$\mathfrak{A}[\bar{f}_0^{(1)}(1)]=\nabla_{p_1}\cdot\{[(\mathbf{p}_1/m)-\mathbf{u}^{(0)}]\bar{f}_0^{(1)}(1)+kT^{(0)}\nabla_{p_1}\bar{f}_0^{(1)}(1)\} \quad (33)$$

$$\mathfrak{A}[\bar{f}_1^{(1)}(1),\,\bar{f}_0^{(1)}(1)]=\nabla_{p_1}\cdot\{[(\mathbf{p}_1/m)-\mathbf{u}^{(0)}]\bar{f}_1^{(1)}(1)+kT^{(0)}\nabla_{p_1}\bar{f}_1^{(1)}(1)\}+\nabla_{p_1}\cdot\{-\mathbf{u}^{(1)}\bar{f}_0^{(1)}(1)+kT^{(1)}\nabla_{p_1}\bar{f}_0^{(1)}(1)\}. \quad (34)$$

The remaining undefined symbols are:

$$\mathbf{u}^{(0)}=(n^{(0)}m)^{-1}\int \mathbf{p}_1\bar{f}_0^{(1)}(1)\,d\mathbf{p}_1$$

$$n^{(0)}=\int \bar{f}_0^{(1)}(1)\,d\mathbf{p}_1$$

$$kT^{(0)}=(3n^{(0)})^{-1}\int m[(\mathbf{p}_1/m)-\mathbf{u}^{(0)}]^2\bar{f}_0^{(1)}(1)\,d\mathbf{p}_1 \tag{35}$$

$$\mathbf{u}^{(1)}=\frac{1}{n^{(0)}}\int[(\mathbf{p}_1/m)-\mathbf{u}^{(0)}]\bar{f}_1^{(1)}(1)\,d\mathbf{p}_1$$

$$kT^{(1)}=\frac{1}{n^{(0)}}\left[\tfrac{1}{3}\int m[(\mathbf{p}_1/m)-\mathbf{u}^{(0)}]^2\bar{f}_1^{(1)}(1)\,d\mathbf{p}_1-n^{(1)}kT^{(0)}\right]$$

$$n^{(1)}=\int \bar{f}_1^{(1)}(1)\,d\mathbf{p}_1. \tag{36}$$

A solution of Eq. (31) is

$$\bar{f}_0^{(1)}(1)=n^{(0)}\{2\pi kT^{(0)}m\}^{-\frac{3}{2}}\exp[-(\mathbf{p}_1-m\mathbf{u}^{(0)})^2/2mkT^{(0)}]. \tag{37}$$

The equations for $\bar{f}_j^{(1)}(j>0)$ determine the velocities $\mathbf{u}^{(j)}$, temperatures $T^{(j)}$, and number densities $n^{(j)}$ only up to linear combinations of quantities conserved by $[J_1+J_2+\mathcal{A}(f)]$, and this flexibility allows one to take $n^{(1)}$, $\mathbf{u}^{(1)}$, and $T^{(1)}$ as zero and $n^{(0)}$, $\mathbf{u}^{(0)}$, and $T^{(0)}$ as the local equilibrium values. Equation (37) is thus the local equilibrium distribution function. Equation (34) can therefore be written as

$$\begin{aligned}\mathcal{A}(\bar{f}_1^{(1)}(1),\,\bar{f}_0^{(1)}(1))&=\nabla_{p_1}\cdot\{[(\mathbf{p}_1/m)-\mathbf{u}]\bar{f}_1^{(1)}(1)+kT\nabla_{p_1}\bar{f}_1^{(1)}(1)\}\\&=kT\nabla_{p_1}\cdot\{\bar{f}_0^{(1)}(1)\nabla_{p_1}(\bar{f}_1^{(1)}(1)/\bar{f}_0^{(1)}(1))\}.\end{aligned} \tag{38}$$

The solution of Eq. (32) may now be made by substituting from Eq. (38) and writing

$$\bar{f}_1^{(1)}(1)=\bar{f}_0^{(1)}(1)\Phi_1. \tag{39}$$

The terms in $D\bar{f}_0^{(1)}$ and J_1 and J_2 have been previously evaluated by Rice.[4] The linear form of the equation for the perturbation function so obtained, indicates that the perturbation function can depend only upon the gradient of the temperature and the gradient of the mean velocity. The perturbation function can therefore be taken to be of the form

$$\Phi_1=-\mathbf{A}_1\cdot\nabla_{R_1}\ln T-\mathbf{B}_1:\nabla_{R_1}\mathbf{u}, \tag{40}$$

and by substitution

$$\iiint \bar{f}_0^{(1)}(1)\,\bar{f}_0^{(1)}(2)[\mathbf{A}_1^*+\mathbf{A}_2^*-\mathbf{A}_1-\mathbf{A}_2](p_{12}/\mu)\,bdbded^3p_2+kT\zeta\nabla_{p_1}\cdot\{\bar{f}_0^{(1)}(1)\nabla_{p_1}\mathbf{A}_1\}/g(\sigma)=\mathbf{K} \tag{41}$$

$$\iiint \bar{f}_0^{(1)}(1)\,\bar{f}_0^{(1)}(2)[\mathbf{B}_1^*+\mathbf{B}_2^*-\mathbf{B}_1-\mathbf{B}_2](p_{12}/\mu)\,bdbded^3p_2+kT\zeta\nabla_{p_1}\cdot\{\bar{f}_0^{(1)}(1)\nabla_{p_1}\mathbf{B}_1\}/g(\sigma)=\mathbf{L}, \tag{42}$$

where an asterisk (*) denotes a value after a collision. The hard-sphere terms $\mathbf{K}$ and $\mathbf{L}$ have been evaluated by Rice.[4] The values are

$$\mathbf{K}=[\bar{f}_0^{(1)}(1)/g(\sigma)](2kT/m)^{\frac{1}{2}}[\tfrac{3}{2}+\alpha T-W_1^2]\mathbf{W}_1+\bar{f}_0^{(1)}(1)(\pi\sigma^3/15v)(2kT/m)^{\frac{1}{2}}[5+20\alpha T-6W_1^2]\mathbf{W}_1 \tag{43a}$$

$$\mathbf{L}=-[\bar{f}_0^{(1)}(1)/g(\sigma)]\{2\mathbf{b}+[(v/C_v)(\partial p/\partial T)_\rho-\tfrac{2}{3}](\tfrac{3}{2}-W_1^2)\mathbf{1}\}-\bar{f}_0^{(1)}(1)(2\pi\sigma^3/15v)\{[-5+2W_1^2]\mathbf{1}+4\mathbf{W}_1\mathbf{W}_1\}, \tag{43b}$$

where

$$\mathbf{W}_1=(m/2kT)^{\frac{1}{2}}[\mathbf{p}_1/m-\mathbf{u}] \tag{44}$$

is a reduced peculiar velocity, and $\mathbf{b}_1$ is the traceless dyadic $(\mathbf{W}_1\mathbf{W}_1-\frac{1}{3}W_1^2\mathbf{1})$.

To evaluate **A** and **B** we expand them as finite sums of Sonine polynomials in the square of the reduced velocity just as for the hard-sphere problem. We write the vector **A** as

$$\mathbf{A}=\mathbf{W}A(|W|)$$

$$A=\sum_{m=0}^{s}a^{(m)}S_{\frac{1}{2}}^{(m)}(W^2). \tag{45}$$

From the restriction previously noted (that $n^{(1)}$, $\mathbf{u}^{(1)}$, and $T^{(1)}$ are each zero) and the properties of the Sonine polynomials, it is found that $a^{(0)}=0$. We approximate A by taking only the first two terms in the expansion,

$$A=a^{(1)}S_{\frac{1}{2}}^{(1)}(W^2)=a^{(1)}(\tfrac{5}{2}-W^2). \tag{46}$$

Substituting in Eq. (41), multiplying by $\mathbf{W}_1S_{\frac{1}{2}}^{(1)}(W_1^2)$ and integrating over d^3p_1 leads to

$$a^{(1)}=-(2kT/m)^{\frac{1}{2}}\frac{\{[v/g(\sigma)]+(2\pi\sigma^3/5)\}\times\frac{15}{4}}{\{4\Omega^{(2,2)}+[45\zeta v/4mg(\sigma)]\}}, \tag{47}$$

where $\Omega^{(2,2)}$ is the reduced collision cross section for the hard-core part of the potential. The hard-sphere term and the term involving **K** have been evaluated by Rice[4]; the remaining integral is quite straightforward.

To evaluate the parameter **B**, the procedure followed for the rigid-sphere fluid can again be used. The tensor **L** is divided into two parts, a traceless dyadic and a scalar multiple of the unit tensor

$$\mathbf{L}=\mathbf{L}^{(1)}+\mathbf{L}^{(2)}\mathbf{1}, \tag{48}$$

and similarly for $\mathbf{B}_1$,

$$\mathbf{B}_1=\mathbf{B}_1^{(1)}+\mathbf{B}_1^{(2)}$$

$$=B_1^{(1)}[\mathbf{W}_1\mathbf{W}_1-\tfrac{1}{3}W_1^2\mathbf{1}]+B_1^{(2)}\mathbf{1}. \tag{49}$$

Substituting Eqs. (48) and (49) in (42) the equations determining $\mathbf{B}^{(1)}$ and $\mathbf{B}^{(2)}$ are found to be

$$\iiint\bar{f}_0^{(1)}(1)\,\bar{f}_0^{(1)}(2)[\mathbf{B}_1^{(1)*}+\mathbf{B}_2^{(1)*}-\mathbf{B}_1^{(1)}-\mathbf{B}_2^{(1)}](p_{12}/\mu)\,bdbd\epsilon d^3p_2=\mathbf{L}^{(1)}-kT\zeta\nabla_{p_1}\cdot\{\bar{f}_0^{(1)}(1)\nabla_{p_1}\mathbf{B}_1^{(1)}\}/g(\sigma) \tag{50}$$

$$\iiint\bar{f}_0^{(1)}(1)\,\bar{f}_0^{(1)}(2)[\mathbf{B}_1^{(2)*}+\mathbf{B}_2^{(2)*}-\mathbf{B}_1^{(2)}-\mathbf{B}_2^{(2)}](p_{12}/\mu)\,bdbd\epsilon d^3p_2=L^{(2)}\mathbf{1}-kT\zeta\nabla_{p_1}\cdot\{\bar{f}_0^{(1)}(1)\nabla_{p_1}\mathbf{B}_1^{2}\}/g(\sigma). \tag{51}$$

As before, the perturbation parameters are expanded as a power series in Sonine polynomials retaining only the first nonvanishing term,

$$B^{(1)}=b_0^{(1)}S_{5/2}^{(0)}(W^2)=b_0^{(1)}$$

$$B^{(2)}=b_2^{(2)}S_{\frac{1}{2}}^{(2)}(W^2)=b_2^{(2)}(\tfrac{15}{8}-\tfrac{5}{2}W^2+\tfrac{1}{2}W^4); \tag{52}$$

$b_0^{(1)}$ is evaluated by introducing $b_0^{(1)}(\mathbf{WW}-\frac{1}{3}W^2\mathbf{1})$ into Eq. (50), multiplying by $(\mathbf{WW}-\frac{1}{3}W^2\mathbf{1})$ and integrating over d^3p_1. The result is

$$b_0^{(1)}=5v\frac{\{[1/g(\sigma)]+(4\pi\sigma^3/15v)\}}{\{4\Omega^{(2,2)}+[5\zeta v/mg(\sigma)]\}}. \tag{53}$$

The coefficient $b_2^{(2)}$ may be determined in the same way, and is found to be zero as in the case of the rigid-sphere

fluid. The final expression for the singlet distribution function is therefore

$$\bar{f}^{(1)}(1)=\bar{f}_0^{(1)}(1)\left\{1+(2kT/m)^{\frac{1}{2}}\frac{15}{4}\frac{\{[v/g(\sigma)]+(2\pi\sigma^3/5)\}}{\{4\Omega^{(2,2)}+\frac{4.5}{4}[\zeta v/mg(\sigma)]\}}(\tfrac{5}{2}-W_1^2)\mathbf{W}_1\cdot\nabla_{R_1}\ln T\right.$$

$$\left.-5v\frac{\{[1/g(\sigma)]+(4\pi\sigma^3/5v)\}}{\{4\Omega^{(2,2)}+[5\zeta v/mg(\sigma)]\}}(\mathbf{W}_1\mathbf{W}_1-\tfrac{1}{3}W_1^2\mathbf{1}):\nabla_{R_1}\mathbf{u}\right\}. \quad (29')$$

Note that in the limit of the pure Fokker-Planck equation this relation reduces to the value given by Lebowitz, Frisch, and Helfand,[9] and in the hard-sphere limit to the equation of RKRZ.

IV. KINETIC CONTRIBUTIONS TO THE FLUX VECTORS

Using the expression for the singlet distribution functions, the kinetic contributions to the thermal conductivity and shear viscosity may be calculated. The kinetic contribution to the heat flux is[10]

$$\mathbf{q}_K=(m/2)\int\bar{f}^{(1)}(1)\,|\,(\mathbf{p}_1/m)-\mathbf{u}\,|^2[(\mathbf{p}_1/m)-\mathbf{u}]d^3p_1. \quad (54)$$

The integrals to be evaluated are exactly the same as those in the paper of RKRZ.[3] The term in $\mathbf{B}:\nabla_{R_1}\mathbf{u}$, as well as the term unity in the distribution function, vanish by symmetry. The remaining term may be readily evaluated with the result that

$$\kappa_K=\frac{75k^2T}{32mg(\sigma)}\frac{[1+(2\pi\sigma^3/5v)g(\sigma)]}{\{\Omega^{(2,2)}+\frac{4.5}{16}[\zeta v/mg(\sigma)]\}}. \quad (55)$$

The kinetic contribution to the stress tensor may be written[10]

$$\mathbf{\sigma}_K=-\int\bar{f}^{(1)}(1)[(\mathbf{p}_1/m)-\mathbf{u}][(\mathbf{p}_1/m)-\mathbf{u}]d^3p_1, \quad (56)$$

with σ related to the viscosity by the Newtonian form of the macroscopic stress tensor

$$\mathbf{\sigma}=-[p+(\tfrac{2}{3}\eta-\phi)\nabla\cdot\mathbf{u}]\mathbf{1}+2\eta\epsilon. \quad (57)$$

In Eq. (57) ϕ is the coefficient of bulk viscosity, η the coefficient of shear viscosity and ϵ the rate of strain tensor defined by

$$\epsilon=\tfrac{1}{2}(\nabla_{R_1}\mathbf{u}+\nabla_{R_1}\mathbf{u}^+), \quad (58)$$

where the superscript dagger denotes the transpose. The integrals may again be evaluated in the manner described by RKRZ.[3] The kinetic contribution to the shear viscosity is found to be

$$\eta_K=\frac{5kT\{1+[4\pi\sigma^3g(\sigma)/15v]\}}{8g(\sigma)\{\Omega^{(2,2)}+[5\zeta v/4mg(\sigma)]\}}. \quad (59)$$

Note that the kinetic contributions η_K and K_K reduce properly to both the hard-sphere and Brownian motion values in the two limiting cases that $\zeta=0$ or $V^{(R)}=0$.

V. RELAXATION TIME IN MOMENTUM SPACE

In this section we calculate the longest relaxation time for a system which is at equilibrium in configuration space but perturbed in momentum space, using the method previously employed by Harris and Rice[5] for the rigid-sphere fluid. We write the perturbed distribution function as

$$\bar{f}^{(1)}(\mathbf{p}_1;t)=\bar{f}_0^{(1)}(\mathbf{p}_1)[1+e^{-\lambda t}\Psi(p_1^2)]$$

$$\bar{f}_0^{(1)}(\mathbf{p}_1)=[(2\pi mkT)^{-\frac{3}{2}}/v]\exp[-(\mathbf{p}_1-m\mathbf{u})^2/2kT]. \quad (60)$$

[9] J. L. Lebowitz, H. L. Frisch, and E. Helfand, Phys. Fluids **3**, 325 (1960).
[10] J. H. Irving and J. G. Kirkwood, J. Chem. Phys. **18**, 817 (1950).

Substituting in the transport equation (Eq. 26) we find

$$-\lambda e^{-\lambda t}\psi(p_1^2)\bar{f}_0^{(1)}(p_1)+\mathbf{F}_1^*\cdot\nabla_{p_1}\{\bar{f}_0^{(1)}(p_1)[1+e^{-\lambda t}\psi(p_1^2)]\}$$

$$=e^{-\lambda t}g(\sigma)\int\bar{f}_0^{(1)}(1)\bar{f}_0^{(1)}(2)[\psi(p_1^{*2})+\psi(p_2^{*2})-\psi(p_1^2)-\psi(p_2^2)](p_{12}/\mu)bdbd\epsilon d^3p_2$$

$$+\zeta\nabla_{p_1}\cdot\{[(\mathbf{p}_1/m)-\mathbf{u}^{(0)}]\bar{f}_1^{(1)}(p_1)+kT^{(0)}\nabla_{p_1}\bar{f}_1^{(1)}(p_1)\}+\zeta\nabla_{p_1}\cdot\{-\mathbf{u}^{(1)}\bar{f}_0^{(1)}(\mathbf{p}_1)+kT^{(1)}\nabla_{p_1}\bar{f}_0^{(1)}(\mathbf{p}_1)\}, \quad (61)$$

where $\mathbf{u}^{(0)}$ and $T^{(0)}$ are defined in Eq. (35), and $\mathbf{u}^{(1)}$ and $T^{(1)}$ are defined in Eq. (36), and we write $\bar{f}_0^{(1)}(\mathbf{p}_1)e^{-\lambda t}\psi(\mathbf{p}_1^2)$ for the perturbation $\bar{f}_1^{(1)}(1)$. As in the previous section we take $\mathbf{u}^{(1)}$, $T^{(1)}$, and $\eta^{(1)}$ as zero and replace $\mathbf{u}^{(0)}$, $T^{(0)}$, and $n^{(0)}$ by their local equilibrium values. On using Eq. (38), Eq. (61) becomes

$$-\lambda e^{-\lambda t}\psi(p_1^2)\bar{f}_0^{(1)}(p_1)+\mathbf{F}_1^*\cdot\nabla_{p_1}\{\bar{f}_0^{(1)}(p_1)[1+e^{-\lambda t}\psi(p_1^2)]\}$$

$$=e^{-\lambda t}g(\sigma)\int\bar{f}_0^{(1)}(\mathbf{p}_1)\bar{f}_0^{(1)}(\mathbf{p}_2)[\psi(p_1^{*2})+\psi(p_2^{*2})-\psi(p_1^2)-\psi(p_2^2)](p_{12}/\mu)bdbd\epsilon d^3p_2$$

$$+e^{-\lambda t}\zeta kT\nabla_{p_1}\cdot\{\bar{f}_0^{(1)}(p_1)\nabla_{p_1}\psi(p_1^2)\}. \quad (62)$$

We now expand the perturbation function ψ in terms of a set of Sonine polynomials whose argument is the square of the reduced velocity defined in Eq. (44),

$$\psi(p_1^2)=\sum_m b_m S_{\frac{1}{2}}^{(m)}(W^2). \quad (63)$$

The polynomials form an orthonormal set, i.e.,

$$\int S_{\frac{1}{2}}^{(m)}(W^2)\,S_{\frac{1}{2}}^{(n)}(W^2)\,\bar{f}_0^{(1)}(\mathbf{p}_1)d^3p_1=C\delta_{im}/\nu, \quad (64)$$

where C is a normalization constant. Substitution of Eq. (63) in Eq. (62) multiplication by $\sum_n b_n S_{\frac{1}{2}}^{(n)}(W_1^2)$ and integration over d^3p_1 gives

$$-\lambda\int\bar{f}_0^{(1)}(p_1)\sum_m b_m b_n S_{\frac{1}{2}}^{(m)}(W_1^2)\,S_{\frac{1}{2}}^{(n)}(W_1^2)d^3p_1=g(\sigma)\int\bar{f}_0^{(1)}(\mathbf{p}_1)\bar{f}_0^{(1)}(\mathbf{p}_2)\sum_n b_n S_{\frac{1}{2}}^{(n)}(W_1^2)\{\sum_m b_m[S_{\frac{1}{2}}^{(m)}(W_1^{*2})$$

$$+S_{\frac{1}{2}}^{(m)}(W_2^{*2})-S_{\frac{1}{2}}^{(m)}(W_1^2)-S_{\frac{1}{2}}^{(m)}(W_2^2)]\}(p_{12}/\mu)bdbd\epsilon d^3p_1d^3p_2$$

$$+\sum_n\zeta kT\int\nabla_{p_1}\cdot[\bar{f}_0^{(1)}(\mathbf{p}_1)\nabla_{p_1}(\sum_m b_m S_{\frac{1}{2}}^{(m)}(W_1^2)]b_n S_{\frac{1}{2}}^{(n)}(W_1^2)d^3p_1. \quad (65)$$

The left-hand side of this equation vanishes unless $m=n$.

To determine the longest relaxation time, corresponding to the minimum value of λ, we perform variations with respect to the coefficients b_k, using the condition $(\partial\lambda/\partial b_k)=0$, $(k=0, 1, \cdots)$. We thus obtain a secular equation

$$\sum_m b_m[g(\sigma)\{m, k\}+\zeta kT([k, m]+[m, k])+\lambda(m, m)\delta_{mk}]=0. \quad (66)$$

The values of λ and of the coefficients b_m are determined by the normalization conditions and the roots of the corresponding determinant,

$$\|g(\sigma)\{m, k\}+\zeta kT([k, m]+[m, k])+\lambda(m, m)\delta_{mk}\|=0. \quad (67)$$

The quantities $\{m, k\}$, (m, m), and $[m, k]$ are defined by

$$\{m, k\} = \int \bar{f}_0^{(1)}(\mathbf{p}_1)\, \bar{f}_0^{(1)}(\mathbf{p}_2)\left[S_{\frac{1}{2}}^{(m)}(W_1^{*2}) + S_{\frac{1}{2}}^{(m)}(W_2^{*2}) - S_{\frac{1}{2}}^{(m)}(W_1^2) - S_{\frac{1}{2}}^{(m)}(W_2^2)\right] S_{\frac{1}{2}}^{(k)}(W_1^2)\,(p_{12}/\mu)\, bdbd\epsilon d^3p_1 d^3p_2 \tag{68}$$

$$(m, m) = \int \bar{f}_0^{(1)}(p_1)\,(S_{\frac{1}{2}}^{(m)}(W_1^2))^2 d^3p_1 \tag{69}$$

$$[m, k] = \int \nabla_{p_1} \cdot \left[\bar{f}_0^{(1)}(p_1)\, \nabla_{p_1} S_{\frac{1}{2}}^{(m)}(W_1^2)\right] S_{\frac{1}{2}}^{k}(W_1^2)\, d^3p_1. \tag{70}$$

The brackets $\{m, k\}$, (m, m), have been evaluated by Harris and Rice. The brackets $\{m, k\}$ vanish identically for $m=0, 1$. For the rigid-sphere model, retention of the first four terms in the series of Eq. (4) therefore yields only a quadratic equation. If only three terms are retained the value of the root is within 9% of the value for four terms. When the rigid-sphere terms are taken as zero then retention of three terms yields a value for the smallest root differing by only 2% from the value obtained with two terms. We give here the 4×4 determinant for the present equation. Depending on the relative magnitudes of the hard-sphere and friction terms a 3×3 determinant may actually suffice:

$$\begin{vmatrix} \lambda & B & 2B & 3B \\ B & (-B+\frac{5}{2}\lambda) & \frac{3}{2}B & 4B \\ 2B & \frac{3}{2}B & (-4A-\frac{7}{2}B+\frac{35}{8}\lambda) & (-3A+\frac{7}{8}B) \\ 3B & 4B & (-3A+\frac{7}{8}B) & (-\frac{2709}{10}A-\frac{63}{8}B+\frac{105}{16}\lambda) \end{vmatrix} = 0, \tag{71}$$

where

$$A = (\pi kT/m)^{\frac{1}{2}}[\sigma^2 g(\sigma)/v], \qquad B = \zeta/m. \tag{72}$$

For purposes of illustration we restrict present considerations to the cubic equation formed by omitting the bottom row and right-hand column of Eq. (71). This may be solved by successive approximation using a standard procedure. As a zero approximation we take $\frac{35}{8}\lambda = 4A + \frac{7}{2}B$ and substitute for λ except in the (3, 3) element. The value of λ calculated from this equation is used as the starting point for the next approximation. Successive approximations obey the formulas

$$\lambda_n = \tfrac{32}{35}A + \tfrac{4}{5}B + E_n,$$

where

$$E_n = \frac{8[392A - 7B + \frac{1715}{4}E_{n-1}]}{35[\frac{512}{7}(A/B)^2 + 96(A/B) - 7 + (E_{n-1}/B^2)(160A + 105B) + \frac{175}{2}(E_{n-1}/B)^2]} \tag{73}$$

and

$$E_0 = 0.$$

The other roots must be found from the corresponding quadratic equation to ascertain which is smaller.

The exact value of ζ to be used must await a further development of the theory. For the purpose of illustration we consider liquid argon at 89°K and take ζ as one-half the value of the friction constant in Kirkwood's theory, which is 4.84×10^{-10} g/sec^{-1}. We find a relaxation time of 3.3×10^{-13} sec compared with the value of 6.0×10^{-13} sec, for the rigid-sphere fluid, and 1.55×10^{-13} sec for Kirkwood's Fokker-Planck equation. (In each case three terms were taken. See remarks above.) This is in the direction one would have anticipated. In a real fluid one would expect the relaxation time to be less than or equal to that for the rigid-sphere fluid at the same density since in the real fluid a molecule is continuously undergoing transfer of energy because of the attractive forces.

VI. DISCUSSION

The purpose of this paper has been to present an analysis of the nonequilibrium steady state for a simple model of a dense fluid. The advantage which the proposed model possesses, lies in the ease of separation of large and small momentum transfers. As a result of this separation it has been possible to obtain and solve a new integro-differential equation for the singlet distribution function. It will be shown in a forthcoming paper, that an analogous analysis can be made for the

doublet distribution function. We are aware that our analysis contains a number of delicate points which we have handled in an intuitive manner rather than by rigorous mathematics.[11] Nevertheless, the authors believe that the physical picture is sufficiently clear so that the intuitive arguments used can claim a wide range of validity. Of course, rigorous justification awaits more detailed treatment.

The physical situation to which our model corresponds is easily visualized. A given molecule undergoes a hard-core collision with a second molecule. This collision is followed by a trajectory determined by the rapidly fluctuating attractive force field generated by all the near neighbors. Although we have postulated that a time τ can be found such that the basic dynamical event consists of one hard-core collision and the quasi-random walk, we do not consider the time smoothing to be a philosophic principle. Rather we regard the time smoothing as a convenient mathematical method for selecting the basic dynamical event and rendering it independent of both prior and future events. The fact that the computed relaxation time for the return to equilibrium in momentum space is much shorter than the time between hard-core collisions strongly supports the contention that a time τ can be specified.

A major problem is, of course, the calculation of the singlet frictional constant ζ. Previous derivations[12,13] have in various ways made use of the fact that at equilibrium the mean force on a molecule vanishes. Since the ζ defined by Eq. (24) is determined only by the soft part of the potential, this condition no longer holds. It is, indeed, necessary to proceed by an examination of the momentum autocorrelation function, with proper attention given to the nonvanishing of the mean attractive force.

In a certain sense, the intuitive picture presented here, has a similarity to the Bogolubov[14] analysis of the approach to equilibrium. The crux of this analysis is that the *chaotization* occurs in different stages provided that the system under consideration has a number of basic relaxation times. The solution to the singlet equation presented here corresponds to a state of the system in which the initial, very rapid relaxation, has already occurred. In the succeeding interval of time, the hard-core interactions have a characteristic relaxation time different from that of the soft attractive interactions. In Bogolubov's analysis, each such stage of analysis is characterized by fewer and fewer variables. This situation is put to practical use in the sense that the diffusive trajectory followed in the Brownian motion is an average description requiring less detailed specification than the mechanical trajectory defining the hard-core collisions. However, in contrast with Bogolubov, since the approximation of Brownian motion is not valid at low densities for short-ranged potentials, the recasting of the transport equation into a virial series does not appear to be profitable in the case discussed in this paper.

Finally, we note that the notion of treating attractive forces as a weak perturbation on strong repulsions has been used on gases at equilibrium,[15] and turns out to be valid there only at high temperatures. For the case considered in this paper we have not really made any assumption that the attractive forces are small. Rather we have assumed that the momentum transfer due to attractive interactions is small relative to the mean momentum per molecule. This implies that the rate of change of $V^{(S)}$ with intermolecular separation is small relative to that of $V^{(R)}$. Such an approximation does not necessitate that $(V^{(S)}/kT)<1$ as the simple example of the Coulomb interaction readily shows.

ACKNOWLEDGMENTS

The authors wish to thank the Alfred P. Sloan Foundation and the Petroleum Research Fund of the American Chemical Society for generous support of this research.

[11] See for example, the analysis between Eqs. (17) and (18).
[12] S. A. Rice and J. G. Kirkwood, J. Chem. Phys. **31**, 901 (1959).
[13] S. A. Rice, J. Chem. Phys. (to be published).
[14] N. Bogolubov, J. Phys. (U.S.S.R.) **10**, 265 (1946).
[15] R. W. Zwanzig, J. Chem. Phys. **22**, 1420 (1954).

On the Kinetic Theory of Dense Fluids. VII. The Doublet Distribution Function for Rigid Spheres with an Attractive Potential

ALAN R. ALLNATT* AND STUART A. RICE†

Department of Chemistry and Institute for the Study of Metals, University of Chicago, Chicago, Illinois

(Received August 31, 1960)

A new integro-differential equation for the doublet distribution function of a model dense fluid is derived and solved. In this model, the intermolecular pair potential is represented as a rigid core plus an attraction. Interactions involving rigid cores are handled as in the theory of the dense rigid-sphere fluid and attractive interactions are handled as in the Fokker-Planck theory. The resultant doublet distribution function is compared with the singlet distribution function calculated for the same model.

I. INTRODUCTION

IN a dilute gas, molecules move along free-particle trajectories with only occasional interruptions due to collisions with other molecules. As a result, the dominant mode of energy and momentum transfer is "piggy-back" carriage in the free flights between collisions. On the other hand, in a dense fluid every molecule is in continuous interaction with its neighbors. In this case the dominant mode of energy and momentum transport is through fluctuations in the force field surrounding each molecule. The computation of the fluxes of energy and momentum thus requires the knowledge of multibody distribution functions. This observation holds for the formulation of transport coefficients in terms of autocorrelation functions in an equilibrium ensemble, as well as for the Kirkwood theory[1] which attempts to directly describe the stationary nonequilibrium state.

In the preceding paper of this series[2] we described a model of the liquid which permitted facile description of the nonequilibrium singlet distribution function. Briefly, each particle is assumed to interact with others through a pair interaction potential which consists of an impenetrable core and a "soft" attraction. It is further assumed that it is possible to define a time interval of length τ such that events which occur during this interval are independent of both prior and future events. In the model liquid considered, the basic dynamical event is taken to be a collision between two rigid cores followed by a Brownian motion of one of the particles in the fluctuating field of its neighbors. The rigid-core interactions are handled as in the theory of the dense rigid-sphere fluid,[3,4] while the subsequent Brownian motion is handled, following Kirkwood,[1] in terms of a Fokker-Planck equation. The resultant transport equation can be solved by the Chapman-Enskog method and the perturbations to the singlet distribution function explicitly computed. The self-consistency of the model and theory is strongly supported by the fact that the relaxation time for return to equilibrium in momentum space is short compared to the time between rigid-core encounters.

It is the purpose of the present paper to derive and solve, for the same model liquid, an integro-differential equation for the doublet distribution function. As in the previous case, the model chosen permits facile description of the physical situation.

II. THE INTEGRO-DIFFERENTIAL EQUATION

As usual, we describe a system containing N structureless molecules in terms of the normalized distribution function, $f^{(N)}$, which satisfies the Liouville equation

$$(\partial f^{(N)}/\partial t)+\sum_i[(\mathbf{p}_i/m)\cdot\nabla_{R_i}f^{(N)}+(\mathbf{X}_i+\mathbf{F}_i)\cdot\nabla_{p_i}f^{(N)}]=0, \quad (1)$$

with $\mathbf{p}_i$, $\mathbf{R}_i$, and m_i the momentum, position, and mass of molecule i, $\mathbf{X}_i$ the external force, and $\mathbf{F}_i$ the intermolecular force. We seek an integro-differential equation specifying the behavior of the doublet distribution function $f^{(2)}$ where

$$f^{(n)}=(N-n)!^{-1}\int f^{(N)}(\mathbf{R}^{(N)}\mathbf{P}^{(N)};t)d\mathbf{R}^{(N-n)}d\mathbf{P}^{(N-n)}. \quad (2)$$

A formal relation of the form sought is obtained by integration of Eq. (1), $2(N-2)$ times, and the use of Green's theorem. The result is

$$\mathfrak{L}^{(2)}\bar{f}^{(2)}=-\frac{1}{(N-2)!\tau}\int_0^\tau\int\cdots\int[\mathbf{F}_1\cdot\nabla_{r_1}f^{(N)}+\mathbf{F}_2\cdot\nabla_{p_2}f^{(N)}]d\mathbf{R}^{(N-2)}d\mathbf{p}^{(N-2)}ds, \quad (3)$$

where the doublet operator $\mathfrak{L}^{(2)}$ is defined in the absence of external forces by

$$\mathfrak{L}^{(n)}=\partial/\partial t+\sum_{i=1}^{n}(\mathbf{p}_i/m)\cdot\nabla_{R_i}, \quad (4)$$

and we have introduced a coarse graining in time in

* NATO Fellow.
† Alfred P. Sloan Fellow.
[1] J. G. Kirkwood, J. Chem. Phys. **14**, 180 (1946).
[2] S. A. Rice and A. R. Allnatt, J. Chem. Phys. **35**, 2144 (1961).
[3] S. A. Rice, J. G. Kirkwood, J. Ross, and R. W. Zwanzig, J. Chem. Phys. **31**, 575 (1959).
[4] S. A. Rice, J. Chem. Phys. **31**, 584 (1959).

order to isolate the basic dynamical event. This coarse graining is specified by

$$\bar{f}^{(n)}(t)=\tau^{-1}\int_0^\tau f^{(n)}(t+s)\,ds. \tag{5}$$

Consider now that the force acting on molecule one (or two) is decomposable into a sum of pair forces. With the use of Eq. (2) and the pairwise decomposition of the intermolecular force, Eq. (3) may be written in the form

$$\mathfrak{L}^{(2)}\bar{f}^{(2)}+\mathbf{F}_{12}\cdot\nabla_{p_1}\bar{f}^{(2)}+\mathbf{F}_{21}\cdot\nabla_{p_2}\bar{f}^{(2)}=\Omega_R^{(2)}+\Omega_s^{(2)}, \tag{6}$$

where

$$\Omega_R^{(2)}=-\tau^{-1}\int_0^\tau\iint[\mathbf{F}_{13}^{(R)}\cdot\nabla_{p_1}f^{(3)}(\mathbf{R}_1\mathbf{R}_2\mathbf{R}_3\mathbf{p}_1\mathbf{p}_2\mathbf{p}_3;\,t+s)\,d\mathbf{R}_3d\mathbf{p}_3ds$$

$$-\tau^{-1}\int_0^\tau\iint[\mathbf{F}_{24}^{(R)}\cdot\nabla_{p_2}f^{(3)}(\mathbf{R}_1\mathbf{R}_2\mathbf{R}_4\mathbf{p}_1\mathbf{p}_2\mathbf{p}_4;\,t+s)\,d\mathbf{R}_4d\mathbf{p}_4ds, \tag{7}$$

$$\Omega_s^{(2)}=-\tau^{-1}\int_0^\tau\iint[\mathbf{F}_{13}^{(s)}\cdot\nabla_{p_2}f^{(3)}(\mathbf{R}_1\mathbf{R}_2\mathbf{R}_3\mathbf{p}_1\mathbf{p}_2\mathbf{p}_3;\,t+s)]\,d\mathbf{R}_3d\mathbf{p}_3ds$$

$$-\tau^{-1}\int_0^\tau\iint[\mathbf{F}_{24}^{(s)}\cdot\nabla_{p_2}f^{(3)}(\mathbf{R}_1\mathbf{R}_2\mathbf{R}_4\mathbf{p}_1\mathbf{p}_2\mathbf{p}_4;\,t+s)]\,d\mathbf{R}_4d\mathbf{p}_4ds. \tag{8}$$

In Eqs. (6), (7), and (8), the intermolecular pair force $\mathbf{F}_{ij}$ has been represented as the sum of a repulsive component $\mathbf{F}_{ij}^{(R)}$ and an attractive component $\mathbf{F}_{ij}^{(S)}$. It will be convenient to write the integrals of Eq. (7) in the form

$$\Omega_R^{(2)}=\Omega_{R3}^{(2)}+\Omega_{R4}^{(2)}, \tag{9}$$

a notation which temporarily identifies molecules. The utility of this artifice will become apparent shortly.

Equation (6) describes the averaged distribution function of a pair of molecules subject to interactions with the remaining $N-2$ molecules of the system. In obtaining this relation we have as yet made no use of the special properties of the intermolecular potential for our model. Equation (6) is therefore valid for any continuous, pairwise decomposable interaction potential. Consider now that the repulsive portion of the pair interaction potential is of the form

$$V_{ij}^{(R)}=(\sigma/R_{ij})^n, \tag{10}$$

and examine the limit to which $f^{(2)}$ tends as $n\to\infty$. In this limit the pair distribution function vanishes whenever $R_{ij}\leq\sigma$, and $\mathbf{F}_{ij}^{(R)}$ vanishes whenever $R_{ij}>\sigma$. With these observations, the substitution of (10) into (6) and subsequent passage to the limit of $n\to\infty$ gives

$$\mathfrak{L}^{(2)}\bar{f}^{(2)}+\mathbf{F}_{12}^{(s)}\cdot\nabla_{p_1}\bar{f}^{(2)}+\mathbf{F}_{21}^{(s)}\cdot\nabla_{p_2}\bar{f}^{(2)}=\Omega_R^{(2)}+\Omega_s^{(2)}. \tag{11}$$

During the time interval 0 to τ the pair of molecules labeled 1, 2 may of course collide with other molecules, $3\cdots N$, in the system. The definition of the rigid-core potential implies, however, that $\mathbf{F}_{1j}^{(R)}$ and $\mathbf{F}_{2k}^{(R)}$ ($j\geq3$, $k\geq3$) cannot *simultaneously* be nonzero. Thus, when $\mathbf{F}_{13}^{(R)}\neq0$, $\mathbf{F}_{24}^{(R)}=0$, and vice versa.

It is now appropriate to consider the time evolution of $f^{(N)}$. If the conditional probability density of finding the system of N molecules at $\{\mathbf{Rp}\}$ in phase space at time $(t+s)$ if it was at $\{\mathbf{R'p'}\}$ at time t, is denoted $K^{(N)}(\mathbf{Rp}/\mathbf{R'p'};s)$, then

$$f^{(N)}(\mathbf{RP};t+s)=\int\cdots\int K^{(N)}(\mathbf{RP}/\mathbf{R'P'};s)f^{(N)}(\mathbf{R'P'};t)\,d\mathbf{R'}d\mathbf{P'}. \tag{12}$$

Now, it may readily be shown that $K^{(N)}$ satisfies the Liouville equation so that

$$(\partial K^{(N)}/\partial s)+\sum_i[(\mathbf{p}_i/m)\cdot\nabla_{R_i}K^{(N)}+\mathbf{F}_i\cdot\nabla_{p_i}K^{(N)}]=0. \tag{13}$$

To study the time evolution of the n-body distribution function we require, by analogy with Eq. (12), the n-body transformation function $K^{(n)}$. To this end, define the conditional probability density

$$f^{(n/N-n)}(\mathbf{rp}/\mathbf{QP};t)=f^{(N)}(\mathbf{rQpP};t)/f^{(n)}(\mathbf{rp};t), \tag{14}$$

whereupon

$$K^{(n)}(\mathbf{rp}/\mathbf{r}'\mathbf{p}';s)=\int\cdots\int K^{(N)}(\mathbf{rpQP}/\mathbf{r}'\mathbf{p}'\mathbf{Q}'\mathbf{P}';s)f^{(n/N-n)}(\mathbf{r}'\mathbf{p}'/\mathbf{Q}'\mathbf{P}';t)d\mathbf{P}d\mathbf{Q}d\mathbf{P}'d\mathbf{Q}', \tag{15}$$

and

$$f^{(n)}(\mathbf{rp};t+s)=\int\cdots\int K^{(n)}(\mathbf{rp}/\mathbf{r}'\mathbf{p}';s)f^{(n)}(\mathbf{r}'\mathbf{p}';t)d\mathbf{r}'d\mathbf{p}'. \tag{16}$$

Consider the three-body distribution function $f^{(3)}$ the evolution of which is determined by $K^{(3)}$ which, in turn, is constrained to satisfy the contracted Liouville equation

$$(\partial K^{(3)}/\partial s)+(\mathbf{p}_1/m)\cdot\nabla_{R_1}K^{(3)}+(\mathbf{p}_2/m)\cdot\nabla_{\mathbf{p}_3}K^{(3)}$$
$$=-\iint\sum_{j=3}^{N}F_j\cdot\nabla_{p_j}K^{(N)}f^{(3/N-3)}(\mathbf{R}_1'\mathbf{R}_2'\mathbf{R}_3'\mathbf{p}_1'\mathbf{p}_2'\mathbf{p}_3'/\mathbf{Q}'\mathbf{P}';t)d\mathbf{P}d\mathbf{Q}d\mathbf{P}'d\mathbf{Q}'. \tag{17}$$

After introduction of the pair forces $\mathbf{F}_{ij}$ **Eq. (17)** reduces to the form

$$\mathfrak{L}^{(3)}K^{(3)}+\mathbf{F}_{12}\cdot\nabla_{p_1}K^{(3)}+\mathbf{F}_{13}\cdot\nabla_{p_1}K^{(3)}+\mathbf{F}_{21}\cdot\nabla_{\mathbf{p}_2}K^{(3)}+\mathbf{F}_{23}\cdot\nabla_{p_2}K^{(3)}+\mathbf{F}_{31}\cdot\nabla_{p_3}K^{(3)}+\mathbf{F}_{32}\cdot\nabla_{p_3}K^{(3)}$$
$$=-\iint\sum_{j=4}^{N}[\mathbf{F}_{1j}\cdot\nabla_{p_1}+\mathbf{F}_{2j}\cdot\nabla_{p_2}+\mathbf{F}_{3j}\cdot\nabla_{p_3}]K^{(N)}(s)f^{(3/N-3)}d\mathbf{P}d\mathbf{Q}d\mathbf{P}'d\mathbf{Q}'. \tag{18}$$

To separate the rigid-core and soft-attraction effects, we consider a very short time interval 0 to $+0$. As we have previously noted, it follows from the definition of the rigid-core potential, that if a collision occurs between molecules one and three we may take $\mathbf{F}_{1j}^{(R)}=\mathbf{F}_{3j}^{(R)}=0(j\geq 4)$. We shall assume, as in the case of the singlet distribution function that $V^{(S)}\approx$ constant in the time interval considered. With these assumptions $\Omega_{R3}^{(2)}$ may be evaluated by substitution for $\mathbf{F}_{13}^{(R)}\cdot\nabla_{p_1}f^{(3)}$ in the expression for $\Omega_{R3}^{(2)}$ using Eq. (18) and the definition of Eq. (15). With due cognizance of the vanishing of the various repulsive potentials in the interval $+0$, we find

$$\Omega_{R3}^{(2)}=\tau^{-1}\int_0^\tau\int\cdots\int[(\partial K_0^{(3)}/\partial s+(\mathbf{p}_1/m)\cdot\nabla_{R_1}K_0^{(3)}+(\mathbf{p}_2/m)\cdot\nabla_{R_2}K_0^{(3)}+(\mathbf{p}_3/m)\cdot\nabla_{R_3}K_0^{(3)}]$$
$$\times f^{(3)}(\mathbf{R}_1'\mathbf{R}_2'\mathbf{R}_3'\mathbf{p}_1'\mathbf{p}_2'\mathbf{p}_3';t)d\mathbf{R}_3d\mathbf{p}_3dsd\mathbf{R}_1'd\mathbf{R}_2'd\mathbf{R}_3'd\mathbf{p}_1'd\mathbf{p}_2'd\mathbf{p}_3', \tag{19}$$

with

$$\mathfrak{L}^{(3)}K_0^{(3)}(s)+\mathbf{F}_{12}\cdot\nabla_{p_1}K_0^{(3)}+\mathbf{F}_{21}\cdot\nabla_{p_2}K_0^{(3)}+\mathbf{F}_{13}\cdot\nabla_{p_1}K_0^{(3)}+\mathbf{F}_{31}\cdot\nabla_{p_3}K_0^{(3)}+\mathbf{F}_{23}\cdot\nabla_{p_2}K_0^{(2)}+\mathbf{F}_{32}\cdot\nabla_{p_3}K_0^{(3)}=0 \tag{20}$$

for the time interval 0 to $+0$.

We have assumed that molecule one collides with molecule three between the times 0 and $+0$, and that during the remainder of the interval 0 to τ it undergoes a kind of Brownian notion due to the attractive forces of the other molecules. We shall assume that if the molecule one undergoes such a collision in the time 0 to τ then the second molecule of the pair, molecule 2, does not, so that $\Omega_{R4}^{(2)}$ is zero. (Clearly since one and two are indistinguishable we might equally well take $\Omega_{R4}^{(2)}\neq 0$, and $\Omega_{R3}^{(2)}=0$. It is convenient for the manipulations which follow not to symmetrize the expression for $\Omega_R^{(2)}$ at this point.) Now the solution of the three-body Liouville equation (20) is readily expressed in the form

$$K_0^{(3)}=\prod_{i=1}^{3}\delta[\mathbf{R}_i-\mathbf{R}_i'-\Delta\mathbf{R}_i(s)]\delta[\mathbf{p}_i-\mathbf{p}_i'-\Delta\mathbf{p}_i(s)], \tag{21}$$

from which it follows by manipulation similar to that outlined in the preceding paper[2]

$$\Omega_R^{(2)}=\iint[f^{(3)}(\mathbf{R}_1-\Delta\mathbf{R}_1,\mathbf{R}_2-\Delta\mathbf{R}_2,\mathbf{R}_1+\sigma\mathbf{k},\mathbf{p}_1-\Delta\mathbf{p}_1,\mathbf{p}_2-\Delta\mathbf{p}_2,\mathbf{p}_3-\Delta\mathbf{p}_3;t)$$
$$-f^{(3)}(\mathbf{R}_1,\mathbf{R}_2,\mathbf{R}_1-\sigma\mathbf{k},\mathbf{p}_1,\mathbf{p}_2,\mathbf{p}_3;t)]bdbd\epsilon d\mathbf{p}_3, \tag{22}$$
$$\mathbf{k}\cdot\mathbf{p}_{13}>0. \tag{23}$$

In order to proceed further with the evaluation of the hard-core term $\Omega_R^{(2)}$ a relationship between the triplet

and pair distribution functions is required. We shall assume that the superposition approximation

$$f^{(3)}(\mathbf{R}_1\mathbf{R}_2\mathbf{R}_3\mathbf{p}_1\mathbf{p}_2\mathbf{p}_3;\, t)=\frac{f^{(2)}(\mathbf{R}_1\mathbf{R}_2\mathbf{p}_1\mathbf{p}_2;\, t)f^{(2)}(\mathbf{R}_1\mathbf{R}_3\mathbf{p}_1\mathbf{p}_3;\, t)f^{(2)}(\mathbf{R}_2\mathbf{R}_3\mathbf{p}_2\mathbf{p}_3;\, t)}{f^{(1)}(\mathbf{R}_1\mathbf{p}_1;\, t)f^{(1)}(\mathbf{R}_2\mathbf{p}_2;\, t)f^{(1)}(\mathbf{R}_3\mathbf{p}_3;\, t)} \tag{24}$$

is valid. In making this assumption in phase space we generalize the original intent of the Kirkwood superposition approximation. At equilibrium, the momentum space triplet distribution function identically satisfies superposition. Moreover, there can be no spatial dependence of the approximation in momentum space and we therefore suggest that superposition in momentum space is at least as valid an approximation as superposition in configuration space. On substituting Eq. (24) in Eq. (23) and performing a final time smoothing we have

$$\Omega_R^{(2)}=\int\cdots\int\left[\frac{\bar{f}^{(2)}(1,2)^*\bar{f}^{(2)}(1,3)^*\bar{f}^{(2)}(2,3)^*}{\bar{f}^{(1)}(1)^*\bar{f}^{(1)}(2)^*\bar{f}^{(1)}(3)^*}-\frac{\bar{f}^{(2)}(1,2)\bar{f}^{(2)}(1,3)\bar{f}^{(2)}(2,3)}{\bar{f}^{(1)}(1)\bar{f}^{(1)}(2)\bar{f}^{(1)}(3)}\right]d\mathbf{R}_3d\mathbf{p}_3 \tag{25}$$

$$\bar{f}^{(2)}(i,j)\equiv\bar{f}^{(2)}(\mathbf{R}_i\mathbf{R}_j\mathbf{p}_i\mathbf{p}_j;\, t), \tag{26}$$

where the asterisk (*) refers to the quantity evaluated with coordinates corresponding to these in the first term of Eq. (22). This function is zero except in the time 0 to +0, when the positions of 1 and 3 differ by one hard-sphere diameter σ. We erect a cylindrical coordinate system (z, b, ϵ) with origin on molecule one and z axis antiparallel to the initial relative momentum vector. Complete collisions occur in an interval τ' corresponding to a filamentary volume in relative configuration space

$$(p_{13}/\mu)\tau' bdbd\epsilon,$$

and in the usual case we should take $\tau'=+0$. However, since in the interval 0 to +0 the molecule undergoes only one rigid-core collision we can extend the length of the cylinder within which no completed collision occurs to

$$(p_{13}/\mu)\tau bdbd\epsilon,$$

without altering the result. Our expression for the hard core therefore becomes

$$\Omega_R^{(2)}=\iint\left[\frac{\bar{f}^{(2)}(1,2)^*\bar{f}^{(2)}(1,3)^*\bar{f}^{(2)}(2,3)^*}{\bar{f}^{(1)}(1)^*\bar{f}^{(1)}(2)^*\bar{f}^{(1)}(3)^*}-\frac{\bar{f}^{(2)}(1,2)\bar{f}^{(2)}(1,3)\bar{f}^{(2)}(2,3)}{\bar{f}^{(1)}(1)\bar{f}^{(1)}(2)\bar{f}^{(1)}(3)}\right](p_{13}/\mu)bdbd\epsilon d^3p_3. \tag{27}$$

Finally we note that in this equation

$$\bar{f}^{(2)}(i,j)^*\equiv\bar{f}^{(2)}(\mathbf{R}_i-\Delta\mathbf{R}_i,\, \mathbf{R}_j-\Delta\mathbf{R}_j,\, \mathbf{p}_i-\Delta\mathbf{p}_i,\, \mathbf{p}_j-\Delta\mathbf{p}_j;\, t)$$

and in the limit of an infinitesimally small time interval the increments $\Delta\mathbf{R}$ approach zero.

The pair distribution function $\bar{f}^{(2)}(1,3)$ appearing in the integral $\Omega_R^{(2)}$ is conveniently expanded by introducing the pair correlation function $g^{(2)}$ defined by the equation

$$\bar{f}^{(2)}(\mathbf{R}_1\mathbf{R}_3\mathbf{p}_1\mathbf{p}_3;\, t)=g^{(2)}(\mathbf{R}_1\mathbf{R}_3\mathbf{p}_1\mathbf{p}_3;\, t)\,\bar{f}^{(1)}(\mathbf{R}_1\mathbf{p}_1;\, t)\,\bar{f}^{(1)}(\mathbf{R}_3\mathbf{p}_3;\, t). \tag{28}$$

Expanding the singlet distribution function centered on $\mathbf{R}_3$ in a Taylor series about $\mathbf{R}_1$ and retaining only first-order terms, Eq. (28) becomes

$$\bar{f}^{(2)}(\mathbf{R}_1,\, \mathbf{R}_1-\sigma\mathbf{k},\, \mathbf{p}_1,\, \mathbf{p}_3;\, t)=g^{(2)}(\mathbf{R}_1,\, \mathbf{R}_1-\sigma\mathbf{k},\, \mathbf{p}_1,\, \mathbf{p}_3;\, t)\,\bar{f}^{(1)}(\mathbf{R}_1\mathbf{p}_1;\, t)\,\bar{f}^{(1)}(\mathbf{R}_1\mathbf{p}_1;\, t)$$

$$-g^{(2)}(\mathbf{R}_1,\, \mathbf{R}_1-\sigma\mathbf{k},\, \mathbf{p}_1,\, \mathbf{p}_3;\, t)\,\bar{f}^{(1)}(\mathbf{R}_1,\, \mathbf{p}_1;\, t)\sigma\mathbf{k}\cdot\nabla_{R_1}\bar{f}^{(1)}(\mathbf{R}_1\mathbf{p}_3;\, t). \tag{29}$$

In the equations which follow we shall write

$$g^{(2)}(\mathbf{R}_1\mathbf{R}_3\mathbf{p}_1\mathbf{p}_3;\, t)\,\bar{f}^{(1)}(\mathbf{R}_1\mathbf{p}_1;\, t)\,\bar{f}^{(1)}(\mathbf{R}_1\mathbf{p}_3;\, t)\equiv\bar{f}^{(2)}(1,3), \tag{30}$$

which defines the quantity denoted by $\bar{f}^{(2)}(1,3)$, the remaining quantities $\bar{f}^{(2)}(i,j)$ appearing in Eq. (27) being

defined, as before by Eq. (26). The final expression for Ω_R is seen from Eqs. (27) and (29) to be

$$\Omega_R^{(2)} = \iint \left\{ \frac{\bar{f}^{(2)}(1,2)^* \bar{f}^{(2)}(1,3)^* \bar{f}^{(2)}(2,3)^*}{\bar{f}^{(1)}(1)^* \bar{f}^{(1)}(2)^* \bar{f}^{(1)}(3)^*} - \frac{\bar{f}^{(2)}(1,2)\bar{f}^{(2)}(1,3)\bar{f}^{(2)}(2,3)}{\bar{f}^{(1)}(1)\bar{f}^{(1)}(2)\bar{f}^{(1)}(3)} \right\} (p_{13}/\mu) b db d\epsilon d^3 p_3$$

$$+ \iint \left\{ \frac{\bar{f}^{(2)}(1,2)^* \bar{f}^{(2)}(2,3)^* g_0^{(2)}(\mathbf{R}_1, \sigma)\sigma\mathbf{k}\cdot\nabla_{R_1}\bar{f}^{(1)}(\mathbf{R}_1, \mathbf{p}_3 - \Delta\mathbf{p}_3, t)}{\bar{f}^{(1)}(2)^* \bar{f}^{(1)}(3)^*} \right.$$

$$\left. - \frac{\bar{f}^{(2)}(1,2)\bar{f}^{(2)}(2,3) g_0^{(2)}(\mathbf{R}_1, \sigma)\sigma\mathbf{k}\cdot\nabla_{R_1}\bar{f}^{(1)}(\mathbf{R}_1, \mathbf{p}_3; t)}{\bar{f}^{(1)}(2)\bar{f}^{(1)}(3)} \right\} \mathbf{p}_{13} b db d\epsilon d^3 p_3 = J_1 + J_2. \tag{31}$$

In writing the second term of Eq. (31) we have assumed, as in the treatment of the singlet distribution function, that $g^{(2)}$ can be approximated by the local equilibrium pair correlation function $g_0^{(2)}$.

The integral containing the attractive forces $\Omega_a^{(2)}$ can be evaluated in a manner similar to that described by Ross,[5] and by Kirkwood.[1] We refer the reader to these papers for a description of the methods to be employed. Using the value for $\Omega_a^{(2)}$ so obtained and combining with Eqs. (6) and (31) the final equation for the pair distribution function can be written in the form

$$D_2\bar{f}^{(2)}(1,2) = J_1 + J_2 + \zeta(\mathbf{R}_1)\mathcal{A}_1[\bar{f}^{(2)}(1,2)] + \zeta(\mathbf{R}_2)\mathcal{A}_2[\bar{f}^{(2)}(1,2)] = J[\bar{f}^{(2)}(1,2)], \tag{32}$$

where

$$D_2\bar{f}^{(2)} = (\partial\bar{f}^{(2)}/\partial t) + (\mathbf{p}_1/m)\cdot\nabla_{R_1}\bar{f}^{(2)} + (\mathbf{p}_2/m)\cdot\nabla_{R_2}\bar{f}^{(2)} + \mathbf{F}_1^{(2)}\cdot\nabla_{p_1}\bar{f}^{(2)} + \mathbf{F}_2^{(2)}\cdot\nabla_{p_2}\bar{f}^{(2)} \tag{33}$$

$$\mathcal{A}_j[\bar{f}^{(2)}(1,2)] = \nabla_{p_j}\cdot\{[(\mathbf{p}_j/m) - \mathbf{u}(\mathbf{R}_j)]\bar{f}^{(2)}(1,2) + kT(\mathbf{R}_j)\nabla_{p_j}\bar{f}^{(2)}(1,2)\} \tag{34}$$

$$\mathbf{F}_1^{(2)} = {}^{(2)}\langle \mathbf{F}_1^{(a)} \rangle^0 + {}^{(2)}\mathbf{F}_1^+$$

$$\mathbf{F}_2^{(2)} = {}^{(2)}\langle \mathbf{F}_2^{(a)} \rangle^0 + {}^{(2)}\mathbf{F}_2^+, \tag{35}$$

where ${}^{(2)}\langle \mathbf{F}_1^{(a)} \rangle^0$ is the average total attractive intermolecular force on a molecule at $\mathbf{R}_1$ where a pair of molecules is fixed at $\mathbf{R}_1$ and $\mathbf{R}_2$ and the average performed in a canonical ensemble over the rest of the molecules, and ${}^{(2)}\mathbf{F}_1^+$ is a perturbation arising from the departure of $f^{(3/N-3)}$ from its equilibrium value. Here $\zeta(\mathbf{R}_1)$ is the friction constant for a molecule at $\mathbf{R}_1$ defined, as in the previous paper,

$$\zeta(\mathbf{R}_1) = (3kT\tau)^{-1}\int_{+0}^{\tau}\int_{-s}^{+0}\iint \mathbf{F}_{12}^{(a)}(\mathbf{R}_{12})\,\mathbf{F}_1^{(a)}[\mathbf{R}_1 + (s+s')(\mathbf{p}/m)]\, f_0^{(1/N-1)}(\mathbf{R}_1\mathbf{p}_1/PQ)\, d\mathbf{p}d\mathbf{Q}dsds'. \tag{36}$$

III. THE PERTURBATION SOLUTION

The equation for the pair distribution function can be solved by the Chapman-Enskog procedure. The pair space density $n_2(\mathbf{R}_1\mathbf{R}_2)$, defined by

$$n_2(\mathbf{R}_1\mathbf{R}_2) = \int \bar{f}^{(2)}(1,2)\, d\mathbf{p}_1 d\mathbf{p}_2 \tag{37}$$

and the variables $\mathbf{u}(\mathbf{R}_1)$, $\mathbf{u}(\mathbf{R}_2)$, $T(\mathbf{R}_1)$, and $T(\mathbf{R}_2)$ are invariants of the collision operator $J(\bar{f}^{(2)})$ of Eq. (32).[6] We denote the quantities by ρ,

$$\rho = \{n_2, \mathbf{u}(\mathbf{R}_1), \mathbf{u}(\mathbf{R}_2), T(\mathbf{R}_1), T(\mathbf{R}_2)\}. \tag{38}$$

The distribution functions are expanded as a series in a perturbation parameter ϵ,

$$\bar{f}^{(2)} = \sum_{l=0}^{\infty} \epsilon^l \bar{f}_l^{(2)} \tag{39}$$

$$\bar{f}^{(1)} = \sum_{l=0}^{\infty} \epsilon^l \bar{f}_l^{(1)}, \tag{40}$$

[5] J. Ross, J. Chem. Phys. **24**, 375 (1956).
[6] J. L. Lebowitz, H. L. Frisch, and E. Helfand, J. Phys. Fluids **3**, 325 (1960).

and Eq. (27) written in the form

$$D_2\bar{f}^{(2)}=\epsilon^{-1}[J(\bar{f}^{(2)})-J_2]+J_2. \tag{41}$$

Utilizing the expansions of Eqs. (39) and (40), and the definitions of the various quantities ρ_r these functions may be similarly expressed in a series of the form

$$\rho_r=\sum_{l=0}^{\infty}\epsilon^l\rho_r^{(l)}. \tag{42}$$

On substituting Eqs. (39), (40), and (42) in the right-hand side of Eq. (41) and equating the coefficients of equal powers of an ϵ infinite set of equations is obtained. These equations determine $\bar{f}^{(2)}$ only up to linear combinations of those quantities conserved by $J(\bar{f}^{(2)})$. This flexibility allows one to require that

$$\rho_r^{(0)}=\rho, \qquad \rho^{(l)}=0 \qquad (l>0). \tag{43}$$

With this simplification the zero-order equation has a solution which is the locally Maxwellian distribution

$$\bar{f}_0^{(2)}=\frac{n_2(\mathbf{R}_1\mathbf{R}_2)\,\exp\left[-\frac{[\mathbf{p}_1-m\mathbf{u}(\mathbf{R}_1)]^2}{2mkT(\mathbf{R}_1)}-\frac{[\mathbf{p}_2-m\mathbf{u}(\mathbf{R}_2)]^2}{2mkT(\mathbf{R}_2)}\right]}{(2\pi mk)^3T(\mathbf{R}_1)^{\frac{1}{2}}T(\mathbf{R}_2)^{\frac{1}{2}}}, \tag{44}$$

and the first-order equation can be written in the form

$$\begin{aligned}D_2\bar{f}_0^{(2)}(1,2)=\zeta(\mathbf{R}_1)\mathfrak{A}_1^{(1)}\bar{f}_1^{(2)}(1,2)+\zeta(\mathbf{R}_2)\mathfrak{A}_2^{(1)}[\bar{f}_1^{(2)}(1,2)]\\ +J_1[\bar{f}_1^{(2)}(1,2)]+J_1[\bar{f}_1^{(2)}(1,3)]+J_1[\bar{f}_1^{(2)}(2,3)]\\ +J_1[\bar{f}_1^{(1)}(1)]+J_1[\bar{f}_1^{(1)}(2)]+J_1[\bar{f}_1^{(1)}(3)]\\ +J_{20},\end{aligned} \tag{45}$$

where

$$\mathfrak{A}_j^{(1)}[\bar{f}_1^{(2)}(1,2)]=\nabla_{pj}\cdot[((\mathbf{p}_j/m)-\mathbf{u}(\mathbf{R}_j))\bar{f}_1^{(2)}(1,2)+kT(\mathbf{R}_j)\bar{f}_1^{(2)}(1,2)] \tag{46}$$

$$J_1(\bar{f}_1^{(2)}(1,2))=\iint\left\{\frac{\bar{f}_1^{(2)}(1,2)^*\bar{f}_0^{(2)}(1,3)^*f_0^{(2)}(2,3)^*}{\bar{f}_0^{(1)}(1)^*\bar{f}_0^{(1)}(2)^*\bar{f}_0^{(1)}(3)^*}-\frac{\bar{f}_1^{(2)}(1,2)\bar{f}_0^{(2)}(1,3)\bar{f}_0^{(2)}(2,3)}{\bar{f}_0^{(1)}(1)\bar{f}_0^{(1)}(2)\bar{f}_0^{(1)}(3)}\right\}(p_{13}/\mu)bdbd\epsilon d^3p_3 \tag{47}$$

$$J_1(\bar{f}_1^{(1)}(1))=-\iint\left\{\frac{\bar{f}_0^{(2)}(1,2)^*\bar{f}_0^{(2)}(1,3)^*\bar{f}_0^{(2)}(2,3)^*\bar{f}_1^{(1)}(1)^*}{\bar{f}_0^{(1)}(1)^*\bar{f}_0^{(1)}(2)^*\bar{f}_0^{(1)}(3)^*}-\frac{\bar{f}_0^{(2)}(1,2)\bar{f}_0^{(2)}(1,3)\bar{f}_0^{(2)}(2,3)}{\bar{f}_0^{(1)}(1)\bar{f}_0^{(1)}(2)\bar{f}_0^{(1)}(3)}\frac{\bar{f}_1^{(1)}(1)}{\bar{f}_0^{(1)}(1)}\right\}$$

$$\times(p_{13}/\mu)bdbd\epsilon d^3p_3 \tag{48}$$

$$J_{20}=\sigma g^{(2)}(\mathbf{R}_1,\sigma)\iint\left\{\frac{\bar{f}_0^{(2)}(1,2)^*\bar{f}_0^{(2)}(2,3)^*\mathbf{k}\cdot\nabla_{R_1}\bar{f}_0^{(1)}(\mathbf{R}_1,\mathbf{p}_3-\Delta\mathbf{p}_3;t)}{\bar{f}_0^{(1)}(2)^*\bar{f}_0^{(1)}(3)^*}-\frac{\bar{f}_0^{(2)}(1,2)\bar{f}_0^{(2)}(2,3)\mathbf{k}\cdot\nabla_{R_1}\bar{f}_0^{(1)}(\mathbf{R}_1\mathbf{p}_3;t)}{\bar{f}_0^{(1)}(2)\bar{f}_0^{(1)}(3)}\right\}$$

$$\times(p_{13}/\mu)bdbd\epsilon d^3p_3. \tag{49}$$

The left-hand side of Eq. (45) can be evaluated using the distribution function of Eq. (44) and the equations of change for n_2, $\mathbf{u}$, T and the number density of molecules, n. The equation of change for n_2 is

$$\partial n_1/\partial t=-[\nabla_{R_1}\cdot\mathbf{j}_1+\nabla_{R_2}\cdot\mathbf{j}_2], \tag{50}$$

where

$$\mathbf{j}_i=\int(\mathbf{p}_i/m)\bar{f}^{(2)}d\mathbf{p}_1d\mathbf{p}_2. \tag{51}$$

Utilizing the fact that n_2 is a collision invariant so that we can take $n_2^{(0)}=n_2$, $n_2^{(l)}=0$ $(l>0)$, it is found that Eq. (50) becomes

$$\partial n_2/\partial t=-\{\nabla_{R_1}\cdot[n_2\mathbf{u}(\mathbf{R}_1)]+\nabla_{R_2}\cdot[n_2\mathbf{u}(\mathbf{R}_2)]\}. \tag{52}$$

The remaining equations of change are

$$\partial n(\mathbf{R}_i)/\partial t+\nabla_{R_i}\cdot[\mathbf{u}(\mathbf{R}_i)n(\mathbf{R}_i)]=0 \tag{53}$$

$$(\partial\mathbf{u}/\partial t)(\mathbf{R}_i)+\mathbf{u}(\mathbf{R}_i)\cdot\nabla_{R_i}\mathbf{u}(\mathbf{R}_i)+\rho^{-1}\nabla_{R_i}p-(\mathbf{F}_i^*/m)(\mathbf{R}_i)=0 \tag{54}$$

$$\partial T(\mathbf{R}_i)/\partial t+\mathbf{u}(\mathbf{R}_i)\cdot\nabla_{R_i}T(\mathbf{R}_i)+(Tv/c_v)(\partial p/\partial T)_\rho\nabla_{R_i}\cdot\mathbf{u}(\mathbf{R}_i)=0, \tag{55}$$

where v is the volume per molecule, ρ is the mass density, and p the hydrostatic pressure. The quantity $\mathbf{F}_1^*$ is given by

$$\mathbf{F}_1^*(\mathbf{R}_i)={}^{(1)}\langle\mathbf{F}_1^{(s)}\rangle^0+{}^{(1)}\mathbf{F}_1^+, \tag{56}$$

where, as before, ${}^{(1)}\langle\mathbf{F}_1^{(s)}\rangle^0$ is the average total intermolecular attractive force on a molecule at $\mathbf{R}_1$, when the average is performed in a canonical ensemble over all other molecules, and ${}^{(1)}\mathbf{F}_1^+$ is a perturbation arising from the departure of $f^{(2/N-2)}$ from its equilibrium value. Using the relation

$$n_2(\mathbf{R}_1\mathbf{R}_2)=n(\mathbf{R}_1)n(\mathbf{R}_2)g(\mathbf{R}_1\mathbf{R}_2) \tag{57}$$

the additional constraint

$$\nabla_{R_j}\cdot\mathbf{d}=0 \tag{58}$$

and Eqs. (52) to (55), it is found that

$$\begin{aligned}D_2\bar{f}_0^{(2)}(1,2)=\bar{f}_0^{(2)}(1,2)\Bigg[\sum_{j=1}^{2}\Big\{2\mathbf{b}_j+[(v/C_v)(\partial p/\partial T)_\rho-\tfrac{2}{3}](\tfrac{3}{2}-W_j^2)\mathbf{1}\Big\}:\nabla_{R_j}\mathbf{u}(R_j)\\ -(\tfrac{3}{2}+\alpha T-W_j^2)[(\mathbf{p}_j/m)-\mathbf{u}(\mathbf{R}_j)]\cdot\nabla_{R_j}\ln T(\mathbf{R}_j)\\ -[(\mathbf{p}_j/m)-\mathbf{u}(\mathbf{R}_j)]\cdot({}^{(2)}\mathbf{G}_j-kT(\mathbf{R}_j)\nabla_{R_j}\ln g)\frac{1}{kT(R_j)}\Bigg],\end{aligned} \tag{59}$$

where

$${}^{(2)}\mathbf{G}_j=\mathbf{F}_j^{(2)}-\mathbf{F}_j^*(R_j) \tag{60}$$

and $\mathbf{W}_j$ is a reduced peculiar velocity defined by

$$\mathbf{W}_j=(m/2kT)^{\frac{1}{2}}[(\mathbf{p}_j/m)-\mathbf{u}(\mathbf{R}_j)]. \tag{61}$$

The tensor $\mathbf{b}_j$ is a traceless dyadic defined by

$$\mathbf{b}_j=[\mathbf{W}_j\mathbf{W}_j-\tfrac{1}{3}W_j^2\mathbf{1}], \tag{62}$$

and α is the coefficient of thermal expansion.

To obtain the perturbation solution of Eq. (45) we now write

$$\bar{f}_1^{(2)}(i,j)=\bar{f}_0^{(2)}(i,j)\Phi(i,j) \tag{63}$$

$$\bar{f}_1^{(1)}(i)=\bar{f}_0^{(1)}(i)\Phi_i \tag{64}$$

$$\bar{f}_0^{(1)}(i)=\frac{(2\pi mkT)^{-\frac{3}{2}}}{v}\exp[-(p_i-m\mathbf{u})^2/2mkT]. \tag{65}$$

It is consistent with our previous analysis of the singlet equation to assume that we may approximate $g^{(2)}$ by the local equilibrium pair correlation function in evaluating the collision terms J_1 and J_2 of Eq. (45). We may therefore write

$$\frac{\bar{f}_0^{(2)}(1,3)\bar{f}_0^{(2)}(2,3)}{\bar{f}_0^{(1)}(1)\bar{f}_0^{(1)}(2)\bar{f}_0^{(1)}(3)}\bar{f}_0^{(2)}(1,2)=g_0^{(2)}(\mathbf{R}_1\mathbf{R}_3)g_0^{(2)}(\mathbf{R}_2\mathbf{R}_3)g_0^{(2)}(\mathbf{R}_1\mathbf{R}_2)\bar{f}_0^{(1)}(1)\bar{f}_0^{(1)}(2)\bar{f}_0^{(1)}(3_1), \tag{66}$$

where on the right-hand side of Eq. (66) we define

$$\bar{f}_0^{(1)}(3_1)\equiv\bar{f}_0^{(1)}(\mathbf{R}_1\mathbf{p}_3;t),$$

and on the left-hand side

$$\bar{f}_0^{(1)}(3)\equiv\bar{f}_0^{(1)}(\mathbf{R}_3\mathbf{p}_3;t). \tag{67}$$

For the collision between molecules 1 and 3 we have

$$\bar{f}_0^{(1)}(1)^*\bar{f}_0^{(1)}(3_1)^* = \bar{f}_0^{(1)}(1)\bar{f}_0^{(1)}(3_1) \tag{68}$$

$$\bar{f}_0^{(1)}(2) = \bar{f}_0^{(1)}(2). \tag{69}$$

From Eqs. (45) to (49), (59), and (63) to (69) the following integral equation is readily found,

$$\bar{f}_0^{(1)}(1)\Big[\sum_{j=1}^{2}\Big\{2\mathbf{b}_j+[(v/C_v)(\partial p/\partial T)_\rho-\tfrac{2}{3}](\tfrac{3}{2}-W_j^2)\mathbf{1}\Big\}:\nabla_{R_j}\mathbf{u}(\mathbf{R}_j)-(\tfrac{3}{2}+\alpha T-W_j^2)[(\mathbf{p}_j/m)-\mathbf{u}(\mathbf{R}_j)]\cdot\nabla_{R_j}\ln T(R_j)$$

$$-[(\mathbf{p}_j/m)-\mathbf{u}(\mathbf{R}_j)]\cdot[{}^{(2)}\mathbf{G}_j-kT(\mathbf{R}_j)\nabla_{R_j}\ln g]\frac{1}{kT(R_j)}$$

$$=g_0^{(2)}(\mathbf{R}_1,\sigma)g_0(\mathbf{R}_2,\mathbf{R}_3)\iint\bar{f}_0^{(1)}(1)\bar{f}_0^{(1)}(3_1)\{[\Phi(1,2)^*+\Phi(1,3)^*$$

$$+\Phi(2,3)^*-\Phi(1,2)-\Phi(1,3)-\Phi(2,3)]-(\Phi_1{}^*+\Phi_2{}^*+\Phi_3{}^*-\Phi_1-\Phi_2-\Phi_3)\}(p_{13}/\mu)bdbd\epsilon d^3p_3$$

$$+\sum_{j=1}^{2}\zeta(\mathbf{R}_j)kT(\mathbf{R}_j)\nabla_{r_j}\cdot[\bar{f}_0^{(1)}(1)\nabla_{p_j}\Phi(1,2)]$$

$$+g_0^{(2)}(\mathbf{R}_1,\sigma)g_0^{(2)}(\mathbf{R}_2,\mathbf{R}_3)\iint[\bar{f}_0^{(1)}(1)^*\sigma\mathbf{k}\cdot\nabla_{R_1}\bar{f}^{(1)}(3)^*+\bar{f}_0^{(1)}(1)\sigma\mathbf{k}\cdot\nabla_{R_1}\bar{f}^{(2)}(3)](p_{13}/\mu)bdbd\epsilon d^3p_3\Big]. \tag{70}$$

The last integral of this equation is evaluated in the paper by Rice.[4]

To solve the integral equation we take the perturbation functions in the form:

$$\Phi(1,3) = -(\mathbf{A}_1+\mathbf{A}_3)\cdot\nabla_{R_1}\ln T(\mathbf{R}_1)-(\mathbf{B}_1+\mathbf{B}_3):\nabla_{R_1}\mathbf{u}(\mathbf{R}_1)$$
$$-(\mathbf{C}_1+\mathbf{C}_3)\cdot{}^{(2)}\mathbf{G}_1{}^F \tag{71}$$

$$\Phi(2,3) = -\mathbf{A}_2\cdot\nabla_{R_2}\ln T(\mathbf{R}_2)-\mathbf{B}_2:\nabla_{R_2}\mathbf{u}(\mathbf{R}_2)-\mathbf{C}_2\cdot{}^{(2)}\mathbf{G}_2{}^F$$
$$-\mathbf{A}_3\cdot\nabla_{R_1}\ln T(\mathbf{R}_3)-\mathbf{B}_3:\nabla_{R_3}\mathbf{u}(\mathbf{R}_3)-\mathbf{C}_3\cdot{}^{(2)}\mathbf{G}_3{}^F \tag{72}$$

$${}^{(2)}\mathbf{G}_j{}^F = {}^2\mathbf{G}_j-kT(\mathbf{R}_j)\nabla_{R_j}\ln g(\mathbf{R}_1\mathbf{R}_2). \tag{73}$$

The perturbation to the singlet distribution function has been shown to be[2]

$$\Phi_j = -a_j{}^{(1)}(\tfrac{5}{2}-W_j^2)\mathbf{W}_j\cdot\nabla_{R_j}\ln T$$
$$-b_{0j}{}^{(1)}(\mathbf{W}_j\mathbf{W}_j-\tfrac{1}{3}W_j\mathbf{1}):\nabla_{R_j}\mathbf{u}, \tag{74}$$

where

$$a_j{}^{(1)} = -\left(\frac{2kT}{m}\right)^{\frac{1}{2}}\left\{\frac{v}{g(\mathbf{R}_j,\sigma)}+\frac{2\pi\sigma^3}{5}\right\}\frac{15}{4}\Big/\left\{4\Omega^{(2,2)}+\frac{45\zeta(\mathbf{R}_j)v}{4mg(\mathbf{R}_j,\sigma)}\right\}$$

$$b_{0j}{}^{(1)} = 5\left\{\frac{v}{g(\mathbf{R}_j,\sigma)}+\frac{4\pi\sigma^3}{15}\right\}\Big/\left\{4\Omega^{(2,2)}+\frac{5\zeta(\mathbf{R}_j)v}{mg(\mathbf{R}_j,\sigma)}\right\}, \tag{75}$$

and $\Omega^{(2,2)}$ is a reduced collisional cross section.

Substitution of Eqs. (64) to (67) in Eq. (63) gives three independent equations for **A**, **B**, and **C**. The equation for **A** is

$$\mathbf{K}_1/g(\mathbf{R}_1\mathbf{R}_2) = \iint\bar{f}_0^{(1)}(1)\bar{f}_0^{(1)}(3_1)[2(\mathbf{A}_1{}^*+\mathbf{A}_3{}^*-\mathbf{A}_1-\mathbf{A}_3)$$

$$-a_1{}^{(1)}\{(\tfrac{5}{2}-W_3{}^{*2})\mathbf{W}_3{}^*+(\tfrac{5}{2}-W_1{}^{*2})\mathbf{W}_1{}^*-(\tfrac{5}{2}-W_3^2)\mathbf{W}_3-(\tfrac{5}{2}-W_1^2)\mathbf{W}_1\}](p_{13}/\mu)bdbd\epsilon d^3p_3$$

$$+\frac{\zeta(\mathbf{R}_1)kT(\mathbf{R}_1)}{g_0^{(2)}(\mathbf{R}_1\mathbf{R}_2)g_0^{(2)}(\mathbf{R}_1,\sigma)}\nabla_{p_1}\cdot[\bar{f}_0^{(1)}(1)\nabla_{p_1}\mathbf{A}_1], \tag{76}$$

where

$$\mathbf{K}_1=\frac{\bar{f}_0^{(1)}(1)}{g(\mathbf{R}_1,\sigma)}\left(\frac{2kT(\mathbf{R}_1)}{m}\right)[\tfrac{3}{2}+\alpha T(\mathbf{R}_1)-W_1^2]\mathbf{W}_1+\bar{f}_0^{(1)}(1)\frac{\pi\sigma^2}{15v}\left(\frac{2kT(\mathbf{R}_1)}{m}\right)^{\frac{1}{2}}[5+20\alpha T-6W_1^2]\mathbf{W}_1. \tag{77}$$

This equation may be solved by the usual procedure of expanding $\mathbf{A}$ in Sonine polynomials, retaining only the first nonvanishing term,

$$\mathbf{A}=\mathbf{W}\{\sum_{m=0}^{\infty}\mathfrak{A}^{(m)}S_{\frac{1}{2}}^{(m)}(W^2)\}$$

$$=\mathbf{W}\mathfrak{A}^{(1)}(\tfrac{5}{2}-W^2). \tag{78}$$

By substituting in Eq. (76), multiplying by $\mathbf{W}_1\cdot S_{\frac{1}{2}}^{(1)}(W_1^2)$ and integrating over d^3p_1 the constant $\mathfrak{A}^{(1)}$ can be evaluated. The integrals are the same as those in the singlet case. The result is

$$\mathfrak{A}_1^{(1)}=\frac{-\left(\frac{2kT(\mathbf{R}_1)}{m}\right)^{\frac{1}{2}}\left\{\frac{v}{g(\mathbf{R}_1,\sigma)}+\frac{2\pi\sigma^3}{5}\right\}(15/4)}{g(\mathbf{R}_1,\mathbf{R}_2)\left\{8\Omega^{(2,2)}+\frac{45\zeta(\mathbf{R}_1)v}{4mg(\mathbf{R}_1,\mathbf{R}_2)g(\mathbf{R}_1,\sigma)}\right\}\left\{\frac{1+4\Omega^{(2,2)}g(\mathbf{R}_1,\mathbf{R}_2)}{\left[4\Omega^{(2,2)}+\frac{45\zeta(\mathbf{R}_1)v}{4mg(\mathbf{R}_1,\sigma)}\right]}\right\}}. \tag{79}$$

The corresponding integral equation for $\mathbf{B}$ can be set up and again solved using the same procedure as in the treatment of the analogous equation for the singlet distribution function, the integrals being the same in the two equations. The result is

$$B_1=B_{01}^{(1)}[\mathbf{W}_1\mathbf{W}_1-\tfrac{1}{3}W_1^2\mathbf{1}] \tag{80}$$

$$B_{01}^{(1)}=\frac{5v\left\{\frac{1}{g(\mathbf{R}_1,\sigma)}+\frac{4\pi\sigma^3}{15v}\right\}\left\{1+\frac{4\Omega^{(2,2)}g(\mathbf{R}_1,\mathbf{R}_2)}{4\Omega^{(2,2)}+[5\zeta(R_1)v/mg(\mathbf{R}_1,\sigma)]}\right\}}{g(\mathbf{R}_1,\mathbf{R}_2)\left\{8\Omega^{(2,2)}+\frac{5\zeta(R_1)v}{mg(\mathbf{R}_1,\sigma)g(\mathbf{R}_1,\mathbf{R}_2)}\right\}}. \tag{81}$$

The equation for $\mathbf{c}$ is

$$[(\mathbf{p}_1/m)-\mathbf{u}(\mathbf{R}_1)]\frac{\bar{f}_0^{(1)}(1)}{kT(\mathbf{R}_1)g(\mathbf{R}_1,\sigma)g(\mathbf{R}_1,\mathbf{R}_2)}=2\iint\bar{f}_0^{(1)}(1)\bar{f}_0^{(1)}(3_1)[\mathbf{c}_1^*+\mathbf{c}_3^*-\mathbf{c}_1-\mathbf{c}_3](\mathbf{p}_{13}/\mu)bdbd\epsilon d^3p_3$$

$$+\frac{\zeta(\mathbf{R}_1)kT(\mathbf{R}_1)}{g(\mathbf{R}_1,\sigma)g(\mathbf{R}_1,\mathbf{R}_2)}\nabla_{p1}\cdot[\bar{f}_0^{(1)}(1)\nabla_{p1}\mathbf{c}_1]. \tag{82}$$

Making the substitution

$$\mathbf{c}=c\mathbf{W}, \tag{83}$$

multiplying by $\mathbf{W}_1$ and integrating over d^3p_1 it is easily found that

$$\mathbf{c}_1=-\mathbf{W}_1(2m/kT(\mathbf{R}_1))^{\frac{1}{2}}[1/\zeta(\mathbf{R}_1)]. \tag{84}$$

Note that the final expression for the distribution function

$$\bar{f}_1^{(2)}(1,2)=\bar{f}_0^{(2)}(1,2)\{\sum_{j=1}^{2}(-\mathfrak{A}_j^{(1)}(\tfrac{5}{2}-W_j^2)\mathbf{W}_j\cdot\nabla_{R_j}\ln T(R_j)-B_{0j}^{(1)}(\mathbf{W}_j\mathbf{W}_j-\tfrac{1}{3}W_j^2\mathbf{1}):\nabla_{R_j}\mathbf{u}(\mathbf{R}_j)-c_j\mathbf{W}_j\cdot^{(2)}\mathbf{G}_j^F, \tag{85}$$

reduces in the limit of the pure Fokker-Planck equation to that recently derived by Lebowitz, Frisch, and Helfand.[6]

IV. DISCUSSION

We have presented in this paper an analysis of the pair distribution function for a model dense fluid. As in the case of the singlet distribution function, our approach has been guided by intuitive arguments at several points, and detailed mathematical verification has yet to be given. Nevertheless, we believe that the model suggested and the method used will prove to be of considerable interest.

The nonequilibrium pair distribution function computed in this paper contains a perturbation not found in the singlet distribution function. This term, which arises from the deviation from equilibrium of the three-body relative probability density $f^{(3/N-3)}$, enters the integro-differential equation linearly. For this reason, it may be separated from the more ordinary gradient terms, even though an ultimate analysis of $f^{(3/N-2)}$ and $\nabla \ln g^{(2)}$ would probably yield dependence upon ∇T and $\nabla \mathbf{u}$. The distribution function may therefore be considered to be parametric in the friction constant and ${}^{(2)}\mathbf{G}_j{}^F$. The completion of the molecular calculation awaits the evaluation of these quantities.

The major obstacle standing in the path of completion of the projected program is the difficulty of describing the autocorrelation function for momentum. We anticipate that the deviation from equilibrium of the pair correlation function and the three-body relative probability density can be handled with techniques introduced by Kirkwood.[7] However, calculation of the momentum autocorrelation function appears to require a more detailed study of molecular dynamics than we have been able to make. In particular, the negative correlations would appear to be of great importance[8] and we have as yet not succeeded in inventing a reliable method of computing these. With the distribution function presented herein we can test internal consistency by examining the thermal conductivity in terms of the frictional constant obtained from viscosity, etc. Such a parametric representation of experimental data would still, in our opinion, represent a valuable addition to our meager understanding of the molecular basis of transport in dense fluids.

ACKNOWLEDGMENTS

We wish to thank the Alfred P. Sloan Foundation and the Petroleum Research Fund of the American Chemical Society for financial support.

[7] See for example, R. W. Zwanzig, J. G. Kirkwood, I. Oppenheim, and B. J. Alder, J. Chem. Phys. **22**, 783 (1954).
[8] S. A. Rice, J. Chem. Phys. (to be published).

THE JOURNAL OF CHEMICAL PHYSICS VOLUME 34, NUMBER 6 JUNE, 1961

Distortable Double Well. A Prototype for the Analysis of Relaxation Spectra*

R. FUCHS AND A. VON HIPPEL

Laboratory for Insulation Research, Massachusetts Institute of Technology, Cambridge 39, Massachusetts

(Received November 8, 1960)

The origin of dielectric relaxation spectra is frequently not the rotation of dipoles as visualized in the Debye and Onsager models but the reversible transfer of ions or electrons between equilibrium sites. The displacement of such charge carriers corresponds to a reversal of dipole moments and had been treated previously as a shifting of charges between fixed equal or unequal double wells. The reversal of dipole moments in condensed phases, however, frequently has decisive after effects: The electrical unbalance created leads to a compensating action of the surroundings, lowering the free energy and tending to freeze in the charge in the occupied well site. Thus the double well becomes unequal because of the reaction of the embedding medium. This model of a distortable double well is here treated, first in its stationary state with and without superposed dc field and then in its ac response, under the simplifying assumption that the surroundings react by an exponentially decaying distortion described by a time constant and final well depth. The characteristics of the model are that it incorporates the equal and unequal fixed double well as special cases but in addition shows an inherent distribution of relaxation times and—for long observation periods—an anomalously large polarizability, since eventually the wells can be turned with their deepened sites in the favorable field direction.

INTERPRETATIONS OF ELECTRIC RELAXATION PHENOMENA

THE relaxation spectra of electric polarization in condensed phases are normally attributed to one of two causes: orientation of dipoles by rotation (as visualized in the pioneering models of Debye[1] and of Onsager[2]) or field distortion resulting from the piling up of charge carriers (a process first exemplified by the Maxwell-Wagner two-layer capacitor[3]). The transient

* Sponsored by the U. S. Office of Naval Research, the Army Signal Corps, and the Air Force.

[1] P. Debye, *Polar Molecules* (Chemical Catalog Company, Inc., New York, 1929).
[2] L. Onsager, J. Am. Chem. Soc. **58**, 1486 (1936).
[3] K. W. Wagner, Arch. Elektrotech. **2**, 371 (1914).

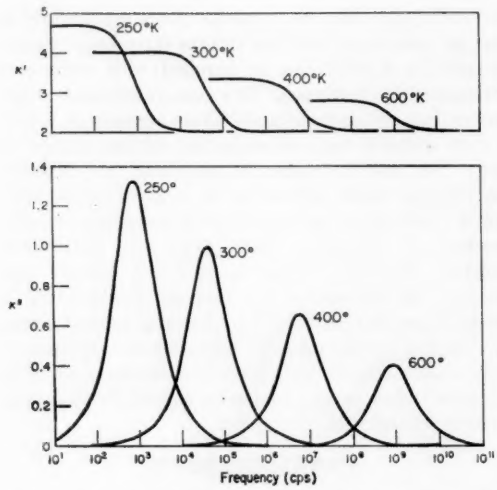

FIG. 1. Typical Debye relaxation spectrum as function of frequency and temperature.

buildup or decay of such polarization phenomena caused by orientation of space-charge formation is characterized by a time constant τ or a distribution of such time constants. The interrelation of dielectric constant κ' and loss factor κ'' in the frequency domain can often be represented by the circular arc locus of a Cole-Cole diagram.[4]

In the Debye as well as in the Onsager treatment of orientation polarization the electric dipole is visualized as immersed in a dielectric continuum; the decisive difference of the models concerns the electric field acting on the polar molecule. While in gases at normal pressures the acting field strength $\mathbf{E}'$ may be approximated by the applied field $\mathbf{E}$, for liquids Debye used the Mosotti (or Lorentz) field

$$\mathbf{E}'=\mathbf{E}+(\mathbf{P}/3\epsilon_0), \qquad (1)$$

which prevails in the center of a spherical virtual cavity when the dielectric assumes the polarization $\mathbf{P}$ in the homogeneous field $\mathbf{E}$. Obviously, Eq. (1) introduces a feedback action between field and polarization. If the field has only to overcome the randomizing action of thermal agitation, as assumed in the derivation of the Langevin function,[5] a spontaneous alignment of the dipole molecules must occur at a critical temperature, as prescribed by the Curie-Weiss law.[6] Hence, ferroelectricity is predicted for all polar materials. Onsager realized that this catastrophic result must be produced by a conceptual mistake: The reference point in the center of the cavity is not a mathematical abstraction but a dipole molecule, located in a real cavity, that in turn polarizes the dielectric and thus causes a reaction field from the surroundings. This field, oriented parallel to the dipole, cannot contribute to the torque on the polar molecule but may increase the dipole moment by induction. The feedback action postulated in Eq. (1) disappears in Onsager's calculation and with it the chance for spontaneous polarization.

Offhand this outcome is also not satisfactory, since ferroelectrics do exist. However, a closer scrutiny of the polarization of crystals, where spontaneous alignment occurs, shows that the whole concept of preformed polar molecules responding by rotation does not normally apply to crystal lattices. Electric dipole moments are integral construction elements of polar crystals. There are cases where individual dipole molecules are clearly discernible and sufficiently small and spherical to retain at higher temperatures some chance for hindered rotation. In general, however, these molecules have been dissolved into an array of polar lattice points. Thus their freedom of rotation has been lost and replaced by the vibration modes of the coupled lattice structure. A concerted displacement of the ions, stemming from these vibratory modes, can cause electric unbalance and thus oriented dipole arrays.[7]

The fact that electric dipoles can invert their moment by flip-flop vibrations across the barrier of a double well is well known from the example of the ammonia molecule or the orientation of hydrogen bonds. In fact, Slater[8] was first to explain a case of ferroelectricity, the behavior of KH_2PO_4, by the ordering of hydrogen bonds. Furthermore, equal or unequal double wells have been invoked in all kinds of rate processes,[9] including dielectric polarization.[10] Mathematically, the transition from dipole rotation to flip-flop vibration can be made by simply admitting only parallel and antiparallel orientations instead of all angles relative to the field direction. The physical difference between the two processes, however, is profound: Rotation requires excess space, vibration does not. In consequence, we expect and find for example that the relaxation spectra of rotation in liquid dielectrics are very pressure sensitive and move to lower frequencies as the voids are being squeezed out, while those of flip-flop vibrations prove relatively insensitive to compression.[11]

The case of equal vs unequal double wells becomes of great importance for relaxation spectra when one considers the temperature dependence of the phenomenon. Temperature increase in the case of dipole rota-

[4] K. S. Cole and R. H. Cole, J. Chem. Phys. **9**, 341 (1941).
[5] P. Langevin, J. phys. radium **4**, 678 (1905).
[6] P. Weiss, J. phys. radium **6**, 667 (1907).
[7] A. von Hippel, *Dielectrics and Waves* (John Wiley & Sons, Inc., New York, 1954), pp. 202–213.
[8] J. C. Slater, J. Chem. Phys. **9**, 16 (1941).
[9] S. Glasstone, K. J. Laidler, and H. Eyring, *The Theory of Rate Processes* (McGraw-Hill Book Company, New York, 1941).
[10] Cf. H. Fröhlich, *Theory of Dielectrics* (Clarendon Press, Oxford, 1949); C. J. F. Böttcher, *Theory of Electric Polarization* (Elsevier Publishing Company, New York, 1952).
[11] A. von Hippel, *Molecular Science and Molecular Engineering* (The Technology Press, Cambridge, Massachusetts, and John Wiley and Sons, New York, 1959), pp. 256 and 257.

tion or inversion between equal double wells produces two effects: it reduces the relaxation time causing the spectrum to move to shorter wavelengths and it increases the randomizing action of the thermal agitation relative to the ordering action of the electric field, resulting in a decrease of polarization (Fig. 1). For unequal wells a third effect appears: with decreasing temperature the relative occupation density of the lower well increases; i.e., the number of participating dipoles diminishes until finally all are frozen into the lower well and the spectrum disappears. This freezing out of relaxation spectra has been observed experimentally in a variety of cases. Typical examples, of different origin, are a hydrogen-bond spectrum in crystalline picric acid, observed by Meakins[12] (Fig. 2), and a dipolar spectrum caused by the motion of Ba^{2+} ions in the tunnel structure of a $Ba(Ti_7Mg)O_{16}$ compound[13] (Fig. 3).

In many of these cases it is not clear *a priori* why the model of an unequal double well should apply, since the two positions of choice have structurally identical surroundings. Obviously, the inequality in such situations must arise because one well site is occupied while the other is empty, and because the surroundings can react to this configuration by a compensating distortion and charge-carrier motion. In analogy to the ionic atmosphere forming around ions in electrolytes (Debye-Hückel theory,[14] Wien effect[15]) or the polarization halo forming around electrons and holes in crystals[16] (the polaron[17]), we have to visualize a dipole halo around the dipolar group, which deepens the occupied well site and, at sufficiently low temperature, immobilizes the dipole moment by self-trapping.[18]

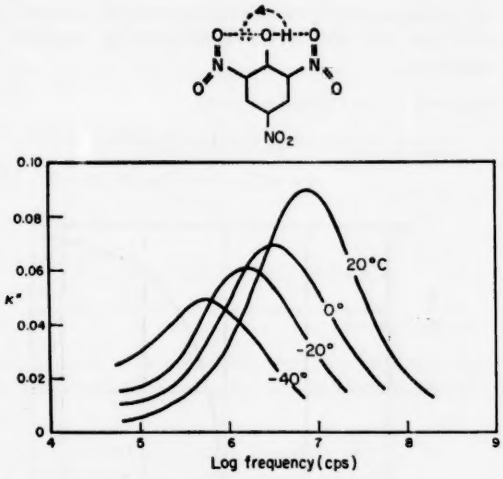

FIG. 2. Hydrogen-bond spectrum in crystalline picric acid (see work cited in reference 12).

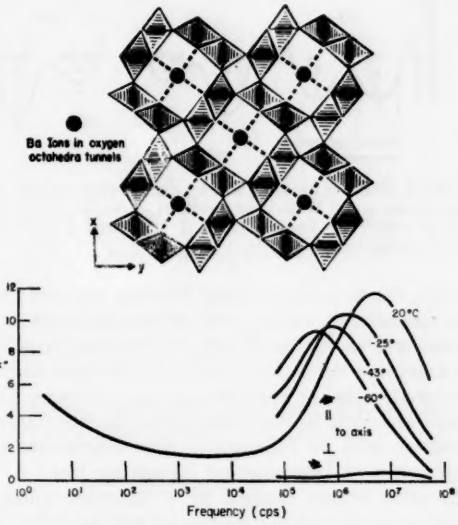

FIG. 3. Dipolar spectra in $Ba(Ti_7Mg)O_{16}$ compound (see work cited in reference 13.)

If this process is of importance and the model of a double well applies, the fixed double well has to be replaced by a distortable double well, a prototype with several unusual features: the embedding medium can still be visualized as a continuum but its response may now be specified in detail by characteristic parameters, a distribution of relaxation times appears as an inherent property, and feedback coupling can be introduced possibly leading to a better model for ferroelectrics. In the present first treatment we make the simple assumption that the deformation is describable as an exponential decay process and therefore by a relaxation time of the distorting surroundings and a final well depth.

STATIONARY STATE OF A DISTORTABLE DOUBLE-WELL SYSTEM

Given a system of equal double wells dispersed in a dielectric medium, uncoupled but with their axes aligned in the x direction. Each is occupied by one particle of the same charge in random distribution. Indices 1 and 2 designate the left and the right well site, respectively; when the particles jumps from site 1 to site 2, the dipole moment of that double well inverts from the $-x$ to the $+x$ direction, and vice versa. Initially all wells shall be clamped in a state of equal

[12] R. J. Meakins, Trans. Faraday Soc. **51**, 371 (1955).
[13] J. S. Dryden and A. D. Wadsley, Trans. Faraday Soc. **54**, 1574 (1958).
[14] P. Debye and E. Hückel, Physik. Z. **24**, 185 (1923).
[15] M. Wien, Ann. Physik [4] **83**, 327 (1927).
[16] A. von Hippel, J. Chem. Phys. **8**, 605 (1940).
[17] S. I. Pekar, *Untersuchungen über die Elektronentheorie der Kristalle* (Akademische Verlagsgesellschaft, Leipzig, Germany, 1954).
[18] A. von Hippel and W. B. Westphal, Tech. Rept. 145, Lab. Ins. Research, M.I.T., December, 1959.

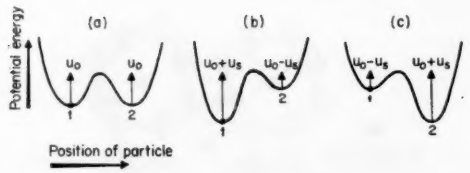

FIG. 4. Shape of a double well for certain values of the distortion energy u. (a) Wells have equal depth ($u=0$); (b) occupied site is completely lowered ($u=u_s$); (c) occupied site is completely raised ($u=-u_s$).

depth; the activation energy between the two sites is u_0, measured in units of kT. When the wells are released and allowed to distort, the occupied sites begin to lower and the empty sites to rise by equal amounts; simultaneously the particles can jump between sites 1 and 2 according to Boltzmann statistics. The distortion proceeds with an exponential time dependence characterized by a time constant (relaxation time) τ_s. The activation energy changes by a distortion energy u, counted positive when the occupied well site is deepened. The maximum amount of distortion energy $\pm u_s$ and the exponential law of distortion with its time constant τ_s characterize the response of the surrounding medium. We want to determine the distribution of well depths and with it that of the particles as a function of u for the stationary state (Fig. 4).

If N designates the total number of double wells of the system and $n_1(u)$ and $n_2(u)$ the respective occupied well sites lying in a distortion range between u and $u+du$,

$$N=\int_{-u_s}^{+u_s}[n_1(u)+n_2(u)]du. \tag{2}$$

The number of occupied well sites 1 can change by three processes: emptying jumps from sites 1 to 2 with a frequency ν_1, filling jumps from sites 2 to 1 with a frequency ν_2, and drift of occupied wells by increasing distortion into the range at u and out of the range at $u+du$. In the stationary state the over-all change must be zero; hence,

$$\frac{dn_1(u)}{dt}du=-n_1(u)\nu_1du+n_2(-u)\nu_2du$$
$$+\left[n_1(u)\frac{du}{dt}\right]_u-\left[n_1(u)\frac{du}{dt}\right]_{u+du}=0. \tag{3}$$

The argument for n_2 is $(-u)$ in this balancing equation, because a lowering of well site 1 of a double well is coupled with a corresponding rise of well site 2. Since the well depth increases as

$$du/dt=-(u-u_s)/\tau_s, \tag{4}$$

the change in the number of occupied wells 1 through distortion becomes

$$\left(n_1\frac{du}{dt}\right)_u-\left(n_1\frac{du}{dt}\right)_{u+du}=-\frac{d}{du}\left(n_1\frac{du}{dt}\right)du$$
$$=\left(\frac{u-u_s}{\tau_s}\frac{dn_1}{du}+\frac{n_1}{\tau_s}\right)du. \tag{5}$$

Furthermore, if we assume the vibration frequency in the individual well to remain at the value ν_0 independent of the distortion, the jump frequencies are

$$\nu_1=\nu_0\exp-(u_0+u),$$
$$\nu_2=\nu_0\exp-(u_0-u). \tag{6}$$

Finally, by introducing the ratio of distortion to maximum distortion depth

$$v\equiv u/u_s \tag{7}$$

as a normalized variable and the ratio of relaxation time to maximum jump time

$$a\equiv\tau_s/\tau_0\exp(u_0+u_s) \tag{8}$$

as a normalized time parameter (where $\tau_0\equiv 1/\nu_0$), we can rewrite with the help of Eqs. (4) to (8) the equilibrium condition (Eq. 3):

$$\tau_s\dot{n}_1(v)=(v-1)[dn_1(v)/dv]+\{1-a\exp[-(v-1)u_s]\}$$
$$\times n_1(v)+a\exp[(v+1)u_s]n_2(-v)=0. \tag{9}$$

For the number of charge carriers $n_2(-v)$ in the right well site, raised to the energy interval $-v$ to $-v-dv$ by the distortion and communicating with the lowered left well site, we obtain the corresponding equilibrium equation

$$\tau_s\dot{n}_2(-v)=(v+1)[dn_2(-v)/dv]$$
$$+\{1-a\exp[(v+1)u_s]\}n_2(-v)$$
$$+a\exp[-(v-1)u_s]n_1(v)=0. \tag{10}$$

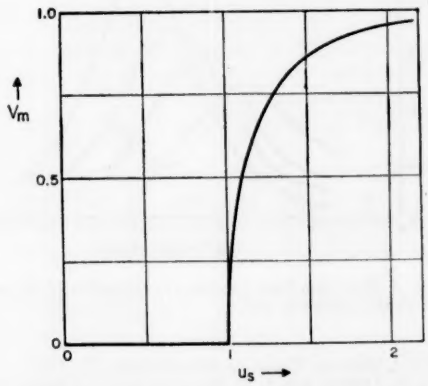

FIG. 5. The dependence of the most likely distortion energies $\pm v_m$ on the maximum distortion energy u_s.

By adding Eqs. (9) and (10) we arrive at the simple relation between $n_1(v)$ and $n_2(-v)$:

$$(d/dv)[(1-v)n_1(v)]=(d/dv)[(1+v)n_2(-v)] \quad (11)$$

or

$$(1-v)n_1(v)=(1+v)n_2(-v). \quad (12)$$

The constant of integration is zero since, without distortion (i.e., for $v=0$), $n_1(0)$ must equal $n_2(-0)$. Now $n_2(-v)$ can be eliminated from Eq. (9) by substitution from Eq. (12), and the final differential equation for $n_1(v)$ results,

$$\frac{dn_1}{n_1}=\left[\frac{1-a\exp[(1-v)u_s]}{1-v}+\frac{a\exp[(1+v)u_s]}{1+v}\right]dv. \quad (13)$$

Integrating from $v=0$ to $v=v'$, we obtain

$$\ln\left[\frac{n_1(v')}{n_1(0)}\right]=a\int_0^{v'}\frac{\exp[(1+v)u_s]}{1+v}dv - a\int_0^{v'}\frac{\exp[(1-v)u_s]}{1-v}dv-\Big[\ln(1-v)\Big]_{v=0}^{v=v'}. \quad (14)$$

The two integrals can be evaluated in terms of the tabulated function

$$Ei(x)\equiv\int_{-\infty}^{x}\frac{e^w}{w}dw. \quad (15)$$

The first, when we substitute $(1+v)u_s=w$, is

$$a\int_0^{v'}\frac{\exp[(1+v)u_s]}{1+v}dv=a\int_{u_s}^{u_s(1+v')}\frac{e^w}{w}dw =a\{Ei[u_s(1+v')]-Ei(u_s)\}, \quad (16)$$

and the second, with $(1-v)u_s=w$, correspondingly becomes

$$a\int_0^{v'}\frac{\exp[(1-v)u_s]}{1-v}dv=-a\{Ei[u_s(1-v')]-Ei(u_s)\}. \quad (17)$$

Hence from Eqs. (14) and (17)

$$\ln\left[\frac{(1-v')n_1(v')}{n_1(0)}\right]=a\{Ei[u_s(1+v')]+Ei[u_s(1-v')] -2Ei(u_s)\}; \quad (18)$$

or the number of occupied left well sites for some relative distortion depth v is in the field-free stationary state

$$n_1(v)=[n_1(0)/(1-v)]\exp a\{Ei[u_s(1+v)] +Ei[u_s(1-v)]-2Ei(u_s)\}. \quad (19)$$

The density $n_1(0)$ of particles at $v=0$ has to be adjusted so that the number of particles in well 1 is one-half the total number N,

$$\int_{-1}^{+1}n_1(v)dv=\tfrac{1}{2}N\equiv N_1. \quad (20)$$

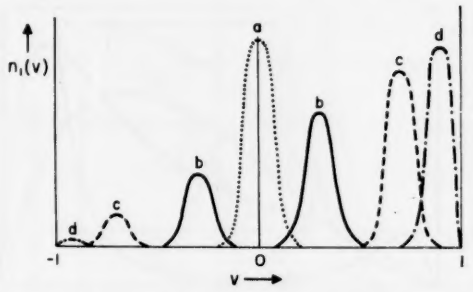

FIG. 6. The effect of a variation of u_s on the distribution $n_1(v)$, for a $\gg 1$. (a) $u_s<1(v_m=0)$; (b) $u_s=1.032(v_m=0.3)$; (c) $u_s=1.237(v_m=0.7)$; (d) $u_s=1.846(v_m=0.95)$.

The occupation densities for the left and right well sites are equal, as already implied in Eq. (6), i.e.,

$$n_1(v)=n_2(v). \quad (21)$$

Obviously, as Eq. (19) specifies, the distribution function $n_1(v)$ for the occupied well sites must depend explicitly on the response time of the embedding medium relative to the jump time represented by the factor of Eq. (8) and on the ratio of maximum distortion depth to kT, given by u_s.

Let us examine some typical situations:

1. The medium has little time to distort before a jump is likely, i.e., $a\gg 1$. In this case the occupied wells 1 will crowd with greatest probability around the distortion depths $v=\pm v_m$; in other words, $n_1(v)$ reaches maxima near the points $v=\pm v_m$ where the symmetric function $\{Ei[u_s(1+v)]+Ei[u_s(1-v)]-2Ei(u_s)\}$ [cf. Eq. (18)] has its two maxima. The equation connecting v_m with u_s is (Fig. 5)

$$u_s=(2v_m)^{-1}\ln[(1+v_m)/(1-v_m)]. \quad (22)$$

For $u_s\leq 1$ the maxima coalesce at the undistorted well position ($v=0$); for $u_s>1$ toward distortion depths $\gg kT$ the maxima move rapidly apart (Fig. 6), and the magnitude of the one at the right (representing the probability of finding the particle in the deepened well) becomes more and more dominant. Obviously, the return jumps from the flattened well site become increasingly likely; hence, its occupation density soon becomes negligible. Finally, as $u_s\to\infty$, $v_m\to\pm 1$, and the peak at $v_m=-1$ disappears; that is, all particles are trapped in the lower well site.

2. As the distortion time of the surroundings is made shorter and begins to approach the jump time (i.e., a moves from $\gg 1$ toward 1), $n_1(v)$ peaks less sharply and the trapping occurs less suddenly (Fig. 7), but the general phenomenon remains the same.

3. Finally, when the embedding medium distorts much faster than jumps are likely to occur ($a\ll 1$), the distribution function for the occupied well sites near

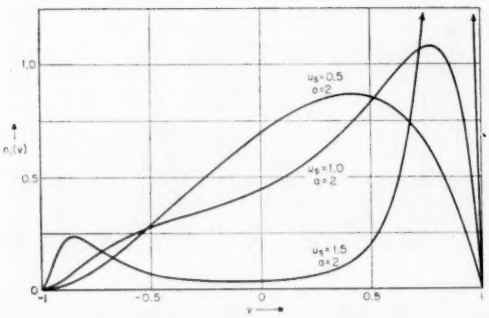

FIG. 7. The effect of a variation of u_s on the distribution $n_1(v)$, for $a=2$.

$v=1$ assumes the form

$$n_1(v)=1/(1-v)^{1-a}; \tag{23}$$

i.e., it approaches infinity at $v=1$. Practically all the particles are found in wells deepened to the maximum amount, as should be expected. Figure 8 indicates the transition to this situation.

STATIC SOLUTION WITH A dc FIELD APPLIED

A uniform dc field applied in the $+x$ direction raises the potential for well 1 by $\phi/2$ and lowers it for well 2 by the same amount; hence, the jump frequencies of Eq. (6) change to

$$\nu_1'=\nu_0\exp-(u_0+u-\phi/2)=\nu_1\exp(\phi/2);$$
$$\nu_2'=\nu_0\exp-(u_0+u+\phi/2)=\nu_2\exp(-\phi/2). \tag{24}$$

The equations determining the new time-independent distributions $n_1'(v)$ and $n_2'(v)$ are the same as the zero-field Eqs. (9) and (10), except for the additional factors $\exp(\phi/2)$ and $\exp(-\phi/2)$:

$$\tau_s\dot{n}_1'(v)=(v-1)\frac{dn_1'(v)}{dv}$$
$$+\{1-a\exp(\phi/2)\exp[-(v-1)u_s]\}n_1'(v)$$
$$+a\exp(-\phi/2)\exp[(v+1)u_s]n_2'(-v)=0; \tag{25}$$

$$\tau_s\dot{n}_2'(-v)=(v+1)\frac{dn_2'(-v)}{dv}$$
$$+\{1-a\exp(-\phi/2)\exp[(v+1)u_s]\}n_2'(-v)$$
$$+a\exp(\phi/2)\exp[-(v-1)u_s]n_1'(v)=0. \tag{26}$$

By adding Eqs. (25) and (26) we again obtain the relation [cf. Eq. (12)]

$$(1-v)n_1'(v)=(1+v)n_2'(-v), \tag{27}$$

which we use to eliminate $n_1'(-v)$. The final solution of these equations, replacing Eq. (19), is

$$n_1'(v)=[n_1'(0)/(1-v)]$$
$$\times\exp a(\exp(-\phi/2)\{Ei[u_s(1+v)]-Ei(u_s)\}$$
$$+\exp(\phi/2)\{Ei[u_s(1-v)]-Ei(u_s)\}). \tag{28}$$

If we keep only the first-order terms in ϕ, this becomes

$$n_1'(v)=n_1(v)(1-a(\phi/2)\{Ei[u_s(1+v)]$$
$$-Ei[u_s(1-v)]\}). \tag{29}$$

Equation (29) can be integrated numerically to find the total number of particles in well 1,

$$N_1'=\int_{-1}^{+1}n_1'(v)dv.$$

Approximate expressions for the change of the number of particles in well 1 from the zero-field number N_1 are

$$N_1'-N_1=-N_1(\phi/2)(1+av_m\{Ei[u_s(1+v_m)]$$
$$-Ei[u_s(1-v_m)]\}), \qquad a\gg1, \tag{30}$$

$$N_1'-N_1=-N_1(\phi/2)\{1+a[Ei(2u_s)-\gamma-\ln2u_s]\},$$
$$a\ll1, \tag{31}$$

where $\gamma=0.5772$.

Obviously we return to the case of equal double wells ($N_1'-N_1=-N_1\phi/2$) either when the distortion occurs very fast in comparison to the jump time ($a\to0$) or when the distortion energy vanishes ($u_s\to0$). For Eq. (30) in the latter case $v_m=0$ or $u_s<1$; for Eq. (31) the expression $Ei(2u_s)-\ln2\gamma u_s\to0$ as $u_s\to0$. On the other hand, when the distortion ($u_s\geq1$, $a>1$) comes into play, we obtain, with increasing static field, a rapid buildup of an anomalously large polarization since the combination of field and distortion tends to orient all the unequal double wells so that the dipoles point in the field direction. Differently expressed, if the dipole moment of the individual double well is $\mathbf{u}$, the dipole moment per unit volume, the polarization

$$\mathbf{P}=(N_2'-N_1')\mu, \tag{32}$$

approaches the saturation value

$$\mathbf{P}_s=N\mathbf{u} \tag{33}$$

under the helping influence of the distortion at relatively low field strength (Fig. 9).

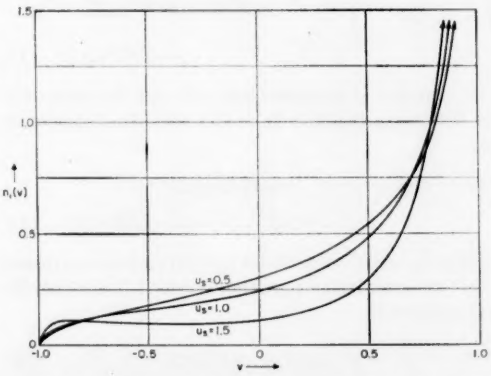

FIG. 8. The effect of a variation of u_s on the distribution $n_1(v)$, for $a=0.5$.

TIME-DEPENDENT POLARIZATION IN ac FIELDS

Returning to Eqs. (25) and (26), we introduce a time dependence of the well occupation by specifying that in an applied sinusoidal field of frequency ω the occupation for the relative well depth v changes from the field-free case $n_1(v)$ and $n_2(-v)$ to

$$n_1'(v)=n_1(v)-p_1(v)\exp(j\omega t);$$
$$n_2'(-v)=n_2(-v)+p_2(-v)\exp(j\omega t). \quad (34)$$

The field-dependent occupation densities $p_1(v)$ and $p_2(-v)$ are complex functions with phase factors ψ in reference to the time phase of the applied field; these phase factors will in general be a function of v, since wells of different distortion depths need not necessarily oscillate mutually in phase.

If we substitute the first time derivatives of Eq. (34) in the left sides of Eqs. (25) and (26) and assume that the potential energy $\phi/2$ introduced by the applied field is small enough to allow the expansion

$$\exp(\pm\phi/2)=1\pm(\phi/2), \quad (35)$$

we obtain

$$j\omega\tau_s p_1(v)=(v-1)[dp_1(v)/dv]+\{1-a\exp[-(v-1)u_s]\}p_1(v)-a\exp[(v+1)u_s]p_2(-v)+a(\phi/2)\{\exp[-(v-1)u_s]n_1(v)+\exp[(v+1)u_s]n_2(-v)\}, \quad (36)$$

and

$$j\omega\tau_s p_2(-v)=(v+1)[dp_2(-v)/dv]+\{1-a\exp[(v+1)u_s]\}p_2(-v)-a\exp[-(v-1)u_s]p_1(v)+a(\phi/2)\{\exp[-(v-1)u_s]n_1(v)+\exp[(v+1)u_s]n_2(-v)\}. \quad (37)$$

These equations can be solved for the case $a\gg1$, $\omega_s\gg1$; the distortion time is very much longer than the jump time as well as the oscillation time; hence, the distribution of well depths is not significantly altered from the zero-field situation. In this limit we can neglect the first two terms on the right side in Eqs. (36) and (37), because they contain neither a nor τ_s; now the right sides of the two equations become identical. Consequently $p_1(v)=p_2(-v)$ and, as in the field-free case, also $p_1(v)=p_2(v)$; in other words, $p_1(v)$ and $p_2(v)$ are symmetrical about $v=0$. Thus we arrive at the expression for $p_1(v)$, the population change in amplitude and phase caused by the ac field,

$$p_1(v)=\frac{n_1(v)\exp(-vu_s)+n_2(-v)\exp(vu_s)}{\exp(-vu_s)+\exp(vu_s)}\times[1+j\omega\tau(v)]^{-1}(\phi/2), \quad (38)$$

where $\tau(v)=(\tau_0e^{u_0})/(2\cosh vu_s)$. The relaxation time $\tau(v)$ characterizes the wells of distortion depth v.

The change in the total number of particles in the right well sites under the influence of the ac field is obtained by integrating $p_1(v)$ between $v=-1$ and $v=+1$ as

$$\Delta N_1=-\int_{-1}^{+1}p_1(v)dv=-\tfrac{1}{2}\phi\int_{-1}^{+1}\frac{2n_1(v)}{1+\exp(2vu_s)}\times[1+j\omega\tau(v)]^{-1}dv. \quad (39)$$

This integral must normally be integrated numerically, but for $a\to\infty$ an exact solution can be found, since $n_1(v)$ peaks sharply about the most probable well depth $\pm v_m$ and can be approximated by δ functions as

$$n_1(v)=(N_1/2)[(1+v_m)\delta(v-v_m)+(1-v_m)\delta(v+v_m)]. \quad (40)$$

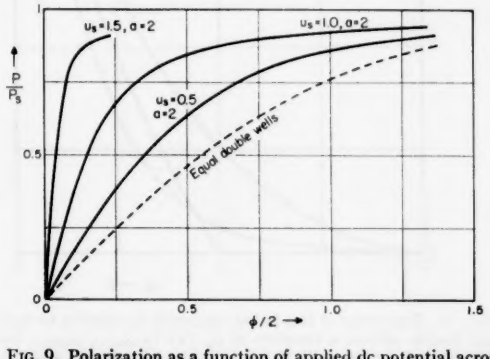

FIG. 9. Polarization as a function of applied dc potential across the half-well ($\phi/2$ expressed in units of kT).

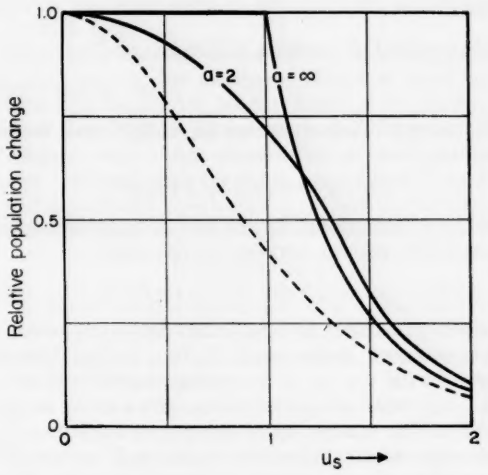

FIG. 10. Relative population change under ac field action as function of u_s, for $\omega\tau>1$. ---- $(\Delta N_1)_u/(\Delta N_1)_e$ for rigid unequal double well; —— $\Delta N_1/(\Delta N_1)_e$ for distortable double well.

Thus,

$$\Delta N_1 = -(\phi/2) N_1 (\cosh u_s v_m)^{-2} [1+j\omega\tau(v_m)]^{-1} \quad \text{for } a \to \infty. \quad (41)$$

The corresponding expression for a rigid equal double well is

$$(\Delta N_1)_e = -(\phi/2) N_1 (1+j\omega\tau_0)^{-1}, \quad (42)$$

and for a rigid unequal double well (with average depth u_0 and difference $2u_s$ between the two sides)

$$(\Delta N_1)_u = -(\phi/2) N_1 (\cosh u_s)^{-2} [1+j\omega\tau(1)]^{-1}. \quad (43)$$

Figure 10 compares, for $\omega\tau \ll 1$, the relative response of a rigid unequal double well $(\Delta N_1)_u/(\Delta N_1)_e$ (dotted curve) with that of a distortable double well $\Delta N_1/(\Delta N_1)_e$, plotted as a function of u_s with a as the parameter. As the relative distortion time a lengthens, the behavior of the distortable double well increasingly resembles a phase transition: A larger u_s corresponds to a lower temperature, since the distortion depth is normalized in reference to kT. Thus, above $u=1$ a very rapid "freezing out" of the dipoles takes place, i.e., fewer and fewer particles respond to the field, because an increasing number remain trapped in the lower well sites. This effect was foreshadowed in Figs. 6 and 7 by the fast approach of the most probable well depth to the extremum and the rapidly increasing population density of the lower well site. Thus, polarization decreases with falling temperature (as shown in Fig. 2) in contrast to the behavior of the Debye spectrum (cf. Fig. 1).

PRINCIPAL DISTINCTION BETWEEN THE RIGID UNEQUAL AND THE DISTORTABLE DOUBLE WELL

While both models, the rigid unequal and the distortable double well, show the "freezing-out" effect, it is more gradual in the former (Fig. 10). As far as a correlation to phase transitions is concerned, the distortable double well at $u_s=1$ may show a discontinuity in the derivative of the dielectric response with respect to temperature; it exhibits a "second-order" transition.

The rigid double well, furthermore, has only a single relaxation time while the distortable double well inherently produces a distribution of relaxation times. This can be seen explicitly by recalling that a relaxation time τ is correlated to every relative well distortion and that the limits are [cf. Eq. (38)]

$$\tau(0) = (2\nu_0 e^{-u_0})^{-1} \to \tau(1) = \operatorname{sech} u_s / 2\nu_0 e^{-u_0}. \quad (44)$$

Thus,

$$v(\tau) = (1/u_s) \cosh^{-1}[\tau(0)/\tau], \quad (45)$$

and the change in the total number of particles in the left well sites under the influence of an ac field can be expressed as an integration over τ, in place of Eq. (39);

$$\Delta N_1 = -\frac{\phi}{2} \int_{\tau(1)}^{\tau(0)} F(\tau) (1+j\omega\tau)^{-1} d\tau, \quad (46)$$

where

$$F(\tau) = \left\{ \frac{2n_1[v(\tau)]}{1+\exp[2u_s v(\tau)]} + \frac{2n_1[-v(\tau)]}{1+\exp[-2u_s v(\tau)]} \right\} \times \frac{1}{u_s} \frac{1}{\{1-[\tau/\tau(0)]^2\}^{\frac{1}{2}}} \quad (47)$$

is the unnormalized distribution of relaxation times. This inherent distribution of relaxation times leads to skewed characteristics in Cole-Cole plots of the imaginary vs the real part of ΔN_1. For $a \geq 2$, however, these plots differ from a semicircle by less than 1%. This deviation becomes greater if $a<2$, but in this region Eqs. (46) and (47) are no longer strictly valid, and a different analytical approach is required.

The complex dielectric constant is given as

$$\kappa^* = 1 + (\mathbf{P}/\epsilon_0 \mathbf{E}) = 1 + (\Delta N_1 \mu / \epsilon_0 \mathbf{E}), \quad (48)$$

where $\mathbf{E}$ is the applied field. If d designates the width of the double well between the two minima, e the charge of the particle, and if the local field is equal to the applied field, we obtain

$$\mu = e(d/2),$$
$$\phi/2 = eE(d/2kT); \quad (49)$$

hence,

$$\kappa^* = 1 + (ed/2)^2 (\epsilon_0 kT)^{-1} (\Delta N_1 / \tfrac{1}{2}\phi). \quad (50)$$

The frequency ω_{max} at which the loss factor κ'' reaches its maximum is

$$\omega_{max} = 2\nu_0 e^{-u_0} \cosh(v_m u_s), \quad \text{for } a \gg 1, \quad (51)$$

in contrast to the expressions for the rigid equal and the rigid unequal double wells, respectively, which are

$$(\omega_{max})_e = 2\nu_0 e^{-u} \quad (52)$$

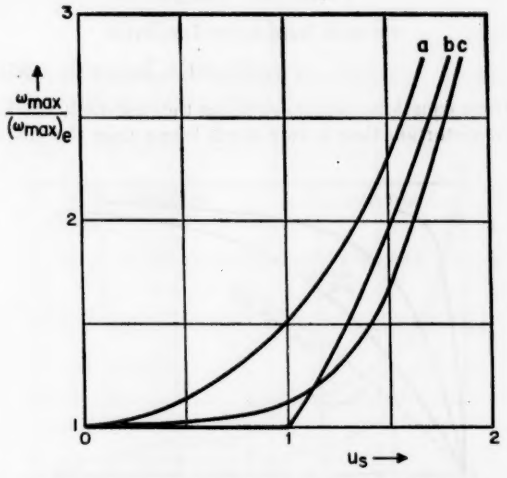

FIG. 11. Frequency of loss-factor maximum in relation to rigid equal double well as a function of u_s. (a) $(\omega_{max})_u/(\omega_{max})_e$ for rigid unequal double well; (b) $(\omega_{max})/(\omega_{max})_e$, $a \to \infty$; and (c) $(\omega_{max})/(\omega_{max})_e$, $a=2$ for distortable double well.

and

$$(\omega_{max})_u = 2\nu_0 e^{-u_0} \cosh u_s. \quad (53)$$

Figure 11 illustrates the trends for specific situations.

The distortable double well has, in addition, one unique feature not contained in the approximation, Eq. (39), but foreshadowed by the dc case [Eqs. (29) and (31)]. While fixed double wells have an orientation permanently built into the dielectric structure, distortable double wells can turn their low well sites into the favorable field direction, if given sufficient time between field reversals. Thus, a second spectrum must appear at sufficiently low frequencies leading to a polarization larger than expected for the Debye case.

If we describe this inversion of the well sites after the application of a dc field as an exponential decay process of orientation characterized by a time constant T_i, we can estimate this relaxation time as follows: There are many deep wells oriented in the wrong direction; jumps out of these wells occur with long time constants, followed normally by a rapid rebound from the flat into the deep well site; but slowly the wells flatten and then invert. The case of equal double wells ($v=0$) is rare for $u_s>1$ and $a\gg1$ (cf. Fig. 7), but here we know the time constant of distortion τ_s and can estimate the density of the wells $n_1(0)$ from Eq. (28). Hence, since the inversion of the wells occurs as a continuous flow process, the drift rate of occupied wells $(dN_1/dt)_{drift}$ is about

$$(dN_1/dt)_{drift} \cong n_1(0)/\tau_s \quad (54)$$

and

$$T_i \cong [N_1/n_1(0)]\tau_s. \quad (55)$$

The inversion time T_i can obviously become much larger than τ_s, since for $a>1$ and $u_s>1$ the expression $N_1/n_1(0)$ is large.

When the undistorted well depth u_0, the corresponding jump time τ_0, the maximum distortion depth u_s, and the time constant τ_s for the distortion are known, the low- and high-frequency spectra are in principle determined; vice versa, observation of the high-frequency spectrum with its freezing-out effect gives a, u_s, and u_0 and hence τ_s/τ_0 from Eq. (8), τ_0 from the high-temperature spectrum, and T_i from Eq. (55).

CONCLUSION

The distortion of a double well, due to the reaction of the surroundings, has been characterized by a distortion energy u_s and a time constant τ_s for reasons of simplicity. When applying the model to definite systems, it becomes necessary to describe the physical nature of the surroundings in detail and to ascertain how well this approximation applies; furthermore, to show how the parameters u_s and τ_s arise, and to determine their temperature dependence.

The surroundings may contain charges that can migrate by thermal activation or by band conduction. Either situation leads to the formation of a Debye-Hückel cloud about a charge in a double well. Alternatively, the model may be applied to the Onsager local-field treatment of dipole-dipole interactions. The reaction field and its response time can be related to u_s and τ_s in our model.

We hope to come back to such extensions and detailed applications of the model in the near future.

ACKNOWLEDGMENT

The authors are grateful to the Computation Center at the Massachusetts Institute of Technology for assistance with the numerical calculations.

Development of the Liquid Equation and the Partial Structure of Water

ROBERT GINELL*

Department of Chemistry, University of Utah, Salt Lake City, Utah

(Received December 9, 1960)

In a previous publication where the derivation of the Tait equation for liquids is given, the number average degree of association and the volume of holes depended on a sum

$$\phi=\sum_{x=1}^{\infty}s_x(1/v)^x.$$

This sum is transformed here into a closed expression. Hence, these quantities can now be evaluated numerically along any isobar or isotherm in terms of one undetermined constant at a particular reference temperature. In terms of this development, the structure of water is analyzed along an isobar (1 atm) from 20°–75°C and along an isotherm (20°C) from 1–200 atm.

IN a previous publication[1] (referred to hereafter as I) the virial equation of state in closed form was used to derive the Tait equation, which describes the isothermal compressibility behavior of liquids. This derivation showed that the general equation of state was applicable to all fluids, both gases and liquids. With this equation one derives analytical expressions for the volume of holes in the liquid, the number average molecular weight, and the total concentration of particles. All these quantities are obtained directly without the introduction of a specific model. The stumbling block to the use of this theory practically, as developed in I, is the fact that all these quantities are functions of one particular sum (in addition to experimental parameters), namely,

$$\phi=\sum_{x=1}^{\infty}s_x(1/v)^x, \tag{1}$$

where v is the volume and s_x is a function of the equilibrium constants, the weight of sample and the molecular weight of 1 mer. Hence, the problem of analyzing the structure of liquids becomes essentially one of evaluating the sum ϕ.

Since s_x is a rather complicated function of the equilibrium constants in the higher terms, and since further, the equilibrium constants for the formation of the larger species are unknown, it was hoped originally that it might be possible to represent this sum by the first few terms of the series. (The equilibrium constants are derived from a consideration of the virial coefficients of the gas,[2] and the higher virial coefficients are known only imperfectly for even the simplest substances.) Unfortunately, attempts to evaluate the sum directly, even approximately, from a knowledge of the first few equilibrium constants and some theory for simple substances[3] showed that the convergence of the series was very slow and that such a direct approach would be very difficult. Efforts were then directed toward changing the series so as to either transform it to a more rapidly converging sequence or to present it in closed form. The latter attempt was successful and will be the subject of this paper. With this modification, a numerical analysis of the structure of liquids is now practical.

TRANSFORMATION OF ϕ

We start by using Eq. (20) of I, which is

$$d\ln N_1=dv/v-\phi dv, \tag{2}$$

where ϕ is defined by Eq. (1) and where the temperature is constant. On integrating Eq. (2) (including the sum, term by term) we get

$$\ln N_1=\ln v-\left[s_1\ln v-\frac{s_2}{v}-\frac{s_3}{2v^2}-\frac{s_4}{3v^3}-\frac{s_5}{4v^4}-\cdots\right]+\text{const.} \tag{3}$$

On inserting the definition of s_x, namely,

$$s_x=xg_x(w/M^0)^{x-1};\qquad g_1=1, \tag{4}$$

where g_x is a function of the equilibrium constants and is constant at constant temperature; and inserting the definition of

$$\sum_{i=1}^{m}iC_i$$

and changing the summation interval, we obtain

$$\ln N_1=\sum_{x=2}^{\infty}\left[\frac{xg_x(\sum iC_i)^{x-1}}{x-1}\right]+\text{const}$$

$$=\sum_{x=1}^{\infty}\left[\frac{(x+1)g_{x+1}(\sum iC_i)^x}{x}\right]+\text{const.} \tag{5}$$

* Permanent address: Department of Chemistry, Brooklyn College, Brooklyn, New York. On leave 1960–1961.

[1] R. Ginell, J. Chem. Phys. **34**, 1249 (1961).

[2] R. Ginell, J. Chem. Phys. **23**, 2395 (1955).

[3] R. Ginell, J. Chem. Phys. **34**, 992 (1961).

This sum can be separated and becomes

$$\ln N_1=\frac{\sum_{x=1}^{\infty} g_{x+1}(\sum iC_i)^{x+1}}{\sum iC_i}+\sum_{x=1}^{\infty}\frac{g_{x+1}}{x}(\sum iC_i)^x+\text{const.} \quad (6)$$

On rewriting the first sum and inserting the value of[2]

$$\sum_{i=1}^{m} C_i,$$

which is

$$\sum_{i=1}^{m} C_i=\sum_{x=1}^{\infty} g_x(\sum iC_i)^x, \quad (7)$$

and the equation for the number average degree of association [I; Eq. (24)]

$$Z_n=\sum iC_i/\sum C_i=L/Jp\phi, \quad (8)$$

where L and J are the Tait coefficients, we obtain

$$\ln N_1=\frac{Jp\phi}{L}-1+\sum_{x=1}^{\infty}\frac{g_{x+1}}{x}(\sum iC_i)^x+\text{const.} \quad (9)$$

On differentiating Eq. (9) at constant temperature, and substituting Eq. (2) in the left-hand side, and using the definition of $\sum iC_i$, we have

$$v^{-1}-\phi=p\phi\frac{d}{dv}\frac{J}{L}+\frac{J}{L}p\frac{d\phi}{dv}+\frac{J}{L}\phi\frac{dp}{dv}-\sum_{x=1}^{\infty}\frac{g_{x+1}(\sum_i^{\infty} iC_i)^x}{v}. \quad (10)$$

By using Tait's equation, changing the summation interval of the series, and using Eqs. (7) and (8), and rearranging, we obtain

$$-(d/dv)\ln(J/L)-(d\ln\phi/dv)+J^{-1}+v^{-1}=0, \quad (11)$$

which on integration gives

$$\phi=\frac{A_V L}{J}\exp\int dv/J, \quad (12)$$

where A is the constant of integration. Another form of the equation may be obtained if in Eq. (11) we use Eq. (8) to eliminate ϕ. In this case upon integration we obtain

$$Z_n=(L/Bpv)\exp\int dp/(L+p). \quad (13)$$

Equation (13), (8), and (12) yield Tait's equation. If as in most liquids, J and L are constant with changes in pressure, then Eqs. (12) and (13) become, using Eq. (8),

$$\phi=(A_V L/J)e^{v/J}=(Bv/J)[L/(L+p)], \quad (14)$$

which gives us

$$L+p=B/A\ e^{-v/J}, \quad (15)$$

an integrated form of Tait's equation. The constant

TABLE I. Water: Variation with temperature at 1 atm pressure, $J=0.3150$ ml.[a]

°C				$[(v-b)/A_{25}]10^{-5}$	
Temp.	$(\phi/A_{25})10^{-5}$	Z_nA_{25}	$\Sigma C_i/A_{25}$	ml/g	L[a] atm
25	2.2728	0.04130	1.3400	0.3288	2956.8
35	2.3283	0.04111	1.3422	0.3414	3015.0
45	2.3623	0.04086	1.3451	0.3546	3040.7
55	2.3766	0.04058	1.3484	0.3683	3037.7
65	2.3738	0.04028	1.3512	0.3823	3012.1
75	2.3549	0.03998	1.3535	0.3966	2965.7

[a] Data from Gibson and Loeffler, reference 4.

B/A can be evaluated; when $p=1$ atm, $v=v_0$ so that

$$B/A=(L+1)\exp(v_0/J)$$

and

$$(L+p)/(L+1)=\exp[(v_0-v)/J]. \quad (16)$$

We have now transformed the sum ϕ into a closed expression, but we still have the problem that while this gives us ϕ (in terms of an undetermined constant), the expression is only valid along an isotherm and we have thus far no indication as to how ϕ varies with temperature.

TEMPERATURE VARIATION OF ϕ

On taking the derivation of the logarithm of Eq. (12) with respect to temperature at constant pressure, we have

$$\left(\frac{\partial\ln\phi}{\partial T}\right)_p=v^{-1}\left(\frac{\partial v}{\partial T}\right)_p-\left(\frac{\partial\ln(J/L)}{\partial T}\right)_p+\left(\frac{\partial(v/J)}{\partial T}\right)_p, \quad (17)$$

which can be rewritten as

$$\left(\frac{\partial\ln\phi}{\partial T}\right)_p=(1+v/J)\beta-\frac{v}{J^2}\left(\frac{\partial J}{\partial T}\right)_p-\left(\frac{\partial\ln(J/L)}{\partial T}\right)_p, \quad (18)$$

where β is the coefficient of instantaneous cubical expansion

$$\beta=v^{-1}(\partial v/\partial T)_p. \quad (19)$$

This equation can be integrated numerically since all the quantities on the right are experimentally determinable. Thus, at constant pressure

$$\phi_T=\phi_0\exp\left\{\int_{T_0}^{T}[1+(v/J)]\beta dT-\int_{T_0}^{T}\left(\frac{\partial\ln(J/L)}{\partial T}\right)_p dT-\int_{T_0}^{T}\frac{v}{J^2}\left(\frac{\partial J}{\partial T}\right)_p dT\right\}, \quad (20)$$

with ϕ_0 equal to the value of ϕ at some reference temperature. If J is independent of temperature, as it is

TABLE II. Water: Variation with pressure at 20°C, $J=0.3150$ ml, $L=2911.4$ atm.[a]

p atm	v[b]	Z_nA_{25}	$\Sigma C_i/A_{25}$	$[(v-b)/A_{25}]10^{-6}$ ml/g
1	1.0020	0.04156	1.3328	0.3267
25	1.0009	0.001670	33.204	0.3252
50	0.9998	0.0008389	66.177	0.3237
100	0.9976	0.0004233	131.43	0.3208
200	0.9934	0.0002154	259.38	0.3152

[a] Extrapolation from data given by Gibson and Loeffler, reference 4.
[b] Data of L. B. Smith and F. G. Keyes, Proc. Am. Acad. Arts Sci. **69**, 285 (1934).
[c] $A_{20}=0.99759\ A_{25}$

in many liquids (e.g., water, benzene) then

$$\phi_T=\phi_0\exp\left\{\int_{T_0}^{T}[1+(v/J)]\beta dT-\int_{T_0}^{T}\left(\frac{\partial\ln(J/L)}{\partial T}\right)_p dT\right\}. \tag{21}$$

Thus, we have now principly determined the value of ϕ as a function of temperature and at the reference temperature we know ϕ, except for an undetermined constant.

The number average degree of association Z_n the volume of holes $(v-b)$ and the total number of particles $\sum C_i$ now become for liquids (where J and L are constant along an isotherm)

$$Z_n=\frac{L}{Jp\phi}=\frac{e^{-v/J}}{Apv} \tag{22}$$

$$(v-b)=\frac{RTwJ\phi}{LM^0}=\frac{ARTwve^{v/J}}{M^0} \tag{23}$$

$$\sum C_i=\frac{w}{M^0}\frac{J}{L}\frac{p}{v}\phi=\frac{Awpe^{v/J}}{M^0}. \tag{24}$$

By using Eqs. (22)–(24) with Eq. (21) we can determine these quantities in terms of a constant A_T at some reference temperature, t.

PARTIAL DETERMINATION OF THE STRUCTURE OF WATER

To gain some insight into the structure of water we have calculated the above quantities along an isobar ($p=1$ atm) for the temperature range 20°–75°C (Table I), also along an isotherm (20°C) for the pressure range 1–200 atm (Table II). The J and L coefficients were determined by Gibson and Loeffler.[4] As can be seen from Table I, with increased temperature at constant pressure, the degree of association decreases, the volume of holes increases, and the number of particles increases. All these conclusions seem reasonable enough. More interesting are the conclusions to be drawn from Table II. Here, upon increase in pressure along an isothermal line, the volume of holes decreases; this is to be expected. However, the degree of association also decreases, while the number of particles increases. In a way this is not surprising. At low pressures the molecules in the liquid are large, loose arrays with an approximate coordination number of 12 and rough fivefold symmetry,[3] having many small holes in the structure. As the pressure increases and the volume of holes decreases, the molecules are sheared and compressed and the individual kinetic unit becomes smaller.

Further work on this problem is in progress.

ACKNOWLEDGMENT

Thanks are due for the useful and stimulating conversations I have had with Dr. Henry Eyring.

[4] R. E. Gibson and O. H. Loeffler, Ann. N. Y. Acad. Sci. **51**, 727 (1949).

Surface-Catalyzed Excitations in the Oxygen System*

GENE MANNELLA† AND PAUL HARTECK

Chemistry Department, Rensselaer Polytechnic Institute, Troy, New York

(Received November 21, 1960)

A luminosity is produced over Ni maintained at approximately 20°C in a stream of O atoms. Spectroscopic investigation shows the strongly forbidden $b\,^1\Sigma_g^+ - X\,^3\Sigma_g^-$ atmospheric system and $A\,^3\Sigma_u^+ - X\,^3\Sigma_g^-$ Herzberg system of the O_2 molecule plus four strong heads of the (0, 0) band of the OH $A\,^2\Sigma^+ - X\,^2\Pi$ interaction. Certain spectral features in the region of the (0, 0) atmospheric band could not be resolved for positive identification but are suggested to be the vibrational-rotational bands of OH. The Herzberg and atmospheric bands appear to be primary products of the surface catalysis while the OH molecule can be either a surface product or the result of chemical reactions of certain excited species present.

INTRODUCTION

OXYGEN does not normally act as a strong light emitter. Of all the possible interactions for excited states of the O_2 molecule, most are strongly forbidden by selection rules. Therefore, most of the older literature on the spectroscopy of this molecule is relative to its role as a light absorber, particularly in the well-known Schumann-Runge system. Of the known band systems for oxygen, all were first discovered in absorption and, more recently, many have been seen under special conditions in emission. The Herzberg and atmospheric bands are of special interest in this paper and will be briefly discussed.

The forbidden $A\,^3\Sigma_u^+ - X\,^3\Sigma_g^-$ system was first observed by Herzberg[1] in 1932 in absorption using very long path lengths and this system subsequently bears his name. Broida and Gaydon[2] examined the afterglow of an uncondensed discharge through oxygen at around 2 mm pressure and first found this system in emission; however, they suggested that Herzberg's assignments of v' be raised one unit. Barth and Kaplan[3] examined the spectrum of the oxygen afterglow in the 3350–4500 A region and obtained sufficient resolution to resolve the rotational structure of the Herzberg bands.

The atmospheric bands of oxygen arise from the $b\,^1\Sigma_g^+ - X\,^3\Sigma_g^-$ interaction with a reported[4] transition probability of 0.14 sec^{-1}. This system was first detected in emission by Kaplan[5] in 1947 in oxygen-enriched nitrogen afterglow; the (0, 0) and (1, 0) transitions were observed. Herman *et al.*[6] obtained the (0, 0) (1, 1) and (2, 2) bands of the atmospheric system in emission from CO–O_2 explosions. Using a static system and spectroscopically pure O_2 at about 1 cm pressure, Branscomb[7] studied the 3000–9000-A region and found only the (0, 0) and (0, 1) atmospheric bands and a weak continuum. Bryan *et al.*[8] also studied the oxygen afterglow; they detected the (0, 0) atmospheric band but found that most of the light observed was in the 3500–4500-A region and was a continuum with no bands present.

Surface-catalyzed excitation is a new development which has recently been observed in our laboratory and reported in the literature.[9] The first observations on surface-catalyzed excitation (SCE) were made using various metal samples in mixed N- and O-atom streams. In these experiments, it was found that a luminosity was produced over the metal samples which was due to the formation of electronically excited species on the metal surface. These species, the N_2 ($A\,^3\Sigma_u^+$) and NO($B\,^2\Pi$), then diffused into the gas phase and radiated their characteristic band spectra. In a later publication[10] the observed intensity distribution of the N_2 first positive system was explained by a crossing over of $A\,^3\Sigma_u^+$ molecules into the $B\,^3\Pi_g$ configuration. This note also reported SCE of N atoms over a Cu sample. In this case, the radiation observed was the second positive system, which is due to the formation of the $C\,^3\Pi_u$ state.

In light of these developments, particularly the fact that three separate excited molecules were quickly detected, it appeared that SCE was a general phenomenon and that many more examples could be found and studied in the laboratory if the correct conditions for surface catalysis could be determined. Ni and Co appear to be very suitable for SCE and are also generally known as good catalysts for many chemical reactions. Accordingly, further study was directed to the oxygen

* The research reported in this document has been sponsored jointly by the Geophysics Research Directorate of the Air Force Cambridge Research Center and the Office of Scientific Research, Air Research and Development Command.

† Present address: Battelle Memorial Institute, Columbus, Ohio.

[1] G. Herzberg, Naturwissenschaften **20**, 577 (1932).

[2] H. P. Broida and A. G. Gaydon, Proc. Roy. Soc. (London) **A222**, 181 (1954); Trans. Faraday Soc. **49**, 1190 (1953).

[3] C. A. Barth and J. Kaplan, J. Mol. Spectroscopy **3**, 583 (1959).

[4] G. Herzberg, *Spectra of Diatomic Molecules* (D. Van Nostrand Company, Inc., Princeton, New Jersey, 1950), 2nd ed., p. 378; W. H. J. Childs and R. Mecke, Z. Physik **68**, 344 (1931).

[5] J. Kaplan, Nature **159**, 673 (1947); Phys. Rev. **71**, 274 (1947).

[6] R. C. Herman, H. S. Hopfield, G. A. Hornbeck, and S. Silverman, J. Chem. Phys. **17**, 220, 982 (1949).

[7] L. M. Branscomb, Phys. Rev. **86**, 258 (1952).

[8] R. B. Bryan, R. B. Holt, and O. Oldenberg, Phys. Rev. **106**, 83 (1957).

[9] R. R. Reeves, G. Mannella, and P. Harteck, J. Chem. Phys. **32**, 946 (1960).

[10] G. G. Mannella, R. R. Reeves, and P. Harteck, J. Chem. Phys. **33**, 636 (1960).

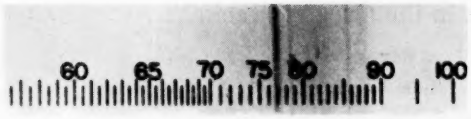

FIG. 1. Oxygen afterglow, 16-hr exposure with 200-μ slit, Kodak I-N plate. The (0, 0) atmospheric oxygen band and the two OI lines can be seen. For comparison purposes, the total exposure is at least twice that of Fig. 2.

system and it was subsequently defined that a red glow could be produced over a Ni sample maintained at room temperature in a stream of O atoms. Spectroscopic investigation of this glow showed its primary feature to be the forbidden atmospheric oxygen band; the sensitivity of the eye in this spectral region is such that the excited molecules must be strongly catalyzed in order for it to be seen. In addition, it is likely, but not completely verified, that the visually observed red glow is at least partially due to the rotational-vibrational OH bands. Unexpectedly, the glow also contained important ultraviolet features which were identified as extensive bands belonging to the Herzberg O_2 system and the four heads of the persistent (0, 0) band of the OH $A\,^2\Sigma^+ - X\,^2\Pi$ interaction.

Thus, it was possible to catalyze even a weak emitter such as O_2 to such an extent that two electronically excited species were observed in emission, plus the strong OH emitter. Without SCE, under our experimental conditions, these bands are at least an order of magnitude less intense or else completely missing in the gas phase.

EXPERIMENTAL TECHNIQUE

The apparatus used employed a fast-pumping flow system which was originally designed for kinetic studies.[11] The main features of this equipment consisted of two discharge tubes of the Wood-Bonhoeffer type connected to a 2-m length of 42-mm-i.d. glass tubing and hence through a trap to a Welch mechanical pump of 375 liter/min capacity. One discharge tube was connected to a variable-output ac source of approximately 8000 v and 250 ma on the secondary. The other discharge tube was connected to a dc power supply and was not used in this work.

High-purity cylinder oxygen was used for most experiments since the long exposures in the flow system would have required considerable amounts of spectroscopically pure or specially prepared oxygen. The regular oxygen afterglow acted as a background and made spectral identification very difficult; use of spectroscopically pure O_2 did not help appreciably since in spite of our safeguards enough nitrogen got into the system to form minute amounts of NO which reacted with the O atoms and gave a visible afterglow. The oxygen was leaked into the system through capillary tubing; decreasing the forepressure on the capillary permitted some control over the total pressure in the system. Experiments were made from 250 μ down to 50 μ, although the best glows were obtained in the 50–100-μ region. Once the system stabilized it was possible to maintain the faint red glow over the Ni sample for days at a time, thus permitting long exposures.

Two spectrographs were employed, Hilger E-498 (F_D 60 cm) medium and E-484 (F_D 20 cm) small quartz instruments. Various methods of increasing speed were tried, including hypersensitizing with ammonia; however, the simplest and most reliable method was the use of SD-19a developer.[12] Hypersensitizing with ammonia is frequently preferred since it is most effective at longer wavelengths; however, it is not reproducible and requires extensive handling of the plate prior to exposure. Identification of the (0, 0) atmospheric oxygen band was accomplished by calibration with *K* and *Cs* lines.

The 42-mm tube was conditioned by cleaning with HNO_3, and then a coating of dilute orthophosphoric acid was applied. This proved to be quite effective, since the oxygen afterglow was observed to travel all the way to the cold trap, a distance of over 2 m, without appreciable decrease in intensity. To minimize ozone formation, Ag foil was placed ahead of the trap to recombine the O atoms. Liquid oxygen was used as a coolant for the trap instead of liquid nitrogen to avoid condensation of the small amounts of O_3 that might be formed. It appears that the small amount of water present in the orthophosphoric coating furnishes a small but finite amount of water vapor during the experiments.

In the present work as well as in previous work it was necessary to avoid conditions where the catalytic recombination of the atoms took place in the ground state. To accomplish this, a special cooling arrangement of glass was blown into the 71/60 cap on the end of the 42-mm tube, which permitted the metal sample to be positioned in the atom stream while cooling water was circulating through the structural members of the sample holder. This proved a simple and effective way to maintain the sample at a reasonably low temperature. Circulating ice water or dry ice-trichloroethylene mixtures did not improve upon the original system.

FIG. 2. SCE of O atoms over Ni, 48-hr exposure with 125-μ slit, Kodak I-N plate. The (0, 0) atmospheric oxygen band and features suspected to be vibrational-rotational OH bands are evident.

[11] P. Harteck, R. R. Reeves, and G. Mannella, J. Chem. Phys. **29,** 608, 1333 (1958); **32,** 532 (1960).

[12] An excellent discussion on increasing film sensitivity can be found in the paper by H. A. Miller, R. W. Henn, and J. I. Crabtree, Photographic Soc. Am. **12,** 586 (1946).

DISCUSSION

The luminosity produced over a Ni sample in an O-atom stream was relatively weak compared to other examples of SCE previously reported.[9] The oxygen afterglow background also interfered with the spectrographic analysis, since long exposures were required to bring all the spectral features in this wavelength region to a reasonable intensity. During these long exposures, the Herzberg bands and the OH band also became sufficiently resolved for positive identification. Each of these will be discussed in turn.

The Oxygen Afterglow

As pointed out earlier, much work has been done to identify the various spectral features of the products of an oxygen discharge. Several blanks with path lengths corresponding to those used in the SCE exposures were taken on both I-D(2) and I-N plates. These plates showed a faint OH band at approximately 3060 A and the (0, 0) O_2 atmospheric band at 7594 A. In addition, the OI lines at 7774 A ($3^5S^0-3^5P$) and at 8446 A ($3^3S^0-3^3P$) also were identified. The red portion of the spectrum for one of these blanks is reproduced in Fig. 1. In exposures taken of the gas phase with path length and exposure time equivalent to the spectrograms of the red glow, it was evident that the oxygen systems and the OH bands were being strongly catalyzed over the Ni. No trace of Herzberg bands was detected in our system without SCE.

The Atmospheric $b\ ^1\Sigma_g^+-X\ ^3\Sigma_g^-$ System

A typical exposure is reproduced in Fig. 2. The (0, 0) band is seen to be very strongly evident, while the *OI* lines appear to be absent. Presumably the metastable O-atom states quench on the Ni surface whereas they do not on the coated glass, since they are present in the gas phase in sufficient concentration that they are excited to levels from which allowed transitions are observed. There are other spectral features in this wavelength region that arise from catalyzed molecules. It was thought at first that these might be lower members of the $a\ ^1\Delta_g-X\ ^3\Sigma_g^-$ infrared atmospheric oxygen bands, whose (0, 0) transition lies at about 12 687 A. Unfortunately our emulsion was sensitive only to about 8700 A, and attempts to fit some of the more prominent spectral features into a table of band origins calculated from Herzberg[13,14] for this system were not successful.[15]

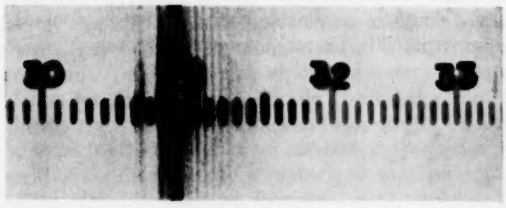

FIG. 3. SCE of O atoms over Ni, 12-hr exposure with 125-μ slit, Kodak I-N plate showing the four heads of the strong (0, 0) band of the OH $A\ ^2\Sigma^+-X\ ^2\Pi$ transition.

FIG. 4. SCE of O atoms over Ni, 120-hr exposure with 100-μ slit, Kodak I-N plate showing the strong (0, 0) OH band and fainter members of the Herzberg oxygen system.

Since the surface was not apparently attacked by O atoms, it seemed unlikely that these could be NiO bands; indeed they did not fit the scheme reported by Rosen.[16] Since they did not appear to fit any known O_2 system, it was attempted to see if they belonged to an H_2O or OH system. (Molecules with strong dipoles when present in minute amounts with these metastable molecules may be easily excited and may radiate to such an extent that they overshadow the vastly more predominant species in respect to light emission.) Gaydon[17] has recorded H_2O bands in the 6000–10 000-A interval, but assignment to this system did not succeed. Attempts to enhance these bands by adding H_2 or H_2O to the oxygen input were unsuccessful, largely since a concentration of H-atoms of about 1% or less was detrimental to the glow and apparently stopped any catalytic activity of the Ni that leads to excited atoms. Instead, the afterglow was extinguished with considerable generation of heat, indicating that the O atoms were recombining in their ground state.

The most probable assignment that can be made without a more detailed study is that these bands are part of the rotational-vibrational structure of the OH molecule. This is supported by the fact that the (0, 0) band of the $A\ ^2\Sigma^+-X\ ^2\Pi$ system of OH is also catalyzed strongly in these experiments. In spite of the fact that much experimental work and very exact measurements have been made on the OH rotational-vibrational bands,[18–21] no definite assignment was possible with the resolution we obtained with our spectrograph.

The OH $A\ ^2\Sigma^+-X\ ^2\Pi$ System

The degree to which the OH $A\ ^2\Sigma^+$ state is catalyzed is indicated in Fig. 3 where the four bands leads of the (0, 0) transition to the ground $X\ ^2\Pi$ state can be seen,

[13] G. Herzberg, see work cited in reference 4, p. 560.
[14] L. Herzberg and G. Herzberg, Astrophys. J. **105**, 353 (1947).
[15] In view of the fact that transitions from the other two states below the dissociation level of O_2, the $^3\Sigma_u^+$ and $^1\Sigma_g^+$, were detected, it seemed reasonable to assume that the $^1\Delta_g^-$ state was also being formed. Investigation out to longer wavelengths is planned when suitable spectrographic equipment is available.
[16] B. Rosen, Nature **156**, 570 (1955).
[17] A. G. Gaydon, Proc. Roy. Soc. (London) **181**, 197 (1942).
[18] J. W. Chamberlain and N. J. Oliver, Phys. Rev. **90**, 1181 (1953).
[19] A. B. Meinel, Astrophys. J. **111**, 555 (1950).
[20] R. C. Herman and G. A. Hornbeck, Astrophys. J. **118**, 214 (1953).
[21] J. W. Chamberlain and F. L. Roesler, Astrophys. J. **121**, 541 (1955).

along with rotational structure that degrades to longer wavelengths. The intensity distribution here is such that the 3089-A head appears most intense. This molecule has been the subject of much study and its radiative lifetime was recently confirmed as 5.5×10^{-7} sec.[22]

The Herzberg $A\ ^3\Sigma_u^+ - X\ ^3\Sigma_g^-$ System

Figure 4 shows members of this system along with the strong OH band. The reproduction of this plate is only fair; bands up to 4700 A can be detected on the original. The dominant bands appear to be from the zero and first vibrational level of the upper $A\ ^3\Sigma_u^+$ state. The spectrogram was obtained by shooting through the 42-mm tube and no quartz window could be conveniently positioned without sacrificing optimum geometric positions. Therefore, the (0, 0) transition around 2800 A could not be picked up, since the cutoff occurred above this wavelength. Nevertheless, other transitions from $v'=0$ and 1 are quite strong.

The Schumann-Runge System

No members of this system, corresponding to the $B\ ^3\Sigma_u^- - X\ ^3\Sigma_g^-$ transition have been detected as yet. It is not unreasonable to suspect that under proper conditions the $B\ ^3\Sigma_u^-$ would be observed also, in spite of the fact that its lower vibrational levels are about 1 ev above D_{O_2}. Its reported[23] lifetime is the order of 10^{-8} sec. This situation would be analogous to the formation of the N_2 ($C\ ^3\Pi_u$) state which was reported earlier[10] and this seems to warrant further investigation.

Mechanisms

It is difficult to make well-founded statements concerning the exact nature of the reactions occurring on the surface of the catalyst until we have more information concerning the fundamental behavior of atoms and molecules adjoining a surface. The surface appears to require some sort of conditioning for SCE. If oxygen attacks the metal, the reaction is

$$\mathrm{Ni}+\tfrac{1}{2}\,\mathrm{O_2}\rightarrow\mathrm{NiO}+59\ \text{kcal}. \qquad (1)$$

If the attack occurs via O atoms, the binding energy of the O atom is virtually equal to the dissociation energy of O_2. Stripping off of this chemically bound atom by another gas-phase atom via

$$\mathrm{NiO}+\mathrm{O}\rightarrow\mathrm{Ni}+\mathrm{O_2}, \qquad (2)$$

is thermally neutral and could not result in an excited molecule. If an O atom were loosely bound to a NiO molecule on the surface as

$$\mathrm{NiO\ (surface)}+\mathrm{O}\rightarrow\mathrm{NiO\cdot O\ (adsorbed)}, \qquad (3)$$

the adsorbed atom could then be taken off by a gas-phase atom, resulting in an excited O_2 molecule,

$$\mathrm{NiO\cdot O\ (adsorbed)}+\mathrm{O\ (gas\ phase)}\rightarrow\mathrm{NiO}+\mathrm{O_2}^*. \qquad (4)$$

The O_2^* could retain almost all its dissociation energy, minus a given amount of surface binding energy. The minimum surface binding energy can be assessed at about 0.5 ev from examination of the spectra of the excited molecules.

This type of mechanism is plausible for the Herzberg and atmospheric bands, which must arise from surface catalysis. The analogous process is not necessarily valid for the OH molecule, since it could be formed either by surface catalysis or by reaction of the metastable species present. For example, transitions from $v'=4$ of the O_2 ($A\ ^3\Sigma_u^+$) molecule are observed. If this molecule in the third or fourth vibrational level reacts with a H atom,

$$\mathrm{O_2}\ (A\ ^3\Sigma_u^+)_{v=3,4}+\mathrm{H}\rightarrow\mathrm{O}+\mathrm{OH}^*,$$

the resultant OH^* molecule could have about 100 kcal, ample to excite the observed $A\ ^2\Sigma^+$ state of OH, which requires 94 kcal.

CONCLUSIONS

Surface-catalyzed excitation of the $A\ ^3\Sigma_u^+$ and $b\ ^1\Sigma_g^+$ states of the O_2 molecule and the $A\ ^2\Sigma^+$ state of OH have been observed. These states, along with the N_2 ($A\ ^3\Sigma_u^+$) and $C\ ^3\Pi_u$ and the NO ($B\ ^2\Pi$) reported earlier,[9,10] constitute an imposing array of excited species which have been detected so far by SCE. It appears that in any system where excited states lie about 0.5 ev below the dissociation level these states could be surface catalyzed, under the right conditions. The 0.5 ev is apparently connected with the loose binding of one atom to the surface until a second atom from the gas phase unites with it to form an excited molecule. The possibility of producing a variety of known excited states in reasonable concentration is obviously an important kinetic tool for future research.

[22] T. Carrington, J. Chem. Phys. **31**, 1243 (1959).
[23] J. C. Keck, J. C. Camm, B. Kivel, and T. Wentink, Jr., Ann. Phys. **7**, 1 (1959).

Letters to the Editor

THE Letters to the Editor section is subdivided into three parts entitled Communications, Comments and Errata, and Notes. These three sections are all subject to the same limitations on length. The textual material of each Letter is limited to a number of words equal to 950 minus the following; (a) 200 words for each average-sized figure: (b) 50 words for each displayed equation: (c) 7 words for each line of table including headings and horizontal rulings. No proof will be sent to the authors of "Communications" and "Comments and Errata." Proof will be sent to the authors of "Notes." The publication charge for Letters is $30 per page, with a minimum of $30 per Letter, If honored, the Institution will be entitled to 100 reprints without covers. See issues of May–September, 1957, for descriptions of categories.

Communications

Energy Transfer in Hydrogen-Bonded *N*-Heterocyclic Complexes and Their Possible Role as Energy Sinks*

M. ASHRAF EL-BAYOUMI AND M. KASHA

Institute of Molecular Biophysics and Department of Chemistry, Florida State University, Tallahassee, Florida

(Received March 20, 1961)

EXCITON theory[1] provides a general mechanism of electronic energy transfer for weakly interacting molecular systems. For such systems the intermolecular overlap between orbitals of two neighboring molecules is negligible. The theory has been previously applied to molecular crystals,[2] dispersion force aggregates,[3,4] and more recently, hydrogen-bonded dimers.[5] In all these cases, shifts or splitting of electronic absorption bands due to exciton-type interaction are satisfactorily explained. The probability of energy transfer depends on the magnitude of the exciton splitting ΔE. However, the detailed mechanism of energy transfer depends on other factors,[6] in particular the relative magnitude of intramolecular vibrational-electronic coupling compared with ΔE, as well as the rate of loss of vibrational energy in the excited state.

In our research we have studied spectral shifts and energy transfer for hydrogen-bonded molecular complexes, especially those composed of *N*-heterocyclic base pairs. In this note we report the energy transfer results for the acridine-carbazole H-bonded complex. Energy transfer in the acridine-carbazole complex may be expected to appear as an increase in the emission yield of acridine (energy acceptor), or as a quenching of the carbazole emission (energy donor), or both. In systems of like molecules, depolarization of fluorescence is used as a direct measure of energy transfer.[7]

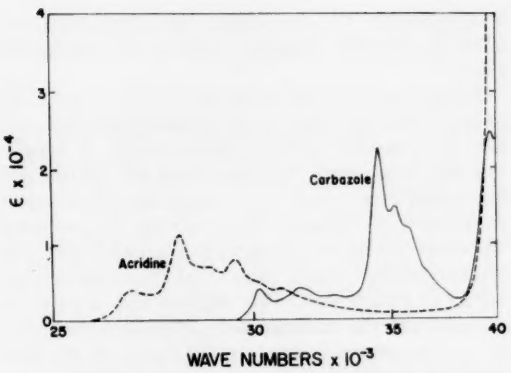

FIG. 1. Absorption spectra of acridine and carbazole in methylcyclohexane solution at 20°C.

The structure of the acridine-carbazole complex is shown to be

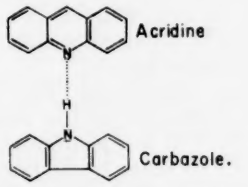

The absorption spectra of acridine and carbazole in methylcyclohexane solution at 20°C are given in Fig. 1.

The emission spectra of carbazole alone and in the presence of acridine in a rigid transparent glass solution at 77°K were recorded in different media, using a Perkin-Elmer model 99 double-pass monochromator. The exciting light in all of our experiments consisted of a narrow band in the region of the second absorption band of carbazole. For a solution containing equimolar quantities of carbazole and acridine almost all the exciting light is absorbed by carbazole without appreciable absorption by acridine.

Solutions of carbazole in hydrocarbon-glass solution at an initial concentration of 1×10^{-4} mole/liter exhibit strong fluorescence ($S'\rightarrow S$) and phosphorescence ($T\rightarrow S$). In the presence of equimolar quantities of acridine in hydrocarbon-glass solution, the emission recorded under identical conditions shows a strong quenching of carbazole emission. However, in alcohol-glass solution, acridine has only a very small effect on the carbazole emission.

Hydrocarbon-glass solution favors the formation of acridine-carbazole hydrogen-bonded complexes; in contrast, in hydroxylic glass solution (EPA) hydrogen bonding of each solute molecule with the solvent occurs. The results can be understood in terms of the acridine-carbazole hydrogen-bonded complex formation and the consequent molecular exciton interaction of the π systems of the two molecules. This interpretation

is supported by the observation that acridine has little effect on *N*-ethyl carbazole emission in hydrocarbon glass.

Strong quenching of carbazole (1×10^{-4} mole/liter) emission was also observed in hydrocarbon-glass solution at a smaller relative concentration of acridine (1×10^{-5} mole/liter). The quenching was greater than one would expect even if it is assumed that complete association of carbazole with acridine has occurred. Therefore, the emission of some free carbazole molecules is also quenched, which means that the complex is acting as an energy sink. This suggests that a collective excitation of the uncomplexed carbazole molecules by an exciton model is involved (probably in the weak coupling approximation, according to Simpson and Peterson's criteria[8]). If an acridine-carbazole complex is present within such a region, the excitation energy can become localized and trapped by the complex. Since the quenching of carbazole emission was not accompanied by a corresponding increase in the emission of acridine, one concludes that the nonradiative decay is favored in this case. Research in our laboratory is being continued to determine the role of complexes as energy sinks in other systems.

The authors acknowledge with thanks several stimulating conversations on this research with Professor J. R. Platt. It is a pleasure to acknowledge a special grant to M. Kasha by the Petroleum Research Fund, American Chemical Society. This grant aided considerably in providing instrumentation used in this research.

* This work was supported by the Division of Biology and Medicine, U. S. Atomic Energy Commission and the Chemistry Division, U. S. Air Force Office of Scientific Research.

[1] Cf. A. S. Davydov, *Theory of Molecular Exciton*, translated by M. Oppenheimer, Jr., and M. Kasha (McGraw-Hill Book Company, Inc., New York, to be published).

[2] Cf. D. S. McClure, *Solid State Physics* (Academic Press, Inc., New York, 1959), vol. 8, pp. 1–47; M. Kasha, Revs. Modern Phys. **31,** 162 (1959).

[3] G. S. Levinson, W. T. Simpson, and W. Curtis, J. Am. Chem. Soc. **79,** 4314 (1957).

[4] E. G. McRae and M. Kasha, J. Chem. Phys. **28,** 721 (1958).

[5] M. Ashraf El-Bayoumi and M. Kasha (to be published).

[6] T. Förster, *Comparative Effects of Radiation* (John Wiley & Sons, Inc., New York, 1960), pp. 300–320.

[7] T. Förster, Ann. Physik **2,** 55 (1948).

[8] W. T. Simpson and D. L. Peterson, J. Chem. Phys. **26,** 588 (1957).

On the Classical Approximation in the Statistical Theory of Mass Spectra

H. M. Rosenstock

Physical Chemistry Division, National Bureau of Standards, Washington 25, D. C.

(Received April 13, 1961)

RECENT photoionization studies have revealed serious discrepancies between experiment and the predictions of mass spectra theory.[1,2] Similar difficulties arise in the interpretation of appearance potentials.[3] The difficulties are that the measured energy dependence of the unimolecular rate constant is much more rapid than predicted theoretically and, with appearance potentials, the rate equations of the theory predict an excitation energy frequently far in excess of the activation energy in order to produce fragmentation in the ion source. Up to now these difficulties have been empirically resolved by assuming that only a fraction of the oscillators, one-third or even less, are kinetically effective or that energy equilibration is incomplete.

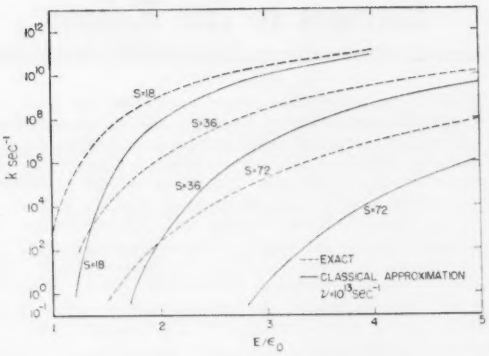

FIG. 1. Comparison of rate constants calculated with and without the classical approximation.

A major approximation in the theory is the computation of the vibrational density of states by the Dirichlet integral. Marcus[4] has pointed out that this classical approximation can be quite poor at low excitation energies, particularly for the activated complex. In the Kassel treatment of unimolecular reactions[5] the equivalent approximation is that the number of quanta is much larger than the number of oscillators. The mass spectrometric processes in question are low-excitation-energy phenomena which do not satisfy the conditions of validity of this approximation. Accordingly, some model calculations were made to assess the

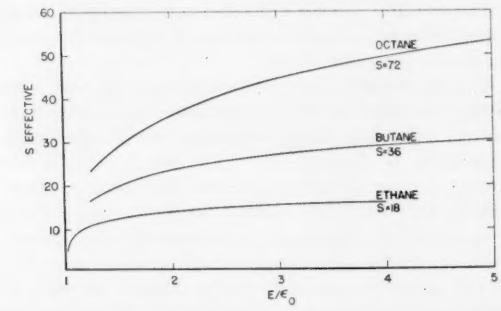

FIG. 2. Energy dependence of the "effective number of oscillators."

extent of the error. It was found that in the region of interest the approximation leads to enormous errors.

A Kassel-type formulation was used for the computations, with the number of oscillators taken equal to those in ethane, butane, and octane, respectively, and a frequency factor of 10^{13} sec^{-1}. The remaining parameter is the number of quanta representing the activation energy for unimolecular reaction. A value of 20 was chosen, roughly representative of the number of discrete vibrational levels in a Morse oscillator. Rate constants were calculated at various energies both with the classical approximation and with an exact combinational enumeration for the vibrational density of states. The results are shown in Fig. 1. For rates of mass spectrometric interest (10^5 sec^{-1}) the errors are very large.

Using now the approximate rate expression with the number of oscillators as a free parameter, the "effective number of oscillators" can be computed (see Fig. 2). They are energy dependent and in the mass spectrometer range they equal approximately one-half the number of physical oscillators. Further calculation on butane indicates that these results depend only moderately on the critical number of quanta representing the excitation energy.

In summary:

(1) The classical approximation is seriously in error, particularly near threshold.

(2) This error leads to a significant reduction in the number of "effective oscillators."

Further work on enumeration of vibrational levels is in progress.

[1] W. A. Chupka and J. Berkowitz, J. Chem. Phys. **32,** 1546 (1960).
[2] B. Steiner, C. F. Giese, and M. G. Inghram, J. Chem. Phys. **34,** 189 (1961).
[3] L. Friedman, F. A. Long, and M. Wolfsberg, J. Chem. Phys. **26,** 714 (1957).
[4] R. A. Marcus and O. K. Rice, J. Phys. & Colloid Chem. **55,** 894 (1951).
[5] L. S. Kassel, *Kinetics of Homogeneous Gas Reactions* (Chemical Catalog Company, New York, 1932).

ESR Detection of the Hydrolysis of Solid CaF_2†

JEROME SIERRO

Institute of Theoretical Physics, University of Geneva, Geneva, Switzerland

(Received February 21, 1961)

SEVERAL works[1–5] have shown that trivalent rare-earth ions are substituted for the bivalent calcium ions in CaF_2. The charge excess of the trivalent ion can be compensated by a fluorine ion located at an interstitial site. Feofilov[6] has pointed out another possibility for charge compensation; he admits that an O^{2-} ion can be substituted for a F^- ion near the trivalent ion. We have tried to make this charge compensation by means of the hydrolysis of CaF_2. This reaction on pure CaF_2 has been already studied by Bontinck.[7]

We have studied the hydrolysis of solid CaF_2 at high temperatures (900–1200°C) by means of the electron spin resonance (ESR) of trivalent gadolinium. We have used a synthetic single crystal doped with 0.01% gadolinium,[8] several natural crystals containing gadolinium as impurities, and crystalline powders doped by thermal diffusion. The ESR spectrum was measured with an X-band spectrometer.[3] The magnetic field was rotated in a (110) plane.

The observed spectra depended on the temperature and duration of the thermal treatment. At the beginning of the hydrolysis reaction, the cubic and tetragonal spectra decreased and several lines with trigonal symmetry appeared. After a 2 to 4 hr treatment, the cubic and tetragonal lines disappeared completely. During this process 28 lines of the trigonal spectrum decreased and disappeared. Thus we conclude that there are two different spectra with trigonal symmetry. After this initial stage of the reaction the remaining trigonal spectrum maintained its intensity. Furthermore a narrow isotropic line appeared and grew slowly.

We can explain the observed spectra as follows. Crystals of CaF_2 belong to the O_h^5 space group, and the structure may be regarded as a regular cubic array of fluorine ions with calcium ions at every other body center. Thus each gadolinium ion is at the center of a cube of eight fluorine ions. At the beginning of the hydrolysis reaction, water molecules dissociate at the crystal surface into H^+ and OH^- ions. Gaseous HF is formed and the OH^- ions take the place of the removed F^- ions. When an hydroxyl ion is substituted for a nearest neighbor of a Gd^{3+} ion, the previous symmetry of the crystalline field will be destroyed because of the electrical dipole of OH^-. Near a Gd^{3+} center, there are eight equal possible sites for OH^-, and as opposite sites are equivalent, there are four distinguishable magnetic centers. A detailed study of the 28 lines trigonal spectrum has shown that it arises from such Gd^{3+}-OH^- centers. If the thermal treatment is continued, the OH^- ions dissociate into O^{2-} and H^+ ions. The charge compensation of a Gd^{3+} is then achieved by an O^{2-} ion substituted for a neighboring F^- ion. There are again four distinguishable magnetic centers. Since O^{2-} and F^- have nearly the same ionic radius, the O^{2-} ions can easily diffuse in CaF_2 and compensate all the Gd^{3+} ions. This explains the complete disappearance of all other spectra previously present. When more O^{2-} ions than Gd^{3+} ions are diffused into the crystal, anion vacancies are formed. Electrons freed during the heat treatment are trapped at these F^- vacancies and form F centers. The immediate environment of a F^- vacancy consists of a regular tetrahedron of calcium ions with zero nuclear spin. The observed narrow isotropic line

with a g value of 1.991 ± 0.001 is consistent with this model.

Using an Hamiltonian of the form $g\,H\cdot S+V$, where V is the crystalline field, we have obtained the following zero-field splittings for the trigonal spectra

OH^-–Gd^{3+} spectrum, $E=0.465\pm0.005$ cm^{-1}

O^{2-}–Gd^{3+} spectrum, $E=1.97\pm0.02$ cm^{-1} .

When the static magnetic field H is rotated perpendicular to the axis of the trigonal crystalline field, the lines showed no angular variation. This fact is in agreement with the theory and allows one to observe the hydrolysis effects on powders, some lines being visible. The hydrolysis reaction is more rapid on powders than on single crystals, showing that the dissociation of the H_2O molecules into O^{2-} and $2H^+$ ions takes place at the contact surface, and that only O^{2-} diffuse into the crystal.

A similar study on SrF_2 and BaF_2 is undertaken and will be reported later. We wish to thank Dr. R. Lacroix for suggesting this study and for many helpful discussions.

† This work was supported by the Swiss National Foundation for the Scientific Research.

[1] E. Zintl and A. Udgard, Z. anorg. u. allgem. Chem. **240,** 150 (1939).
[2] B. Bleaney, P. M. Llewellyn, and D. A. Jones, Proc. Phys. Soc. (London) **A69,** 858 (1956).
[3] C. Ryter, Helv. Phys. Acta **30,** 353 (1957).
[4] J. M. Baker, B. Bleaney, and W. Hayes, Proc. Roy. Soc. (London) **A247,** 141 (1958).
[5] J. Sierro and R. Lacroix, Compt. rend. **250,** 2686 (1960).
[6] P. P. Feofilov, J. phys. radium **17,** 656 (1956).
[7] W. Bontinck, Physica **24,** 650 (1958).
[8] We are grateful to Dr. D. A. Jones of the University of Aberdeen for sending us this single crystal.

Electrical Conductivities of α- and β-Phthalocyanine

K. Wihksne and A. E. Newkirk

General Electric Research Laboratory, Schenectady, New York

(Received March 28, 1961)

THE electrical properties of phthalocyanines have aroused considerable interest since the initial work of Eley,[1] but all measurements appear to have been made on the β form except for a few by Eley and Parfitt[2] which indicated that the conductivity of the α form was approximately 10 times greater than the conductivity of the β form. This difference in conductivity is of interest because it may be ascribed to the influence of the differences in the molecular arrangement of the two forms. A more exact measure of the difference in conductivity is therefore desirable.

We have now observed (Fig. 1) that the electrical conductivity of the α form as conventionally prepared is more nearly 100 000 times greater than that of the

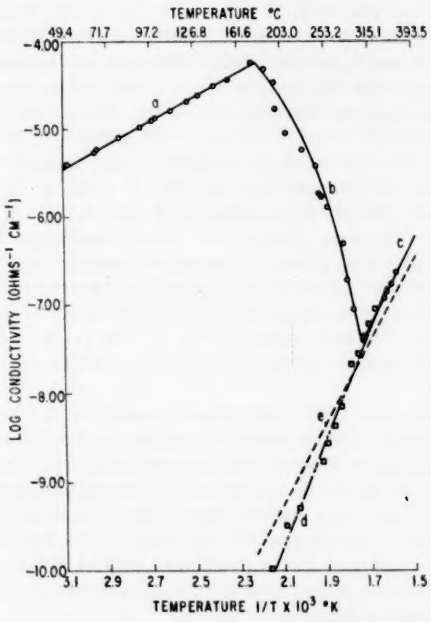

FIG. 1. Electrical conductivities of α- and β-phthalocyanine. Curve a: α-phthalocyanine at increasing temperature, b: transition region, c: increasing temperature past transition region, d: decreasing temperature, e: conductivity of a sample which was originally β.

β form at the transition temperature, and that the transformation from α to β may be followed electrically on heating. The reverse transformation does not occur on cooling, the sample remaining in the β form and having a conductivity similar to that of the β form measured directly.

The irreversibility of the transformation is in accord with the common observation that finely divided α-phthalocyanine transforms rapidly to β-phthalocyanine at room temperature in organic liquids used as paint vehicles and thinners.

The conductivities for the α- and β-phthalocyanine may be represented by the equation $\sigma=\sigma_0\exp(-E/kT)$ and the slopes of curves (a) and (e) (Fig. 1) yield values of the activation energy of 0.25 ev for α and 0.9 ev for β. Fielding and Gutman[3] obtained $E=0.86$ ev, as the mean value for single crystals of β-phthalocyanine. The large differences in conductivity and activation energy between the α and β forms are surprising, but cannot clearly be ascribed only to differences in molecular arrangement in view of a sharp electron spin resonance absorption observed in the α sample. However, the temperature dependence of the electron spin resonance absorption did not parallel the temperature dependence of the conductivity.

The β form was prepared from a commercial phthalocyanine by extraction with nitrobenzene and repeated

sublimation in nitrogen at 500–550°C and 4–5 mm Hg pressure. The crystals thus obtained showed no electron spin resonance absorption, and gave the reported infrared spectrum[4] and x-ray diffraction pattern.[5] The α form was prepared in the conventional manner, as follows: Purified β crystals were dissolved in reagent-grade concentrated sulfuric acid, precipitated by pouring into a large quantity of water, and thoroughly washed. The material thus obtained gave the reported infrared spectrum,[4] a characteristic x-ray diffraction pattern with very diffuse lines, and a strong, sharp electron spin resonance absorption line. The intensity of this line decreased on heating above 120°, but was independent of temperature below this. Analysis of the α sample by x-ray emission showed 0.003% Cl, <0.01% Fe, <0.01% Cu, and no other elements of atomic number greater than titanium (with a lower detection limit of 0.01 to 0.001%).

Electrical measurements were made on a pressed block of powder using a four-point probe method.[6] Both forms showed some reversible sensitivity to air and the measurements of Fig. 1 were made in flowing nitrogen. The conductivity of the α form was reversible with temperature up to at least 135°C, and that of the β form was reversible over the entire range shown.

We are indebted to Dr. C. M. Huggins and Dr. O. H. LeBlanc, Jr., for information about the electron spin resonance absorption of the two forms which they expect to publish in detail.

[1] D. D. Eley, Nature **162,** 819 (1948).
[2] D. D. Eley and G. D. Parfitt, Trans. Faraday Soc. **51,** 1529 (1955).
[3] P. E. Fielding and F. Gutman, J. Chem. Phys. **26,** 411 (1957).
[4] A. A. Ebert and H. B. Gottlieb, J. Am. Chem. Soc. **74,** 2806 (1952).
[5] F. W. Karasek and J. C. Decius, J. Am. Chem. Soc. **74,** 4716 (1952).
[6] C. M. Huggins, J. H. Lupinski, and O. H. LeBlanc, Jr. (unpublished).

Concerning the Feasibility of Nuclear Cooling with Palladium Hydride*

J. J. Fritz, H. J. Maria, and J. G. Aston

Cryogenic Laboratory, College of Chemistry and Physics, The Pennsylvania State University, University Park, Pennsylvania

(Received February 20, 1961)

ATTEMPTS to obtain nuclear cooling of protons in palladium hydride (formal composition Pd_2H) were frustrated by energy evolution in this system below 1°K. The negative results were not unexpected; details of the energy evolution are given below. The palladium hydride specimen, containing 0.2 mole of 99.999% palladium, was attached, as a bundle of No. 30 wires, to the copper "heat link" of an apparatus essentially the same as that used for nuclear demagnetization of copper,[1] and cooled by demagnetization

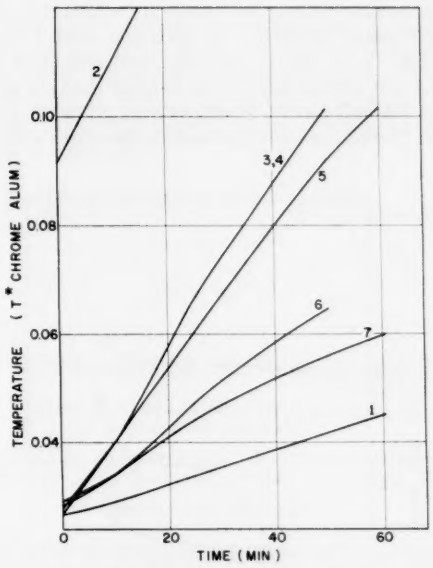

FIG. 1. Warming curves $4Pd_2H=PdH_4\cdot 7Pd$ (*: unannealed, **: partially annealed, ***: annealed): 1—Pd*, 2—Pd_2H*, 3—Pd_2H* (8/17/60), 4—Pd_2H* (9/2/60), 5—Pd_2H** (9/2/60), 6—Pd_2H*** 16 hr 20°–80° (11/17/60), 7—Pd_2H*** 3 days 20°–80° (12/3/60).

of chrome alum. Ten experiments were performed on metallic palladium and 25 on palladium hydride. After cooling below 1°K, the temperature of the alum was followed magnetically for 40 to 120 min. Some representative results are given in Figs. 1 and 2 which give the (magnetic) temperature of the alum and our estimate of the rate of energy input, respectively, as a function of time.

The metallic specimen (curve 1) warmed at about 0.0003° (C)/min, corresponding to a total heat influx of 10 to 20 erg min^{-1}. The warming rate for the palladium hydride specimens was from 3 to 60 times greater, decreasing with the extent of "annealing" of the specimen below 77°K. Curves 3 and 4 represent the warming of the specimens when cooled to 0.03° (C) after rapid cooling from 77° to 4.2°K ("unannealed"). Curve 5 was obtained on the same day as Curve 4, after an additional 6 hr below 4.2°K. Curves 6 and 7 were obtained for a specimen "annealed" by slow cooling from 77° to 20°K.

The annealing procedure reduced the rate of energy influx almost to that obtained with metallic palladium and with copper, but attempts to obtain nuclear demagnetization were uniformly unsuccessful. This indicates that the nuclear spin system must be involved in the energy production, since the amounts of energy transmitted to the lattice in (6) and (7) should not have prevented nuclear cooling.

We believe that the energy evolution is due to transi-

tions between nuclear spin states of the bound hydrogen in palladium hydride.[2] A specimen cooled rapidly through the region of the rotational transition (near 50°K) will contain units in states other than the ground state, and will give off energy as these go to the ground state. The rate of energy evolution decreases with time

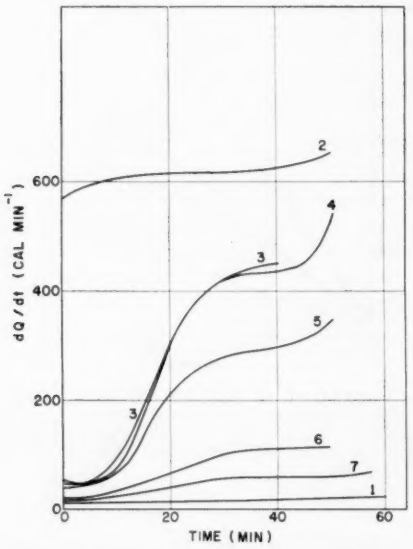

FIG. 2. Rate of energy production (*:unannealed, **: partially annealed, ***: annealed): 1—Pd*, 2—Pd_2H*, 3—Pd_2H* (8/17/60), 4—Pd_2H* (9/2/60), 5—Pd_2H** (9/2/60), 6—Pd_2H*** 16 hr 20°–80° (11/17/60), 7—Pd_2H*** 3 days 20°–80° (12/3/60).

as the conversion occurs. "Annealing" above 20°K permits better approach to equilibrium on the cooling and decreases the rate of energy evolution below 1°K.

Correlation of the rates of energy evolution indicate that the conversion process is probably second order, with a rate constant independent of temperature above 0.1°K. Analysis of the data on this basis indicates that the equilibrium at 4.2°K probably corresponds to about 99% conversion to the ground state, with several times as large a population of higher states "frozen into" unannealed specimens.

An "induction period" of slow energy evolution was observed below, but not above 0.1°K, indicating that the rate constant may drop below this temperature. Further experiments are being carried out on the conversion process. At present it is difficult to imagine any process other than spin conversion proceeding at an appreciable rate below 0.05°K.

* Communication No. 118.

[1] J. J. Fritz, H. J. Maria, and J. G. Aston, J. Chem. Phys. **34,** 344 (1961).

[2] D. M. Nace and J. G. Aston, J. Am. Chem. Soc. **79,** 3619 (1959).

Comments and Errata

Pre-Exponential Factor of Temperature in the Diffusion Equation

R. H. DOREMUS

General Electric Research Laboratory, Schenectady, New York

(Received March 29, 1961)

SWETS, Lee, and Frank[1] described their results on the diffusion of helium in fused silica by two intersecting straight lines on a log diffusion coefficient D versus reciprocal temperature plot. However, when the logarithm of the ratio D/T, where T is the absolute

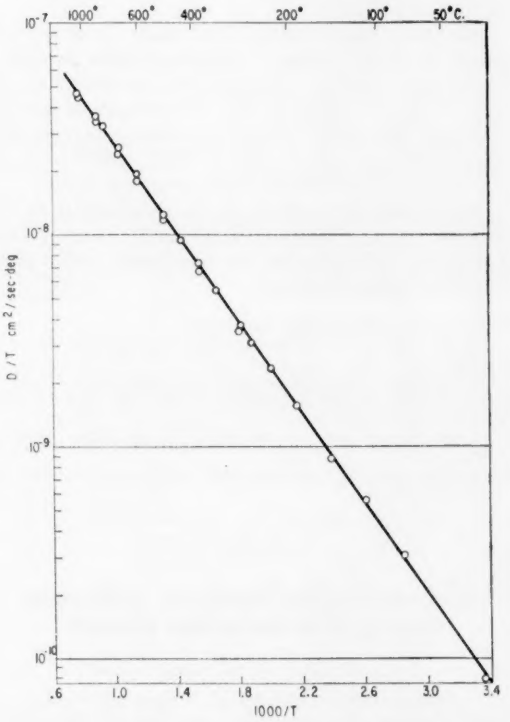

FIG. 1.

temperature, is plotted against $1/T$, the data fit on a single straight line over the entire temperature range examined, as shown in Fig. 1. This line follows the equation

$$D=2.7(10)^{-7}T\exp-(4810/RT),$$

in which R is the gas constant.

Eyring and his co-workers[2] have derived an equation for diffusion in which a pre-exponential factor of temperature appears. However, Zener[3] has criticized this

expression because the free energy of activation in it is not a true free energy, since it refers to a ratio of partition functions having a different number of degrees of freedom. Zener[3] derived an equation similar to that of Eyring, but not containing a pre-exponential factor of temperature. Recently from quite different considerations Rice[4] has derived an equation for diffusion that does not have a pre-exponential factor of temperature.

The only other diffusion data known to the author of sufficient accuracy and over a wide enough temperature range to check the pre-exponential factor of temperature are on the diffusion of carbon in α-iron.[5] In this case it appears that there is not a factor of T in the pre-exponential. However these data were taken in two different temperature ranges, and those at higher temperatures were not particularly accurate.

It is not clear that the data of Swets *et al.* confirm the assumptions and derivation of Eyring, but any general theory for diffusion must explain the presence of the pre-exponential factor of temperature in the results of Swets, Lee, and Frank. A discussion of the application of theories of diffusion to other results on diffusion in glasses will appear shortly in a review article.[6]

[1] D. E. Swets, R. W. Lee, and R. C. Frank, J. Chem. Phys. **34,** 17 (1961).
[2] S. Glasstone, K. J. Laidler, and H. Eyring, *The Theory of Rate Processes* (McGraw-Hill Book Company, Inc., New York, 1941), p. 523 ff.
[3] C. Zener in *Imperfections in Nearly Perfect Crystals* (John Wiley & Sons, Inc., New York, 1952), p. 289.
[4] S. A. Rice, Phys. Rev. **112,** 804 (1958).
[5] C. Wert, Phys. Rev. **79,** 601 (1950).
[6] R. H. Doremus, "Diffusion in noncrystalline silicates" in *Modern Aspects of the Vitreous State* (to be published by Butterworths Scientific Publications, Ltd., London), Vol. II.

Comments on Dr. Doremus' Letter

D. E. Swets, R. W. Lee, and R. C. Frank

General Motors Research Laboratories, Warren, Michigan

(Received April 7, 1961)

We appreciate the interesting observation of Doremus and agree that it is possible to fit our data with an equation containing a pre-exponential temperature factor. We had previously checked for a pre-exponential factor of $T^{\frac{1}{2}}$ in the permeation equation, as was suggested in the work of Jones.[1] It was noted that our permeability data could be fitted by an equation having a pre-exponential factor of $T^{\frac{1}{2}}$ but our diffusion coefficients could not. If it is assumed that the pre-exponential factor for the diffusion coefficients is T and for the permeabilities is $T^{\frac{1}{2}}$, this would imply a factor of $T^{-\frac{1}{2}}$ in the solubility equation, assuming $P=DS$. Thus three different pre-exponential factors would be required, making theoretical interpretation more complicated.

It would seem that either our original interpretation[2] or the one suggested by Doremus could be postulated on the basis of the present data; each interpretation has some advantages. Perhaps further studies at lower temperatures are needed before a proper decision between the two can be made.

[1] W. M. Jones, J. Am. Chem. Soc. **75,** 3093 (1953).
[2] D. E. Swets, R. W. Lee, and R. C. Frank, J. Chem. Phys. **34,** 17 (1961).

On the Structure of the Isomers of N_2F_2

Raymond Ettinger, Frederic A. Johnson, and Charles B. Colburn

Rohm and Haas Company, Redstone Arsenal Research Division, Huntsville, Alabama

(Received March 2, 1961)

The infrared spectra and structure of the isomers of difluorodiazine (N_2F_2) were the subject of a recent paper by Sanborn.[1]

First, it should be pointed out that the isomers have been characterized in the past not only by their reactivity towards mercury but also by their (1) vapor pressures, (2) boiling points, (3) heats of vaporization, (4) critical temperatures, (5) melting points, (6) mass spectral cracking patterns, (7) NMR spectra, (8) infrared spectra, (9) heat of isomerization, and (10) reactivity not only with mercury but also with glass.[2]

Second, we agree with Sanborn that the less active (lower boiling -111.4°C) isomer[1,2] is described by the *trans* configuration, although our acceptance of his infrared spectral assignment of *trans*-1,2-difluorodiazine is not unqualified. For example, he derives the inactive fundamental ν_2 (N=N stretch, A_g 1636 cm^{-1}) from a single observed combination frequency at 1996 cm^{-1} with the assignment $\nu_2+\nu_6$ (torsion, Au 360 cm^{-1}). Couldn't this combination frequency have equally well arisen from ν_2 (1575 cm^{-1})$+\nu_5$ (NNF asym. bend, Bu 421 cm^{-1}); or, for that matter from ν_1 (NF sym. stretch, Ag 1010 cm^{-1})$+\nu_4$ (NF asym. stretch, Bu 989 cm^{-1})?

We do however believe that the structure of the more active (higher boiling, -105.7°C) isomer is still very much in doubt for the following reasons:

(1) The scanty chemical evidence[1-3] available shows only that the two isomers are quite different in their reactivity. No reaction is known in which either the

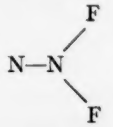

or the FNNF system is retained (other than the reversible isomerization of the isomers[2])

(2) The dipole moment of the active (higher boiling) isomer has not been measured. Since no lines were found in a search of the microwave spectrum, Professor R. J. Myers[1] concluded that the dipole moment must be less than 0.1 debye units. The *cis*-isomer is expected to have a small moment similar to that found for NF_3 and N_2F_4. The unsymmetrical 1,1 isomer, however, will have separated partial charges which must balance in a rather fortuitous way in order for the molecule to have such a small dipole moment.

(3) The mass spectral patterns given by Sanborn show an NF_2^+ peak of less than 0.01% (relative to the N_2F^+ peak as 100%). We have confirmed the intensity of this peak as less than 0.07% using a more sensitive instrument than was available to us previously.[2] This peak (m/e 52 NF_2^+) is expected to be weaker than the others due to the difficulty of breaking the $N^+{=}N^-$ bond as Sanborn[1] argues, but its absence at the 0.01% level is surprising in view of our finding that the isoelectronic COF_2 has a CF_2^+ peak which is 2.5% of the COF^+ peak.

(4) Sanborn's[1] infrared-spectral evidence in favor of 1,1-difluorodiazine as the structure for the high-boiling isomer is also open to question. His crucial observation is that only infrared bands with *P* and *R* branches are found in the N=N double-bond stretching region. Sanborn[1] states that the N=N stretch vibration of the *cis*-isomer should show appreciable *PQR* structure[4] because the dipole moment change is along the least moment of inertia, which is parallel to the NN bond. However, the NN bond stretching of the *cis*-isomer is of symmetry species A_1, and, this being a totally symmetric representation, the dipole-moment change must lie along the C_2 axis; the latter is the *x* axis in Sanborn's coordinate system, and the direction of the intermediate moment of inertia. Hence, the double-bond stretch vibration of the *cis*-isomer would be expected to exhibit *PR* structure just as in the model of 1,1-difluorodiazine.[1] Sanborn states that the observed NF stretch vibrations could be accommodated "nicely" with the *cis*-structure.

(5) W. D. Phillips[5] has recently investigated the ^{14}N NMR spectra of the isomers of N_2F_2 and in both the high- and low-boiling isomers found only one nitrogen resonance. While this is negative evidence one would not be surprised to find two nitrogen resonances in a structure such as 1,1-difluorodiazine

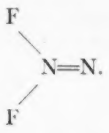

The purpose of this note is simply to point out that the structure of the high-boiling isomer of difluorodiazine has not been established and that further work on this problem is in order.

The authors wish to express their thanks to Al Kennedy for obtaining the mass spectral cracking pattern of COF_2 referred to above. We also wish to acknowledge several helpful discussions on this subject with Dr. W. D. Phillips. This work was done under the sponsorship of the U. S. Army Ordnance Corps.

[1] R. H. Sanborn, J. Chem. Phys. **33,** 1855 (1960).
[2] C. B. Colburn, F. A. Johnson, A. Kennedy, K. McCallum, L. C. Metzger, and C. O. Parker, J. Am. Chem. Soc. **81,** 6397 (1959).
[3] J. W. Fraser, J. Inorg. & Nuclear Chem. **11,** 166 (1959).
[4] R. M. Badger and L. R. Zumwalt, J. Chem. Phys. **6,** 711 (1938).
[5] W. D. Phillips (private communication to one of the authors, C. B. C.).

Comments on "On the Structure of the Isomers of N_2F_2"†

RUSSELL H. SANBORN

University of California, Lawrence Radiation Laboratory, Livermore, California

(Received March 22, 1961)

ETTINGER, Johnson, and Colburn[1] in the preceding paper are quite correct in their point (4) that the dipole moment change in the NN double-bond stretch in a *cis*-isomer of N_2F_2 is along the axis of the intermediate moment of inertia. The shapes of the infrared bands no longer rule out a *cis*-isomer.[2] However, we prefer to defer discussion of their other points until more complete physical and chemical information on the N_2F_2 systems is available.

When the vibrational sum rule of Mizushima, Shimanouchi, Nakagawa, and Miyake[3] for rotational isomers is applied to the N_2F_2 systems, the conclusion is reached that the infrared band at 737 cm^{-1} in active N_2F_2 must be a fundamental vibration. Since it can only be a bending fundamental, it is completely out of position for a *cis*-isomer, but fits perfectly for 1,1-difluorodiazine.

To help clarify the N_2F_2 systems, we intend to measure the Raman spectra and to conduct spectral investigations of the isomers in matrix isolation at liquid-helium temperatures.

† This work was performed under the auspices of the U. S. Atomic Energy Commission.
[1] R. Ettinger, F. A. Johnson, and C. B. Colburn, J. Chem. Phys. **34,** 2187 (1961), preceding paper.
[2] R. H. Sanborn, J. Chem. Phys. **33,** 1855 (1960).
[3] S. Mizushima, T. Shimanouchi, I. Nakagawa, and A. Miyake, J. Chem. Phys. **21,** 215 (1953).

Erratum: Lattice Energies of the Alkali Halides and the Electron Affinities of the Halogens

[J. Chem. Phys. **31**, 1646 (1959); **33**, 1579 (1960)]

DANIEL CUBICCIOTTI

Stanford Research Institute, Menlo Park, California

A MISTAKE was made in the calculation of the zero-point energies and brought to the author's attention by Professor E. A. Guggenheim. Since there are two moles of ions in a formula weight of an alkali halide, the zero-point energy should be just twice as great as the value calculated by Eq. (14). Correcting that mistake gives the following values for the lattice energies (kcal/mole) (see Table I).

TABLE I

	F	Cl	Br	I
Li	246.8	202.0	190.7	176.8
Na	218.7	185.9	176.7	165.4
K	194.4	169.4	162.4	153.0
Rb	185.9	164.0	157.5	148.7
Cs	178.7	155.9	151.1	143.7

Some revisions of the heats of reaction used in the calculation of the electron affinities have been brought to the author's attention by Professor Leo Brewer. The revised values are given in Appendix 7 (second edition) of the work by Lewis and Randall.[1] In particular: (a) the new heats of formation used for LiF and LiCl were 145.7 and 96.0; (b) −0.5 was added to all Rb and −3.4 to all Cs heats of formation; (c) the new heats of sublimation used for Rb and Cs were 19.5 and 18.7; and (d) the new heats of dissociation used for Cl_2 and Br_2 were 28.94 and 26.76.

TABLE II

	F	Cl	Br	I
Li	79.1	84.5	81.6	75.7
Na	79.7	85.1	80.2	73.3
K	79.8	85.1	79.6	72.5
Rb	80.1	84.2	78.8	71.9
Cs	78.6	88.7	82.3	74.6
Average	79.5	85.5	80.5	73.6

The revised values for the electron affinities of the halogens are given in Table II.

A mistake was made in copying the values of l (Table III, column 5) from the computer sheets. The values from KF to the bottom of the column should have the first *one* deleted and the decimal moved one digit to the right. The correct value of l was used in the calculation.

[1] G. N. Lewis and M. Randall, *Thermodynamics*, revised by K. S. Pitzer and L. Brewer (McGraw-Hill Book Company, Inc., New York, 1961).

Notes

Separation of the Isotopes HT and ortho-D_2 by Adsorption at Low Temperatures*

ANTHONY KATORSKI, J. G. EBERHART, AND DAVID WHITE

Contribution of the Cryogenic Laboratory, Department of Chemistry, The Ohio State University, Columbus, Ohio

(Received February 6, 1961)

RECENTLY, a theory[1] has been developed to account for the separation of homonuclear isotopic diatomics by adsorption at low temperatures. We have now extended this theory to include heteronuclear isotopic species. A detailed description of the theory and calculations will be presented shortly. In this note the predictions of the theory concerning the sepration of the two isotopes of the same mass HT and ortho-D_2 are presented.

It has been demonstrated by Bigeleisen and Kerr[2] that the vapor pressures of the two isotopes are not identical. In fact, HT is more volatile than D_2 at a given temperature. This has also been discussed theoretically by A. Babloyantz.[3] One should expect a similar phenomenon to occur on adsorption of these two isotopes at low temperatures. This provides a method for the separation of these species.

The separation factor S is defined by the expression

$$S=\left(\frac{N_{D_2}}{N_{HT}}\right)^{ads}\times\left(\frac{N_{HT}}{N_{D_2}}\right)_{gas}$$

$$=\left(\frac{Q_{D_2}}{Q_{HT}}\right)_{ads}\times\left(\frac{Q_{HT}}{Q_{D_2}}\right)_{gas}\approx\left(\frac{Q^1{}_{D_2}}{Q^1{}_{HT}}\right)_{ads}, \quad (1)$$

where N and Q refer to the mole fraction and partition function, respectively, of the isotopes HT and ortho-D_2 and the subscripts "ads" and "gas" refer to the adsorbed phase and gaeous phase, respectively. If the partition functions of both the adsorbed phase and gas phase are assumed separable, at least so far as electronic energy, intramolecular vibration, and translation[4] are concerned, then because the masses of the isotopes are

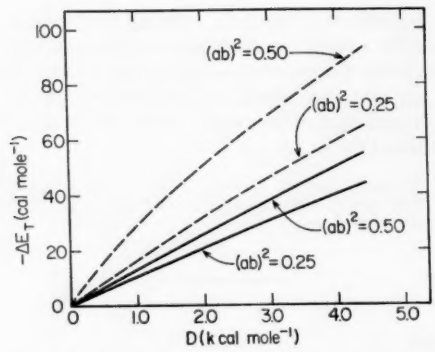

FIG. 1. Solid line, variation of difference in zero-point energy between o-D_2 and HT, as a function of surface barrier. Dotted line, see text.

the same, the separation factor reduces to a simple ratio involving Q^1's for the adsorbed phase, where Q^1 refers to the partition function for rotation of the adsorbed molecule and vibration normal to the surface. This expression is valid if only the ground states in both the gas and adsorbed phases are considered. This is a reasonable approximation to the physical situation at low temperatures.

In order to calculate the ground state energy for the adsorbed heteronuclear HT, we have used the same model as outlined in reference 1 Sec. IV. (The ground state for ortho-D_2 is given in this reference.) Each atom of the adsorbed molecule is assumed to interact with the plane surface on accordance with a Morse potential. We have assumed as before[1] that the rotations of the molecule and vibrations normal to the surface are coupled, and we have used the same variation method to separate the variables in the Schrödinger equation. The potential for the interaction is again represented as an expansion in a power series of $\eta = \cos\theta$; however, unlike the homonuclear case, this expansion now contains both even and odd powers of η because of lack of symmetry. This complicates the solution of the resulting two differential equations; however, satisfactory solutions have been obtained with the aid of an IBM 704 computer and graphical interpolations. The results are shown in Fig. 1. The difference in zero-point energies, ΔE_T, between ortho-D_2 and HT ($E_{D_2} - E_{HT}$)[5] are plotted as a function of D and $(ab)^2$. D and "a" are constants of the Morse potential and "b" is one-half the internuclear distance. It is evident from the figure that adsorbed HT is more volatile than adsorbed D_2 as in the case of the liquids. The dotted line in Fig. 1 represents the difference in zero point energies between ortho-D_2 and HT, if the odd powers of η in the potential function are not included in the HT calculations. This assumes that the only difference between HT and D_2 is the moment of inertia. The difference between the dotted line and solid line for a given $(ab)^2$ gives an estimate of the effect of asymmetry. It is of interest to note that the effect of asymmetry is to reduce the difference in zero-point energies.

In order to calculate the isotope separation factor it is necessary to assume a value for D. We have chosen a value which gives a zero-point energy of D_2 equal to 2.0 kcal/mole. This is approximately the experimental value for the heat of adsorption on alumina.[6] The separation factors at 20°K are as follows: $(ab)^2 = 0.25$ $S = 1.6$; $(ab)^2 = 0.50$ $S = 1.9$.

Another interesting prediction of the theory is that HD cannot be easily separated from hydrogen which has appreciable ortho content. This is in accord with the chromatographic studies by a number of investigators.[7]

We are indebted to Professor E. N. Lassettre for helpful discussions and comments, and Dr. J. Bigeleisen who suggested that the separation of the isotopes might be significant.

* This work is supported by the Division of Research, U. S. Atomic Energy Commission.

[1] D. White and E. N. Lassettre, J. Chem. Phys. **32,** 72 (1960).
[2] J. Bigeleisen and E. C. Kerr, J. Chem. Phys. **23,** 2442 (1955).
[3] A. Babloyantz, J. Mol. Phys. **2,** 39 (1958).
[4] In the adsorbed phase the molecule may not undergo translations in the plane of the surface if the adsorption is localized. It is, however, not necessary to make any assumption as to whether the adsorbed layer is localized or mobile if the partition function is separable, since center of mass motions for the two isotopes will cancel.
[5] The uncertainty in ΔE is of the order of ± 4–5 cal/mole.
[6] P. Radhakrishna, W. J. Haubach, and D. White (unpublished results of the laboratory).
[7] W. R. Moore and H. R. Ward, J. Phys. Chem. **64,** 832 (1960); W. A. Van Hook and P. H. Emmett, *ibid.* 673 (1960).

Method for Distinguishing between Overlapping Transitions in Electronic Absorption Spectra, with Application to Azulene

W. W. ROBERTSON AND A. D. KING, JR.

Department of Physics, The University of Texas, Austin 12, Texas

(Received February 13, 1961)

IN electronic absorption spectra it is sometimes difficult to tell whether a given region of absorption is the result of one or of more than one transition. However, if the overlapping transitions have different oscillator strengths, or for polar absorbers, if the dipole moments of the excited states are not the same, then the different responses of the transitions to an environmental change can be used to distinguish between them.

For nonhydrogen bonding molecules the frequency shift of a polar absorber in a polar solvent can be expressed in terms of the following types of interaction:

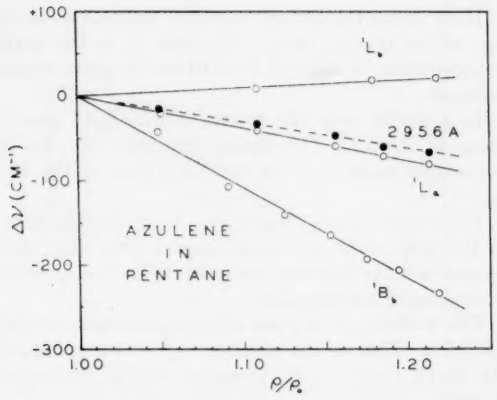

FIG. 1. Frequency shifts of four transitions of azulene with relative density of the *n*-pentane solvent.

induced dipole-induced dipole, solute dipole-solvent induced dipole, dipole-dipole, and solvent dipole-solute induced dipole.[1] The first of these is present whether or not polar molecules are involved and is measured in terms of the transition oscillator strength and the solvent index of refraction. The second type of interaction depends upon the change in dipole moment of the absorber upon excitation and upon the solvent index. The third depends upon the change in absorber dipole moment, solvent index and dielectric constant. The fourth type is usually negligibly small.[1] Thus, for transitions of different oscillator strengths or for transitions to states with different dipole moments, varying frequency shifts will result from a change in the solvent index or dielectric constant.

These changes in solvent properties may be produced stepwise by a change in the solvent or continuously by a change in either the temperature of or the pressure upon the solvent. A change in solvent occasionally leads to a broadening of bands and a loss of structure that obscures the frequency shift. A change in temperature not only produces a shift due to a density change but also a change in band shape. As a result an apparent shift occurs that is not correlated with transistor strength or dipole moment changes. Density changes produced by hydrostatic pressure are perhaps best for the present purpose, but, of course, necessitate the availability of pressure equipment. Frequency shifts might also be observed in going from vapor to solution, but the large shifts and the changes in band appearance may make the correlation of the spectra uncertain.

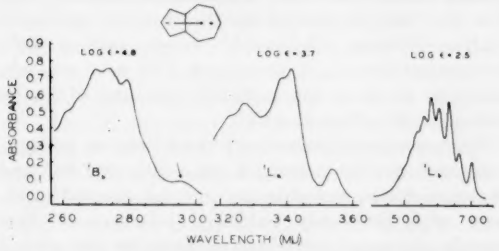

FIG. 2. The four transitions of azulene as recorded on a Beckman DK spectrophotometer. With a 1-cm cell, the concentrations of azulene in pentane were 1.2×10^{-5}, 1.5×10^{-4}, and 1.9×10^{-3} *M*, respectively, for the ^1B_b, ^1L_a, and ^1L_b transitions. The arrow indicates the transition in question.

In the present example, Fig. 1 shows the frequency shifts as a function of solvent density of three distinct transitions in azulene. These are labeled in Fig. 2 as ^1L_b, ^1L_a, and ^1B_b, in Platt's notation. It is observed that the greater slopes are associated with the larger extinction coefficients, as has been shown previously in a number of examples.[2] The relatively weak band at 2956 A has been tentatively assigned by Pariser,[3] on the basis of a calculation, to a transition different from the ^1B_b. If it were a part of the ^1B_b transition, its rate of frequency shift with density (or index) would be the same as for any other band in the transition. However, since its rate of frequency shift, as seen in Fig. 1, is much smaller than that of the ^1B_b, its existence as a separate transition is experimentally established.

[1] E. G. McRae, J. Phys. Chem. **61,** 562 (1957).
[2] W. W. Robertson, O. E. Weigang, Jr., and F. A. Matsen, J. Mol. Spectroscopy **1,** 1 (1957).
[3] R. Pariser, J. Chem. Phys. **25,** 1112 (1956).

Distribution of Silver Ions in Melt-Grown Alkali Halides

W. GOMES

Laboratorium voor Kristalkunde en Studie van Vaste Stoffen, Rozier 6, Ghent, Belgium

(Received February 20, 1961)

ONE of the techniques, used in this laboratory for the decoration of dislocations in alkali halides, consisted in treating crystals doped with silver chloride in a stream of hydrogen at high temperature.[1] We are now studying this reaction in some detail in order to establish the kinetics. Large single crystals are grown in this laboratory by the Kyropoulos method; the silver chloride is added to the melt. Their formula is $Na_{1-\delta}Ag_\delta Cl$, respectively, $K_{1-\delta}Ag_\delta Cl$. For this work it was necessary to determine the distribution of silver ions in such crystals and in this note we comment the results obtained.

At each moment the concentration of silver ions, incorporated in the growing crystal, is determined by a distribution equilibrium. When the concentrations of admixture in the crystal and in the melt at the same stage of growth are represented, respectively, by C_c and C_m the distribution coefficient A is defined by $A=C_c/C_m$. The A is dependent on the host crystal, the

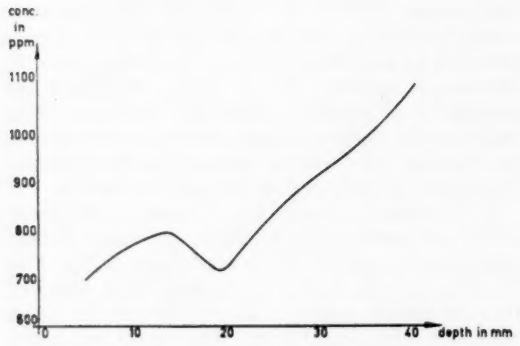

FIG. 1. Typical distribution curve.

admixture, the temperature gradient, the rate of growth, and the crystallographic direction.

In this case, this value is smaller than 1. Thus, the concentration of admixture in the melt rises during growth, so that it must increase in the crystal with depth.

Several authors[2,3] assuming A constant, calculated theoretically the distribution in function of depth. The obtained results were confirmed by the experiments of McFee[2] on the distribution of K^+ and Cu^{++} in NaCl crystals, grown by the Bridgman method. We determined the concentration of Ag^+ in $K_{1-\delta}Ag_\delta Cl$ crystals as a function of depth by polarographic analysis. The samples were dissolved (1g/10 ml) in $1M$ NH_3 solution. The KCl from the crystal served as indifferent electrolyte. Sodium sulphite was added in order to remove oxygen. A Radiometer polarograph PO4-c with dropping mercury electrode, was used for the determinations. As the Ag^+ wave has no residual current, the average limiting diffusion current i_d was measured at constant voltage [$d-0.6$v vs saturated calomel electronic (SCE)] as recommended in such cases by several authors.[4,5] Correction was made for the blank.

The value of k in the relation $i_d = k \cdot c$ (c = concentration in mole/liter) was determined from a series of standard solutions. A mean value of $k = 3.82 \cdot 10^3$ at 25°C was found. The procentual error was 1.3% for the range of concentration from $2 \cdot 10^{-5}M$ to $5 \cdot 10^{-3}M$ and 0.75% from $10^{-4}M$ to $5 \cdot 10^{-3}M$.

The $K_{1-\delta}Ag_\delta Cl$ crystals (diameter$\simeq$10 cm, height$\simeq$ 6.5 cm) under investigation had been grown from a melt, containing 2% Ag^+ (weight %). The crystals were pulled up at regular intervals in order to obtain a constant growth rate. The lower part ($\simeq$2 cm) of the crystals, being opaque on account of the presence of AgCl particles, was not analyzed.

The results are reproducible but do not obey theory. A typical distribution curve is shown in Fig. 1.

Anomalies can possibly be explained in terms of variation in temperature gradient during growth by the Kyropoulos method.

Here A can be derived from the value of C_c in the top of the crystal, for in that case C_m is the initial concentration. A value of $A = 0.04$ for the given system is found.

In a similar way the system NaCl+AgCl gives a value of $A = 0.22$. This means that Ag^+ ions are incorporated more easily in the NaCl than in the KCl lattice.

This result is rather surprising. From considerations of the ionic radii one should expect that silver ions should be taken up more easily by KCl. This question is now under investigation.

This work is part of a research program sponsored by I.R.S.I.A. (Brussels) to which we express our gratitude. We thank Professor W. Dekeyser for his continuous interest.

[1] W. Van der Vorst and W. Dekeyser, Phil. Mag. **1**, 882 (1956).
[2] R. H. McFee, J. Chem. Phys. **15**, 856 (1947).
[3] G. Schreiber and R. Schubert, Z. physik. Chem. **206**, 102 (1956).
[4] I. Israël and A. Vromen, Anal. Chem. **31**, 1470 (1959).
[5] G. C. B. Cave and D. N. Hume, Anal. Chem. **24**, 588 (1952).

Some Structural Data for Cubic Metaboric Acid

J. L. PARSONS, A. H. SILVER, AND M. E. MILBERG

Scientific Laboratory, Ford Motor Company, Dearborn, Michigan

(Received February 23, 1961)

As part of a study of boron oxide glasses and related crystalline materials, the stable cubic phase of metaboric acid, HBO_2(I), was prepared by a method similar to one first reported by Kracek, Morey, and Merwin,[1] and more recently by Kilday and Prosen.[2] Minor variations in preparative procedure yielded HBO_2(I) either in the form of brilliant rhombic dodecahedra up to about 1 mm in diam which were very slowly attacked by water at room temperature, or in the form of cubes which were less resistant to hydrolysis.

The product was identified by x-ray diffraction and density measurements, and by its chemical composition. The last was determined by the titration method,[1,2] analyses yielding 79.43±0.15 weight percent B_2O_3 (theoretical 79.45). A density of 2.49 g/cc was obtained by the float-sink method in mixtures of diiodomethane and xylene at 25°C.

Weissenberg and precession x-ray diffraction patterns confirmed that the material is cubic with $a = 8.86$A and 24 stoichiometric molecules per unit cell, in good agreement with previously published information.[1] Systematic absences were observed only for $h00$ with h odd. Since the Laue symmetry is $m3m$, the probable space group is O^2–$P4_232$. It should be noted that only a few very weak reflections of the type hhl with l odd appeared on the diffraction patterns. Had they been

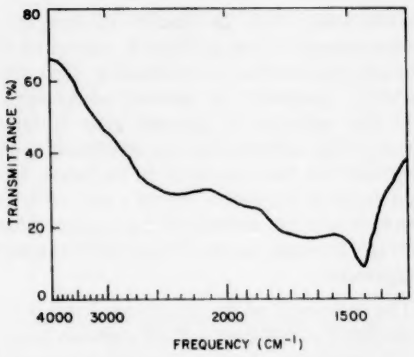

FIG. 1. The infrared spectrum of cubic metaboric acid. The spectrum is compounded from measurements made with Nujol and hexachlorobutadiene mulls.

absent, the probable space groups would have been T_d^4–$P\bar{4}3n$ and O_h^3–$Pm3n$.

In view of the high density, it is not surprising to find evidence for quite short hydrogen bonds. Broad absorption maxima have been observed in the 2800–1500 cm^{-1} region of the infrared absorption spectra of compounds which have hydroxyl groups involved in very strong hydrogen bonds.[3] As shown in Fig. 1, this characteristic absorption pattern for the strong hydrogen bond appears in the infrared spectrum of cubic metaboric acid, along with the complete absence of absorption maxima above 3000 cm^{-1} where OH absorptions are usually found. Correlations have been made indicating a linear relationship between the shift from the normal OH stretching frequency and the O—H—O distance in hydrogen bonded crystals.[4,5] Using the correlation data in reference 4 and $\Delta\nu\simeq1500$ cm^{-1} for the very broad OH absorption in the spectrum of HBO_2(I), the indicated O—H—O distance is approximately 2.5 A. Several attempts were made to crystallize DBO_2(I) in order to verify the assignment of the absorptions in the 2800–1500 cm^{-1} region to O—H vibrations, but only monoclinic DBO_2 was obtained. This would appear to be a manifestation of the hydrogen-deuterium isotope effect in crystals, similar to that experienced by Ubbelohde with KD_2PO_4.[6]

The nuclear magnetic resonances of both B^{11} and H^1 were observed in the polycrystalline material with a Pound-Watkins-type spectrometer at room temperature. The B^{11} resonance was observed at Larmor frequencies of 22.6, 14.2, 10.6, and 5.0 Mc/sec. In all cases a single, symmetric line was observed. The width of the line, measured by the separation of the extrema in the derivative of the absorption, is 10 kc/sec and independent of magnetic field. This line is interpreted as the $m=\frac{1}{2}\leftrightarrow-\frac{1}{2}$ transition of the B^{11} nuclei. An electric quadrupole interaction will affect this transition in second order[7] and an upper limit on the quadrupole coupling may be estimated from this fact. From Eq. (7) of reference 7, $eq\,Q)<0.7$ Mc/sec, where the Larmor frequency, ν_0, is taken as 5.0 Mc/sec and $\nu_{HF}-\nu_0=5$ kc/sec. This result should be compared with that in the other boric acids[8] and the boron oxide glasses.[7,9] The presence of a single, symmetric boron resonance implies that all boron atoms in HBO_2(I) are tetrahedrally coordinated. This is based on the tacit assumption that the covalent nature of the B—O bonds does not change appreciably from one acid to the next. On the same assumption, however, it is also conceivable that the boron atoms are bonded to three oxygen atoms such that the O—B—O angle is much less than 120°. By comparison with the other acids and the glasses, it is concluded that there are no planar BO_3 groups in cubic HBO_2. Since only BO_3 triangles are present in the low-density (1.784 g/cc) orthorhombic form[10] HBO_2(III), and both triangles and BO_4 tetrahedra in the intermediate density (2.045 g/cc) monoclinic form[11] HBO_2(II), it is reasonable that all the boron atoms in the high-density cubic form should be tetrahedrally coordinated.

The nuclear resonance of H^1 was observed at 19.9 Mc/sec. It is 10 gauss wide between the derivative extrema and has only the slightest indication of a splitting due to H^1–H^1 spin interaction. The linewidth is comparable to that observed in orthoboric[8,12] and the other metaboric acids.[13]

[1] F. C. Kracek, G. W. Morey, and H. E. Merwin, Am. J. Sci. **35A,** 143 (1938).
[2] M. V. Kilday and E. J. Prosen, J. Am. Chem. Soc. **82,** 5508 (1960).
[3] J. T. Braunholtz, G. E. Hall, F. G. Mann, and N. Sheppard, J. Chem. Soc. **1959,** 868.
[4] G. C. Pimentel and C. H. Sederholm, J. Chem. Phys. **24,** 639 (1956).
[5] R. C. Lord and R. E. Merrifield, J. Chem. Phys. **21,** 166 (1953).
[6] A. R. Ubbelohde, Proc. Roy. Soc. (London) **173A,** 417 (1939).
[7] A. H. Silver and P. J. Bray, J. Chem. Phys. **29,** 984 (1958).
[8] A. H. Silver, J. Chem. Phys. **32,** 959 (1960).
[9] M. E. Milberg, R. K. Belitz, and A. H. Silver, Phys. Chem. Glasses **1,** 155 (1960).
[10] H. Tazaki, J. Sci. Hiroshima University **A10,** 55 (1940).
[11] W. H. Zachariasen, Acta Cryst. **5,** 68 (1952).
[12] K. Kume and Y. Kakiuchi, J. Phys. Soc. Japan **15,** 1277 (1960).
[13] A. H. Silver (unpublished data).

Luminescence of Chromium(III) Complexes*

LESLIE S. FORSTER AND KEITH DEARMOND
Department of Chemistry, University of Arizona, Tucson, Arizona

(Received February 6, 1961)

THE emission of Cr(III) in Al_2O_3 (ruby) consists of two lines at 14 420 and 14 450 cm^{-1}.[1] These lines arise from transitions between the components of the ^2G state, split by the combined effect of the trigonal field and spin-orbit interaction,[1] and the ground state,

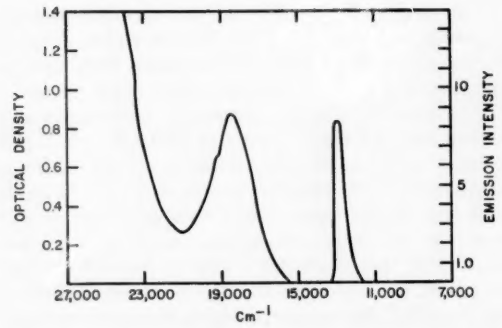

FIG. 1. The absorption and emission spectra of *tris*-acetylacetonatochromium(III) at −183°C.

$^4A_2$. We have observed a broad emission band from the chelates, *tris*-acetylacetonatochromium (III) [$Cr(aca)_3$], a Union Carbide product, and *tris*-(8-hydroxy)-quinolinochromium (III) [$Cr(hq)_3$], prepared by the method of Ablov.[2] The $Cr(aca)_3$ emission was observed in an EPA glass while the $Cr(hq)_3$ was dissolved in a methanol, ethanol, isopropanol glass (8:1:1, by volume) at −183°. The chelate concentrations were less than 0.01 *M* and the glassy solutions remained transparent with minimal cracking. The emission disappeared when the glass melted. The −183° absorption and emission spectra of $Cr(aca)_3$ are shown in Fig. 1. The spectra were obtained by placing the solution in a 1-cm cuvette into a cryostat[3] which was then placed into a Cary model 11 spectrophotometer or a grating spectrophotofluorometer equipped with a DuMont 6911 photomultiplier detector. The $Cr(aca)_3$ emission was also recorded photographically with a grating spectrograph. The crystal field absorption band in $Cr(hq)_3$ is not as well resolved as in $Cr(aca)_3$ and the emission ($\tilde{\nu}_{max}$ = 13 200 cm^{-1}) is more asymmetric with tailing on the low-frequency side.

The emission can be excited with 3660, 4358, and 5460 A radiation and the near independence of the emission band position of the nature of the ligand indicates that it is essentially localized in the Cr(III) ion. Emission from the glassy solvents was absent at −183°.

The importance of trigonal distortion in $Cr(aca)_3$ and *tris*-oxalatochromium (III)[$Cr(ox)_3$] has been demonstrated[4–6] and the appearance of the shoulder at 19 400 cm^{-1} in the −183° absorption spectrum of the $Cr(aca)_3$ solution is probably due to this splitting of the $^4T_{2g}$ into $^4A_1$ and ^4E. The breadth and position of the emission band makes the assignment of this luminescence to $^2E \rightarrow {}^4A_2$ questionable. An alternative would be the assignment $^4E \rightarrow {}^4A_2$. This is preferred to $^4A_1 \rightarrow {}^4A_2$ because of the general observation that emission occurs from the lowest level of a given multiplicity.[7] The ^4E state lies below $^4A_1$ in the acetylacetonate.[4,6]

If our assignment is correct it would be expected that with increasing *Dq* both the absorption and emission bands would shift to shorter wavelengths. The absorption corresponding to $^4E \leftarrow {}^4A_2$ occurs at 22 300 cm^{-1} in *tris*-ethylenediamine chromium (III) chloride [$Cr(en)_3Cl_3$], prepared by method of Linhard and Weigel.[8] The emission in glycerol glass is found at 15 000 cm^{-1}. The half-width of the absorption spectrum is comparable to that observed in $Cr(aca)_3$, but the emission band is somewhat sharper and coincides in position with $^2E \leftarrow {}^4A_2$ and may be an intercombination.

There are, however, several difficulties that arise from this assignment:

(i) The half-width of the absorption band is ∼3200 cm^{-1} compared to 600 cm^{-1} for the emission band.

(ii) The separation between the low-frequency limit of the absorption band and the high-frequency limit of the emission band is ∼2000 cm^{-1} for $Cr(aca)_3$.

(iii) The lifetime of the $Cr(aca)_3$ emission is 400 μsec, a magnitude to be expected for an intercombination.

In O_h symmetry the $^4T_{2g} \leftrightarrow {}^4A_{2g}$ transition is parity forbidden. The reduction of the symmetry to D_3 or C_3 removes this restriction and it has been shown that $^4E \leftarrow {}^4A_2$ is electronically allowed in $Cr(ox)_3$[6] and ruby.[9] The excitation of many vibrational quanta is probably involved in the emission. This may be due to a Jahn-Teller distortion of the ^4E state such as that observed in ruby.[9] If one of the minima that results from this splitting is lower than the ^2E state, the absence of the intercombination lines would be expected.

The absorption spectrum of $Cr(hq)_3$ does show considerable tailing to low frequencies and there appear to be several weak transitions in this tail. The separation between the emission and absorption spectra disappears but the shapes and half-widths are considerably different.

* Supported by the U. S. Atomic Energy Commission.

[1] W. A. Runciman, Repts Progr. Phys. **21,** 40 (1958).
[2] A. Ablov, Bull. Soc. Chim. France [4] **53,** 234 (1933).
[3] T. O. Jones and J. E. Willard, Rev. Sci. Instr. **27,** 1037 (1956).
[4] A. Chakravorty and S. Basu, J. Chem. Phys. **33,** 1266 (1960).
[5] H. S. Jarrett, J. Chem. Phys. **27,** 1298 (1957).
[6] T. S. Piper and R. L. Carlin, J. Chem. Phys. **33,** 608 (1960).
[7] M. Kasha, Discussions Faraday Soc. **9,** 14 (1950).
[8] M. Linhard and M. Weigel, Z. anorg. u. allgem. Chem. **271,** 115 (1953).
[9] R. A. Ford and O. F. Hill, Spectrochim. Acta **16,** 493 (1960).

Superconductivity in the In-Sn System

J. H. WERNICK AND B. T. MATTHIAS
Bell Telephone Laboratories, Inc., Murray Hill, New Jersey

(Received January 26, 1961)

THE search for new superconductors has been confined chiefly to the identification of superconductivity in binary alloys and compounds of transition elements. In many cases, these compounds have critical

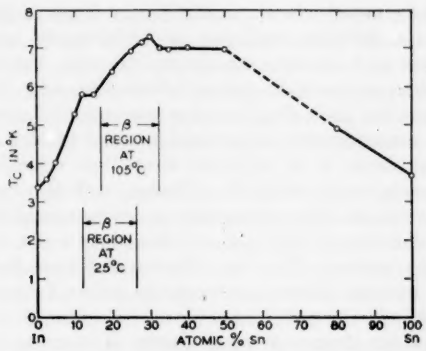

FIG. 1. Superconducting transition temperature vs composition in the In-Sn system.

temperatures much higher than either of the end members; Nb–Zr is a good example of such a system.

On the other hand, comparatively little work has been done in regard to systematic studies of superconductivity of binary systems in which both constituents are soft superconductors. Meissner *et al.*[1] studied binary allows in which both components are superconductors (In–Pb, Sn–Tl, Pb–Hg, In–Tl), while McLennan *et al.*[2] and Allen[3] studied alloys in which one element is a superconductor (Pb, Sn, and Tl). No substantial increase in the critical temperature above that of the component having the highest critical temperature was observed.

We have determined the superconducting transition temperatures T_c for a number of alloys in the In–Sn system. The alloys were prepared in quartz crucibles in argon from 99.999% In and Sn by induction heating. The critical temperatures were determined by the inductance method.[4] The critical temperature was taken as the temperature at which the induction first starts to drop steeply. X-ray powder photographs[5] were taken to verify the constitution of the alloys.

The In–Sn system (T_c=3.37° and 3.69°K, respectively) is characterized by the presence of two intermediate phases, the β and γ phases.[6] The β phase, probable ideal composition $In_{0.75}Sn_{0.25}$, can exist over a wide range of composition (12.5 to 26 at % Sn at 25°C).[7] There is still some uncertainty in the literature regarding the crystal structure of this phase. It has been reported to be simple face-centered tetragonal, with two atoms per unit cell.[8,9] Fink *et al.*[10] reported an equivalent but smaller body-centered tetragonal cell. However, Screaton and Ferguson[11] reported that the intensity data were not consistent with the body-centered cell, but this criticism in turn has been questioned.[7] The γ-phase, ideal composition $In_{0.2}Sn_{0.8}$, is hexagonal, $P6/mmm$.[10]

The critical temperature as a function of composition is shown on Fig. 1. A maximum at T_c=7.30°K occurs for the β alloy $In_{0.7}Sn_{0.3}$. This alloy is single phase at 105°C and contains a small amount of Sn-rich precipitate at room temperature under equilibrium conditions.[7] The x-ray pattern indicates also the presence of some γ as second phase. This composition corresponds to a valence electron per atom ratio of 3.3, which is in fair agreement with similar results involving the transition elements. It is difficult to decide at present whether the total observed variation in transition temperature is a function of the change in number of valence electrons or to the presence of other phases.

It should be mentioned that Meissner,[12] in a study of superconducting contacts, reported T_c=5.5°K for $In_{0.75}Sn_{0.25}$, which is lower than our value. We believe this discrepancy may be due either to the preparation of the samples or that resistance measurements give a somewhat lower temperature.

The authors wish to thank D. Dorsi, S. E. Haszko, and E. Corenzwit for experimental assistance, and V. B. Compton for comments.

[1] W. Meissner, H. Franz, and H. Westerhof, Ann. Physik **13,** 505 (1932).
[2] J. C. McLennan, J. F. Allen, and J. O. Wilhelm, Trans. Roy. Soc. Canada **24,** 53 (1930).
[3] J. F. Allen, Phil. Mag. **16,** 1005 (1933).
[4] B. T. Matthias, and J. K. Hulm, Phys. Rev. **87,** 799 (1952).
[5] CuKα radiation, Straumanis-type Norelco cameras of 114.6 mm diameter.
[6] The β phase forms peritectically at 126°C and the γ phase peritectoidally at approximately 70°C (see work cited in reference 7).
[7] M. Hansen, *Constitution of Binary Alloys,* (McGraw-Hill Book Company, Inc., New York, 1958).
[8] S. Valentiner, Z. Metallk. **32,** 31 (1940); Z. Physik **115,** 11 (1940).
[9] W. Klemm, and E. Orlamünder, Z. anorg. Chem. **256,** 245 (1948).
[10] C. G. Fink, E. R. Jette, S. Katz, and F. J. Schnettler, Trans. Electrochem. Soc. **88,** 229 (1945).
[11] R. M. Screaton, and R. B. Ferguson, Acta Cryst. **7,** 364 (1954).
[12] H. Meissner, Phys. Rev. **109,** 686 (1958).

Nitrosyl Chloride Structure

JOHN D. ROGERS

University of California, Los Alamos Scientific Laboratory, Los Alamos, New Mexico

AND

DUDLEY WILLIAMS

Physics Department, Ohio State University, Columbus, Ohio

(Received March 9, 1961)

THE rotational constants obtained earlier[1] from microwave measurements were used to compute the bond angle and distances for NOCl. The methods of Weatherly and Williams[2] and Kraitchman[3] were used. Results from the latter were not precise because of the large uncertainty introduced in taking differences of nearly like-valued numbers for I_x and I_x'. The rigid-rotor plane body assumption with the sum of the

TABLE I. Bond distances and angle of NOCl.

Parameter	This work	K and P
r(N—Cl)	1.95±0.06 A	1.95±0.01 A
r(N—O)	1.17±0.06	1.14±0.02
r(O—Cl)	2.65±0.03	2.65±0.01
∠(ONCl)	114°±3°	116°±2°

moments of inertia giving the third was used. The results obtained from the method of the work cited in reference 2 and those of Ketelaar and Palmer,[4] who obtained electron-diffraction data, are presented in Table I. The agreement between the structure from the two experimental approaches is demonstrated.

[1] J. D. Rogers, W. J. Pietenpol, and D. Williams, Phys. Rev. **83**, 431 (1951).
[2] T. L. Weatherly, and Q. Williams, J. Chem. Phys. **25**, 717 (1956).
[3] J. Kraitchman, Am. J. Phys. **21**, 17 (1953).
[4] J. A. A. Ketelaar and K. J. Palmer, J. Am. Chem. Soc. **59**, 2629 (1937).

Measurement of the O-O_2 Diffusion Coefficient

R. E. WALKER

Applied Physics Laboratory, The Johns Hopkins University, Silver Spring, Maryland

(Received December 27, 1960)

THERE have recently appeared in the literature several papers dealing with reactions of oxygen atoms in the gas phase[1] and on surfaces.[2] Surface catalytic studies are generally performed with closed-end side arms (Smith[3]) and gas kinetic studies are usually accomplished in tubular flow reactors. The author has found that if the flow velocity is sufficiently reduced in a tubular flow rector, one-dimensional flow can be retained wherein axial diffusion is not negligible and the diffusion coefficient of labile species can be treated as a separate measurable quantity. Providing the disappearance of reactant follows first-order chemical kinetics (as it does for trace amounts of O atoms), only a measurement of the axial decay of relative atom concentration ψ for different mean flow velocities is necessary to determine the diffusion coefficient for the labile species. The appropriate one-dimensional diffusion equation is $U\psi_z - D\psi_{zz} = -k\psi$, where z is the distance coordinate, D is the diffusion coefficient for the *trace* reactant diffusing through the ambient mixture,[4] and k is the lumped first-order rate constant. For the case where there is a steady source of atoms at some point (subscript "0") in a tube of infinite length, the solution downstream of the source is $\psi = \psi_0 \exp(-\lambda z)$, where $\lambda = -(U/2D) + [(U/2D)^2 + \alpha^2]^{\frac{1}{2}}$ with $\alpha^2 = k/D$. λ and α thus represent the slopes of plots of $\ln\psi$ vs z when the flow velocity is U and zero, respectively. Solving for D one gets

$$D = U\lambda/(\alpha^2 - \lambda^2). \quad (1)$$

Similar equations can be developed for different finite values of U or for the decay of reactant upstream and downstream of the source.

This method has been used by the author to measure the diffusion of O atoms through O_2 containing trace amounts of NO. The latter was introduced to the O—O_2 mixture as a very sensitive photometric indicating "catalyst." The O—NO reactions are also first order in O atom removal and the afterglow intensity which was measured with a movable 931 A photomultiplier tube is directly proportional to the O atom concentration (Kaufman[1]). A 90-w, 28-Mc rf electrodeless discharge was used to generate the O atoms and a transfer stopcock permitted the reacting mixture either to be passed by, or through, the 1.01 cm diam by 80-cm long Pyrex tube used for measurement. The pressure was controlled by a constriction (valve) just upstream of the vacuum

TABLE I. Measured values of D_{O-O_2} using the side-arm-with-flow method (T=25°C).

P (mm Hg)	X_{NO} (mole fraction of NO)	U (cm/sec at 1 atm)	D (cm²/sec at 1 atm)	k (sec⁻¹) Exptl	k (sec⁻¹) Literature[a]
1.17	0.0066	0.135	0.311	4.4	4.3
1.79	0.0066	0.135	0.317	8.3	6.7
1.70	0.0061	0.163	0.253	7.2	6.2
1.42	0.0052	0.165	0.305	4.7	4.8
1.60	0.0052	0.165	0.292	5.0	5.5
1.60	0.0053	0.165	0.300	4.9	5.5
1.37	0.0052	0.170	0.311	6.2	4.8
1.86	0.0051	0.223	0.305	6.6	6.5
2.17	0.0051	0.223	0.288	7.4	7.9
1.54	0.0051	0.223	0.318	5.1	5.2
1.05	0.0051	0.223	0.312	3.4	3.8
1.93	0.0051	0.223	0.296	6.6	6.8
			Av 0.302±0.012		

[a] Assuming reactions: (1) O+wall→½O_2+wall, k_1=2.5 sec⁻¹; (2) O+O_2+O_2→O_3+O_2, k_2=1.0×10¹⁴ cc² mole⁻² sec⁻¹; (3) O+O_3→O_2+O_2, stationary state for [O_3]; (4) O+NO→NO_2+$h\nu$, negligible; (5) O+NO+O_2→NO_2+O_2, k_5=2.0×10¹⁶ cc² mole⁻² sec⁻¹; (6) NO_2+O→NO+O_2, stationary state for [NO_2].

pump. Compressed gases were used without any purification. The O_2 and NO were accurately metered and with the measured area of the tube the flow velocity was computed from mass conservation. A reference pressure of one atomosphere was used in calculations with Eq. (1) which does not require the measured value of p.

Although the experiment suffered from occasional irregularities which were probably due to trace impurities, several reasonably satisfactory measurements of diffusion coefficients have been made and are reported in Table I. Where necessary, small corrections for viscous pressure drop have been made. In these experiments the concentration of NO was sufficiently small so that the measured diffusion coefficient was that of O atoms diffusing essentially through O_2. The average value obtained is in good agreement with that reported by Krongelb and Strandberg[1] (0.296–0.315 cm²/sec). Also included in Table I are the experimental values for the lumped first order rate constant k. Comparison is made with computed values of k using average homogeneous rate constants published in the literature[1] and a first order heterogeneous rate constant of 2.5 sec^{-1} ($\gamma = 4.1 \times 10^{-5}$) indicated by the data. The limited range of p and X_{NO} used in these experiments did not permit a separate evaluation of the various rate constant involved.

The author wishes to thank Dr. A. A. Westenberg for suggesting this problem, Dr. F. Kaufman for pointing out the unique features of using NO to measure relative O atom concentration, and N. deHaas for his assistance in the laboratory.

[1] F. Kaufman, Proc. Roy. Soc. (London) **A247,** 123 (1958); L. Elias, E. A. Ogryzle, and H. I. Schiff, Can. J. Chem. **37,** 1680, 1690 (1959); P. G. Dickens, *et al.*, Nature **187,** 686 (1960); S. Kronegelb and M. W. P. Strandberg, J. Chem. Phys. **31,** 1196 (1959); P. Harteck, R. P. Reeves, and G. Mannella, *ibid.* 1333 (1958).

[2] J. W. Linnett and D. G. H. Marsden, Proc. Roy. Soc. (London) **A234,** 489 (1956); J. C. Greaves and J. W. Linnett, Trans. Faraday Soc. **54,** 1323 (1958); **55,** 1338, 1346, 1355 (1959). Also see papers in reference 1.

[3] W. V. Smith, J. Chem. Phys. **11,** 110 (1943).

[4] R. E. Walker, N. deHaas, and A. A. Westenberg, J. Chem. Phys. **32,** 1314 (1960).

Vaporization of the Rare Earth Oxides*

MORTON B. PANISH

Research and Advanced Development Division, Avco Corporation, Wilmington, Massachusetts

(Received February 9, 1961)

THE vaporization modes of most of the sesquioxides of the lighter rare earth metals have previously been shown to change from

$$M_2O_3 \rightarrow 2MO_{(g)} + O_{(g)} \quad (1)$$

to

$$M_2O_3 \rightarrow 2M_{(g)} + 3O_{(g)} \quad (2)$$

with increasing atomic number of the metal.[1]

In this work, we have studied the vaporization of Gd_2O_3, Tb_2O_3, Dy_2O_3, Ho_2O_3, Er_2O_3, Tm_2O_3, Yb_2O_3, and Lu_2O_3 at temperatures ranging from 2000 to 2500°K by analyzing the species effusing from an iridium effusion cell with a Bendix time-of-flight mass spectrometer. Experimental details of the heating and temperature measuring techniques have been described elsewhere.[2]

The ratios of the ion currents due to the metal and the monoxide, I_{M^+}/I_{MO^+}, are shown in Fig. 1 for ions produced with a 20-ev electron beam. The previously reported data on La_2O_3, Pr_2O_3, Nd_2O_3, Sm_2O_3, and Eu_2O_3[1,3] are also included in the figure. The effusing species were observed at several temperatures and electron-beam energies for each of the compounds studied, and the variation of the ion-current ratio with temperature over several hundred degrees was found to be within the limits shown about each point in Fig. 1. The limits shown for the vaporization of Eu_2O_3 and Tm_2O_3 are quite large because the low concentration of MO obtained with these oxides necessitated measurements at low signal-noise levels. In the case of Yb_2O_3 only Yb^+ ions were observed.

The possibility that the results might have been seriously influenced by dissociative ionization or ion molecule recombinations within the ion source was examined in a manner identical to that described previously,[1] and these processes were found to be insignificant. It thus appears, that the rare earth sesquioxides may be divided into two groups, within each of which the vaporization mode changes from that shown in Eq. (1) to that shown in Eq. (2) with increasing atomic number of the rare earth metal. It is of interest to note the abrupt change in the vaporization mode which occurs after Eu and Yb; the rare earth metals in which the 4*f* electron shell is half and completely filled.

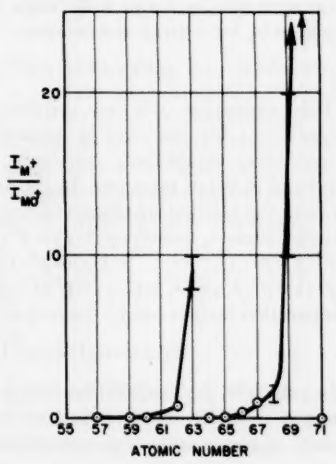

FIG. 1. Ion-current ratios I_{M^+}/I_{MO^+} vs atomic number of M for the vaporization of M_2O_3.

It is also of interest to note that, except for Lu_2O_3, the classification of the oxides into groups according to their vaporization modes is identical to the separation of the rare earths into so-called cerium and yttrium groups according to their behavior in various separation schemes.[4]

The approximate vapor pressures of the major species vaporizing from the yttrium group of oxides were determined in a manner similar to that described previously for the cerium group. The equilibrium partial pressures over M_2O_3 at 2300°K were: TbO, DyO, HoO, ErO, $LuO \approx 10^{-7}$ atm; Tm and $Yb \approx 10^{-6}$ atm. In order to obtain the approximate pressures, the iridium-ion current from the vaporization of the iridium effusion cell was used for the calibration of the M^+ and MO^+ ion currents.

* This work was supported by the Advanced Research Projects Agency and by the Materials Central, Wright Air Development Division, Wright-Patterson Air Force Base, Ohio.

[1] M. B. Panish, J. Chem. Phys. **34**, 1079 (1961).

[2] M. B. Panish and L. Reif, J. Chem. Phys. **34**, 1915 (1961), this issue.

[3] P. N. Walsh, H. W. Goldstein, and D. White, J. Am. Ceram. Soc. **43**, 229 (1960).

[4] D. M. Yost, H. Russel, Jr., and C. S. Garner, *The Rare Earth Elements and Their Compounds* (John Wiley & Sons, Inc., New York, 1947).

Separation Factors in Multicomponent Mixtures of Isotopes*

ALFRED NARTEN

Department of Chemistry, Columbia University, New York, New York

(Received February 6, 1961)

IN a liquid mixture of j isotopic species, each of the components has a vapor pressure $p^\circ(1) > p^\circ(2) > \cdots > p^\circ(i) > p^\circ(k) > \cdots > p^\circ(j)$. By definition, the single-stage separation factor for the distribution of the isotopic species i and k between the gas and liquid phases is, for a given temperature,

$$\alpha(i/k) = p^\circ(i)/p^\circ(k). \tag{1}$$

This discussion will be restricted to vapor-liquid equilibria; for the case of general isotopic exchange equilibria, equilibrium constants have to be used instead of vapor pressures. In the j-component system, out of the existing separation factors, $j-1$ are of fundamental interest, namely, $\alpha(1/2) = p^\circ(1)/p^\circ(2)$, $\alpha(1/3) = p^\circ(1)/p^\circ(3)$, $\cdots$, $\alpha(1/i) = p^\circ(1)/p^\circ(i)$, $\alpha(1/k) = p^\circ(1)/p^\circ(k)$, $\cdots$, $\alpha(1/j) = p^\circ(1)/p^\circ(j)$. All the other separation factors can be derived according to

$$\alpha(i/k) = \alpha(1/k)/\alpha(1/i). \tag{2}$$

In principle, $j-1$ separation factors have to be determined in order to allow further mathematical treatment of the j-component separation problem.

Things are greatly simplified in multicomponent mixtures consisting of mixed isotopic molecules, if the distribution of the isotopic atoms among the molecules in the gas phase is statistical. In this case, the vapor pressures of the mixed isotopic molecules can be represented in terms of the vapor pressures of the isotopically pure species (rule of the geometric mean). It was shown by Bigeleisen[1] that the rule of the mean is a direct statistical mechanical consequence of the $u^2/24$ law and the fact that the difference in the sums of the squares of the frequencies of the isotopic molecules depends only on the masses of the isotopic molecules.

In the practice of isotope separation, the problem of producing pure isotopic compounds is irrelevant in most cases. Instead, one is interested in the production of one particular nuclide. If in the j-component mixture x components contain the nuclide X, and y the nuclide Y, the *effective separation factor* is usually defined as

$$\alpha(X/Y) = \frac{[N(X)/N(Y)]_l}{[N(X)/N(Y)]_g}, \tag{3}$$

N denotes mole fractions, and the indices l and g the liquid and gas phases. Assuming Raoult's law to hold for the mixture, and using definition (1), we obtain

$$\alpha(X/Y) = \frac{\sum_y N(i) \sum_x N(i)\alpha(1/i)}{\sum_x N(i) \sum_y N(i)\alpha(1/i)}. \tag{4}$$

The $N(i)$ in (4) denote mole fractions in the gas phase. Equation (4) gives the dependence of the effective separation factor on the individual separation factors as defined by (1) and on the concentration of the individual isotopic species in the mixture. A discussion of (4) shows, that in cases where the rule of the mean holds, the effective α will be concentration independent (if Raoult's law is obeyed); in cases where the rule of the mean does not hold, the effective α will be concentration dependent.

For the system of isotopic nitric oxides at 121°K, it was clearly shown[2,3] that the rule of the mean holds. It was also shown for this system, that Raoult's law is obeyed.[4] It follows from (4), that the effective separation factors for the production of nitrogen-15 and oxygen-18 by distillation of nitric oxide are

$$\alpha(N^{14}/N^{15}) = p^\circ(N^{14}O^{16})/p^\circ(N^{15}O^{16})$$

and $\alpha(O^{16}/O^{18}) = p^\circ(N^{14}O^{16})/p^\circ(N^{14}O^{18})$. It has been maintained[2] that in the fractionation of nitric oxide the large $\alpha(N^{14}O^{16}/N^{15}O^{18})$ would contribute considerably to the effective separation factor at appreciable concentrations of $N^{15}O^{18}$. This is not the case. The effective separation factors $\alpha(N^{14}/N^{15})$ and $\alpha(O^{16}/O^{18})$ which are relevant for the design calculations of a nitrogen-15 and (or) oxygen-18 distillation cascade are independent of the N^{15} or O^{18} or any other concentration.

For the system of isotopic water molecules at 373°K, it was shown that the rule of the mean does not hold.[5]

In this case the concentration dependence of $\alpha(H/D)$ and $\alpha(O^{16}/O^{18})$ is given by Eq. (4).

The author is indebted to Professor T. I. Taylor and Dr. E. U. Monse for stimulating discussions and for reading the manuscript.

* Supported in part by a grant from the U. S. Atomic Energy Commission.

[1] J. Bigeleisen, J. Chem. Phys. **23,** 2264 (1955).
[2] K. Clusius, K. Schleich, and M. Vecchi, Helv. Chim. Acta **42,** 2654 (1959).
[3] J. Bigeleisen, J. Chem. Phys. **33,** 1775 (1960).
[4] K. Clusius, M. Vecchi, A. Fischer, and U. Piesbergen, Helv. Chim. Acta **42,** 1975 (1959).
[5] P. W. Schultz, and W. C. Zmachinski, SAM Report A-595, April 12, 1943; E. Whalley, *Proceedings of the Joint Conference on the Thermodynamic and Transport Properties of Fluids* (The Institute of Mechanical Engineers, London, England, 1958), p. 15; P. Baertschi and M. Thuerkauf, Helv. Chim. Acta **43,** 80 (1960).

Maximum-Overlap Directed-Hybrid Orbitals*

T. L. Gilbert and P. G. Lykos†
Argonne National Laboratory, Argonne, Illinois

(Received January 3, 1961)

RECENTLY, J. N. Murrell[1] discussed a method for constructing best hybrid orbitals based on the principle of maximum overlap. Within valence-bond theory, the total energy of a molecule is expressible as a sum of essentially atomic terms and a sum of interaction terms between different atoms. The interaction terms are considered to be essentially proportional to the overlap between the atomic orbitals involved in the bonding. Hence, where any degrees of freedom exist in the form of the bonding orbitals, these may be taken up by a variational calculation on the total energy of the molecule. Alternatively, consistent with the assumption that the binding-energy terms are proportional to overlap, the remaining degrees of freedom may be taken up by maximizing the overlap between the bonding orbitals.

Murrell concerned himself with a molecule of the type $M—(X_1, \cdots, X_k)$ where all the groups are attached directly to atom M and where there is a set of atomic orbitals, $\phi_1, \phi_2, \cdots, \phi_n$, $n \geq k$, on atom M and a set of bonding atomic orbitals, $\theta_1, \theta_2, \cdots, \theta_k$, on the substituents, $\mathbf{X}_i$. He constructs the hybrid orbitals,

$$\psi_i = \sum_{j=1}^{n} a_{ij}\phi_j,$$

$i = 1, 2, \cdots, k$, by maximizing the sum of the overlap integrals,

$$\sum_{i=1}^{k} \langle \psi_i \theta_i \rangle.$$

This is done by first constructing an orthogonal set,

$$\chi_i = \sum_{j=1}^{n} b_{ij}\phi_j,$$

such that $\chi_{k+1}, \cdots, \chi_n$ are orthogonal to all θ_i, and then using the fact that $\langle \psi_i \theta_j \rangle = \langle \psi_j \theta_i \rangle$ to construct the transformation

$$\psi_i = \sum_{j=1}^{k} c_{ij}\chi_j.$$

The purpose of this note is to outline a simpler and more general procedure for constructing maximum-overlap hybrid orbitals from which Murrell's orbitals are obtained as a special case.

The first step is to determine the orbitals,

$$\lambda^{(i)} = \sum_{j=1}^{n} d_j^{(i)}\phi_j,$$

$i = 1, 2, \cdots, k$, for which the square of the overlap, $\langle \lambda^{(i)} \theta_i \rangle \langle \theta_i \lambda^{(i)} \rangle$, is maximum. If the ϕ_j are mutually orthogonal, the transformation is given by a column vector, $\mathbf{d}^{(i)} = \{d_j^{(i)}\}$, which is that eigenvector of the square matrix, $\mathbf{\Omega}^{(i)} = [\Omega_{jl}^{(i)}] = [\langle \phi_j \theta_i \rangle \langle \theta_i \phi_l \rangle]$, with the largest (and only nonzero) eigenvalue $\omega^{(i)}$. The eigenvectors and eigenvalues of interest are, explicitly,

$$\{d_j^{(i)}\} = \{\langle \phi_j \theta_i \rangle / \sum_{j=1}^{n} |\langle \phi_j \theta_i \rangle|^2\}$$

and

$$\omega^{(i)} = \sum_{j=1}^{n} |\langle \phi_j \theta_i \rangle|^2 = \text{Trace } \mathbf{\Omega}^{(i)}.$$

It is clear, by construction, that the k hybrid orbitals obtained in this manner have all the desired properties except orthogonality. One can readily show that $\lambda^{(1)}, \lambda^{(2)}, \cdots, \lambda^{(k)}$ span the same manifold as Murrell's $\chi_1, \chi_2, \cdots, \chi_k$, i.e.,

$$\lambda^{(i)} = \sum_{j=1}^{k} f_{ij}\chi_j.$$

The above procedure for constructing the manifold is, however, simpler than that given by Murrell.

Use may be made of the Carlson-Keller theorem[2] in order to obtain an orthogonal set without reducing the overlap of the individual orbitals any more than necessary. This theorem states that the orthonormal orbitals $\{\psi_i\}$, which minimize the weighted mean difference,

$$M = \sum_{i=1}^{k} w_i \langle \psi_i - \lambda^{(i)}, \psi_i - \lambda^{(i)} \rangle,$$

are explicitly given by

$$\psi_i = \sum_{j=1}^{k} \lambda^{(j)} w_j (\mathbf{WSW})_{ji}^{-\frac{1}{2}},$$

where $\mathbf{S} = [\langle \lambda^{(i)} \lambda^{(j)} \rangle]$ is the overlap matrix and $\mathbf{W} =$

$[w_i\delta_{ij}]$ is a square matrix constructed from the weighting factors w_i.

The increased generality in the above method lies in the freedom of choice of the weighting factors. If the choice $w_i=[\omega^{(i)}]^{\frac{1}{2}}$ is made, the resulting hybrid orbitals are the same as those obtained by Murrell. Other choices [e.g., $w_i=1$ or $w_i=\omega^{(i)}$], are possible, however. If the total energy of the molecule is directly proportional to the overlap with the bonding orbitals, then Murrell's choice of orbitals is optimum. More extensive *ab initio* calculations or semiempirical studies will be required to settle this point.

The most difficult part of the calculation is the evaluation of the inverse root, $(\mathbf{WSW})^{-\frac{1}{2}}$. This involves calculation of the eigenvalues s_i and eigenvectors $\mathbf{u}_i=\{u_{ij}\}$, of the symmetric matrix **WSW**. The matrix elements of the inverse root are then explicitly given by

$$(\mathbf{WSW})_{ij}^{-\frac{1}{2}}=\sum_{l=1}^{k}u_{li}s_l^{-\frac{1}{2}}u_{lj}.$$

There is no ambiguity in this result because the Carlson-Keller theorem requires that the positive roots be used. This suggests that the ambiguity in the choice of the root for maximizing the trace in the procedure outlined by Murrell can be resolved by the same prescription.

Note added in proof. We have discovered that Dr. A. Golebiewski, Jagellonian University, Krakow, Poland, has, independently, completed a very similar analysis which will be published in the *Transactions of the Faraday Society*.

* Based on work performed under the auspices of the U. S Atomic Energy Commission.

† Permanent address: Department of Chemistry, Illinois Institute of Technology, Chicago 16, Illinois.

[1] J. N. Murrell, J. Chem. Phys. **32**, 767 (1960).
[2] B. C. Carlson and J. M. Keller, Phys. Rev. **105**, 102 (1957)

Effect of Pressure on the Spectra of MnO_4^- and $CrO_4^=$ †

W. H. Bentley and H. G. Drickamer

Department of Chemistry and Chemical Engineering, University of Illinois, Urbana, Illinois

(Received February 8, 1961)

THE effect of pressure has been measured on the intense allowed transitions in $KMnO_4$ and K_2CrO_4 in the solid state. The chemicals were C. P. material. The high-pressure optical techniques have been described elsewhere.[1,2] In each case only the lower energy of the two large charge-transfer peaks was observed. The $KMnO_4$ absorption showed considerable structure with three easily distinguishable peaks and several shoulders. All three peaks shifted identically within the accuracy of our observations. The shifts are shown in Fig. 1. In both compounds a blue shift with increasing pressure was observed. The shifts were nearly the same for $KMnO_4$ and K_2CrO_4, with the latter being perhaps slightly less. There seemed to be no significant change in half-width or integrated intensity, although it was difficult to obtain the entire peaks, and changes of 10–20% would have been difficult to distinguish.

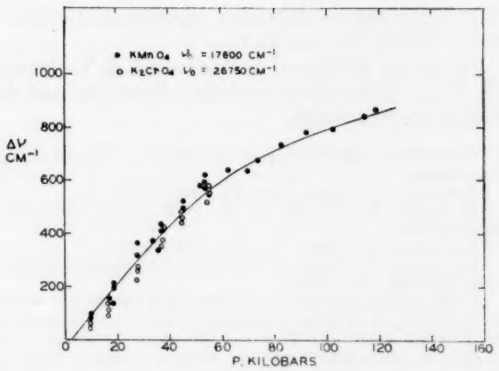

FIG. 1. Shift of charge transfer peaks $KMnO_4$ and K_2CrO_4.

From the blue shift it is clear that the transition observed is due to the jump of an electron from a nonbonding (or very weakly bonding) orbital to an antibonding orbital. This is consistent with the theoretical assignments made by a number of writers.[3–5] In particular, in the energy level diagram of Ballhausen and Liehr[5] the transition is from the π oxygen orbital of symmetry t_1 to the complex antibonding orbital made up from the metal ion $3d(e)$ state and the oxygen $\pi(e)$ orbital. This antibonding orbital increases in energy with increasing pressure (relative to the ligand orbital). This gives a measure of the decrease in energy (increase of bonding) of the corresponding bonding $\pi(e)$ orbital.

† This work was supported in part by the U. S. Atomic Energy Commission.

[1] R. A. Fitch, T. E. Slykhouse, and H. G. Drickamer, J. Opt. Soc. Am. **47**, 1015 (1957).
[2] H. G. Drickamer, Rev. Sci. Instr. **32**, 212 (1961).
[3] M. Wolfsberg and L. Helmholtz, J. Chem. Phys. **20**, 837 (1952).
[4] L. Helmholtz, H. Brennan, and M. Wolfsberg, J. Chem. Phys. **23**, 853 (1955).
[5] C. J. Ballhausen and A. D. Liehr, Mol. Spectroscopy **2**, 342 (1958).

Absorption and Luminescence Origins in Anthracene Crystals

P. W. Alexander, A. R. Lacey, and L. E. Lyons

Department of Physical Chemistry, University of Sydney, Sydney, N.S.W., Australia

(Received February 20, 1961)

THE bands at the long wavelength edge of the first strong absorption system in anthracene crystals at 4° or 20°K, although often observed previously,[1–9]

have not yet been definitely explained. Whether they are due to (i) indirect transitions involving lattice vibrations[10]; (ii) impurities of some unspecified nature[11]; (iii) defects in the crystal lattice[5,6]; or (iv) trapped excitons[3] has not been settled.

Using zone refining we have now shown at 4°K that at least some of the bands are associated with the presence of very small amounts of impurities such as anthraquinone. Crystals about 10μ thick of various purities were examined. In the region 24800–25030 cm^{-1} the purest anthracene showed no absorption, but less pure material showed bands at 24906, 24926, and 25029. More impurity still results in continuous absorption. Two sublimations in air of the purest material caused bands to appear at 24926 and 25010 cm^{-1}. Sublimation in the absence of oxygen of a mixture of pure material and a small amount of anthraquinone caused bands to appear at 24916 and 24804 cm^{-1}.

The free exciton (b) origin in pure anthracene crystals was recently placed at 25150 cm^{-1}.[12] By removing other possible claimants to identification as the free exciton (b) origin, our work confirms the earlier results.

Free exciton luminescence from pure anthracene crystals is thus expected to have an origin at 25150 cm^{-1} (b polarized). Such luminescence at 4°K has been observed only feebly if at all in the crystals previously examined.[3,11] The effective origins have lain at lower energies. These origins are now seen to be due to impurities or to lattice defects caused by the presence of impurities. Such a conclusion is confirmed by comparing the luminescence at 4°K from a crystal which exhibited edge bands in absorption with that from a purer crystal in which absorption edge bands were not present. The luminescent band of greatest energy lay at 24840 cm^{-1} in the first case and at 25040 cm^{-1} in the second. The difference between the free exciton region observed at 25040 cm^{-1} and that expected at 25150 cm^{-1} is attributed (apart from an experimental error of $\pm$50 cm^{-1}) to reabsorption, since bands were observed both at 23740 and 22360 cm^{-1} differing by one and two quanta of a 1400 cm^{-1} vibration from 25150 cm^{-1}.

The pure crystal spectrum is thus relatively simple. The large difference once supposed to exist between fluorescence and absorption origins in anthracene crystals is not a property of the pure crystal. Explanations of the origins involving Franck-Condon effects[13] or Frenkel-type trapped excitons[3] are now almost if not quite unnecessary. The present work also explains the temperature dependence[14] of luminescence from anthracene which is now seen to arise from impurity centers acting as traps for the energy. The same impurities are likely also to trap carriers in the photoconductivity observed[15] in anthracene crystals.

[1] I. V. Obreimov and A. F. Prikhotjko, Phys. Z. Sowjetunion **9,** 48 (1936).
[2] D. P. Craig and P. C. Hobbins, J. Chem. Soc. **1955,** 2309.
[3] J. Sidman, Phys. Rev. **102,** 96 (1956).
[4] J. Ferguson and W. G. Schneider, J. Chem. Phys. **28,** 761 (1958).
[5] A. F. Prikhotjko and I. Ya. Fugol, Optika i Spektroskopia **4,** 335 (1958).
[6] I. Ya. Fugol and I. Shulga, Optika i Spektroskopia **5,** 34 (1958).
[7] I. V. Obreimov, A. F. Prikhotjko, and C. G. Shabaldas, J. Exptl. Theoret. Phys. (U.S.S.R) **6,** 1061 (1936).
[8] P. Pesteil and M. Barbaron, J. phys. radium **15,** 92 (1954).
[9] J. Ferguson and W. G. Schneider, Can. J. Chem. **36,** 1070 (1958).
[10] L. E. Lyons, Proceedings of the Conference on Electronic Conductivity in Organic Solids, Duke University (April, 1960), to be published.
[11] H. C. Wolf, Z. Naturforsch., **13a,** 414 (1958).
[12] A. R. Lacey and L. E. Lyons, Proc. Chem. Soc. **1960,** 414.
[13] D. S. McClure, J. Chem. Phys. **25,** 481 (1956).
[14] L. E. Lyons and J. W. White, J. Chem. Phys. **29,** 447 (1958); J. Chem. Soc. **1960,** 5213.
[15] e. g., L. E. Lyons and G. C. Morris, J. Chem. Soc. **1957,** 3648.

Cation Mobility and Thermal Contraction in AgI

R. T. Payne and A. W. Lawson

Department of Physics and Institute for the Study of Metals, University of Chicago, Chicago 37, Illinois

(Received March 6, 1961)

According to the continuum theory of diffusion,[1–3] the enthalpy of activation ΔH^+, the entropy of action ΔS^+ and the volume of activation ΔV^+ are related by the pseudothermodynamic relations

$$\Delta S^+ = (\alpha/\beta)\Delta V^+ \quad (1)$$

$$\Delta V^+ = 2(\gamma - \tfrac{1}{3})\beta\Delta H^+ \quad (2)$$

$$\Delta S^+ = 2\alpha(\gamma - \tfrac{1}{3})\Delta H^+, \quad (3)$$

where α is the isobaric coefficient of thermal expansion, β the isothermal compressibility, and γ the Gruniesen constant given by

$$\gamma = (\alpha/\beta)(V_m/c_m), \quad (4)$$

where c_m is the molar specific heat and V_m is the molar volume. These semiempirical relations may be subjected to a severe test by consideration of abnormal substances in which, for instance, α is negative.

The recent data of Wagener[4] relating to the effect of pressure on the ionic conductivity of AgI provide the possibility of such a test. AgI is known to contract on heating.[5] Hence α is negative. According to Wagener the effect of pressure P is to increase the conductivity σ of pure and doped material below 137°C. Hence, because

$$\Delta V^+ = -RT(\partial \ln\sigma/\partial P), \quad (5)$$

the volume of activation is negative. From Eq. (4), γ is negative and Eq. (2) is accordingly satisfied since both β and ΔH^+ are intrinsically positive. From Eq.

(3), ΔS^+ must be positive, and, of course, because Eq. (1) is the ratio of Eq. (2) and Eq. (3), it is automatically satisfied.

A more quantitative comparison is subject to a variety of uncertainties. First, the pressure data on AgI are spotty. Second, considerable confusion still exists concerning the crystal structure of AgI. However, assuming Majumdar and Roy's data[5] on the thermal expansion of what they consider to be a wurtzite form of AgI is a crude measure of the highly disordered combination of both wurtzite and sphaleritic phases usually obtained, we may set $\alpha=-1.0\times10^{-4}$°C^{-1}. The compressibility of AgI is $+4.1\times10^{-12}$ cm^2/d.[6] Thus from Eq. (4) we have $\gamma=-1.9$. For highly doped samples at 110°C, Wagener reports $\partial \ln\sigma/\partial P=3.2\times10^{-4}$ bar^{-1}, corresponding to an activation volume for diffusion of the Ag^+ vacancies of approximately 9.6 cc/mole. Coupling the value of ΔV^+ with our estimate of γ, we find ΔH^+ from Eq. (2) to be 0.59 ev. This value compares favorably with the value of ΔH^+ of 0.68 ev reported by Mrgudich[7] for the temperature range between 30° and 80°C where one might expect residual divalent impurities to give rise to extrinsic vacancy conduction. However, clearly more experiments are needed before a satisfactory quantitative comparison can be carried out.

[1] A. W. Lawson, J. Phys. Chem. Solids **3,** 250 (1957).
[2] R. W. Keyes, J. Chem. Phys. **29,** 467 (1958).
[3] A. W. Lawson, S. A. Rice, R. D. Corneliussen, and N. H. Nachtrieb, J. Chem. Phys. **32,** 447 (1960).
[4] K. Wagener, Z. physik. Chem. **23,** 305 (1960).
[5] A. J. Majumdar and R. Roy. J. Phys. Chem. **63,** 1858 (1959).
[6] *International Critical Tables* (McGraw-Hill Book Company, Inc., New York, 1930), Vol. III, p. 50.
[7] J. N. Mrgudich, Laboratory for Insulation Research, Technical Report 138, M.I.T., June, 1959.

Infrared Spectra of Some Group IV Halides*

ALFRED BÜCHLER, J. B. BERKOWITZ-MATTUCK, AND DONALD H. DUGRE†

Arthur D. Little, Inc., Cambridge 40, Massachusetts

(Received December 29, 1960)

THE purpose of this note is to report values of the asymmetric stretching frequencies ν_3 of the gaseous tetrafluorides and tetrachlorides of zirconium, hafnium, and thorium. These compounds are assumed to have tetrahedral symmetry and will thus have four normal modes of vibration, two of which, the stretching frequency ν_3 and the bending frequency ν_4, will be infrared active, while all will be Raman active. In the case of $ZrCl_4$, the tetrahedral structure has been confirmed by electron diffraction.[1,2] Until very recently, the only spectroscopic work on these compounds was that of Delwaulle and François,[3] who obtained the Raman spectrum of $ZrCl_4$ in solution in PCl_5 and $POCl_3$. They observed the symmetric stretching vibration ν_1 at 383 cm^{-1}, as well as a broad band between 117 and 123 cm^{-1} which they assigned to the bending vibrations ν_2 and ν_4. While the present work was in progress, values of ν_3 were reported by Blander and Morgan[4] for ZrF_4 and HfF_4 and by Wilmshurst[5] for $ZrCl_4$. From an examination of overtone and combination bands, the latter also obtained values of 388, 102, and 112 cm^{-1} for, respectively, ν_1, ν_2, and ν_4 of $ZrCl_4$.

The spectrometer used in this study was a modified Perkin-Elmer model 12C infrared spectrometer with cesium bromide and cesium iodide optics. The technique followed closely that described by Klemperer and associates.[6] A nickel tube with cesium iodide or polyethylene windows served as sample cell. The tube was surrounded by a molybdenum-wound, Alundum-core resistance furnace that was used to heat the sample. Samples were obtained from Var-La-Coid Chemical Corporation (ZrF_4, $HfCl_4$, $ThCl_4$); Matheson, Coleman, and Bell ($ZrCl_4$); and A. D. Mackay, Inc. (ThF_4). We are indebted to Dr. H. W. Morgan, Oak Ridge National Laboratory, for a sample of HfF_4. The temperatures of the experiments were of the order of 250° for $ZrCl_4$ and $HfCl_4$; 675° fro $ThCl_4$; 800° for ZrF_4 and and 1200° for ThF_4.

TABLE I. Asymmetric stretching vibrations ν_3 of group IV halides XY_4, cm^{-1}.

X / Y	Zr	Hf	Th
F	668; 670[a]	645; 650[a]	520
Cl	423; 421[b]	393	335

[a] Reference 4.
[b] Reference 5.

TABLE II. Predicted and observed vibrational frequencies of ZrF_4 and $ZrCl_4$, cm^{-1}.

	ZrF_4		$ZrCl_4$	
Frequency	Calc.[a]	Obs.	Calc.[a]	Obs.
ν_1	600–725	...	382	383[d]; 388[e]
ν_2	150–200	...	108	117–123[d]; 102[e]
ν_3	?	668[b]; 670[c]	423	423[b]; 421[e]
ν_4	180–230	190±20[b]	114	117–123[d]; 112[e]

[a] Reference 7.
[b] This work.
[c] Reference 4.
[d] Reference 3.
[e] Reference 5.

The values of ν_3 obtained are listed in Table I, together with those given in other investigations; the agreement among the various experimental studies is very satisfactory. In the case of ZrF_4, an attempt was made to observe the bending vibration ν_4. The high-frequency wing of an absorption band was observed near the cutoff (200 cm^{-1}) of the cesium iodide prism,

the onset of total absorption shifting to higher frequencies as the temperature was raised from 800° to 890°C. We thus assign 190±20 cm^{-1} as the value of ν_4 for ZrF_4.

Table II lists the observed frequencies of ZrF_4 and $ZrCl_4$, together with those predicted by Godnev[7] from data for related group IV halides through the use of a 5-parameter potential function. The uncertainty in the case of the fluoride reflects the relative lack of data for related group IV fluorides. In the case of the chloride the agreement between calculated and experimental values is very good. In particular, the experimentally observed separation of about 40 cm^{-1} between ν_1 and ν_3 is correctly predicted; a simple valence force field would predict a separation of about 100 cm^{-1}.

* This work was supported by the Office of Ordnance Research, U. S. Army, with funds provided by the Advanced Research Projects Agency.

† Present Address: Department of Chemical Engineering, University of Massachusetts, Amherst, Massachusetts.

[1] M. W. Lister and L. E. Sutton, Trans. Faraday Soc. **37**, 393 (1941).

[2] M. Kimura, K. Kimura, M. Aoki, and S. Shibata, Bull. Chem. Soc. (Japan) **29**, 95 (1956).

[3] M. L. Delwaulle and F. François, Bull. soc. chim. **13**, 205 (1946); J. phys. radium **7**, 15 (1946).

[4] M. Blander and H. W. Morgan, presented at the 138th Meeting, American Chemical Society, New York, September 1960.

[5] J. K. Wilmshurst, J. Mol. Spectroscopy **5**, 343 (1960).

[6] W. Klemperer, J. Chem. Phys. **24**, 353 (1956); W. Klemperer and S. A. Rice, *ibid.* **26**, 618 (1957).

[7] I. V. Godnev, A. M. Aleksandrovskaya, and I. V. Regina, Optika i Spektroskopia **7**, 271 (1959); (translation) Optics and Spectroscopy **7**, 172 (1959). The last sentence of the translated version should read "In the case of zirconium halides the calculated frequency ν_1=382 cm^{-1} likewise agrees well with the experimental (383 cm^{-1})."

Electrical Conduction in Polycrystalline Lead Zirconate-Titanate

C. V. STEPHENSON AND C. E. FLANAGAN*

Southern Research Institute, Birmingham, Alabama

(Received December 16, 1960)

POLYCRYSTALLINE lead zirconate-titanate is well known for its exceptional piezoelectric properties.[1] This material has also been reported to have an anomalous pyroelectric behavior.[1,2] An investigation of the anomalous pyroelectric effect has revealed that lead zirconate-titanate is probably an ionic conductor and that the ionic conduction is possibly the cause of its anomalous behavior.

To test the conclusion that ionic conduction exists, the emf of the cell

$$Pt\,|\,Pb, \quad PbO\,|\,PbZr_{.53}Ti_{.47}O_3\,|\,Cu, \quad Cu_2O\,|\,Pt$$

in purified nitrogen has been measured. The emf of this cell was found to be 0.205±0.005 v at 250°C. Steady-state values were reached after about ten hours. The observed value of the emf is close to the theoretical value of 0.200 calculated from free energy of formation curves of PbO and Cu_2O published by Glassner[3] and Rossini, *et al.*[4] The composition of the lead zirconate-titanate used in this experiment was 53 molar percent lead zirconate and 47 molar percent lead titanate. It was obtained from the Clevite Corporation and is designated by Clevite as PZT-1.

Although there is no conclusive evidence as to whether the ionic conduction is due to cation migration or anion migration, there is at least some evidence that part of the conduction is due to oxygen ion migration—possibly via anion vacancies similar to that found by Kiukkola and Wagner[5] in ZrO_2–CaO electrolytes. This evidence comes from experiments in which lead zirconate-titanate is used as the electrolyte in an oxygen-hydrogen fuel cell. In these experiments the ceramic element was used to separate two chambers, one filled with hydrogen, the other with oxygen. The potential of this cell was measured with a Keithley Model 610 electrometer. Under the conditions which prevailed, the steady-state potential of the cell varied from 0.81 v at 325° to about 0.41 v at 700°C. These values should not be construed as ultimate values since they were found to be dependent on the pressure of the oxygen and hydrogen, and our cell was not designed for high pressures. During the operation of the fuel cell, the temperature of the gas in the hydrogen chamber, as measured by a thermocouple placed about 0.25 cm from the surface of the electrolyte, was 5–10°C higher than the temperature of the oxygen as measured by a similarly placed thermocouple, when the cell was operated at high temperatures. When the gases were reversed in the chambers the temperature differential reversed. The reaction then seemed to be going on in the hydrogen chamber. The temperature recorded in the oxygen chamber was always the same as was found in both chambers when both chambers were filled with nitrogen. The hydrogen chamber was kept at a somewhat higher pressure than the oxygen, both being slightly above atmospheric pressure. There was no detectable leak by or through the electrolyte from one chamber to the other. The temperature differential itself would indicate that there was no leak of this type—either that or one would have to explain a unidirectional leak. The temperature differential would not eliminate the possibility of small leaks in the individual chambers; however such were not detected. The current in the electrolyte is estimated to be a few milliamperes per square centimeter at the time of detection of the temperature differential. The heat of reaction of the amount of oxygen needed to produce this current is at least of the right order of magnitude to produce the observed temperature difference. These results would indicate that at least some of the conduction is by oxygen ion migration.

It has also been possible to obtain voltages by a careful selection of electrode materials. When lead zirconate-titanate elements were placed between two electrodes of the same metal—one oxidized, the other unoxidized—small voltages were developed by heating the element to temperatures in the range of 200°C to 500°C. These voltages were always short lived and varied from about 10 mv to about 100 mv for different metals. The current flow during these outputs was usually several orders of magnitude below the measured galvanic currents at the same temperature. Smaller voltages of unpredictable polarity are obtained if both electrodes are either oxidized or unoxidized. This potential presumably arises from the oxidation of the metal electrode and is probably the origin of at least part of the so-called anomalous pyroelectric effect previously observed in lead zirconate-titanate ceramic elements.

* Present address: Muscle Shoals Electrochemical Corporation, Tuscumbia, Alabama.

[1] For references see D. A. Berlincourt, C. Cmolik, and H. Jaffe, Proc. Inst. Radio Engrs. **48,** 220 (1960).

[2] C. V. Stephenson, Bull. Am. Phys. Soc. **3,** 299 (1958).

[3] A. Glassner, U. S. Atomic Energy Commission, Argonne National Laboratory Report ANL-5750 (1957).

[4] F. D. Rossini, D. D. Wagman, W. H. Evans, S. Levine, and I. Jaffe, Natl. Bur. Standards Circ. No. **500,** 158, 207 (1952).

[5] K. Kiukkola and C. Wagner, J. Electrochem. Soc. **104,** 379 (1957).

Nuclear Quadrupole Resonance of BrCl†

M. A. Whitehead and H. H. Jaffé

Department of Chemistry, University of Cincinnati, Cincinnati 21, Ohio

(Received February 3, 1961)

THE ratio (F) of the NQR frequency (F_M) of an atom in a molecule to that (F_A) in the free atom,

$$F = F_M/F_A,$$

has frequently been expressed as

$$F = 1 \pm i - s^2 + d^2 - \pi, \tag{1}$$

where i is the ionic character, s and d are the % s and d character, respectively, in the bonding hybrid orbital, and the plus or minus applies according to whether the atom concerned is the positive or negative end of the dipole, and π is the fractional π bond character.[1] The contributions of d orbitals have frequently been ignored, and in a molecule such as BrCl π must be zero. Equation (1), with neglect of d and π, actually is obtained by neglecting the presumable small term is^2 in Eq. (2);

$$F = (1 \pm i)(1 - s^2). \tag{2}$$

In BrCl, two frequencies are observed, one for each atom, and each may be expected to be determined by an expression of the form of Eq. (2). In these two expressions

$$F_{Cl} = (1 - i)(1 - s_{Cl}^2) \tag{3}$$

$$F_{Br} = (1 + i)(1 - s_{Br}^2), \tag{4}$$

i is the same, but s_{Cl} and s_{Br} may be different, since the two atoms may be differently hybridized. Multiplication of (3) and (4) yields

$$F_{Cl}F_{Br} = (1 - i^2)(1 - s_{Cl}^2)(1 - s_{Br}^2) \leq 1. \tag{5}$$

The limit of $F_{Cl}F_{Br} = 1$ implies $i = s_A = s_B = 0$, and hence $F_{Cl} = F_{Br} = 1$.

The experimental values obtained for this molecule are: $F_M^{Cl} = 51.8$ Mc, $F_A^{Cl} = 54.87$ Mc, $F_M^{Br} = 438.3$ Mc, $F_A^{Br} = 384.9$ Mc,[2] hence, $F_{Cl} = 0.944$, $F_{Br} = 1.139$, $F_{Cl} \cdot F_{Br} = 1.075$, violating the condition of Eq. (5). The validity of neglecting π cannot be questioned unless some $p\pi - d\pi$ resonance were postulated. The discrepancy from $F_{Cl}F_{Br} = 1$ cannot be ascribed to experimental error, not only because the magnitudes of the shifts are too large, but also $F_{Cl} \cdot F_{Br} = 1$ would imply $F_{Cl} = F_{Br} = 1$, which is obviously not the case. Consequently, the only alternative appears to be to assume involvement of d orbitals. Although use of $p\pi d\pi$ hybridization cannot be excluded, it seems more attractive to postulate use of d orbital in the bromine σ bonding orbital. This is partially justified since Br is the positive end of the dipole, and consequently its d orbitals are contracted.[3] Crude estimation shows that use of a few percent of d character is sufficient to explain the observed Cl frequency, without involvement of Cl s electrons, since the Br electronegativity is lowered and hence i increased. The Br frequency is similarly explained, *provided* hybridization with d electrons *exceeds* that with s electrons.

† Support of this work by Wright Air Development Division, U. S. Air Force is gratefully acknowledged.

[1] T. P. Das and E. L. Hahn, *Nuclear Quadrupole Resonance Spectroscopy* (Academic Press, Inc., New York, 1958), p. 138.

[2] W. Gordy, W. V. Smith, and R. F. Trambarulo, *Microwave Spectroscopy* (John Wiley & Sons, Inc., New York, 1953), p. 363.

[3] D. P. Craig, A. Maccoll, R. S. Nyholm, L. E. Orgel, and L. E. Sutton, J. Chem. Soc. **1954,** 332; cf. R. S. Mulliken, J. Am. Chem. Soc. **77,** 884 (1955).

Dependence of Vibrational Relaxation Time on the Vibrational Quantum Number. Experimental Verification for NO($A\ ^2\Sigma^+$) behind Shock Waves*

Walter Roth

Physics Division, Armour Research Foundation, Chicago 16, Illinois

(Received February 23, 1961)

THE theoretical dependence of the vibrational transition probability on vibrational quantum number v was reported[1,2] and more recently was derived in detail

by Penner.[3] For a nonrotating harmonic oscillator, the transition probability, $A_{v,v-1}$ is proportional to $|X_{v,v-1}|^2$ where $X_{v,v-1}$ is the matrix element for the x component of the dipole moment. The dipole moment, may be represented by the series expansion

$$\mu=\sum_i \mu_i(r-r_e)^i.$$

However, it has been shown[4] that μ is approximately a linear function of r for values of r not much different from the equilibrium internuclear distance, r_e. Thus, for transitions originating from vibrational levels of low v, the dipole moment may be represented to a good approximation by

$$\mu=\mu_0+\mu_1(r-r_e).$$

Substituting this into the expression for $X_{v,v-1}$ leads to the result

$$X_{v,v-1}=\mu_1(v/2\alpha)^{\frac{1}{2}},$$

where μ_1 and α are constants. It follows that $A_{v,v-1}$ is proportional to v and $A_{v,v-1}=vA_{1,0}$. From this it is clear that collision-induced vibrational relaxation times, at constant temperature and density, are related by

$$\tau_{v,v-1}=\tau_{1,0}/v.$$

This relationship is valid only for the harmonic oscillator and for small $(r-r_e)$ and is therefore applicable only to transitions involving low v.

In a recent shock-tube study[5] of vibrational relaxation in the $A\ ^2\Sigma^+$ state of NO, it was shown that

$$\tau_{1,0}=t/\ln\left\{\frac{[\mathrm{NO}(A\ ^2\Sigma^+)_{v'=1}]_0}{[\mathrm{NO}(A\ ^2\Sigma^+)_{v'=1}]_t}\right\}\equiv t/\ln R,$$

where t is the time between nonequilibrium emission intensity peaks from $\gamma(1,1)$ and $\gamma(0,0)$ bands and the ratio in the denominator R is merely a measure of the decay of $v'=1$ population in NO$(A\ ^2\Sigma^+)$. In continuation of the study on NO, measurements were made of the temporal behavior of $\gamma(2,7)$ and $\gamma(1,6)$ at 2763 and 2810 A, respectively, behind shock waves in Xe+5% air. The ratio R was determined by observing the decay of $\gamma(2,6)$ at 2630 A. The measurements were used to calculate $\tau_{2,1}$ for NO$(A\ ^2\Sigma^+)$. All of the measurements were made under conditions such that temperatures and total densities behind incident shock waves were about 6950°K and 1.29×10^{17} cm^{-1}. Under these conditions $\tau_{2,1}$ was 6.7μsec. The earlier work[5] indicated that, under the same conditions, $\tau_{1,0}$ was 12.5 μsec. Thus $\tau_{1,0}/\tau_{2,1}\approx1.9$ in good agreement with the theoretical prediction of a value of 2.

* Work supported by The Bendix Corporation under contract to the U. S. Army Rocket and Guided Missile Agency.

[1] H. A. Bethe and E. Teller, Ballistic Research Labs., Report X 117 (1941), p. 30.

[2] K. E. Herzfeld and T. A. Litovitz, *Absorption and Dispersion of Ultrasonic Waves* (Academic Press, Inc., New York, 1959), p. 348.

[3] S. S. Penner, *Quantitative Molecular Spectroscopy and Gas Emissivities* (Addison-Wesley Publishing Company, Reading, Massachusetts, 1959), p. 124.

[4] G. Herzberg, *Spectra of Diatomic Molecules* (D. Van Nostrand Company, Princeton, New Jersey, 1950), p. 97.

[5] W. Roth, J. Chem. Phys. **34**, 999 (1961).

Electron Spin Resonance of Crystalline Free Radicals

JEROME I. KAPLAN

Brandeis University, Waltham, Massachusetts

(Received January 12, 1961)

IN this note we wish to point out how Van Vleck's spin Hamiltonian[1]

$$H=g\beta H_0\sum_i S_{z_i}+\sum_{i\pm j}A_{ij}\mathbf{S}_i\cdot\mathbf{S}_j+g^2\cdot\beta^2\sum_{i\neq j}\frac{\mathbf{S}_i\cdot\mathbf{S}_j}{r_{ij}^3}-\frac{3(\mathbf{S}_i\cdot\mathbf{r}_{ij})(\mathbf{S}_j\cdot\mathbf{r}_{ij})}{r_{ij}^5} \quad (1)$$

for the computation of spin resonance linewidths in solids must be modified if the local "spin sites" are not ions but molecules.

We take as our physical picture an ordered array of molecules, each with one unpaired electron. It is assumed the wave function for this one electron can be represented by a molecular orbital which is the product of a spin and orbital part. The total wave function for the crystal will be a linear combination of Slater determinants made up of the above defined one-particle wave functions.

The interaction between two electrons is given by

$$\frac{e^2}{r_{ij}}+g^2\beta^2\left[\frac{S_iS_j}{r_{ij}^3}-\frac{3(\mathbf{S}_i\cdot\mathbf{r}_{ij})(\mathbf{S}_j\cdot\mathbf{r}_{ij})}{r_{ij}^5}\right]. \quad (2)$$

As is well known the first term gives rise to an exchange spin interaction $A_{ij}S_i\cdot S_j$ as a result of the antisymmetric character of the Slater determinant. The second term will give rise to a direct interaction

$$\iint d\tau_i d\tau_j\psi_i^*\psi_i\left[\frac{\mathbf{S}_i\cdot\mathbf{S}_j}{r_{ij}^3}-\frac{3(\mathbf{S}_i\cdot\mathbf{r}_{ij})(\mathbf{S}_j\cdot\mathbf{r}_{ij})}{r_{ij}^5}\right]\psi_j^*\psi_j \quad (3)$$

and an "exchange interaction" which being much smaller we will neglect. The ψ_i and ψ_j are the orbital parts of the spin wave function on sites i and j, respectively. If ψ_i and ψ_j are atomic wave functions centered at sites i and j then Eq. (1) will be very nearly correct if the r_{ij} are taken to be the internuclear distances. Only in the case that ψ_i and ψ_j are delta functions (i.e., for the nuclear dipole interactions) centered at nuclear sites i and j will r_{ij} be the exact internuclear distance. We will ignore the distinction and treat each atomic wave function as if it were a delta function.

For the general case of a molecule one can approximately represent ψ_i as a linear combination of atomic orbitals or

$$\psi_i=\sum_n C_{n(i)}\phi_n. \tag{4}$$

Substituting the atomic orbital form of ψ_i in Eq. (3) one obtains the second moment of the line shape to be given as[1]

$$\Delta\nu^2=\tfrac{1}{3}S(S+1)h^{-2}\sum_k B_{jk}^2, \tag{5}$$

where

$$B_{jk}=-3g^2\beta^2\sum_{n(j),m(k)} r^{-3}[\tfrac{3}{2}\gamma^2_{n(j)m(k)}-\tfrac{1}{2}]C_{n(j)}^2C_{m(k)}^2,$$

where $\gamma_{n(j)m(k)}$ is the cosine of the angle between the magnetic field and the radius vector between atoms located at sites $n(j)$ and $m(k)$. For nearby spins there will be an appreciable alteration in B_{jk}^2 depending on whether the spin is localized or spread out. Consider as an example two wheel-like molecules of radius l located l units apart on an imaginary axle. For the localized spin the orbital part of the wave function is taken to be $\psi_\pm=\delta(r\pm\mathbf{i}l/2)$ and for the nonlocalized spins

$$\psi_\pm=\frac{1}{(5)^{\frac{1}{2}}}\delta(r\pm\mathbf{i}l/2)$$

$$+\frac{1}{(5)^{\frac{1}{2}}}\sum_{\epsilon_1,\epsilon_2=\pm1}\delta(r\pm\mathbf{i}l/2+\mathbf{j}\epsilon_1 l/\sqrt{2}+\mathbf{k}\epsilon_2 l/\sqrt{2}).$$

The ratio of B_{jk}^2 for the nonlocalized spin to the localized spin will be about 1:20.

The point to be made is that for near neighbors some approximation to the true spin distribution must be used or else one may obtain an entirely false value for the linewidth.

[1] J. H. Van Vleck, Phys. Rev. **74**, 1168 (1948).

Crystal Spectra of Metal Coordination Compounds. V. The Five-Coordinated Salicylaldehyde-ethylenediimine Copper(II) Complex.

J. FERGUSON

Division of Chemical Physics, C. S. I. R. O. Chemical Research, Laboratories, Melbourne, Australia

(Received February 6, 1961)

THE crystal structure of *bis*-salicylaldehyde-ethylenediimine-copper has recently been reported.[1,2] It is of unusual interest because the molecules of the complex occur in pairs and there is a significant distortion which results in a five-coordinated pyramidal copper ion. The lack of definite cases of five-coordinated copper makes it of some interest to record the absorption spectrum of the crystal even if only for its diagnostic use.

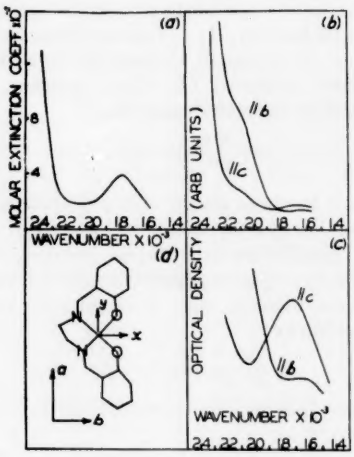

FIG. 1. (a) Absorption spectrum in chloroform; (b) absorption spectrum of a single crystal about 5 μ thick, light incident on the (100) face; (c) same as (b) except that crystal is about 25 μ thick; (d) projection of the molecule on the (001) face.

The compound was prepared by a standard method[3] and crystals were grown from chloroform. The monoclinic plates have the (100) face predominant[4] and the axes in this face were determined by x-ray methods.[5] The crystals were examined under a reflecting microscope and the spectra recorded with a Hilger constant-deviation spectrometer.[6] Three crystal faces were used: (100), (001), and (010), the latter two being obtained by embedding the crystals in paraffin wax and cutting sections with a hand microtome.

The molecule does not possess a center of symmetry and this accounts for the relatively high intensity ($\epsilon\sim400$) of the visible band (17 900 cm^{-1}) in solution [Fig. 1(a)]. The spectrum of the crystal is quite different and there are two bands in place of the one in solution. Figures 1(b) and 1(c) show spectra for light incident on the (100) face for two crystals of different thickness. These spectra show that there are two bands in the crystal, one at 20 800 cm^{-1}, overlapped by ligand absorption, and the other at 17 300 cm^{-1}.

It is possible to determine the polarization of the two bands from observations with the different crystal faces and, to help see the relation between the polarization of the bands and the molecular orientation, one of the relevant projections is shown in Fig. 1(d). Other projections and atomic coordinates are given by Hall and Waters.[1] The length of the molecule lies along the a axis and, in addition, the mean molecular plane is close to the (001) plane.

The band at 20 800 cm^{-1} absorbs strongly in the (100) plane mainly along the b axis. This means that

the absorption band is polarized along the x direction. If there is any z component, then it must be much less than the x component, while the projection cannot give a clear decision as to whether the band has a y component, because of the very small projection that this vector makes on the (100) plane.

The band at 17 300 cm^{-1} appears weakly in thin crystals but is clearly seen with crystals about 30 μ thick. The band is polarized more strongly perpendicular to the b axis than parallel to it. This is expected for a band polarized along the y direction in the molecule and was confirmed when observations were made with the (001) and (010) sections. These were about 15 μ thick and in both of them absorption was complete for light polarized along the a axis but light was transmitted perpendicular to this axis. The band is then strongly polarized along the molecular y axis and this explains the weak absorption for light incident on the (100) face.

It is hoped that some theoretical study of the problem might be stimulated by the results of this investigation. The configuration of the ligands around the copper ion is certainly an unusual one and the absorption spectrum is markedly different from that in solution (square-planar). Instead of one band in solution, two are found in the crystal. Unlike other copper complexes, which have centers of symmetry, the bands are not of mixed molecular polarization but are strongly polarized in the mean molecular plane and there is no significant absorption normal to the plane.

The closely related complex *bis*-acetylacetone-ethylenediimine-copper was also studied but the crystal absorption was found to be unchanged from that in solution and it must be concluded that there is no change in the configuration of the copper ion in this crystal.

[1] D. Hall and T. N. Waters, J. Chem. Soc. **1960,** 2644.
[2] K. Pachler and M. V. Stackelberg, Z. anorg. u. allgem. Chem. **305,** 286 (1960).
[3] P. Pfeiffer and E. Breith, Ann. Phys. **503,** 110 (1933).
[4] M. V. Stackelberg, Z. anorg. u. allgem. Chem. **253,** 136 (1947).
[5] This determination was kindly made by Dr. A. McL. Mathieson of this Division.
[6] J. Ferguson, J. Chem. Phys. **34,** 611 (1961).

Nuclear Magnetic Resonance of Proton Complexes of Weak Bases

C. MacLean and E. L. Mackor

Koninklijke/Shell-Laboratorium, Amsterdam, Netherlands

(Received December 20, 1960)

PROTON exchange often impedes the detection of the proton resonance of conjugate acids of weak bases. A combination of a very strong acid and a low temperature will reduce the exchange rate.[1] Well-defined NMR spectra at 40 Mc/sec were obtained for the proton complexes of water, ethyl alcohol, and acetone when solutions in anhydrous hydrogen fluoride saturated with boron trifluoride were cooled down to about $-75°C$.

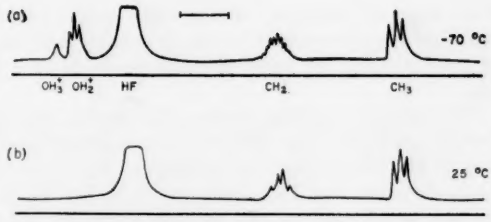

FIG. 1. NMR spectra of $C_2H_5OH_2^+$ (6.9 mole %) in $HF+BF_3$ at $-70°C$ (a) and at room temperature (b). The magnetic field increases from left to right. The scale 50 cps is indicated in the spectrum. Values of chemical shifts at 70°C, with respect to the CH group, are: OH_3^+ (353 cps); OH_2^+ (332 cps); CH_2 (122 cps).

For solutions of water the equilibrium constant of the exothermic reaction

$$HF+H_2O+BF_3 \rightleftharpoons H_3O^+ + BF_4^- + \backsim 15 \text{ kcal/mole},$$

is about 10^4 liter/mole at 20°C, which may mean that the rate of this reaction is sufficiently high to cause fusion of the NMR lines of solvent and ions. At $-75°C$ a well-defined quadruplet structure of the fluorine resonance of the BF_4^- ion is displayed at -1670 cps from the solvent peak. At temperatures above $-50°C$ the proton resonance of the solution is a single peak which is the combined signal of the acid and the hydronium ion. As the temperature is decreased below $-50°C$ the peaks of HF and H_3O^+ separate gradually and at $-75°C$ the exchange rate is smaller than 10 sec^{-1}. This is in agreement with a greatly increased equilibrium constant estimated to be 10^9 liter/mole at $-75°C$.

The chemical shift at $-75°C$ of the H_3O^+ ion is -71 cps with respect to the solvent peak or -173 cps with respect to liquid water at room temperature. This value, which corresponds to -4.3 ppm is much smaller than the extrapolated values of -9.2 to -11.8 ppm obtained from NMR measurements on mixtures of acids and water at room temperature.[2]

The spectra of solutions of ethyl alcohol are reproduced in Fig. 1(a) and (b). Both the intensities and the multiplet structure prove the spectrum in Fig. 1(a) to belong to a stable $C_2H_5OH_2^+$ ion. The coupling constant of the CH_2 group with the OH_2^+ group is smaller than the corresponding one in ethyl alcohol (2.6 cps and 4.8 cps, respectively). The multiplet structure of the CH_2 group gradually changes owing to coupling with the two neighboring groups. The small peak at the extreme left of the spectrum belongs to the hydronium ion. Thus the shielding of the protons is smaller in the H_3O^+ ion than in the OH_2^+ group.

An example of the proton complex of a ketone is furnished by a solution of acetone in HF-BF_3 at $-75°C$.

The magnetic shielding of the OH^+ group (-225 cps from the solvent peak) is much smaller than that of the H_3O^+ ion, the signal of which is visible at -75 cps.

The spin-spin coupling between the proton and the fluorine nucleus in the HF molecule is generally obscured by lifetime-limiting processes. In favorable cases, however, the HF resonance, both for ^1H and ^{19}F, has been found to split up into a doublet at low temperatures. The separation of the pair in these doublets was determined to be 521 cps. A less accurate value of this coupling constant (615 cps) has been very ingeniously obtained by Solomon and Bloembergen[3] using an indirect technique.

[1] C. MacLean, J. H. van der Waals, and E. L. Mackor, Mol. Phys. **1**, 247 (1958).
[2] H. S. Gutowsky and A. Saika, J. Chem. Phys. **21**, 1688 (1953); G. C. Hood, O. Redlich, and C. Reilly, *ibid.* **22**, 2067 (1954).
[3] I. Solomon and N. Bloembergen, J. Chem. Phys. **25**, 261 (1956).

Proton Exchange in Carbonium Ions of Methyl-Substituted Benzenes

C. MacLean and E. L. Mackor

Koninklijke/Shell-Laboratorium, Amsterdam, Netherlands

(Received December 20, 1960)

NUCLEAR magnetic resonance experiments at 40 Mc/sec on proton complexes of methyl-substituted benzenes have demonstrated an interesting type of proton exchange in which the exchanging proton distributes its time over different positions within one ion.

The spectra of mesitylene dissolved as its proton complex in anhydrous hydrogen fluoride, saturated with boron trifluoride, are reproduced in Fig. 1. These spectra can be understood in terms of the following proton exchange reaction:

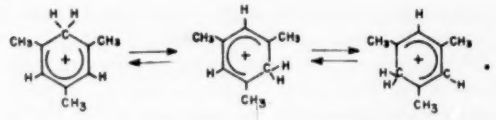

At $-75°C$ the exchange is slow and four separate peaks are observed. In the order of increasing field these are the broadened peak of HF, that of the ring protons, the H—C—H group and the protons of the methyl groups in ortho position with a shoulder of the methyl group in para position.[1] Only two lines are observed at room temperature; one caused by the four ring protons and one by the three methyl groups. The position of the first peak is halfway between the peaks of the ring protons and of the CH_2 group as measured at $-75°C$. These results prove unambiguously that the

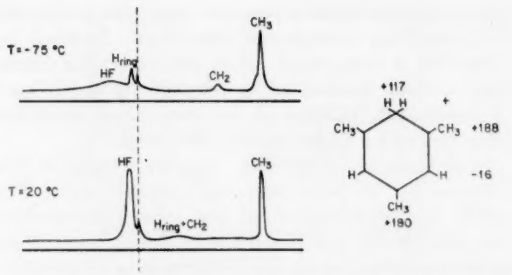

FIG. 1. Spectra at 40 Mc/sec of the proton complex of mesitylene (5 mole %) in $HF+BF_3$. The dotted line represents the chemical shift of benzene which was used as an internal reference. Peaks on the extreme left are solvent lines. The chemical shifts with respect to benzene are indicated in the diagram.

proton exchange does not proceed via the acid, but that the captured proton remains on the ion while it jumps between positions of equal proton affinity.

The energy of activation for this process, as determined from the temperature variation of the spectra, is about 10 kcal/mole. This value is somewhat smaller than the heat of formation of the compound of 14 kcal/mole at 0°C.[2]

The exchange proceeds at about the same rate in hexamethylbenzene as in mesitylene. No exchange is observed in pentamethylbenzene, where the unsubstituted carbon atom possesses the highest proton affinity.

The results of our measurements on mesitylene, 1,3,4-trimethylbenzene, durene, and 1,3,4,5-tetramethylbenzene can be summarized as follows. The chemical shifts at $-75°C$ of ring protons in the para and the meta position with respect to the CH_2 group are -52 cps and -16 cps from benzene used as internal reference. These shifts to lower field are caused by positive charges on the adjacent carbon atoms. The "pure" charge shifts should be taken with respect to the resonance of a proton bonded to a sp^2 carbon atom ($\sim+75$ cps from benzene), because the ring current effect is not operative in the ion. This leads to -127 cps and -91 cps for the charge shifts of para and meta ring protons and to about -113 cps for the value of the ortho shift.[3] This adds up to a shift of -535 cps (13.4 ppm) per unit charge. Fraenkel, Carter, McLachlan, and Richards[4] have determined charge shifts in the systems $C_5H_5^-$, C_6H_6, and $C_7H_7^+$. Assuming that the charge shift is proportional to the excess charge on the adjacent carbon atom they calculate a shift of 10 ppm per unit charge. The sign of the shift is determined by the sign of the excess charge and therefore a description of the charge shifts in terms of a simple electrostatic model[5,6] cannot be adequate. This model would lead to a negative charge shift which is proportional to the square of the excess charge; although in the CH fragment it gives the reasonable value 14 ppm for the calculated charge shift per (unit charge)^2, the experi-

mental shifts, if described in terms of this model would correspond to about 70 ppm per (unit charge).[2]

If the shifts of −127, −113, and −91 cps of the ring protons in para, ortho, and meta position are attributed exclusively to the excess charges on the adjacent carbon atoms, the following charge densities emerge:

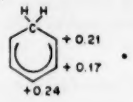

The charge distribution is much more even than that according to calculations with the Hückel method. Calculations according to Wheland and Mann[7] give fair agreement.

[1] C. MacLean, J. H. van der Waals, and E. L. Mackor, Mol. Phys. **1,** 247 (1958).
[2] E. L. Mackor, A. Hofstra, and J. H. van der Waals, Trans. Faraday Soc. **54,** 186 (1958).
[3] C. MacLean and E. L. Mackor (to be published).
[4] G. Fraenkel, R. E. Carter, A. McLachlan, and J. H. Richards, J. Am. Chem. Soc. **82,** (1960) 5846.
[5] H. S. Gutowsky, J. Chem. Phys. **31,** 1683 (1959).
[6] T. W. Marshall and J. A. Pople, Mol. Phys. **1,** 199 (1958).
[7] G. W. Wheland and D. E. Mann, J. Chem. Phys. **17,** 264 (1949).

Announcement

The Division of Chemical Physics of the American Chemical Society, in accordance with its By-Laws, hereby announces the result of the election of new officers: for Vice-Chairman, H. P. Broida; for Secretary-Treasurer, J. C. Decius; for Member of the Executive Committee, D. A. Ramsay.

The complete new list of officers, with the years of retirement, is as follows:

H. McConnell, Chairman (1962)
H. P. Broida, Vice-Chairman (1962)
J. C. Decius, Secretary-Treasurer (1964)
D. A. Ramsay, Executive Committee (1964)
R. Herman, Executive Committee (1963)
T. R. Berlin, Executive Committee (1962)
J. R. Platt (Ex-Chairman), Executive Committee (1962)

Arthur A. Frost
Retiring Secretary-Treasurer

Author Index to Volume 34

(References with (L) are to Letters to the Editor.)

Abraham, R. J. Solvent effects in nuclear magnetic resonance—1062(L)

Acquista, N. (see Mann, D. E.)—420

Adams, O.W. and P. G. Lykos. Open- and closed-shell SCF method for conjugated systems—1444(L)

Adams, William H. On the solution of the Hartree-Fock equation in terms of localized orbitals—89

Adrian, F. J. (see Cochran, E. L.)—1161

Akon, C. D. and T. Iredale. Nuclear quadrupole and electron spin resonance spectra of some chlorine compounds including $(Me_3PhN)(FeCl_4)$—340(L)

Albrecht, Andreas C. On the theory of Raman intensities—1476

Alexander, P. W., A. R. Lacey, and L. E. Lyons. Absorption and luminescence origins in anthracene crystals—2200(L)

Alexander, S. Spin-spin interactions in nuclear magnetic resonance. Contact contribution—106

Alire, R. M. (see Crosby, G. A.)—743

Allen, Leland C. Wave functions and correlation energies for F, F^-, and Ne—1156

Allnatt, Alan R. and Stuart A. Rice. On the kinetic theory of dense fluids. VII. Doublet distribution function for rigid spheres with an attractive potential—2156

—— (see Rice, Stuart A.)—409, 2144

Amat, Gilbert and Harald H. Nielsen. Erratum: Higher order rotation-vibration energies of polyatomic molecules. IV—339(L)

Amdur, I., J. E. Jordan, and S. O. Colgate. Scattering of high-velocity neutral particles. XI. Further study of the He-He potential—1525

Amma, E. L. and G. A. Jeffrey. Study of the Wurtzite-type compounds. V. Structure of aluminum oxycarbide, Al_2CO; a short-range Wurtzite-type superstructure—252

Amstutz, G. C. (see Petz, John I.)—526

Anbar, Michael, Shmuel Guttmann, and Gabriel Stein. Radiolysis of aqueous solutions highly enriched in O^{18}—703

Anderson, Ernest W. (see Douglass, Dean C.)—152

—— (see McCall, David W.)—804

Anthrop, Donald F. (see Davis, Stanley G.)—659

Arajs, Sigurds, R. V. Colvin, and J. M. Peck. Paramagnetic susceptibility of polycrystalline praseodymium metal—1959

Arbell, H. (see Halperin, A.)—879

Aston, J. G. (see Fritz, J. J.)—344(L), 2185(L)

Balchan, A. S. and H. G. Drickamer. Effect of pressure on the resistance of iodine and selenium—1948

Baldeschweiler, John D. Quadrupole relaxation effects in nuclear magnetic double resonance—718

—— (see Fulton, Robert L.)—1075(L)

Balk, P. (see Benson, G. C.)—157

Ball, J. J. (see Mann, D. E.)—420

Banyard, K. E. Diamagnetic susceptibility of Ne, NH_3, and CH_4—338(L)

—— "Floating" hydrogen densities in some molecules of the type XH_n—2105

Bartz, Kenneth W. (see Stehling, Ferdinand C.)—1076(L)

Baum, Lillian H. (see Siegel, Seymour)—339(L), 1782

Bauman, Robert P. and James P. Considine. Derivation of interelectronic screening parameters from statistical considerations—1388

Beal, James B., Jr. (see Hilton, A. Ray, Jr.)—1137

Bearman, Richard J. and V. S. Vaidhyanathan. Composition dependence of the thermal conductivity of regular solutions—264

Beaumont, R. H., H. Chihara, and J. A. Morrison. Transitions between different forms of ice—1456(L)

Belford, Geneva (see Belford, R. Linn)—1330

Belford, R. Linn. Paramagnetism of uranyl ion. Effect of $6d$ orbitals and pi bonding—318

—— **and Geneva Belford.** Pi bonding in uranyl ion—1330

Benson, G. C., E. Dempsey, and P. Balk. Distortion correction to the surface energy of the {110} face of alkali halide crystals—157

Benson, Sidney W. Reaction of cyclopropane with iodine and some observations on the isomerization of cyclopropane—521

—— **and Edward O'Neal.** Kinetics of the reactions of alkyl iodides with HI—514

Bentley, W. H. and H. G. Drickamer. Effect of pressure on the spectra of MnO_4^- and $CrO_4^=$—2200(L)

Berkowitz-Mattuck, J. B. (see Büchler, Alfred)—2202(L)

Berlman, Isadore B. Luminescence in a scintillation solution excited by α and β particles and related studies in quenching—598

—— Transient dimer formation by 2,5-diphenyloxazole—1083(L)

Bernal, Ivan and S. E. Harrison. Electron spin resonance and optical absorption of $K_3[Cr(CN)_5NO]\cdot H_2O$—102

Bernheim, Robert A., H. S. Gutowsky, and Ian J. Lawrenson. Temperature dependence of the proton spin-lattice relaxation time in liquid butyl alcohols—565

Bernstein, Richard B. Quantum calculations of the velocity dependence of the differential and total cross sections for elastic scattering of molecular beams—361

Berry, R. S., R. Dehl, and W. R. Vaughan. Nuclear magnetic resonance spectrum of the triphenylcarbonium ion—1460(L)

Besnainou, S. (see Bratož, S.)—1142

Bigeleisen, Jacob. Statistical mechanics of isotope effects on the thermodynamic properties of condensed systems—1485

Bingel, Werner A. Spin dependence of the first-order transition density matrix—1066(L)

Blander, Milton. Quasi-lattice model of reciprocal salt systems. A generalized calculation—432

—— Some calculations for a one-dimensional salt mixture—697(L)

Blau, Edmund J., Bernard F. Hochheimer, and Hilbert J. Unger. Infrared spectrum of diimide—1060(L)

Blinder, S. M. (see Lord, N. W.)—1693

Bloembergen, N. and L. O. Morgan. Proton relaxation times in paramagnetic solutions. Effects of electron spin relaxation—842

Blomgren, George E. An extended hole theory of liquids—1307

Bloom, M. (see Lipsicas, M.)—1813

Bloomfield, Philip, A. W. Lawson, and Charles Rey. Crystal field splitting and covalent bonding in Fe^{++} silicate garnets—749

Boll, R. H. Calculation of complex equilibrium with an unknown number of phases—1108

Boozer, C. E. (see Reddy, G. S.)—700(L)

Boston, Charles R. (see Smith, G. Pedro)—1396

Bottger, G. (see Dows, David A.)—689(L)

Bowen, William A., Jr. (see Buchanan, Robert A.)—348(L)

Bowers, V. A. (see Cochran, E. L.)—1161

Brackman, R. T. and Wade L. Fite. Condensation of atomic and molecular hydrogen at low temperatures—1572

Brady, George W. and John I. Petz. Clustering in the critical region—332(L)

Bratož, S. and S. Besnainou. Influence of the molecular environment on the carbonyl frequency. Electronic calculation—1142

Bredig, M. A. (see Bronstein, H. R.)—1843(L)
Bree, A. and W. G. Schneider. "Sub-threshold" photocurrents of high-quantum yield in 9,10-dichloroanthracene—1453(L)
Brient, S. J. (see Brigman, G. H.)—958
Briglia, Donald D. (see Hertzberg, Martin)—343(L)
Brigman, G. H., S. J. Brient, and F. A. Matsen. Interaction of a triplet and a normal helium atom—958
Broida, H. P. (see Krisnamachari, S. L. N. G.)—1709
Bronstein, H. R., A. S. Dworkin, and M. A. Bredig. Electrical conductance of solutions of salts in liquid metals. Potassium iodide in potassium—1843(L)
Brown, Robert J. S. and Don D. Thompson. Second-order effects in low-field NMR for ammonium ion solutions—1580
Broyles, A. A. Radial distribution function from the Percus-Yevick equation—1068(L)
—— Solution at high density to the Born-Green equation—359
Brush, Stephen G. Statistical thermodynamics of mixtures. II. Convergence of the quasi-chemical method for the Ising square lattice—1852(L)
Buchanan, Robert A. and William A. Bowen, Jr. LiOH hydration effects in pressed alkali halide pellets—348(L)
Büchler, Alfred, J. B. Berkowitz-Mattuck, and Donald H. Dugre. Infrared spectra of some group IV halides—2202(L)
Buckingham, A. D., T. Schaefer, and W. G. Schneider. Solvent effects in nuclear magnetic resonance—1064(L)
Buijs, K. (see Strasheim, A.)—691(L)
Burns, R. P. (see Grimley, R. T.)—664
Burton, M. (see Nosworthy, J. M.)—83

Calvin, Melvin (see Kearns, David R.)—2022, 2026
Camac, Morton. O_2 vibration relaxation in oxygen-argon mixtures—448
—— **and Arthur Vaughan.** O_2 dissociation rates in O_2–Ar mixtures—460
Carlson, E. H. and G. H. Dieke. State of the Nd^{3+} ion as derived from the absorption and fluorescence spectra of $NdCl_3$ and their Zeeman effects—1602
Carlson, F. F. (see King, G. J.)—1499
Carter, R. E. Kinetic model for solid-state reactions—2010
Cassel, H. M. and I. Liebman. Note on the sublimation of ammonium perchlorate—343(L)
Castellano, S. and J. S. Waugh. Strong coupling in nuclear resonance spectra. IV. Exact analysis of three-spin spectra —295
Caughey, W. S. (see Roberts, E. M.)—591
Cavanaugh, James R. and B. P. Dailey. NMR spectra of propyl derivatives—1094
—— **and B. P. Dailey.** Proton chemical shifts for the alkyl derivatives—1099
Chan, Sunney I., John Zinn, and William D. Gwinn. Trimethylene oxide. II. Structure, vibration-rotation interaction, and origin of potential function for ring-puckering motion—1319
Chang, Ike Y. (see Ferguson, E. E.)—628
Chantry, G. W. and R. A. Plane. Raman intensities and the structure of some oxyanions of group VII—1268
Chen, Mei Chio and H. Austin Taylor. Reaction of nitrogen atoms with ozone—1344
Chesnut, D. B., H. Foster, and W. D. Phillips. EPR studies of spin correlation in some ion radical salts—684(L)
Chihara, H. (see Beaumont, R. H.)—1456(L)
Chin, David and Paul A. Giguère. Torsional oscillation frequency of H_2O_2—690(L)
Choi, Q. Won and W. Gilbert Clark. Spin-lattice relaxation time of F^{19} nuclei in Ag_2F—1584
Christy, R. W. Thermoelectric power of silver halides—1148
Clark, W. Gilbert (see Choi, Q. Won)—1584
Clayton, Glen T. (see Kim, Young Soo)—1464(L)
Clayton, Robert N. Oxygen isotope fractionation between calcium carbonate and water—724
Clementi, Enrico. Ground-state wave functions for linear molecules—1468(L)
Clinton, William L. Sum rule for transition probabilities—273
Cochran, E. L., F. J. Adrian, and V. A. Bowers. Anisotropic hyperfine interactions in the ESR spectra of alkyl radicals—1161
Coggeshell, N. D. (see Saraceno, A. J.)—260
Cohan, Norah V. (see Tschudi, Carman S.)—401
Cohen, Morrel H. (see Turnball, David)—120
Colburn, Charles B. (see Ettinger, Raymond)—2187(L)
Cole, G. H. A. Fluid superposition approximation and the fourth virial coefficient—2016
Cole, T. and C. Heller. Hyperfine splittings in the $(HOOC)C^{13}H(COOH)$ radical—1085(L)
——, **C. Heller, and J. Lambe.** Electron nuclear double resonance in irradiated organic crystals—1447(L)
Colgate, S. O. (see Amdur, I.)—1525
Collins, R. L. Complex cyclotron resonance in dilute gases—1425
Colvin, R. V. (see Arajs, Sigurds)—1959
Considine, James P. (see Bauman, Robert P.)—1388
Conway, John G. (see Gruber, John B.)—632
Coogan, C. K. (see Stalinski, B.)—1191
Cormia, Robert L. (see Turnbull, David)—820
Cox, James R., Jr., and James D. Ray. *Bis*-liganded nitrosyl as a reaction intermediate—1072(L)
Crawford, Bryce, Jr., and I. Oppenheim. Second law of thermodynamics—1621
Crosby, G. A., R. E. Whan, and R. M. Alire. Intramolecular energy transfer in rare earth chelates. Role of the triplet state—743
Crowell, A. D. and R. B. Steele. Interaction potentials of simple nonpolar molecules with graphite—1347
Cubicciotti, Daniel. Erratum: Lattice energies of the alkali halides and the electron affinities of the halogens—2189(L)
Curl, R. F., Jr. (see Miller, Ronald F.)—1847(L)
Curran, R. K. Low-energy process for F^- formation in SF_6—1069(L)
—— Positive and negative ion formation in CCl_3F—2007
—— **and R. E. Fox.** Mass spectrometer investigation of ionization of N_2O by electron impact—1590
—— (see Fox, R. E.)—1595
Curtis, A. J. Dielectric properties of polyamides—1849(L)

Dahl, A. J. (see Weigang, O. E., Jr.)—1845(L)
Daiber, J. W. (see Freedman, E.)—1271
Dailey, B. P. (see Cavanaugh, James R.)—1094, 1099
—— (see Gordon, Sidney)—1084(L)
Daniels, Farrington (see Johnson, Noye M.)—1434
Das, T. P. (see Karplus, M.)—1683
Datz, Sheldon, William T. Smith, Jr., and Ellison H. Taylor. Molecular association in alkali halide vapors—558
Davidson, Ernest R. Comparison of theoretical calculations on diatomic molecules with experiment—1240
Davies, William O. (see Steinberg, Martin)—1373
Davis, Stanley G., Donald F. Anthrop, and Alan W. Searcy. Vapor pressure of silicon and the dissociation pressure of silicon carbide—659
Dearman, Henry H. and Ronald Lefebvre. Method of alternant orbitals for allyl—72
——, **W.W. Porterfield, and H. M. McConnell.** Paramagnetic resonance of *bis*-cyclopentadienyl vanadium in ferrocene—696(L)
DeArmond, Keith (see Forster, Leslie S.)—2193(L)
Dehl, R. (see Berry, R. S.)—1460(L)
Dempsey, E. (see Benson, G. C.)—157
De Rocco, Andrew G. (see Hoover, William G.)—1059(L)
de Vries, A. E. (see van der Valk, F.)—345(L)

DeVries, R. C. and G. W. Sears. Step formation during the growth of $BaTiO_3$ crystals—616
—— (see Sears, G. W.)—2142
Dewar, Michael J. S. and N. L. Hojvat. The SPO (split *p*-orbital) method and its application to ethylene—1232
Diehl, P. and I. Gränacher. Determination of relative signs of spin coupling constants in an AB_2X nuclear magnetic resonance spectrum—1846(L)
Dieke, G. H. (see Carlson, E. H.)—1602
Dillard, Clyde R. (see May, Leopold)—694(L)
Doering, John P. and Bruce H. Mahan. Photolysis of nitrous oxide. I. 1236 A—1617
Doremus, R. H. Pre-exponential factor of temperature in the diffusion equation—2186(L)
Dorman, F. H. and J. D. Morrison. Determination of relative electronic transition probabilities by impact methods—578
—— **and J. D. Morrison.** Ionization potentials of multiply charged krypton, xenon, and mercury—1407
Douglass, Dean C., David W. McCall, and Ernest W. Anderson. Self-diffusion of nearly spherical molecules. Neopentane and tetramethyl silane—152
Dows, David A. and G. Bottger. Infrared spectrum of crystalline boron trichloride—689(L)
—— (see Hollenberg, J. L.)—1061(L)
—— (see Schatz, P. N.)—175
Dravnieks, F. (see Reitz, D. C.)—1457(L)
Dressler, Kurt (see Milligan, Dolphus E.)—1009
Drickamer, H. G. (see Balchan, A. S.)—1948
—— (see Bentley, W. H.)—2200(L)
—— (see Keating, K. B.)—140, 143
—— (see Minomura, S.)—670
—— (see Stephens, D. R.)—937
Drury, J. S. (see Garretson, H. H.)—1957
Duff, Russell E. (see Rink, John P.)—1942
Duffey, George H. (see Macek, Joseph H.—228, 682
Dugre, Donald H. (see Büchler, Alfred)—2202(L)
Duncan, A. B. F. (see La Paglia, S. R.)—125, 350(L), 1003
Dunford, H. B. (see Milton, Earl R. V.)—51
Dworkin, A. S. (see Bronstein, H. R.)—1843(L)

Eargle, Dolan H., Jr., and S. I. Weissman. Spin and charge exchange in anions of biphenyl ether—1840(L)
Eberhart, J. G. (see Katorski, Anthony)—2189(L)
Economou, Nicolaos A. (see Heller, Wilfried)—971
—— (see Pangonis, William J.)—960
Ehrenson, S. and P. E. Phillipson. Theoretical molecular transition probabilities. I. The *V-N* transition in H_2—1224
Ehrlich, Gert. Low-temperature chemisorption. I. Flash desorption of nitrogen—29
—— Low-temperature chemisorption. II. Flash desorption of carbon monoxide—39
Eisenstein, J. C. Absorption spectrum and magnetic properties of osmium hexafluoride—310
—— Magnetic properties and optical absorption spectrum of K_2ReCl_6—1628
Eisner, M. (see Mitchell, R. W.)—651
El-Bayoumi, M. Ashraf and M. Kasha. Energy transfer in hydrogen-bonded *N*-heterocyclic complexes and their possible role as energy sinks—2181(L)
Ellison, Frank O. Role of exchange energy in intermediate-range interactions—2100
El-Sayed, Mostafa F. Amr, M. Kasha, and Y. Tanaka. Ionization potentials of benzene, hexadeuterobenzene, and pyridine from their observed Rydberg series in the region 600–200 A—334(L)
—— **and G. W. Robinson.** Excitation transfer splitting in the $n\rightarrow\pi^*$ transitions of the diazines—1840(L)
Epstein, Lawrence M. (see Gardner, Donald G.)—1653
Erath, Edward H. Crystal field parameters for erbium in $Er(C_2H_5SO_4)_3\cdot 9H_2O$—1985
Ettinger, Raymond, Frederic A. Johnson, and Charles B. Colburn. On the structure of the isomers of N_2F_2—2187(L)
Ewing, George E., Warren E. Thompson, and George C. Pimentel. Erratum: Infrared detection of the formyl radical HCO—1067(L)
Eyring, Edward M. and Austin L. Wahrhaftig. Dependence of calculated and experimental propane mass spectra upon electron voltage—23

Fabricand, Burton P. and Sigmund Goldberg. Proton resonance shifts in alkali halide solutions—1624
Falk, M. and E. Whalley. Infrared spectra of methanol and deuterated methanols in gas, liquid, and solid phases—1554
—— (see Whalley, E.)—1569
Fallon, Robert J., Irwin Tobias, and Joseph T. Vanderslice. Potential energy curves for OH—167
Farmer, J. B., C. L. Gardner, and C. A. McDowell. Energy transfer between triplet states detected by electron spin resonance spectroscopy—1058(L)
Farnsworth, H. E. (see Madden, H. H.)—1186
Ferguson, E. E. and Ike Y. Chang. Intensities of infrared bands of some I_2-alkylbenzene charge-transfer complexes—628
Ferguson, J. Crystal spectra of metal coordination compounds. III. Nickel complexes with salicylaldehyde and its imines—611
—— Crystal spectra of metal coordination compounds. IV. *Bis*-acetylacetonato-copper(II)—1609
—— Crystal spectra of metal coordination compounds. V. The five-coordinated salicylaldehyde-ethylenediimine copper(II) complex—2206(L)
Fine, M. E. (see Greener, E. H.)—1017
Fisher, Michael E. and Basil J. Hiley. Configuration and free energy of a polymer molecule with solvent interaction—1253
Fite, Wade L. (see Brackmann, R. T.)—1572
Fixman, Marshall. Vibrational relaxation in liquids—369
Flanagan, C. E. (see Stephenson, C. V.)—2203(L)
Flotow, Howard E. and Darrell W. Osborne. Heat capacities and thermodynamic functions of ZrH_2 and ZrD_2 from 5 to 350°K and the hydrogen vibration frequency in ZrH_2—1418
Flournoy, John M. (see Siegel, Seymour)—339(L), 1782
Forster, Leslie S. and Keith DeArmond. Luminescence of chromium (III) complexes—2193(L)
Foster, H. (see Chestnut, D. B.)—684(L)
Fox, R. E. and R. K. Curran. Ionization processes in CCl_4 and SF_6 by electron beams—1595
—— (see Curran, R. K.)—1590
Fraenkel, George K. (see Schreurs, Jan W. H.)—756
—— (see Vincow, Gershon)—1333
Fraenkel, Gideon. Site of protonation in methyl formate—1466(L)
Fraga, Serafin and Bernard J. Ransil. Studies in molecular structure. III. Populations analyses for selected first-row diatomic molecules—727
Frank, Henry S. and Arvin S. Quist. Pauling's model and the thermodynamic properties of water—604
Frank, R. C. (see Swets, D. E.)—17, 2187(L)
Freedman, E. and J. W. Daiber. Decomposition rate of nitric oxide between 3000 and 4300°K—1271
Freedman, J. F. and W. D. Robertson. Electrical resistivity of liquid sodium, liquid lithium, and dilute liquid sodium solutions—769
Freeman, G. R. (see Ramaradhya, J. M.)—1726
Fricke, Hugo and David L. Phillips. High-speed computations in diffusion kinetics. III. Solute depletion in the cylindrical one radical-one solute model—905
Friedman, Harold L. Density expansions of correlation functions for equilibrium systems—73
Friedman, L. (see Irsa, A. P.)—330(L)
Fries, R. J. (see Kempter, C. P.)—1994
Frisch, H. L. (see Helfand, E.)—1037

Fritz, J. J., H. J. Maria, and J. G. Aston. Concerning the feasibility of nuclear cooling with palladium hydride—2185(L)
——, **H. J. Maria, and J. G. Aston.** Nuclear cooling with metallic copper—344(L)
Fuchs, R. and A. von Hippel. Distortable double well. A prototype for the analysis of relaxation spectra—2165
Fujita, Hiroshi and Akira Kishimoto. Interpretation of viscosity data for concentrated polymer solutions—393
Fujiwara, Shizuo (see Shimizu, Hiroshi)—1467(L), 1501
Fulton, Robert L. and John D. Baldeschwieler. Spin inversion operator in nuclear magnetic resonance—1075(L)
Funabashi, Koichi (see Magee, John L.)—1715

Gardiner, W. C., Jr., and G. B. Kistiakowsky. Density measurements in reflected shock waves—1080(L)
Gardner, C. L. (see Farmer, J. B.)—1058(L)
Gardner, Donald G. and Lawrence M. Epstein. Protection against radiation damage in polymethylmethacrylate by high-energy electrons and by ultraviolet light—1653
Garland, C. W. and J. Silverman. Analysis of specific heat data for zinc. Resolution of the calorimetric and elastic Θ_0 discrepancy—781
Garretson, H. H. and J. S. Drury. Isotopic separation factor for the system potassium amalgam-aqueous potassium hydroxide—1957
Giese, Clayton F. (see Steiner, Bruce)—189
Giguère, Paul A. (see Chin, David)—690(L)
Gilbert, T. L. and P. G. Lykos. Maximum-overlap directed-hybrid orbitals—2199(L)
Ginell, Robert. Derivation of the Tait equation and its relation to the structure of liquids—1249
—— Geometric basis of phase change—992
—— Development of the liquid equation and the partial structure of water—2174
Gingrich, N. S. and LeRoy Heaton. Structure of alkali metals in the liquid state—873
Glasel, Jay Arthur. Near-infrared absorption spectrum of solid methane at the λ point—1649
Glaze, William (see West, Robert)—685(L)
Goldberg, H. (see Herzfeld, C. M.)—643
Goldberg, Sigmund (see Fabricand, Burton P.)—1624
Goldstein, J. H. (see Reddy, G. S.)—700(L)
—— (see Whipple, E. B.)—2136
Gomer, R. (see Melmed, A. J.)—1802
Gomes, W. Distribution of silver ions in melt-grown alkali halides—2191(L)
Goodman, F. O. Application of a theory of nonideal solutions to results of ultrasonic absorption measurements—1585
Goodman, Lionel (see Hoyland, J. R.)—1446(L)
Gordon, Alvin S. and S. Ruven Smith. Elimination of molecular hydrogen from alkyl free radicals—331(L)
Gordon, Sidney and B. P. Dailey. Density versus chemical shift in NMR spectra—1084(L)
Gordus, Adon A. (see Hsiung, Chi-hua)—535
—— (see Rack, Edward P.)—1855
Gordy, Walter (see Kurita, Yukio—282, 1285
Gränacher, I. (see Diehl, P.)—1846(L)
Granquist, W. T. (see Hollingsworth, C. A.)—1814
Grant, David M. and H. S. Gutowsky. Effect of magnetic nonequivalence in A_2B_2 NMR spectra—699(L)
Gray, B. F. and R. Whitehead. Second-order perturbation theory of helium-like ions—1243
Greener, E. H., D. H. Whitmore, and M. E. Fine. Electrical conductivity of near-stoichiometric α-Nb_2O_5—1017
Greenschlag, Samuel (see Hill, Terrell L.)—1538
Grimley, R. T., R. P. Burns, and Mark G. Inghram. Thermodynamics of the vaporization of Cr_2O_3: dissociation energies of CrO, CrO_2, and CrO_3—664
Grossweiner, L. I. and E. F. Zwicker. Transient measurements of photochemical processes in dyes. I. The photosensitized oxidation of phenol by eosin and related dyes—1411
Gruber, John B. and John G. Conway. Evaluation of electrostatic energy levels of f^n—632
Gutowsky, H. S. (see Bernheim, Robert A.)—565
—— (see Grant, David M.)—699(L)
—— (see Porte, A. L.)—66
—— (see Stalinski, B.)—1191
Guttman, Lester. Monte Carlo computations on the Ising model. The body-centered cubic lattice—1024
Guttman, Shmuel (see Anbar, Michael)—703
Gwinn, William D. (see Chan, Sunney I.)—1319

Hadži, D. Far-infrared bands of some crystals with strong hydrogen bonds—1445(L)
Hall, Frances R. (see Kommandeur, J.)—129
Halperin, A. and H. Arbell. Transients in the blue and green luminescence of ZnS:Cu:Cl crystals—879
—— **and R. Pinker.** Color centers in ZnS single crystals—2031
Hamano, H. Polarity of the C—H bonds in acetylene and its molecular quadrople moment—1678
Hameka, H. F. Calculation of the diamagnetic susceptibility of N_2—366
—— Calculation of the lower excited energy levels of helium—884
—— Theory of the diamagnetic susceptibilities of the alkanes—1996
Hamilton, J. R. (see Hemstreet, R. A.)—948
Harris, G. M. (see Porte, A. L.)—66
Harris, Robert A. (see McLachlan, Andrew D.)—1451(L)
Harrison, S. E. (see Bernal, Ivan)—102
Hart, Edward W. Thermodynamic theory of the pair correlation function—1471
Harteck, Paul (see Mannella, Gene)—2177
Hatcher, Robert D. (see Neuberger, Jacob)—1733
Heaton, LeRoy (see Gingrich, N. S.)—873
Heicklen, Julian and Gerald B. Porter. Photodecomposition of biacetyl vapor—686(L)
Helfand, E., H. L. Frisch, and J. L. Lebowitz. Theory of the two- and one-dimensional rigid sphere fluids—1037
Heller, C. (see Cole, T.)—1085(L), 1447(L)
Heller, Wilfried, William J. Pangonis, and Nicolaos A. Economou. Theoretical investigations on the light scattering of colloidal spheres. X. "Scattering ratio" and depolarization of light scattered at an angle of observation of 90°—971
—— (see Pangonis, William J.)—960
—— (see Stevenson, Arthur F.)—1789
—— (see Wallach, Morton L.)—1796
Hemkar, M. P. (see Joshi, S. K.)—1458(L)
Hemstreet, R. A. and J. R. Hamilton. Evidence of multiple trapping sites for excited nitrogen atoms in solid molecular nitrogen—948
Henderson, William D. (see Hilton, A. Ray, Jr.)—1137
Hermsen, R. W. and J. M. Prausnitz. Entropies of vaporization of hydrocarbons and the Hildebrand rule—1081(L)
Herschbach, D. R., G. H. Kwei, and J. A. Norris. Reactive scattering in crossed molecular beams. K atoms with CH_3I and C_2H_5I—1842(L)
Hersh, L. S. (see Kleppa, O. J.)—351
Hertzberg, Martin, Donald Rapp, Irene B. Ortenburger, and Donald D. Briglia. Ion-neutral reactions in the helium-hydrogen system—343(L)
Herzfeld, C. M. and H. Goldberg. On the nautre of the crystal field approximation—643
Hexter, Robert M. Infrared spectrum of single crystals of LiOH, LiOD, and LiOH·LiOD—941
—— (see Milligan, Dolphus E.)—1009

Hijikata, Katsunori. On the fluorine molecule. Part I. The pilot calculation—221
—— On the fluorine molecule. II. Energy levels of F_2 and F_2^+—231
—— (see Yamazaki, M.)—1926
Hiley, Basil J. and M. F. Sykes. Probability of initial ring closure in the restricted random-walk model of a macromolecule—1531
—— (see Fisher, Michael E.)—1253
Hill, Emma (see Jennings, L. D)—2082
Hill, Terrell L. Theory of solutions. III. Thermodynamics of aggregation or polymerization—1974
—— **and Samuel Greenschlag.** Statistical mechanics of monatomic systems in an external periodic potential field. I. Introduction, virial expansion, and classical second virial coefficient—1538
—— **and Nobuhiko Saitô.** Statistical mechanics of monatomic systems in an external periodic potential field. II. Distribution function theory for fluids—1543
Hilton, A. Ray, Jr., Albert W. Jache, James B. Beal, Jr., William D. Henderson, and R. J. Robinson. Millimeter wave spectrum and molecular structure of oxygen difluoride—1137
Hirschfelder, Joseph O. and George V. Nazaroff. Applicability of approximate quantum-mechanical wave functions having discontinuities in their first derivatives—1666
Hirt, R. C. (see Paris, J. P.)—1851(L)
Hirth, J. P. (see Rapp, R. A.)—184
Hobson, J. P. Physical adsorption of nitrogen on Pyrex at very low pressures—1850(L)
Hochheimer, Bernard F. (see Blau, Edmund J.)—1060(L)
Hoerni, J. A. Application of the free-electron theory to three-dimensional networks—508
Hogg, B. G. (see Ormrod, J. H.)—624
Hoijtink, G. J., J. Townsend, and S. I. Weissman. Spin density in pyrene negative ion—507
Hojvat, N. L. (see Dewar, Michael J. S.)—1232
Hollahan, J. R. (see Reitz, D. C.)—1457(L)
Hollenberg, J. L. and David A. Dows. Measurement of absolute infrared absorption intensities in crystals—1061(L)
—— (see Schatz, P. N.)—175
Hollingsworth, C. A. and W. T. Granquist. Relaxation of laminar flow with reference to streaming birefringence decay—1814
Hoover, William G. and Andrew G. De Rocco. Sixth virial coefficients for gases of parallel hard lines, hard squares, and hard cubes—1059(L)
Hornig, D. F. (see Miller, R. L.)—265
Horrocks, W. D., Jr. (see McDowell, Robin S.)—530
Houghen, Jon T., George E. Leroi, and Thomas C. James. Application of ligand field theory to the electronic spectra of gaseous $CuCl_2$, $NiCl_2$, and $CoCl_2$—1670
Howe, John A. Microwave spectrum of *cis* 1-chloro-2-fluoroethylene—1247
Hoyland, J. R. and Lionel Goodman. Open-shell wave functions for conjugated hydrocarbons—1446(L)
Hsiung, Chi-hua, Hsien-chih Hsiung, and Adon A. Gordus. A closed general solution of the probability distribution function for three-dimensional random walk processes—535
Hsiung, Hsien-chih (see Hsiung, Chi-hua)—535
Huffine, C. (see Sears, G. W.)—2142
Huggins, Charles M. (see McCall, David W.)—804
Hunt, G. R. and M. Kent Wilson. Infrared spectra and potential constants of some monohaloacetylenes—1301
Hurlbert, R. C. and J. O. Konecny. Diffusion of hydrogen through palladium—655
Hurley, A. C. and V. W. Maslen. Potential curves for doubly positive diatomic ions—1919
Hurst, R. P. and J. M. H. Levelt. Quantum-mechanical cell model of the liquid state. II. Application to the zero-point properties of close-packed crystals—54
Hutchison, Clyde A., Jr., and Billy W. Mangum. Paramagnetic resonance absorption in naphthalene in its phosphorescent state—908
——, **and Donald E. O'Reilly.** Densities of solutions of potassium in liquid ammonia and deutero-ammonia—163
——, **and Donald E. O'Reilly.** Electronic paramagnetic relaxation times in potassium-ammonia and potassium-deutero-ammonia solutions—1279

Inghram, Mark G. (see Grimley, R. T.)—664
—— (see Steiner, Bruce)—189
Iredale, T. (see Akon, C. D.)—340(L)
Irsa, A. P. and L. Friedman. Collision-induced dissociation of HD^+—330(L)
Ito, Kazuo, Haruyuki Watanabe, and Masaji Kubo. Proton magnetic resonances of some borazole derivatives—1043

Jache, Albert W. (see Hilton, A. Ray, Jr.)—1137
Jackson, P. J. Electrostatic binding energy in a body-centered structure of parallel charge doublet chains—2119
Jaffé, H. H. (see Whitehead, M. A.)—2204(L)
James, Thomas C. (see Houghen, Jon T.)—1670
Jeffrey, G. A. (see Amma, E. L.)—252
Jennings, L. D., Emma Hill, and F. H. Spedding. Heat capacity of thulium from 15° to 360°K—2082
Johnson, Frederic A. (see Ettinger, Raymond)—2187(L)
Johnson, Noye M. and Farrington Daniels. Luminescence during annealing and phase change in crystals—1434
Johnson, Quintin C. and David H. Templeton. Madelung constants for several structures—2004
Jordan, J. E. (see Amdur, I.)—1525
Jortner, Joshua. Cation-electron interaction in metal-ammonia solutions—678
——, **Baruch Raz, and Gabriel Stein.** Spectrum and radius of OH^- in solution—1455(L)
Joshi, S. K. and M. B. Hemkar. Dispersion of lattice waves in copper—1458(L)
—— (see Mitra, S. S.)—1462(L)

Kanda, Seiichi and Shinichi Kawaguchi. Electrical conductivity of some coordination polymers—1070(L)
Kaplan, Jerome I. Electron spin resonance of crystalline free radicals—2205(L)
Karplus, M. and T. P. Das. Theory of localized contributions to the chemical shift. Application to fluorobenzenes—1683
Kasha, M. (see El-Bayoumi, M. Ashraf)—2181(L)
—— (see El-Sayed, Mostafa F. Amr)—334(L)
—— (see Strickler, S. J.)—1077(L)
Kaskan, W. E., J. D. Mackenzie, and R. C. Millikan. Origin of the green bands in the boron-oxygen system—570
Kato, Yoshifumi. Nuclear quadrupole coupling in the NH_3 molecule—619
Katorski, Anthony, J. G. Eberhart, and David White. Separation of the isotopes HT and ortho-D_2 by adsorption at low temperatures—2189(L)
Kauder, Lois Nash (see Stern, Marvin J.)—333(L)
Kawaguchi, Shinchi (see Kanda, Seiichi)—1070(L)
Kearns, David R. and Melvin Calvin. Electrical properties of organic solids. IV. Charge carrier diffusivity in metal-free phthalocyanine—2022
—— **and Melvin Calvin.** Solid-state ionization potentials of some aromatic organic compounds—2026
Keating, K. B. and H. G. Drickamer. Effect of pressure on the spectra of crystalline UF_4 and UF_3—140
—— **and H. G. Drickamer.** Effect of pressure on the spectra of rare earth ions in crystals—143
Kempter, C. P. and R. J. Fries. Crystallography of the Ru-B and Os-B systems—1994
Kim, Young Soo, C. L. Standley, R. F. Kruh, and Glen T. Clayton. X-ray diffraction study of liquid mercury-indium alloys—1464(L)

King, A. D., Jr. (see Robertson, W. W.)—1511, 2190(L)
King, G. J., F. F. Carlson, B. S. Miller, and R. C. McMillan. Evidence of trapped N atoms in x-ray irradiated NaN_3—1499
Kingery, W. D. (see Oishi, Y.)—688(L)
Kinsinger, Jack B. (see Meyer, Victor E.)—1429
Kishimoto, Akira (see Fujita, Hiroshi—393
Kistiakowsky, G. B. and C. E. Klots. Kinetics of coordinate bond formation. IV. Kinetic isotope effect in the reaction NH_3+BF_3—712
—— **and C. E. Klots.** Kinetics of coordinate bond formation. V. Kinetics of the reaction $P(CH_3)_3+BF_3$—715
—— (see Gardiner, W. C., Jr.)—1080(L)
Klaboe, Peter and J. Rud Nielsen. Infrared and Raman spectra of fluorinated ethanes. XIV. CF_2Cl—CHF, and CF_2Br—CHF_2—1819
Klein, Fritz S. and Max Wolfsberg. Competitive reaction rates of hydrogen atoms with HCl and Cl_2 entropy considerations of the HCl_2 transition state—1494
Klemperer, William and Wilfred G. Norris. Infrared spectra of the lithium halide dimers—1071(L)
Kleppa, O. J. and L. S. Hersh. Heats of mixing in liquid alkali nitrate systems—351
Klots, C. E. (see Kistiakowsky, G. B.)—712, 715
Knight, Herbert T. (see Rink, John P.—1942
Kommandeur, J. and Frances R. Hall. Electronic conduction in complexes of aromatic hydrocarbons with iodine—129
—— (see Singer, L. S.)—133
Konecny, J. O. (see Hurlbert, R. C.)—655
Konitzer, John D. (see Markham, Jordan J.)—1936
Koski, W. S. (see Roberts, E. M.)—591
Krauss, M. Use of Gaussian orbitals for atoms-in-molecule calculations—692(L)
—— (see Wallenstein, M. B.)—929
Krebs, James J. Proton spin polarization of water adsorbed on sucrose chars—326
Krisnamachari, S. L. N. G. and H. P. Broida. Effect of molecular oxygen on the emission spectra of atomic oxygen-acetylene flames—1709
Kroh, J. and J. W. T. Spinks. Tritium as an internal source of radiation in EPR studies of organic materials—1853(L)
Kruh, R. F. (see Kim, Young Soo)—1464(L)
—— (see Petz, John I.)—526
—— (see Standley, C. L.)—1450(L)
Kubo, Masaji (see Ito, Kazuo)—1043
Kurita, Yukio and Walter Gordy. Electron spin resonance in a gamma-irradiated single crystal of *L*-cystine dihydrochloride—282
—— **and Walter Gordy.** Electron spin resonance in a gamma-irradiated single crystal of thiodiglycolic acid—1285
Kusch, P. (see Rao, V. S.)—832
Kwei, G. H. (see Herschbach, D. R.)—1842(L)
Kydd, Paul H. (see Lyon, Richard K.)—1069(L)
—— (see Miyama, Hajime)—2038

Lacey, A. R. (see Alexander, P. W)—2200(L)
Laidler, Keith J. (see Steel, Colin)—1827
Lambe, J. (see Cole, T.)—1447(L)
La Paglia, S. R. and A. B. F. Duncan. Vacuum ultraviolet absorption spectra of hexafluoroacetone and hexachloroacetone—350(L)
—— **and A. B. F. Duncan.** Vacuum ultraviolet absorption spectrum and dipole moment of nitrogen trifluoride—1003
—— **and A. B. F. Duncan.** Vacuum ultraviolet absorption spectrum of phosgene—125
Laurie, Victor W. Microwave spectrum of *cis*-difluoroethylene. Structures and dipole moments of fluoroethylenes—291
—— Microwave spectrum of isobutylene. Dipole moment, internal barrier, equilibrium conformation, and structure—1516
Lawrenson, Ian J. (see Bernheim, Róbert A.)—565
Lawson, A. W. (see Bloomfield, Philip—749
—— (see Payne, R. T.)—2201(L)
Layton, E. Miller, Jr. (see Ruedenberg, Klaus)—1896
Leask, M. J. M., Darrell W. Osborne, and W. P. Wolf. Magnetic properties of uranium tetrafluoride—2090
Lebowitz, J. L. (see Helfand, E.)—1037
Lee, Betty (see Wilson, David J.)—1392
Lee, R. W. (see Swets, D. E.)—17, 2187(L)
Lees, J., B. H. Muller, and J. D. Noble. Degassing of liquids for nuclear spin-lattice relaxation studies—341(L)
Lefebvre, Roland. Proton resonance line shape for a polycrystalline aromatic radical—2035
—— (see Dearman, Henry H.)—72
Lefebvre-Brion, Hélène, C. M. Moser, and R. K. Nesbet. Calculation of the potential energy curves for some electronic states of carbon monoxide—1950
Lehmann, Walter J., Charles O. Wilson, Jr., and I. Shapiro. Infrared spectra of alkyldiboranes. IV. 1,1-dimethyl- and 1,1-diethyldiboranes—476
——, **Charles O. Wilson, Jr., and I. Shapiro.** Infrared spectra of alkyldiboranes. V. Tri- and tetramethyl- and ethyldiboranes—783
Leroi, George E. (see Houghen, Jon T.)—1670
Levelt, J. M. H. (see Hurst, R. P.)—54
Levitt, Leonard S. Extreme pressures. II. Volume-temperature relationship for gases—1440
Lide, D. R., Jr. (see Mann, D. E.)—420
Liebman, I. (see Cassel, H. M.)—343(L)
Lien, William H. and Norman E. Phillips. Heat capacity anomaly in solid air—1073(L)
Lifson, Shneior and A. Roig. On the theory of helix-coil transition in polypeptides—1963
Lin, Chun C. (see Yamazaki, M.)—1926
Linevsky, Milton J. Infrared spectrum of lithium fluoride monomer by matrix isolation—587
Linnell, Robert H. Near-ultraviolet solution spectra of pyridazine-698(L)
Lippincott, E. R., R. Schroeder, and D. Steele. Dissociation energies of diatomic molecules—1448(L)
Lipsicas, M., M. Bloom, and B. H. Muller. NMR measurement of gas compressibility—1813
Litovitz, T. A. (see Madigosky, W. M.)—489
Little, L. H. ν_5 vibration of adsorbed ethylene—342(L)
Livingston, Ralph (see Zeldes, Henry)—247
Lord, N. W. and S. M. Blinder. Isotropic and anisotropic hyperfine interactions in hydrazyl and carbazyl—1693
Loshaek, Samuel (see Sandler, Stanley R.)—439, 445
Lund, L. H. Erratum: X-ray scattering by a cell-model liquid—688(L)
Lykos, P. G. (see Adams, O. W.)—1444(L)
—— (see Gilbert, T. L.)—2199(L)
Lyon, Richard K. and Paul H. Kydd. Gaseous detonations. XIV. The CH radical in acetylene oxygen detonations—1069(L)
Lyons, L. E. (see Alexander, P. W.)—2200(L)

Macek, Joseph H. and George H. Duffey. Bonding in cubic complexes—682
—— **and George H. Duffey.** Bonding in icosahedral complexes—288
Mackenzie, J. D. (see Kaskan, W. E.)—570
Mackor, E. L. (see MacLean, C.)—2207(L), 2208(L)
MacLean, C. and E. L. Mackor. Nuclear magnetic resonance of proton complexes of weak bases—2207(L)
—— **and E. L. Mackor.** Proton exchange in carbonium ions of methyl-substituted benzenes—2208(L)
Madden, H. H. and H. E. Farnsworth. Tests for chemisorption of nitrogen on a clean (100) nickel surface—1186
Madigosky, W. M. and T. A. Litovitz. Mean free path and ultrasonic vibrational relaxation in liquids and dense gases—489

Maeda, Shiro (see Schatz, P. N.)—175
Magee, John L. and Koichi Funabashi. Dissociation processes in electronically excited molecules. Linear chain model—1715
—— (see Nosworthy, J. M.)—83
Mahan, Bruce H. (see Doering, John P.)—1617
Maki, A. H. (see Melchior, M. T.)—471
Mangum, Billy W. (see Hutchison, Clyde A., Jr.)—908
Mann, D. E., B. A. Thrush, D. R. Lide, Jr., J. J. Ball, and N. Acquista. Spectroscopy of fluoride flames. I. Hydrogen-fluorine flame and the vibration-rotation emission spectrum of HF—420
Mannella, Gene and Paul Harteck. Surface-catalyzed excitations in the oxygen system—2177
Marcus, R. A. (see Slagg, N.)—1013
Maria, H. J. (see Fritz, J. J.)—344(L), 2185(L)
Markham, Jordan J. and John D. Konitzer. Experimental study of the shape of the *F* band absorption in NaCl—1936
Maslen, V. W. (see Hurley, A. C.)—1919
Matarrese, L. M. Comments on the EPR spectrum of Mn^{++} in calcite—336(L)
Matlow, Sheldon L. Three dimensional Fe-Mo model. I. ΔH of dissociation of homonuclear diatomic molecules—1187
Matsen, F. A. Dipole moment of lithium hydride—337(L)
—— (see Brigman, G. H.)—958
Matthews, D. L. Vibrational relaxation of carbon monoxide in the shock tube—639
Matthias, B. T. (see Wernick, J. H.)—2194(L)
May, Leopold and Clyde R. Dillard. Infrared spectrum of stannane—694(L)
Mayer, J. E. Approach to thermodynamic equilibrium—1207
Mayer, S. W. (see Reiss, H.)—2001
Mazo, R. M. Linewidths in the electron paramagnetic resonance spectrum of gaseous atomic hydrogen—169
McCall, David, W., Ernest W. Anderson, and Charles M. Huggins. Self-diffusion in linear dimethylsiloxanes—804
—— (see Douglass, Dean C.)—152
McConnell, Harden M. Spin-orbit coupling in orbitally degenerate states of aromatic ions—13
—— **and A. D. McLachlan.** Nuclear hyperfine interactions in orbitally degenerate states of aromatic ions—1
—— (see Dearman, H. H.)—696(L)
McDowell, C. A. (see Farmer, J. B.)—1058(L)
McDowell, Robin S. Coupled anharmonic vibrations and spectral band broadening—1065(L)
——, **W. D. Horrocks, Jr., and John T. Yates.** Infrared spectrum of $Co(CO)_3NO$—530
McEwen, K. Lenore. Electronic structures and spectra of some nitrogen-oxygen compounds—547
McGrath, J. W. and A. A. Silvidi. Structure of the water molecule in solid hydrated compounds—322
McInteer, B. B. and M. J. Reisfeld. Erratum: Thermal-diffusion-column shape factors for the Lennard-Jones (12–6) potential—1844(L)
McLachlan, A. D. (see McConnell, H. M.)—1
McLachlan, Andrew D. and Robert A. Harris. Mayer's ensembles of maximum entropy—1451(L)
McLellan, A. G. Eigenfunctions for integer and half-odd integer values of *J* symmetrized according to the icosahedral group and the group C_{3v}—1350
McMillan, R. C. (see King, G. J.)—1499
McNesby, J. R. (see Okabe, H.)—668
McWeeny, R. Comment on the calculation of zero-field splittings—1065(L)
—— Zero-field splitting of molecular Zeeman levels—399
Medlin, W. L. Thermoluminescence in dolomite—672
Meiboom, S. Nuclear magnetic resonance study of the proton transfer in water—375
Meijer, Paul H. E. Line shape of ultraviolet absorption in solid noble gases—2078
Melchior, M. T. and A. H. Maki. Electron spin resonance study of *p*-phenylene-diamine positive ion—471
Melmed, A. J. and R. Gomer. Field emission from whiskers—1802
Melton, C. E. (see Ropp, Gus A.)—688(L)
Merrifield, R. E. Ionized states in a one-dimensional molecular crystal—1835
Meyer, Richard T. and Rollie J. Myers. Dipole moment of the OH radical from the stark effect of its microwave spectrum —1074(L)
Meyer, Victor E., Jack B. Kinsinger, and Paul M. Parker. Expected square of the length of isotactic vinylic hydrocarbon-type chains—1429
Meyerson, Seymour. Effect of electron energy on some electron-impact processes—2046
Milberg, M. E. (see Parsons, J. L.)—2192(L)
Miller, B. S. (see King, G. J.)—1499
Miller, R. L. and D. F. Hornig. Infrared spectrum and force field of crystalline hydrogen peroxide—265
Miller, Ronald F. and R. F. Curl, Jr. Microwave spectrum of O^{18} formyl fluoride and the structure of formyl fluoride—1847(L)
Milligan, Dolphus E., Robert M. Hexter, and Kurt Dressler. Infrared spectroscopic evidence for the rotation of the ammonia molecule in solid argon and nitrogen—1009
Millikan, R. C. (see Kaskan, W. E.)—570
Milton, Earl R. V. and H. B. Dunford. Reactions of active nitrogen with hydrogen bromide, bromine, and ethylene—51
Minomura, S. and H. G. Drickamer. Pressure induced color centers in CaF_2 and BaF_2—670
Mitchell, R. W. and M. Eisner. Concentration dependence of NMR spin-lattice relaxation times in solutions—651
Mitra, S. S. and S. K. Joshi. Thermal expansion of metals—1462(L)
Miyama, Hajime and Paul Kydd. Gaseous detonations. XV. Expansion waves in gaseous detonations—2038
Moore, Donald W. Proton magnetic resonance spectrum of diketene—1470(L)
Moran, T. I. and J. W. Trischka. New determinations of the vibrational constants of Li^6F and Li^6Cl^{35} by the molecular beam electric resonance method—923
Morelock, C. R. and G. W. Sears. Growth of whiskers by chemical reactions—1008
Morgan, L. O. (see Bloembergen, N.)—842
Morino, Yonezo (see Shimizu, Hiroshi)—1467(L)
Morris, John R., II (see Pilar, Frank L.)—389
Morrison, J. A. (see Beaumont, R. H.)—1456(L)
Morrison, J. D. (see Dorman, F. H.)—578, 1407
Mortensen, Earl M. (see Sinanoğlu, Oktay—1078(L)
Moser, C. M. (see Lefebvre-Brion, Hélène)—1950
Muller, B. H. (see Lees, J.)—341(L)
—— (see Lipsicas, M.)—1813
Murrell, J. N. and L. Salem. Energies of excited electronic states as calculated with the zero differential overlap approximation—1914
Musher, J. I. NMR spectra of 1,1,4,4-tetramethylcyclohexyl-*cis* and *trans*-2,6-diacetate—594
Muzyka, A. (see Ullman, Robert)—1461(L)
Myers, Rollie J. (see Meyer, Richard T.)—1074(L)

Nagai, Kazuo. Dimensional change of polypeptide molecules in the helix-coil transition region. II—887
Narasimhan, P. T. and Max T. Rogers. Proton magnetic resonance spectra of compounds of the type $X(C_2H_5)_n$. Relative signs of the X–H spin coupling constants—1049
Narten, Alfred. Fractionation of nitrogen isotopes between nitrosonium salt solutions and nitrogen oxides—1056
—— Separation factors in multicomponent mixtures of isotopes—2198(L)
Nazaroff, George V. (see Hirschfelder, Joseph O.)—1666

Nesbet, R. K. (see Lefebvre-Brion, Hélène)—1950
Neuberger, Jacob and Robert D. Hatcher. Infrared optical constants of NaCl—1733
Newkirk, A. E. (see Wihksne, K.)—2184(L)
Nielsen, Harald H. (see Amat, Gilbert)—339(L)
Nielsen, J. Rud (see Klaboe, Peter)—1819
Noble, Barbara (see Wilson, David J.)—1392
Noble, J. D. (see Lees, J.)—341(L)
Norris, J. A. (see Herschbach, D. R.)—1842(L)
Norris, Wilfred G. (see Klemperer, William)—1071(L)
Nosworthy, J. M., John L. Magee, and M. Burton. On the luminescence minimum in certain scintillator solutions—83
Noyes, Richard M. Entropy of mixing of interconvertible species. Some reflections on the Gibbs paradox—1983

Oishi, Y. and W. D. Kingery. Erratum: Oxygen diffusion in periclase crystals—688(L)
Okabe, H. and J. R. McNesby. Vacuum ultraviolet photolysis of ethane: molecular detachment of hydrogen—668
Okano, K. and E. Wade. Theory of light scattering by thin rodlike macromolecules in a liquid subjected to shear—405
O'Neal, Edward (see Benson, Sidney W.)—514
Oppenheim, I. (see Crawford, Bryce, Jr.)—1621
O'Reilly, Donald E. (see Hutchison, Clyde A., Jr.)—163, 1279
O'Reilly, James M. and Louis Pierce. Microwave spectrum, structure, dipole moment, and internal barrier of vinyl silane—1176
Oriani, R. A. Delineation of the problem of Soret diffusion—1773
Ormrod, J. H. and B. G. Hogg. Time spectra of positrons annihilating in organic liquids containing halogens—624
Ortenburger, Irene B. (see Hertzberg, Martin)—343(L)
Ortner, M. H. Infrared spectrum and thermodynamic properties of ruthenium tetroxide—556
Osborne, Darrell W. (see Flotow, Howard E.)—1418
——(see Leask, M. J. M.)—2090
Otterson, Dumas A. Neutralization of hydroxide ion in melt-grown NaCl crystals—1849(L)
Overend, John and James R. Scherer. Transferability of Urey-Bradley force constants. VI. The silyl halides—574

Pangonis, William J., Wilfried Heller, and Nicolaos A. Economou. Theoretical investigations on the light scattering of colloidal spheres. IX. Lateral scattering at 90° from incident natural and linearly polarized light—960
—— (see Heller, Wilfried)—971
Panish, Morton B. Vaporization of several rare earth oxides—1079(L)
—— Vaporization of the rare earth oxides—2197(L)
—— **and Liane Reif.** Vaporization of iridium and rhodium—1915
Papazian, Harold A. Infrared spectra of alkali metal azide crystals—1614
Pappalardo, R. Cubic-field splitting and cubic-symmetry orthonormal sets of wave functions for *J*-manifolds (*J*-half-integer)—1380
Paris, J. P., R. C. Hirt, and R. G. Schmitt. Observed phosphorescence and singlet-triplet absorption in *s*-triazine and trimethyl-*s*-triazine—1851(L)
Parker, J. G. Effect of several light molecules on the vibrational relaxation time of oxygen—1763
Parker, Paul M. Note concerning ruby maser-type hamiltonians—1459(L)
—— (see Meyer, Victor E.)—1429
Parks, John R. Criticality criteria for various configurations of a self-heating chemical as functions of activation energy and temperature of assembly—46
Parr, Robert G. (see Snyder, Lawrence C.)—837, 1661
Parsons, J. L., A. H. Silver, and M. E. Milberg. Some structural data for cubic metaboric acid—2192(L)
Pasternak, R. A. and Hans U. D. Wiesendanger. Interaction of hydrogen and of nitrogen with a molybdenum ribbon—2062
Payne, R. T. and A. W. Lawson. Cation mobility and thermal contraction in AgI—2201(L)
Peck, J. M. (see Arajs, Sigurds)—1959
Peterlin, A. and M. Pintar. Temperature dependence of NMR absorption in solid acetic acid and in some of its chloro and acid chloride derivatives—1730
Petersen, R. G. and Norman E. Phillips. Heat capacity of antiferromagnetic $CuCl_2 \cdot 2H_2O$ in the spin wave region—1463(L)
Petruska, John. Changes in the electronic transitions of aromatic hydrocarbons on chemical substitution. I. Perturbation theory for substituted cyclic polyenes—1111
—— Changes in the electronic transitions of aromatic hydrocarbons on chemical substitution. II. Application of perturbation theory to substituted-benzene spectra—1120
Petz, John I., R. F. Kruh, and G. C. Amstutz. X-ray diffraction study of lead sulfide-arsenic sulfide glasses—526
—— (see Brady, George W.)—332(L)
Phillips, David L. (see Fricke, Hugo)—905
Phillips, Norman E. (see Lien, William H.)—1073(L)
—— (see Petersen, R. G.)—1463(L)
Phillips, W. D. (see Chestnut, D. B.)—684(L)
Phillipson, P. E. (see Ehrenson, S.)—1224
Pierce, Louis. Energy levels for internal and over-all rotation of two-top molecules. I. Microwave spectrum of dimethyl silane—498
—— (see O'Reilly, James M.)—1176
Pilar, Frank L. and John R. Morris, II. Choice of parameters for the Hückel π-electronic strucutre of furan: tentative extension to pyrrole and thiophene—389
Pimentel, George C. (see Ewing, George E.)—1067(L)
Pinker, R. (see Halperin, A.)—2031
Pintar, M. (see Peterlin, A.)—1730
Piotrowski, Edward A. (see Ziomek, Joseph S.)—1087
Plane, R. A. (see Chantry, G. W.)—1268
Platt, John R. Electrochromism, a possible change of color producible in dyes by an electric field—862
Polanyi, J. C. Proposal for an infrared maser dependent on vibrational excitation—347(L)
Pollak, Victor L. Electron spin relaxation in metal-ammonia solutions—864
Porte, A. L., H. S. Gutowsky, and G. M. Harris. Proton magnetic resonance study of crystalline potassium trisoxalatorhodium (III) hydrate—66
Porter, Gerald B. (see Heicklen, Julian)—686(L)
Porter, Richard F. Stabilities of gaseous molecules in the Pb–Se and Pb–Te systems—585
Porterfield, W. W. (see Dearman, H. H.)—696(L)
Pound, G. M. (see Rapp, R. A.)—184
Prausnitz, J. M. (see Hermsen, R. W.)—1081(L)

Quist, Arvin S. (see Frank, Henry S.)—604

Rack, Edward P. and Adon A. Gordus. Effect of inert-gas moderators on the (n,γ) activated reaction of I^{128} with CH_4—1855
Radford, Loren E. Limit of stability of crystalline helium—182
Ramaradhya, J. M. and G. R. Freeman. Radiolysis of cyclohexane. III. Vapor phase—1726
Randić, Milan. Comment on the difference between the bond orders calculated by SCF MO and simple MO method—693(L)
Ransil, Bernard J. Studies in molecular structure. IV. Potential curve for the interaction of two helium atoms in single-configuration LCAO MO SCF approximation—2109
—— (see Fraga, Serafin)—727

Rao, V. S. and P. Kusch. Alkali-iron group-halogen complexes. Dissociation energies of $KClFeCl_2$ and $CsClFeCl_2$—832
Rapp, Donald (see Hertzberg, Martin)—343(L)
Rapp, R. A., J. P. Hirth, and G. M. Pound. Condensation coefficients in the growth of cadmium and zinc from the vapor—184
Raw, C. J. G. Second virial coefficient of boron trifluoride—1452(L)
Ray, James D. (see Cox, James R., Jr.)—1072(L)
Raz, Baruch (see Jortner, Joshua)—1455(L)
Reddy, G. S., C. E. Boozer, and J. H. Goldstein. Correlation of proton magnetic resonance shifts with group dipole moments in substituted ethylenes—700(L)
—— (see Whipple, E. B.)—2136
Reeves, L. W. and K. O. Strømme. Studies of rates of conversion and populations of conformations in saturated ring compounds. III. *NN'* dimethyl piperazine—1711
Reif, Liane (see Panish, Morton B.)—1915
Reilly, C. A. and J. D. Swalen. NMR spectra of glycidaldehyde—980
—— (see Swalen, J. D.)—2122
Reisfeld, M. J. (see McInteer, B. B.)—1844(L)
Reiss, H. and S. W. Mayer. Theory of the surface tension of molten salts—2001
Reitz, D. C. Proton hyperfine splittings and spin densities of pentaphenylcyclopentadienyl—701(L)
——, **J. R. Hollahan, F. Dravnieks, and J. E. Wertz.** Electron spin resonance studies of some quinone reactions—1457(L)
Rey, Charles (see Bloomfield, Phillip)—749
Rice, Stuart A. and Alan R. Allnatt. Approximate theory of transport in simple dense fluid mixtures—409
—— **and Alan R. Allnatt.** On the kinetic theory of dense fluids. VI. Singlet distribution function for rigid spheres with an attractive potential—2144
—— (see Allnatt, Alan R.)—2156
Richman, Isaac (see Wong, Eugene Y.)—1182
Rink, John P., Herbert T. Knight, and Russell E. Duff. Shock tube determination of dissociation rates of oxygen—1942
Roberts, E. M., W. S. Koski, and W. S. Caughey. Electron spin resonance of some vanadyl porphyrins—591
Robertson, W. D. (see Freedman, J. F.)—769
Robertson, W. W. and A. D. King, Jr. Calculation of pressure shifts of optical absorption spectra from solvent data—1511
—— **and A. D. King, Jr.** Method for distinguishing between overlapping transitions in electronic absorption spectra, with application to azulene—2190(L)
Robinson, G. W. (see El-Sayed, M. A.)—1840(L)
Robinson, R. J. (see Hilton, A. Ray, Jr.)—1137
Rogers, John D. and Dudley Williams. Nitrosyl chloride structure—2195(L)
Rogers, Max T. (see Narasimhan, P. T.)—1049
Roig, A. (see Lifson, Shneior)—1963
Ropp, Gus A., C. E. Melton, and P. S. Rudolph. Mass spectrometric test for an intermediate in a photochemical reaction involving chlorine—688(L)
Rosenberg, Barnett. Effect of oxygen adsorption on photo- and semiconduction of β-carotene—812
—— Photoconduction activation energies in *cis-trans* isomers of β-carotene—63
Rosenstock, H. M. On the classical approximation in the statistical theory of mass spectra—2182(L)
Ross, Marvin (see Steele, William A.)—1067(L)
Roth, Walter. Dependence of vibrational relaxation time on the vibrational quantum number. Experimental verification for NO($A^2\Sigma^+$) behind shock waves—2204(L)
—— Shock tube study of vibrational relaxation in the $A^2\Sigma^+$ state of NO—999
Rothberg, G. M. Binding energies of alkali halide molecules—2069
Rudolph, P. S. (see Ropp, Gus A.)—688(L)
Ruedenberg, Klaus. Quantum mechanics of mobile electrons in conjugated bond systems. I. General analysis in the tight-binding formulation—1861
—— Quantum mechanics of mobile electrons in conjugated bond systems. II. Augmented tight-binding formulation—1878
—— Quantum mechanics of mobile electrons in conjugated bond systems. III. Topological matrix as generatrix of bond orders—1884
—— Quantum mechanics of mobile electrons in conjugated bond systems. IV. Integral formulas—1892
—— **and E. Miller Layton, Jr.** Quantum mechanics of mobile electrons in conjugated bond systems. V. Empirical determination of integrals between carbon atomic orbitals from experimental data on benzene—1897
—— Quantum mechanics of mobile electrons in conjugated bond systems. VI. Theoretical evaluation of energy contributions—1907
Saitô, Nobuhiko (see Hill, Terrell L.)—1543
Sakamoto, M. (see Yamazaki, M.)—1926
Salem, L. (see Murrell, J. N.)—1914
Sanborn, Russell H. Comments on "On the structure of the isomers of N_2F_2"—2188(L)
Sandler, Stanley R. and Samuel Loshaek. Effect of solvent and solute structure on scintillator pulse heights. I. Correlation of pulse heights for ring substituted styrene plastic scintillators with Hammett substituent constants—439
—— **and Samuel Loshaek.** Effect of solvent and solute structure on scintillator pulse heights. II. Correlation of pulse heights for aromatic liquid organic scintillators with Hammett substituent constants—445
Saraceno, A. J. and N. D. Coggeshall. Effect of dissolved oxygen on the spin-lattice relaxation time of free radicals in petroleum oils—260
Schaefer, T. (see Buckingham, A. D.)—1064(L)
Schatz, P. N., Shiro Maeda, J. L. Hollenberg, and David A. Dows. Reflection spectra and absolute infrared intensities in pure liquids: benzene, chloroform, bromoform, carbon disulfide, and carbon tetrachloride—175
Scherer, James R. (see Overend, John)—574
Schmidt, Hartland H. Half-crystal energy constants—1520
Schmitt, R. G. (see Paris, J. P.)—1851(L)
Schneider, W. G. (see Bree, A.)—1453(L)
—— (see Buckingham, A. D.)—1064(L)
Schomaker, Verner (see Verdier, Peter H.)—118
Schreurs, Jan W. H. and George K. Fraenkel. Anomalous relaxation of hyperfine components in electron spin resonance. II—756
Schroeder, R. (see Lippincott, E. R.)—1448(L)
Schulz, G. J. Study of the N_2O molecule using electron beams—1778
Searcy, Alan W. (see Davis, Stanley G.)—659
Sears, G. W., R. C. DeVries, and C. Huffine. Twist in alumina whiskers—2142
—— (see DeVries, R. C.)—616
—— (see Morelock, C. R.)—1008
Secco, E. A. Erratum: Diffusion and exchange of Zn in crystalline ZnS—1844(L)
Shapiro, I. (see Lehmann, Walter J.)—476, 783
Sharn, Charles F. High-energy radiation damage to fluorescent organic solids—240
Shimanouchi, Takehiko and Mitsuo Tasumi. Dichroism of 603 cm^{-1} band of polyvinyl chloride—687(L)
Shimizu, Hiroshi and Shizuo Fujiwara. Nuclear relaxation processes of a nonequivalent two-spin system—1501
——, **Shizuo Fujiwara, and Yonezo Morino.** Molecular structure of diphenylethers—1467(L)

Siegel, Seymour, L. H. Baum, Sol Skolnik, and John M. Flournoy. Erratum: Observations of the thermal behavior of radicals in gamma-irradiated ice—339(L)
——, **John M. Flournoy, and Lillian H. Baum.** Irradiation yields of radicals in gamma-irradiated ice at 4.2° and 77°K—1782
Sierro, Jerome. ESR detection of the hydrolysis of solid CaF_2—2183(L)
Silver, A. H. (see Parsons, J. L.)—2192(L)
Silverman, J. (see Garland, C. W.)—781
Silvidi, A. A. (see McGrath, J. W.)—322
Sinanoğlu, Oktay. Relation of perturbation theory to variation method—1237
—— **and Earl M. Mortensen.** Core polarization in Li_2—1078(L)
Singer, L. S. and J. Kommandeur. Electron spin resonance in complexes of aromatic hydrocarbons with iodine—133
Sinnott, K. M. Microwave spectrum of acetyl chloride—851
Skolnik, Sol (see Siegel, Seymour)—339(L)
Slagg, N. and R. A. Marcus. Photochemical studies in flash photolysis. II. Photolysis of acetone with filtered light—1013
Smith, Felix T. Capacitive energy and the ionization of aromatic hydrocarbons—793
Smith, G. Pedro and Charles R. Boston. $n \rightarrow \pi^*$ electronic transition in pure alkali nitrate melts—1396
Smith, S. Ruven (see Gordon, Alvin S.)—331(L)
Smith, William T., Jr. (see Datz, Sheldon)—558
Snyder, Lawrence C. and Robert G. Parr. Extraordinary basic functions in valence theory—1661
—— **and Robert G. Parr.** Problems in perturbation theory calculation of diamagnetic susceptibility and nuclear magnetic shielding in molecules. Illustration with the hydrogen atom—837
Soden, R. R. (see Van Uitert, L. G.)—276
Somayajulu, G. R. Dissociation energies of diatomic molecules—1449(L)
Spedding, F. H. (see Jennings, L. D.)—2082
Spindel, W. (see Stern, Marvin J.)—333(L)
Spinks, J. W. T. (see Kroh, J.)—1853(L)
Stalinski, B., C. K. Coogan, and H. S. Gutowsky. Proton magnetic resonance studies of structure, diffusion, and resonance shifts in titanium hydride—1191
Standley, C. L. and R. F. Kruh. On the structure of ferric chloride solutions—1450(L)
—— (see Kim, Young Soo)—1464(L)
Steel, Colin and Keith J. Laidler. High frequency factors in unimolecular reactions—1827
Steele, D. (see Lippincott, E. R.)—1448(L)
Steele, R. B. (see Crowell, A. D.)—1347
Steele, William A. Vapor pressure of nearly classical liquids—802
—— **and Marvin Ross.** Erratum: Distribution functions of a fluid in an external potential field. Application to physical adsorption—1067(L)
Stehling, Ferdinand C. and Kenneth W. Bartz. Identification of perinaphthene radical in petroleum product—1076(L)
Stein, Gabriel (see Anbar, Michael)—703
—— (see Jortner, Joshua)—1455(L)
Steinberg, Martin and William O. Davies. High-temperature absorption of carbon dioxide at 4.40μ—1373
Steiner, Bruce, Clayton F. Giese, and Mark G. Inghram. Photoionization of alkanes. Dissociation of excited molecular ions—189
Stephen, M. J. Note on the calculation of saturation effects in magnetic resonance—484
Stephens, D. R. and H. G. Drickamer. Effect of pressure on the spectra of five nickel complexes—937
Stephenson, C. V. and C. E. Flanagan. Electrical conduction in polycrystalline lead zirconate-titanate—2203(L)
Stern, Marvin J., Lois Nash Kauder, and W. Spindel. Temperature dependence of the isotopic fractionation of nitrogen in the NO–NO^{-3} system—333(L)
Stevenson, Arthur F., Wilfried Heller, and Morton L. Wallach. Theoretical investigations on the light scattering of colloidal spheres. XI. Determination of size distribution curves from spectra of the scattering ratio or from depolarization spectra—1789
—— (see Wallach, Morton L.)—1796
Stevenson, Richard. Phase transition in ammonium fluoride—346(L)
—— Phase transitions in the ammonium halides—1757
Stewart, W. E. (see Whipple, E. B.)—2136
Strasheim, A. and K. Buijs. Infrared absorption of nitrate ions dissolved in solid alkali halides—691(L)
Strickler, S. J. and M. Kasha. Solvent effects on the spectra of halide ions—1077(L)
Strømme, K. O. (see Reeves, L. W.)—1711
Subbarao, E. C. Ferroelectricity in mixed bismuth oxides with layer-type structure—695(L)
Suzuki, Yasutaka. Molecular statistics of vinyl polymers—79
Swalen, J. D. and C. A. Reilly. NMR spectra of some halogenated propenes—2122
—— (see Reilly, C. A.)—980
Swets, D. E., R. W. Lee, and R. C. Frank. Comments on Dr. Doremus' Letter—2187(L)
——, **R. W. Lee, and R. C. Frank.** Diffusion coefficients of helium in fused quartz—17
Sykes, M. F. (see Hiley, B. J.)—1531

Tanaka, Y. (see El-Sayed, Mostafa F. Amr)—334(L)
Tasumi, Mitsuo (see Shimanouchi, Takehiko)—687(L)
Taylor, Ellison H. (see Datz, Sheldon)—558
Taylor, H. Austin (see Chen, Mei Chio)—1344
Templeton, David H. (see Johnson, Quintin C.)—2004
Thompson, Don D. (see Brown, Robert J. S.)—1580
Thompson, Warren E. (see Ewing, George E.)—1067(L)
Thorson, Walter R. Inelastic scattering of atoms. I. Intermultiplet transitions—1744
Thrush, B. A. (see Mann, D. E.)—420
Tietz, T. Interaction energy in the Amaldi-Fermi theory for a pair of simple negative ions of the same kind with filled electronic shells—1848(L)
Tinoco, Ignacio, Jr. Erratum: Optical and other electronic properties of polymers—1067(L)
Tobias, Irwin (see Fallon, Robert J.)—167
Townsend, J. (see Hoijtink, G. J.)—507
Trischka, J. W. (see Moran, T. I.)—923
Tschudi, Carmen S. and Norah V. Cohan. Valence bond treatment on the *B* state of the hydrogen molecule—401
Turnbull, David and Morrel H. Cohen. Free-volume model of the amorphous phase: glass transition—120
—— **and Robert L. Cormia.** Kinetics of crystal nucleation in some normal alkane liquids—820

Ullman, Robert and A. Muzyka. Intrinsic viscosity of stiff chains—1461(L)
Unger, Hilbert J. (see Blau, Edmund J.)—1060(L)

Vaidhyanathan, V. S. (see Bearman, Richard J.)—264
Vanderslice, Joseph T. (see Fallon, Robert J.)—167
van der Valk, F. and A. E. de Vries. Thermal diffusion factor of helium—345(L)
Van Uitert, L. G. and R. R. Soden. Emission spectra of trivalent thulium—276
Vaughan, Arthur (see Camac, Morton)—460
Vaughan, W. R. (see Berry, R. S.)—1460(L)
Verdier, Peter H., E. B. Whipple, and Verner Schomaker. Moment analysis of magnetic resonance signals—118

Vincow, Gershon and George K. Fraenkel. Molecular orbital theory and hyperfine splitting in electron spin resonance spectra of semiquinones—1333
von Hippel, A. (see Fuchs, R.)—2165
Vratny, F. Reflectance spectra of terbium oxides in the range Tb_2O_3 to Tb_4O_7—1377

Wada, E. (see Okano, K.)—405
Wahrhaftig, Austin L. (see Eyring, Edward M.)—23
Walker, R. E. Measurement of the O–O_3 diffusion coefficient—2196(L)
Wallach, Morton L., Wilfried Heller, and Arthur F. Stevenson. Theoretical investigations on the light scattering of colloidal spheres. XII. Determination of size distribution curves from turbidity spectra—1796
—— (see Stevenson, Arthur F.)—1789
Wallenstein, M. B. and M. Krauss. Interpretation of the appearance potentials of secondary ions—929
Watanabe, Haruyuki (see Ito, Kazuo—1043
Waugh, J. S. (see Castellano, S.—(295)
Weigang, O. E., Jr., and A. J. Dahl. Vibration perturbations in electronically excited monosubstituted benzenes—1845(L)
Weinreb, A. Energy transfer and quenching processes in the system cyclohexane-benzene-terphenyl-oxygen—1316
Weissman, S. I. (see Eargle, Dolan H., Jr.)—1840(L)
—— (see Hoijtink, G. J.)—507
Wentorf, R. H., Jr. Synthesis of the cubic form of boron nitride—809
Wernick, J. H. and B. T. Matthias. Superconductivity in the In-Sn system—2194(L)
Wertz, J. E. (see Reitz, D. C.)—1457(L)
West, Robert and William Glaze. Lithium kinetic isotope effect in the reaction of ethyllithium with benzyl chloride—685(L)
Whalley, E. and M. Falk. Difference of intermolecular potentials of CH_3OH and CH_3OD—1569
—— (see Falk, M.)—1554
Whan, R. E. (see Crosby, G. A.)—743
Whipple, E. B., W. E. Stewart, G. S. Reddy, and J. H. Goldstein. NMR spectra of vinyl chloride and the chloroethylenes—2136
—— (see Verdier, Peter H.)—118
White, David (see Katorski, Anthony)—2189(L)
Whitehead, M. A. and H. H. Jaffé. Nuclear quadrupole resonance of BrCl—2204(L)
Whitehead, R. (see Gray, B. F.)—1243
Whitmore, D. H. (see Greener, E. H.)—1017
Widom, B. Deviations from thermal equilibrium among reactant molecules—2050
Wiesendanger, Hans U. D. (see Pasternak, R. A.)—2062
Wihksne, K. and A. E. Newkirk. Electrical conductivities of α- and β-phthalocyanine—2184(L)
Wijnen, M. H. J. Decomposition of dimethyl carbonate on quartz—1465(L)
Williams, Dudley (see Rogers, John D.)—2195(L)
Wilson, Charles O., Jr. (see Lehmann, Walter J.)—476, 783
Wilson, David J., Barbara Noble, and Betty Lee. Pressure dependence of fluorescence spectra—1392
Wilson, M. Kent (see Hunt, G. R.)—1301
Wise, Henry. Diffusional transport of atomic hydrogen through molecular hydrogen at elevated temperatures—2139
Woessner, D. E. Effects of diffusion in nuclear magnetic resonance spin-echo experiments—2057
Wolf, W. P. (see Leask, M. J. M.)—2090
Wolfsberg, Max (see Klein, Fritz S.)—1494
Wong, Eugene Y. Analysis of the absorption and fluorescence spectrum of $NdCl_3$ diluted with $LaCl_3$—1989
—— **and Isaac Richman.** Analysis of the absorption spectrum and Zeeman effect of thulium ethylsulphate—1182
Wybourne, B. G. Composition of the electronic states of Nd(IV) and Er(IV)—279

Yamakawa, Hiromi. Concentration dependence of polymer chain configurations in solution—1360
Yamazaki, M., M. Sakamoto, K. Hijikata, and Chun C. Lin. Effect of configuration interactions on the dissociation energy and hyperfine structure constants of the NO molecule—1926
Yates, John T. (see McDowell, Robin S.)—530
Young, Robert A. Erratum: Pressure dependence of some infrared and vacuum ultraviolet bands occurring in active nitrogen—339(L)
—— Measurements of the diffusion coefficient of atomic nitrogen in molecular nitrogen and the catalytic efficiency of silver and copper oxide surfaces—1295
—— Pressure dependence of the absolute catalytic efficiency of surfaces for removal of atomic nitrogen—1292

Zeldes, Henry and Ralph Livingston. Paramagnetic resonance study of irradiated single crystals of calcium tungstate—247
Zinn, John (see Chan, Sunney I.)—1319
Ziomek, Joseph S. and Edward A. Piotrowski. Normal coordinate treatments and calculated thermodynamic properties of phosphoryl chloride, thiophosphoryl chloride, and phosphoryl fluoride—1087
Zmerli, Adnan. Phosphorescence spectra of acenaphthene at low temperatures—2130
Zwanzig, Robert. Theory of vibrational relaxation in liquids—1931
Zwicker, E. F. (see Grossweiner, L. I.)—1411

Analytic Subject Index to Volume 34

(References with (L) are to Letters to the Editor)

Absorption Spectra, Infrared

Comments on "On the structure of the Isomers of N_2F_2," Russell H. Sanborn—2188(L)
Coupled anharmonic vibrations and spectral band broadening, Robin S. McDowell—1065(L)
Dichroism of 603 cm^{-1} band of polyvinyl chloride, Takehiko Shimanouchi and Mitsuo Tasumi—687(L)
Erratum: Infrared detection of the formyl radical HCO [J. Chem. Phys. **32,** 927 (1960)], George E. Ewing, Warren E. Thompson, and George C. Pimental—1067(L)
Erratum: Pressure dependence of some infrared and vacuum ultraviolet bands occurring in active nitrogen [J. Chem. Phys. **33,** 1112 (1960)], Robert A. Young—339(L)
Far-infrared bands of some crystals with strong hydrogen bonds, D. Hadži—1445(L)
High-temperature absorption of carbon dioxide at 4.40μ, Martin Steinberg and William O. Davies—1373
Infrared absorption of nitrate ions dissolved in solid alkali halides, A. Strasheim and K. Buijs—691(L)
Infrared and Raman spectra of fluorinated ethanes. XIV. CF_2Cl—CHF_2 and CF_2Br—CHF_2, Peter Klaboe and J. Rud Nielsen—1819
Infrared optical constants of NaCl, Jacob Neuberger and Robert D. Hatcher—1733
Infrared spectra and potential constants of some monohaloacetylenes, G. R. Hunt and M. K. Wilson—1301
Infrared spectra of alkali metal azide crystals, Harold A. Papazian—1614
Infrared spectra of alkyldiboranes. IV. 1,1-dimethyl- and 1,1-diethyldiboranes, Walter J. Lehmann, Charles O. Wilson, Jr., and I. Shapiro—476
Infrared spectra of alkyldiboranes. V. Tri- and tetramethyl- and ethyldiboranes, Walter J. Lehmann, Charles O. Wilson, Jr., and I. Shapiro—783
Infrared spectra of methanol and deuterated methanols in gas, liquid, and solid phases, M. Falk and E. Whaley—1554
Infrared spectra of some group IV halides, Alfred Büchler, J. B. Berkowitz-Mattuck and Donald H. Dugre—2202(L)
Infrared spectra of the lithium halide dimers, William Klemperer and Wilfried G. Norris—1071(L)
Infrared spectroscopic evidence for the rotation of the ammonia molecule in solid argon and nitrogen, Dolphus E. Milligan, Robert M. Hexter and Kurt Dressler—1009
Infrared spectrum and force field of crystalline hydrogen peroxide, R. L. Miller and D. F. Hornig—265
Infrared spectrum and thermodynamic properties of ruthenium tetroxide, M. H. Ortner—556
Infrared spectrum of $Co(CO)_3NO$, Robin S. McDowell, W. D. Horrocks, Jr., and John T. Yates—530
Infrared spectrum of crystalline boron trichloride, David A. Dows and G. Bottger—689(L)
Infrared spectrum of diimide, Edmund J. Blau, Bernard F. Hochheimer and Hilbert J. Unger—1060(L)
Infrared spectrum of lithium fluoride monomer by matrix isolation, Milton J. Linevsky—587
Infrared spectrum of single crystals of LiOH, LiOD and LiOH·LiOD, R. M. Hexter—941
Infrared spectrum of stannane, Leopold May and Clyde R. Dillard—694(L)
Intensities of infrared bands of some l_2-alkylbenzene charge-transfer complexes, E. E. Ferguson and Ike Y. Chang—628
LiOH hydration effects in pressed alkali halide pellets, Robert A. Buchanan and William A. Bowen, Jr.—348(L)
Measurement of absolute infrared absorption intensities in crystals, J. L. Hollenberg and David A. Dows—1061(L)
Near-infrared absorption spectrum of solid methane at the λ point, Jay Arthur Glasel—1649
ν_3 vibration of adsorbed ethylene, L. H. Little—342(L)
On the structure of the isomers of N_2F_2, Raymond Ettinger, Frederic A. Johnson and Charles B. Colburn—2187(L)
Proposal for an infrared maser dependent on vibrational excitation, J. C. Polanyi—347(L)
Torsional oscillation frequency of H_2O_2, David Chin and Paul A. Giguere—690(L)

Absorption Spectra, Microwave

Dipole moment of the OH radical from the Stark effect of its microwave spectrum, Richard T. Meyer and Rollie J. Myers—1074(L)
Effect of dissolved oxygen on the spin-lattice relaxation time of free radicals in petroleum oils, A. J. Saraceno and N. D. Coggeshall—260
Electron spin resonance and optical absorption of $K_{35}Cr(CN)[NO]\cdot H_2O$, Ivan Bernal and S. E. Harrison—102
Electron spin resonance in complexes of aromatic hydrocarbons with iodine, L. S. Singer and J. Kommandeur—133
Electron spin resonance of some vanadyl porphyrins, E. M. Roberts, W. S. Koski and W. S. Caughey—591
Energy levels for internal and over-all rotation of two-top molecules. I. Microwave spectrum of dimethyl silane, Louis Pierce—498
Infrared spectra of alkyldiboranes. IV. 1,1-dimethyl- and 1,1-diethyldiboranes, Walter J. Lehmann, Charles O. Wilson, Jr., and I. Shapiro—476
Microwave spectrum of acetyl chloride, K. M. Sinnott—851
Microwave spectrum of *cis*-difluoroethylene. Structures and dipole moments of fluoroethylenes, Victor W. Laurie—291
Microwave spectrum of *cis* 1-chloro-2-fluoroethylene, John A. Howe—1247
Microwave spectrum of isobutylene. Dipole moment, internal barrier, equilibrium conformation, and structure, Victor W. Laurie—1516
Microwave spectrum of O^{18} formyl fluoride and the structure of formyl fluoride, Ronald F. Miller and R. F. Curl, Jr.—1847(L)
Microwave spectrum, structure, dipole moment, and internal barrier of vinyl silane, James M. O'Reilly and Louis Pierce—1176
Millimeter wave spectrum and molecular structure of oxygen difluoride, A. Ray Hilton, Jr., Albert W. Jache, James B. Beal, Jr., William D. Henderson and R. J. Robinson—1137
Spin density in pyrene negative ion, G. J. Hoijtink, J. Townsend and S. I. Weissman—507
Trimethylene oxide. II. Structure, vibration-rotation interaction, and origin of potential function for ring-puckering motion, Sunney I. Chan, John Zinn, and William D. Gwinn—1319

Absorption Spectra of Crystals

Analysis of the absorption and fluorescence spectrum of $NdCl_3$ diluted with $LaCl_3$, Eugene Y. Wong—1989
Analysis of the absorption spectrum and Zeeman-effect of thulium ethylsulphate, Eugene Y. Wong and Isaac Richman—1182

Color centers in ZnS single crystals, A. Halperin and R. Pinker—2031
Composition of the electronic states of Nd(IV) and Er(IV), B. G. Wybourne—279
Crystal field parameters for erbium in $Er(C_2H_5SO_4)_3 \cdot 9H_2O$, Edward H. Erath—1985
Crystal field splitting and covalent bonding in Fe^{++} silicate garnets, Philip Bloomfield, A. W. Lawson, and Charley Rey—749
Crystal spectra of metal coordination compounds. III. Nickel complexes with salicylaldehyde and its imines, J. Ferguson—611
Crystal spectra of metal coordination compounds. IV. Bis-acetylacetonato-copper (II), J. Ferguson—1609
Crystal spectra of metal coordination compounds. V. The 5 coordinated salicylaldehyde-ethylenediimine copper (II) complex, J. Ferguson—2206(L)
Effect of pressure on the spectra of five nickel complexes, D. R. Stephens and H. G. Drickamer—937
Effect of pressure on the spectra of MnO_4^- and $CrO_4^=$, W. H. Bentley and H. G. Drickamer—2200(L)
Effect of pressure on the spectra of rare-earth ions in crystals, K. B. Keating and H. G. Drickamer—143
Experimental study of the shape of The *F* band absorption in NaCl, Jordan J. Markham and John D. Konitzer—1936
Far-infrared bands of some crystals with strong hydrogen bonds, D. Hadži—1445(L)
Infrared absorption of nitrate ions dissolved in solid alkali halides, A. Strasheim and K. Buijs—691(L)
Infrared spectra of alkali metal azide crystals, H. A. Papazian—1614
Infrared spectra of alkyldiboranes. IV. 1,1-dimethyl- and 1,1-diethyldiboranes, Walter J. Lehmann, Charles O. Wilson, Jr., and I. Shapiro—476
Infrared spectrum and force field of crystalline hydrogen peroxide, R. L. Miller and D. F. Hornig—265
Infrared spectrum of crystalline boron trichloride, David A. Dows and G. Bottger—689(L)
Infrared spectrum of single crystals of LiOH, LiOD and LiOH·LiOD, R. M. Hexter—941
Luminescence of chromium (III) complexes, Leslie S. Forster and Keith DeArmond—2193(L)
Measurement of absolute infrared absorption intensities in crystals, J. L. Hollenberg and David A. Dows—1061(L)
Near-infrared absorption spectrum of solid methane at the λ point, Jay Arthur Glasel—1649
Reflectance spectra of terbium oxides in the range Tb_2O_3 to Tb_4O_7, F. Vratny—1377
State of the Nd^{3+} ion as derived from the absorption and fluorescence spectra of $NdCl_3$ and their Zeeman effects, E. H. Carlson and G. H. Dieke—1602

Absorption Spectra, Visible or Ultraviolet

Absorption spectrum and magnetic properties of osmium hexafluoride, J. C. Eisenstein—310
Analysis of the absorption and fluorescence spectrum of $NdCl_3$ diluted with $LaCl_3$, Eugene Y. Wong—1989
Application of ligand field theory to the electronic spectra of gaseous $CuCl_2$, $NiCl_2$, and $CoCl_2$, Jon T. Hougen, George E. Leroi, and Thomas C. James—1670
Calculation of pressure shifts of optical absorption spectra from solvent data, W. W. Robertson and A. D. King, Jr.—1511
Calculation of the lower excited energy levels of helium, H. F. Hameka—884
Changes in the electronic transitions of aromatic hydrocarbons on chemical substitution. I. Perturbation theory for substituted cyclic polyenes, John Petruska—1111
Changes in the electronic transitions of aromatic hydrocarbons on chemical substitution. II. Application of perturbation theory to substituted-benzene spectra, John Petruska—1120
Crystal field parameters for erbium in $Er(C_2H_5SO_4)_3 \cdot 9H_2O$, Edward H. Erath—1985
Crystal spectra of metal coordination compounds. III. Nickel complexes with salicylaldehyde and its imines, J. Ferguson—611
Crystal spectra of metal coordination compounds. IV. Bis-acetylacetonato-copper (II), J. Ferguson—1609
Crystal spectra of metal coordination compounds. V. The 5 coordinated salicylaldehyde-ethylenediimine copper (II) complex, J. Ferguson—2206(L)
Effect of pressure on the spectra of crystalline UF_4 and UF_3, K. B. Keating and H. G. Drickamer—140
Effect of pressure on the spectra of five nickel complexes, D. R. Stephens and H. G. Drickamer—937
Effect of pressure on the spectra of MnO_4^- and $CrO_4^=$, W. H Bentley and H. G. Drickamer—2200(L)
Effect of pressure on the spectra of rare-earth ions in crystals, K.B. Keating and H. G. Drickamer—143
Electrochromism, a possible change of color producible in dyes by an electric field, John R. Platt—862
Electron spin resonance and optical absorption of $K_2Cr(CN)[NO] \cdot H_2O$, Ivan Bernal and S. E. Harrison—102
Energy transfer in hydrogen-bonded *N*-heterocyclic complexes and their possible role as energy sinks, M. Ashraf El-Bayoumi and M. Kasha—2181(L)
Erratum: Pressure dependence of some infrared and vacuum ultraviolet bands occurring in active nitrogen [J. Chem. Phys. **33,** 1112 (1960)], Robert A. Young—339(L)
Evalulation of electrostatic energy levels of f^n, John B. Gruber and John G. Conway—632
Excitation transfer splitting in the $n \rightarrow \pi^*$ transitions of the diazines, M. A. El-Sayed and G. W. Robinson—1840(L)
Experimental study of the shape of the *F* band absorption in NaCl, Jordan J. Markham and John D. Konitzer—1936
Gaseous detonations XV. Expansion waves in gaseous detonations, Hajime Miyama and Paul Kydd—2038
Ionization potentials of benzene, hexadeuterobenzene, and pyridine from their observed Rydberg series in the region 600–2000 A, Mostafa F. Amr El-Sayed, M. Kasha and Y. Tanaka—334(L)
Line shape of ultraviolet absorption in solid noble gases, Paul H. E. Meijer—2078
Luminescence of chromium (III) complexes, Leslie S. Forster and Keith DeArmond—2193(L)
Magnetic properties and optical absorption spectrum of K_2ReCl_6, J. C. Eisenstein—1628
Method for distinguishing between overlapping transitions in electronic absorption spectra—with application to azulene, W. W. Robertson and A. D. King, Jr.—2190(L)
$n \rightarrow \pi^*$ electronic transition in pure alkali nitrate melts, G. Pedro Smith and Charles R. Boston—1396
Near-ultraviolet solution spectra of pyridazine, Robert H. Linnell—698(L)
Observed phosphorescence and singlet-triplet absorption in *s*-triazine and trimethyl-*s*-triazine, J. P. Paris, R. C. Hirt and R. G. Schmitt—1851(L)
Origin of the green bands in the boron-oxygen system, W. E. Kaskan, J. D. Mackenzie, and R. C. Millikan—570
Photoconduction activation energies in *cis-trans* isomers of β-carotene, Barnett Rosenberg—63
Pressure induced color centers in CaF_2 and BaF_2, S. Minomura and H. G. Drickamer—670
Reflectance spectra of terbium oxides in the range Tb_2O_3 to Tb_4O_7, F. Vratny—1377
Solvent effects on the spectra of halide ions, S. J. Strickler and M. Kasha—1077(L)
Spectrum of radius of OH^- in solution, Joshua Jortner, Baruch Raz, and Gabriel Stein—1455(L)

State of the Nd^{3+} ion as derived from the absorption and fluorescence spectra of $NdCl_3$ and their Zeeman effects, E. H. Carlson and G. H. Dieke—1602
Sum rule for transition probabilities, William L. Clinton—273
Transient dimer formation by 2,5-diphenyloxazole, Isadore B. Berlman—1083(L)
Transient measurements of photochemical processes in dyes. I. The photosensitized oxidation of phenol by eosin and related dyes, L. I. Grossweiner and E. F. Zwicker—1411
Vacuum ultraviolet absorption spectra of hexafluoroacetone and hexachloroacetone, S. R. La Paglia and A. B. F. Duncan—350(L)
Vacuum ultraviolet absorption spectrum and dipole moment of nitrogen trifluoride, S. R. La Paglia and A. B. F. Duncan—1003
Vacuum ultraviolet absorption spectrum of phosgene, S. R. La Paglia and A. B. F. Duncan—125
Vibration perturbations in electronically excited monosubstituted benzenes, O. E. Weigang, Jr. and A. J. Dahl—1845

Accommodation Coefficients

Condensation coefficients in the growth of cadmium and zinc from the vapor, R. A. Rapp, J. P. Hirth, and G. M. Pound—184
Condensation of atomic and molecular hydrogen at low temperatures, R. T. Brackmann and Wade L. Fite—1572
Observed phosphorescence and singlet-triplet absorption in *s*-triazine and trimethyl-*s*-triazine, J. P. Paris, R. C. Hirt and R. G. Schmitt—1851(L)

Announcements

Announcement—2209

Adsorption (see Surface Phenomena)

Low-temperature chemisorption. I. Flash desorption of nitrogen, Gert Ehrlich—29
Low-temperature chemisorption. II. Flash desorption of carbon monoxide, Gert Ehrlich—39

Beams, Atomic and Molecular

Alkali-iron group-halogen complexes. The dissociation energies of $KClFeCl_2$ and $CsClFeCl_2$, V. S. Rao and P. Kusch—832
Condensation of atomic and molecular hydrogen at low temperatures, R. T. Brackmann and Wade L. Fite—1572
Reactive scattering in crossed molecular beams: K atoms with CH_3I and C_2H_5I, D. R. Herschbach, G. H. Kwei and J. A. Norris—1842(L)
Scattering of high velocity neutral particles. XI. A further study of the He-He potential, I. Amdur, J. E. Jordan, and S. O. Colgate—1525
Study of the N_2O molecule using electron beams, G. J. Schulz—1778

Catalysis

Measurements of the diffusion coefficient of atomic nitrogen in molecular nitrogen and the catalytic efficiency of silver and copper oxide surfaces, Robert A. Young—1295
Pressure dependence of the absolute catalytic efficiency of surfaces for removal of atomic nitrogen, Robert A. Young—1292

Chemical Reactions (see Kinetics of Reactions)

Conductance

Electrical conductivity of near-stoichiometric α-Nb_2O_5, E. H. Greener, D. H. Whitmore, and M. E. Fine—1017
Electronic conduction in complexes of aromatic hydrocarbons with iodine, J. Kommandeur and Frances R. Hall—129
Photoconduction activation energies in *cis-trans* isomers of β-carotene, Barnett Rosenberg—63

Crystal Growth

Condensation coefficients in the growth of cadmium and zinc from the vapor, R. A. Rapp, J. P. Hirth, and G. M. Pound—184
Distribution of silver ions in melt-grown alkali halides, W. Gomes—2191(L)
Growth of whiskers by chemical reactions, C. R. Morelock and G. W. Sears—1008
Kinetics of crystal nucleation in some normal alkane liquids, David Turnbull and Robert L. Cormia—820
Step formation during the growth of $BaTiO_3$ crystals, R. C. DeVries and G. W. Sears—616

Crystalline State

Analysis of specific heat data for zinc: Resolution of the calorimetric and elastic H_0 discrepancy. C. W. Garland and J. Silverman—781
Analysis of the absorption and fluorescence spectrum of $NdCl_3$ diluted with $LaCl_3$, Eugene Y. Wong—1989
Application of the free-electron theory to three-dimensional networks, J. A. Hoerni—508
Color centers in ZnS single crystals, A. Halperin and R. Pinker—2031
Crystal field splitting and covalent bonding in Fe^{++} silicate garnets, Philip Bloomfield, A. W. Lawson and Charley Rey—749
Crystal spectra of metal coordination compounds. IV. Bis-acetylacetonato-copper (II), J. Ferguson—1609
Cubic field splitting and cubic-symmetry orthonormal sets of wavefunctions for J-manifolds (J half-integer), R. Pappalardo—1380
Dispersion of lattice waves in copper, S. K. Joshi and M. P. Hemkar—1458(L)
Distortion correction to the surface energy of the {110} face of alkali halide crystals, G. C. Benson, E. Dempsey, and P. Balk—157
Effect of pressure on the spectra of crystalline UF_4 and UF_3, K. B. Keating and H. G. Drickamer—140
Effect of pressure on the spectra of five nickel complexes, D. R. Stephens and H. G. Drickamer—937
Effect of pressure on the spectra of MnO_4^- and $CrO_4^=$, W. H. Bentley and H. G. Drickamer—2200(L)
Eigenfunctions for integer and half-odd integer values of J symmetrized according to the icosahedral group and the group C_{3v}, A. G. McLellan—1350
Electrical conductivity of near-stoichiometric α-Nb_2O_5, E. H. Greener, D. H. Whitmore, and M. E. Fine—1017
ESR detection of the hydrolysis or solid CaF_2, Jerome Sierro—2183(L)
Electrostatic binding energy in a body centered structure of parallel charge doublet chains, P. J. Jackson—2119
Erratum: Lattice energies of the alkali halides and the electron affinities of the halogens [J. Chem. Phys. **31,** 1646 (1959); **33,** 1579 (1960)], Daniel Cubicciotti—2189(L)
Experimental study of the shape of the F band absorption in NaCl, Jordan J. Markham and John D. Konitzer—1936
Far-infrared bands of some crystals with strong hydrogen bonds, D. Hadži—1445(L)
Ferroelectricity in mixed bismuth oxides with layer-type structure, E. C. Subbarao—695(L)
Half-crystal energy constants, Hartland H. Schmidt—1520
Infrared optical constants of NaCl, Jacob Neuberger and Robert D. Hatcher—1733
Infrared spectra of alkali metal azide crystals, Harold A. Papazian—1614

Infrared spectrum and force field of crystalline hydrogen peroxide, R. L. Miller and D. F. Hornig—265
Ionized states in a one-dimensional molecular crystal, R. E. Merrifield—1835
Limit of stability of crystalline helium, Loren E. Radford—182
Line shape of ultraviolet absorption in solid noble gases, Paul H. E. Meijer—2078
Madelung constants for several structures, Quintin C. Johnson and David H. Templeton—2004
Magnetic properties and optical absorption spectrum of K_2ReCl_6, J. C. Eisenstein—1628
Measurement of absolute infrared absorption intensities in crystals, J. L. Hollenberg and David A. Dows—1061(L)
Monte Carlo computations on the Ising model: The body-centered cubic lattice, Lester Guttman—1024
Near-infrared absorption spectrum of solid methane at the λ point, Jay Arthur Glasel—1649
Neutralization of hydroxide ion in melt-crown NaCl crystals, Dumas A. Otterson—1849(L)
Note concerning ruby master-type Hamiltonians, Paul M. Parker—1459(L)
Paramagnetic resonance of bis-cyclopentadienyl vanadium in ferrocene, H. H. Dearman, W. W. Porterfield and H. M. McConnell—696(L)
Pressure induced color centers in CaF_2 and BaF_2, S. Minomura and H. G. Drickamer—670
Proton magnetic resonance studies of structure, diffusion and resonance shifts in titanium hydride, B. Stalinski, C. K. Coogan and H. S. Gutowsky—1191
Proton magnetic resonance study of crystalline potassium trisoxalatorhodium(III) hydrate, A. L. Porte, H. S. Gutowsky and G. M. Harris—66
"Subthreshold" photocurrents of high-quantum yield in 9,10-dichloroanthracene, A. Bree and W. G. Schneider—1453(L)
Synthesis of the cubic form of boron nitride, R. H. Wentorf, Jr.—809
Temperature dependence of NMR absorption in solid acetic acid, and in some of its chloro and acid chloride derivatives, A. Peterlin and M. Pintar—1730
Thermoluminescence in dolomite, W. L. Medlin—672
Twist in alumina whiskers, G. W. Sears, R. C. DeVries, and C. Huffine—2142

Crystal Structure

Crystallography of the Ru-B and Os-B systems, Charles P. Kempter and R. Jay Fries—1994
Some structural data for cubic metaboric acid, J. L. Parsons, A. H. Silver and M. E. Milberg—2192(L)
Study of the Wurtzite-type compounds. V. Structure of aluminum oxycarbide, Al_2CO; a short-range Wurtzite-type superstructure, E. L. Amma and G. A. Jeffrey—252

Detonation (see also Shock Waves)

Gaseous detonations. XIV. The CH radical in acetylene oxygen-detonations, Richard K. Lyon and Paul H. Kydd—1069(L)
Gaseous detonations. XV. Expansion waves in gaseous detonations, Hajime Miyama and Paul Kydd—2038

Deuterium (see Isotopes)

Dielectrics

Dielectric properties of polyamides, A. J. Curtis—1849(L)
Dipole moment of lithium hydride, F. A. Matsen—337(L)
Dipole moment of the OH radical from the Stark effect of its microwave spectrum, Richard T. Meyer and Rollie J. Myers—1074(L)
Distortable double well, a prototype for the analysis of relaxation spectra, R. Fuchs and A. von Hippel—2165
Ferroelectricity in mixed bismuth oxides with layer-type structure, E. C. Subbarao—695(L)
Solvent effects in nuclear magnetic resonance, R. J. Abraham—1062(L)
Solvent effects in nuclear magnetic resonance, A. D. Buckingham, T. Schaefer and W. G. Schneider—1064(L)

Diffusion

Approximate theory of transport in simple dense fluid mixtures, Stuart A. Rice and Alan R. Allnatt—409
Cation mobility and thermal contraction in AgI, R. T. Payne and A. W. Lawson—2201(L)
Closed general solution of the probability distribution function for three-dimensional random walk processes, Chi-hua Hsiung, Hsien-Chih Hsiung, and Adon A. Gordus—535
Comments on Dr. Doremus letter, D. E. Swets, R. W. Lee, and R. C. Frank—2187(L)
Criticality criteria for various configurations of a self-heating chemical as functions of activation energy and temperature of assembly, John R. Parks—46
Delineation of the problem of Soret diffusion, R. A. Oriani—1773
Diffusion coefficients of helium in fused quartz, D. E. Swets, R. W. Lee, and R. C. Frank—17
Diffusion of hydrogen through palladium, R. C. Hurlbert and J. O. Konecny—655
Diffusional transport of atomic hydrogen through molecular hydrogen at elevated temperatures, Henry Wise—2139
Erratum: Diffusion and exchange of Zn in crystalline ZnS [J. Chem. Phys. **29,** 406 (1958)], E. A. Secco—1844(L)
Erratum: Oxygen diffusion in periclase crystals [J. Chem. Phys. **33,** 905 (1960)], Y. Oishi and W. D. Kingery—688(L)
High-speed computations in diffusion kinetics. III. Solute depletion in the cylindrical one radical—one solute model, Hugo Fricke and David L. Phillips—905
Measurement of the O–O_2 diffusion coefficient, R. E. Walker—2196(L)
Measurements or the diffusion coefficient of atomic nitrogen in molecular nitrogen and the catalytic efficiency of silver and copper oxide surfaces, Robert A. Young—1295
Pre-exponential factor of temperature in the diffusion equation, R. H. Doremus—2186(L)
Pressure dependence of the absolute catalytic efficiency of surfaces for removal of atomic nitrogen, Robert A. Young—1292
Proton magnetic resonance studies of structure, diffusion and resonance shifts in titanium hydride, B. Stalinski, C. K. Coogan and H. S. Gutowsky—1191
Self-diffusion in linear dimethyl-siloxanes, David W. McCall, Ernest W. Anderson and Charles M. Huggins—804
Self-diffusion of nearly spherical molecules. Neopentane and tetramethyl silane, Dean C. Douglass, David W. McCall, and Ernest W. Anderson—152

Electrical Properties

Cation mobility and thermal contraction in AgI, R. T. Payne and A. W. Lawson—2201(L)
Effect of oxygen adsorption on photo- and semiconduction of β-carotene, Barnett Rosenberg—812
Effect of pressure on the resistance of iodine and selenium, A. S. Balchan and H. G. Drickamer—1948
Electrical conductance of solutions of salts in liquid metals: Potassium iodide in potassium, H. R. Bronstein, A. S. Dworkin and M. A. Bredig—1843(L)
Electrical conduction in polycrystalline lead zirconate-titanate, C. V. Stephenson and C. E. Flanagan—2203(L)
Electrical conductivities of α- and β-phthalocyanine, K. Wihksne and A. E. Newkirk—2184(L)
Electrical conductivity of some coordination polymers, Seiichi Kanda and Shinichi Kawaguchi—1070(L)

Electrical resistivity of liquid sodium, liquid lithium and dilute liquid sodium solutions, J. F. Freedman and W. D. Robertson —769
Electrochromism, a possible change of color producible in dyes by an electric field, John R. Platt—862
Photoconduction activation energies in *cis-trans* isomers of β-carotene, Barnett Rosenberg—63
"Subthreshold" photocurrents of high-quantum yield in 9,10-dichloroanthracene, A. Bree and W. G. Schneider—1453(L)
Superconductivity in the In–Sn system, J. H. Wernick and B. T. Matthias—2194(L)
Thermoelectric power of silver halides, R. W. Christy—1148

Electrochemistry

Electrical conduction in polycrystalline lead zirconate-titanate, C. V. Stephenson and C. E. Flanagan—2203(L)

Electron Affinity

Erratum: Lattice energies of the alkali halides and the electron affinities of the halogens [J. Chem. Phys. **31,** 1646 (1959); **33,** 1579 (1960)], Daniel Cubicciotti—2189(L)

Emission Spectra

Effect of molecular oxygen on the emission spectra of atomic oxygen-acetylene flames, S. L. N. G. Krishnamachari and H. P. Broida—1709
Emission spectra of trivalent thulium, L. G. Van Uitert and R. R. Soden—276
Evidence of multiple trapping sites for excited nitrogen atoms in solid molecular nitrogen, R. A. Hemstreet and J. R. Hamilton—948
Gaseous detonations XIV. The CH radical in acetylene oxygen-detonations, Richard K. Lyon and Paul H. Kydd—1069(L)
Luminescence of chromium (III) complexes, Leslie S. Forster and Keith DeArmond—2193(L)
Observed phosphorescence and singlet-triplet absorption in *s* triazine and trimethyl-*s*-triazine, J. P. Paris, R. C. Hirt and R. G. Schmitt—1851(L)
Phosphorescence spectra of acenaphthene at low temperatures, Adnan Zmerli—2130
Proposal for an infrared maser dependent on vibrational excitation, J. C. Polanyi—347(L)
Shock tube study of vibrational relaxation in the $A^3\Sigma^+$ state of NO, W. Roth—999
Spectroscopy of fluoride flames. I. Hydrogen-fluoride flame and the vibration-rotation emission spectrum of HF, D. E. Mann, B. A. Thrush, D. R. Lide, Jr., J. J. Ball, and N. Acquista—420
Surface catalyzed excitations in the oxygen system, Gene Mannella and Paul Harteck—2177
Transient dimer formation by 2,5-diphenyloxazole, Isadore B. Berlman—1083(L)
Transients in the blue and green luminescence of ZnS:Cu:Cl crystals, A. Halperin and H. Arbell—879

Energy Transfer

Dependence of vibrational relaxation time on the vibrational quantum number-experimental verification for NO($A^2\Sigma^+$) behind shock waves, Walter Roth—2204(L)
Effect of several light molecules on the vibrational relaxation time of oxygen, J. G. Parker—1763
Electron spin relaxation in metal-ammonia solutions, Victor L. Pollack—864
Energy transfer in hydrogen-bonded *N*-heterocyclic complexes and their possible role as energy sinks, M. Ashraf El-Bayoumi and M. Kasha—2181(L)
Inelastic scattering of atoms. I. Inter-multiplet transitions, Walter R. Thorson—1744
New determinations of the vibrational constants of Li^6F and Li^6Cl^{35} by the molecular beam electric resonance method, T. I. Moran and J. W. Trischka—923
O_3 vibration relaxation in oxygen-argon mixtures, Morton Camac—448
Photoionization of alkanes. Dissociation of excited molecular ions, Bruce Steiner, Clayton F. Giese, and Mark G. Inghram —189
Spin-lattice relaxation time of F^{19} nuclei in Ag_2F, Q. Won Choi and W. Gilbert Clark—1584
Vibrational relaxation in liquids, Marshall Fixman—369
Vibrational relaxation of carbon monoxide in the shock tube, D. L. Matthews—639

Errata

Erratum: Diffusion and exchange of Zn in crystalline ZnS [J. Chem. Phys. **29,** 406 (1958)], E. A. Secco—1844(L)
Erratum: Distribution functions of a fluid in an external potential field: Application to physical adsorption [J. Chem. Phys. **33,** 464 (1960)], William A. Steele and Marvin Ross—1067(L)
Erratum: High-order rotation-vibration energies of polyatomic molecules. IV. [J. Chem. Phys. **29,** 665 (1958)], Gilbert Amat and Harald H. Nielsen—339(L)
Erratum: Infrared detection of the formyl radical HCO [J. Chem. Phys. **32,** 927 (1960)], George E. Ewing, Warren E. Thompson, and George C. Pimentel—1067(L)
Erratum; Lattice energies of the alkali halides and the electron affinities of the halogens [J. Chem. Phys. **31,** 1646 (1959); **33,** 1579 (1960)], Daniel Cubicciotti—2189(L)
Erratum: Observations of the thermal behavior of radicals in gamma-irradiated ice [J. Chem. Phys. **32,** 1249 (1960)], Seymour Siegel, L. H. Baum, Sol Skolnik, and John M. Flournoy—339(L)
Erratum: Optical and other electronic properties of polymers [J. Chem. Phys. **33,** 1532 (1960)], Ignacio Tinoco, Jr.—1067(L)
Erratum: Oxygen diffusion in periclase crystals [J. Chem. Phys. **33,** 905 (1960)], Y. Oishi and W. D. Kingery—688(L)
Erratum: Pressure dependence of some infrared and vacuum ultraviolet bands occurring in active nitrogen [J. Chem. Phys. **33,** 1112 (1960)], Robert A. Young—339(L)
Erratum: Thermal-diffusion-column shape factors for the Lennard-Jones (12–6) potential [J. Chem. Phys. **33,** 570 (1960)], B. B. McInteer and M. J. Reisfield—1844(L)
Erratum: X-ray scattering by a cell-model liquid [J. Chem. Phys. **33,** 1086 (1960)], L. H. Lund—688(L)

Field Emission Microscopy

Field emission from whiskers, A. J. Melmed and R. Gomer—1802

Films (see Surface Phenomena)

Flames

Origin of the green bands in the boron-oxygen system, W. E. Kaskan, J. D. Mackenzie, and R. C. Millikan—570
Reactions of active nitrogen with hydrogen bromide, bromine, and ethylene, Earl R. V. Milton and H. B. Dunford—51

Fluorescence

Emission spectra of trivalent thulium, L. G. Van Uitert and R. R. Soden—276
High-energy radiation damage to fluorescent organic solids, Charles F. Sharn—240

Intramolecular energy transfer in rare-earth chelates. The role of the triplet state, G. A. Crosby, R. E. Whan and R. M. Alire—743
Luminescence in a scintillation solution excited by α and β particles and related studies in quenching, Isadore B. Berlman—598
Pressure dependence of fluorescence spectra, David J. Wilson, Barbara Noble and Betty Lee—1392
State of the Nd^{3+} ion as derived from the absorption and fluorescence spectra of $NdCl_3$ and their Zeeman effects, E. H. Carlson and G. H. Dieke—1602
Transients in the blue and green luminescence of ZnS:Cu:Cl crystals, A. Halperin and H. Arbell—879

Free Radicals

Effect of dissolved oxygen on the spin-lattice relaxation time of free radicals in petroleum oils, A. J. Saraceno and N. D. Coggeshall—260
Electron spin resonance and optical absorption of $K_{3a}Cr(CN)[NO]\cdot H_2O$, Ivan Bernal and S. E. Harrison—102
Electron spin resonance of crystalline free radicals, Jerome I. Kaplan—2205(L)
Electron spin resonance study of *p*-phenylene-diamine positive ion, M. T. Melchior and A. H. Maki—471
Elimination of molecular hydrogen from alkyl free radicals, Alvin S. Gordon and S. Ruven Smith—331(L)
Erratum: Infrared detection of the formyl radical HCO [J. Chem. Phys. **32,** 927 (1960)], George E. Ewing, Warren E. Thompson, and George C. Pimentel—1067(L)
Erratum: Observations of the thermal behavior of radicals in gamma-irradiated ice [J. Chem. Phys. **32,** 1249 (1960)], Seymour Siegel, L. H. Baum, Sol Skolnik, and John M. Flournoy—339(L)
Evidence of multiple trapping sites for excited nitrogen atoms in solid molecular nitrogen, R. A. Hemstreet and J. R. Hamilton—948
Evidence of trapped *N* atoms in X-ray irradiated NaN_3, G. J. King, F. F. Carlson, B. S. Miller and R. C. McMillan—1499
Gaseous detonations. XIV. The CH radical in acetylene oxygen-detonations, Richard K. Lyon and Paul H. Kydd—1069(L)
Identification of perinaphthene radical in petroleum product, Ferdinand C. Stehling and Kenneth W. Bartz—1076(L)
Irradiation yields of radicals in gamma-irradiated ice at 4.2° and 77°K, Seymour Siegel, John M. Flournoy, and Lillian H. Baum—1782
Proton hyperfine splittings and spin densities of pentaphenylcyclopentadienyl, D. C. Reitz—701(L)

Free Rotation (see Rotation)

Gases

Mean free path and ultrasonic vibrational relaxation in liquids and dense gases, W. M. Madigosky and T. A. Litovitz—489
Measurement of the O–O_2 diffusion coefficient, R. E. Walker—2196(L)
NMR measurement of gas compressibility, M. Lipsicas, M. Bloom and B. H. Muller—1813
Second virial coefficient of boron trifluoride, C. J. G. Raw—1452(L)
Sixth virial coefficients for gases of parallel hard lines, hard squares and hard cubes, William G. Hoover and Andrew G. DeRocco—1059(L)

Glasses

Diffusion coefficients of helium in fused quartz, D. E. Swets, R. W. Lee, and R. C. Frank—17
Free-volume model of the amorphous phase: Glass transition, David Turnbull and Morrel H. Cohen—120
X-ray diffraction study of lead sulfide-arsenic sulfide glasses, John I. Petz, R. F. Kruh and G. C. Amstutz—526

Heat Capacity (see Thermodynamic Properties)

High Pressures

Calculation of pressure shifts of optical absorption spectra from solvent data, W. W. Robertson and A. D. King, Jr.—1511
Cation mobility and thermal contraction in AgI, R. T. Payne and A. W. Lawson—2201(L)
Effect of pressure on the resistance of iodine and selenium, A. S. Balchan and H. G. Drickamer—1948
Effect of pressure on the spectra of crystalline UF_4 and UF_5, K. B. Keating and H. G. Drickamer—140
Effect of pressure on the spectra of five nickel complexes, D. R. Stephens and H. G. Drickamer—937
Effect of pressure on the spectra of MnO_4^- and CrO_4^-, W. H. Bentley and H. G. Drickamer—2200(L)
Effect of pressure on the spectra of rare-earth ions in crystals, K. B. Keating and H. G. Drickamer—143
Extreme pressures. II. Volume-temperature relationship for gases, Leonard S. Levitt—1440
Phase transitions in the ammonium halides, Richard Stevenson—1757
Pressure induced color centers in CaF_2 and BaF_2, S. Minomura and H. G. Drickamer—670

Hindered Rotation (see Rotation)

NMR spectra of glycidaldehyde, C. A. Reilly and J. D. Swalen—980

Infrared Spectra (see Absorption Spectra)

Potential energy curves for OH, Robert J. Fallon, Irwin Tobias, and Joseph T. Vanderslice—167
Reflection spectra and absolute infrared intensities in pure liquids: Benzene, chloroform, bromoform, carbon disulfide and carbon tetrachloride, P. N. Schatz, Shiro Maeda, J. L. Hollenberg and David A. Dows—175
Spectroscopy of fluorine flames. I. Hydrogen-fluorine flame and the vibration-rotation emission spectrum of HF, D. E. Mann, B. A. Thrush, D. R. Lide, Jr., J. J. Ball, and N. Acquista—420

Intensities of Spectra

Intensities of infrared bands of some 1,2-alkylbenzene charge-transfer complexes, E. E. Ferguson and Ike Y. Chang—628

Isotope Effects

Effect of electron energy on some electron-impact processes, Seymour Meyerson—2046
Fractionation of nitrogen isotopes between nitrosonium salt solutions and nitrogen oxides, Alfred Narten—1056
Heat capacities and thermodynamic functions of ZrH_2 and ZrD_2 from 5 to 350°K, and the hydrogen vibration frequency in ZrH_2, Howard E. Flotow and Darrell W. Osborne—1418
Isotopic separation factor for the system potassium amalgam-aqueous potassium hydroxide, H. H. Garretson and J. S. Drury—1957
Kinetics of coordinate bond formation. IV. Kinetic isotope effect in the reaction NH_3+BF_3, G. B. Kistiakowsky and C. E. Klots—712
Kinetics of coordinate bond formation. V. Kinetics of the reaction $P(CH_3)_3+BF_3$, G. B. Kistiakowsky and C. E. Klots—715

Lithium kinetic isotope effect in the reaction of ethyllithium with benzyl chloride, Robert West and William Glaze—685(L)
Microwave spectrum of acetyl chloride, K. M. Sinnott—851
Microwave spectrum of O^{18} formyl fluoride and the structure of formyl fluoride, Ronald F. Miller and R. F. Curl, Jr.—1847(L)
Oxygen isotope fractionation between calcium carbonate and water, Robert N. Clayton—724
Photolysis of nitrous oxide. I. 1236 A, John P. Doering and Bruce H. Mahan—1617
Radiolysis of aqueous solutions highly enriched in O^{18}, Michael Anbar, Shmuel Guttmann and Gabriel Stein—703
Separation factors in multicomponent mixtures of isotopes, Alfred Narten—2198(L)
Separation of the isotopes HT and ortho-D_2 by adsorption at low temperatures, Anthony Katorski, J. G. Eberhart, and David White—2189(L)
Statistical mechanics of isotope effects on the thermodynamic properties of condensed systems, Jacob Bigeleisen—1485
Temperature dependence of the isotopic fractionation of nitrogen in the NO-NO^{-3} system, Marvin J. Stern, Lois Nash Kauder, and W. Spindel—333(L)

Kinetics of Reaction

Bis-liganded nitrosyl as a reaction intermediate, James R. Cox, Jr. and James D. Ray—1072(L)
Collision-induced dissociation of HD^+, A. P. Irsa and L. Friedman—330(L)
Competitive reaction rates of hydrogen atoms with HCl and Cl_2. Entropy considerations of the HCl_2 transition state, Fritz S. Klein and Max Wolfsberg—1494
Criticality criteria for various configurations of a self-heating chemical as functions of activation energy and temperature of assembly, John R. Parks—46
Decomposition of dimethyl carbonate on quartz, M. H. J. Wijnen—1465(L)
Decomposition rate of nitric oxide between 3000 and 4300°K, E. Freedman and J. W. Daiber—1271
Deviations from thermal equilibrium among reactant molecules, B. Widom—2050
Dissociation processes in electronically excited molecules. Linear chain-model, John L. Magee and Koichi Funabashi—1715
Effect of inert-gas moderators on the (n, γ) activated reaction of I^{128} with CH_4, Edward P. Rack and Adon A. Gordus—1855
Elimination of molecular hydrogen from alkyl free radicals, Alvin S. Gordon and S. Ruven Smith—331(L)
High-frequency factors in unimolecular reactions, Colin Steel and Keith J. Laidler—1827
Kinetics of coordinate bond formation. IV. Kinetic isotope effect in the reaction NH_3+BF_3, G. B. Kistiakowsky and C. E. Klots—712
Kinetics of coordinate bond formation. V. Kinetics of the reaction $P(CH_3)_3+BF_3$, G. B. Kistiakowsky and C. E. Klots—715
Kinetics of the reaction of alkyl iodides with HI, Sidney W. Benson and Edward O'Neal—514
Lithium kinetic isotope effect in the reaction of ethyllithium with benzyl chloride, Robert West and William Glaze—685(L)
Low-temperature chemisorption. I. Flash desorption of nitrogen, Gert Ehrlich—29
Low-temperature chemisorption. II. Flash desorption of carbon monoxide, Gert Ehrlich—39
Nuclear magnetic resonance study of the proton transfer in water, S. Meiboom—375
On the classical approximation in the statistical theory of mass spectra, H. M. Rosenstock—2182(L)
O_2 dissociation rates in O_2–Ar mixtures, Morton Camac and Arthur Vaughan—460
O_2 vibration relaxation in oxygen-argon mixtures, Morton Camac—448
Photoionization of alkanes. Dissociation of excited molecular ions, Bruce Steiner, Clayton F. Giese, and Mark G. Inghram—189
Photolysis of nitrous oxide. I. 1236 A, John P. Doering and Bruce H. Mahan—1617
Reaction of cyclopropane with iodine and some observations on the isomerization of cyclopropane, Sidney W. Benson—521
Reaction of nitrogen atoms with ozone, Mei Chio Chen and H. Austin Taylor—1344
Reactions of active nitrogen with hydrogen bromide, bromine, and ethylene, Earl R. V. Milton and H. B. Dunford—51
Shock tube determination of dissociation rates of oxygen, John P. Rink, Herbert T. Knight and Russell E. Duff—1942
Site of protonation in methyl formate, Gideon Fraenkel—1466(L)
Transient dimer formation by 2,5-diphenyloxazole, Isadore B. Berlman—1083(L)

Large Molecules (see Polymers)

Light Scattering

Theoretical investigations on the light scattering of colloidal spheres. IX. Lateral scattering at 90° from incident natural and linearly polarized light, William J. Pangonis, Wilfried Heller and Nicolaos A. Economou—960
Theoretical investigations on the light scattering of colloidal spheres. X. The "scattering ratio" and depolarization of light scattered at an angle of observation of 90°, Wilfried Heller, William J. Pangonis and Nicolaos A. Economou—971
Theoretical investigations on the light scattering of colloidal spheres. XI. Determination of size distribution curves from spectra of the scattering ratio or from depolarization spectra, Arthur F. Stevenson, Wilfried Heller and Morton L. Wallach—1789
Theoretical investigations on the light scattering of colloidal spheres. XII. The determination of size distribution curves from turbidity spectra, Morton L. Wallach, Wilfried Heller and Arthur F. Stevenson—1796
Theory of light scattering by thin rod-like macromolecules in a liquid subjected to shear, K. Okano and E. Wada—405

Liquids

Approximate theory of transport in simple dense fluid mixtures, Stuart A. Rice and Alan R. Allnatt—409
Densities of solutions of potassium in liquid ammonia and deutero-ammonia, Clyde A. Hutchison, Jr. and Donald E. O'Reilly—163
Derivation of the Tait equation and its relation to the structure of liquids, Robert Ginell—1249
Electrical resistivity of liquid sodium, liquid lithium and dilute liquid sodium solutions, J. F. Freedman and W. D. Robertson—769
Entropies of vaporization of hydrocarbons and the Hildebrand rule, R. W. Hermsen and J. M. Prausnitz—1081(L)
Erratum: X-ray scattering by a cell-model liquid [J. Chem. Phys. **33,** 1086 (1960)], L. H. Lund—688(L)
Extended hole theory of liquids, George E. Blomgren—1307
Free-volume model of the amorphous phase: Glass transition, David Turnbull and Morrel H. Cohen—120
Geometric basis of phase change, Robert Ginell—992
Limit of stability of crystalline helium, Loren E. Radford—182
Mean free path and ultrasonic vibrational relaxation in liquids and dense gases, W. M. Madigosky and T. A. Litovitz—489
$n \rightarrow \pi^*$ electronic transition in pure alkali nitrate melts, G. Pedro Smith and Charles R. Boston—1396
Pauling's model and the thermodynamic properties of water, Henry S. Frank and Arvin S. Quist—604

Quantum-mechanical cell model of the liquid state. II. Application to the zero-point properties of close-packed crystals, R. P. Hurst and J. M. H. Levelt—54
Relaxation of laminar flow with reference to streaming birefringence decay, C. A. Hollingsworth and W. T. Granquist—1814
Solution at high density to the Born-Green equation, A. A. Broyles—359
Structure of alkali metals in the liquid state, N. S. Gingrich and LeRoy Heaton—873
Theory of the surface tension of molten salts, H. Reiss and S. W. Mayer—2001
Theory of the two- and one-dimensional rigid sphere fluids, E. Helfand, H. L. Frisch and J. L. Lebowitz—1037
Theory of vibrational relaxation in liquids, Robert Zwanzig—1931
Vibrational relaxation in liquids, Marshall Fixman—369
X-ray diffraction study of liquid mercury-indium alloys, Young Soo Kim, C. L. Standley, R. F. Kruh and Glen T. Clayton—1464(L)

Magnetic Cooling

Concerning the feasibility of nuclear cooling with palladium hydride, J. J. Fritz, H. J. Maria, and J. G. Aston—2185(L)
Nuclear cooling with metallic copper, J. J. Fritz, H. J. Maria, and J. G. Aston—344(L)

Magnetic Resonance

Anisotropic hyperfine interactions in the ESR spectra of alkyl radicals, E. L. Cochran, F. J. Adrian and V. A. Bowers—1161
Anomalous relaxation of hyperfine components in electron spin resonance II., Jan W. H. Schreurs and George K. Fraenkel—756
Comment on the calculation of zero-field splittings, R. McWeeny—1065(L)
Comments on the EPR spectrum of Mn^{++} in calcite, L. M. Matarrese—336(L)
Complex cyclotron resonance in dilute gases, R. L. Collins—1425
Concentration dependence of NMR spin-lattice relaxation times in solutions, R. W. Mitchell and M. Eisner—651
Correlation of proton magnetic resonance shifts with group dipole moments in substituted ethylenes, G. S. Reddy, C. E. Boozer and J. H. Goldstein—700(L)
Degassing of liquids for nuclear spin-lattice relaxation studies, J. Lees, B. H. Muller and J. D. Noble—341(L)
Densities of solutions of potassium in liquid ammonia and deutero-ammonia, Clyde A. Hutchison, Jr. and Donald E. O'Reilly—163
Density vs chemical shift in NMR spectra, Sidney Gordon and B. P. Dailey—1084(L)
Determination of relative signs of spin coupling constants in an AB_2X nuclear magnetic resonance spectrum, P. Diehl and I. Gränacher—1846(L)
Effect of dissolved oxygen on the spin-lattice relaxation time of free radicals in petroleum oils, A. J. Saraceno and N. D. Coggeshall—260
Effect of magnetic nonequivalence in A_2B_2 NMR spectra, David M. Grant and H. S. Gutowsky—699(L)
Effects of diffusion in nuclear magnetic resonance spin-echo experiments, D. E. Woessner—2056
Electron nuclear double resonance in irradiated organic crystals, T. Cole, C. Heller and J. Lambe—1447(L)
Electron spin relaxation in metal-ammonia solutions, Victor L. Pollak—864
Electron spin resonance and optical absorption of $K_{3}Cr(CN)[NO]\cdot H_2O$, Ivan Bernal and S. E. Harrison—102
ESR detection of the hydrolysis of solid CaF_2, Jerome Sierro—2183(L)
Electron spin resonance in a gamma-irradiated single crystal of *L*-cystine dihydrochloride, Yukio Kurita and Walter Gordy—282
Electron spin resonance in a gamma-irradiated single crystal of thiodiglycolic acid, Yukio Kurita and Walter Gordy—1285
Electron spin resonance in complexes of aromatic hydrocarbons with iodine, L. S. Singer and J. Kommandeur—133
Electron spin resonance of crystalline free radicals, Jerome I. Kaplan—2205(L)
Electron spin resonance of some vanadyl porphyrins, E. M. Roberts, W. S. Koski, and W. S. Caughey—591
Electron spin resonance studies of some quinone reactions, D. C. Reitz, J. R. Hollahan, F. Dravnieks, and J. E. Wertz—1457(L)
ERP studies of spin correlation in some ion radical salts, D. B. Chestnut, H. Foster and W. D. Phillips—684(L)
Electron spin resonance study of *p*-phenylene-diamine positive ion, M. T. Melchior and A. H. Maki—471
Electronic paramagnetic relaxation times in potassium-ammonia and potassium-deuteroammonia solutions, Clyde A. Hutchison, Jr. and Donald E. O'Reilly—1279
Energy transfer between triplet states detected by electron spin resonance spectroscopy, J. B. Farmer, C. L. Gardner and C. A. McDowell—1058(L)
Erratum: Observations of the thermal behavior of radicals in gamma-irradiated ice [J. Chem. Phys. **32,** 1249 (1960)], Seymour Siegel, L. H. Baum, Sol Skolnik, and John M. Flournoy—339(L)
Evidence of trapped N atoms in x-ray irradiated NaN_3, G. J. King, F. F. Carlson, B. S. Miller and R. C. McMillan—1499
Hyperfine splittings in the $(HOOC)C^{13}H(COOH)$ radical, T. Cole and C. Heller—1085(L)
Identification or perinaphthene radical in petroleum product, Ferdinand C. Stehling and Kenneth W. Bartz—1076(L)
Irradiation yields or radicals in gamma-irradiated ice at 4.2° and 77°K, Seymour Siegel, John M. Flournoy, and Lillian H. Baum—1782
Isotropic and anisotropic hyperfine interactions in hydrazyl and carbazyl, N. W. Lord and S. M. Blinder—1693
Line widths in the electron paramagnetic resonance spectrum of gaseous atomic hydrogen, R. M. Mazo—169
Molecular orbital theory and hyperfine splitting in electron spin resonance spectra of semiquinones, Gershon Vincow and George K. Fraenkel—1333
Molecular structure of diphenylethers, Hiroshi Shimizu, Shizuo Fujiwara and Yonezo Morino—1467(L)
Moment analysis of magnetic resonance signals, Peter H. Verdier, E. B. Whipple, and Verner Schomaker—118
Note on the calculation of saturation effects in magnetic resonance, M. J. Stephen—484
Nuclear hyperfine interactions in orbitally degenerate states of aromatic ions, H. M. McConnell and A. D. McLachlan—1
NMR measurement of gas compressibility, M. Lipsicas, M. Bloom and B. H. Muller—1813
Nuclear magnetic resonance of proton complexes of weak bases, C. MacLean and E. L. Mackor—2207(L)
NMR spectra of glycidaldehyde, C. A. Reilly and J. D. Swalen—980
NMR spectra of 1,1,4,4-tetramethylcyclohexyl-cis- and trans-2,6-diacetate, J. I. Musher—594
NMR spectra of propyl derivatives, James R. Cavanaugh and B. P. Dailey—1094
NMR spectra of some halogenated propenes, J. D. Swalen and C. A. Reilly—2122
NMR spectra of vinyl chloride and the chloroethylenes, E. B. Whipple, William E. Stewart, G. S. Reddy and J. H. Goldstein— 2136

Nuclear magnetic resonance spectrum of the triphenylcarbonium ion, R. S. Berry, R. Dehl and W. R. Vaughan—1460(L)
Nuclear magnetic resonance study of the proton transfer in water, S. Meiboom—375
Nuclear relaxation processes of a nonequivalent two-spin system, Hiroshi Shimizu and Shizuo Fujiwara—1501
Paramagnetic resonance absorption in napthalene in its phosphorescent state, Clyde A. Hutchison, Jr. and Billy W. Mangum—908
Paramagnetic resonance of bis-cyclopentadienyl vanadium ferrocene, H. H. Dearman, W. W. Porterfield and H. M. McConnell—696(L)
Paramagnetic resonance study of irradiated single crystals of calcium tungstate, Henry Zeldes and Ralph Livingston—247
Problems in perturbation theory calculation of diamagnetic susceptibility and nuclear magnetic shielding in molecules: Illustration with the hydrogen atom, Lawrence C. Snyder and Robert G. Parr—837
Proton chemical shifts for the alkyl derivatives, James R. Cavanaugh and B. P. Dailey—1099
Proton exchange in carbonium ions of methyl-substituted benzenes, C. MacLean and E. L. Mackor—2208(L)
Proton hyperfine splittings and spin densities or pentaphenylcyclopentadienyl, D. C. Reitz—701(L)
Proton magnetic resonance spectra of compounds of the type $X(C_2H_5)_n$: Relative signs of the X-H spin coupling constants, P. T. Narasimhan and Max T. Rogers—1049
Proton magnetic resonance spectrum of diketene, Donald W. Moore—1470(L)
Proton magnetic resonance studies of structure, diffusion and resonance shifts in titanium hydride, B. Stalinski, C. K. Coogan and H. S. Gutowsky—1191
Proton magnetic resonance study of crystalline potassium trisoxalator-hodium(III) hydrate, A. L. Porte, H. S. Gutowsky and G. M. Harris—66
Proton magnetic resonances of some borazole derivatives, Kazuo Ito, Haruyuki Watanabe, and Masaji Kubo—1043
Proton relaxation times in paramagnetic solutions; effects of electron spin relaxation, N. Bloembergen and L. O. Morgan—842
Proton resonance line shape for a polycrystalline aromatic radical, Roland Lefebvre—2035
Proton resonance shifts in alkali halide solutions, Burton P. Fabricand and Sigmund Goldberg—1624
Proton spin polarization of water adsorbed on sucrose chars, James J. Krebs—326
Quadrople relaxation effects in nuclear magnetic double resonance, John D. Baldeschwieler—718
Second-order effects in low-field NMR for ammonium ion solutions, Robert J. S. Brown and Don D. Thompson—1580
Site of protonation in methyl formate, Gideon Fraenkel—1466(L)
Solvent effects in nuclear magnetic resonance, R. J. Abraham—1062(L)
Solvent effects in nuclear magnetic resonance, A. D. Buckingham, T. Schaefer and W. G. Schneider—1064(L)
Spin and charge exchange in anions or biphenylyl ether, Dolan H. Eargle, Jr. and S. I. Weissman—1840(L)
Spin density in pyrene negative ion, G. J. Hoijtink, J. Townsend and S. I. Weissman—507
Spin inversion operator in nuclear magnetic resonance, Robert L. Fulton and John D. Baldeschwieler—1075(L)
Spin-lattice relaxation time of F^{19} nuclei in Ag_2F, Q. Won Choi and W. Gilbert Clark—1584
Spin-orbit coupling in orbitally degenerate states of aromatic ions, Harden M. McConnell—13
Spin-spin interactions in nuclear magnetic resonance. Contact contribution, S. Alexander—106
Strong coupling in nuclear resonance spectra. IV. Exact analysis of three-spin spectra, S. Castellano and J. S. Waugh—295
Structure of the water molecule in solid hydrated compounds, J. W. McGrath and A. A. Silvidi—322
Studies of rates of conversion and populations of conformations in saturated ring compounds. III. *NN'* dimethyl piperazine, L. W. Reeves and K. O. Strømme—1711
Temperature dependence of NMR absorption in solid acetic acid, and in some of its chloro and acid chloride derivatives, A. Peterlin and M. Pintar—1730
Temperature dependence of the proton spin-lattice relaxation time in liquid butyl alcohols, Robert A. Bernheim, H. S. Gutowsky and Ian J. Lawrenson—565
Theory of localized contributions to the chemical shift. Application to fluorobenzenes, M. Karplus and T. P. Das—1683
Tritium as an internal source of radiation in EPR studies of organic materials, J. Kroh and J. W. T. Spinks—1853(L)
Zero-field splittings of molecular Zeeman effects, R. McWeeny—399

Magnetic Susceptibilities

Absorption spectrum and magnetic properties of osmium hexafluoride, J. C. Eisenstein—310
Calculation or the diamagnetic susceptibility of N_2, H. F. Hameka—366
Diamagnetic susceptibility of Ne, NH_3 and CH_4, K. E. Banyard—338(L)
Heat capacity anomaly in solid air, William H. Lien and Norman E. Phillips—1073(L)
Heat capacity of antiferromagnetic $CuCl_2 \cdot 2H_2O$ in the spin wave region, R. G. Petersen and Norman E. Phillips—1463(L)
Magnetic properties and optical absorption spectrum of K_2ReCl_6, J. C. Eisenstein—1628
Magnetic properties or uranium tetrafluoride, M. J. M. Leask, Darrell W. Osborne and W. P. Wolf—2090
Paramagnetic susceptibility or polycrystalline praseodymium metal, Sigurds Arajs, R. V. Colvin, and J. M. Peck—1959
Paramagnetism or uranyl ion. Effect of 6*d* orbitals and pi bonding, R. Linn Belford—318
Problems in perturbation theory calculation of diamagnetic susceptibility and nuclear magnetic shielding in molecules: Illustration with the hydrogen atom, Lawrence C. Snyder and Robert G. Parr—837
Theory of the diamagnetic susceptibilities or the alkanes, H. F. Hameka—1996

Mass Spectra

Collision-induced dissociation of HD^+, A. P. Irsa and L. Friedman—330(L)
Dependence of calculated and experimental propane mass spectra upon electron voltage, Edward M. Eyring and Austin L. Wahrhaftig—23
Determination or relative electronic transition probabilities by impact methods, F. H. Dorman and J. D. Morrison—578
Effect of electron energy on some electron-impact processes, Seymour Meyerson—2046
Interpretation of the appearance potentials of secondary ions, M. B. Wallenstein and M. Krauss—929
Ionization potentials of multiply charged krypton, xenon and mercury, F. H. Dorman and J. D. Morrison—1407
Ionization processes in CCl_4 and SF_6 by electron beams, R. E. Fox and R. K. Curran—1595
Ion-neutral reactions in the helium-hydrogen system, Martin Hertzberg, Donald Rapp, Irene B. Ortenburger and Donald D. Briglia—343(L)
Low-energy process for F^- formation in SF_6, R. K. Curran—1069(L)
Mass spectrometric investigation of ionization or N_2O by electron impact, R. K. Curran and R. E. Fox—159

Mass spectrometric test for an intermediate in a photochemical reaction involving chlorine, Gus A. Ropp, C. E. Melton and P. S. Rudolph—688(L)
On the classical approximation in the statistical theory of mass spectra, H. M. Rosenstock—2182(L)
Photoionization of alkanes. Dissociation of excited molecular ions. Bruce Steiner, Clayton F. Giese, and Mark G. Inghram —189
Positive and negative ion formation in CCl_3F, R. K. Curran— 2007
Stabilities of gaseous molecules in the Pb–Se and Pb–Te systems, Richard F. Porter—583
Study of the N_2O molecule using electron beams, G. J. Schulz— 1788
Thermodynamics of the vaporization of Cr_2O_3: Dissociation energies of CrO, CrO_2, and CrO_3, R. T. Grimley, R. P. Burns, and Mark G. Inghram—664
Vaporization of several rare-earth oxides, Morton B. Panish— 1079(L)

Mechanics, Quantum

Absorption spectrum and magnetic properties or osmium hexafluoride, J. C. Eisenstein—310
Applicability of approximate quantum-mechanical wave functions having discontinuities in their first derivatives, Joseph O. Hirschfelder and George V. Nazaroff—1666
Application of the free-electron theory to three-dimensional networks, J. A. Hoerni—508
Binding energies of alkali halide molecules, G. M. Rothberg— 2069
Bonding in cubic complexes, Joseph H. Macek and George H. Duffey—682
Bonding in icosahedral complexes, Joseph H. Macek and George H. Duffey—288
Calculation of the diamagnetic susceptibility of N_2, H. F. Hameka—366
Calculation or the lower excited energy levels of helium, H. F. Hameka—884
Calculation of the potential energy curves for some electronic states of carbon monoxide, Hélène Lefebvre-Brion, C. M. Moser and R. K. Nesbet—1950
Cation—electron interaction in metal-ammonia solutions, J. Jortner—678
Changes in the electronic transitions of aromatic hydrocarbons on chemical substitution. I. Perturbation theory for substituted cyclic polyenes, John Petruska—1111
Changes in the electronic transitions of aromatic hydrocarbons on chemical substitution. II. Application or perturbation theory to substituted-benzene spectra, John Petruska—1120
Choice of parameters for the Hückel π-electronic structure of furan: Tentative extension to pyrrole and thiophene, Frank L. Pilar and John R. Morris, II—389
Comparison of theoretical calculations on diatomic molecules with experiment, Ernest R. Davidson—1240
Composition of the electronic states of Nd(IV) and Er(IV), B. G. Wybourne—279
Core polarization in Li_2, Oktay Sinanoğlu and Earl M. Mortensen—1078(L)
Crystal field parameters for erbium in $Er(C_2H_5SO_4)_3 \cdot 9H_2O$, Edward H. Erath—1985
Cubic-field splitting and cubic-symmetry orthonormal sets of wavefunctions for J-manifolds (J half-integer), R. Pappalardo —1380
Derivation of interelectronic screening parameters from statistical considerations, Robert P. Bauman and James P. Considine—1388
Diamagnetic susceptibility of Ne, NH_3 and CH_4, K. E. Banyard —338(L)
Dipole moment of lithium hydride, F. A. Matsen—337(L)
Dissociation processes in electronically excited molecules. Linear chain model, John L. Magee and Koichi Funabashi— 1715
Eigen-functions for integer and half-odd integer values of J symmetrized according to the icosahedral group and the group C_{2v}, A. G. McLellan—1350
Electron spin resonance of crystalline free radicals, Jerome I. Kaplan—2205(L)
Electronic structures and spectra of some nitrogen-oxygen compounds, K. Lenore McEwen—547
Energies of excited electronic states as calculated with the zero differential overlap approximation, J. N. Murrell and L. Salem—1914
Erratum: High order rotation-vibration energies or polyatomic molecules. IV. [J. Chem. Phys. **29,** 665 (1958)], Gilbert Amat and Harald H. Nielsen—339(L)
Evaluation or electrostatic energy levels of f^6, John B. Gruber and John G. Conway—632
Extraordinary basic functions in valence theory, Lawrence C. Snyder and Robert G. Parr—1661
"Floating" hydrogen densities in some molecules of the type XH_n, K. E. Banyard—2105
Ground state wave functions for linear molecules, Enrico Clementi—1468(L)
Inelastic scattering of atoms. I. Inter-multiplet transitions, Walter R. Thorson—1744
Influence of the molecular environment on the carbonyl frequency. An electronic calculation, S. Bratoz and Mme. S. Besnainou—1142
Interaction energy in the Amaldi-Fermi theory for a pair of simple negative ions of the same kind with filled electronic shells, T. Tietz—1848(L)
Interaction of a triplet and a normal helium atom, G. H. Brigman, S. J. Brient and F. A. Matsen—958
Interaction potentials of simple nonpolar molecules with graphite, A. D. Crowell and R. B. Steele—1347
Ionized states in a one-dimensional molecular crystal, R. E. Merrifield—1835
Limit or stability or crystalline helium, Loren E. Radford—182
Line widths in the electron paramagnetic resonance spectrum of gaseous atomic hydrogen, R. M. Mazo—16,
Maximum overlap directed hybrid orbitals, T. L. Gilbert and P. G. Lykos—2199(L)
Method of alternant orbitals for allyl, Henry H. Dearman and Roland Lefebvre—72
Note concerning ruby maser-type Hamiltonians, Paul M. Parker—1459(L)
Nuclear hyperfine interactions in orbitally degenerate states of aromatic ions, H. M. McConnell and A. D. McLachlan—1
NMR spectra of propyl derivatives, James R. Cavanaugh and B. P. Dailey—1094
Nuclear relaxation processes of a nonequivalent two-spin system, Hiroshi Shimizu and Shizuo Fujiwara—1501
On the fluorine molecule. Part I. The pilot calculation, Katsunori Hijikata—221
On the fluorine molecule. II. Energy levels of F_2 and F_2^+, Katsunori Hijikata—231
On the nature of the crystal field approximation, C. M. Herzfeld and H. Goldberg—643
On the solution of Hartree-Fock equation in terms of localized orbitals, William H. Adams—89
On the theory of Raman intensities, Andreas C. Albrecht—1476
Open and closed shell SCF method for conjugated systems, O. W. Adams and P. G. Lykos—1444(L)
Open-shell wave functions for conjugated hydrocarbons, J. R. Hoyland and Lionel Goodman—1446(L)
Pi bonding in uranyl ion, R. Linn Belford and Geneva Belford— 1330

Potential curves for doubly positive diatomic ions, A. C. Hurley and V. N. Maslen—1919
Potential energy curves for OH, Robert J. Fallon, Irwin Tobias, and Joseph T. Vanderslice—167
Problems in perturbation theory calculation of diamagnetic susceptibility and nuclear magnetic shielding in molecules: Illustration with the hydrogen atom, Lawrence C. Snyder and Robert G. Parr—837
Proton chemical shifts for the alkyl derivatives, James R. Cavanaugh and B. P. Dailey—1099
Quantum calculations of the velocity dependence of the differential and total cross sections for elastic scattering of molecular beams, Richard B. Bernstein—361
Quantum-mechanical cell model of the liquid state. II. Application to the zero-point properties of close-packed crystals, R. P. Hurst and J. M. H. Levelt—54
Quantum mechanics of mobile electrons in conjugated bond systems. III. Topological matrix as generatrix of bondorders in homonuclear conjugated systems, Klaus Ruedenberg—1883
Relation of perturbation theory to variation method, Oktay Sinanoglu—1237
Role of exchange energy in intermediate-range interactions, Frank O. Ellison—2100
Second-order perturbation theory of helium-like ions, B. F. Gray and R. Whitehead—1243
Spin density in pyrene negative ion, G. J. Hoijtink, J. Townsend and S. I. Weissman—507
Spin-dependence of the first-order transition density matrix, Werner A. Bingle—1066(L)
Spin inversion operator in nuclear magnetic resonance, Robert L. Fulton and John D. Baldeschwieler—1075(L)
Spin-orbit coupling in orbitally degenerate states of aromatic ions, Harden M. McConnell—13
Spin-spin interactions in nuclear magnetic resonance. Contact contribution, S. Alexander—106
SPO (split *p*-orbital) method and its application to ethylene, Michael J. S. Dewar and N. L. Hojvat—1232
Strong coupling in nuclear resonance spectra. IV. Exact analysis of three-spin spectra, S. Castellano and J. S. Waugh—295
Studies in molecular structure. III. Populations analyses for selected first-row diatomic molecules, Serafin Fraga and Bernard J. Ransil—727
Studies in molecular structure. IV. Potential curve for the interaction of two helium atoms in single-configuration LCAO–MO–SCF approximation, Bernard J. Ransil—2109
Sum rule for transition probabilities, William L. Clinton—273
Theoretical molecular transition probabilities. I. The V–N transition in H_2, S. Ehrenson and P. E. Phillipson—1224
Theory of localized contributions to the chemical shift. Application to fluorobenzenes, M. Karplus and T. P. Das—1683
Theory of the diamagnetic susceptibilities of the alkanes, H. F. Hameka—1996
Three-dimensional FE–MO model. I. ΔH of dissociation of homonuclear diatomic molecules, Sheldon L. Matlow—1187
Use of Gaussian orbitals for atoms-in-molecule calculations, M. Krauss—692(L)
Valence bond treatment on the *B* state of the hydrogen molecule, Carmen S. Tschudi and Norah V. Cohan—401
Wave functions and correlation energies for F, F^-, and Ne, Leland C. Allen—1156

Mechanics, Statistical

Approach to thermodynamic equilibrium, J. E. Mayer—1207
Approximate theory of transport in simple dense fluid mixtures, Stuart A. Rice and Alan R. Allnatt—409
Closed general solution of the probability distribution function for three-dimensional random walk processes, Chi-hua Hsiung, Hsien-Chih Hsiung, and Adon A. Gordus—535
Composition dependence of the thermal conductivity of regular solutions, Richard J. Bearman and V. S. Vaidhyanathan—264
Concentration dependence of polymer chain configurations in solution, Hiromi Yamakawa—1360
Configuration and free energy of a polymer molecule with solvent interaction, Michael E. Fisher and Basil J. Hiley—1253
Density expansions of correlation functions for equilibrium systems, Harold L. Friedman—73
Derivation of the Tait equation and its relation to the structure of liquids, Robert Ginell—1249
Development of the liquid equation and the partial structure of water, Robert Ginell—2174
Deviations from thermal equilibrium among reactant molecules, B. Widom—2050
Dimensional change of polypeptide molecules in the helix-coil transition region. II., Kazuo Nagai—887
Distortion correction to the surface energy of the {110} face of alkali halide crystals, G. C. Benson, E. Dempsey and P. Balk—157
Erratum: Distribution functions of a fluid in an external potential field: Application to physical adsorption [J. Chem. Phys. **33,** 464 (1960)], William A. Steele and Marvin Ross—1067(L)
Expected square of the length of isotactic vinylic hydrocarbon-type chains, Victor E. Meyer, Jack B. Kinsinger and Paul M. Parker—1429
Extended hole theory of liquids, George E. Blomgren—1307
Free-volume model of the amorphous phase: Glass transition, David Turnbull and Morrel H. Cohen—120
Intrinsic viscosity of stiff chains, Robert Ullman and A. Muzyka—1461(L)
Limit of stability of crystalline helium, Loren E. Radford—182
Mayer's ensembles of maximum entropy, Andrew D. McLachlan and Robert A. Harris—1451(L)
Mean free path and ultrasonic vibrational relaxation in liquids and dense gases, W. M. Madigosky and T. A. Litovitz—489
Molecular statistics of vinyl polymers, Yasutaka Suzuki—79
Monte Carlo computations on the Ising model: The body-centered cubic lattice, Lester Guttman—1024
On the kinetic theory or dense fluids. VI. The singlet distribution function for rigid spheres with an attractive potential, Stuart A. Rice and Alan R. Allnatt—2144
On the kinetic theory of dense fluids. VII. The doublet distribution function for rigid spheres with an attractive potential, Alan R. Allnatt and Stuart A. Rice—2156
On the theory of helix-coil transition in polypeptides, Shneior Lifson and A. Roig—1963
Pauling's model and the thermodynamic properties of water, Henry S. Frank and Arvin S. Quist—604
Probability of initial ring closure in the restricted random walk model of a macromolecule, B. J. Hiley and M. F. Sykes—1531
Quantum-mechanical cell model of the liquid state. II. Application to the zero-point properties of close-packed crystals, R. P. Hurst and J. M. H. Levelt—54
Quasi-lattice model of reciprocal salt systems. A generalized calculation, Milton Blander—432
Radial distribution function from the Percus-Yevick equation, A. A. Broyles—1068(L)
Sixth virial coefficients for gases of parallel hard lines, hard squares and hard cubes, William G. Hoover and Andrew G. De Rocco—1059(L)
Solution at high density to the Born-Green equation, A. A. Broyles—359
Statistical mechanics of isotope effects on the thermodynamic properties of condensed systems, Jacob Bigeleisen—1485
Statistical mechanics of monatomic systems in an external periodic potential field. I. Introduction, virial expansion, and classical second virial coefficient, Terrell L. Hill and Samuel Greenschlag—1538

Statistical mechanics of monatomic systems in an external periodic potential field. II. Distribution function theory for fluids, Terrell L. Hill and Nobuhiko Saitô—1543
Statistical thermodynamics of mixtures. II. Convergence of the quasi-chemical method for the Ising square lattice, Stephen G. Brush—1852(L)
Theory of the surface tension of molten salts, H. Reiss and S. W. Mayer—2001
Theory of the two- and one-dimensional rigid sphere fluids, E. Helfand, H. L. Frisch and J. L. Lebowitz—1037
Theory of vibrational relaxation in liquids, Robert Zwanzig—1931
Thermodynamic theory of the pair correlation function, Edward W. Hart—1471
Vapor pressure of nearly classical liquids, William A. Steele—802
Vibrational relaxation in liquids, Marshall Fixman—369

Metals

Analysis of specific heat data for zinc: Resolution of the calorimetric and elastic H_0 discrepancy, C. W. Garland and J. Silverman—781
Cation-electron interaction in metal-ammonia solutions, J. Jortner—678
Concerning the feasibility of nuclear cooling with palladium hydride, J. J. Fritz, H. J. Maria, and J. G. Aston—2185(L)
Dispersion of lattice waves in copper, S. K. Joshi and M. P. Hemkar—1458(L)
Electrical resistivity of liquid sodium, liquid lithium and dilute liquid sodium solutions, J. F. Freedman and W. D. Robertson—769
Field emission from whiskers, A. J. Melmed and R. Gomer—1802
Heat capacity of thulium from 15° to 360°K, L. D. Jennings, Emma Hill and F. H. Spedding—2082
Monte Carlo computations on the Ising model; The body-centered cubic lattice, Lester Guttman—1024
Proton magnetic resonance studies of structure, diffusion and resonance shifts in titanium hydride, B. Stalinski, C. K. Coogan and H. S. Gutowsky—1191
Structure of alkali metals in the liquid state, N. S. Gingrich and LeRoy Heaton—873
Thermal expansion or metals, S. S. Mitra and S. K. Joshi—1462(L)
Twist in alumina whiskers, G. W. Sears, R. C. DeVries, and C. Huffine—2142
X-ray diffraction study of liquid mercury-indium alloys, Young Soo Kim, C. L. Standley, R. F. Kruh and Glen T. Clayton—1464(L)

Microwave Spectra (see Absorption Spectra)

Molecular Beams

New determinations of the vibrational constants of Li^6F and Li^6Cl^{35} by the molecular beam electric resonance method, T. I. Moran and J. W. Trischka—923

Molecular Films (see Surface Phenomena)

Microwave spectrum of cis 1-chloro-2-fluoroethylene, John A. Howe—1247

Molecular Spectra (see Absorption Spectra, Emission Spectra, Fluorescence and Raman Spectra)

Comment on the calculation of zero-field splittings, R. McWeeny—1065(L)
Composition of the electronic states of Nd(IV) and Er(IV), B. G. Wybourne—279
Determination of relative electronic transition probabilities by impact methods, F. H. Dorman and J. D. Morrison—578
Effect of pressure on the spectra of crystalline UF_4 and UF_3, K. B. Keating and H. G. Drickamer—140
Electron spin resonance in complexes of aromatic hydrocarbons with iodine, L. S. Singer and J. Kommandeur—133
Electronic conduction in complexes of aromatic hydrocarbons with iodine, J. Kommandeur and Frances R. Hall—129
Infrared spectrum of $CO(CO)_3NO$, Robin S. McDowell, W. D. Horrocks, Jr., and John T. Yates—530
Microwave spectrum of *cis*-difluoroethylene. Structures and dipole moments of fluoroethylenes, Victor W. Laurie—291
Origin of the green bands in the boron-oxygen system, W. E. Kaskan, J. D. Mackenzie, and R. C. Millikan—570
Potential energy curves for OH, Robert J. Fallon, Irwin Tobias, and Joseph T. Vanderslice—167
Quantum mechanics of mobile electrons in conjugated bond systems. I. General analysis in the tight-binding formulation, Klaus Ruedenberg—1861
Quantum mechanics of mobile electrons in conjugated bond systems. II. Augmented tight-binding formulation, Klaus Ruedenberg—1877
Quantum mechanics of mobile electrons in conjugated bond systems. III. Topological matrix as generatrix of bondorders in homonuclear conjugated systems, Klaus Ruedenberg—1883
Quantum mechanics of mobile electrons in conjugated bond systems. IV. Integral formulas, Klaus Ruedenberg—1891
Quantum mechanics of mobile electrons in conjugated bond systems. V. Empirical determination of integrals between carbon atomic orbitals from experimental data on benzene, Klaus Ruedenberg and E. Miller Layton, Jr.—1896
Quantum mechanics of mobile electrons in conjugated bond systems. VI. Theoretical evaluation or energy contributions, Klaus Ruedenberg—1907
Strong coupling in nuclear resonance spectra. IV. Exact analysis of three-spin spectra, S. Castellano and J. S. Waugh—295
Vacuum ultraviolet absorption spectrum of phosgene, S. R. La Paglia and A. B. F. Duncan—125
Zero-field splittings of molecular Zeeman effects, R. McWeeny—399

Molecular Structure and Constants (see also Absorption Spectra, Fluorescence, Raman Spectra, Electron and X-ray Diffraction

Application of ligand field theory to the electronic spectra of gaseous $CuCl_2$, $NiCl_2$, and $CoCl_2$, Jon T. Hougen, George E. Leroi and Thomas C. James—1670
Binding energies of alkali halide molecules, G. M. Rothberg—2069
Bonding in icosahedral complexes, Joseph H. Macek and George H. Duffey—288
Calculation of the potential energy curves for some electronic states of carbon monoxide, Hélène Lefebvre-Brion, C. M. Moser and R. K. Nesbet—1950
Capacitive energy and the ionization of aromatic hydrocarbons, Felix T. Smith—793
Changes in the electronic transitions of aromatic hydrocarbons on chemical substitution. I. Perturbation theory for substituted cyclic polyenes, John Petruska—1111
Changes in the electronic transitions of aromatic hydrocarbons on chemical substitution. II. Application of perturbation theory to substituted-benzene spectra, John Petruska—1120
Choice of parameters for the Hückel π-electronic structure of furan: Tentative extension to pyrrole and thiophene, Frank L. Pilar and John R. Morris, II—389
Comment on the calculation of zero-field splittings, R. McWeeny—1065(L)
Comments on "On the structure of the Isomers of N_2F_2, Russell H. Sanborn—2188(L)
Comparison of theoretical calculations on diatomic molecules with experiment, Ernest R. Davidson—1240

Core polarization in Li_2, Oktay Sinanoğlu and Earl M. Mortensen—1078(L)
Difference of intermolecular potentials of CH_3OH and CH_3OD, E. Whalley and M. Falk—1569
Dipole moment or the OH radical from the Stark effect of its microwave spectrum, Richard T. Meyer and Rollie J. Myers—1074(L)
Dissociation energies of diatomic molecules, E. R. Lippincott, R. Schroeder, and D. Steele—1448(L)
Dissociation energies or diatomic molecules, G. R. Somayajulu—1449(L)
Energies of excited electronic states as calculated with the zero differential overlap approximation, J. N. Murrell and L. Salem—1914
Energy levels for internal and over-all rotation of two-top molecules. I. Microwave spectrum of dimethyl silane, Louis Pierce—498
EPR studies of spin correlation in some ion radical salts, D. B. Chestnut, H. Foster, and W. D. Phillips—684(L)
Excitation transfer splitting in the $n\rightarrow\pi^*$ transitions of the diazines, M. A. El-Sayed and G. W. Robinson—1840(L)
Ground state wave functions for linear molecules, Enrico Clementi—1468(L)
Hyperfine splittings in the (HOOC)C^{13}H(COOH) radical, T. Cole and C. Heller—1085(L)
Influence of the molecular environment on the carbonyl frequency. An electronic calculation, S. Bratoz and Mme S. Besnainou—1142
Infrared and Raman spectra of fluorinated ethanes. XIV. CF_2Cl—CHF_2 and CF_2Br—CHF_2, Peter Klaboe and J. Rud Nielsen—1819
Infrared spectra and potential constants of some monohaloacetylenes, G. R. Hunt and M. K. Wilson—1301
Infrared spectra of alkyldiboranes. IV. 1,1-dimethyl- and 1,1-diethyldiboranes, Walter J. Lehmann, Charles O. Wilson, Jr. and I. Shapiro—476
Infrared spectra of alkyldiboranes. V. Tri- and tetramethyl- and ethyldiboranes, Walter J. Lehmann, Charles O. Wilson, Jr. and I. Shapiro—783
Infrared spectra of methanol and deuterated methanols in gas, liquid, and solid phases, M. Falk and E. Whalley—1554
Infrared spectra of the lithium halide dimers, William Klemperer and Wilfried G. Norris—1071(L)
Infrared spectrum and thermodynamic properties or ruthenium tetroxide, M. H. Ortner—556
Infrared spectrum of diimide, Edmund J. Blau, Bernard F. Hochheimer and Hilbert J. Unger—1060(L)
Infrared spectrum or stannane, Leopold May and Clyde R. Dillard—694(L)
Ion-neutral reactions in the helium-hydrogen system, Martin Hertzberg, Donald Rapp, Irene B. Ortenburger and Donald D. Briglia—343(L)
Ionization potentials of benzene, hexadeuterobenzene, and pyridine from their observed Rydberg series in the region 600–2000 A, Mostafa F. Amr El-Sayed, M. Kasha and Y. Tanaka—334(L)
Isotropic and anisotropic hyperfine interactions in hydrazyl and carbazyl, N. W. Lord and S. M. Blinder—1693
Mass spestrometric investigation of ionization of N_2O by electron impact, R. K. Curran and R. E. Fox—1590
Method of alternant orbitals for allyl, Henry H. Dearman and Roland Lefebvre—72
Microwave spectrum of acetyl chloride, K. M. Sinnott—851
Microwave spectrum of *cis*-difluoroethylene. Structures and dipole moments of fluoroethylenes, Victor W. Laurie—291
Microwave spectrum of cis 1-chloro-2-fluoroethylene, John A. Howe—1247
Microwave spectrum of isobutylene. Dipole moment, internal barrier, equilibrium conformation, and structure, Victor W. Laurie—1516
Microwave spectrum of O^{18} formyl fluoride and the structure of formyl fluoride, Ronald F. Miller and R. F. Curl, Jr.—1847(L)
Microwave spectrum, structure, dipole moment, and internal barrier of vinyl silane, James M. O'Reilly and Louis Pierce—1176
Millimeter wave spectrum and molecular structure of oxygen difluoride, A. Ray Hilton, Jr., Albert W. Jache, James B. Beal, Jr., William D. Henderson and R. J. Robinson—1137
Molecular orbital theory and hyperfine splitting in electron spin resonance spectra of semiquinones, Gershon Vincow and George K. Fraenkel—1333
Molecular structure of diphenylethers, Hiroshi Shimizu, Shizuo Fujiwara and Yonezo Morino—1467(L)
New determinations of the vibrational constants of Li^6F and Li^6Cl^{35} by the molecular beam electric resonance method, T. I. Moran and J. W. Trischka—923
Nitrosyl chloride structure, John D. Rogers and Dudley Williams—2195(L)
Normal coordinate treatments and calculated thermodynamic properties of phosphoryl chloride, thiophosphoryl chloride, and phosphoryl fluoride, Joseph S. Ziomek and Edward A. Piotrowski—1087
NMR spectra of glycidaldehyde, C. A. Reilly and J. D. Swalen—980
NMR spectra of 1,1,4,4-tetramethylcyclohexyl-cis- and trans-2,6-diacetate, J. I. Musher—594
NMR spectra of some halogenated propenes, J. D. Swalen and C. A. Reilly—2122
NMR spectra of vinyl chloride and the chloroethylenes, E. B. Whipple, William E. Stewart, G. S. Reddy and J. H. Goldstein—2136
Nuclear quadropole coupling in the NH_3 molecule, Yoshifumi Kato—619
On the fluoreine molecule. Part I. The pilot calculation, Katsunori Hijikata—221
On the fluorine molecule. II. Energy levels of F_2 and F_2^+, Katsunori Hijikata—231
On the nature or the crystal field approximation, C. M. Herzfeld and H. Goldberg—643
On the structure or the isomers of N_2F_2, Raymond Ettinger, Frederic A. Johnson and Charles B. Colburn—2187(L)
Open and closed shell SCF method for conjugated systems, O. W. Adams and P. G. Lykos—1444(L)
Open-shell wave functions for conjugated hydrocarbons, J. R. Hoyland and Lionel Goodman—1446(L)
Pi bonding in uranyl ion, R. Linn Belford and Geneva Belford—1350
Polarity of the C—H bonds in acetylene and its molecular quadrupole moment, H. Hamano—1678
Proton hyperfine splittings and spin densities of pentaphenylcyclopentadienyl, D. C. Reitz—701(L)
Potential curves for doubly positive diatomic ions, A. C. Hurley and V. W. Maslen—1919
Proton magnetic resonance spectra of compounds of the type $X(C_2H_3)_n$: Relative signs of the X-H spin coupling constants, P. T. Narasimhan and Max T. Rogers—1049
Quantum mechanics of mobile electrons in conjugated bond systems. I. General analysis in the tight-binding formulation, Klaus Ruedenberg—1861
Quantum mechanics of mobile electrons in conjugated bond systems. II. Augmented tight-binding formulation, Klaus Ruedenberg—1877
Quantum mechanics of mobile electrons in conjugated bond systems. III. Topological matrix as generatrix of bondorders in homonuclear conjugated systems, Klaus Ruedenberg—1883
Quantum mechanics or mobile electrons in conjugated bond systems. IV. Integral formulas, Klaus Ruedenberg—1891

Quantum mechanics of mobile electrons in conjugated bond systems. V. Empirical determination of integrals between carbon atomic orbitals from experimental data on benzene, Klaus Ruedenberg and E. Miller Layton, Jr.—1896
Quantum mechanics of mobile electrons in conjugated bond systems. VI. Theoretical evaluation of energy contributions, Klaus Ruedenberg—1907
Raman intensities and the structure of some oxyanions of group VII, G. W. Chantry and R. A. Plane—1268
Spin and charge exchange in anions of biphenylyl ether, Dolan H. Eargle, Jr. and S. I. Weissman—1840(L)
SPO (split p-orbital) method and its application to ethylene, Michael J. S. Dewar and N. L. Hojvat—1232
Structure of the water molecule in solid hydrated compounds, J. W. McGrath and A. A. Silvidi—322
Studies in molecular structure. III. Populations analyses for selected first-row diatomic molecules, Serafin Fraga and Bernard J. Ransil—727
Studies in molecular structure. IV. Potential curve for the interaction of two helium atoms in single-configuration LCAO-MO-SCF approximation, Bernard J. Ransil—2109
Studies of rates of conversion and populations of conformations in saturated ring compounds. III. NN' dimethyl piperazine, L. W. Reeves and K. O. Strømme—1711
Study of the N_2O molecule using electron beams, G. J. Schulz—1778
Theoretical molecular transition probabilities. I. The V–N transition in H_2, S. Ehrenson and P. E. Phillipson—1224
Torsional oscillation frequency of H_2O_2, David Chin and Paul A. Giguere—690(L)
Transferability of Urey-Bradley force constants VI. The silyl halides, John Overend and James R. Scherer—574
Trimethylene oxide. II. Structure, vibration-rotation interaction, and origin of potential function for ring-puckering motion, Sunney I. Chan, John Zinn, and William D. Gwinn—1319
Vacuum ultraviolet absorption spectrum and dipole moment of nitrogen trifluoride, S. R. La Paglia and A. B. F. Duncan—1003
Valence bond treatment on the B state of the hydrogen molecule, Carmen S. Tschudi and Norah V. Cohan—401
Zero-field splittings of molecular Zeeman effects, R. McWeeny—399

Neutron Diffraction

Structure of alkali metals in the liquid state, N. S. Gingrich and LeRoy Heaton—873

Nuclear Quadrupole Resonance

Nuclear quadrupole and electron spin resonance spectra of some chlorine compounds including (Me_3PhNc)($FeCl_4$), C. D. Akon and T. Iredale—340(L)
Quadrupole relaxation effects in nuclear magnetic double resonance, John D. Baldeschwieler—718

Nuclear Resonance (see Magnetic Resonance)

Concentration dependence of NMR spin-lattice relaxation times in solutions, R. W. Mitchell and M. Eisner—651
NMR spectra of glycidaldehyde, C. A. Reilly and J. D. Swalen—980
NMR spectra of 1,1,4,4-tetramethylcyclohexyl-cis- and trans-2,6-diacetate, J. I. Musher—594
Nuclear magnetic resonance study of the proton transfer in water, S. Meiboom—375
Strong coupling in nuclear resonance spectra. IV. Exact analysis of three-spin spectra, S. Castellano and J. S. Waugh—295
Structure of the water molecule in solid hydrated compounds, J. W. McGrath and A. A. Silvidi—322

Nucleation

Kinetics of crystal nucleation in some normal alkane liquids, David Turnbull and Robert L. Cormia—820

Optical Activity

Erratum: Optical and other electronic properties of polymers [J. Chem. Phys. **33,** 1532 (1960)], Ignacio Tinoco, Jr.—1067(L)

Phase Transitions

Clustering in the critical region, George W. Brady and John I. Petz—332(L)
Geometric basis or phase change, Robert Ginell—992
Limit of stability of crystalline helium, Loren E. Radford—182
Note on the sublimation of ammonium perchlorate, H. M. Cassel and I. Liebman—343(L)
Phase transition in ammonium fluoride, Richard Stevenson—346(L)
Phase transitions in the ammonium halides, Richard Stevenson—1757
Transitions between different forms of ice, R. H. Beaumont, H. Chihara and J. A. Morrison—1456(L)

Phosphors

Paramagnetic resonance absorption in naphthalene in its phosphorescent state, Clyde A. Hutchison, Jr. and Billy W. Mangum—908
Phosphorescence spectra of acenaphthene at low temperatures, Adnan Zmerli—2130

Photochemistry

Decomposition of dimethyl carbonate on quartz, M. H. J. Wijnen—1465(L)
Electric properties of organic solids. IV. Charge carrier diffusivity in metal free phthalocyanine, David R. Kearns and Melvin Calvin—2022
Mass spectrometric test for an intermediate in a photochemical reaction involving chlorine, Gus A. Ropp, C. E. Melton and P. S. Rudolph—688(L)
Paramagnetic resonance absorption in naphthalene in its phosphorescent state, Clyde A. Hutchison, Jr. and Billy W. Mangum—908
Photochemical studies in flash photolysis. II. Photolysis of acetone with filtered light, N. Slagg and R. A. Marcus—1013
Photodecomposition of biacetyl vapor, Julian Heicklen and Gerald B. Porter—686(L)
Photolysis of nitrous oxide. I. 1236 A, John P. Doering and Bruce H. Mahan—1617
Pressure dependence of fluorescence spectra, David J. Wilson, Barbara Noble and Betty Lee—1391
Solid state ionization potentials of some aromatic organic compounds, David R. Kearns and Melvin Calvin—2026
"Subthreshold" photocurrents of high-quantum yield in 9,10-dichloroanthracene, A. Bree and W. G. Schneider—1453(L)
Transient dimer formation by 2,5-diphenyloxazole, Isadore B. Berlman—1083(L)
Transient measurements of photochemical processes in dyes. I. The photosensitized oxidation of phenol by eosin and related dyes, L. I. Grossweiner and E. F. Zwicker—1411
Vacuum UV photolysis of ethane: Molecular detachment of hydrogen, H. Okabe and J. R. McNesby—668

Photoconductivity

Effect of oxygen adsorption on photo- and semiconduction of β-carotene, Barnett Rosenberg—812

Electrical properties of organic solids. IV. Charge carrier diffusivity in metal free phthalocyanine, David R. Kearns and Melvin Calvin—2022
Photoconduction activation energies in *cis-trans* isomers of β-carotene, Barnett Rosenberg—63
"Subthreshold" photocurrents of high-quantum yield in 9,10-dichloroanthracene, A. Bree and W. G. Schneider—1453(L)

Photoionization

Solid state ionization potentials of some aromatic organic compounds, David R. Kearns and Melvin Calvin—2026

Polymers

Concentration dependence of polymer chain configurations in solution, Hiromi Yamakawa—1360
Configuration and free energy of a polymer molecule with solvent interaction, Michael E. Fisher and Basil J. Hiley—1253
Dichroism of 603 cm^{-1} band of polyvinyl chloride, Takehiko Shimanouchi and Mitsuo Tasumi—687(L)
Dimensional change of polypeptide molecules in the helix-coil transition region. II., Kazuo Nagai—887
Electrostatic binding energy in a body centered structure of parallel charge doublet chains, P. J. Jackson—2119
Erratum: Optical and other electronic properties of polymers [J. Chem. Phys. **33,** 1532 (1960)], Ignacio Tinoco, Jr.—1067(L)
Expected square of the length of isotactic vinylic hydrocarbon-type chains, Victor E. Meyer, Jack B. Kinsinger and Paul M. Parker—1429
Interpretation of viscosity data for concentrated polymer solutions, Hiroshi Fujita and Akira Kishimoto—393
Intrinsic viscosity of stiff chains, Robert Ullman and A. Muzyka—1461(L)
Molecular statistics or vinyl polymers, Yasutaka Suzuki—79
On the theory of helix-coil transition in polypeptides, Shneior Lifson and A. Roig—1963
Probability of initial ring closure in the restricted random walk model of a macromolecule, B. J. Hiley and M. F. Sykes—1531
Protection against radiation damage in polymethylmethacrylate by high-energy electrons and by ultraviolet light, Donald G. Gardner and Lawrence M. Epstein—1653
Theoretical investigations on the light scattering of colloidal spheres. IX. Lateral scattering at 90° from incident natural and linearly polarized light, William J. Pangonis, Wilfried Heller and Nicolaos A. Economou—960
Theoretical investigations on the light scattering of colloidal spheres. X. The "scattering ratio" and depolarization of light scattered at an angle of observation of 90°, Wilfried Heller, William J. Pangonis and Nicolaos A. Economou—971
Theory of light scattering by thin rodlike macromolecules in a liquid subjected to shear, K. Okano and E. Wada—405
Theory of solutions. III. Thermodynamics of aggregation or polymerization, Terrell L. Hill—1974

Proteins

Dimensional change of polypeptide molecules in the helix-coil transition region. II., Kazuo Nagai—887

Quadropole Resonance (see Nuclear Quadrupole Resonance)

Nuclear quadrupole coupling in the NH_3 molecule, Yoshifumi Kato—619

Quantum Mechanics (see Mechanics, Quantum)

Comment on the calculation of zero-field splittings, R. McWeeny—1065(L)
Electron spin resonance of some vanadyl porphyrins, E. M. Roberts, W. S. Koski and W. S. Caughey—591
Nuclear quadrupole coupling in the NH_3 molecule, Yoshifumi Kato—619
Quantum mechanics of mobile electrons in conjugated bond systems. I. General analysis in the tight-bonding formulation, Klaus Ruedenberg—1861
Quantum mechanics or mobile electrons in conjugated bond systems. II. Augmented tight-binding formulation, Klaus Ruedenberg—1877
Quantum mechanics of mobile electrons in conjugated bond systems. III. Topological matrix as generatrix of bondorders in homonuclear conjugated systems, Klaus Ruedenberg—1883
Quantum mechanics of mobile electrons in conjugated bond systems. IV. Integral formulas, Klaus Ruedenberg—1891
Quantum mechanics of mobile electrons in conjugated bond systems. V. Empirical determination of integrals between carbon atomic orbitals from experimental data on benzene, Klaus Ruedenberg and E. Miller Layton, Jr.—1896
Quantum mechanics or mobile electrons in conjugated bond systems. VI. Theoretical evaluation of energy contributions, Klaus Ruedenberg—1907
Valence bond treatment on the *B* state of the hydrogen molecule, Carmen S. Tschudi and Norah V. Cohan—401
Zero-field splittings of molecular Zeeman effects, R. McWeeny—399

Radiation Chemistry

Effect of inert-gas moderators on the (n, γ) activated reaction of I^{128} with CH_4, Edward P. Rack and Adon A. Gordus—1855
Electron spin resonance in a gamma-irradiated single crystal or thiodiglycolic acid, Yukio Kurita and Walter Gordy—1285
Energy transfer and quenching processes in the system cyclohexane-benzene-terphenyl-oxygen, A. Weinreb—1316
Evidence of trapped N atoms in X-ray irradiated NaN_3, G. J. King, F. F. Carlson, B. S. Miller, and R. C. McMillan—1499
High-energy radiation damage to fluorescent organic solids, Charles F. Sharn—240
Irradiation yields of radicals in gamma-irradiated ice at 4.2° and 77°K, Seymour Siegel, John M. Flournoy, and Lillian H. Baum—1782
Luminescence in a scintillation solution excited by α and β particles and related studies in quenching, Isadore B. Berlman—598
On the luminescence minimum in certain scintillator solutions, J. M. Nosworthy, John L. Magee, and M. Burton—83
Paramagnetic resonance study of irradiated single crystals of calcium tungstate, Henry Zeldes and Ralph Livingston—247
Protection against radiation damage in polymethylmethacrylate by high-energy electrons and by ultraviolet light, Donald G. Gardner and Lawrence M. Epstein—1653
Radiolysis of aqueous solutions highly enriched in O^{18}, Michael Anbar, Shmuel Guttmann and Gabriel Stein—703
Radiolysis of cyclohexane. III. Vapor phase, J. M. Ramaradhya and G. R. Freeman—1726
Time spectra of positrons annihilating in organic liquids containing halogens, J. H. Ormrod and B. G. Hogg—624
Tritium as an internal source of radiation in EPR studies of organic materials, J. Kroh and J. W. T. Spinks—1853(L)

Radiochemistry

Closed general solution of the probability distribution function for three-dimensional random walk processes, Chi-hua Hsiung, Hsien-Chih Hsiung, and Adon A. Gordus—535
Effect of solvent and solute structure on scintillator pulse heights. I. Correlation of pulse heights for ring substituted styrene plastic scintillators with Hammett substituent constants, Stanley R. Sandler and Samuel Loshaek—439

Effect of solvent and solute structure on scintillator pulse heights. II. Correlation of pulse heights for aromatic liquid organic scintillators with Hammett substituent constants, Stanley R. Sandler and Samuel Loshaek—445

Raman Spectra

Infrared and raman spectra of fluorinated ethanes. XIV. CF_3Cl—CHF_2 and CF_2Br—CHF_2, Peter Klaboe and J. Rud Nielsen—1819
Infrared spectra of methanol and deuterated methanols in gas, liquid, and solid phases, M. Falk and E. Whalley—1554
On the theory of raman intensities, Andreas C. Albrecht—1476
Raman intensities and the structure of some oxyanions of group VII, G. W. Chantry and R. A. Plane—1268

Reaction Rates (see Kinetics of Reaction)

Rotation

Energy levels for internal and over-all rotation of two-top molecules. I. Microwave spectrum of dimethyl silane, Louis Pierce —498
Infrared spectroscopic evidence for the rotation of the ammonia molecule in solid argon and nitrogen, Dolphus E. Milligan, Robert M. Hexter and Kurt Dressler—100
Microwave spectrum, structure, dipole moment, and internal barrier of vinyl silane, James M. O'Reilly and Louis Pierce —1176

Scattering

Quantum calculations of the velocity dependence of the differential and total cross sections for elastic scattering of molecular beams, Richard B. Bernstein—361
Reactive scattering in crossed molecular beams: K atoms with CH_3I and C_2H_5I, D. R. Herschbach, G. H. Kwei and J. A. Norris—1842(L)
Scattering of high velocity neutral particles. XI. A further study of the He-He potential, I. Amdur, J. E. Jordan, and S. O. Colgate—1525

Semi-conductors

Effect of oxygen adsorption on photo- and semiconduction of β-carotene, Barnett Rosenberg—812
Effect of pressure on the resistance of iodine and selenium, A. S. Balchan and H. G. Drickamer—1948
Electrical conductivity of some coordination polymers, Seiichi Kanda and Shinichi Kawaguchi—1070(L)

Shock Waves (see also Detonation)

Density measurements in reflected shock waves, W. C. Gardiner, Jr. and G. B. Kistiakowsky—1080(L)
Dependence of vibrational relaxation time on the vibrational quantum number—experimental verification for NO($A\ ^2\Sigma^+$) behind shock waves, Walter Roth—2204(L)
Gaseous detonations. XV. Expansion waves in gaseous detonations, Hajime Miyama and Paul Kydd—2038
High temperature absorption of carbon dioxide at 4.40μ, Martin Steinberg and William O. Davies—1373
Shock tube determination of dissociation rates of oxygen, John P. Rink, Herbert T. Knight and Russell E. Duff—1942
Shock tube study of vibrational relaxation in the $A^3\Sigma^+$ state of NO, W. Roth—999
Vibrational relaxation of carbon monoxide in the shock tube, D. L. Matthews—639

Solutions (see also liquids)

Application of a theory of nonideal solutions to results of ultrasonic absorption measurements, F. O. Goodman—1585
Approximate theory of transport in simple dense fluid mixtures, Stuart A. Rice and Alan R. Allnatt—409
Cation—electron interaction in metal-ammonia solutions, J. Jortner—678
Electrical conductance of solutions of salts in liquid metals: Potassium iodide in potassium, H. R. Bronstein, A. S. Dworkin and M. A. Bredig—1843(L)
Electron spin relaxation in metal-ammonia solutions, Victor L. Pollak—864
Electronic paramagnetic relaxation times in potassium-ammonia and potassium-deuteroammonia solutions, Clyde A. Hutchison, Jr. and Donald E. O'Reilly—1279
Heats of mixing in liquid alkali nitrate systems, O. J. Kleppa and L. S. Hersh—351
Near-ultraviolet solution spectra of pyridazine, Robert H. Linnell—698(L)
Nuclear hyperfine interactions in orbitally degenerate states of aromatic ions, H. M. McConnell and A. D. McLachlan—1
On the structure of ferric chloride solutions, C. L. Standley and R. F. Kruh—1450(L)
Proton resonance shifts in alkali halide solutions, Burton P. Fabricand and Sigmund Goldberg—1624
Quasi-lattice model or reciprocal salt systems. A generalized calculation, Milton Blander—432
Solvent effects on the spectra of halide ions, S. J. Strickler and M. Kasha—1077(L)
Some calculations for a one-dimensional salt mixture, Milton Blander—697(L)
Spectrum of radius of OH^- in solution, Joshua Jortner, Baruch Raz, and Gabriel Stein—1455(L)
Spin-orbit coupling in orbitally degenerate states of aromatic ions, Harden M. McConnell—13
Theory of solutions. III. Thermodynamics of aggregation or polymerization, Terrell L. Hill—1974
Vibration perturbations in electronically excited monosubstituted benzenes, O. E. Weigang, Jr. and A. J. Dahl—1845

Spectra (see Absorption Spectra, Emission Spectra Fluorescence, Raman Spectra)

Composition of the electronic states of Nd(IV) and Er(IV), B. G. Wybourne—279
Determination of relative electronic transition probabilities by impact methods, F. H. Dorman and J. D. Morrison—578
Emission spectra of trivalent thulium, L. G. Van Uitert and R. R. Soden—276
Reflection spectra and absolute infrared intensities in pure liquids: Benzene, chloroform, bromoform, carbon disulfide and carbon tetrachloride, P. N. Schatz, Shiro Maeda, J. L. Hollenberg and David A. Dows—175
Spectroscopy of fluorine flames. I. Hydrogen-fluoride flame and the vibration-rotation emission spectrum of HF, D. E. Mann, B. A. Thrush, D. R. Lide, Jr., J. J. Ball, and N. Acquista—420
Spin density in pyrene negative ion, G. J. Hoijtink, J. Townsend and S. I. Weissman—507

Sputtering

Statistical Mechanics (see Mechanics, Statistical)

Surface Phenomena

Distortion correction to the surface energy of the [110] face of alkali halide crystals, G. C. Benson, E. Dempsey, and P. Balk—157
Erratum: Distribution functions of a fluid in an external potential field: Application to physical adsorption [J. Chem. Phys. **33,** 464 (1960)], William A. Steele and Marvin Ross—1067(L)
Half-crystal energy constants, Hartland H. Schmidt—1250

Interaction of hydrogen and of nitrogen with a molybdenum ribbon, R. A. Pasternak and Hans U. D. Wiesendanger—2062
Interaction potentials of simple nonpolar molecules with graphite, A. D. Crowell and R. B. Steele—1347
Low-temperature chemisorption. I. Flash desorption of nitrogen, Gert Ehrlich—29
Low-temperature chemisorption. II. Flash desorption of carbon monoxide, Gert Ehrlich—39
Measurements of the diffusion coefficient of atomic nitrogen in molecular nitrogen and the catalytic efficiency of silver and copper oxide surfaces, Robert A. Young—1295
ν_3 vibration of adsorbed ethylene, L. H. Little—342(L)
Physical adsorption of nitrogen on pyrex at very low pressures, J. P. Hobson—1850(L)
Pressure dependence of the absolute catalytic efficiency of surfaces for removal of atomic nitrogen, Robert A. Young—1292
Proton-spin polarization of water adsorbed on sucrose chars, James J. Krebs—326
Separation of the isotopes HT and ortho-D_2 by adsorption at low temperatures, Anthony Katorski, J. G. Eberhart, and David White—2189(L)
Statistical mechanics of monatomic systems in an external periodic potential field. I. Introduction, virial expansion and classical second virial coefficient, Terrell L. Hill and Samuel Greenschlag—1538
Statistical mechanics of monatomic systems in an external periodic potential field. II. Distribution function theory for fluids, Terrell L. Hill and Nobuhiko Saitô—1543
Surface catalyzed excitations in the oxygen system, Gene Mannella and Paul Harteck—2177
Tests for chemisorption of nitrogen on a clean (100) nickel surface, H. H. Madden and H. E. Farnsworth—1187
Theory of the surface tension of molten salts, H. Reiss and S. W. Mayer—2001

Thermal Conductivity

Composition dependence of the thermal conductivity of regular solutions, Richard J. Bearman and V. S. Vaidhyanathan—264

Thermal Diffusion

Delineation of the problem of Soret diffusion, R. A. Oriani—1773
Erratum: Thermal-diffusion-column shape factors for the Lennard-Jones (12–6) potential [J. Chem Phys. **33,** 570 (1960)], B. B. McInteer and M. J. Reisfeld—1844(L)
Thermal diffusion factor of helium, F. van der Valk and A. E. de Vries—345(L)

Thermodynamic Properties

Alkali-iron group-halogen complexes. The dissociation energies of $KClFeCl_2$ and $CsClFeCl_2$, V. S. Rao and P. Kusch—832
Analysis of specific heat data for zinc: Resolution of the calorimetric and elastic H_0 discrepancy, C. W. Garland and J. Silverman—781
Densities of solutions of potassium in liquid ammonia and deutero-ammonia, Clyde A. Hutchison, Jr. and Donald E. O'Reilly—163
Distribution of silver ions in melt-grown alkali halides. W. Gomes—2191(L)
Electrical conductions in polycrystalline lead zirconate-titanate, C. V. Stephenson and C. V. Flanagan—2203(L)
Entropies of vaporization of hydrocarbons and the Hildebrand rule, R. W. Hermsen and J. M. Prausnitz—1081(L)
Extreme pressures. II. Volume-temperature relationship for gases, Leonard S. Levitt—1440
Heat capacities and thermodynamic functions of ZrH_2 and ZrD_2 from 5 to 350°K, and the hydrogen vibration frequency in ZrH_2, Howard E. Flotow and Darrell W. Osborne—1418
Heat capacity anomaly in solid air, William H. Lien and Norman E. Phillips—1073(L)
Heat capacity of antiferromagnetic $CuCl_2 \cdot 2H_2O$ in the spin wave region, R. G. Petersen and Norman E. Phillips—1463(L)
Heat capacity of thulium from 15° to 360°K, L. D. Jennings, Emma Hill and F. H. Spedding—2082
Heats of mixing in liquid alkali nitrate systems, O. J. Kleppa and L. S. Hersh—351
Infrared spectrum and thermodynamic properties of ruthenium tetroxide, M. H. Ortner—556
Molecular association in alkali halide vapors, Sheldon Datz, William T. Smith, Jr., and Ellison H. Taylor—558
Monte Carlo computations on the Ising model: The body-centered cubic lattice, Lester Guttman—1024
Normal coordinate treatments and calculated thermodynamic properties of phosphoryl chloride, thiophosphoryl chloride, and phosphoryl fluoride, Joseph S. Ziomek and Edward A. Piotrowski—1087
Oxygen isotope fractionation between calcium carbonate and water, Robert N. Clayton—724
Pauling's model and the thermodynamic properties of water, Henry S. Frank and Arvin S. Quist—604
Phase transition in ammonium fluoride, Richard Stevenson—346(L)
Second virial coefficient of boron trifluoride, C. J. G. Raw—1452(L)
Stabilities of gaseous molecules in the Pb–Se and Pb–Te systems, Richard F. Porter—583
Statistical mechanics of isotope effects on the thermodynamic properties of condensed systems, Jacob Bigeleisen—1485
Temperature dependence of the isotopic fractionation of nitrogen in the NO–NO^{-3} system, Marvin J. Stern, Lois Nash Kauder, and W. Spindel—333(L)
Thermodynamics of the vaporization of Cr_2O_3: Dissociation energies of CrO, CrO_2, and CrO_3, R. T. Grimley, R. P. Burns, and Mark G. Inghram—664
Thermoelectric power of silver halides, R. W. Christy—1148
Vapor pressure of nearly classical liquids, William A. Steele—802
Vapor pressure of silicon and the dissociation pressure of silicon carbide, Stanley G. Davis, Donald F. Anthrop, and Alan W. Searcy—659
Vaporization of iridium and rhodium, Morton B. Panish and Liane Reif—1915
Vaporization of several rare earth oxides, Morton B. Panish—1079(L)
Vaporization of the rare earth oxides, Morton B. Panish—2197(L)

Thermodynamics

Approach to thermodynamic equilibrium, J. E. Mayer—1207
Calculation of complex equilibrium with an unknown number of phases, R. H. Boll—1108
Density expansions of correlation functions for equilibrium systems, Harold L. Friedman—73
Entropy of mixing of interconvertible species; some reflections on the Gibbs paradox, Richard M. Noyes—1982
Mayer's ensembles of maximum entropy, Andrew D. McLachlan and Robert A. Harris—1451(L)
Quasi-lattice model of reciprocal salt systems. A generalized calculation, Milton Blander—432
Second law of thermodynamics, Bryce Crawford, Jr. and I. Oppenheim—1621
Thermodynamic theory of the pair correlation function, Edward W. Hart—1471

Thermoluminescence

Luminescence during annealing and phase change in crystals, Noye M. Johnson and Farrington Daniels—1434
Thermoluminescence in dolomite, W. L. Medlin—672

Transport Phenomena

Approximate theory of transport in simple dense fluid mixtures, Stuart A. Rice and Alan R. Allnatt—409
Composition dependence of the thermal conductivity of regular solutions, Richard J. Bearman and V. S. Vaidhyanathan—264
On the kinetic theory of dense fluids. VI. The singlet distribution function for rigid spheres with an attractive potential, Stuart A. Rice and Alan R. Allnatt—2144
On the kinetic theory of dense fluids. VII. The doublet distribution function for rigid spheres with an attractive potential, Alan R. Allnatt and Stuart A. Rice—2156
O_2 vibration relaxation in oxygen-argon mixtures, Morton Camac—448
Self-diffusion of nearly spherical molecules. Neopentane and tetramethyl silane, Dean C. Douglass, David W. McCall, and Ernest W. Anderson—152

Ultrasonics

Application of a theory of nonideal solutions to results of ultrasonic absorption measurements, F. O. Goodman—1585
Effect of several light molecules on the vibrational relaxation time of oxygen, J. G. Parker—1763
Mean free path and ultrasonic vibrational relaxation in liquids and dense gases, W. M. Madigosky and T. A. Litovitz—489

Valence and Chemical Bond

Applicability of approximate quantum mechanical wave functions having discontinuities in their first derivatives, Joseph O. Hirschfelder and George V. Nazaroff—1666
Comment on the difference between the bond orders calculated by SCF MO and simple MO method, Milan Randić—693(L)
Extraordinary basic functions in valence theory, Lawrence C. Snyder and Robert G. Parr—1661
Far-infrared bands of some crystals with strong hydrogen bonds, D. Hadži—1445(L)
'Floating' hydrogen densities in some molecules of the type XH_n, K. E. Banyard—2105
Low energy process for F^- formation in SF_6, R. K. Curran—1069(L)
Nuclear quadrople resonance of BrCl, M. A. Whitehead and H. H. Jaffé—2204(L)
Paramagnetism of uranyl ion. Effect of 6*d* orbitals and pi bonding, R. Linn Belford—318
Polarity of the C—H bonds in acetylene and its molecular quadrupole moment, H. Hamano—1688
Quantum mechanics of mobile electrons in conjugated bond systems. III. Topological matrix as generatrix or bondorders in homonuclear conjugated systems, Klaus Ruedenberg—1883
Theory of localized contributions to the chemical shift. Application to fluorobenzenes, M. Karplus and T. P. Das—1683

Viscosity

Approximate theory of transport in simple dense fluid mixtures, Stuart A. Rice and Alan R. Allnatt—409
Interpretation of viscosity data for concentrated polymer solutions, Hiroshi Fujita and Akira Kishimoto—393

X-ray Diffraction

Clustering in the critical region, George W. Brady and John I. Petz—332(L)
Crystallography of the Ru–B and Os–B systems, Charles P. Kempter and R. Jay Fries—1994
Erratum: X-ray scattering by a cell-model liquid [J. Chem. Phys. **33,** 1086 (1960)], L. H. Lund—688(L)
On the structure of ferric chloride solutions, C. L. Standley and R. F. Kruh—1450(L)
Some structural data for cubic metaboric acid, J. L. Parsons, A. H. Silver and M. E. Milberg—2192(L)
Study of the Wurtzite-type compounds. V. Structure or aluminum oxycarbide, Al_2CO; a short-range Wurtzite-type superstructure, E. L. Amma and G. A. Jeffrey—252
Transitions between different forms of ice, R. H. Beaumont, H. Chihara and J. A. Morrison—1456(L)
X-ray diffraction study of lead sulfide-arsenic sulfide glasses John I. Petz, R. F. Kruh and G. C. Amstutz—526
X-ray diffraction study of liquid mercury-indium alloys, Young Soo Kim, C. L. Standley, R. F. Kruh and Glen T. Clayton—1464(L)